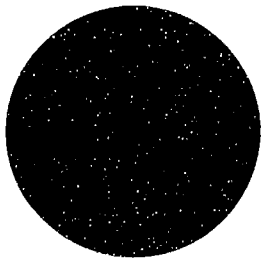
Technical Memorandum
of PWRI No. 3387

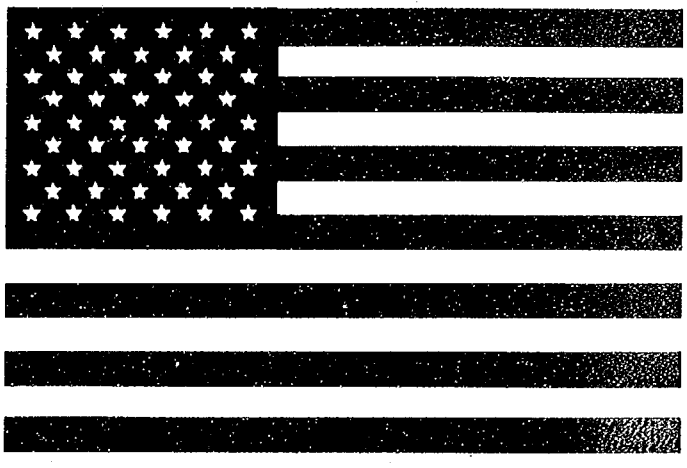
UJNR

Tsukuba, Japan

Wind and Seismic Effects

Proceedings of the 27th Joint Meeting





May, 1995

Copyright ©1995 by P.W.R.I.

All rights reserved. No part of this book may be reproduced by any means, nor translated into a machine language without the written permission of the Director General of P.W.R.I.

この報告書は，土木研究所長の承認を得て刊行したものである。したがって，本報告書の全部又は一部の転載，複製は，土木研究所長の文書による承認を得ずしてこれを行ってはならない。

Wind and Seismic Effects

PROCEEDINGS OF
THE 27TH JOINT
MEETING OF
THE U.S.–JAPAN
COOPERATIVE PROGRAM
IN NATURAL RESOURCES
PANEL ON WIND AND
SEISMIC EFFECTS

CONTENTS

PREFACE
AGENDA OF JOINT TECHNICAL MEETING AND SITE VISITS 1
LIST OF PANEL MEMBERS 13
LIST OF TASK COMMITTEE MEMBERS 33
RESOLUTIONS 39
PAPERS 45

THEME 1. Earthquake Engineering

Analysis of Dynamic Characteristics of Prestressed Concrete Cable-Stayed Bridge (Aomori Bay Bridge) Using Strong Motion Observation Data
Takamasa Inatomi and Sachito Tanaka 49

USGS Northridge Earthquake Digitized Recordings
A. Gerald Brady 61

Shaking Table Damage Tests of 3 Story RC Frames
Chikahiro Minowa, Shinichi Miyasita, Keiji Kitajima, Hiroshi Hosoya and Tsuneo Okada 67

Test Requirements for Base Isolation
H. W. Shenton, A. W. Taylor and H. S. Lew 81

Damage to Infrastructures by the 1994 Hokkaido-Toho-Oki Earthquake
Yasuyuki Koga, Ryoji Hagiwara, Hisanori Otsuka and Osamu Matsuo 89

Cost-effective Ground Improvement for Liquefaction Remediation near Existing Lifelines
Ronald D. Andrus and Riley M. Chung (Presented by H. S. Lew) 115

Shear Modulus and Radiation Damping Ratio of Rockfill Dams Estimated by Laboratory Test, In-Situ Test and Back Analysis of Earthquake Motions
Tadahiko Fujisawa, Akira Nakamura, Tomoya Iwashita and Nario Yasuda 125

Seismic Safety Evaluation of Sanitary Landfills
Ellis L. Krinitzsky, Mary Ellen Hynes and Arley G. Franklin 137

Evaluation Method of Ground Motion Amplification due to Irregularity of Ground Condition
Ryoji Hagiwara and Riki Honda 155

The Use of Seismic Hazard Maps for Improved Earthquake Risk Reduction
Richard J. McCarthy and James E. Slosson 169

Experimental Research on the Use of Viscoelastic Dampers in the Rehabilitation of Lightly Reinforced Concrete Frames
John R. Hayes, Jr. and Pamalee A. Brady (Presented by Steven C. Sweeney) 181

A Study on the Deformation Characteristics of Precast Hollow Piers during Earthquakes
Masanori Nakano, Shigeru Takagi and Moriyuki Okoshi 217

Response of On-netoh Bridge during Hokkaido Toho-oki Earthquake of October 1994
Masashi Sato, Hiroaki Nishi and Atsushi Nishimura 239

Comparison of U.S. and Japanese Highway Bridge Seismic Design Criteria
W. Phillip Yen, James D. Cooper and Ian M. Friedland 249

Verification of Stone Column Construction Using Field Instrumentation Data
Francis G. McLean, Michael G. Stevens and Richard H. Kelsic (Presented by John Ake) 263

New Developments in Civil Infrastructure Systems
K. P. Chong and S. C. Liu 287

Development of Hybrid Seismic Response Control of Bridges
Kazuhiko Kawashima, Hisanori Otsuka, Shigeki Unjoh and Hidetoshi Mukai 295

Shape Memory Alloy Dampers for Seismic Rehabilitation of Existing Buildings
Steven C. Sweeney and John R. Hayes 317

U.S.-Japan Cooperative Research Program on Composite and Hybrid Structures
–Research Plan and Progress–
Isao Nishiyama and Hiroyuki Yamanouchi 333

THEME 2. Wind Engineering

Offshore Research Results from Hurricane Andrew
Charles E. Smith 347

Wind-Induced Vibrations of a Super Long-Span Cable-Stayed Bridge in Turbulent Flow Generated by Surrounding Islands
Hiroshi Sato, Makoto Kitagawa, Ryuichi Toriumi and Hiroshi Katsuchi 357

First Five Years of NSF's Collaborative Program in Wind Engineering
–Results and Future Activities–
B. Bienkiewicz 371

THEME 3. Hyogoken Nanbu Earthquake

A Preliminary Report on the Hyogo-ken Nanbu Earthquake 1995
Hidemi Ito, Sumio Yoshikawa, Tetsuo Hashimoto and Akio Yoshida 395

Relationships between Geomorphologic Condition and Disasters at 1995 Hyogoken-nanbu Earthquake
Masaharu Tsuzawa, Masakatsu Horino and Hidetoshi Nakajima 403

Evaluation of Strong Ground Motion in Kobe Area of 1995 Hyogoken Nanbu Earthquake
Yoshikazu Kitagawa, Izuru Okawa, Toshihide Kashima and Shin Koyama 411

Infrastructure Damage by the 1995 Hyogoken Nanbu Earthquake
Takashi Iijima, Tomonobu Nakaoka and Yasuyuki Koga 421

Damages of Buildings Caused by the 1995 Hyogoken Nanbu Earthquake
Hisahiro Hiraishi, Toshibumi Fukuta and Motoi Yasumura 471

THEME 4. Technology Needs for Emergency Management Agency in Response, Recovery and Mitigation Operations Following Natural Disasters

Technology Applications by the U.S. Federal Emergency Management Agency in Response, Recovery, and Mitigation Operations Following Natural Disasters
Bruce Price and Bob Fox (Presented by James D. Cooper) 485

Collection and Distribution of Road Information in Disasters
–Kushiro-oki Earthquake, Hokkaido Nansei-oki Earthquake, and Hokkaido Touhou-oki Earthquake–
Yasuhiko Kajiya, Hideki Abe and Keishi Ishimoto 503

Epidemiologic Methods for Assessing Wind- and Seismic-related Health Effects in Disaster Response
Josephine Malilay and Eric Noji 507

THEME 5. Storm Surge and Tsunamis

Virtual Reality Expression System forTsunami Prevention
Hironao Takahashi, Kouji Sakai, Tetsuya Hiraishi and Toshihiko Nagai 517

Tsunami Reconnaissance Procedures
Harry Yeh 527

Propagation of Hokkaido Nansei-Oki Earthquake Tsunami around Cape Aonae
–nonlinear propagation of tsunami in shallow water–
Kenji Noguchi, Shinji Sato and Shigenobu Tanaka 545

Breakwater Armor Design Advances
William E. Roper 553

MANUSCRIPTS AUTHORED FOR THE PANEL MEETING BUT NOT PRESENTED ORALLY

A Review of Wind Research Currently Underway in the Vincent Aerodynamics Laboratory
Harold R. Bosch and Dryver R. Huston 571

Earthquake Engineering Research for Reservoir Dams
William E. Roper 583

Durability of Structural Retrofit with Carbon Fiber Reinforced Plastics (CFRPs)
L. C. Muszynski and R. L. Sierakowski 607

Concrete Beams and Aerospace Composite Material
C. A. Ross, M. L. Hughes, R. L. Sierakowski, J. W. Tedesco and W. C. Naylor 615

Probabilistic Assessment of Soil Liquefaction
Nikolaos Simos, Carl J. Costantino, Morris Reich and Thomas McSpadden 623

Impedance Functions of Footings Embedded in Saturated Strata
A. J. Philippacopoulos, Nikolaos Simos and Thomas McSpadden 635

Performance of Multi-Unit Residential Buildings During the 17 January 1994 Northridge Earthquake
Diana Todd and Riley Chung 647

Strength of Concrete Frames with Masonry Infill
Steven C. Sweeney and Ghassan Al-chaar 657

Use of Experience Data for Seismic Evaluations at Department of Energy Facilities
James R. Hill, Dan J. Guzy, Jeffrey K. Kimball and Robert C. Murray 675

Triaxial Upgrade of USACERL Shaking Table
John R. Hayes, Jr. and James B. Gambill 685

Seismic Response Properties of Concrete Gravity Dam with Interaction of Dam and Foundation Rock
Isao Nagayama and Takashi Sasaki 697

River Embankment Damage Caused by the 1993 Hokkaido Kushiro-oki and Hokkaido Nansei-oki Earthquakes and Their Restoration Methods
Akihiro Yamakoshi, Yasuro Ide and Masahide Kaji 707

Strong Motion Records of Hokkaido Toho-oki Earthquake in 1994
Masashi Sato, Takeshi Shimada and Manabu Kaneko 721

Features of Damages to Road Embankments by Recent Earthquakes in Hokkaido, Japan
Jun'ichi Nishikawa and Yasuaki Matsuda 733

Damage and Soil Liquefaction Caused by the 1994 Hokkaido Tohooki Earthquake
Katsuyoshi Suzuki and Yoshitaka Yamada 739

The Relationships between Physical Conditions and Various Damage Caused by the 1994 Sanriku-haruka-oki Earthquake
Masakatsu Horino, Seiji Ichikawa and Yasushi Ono 753

Characteristics of Water Level in Rivers Before the 1993 Hokkaido Nansei-oki Earthquake
Masashi Sato, Tadayuki Shirono and Takashi Sato 765

APPENDIX
TASK COMMITTEES REPORTS 781
TECHNICAL SITE VISITS 807

PREFACE

This publication is the proceedings of the 27th Joint Meeting of the U.S.–Japan Panel on Wind and Seismic Effects. The meeting was held at the Public Works Research Institute, Tsukuba, Japan, during May 16–19, 1995. The proceedings include the program, list of members, panel resolutions, task committee reports and technical papers submitted to the Joint Panel Meeting, and summary of the technical site visits.

BACKGROUND

Responding to the need for improved engineering and scientific practices through exchange of technical data and information, research personnel, and research equipment, the United States and Japan in 1961 created the U.S.–Japan Cooperative Science Program. Three collateral programs comprise the Cooperative Science Program. The U.S.–Japan Cooperative Program in Natural Resources (UJNR), one of the three, was created in January 1964. The objective of UJNR is to exchange information on research results and exchange scientists and engineers in the area of natural resources for the benefit of both countries. UJNR is composed of 16 Panels each responsible for specific technical subjects.

The Panel in Wind and Seismic Effects was established in 1969. Seventeen U.S. and seven Japanese agencies participated with representatives of private sector organizations to develop and exchange technologies aimed at reducing damages from high winds, earthquakes, storm surge, and tsunamis. This work is produced through collaboration between U.S. and Japanese member researchers working in 10 task committees. Each committee focuses on specific technical issues, e.g., earthquake strong motion data. The Panel provides the vehicle to exchange technical data and information on design and construction of civil engineering lifelines, buildings and waterfront structures, and to exchange high wind and seismic measurement records. Annual meetings alternate between Japan and United States(odd numbered years in Japan; even numbered years in U.S.). These one–week technical meetings provide the forum to discuss ongoing research and research results; one–week technical study tours follow the meetings.

The National Institute of Standards and Technology (NIST) provides the U.S.–side chairman and secretariat. The Public Works Research Institute (PWRI), Japan, provides the Japan–side chairman and secretariat.

Cooperative research is performed through formal Panel Programs. In 1981, cooperative research in Large–scale Testing was started under the auspices of the Panel. Also in 1981, joint research on Reinforced Concrete Structures was initiated. Full–scale testing was performed at the Building Research Institute (BRI), one of the six Japanese member organizations, with supporting tests in Japan and in the United States. Two years later, a joint research program on Steel Structures was initiated. Full–scale testing again was led by BRI with supporting tests in the United States and Japan. The U.S.–Japan coordinated program for Masonry Building Research was started in 1985. A U.S.–Japan coordinated program on Precast Seismic Structural Systems was initiated in 1991. A joint program on

Seismic Performance of Composite and Hybrid Structures was initiated in 1993. In 1994, a joint program was initiated on Physical and Numerical Simulation of Structural Damages Due to Liquefaction and Development of Countermeasure Techniques.

Task Committee meetings, exchanges of data and information through technical presentations at annual Panel meetings, exchanges of guest researchers, visits to respective research laboratories and informal interactions between Panel meetings, joint workshops and seminars, and joint cooperative research programs all contribute to the development and effective delivery of knowledge that has influenced design and construction practices in both countries. Guest research exchanges have advanced the state of technology in areas of steel, concrete, and masonry structures under seismic forces; developed techniques to analyze risks from liquefaction; modeled water seepage in dam foundations; performed comparative analyses of seismic design of U.S. and Japanese bridges.

Direct communication between counterpart country organizations is the cornerstone of the Panel. Effective information exchanges and exchanges of personnel and equipment have strengthened domestic programs of both countries. There are opportunities for experts in various technical fields to get to know their foreign counterparts, conduct informal exchanges, bring their respective views to the frontiers of knowledge, and advance knowledge of their specialities.

The Panel's activities resulted in improved building and bridge standards and codes and design and construction practices in hydraulic structures in both countries, for example:

- created and exchanged digitized earthquake records used as the basis of design and research for Japan and the United States;
- transferred earthquake engineering information and strong-motion measurement techniques for use by seismically active countries, e.g., Australia, Canada, Italy, Mexico, Peru, Taiwan, Turkey, and North Africa;
- produced data that advanced retrofit techniques for bridge structures;
- developed field test data for use in aerodynamic retrofit of bridge structures;
- produced full-scale test data that advanced seismic design standards for buildings;
- advanced technology for repairing and strengthening reinforced concrete,steel,and masonry structures;
- improved in-situ measurement methods for soil liquefaction and stability under seismic loads;
- created a database comparing Japanese and U.S. standard penetration tests to improve prediction of soil liquefaction;
- created database on storm surge and tsunamis and verified mathematical models of tsunami and storm surge warning systems;
- established a library resource of current research on wind and earthquake engineering and on storm surge and tsunamis;
- published proceedings of Panel meetings, Task Committee Workshops, and special publications such as List of Panel Publications and translated two-volume series on earthquake resistant construction using base isolation systems;
- gained better knowledge of both countries' research, design, and construction capabilities

from indepth visits to host country's laboratories and building and public works projects. Results of such visits contribute to creation of new Task Committees, agendas for Joint Panel meetings and task committee workshops, special visits of U.S.–Japan researchers, and joint collaborative research.

HIGHLIGHTS OF THE 27TH JOINT PANEL MEETING

Thirty–four papers were presented orally. The papers were organized into five themes: Wind Engineering; Earthquake Engineering; Storm Surge and Tsunamis; Hyogo–ken Nanbu Earthquake; and Technology Needs for Emergency Response and Recovery.

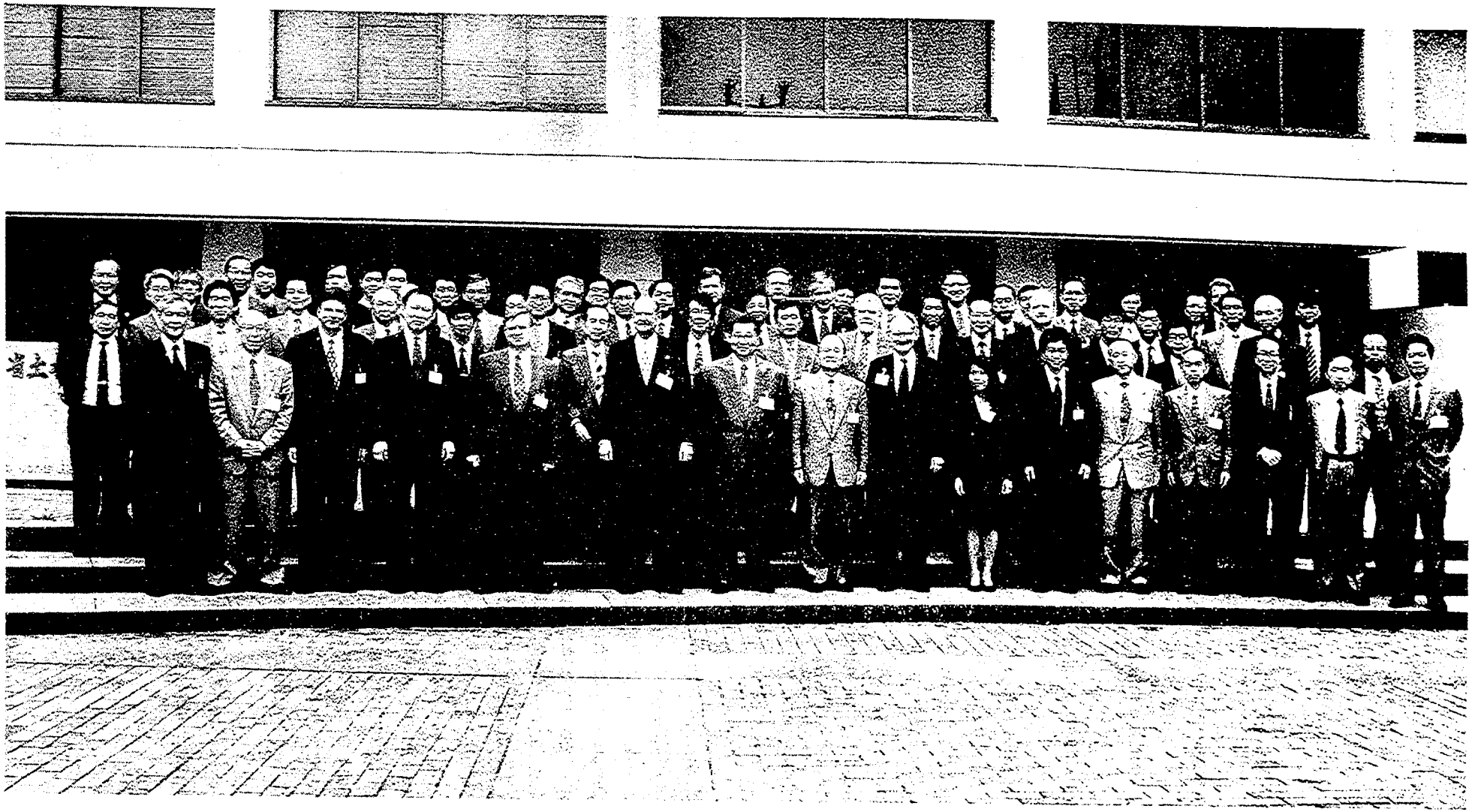
Highlights include:

- Technical presentations:
  - highlighted important work by the U.S. and Japan Panel.
  - important knowledge was exchanged for research and practice, e.g., analytical and experimental research results on wind engineering; seismic design of bridges and dams; active and passive control of structural response; recent earthquake disasters caused by Northridge Earthquake, Hokkaido Nansei–oki Earthquake, and Hyogo–ken Nanbu Earthquake.
  - information was exchanged about extensive U.S./Japanese public works projects, civil engineering research, and their applications into practice.

- Excellent projects are being performed by both sides in intelligent and smart materials and systems technologies. Panel participants advance their competence by becoming more familiar with these research projects and through direct participation in appropriate research.
- Reports on reconnaissance of recent earthquakes show the need of strength design method for concrete and steel structures.
- Task Committee activities grow in strength.The T/C structure is an extremely effective vehicle to explore in depth the technologies and methods being used by both countries.
  - Two Task Committee workshops/conferences were held in the past year and eight workshops are planned for the coming year.
- Cooperative Research Programs continue to be productive. Since the 24th Joint Panel Meeting cooperative research has led to Japan–side publications of:
  - Precast Connection Design Manual, and
  - Design Guidelines for New Precast Concrete Systems.

A new Cooperative Research Program was approved on Seismic Performance of Composite and Hybrid Structures.

Tomonobu Nakaoka, Secretary–General
Japan–Side Panel on Wind and Seismic Effects



U.S. Side and Japan Side Attendance
27th Joint Meeting of the U.S.–Japan Panel on Wind and Seismic Effects

Agenda of Joint Meeting and Site Visits

AGENDA OF JOINT TECHNICAL MEETING AND SITE VISITS

TECHNICAL MEETING

May 16 (Tue) 10:30 ~ 12:00

10:30 OPENING CEREMONIES
(8TH Floor Conference Room, Main Building)

Call to order by Tomonobu NAKAOKA, Secretary-General, Japan Side

Opening remarks by Haruho FUJII, Vice-Minister of Construction for Engineering Affairs

Remarks by Dr. M. A. G. MICHAUD, Minister-Counselor for Environmental, Scientific and Technological Affairs, Embassy of the United States of America

Remarks by Shinichiro OGURA, International Affairs Division, Science and Technology Promotion Bureau, Science and Technology Agency

Remarks by Takashi IIJIMA, Chairman JAPAN-Side, Panel on Wind and Seismic Effects, Director-General, Public Works Research Institute, Ministry of Construction

Remarks by Richard N. WRIGHT, Chairman U. S. -Side, Panel on Wind and Seismic Effects, Director, Building and Fire Research Laboratory, National Institute of Standards and Technology, Department of Commerce

Introduction of JAPAN Members by Japan Panel Chairman

Introduction of U. S. Members by U. S. Panel Chairman

Elect Joint Meeting Chairman

Adopt Agenda

Adjourn

11:45 Group Photograph

May 16 (TUE)

10:30 Opening Ceremonies [8F Conference Room]

11:45 Group Photograph

12:00 Lunch [1F Conference Room]

13:00 Session 1 (Earthquake Engineering 1) Chairman—R. N. Wright

13:00 Analysis of Dynamic Characteristics of Prestressed Concrete Cable-Stayed Bridge (Aomori Bay Bridge) Using Strong Motion Observation Data
Takamasa Inatomi, Sachito Tanaka, PHRI

13:20 USGS Northridge Earthquake Digitized Recordings
Gerald Brady, USGS

13:40 Shaking Table Damage Tests of Three Story RC Frames
Chikahiro Minowa, NRIESD, Tsuneo Okada, Univ. of Tokyo, et al.

14:00 Test Requirements for Base Isolation
H. W. Shenton, UD, A. W. Taylor and H. S. Lew, NIST

14:20 Discussion

14:40 Break

15:00 Task Committee Meetings
A: Strong-Motion Data and Applications [5F Room 524]
B : Testing and Evaluation Procedures for Building Systems [5F Room 531A]
C : Design Evaluation and Improvement of Structures
D : Dam Earthquake Engineering [5F Room 531B]
G : Structural Control and Intelligent Material Systems [5F Room 526]
K : Wind and Earthquake Engineering for offshore and Coastal Facilities [5F Room 531C]

16:40 Adjourn

18:00 Reception Hosted by Vice-Minister of Construction for Engineering Affairs
(Hotel Tsukuba Sun-Route, Tel. 0298-58-1151)

May 17 (WED)

9 : 0 0 Session 2 (Earthquake Engineering 2) Chairman－Takashi Ijima

9 : 0 0 Damage to Infrastructures by the 1994 Hokkaido－Toho－Oki Earthquake
Yasuyuki Koga, Ryoji Hagiwara, Hisanori Otsuka
and Osamu Matsuo, PWRI

9 : 2 0 Cost－effective Ground Improvement for Liquefaction Remediation near Existing Lifelines
Ronald D. Andrus and Riley Chung, NIST (Presented by H. S. Lew)

9 : 4 0 Shear Modulus and Radiation Damping Ratio of Rockfill Dams Estimated by Laboratory Test, In－Situ Test and Back Analysis of Earthquake Motions
Tadahiko Fujisawa, Akira Nakamura, Nario Yasuda,
Tomoya Iwashita, PWRI

1 0 : 0 0 Seismic Safety Evaluation of Sanitary Landfills
Ellis Krinitzsky, Mary Ellen Hynes and Arley Franklin, WES

1 0 : 2 0 Discussion

1 0 : 4 0 Break

1 1 : 0 0 Session 3 (Earthquake Engineering 3) Chairman－Takashi Ijima

1 1 : 0 0 Evaluation Method of Ground Motion Amplification due to Irregularity of Ground Condition
Ryoji Hagiwara, Riki Honda , PWRI

1 1 : 2 0 The Use of Seismic Hazard Maps for Improved Earthquake Risk Reduction
Richard J. McCarthy , CA Seismic Safety Commission, and James Slosson,
Slosson & Assoc

1 1 : 4 0 Experimental Research on the Use of Viscoelastic Dampers in the Rehabilitation of Lightly Reinforced Concrete Frames
John Hayes and Pamalee Brady, CERL (Presented by Steven Sweeney)

1 2 : 0 0 Discussion

1 2 : 2 0 Lunch [1F Conference Room]

1 3 : 2 0 Session 4 (Earthquake Engineering 4) Chairman－Takashi Ijima

1 3 : 2 0 A Study on the Deformation Characteristics of Precast hollow Piers during Earthquakes
Masanori Nakano, Shigeru Takagi, Moriyuki Okoshi , PWRI

1 3 : 4 0 Response of On－netoh Bridge during Hokkaido Toho－oki Earthquake of

October 1994
Masashi Sato, Hiroaki Nishi, Atsushi Nishimura, CERI

14 : 00 Comparison of U. S. and Japanese Highway Bridge Seismic Design Criteria
W. Phillip Yen, James D. Cooper, FHWA, and Ian Friedland, UNYB

14 : 20 Verification of Stone Column Construction Using Field Instrumentation Data
Rick Kelsic, Mike Stevens and Frank McLean, BUREC
(presented by John Ake)

14 : 40 New Developments in Civil Infrastructure Systems
K. P. Chong and S. C. Liu, NSF

15 : 00 Discussion

15 : 20 Break

15 : 40 Task Committee Meetings
F : Disaster Prevention Methods for Lifelines Systems [5F Room 524]
H : Soil Behavior and Stability During Earthquakes [5F Room 531A]
I : Storm Surge and Tsunami [5F Room 531B]
J : Wind and Earthquake Engineering for Transportation Systems [5F Room 526]

17 : 20 Adjourn

18 : 30 Reception Hosted by Director-General of Public Works Research Institute
(Ushiku-Chateau, Tel. 0298-73-3151)

May 18 (THU)

9 : 0 0 Session 5 (Earthquake Engineering 5) Chairman– R. N. Wright

9 : 0 0 Development of Hybrid Seismic Response Control of Bridges
Kazuhiko Kawashima, Hisanori Otsuka, Shigeki Unjoh,
Hidetoshi Mukai, PWRI

9 : 2 0 Shape Memory Alloy Dampers for Seismic Rehabilitation of Existing Buildings
Steven Sweeney and Jack Hayes, CERL

9 : 4 0 U. S. –Japan Cooperative Research Program on Composite and Hybrid Structures – Research Plan and its Progress–
Isao Nishiyama, Hiroyuki Yamanouchi, BRI

1 0 : 0 0 Discussion

1 0 : 2 0 Break

1 0 : 4 0 Session 6 (Wind Engineering) Chairman– R. N. Wright

1 0 : 4 0 Offshore Research Results from Hurricane Andrew
Charles Smith, MMS

1 1 : 0 0 Wind– Induced Vibrations of a Super Long–Span Cable–Stayed Bridge in Turbulent Flow Generated by Surrounding Islands
Hiroshi Sato, PWRI
Makoto Kitagawa, Ryuichi Toriumi, Hiroshi Katsuchi, HSBA

1 1 : 2 0 First Five Years of NSF's Collaborative Program in Wind Engineering: Results and Future Activities
Bogusz Bienkiewicz, CSU

1 1 : 4 0 Discussion

1 2 : 0 0 Lunch [1F Conference Room]

1 3 : 0 0 Session 7 (Hyogo–ken Nanbu Earthquake 1) Chairman– R. N. Wright

1 3 : 0 0 A Preliminary Report on the Hyogo–ken Nanbu Earthquake 1995
Hidemi Ito, Sumio Yoshikawa, JMA
Tetsuo Hashimoto, Akio Yoshida, MRI

1 3 : 2 0 Relationships between Geomorphologic Condition and Disasters at 1995 Hyogoken– nanbu Earthquake
Masaharu Tsuzawa, Masakatsu Horino, Hidetoshi Nakajima, and GSI Team, GSI

13：40 Evaluation of Strong Ground Motion in Kobe Area of 1995 Hyogoken Nanbu Earthquake
Yoshikazu Kitagawa, Izuru Okawa, Toshihide Kashima, Shin Koyama, BRI

14：00 Discussion

14：20 Break

14：40 Session 8 (Hyogo-ken Nanbu Earthquake 2) Chairman-R. N. Wright

14：40 Infrastructure Damage by the 1995 Hyogoken Nanbu Earthquake
Takashi Iijima and PWRI Team , PWRI

15：20 Damages of Buildings Caused by the 1995 Hyogoken Nanbu Earthquake
Hisahiro Hiraishi, Toshibumi Fukuta, Motoi Yasumura, BRI

15：40 Discussion

16：00 Break

16：20 Report of Workshop Chairman-R. N. Wright

17：20 Adjourn

18：00 Individually Hosted Dinner

MAY 19 (FRI)

9 : 0 0 Session 9 (Technology Needs for Emergency Response and Recovery Following Natural Disasters) Chairman–Takashi Ijima

9 : 0 0 Technology Applications by the U. S. Federal Emergency Management Agency in Response, Recovery, and Mitigation Operations Following Natural Disasters
Bruce Price and Bob Fox, FEMA (presented by James Cooper, FHWA)

9 : 2 0 Collection and Distribution of Road Information in Disasters
–Kushiro–oki Earthquake, Hokkaido Nansei–oki Erathquake, and Hokkaido–Touhou–oki Earthquake –
Yasuhiko Kajiya, Hideki Abe, Keishi Ishimoto, CERI

9 : 4 0 Epidemiologic Methods for Assessing Wind–and Seismic–related Health Effects in Disaster Response
Josephine Malilay and Eric Noji, CDC

1 0 : 0 0 Discussion

1 0 : 2 0 Break

1 0 : 4 0 Session 1 0 (Storm Surge and Tsunamis) Chairman–Takashi Ijima

1 0 : 4 0 Virtual Reality Expression System for Tsunami Prevention
Hironao Takahashi, Kouji Sakai, Tetsuya Hiraishi, Toshihiko Nagai, PHRI

1 1 : 0 0 Tsunami Reconnaissance Procedures
Harry Yeh, Univ of Wash

1 1 : 2 0 Propagation of Hokkaido Nan–sei Oki Earthquake Tsunami around Cape Aonae –nonlinear propagation of tsunami in shallow water –
Kenji Noguchi, Shinji Sato, Shigenobu Tanaka, PWRI

1 1 : 4 0 Breakwater Armor Design Advances
William Roper, CORPS

12：00 Discussion

12：20 Lunch [1F Conference Room]

13：20 Reports of Task Committees

A : Strong-Motion Data and Applications
B : Testing and Evaluation Procedures for Building Systems
C : Evaluation and Improvement of Structures
D : Dam Earthquake Engineering
F : Disaster Prevention Methods for Lifelines Systems
G : Structural Control and Intelligent Material Systems
H : Soil Behavior and Stability During Earthquakes
I : Storm Surges and Tsunami
J : Wind and Earthquake Engineering for Transportation Systems
K : Wind and Earthquake Engineering for offshore and Coastal Facilities

15：20 Break

15：40 Adoption of Final Resolution

16：30 Break

16：40 Closing Ceremony

18：00 Reception Hosted by U. S. Members
(Hotel Grand Shinonome, Tel. 0298-56-2211)

CLOSING CEREMONIES

May 19 (Fri) 16:40 ～ 17:00
(8TH Floor International Conference Room)

16 : 40

Call to Order by Tomonobu NAKAOKA, Secretary-General, Japan-Side Panel

Closing Remarks by Richard N. WRIGHT, Chairman U. S. – Side Panel

Closing Remarks by Takashi IIJIMA, Chairman JAPAN – Side Panel

TECHNICAL STUDY TOUR

May 15 (Monday)

Visit to Trans−Tokyo Bay Highway (under construction)

May 20 (Saturday)

Visit to Kangawa Bridge
Inspection of Kangawa Bridge (Arch Bridge, under construction)
Visit to stadium for Nagano Olympic
Dinner (hosted by Nagano National Highway Construction Office)

May 21 (Sunday)

Visit to Kamikochi
Dinner (hosted by Takayama National Highway Construction Office)

May 22 (Monday)

Visit to Abou Tunnel (under construction)
Visit to Tsumago, Magome (old town)

May 23 (Tuesday)

Visit to Akashi−straight Bridge 4A
Visit Nojima fault and striken area in Awaji Island caused by Great Hanshin−Awaji Earthquake
Visit to Akashi−straight Bridge 2P
Reception (hosted by Honshu−Shikoku Bridge Authority)

May 24 (Wednesday)

Visit to Matsumura Research Institute (Seismic Isolation Buildings)
Investigation of damage to highway bridges around Kobe
Reception

May 25 (Thursday)

Investigation of damage to port facilities around Kobe
Investigation of damage to buildings around Kobe

May 26 (Friday)

Visit to Horyuji−Temple (the oldest wooden building in the world)
Visit to Todaiji−Temple (The great image of Buddha at Nara etc.)

May 27 (Saturday)

Visit to Kansai International Airport

List of Panel Members

JAPAN-SIDE PANEL ON WIND AND SEISMIC EFFECTS MEMBERSHIP LIST

STEERING COMMITTEE

Dr. Takashi Iijima
Chairman, Japan-side
Panel on Wind and Seismic Effects,
UJNR
Director-General
Public Works Research Institute
Ministry of Construction
1, Asahi, Tsukuba-shi,
Ibaraki-ken 305

Mr. Tomonobu Nakaoka
Secretary-General, Japan-side
Panel on Wind and Seismic Effects,
UJNR
Deputy Director-General
Public Works Research Institute
Ministry of Construction
1, Asahi, Tsukuba-shi,
Ibaraki-ken 305

Mr. Naotoshi Baba
Director, Planning Divison
Road Disaster Prevention Section
Road Bureau
Ministry of Construction
2-1-3, Kasumigaseki, Chiyoda-ku,
Tokyo 100

Mr. Kunio Enoshima
Senior Assistant for Disaster Prevention
Planning Division
Administration Department
Japan Meteorological Agency
1-3-4, Otemachi, Chiyoda-ku
Tokyo 100

Mr. Tadahiko Fujisawa
Director, Dam Department
Public Works Research Institute
Ministry of Construction
1, Asahi, Tsukuba-shi,
Ibaraki-ken 305

Mr. Ryoji Hagiwara
Head, Ground Vibration Division
Earthquake Disaster Prevention
Department
Public Works Research Institute
Ministry of Construction
1, Asahi, Tsukuba-shi,
Ibaraki-ken 305

Mr. Takeshi Hashimoto
Director, Earthquake Disaster
Countermeasures Division
Prevention Bureau
National Land Agency
1-2-2, Kasumigaseki, Chiyoda-ku,
Tokyo 100

Dr. Hisahiro Hiraishi
Structural Engineering Department
Building Research Institute
Ministry of Construction
1, Takehara, Tsukuba-shi,
Ibaraki-ken 305

Dr. Susumu Iai
Chief, Geotechnical Earthquake
Engineering Laboratory
Port and Harbour Research Institute
Ministry of Transport
3-1-1, Nagase, Yokosuka-shi
Kanagawa-ken 239

Dr. Takamasa Inatomi
Director, Structural Engineering Division
Port and Harbour Research Institute
Ministry of Transport
3-1-1, Nagase, Yokosuka
Kanagawa-ken, 239

Dr. Toshio Iwasaki
President
Civil Engineering Research Laboratory
Kyodo Building 5F 3-3-4 Kanda Kaji-cho
Chiyoda-ku Tokyo 101

Dr. Kazuhiko Kawashima
Professor Department of Civil Engineering
Tokyo Institute of Technology
2-12-1 O-okayama
Meguro-ku Tokyo 152

Dr. Yoshikazu Kitagawa
Director, International Institute of
Seismology and Earthquake Engineering
Building Research Institute
Ministry of Construction
1, Tatehara, Tsukuba-shi,
Ibaraki-ken 305

Dr. Yasuyuki Koga
Director, Earthquake Disaster
Prevention Department
Public Works Research Institute
Ministry of Construction
1, Asahi, Tsukuba-shi,
Ibaraki-ken 305

Mr. Kiyoshi Mimura
Directer, Geographic Department
Geographical Survey Institute
Ministry of Construction
1, Kitasato, Tsukuba-shi
Ibaraki-ken 305

Dr. Chikahiro Minowa
Cooperative Research Officer
National Research Institute for
Earth Science and Disaster
Prevention
Science and Technology Agency
3-1, Tennodai, Tsukuba-shi,
Ibaraki-ken, 305

Mr. Hatsukazu Mizuno
Program Director of International Codes and
Standards Research
Codes and Evaluation Research Center
Building Research Institute
Ministry of Construction
1, Tatehara, Tsukuba-shi,
Ibaraki-ken 305

Mr. Eishi Mochizuki
Director, Seismology and Volcanology
Research Department
Meteorological Research Institute
Japan Meteorological Agency
1-1, Nagamine, Tsukuba-shi
Ibaraki-ken 305

Mr. Akira Nakamura
Head, Fill Type Dam Division
Public Works Research Institute
Ministry of Construction
1, Asahi, Tsukuba-shi,
Ibaraki-ken 305

Dr. Tadahiko Nakao
Director, River Division
Public Works Research Institute
Ministry of Construction
1, Asahi, Tsukuba-shi,
Ibaraki-ken 305

Dr. Shinsuke Nakata
Director, Production
Department
Building Research Institute
Ministry of Construction
1, Tatehara, Tsukuba-shi,
Ibaraki-ken 305

Dr. Nobuyuki Narita
Professor, Tokyo Metropolitan University
17-15 Yawata-6 Ichikawa-shi
Chiba-ken 272

Dr. Setsuo Noda
Director- General
Port and Harbour Research
Institute
Ministry of Transport
3-1-1, Nagase, Yokosuka,
Kanagawa-ken 239

Dr. Shigeyuki Noto
Director, Structures Division
Civil Engineering Research Institute
Hokkaido Development Agency
1-3, Hiragishi, Toyohira-ku
Sapporo, Hokkaido, 062

Dr. Tsuneo Okada
Professor, University of Tokyo
7-22-1, Roppongi, Minato-ku,
Tokyo 106

Mr. Masao Okamoto
Director, Disaster Prevention
Investigation Section
River Bureau
Ministry of Construction
2-1-3, Kasumigaseki, Chiyoda-ku,
Tokyo 100

Mr. Keiichi Ohtani
Director, Disaster Prevention
Research Division
National Research Institute for
Earth Science and Disaster Prevention
Science and Technology Agency
3-1, Tennodai, Tsukuba-shi,
Ibaraki-ken, 305

Dr. Hisanori Ohtsuka
Head, Earthquake Engineering
Division
Earthquake Disaster Prevention
Department
Public Works Research Institute
Ministry of Construction
1, Asahi, Tsukuba-shi,
Ibaraki-ken 305

Mr. Shin Ootsuka
Director, Typhoon Research Division
Meteorological Research Institute
Japan Meteorological Agency
1-1, Nagamine, Tsukuba-shi
Ibaraki-ken 305

Mr. Hiroshi Sasaki
Director, Building Guidance Divison
Building Disaster Prevention Section
Housing Bureau
Ministry of Construction
2-1-3, Kasumigaseki, Chiyoda-ku,
Tokyo 100

Mr. Yuji Sakakibara
Director
Office of Disaster Prevention Research
Policy Division
Research and Development Bureau
1-2-2, Kasumigaseki Chiyoda-ku
Tokyo 100

Dr. Hiroshi Sato
Head, Structure Division
Structure and Bridge Department
Public Works Research Institute
Ministry of Construction
1, Asahi, Tsukuba-shi,
Ibaraki-ken 305

Mr. Shigenobu Tanaka
Head, Coastal Engineering Division
River Department
Public Works Research Institute
Ministry of Construction
1, Asahi, Tsukuba-shi,
Ibaraki-ken 305

Dr. Tatsuo Uwabe
Chief, Earthquake Disaster Prevention Laboratory
Structural Engineering Division
Port and Harbour Research Institute
Ministry of Transport
3-1-1, Nagase, Yokosuka-shi,
Kanagawa-ken 239

Mr. Makoto Wada
Director, Disaster Countermeasure Office
Coast Administration and Disaster Prevention Division
Ports and Harbours Bureau,
Ministy of Transport
2-1-3, Kasumigaseki, Chiyoda-ku,
Tokyo 100

Dr. Makoto Watabe
Senior Managing Director
Shimizu Corporation
2-25-5, Tokiwadai, Itabashi-ku,
Tokyo 173

Mr. Asao Yamakawa
Director, International Affairs Division
Economic Affairs Bureau
Ministry of Construction
2-1-3, Kasumigaseki, Chiyoda-ku,
Tokyo 100

Dr. Hiroyuki Yamanouchi
Director, Structural Engineering Department
Building Research Institute
Ministry of Construction
1, Takehata, Tsukuba-shi,
Ibaraki-ken 305

Dr. Koichi Yokoyama
Director, Structure and Bridge Department
Public Works Research Institute
Ministry of Construction
1, Asahi, Tsukuba-shi,
Ibaraki-ken 305

SECRETARIES COMMITTEE

Mr. Tomonobu Nakaoka
Secretary-General, Japan-side
Panel on Wind and Seismic Effects,
UJNR
Deputy Director-General
Public Works Research Institute
Ministry of Construction
1, Asahi, Tsukuba-shi,
Ibaraki-ken 305

Mr. Takekazu Akagiri
Head, Planning Divison
Geographic Department
Geographical Survey Institute
1, Kitasato, Tsukuba-shi,
Ibarakiken 305

Mr. Ryoji Hagiwara
Head, Ground Vibration Division
Earthquake Disaster Prevention
Department
Public Works Research Institute
Ministry of Construction
1, Asahi, Tsukuba-shi,
Ibaraki-ken 305

M r. Koichi Honda
Director,
Research Planning and Coordination Section
Administration Divison
Civil Engineering Research Institute of
Hokkaido Development Bureau
1-3, Hiragishi, Toyohiraku, Sapporo,
Hokkaido 062

Dr. Susumu Iai
Chief, Geotechnical Earthquake
Engineering Laboratory
Port and Harbour Research Institute
Ministry of Transport
3-1-1, Nagase, Yokosuka-shi
Kanagawa-ken 239

Dr. Kazuhiko Kawashima
Professor Department of Civil Engineering
Tokyo Institute of Technology
2-12-1 O-okayama
Meguro-ku Tokyo 152

Dr. Yoshikazu Kitagawa
Director, International Institute of
Seismology and Earthquake Engineering
Building Research Institute
Ministry of Construction
1, Tatehara, Tsukuba-shi,
Ibaraki-ken 305

Dr. Yasuyuki Koga
Director, Earthquake Disaster
Prevention Department
Public Works Research Institute
Ministry of Construction
1, Asahi, Tsukuba-shi,
Ibaraki-ken 305

Mr. Osamu Matsuo
Head, Soil Dynamics Division
Earthquake Disaster Prevention
Department
Public Works Research Institute
Ministry of Construction
1, Asahi, Tsukuba-shi,
Ibaraki-ken 305

Dr. Chikahiro Minowa
Cooperative Research Officer
National Research Institute for
Earth Science and Disaster
Prevention
3-1, Tennodai, Tsukuba-shi,
Ibaraki-ken, 305

Mr. Akira Nakamura
Head, Fill Type Dam Division
Public Works Research Institute
Ministry of Construction
1, Asahi, Tsukuba-shi,
Ibaraki-ken 305

Mr. Masanori Nakano
Head, Foundation Engineering Division
Structure and Bridge Department
Public Works Research Institute
Ministry of Construction
1, Asahi, Tsukuba-shi,
Ibaraki-ken 305

Mr. Kazuhiro Nishikawa
Head, Bridge Division
Structure and Bridge Department
Public Works Research Institute
Ministry of Construction
1, Asahi, Tsukuba-shi,
Ibaraki-ken 305

Dr. Nobuyuki Ogawa
Head, Earthquake Engineering Laboratory
National Research Institute for
Earth Science and Disaster Prevention
Science and Technology Agency
3-1, Tennodai, Tsukuba-shi,
Ibaraki-ken 305

Dr. Hisashi Okada
Head of Aerodynamics Divison
Structural Engineering Department
Building Research Institute
Ministry of Construction
1, Tatehara, Tsukuba-shi,
Ibaraki-ken 305

Mr. Masami Okada
Head
The First Research Laboratory,
Seismology and Volcanology Research Department
Meteorological Research Institute
Japan Meteorological Agency
Ministry of Transport
1-1, Nagamine, Tsukuba-shi,
Ibaraki-ken 305

Dr. Izuru Okawa
Head, Geotechnical Engineering Division
Structural Engineering Department
Building Research Institute
Ministry of Construction
1, Tatehara, Tsukuba-shi,
Ibaraki-ken 305

Mr. Keiichi Ohtani
Director, Disaster Prevention Research Division
National Research Institute for
Earth Science and Disaster Prevention
Science and Technology Agency
3-1, Tennodai, Tsukuba-shi,
Ibaraki-ken, 305

Dr. Hisanori Ohtsuka
Head, Earthquake Engineering Division
Earthquake Disaster Prevention Department
Public Works Research Institute
Ministry of Construction
1, Asahi, Tsukuba-shi,
Ibaraki-ken 305

Dr. Hiroshi Sato
Head, Structure Division
Structure and Bridge Department
Public Works Research Institute
Ministry of Construction
1, Asahi, Tsukuba-shi,
Ibaraki-ken 305

Dr. Koichi Yokoyama
Director, Structure and Bridge
Department
Public Works Research Institute
Ministry of Construction
1, Asahi, Tsukuba-shi,
Ibaraki-ken 305

Mr. Masashi Satou
Head, Structures Section
Civil Engineering Research Institute
Hokkaido Development Bureau
Hokkaido Development Agency
1-3, Hiragishi, Toyohira-ku
Sapporo, Hokkaido, 062

Mr. Shigenobu Tanaka
Head, Coastal Engineering Division
River Department
Public Works Research Institute
Ministry of Construction
1, Asahi, Tsukuba-shi,
Ibaraki-ken 305

Dr. Tatsuo Uwabe
Chief, Earthquake Disaster Prevention
Laboratory
Structural Engineering Division
Port and Harbour Research Institute
Ministry of Transport
3-1-1, Nagase, Yokosuka-shi
Kanagawa-ken 239

Dr. Hiroyuki Yamanouchi
Director, Structural Engineering
Department
Building Research Institute
Ministry of Construction
1, Takehata, Tsukuba-shi
Ibaraki-ken 305

ASSOCIATE MEMBERS

Dr. Minoru Fujiwara
Professor
Tohoku University
Aoba, Aramakiaza, Aoba-Ku, Sendai-shi,
Miyagi-ken, 980
TEL:022-222-1800

Dr. Masami Fukuoka
Professor
Department of Civil Engineering
Science University of Tokyo
2641, Yamazaki, Noda-shi,
Chiba-ken 278
TEL:0471-24-1501

Dr. Masaya Hirosawa
Professor
Kogakuin University
1-24-2-91, Nishishinjyuku, Shinjyuku-ku
Tokyo 163
TEL:03-3342-1211

Dr. Shiro Ibukiyama
President
Kogyokusha College of Technology
5-14-2, Nishigotanda, Shinagawa-ku,
Tokyo141
TEL:03-3493-5671

Dr. Kaoru Ichihara
President
Public Works Research Center
1-6-4, Taito, Taito-ku,
Tokyo 110
TEL:03-3835-3609

Dr. Ryuichi Iida
President
Japan Dam Engineering Center
2-4-5, Azabudai, Minato-ku,
Tokyo 110
TEL:03-3433-7811

Dr. Toshio Iwasaki
President
Civil-work Research Laboratory
1-25-5, Toranomon, Minato-ku,
Tokyo 106
TEL:03-3254-9481

Mr. Shunichiro Kamijo
Managing Director
Mitsui Construction Company, Ltd.
3-10-1, Iwamoto-cho, Chiyoda-ku,
Tokyo 106
TEL:03-5821-7100

Mr. Kenji Kawakami
Adviser
Kubota Corporation
3-1-3, Nihonbashimuromachi, Cyuoh-ku,
Tokyo 103
TEL:03-3245-3050

Dr. Eiichi Kuribayashi
Professor
Toyohashi University of Technology
1-1, Hibarigaoka, Tenpaku-cho,
Toyohashi-shi 440
TEL:0532-47-0111

Mr. Mitsuru Nagao
President
Japan Construction Mechanization Association
3-5-8, Shibakoen, Minato-ku,
Tokyo 105
TEL:03-3433-1501

Dr. Seiji Nakano
Professor
Tokyo Denki University
2-2, Kandanishiki-cho, Chiyoda-ku,
Tokyo 101
TEL:03-5280-3501

Dr. Kazuo Nakazawa
Chairman
Civil-work Research Laboratory
3-3-4, Kandakaji-cho, Chiyoda-ku,
Tokyo 101
TEL:03-3254-9481

Dr. Nobuyuki Narita
Professor, Department of Civil Engineering
Tokyo Metropolitan University
1-1, Minamiohsawa, Hachiohji-shi,
Tokyo 192-03
TEL:0426-77-1111

Dr. Shin Okamoto
Directer General
Building Technology Research Institute
The Building Center of Japan
3-2-2, Toranomon, Minato-ku,
Tokyo 105
TEL:03-3434-7164

Mr. Yoshijiro Sakagami
President
Rinkai Construction Co., Ltd
2-3-8, Shiba, Minato-ku,
Tokyo 105
TEL:03-3453-4111

Dr. Yasushi Sasaki
Professor
Hiroshima University
1-4-1, Kagamiyama, Higashihiroshima-shi,
Hiroshima- ken 739
TEL:0824-24-7783

Dr. Yukihiko Sumiyoshi
Executive Counselor
Nippon Steel Co., Ltd
2-6-3, Ohte-machi, Chiyoda-ku,
Tokyo 100-71
TEL:03-3275-5868

Mr. Jiro Taguchi
Managing Director
Trans-Tokyo Bay Highway Co., Ltd
15-5, Ichiban-cho, Chiyoda-ku,
Tokyo 102
TEL:03-3239-6584

Dr. Hiroshi Takahashi
Adviser
Engineering Department
Sato Kogyo Co., Ltd
4-12-20, Nihonbashihon-cho, Cyuo-ku,
Tokyo 103
TEL:03-3661-2296

Dr. Masateru Tominaga
President
Central Consultant Inc.
2-16-2, Minamikamata, Ohta-ku,
Tokyo 144
TEL:03-5703-6161

Dr. Hajime Tsuchida
President
Coastal Development Institute of Technology
3–16, Hayabusa–cho, Chiyoda–ku,
Tokyo 102
TEL:03–3234–5861

Dr. Makoto Watabe
Senior managing Directer
Shimizu Corp.
1–2–3, Shibaura, Minato–ku,
Tokyo 105–07
TEL:03–5441–1111

UNITED STATES-SIDE PANEL ON WIND AND SEISMIC EFFECTS MEMBERSHIP LIST

Dr. Richard N. Wright
Chairman, U. S. Side Panel on Wind and Seismic Effects
Director, Building and Fire Research Laboratory
National Institute of Standards and Technology
U. S. Department of Commerce
Gaithersburg, MD 20899
USA
TEL: 301-975-5900
FAX: 301-975-4032
e-mail: wright@micf. nist. gov

Mr. Noel J. Raufaste
Secretary-General, U. S. Side Panel on Wind and Seismic Effects
Head, Cooperative Research Programs
Building and Fire Research Laboratory
National Institute of Standards and Technology
U. S. Department of Commerce
Gaithersburg, MD 20899
USA
TEL: 301-975-5905
FAX: 301-975-4032
e-mail: raufaste@micf. nist. gov

Dr. Kharaiti L. Abrol
Acting Director
Structural Engineering Service (088475)
Department of Veterans Affairs
810 Vermont Avenue, NW
Washington, DC 20420
USA
TEL: 202-233-7379
FAX: 202-233-2115

Dr. John Ake
Geophysicist
Seismotectonics and Geophysics Section
P. O. Box 25007
Bureau of Reclamation
U. S. Department of the Interior
Denver, CO 80225
USA
TEL: 303-236-4195
FAX: 303-236-9127

Dr. S. T. Algermissen
Deputy for Geologic Hazard & Risk Assessment
Office of International Geology
U. S. Geological Survey, 917 National Center
12201 Sunrise Valley Drive
U. S. Department of the Interior
Reston, VA 22092
USA
TEL: 703-648-6051
FAX: 703-648-4227

Mr. Charles E. Anderson
Seismic Safety Coordinator
P. O. Box 25007 (D-8110)
Bureau of Reclamation
U. S. Department of the Interior
Denver, CO 80225
USA
TEL: 303-236-3999
FAX: 303-236-9099
e-mail: canderso@do. usbr. gov

Dr. Celso S. Barrientos
Supervisory Physical Scientist
National Environmental Satelite Data
Information Service – Code E/RA28
National Oceanic and Atmospheric
Administration
U. S. Department of Commerce
5200 Auth Road
Camp Springs, MD 20746
USA
TEL: 301-763-8102
FAX: 301-763-8108

Dr. Eddie N. Bernard
Director, Pacific Marine Environmental
Laboratory
National Oceanic and Atmospheric
Administration
U. S. Department of Commerce
7600 Sand Point Way, NE
BIN C15700/Building 3
Seattle, WA 98115-0070
USA
TEL: 206-526-6800
FAX: 206-526-6815
e-mail: bernard@pmel. noaa. gov

Mr. Mike Blackford
Director, Pacific Tsunami Warning Center
National Oceanic and Atmospheric
Administration
U. S. Department of Commerce
91270 Fort Weaver Road
Ewa Beach, HI 96706-2928
USA
TEL: 808-689-8207
FAX: 808-689-4543
e-mail: mike@ptwc. noaa. gov

Dr. Roger D. Borcherdt
Branch of Seismology
U. S. Geological Survey
U. S. Department of the Interior
345 Middlefield Road, MS 977
Menlo Park, CA 94025
USA
TEL: 415-329-5619
FAX: 415-329-5163
e-mail: bernard@pmel. noaa. gov

Dr. A. Gerald Brady
Research Civil Engineer
Branch of Earthquake and Geomagnetic
Information
U. S. Geological Survey
U. S. Department of the Interior
345 Middlefield Road, MS 977
Menlo Park, CA 94025
USA
TEL: 415-329-5664
FAX: 415-329-5163
e-mail: brady@samoa. WR. USGS. gov

Mr. H. Lee Butler
Chief, Research Division
Coastal Engineering Research Center
U. S. Army Engineer Waterways
Experiment Station
Office CEWES-CR
3909 Halls Ferry Road
Vicksburg, MS 39180-6199
USA
TEL: 601-634-2405
FAX: 601-634-4314

Dr. Ken P. Chong
Program Director, Mechanical & Structural Systems
National Science Foundation
4201 Wilson Boulevard – Room 545
Arlington, VA 22230
USA
TEL: 703–306–1361
FAX: 703–306–0291
e–mail: KChong@NSF. gov

Dr. Riley M. Chung
Group Leader, Earthquake Engineering Structures Division
Building and Fire Research Laboratory
National Institute of Standards and Technology
U. S. Department of Commerce
Gaithersburg, MD 20899
USA
TEL: 301–975–6056
FAX: 301–869–6275

Mr. James D. Cooper
Deputy Chief, Structures Division HNR–10
Federal Highway Administration
U. S. Department of Transportation
6300 Georgetown Pike
McLean, VA 22101
USA
TEL: 703–285–2060
FAX: 703–285–2766

Dr. A. G. Franklin
Chief, Earthquake Engineering & Geophysics Division
CEWES–GH Geotechnical Laboratory
U. S. Army Engineer Waterways Experiment Station
3909 Halls Ferry Road
Vicksburg, MS 39180–6199
USA
TEL: 601–634–2658
FAX: 601–634–4134
e–mail: FRANKLA@EX1. wes. army. mil

Mr. G. Robert Fuller
Senior Environmental Specialist
Housing Operations
Room 9138 HO
U. S. Department of Housing and Urban Development
Washington, DC 20410–8000
USA
TEL: 202–708–1104
FAX: 202–708–2387
e–mail: grobert_fuller@hud. gov

Mr. James H. Gates
Caltrans – Structures
P. O. Box 942874
Sacramento, CA 94274
USA
TEL: 916–227–8773
FAX: 916–227–8174

Mr. Peter E. Gurvin
Director, Building Design and Engineering Division
Foreign Building Operations
Building SA–6, Room 335
U. S. Department of State
Washington, DC 20520
USA
TEL: 703–875–6117
FAX: 703–875–6204

Dr. Walter W. Hays
Deputy for Research Applications
Office of Earthquake, Volcanoes and Engineering
905 National Center
U. S. Geological Survey
U. S. Department of the Interior
Reston, VA 22092
USA
TEL: 703–648–6711
FAX: 703–648–6717

Mr. James R. Hill
Manager, Natural Hazards Mitigation Programs
Office of Field Engineering and Site Interface
EH-34
U. S. Department of Energy
Washington, DC 20545
USA
TEL: 301-903-4508
FAX: 301-903-8585
e-mail: Jim. Hill@HQ. DOE. gov

Mr. Larry C. Hultengren
Senior Structural Engineer
Office of Civil/Structural Engineering
Foreign Building Operations
U. S. Department of State
Washington, DC 20520
USA
TEL: 703-875-6194
FAX: 703-875-6204

Dr. William B. Joyner
Geophysicist
Branch of Seismology
U. S. Geological Survey
U. S. Department of the Interior
345 Middlefield Road, MS 977
Menlo Park, CA 94025
USA
TEL: 415-329-5640
FAX: 415-329-5163
e-mail: joyner@samoa. wr. usgs. gov

Mr. Roger M. Kenneally
Structural Engineer
Structural and Seismic Engineering Branch
Mail Stop T10-L1
U. S. Nuclear Regulatory Commission
Washington, DC 20555
USA
TEL: 301-415-6303
FAX: 301-415-5074
e-mail: rmk@nrc. gov

Dr. H. S. Lew
Chief, Structures Division
Building and Fire Research Laboratory
National Institute of Standards and Technology
U. S. Department of Commerce
Gaithersburg, MD 20899
USA
TEL: 301-975-6061
FAX: 301-869-6275

Dr. Shih-Chi Liu
Program Director, Structural Systems
Division of Biological and Critical Systems
National Science Foundation
4201 Wilson Boulevard - Room 545
Arlington, VA 22230
USA
TEL: 703-306-1362
FAX: 703-306-0291

Dr. Francis G. McLean
Value Engineer & Review Coordinator
Code D-8170
P. O. Box 25007
Bureau of Reclamation
U. S. Department of the Interior
Denver, CO 80225
USA
TEL: 303-236-8546
FAX: 303-236-8044

Dr. Raymond E. Meyer
Senior Program Manager
Office of Foreign Disaster Assistance
N/S Room 1262A
Department of State
320 21st Street, NW
Washington, DC 20523-0008
USA
TEL: 202-647-7530
FAX: 202-647-4036

Mr. Ugo Morelli
Policy Manager for Seismology
Federal Emergency Management Agency
500 C Street, SW
Washington, DC 20472
USA
TEL: 202-646-2810
FAX: 202-646-3104

Mr. Howard D. Nickerson
Earthquake Engineering and Weapons Specialist
Naval Facilities Engineering Command
Hoffman Building #2, Room 12S63,
Code 04 B2
200 Stovall Street
Alexandria, VA 22332
USA
TEL: 202-433-8599
FAX: 202-433-8777

Dr. William E. Roper
Assistant Director
Research and Development (Civil Works)
U. S. Army Corps of Engineers
20 Massachusetts Avenue, N. W.
Washington, DC 20314-1000
USA
TEL: 202-272-0257
FAX: 202-272-0907

Dr. John B. Scalzi
Program Director, Structures and Building Systems
National Science Foundation
4201 Wilson Boulevard - Room 545
Arlington, VA 22230
USA
TEL: 703-306-1361
FAX: 703-306-0291

Dr. Charles E. Smith
Research Program Manager Offshore Minerals Management
Technology Assessment and Research Branch
Minerals Management Service
U. S. Department of the Interior
381 Elden Street, MS 4800
Herndon, VA 22070-4817
USA
TEL: 703-787-1559
FAX: 703-787-1010

Dr. T. T. Soong
Samuel P. Capen Professor
Department of Civil Engineering
National Center for Earthquake Engineering Research
State University of New York at Buffalo
212 Ketter Hall
Buffalo, NY 14260
USA
TEL: 716-645-2469
FAX: 716-645-3733

Mr. Stan Strickland
Chief, Air Base Systems Branch
Stop 37, WL/FIVC/OL, Bldg. 1120
139 Barnes Drive, STE 2
Tyndall AFB, FL 32403-6001
USA
TEL: 904-283-3709
FAX: 904-283-3722

ALTERNATE MEMBERS

Dr. Clifford J. Astill
Program Director
Division of Biological and Critical Systems
National Science Foundation
4201 Wilson Boulevard – Room 545
Arlington, VA 22230
TEL: 703–306–1361
FAX: 703–306–0291

Dr. Mehmet K. Celebi
Research Civil Enginieer
Branch of Earthquake and Geomagnetic Information
U. S. Geological Survey
U. S. Department of the Interior
345 Middlefield Road MS 977
Menlo Park, CA 94025
TEL: 415–329–5623
FAX: 415–329–5163

Mr. Michael Changery
Chief, Global Analysis Branch
National Climatic Data Center
National Oceanic and Atmospheric Administration
U. S. Department of Commerce
Federal Building
Ashville, NC 28801
TEL: 704–271–4765
FAX: 704–271–4246

Mr. C. Y. Chen
Senior Civil/Geotechnical Engineer
Office of Foreign Buildings
Department of State
Code SA–6, Rm. 327
Washington, DC 20520
TEL: 703–875–6207
FAX: 703–875–6204

Mr. Vincent P. Chiarito
Research Structural Engineer
Structural Mechanics Division
Structures Laboratory
U. S. Army Engineer Waterways Experiment Station
3909 Halls Ferry Road
Vicksburg, MS 39180–6199
TEL: 601–634–2714
FAX: 601–634–3412

Dr. James F. Costello
Senior Structural Engineer
Structural and Seismic Engineering Branch
Structural Section
Office of Nuclear Regulatory Research
U. S. Nuclear Regulatory Commission
Mail Stop T10–L1
Washington, DC 20555
TEL: 301–492–3818
FAX: 301–415–5074

Mr. Lucian G. Guthrie
Structural Engineer
Office of Chief of Engineers
Headquarters U. S. Army Corps of Engineers
Corps of Engineers Civil Works Engineering Div.
U. S. Department of the Army
20 Massachusetts Avenue, N. W.
Washington, DC 20314–1000
TEL: 202–272–8673
FAX: 202–272–1485

Dr. Robert L. Hall
Chief, Structural Analysis Group
U. S. Army Engineer Waterways Experiment Station
3909 Halls Ferry Road
Vicksburg, MS 39180–6199
TEL: 601–634–2567
FAX: 601–634–3412

Dr. James R. Houston
Director, Coastal Engineering Research Center
U. S. Army Engineer Waterways Experiment Station/WESCV-Z
3909 Halls Ferry Road
Vicksburg, MS 39180-6199
TEL: 601-634-2000
FAX: 601-634-2055
e-mail: houston@coafsl. wes. army. mil

Mr. James Lander
Geophysicist
Cooperative Institute for Research in Environmental Sciences
University of Colorado
Campus Box 449, Room 152 RL3
3100 Marine Street
Boulder, CO 80309
TEL: 303-497-6446
FAX: 303-497-6513

Mr. Tingley K. Lew
Research Structural Engineer
Structures Division
Naval Facilities Engineering Service Center - ESC 62
560 Center Drive
Port Hueneme, CA 93043-4328
TEL: 805-982-1234
FAX: 805-982-1418

Mr. Michael Mahoney
Physical Scientist
Federal Emergency Management Agency
500 C Street, SW
Washington, DC 20472
TEL: 202-646-2794
FAX: 202-646-4387

Dr. J. Eleonora Sabadell
Director, Natural and Manmade Hazards Mitigation Program
Directorate of Engineering
National Science Foundation
4201 Wilson Boulevard - Room 545-03
Arlington, VA 22230
TEL: 703-306-1361
FAX: 703-306-0291
e-mail: esabadel@nsf. gov

Dr. Erdal Safak
Research Structural Engineer
U. S. Geological Survey
U. S. Department of the Interior
922 National Center
Reston, VA 22092
TEL: 703-648-6534
FAX: 703-648-6717

List of Task Committee Members

TASK COMMITTEE MEMBERSHIP LIST

Task Committee	US Side	Japanese Side
A. Strong-Motion Data and Applications	A. G. Brady*	S. Noda*
	C. J. Astill	Y. Kitagawa
	R. D. Borcherdt	R. Hagiwara
	M. K. Celebi	K. Horai
	A. G. Franklin	K. Mimura
	W. B. Joyner	S. Iai
	R. B. MacDonald	H. Mizuno
	F. G. McLean	K. Ohtani
	J. R. Hill	
	S. T. Algermissen	
	C. S. Barrientos	
	G. R. Fuller	
	T. K. Lew	
	E. Safak	
	J. Kimball	
	J. Hunt	
B. Testing and Evaluation Procedures for Building Systems	H. S. Lew*	K. Ohtani*
	V. P. Chiarito	O. Matsuo
	J. E. Sabadell	H. Mizuno
	C. E. Smith	S. Noda
	K. Abrol	I. Ohkawa
	S. Sweeney	H. Sato
	A. Bieniawski	

Task Committee	US Side	Japanese Side
C. Evaluation and Improvement of Structures	K. P. Chong*	H. Yamanouchi*
	P. A. Brady	H. Hiraishi
	J. O. Jirsa	K. Yokoyama
	H. S. Lew	Y. Koga
	T. K. Lew	M. Nakano
	H. D. Nickerson	T. Fujitani
	D. H. Oh	S. Nakata
	J. B. Scalzi	S. Ohtsuka
	D. Eagling	I. Ohkawa
	S. Woodson	H. Sato
	M. A. Phipps	
	S. A. Asar	
	M. K. Celebi	
	G. R. Fuller	
	K. L. Abrol	
	R. L. Hall	
	D. Ellsworth	
	A. Bieniawski	
	K. Mutreja	
D. Earthquake Engineering for Dams	W. E. Roper*	S. Nakamura*
	R. L. Hall	R. Hagiwara
	J. R. Hill	K. Kawashima
	L. G. Guthrie	H. Ohtsuka
	R. Davidson	
	M. E. Hynes	
	A. G. Franklin	
	R. Navidi	
	L. Von Thun	
	W. Allerton	
	F. G. Mclean	
F. Disaster Prevention Methods for Lifeline Systems	R. M. Chung*	Y. Koga*
	C. J. Astill	K. Kawashima
	M. K. Celebi	R. Hagiwara
	J. D. Cooper	N. Ogawa
	T. K. Lew	H. Ohtsuka
	J. B. Scalzi	T. Uwabe
	J. S. Spencer	S. Noto
	S. Wu	M. Sato
	G. Al-Chaar	
	J. R. Hill	
	S. Sommer	

Task Committee	US Side	Japanese Side
G. Structural Control and Intelligent Material Systems	S. C. Liu* K. P. Chong L. C. Hultengren T. T. Soong V. P. Chiarito J. R. Hayes	Y. Kitagawa* K. Kawashima N. Ogawa H. Yamanouchi H. Sato C. Minowa H. Ohtsuka
H. Soil Behavior and Stability During Earthquakes	A. G. Franklin* C. J. Astill R. D. Borcherdt C. Y. Chen F. G. McLean C. E. Smith R. M. Chung	R. Hagiwara* A. Nakamura O. Mastuo H. Mizuno S. Iai Y. Koga S. Noto T. Inatomi M. Nakano
I. Stom Surge and Tsunami	M. Blackford* C. J. Astill C. S. Barrientos E. N. Bernard L. Butler J. Lander W. E. Roper	S. Tanaka* S. Ohstuka T. Tayayama S. Ohtsuka
J. Wind and Earthquake Engineering for Transportation System	J. D. Cooper* A. G. Franklin J. H. Gates J. B. Scalzi H. S. Lew P. Yen H. R. Bosch	K. Yokoyama* T. Fujitani R. Hagiwara K. Nishikawa K. Kazuhiko H. Ohtsuka H. Sato M. Nakano Y. Koga M. Sato
K. Wind and Earthquake Engineering for Offshore and Coastal Facilities	C. E. Smith* C. S. Barrientos W. E. Roper J. E. Sabadell M. C. Miller M. K. Celebi	T. Uwabe* T. Fujitani M. Nakano S. Noda T. Inatomi S. Iai

* Chairman

Resolutions

Copyright

RESOLUTIONS OF THE TWENTY-SEVENTH JOINT MEETING U.S.-JAPAN PANEL ON WIND AND SEISMIC EFFECTS (UJNR)

Public Works Research Institute
Tsukuba, Japan
May 16-19, 1995

The following resolutions are hereby adopted:

1. The Twenty-Seventh Joint Panel Meeting provided the forum to exchange valuable technical information that was beneficial to both countries. In view of the importance of cooperative programs on the subject of wind and seismic effects, the continuation of Joint Panel Meetings is considered essential.

2. The following activities have been conducted since the Twenty-Sixth Joint Meeting:
   a. Guest Researcher Exchanges
      Five guest researches were exchanged : Mr. H. Shiobara from BRI performed earthquake engineering assignments as a guest researcher at Virginia Polytechnic Institute; Dr. N. Matsumoto from PWRI visited U.S. Army Engineer Waterways Experiment Station for exchange of technical information; and three U.S. researchers performed bridge and earthquake engineering assignments as guest researchers in Japan: Mr. M. Yashinsky from Caltrans and Dr. P. Yen and Mr. M. Britt from FHWA worked at PWRI.
      Also, five U.S. researchers including Dr. H.S. Lew participated in the International Workshop on Seismic Design of Bridges that was held at PWRI, on 13-14 March 1995.
   b. Technology Exchanges
      Technical documents, research reports, and proceedings of workshops have been exchanged. These exchanges contributed to the development of research programs and enhanced on-going research in both countries.
   c. Task Committee Workshops
      Two workshops were held:
      (1) The 4th Joint Workshop on Remedial Treatment of Potentially Liquefiable Soils, Task Committee (H), 4-8 July 1994, Tsukuba, Japan
      (2) The 2nd Workshop on Wind and Earthquake Engineering for Offshore and Coastal Facilities, Task Committees (K&I), 17-19 January 1995, Berkeley, USA

3. The Panel will continue to seek methods to contribute to the IDNDR such as exchanging Proceedings of Joint Panel Meetings and of Task Committee Workshops with their respective country's National Committees for the IDNDR.

4. Japanese and U.S. members performed two joint damage investigations of the 17 January 1995 Hyogo-ken-nanbu Earthquake. The first investigation was performed during 23-28 January by 2 Japanese researchers headed by Dr. Yokoyama (PWRI), and 3 U.S. researchers headed by Dr. H. S. Lew (NIST). The second investigation was performed during 13-17 February by 13 Japanese researchers headed by Mr. Nakaoka (PWRI), and 18 U.S. researchers headed by Dr. R. Chung (NIST). In addition three U.S. researchers visited Hyogo-Prefecture to perform field investigations and to exchange information following the Hyogo-ken-nanbu Earthquake. Drs. Krinitzsky, Hall and Koester from U.S. Army Engineer Waterways Experiment Station. The Japan-side presentations at the 27th Joint Panel Meeting on the Hyogo-ken-nanbu Earthquake presented important data and information about the reasons for building and infrastructure damages. The Panel recognizes the

importance of using these findings in its on-going work and of the need to continue performing future joint post-disaster investigations to improve engineering and construction practices.

5. The Panel approved the Task Committee reports developed and presented during the 27th Joint Panel Meeting. Each report included objectives, scope of work, accomplishments, future plans, and other information.

6. The Panel endorsed the following eight proposed Task Committee Workshops and Joint Meetings during the coming year.
   a. Task Committee (A) plans its Workshop on Strong-Motion Data/ Local Site Effects, January 1996, Yokosuka, Japan.
   b. Task Committee (B) plans its 2nd Joint Technical Coordinating Committee Meeting on Composite and Hybrid Structural Systems, June 1995, Berkeley, USA
   c. Task Committees (C&G) plan their 2nd workshop on Structural Control and Intelligent Material Systems , 1996 , USA.
   d. Task Committee (D) plans its Workshop on State-of-the Art Review of U.S.-Japan Research on Earthquake Engineering for Dams, during 1996, USA.
   e. Task Committee (F) plans its 6th Joint Workshop on Disaster Prevention for Lifeline Systems, 18-19 July 1995, Osaka, Japan.
   f. Task Committee (I) plans a Tsunami Symposium, April 1996, Hawaii, USA.
   g. Task Committee (J) plans its 11th Bridge Workshop, 30-31 May 1995, Tsukuba, Japan.
   h. Task Committee (J) plans its 12th Bridge Workshop, 1996, USA.

   Scheduling for the Workshops shall be performed by the U.S. and Japan Chairmen of the respective Task Committees with concurrence of the Joint Panel Chairmen. Both sides' Secretaries- General shall be kept informed of the planning. Results of each activity conducted before the 28th Joint Meeting shall be presented at the 28th Joint Panel Meeting.

7. The Panel recognizes the importance of continuing its joint research programs on Composite and Hybrid Structures and on Soil Liquefaction and Countermeasures. The Panel also recommends performing a feasibility study of creating a Task Committee on Design for Wind and Wind Hazard Mitigation.

8. The Panel published its second issue of Wind and Seismic Effects Newsletter in March 1995. The newsletter summarized the Northridge Earthquake, Hokkaido-Nansei-Oki Earthquake and 26th Joint Panel Meeting. The Panel endorses continuation of publishing its newsletter. Hence, the third newsletter issue will be published by the Japan-side during the fall of 1995.

9. The Panel recognizes the importance of continued exchange of personnel, technical information, research results, and recorded data that lead to mitigating losses from strong winds and earthquakes. During the coming year the Panel Secretaries-General will explore the feasibility of exchanging Panel information using the INTERNET and considering developing Home Page and Discussion Groups. The Panel also recognizes the importance of using available large-scale testing facilities in both countries. Thus, these activities should be continued, strengthened, and expanded. The Panel will provide official endorsement to facilitate these exchanges.

10. The Twenty-Eighth Joint Panel Meeting of the UJNR Panel on Wind and Seismic Effects will be held at National Institute of Standards and Technology, Gaithersburg, Maryland, USA, in May 1996. Specific dates, program, and itinerary will be proposed by the U.S.-Side with concurrence of the Japan-Side Panel.

Papers

Theme 1

Analysis of Dynamic Characteristics of Prestressed Concrete Cable-Stayed Bridge (Aomori Bay Bridge) using Strong Motion Observation Data

Takamasa Inatomi[1] and Sachito Tanaka[2]

ABSTRACT

Strong motions observed at a prestressed concrete cable-stayed bridge (Aomori Bay Bridge) during the Kushiro-oki Earthquake (January 15,1993) were analyzed to evaluate the validity of the structural modeling method used in seismic design for the bridge and the damping ratio of the superstructure.
Comparison of observed and computed vibrations confirmed that they agreed well in both natural frequency and mode, and that the modeling method used was valid. Earthquake response calculation using observed acceleration data in the longitudinal direction revealed that the damping ratio of the superstructure during the above earthquake was about 2%.
Key Words:
Seismic Response Anaysis, Cable-Stayed Bridge, Strong Motion Obsevation, Damping Ratio.

1. INTRODUCTION

The Aomori Bay Bridge (length: 498m) is one of the largest prestressed concrete cable-stayed bridges in Japan. Consisting of alternating layers of sedimentary clay and sandy soil, the site of the bridge, which is a typical soft ground composed of alluvial soil often found in coastal areas in Japan, does not have any hard soil layer (within several tens of meters from ground surface) that is regarded as bedrock in seismic design.

Japan is one of the most seismically active countries in the world. The cross sections of members of bridges, therefore,are often designed according to the seismic loading. Particularly, in areas like the site of the Aomori Bay Bridge, where ground motion is usually amplified, earthquake resistance is an important consideration in designing structures. In the design of the Aomori Bay Bridge, too, various analysis and studies were undertaken. Since the completion of the bridge, strong motion observation has been continued to compare the bridge's actual behavior during earthquakes with the results of analyses conducted at the design stage and verify the validity of the seismic design method employed for the bridge.

In this paper, strong motions recorded at the bridge during the Kushiro-oki Earthquake (January 15, 1993) are analyzed, and the validity of

1) Director, Port and Harbor Research Institute, Yokosuka, 239 Japan.
2) Senior Research Engineer, ditto.

the structural modeling method used in design and the damping ratio of the bridge's superstructure are discussed.

2. STRUCTURE AND EARTHQUAKE RESISTANCE

Fig.1 shows the structure of the Aomori Bay Bridge. The Bridge is a three-span, continuous prestressed concrete cable-stayed bridge having a center span length of 240m and a side span length of 128m.

The girder,which measures 25m in width and 3.5-2.5m in depth, is a prestressed concrete structure that has a three-cell trapezoidal cross section. The 81.6m high tower consists of inward leaning piers and inverted-Y-shaped towers made of reinforced concrete. The bridge has a fan-shaped multi-cable system with 10 levels of stay cables, which are arranged in a single vertical plane. The piers are built on a 42m deep, cast-in-situ diaphragm wall foundation that has a six-cell cross section (30m x 20.5m, wall thickness 1.5m), the largest of its kind in Japan.

For superstructure, a continuous girder system using supports at piers was adopted because under this system earthquake response at the girder and the bottom of the tower, whose cross sections must be designed under many restrictions, is relatively small. The biggest problems that had to be addressed in the seismic design of this continuous girder structure were the coupled vibration of torsion and bending of the girder during earthquakes in the transverse direction. Generally a girder supported elastically by a large number of cables is subject to torsional vibration stemming from the gap between the center of gravity of the girder and the supporting point. If this vibration is coupled with out-of-plane vibration of the girder, earthquake response becomes considerably large. For this reason, efforts were made to separate the natural frequencies of these two types of vibration wherever possible.

3. KUSHIRO-OKI EARTHQUAKE AND STRONG MOTION OBSERVATION

At 8:07 p.m. on January 15, 1993, an earthquake registering a magnitude(M) of 7.8 occurred off the coast of Kushiro, Hokkaido. The epicenter was at lat. 42°51'N and long. 144°23'E (depth:107km). At Aomori, 380km from the epicenter, this earthquake measured IV on the Japan Meteorological Agency's scale of seismic intensity. Fig.2 shows the location of the epicenter.

Accelerometers were installed at 15 locations to measure 31 components. Fig.3 shows the locations of observation points and the maximum amplitudes recorded. The measured maximum amplitudes at all points were about one-seventh of the calculated values used in seismic design, and the ground motions can be considered to be very small ones that do not cause any cracks in concrete.

Fig.4(a)-(d) show accelerations recorded at represen-

tative observation points, namely, on the ground (G1-X, depth 43.5m; G3-X, depth 1.5m), at a tower top (T1-X) and on the girder (K4-Z, 1/4 of center span).

4. VERIFICATION OF VALIDITY OF STRUCTURAL MODELING METHOD THROUGH ANALYSIS OF PREDOMINANT FREQUENCY AND MODE OF VIBRATION

Fig.5 shows Fourier spectra of the recorded accelerations in longitudinal vibration (in-plane vibration mode)(for 82 seconds during which major accelerations were recorded). As shown in Fig.5, the predominant frequencies of the superstructure appear at 0.59 Hz, 0.83 Hz, 1.02 Hz and 1.23 Hz.
Similarly, examination of observed vibrations in the transverse direction (out-of-plane vibration mode) revealed predominant components at 0.56 Hz, 0.82 Hz, 1.45 Hz and 2.97 Hz. Torsional Vibration of the girder at 1/4 of the center span had predominant components at 0.58 Hz, 0.81 Hz, 1.02 Hz and 1.32 Hz.
The acceleration records were processed with bandpass-filters at the predominant frequencies of Fourier spectrum, and the amplitudes were plotted. Thus, the modes of vibration were obtained,and were compared with those determined analytically. The analytical model used here was the same as the one used in the design stage. Because of the symmetry of the bridge structure, only half of the bridge was modeled considering the influence of the surrounding ground by springs (Ishibasi et al, 1991).

Fig. 6(a) and 6(b) compare observed modes of vibration in the longitudinal direction and in the transverse direction with those determined through analysis. Fig.7 compares observed frequencies and calculated frequencies. As shown, all vibration modes determined through analysis and observation agree well. The observed frequencies tended to be 2-16% higher than the corresponding calculated frequencies. On the whole, however, it can be said that they show good agreement.

These results confirm the validity of the structural modeling method employed in design. Although the coupling of the bending vibration (0.82 Hz) and torsional vibration (1.32 Hz) of the girder posed major problems in the seismic design, good agreement between the observed modes and the calculated modes indicates that these vibrations were separated just as designed.

The measured predominant frequencies of 1.23 Hz (in-plane) and 1.45 Hz (out of plane) are 12% and 16% higher than the calculated values respectively; these are vibration modes where rotating movement of the foundation is greater than in the remaining modes. The reason why the observed frequency is higher than the calculated frequency in the vibration modes in which the foundation rotates may be that the evaluation of the soil springs was not very accurate. These, however, are yet to be determined.

5. DAMPING RATIO BASED ON SEISMIC RESPONSE ANALYSIS USING OBSERVED ACCELERATION DATA

Earthquake response analysis for the longitudinal direction considering vertical vibration was conducted using accelerations measured at the foundation. Then damping characteristics of the superstructure were examined by comparing the calculated responses with the measured ones.

The analytical model used here was constructed by reducing the numbers of nodes and elements of the model used in the design stage. It was confirmed that vibration characteristics (natural period, vibration mode) of the simplified model did not differ substantially from those of the design model.
As mentioned earlier, the natural frequencies of the design model deviated from the predominant frequencies of the observed accelerations by about several percent. Therefore, the stiffness of the model was corrected so that the calculated predominant frequencies of the vibration components at 0.59 Hz, which were predominant components in the longitudinal direction, agreed with those of observed ones.

As inputs, longitudinal seismic waves at the top of the pier and longitudinal and vertical seismic waves at the top and bottom of the foundation were used, and they were input directly into two piers in phase. Seismic waves at the top and bottom of the foundation were used here in order to consider the vertical and rotational vibration of the foundation. The accelerations at the top and bottom of the foundation were calculated from the measured values of eight components obtained at pier P9, assuming that the diaphragm wall foundation was a rigid body.

Rayleigh damping was assumed, as shown below. Since the input seismic waves were input directly at the foundation, the damping of the structure included the structural damping of the superstructure, but not damping associated with energy dissipation at the foundation.

$$[C]=\alpha[M]+\beta[K] \quad (1)$$

where, $[C]$: damping matrix, $[M]$: mass matrix, $[K]$: stiffness matrix, α, β: constant

$hn=(\alpha/2\omega n)+(\beta\omega n/2)$, hn: modal damping ratio in n^{th} mode, and ωn: natural circular frequency in n^{th} mode.

In the seismic response analysis, damping ratios of critical for the natural periods of the first and second modes were selected as 1%, 2% and 3%. The calculated responses at the tower top in the longitudinal direction (T1-X), at 1/2 of the side span in the vertical direction (K1-Z), and at 1/4 of the center span in the vertical direction (K4-Z) were compared with the measured values.

Fig. 8 shows the accelerations. The calculated and measured values for the three locations show the best agreement at the damping ratio of 2%. Fig.9 compares the calculated maximum responses with the measured values. Although

the time when the maximum response occurs obtained through analysis does not necessarily correspond to the actual time of occurrence, it can be seen that the best agreement between the calculated value and the measured value is obtained at the damping ratio of 2%.
Thus,it can be confirmed that the damping ratio (not including the damping associated with energy dissipation at the foundation and cracking of concrete) of the superstructure corresponding to the magnitude of vibration caused by the Kushiro-oki Earthquake is about 2%.

Fig. 10 compares the Fourier spectra of the calculated responses in the case of damping ratio of 2% with those of the measured responses. The Fourier spectra of the measured values for all locations have peak at 0.59 Hz, and in the case of K1-Z and K4-Z (girder) other predominant components appear at 1.02 Hz.

As shown in Fig.6(a), the vibration at 1.02 Hz had a vertical vibration mode in which the side span and the center span of the girder vibrate synchronously in the vertical direction, while the tower and the foundation move little. This mode of vibration cannot be caused by uniform ground motion in the vertical direction because the right and left sides of the midpoint of the center span vibrate in the vertical direction antisymmetrically.
Therefore, vibration of this kind shown by the measured responses is thought to have been caused by phase difference between the two sides of the foundation. The percentage of response due to this type of vibration to overall response is low,and hence does not have a major influence, but it has been found that vibration that does not result from uniform inputs can occur in three-span continuous cable-stayed bridges.

6.CONCLUSION

The validity of the structural modeling method used in design and the damping ratio of the superstructure have been discussed on the basis of observation data obtained at the Aomori Bay Bridge during the Kushiro-oki Earthquake. The conclusions can be summarized as follows:

1) The predominant modes of observed vibration agreed well with the modes obtained from the analytical model in the design stage, confirming the validity of the method of modeling the ground and the structure employed in design. In vibration modes involving the rotation of the foundation, however, the analysis tended to underestimate frequency. This was because the evaluation of soil spring at the foundation may not be very accurate. Since the evaluation of soil springs at the foundation greatly affect the earthquake response of structural members,it is necessary to continue quantitative evaluation based on earthquake observation data.

2) Response calculation using measured values revealed that the damping ratio (not including damping associated with

energy dissipation at the foundation and cracking of concrete) of the superstructure corresponding to the magnitude of vibration caused by the Kushiro-oki Earthquake is about 2%.

3) Phase difference between the seismic motion at different foundation may cause vibration that will not occur in the case when uniform ground motion in the vertical direction is considered. Although the percentage of these vibrations was low, they had not been anticipated in the design stage.

Since the damping ratio is thought to be dependent on the amplitude of vibration, the authors will continue earthquake observation to acquire data for further quantitative evaluation.

ACKNOWLEDGMENT

The authors would like to express their appreciation to Aomori Port Management Office, Port and Harbor Division, of Aomori prefectural government for invaluable assistance in connection with the earthquake observation.

REFERENCE

(1) Ishibashi, T., et al.: A seismic design of long-span prestressed concrete cable-stayed bridge on the soft ground, Bridges and Foundations, Vol. 25, No.9, Sept. 1991 (in Japanese).

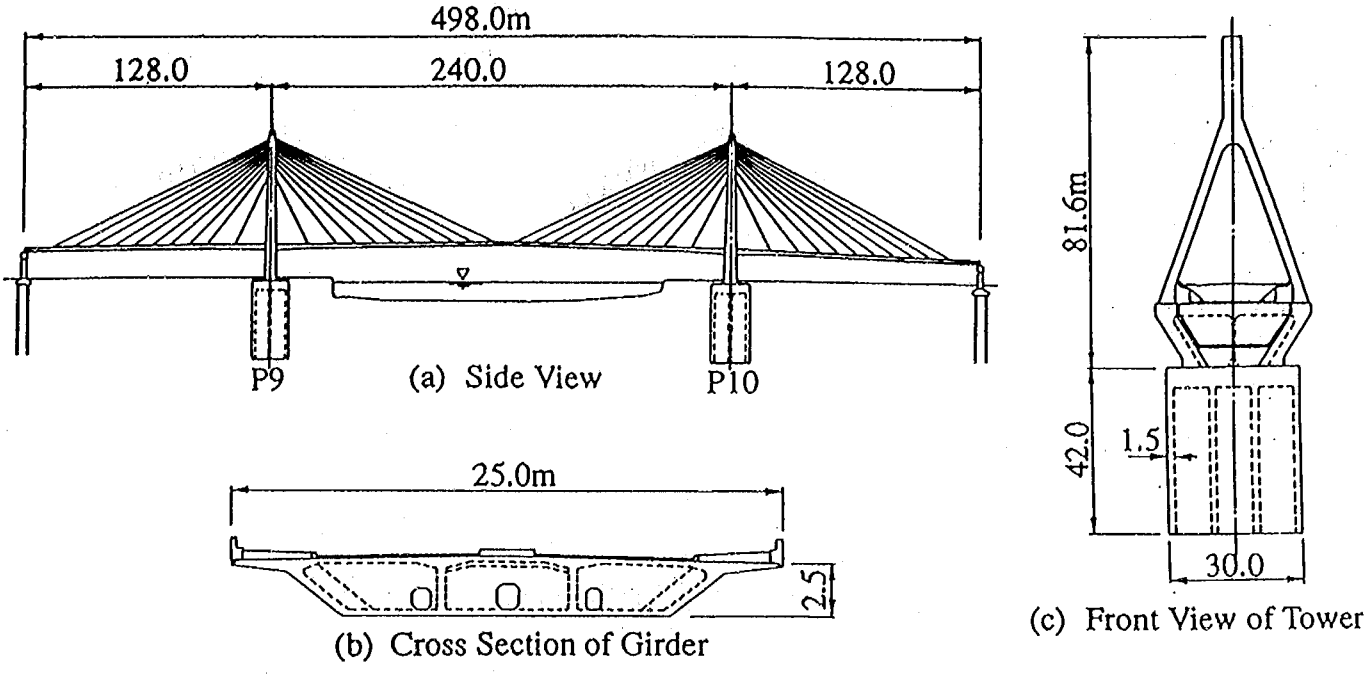


Fig.1 Aomori Bay Bridge

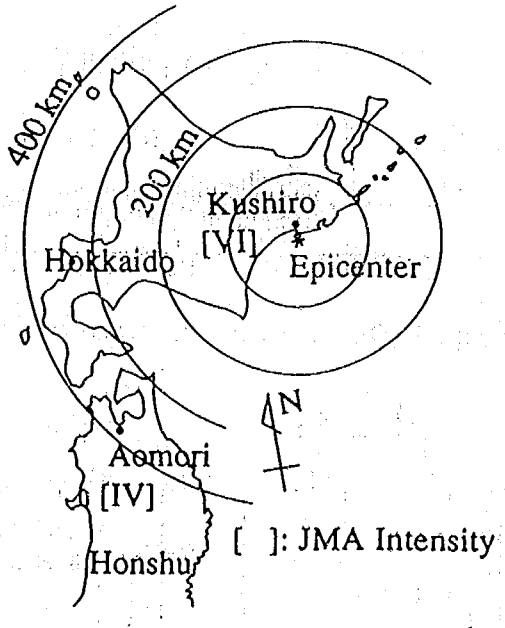


Fig.2 Location of epicenter

Peak Acceleration (cm/sec²)

	x	y	z		x	y	z
G1	25	23	13	K1	-	79	104
G2	20	22	-	K2	-	38	-
G3	51	50	17	K3	-	-	98
G4	35	47	-	K4	-	78	95
B1	22	19	19	P1	47	-	-
B2	30	24	19	T1	127	119	-
B3	32	24		T2	-	136	-
B4	20	27					

X, Y and Z represent peak acceleration in longitudinal, transverse and vertical direction, respectively.

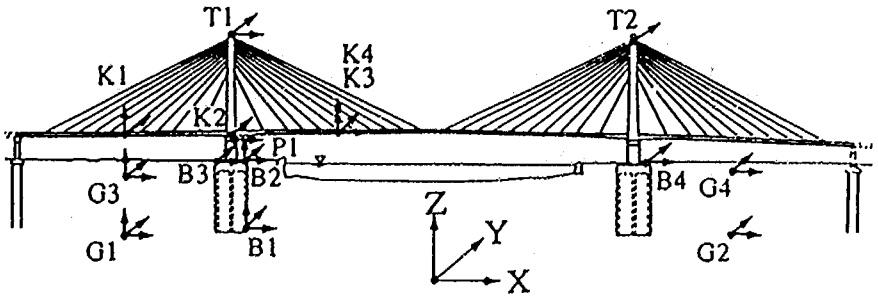


Fig.3 Location of acceleration and observed maximum acceleration

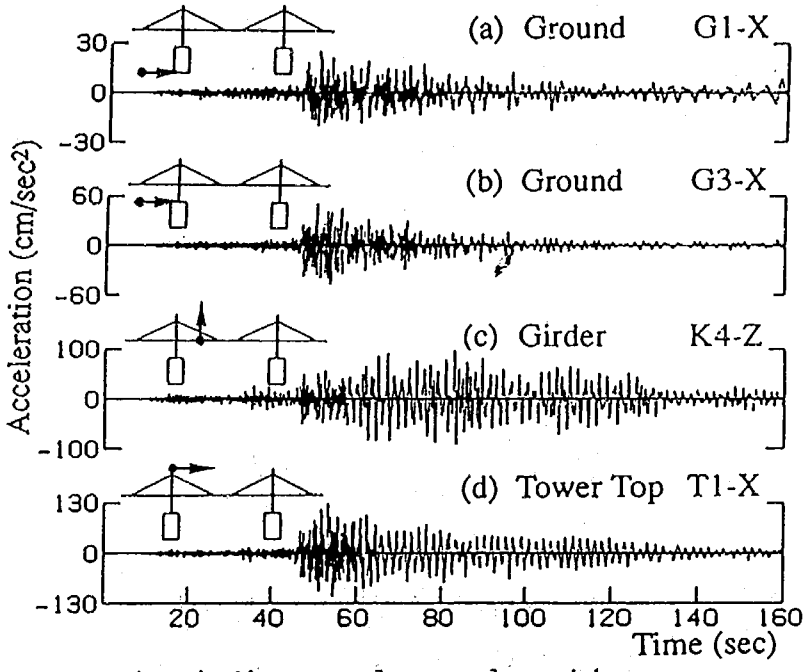
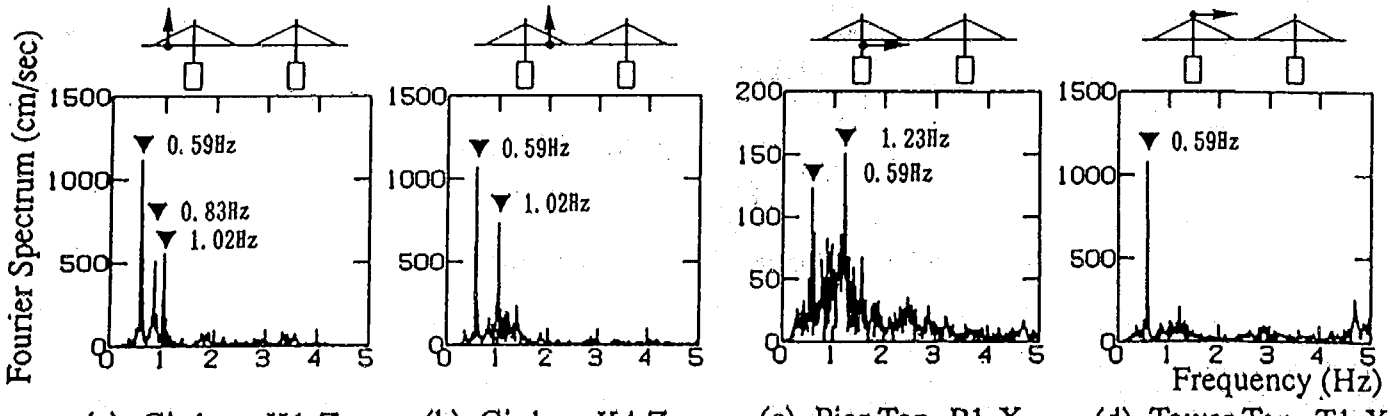
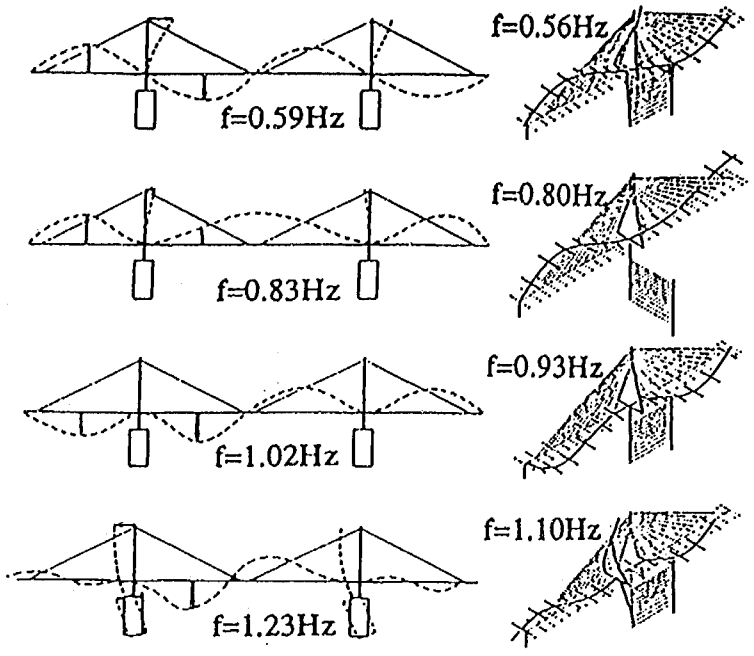


Fig.4 Observed acceleration

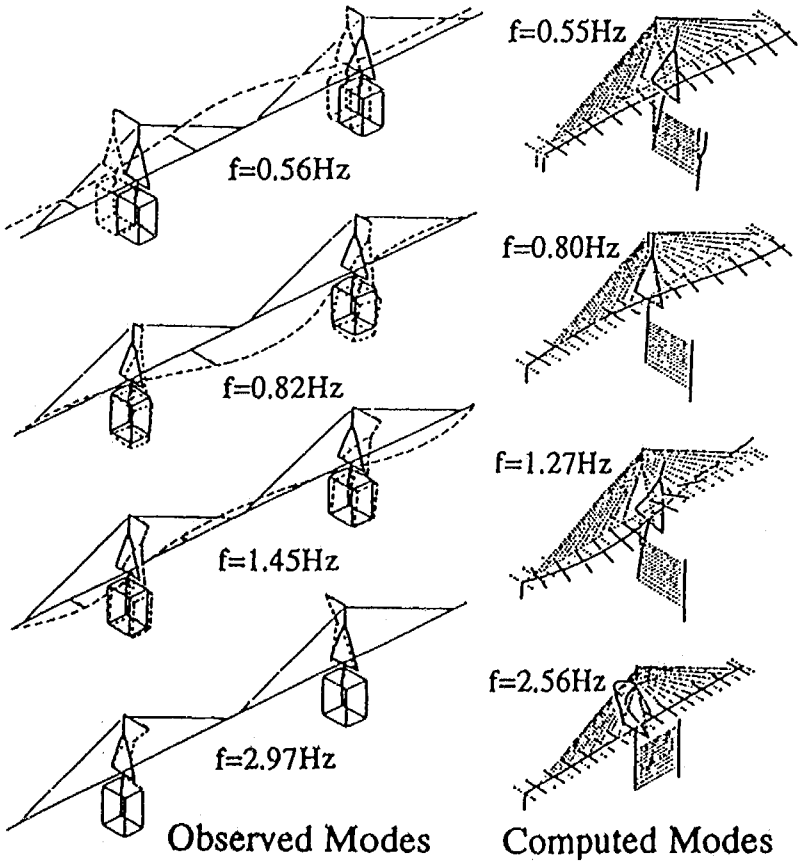


(a) Girder K1-Z (b) Girder K4-Z (c) Pier Top P1-X (d) Tower Top T1-X

Fig.5 Fourier spectra of obseved acceleration in longitudinal vibration

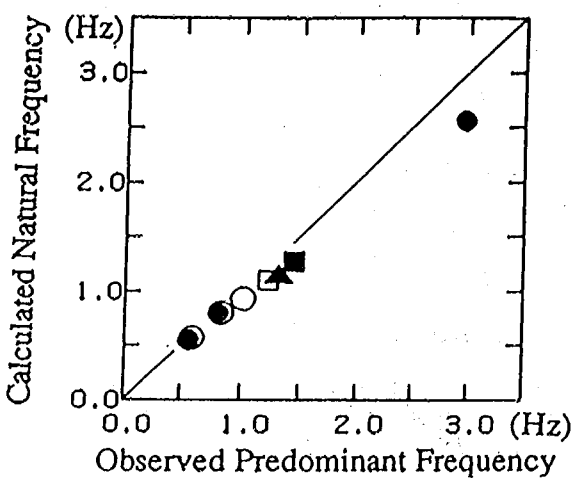


(a) Longitudinal Direction



(b) Transverse Direction

Fig.6 Comparison of observed and computed vibration modes



Legend

	Rotation of Foundation	
	Small	Large
In-plane	○	□
Out-of-plane	●	■
Torsion of girder	▲	

Fig.7 Comparison of observed and computed frequency

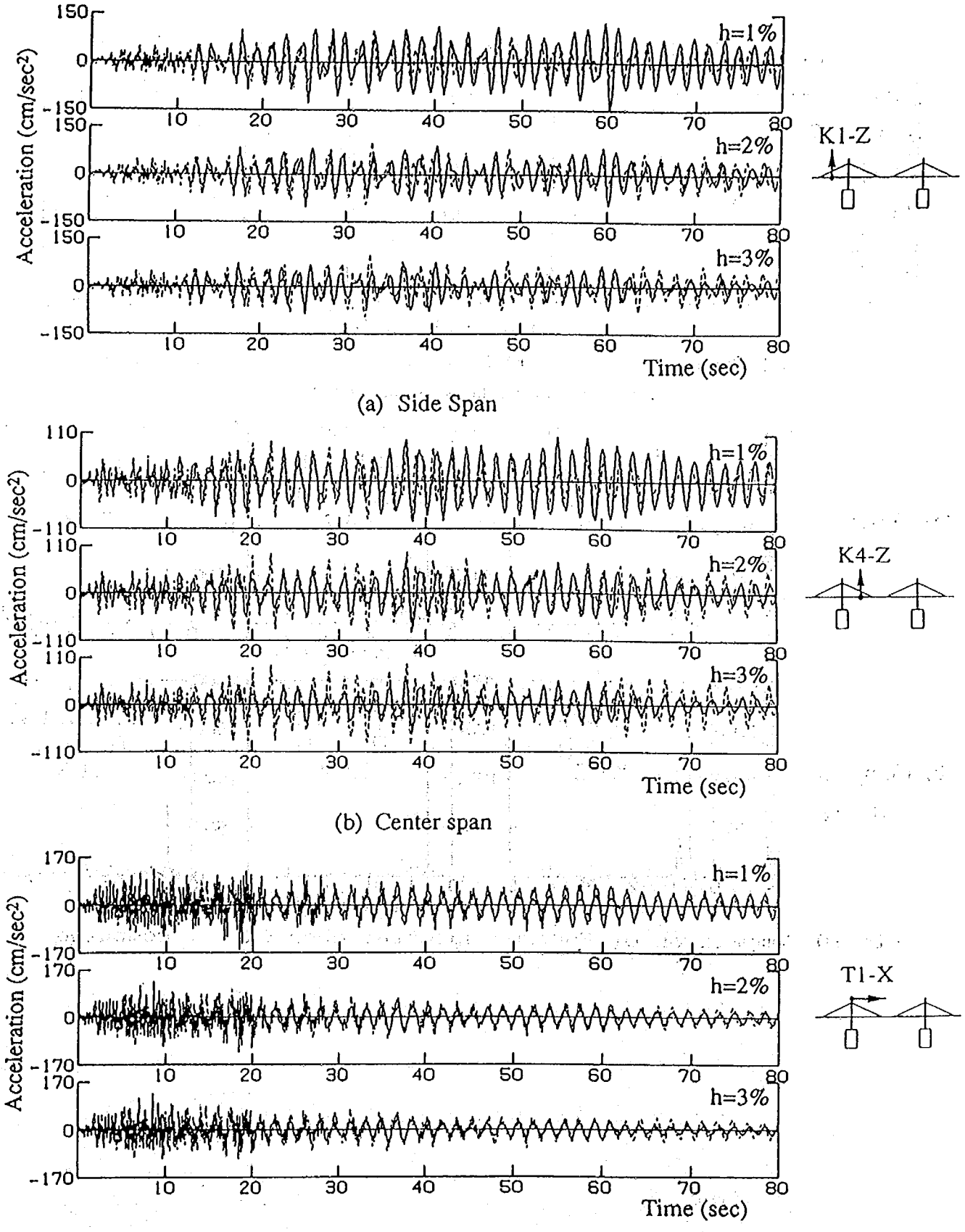
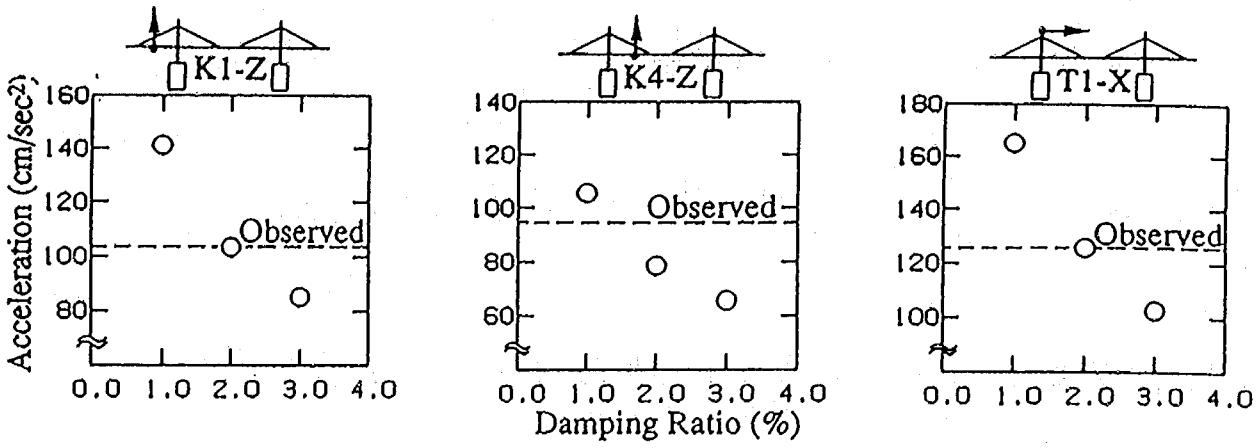


Fig.8 Computed acceleration response



(a) Side Span (b) Center Span (c) Tower Top

Fig.9 Computed maximum response

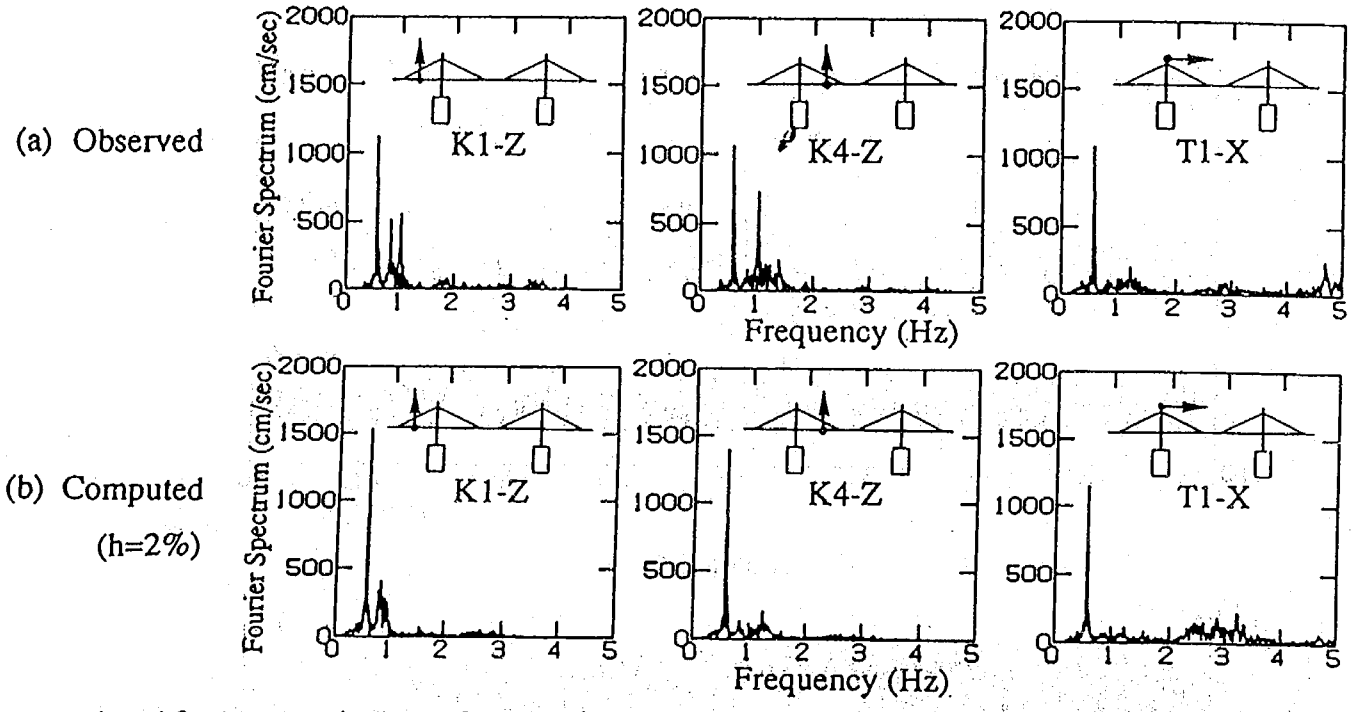


Fig.10 Comparison of Fourier spectra: obseved vs. computed

USGS Northridge Earthquake Digitized Recordings

by

A. Gerald Brady*

ABSTRACT

The US Geological Survey Northridge earthquake strong-motion records have been digitized commercially on a newly-designed complete desk-top digitization system. Scanning is based on existing software. The digitizing system is now installed at Menlo Park. The Northridge records demonstrate, in a limited fashion, the existence of a potentially destructive transverse shear wave pulse. Some damage in Kobe may be explained by this wave. Recordings in El Centro show it.

KEYWORDS: Northridge earthquake; strong-motion records; transverse shear wave.

1. INTRODUCTION

The USGS administers the National Strong-Motion Program in the US. This Program designs, develops and operates an accelerograph network to record potentially damaging ground motion and to monitor structural response. Data are disseminated world-wide. Northridge preliminary data is on Internet.

The network consists of the equivalent of 1000 accelerographs at 600 ground sites, 56 dams, 5 bridges and 60 large buildings. Primary participants are the Army Corps of Engineers, the Department of Veterans Affairs, and the Metropolitan Water District of Southern California.

2. THE NORTHRIDGE EARTHQUAKE

The Mw 6.7 (moment magnitude) Northridge earthquake of January 17, 1994 produced 150 accelerograms from 100 stations in the Program (Porcella and others, 1994). Parenthetically, the total count including records from other networks is several hundred accelerograms. Program stations include 30 high-rise buildings, 7 major hospitals, 12 dams, a bridge structure, 7 water or power distribution facilities, and 60 sites at ground level.

Peak horizontal ground accelerations exceeded a quarter-g at 11 sites within a 30km epicentral distance and two sites to the north were close to 1g. In general, peak acceleration attenuation follows the expected curves of Joyner and Boore (personal communication) and other statisticians, beyond the immediate source area. The rupture occurred on a blind thrust fault, steeply rising to the north. It commenced at a depth of 18km and did not reach the surface.

3. USGS DESKTOP PROCESSING SYSTEM

The USGS recently contracted for the engineering design of a new in-house digitizing system for processing film accelerograms. It is based on commercially available processing software. The system will scan records at a resolution of 600 dots-per-inch (dpi) and plots on a laser printer of the same resolution. We had hoped the system would be for processing occasional records, but personnel and funding constraints might force it to be our primary digitizing source.

For 600 samples-per-inch digitizing, with a possible increase to twice this rate, a typical scanned 12-trace record requires a 1.2GB disk drive and a fast processor. For archiving, a magneto-optical system was chosen, and for low volume data distribution, a CD-ROM mastering system.

Quality control of the digitizing is maintained by comparing each original record with its

---

* US Geological Survey, Menlo Park, Calif. 94025

digitized version, plotted to the same scale. Discrepancies are fixed by editing on the screen, and redigitizing where required.

3.1 Northridge digitization

Film records from the Northridge earthquake, and from the backlog of other California earthquakes occurring after the Loma Prieta earthquake of 1989, have been digitized in a follow-up contract which included training of USGS personnel in the system's use. Records at Northridge stations for which peak ground accelerations exceeded 0.1g or for which peak structural accelerations exceeded 0.2g were digitized. The data have been interpolated at 200 samples per second. This preliminary data set was made available on Internet (agram.wr.usgs.gov) with the understanding that its useful frequency range might be narrower than that of subsequent corrected data. There has been no high-frequency filtering or instrument correction, and no filtering for long-period noise removal.

A preliminary check of the corrected data set involved the use of a long period filter of 10 seconds for the closer recordings. Initial processing indicates that the high-frequency content will be satisfactory to about 15 Hz, and that the long-period content will be generally good to about 10 seconds or more for close-in records and to about 5 seconds for the most distant records.

4. NEAR-SOURCE GROUND MOTION AND RECORDINGS

Several of the recent damaging earthquakes in California and Japan have triggered a hundred or more strong-motion records (1989 Loma Prieta, 1994 Northridge, and 1995 Kobe, for example). As soon as peak values of acceleration are made available, their attenuation is plotted against a relevant distance (epicentral distance, fault distance, perpendicular distance to the line of intersection of the rupture and the ground surface, etc.). Not surprisingly, the plotted values lie sufficiently close to the statistically-obtained, expected or average curves, or one standard deviation away from this average, that the earthquake accelerations are often described as not unusual. High accelerations on soft soil at great distances attract careful research on the extent to which soil amplification has occurred. An earthquake occurring on a thrust fault produces a group of records having high accelerations, stressing the significance of the high friction forces associated with these faults. But even as the number of instruments in highly seismic areas rises, the number of records from within a few kilometers of a rupture remains few, and the broad statistical results of the preponderance of data do not address this most damaging area. The probability that transverse shear waves developing at the head of the rupture were involved in some of the damage in Kobe and surrounding areas invites an investigation of these waves in Northridge.

5. THE TRANSVERSE SHEAR WAVE

We compare the production of transverse shear waves at the head of the ruptures that caused earthquakes in El Centro (a 1979 aftershock), Northridge (1994) and Kobe(1995), verifying their existence with records or incredible damage.

A number of introductory diagrams are necessary before the significance of these waves both in Northridge and Kobe becomes apparent.

Figure 1 is a view looking down or along a fault plane to show the directions of pre-event crustal shearing displacements. It is a plan view for strike-slip faults like the San Andreas, and an elevation view for thrust events like Northridge.

Figure 2 is a view in the same direction of an elemental volume, with crustal shear forces and associated equilibrating shear forces. Perpendicular to the this, the element dimension is the distance across the fault. We assume that these are the significant stresses acting on the elemental volume and disregard any stresses acting on faces parallel to the plane of the fig-

ure, and any stresses perpendicular to the plane of the figure.

Figure 3 indicates the directions of the routine P and S wave fronts generated by an elemental slip, and the directions of the initial "particle motion". The first P-waves, whose arrivals are measured around the world, are used for earthquake locations and source mechanism.

At the same time as this elemental slip is occurring on the fault, the driving stress drops in value, and without loss of generality, we assume it drops to zero. The equilibrating stresses of Figure 2, now unbalanced, act on the elemental mass, accelerating it transversely until these stresses also drop to zero.

Figure 4 indicates the directions of transverse first motions and of the transverse shear wave fronts, after the equilibrating transverse shear forces act.

The transverse shear displacements weaken the neighboring fault ahead of the rupture, allowing the rupture front to travel close behind the generated shear wave. Freshly generated shears are added to the shears from all earlier rupturing, although perfect coordination is not likely. In spite of this, continuing transverse shear displacement production is largely cumulative -- a large transverse displacement pulse is generated at the head of the rupture. None of the other displacements are cumulative during the rupturing process. It is this displacement pulse that we investigate more fully.

5.1 Aftershock of the 1979 Imperial Valley earthquake.

The El Centro Array is an array of 13 stations installed in the 1970s transverse to the Imperial Fault, covering a total length of 44 km, equally spaced on both sides of the fault. An aftershock of the 1979 Imperial Valley earthquake produced records with radio time at six of the stations. Transverse displacements, calculated from the recorded accelerations, attained an amplitude of 4cm in a lone pulse, measured very close to the fault rupture. This was the first indication to the Program that this displacement pulse might be damaging for a large earthquake. At a distance of 4km from the fault, the amplitude has dropped by one half.

Figure 5 is a composite of the transverse displacements, plotted on a common time scale, so that they are offset according to their trigger times.

5.2 The 1994 Northridge earthquake.

Figure 6 is a diagram of the Northridge earthquake rupture surface, considered for simplicity to be on a planar fault steeply sloped upwards (42 deg) to the north, and striking at 122 deg. The diagram of Figure 1 in this case becomes a horizontal view looking approximately west. The transverse shear wave of Figure 4 which is still a view to the west, would on reaching the surface, have initial motion to the south and upwards. The shear wave, however, is bent towards the vertical as it travels through layers of decreasing velocity, and the initial displacement pulse from the transverse shear is mostly southward.

Three instruments are installed at different sites at the Jensen Filter Plant, a facility of the Metropolitan Water District of Southern California. The southward ground displacements calculated from the records while retaining all long periods out to 10 seconds, are remarkably similar, and are typified by the plot in Figure 7. The southward pulse has an amplitude of 80cm.

At the Sepulveda VA Hospital, a facility of the Department of Veterans Affairs further south from the ground intercept, the southward displacement amplitude is 20cm.

No other records from the USGS network are suitably placed to investigate this pulse, or any other simple, deterministic motion. But the Northridge records have been used in damage surveys, attenuation studies, and urban seismic zoning.

5.3 Earthquake damage at Kobe, 1995.

Among the impressive damage on the elevated Hanshin Expressway were two sections in which spans were dropped to the ground, one of 800m length running parallel to the fault almost on the same alignment as the fault, and one section, consisting of two downed spans, running perpendicular to the fault close to the northeastern extremity of the rupture.

On the first section, the bridge was knocked on its side. This could have been primarily caused by the transverse shear wave pulse travelling down the length of the expressway at the velocity of the rupture, destroying each pier in turn. The final position, a fall to the northwest, requires that the elastic rebound of the ground, to the southeast, be called on to initiate the collapse.

On the second section, the deck girders lost their seatings on the pier caps by excessive relative motion in the longitudinal direction of the bridge. Damage to the piers indicates excessive southeast ground accelerations, in accordance with damage to the first section.

In both cases, there is no evidence of damaging motion in any other direction, implying that the transverse shear wave and its elastic rebound, close to the source, had much greater amplitudes than expected, and was preceded and followed by less shaking.

CONCLUSIONS

The USGS has installed a complete desktop digitizing system after its satisfactory testing on the Northridge film recordings. Preliminary processing of these digitized records indicates that the data are good. Evidence of a potentially damaging transverse shear wave pulse is shown by two stations located fortuitously in suitable positions to the north of the Northridge epicenter. Some of the Kobe damage may be attributed to the transverse shear wave generated on the fault beneath the city as the rupture approached.

REFERENCES

1. Porcella et al (1994). Accelerograms recorded at USGS National Strong-Motion Network stations during the Ms=6.6 Northridge, California earthquake of January 17, 1994. USGS Open-File Report No. 94-141.

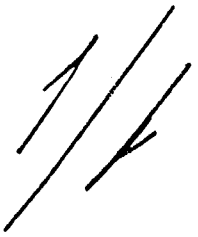


Figure 1. Pre-event shear displacement, strain, or forces acting on a fault.

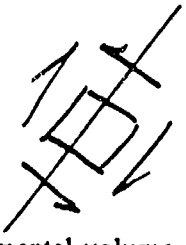


Figure 2. Elemental volume, with tectonic shears and equilibrating shears

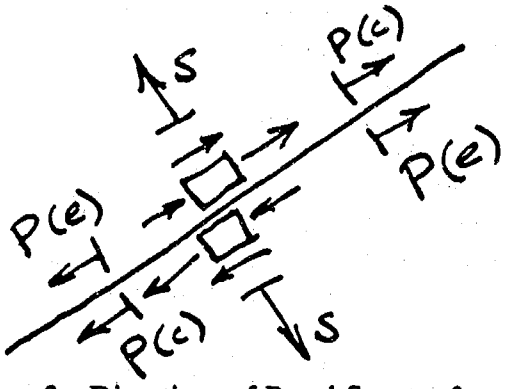


Figure 3. Directions of P and S wave fronts and of initial particle motion when slip occurs.

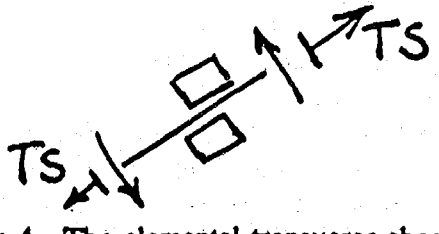


Figure 4. The elemental transverse shear wave initial particle motion and its wave front direction.

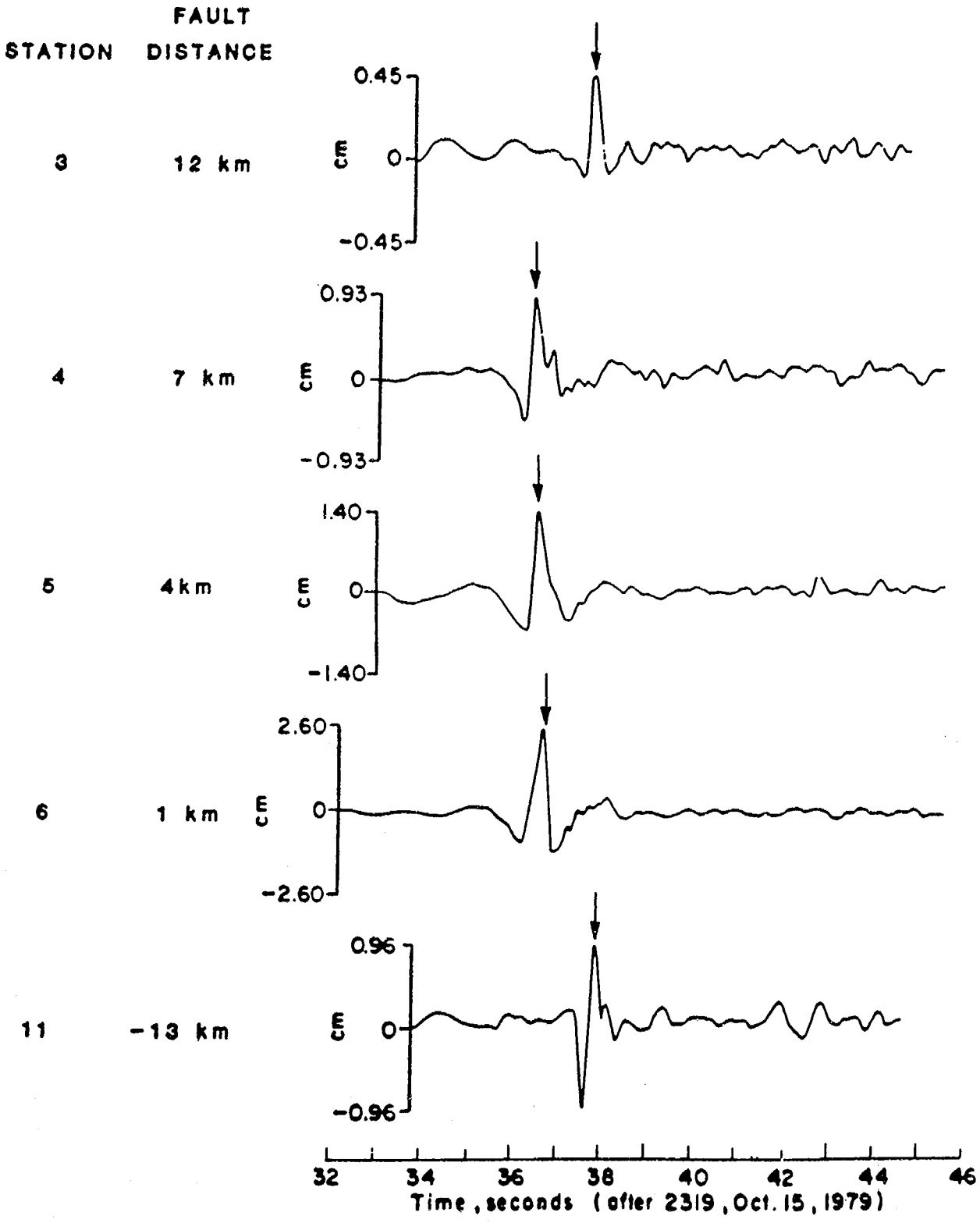


Figure 5. The transverse shear wave (230 deg component) from an aftershock of the 1979 Imperial Valley earthquake, shown on five stations between 1 and 13 km from the fault.

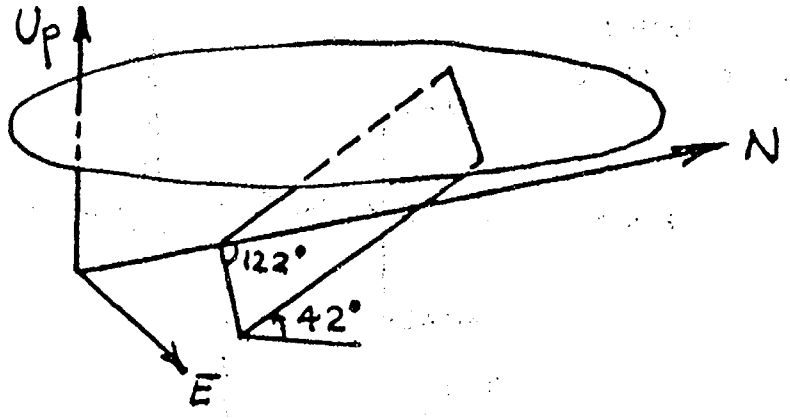


Figure 6. Diagram of the approximate Northridge earthquake rupture surface.

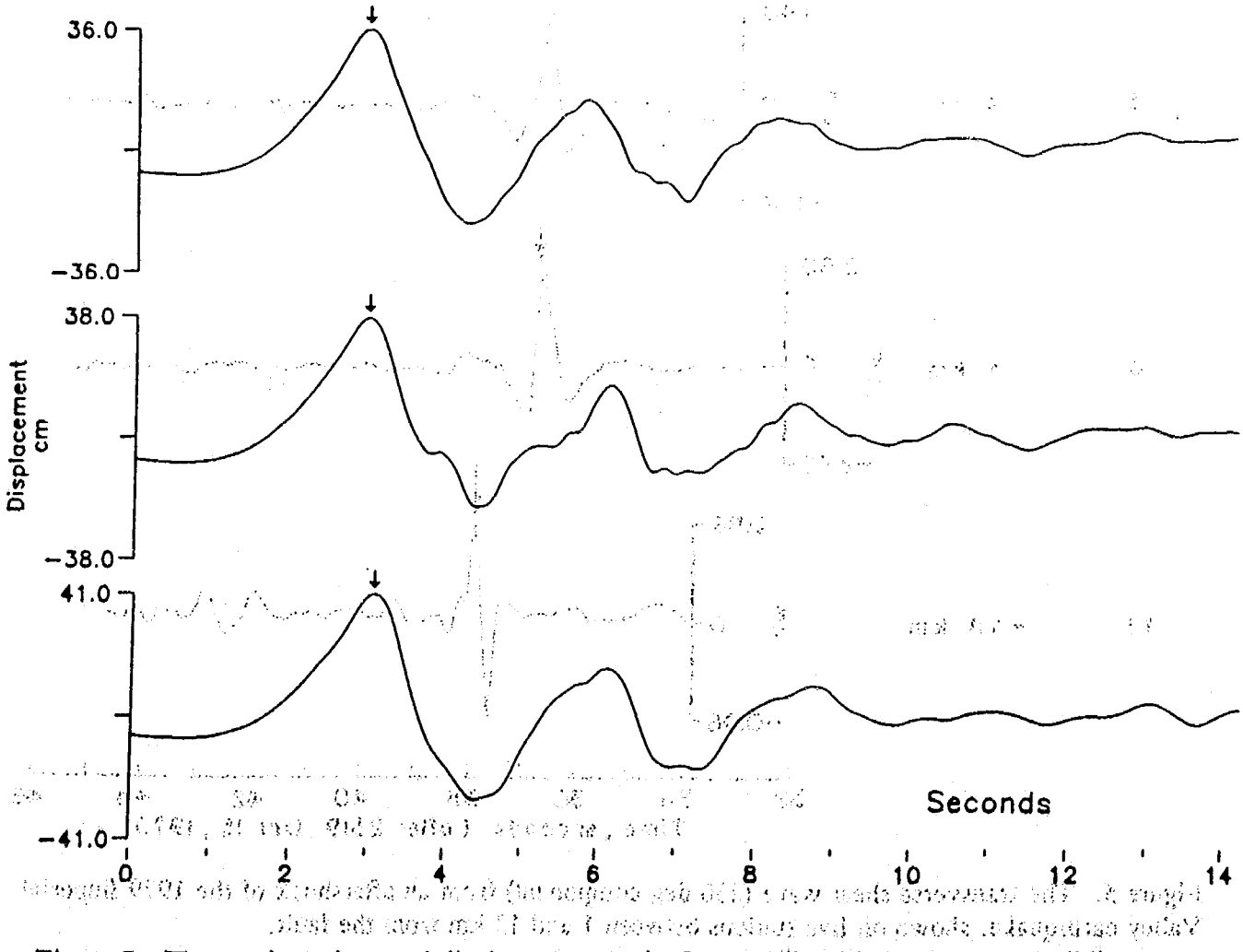


Figure 7. The southward ground displacements at the Jensen Filter Plant: generator building ground level (top), reservoir roof, and administration building basement.

Shaking Table Damage Tests of 3 Story RC Frames

By

Chikahiro Minowa[1], Shinichi Miyashita[2], Keiji Kitajima[3], Hiroshi Hosoya[4]
Tuneo Okada[5]

ABSTRACT

Dynamic damage tests of acutely size 3 story reinforced concrete frames (one bay x one bay) were carried out. Two RC frame of three stories were tested on the NIED large scale shaking table of one horizontal movement. Two RC frames were designed so as to make the girders yield prior to the columns. The Kobe JMA NS record of the Hyogo-ken Nanbu Earthquake, and Hachinohe EW record of 1968 Tokachi-oki Earthquake were used in the tests. The failure modes of shaking table tests agreed to the predicted modes. The girders which were normal to excitation direction, sustained the failures at the connections. The maximum story displacement angle was about 1/21 in Kobe JMA excitations.

Key Words : Reinforce Concrete
Shaking Table Test
Damping Ratio
Damage Test
Earthquake Motion

1. INTRODUCTION

It is important to study the dynamic failure process of structures, for the aseismic design, the damage judgement of buildings, the evacuation plan, the planning of earthquake disaster mitigation, the retrofit plan. For the purpose, NIED conducted the study of RC structure damages during the strong earthquake as a STA project of joint research with private companies. In the study, the shaking table damage tests of actual size 3 story RC frames were conducted two times. At the second test, the test frame was excited by Kobe JMA NS record of the Hyogo-ken Nanbu earthquake.

The RC frame dynamic response studies in which the shaking table tests of small models were used, were already conducted by the group of Sozen[1], Abe and Okada[2]. EERC in University of California, and BRI in Japan conducted the shaking table tests of middle size RC frame models. The shaking table tests of actual size RC structures were carried out in Nuclear Power Engineering Test Center and National Research Center for Disaster Prevention.

The shaking table tests of the study made large deformations and damages in actual size 3 story RC frames, and the dynamic damage processes were examined. Considering the capacity of NIED Shaking table, the wall structure damage tests should be impossible. Thus, the beam - column frames were investigated.

The research was carried under the promote board, the chairman; Tuneo Okada.

2. FIRST SHAKING TABLE TEST

TEST FRAME

The outline and reinforcements of a test frame are shown in Photo 1 and Fig.1 and 2. The reinforced concrete test frame of three stories has the total height of 10m, the each story height of 3m, the length of 6m in both (x and y) directions, and 4 columns of section 45cm x 45cm. The girders were designed to be weak in comparison with the columns. The x direction was

1) National Research Institute for Earth Science and Disaster Prevention, Cooperative Research Officer
2) Tokyu Construction Co. Structural Engineering Dept.
3) Akoki Construction Co. Research Institute.
4) Okumura Construction Co. Research Institute.
5) University of tokyo, Institute of Industry and Science, Professor

parallel to the excitation axis, and the y direction was normal to the axis. The south and north elevations coincided with the x direction, the east and west elevations coincided with the y direction. The thickness of each floor slab was 15cm. The each slab had a beam in the x direction. The steel blocks which gave the lively loads corresponding to actual buildings, distributed over the slabs. The weights of the third, second, first story were 39.05ton, 37.07ton, 37.28ton respectively.

The date of shaking table damage test was after 39 days from first story concrete casting (compressive strength 316kg/cm^2, before 3 days of the test), after 29 days from second story concrete casting (400kg/cm^2, before 3 days of the test), after 19 days from third story concrete casting (294kg/cm^2, on next day of the test). The tensile strengths of steel bars were about 3.5tonf/cm^2 in small diameter bars like D10, and about 4tons/cm^2 in large diameter bars like D22. In order to mitigate the shock loads of falling frames in the shaking table during damage excitations, a rigid steel frame was fabricated on the table. The weight of the frame was about 80ton.

TEST METHODS

The shaking table was driven by the strong earthquake motion record of 1968 Tokachioki, Hachinohe E-W, which was mode in the use of FFT band pass filter 0.4Hz-50Hz. The real time scale was used. The pulse excitations were used to observe the change of the stiffness and damping

The one horizontal dimension shaking table of NIED was used in the test. The dimension of shaking table is 12m by 12m. The table weight is 180ton. The maximum power is 360tons.

The deformations of the test frame were measured by potentio meters which were installed in the rigid steel frame. Acceleration and strain responses were measured.

TEST RESULTS

The table movements of the damage test were 169.1mm in the maximum displacement, 69.4cm/sec in the maximum velocity, and 960gal in maximum acceleration, as shown in Fig.3. Maximum exciting force was 341.4tonf. The potentio meter records of each story were 33.3cm in third story, 21.8cn in second story, and 9.6cm in first story, as shown in Fig.4. The acceleration responses of each story were shown in Fig.5. The displacement offsets after the damage excitation ere about 2.3cm in third story. The x direction girder ends on the connections between columns and girder were cracked and the small crushed concrete separated down from the frame, as shown in Fig.6, and Photo 2,3, because of the weak girder design. The damages of columns, as cracks of column foot in bases, were a little in the comparison with the girders. Furthermore, the y direction girders were damaged very much, as shown in Fig.7.

The reinforcement steel bars in x direction girders yielded very much in every stories. However, in second and third stories, the bars of columns were appeared not to yield or to yield in small plastic ratio less than 2. The column ends of first story and bases yielded larger than the columns of other stories. The damage modes which were observed in the test, were anticipated in the design processes.

The response spectra of table acceleration records were shown in Fig.8. The impulse responses before and after the damage excitation, were shown in Fig.9. The estimated modal characteristics were indicated in Table 1. The natural frequency of the rigid steel frame was estimated to be 10Hz.

DISCUSSIONS

The inertia force - story displacement hysteresis loops are shown in Fig.10. The inertia forces were calculated by the acceleration X the story mass. The simulation data were given by the Computer code RESP-F of plane frame elasto - plasto dynamic analysis. The Calculated natural frequencies, using material test data, were described in Table 1. Simulation hysteresis loops are seen to agree with test

results, well. However, the displacement values were a little different from test results. The more study will be necessary.

3. SECOND SHAKING TABLE TEST

TEST FRAME

The most of test frame details were as same as first test frame, except the reinforcements of girders and beams, and the distributions of steel blocks. The section of third story beam was 35cm width by 30cm height. The up side reinforcements of the beam were 3-D16 in the end and center parts, and the lower side reinforcements were 2-D16 in the end part, 4-D22 in the center part. The section of second and first story beam was 30cm width by 35cm height. The up side reinforcements of the beam were 2-D16 in the end and center parts, and the lower side reinforcements were 2-D16 in the end part, 3-D19 in the center part. The y direction girders were made strong by the web reinforcements 2-D16 and straps D-13 with the spacing of 10cm. The lower side reinforcements of third story girders were 2-D13 and 2-D10. The change had been done in order to increase the torsional strengths of girders.

The steel blocks were distributed so as to make the torsional vibrations in the test frame. The steel block positions were near the edges line of south side in each story, as shown in Fig. 11. The weight of each story were as same as the first test. The distance between gravity centers and rigidity centers of each story was about 0.9m.

TEST METHODS

The test schedule of the second test frame was, that the Hachinohe E-W was used in the first excitation so as to compare the results with the first test, and Kobe JMA NS record of the Hyogo-ken Nanbu Earthquake was used in the next excitations. Assuming the after-shocks of, etc., the excitations of Kobe JMA NS were conducted three times. The shaking table input of Kobe JMA NS record of the Hyogo-ken Nanbu Earthquake was obtained, as follows.

In the case of shaking table simulations of earthquake motions, the time histories of the simulated earthquake motions must be kept in the limit performances of shaking tables. The most of strong earthquake motion would be recorded in accelerations. Thus, The integrals of accelerations have to be executed two times so as to get the displacements. Usually, the displacement time histories which were taken by the integrals, would diverge. Therefore, high pass filter would be used for cutting the long period components of source waves and getting the converged displacement time histories. FFT and digital filters would be applied for the purpose. However, in principle, the filter must not be used, because the filter would deform the original waves in excess.

The integrals of Kobe JMA NS acceleration gives a divergent displacement as same as other acceleration records, as shown in Fig. 13. However, the divergent portion of the integrated displacement looks to consist of the linear of quadratic curves. If the displacement would increase linear or quadratic, the velocity would make a zero shift or a linear curve, which will correspond to an impulse or an shift in the acceleration, as shown in Fig.12. The values of impulses and shifts are estimated from the gradients of divergent parts. The impulse and shift may be found as electric noises. Also, the impulse and shift may be given by the shock noise of drop stone and the inclines of base mats. The convergent displacements are obtained by adding the same opposite values of impulses or shifts at the corresponding time positions in acceleration records. The integrated displacements are to leave the offsets. The displacement offsets are to be natural. The displacement time history of Fig.14 was obtained by the presented methods. The offsets of displacement are found in EW and UD components, not in NS component.

Kobe JMA records are understood to be about 820gal, 90cm/sec and 36cm p-p in NS component, and about 613gal, 75cm/sec and 30cm p-p in EW component. The response spectra indicates that the NS component would be destructive. The one horizontal direction shaking table of NIED has maximum velocity of 75cm/sec and maximum displacement of 46cm p-p. The NIED shaking table can't reproduce the maximum velocity of Kobe JMA NS component. In Kobe JMA NS component, the position which is over 75cm/sec, is only one and shorter than 0.3 seconds. If the only velocity peak of 92cm/sec would be reduced under 75cm/sec, the less deformed shaking table input will be obtained. Thus, the modification of acceleration records shown in fig. 15, was attempted. Fortunately, the shaking table input which has the same maximum acceleration and similar displacement and maximum velocity of 72cm/sec was obtained. The input wave modification of the methods shows that the response spectra of original and modified accelerations are almost same. The differences are less than 5%, as shown in Fig.16 and 17.

TEST RESULTS

At the first large amplitude excitation of Hachinohe E-W, the reinforcement steel bars of the test frame were measured to yield, and small cracks were observed around the connections.

From second excitation, the Kobe JMA NS record was applied. The potentio meter displacement records of total excitations in the x-direction, are shown in Fig.18. The maximum response 47cm of an excitation was the record of first Kobe JMA NS at the steel block side, and left the offset 8.4cm.

In next two excitations of Kobe JMA NS, the same amplitude inputs were adopted. The apparent natural frequencies went down by the reduction of stiffness, and shifted from the peak frequencies of response spectra, as a result, the response values decreases in 70% - 80%. By these excitations, the displacement offsets increased in the same direction. And at the end of test, the third story offset resulted in about 15cm on the steel block side, in about 11cm on the opposite side.

The failure occurred in the x-direction girders near the connections, as same as the first test frame, as shown in Photo 4,5. The torsion damage of y-direction girders were small in comparison with the first test. The inertia force - story displacement hysteresis loops are shown in Fig.19. The changes of impulse responses are shown in Fig. 20. The modal characteristics are described in Table 1. The response spectra of the low level excitation 40gal which was conducted before the damage excitation, and of the high level excitation 820gal are shown in Fig.21 and 22. In the low level excitation, the test frame exhibited the elastic response, so the response spectra had a valley at the natural frequency of the test frame. However, in the high level excitation, the same kind of the valley in response spectra was not found, the high frequency components were intense.

DISCUSSIONS

The predicted responses of the second test frame are shown in Fig. 23. The predicted maximum displacement was 38cm at the steel block side of the third story, and the offset was 15cm. The frame torsional responses which were assumed a little in the design, were observed very much in the test. The response calculations to the original Kobe JMA NS record, were diverged.

4. CONCLUSION

It was examined that the structures which were designed to make the girders yield before the columns, were very strong, and it would be difficult for the structures to collapse down.

The dampings increased with the progress of damages. The torsional structures gave the small damping in comparison with the general structures in the large deformation areas.

The damage of y-direction (normal to excitation direction) girders were examined.

ACKNOWLEDGMENT

The strong earthquake motion data were provide by the efforts of Mr. Fujio Kusano; the member of Japan Meteorological Agency, Dr. Hisanobu Akagi; The member of NTT Facilities, Mr. Makoto Miyamoto; the member of NIED. The authors wish to express the appreciations to them.

REFERENCES

1)Takeda T., Sozen M. A., et al., "Reinforce Concrete Response to Simulated Earthquake" Nov. 1970, Proceeding of 3rd JEES 357-364

2)Abe I., Okada T., et al., " Shaking Table Test of 1/7th-Scale Models", Proceeding of AIJ Conference 1988, 633-634

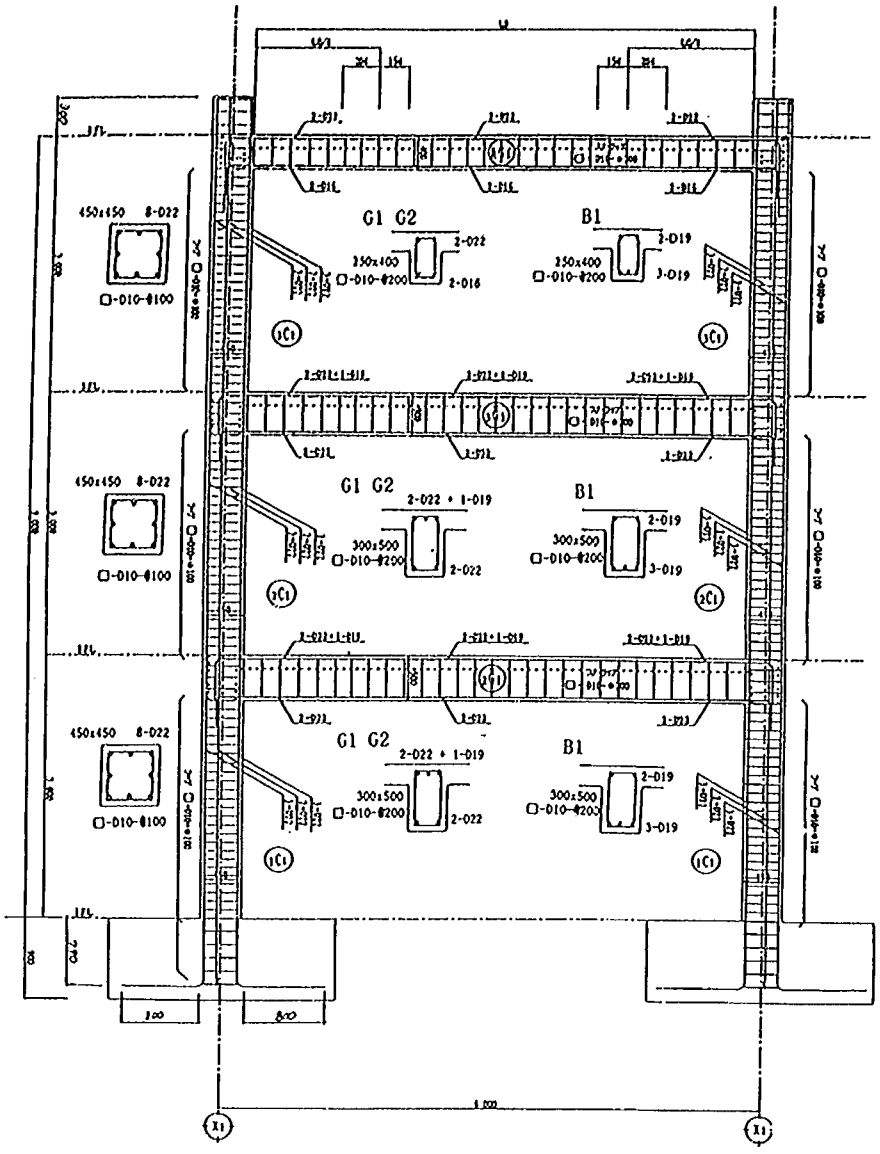


Fig. 1 Steel Bar Distribution of 1st Test Frame Elevation

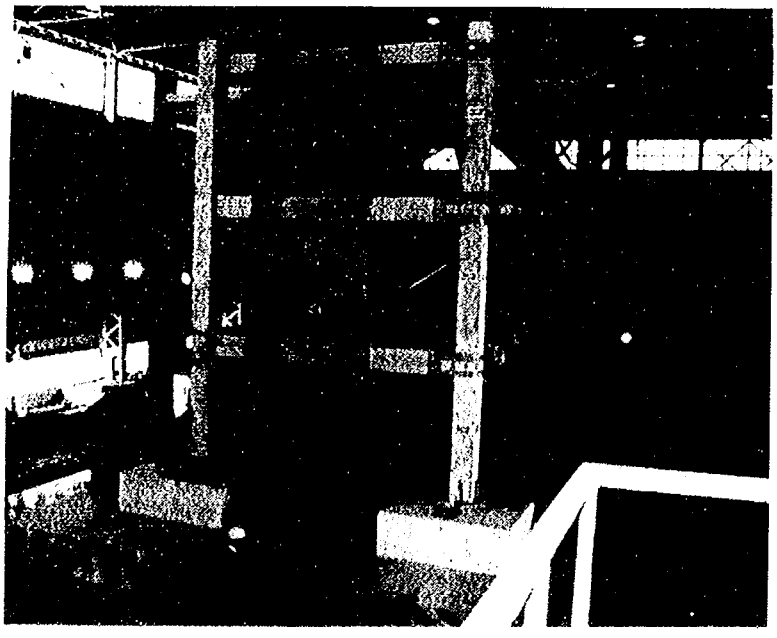


Photo 1 RC Test Frame and Support Frame

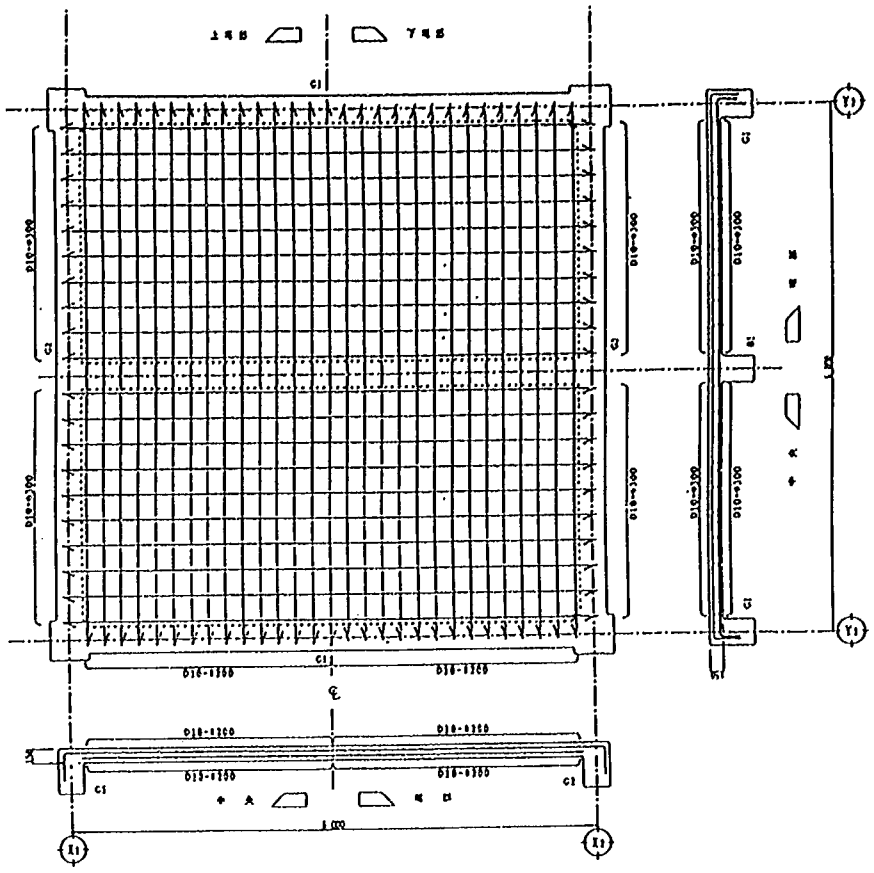


Fig. 2 Slab Steel Bar Distribution

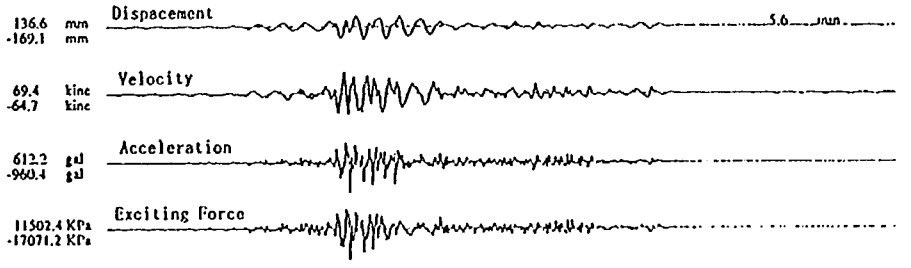


Fig. 3 Hachinohe EW Table Movements

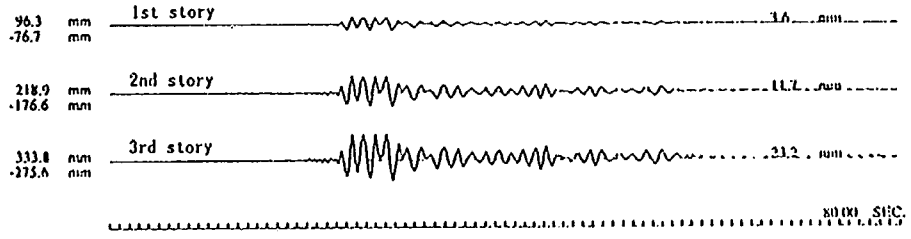


Fig. 4 Hachinohe EW Relative Displacements from Support Frame

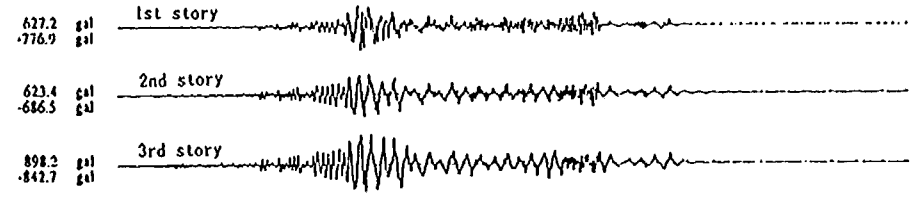


Fig. 5 Hachinohe EW Response Accelerations

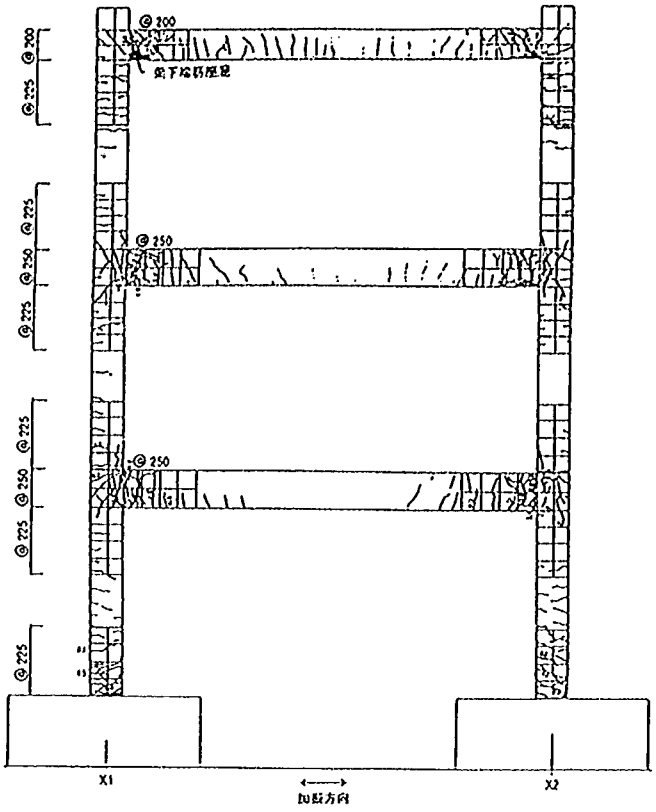


Fig. 6 Crack Sketch of 1st RC Frame South Elevation

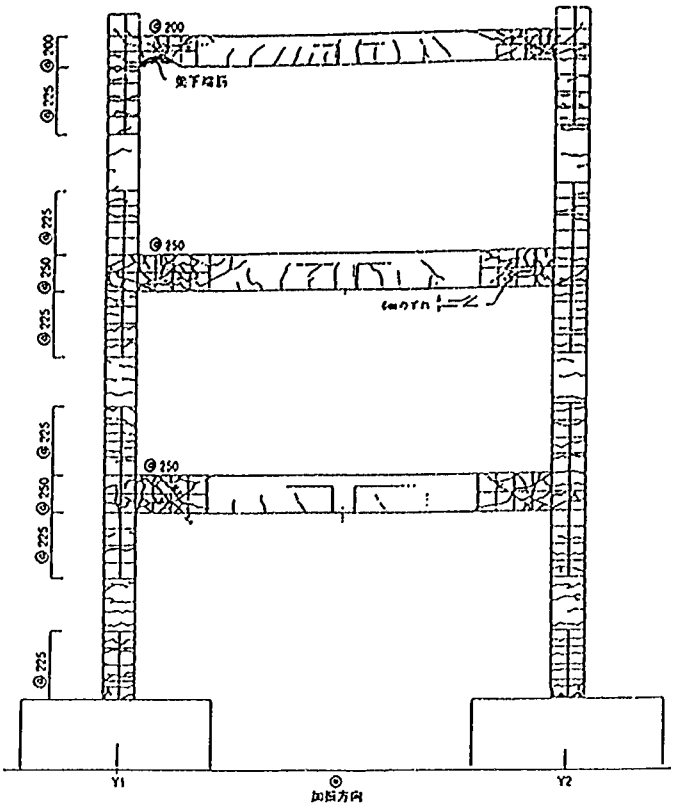


Fig. 7 Crack Sketch of 1st RC Frame East Elevation

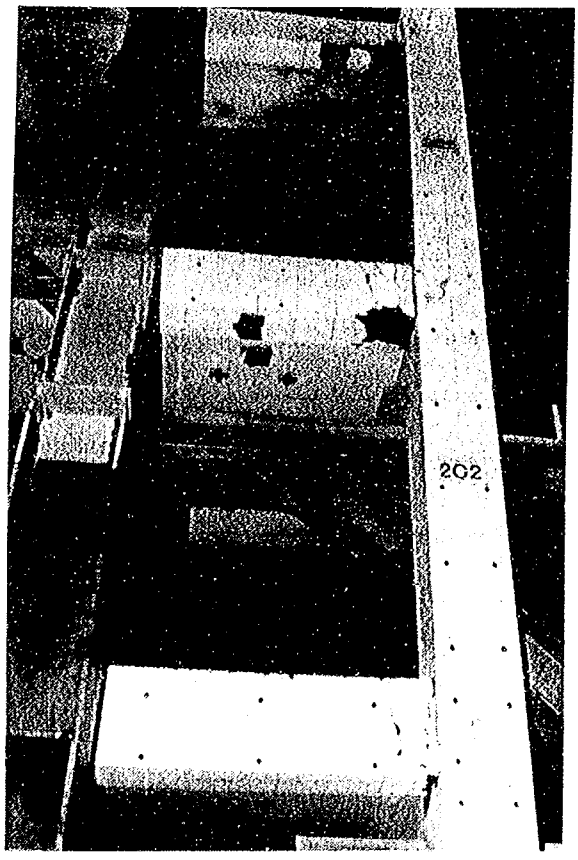


Photo 2 Damaged 1st RC Frame

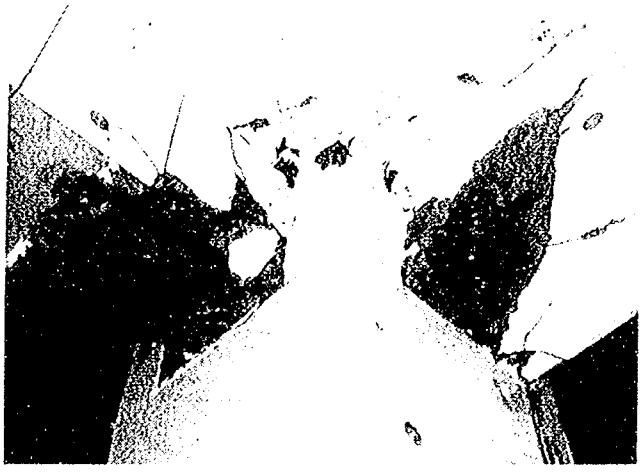


Photo 3 Damaged Girders of 1st RC Frame

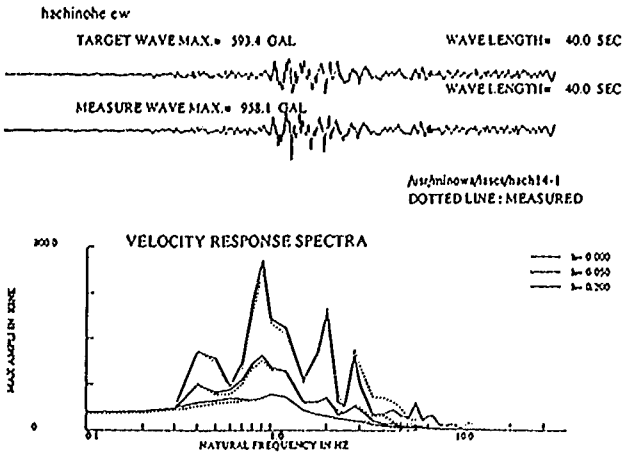


Fig. 8 Velocity Response Spectra of Hachinohe EW

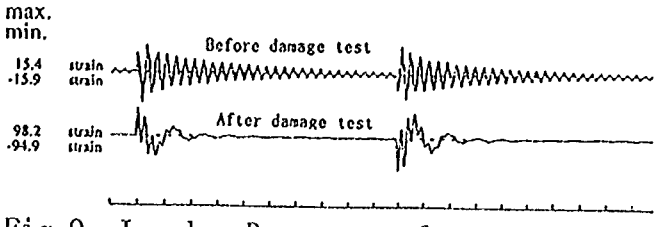


Fig. 9 Impulse Responses of 1st RC Frame

Table 1 Measured Modal Characteristics of 1st RC Test Frame

	1st Mode		2nd Mode		3rd Mode	
	Frequency	Damping	Frequency	Damping	Frequency	Damping
Before Damage	3.0Hz (3.3Hz)	1.3% - 2.0%	9.7Hz (10.1Hz)	2.0% - 3.7%	18.7Hz (20.2Hz)	2.5% - 5.2%
After Damage	0.85Hz	15%	3.7Hz	3% - 6%	8.5Hz	3% - 6%

( ) : Simulation

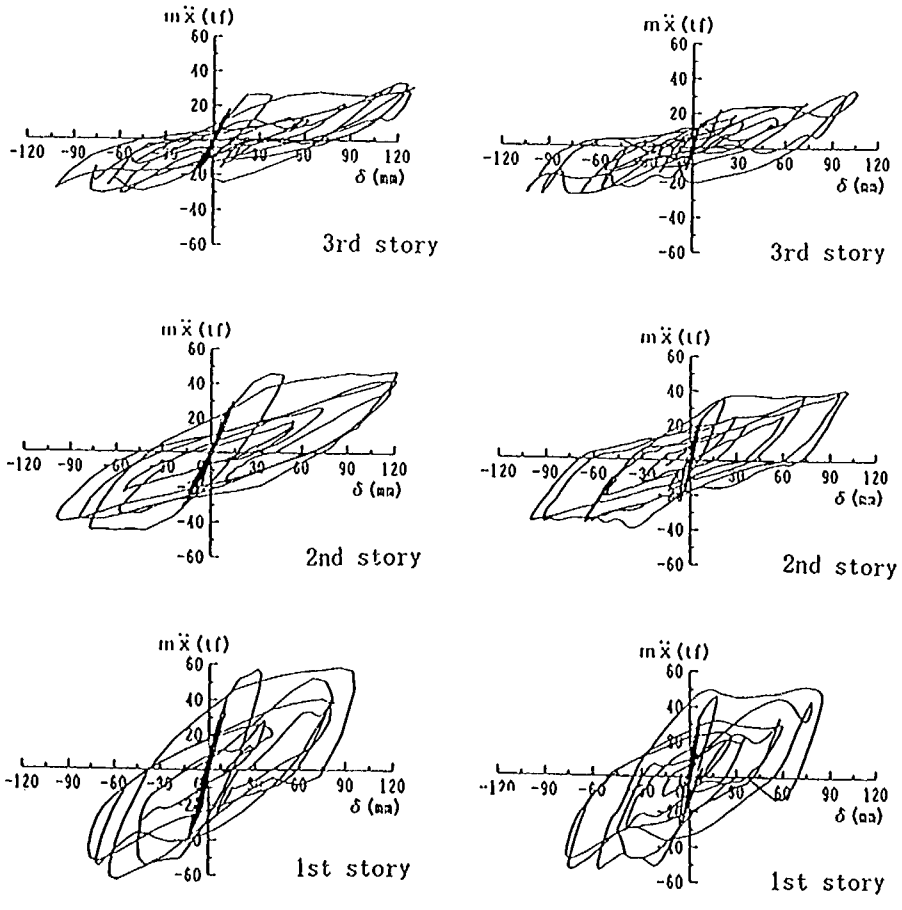


Fig. 10 Story Deformation - Inertia Force Curves of 1st Frame

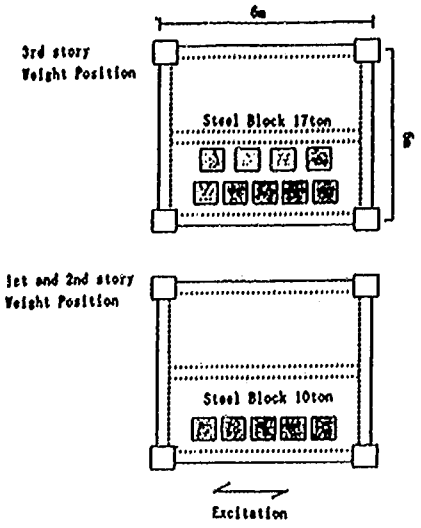


Fig. 11 Weight Block Distribution of 2nd RC Frame

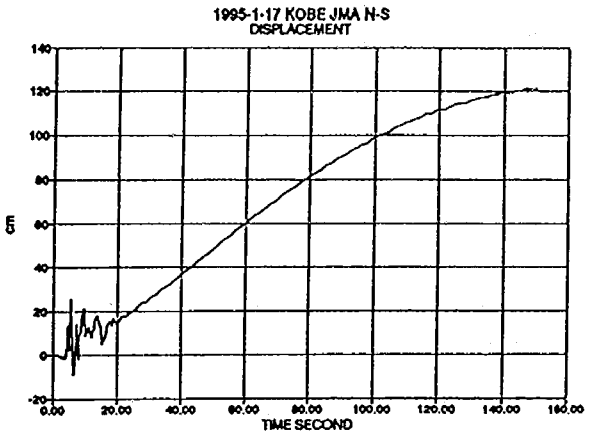


Fig. 13 Integrated Displacement of Source Acceleration Wave

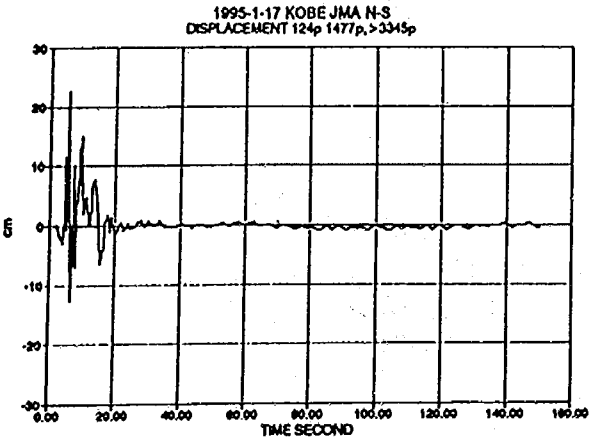


Fig. 14 Integrated Displacement of Corrected Acceleration Wave

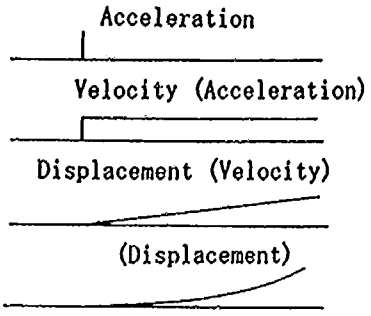


Fig. 12 Outline of Integration

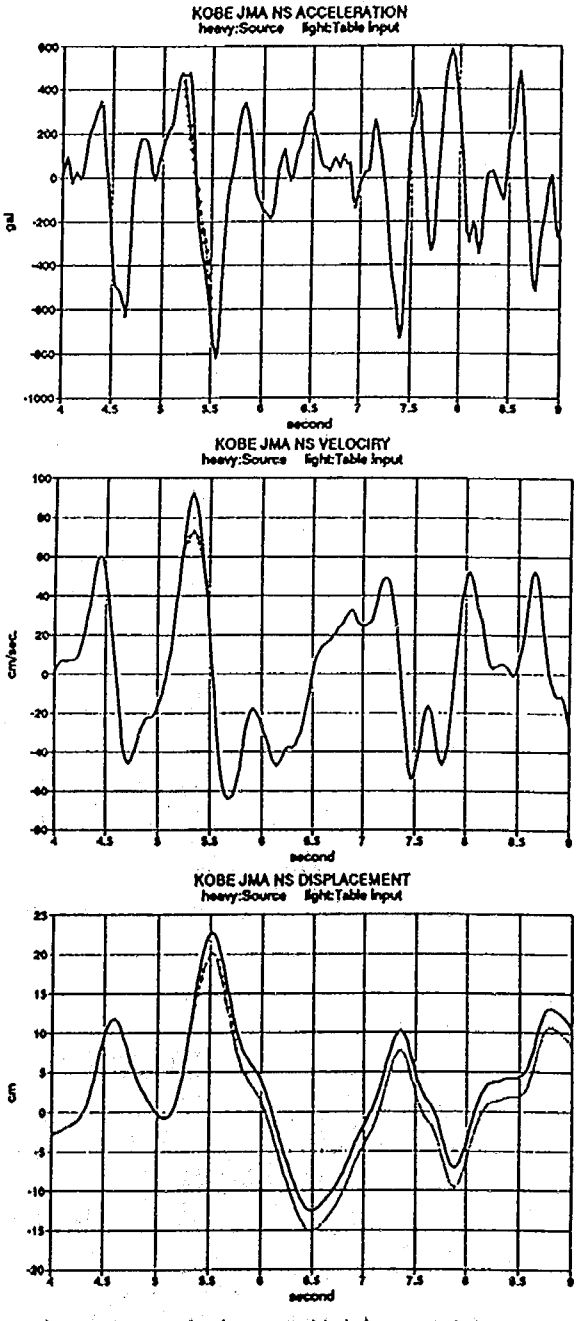
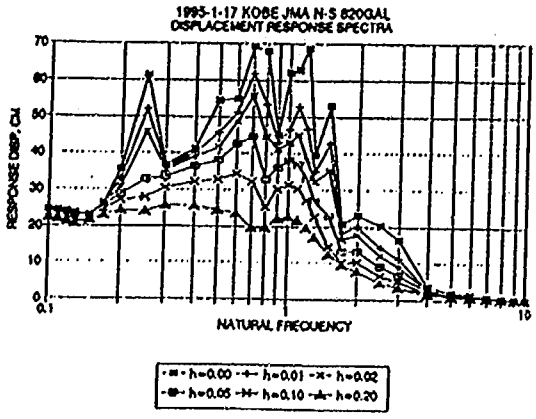


Fig. 15 Explain of Making Table Input



Fig, 16 Response Spectra of Source

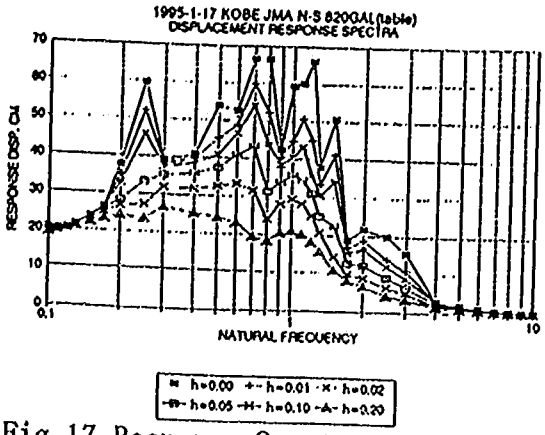


Fig. 17 Response Spectra of Table Input

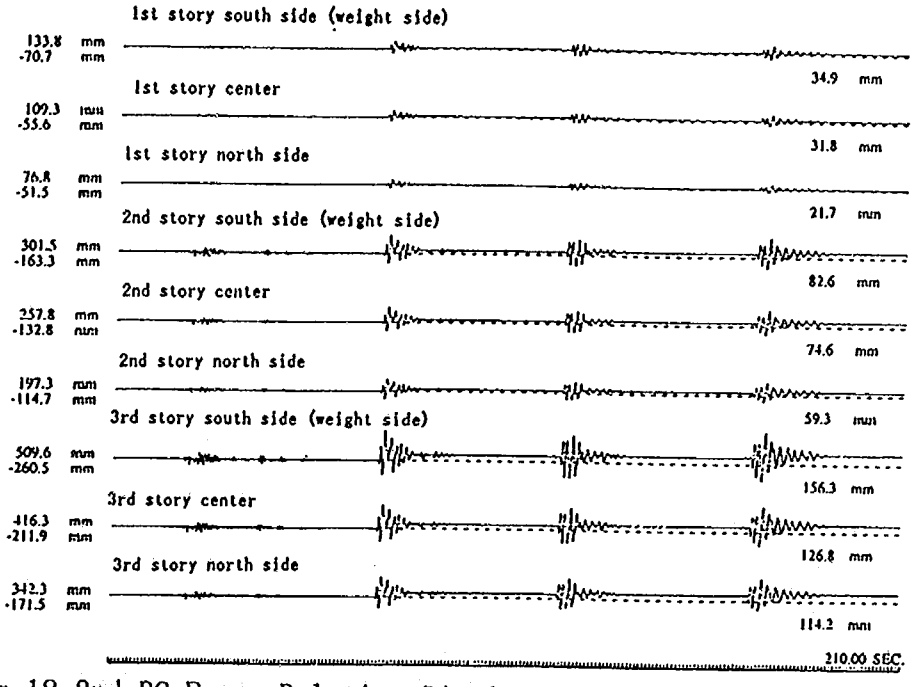


Fig. 18 2nd RC Frame Relative Displacements from Support Frame

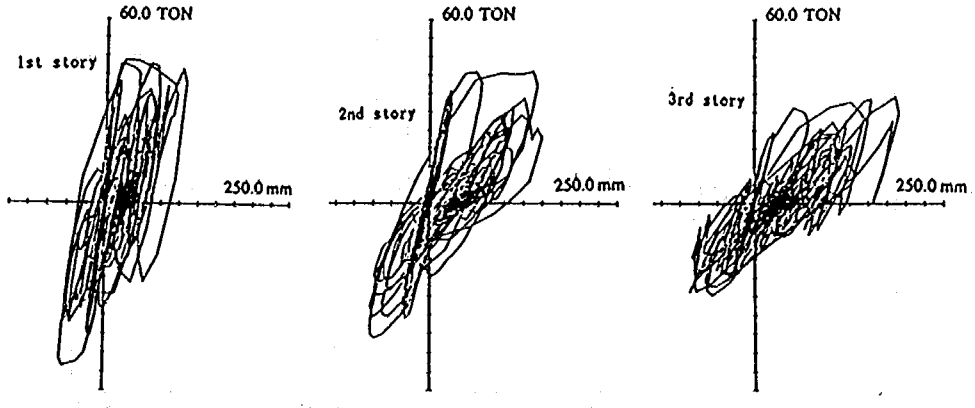


Fig. 19 Story Deformation - Inertia Force Curve of 2nd Frame

Table 2 Rough Modal Estimation of 2nd RC Test Frame

	1st Mode		2nd Mode		3rd Mode	
	Frequency	Damping	Frequency	Damping	Frequncy	Damping
No Damage	2.55Hz	1.60%	8.49Hz	2.12%	15.2Hz	3.57%
After Hachinohe	1.65Hz	6% - 12%	6.1Hz	2.5%-5%	13Hz	3%-6%
After 1st Kobe	0.98Hz	12%	4Hz	2% -3%	9.2Hz	3%
After 2nd Kobe	0.86Hz	11% - 14%	3.5Hz	2%-3.5%	8Hz	2.5%-3%

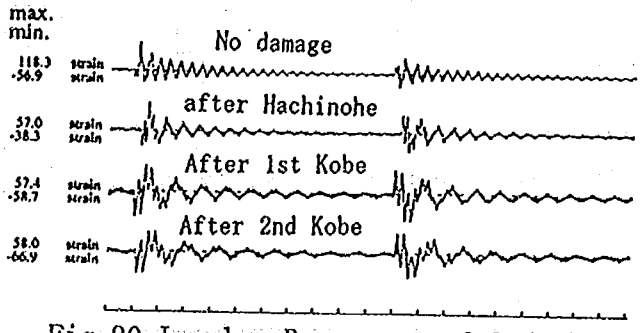
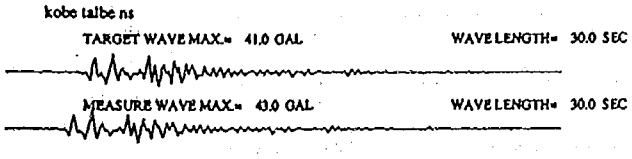
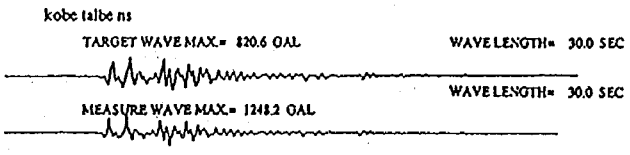


Fig. 20 Impulse Responses of 2nd RC Frame





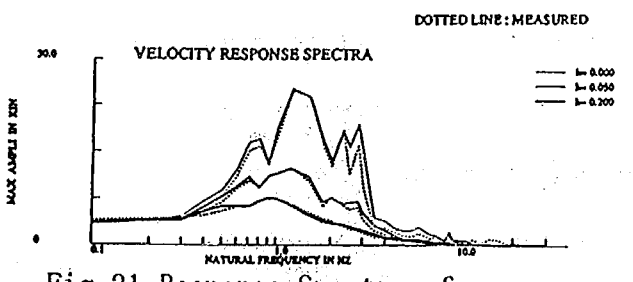


Fig. 21 Response Spectra of High Level Input

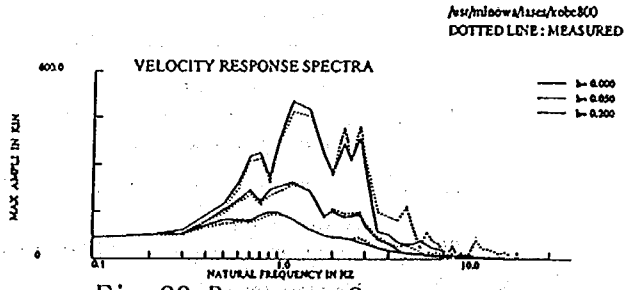


Fig. 22 Response Spectra of Low Level Input

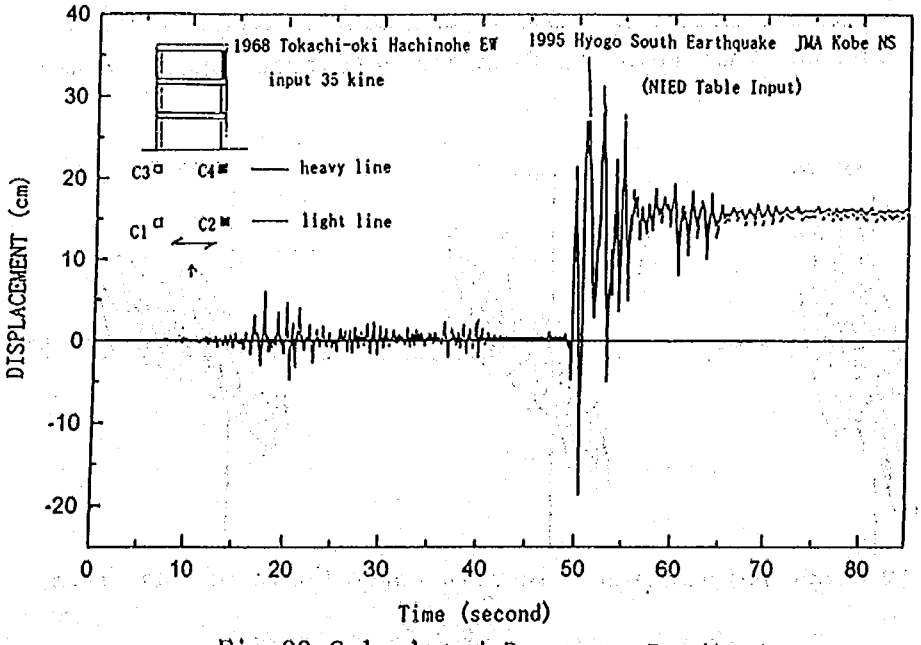


Fig. 23 Calculated Response Prediction

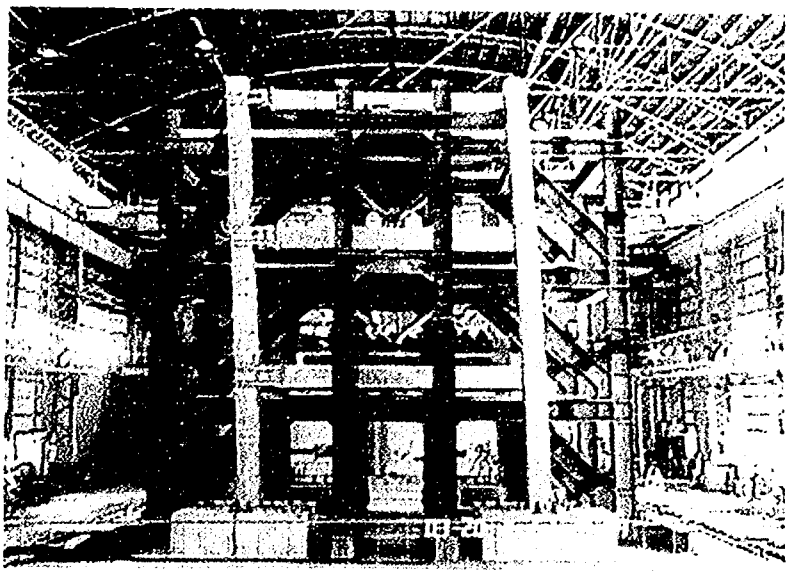


Photo 4 Deformed 2nd RC Frame

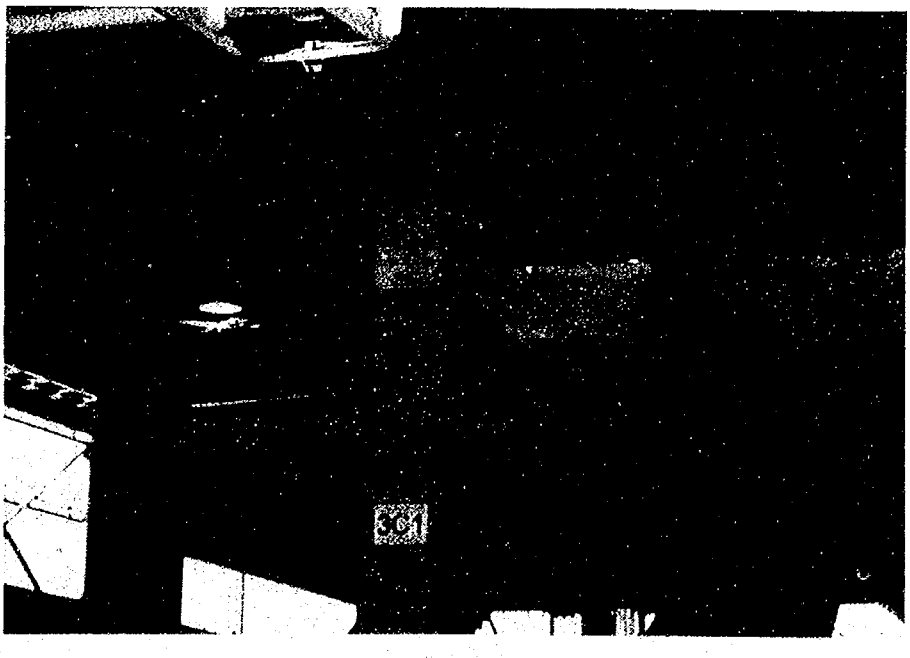


Photo 5 Damaged Girder of 2nd RC Frame

Test Requirements for Base Isolation

by

By H.W. Shenton[1], A.W. Taylor[2], III, and H.S. Lew[3]

ABSTRACT

In the United States there are currently no widely accepted standards for the testing and evaluation of seismic base isolation systems for buildings, bridges and other civil engineering structures. It is difficult for designers to evaluate the characteristics of a given system, or to compare competing systems, since standard test methods and properties of systems have never been clearly defined. This paper describes guidelines, recently developed at the National Institute of Standards and Technology (NIST), for testing and evaluation of seismic isolation systems. The guidelines are intended to apply to any type of base isolation system (elastomeric, sliding, hybrid, or other type); and to any type of civil engineering structure. In this paper the philosophy behind the development of the guidelines is first discussed. Then the guidelines themselves are briefly reviewed, and the three types of tests recommended by the guidelines are described: pre-qualification, prototype, and quality control testing. Finally, future research and standards development activities related to the guidelines are outlined.

KEYWORDS: base isolation; bridges; buildings; earthquake engineering; elastomeric bearings; seismic design; sliding systems; standards; testing

1. INTRODUCTION

In the United States there are currently no widely accepted standards for testing and evaluating seismic base isolation systems. A series of basic performance requirements and tests are described in the national building codes, but these requirements are not defined in detail, so they are open to subjective interpretation. As a result there is considerable confusion and disagreement among designers, owners and manufacturers about how seismic isolation systems should be tested and evaluated. Guidelines are needed to define the types of tests that are required in a given design situation, the details of the test procedures, the physical properties to measure in testing, and methods for evaluating and comparing measured properties.

A comprehensive set of draft guidelines for the testing and evaluation of seismic isolation systems has recently been developed by the Building and Fire Research Laboratory (BFRL) of the National Institute of Standards and Technology (NIST). The guidelines will serve as a resource document for individuals and agencies involved in the design and construction of seismically isolated structures. The guidelines will also serve as a basis for developing a national testing standard.

The NIST guidelines are broadly applicable. Except as described later, the guidelines are not specific to a particular type of isolation system or superstructure. The guidelines can be used in projects that involve buildings, bridges, nuclear plants and equipment, and elastomeric, sliding or hybrid isolation systems. A broadly based guideline has several advantages over system specific procedures. First, the potential of the technology can be maximized by all sub-disciplines of civil engineering. Second, broadly based guidelines will minimize the likelihood of each sub-discipline developing unique standards for their own application, which would only slow further progress of seismic isolation technology. And finally, the guidelines do not favor one isolation system over another. Therefore, the guidelines should encourage competition between various systems, resulting in production of the highest quality systems.

---

[1]Assistant Professor, Department of Civil Engineering, University of Delaware, Newark, Delaware, 19716. (Formerly, Research Structural Engineer, Building and Fire Research Laboratory, National Institute of Standards and Technology, Gaithersburg, Maryland, 20899).

[2]Research Structural Engineer, Structures Division, Building and Fire Research Laboratory, National Institute of Standards and Technology, Gaithersburg, Maryland, 20899.

[3]Chief, Structures Division, Building and Fire Research Laboratory, National Institute of Standards and Technology, Gaithersburg, Maryland, 20899.

The guidelines apply primarily to passive seismic isolation systems which provide isolation in a horizontal plane. Some parts of the guidelines may be applicable to active seismic isolation systems, and systems which provide isolation in a vertical plane, but this is not the intent of the guidelines.

2. DEVELOPMENT OF THE GUIDELINES

The guidelines have been developed in a four step process. Throughout development of the guidelines a concerted effort has been made to solicit the opinions and suggestions of members of the base isolation community. These outreach efforts are expected to strengthen acceptance of the guidelines, and encourage their use and support. The steps followed in development of the guidelines are outlined below.

1. An oversight committee was formed to advise and collaborate with NIST in writing the initial draft of the guidelines. The committee consisted of five experts from the field of seismic isolation, representing the perspectives of designers, researchers, and manufacturers.

2. Once the initial draft guidelines were prepared they were circulated to approximately 200 designers, researchers and manufacturers in the base isolation community. Comments were received from about 40 people.

3. A workshop was held on July 25, 1994 to provide an interactive forum for review and discussion of the draft guidelines. Approximately 35 invited participants attended, representing a range of interests in the base isolation community. The draft guidelines were discussed in small groups and in plenary sessions. The comments and suggestions of the participants were recorded and summarized in notes.

4. As the last step in development of the guidelines, the comments received by mail (step 2) and from the workshop (step 3) will be incorporated in final guidelines. Many constructive comments have been received, and these will be considered in development of the final guidelines. The final guidelines will be published as a NIST technical report in mid 1995.

3. OVERVIEW OF THE GUIDELINES

The guidelines cover three broad categories of testing: pre-qualification, prototype and quality control. These are defined as follows:

> Pre-qualification Tests are usual not related to a specific construction project. Rather, pre-qualification tests are most often related to basic research conducted during development of a new type of isolation system. These tests establish the fundamental characteristics of an isolation system, and determine the extent to which the properties of the system are dependent on the type of loading and environmental factors.
>
> Prototype Tests are related to a specific construction project. These tests are conducted to verify the design properties of an isolation system prior to construction.
>
> Quality Control Tests are also related to a specific construction project. They are conducted to verify the quality and consistency of the manufacturing process, and to measure the as-built properties of the isolation system prior to installation. Quality control tests include production tests on the materials and component, as well as tests on completed isolation units.

Prototype tests and quality control tests are currently required by the 1994 Uniform Building Code (UBC) (*Uniform*, 1994), and the 1991 AASHTO *Guide Specification for Seismic Isolation Design* (*Guide*, 1991). However, the exact nature of the tests and interpretation of the test results are not clearly spelled out. Pre-qualification tests are not formally required by either of these codes; although, in practice tests similar to the pre-qualification series are usually conducted as a new isolation system is developed. Appropriate prototype and quality control tests can only be conducted after a proper series of pre-qualification tests have been conducted.

The guidelines are organized into three separate reports. One report covers pre-qualification and prototype testing (Shenton, 1994a), and the others address quality control testing for elastomeric systems (Shenton, 1994b) and quality control testing for sliding isolation systems (Shenton, 1994c). The guidelines for quality control testing are classified according to the type of isolation

system because of the production tests. These tests must be related to a specific seismic isolation system, since they depend on the materials being used and the unique details of the design.

3.1 Pre-qualification Tests

Pre-qualification tests are exploratory in nature, and are intended to determine the fundamental characteristics of the system. For example, one pre-qualification test is designed to determine the effect of temperature on the effective stiffness and energy dissipation capacity of the device. Another is designed to determine the effect of frequency of cyclic loading. The series also establishes characteristics of the static load carrying capacity of the device. As the name implies, the pre-qualification series is intended to provide preliminary information and data about the isolation system. The results of the tests could be submitted by an isolation system manufacturer in the pre-bid package, so that the designer can judge whether or not the system is suitable for a particular application. It should be noted that there are presently no known plans to develop a formal national pre-qualification or certification program for seismic isolation systems.

The pre-qualification series includes not only initial tests to determine basic system properties, but also a complete series of prototype and quality control tests. These tests are outlined in the subsections that follow. Tests included in the pre-qualification series are shown in Table 1. Note that the tests in Table 1 are grouped into two sub-categories: Preliminary Characterization (I), and Ultimate and Reserve Capacity (II). The procedures in category I determine the effect of load and environmental factors on the system performance. The procedures in category II establish the ultimate or reserve capacity of a device for various load conditions. The pre-qualification series is to be conducted only once, for a system of a given design, material and construction. The series would only be repeated if there were major design changes to the device.

Table 1. Pre-qualification Tests[1]

Category	Test	Purpose
I Preliminary Characterization	I.1	Establish dependence on virgin loading
	I.2	Establish dependence on frequency of load
	I.3	Establish dependence on load cycle history
	I.4	Establish dependence on load cycling
	I.5	Establish dependence on vertical load
	I.6	Establish dependence on load direction
	I.7	Establish dependence on load plane rotation
	I.8	Establish dependence on bilateral load
	I.9	Establish dependence on temperature
	I.10	Establish dependence on creep
	I.11	Establish dependence on aging
II Ultimate and Reserve Capacity	II.1	Ultimate compression under zero lateral load
	II.2	Compression in displaced position
	II.3	Ultimate tension under zero lateral load
	II.4	Tension in displaced position
	II.5	Lateral load and displacement capacity under design vertical load

[1]Pre-qualification shall also include a complete series of prototype tests and quality control tests.

3.2 Prototype Tests

The prototype series is divided into two categories: Seismic Loads (III) and Non-Seismic Loads (IV). This is shown in Table 2. Note that prototype testing includes a full series of quality control tests, as described in the next subsection.

The principal design properties of the isolation system, effective stiffness and energy dissipation capacity (i.e., damping), are measured in prototype test III.1. These properties are essential to the design of the superstructure. The effective stiffness and energy dissipation capacity of the system determine the magnitude of the force that is transmitted to the superstructure, and control

the displacement across the isolation interface. Two other seismic load tests are conducted in series III: one to measure the isolation system degradation (stiffness and energy dissipation) under cyclic loading (III.2), and one to check for stability at maximum seismic displacement (III.3). Test III.2 is significant with regard to the long term performance and durability of the isolation system. Test III.3 checks that the system can maintain its vertical load carrying capacity while in the maximum displaced position.

The extent of testing required in the prototype series, in particular under test III.1, will depend on the outcome of the pre-qualification series (Table 1). For example, if a system is found to be dependent on the frequency of loading, the test matrix in III.1 is augmented to include tests to measure the effective stiffness and energy dissipation for a range of frequencies.

First and foremost, the performance of an isolation system must be stable and predictable under *non-seismic* load conditions, which are imposed over most of the design life of the isolation system. This is addressed with the category IV tests in the prototype series. Non-seismic load tests are included for wind load, thermal displacement, thermal cycling and braking/centrifugal force. The first is most important for large structures, such as buildings, that are exposed to wind load. The latter three are intended principally for bridge applications. There are certainly other non-seismic load conditions that are important in other applications. In such cases the guidelines could be supplemented to include additional non-seismic load tests that are unique to a particular application. Obviously, only those non-seismic load tests deemed to be relevant to a particular application need to be conducted.

There is an exception in the guidelines that exempts prototype tests under certain conditions. It has been included with the intent of minimizing or eliminating duplicate testing of identical units. The exception states that the results of prototype tests previously conducted can be substituted, provided the tests were conducted on a device of essentially the same design, material and construction, the largest overall dimension of the unit is within 10% of the same dimension of the unit previously tested, and all other critical dimensions are within 15% of the same dimensions of the unit previously tested.

Table 2. Prototype Tests[1]

Category	Test	Purpose
III Seismic Loads	III.1	Effective Stiffness and Energy Dissipation Capacity
	III.2	System Degradation Under Cyclic Loading
	III.3	Stability at Maximum Lateral Displacement
IV Non-Seismic Loads	IV.1	Wind Load
	IV.2	Thermal Displacement
	IV.3	Stability with Thermal Cycling
	IV.4	Braking/Centrifugal Force

[1]Prototype Testing shall also include a complete series of quality control tests.

3.3 Quality Control Tests

As mentioned above, the quality control series is divided into production tests and completed unit tests. Tests conducted on the materials or component parts that go into making a unit are considered production tests. Completed units tests are conducted on the assembled isolator unit.

The production tests for elastomeric systems are designed to establish the properties, and consistency of those properties, of the elastomer that is used in fabricating the device. The production tests currently specified in the guidelines include tests for hardness, tensile strength and elongation at break, bond strength, compression set, low temperature properties, high temperature aging, and ozone resistance of the elastomer. These are similar to the material tests that have been used in the past for fabricating non-seismic elastomeric bridge bearings. The completed unit tests for elastomeric systems are presented in Table 3. These are the final tests conducted on the unit before it is installed. The purpose of the sustained compression test is to verify the integrity of the bond between the elastomer and the steel. This is a very time consuming test, lasting generally between twelve and fifteen hours. Research is needed to develop a more efficient method of testing the elastomer/steel bond. One suggested alternative is a shear test with zero compression load.

Table 3. Completed Unit Quality Control Tests for Elastomeric Systems

Test	Purpose
1	Effective Stiffness and Energy Dissipation Capacity
2	Sustained Compression
3	Compression Stiffness

Production tests for sliding systems are designed to ensure the quality of the sliding interface. These include tests for surface roughness, trueness (flatness) of surface, interface material properties, backing material properties, bearing pad attachment and sliding interface attachment. The completed unit tests for sliding systems are shown in Table 4. The sustained compression test in this case is conducted only for systems that are susceptible to creep (as determined by the pre-qualification tests, Table 1).

Table 4. Completed Unit Quality Control Tests for Sliding Systems

Test	Purpose
1	Effective Stiffness and Energy Dissipation Capacity
2	Sustained Compression

Quality control tests, in particular the completed unit tests, can be expensive and time consuming. The extent of testing to be recommended in the final guidelines has generated some debate within the base isolation community. Some would place more emphasis on completed unit tests, requiring every single unit that is manufactured be tested. In this case, few if any production tests would be required. The justification for this approach is that, regardless of how the unit was manufactured, the proof of the performance of the device is the completed unit test. Others would require a rigorous production test program, and fewer completed unit tests. In this case only a certain percentage of units manufactured would be tested, unless some of these failed, in which case all units manufactured would be tested. There are advantages and disadvantages to both of these approaches, with regard to how they may affect the future and growth of seismic isolation technology. On the one hand, a heavy emphasis on completed unit tests may stifle growth, because of the time and expense required for testing each and every isolation unit produced. This could discourage owners from considering isolation. On the other hand, if the emphasis is placed on quality control tests of materials and components during fabrication, and only a few completed units are tested, this leaves open the possibility of substandard completed units being produced. There is concern that failure of a single isolated structure, due to marginal behavior of completed isolation units which had not been thoroughly proof tested, could be devastating to the future of this technology.

3.4 General Requirements and a Typical Test Description

The general requirements for testing are outlined in a separate chapter in the report on pre-qualification and prototype testing (Shenton 1994a). The general requirements cover such things as qualifications of the test facility and instrumentation; calibration of the test facility and instrumentation; data acquisition; analysis of the recorded data; and reporting of results.

To illustrate typical test requirements, a sample test description is presented in figure 1. All of the test descriptions are presented in a similar format. The standard format includes several subsections: Test Designation, Purpose, Sequence, Procedure, Criteria and Special Requirements. The main features and requirements of the test are outlined under the three subsections Sequence, Procedure and Criteria. The load, frequency of load, number of cycles, etc. are given under Sequence. A step by step description of how the test should be conducted is given under Procedure. Finally, performance criteria have been established for each test and are presented in the Criteria subsection. The results of the test are to be evaluated against the performance criteria: isolation units that do not meet or exceed the criteria may not perform satisfactorily in service. Establishing the numeric values for the performance criteria is the most difficult task in developing the guidelines. For this reason, many of these values have simply been expressed in terms of a variable in the draft guidelines (e.g. α and β in fig. 1). One of the major tasks to be undertaken in developing the final guidelines will be to specify the numeric values for the performance criteria. The comments and suggestions received from the base isolation community will be extremely useful in this effort.

4. FUTURE ACTIVITIES

NIST has submitted a proposal to the American Society of Civil Engineers (ASCE) suggesting that ASCE develop a national, consensus based standard for testing seismic isolation systems. ASCE has accepted the proposal, and formation of the standards committee will begin this year. The NIST guidelines will be used as a starting point for development of the consensus standard. ASCE would appear to be the organization best suited to develop a national, consensus based standard, since seismic isolation technology is distributed among various civil engineering sub-disciplines, and seismic isolation has applications in a wide variety of civil type structures.

As a follow up to the development of the NIST guidelines for testing base isolation systems, an experimental program is being planned at NIST. The purpose of test program is to evaluate the testing procedures proposed in the guidelines. In the first phase of the test program the effect of scaling on the ultimate load carrying capacity of isolation bearings in compression will be examined. The work will then be extended to study the ultimate capacity in combined compression and shear.

5. CONCLUSIONS

The development of guidelines for the testing and evaluation of seismic base isolation systems has been described. Draft guidelines have been developed at NIST, and have undergone an extensive review by the base isolation community. Comments and suggestions from the review are currently being incorporated into the draft guidelines, which will then be published as final guidelines. The rationale behind the guidelines has been outlined, and an overview of the structure and content of the guidelines has been presented.

It has been proposed that the final guidelines be used as a model document in the development of a national consensus standard for testing base isolation systems. Future activities at NIST include an experimental program aimed at evaluating the proposed test procedures.

6. REFERENCES

Shenton, H.W., III, 1994a, "Draft Guidelines for Pre-Qualification and Prototype Testing of Seismic Isolation Systems," NISTIR 5359, Building and Fire Research Laboratory, National Institute of Standards and Technology, Gaithersburg, Maryland, 98 pages.

Shenton, H.W., III, 1994b, "Draft Guidelines for Quality Control Testing of Elastomeric Seismic Isolation Systems," NISTIR 5345, Building and Fire Research Laboratory, National Institute of Standards and Technology, Gaithersburg, Maryland, 28 pages.

Shenton, H.W., III, 1994c, "Draft Guidelines for Quality Control Testing of Sliding Seismic Isolation Systems," NISTIR 5371, Building and Fire Research Laboratory, National Institute of Standards and Technology, Gaithersburg, Maryland, 28 pages.

Uniform Building Code, 1994, International Conference of Building Officials, Whittier, California.

Guide Specifications for Seismic Isolation Design, 1991, American Association of State Highway and Transportation Officials, Washington, D.C.

Test Designation: I.5

Purpose: Establish dependence on vertical load.

Sequence: Three fully reversed cycles to peak displacements of ±D. Tests shall be conducted for vertical loads corresponding to P_L, P_D, P_U. The frequency of loading shall be not less than f_L or 0.004 cyc/sec.

Procedure: Place the specimen in the test machine and secure to the supports and loading plate. Apply the full vertical load to the specimen and allow the load to stabilize. Apply the cyclic lateral load to the specimen for the required 3 fully reversed cycles of the test. Remove the vertical load. The test shall be run continuously without pause between cycles. The test shall be conducted at the vertical loads specified in the order P_L, P_D, and P_U. Sufficient time shall be allowed between tests at the different vertical loads to dissipate any heat developed during the previous test.

Criteria: The System, Unit or Component response is considered to be independent of vertical load if:

(1.) the Average Effective Stiffnesses measured at vertical loads corresponding to P_L and P_U are within ±α% of the Average Effective Stiffness measured at the vertical load corresponding to P_D, i.e.,

$$\frac{|K_H^P - K_H|}{K_H} \leq 0.01\alpha$$

where $_PK_H$ is the reference Average Effective Stiffness measured at a vertical load corresponding to P_D, and K_H denotes the Average Effective Stiffness measured at vertical loads corresponding to P_L and P_U.

(2.) the Average Energy Dissipation measured at vertical loads corresponding to P_L and P_U are within ±β% of the Average Energy Dissipation measured at the vertical load corresponding to P_D, i.e.,

$$\frac{|E_H^P - E_H|}{E_H} \leq 0.01\beta$$

where $_PE_H$ is the reference Average Energy Dissipation measured at a vertical load corresponding to P_D, and E_H denotes the Average Energy Dissipation measured at vertical loads corresponding to P_L and P_U.

Special Requirements: None

Figure 1. Typical Test Description (Test for Dependence on Vertical Load)

DAMAGE TO INFRASTRUCTURES BY THE 1994 HOKKAIDO-TOHO-OKI EARTHQUAKE

by

Yasuyuki KOGA[1], Ryoji HAGIWARA[2], Hisanori OHTSUKA[3] and Osamu MATSUO[4]

ABSTRACT

Described is the outline of the damage to infrastructures caused by the 1994 Hokkaido-Toho-Oki Earthquake based on the reconnaissance survey conducted by the PWRI teams.

KEY WORD

Earthquake Damage, Hokkaido-Toho-Oki Earthquake, Road, Bridge, River Facility, Dam, Sewarage System, Lifeline Facility, Slope Failure

1. INTRODUCTION

At around 10:22 PM on October 4, 1994 an earthquake of JMA magnitude 8.1 occurred with its epicenter located in the sea to the east of Hokkaido. The Japan Meteorological Agency has named this the Hokkaido-Toho-Oki Earthquake.

In last two and a half years four large earthquakes occurred in succession around Hokkaido Island, including the Kushiro-Oki Earthquake of Jan. 15, 1993[1], the Hokkaido-Nansei-Oki Earthquake of July 12, 1993[2] and this earthquake, whose source regions are shown in Fig.1. Among these the epicenter and the magnitude of the Kushiro-Oki Earthquake and the Hokkaido-Toho-Oki are relatively close. The damage features of these two earthquakes are roughly compared in the later sections.

This earthquake caused major damage to public infrastructures and lifeline facilities in the eastern region of Hokkaido Island where similar structures were damaged during the Kushiro-Oki Earthquake which occurred just one year and 8 months back. The Public Works Research Institutute, MOC implemented a reconnaissance survey of the heavily damaged districts of Kushiro, Nemuro and Abashiri immediately after the earthquake for the purpose of obtaining data on the status of damage to infrastructures, probing specific causes of damage and identification of problem points for the future.

This report provides an overview of the reconnaissance survey conducted by the PWRI teams focusing on damages to public infrastructures.

2. OUTLINE OF THE EARTHQUAKE

The epicenter was about 170 km east of the city of Nemuro, and the focal depth was about 30 km. The JMA magnitude was 8.1, exceeding both the Kushiro-Oki earthquake which occurred in January, 1993 and the Hokkaido-Nansei-Oki earthquake which occurred in July,1993 both with a magnitude of 7.8. It was the first earthquake in Japan to exceed a magnitude of 8 since the Tokachi-Oki Earthquake of 1952 which measured a magnitude 8.2. However, the damage in this earthquake was on a smaller scale at least in Japan than the previously mentioned earthquakes. The reason is that the epicenter was a little far from the cities in Hokkaido Island, there were no large scale structures in the area which could be easily

1) Director, Earthquake-Disaster Prevention Department, PWRI

2) Head, Ground Vibration Division, PWRI

3) Haed, Earthquake Engineering Division, PWRI

4) Head, Soil Dynamics Division, PWRI

damaged, nor did a large tsunami occur, which is often a factor in adding earthquake damage near coast areas.

Fig.2 shows the distribution of the JMA Seismic Intensity. It was VI at Kushiro and Akkeshi, V at Nemuro, Hiroo, Urakawa, Nakashibetsu and Rausu. The area with felt motion covered a broad area as far away as the Kanto and Chubu regions. According to the survey conducted by the Japan Meteorological Agency after the earthquake, Seismic Intensity VI was also felt in parts of Nemuro City, Hamanakacho, Bekkaicho and Nakashibetsucho.

Strong motion records were obtained in many public infrastructures such as bridges, river dikes and dams in Hokkaido and Tohoku regions. Fig.3 shows the maximum acceleration in various sites. The maximum horizontal acceleration measured was 487gal obtained at the nearby ground of Tokachi River dike, whose distance from the epicenter was 330km. As shown in Fig.4 maximum acceleration during this earthquake within around 500 km of epicentral distance was larger than average trend from past earthquakes[3] and its attenuation rate to the epicentral distance was higher than average trend. This phenomenon needs farther investigation together with the area of source region, focal mechanism, etc.

3. OUTLINE OF DAMAGE

Table 1 shows the outline of damage based on the report by Fire and Disaster Prevention Division of Hokkaido Prefectural Government. Total damages experienced during the Kushiro−Oki Earthquake of 1993 are also included in the Table for comparison. Damage in this earthquake was concentrated in the eastern region of Hokkaido. Damage in monetary terms totalled 42.5 billion yen, an amount equivalent to 89% of the damage experienced in the Kushiro−Oki Earthquake.

Human casualties as a result of the earthquake totalled 435, with 24 serious injuries and 411 minor injuries. There were no fatalities.

Damage to residential houses reached a total of 4,586 houses, with 9 of these totally destroyed, 68 partially destroyed, and 4,489 with local damage. A total of 20 houses were inundated by tsunami. No fires occurred.

Detail on damage to public infrastructures is covered in later sections of this report. An overview is given below.

Damage to roads occurred in locations with embankments and bridges. Major types of damage to embankments were cracks, slump, settlement of embankments and road shoulder failure. Areas where most severe damage was detected were those areas with soft soil, transition zones from cuts to banks, approaching sections to bridges, areas crossing swamps or marshes, and areas where foundation ground is transeversely inclined. Major types of damage to bridges were damage to bearings and failure of abutments. The number of locations suffering damage and the range of damage was limited in comparison to the Kushiro−Oki Earthquake. Termination level of main longitudinal reinforcement of reinforced concrete piers where failure occurred in the Kushiro−Oki Earthquake had been reinforced with jacking by reinforced concrete or steel plate. No damage to these bridges was detected during this earthquake.

Out of four river systems, damage to dikes was detected in 23 locations, and damage to revetments in four locations. Damage consisted almost entirely of longitudinal and transverse cracks and settlement along the crest of dikes, slope failure, and collapse of revetments. Damage overall was less serious in comparison to the Kushiro−Oki Earthquake.

As far as dams are concerned, no damage or abnormal conditions occurred requiring special safety management.

As for sewarage systems, damage occurred in 2 cities and 7 towns. Damage occurred to sewers along a 30km stretch, and is estimated to total 4.5 billion yen. Both range and scale of damage to sewarage systems was larger in comparison to the Kushiro−Oki Earthquake (1 city, 7 towns, approximately 22km affected and an estimated 2.4 billion yen in damage). Nearly half of the total damages to sewarage systems, totalling approximately 2 billion yen, occurred in Shibetsucho.

Damage to other lifeline facilities was also smaller in comparison to the Kushiro−Oki Earthquake. Water service to approximately 9,450 households was cut off in the city of Nemuro where cracks and uncoupling of pipes occurred. However, service of 90% was restored within four days after the earthquake. Transmission of electrical power was shut off automatically at 11 substations in eastern Hokkaido, causing blackouts in approximately 46,000 households, but service was restored quickly. As for telephone lines, congestion conditions continued after earthquake occurrence, but by the evening of the next day these were restored to normal. Optical cable was cut off in two locations as well. Damage to gas lines was limited to leakage from only 12 houses, and restoration of normal service was completed within a day after the earthquake occurred.

4. DAMAGE TO ROADS

Damage to roads occurred in a wide area concentrated mostly in the southeastern region of Hokkaido. Major types of damage were slump, settlement, cracks in road surface, and collapse of road shoulder where roads crossed over banks. Other damage included falling rocks in Sharicho on Highway 344, and collapse of a chimney onto the road in Bekkaicho on Highway 244. Damage to bridges is described in Section 5. Locations of major road damage are shown in Fig. 5.

Damage in this earthquake tended to occur in the following types of places:
1) Areas close to the epicenter and with soft soil(swampland) : Bekkaicho, Nakashibetsu −cho, Shibechacho.
2) Transition zones from cuts to banks.
3) Approaching sections to structures (bridges, culverts).
4) Areas crossing swamps or marshes.
5) Areas where foundation is transeversely inclined.

Damage to highways occurred in 220 locations on 13 routes, with most severe damage to Highway 272. However, locations where damage restoration was performed after the Kushiro−Oki Earthquake incurred no damage during this earthquake.

Road surface slump and collapse of road shoulders occurred intermittently along a 4km stretch of Highway 272 in the Nakachanbetsu district of Shibechacho (Point a in Fig.5). An especially large area collapsed at one transition zone from cut to bank placed on swampland in this section(Photo 1). The collapsed area was 7−8m in width and 200m long located on the bank. The height of the bank was approximately 9m, and the foundation was soft and swampy soil. Emergency measures were taken to open one lane to traffic by October 9.

On Highway 391 in the Takkobu district of Kushirocho (Point b in Fig.5), road shoulder collapsed on a bank where foundation was transeversely inclined. Settlement affected part of the motor lane and the sidewalk in an area running 25m in length and 2m in width. Maximum depth of the settlement was 80cm (Photo 2). Soil type in the surrounding area is peat and silty sand. Damage was observed especially to the

bank which had been built up on top of swampy, and especially low lying foundation ground.

As for Hokkaido prefectural highways and city, town and village roads, major damage was observed in the region of Bekkaicho and Nakashibetsucho, where bank roads collapsed.

In the Koshin district of Bekkaicho on the Izumikawa route of the Hokkaido Highway (Point c in Fig.5), an area where the foundation is transversely inclined, and where there is a transition zone from one side cut–one side bank to both sides bank, the bank collapsed in an area 200m in length at a T–shaped intersection (Photo 3). The road bank slid about 30m to the low lying side, and another part of the bank collapsed near a drainage ditch crossing near the intersection of the road which crosses the Izumikawa Route, causing the drainage ditch to move about 3m in the direction of the crossing. Water flow concentrates at this intersection, and it is considered that high water content in the soil is the cause of the severity of the damage.

Major collapse of a bank built up on swampland occurred at the approaching section to the Bihiro Bridge (Bekkaicho, Point d in Fig.5) on the Nakashunbetsu –Tawarabashi Route of the Hokkaido Highway (Photo 4). A difference in level of 45cm developed at the approaching section to the bridge, and a slump occurred on the road surface 25m long and 2.2m wide. Maximum depth of the slump was 3m. No damage was detected to the bridge abutment. In addition, an accident occurred in the area where two vehicles fell into the slumped portion.

On the Nemuro–Nakashibetsu Route of the Hokkaido Highway (Point e in Fig.5), along a 20.8km stretch running from Nakashibetsucho–Kyowa to the urban area of Bekkaicho, numerous road surface slumps, cracks and road shoulder collapses occurred, leading to a complete closure of traffic through the area (Photo 5). The majority of the damage occurred in transition zones from cut to bank, with an especially large amount of damage observed on bank roads crossing swampland.

A transition zone from cut to bank experienced major collapse in the Nakashibetsucho–Mataochi region of Nakashibetsucho Road 28 (Point f in Fig.5), with slump occurring across the full width of the road measuring 60m (Photo 6). The cracks which appeared in the road surface measured 1.5m in maximum width and 2m in maximum depth. In this section because of a road surface inclination, water tends to flow from the upper cut area down to the lower lying bank area. Therefore water content in the soil in the area where water collects is high, and is thought to be the cause of the severity of the damage.

Road shoulder collapse occurred along an area 50m in length and 3m across in the region of the Kussharoko observatory on the Abashiri–Kawayu Route of the Hokkaido Highway (Point g in Fig.5). The damaged area was a bank on a transeversely inclined slope where the road crossed through swampland. The bank on the low–lying side collapsed. It is thought that high water content in local soil was the cause of the damage.

5. DAMAGE TO ROAD BRIDGES

Road bridges incurring damage in this earthquake totalled 16 bridges in the region administered by the Hokkaido Development Bureau Kushiro Development and Construction Department, one in the area administered by the Abashiri Development and Construction Department of the same bureau, 14 in the area administered by the

Kushiro District Public Works Management Office, Hokkaido Prefectural Government, and 9 bridges in the area administered by the Obihiro District Public Works Management Office. Table 2 shows the locations of bridges incurring major damage.

Damage to bearings was seen especially in mortar on fixed bearings, loosening of anchor bolts, damage to stoppers of displacement-restriction devices, and to the bridge abutment itself. Damage to main body of bridge abutment was observed especially in instances where distance covered by support edges was lacking.

Damage to the main bodies of bridges was limited in this earthquake, while that incurred by embankment portions of approaching to abutments was most noticeable. This type of damage tended to occur to bridges constructed in areas where foundation consists of soft soil, and where a approaching platform was not used. In addition, many instances of settlement occurred to retaining walls and wings at the backfill of the abutment. The most notable damage to bridges which were observed are described below.

Damage occurred to both fixed and moveable bearings on the Rindo Bridge on Highway 272 and to the sole plate of the super structure (a two-box steel bridge) connected to bearings (Photo 7). Damage to the main body of the bridge abutment also occurred(Photo 8). This bridge had been completed recently, in December 1993, and its construction is based on current road bridge specifications. Therefore this case will become a good example to assess the possibility of structural problems and the appropriateness of the seismic strength of the current design.

Retrofitting was performed on reinforced concrete piers of Matsunoe bridge which sustained damage in the Kushiro-Oki Earthquake with jacking by reinforced concrete or steel plate (Photo 9). As can be seen in Photo 10, no damage to these bridges was detected during this earthquake, a fact which confirms the effectiveness of the added reinforcement.

6. DAMAGE TO RIVER FACILITIES

Table 3 shows the locations of damage to river facilities within the area administered by the Hokkaido Development Bureau are shown. Out of four river systems, damage to dikes was detected in 23 locations, and damage to revetments in four locations. Damage consisted almost entirely of longitudinal and transverse cracks and settlement along the crest of dikes, slope failure, and collapse of revetments. Damage overall was less serious in comparison to the Kushiro-Oki Earthquake.

An outline of damage occurring along the Kushiro and Shibetsu rivers, where damage restoration was deemed to be most necessary, is given below.

Major damage occurred to the Kushiro River in the Kushiro-Oki Earthquake, and areas where foundation improvement utilizing sand compaction piles was carried out for the restoration (an area running 2.3km) did not experience damage during this earthquake. However, nearby areas where foundation improvement was not carried out incurred damage in several locations, althogh the degree of the damage was minor. This fact should be taken into consideration when planning future restoration work. Damage was concentrated in the right banks of retarding basins and in dikes in the region where the Osobetsu River converges with the Kushiro River. Longitudinal and transverse cracks 1-3m deep opened up, and slope failure occurred (Photos 11-12). In the previous Kushiro-Oki Earthquake damage was concentrated in riverside area, but this time it was concentrated landside

area. Sand boil was observed in various locations near the damaged area as well, but it will be necessary to perform a more detailed investigation of this and other damage in order to understand the causes more clearly.

Minor cracks appeared along the Shibetsu River in the Kushiro-Oki Earthquake, but this time damage occurred in different locations. Though covering less overall length, damage in this earthquake in several locations was more severe, consisting of numerous longitudinal cracks and slope failures.

7. DEFORMATION IN DAMS

Fourteen dams (including one small reservoir) were surveyed in the areas within Hokkaido experiencing Seismic Intensity IV and above. In all cases, no damage or excessive deformatios occurred requiring special safety measures.

The dam located closest to the epicenter is the Makinouchi Dam on the Nemuro Peninsula. It is a gravity type concrete dam of 18.5 m in height located at a distance of 150km from the epicenter. No seismographs had been installed at the dam. Targets had been installed in nine locations on the crest of the Makinouchi Dam as a means of measuring deformations. Horizontal displacement of 1.8 mm at the maximum to upstream was observed at all targets as a result of measurements taken before and after the earthquake. In addition, a small amount of fresh exfoliation of concrete was discovered on the No.4 joint of the intake tower in the region of the crest on the upstream side.

A small longitudinal crack less than 1mm in width was discovered in the asphalt surface of the administrative-use road on the central area of the crest of Mitsuishi Dam. However, it is possible that this crack existed before the earthquake. In addition, maximum acceleration of over 240 gal was measured at the crest of the Mitsuishi Dam. This is the largest acceleration taken at a dam during this earthquake.

Leakage after the earthquake at the right bank of the Tokachi Dam increased from 15 l/min to 24 l/min, and at the Samani Dam, entire leakage increased from 1.86 l/min to 2.38 l/min. As of November 1, leakage at each dam has stabilized at those amounts. The leakage in the area of the river section of Takami Dam increased from 0.82 l/min to 1.08 l/min. The amount of change in all of the above 3 dams was minimal, and did not cause any particular problems.

8. DAMAGE TO SEWARAGE FACILITIES

Table 4 shows the municipalities which applied for assesment of restoration works to the Hokkaido Prefectural Government, the number of places suffering damage, and the cumulative length of sewers damaged. The cumulative length of sewers damaged in Kushirocho and Shibechacho was one-tenth of that experienced in the Kushiro-Oki Earthquake. However, areas under the administration of the Nemuro District office, which was close to the epicenter, were struck harder. Bekkaicho and Shibetsucho experienced respectively 5 times and nearly 10 times the damage of the previous earthquake. In particular, a length of 10.9km of sewer was damaged in Shibetsucho, a figure which constitutes over 40% of the overall damaged length of 24.6 km.

An explanation of the damage follows below:

1) There were instances of cracks and breakage of sewers, as well as slippage and meandering in many towns and cities. In all such towns and cities, examples of vertical displacement were found more prevalent

than horizontal displacement at the early stage of investigation. However, it will be necessary to assess the overall tendency of displacement after completion of an investigation using a TV camera inside the sewer.

2) Damage, slippage and uplift of manholes was also observed in many towns and cities. Uplifts of manholes seemingly caused by liquefaction were obsereved together with slumps of the surrounding ground. In particular, there were striking examples of slumps of the ground at backfilled portions of the sewer route (Photo 13).

3) Ground settlement and deformation of expansion joint sections within processing and pumping stations were seen in some areas. In addition, in the city of Nemuro, tsunami caused inundation of sea water into the central No. 2 Pumping Station, causing damage to the starter board for private electricity generation.

By one week after the earthquake, all towns and cities were able to assess the damage status more quickly than after the Kushiro-Oki Earthquake.

As for damage restoration, submerged pumps were inserted into manholes in which sewers had collected. Temporary drainage restoration was performed by pumping the waste water downstream forcibly, at 3 spots in Nakashibetsucho and 2 spots in Shibetsucho. Cutting of top part of manholes uplifted by liquefaction was implemented in Kushirocho and Sharicho. The spreading of sand to restore slumped roads was performed in the city of Nemuro and Sharicho, especially in the vicinity of sewer installation sites and manhole caps.

9. DAMAGE TO LIFELINE FACILITIES

Damage to lifeline facilities due to the Hokkaido-Toho-Oki Earthquake was less than that caused by the Kushiro-Oki Earthquake. Even in the city of Kushiro, which recorded an Intensity of VI, impact on the regional society was kept to a minimum. However, in Nemuro, which was closest city to the epicenter, there were many cases of damage to water pipes, and it took ten days to fully restore the city's water supply. The following will report on damage to lifeline facilities other than sewerage facilities.

1) Damage to Water Facilities

The survey of damage to water facilities was conducted in the city of Nemuro. Table 5 shows the number of occurrences of damage caused by the earthquake. Much of the damage was in the form of breaking off of pipe conduits (e.g. asbestos pipes and cast iron pipes) due to cracks and uncoupling. As a result, water supply was cut off to 9,450 homes after the earthquake. There were no occurrences of damage at water purification plants and pumping stations.

Fig. 6 shows the water supply restoration conditions over time. This diagram indicates that over 90% of the water works were restored by the fourth day after the earthquake, but the water supply to regions which receive water for agricultural use was cut off for 10 days. This is because water for agricultural use in Nemuro is taken from Lake Mashu, and pipes of some 130km long are used in the transport and distribution of the water. In addition, some pipes pass through mountain areas, and the inspection of these pipes for leaks required a considerable time.

2) Damage to Electrical Facilities

Transmission of electricity at 11 substations was cut off automatically immediately after the earthquake, causing loss of electricity in some 46,000 houses, mainly in areas in the eastern region of Hokkaido, under the administration of the

District of Kushiro and Nemuro. Inspections confirmed that no damage of a degree that would hinder the supply of electricity was sustained, and transmission of electricity was restarted at all power plants an hour after the earthquake.

Fig. 7 shows the transitions in the number of blacked out houses over time comparing with the situation during the Kushiro-Oki Earthquake.

From this diagram, it can be discerned that restoration of electrical power was completed more quickly in this earthquake. This is probably because, while in the Kushiro-Oki Earthquake, substations at large-scale power plants were damaged, and therefore considerable time was required in order to restore them fully, substations did not sustain damage in this earthquake. In addition, wireless radios, which were introduced after the Kushiro-Oki Earthquake as a communication measure in case of emergency among the road administrators, were used to quickly obtain information regarding road conditions from road maintenance personnel, thus making it possible to effectively guide damage restoration-use vehicles to damaged areas. This is a good example of a lesson being learned from a previous earthquake and put to use.

3) Damage to Telephone Facilities

In the eastern region of Hokkaido, mainly the cities of Kushiro and Nemuro, congestion of telephone lines continued from the occurrence of the earthquake. Due to this situation, the usage of telephone lines was controlled automatically. However, normal conditions were restored by the evening of the fifth day. Damage to equipment occurred in the form of cut-off optical cables at 2 places: in the Kayanuma district along National Highway 391 and the area from Hamabekkai to Odainuma along National Highway 244. As shown in Photo 14, six optical cables were installed in the slope of the road embankment. During the earthquake, the cast iron couplings were broken off and the optic cables inside the pipes were broken. There was evidence that the road embankments had slumped at the point where the damage occurred, and it is estimated that along with this large deformations of the pipeline also occurred.

4) Damage to Gas Facilities

There were only 12 occurrences of gas pipe leaks during this earthquake, a relatively small amount of damage compared to the Kushiro-Oki Earthquake. Most of the damage was to couplings of lead-in pipes to buildings. All of these were restored by the day after the earthquake.

10. MISCELLANEOUS

1) Damage to Houses on Slopes

In this earthquake, houses built on slopes of mountains were damaged by failure of slopes, etc. One house was completely destroyed, one was partially destroyed and six houses were partially damaged in this earthquake. Compared to the Kushiro-Oki Earthquake, in which seven houses were completely destroyed, seven partially destroyed, and one partially damaged, the damage in this earthquake was slight.

The destruction was striking in a housing embankment in Nakashibetsucho in Shibetsugun, where one house was completely destroyed and four were partially damaged. A 20m wide section of a 3m high embankment ($200m^3$ of soil) collapsed. The collapsed soil is assumed to have slid in the shape of a compounded slip, and the house built at the slip head of the top portion of the embankment was completely destroyed. In addition, damage was observed on the neighboring house, where a portion of the foundation was exposed and sunken. The falling soil reached as far as the houses below the embankment where it damaged house walls and stopped.

Slope failure (soil quantity of $20m^3$) and cracks also occurred in the Midorigaoka district of Kushiro city, where an Intensity of VI was observed, and which incurred a great deal of damage in the previous earthquake. However, there was no serious damage during this earthquake.

2) Damage to Coastal Facilities

There are a total of 28 coastal preservation facilities related to the Ministry of Construction, including 14 sites in Nemuro, two in Shibetsucho, 1 in Rausucho, 8 in Bekkaicho, 2 in Hamanakacho and 1 in Shiramekacho. Settlement and damage of crest and slopes of dikes and revetments, damage to parapet sections of tide protection embankments were observed at some sites. All such damage was earthquake related, and not caused by tsunami.

11. AFTERWORD

Hokkaido–Toho–Oki Earthquake was the second of two major earthquakes of a magnitude 8 class that struck the eastern area of Hokkaido twice just within one year and eight months, following the Kushiro–Oki Earthquake of January, 1993. Indeed, it came while the memory of the previous earthquake was still fresh. It is extraordinarily rare that such two large earthquakes attack nearly the same region within such a short period. From the viewpoint of earthquake engineering, valuable knowledge can be obtained by making detailed analyses of the differences in damage caused by each earthquake.

References

1) PWRI : Damage to Infrastructures Caused by the 1993 Kushiro–Oki Earthquake, 25th UJNR, 1993.

2) PWRI : Infrastructure Damage by the 1993 Hokkaido–Nansei–Oki Earthquake, 26th UJNR, 1994.

3) Japan Road Association : Seismic Design Specifications for Highway Bridges, 1990.

Table 1 Summary of Damage and Loss during Hokkaido–Toho–Oki EQ (Compared with Kushiro–Oki EQ)

Category			Hokkaido–Toho–Oki EQ (A)	Kushiro–Oki EQ (B)	A/B (%)
Death		(person)	0	1	0
Seriously Injured		(person)	24	114	21.1
Slight Injured		(person)	411	819	50.2
Number of Residential Houses		(Houses)	4,586	3,474	132
Number of Non–Residential Houses		(Houses)	7	50	14.0
Loss	Agriculture Products	(Thousand Yen)	2,667,511	3,904,820	68.3
	Public Works	(Thousand Yen)	17,903,571	18,800,300	95.2
	Fishery	(Thousand Yen)	2,390,032	1,737,639	138
	Forestry	(Thousand Yen)	1,033,294	1,290,558	80.1
	Sanitation	(Thousand Yen)	950,575	952,057	99.8
	Commerce and Industry	(Thousand Yen)	7,946,035	14,749,189	53.9
	Education	(Thousand Yen)	446,512	1,138,600	39.2
	Others	(Thousand Yen)	5,353,051	2,461,272	217
Total		(Thousand Yen)	42,480,892	47,507,796	89.4

Table 2 Summary of Bridges Damage

Bridge Name	Route	Administrator	Length (m)	Year of Construction	Damage to Superstructure					Damage to Abutment				Damage to Pier		Damage to Bearing Support			
					A	B	C	D	E	F	G	H	I	J	K	L	M	N	O
Pon−river	National Road 244	Hokkaido Development Bureau	30	1972									○				○	○	
Mannen	National Road 244	Hokkaido Development Bureau	99	1972					○	○		○	○				○	○	○
Yubae	National Road 247	Hokkaido Development Bureau	36	1971							○		○						
Rindou	National Road 272	Hokkaido Development Bureau	173	1993						○			○			○	○	○	○
Shari	National Road 334	Hokkaido Development Bureau	197	1960										○				△	△
Show−un	National Road 335	Hokkaido Development Bureau	351	1975									○					○	○
Kumasawa	Prefectural Road Kamimusa−Kenebetsu Line	Hokkaido Government											○					○	○

Note) Damage to Superstructure : A: Slab, B: Girder, C: Expansion Joint, D: Falling−off Prevention Device, E: Handrail
Damage to Abutment : F: Parapet, G: Wing, H: Inclination, I: Subsidence of Embankment
Damage to Pier : J: Pier, K: Inclination
Damage to Bearing Supports : L: Bearing Supports, M: Displacement−Restriction Device, N: Shoe Pedestal Mortar, O: Anchor Bolts
○ : Major Damage
△ : Slight Damage

Table 3 Damage to River Dikes

River System	Part	Number of Damaged Sites	Number of Restoration Sites	Length of Restoration (m)	Major Damaged Sites	Feature of Damage
Kushiro	Dike	8	3	960	·Right Bank of Yasuhara Marsh ·Upper Stream of Shimo−osobetsu−genya Sluice	Crack in the Crest Settlement of Slope
Kushiro	Revetment	4	4	840	·Both of Upper Banks of Kushiro Bridge	
Watenbetsu	Dike	1	0			
Shibetsu	Dike	8	8	420	·Lower Stream of Chashikotsu−daisougen Bridge ·Upper Stream of Shibetsu−gawa Confluence Sluice	Crack in the Crest Settlement, Sliding Failure
Tokachi	Dike	6	0			

Table 4 Summary of Sewerage Facilities

Municipalities Name	Number of Places Suffering Damage	Cumulative Length of Sewers Damaged (km)
Kushiro City	104	8.1
Nemuro City	17	1.5
Kushiro Town	6	0.5
Shibecha Town	9	0.4
Nakashibetsu Town	23	5.0
Bekkai Town	8	1.5
Shibetsu Town	29	10.9
Shari Town	12	0.8
Akan Town	3	1.2
Total	211	29.9

Table 5 Summary of Water Pipeline Damage

	Conduit Pipe	Service Pipe	Total
Water Works	33	113	146
Attoko Small Water–Supply System	1	0	1
Ochiishi Small Water–Supply System	2	3	5
Agricultural Water	9	0	9

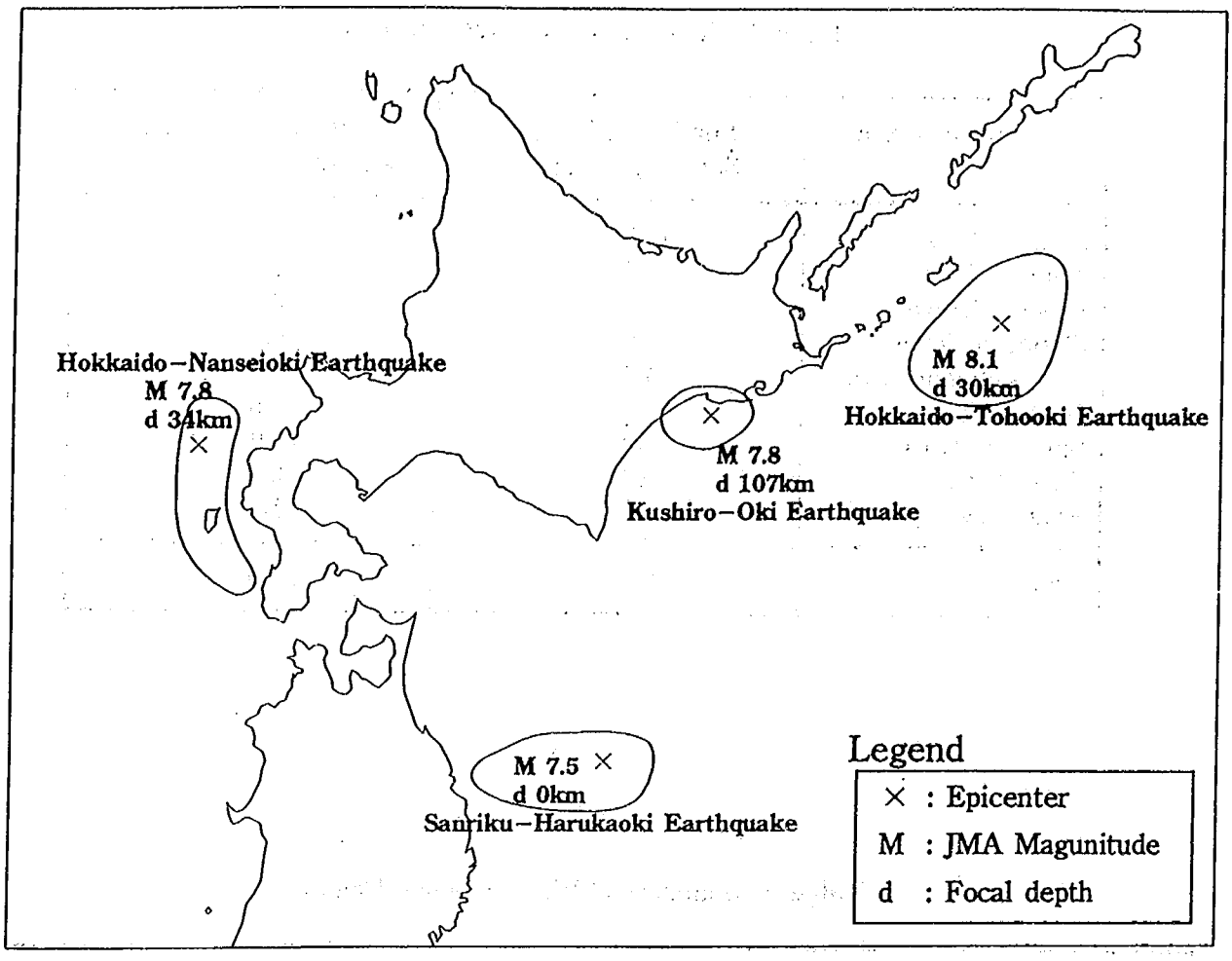


Fig. 1 Distribution of Source Region of 4 Recent Earthquakes Around Hokkaido

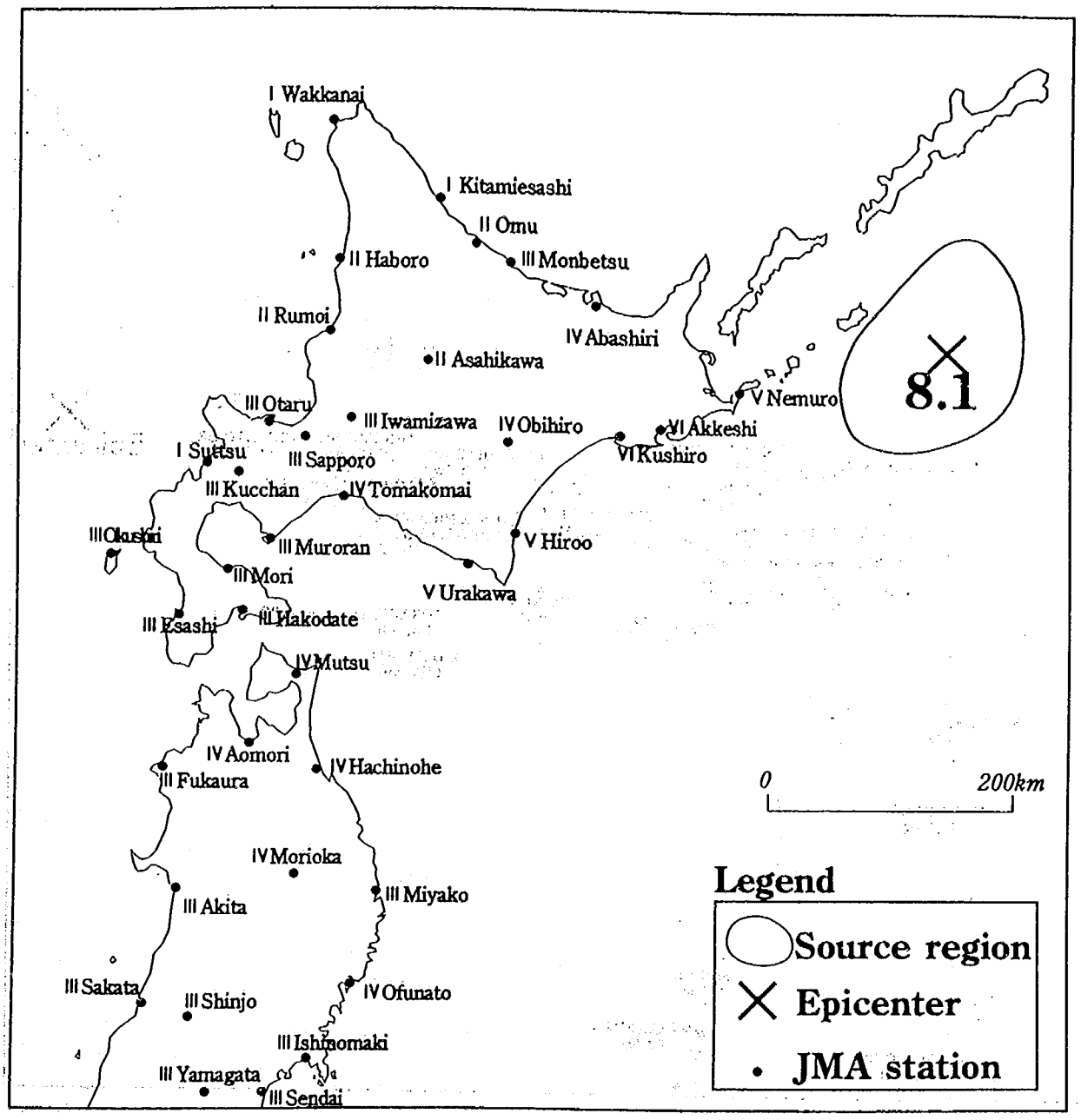


Fig. 2 Distribution of JMA Seismic Intensity

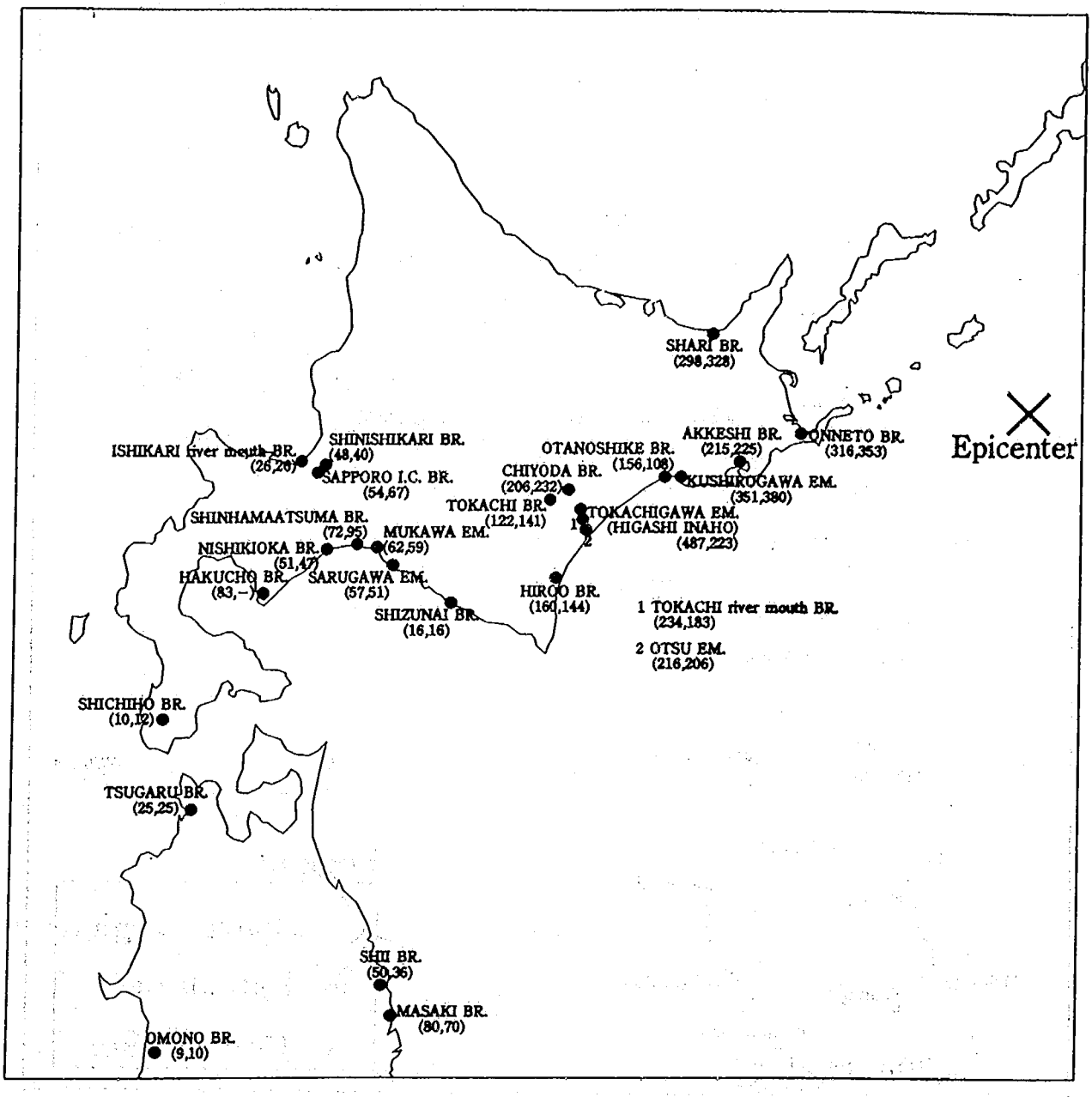


Fig. 3 Distribution of Maximum Acceleration of Horizontal Component

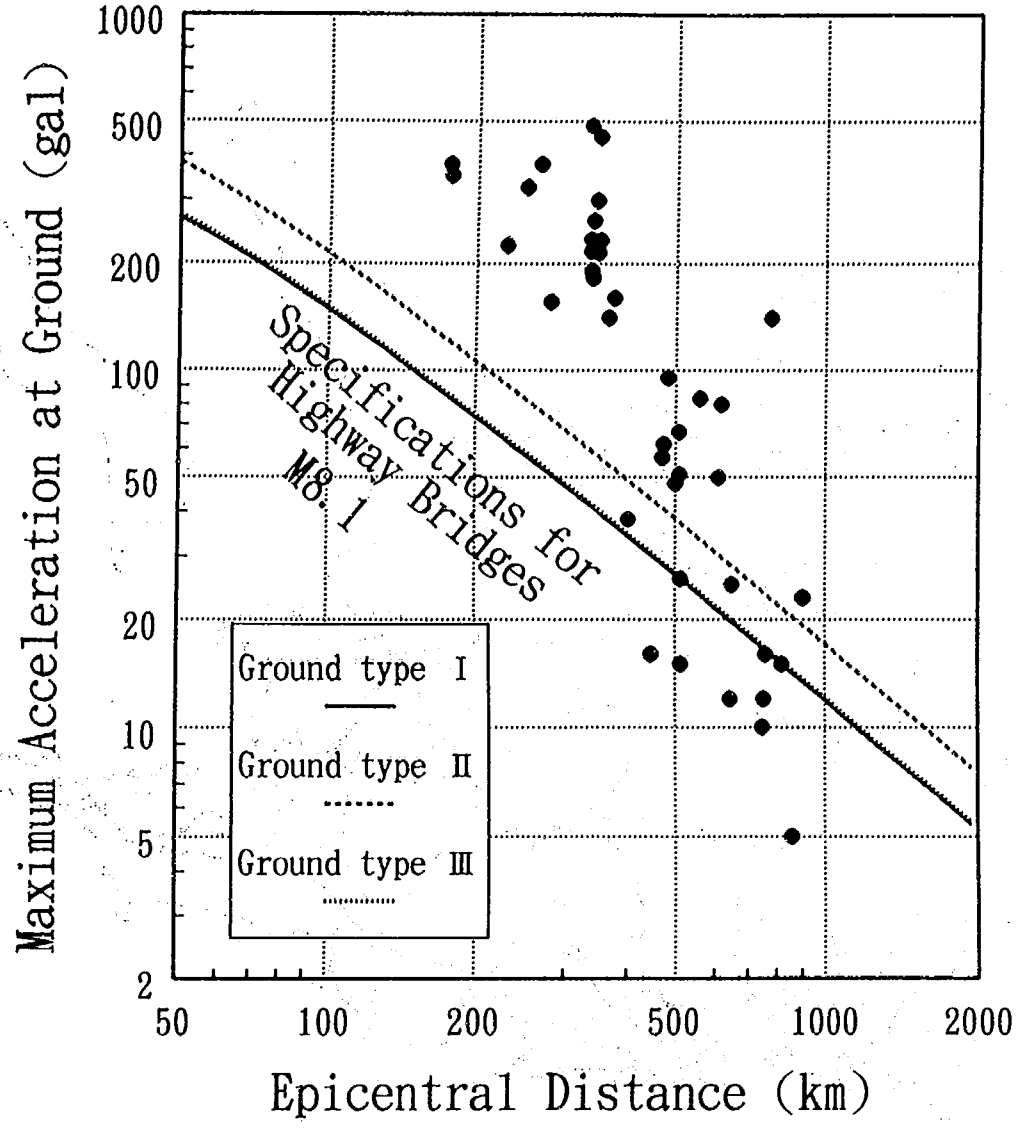


Fig. 4 Attenuation of the Maximum Acceleration of Horizontal Components

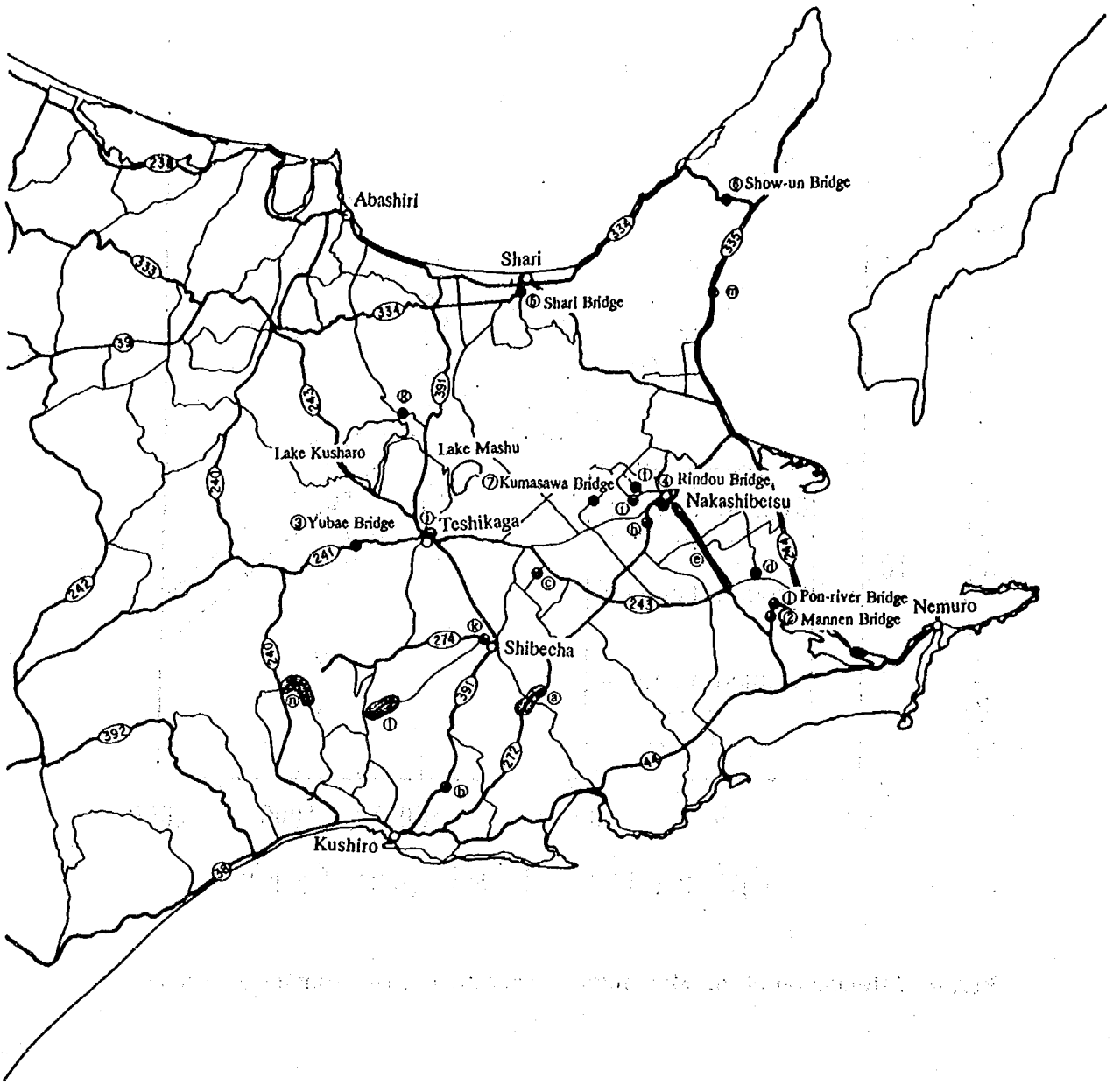


Fig. 5 Location of Damage to Roads and Road Bridges

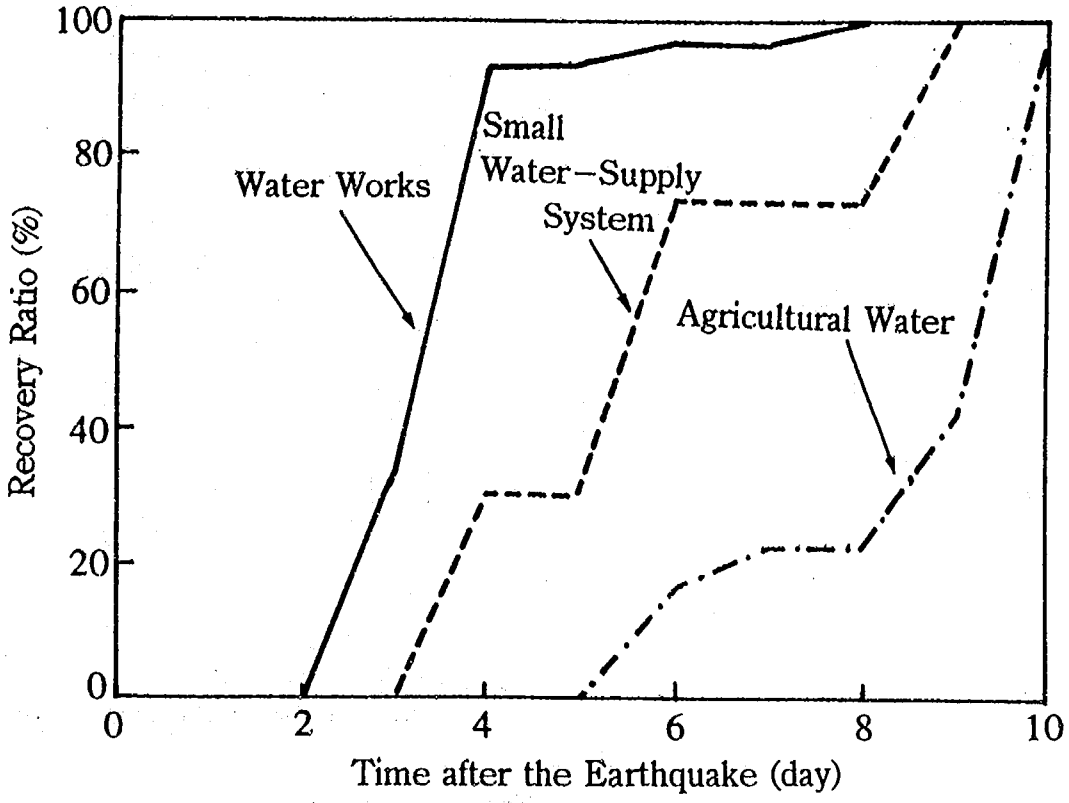


Fig. 6 Restoration Process of Water Supply System in Nemuro City

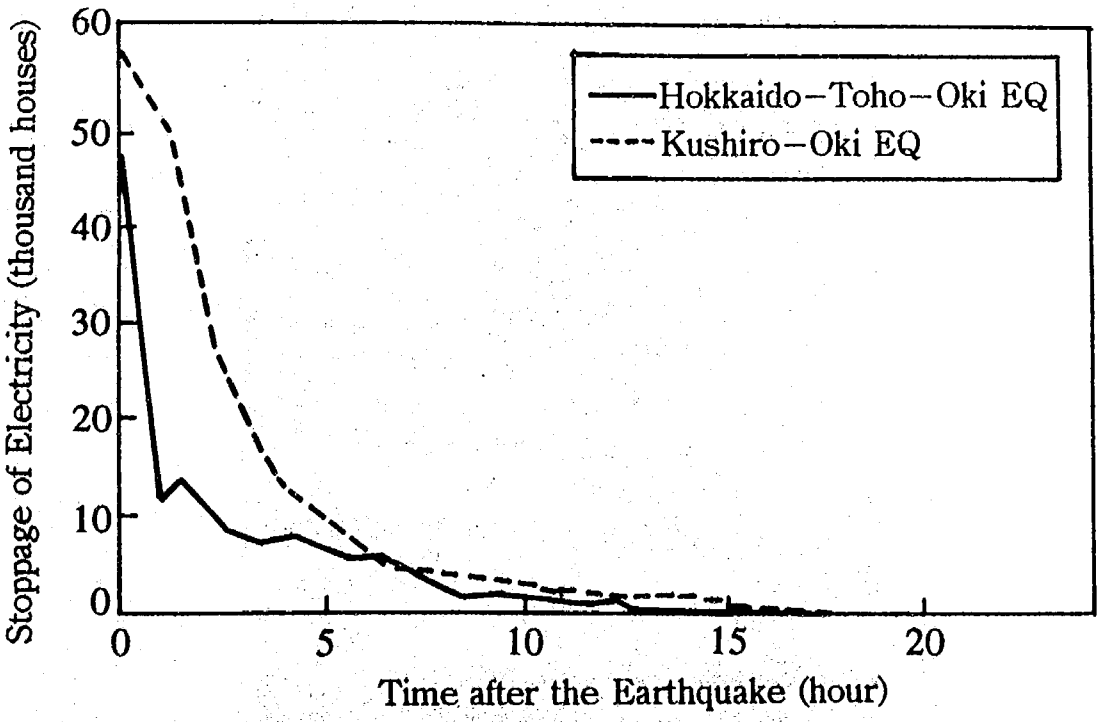


Fig. 7 Restoration Process of Electricity Supplies in the Eastern Hokkaido

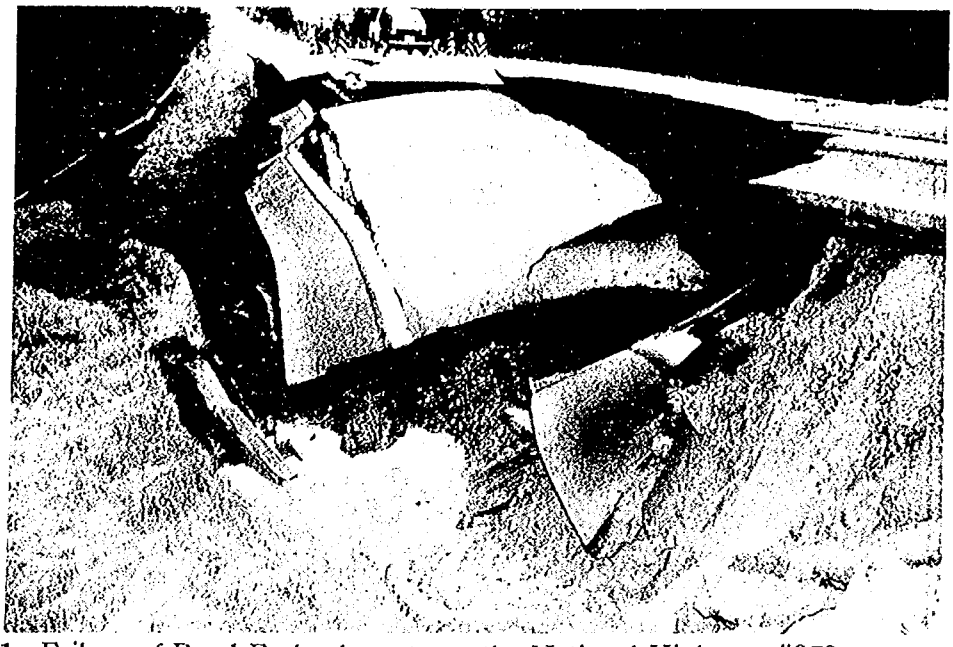


Photo 1 Failure of Road Embankments on the National Highway #272,
at Nakachanbetsu, Shibecha Town

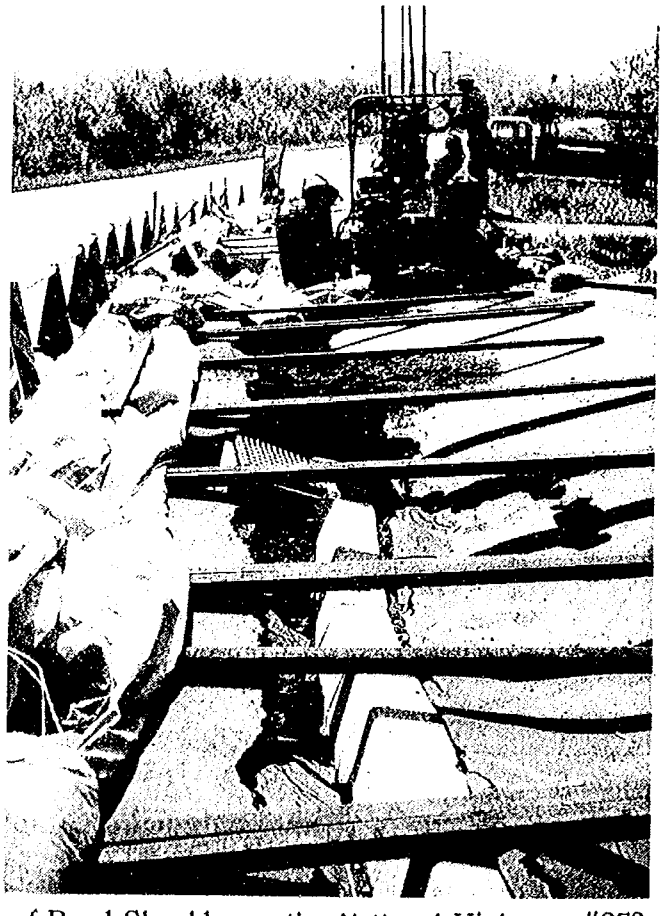


Photo 2 Failure of Road Shoulder on the National Highway #272,
at Takkobu, Kushiro Town



Photo 3 Failure of Road Embankment on the Prefectural Road, the Izumikawa Line, at Bekkai Town



Photo 4 Failure of Approaching Road Embankment to the Bihiro Bridge, on the Prefectural Road, the Shunbetsu–Tawarabashi Line

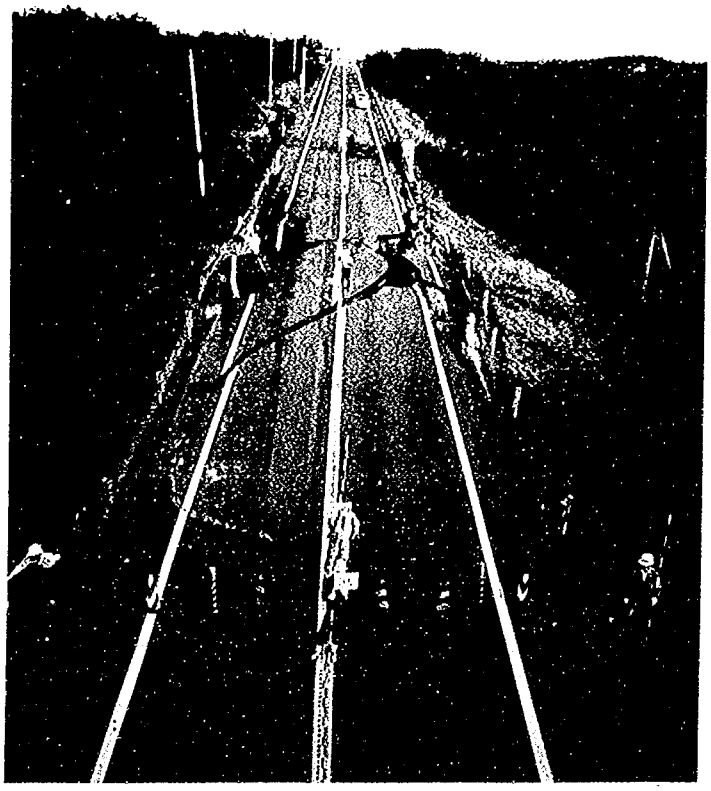


Photo 5 Failure of Road Embankment at Bekkai Town
(the Prefectural Road, the Nakashibetsu−Shibecha Line)

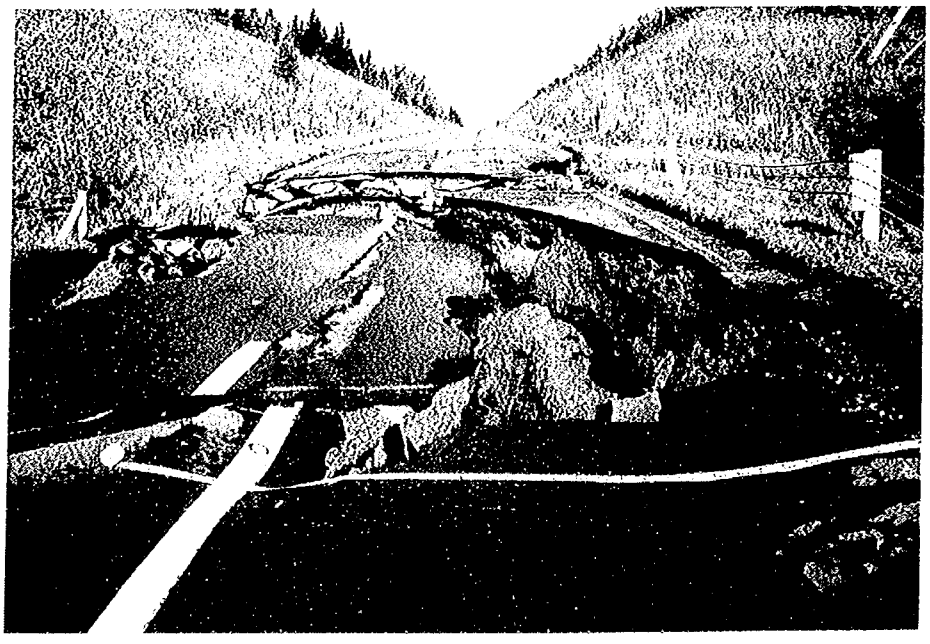


Photo 6 Failure of Road Embankment (the Nakashibetsu City Road #28)



Photo 7 Damage to Fixed Bearing at the Rindo Bridge, the National Road #272 (Exfoliation of Sole Plate and Damage of Displacement-Restriction Device)

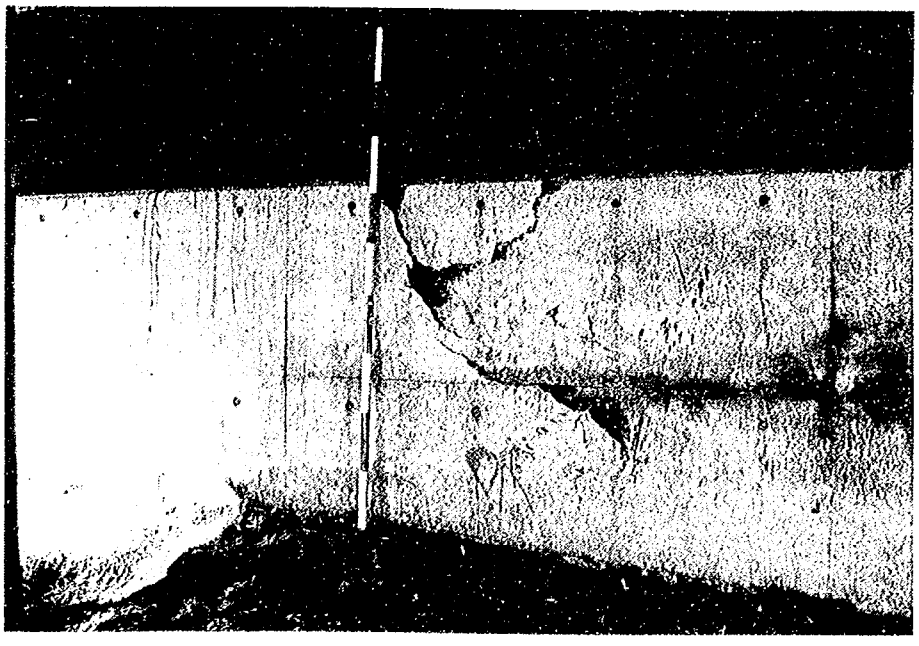


Photo 8 Damage to Abutment in Rindo Bridge

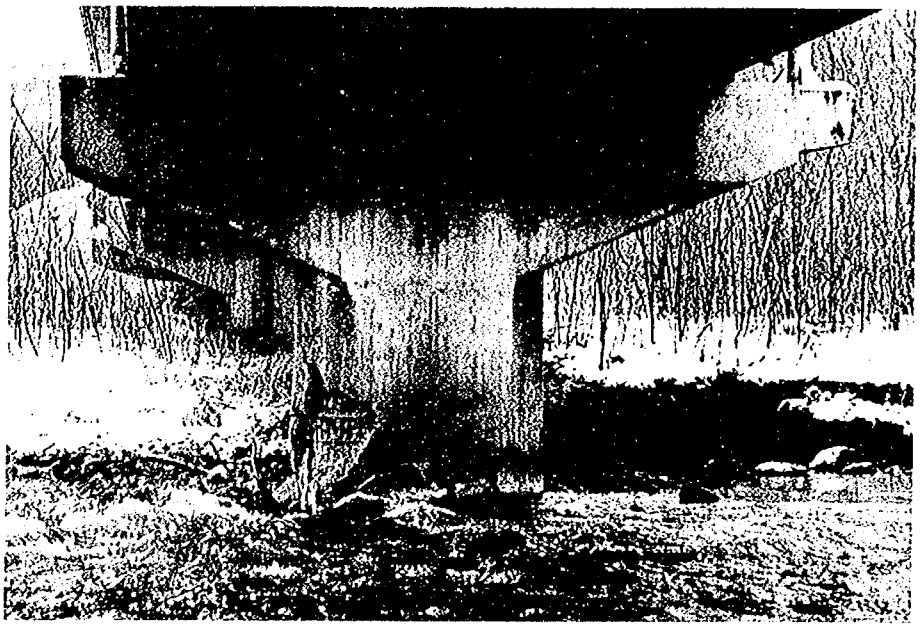


Photo 9 Failure of a Pier in Matsunoe Bridge due to the Kushiro−Oki EQ

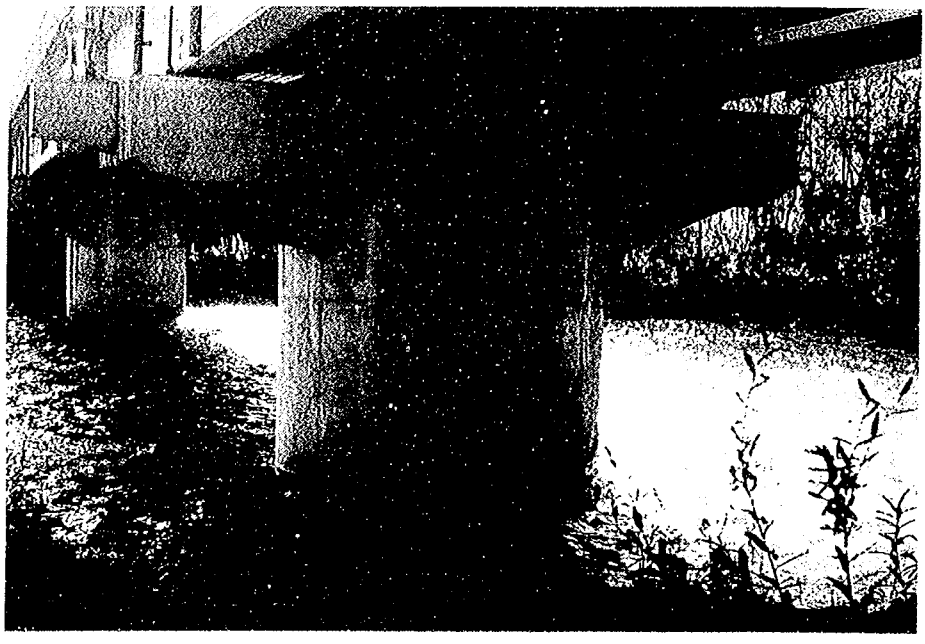


Photo 10 Matsunoe Bridge Reinforced with Reinforced Concrete Jacketing after the Kushiro−Oki EQ



Photo 11 Cracks in the Right Dike of Kushiro Retarding Basin (crack depth = 1.9m, gap=40cm, total length=50m)



Photo 12 Slope Failure of the Osobetsu Dike , Kushiro River

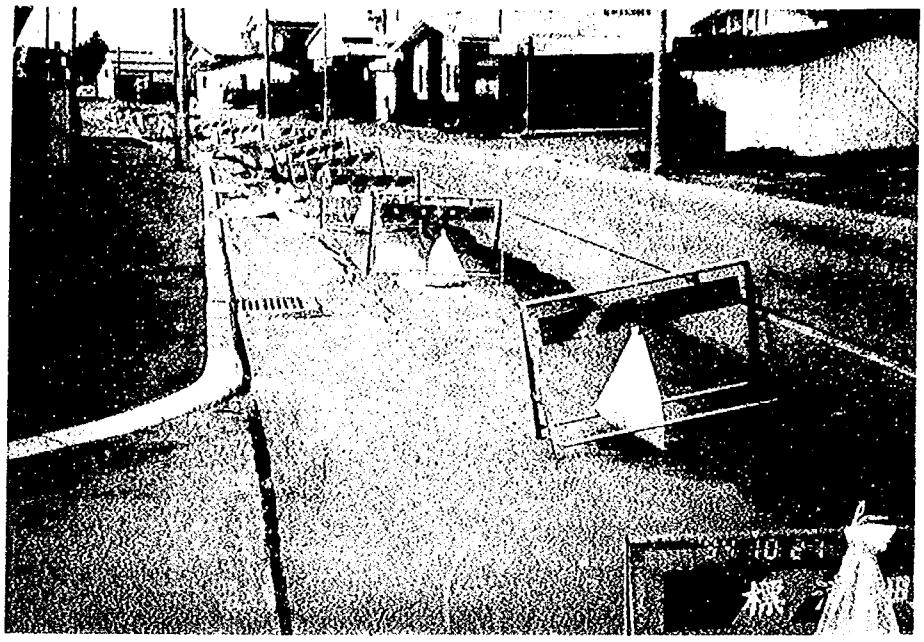


Photo 13 Slumping of Road Surface at a Back−Filled Area along Subsurface Sewer



Photo 14 Broken Telecommunication Line at Kayanuma Area

Cost-effective Ground Improvement for Liquefaction Remediation near Existing Lifelines

by

Ronald D. Andrus and Riley M. Chung*

ABSTRACT

Little information has been gathered on ground improvement near existing lifelines. Five low vibration ground improvement techniques suitable for remedial work near existing structures are discussed. The five techniques are compaction grouting, permeation grouting, jet grouting, *in situ* soil mixing, and drain pile. Cost estimates are given for each technique, except the drain pile technique which is not yet available in the United States. Two reported case histories of ground improvement near buried pipes and conduits are reviewed. A combination of techniques may provide a cost-effective solution for preventing damage to existing lifelines resulting from liquefaction-induced horizontal ground displacement, subsidence, and uplift.

KEYWORDS: building technology; earthquake; ground improvement; lifelines; permanent ground deformation; soil liquefaction.

1. INTRODUCTION

One of the major factors of lifeline damage in earthquakes is horizontal ground displacement caused by liquefaction of granular soils, as illustrated in the case studies for many past earthquakes in the United States and Japan (O'Rourke and Hamada, 1992; Hamada and O'Rourke, 1992). Other important factors of liquefaction-induced damage include local subsidence associated with the ejection of soil and water, and flotation of light weight buried structures. For example, horizontal ground displacement damaged many pipelines, roads, bridges, and buildings during the 1906 San Francisco, California, earthquake. Broken water lines made fire fighting after the earthquake impossible, and much of San Francisco burned. During the 1989 Loma Prieta earthquake, liquefaction, horizontal ground movement, major pipeline damage, and fires occurred at virtually the same locations in San Francisco. Of the 160 breaks in the Municipal Water Supply System of San Francisco in 1989, 123 were in the Marina, where significant liquefaction and ground deformation had occurred (O'Rourke.and Pease, 1992).

Many lifeline structures lie in regions of high liquefaction and ground displacement potential. While it may be feasible to relocate some support facilities on sites which are not susceptible, similar precautions are not always possible for the long linear element of lifeline systems such as pipelines, electrical transmission lines, and communication lines. For some pipeline systems, such as gas and water lines, it may be economical to install modern welded steel pipes that may not break or leak, even after moderate deformation (O'Rourke and Palmer, 1994). For other pipeline systems, such as waste water lines, the segmented pipe used can accommodate very little deformation. Ground improvement may be the most economical solution for these type of systems, or for areas where large ground deformations are anticipated.

This paper reviews five low vibration ground improvement techniques, and discusses their application to existing lifelines, in particular, pipelines supported by ground having high potential for liquefaction and horizontal ground displacement.

2. LIQUEFACTION REMEDIATION BY GROUND IMPROVEMENT

The risk of liquefaction and ground displacement can be reduced by the following types of ground improvement: densification, solidification, drainage, dewatering, and reinforcement (National Research Council, 1985; Kramer and Holtz, 1991; JSSFME, 1994). Soil densification is generally considered highly reliable, and the most standard remedial measure against liquefaction. It reduces the void space, thereby decreasing the potential for volumetric change that would lead to liquefaction. Resistance to shear deformation also increases

*National Institute of Standards and Technology, Building 226, Room B158, Gaithersburg, Maryland 20899, USA.

with increased density. Several sites improved by densification techniques performed well during the 1989 Loma Prieta and the 1994 Northridge, California, earthquakes (Mitchell and Wentz, 1991; Graf, 1992a; Hayden and Baez, 1994).

Solidification is also considered a highly reliable remedial measure against liquefaction. It prevents soil particle movement and provides cohesive strength. During the 1989 Loma Prieta earthquake, the few sites improved by solidification techniques performed well (Mitchell and Wentz, 1991; Graf, 1992a).

While the drainage method has been used for a number of liquefaction remediation projects in Japan, it has found limited use in the United States. Shake table tests (Sasaki and Taniguchi, 1982) indicate that gravel drains can accelerate the dissipation of excess pore water pressures, thereby limiting the loss of shear strength and reducing the uplift pressures acting on buried structures. Following the 1993 Kushiro-Oki, Japan, earthquake, Iai et al. (1994) observed that quay walls having back fill treated by the gravel drain pile and sand compaction pile techniques suffered no damage, while quay walls having untreated backfill were severely damaged due to liquefaction. The drainage method does not prevent seismic-induced subsidence.

Lowering the ground water level by dewatering reduces the degree of saturation, thereby preventing the development of excess pore water pressure which would lead to liquefaction. The dewatering method does not prevent seismic-induced settlement. Dewatering is a difficult task and very expensive, since both upstream and downstream seepage cutoffs are usually required, and pumps must be maintained constantly.

Soil reinforcement provides resistance to ground deformations. Shake table tests reported by Yasuda et al. (1992) indicate that continuous underground walls can control horizontal ground movement. Their effectiveness depends on such factors as quantity, orientation, shear resistances, and excitation direction.

The most commonly used ground improvement techniques are vibro-compaction, vibro-replacement, dynamic compaction, and sand compaction pile. These four techniques improve by densification, and are typically less expensive than other techniques. However, they can produce objectionable levels of work vibration.

3. GROUND IMPROVEMENT TECHNIQUES FOR EXISTING LIFELINES

Techniques selected to improve the ground surrounding or adjacent to existing lifelines should be those that would not cause excessive level of disturbance to the lifelines. Five low vibration techniques which improve ground conditions in one or more of the above ways are discussed in the following paragraphs. A number of advantages and constraints for each technique are listed in Table 1.

3.1 Compaction Grouting

Compaction grouting is the injection of a thick, low mobility grout that remains in a homogenous mass without entering soil pores (Graf, 1992b; Warner et al., 1992; Rubright and Welsh, 1993). As the grout mass expands the surrounding soil is displaced and densified. Recommended grout mixes consist of silty sand, cement, fly ash, and water. Bentonite and other clay materials increase mobility, and their use should be restricted. Cement may not be needed for just soil displacement. For deep injection (greater than about 3 m), final spacings of 2 to 4 m are frequently used. For shallow injection, final spacings usually range from 1 to 2 m. Compaction grouting has been successfully used to correct structural settlement, prevent settlement during soft ground tunneling in urban areas, protect structures against local zones of sinkhole settlement and densify liquefiable soil. The technique is not effective in thick, saturated clayey soils, and may be marginally effective in silt deposits.

3.2 Permeation Grouting

Permeation grouting is the injection under pressure of low viscosity particulate or chemical fluids into soil pore space with little change to the physical structure of the soil (Baker, 1982; Littlejohn, 1993). Particulate grout mixtures may consist of Portland cement, micro-fine cement, clay, fly ash, and water. Chemical grout types include sodium silicates, acrylamides, lignosulfonates, and resins (Karol, 1982). Sodium silicate grouts are the most widely used chemical grout. The acrylamides in solution or powder form, and the catalyst used in all lignosulfonates are toxic. Typical final spacings of grout holes range from 0.5 to 2 m. Permeation grouting has been successfully used to control ground water flow, stabilize excavations in soft ground, underpin existing foundations, and prevent seismic-induced

settlement and liquefaction. As a rule-of-thumb, particulate grouts will not permeate most sands, and chemical grouts will not permeate sands containing more than about 25 percent silt and clay. Grout must resist seepage forces, chemical and biological attack, and cracking. Special handling and mixing procedures may be required to insure the health and safety of workers, and to protect the environment.

3.3 Jet Grouting

In jet grouting, high pressure (typically 40 to 60 MPa) fluid jets are used to erode and mix/replace soil with grout (Bell, 1993; Covil and Skinner, 1994; Stroud, 1994). The installation procedure begins with the drilling of a small hole, usually 90 to 150 mm in diameter, to the final depth. Grout, usually a water-cement slurry, is jetted into the soil through small nozzles, as the drill rod is rotated and withdrawn. Bentonite is typically added where low permeability is critical. A continuous flow of slurry from the jet points to the ground surface is required to prevent ground pressures from building up to the jet pressure, leading to ground deformation. Large quantities of waste slurry accumulates at the ground surface. Columns and panels of soil-cement as wide as 3 m have been formed. The technique has been successfully used to underpin existing foundations, support excavations, control ground water flow, and strengthen liquefiable soils. Careful control of operations is required for consistent results. Site pilot studies are highly recommended for this technique, as well as the other four techniques.

3.4 *In Situ* Soil Mixing

In situ soil mixing is the mechanical mixing of soil and stabilizer using rotating auger and mixing-bar arrangements (Jasperse and Ryan 1992; Stroud, 1994; JSSFME, 1994). As augers penetrate the ground, the stabilizer is pumped through the auger shaft and out the tip. Flat mixing bars attached to the auger shaft mix injected stabilizer and soil. Upon reaching the designed depth, a second mixing occurs as augers are withdrawn. The result is high strength, or low permeability, columns and panels. Large augers (up to 4 m in diameter) require more torque, and are generally limited to depths less than about 8 m. For deeper mixing, a single-row of two to four shafts about 1 m in diameter is typically used. The columns and panels are commonly layout in a lattice pattern. The technique has been successfully used to control ground water flow, support excavations, stabilize embankments and slopes, increase bearing capacity for new foundations, and prevent lateral ground displacement caused by liquefaction. Obstructions such as boulders and logs, and hard strata can be a problem.

3.5 Drain Pile

Ono et al. (1991) described a low vibration system for constructing gravel drain piles using a large casing auger. The casing is screwed down into the ground, while simultaneously pouring water into the casing to prevent hydrostatic imbalance and sediment flow into the casing. Gravel is discharged into the casing upon reaching the final depth. As the casing is unscrewed, gravel is pushed out the end of the casing and compacted by a rod. One study showed standard penetration resistances measured at the midpoint between piles after installation were about 5 blow counts higher than before installation. When drains are installed without the compaction rod, little densification occurs. Design charts for determining drain spacings which take well resistance into account have been proposed by Onque (1988). There is no easy way to install filters around gravel drain piles, and drains may clog when liquefaction occurs (Onque et al., 1987). Systems for installing synthetic drains made of plastic and filter cloth have also been developed. For several liquefaction remediation projects in Japan, a densification technique, such as vibro-compaction or sand compaction pile, was used to densify loose soil to within about 20 m of an existing structure, and gravel or plastic drain piles were installed to within a few meters of the structure (Iai et al., 1994; JSSFME, 1994). There are very few cases in which drains were applied to ground having fines content of over 30 percent and coefficient of permeability of less than 0.001 cm/sec. Careful consideration of seepage conditions is required.

3.6 Cost

Cost estimates for four techniques are given in Table 2. Costs are not provided for the drain pile technique, since it is not available in the United States. These estimates are believed to be reasonable starting values for feasibility studies. The injection labor and materials costs are in terms of dollars per cubic meter of improved soil. For compaction grouting and permeation grouting, the total improved volume is assumed a percentage of the volume of grout injected, as noted below the table. For jet

grouting and soil mixing, the cost of labor and materials is for the mixed volume. Before a meaningful cost comparison can be made, the required volume of treatment to prevent horizontal ground displacement must be determined from seismic stability analyses. Items such as quality control and verification testing are not included in the values provided in Table 2. The cost of improvement near lifelines will likely be higher given the special considerations listed below.

4. EXISTING LIFELINES

Ground improvement near existing lifelines requires special considerations (Glaser and Chung, 1995) because of the following:

- Work vibrations may damage lifeline, which could have very serious consequences;
- Soil needing improvement is obstructed by the lifeline;
- Scope of work is of large areal extent, yet may be limited to a narrow right-of-way;
- Subsurface conditions will vary greatly along alignment;
- Extent of treatment required to protect lifeline is not known;
- Exact location and condition of buried utilities may not be known; and
- Improvement may adversely affect regional hydrology.

4.1 Case Histories

Reported case histories of ground improvement near existing lifelines are not common. The two cases involving buried utilities that the authors are aware of are reviewed below.

Gazaway and Jasperse (1992) discussed the application of jet grouting to construct a section of an impervious cutoff wall where several underground pipes and fragile conduits crossed at a chemical plant in northern Michigan. A typical section of this crossing is showing in Figure 1. The depth of the cutoff wall is as much as 7.3 m. To ensure closure beneath the larger pipes, the drill rod was rotated and withdrawn at slower rates. Near the smaller and more fragile conduits, column spacings were tightened, and rotation and withdrawal rates increased. Jet pressures as low as 35 MPa were sometimes used for short periods in the immediate vicinity of particularly sensitive conduits. Approximately 530 square meters of cutoff wall was installed by jet grouting in three and a half weeks. No detectable damage occurred to any of the underground utilities from the jetting action.

Scherer and Weiner (1993) described a remediation project involving a concrete effluent channel and three buried concrete pipelines connected to the channel that had settled as much as 190 mm. Joints in the pipelines had opened as a result of the settlement. The diameters of the three pipes were 1.22, 1.52, and 2.13 m. To avoid costly excavation, dewatering, and problems posed by other utilities within the area, pipes were supported and raised with compaction grout pile elements at each joint location or at intervals not exceeding 3 m. First, vertical compaction piles were constructed on each side of the concrete pipe extending from a firm layer at depth to the bottom of the pipe, as shown in Figure 2. Grout was then injected beneath the center of the pipe to lift the pipe. Finally, the interface between the vertical grout columns and pipe was filled with additional grout to establish positive support. Fifty-two vertical and angle grout columns were installed.

4.2 Liquefaction Remediation

Conceptual diagrams showing various types of ground improvement near an underground utility are shown in Figure 3. These diagrams suggest that buried utilities could be protected from subsidence and uplift using permeation grouting or jet grouting. Depending on the constrains summarized in Table 1, horizontal ground movement could be prevented by any one of the five techniques. The extent of treatment is determined from seismic stability analyses. The safe application distance depends on the nature and condition of the lifeline, as well as the level of disturbance which occurs during ground improvement.

5. CONCLUSIONS

Compaction grouting, permeation grouting, and jet grouting are well suited for remedial work beneath existing structures. The *in situ* soil mixing and drain pile techniques are suitable for work near existing structures. Of these five techniques, only jet grouting and *in situ* soil mixing can treat all liquefiable soil types. Compaction grouting may be marginally effective in thick silt deposits. Chemical grouts cannot permeate soils with more than about 25

percent fines, silt and clay. It seems that drains would be ineffective in ground with low permeability. All five techniques are very expensive. However, each can provide a highly cost-effective solution for certain situations.

Upon reviewing the available cases of ground improvement near buried utilities, one quickly becomes aware that very little has been gathered on the subject. With great care, and depending on the nature and condition of the lifeline, permeation grouting and jet grouting could improve soil conditions immediately adjacent to lifelines. Compaction grouting could be applied beneath existing lifelines, but may not sufficiently compact soils immediately beneath them. The *in situ* soil mixing and drain pile techniques could be effectively employed a short distance away from lifelines. A combination of techniques may provide the most cost-effective solution for some systems.

6. REFERENCES

1. Baker, W.H. (1982). "Planning and Performing Structural Chemical Grouting," Proc, Grouting in Geotechnical Engineering., held in New Orleans, LA, on 10-12 Feb., W.H. Baker, Ed., ASCE, pp. 515-539.
2. Bell, A.L. (1993). "Jet Grouting," Ground Improvement, M.P. Moseley, Ed., CRC Press, Inc., Boca Raton, FL, pp. 149-174.
3. Covil, C.S., and Skinner, A.E. (1994). "Jet Grouting--A Review of Some of the Operating Parameters that Form the Basis of the Jet Grouting Process," Proc., Grouting in the Ground, held in London, England, on 25-26 Nov. 1992, A.L. Bell, Ed., Thomas Telford, London, pp. 605-629.
4. Glaser, S.D., and Chung, R.M. (1995). "Use of Ground Improvement to Mitigate Liquefaction Potential for Lifelines," Proc., U.S.-Taiwan Geotech. Collaboration Workshop, held in Taipei on 9-11 Jan.
5. Gazaway, H.N., and Jasperse, B.H. (1992). "Jet Grouting in Contaminated Soils," Proc., Grouting, Soil Improvement and Geosynthetics, held in New Orleans, LA, on 25-28 Feb., R.H. Borden, R.D. Holtz and I. Juran, Eds., ASCE, Geotech. Special Publication No. 30, Vol. 1, pp. 206-214.
6. Graf, E.D. (1992a). "Earthquake Support Grouting in Sands," Proc., Grouting, Soil Improvement, and Geosynthetics, held in New Orleans, LA, on 25-28 Feb., R.H. Borden, R.D. Holtz and I. Juran, Eds., ASCE, Geotech. Special Publication No. 30, Vol. 2, pp. 879-888.
7. Graf, E.D. (1992b). "Compaction Grouting, 1992," Proc., Grouting, Soil Improvement, and Geosynthetics, held in New Orleans, LA, on 25-28 Feb., R.H. Borden, R.D. Holtz and I. Juran, Eds., ASCE, Geotech. Special Publication No. 30, Vol. 1, pp. 275-287.
8. Hamada, M., and O'Rourke, T.D., Eds. (1992). "Case Studies of Liquefaction and Lifeline Performance During Past Earthquakes, Japanese Case Studies," Technical Report NCEER-92-0001, National Center for Earthquake Engineering Research, Buffalo, NY.
9. Hayden, P.F., and Beaz, J.I. (1994). "State of Practice for Liquefaction Mitigation in North America," Proc., Int. Workshop on Remedial Treatment of Liquefiable Soils, held in Tsukuba Science City, Japan, on 4-6 July.
10. Iai, S., Matsunaga, Y., Morita, T., and Sakurai, H. (1994). "Effectiveness of Measures Against Liquefaction Confirmed at a Recent Earthquake - A Case History During the 1993 Kushiro-Oki Earthquake, Proc., 26th Joint Meeting of United States-Japan Panel on Wind and Seismic Effects, held in Gaithersburg, MD, on 17-20 May, pp. 213-225.
11. Jasperse, B.H., and Ryan, C.R. (1992). "Stabilization and Fixation Using Soil Mixing," Proc., Grouting, Soil Improvement, and Geosynthetics, held in New Orleans, LA, on 25-28 Feb., R.H. Borden, R.D. Holtz, and I. Juran, Eds., ASCE, Geotech. Special Publication No. 30, Vol. 2, pp. 1273-1284.
12. JSSMFE (1994). Remedial Measure Against Soil Liquefaction -- From Investigation and Design to Implementation, Japanese Society for Soil Mechanics and Foundation Engineering. (in Japanese; translation into English in progress).
13. Karol, R.H. (1982). "Chemical Grouts and Their Properties," Proc., Grouting in Geotechnical Engineering., held in New Orleans, LA, on 10-12 Feb., W.H. Baker, Ed., ASCE, pp. 359-377.

14. Kramer, S.L., and Holtz, R.D. (1991). Soil Improvement and Foundation Remediation with Emphasis on Seismic Hazards, Report of workshop held at the Univ. of Washington, Seattle, on 19-21 Aug., 106 p.

15. Littlejohn, G.S. (1993). "Chemical Grouting," Ground Improvement, M.P. Moseley, Ed., CRC Press, Inc., Boca Raton, FL, pp. 100-130.

16. Mitchell, J.K. and Wentz, F.J., Jr. (1991). "Performance of Improved Ground During the Loma Prieta Earthquake," Report No. UCB/EERC-91/12, Earthquake Engineering Research Center, Univ. of California at Berkeley, 93 p.

17. National Research Council (1985). Liquefaction of Soils During Earthquakes, National Academy Press, Washington, D.C., 240 p.

18. Ono, Y., Ito, K., Nakajima, Y., and Oishi, H. (1991). "Efficient Installation of Gravel Drains;" Proc., 2nd Int. Recent Advances in Geotech. Earthquake Engrg. and Soil Dynamics, held in St. Louis, MO, on 11-15 Mar., S. Prakash, Ed., Vol. 1, pp. 437-444.

19. Onque, A. (1988). "Diagrams Considering Well Resistance for Designing Spacing Ratio of Gravel Drains," Soils and Foundations, JSSMFE, Vol. 28, No. 3, September, pp. 160-168.

20. Onque, A., Mori, N., and Takano, J. (1987). "In-Situ Experiment and Analysis on Well Resistance of Gravel Drains," Soils and Foundations, JSSMFE, Vol. 27, No. 2, June, pp. 42-60.

21. O'Rourke, T.D., and Hamada, M., Eds. (1992). "Case Studies of Liquefaction and Lifeline Performance During Past Earthquakes, United States Case Studies," Technical Report NCEER-92-0002, National Center for Earthquake Engineering Research, Buffalo, NY.

22. O'Rourke, T.D., and Palmer, M.C. (1994). Feasibility Study of Replacement Procedures and Earthquake Performance Related to Gas Transmission Pipelines, Technical Report NCEER-94-0012, National Center for Earthquake Engineering Research, Buffalo, NY.

22. O'Rourke, T.D., and Pease, J.W. (1992). "Large Ground Deformations and Their Effect on Lifeline Facilities: 1989 Loma Prieta Earthquake," Case Studies of Liquefaction and Lifeline Performance During Past Earthquakes, United States Case Studies, Technical Report NCEER-92-0002, T.D. O'Rourke and M. Hamada, Eds., National Center for Earthquake Engineering Research, Buffalo, NY.

23. Rubright, R., and Welsh, J.P. (1993). "Compaction Grouting" Ground Improvement, M.P. Moseley, Ed., CRC Press, Inc., Boca Raton, FL, pp. 131-148.

24. Sasaki, Y., and Taniguchi, E. (1982). "Shaking Table Tests on Gravel Drains to Prevent Liquefaction of Sand Deposits," Soils and Foundations, JSSMFE, Vol. 22, No. 3, Sept., pp. 1-14.

25. Scherer, S.D., and Weiner, E. (1993). "Underpinning and Leveling Settled Pipes and Channel," Proc., 3rd Int. Conf. on Case Histories in Geotech. Engrg., held in St. Louis, MO, on 1-4 June, S. Prakash, Ed., Vol. 2, pp. 1183-1188.

26. Stroud, M.D. (1994). "Report on Sessions 5 and 6: Jet Grouting and Soil Mixing," Proc., Grouting in the Ground, held in London, England, on 25-26 Nov. 1992, A.L. Bell, Ed., Thomas Telford, London, pp. 539-560.

27. Warner, J., Schmidt, N., Reed, J., Shepardson, D., Lamb, R., and Wong, S. (1992). "Recent Advances in Compaction Grouting Technology," Proc., Grouting, Soil Improvement, and Geosynthetics, held in New Orleans, LA, on 25-28 Feb., R.H. Borden, R.D. Holtz and I. Juran, Eds., ASCE, Geotech. Special Publication No. 30, Vol. 1, pp. 252-264.

28. Welsh, J.P. (1992). "Grouting Techniques for Excavation Support," Proc., Excavation and Support for the Urban Infrastructure, held in New York, NY, on 14-15 Sept., T.D. O'Rourke and A.G. Hobelman, Eds., ASCE, Geotech. Special Publication No. 33, pp. 240-261.

29. Welsh, J.P. (1995). Personal communication.

30. Yasuda, S., Nagase, H., and Kiku, H. (1992). "Appropriate Countermeasures against Permanent Ground Displacement due to Liquefaction," Proc., 10th World Conf. on Earthquake Engineering, held in Madrid, Spain, on 19-24 July, Balkema, Rotterdam, pp. 1471-1476.

Table 1. Advantages and Constraints for Five Ground Improvement Techniques.

Advantage or Constraint	Compaction Grouting	Permeation Grouting	Jet Grouting	*In Situ* Soil Mixing	Drain Pile
Produces low levels of work vibration and noise	yes	yes	yes	yes	yes
Soil types not treatable	saturated clayey soils	soils with fines content of over about 25%	irregular geometries in cobbly soils and open gravel	boulders, logs, and hard strata can be a problem	soils with significant fines content and very low permeability
Treatment beneath existing structures possible	yes	yes	yes	earth structures	earth structures
Small diameter drilling	yes	yes	yes	no	no
Low headroom work possible	yes	yes	yes	no	plastic drain pile
Selective treatment possible	yes	yes	yes	no	no
Intimate contact with structure possible	limited	yes	yes	no	no
Treatment at very low confinement possible	marginal	yes	yes	yes	yes
Without care, likely disturbance	significant ground movement; damaged pipes	significant ground movement; damaged pipes	significant ground movement; damaged pipes	significant ground movement; damaged pipes	damaged pipes
Quantity of waste produced	little	little	large	some	some
Prevents seismic-induced subsidence	yes	yes	depends on design	depends on design	no
Well-defined specifications required	yes	yes	yes	yes	yes
Engineered/observational approach required	yes	yes	yes	yes	yes
Quality control during installation required	yes	yes	yes	yes	yes
Other evaluations required	site pilot study	durability; creep; health and safety; site pilot study	durability; site pilot study	durability; site pilot study	seepage; clogging; site pilot study
Can be highly cost-effective	yes	yes	yes	yes	yes
Cost	expensive	expensive	expensive	expensive	expensive

Table 2. Cost Estimates for Low Vibration Ground Improvement Techniques in the United States (based on data from Welsh, 1992; Welsh, 1995).

Method	Mobilization/ Demobilization ($ per drill rig)	Grout Pipe Installation ($ per m of pipe)	Injection Labor and Materials ($ per m^3 of improved soil)
Compaction Grouting	8,000 to 15,000	> 50[a]	> 20[b]
Permeation Grouting			
Micro-fine cement	15,000 to 25,000	> 50[c]	> 130[d]
Silicates	> 25,000	> 50[c]	> 200[e]
Jet Grouting	> 35,000	-----	> 320[f]
In Situ Soil Mixing	100,000[g]	-----	> 100[h] , > 200[i]
Drain Pile	not available	-----	not available

[a]Grout pipe 76 mm in diameter; cost would double for low headroom work.
[b]Assuming volume of grout injected is 10 percent of the total volume treated.
[c]Sleeve port pipes; cost would double for low headroom work.
[d]Assuming clean gravel with sand, 20 percent grout take, and more than 200,000 liters of grout.
[e]Assuming clean sand, 30 percent grout take, and more than 200,000 liters of grout.
[f]Does not include handling and removal of the waste slurry.
[g]Approximate cost for large multi-auger rig and grout plant.
[h]Shallow mixing (say depths less than about 8 m).
[i]Deep mixing (say depths between 8 m and 30 m).

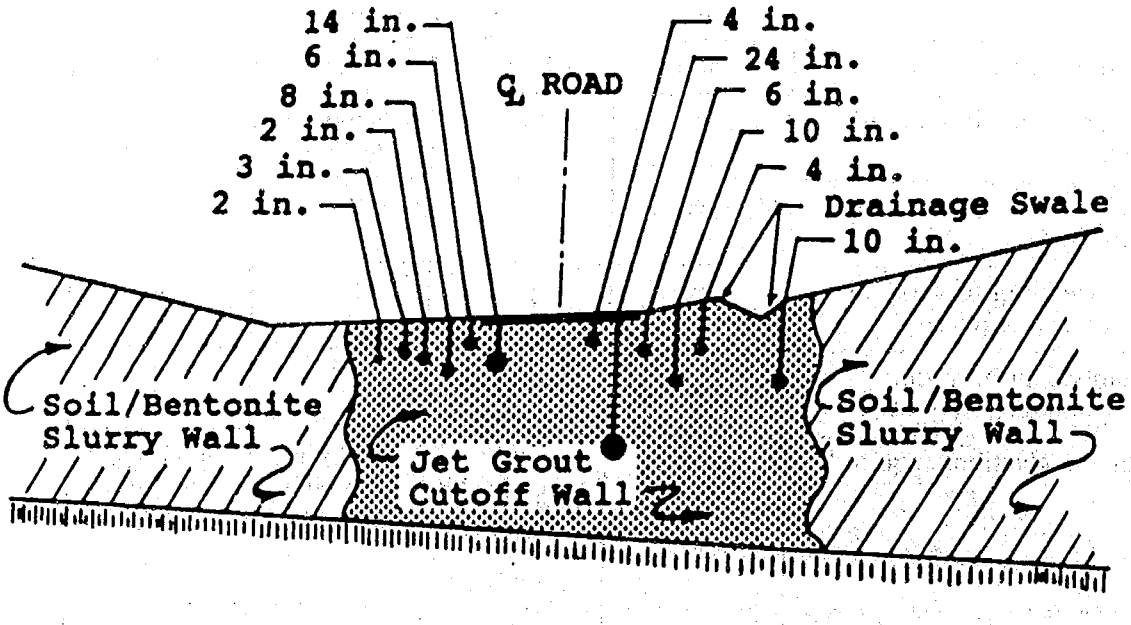


Figure 1. Construction of Cutoff Wall at Utility Crossing by Jet Grouting (Gazaway and Jasperse, 1992). (1 in. ≈ 25 mm.)

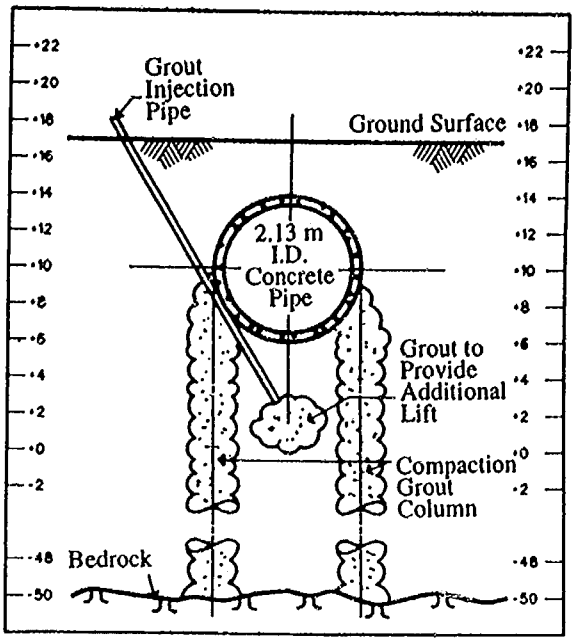


Figure 2. Underpinning and Leveling Settled Pipe by Compaction Grouting (Scherer and Weiner, 1993). (Elevations are in ft; 1 ft ≈ 0.3 m.)

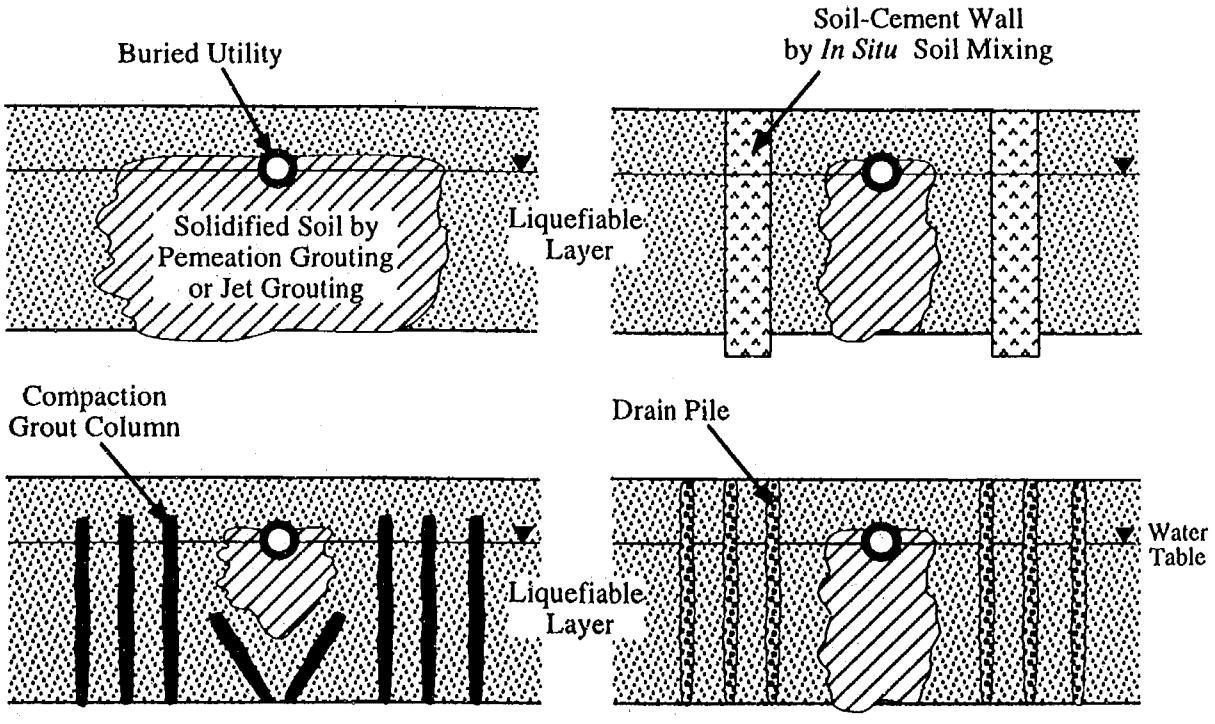


Figure 3. Liquefaction Remediation Near Buried Utility by Combination of Low Vibration Ground Improvement Techniques.



Shear Modulus and Radiation Damping Ratio of Rockfill Dams Estimated by Laboratory Test, In-Situ Test and Back Analysis of Earthquake Motions

by

Tadahiko Fujisawa[1], Akira Nakamura[2], Tomoya Iwashita[3], and Nario Yasuda[4]

ABSTRACT

On dynamic analysis of rockfill dams, dynamic deformation characteristics of rockfill materials such as shear moduli and damping ratios must be known to make analysis with higher accuracy. In this study, large-scale cyclic triaxial tests were carried out using rockfill materials of existing dams, and the results were compared with the dynamic deformation characteristics obtained by in-situ geophysical explorations and back analysis of earthquake motions observed at dams. Furthermore, the radiation damping ratio was estimated from back analysis and laboratory tests, and then the frequency dependent characteristics of the radiation damping were evaluated.

Key Words : *Rockfill Dam, Cyclic Triaxial Test, In-Situ Geophysical Exploration, Back Analysis of Earthquake Motions, Shear Modulus, Radiation Damping Ratio*

1. INTRODUCTION

In Japan, rockfill dams are designed using a seismic coefficient method and a modified seismic coefficient method. Seismic stability, however, is confirmed also by dynamic analysis for the modified seismic coefficient method. On more accurate dynamic analysis, hence, it is important to investigate dynamic deformation characteristics, including the shear moduli and damping ratios of dam materials, over wide shear strain and frequency ranges. Dynamic deformation characteristics of rockfill materials obtained by laboratory tests have been used for dynamic analysis of rockfill dams. However, deformation characteristics from laboratory tests have rarely compared with those from in-situ tests. In this study, we conducted large-scale cyclic triaxial tests using rockfill materials transported from quarry sites and compared the results with the dynamic deformation characteristics obtained by in-situ geophysical explorations and back analysis of earthquake motions observed at dam bodies. Radiation damping by dissipation of wave energy into base rock from the dam body has not been determined quantitatively even though it has more affect to the behavior of the dam during earthquakes than internal damping. We, hence, estimated radiation damping from the total damping of the dam body by back response analysis and hysteresis damping of rockfill materials by laboratory tests. We compared the estimated radiation damping ratio with that from various ground models by other researchers.

2. GENERAL DESCRIPTION OF TEST AND ANALYSIS

2.1 Objective Dams

This study was made on two existing dams: Miho Dam and Oya Dam. These are zoned rockfill dams with a central core of 95.0 m and 56.5 m heights. Figures 1 (a) and (b) show the standard cross sections of each dam.

1) Director, Dam Department, Public Works Research Institute, Ministry of Construction, Tsukuba Science City, 305 Japan
2) Head, Filldam Division, ditto
3) Research Engineer, Filldam Division, ditto
4) Head, Planning Division, ditto

2.2 *Laboratory Test*

We transported rockfill materials from the quarry site of each dam. The materials were inner small grain sized rock for Miho Dam, and inner and outer rock for Oya Dam. We conducted large-scale cyclic triaxial laboratory tests using the materials. The cyclic triaxial testing apparatus is shown in Fig.2. Specimens were 30 cm in diameter and 60 cm in height. We sieved the rockfill materials for a maximum grain size of 63.5 mm and for similar grain size distribution with the banking materials at each dam as shown in Fig.3. Specimens were prepared in six layers, with the same gradation in each layer. The air-dried materials were spread uniformly into a mold so as to avoid segregation, then compacted using an electric vibratory hammer (950 blows/min, weight 320 N, diameter of loading plate 29 cm) to provide the specified relative densities. All tests were conducted in the saturated condition and consolidated drained state under the conditions shown in Table 1. Specimens were consolidated under the specified confining stress, and after consolidation, cyclic load was applied at 0.1 cycles per second and increased in stages (cyclic loading was repeated 12 times for each step and the data of the 10th cycle were used for the analysis). When the generated strain reached approximately 5×10^{-4}, the next confining stress was applied to the specimen and the same procedure was repeated. Micro axial strain was measured, using differential transformer type linear displacement transformers as shown in Fig.4.

2.3 *In-Situ Geophysical Exploration*

We conducted geophysical explorations in the downstream side body of Miho Dam by means of PS logging and refraction method (Fig.5(a)). For PS logging, blasting was executed in the open-standpipe piezometer within the dam body, and reception of S-wave was taken on the downstream surface of the dam. For Oya dam, we conducted elastic wave explorations in the downstream side body of dam by refraction method (Fig.5(b)).

2.4 *Back Analysis of Observed Earthquake Motions*

For Miho Dam seismographs have been installed at the crest and downstream toe as shown in Fig.1 (a), and for Oya Dam seismographs have been installed at the crest and in the limb tunnel on the left abutment as shown in Fig.1 (b). The main features of the used earthquakes are listed in Tables 2. Figures 6 and 7 show the typical time history of acceleration and frequency response function. We estimated the natural frequencies of the dam bodies from the frequency response functions at the dam crest corresponding to the foundation in the upstream-downstream component. In the response analysis, we should use the earthquake motions monitored at the free field. However, earthquake motion at the free field have not been observed at the two dams. We considered that the earthquake motions observed at the downstream toe foundation of Miho Dam were those monitored at the foundation, because the downstream toe motions had little effect on the vibration of the dam body during earthquakes. In the case of Oya dam we used earthquake motions observed in the limb tunnel on the left abutment in the same manner. We smoothed the frequency response functions using a Parzen window with a band width of 0.6 Hz.

3. S-WAVE VELOCITY BY LABORATORY TEST AND IN-SITU GEOPHYSICAL EXPLORATION

Using the result of the laboratory tests of the rockfill materials of Miho Dam and Oya Dam, the relationships between shear modulus G_0 at infinitesimal strain, $\gamma = 10^{-6}$, void ratio e and mean effective principal stress σ'_m are expressed by:

$$G_0 = A \cdot P_{at} \frac{(2.17-e)^2}{1+e} \left(\frac{\sigma'_m}{P_{at}} \right)^B \quad (1)$$

where, P_{at} is the atmospheric pressure, and K is the principal stress ratio (σ_3/σ_1). The constant factors A, B are obtained as in Fig.8 from the large-scale cyclic triaxial tests for both K=1.0 and K=0.5 for Miho Dam. Go and σ'_m have the following relationships respectively.

$$G_0 = \rho_D V_S^2 \quad (2)$$

$$\sigma'_m = \frac{1}{3}(1+2K)\,\sigma'_v \quad (3)$$

$$\sigma'_v = \rho_D \cdot g \cdot D \quad (4)$$

where, ρ_D is the wet density of the rockfill, V_S is the S-wave velocity, σ'_v is the effective vertical stress expressed by (5) and D is the depth from the dam surface.

If (2), (3) and (4) are substituted for (1), and if ρ_D = 2.3 t/m^3 and e = 0.25 on the basis of the results of quality control tests on banking, Figs. 9 (a) and (b) show the distribution of V_S with D in the cases of K=1.0 and 0.5 for Miho Dam, and cases of K=1.0 and 0.667 for Oya Dam. The result of in-situ geophysical explorations conducted in the downstream side of each dam is also shown in these figures. The distribution of V_S from the laboratory tests agreed with that from the in-situ geophysical exploration. The shear modulus of the rockfill dam body can be estimated by laboratory tests on the rockfill materials, since rockfill dams are constructed in a similar process to that for preparing specimens of laboratory tests

4. SHEAR MODULUS BY LABORATORY TEST AND BACK ANALYSIS OF EARTHQUAKE MOTIONS

We calculated the shear moduli of the two dams for each shear strain level during the earthquakes listed in Tables 2. In accordance with shear beam theory, the shear modulus G is in proportion to the square of the i-th natural frequency fi. When the first natural frequency and shear modulus of a dam body at very small shear strain are f_{1*} and G_* respectively, the normalized shear modulus G/G_* is expressed by:

$$\frac{G}{G_*} = \left(\frac{f_1}{f_{1*}} \right)^2 \quad (6)$$

The first natural frequency and the shear modulus at the smallest shear strain level of a dam body among the observed earthquake motions were assumed to be f_{1*} and G_*. We simply calculated the maximum shear strain γ caused in the dam body during each earthquake by the three processes shown below.

1) The average of maximum shear strains for each layer of the dam body model was obtained using the one-dimensional dynamic analysis, SHAKEM (Chugh, 1985).

2) The shear strain was calculated from the maximum displacement dmax by two times integration of the time history of acceleration at the crest.

3) The shear strain was calculated from the maximum acceleration amax at the crest, as expressed by:

$$\gamma = \frac{d_{max}}{H} = \frac{a_{max}}{(2\pi f_1)^2 \cdot H} \quad (7)$$

where, H is the height of dam.

Tables 3 (a) and (b) show the results of calculation γ for Miho Dam and Oya Dam.

Figures 10 (a) and (b) show the dependency of G/G_* with γ during the earthquakes for Miho Dam and Oya Dam respectively. Normalized shear moduli G/G_* decrease as the shear strains γ increase for both the dams. These figures show also the normalized shear moduli G/G_0 obtained by laboratory tests for various confining pressures σ'_c. The G/G_*

obtained by earthquake motions is slightly larger than G/G_0 by laboratory tests, for G_* and G_0 were defined at the different shear strains. The reductive tendency of G/G_* with γ for each dam agreed with that of G/G_0. As a result, the strain dependency of the shear modulus for rockfill dam bodies during earthquakes can be estimated from laboratory tests.

5.QUANTITATIVE ESTIMATION AND FREQUENCY DEPENDENT CHARACTERISTICS OF RADIATION DAMPING RATIO

We estimated the total damping ratio $h_{t,i}$ of dams for the first to third resonance frequencies from the frequency response functions at the dam crest corresponding to the foundation of observed earthquake motions by the half power method as expressed by following equation and as shown in Fig.11.

$$ht,i(\%)=\frac{\Delta f_i}{2\cdot f_i}\times 100 \qquad (8)$$

Figures 12 (a) and (b) show the relationships between the total damping ratio $h_{t,1}$ and shear strain γ_1 for the first natural frequency of each earthquake motion, and also the relationships between the hysteresis damping ratio h_h and shear strain γ obtained from laboratory tests. As shown in Figs.12 (a) and (b), the damping ratio from the back analysis of observed earthquake motions is total damping ratio $h_{t,i}$ at each strain level, which consists of both the internal damping ratio — it is almost covered by the hysteresis damping ratio h_h for earth structures — and the radiation damping ratio $h_{r,i}$..

The shear strain greatly differs at each vibration mode. We calculated the shear strain γ_i for the i-th vibration mode from the rate of Fourier spectrum amplitude of the shear strain for the i-th natural frequency against the peak amplitude (Sugito et al., 1994), as expressed by:

$$\gamma_i=\gamma\cdot\frac{F_{\gamma,i}}{F_{\gamma\max}} \qquad (9)$$

where, $F_{\gamma,i}$ is Fourier spectrum amplitude of the shear strain for the i-th natural frequency and $F_{\gamma max}$ is the peak amplitude of Fourier spectrum of shear strain. We estimated the hysteresis damping ratio $h_h(\gamma_i)$ for the shear strain γ_i of the i-th mode from the result of laboratory tests.

We estimated the radiation damping ratio $h_{r,i}$ by subtracting the hysteresis damping $h_h(\gamma_i)$ from the total damping ratio $h_{t,i}$, as expressed by the following equation.

$$hr,i=ht,i(\gamma_i)-hh(\gamma_i) \qquad (10)$$

Figures.13 (a) and (b) show the radiation damping ratio $h_{r,i}$ for each earthquake motion with the first to third natural frequency of the dam body.

Ohmachi (1981) derived the radiation damping ratio $h_{r,i}$, as expressed by equation (11), by modeling a two-dimensional triangle-shaped elastic dam body on a homogeneous semi-infinite elastic base, and by replacing the equation of motion in the i-th vibration mode for a non-damping shear vibration model with that for a damping free vibration model with a single-degree of freedom.

$$hr,i=\frac{1}{zi}\cdot\beta \qquad (11)$$

where, β is vibration impedance ratio between the dam body and the foundation, and z_i is the i-th value which gives zero in Bessel function of the first kind of order zero.

Toki (1981) derived the radiation damping ratio $h_{r,i}$, as expressed by the equation (12), by equating the resonance amplitude of the surface displacement for a non-damping layer ground model on the elastic base with that for a complex stiffness surface ground model on the rigid base.

$$h_{r,i} = \frac{2}{(2i-1)\cdot\pi} \cdot \frac{\beta}{\sqrt{1-\beta^2}} \qquad (12)$$

Sato (1983) derived the radiation damping ratio $h_{r,i}$, as expressed by the equation (13), by equating the natural circular frequency of a non-damping elastic two-layer ground model with that for a Voigt type viscoelastic surface ground model on the rigid base.

$$h_{r,i} = \frac{1}{(2i-1)\cdot\pi} \cdot \ln\frac{|1+\beta|}{|1-\beta|} \qquad (13)$$

The radiation damping ratios with the parameter γ from the equations (11), (12) and (13) are plotted together in Figs.13 (a) and (b). In these figures, the radiation damping ratio $h_{r,i}$ of the two dams from back analyses and laboratory tests decrease as a higher vibration mode and that these results show a similar dependency to the results by the three researchers.

6. CONCLUSIONS

We compared the shear modulus of rockfill materials and estimated radiation damping ratio of rockfill dams from cyclic triaxial laboratory tests, in-situ explorations and back analyses of observed earthquake motions.

The distributions of S-wave velocities in the direction of depth obtained by laboratory tests and in-situ explorations were in agreement. The reduction of the normalized shear moduli with shear strains from laboratory tests and response analyses of earthquake motions was also in agreement. Therefore, the shear moduli of man-made banking structures such as rockfill dams can be estimated accurately by laboratory tests.

We estimated the radiation damping ratio of rockfill dams by subtracting the hysteresis damping ratio obtained by laboratory tests from the total damping ratio calculated by the half power method from the frequency response function of observed earthquake motions. We, thus, obtained the frequency dependent characteristics where the radiation damping ratio decreased as a higher vibration mode.

REFERENCES

Chugh, A. K. (1985): "Dynamic Response of Embankment Dams", International Journal for Numerical and Analytical Method in Geomechanics, vol.9, pp.101-124.

Ohmachi,T.(1981): "Calculation of Underground Radiation Damping in the Vibration of Embankment Dams", Proceedings of the 36th Annual Conference of the Japan Society of Civil Engineering, 3, pp.570-571. (In Japanese)

Sato, T. (1983): "Effect of the Underground Radiation Damping on Vibration Mode of Ground", Proceedings of the 17th JSCE Earthquake Engineering Symposium, pp.147-150. (In Japanese)

Sugito,M., Goda,H., and Masuda,T. (1994): "Frequency Dependent Equi-linearized Technique for Seismic Response Analysis of Multi-layered Ground", Proceedings of the Japan Society of Civil Engineering, No.493/ III-27, pp.49-58. (In Japanese)

Toki, K. (1981): "Seismic Analysis of Structures, New System Civil Engineering 11", pp.99-101, Gihodo-Publication. (In Japanese)

Table 1 Test condition of the cyclic triaxial tests

	Miho Dam	Oya Dam	
		(Inner Rock)	(Outer Rock)
Principal Stress Ratio	1.0, 0.5	1.0, 0.667	
Relative Density (%)	85	95	100
Confining Stress (MPa)	0.1, 0.2, 0.3, 0.4, 0.6	0.05, 0.1, 0.25, 0.5	
Control Condition	0.1Hz (Sinusoidal) : Stress Control	0.1Hz (Sinusoidal) :Stress Control	

Table 2 (a) Main features of the earthquakes for Miho Dam

Point of Epicenter	Date	Epicentral Distance (km)	Depth (km)	Magnitude
①Izu Peninsula Off	Jun.29, 1980	57	10	6.7
②East Yamanashi Pref.	Apr.14, 1981	13	40	4.5
③West Kanagawa Pref.	Aug. 8, 1983	12	30	6.0
④East Chiba Pref. Off	Dec.17, 1987	131	58	6.7
⑤Hakone	Aug. 5, 1990	24	14	5.1
⑥Tokyo Bay	Feb. 2, 1992	73	90	5.7

Table 2 (b) Main features of the earthquakes for Oya Dam

Point of Epicenter	Date	Epicentral Distance (km)	Depth (km)	Magnitude
①Noto Peninsula Off	Feb. 7,1993	31	25.0	6.6
②Noto Peninsula Off	Feb. 8,1993	37	25.7	4.9
③Noto Peninsula Off	Feb. 16,1993	28	24.8	5.0
④Noto Peninsula Off	Feb. 22,1993	9	26.5	4.8
⑤East Ishikawa Pref.	Dec. 8,1993	42	21.0	5.0
⑥Noto Peninsula Off	Jun. 7,1994	40	20.0	4.9

Table 3 (a) Results of calculation of shear strain γ for Miho Dam

Earthquake No.	Maximum Acceleration a_{max} (gal) Crest	Foundation	1st Natural Frequency f_1 (Hz)	Shear Strain γ by the process 3)
①	66	31	1.904	4.85×10^{-5}
②	87	31	1.855	6.74×10^{-5}
③	257	148	1.709	2.35×10^{-4}
④	66	11	2.002	4.39×10^{-5}
⑤	80	28	1.855	6.20×10^{-5}
⑥	32	12	2.051	2.03×10^{-5}

Table 3 (b) Results of calculation of shear strain γ for Oya Dam

Earthquake No.	Maximum Acceleration a_{max} (gal) Crest	Foundation	1st Natural Frequency f_1 (Hz)	Shear Strain γ by the process 3)
①	192	65	2.124	1.91×10^{-4}
②	38	6	2.271	3.30×10^{-5}
③	29	9	2.466	2.57×10^{-5}
④	53	14	2.393	4.15×10^{-5}
⑤	14	4	2.319	1.24×10^{-5}
⑥	10	4	2.490	7.49×10^{-6}

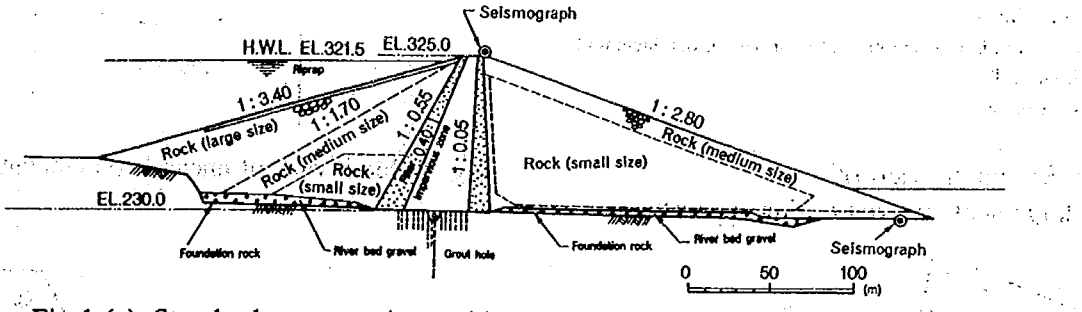


Fig.1 (a) Standard cross section and location of seismographs for Miho Dam

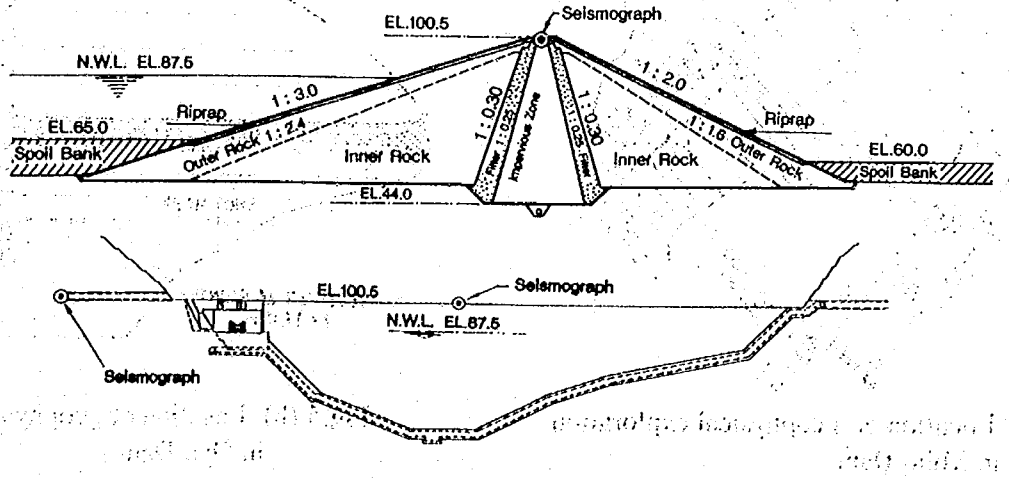
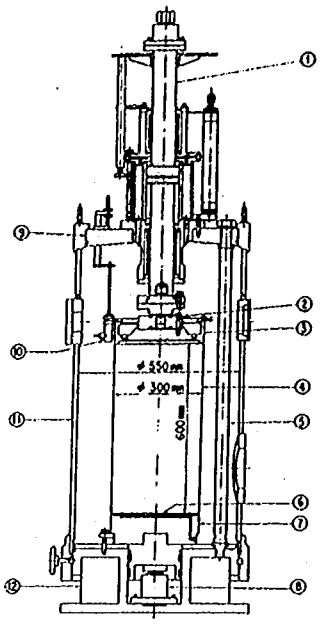


Fig.1 (b) Standard cross section, longitudinal section and location of seismographs for Oya Dam



① loading rod
② load cell for cyclic loading test
③ loading cap
④ specimen
⑤ support
⑥ porous metal disk
⑦ pedestal
⑧ load cell for monotonic loading test
⑨ upper platen
⑩ linear variable differential transformer for displacement
⑪ triaxial cell
⑫ lower platen

Fig.2 Schematic view of large-scale triaxial testing apparatus

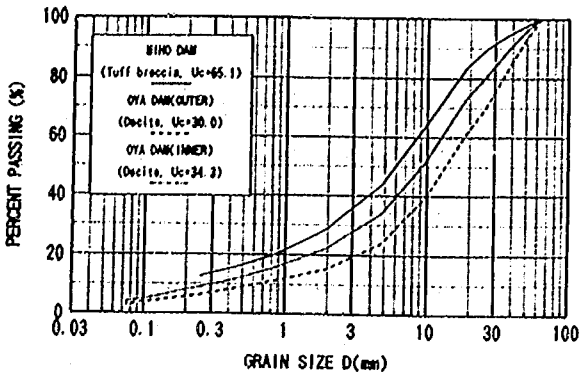


Fig.3 Grain size distribution of rockfill materials for laboratory tests

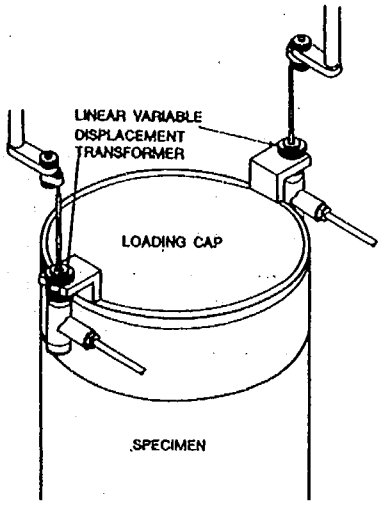


Fig.4 Detail view of linear displacement transformers

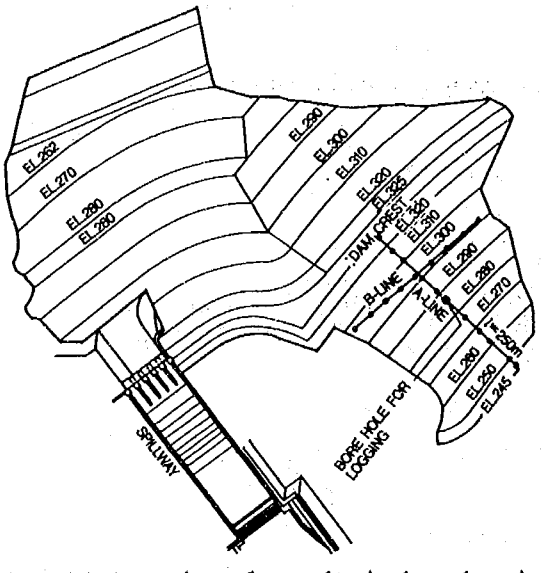


Fig.5 (a) Location of geophysical exploration in Miho Dam

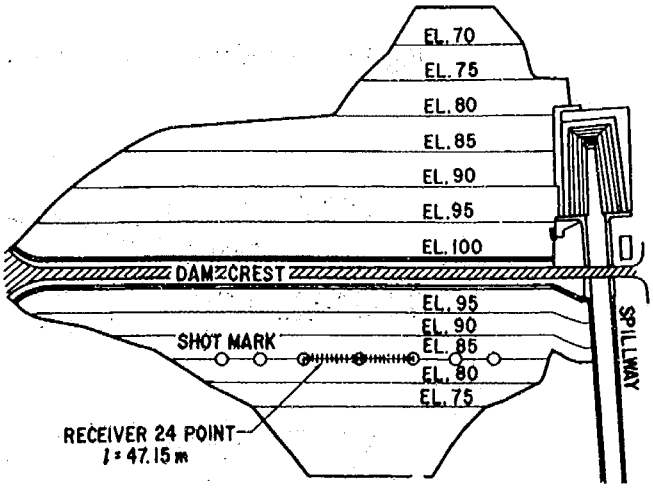


Fig.5 (b) Location of geophysical exploration in Oya Dam

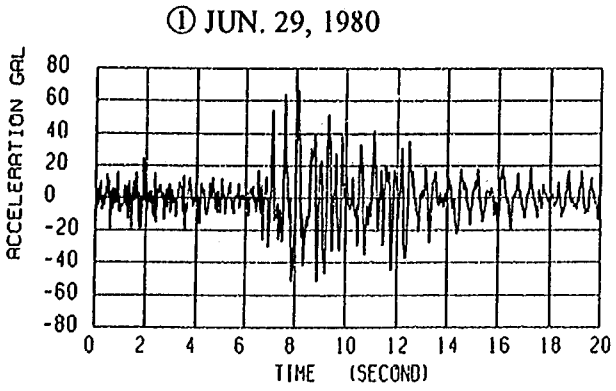


Fig.6 (a) Time history of acceleration observed at the crest of Miho Dam (Upstream-downstream component)

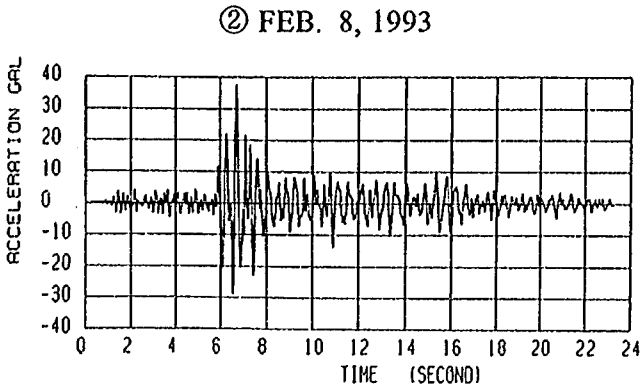


Fig.6 (b) Time history of acceleration observed at the crest of Oya Dam (Upstream-downstream component)

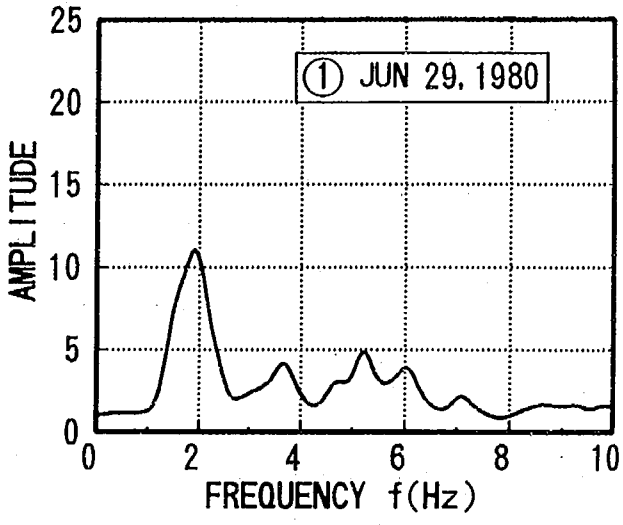


Fig.7 (a) Frequency response function of observed earthquake motion for Miho Dam

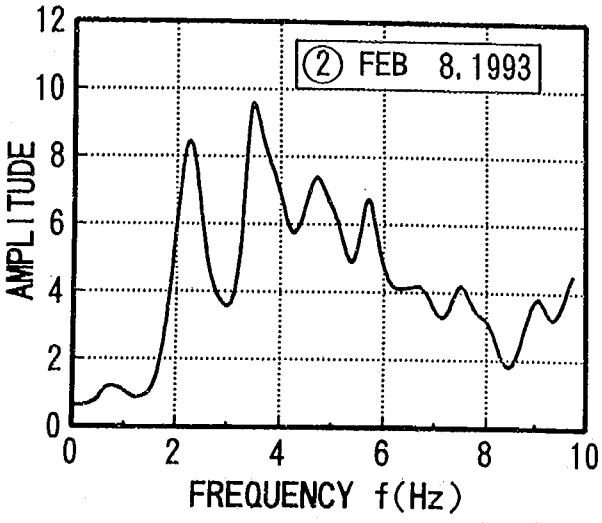


Fig.7 (b) Frequency response function of observed earthquake motion for Oya Dam

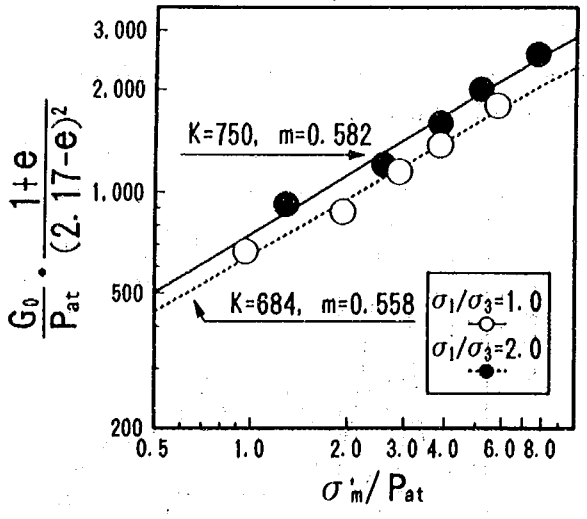


Fig.8 Relationship of $G_0(1+e)/P_{at}(2.17-e)^2$ and σ'_m/P_{at} for rockfill materials of Miho Dam

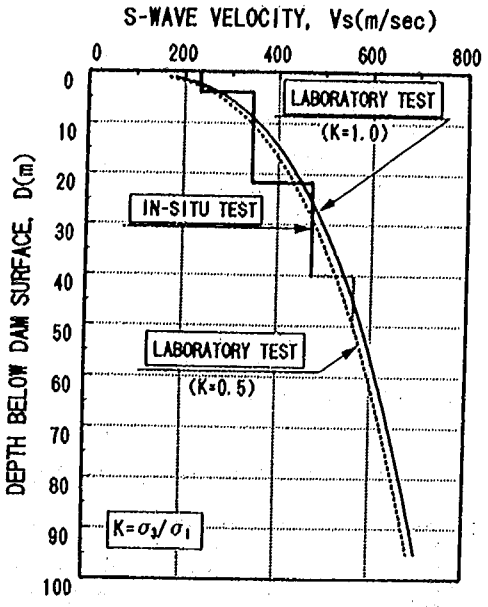


Fig.9 (a) Comparison of S-wave velocity from laboratory test and in-situ geophysical exploration for Miho Dam

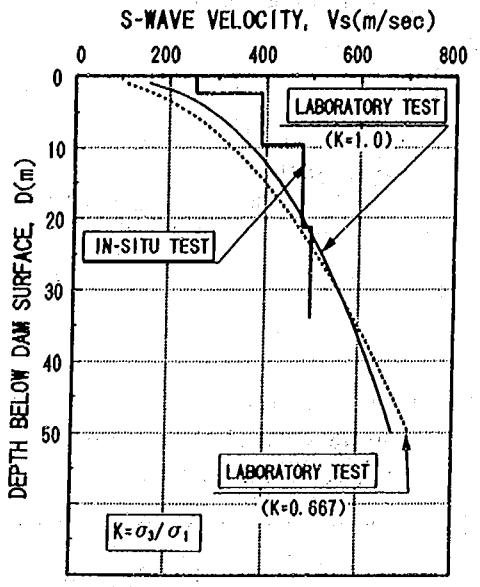


Fig.9 (b) Comparison of S-wave velocity from laboratory test and in-situ geophysical exploration for Oya Dam

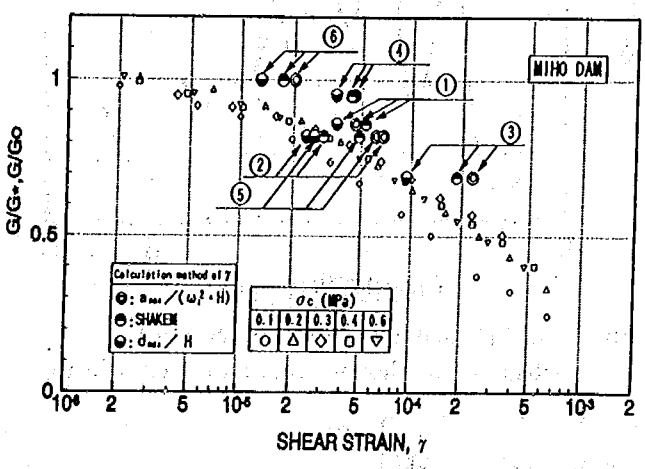


Fig.10 (a) Normalized shear modulus G/G_*, G/G_0 versus shear strain γ relationships for Miho Dam

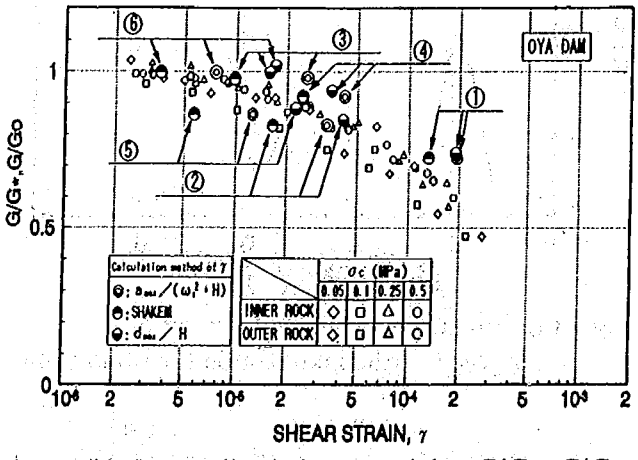


Fig.10 (b) Normalized shear modulus G/G_*, G/G_0 versus shear strain γ relationships for Oya Dam

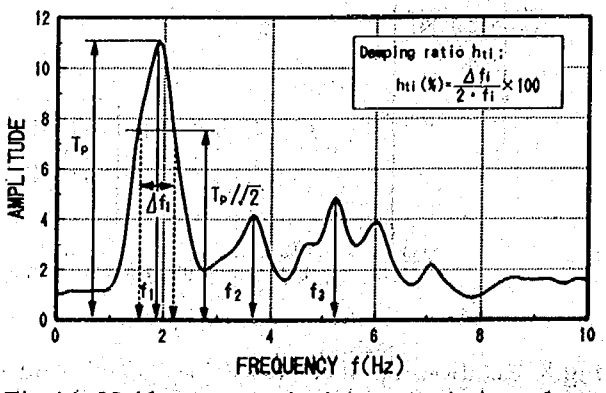


Fig.11 Half power method for calculation of total damping ratio $h_{t,i}$

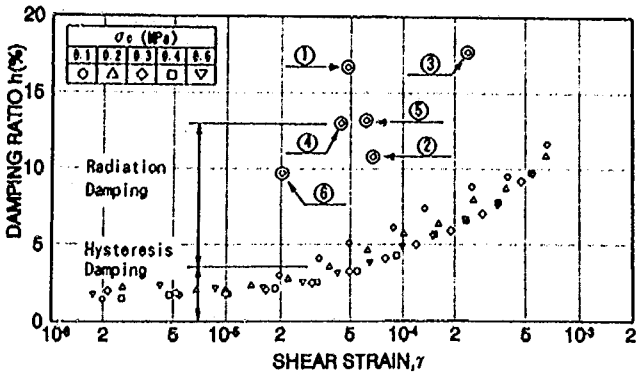


Fig.12 (a) Hysteresis damping ratio obtained by laboratory tests and total damping ratio for the first vibration mode by back analyses of earthquake motions versus shear strain for Miho Dam

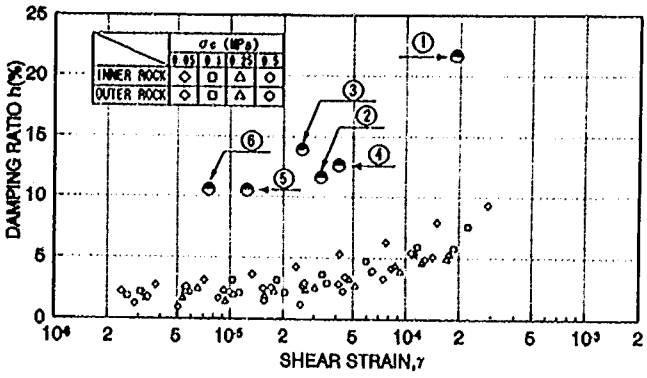


Fig.12 (b) Hysteresis damping ratio obtained by laboratory tests and total damping ratio for the first vibration mode by back analyses of earthquake motions versus shear strain for Oya Dam

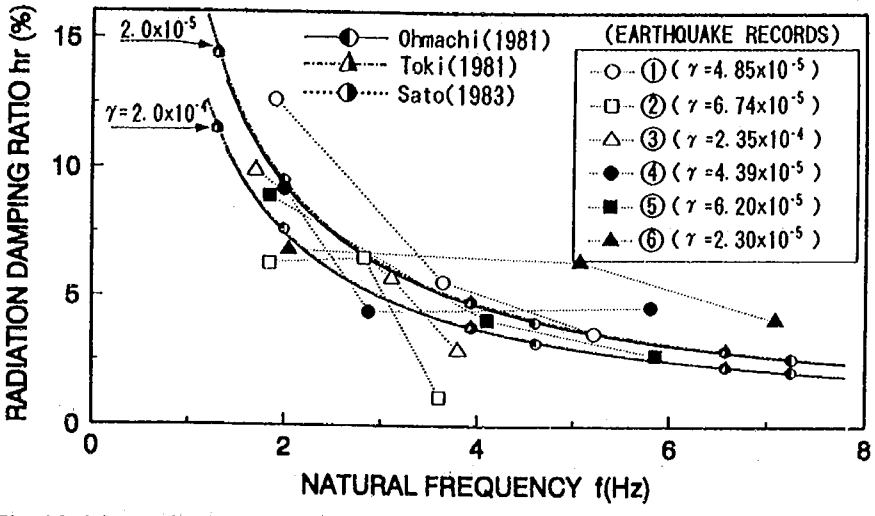


Fig.13 (a) Radiation damping ratio with natural frequency for Miho Dam

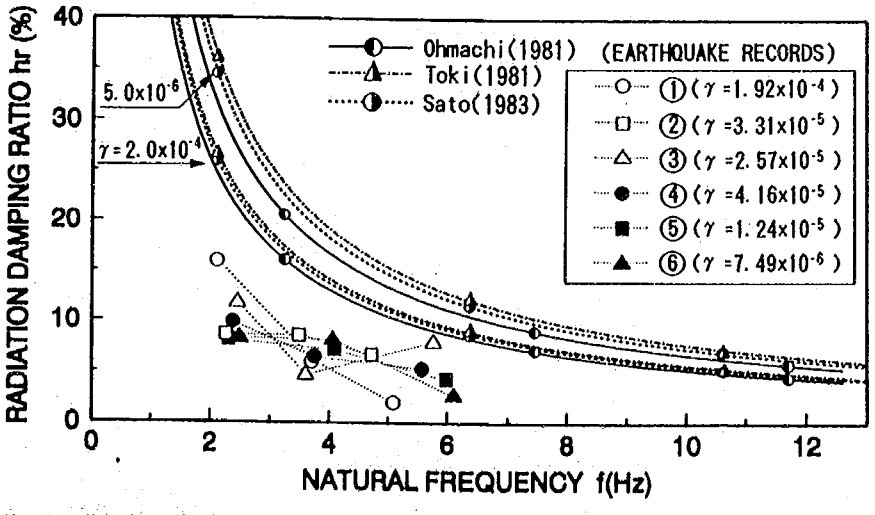


Fig.13 (b) Radiation damping ratio with natural frequency for Oya Dam

Seismic Safety Evaluation of Sanitary Landfills

by

Ellis L. Krinitzsky*
Mary Ellen Hynes*
Arley G. Franklin*

ABSTRACT

Earthquake ground motions at municipal solid waste landfills must be specified according to the level of hazard or criticality of the site along with the type of engineering analysis that is to be performed. The hazard is graded as (1) None to Negligible, (2) Low, (3) Moderate, and (4) Great. For non-critical sites, motions can be obtained from probabilistic maps as part of a non-site specific investigation: for critical sites, a deterministic, site specific evaluation is preferred and motions must be specified appropriately for the type of analysis, whether it is for foundation liquefaction, stability of slopes, integrity of barriers, earth pressures, or the design of appurtenant structures.

1. INTRODUCTION

During the past two decades, geotechnical earthquake engineers have evolved a consensus on a general approach to the evaluation of the stability of embankments under earthquake loading conditions. In broad terms, the approach follows the procedure shown in Figure 1. This approach has very general applicability, extending to sanitary landfills, and engineers working with seismic evaluations of landfills generally consider the specific analytical techniques used in the evaluation of earth structures to be applicable to sanitary landfills. These include conventional slope stability analyses, one-, two-, and three-dimensional dynamic response analyses, Newmark sliding block analyses, and others. However, the properties of the materials in sanitary landfills differ in significant ways from soils, and other characteristics of the "structure" (the landfill) differ in significant ways from conventional embankment or earthfill structures. These differences must be considered in evaluating the propagation of ground motions in the structure as well as the potential modes of failure. The observed performance of sanitary landfills in past earthquakes, considered in the light of observed and measured material properties and other characteristics of landfills, contributes significantly to our understanding of the potential modes of failure.

The seismic evaluation approach shown in Figure 1 is familiar to geotechnical earthquake engineers who deal with seismic effects on dams or other earthfill structures, and need not be elaborated upon in this paper. The paper will instead briefly discuss those characteristics that make the behavior of sanitary landfills differ from that of soil structures, and present the authors' recommendations for seismic hazard assessments at municipal solid waste landfills (MSWL) in accordance with U.S. Federal regulatory requirements for seismic safety (CFR 40, Parts 258.13 to 258.15). Included are methods to obtain earthquake ground motions and to assess earthquake effects on

* U.S. Army Engineer Waterways Experiment Station, Vicksburg, Mississippi 39180

foundations, landfills, liners, cover, gathering systems for leachates and gases, and appurtenant structures.

2. CHARACTERISTICS OF SANITARY LANDFILLS

Composition and Structure

The nature of the waste materials in landfills varies widely in accordance with the source; i.e. industrial wastes of various kinds or the collected wastes of households and small businesses. The composition of household wastes is culture-dependent, but in more industrialized cultures it may be expected to have higher proportions of paper and packaging materials. From samples of 11 U.S. landfills, Rathje (1991) estimates the average composition as:

Type of waste	Average percent
Paper products	50
Organic; includes wood, yard waste, food scraps	13
Plastic	10
Metal	6
Glass	1
Miscellaneous; includes construction and demolition debris, tires, textiles, rubber, disposable diapers	20

In typical U.S. practice, the waste material placed during a working day is covered by a layer of soil at the end of the day, resulting in a cellular structure: discontinuous cells of waste materials separated by continuous cell walls of soil. There may also be membranes of geotextile or impervious plastic for the purposes of improving the strength of the fill or of controlling water movement. This cellular structure is of major significance in the stability of the landfill, since failure surfaces may tend to run through the soil layers along the interfaces of soil or waste with synthetic membranes, or between synthetic components.

The presence of toxic or otherwise hazardous materials in some landfills creates special performance requirements, i.e. preservation of the integrity of barriers to migration or release of those materials.

Decomposition

Because of the usually significant fraction of high-energy organic matter in sanitary landfills, significant biochemical activity is the rule. This results in chemical breakdown of both solid and liquid constituents to liquid and vapor end products. Much of this activity takes place under anaerobic conditions, and methane gas is a common product. Rates of decomposition are highly variable; Chen, et al, (1977) found reported rates of decomposition varying from 0.012 to 0.788/year. However, much of the material, especially the paper products, may endure for surprisingly long times. In some excavated landfills, strata dating to 50 years or more before the present may contain readable newspapers and readily recognizable food items.

Compressibility and Settlement

According to Edil, et al. (1990), the primary mechanisms involved in the settlement in refuse fills are:

1. Mechanical (distortion, bending, crushing, and reorientation; similar to consolidation of organic soils);

2. Ravelling (movement of fines into large voids);

3. Physical-chemical change (corrosion, oxidation and combustion); and

4. Bio-chemical decomposition (fermentation and decay, both aerobic and anaerobic processes).

The authors observed that the rate of settlement was best described by the power creep law:

$$S = H \Delta\sigma m t^n \qquad (1)$$

where
S = settlement
H = initial height of refuse
$\Delta\sigma$ = compressive stress, kPa
m = reference compressibility, 1/kPa
t = time, days
n = rate of compression.

Average values of the empirical parameters m and n obtained from observations of four sites were about 2.5×10^{-5} and 0.65, respectively. Values of m were highly variable, from 7.52×10^{-8} to 1.38×10^{-4}; values of n were less so, varying from 0.264 to 1.17. It has been observed by Edil et al. (1990), and by others, that primary consolidation, i.e. the dissipation of excess pore pressure, is largely complete at the end of placement of the refuse, and that creep dominates the compression behavior afterwards. Chen, et al. (1977) performed consolidation tests on laboratory specimens of saturated milled refuse materials, 2 to 4 inches (5 to 10 cm) in thickness, and found the pore pressure dissipation phase was generally completed in times of one minute or less, and that the settlement thereafter could be described by a creep model.

Density

Density of refuse material varies with composition, depth (overburden pressure), method of placement, and age. Refuse materials experience primary consolidation within the first few days of placement, but continue to settle and densify with time. Decomposition appears to have a negligible effect on density over a period of several decades. Measurements of density have been made from large-scale excavations in landfills, attempts at obtaining undisturbed samples from drill holes, and from laboratory consolidation tests used to simulate in situ materials and stresses. Landva and Clark (1990) developed a procedure for estimating the in situ unit weight of refuse based on the average unit weights of the constituents and the results of consolidation tests. Figure 2 shows recommended values of density for refuse as a function of depth from Kavazanjian et al. (1995) and Landva (1994). Although variation in density typically has little effect on the response of level ground sites and embankments, the dramatic variation in density for landfills has a distinct effect on dynamic response and is important to account for if a dynamic analysis is performed.

Shear Strength

The shear strength of landfill materials is difficult to measure since large-scale testing facilities are needed to accommodate a reasonable sample of the refuse and testing of actual refuse material may require special safety measures. The shear strength of refuse in landfills has been estimated by means such as back-calculation of stable landfill slopes (Kavazanjian et al. 1995), loading of fills in situ (Pagotto and Rimoldi 1987; Richardson and Reynolds 1991), and large-scale laboratory testing of refuse

(Landva and Clark 1990, Landva 1994). Figure 3 shows a recommended shear strength for municipal solid waste materials based on these data: c= 24kPa for normal stresses less than 25 kPa and c= 5kPa with ϕ=33 degrees for normal stresses greater than 25kPa. Landva (1994) recommends a lower range of c = 0 and ϕ = 33 degrees based on direct shear tests. In the field, large landfill slopes are stable at slopes as steep as 1.2:1 to about 2:1, indicating strengths of at least c = 5 kPa and ϕ = 28 degrees (Kavazanjian et al. 1995).

Dynamic Response

The dynamic response of a landfill depends on the nature of the incoming motions, landfill geometry, foundation conditions, stratigraphy or internal structure, density distribution, internal fluid pressures, moduli distribution, and moduli degradation with cyclic loading. This section focuses on in situ measurement of shear wave velocities for moduli estimation and back-calculation of modulus degradation from actual strong motion instrument recordings at a landfill.

Shear Wave Velocity. In situ measurement of shear wave velocities have been made using surface (spectral analysis of surface waves, seismic refraction) and/or subsurface techniques (down-hole, cross-hole, OYO in-hole) at several landfills as shown in Figure 4 (after Kavazanjian et al. 1995). These data indicate that shear wave velocities increase significantly with depth, by a factor of about two over a depth of 100 ft (30m).

Modulus Degradation and Damping. Only one landfill in the United States has been instrumented with strong motion recording equipment, namely the Operating Industries, Inc. (OII) landfill located in Monterey Park, California. The OII landfill is a significant structure, with fill heights of greater than 250 ft (76 m), total area of more than 1 square mile (2600 m^2) and slopes of about 2H:1V. Several recordings of earthquakes have been made with the instruments at OII. The 1994 Northridge, California Earthquake produced the largest motions yet recorded at the site. These recordings have been used to estimate modulus reduction and damping curves to use in equivalent linear dynamic response analyses. The results of back-calculations by Kavazanjian et al. (1995) indicate that the modulus reduction and damping curves for a refuse fill are similar to those for sand.

Performance of Landfills in Past Earthquakes

Anderson and Kavazanjian (1995) summarized observations from field inspections of landfills following three recent California earthquakes: the 1987 M 6.1 Whittier Narrows event, the 1989 M 7.1 Loma Prieta event, and the 1994 M 6.7 Northridge event. For the latter two earthquakes there is an abundance of data on landfill performance, since the earthquakes affected a wide area and numerous landfills were subjected to moderate to severe shaking.

In the Whittier Narrows earthquake, six landfills are known to have been subjected to estimated ground motions in the range of 0.10 to 0.30 g. The OII landfill was located only 4 km from the epicenter, and underwent an estimated free-field PGA of 0.30 g. Following the earthquake, some ground cracking in cover soils was reported at the OII landfill. No damage was reported from any of the others. At three of them, however, there were no post-earthquake inspections reported.

Following the 1989 Loma Prieta earthquake, there were reports of inspections of at least 17 landfills. One of these was 75 m high and subjected to an estimated PGA of 0.5 g. Others up to 45 m high experienced shaking with PGA's from 0.04 to 0.5 g. Only minor damage was reported, consisting typically of cracks 25 to 75 mm wide, occurring mostly at transition zones and at contacts between different materials, e.g. solid waste and natural ground. At one site, minor downslope movement of cover soils was noted.

Reports of investigations of 22 landfills are available following the 1994 Northridge earthquake. Of these, 16 were reported to have experienced motions exceeding 0.24 g (free-field PGA at base), and 6 to have experienced motions exceeding 0.38 g. The most severe damage reported was at the Chiquita Canyon landfill, 26 km from the epicenter, where the PGA was estimated to have been 0.39 g. Two tears were found in geomembrane liners, one 23 m long and one 3 m long. There was also cracking of cover soils, but no disruption of underlying impervious soil liners. In 17 cases the damage was categorized as minor or none. Where damage occurred, it typically consisted of superficial brittle cracking of cover soils and damage to gas recovery systems, including loss of power and breakage of gas and condensate lines and well heads. In all cases, the systems were back in operation within 24 hours.

3. SEISMIC HAZARDS

Seismically-Induced Permanent Displacement

As discussed above, the waste materials in sanitary landfills in general have relatively high shear strength, and experiences of landfills during past earthquakes have not produced any reports of large-scale movement or sliding in the landfill materials themselves. The most serious concern appears to be cracking of liner systems and covers and damage to appurtenances such as gas collection systems. Relatively small movements can pose a threat to the integrity of these systems. According to Anderson and Kavazanjian (1995) permanent displacements of 10 to 30 cm can be tolerated before these threats become serious.

Earthquake engineers generally accept the use of the Newmark sliding block analysis to estimate the potential permanent displacement in an embankment where there is no liquefaction threat. Description of the method, and computed displacements for over three hundred earthquake strong-motion time histories, are given by Franklin and Chang (1977) and Hynes-Griffin and Franklin (1984).

Hynes-Griffin and Franklin used a criterion of 1 m as an upper bound of permanent displacement in earth embankments to arrive at a recommendation for the use of a pseudostatic stability analysis with a seismic coefficient of one-half of the peak base acceleration, and a limiting factor of safety of unity, as a conservative screening method for permanent displacements. The authors have applied similar reasoning to sliding on deep surfaces in landfills, with the following modifications: (1) the mean $+\sigma$ curve for displacements (Hynes-Griffin and Franklin, 1984) is used, rather than the upper bound for all records analyzed; (2) the amplification factor for ground motions propagated into the embankment is graded from upper bound to mean values (Hynes-Griffin and Franklin 1984) as the base motions increase; and (3) a displacement limit of 1 foot (30 cm) is used. This analysis indicates that a pseudostatic analysis with a seismic coefficient of 0.2 $\times$ PGA

+ 0.1 g, with a factor of safety of unity, is suitable for screening against permanent displacement for a deep-seated failure surface. Displacement analyses using a Makdisi and Seed (1978) approach also support a screening seismic coefficient of 0.2 × PGA + 0.1 g for deep-seated surfaces.

This analysis also indicates that if the static factor of safety against slope instability is at least 1.5, then this mode of failure is not of concern for ground motions less than 0.15 to 0.20 g. But considering other mechanisms of seismically induced deformation or settlement leads us to believe a range of 0.10 to 0.15 g is prudent as a threshold below which analysis is not needed.

For permanent displacements near the crest of a landfill involving cover materials, simplified Newmark sliding block analyses either by the Hynes-Griffin and Franklin (1984) approach or by the Makdisi and Seed (1978) approach indicate damaging levels of displacement may occur at low levels of ground motion, ≤ 0.1 g. We believe that cover materials should either be designed so that they can easily be repaired or special features will need to be designed into the cover systems to increase yield acceleration values.

Liquefaction in Foundation Soils

The fibrous materials that dominate in municipal landfills are not themselves susceptible to liquefaction. However, a susceptibility to liquefaction in foundation soils can have a dangerous potential for inducing differential displacement in a landfill. Evaluation of this hazard is discussed in detail by Koester and Franklin (1985) and Carter and Seed (1988).

Fault-Induced Permanent Displacement

MSWL units should not, and under U.S. federal regulations may not, be located within 200 feet (60 meters) of an active fault, i.e. one evidencing Holocene displacement, unless the fault can be proven not to present a threat. The concern is that a fault movement beneath a landfill can result in a permanent displacement for which the fill was not designed. An active fault is considered to be one that is likely to move again with or without an earthquake. Movement will be either along an identifiable trace or within a zone in which fault movement has occurred in the past.

Existing landfills may not have been evaluated for fault hazards. Reexamination of a site should include potentials for fault movement and the extent to which damages may occur.

Karst Instability

In areas where the bedrock is limestone or other soluble rock, sudden collapse of the ground into solution cavities can pose a special hazard. Such collapses are known to have taken place as a result of earthquake shaking. Not only would they be a cause of displacements in fills, but they are invariably connected with groundwater aquifers and pose a threat of contamination.

Activation from Mining, Fluid Extraction, etc.

Similar to the problems with karst, the presence of man-made cavities from mining or other activities may destabilize the foundation of a landfill. Extractions of fluids such as groundwater or petroleum also may cause differential settlements. Fluid extraction has an effect of causing shallow

non-seismic activation of movement along existing fault planes.

Susceptibility to Landslides, Avalanches, and Debris Flows

Landfills often are situated in rugged terrain that is unsuited to other uses. Such areas may be prone to having landslides, avalanches, land slips, and mud flows or debris flows.

The above hazards need to be assessed as part of the general geological evaluation to assure stability at a landfill site. In some cases they can be done routinely, simply by noting their absence as threats to a site. For others, there are no generally accepted procedures. At potentially hazardous sites the investigation should be done in a way that is defensible for each set of circumstances.

4. CLASSIFICATION AND RECOMMENDATIONS FOR ANALYSIS

Seismicity

Federal regulatory guidance (CFR 40, Part 258.14) provides for two methods of investigation of the potential ground motions at the site: The first, which may be termed a non-site-specific evaluation, uses a seismic hazard map (Algermissen, et al. 1990) showing mean values of acceleration on rock with a 90 percent probability of non-exceedance in 250 years.

The 250-year map cannot be site-specific because it must generalize information that is both unevenly distributed and of greatly uneven quality. Microzoning for sensitive local conditions is mostly neglected. Motions assigned very often are effective motions, those that eliminate peak values judged to have the smallest likelihood of being experienced. Effective motions attempt, sometimes crudely, to reduce costs in construction for earthquakes that are uncertain. A critical landfill in an area of seismic threat needs a site-specific evaluation that is tightly focused on conditions pertinent to the local environs.

The second method permits an investigator to perform an analysis by which the maximum expected horizontal acceleration is obtained based on a site-specific seismic evaluation. A site-specific evaluation requires a geological-seismological study that starts at the beginning, reviews all relevant data, defines the earthquake source areas that are meaningful for the site, assigns magnitudes, attenuations, etc., and makes an independent designation of site-specific ground motions. In general, site-specific evaluations may be done by either deterministic or probabilistic methods. At a critical site, the design should accommodate the worst that can reasonably be expected regardless of when it may happen; probability should not be a determining consideration.

A site-specific evaluation may indicate several earthquake sources that can affect a site. Each significant source should be analyzed with its own suite of accelerograms.

In both cases, a Design Level Earthquake (DLE), or earthquakes, are assigned. The DLE may be a mean value or a mean $+\sigma$ value depending on the severity of the hazard and the type of engineering analysis, as indicated in Tables 1 and 2.

Levels of Criticality

The level of criticality of a site determines the minimum extent of investigation that the site requires, whereas economic

considerations normally tend to drive us toward minimizing the investigative effort. We thus focus on the minimum levels of investigation required and the minimum threshold values of ground motion that would trigger the requirement for various kinds of investigations. However, the level of criticality is often a subjective judgment. We approach the issue by asking the question, what are the consequences of failure? If they are intolerable, then the site is a critical one. If they are tolerable, then the site is not critical. At non-critical sites, the consequences of failure will be essentially eeonomic losses, which could range from inconsequential to heavy.

Grade of Seismic Hazard

The U.S. federal regulatory guidance (CFR 40, Part 258.15) requires that potential instabilities in the foundation of the landfill, or that of adjacent areas from which the landfill might be affected, be evaluated. The landfill must be shown to present no hazard from instability at the site, or is adequately protected against whatever instability may exist. The hazards can include unstable foundation soils, nearby landslides or other mass movement, weakness from underlying karst, differential displacement from fluid extraction, collapse in mines or from other underlying cavities, or whatever else may be a source of potential instability at the site.

The guidance (CFR 40, Part 258.14) establishes a basic threshold at which an investigation is mandated: this corresponds to a 90 percent probability that a ground motion of 0.10g will not be exceeded in 250 years. The extent of the investigation that is appropriate needs to be determined by the grade level of the seismic threat.

The potential hazards to the environment and to people due to the presence of MSWL can be highly variable. The possible effects depend on the geometry of the fill and its susceptibility to deformation; the presence of toxic substances, with problems of fluid leakage and emission of gases; danger to the environment due to contamination of groundwater, surface waters, etc; direct threats to populations, and danger to lifelines, transportation, and other essential facilities.

Four grades of seismic hazard are used: (1) None to negligible, (2) Low, (3) Moderate, and (4) Great. Assigning a grade to the seismic hazard is essentially subjective, but it involves consideration of the site seismicity, the criticality of the site, and the potential for loss or injury, including economic losses at non-critical sites. Grading these factors can be either straightforward or highly subjective. Grading needs to be done on a site-specific basis. There are no rules.

Table 1 presents ranges of the grade of seismic hazard associated with the type of threat, or problem, and the criticality of the site. Table 2 gives an approximate relationship between the nature of the hazard and the grade levels of Table 1, and acceleration thresholds and corresponding seismic evaluations that are appropriate for each grade.

The levels of grade discrimination in Table 2 are categorized by whether a site is critical or non-critical. A non-critical site may be evaluated using seismic probability maps in a non-site specific appraisal, provided there is no susceptibility to liquefaction. A critical site requires a site specific evaluation and one should be guided by thresholds of earthquake ground motion that are appropriate for the kind of engineering

analysis being considered. A site that is susceptible to liquefaction, though it is otherwise non-critical, may in some cases require a site specific evaluation. The general rule is that for critical sites the requirements for analysis and design are governed by considerations of public safety; for non-critical sites economic considerations generally govern, and one must balance the present costs of investigations, analysis and earthquake-resistant design against the potential future losses due to earthquake damage.

Pseudostatic Analyses

Earthquake ground motions appropriate for various categories of use in pseudostatic analyses are shown in Table 3. These are based on criticality of the landfill and the seismicity level of the area. The analyses are for stability of slopes, permanent deformations and integrity of soil or membrane barriers, earth pressures on retaining walls, and structures of concrete and/or steel frame. The indicated motions, unless otherwise designated, are intended for use as seismic coefficients. As indicated in Table 3, pseudostatic analyses are not suitable for analysis of foundation liquefaction and are not suitable for motions greater than 0.40 g. Similarly, they are not suitable for analysis of slopes, soil barriers, or earth pressures where the soils involved may be susceptible to liquefaction.

Dynamic Analyses

Earthquake ground motions for use in dynamic analyses are shown in Table 4. This type of analysis is indicated for a critical landfill in an area of moderate to strong seismicity. A threshold acceleration of 0.15 g (mean + σ) on rock is appropriate to analyze deep-seated sliding or deformation. Susceptibility to liquefaction, in any area, requires a threshold for motions as low as 0.05 g on rock. These motions serve as parameters for shaping time histories to provide cyclic shaking for use in the dynamic analyses. The parameters are also levels for entrance into response spectra.

5. CONCLUSIONS

The level of sensitivity to seismic hazard, based subjectively on dangers to people and the environment, is graded as (1) None to Negligible, (2) Low, (3) Moderate, and (4) Great. These are based on considerations of seismicity, the potential consequences of earthquake damage, and whether the site is considered to be Critical or Non-critical. A non-critical site may appropriately be evaluated with a non-site specific study based on ground motions obtained from probabilistic maps and may require an engineering analysis only if there is a liquefaction threat or if the potential economic losses justify it. A critical site in an earthquake-prone area requires site specific earthquake ground motions. Levels of ground motion suitable for various types of engineering analysis, and thresholds calling for their use, are recommended for analysis of foundation liquefaction, stability of slopes, permanent displacements and integrity of barriers, earth pressures, and appurtenant structures.

6. ACKNOWLEDGEMENTS

The studies described, unless otherwise noted, were conducted under research programs of the United States Army Corps of Engineers. Permission was granted by the Chief of Engineers to publish this information. Opinions and recommendations presented in this paper are those of the authors, and do not represent official positions of the Corps of Engineers.

7. REFERENCES

Algermissen, S.T., Perkins, D.M., Thenhaus, P.C., Hanson, S.L., and Bender, B.L. 1990. Probabilistic Earthquake Acceleration and Velocity Maps for the United States and Puerto Rico, U.S. Geological Survey Miscellaneous Field Studies Map MF-2120, 2 sheets, Washington, D.C.

Anderson, D.G. and Kavazanjian, E., Jr. 1995. "Performance of Landfills Under Seismic Loading," Proceedings, Third International Conference on Recent Advances in Geotechnical Earthquake Engineering and Soil Dynamics, Rolla, MO.

Carter, David P. and Seed, H. Bolton 1988. "Liquefaction Potential of Sand Deposit Under Low Levels of Excitation," Report No. UCB/EERC-88/11, University of California at Berkeley.

Chen, W.H., Zimmerman, R.E., and Franklin, A.G. 1977. "Time Settlement Characteristics of Milled Urban Refuse," Proceedings, ASCE Conference on Geotechnical Practice for Disposal of Solid Waste Materials, Ann Arbor, MI, pp. 136-152.

Code of Federal Regulations (CFR) 40, Parts 258.13 to 258.15, Revised as of July 1, 1993. Federal Register, Washington, D.C.

Edil, T.B., Ranguette, V.J., and Wuellner, W.W. 1990. "Settlement of Municipal Refuse," Geotechnics of Waste Fills - Theory and Practice, ASTM STP 1070, Philadelphia, PA, pp. 225-239.

Franklin, A.G. and Chang, F.K. 1977. "Earthquake Resistance of Earth and Rock-Fill Dams; Permanent Displacements of Earth Embankments by Newmark Sliding Block Analysis," Miscellaneous Paper S-71-17, Report 5, U.S. Army Engineer Waterways Experiment Station, Vicksburg, MS.

Harder, L.F., Jr. 1991. "Performance of Earth Dams During the Loma Prieta Earthquake," Proceedings, Second International Conference on Recent Advances in Geotechnical Earthquake Engineering and Soil Dynamics, Vol. II, Shamsher Prakash, ed., Rolla, MO, pp. 1613-1629.

Hynes-Griffin, Mary E. and Franklin, Arley G. 1984. "Rationalizing the Seismic Coefficient Method," Miscellaneous Paper GL-84-13, U.S. Army Engineer Waterways Experiment Station, Vicksburg, MS.

Kavazanjian, Edward Jr., and Matasovic, Neven 1995. "Seismic Analysis of Solid Waste Landfills," Geoenvironment 2000, v. 2, ASCE Geotechnical Special Publication No. 46, pp 1066-1080.

Kavazanjian, Edward Jr.; Matasovic, Neven; Bonaparte, Rudolph; Schmertmann, Gary R. 1995. "Evaluation of MSW Properties for Seismic Analysis," Geoenvironment 2000, v. 2, ASCE Geotechnical Special Publication No. 46, pp. 1126-1141.

Koester, J.P. and Franklin, A.G. 1985. "Current Methodologies for Assessing the Potential for Earthquake-Induced Liquefaction in Soils," Report No. NUREG/CR-4430, U.S. Nuclear Regulatory Commission, Washington, D.C.

Landva, A. O. 1994. Personal Communication.

Landva, A. O. and Clark, J. I. 1990. "Geotechnics of Waste Fill," Geotechnics of Waste Fill - Theory and Practice, STP 1070, ASTM, Philadelphia, PA.

Makdisi, F.I., and Seed, H.B., 1978. "Simplified Procedure for Estimating Dam and Embankment Earthquake Induced Deformations," Journal of the Geotechnical Engineering Division, ASCE, Vol. 104, No. GT7, pp. 849-867.

Pagotto, A., and Rimoldi, P. 1987. "Design and Construction of a Geogrid Reinforced Embankment Over Waste Material," Proceedings of Geosynthetics '87, New Orleans, LA.

Table 1. Relation of Landfill Problem to Grade of Seismic Hazard

Landfill Problem	Grade of Seismic Hazard*	
	Non-Critical**	Critical***
A. Geometry susceptible to deformation	1,2,3	3,4
B. Presence of toxic substances	1,2	3,4
C. Danger to the environment, ground water, other	1,2	3,4
D. Danger to population	1,2	3,4
E. Danger to lifelines, transportation, other	1,2,3	3,4

* 1 = None to negligible
2 = Low
3 = Moderate
4 = Great

** Consequences of failure are tolerable. Damage readily repaired.

*** Consequences of failure are intolerable.

Table 2. Grade of Seismic Hazard with Threshold Acceleration and Corresponding Engineering Analysis

Grade of Seismic Hazard	Seismic Impact Zone CFR 40, Part 258.14	Initial Earthquake Hazard Evaluation	Type of Hazard	Threshold for PHA on rock and Corresponding Analysis Method
1 (None to Negligible)	≥0.10g Mean horizontal motion on rock. 250 year, 90% probability of nonexceedance.	Non-site specific: 250-yr probability map*, 90% probability of nonexceedance. Check against deterministic information for worst-case scenario.	≥0.10 g Potential losses inconsequential	No analysis.
2 (Low)				
3 (Moderate)		Non-site specific: 250-yr probability map. Compare deterministic worst case. Perform geological reconnaissance. Site specific: If site is susceptible to liquefaction, critical, or potential serious economic losses.	a. Foundation materials susceptible to liquefaction. b. Possible damage to liner, cover, or gathering system for leachates or gases. Possible deformation within the landfill.	a. For liquefaction: ≥0.05g to 0.10g (mean + σ); Perform dynamic analysis. b. For deep-seated sliding and deformation: (1) ≥0.10g to 0.15 g (mean + σ); Perform pseudostatic analysis. (2) ≥0.15g (mean + σ); Perform dynamic analysis.
4 (Great)		Site specific: Deterministic investigation: Locate earthquake sources, assign maximum credible earthquakes for each source, attenuate motions to the site, specify free field motions for the site, select analogous time histories for excitation at the site.		

* Algermissen, et al. 1990.

Table 3. Earthquake Ground Motions for Use in Pseudostatic Analyses

	Foundation Liquefaction	Stability of Slopes and Integrity of Barriers	Earth Pressures	Concrete and/or Steel Frame Structures
• Non-critical landfill in any zone of seismic activity. • Critical landfill in an area of low seismicity (Mean + σ PHA <0.15g) • Obtain Design Level Earthquake(s) (DLEs)	Pseudostatic analyses do not apply. Use dynamic analyses.	• Use 0.2 × PHA + 0.1g as seismic coefficient, F.S. ≥1.0. • PHA is obtained from (mean)* values: (a) MM intensity (b) Magnitude-distance attenuation (c) 250-yr, 90% probability of nonexceedance.	• PHA from (mean)* values: (a) MM intensity (b) Magnitude-distance attenuation (c) 250-yr, 90% probability of nonexceedance. • Use 1/2 PHA for backfill.	• Seismic-zone coefficients/factors in building codes • For generating ratio of PHA to A of structure or element, PHA is obtained from (mean)* values: (a) MM intensity (b) Magnitude-distance attenuation (c) 250-yr, 90% probability of nonexceedance.
• Critical landfill in an area of moderate to strong seismicity (Mean + σ PHA ≥0.15g ≤0.40g) • Obtain Design Level Earthquake(s) (DLEs)	Use dynamic analyses.	• Use 0.2 × PHA +0.1g as seismic coefficient, F.S. ≥1.0. • PHA from (mean + σ)* values: (a) MM intensity (b) Magnitude-distance attenuation (c) 250-yr, 90% probability of nonexceedance.	• PHA from (mean + σ)* values: (a) MM intensity (b) Magnitude-distance attenuation (c) 250-yr, 90% probability of nonexceedance. • Use 3/4 PHA for backfill.	• Seismic-zone coefficients/factors in building codes. • PHA from (mean + σ)* values: (a) MM intensity (b) Magnitude-distance attenuation (c) 250-yr, 90% probability of nonexceedance.

* Adjust if necessary for site condition; shallow plate boundary, deep subduction zone, or intraplate area; near field or far field; effective motions when near an earthquake source.

Note: PHA is the free-field Peak Horizontal Acceleration.

Table 4. Earthquake Ground Motions for Use in Dynamic Analyses

	Foundation Liquefaction	Stability of Slopes and Integrity of Barriers	Earth Pressures	Concrete and/or Steel Frame Structures
• Critical landfill in an area of moderate to strong seismicity for sliding and deformation: PHA $\geq$0.15g (mean + σ) for liquefaction in any area: PHA >0.05g (mean + σ) • Obtain Design Level Earthquake(s) (DLEs)	• Peak horizontal motions (mean + σ) • Generate time histories	• Peak horizontal motions (mean + σ)* • Generate time histories.	• Peak horizontal motions (mean + σ)* • Generate time histories.	• Peak horizontal motions (mean + σ)* • Generate time histories. • Obtain response spectra for above time histories. • Alternatively, go directly to response spectra, entering with the above peak motions. • Check response with either frequency or time domain analyses.

* Obtain peak horizontal motions from (a) MM intensity or (b) magnitude-distance attenuation charts. Adjust for site condition; shallow plate boundary, deep subduction zone, or intraplate area; near field or far field effective motions when near an earthquake source.

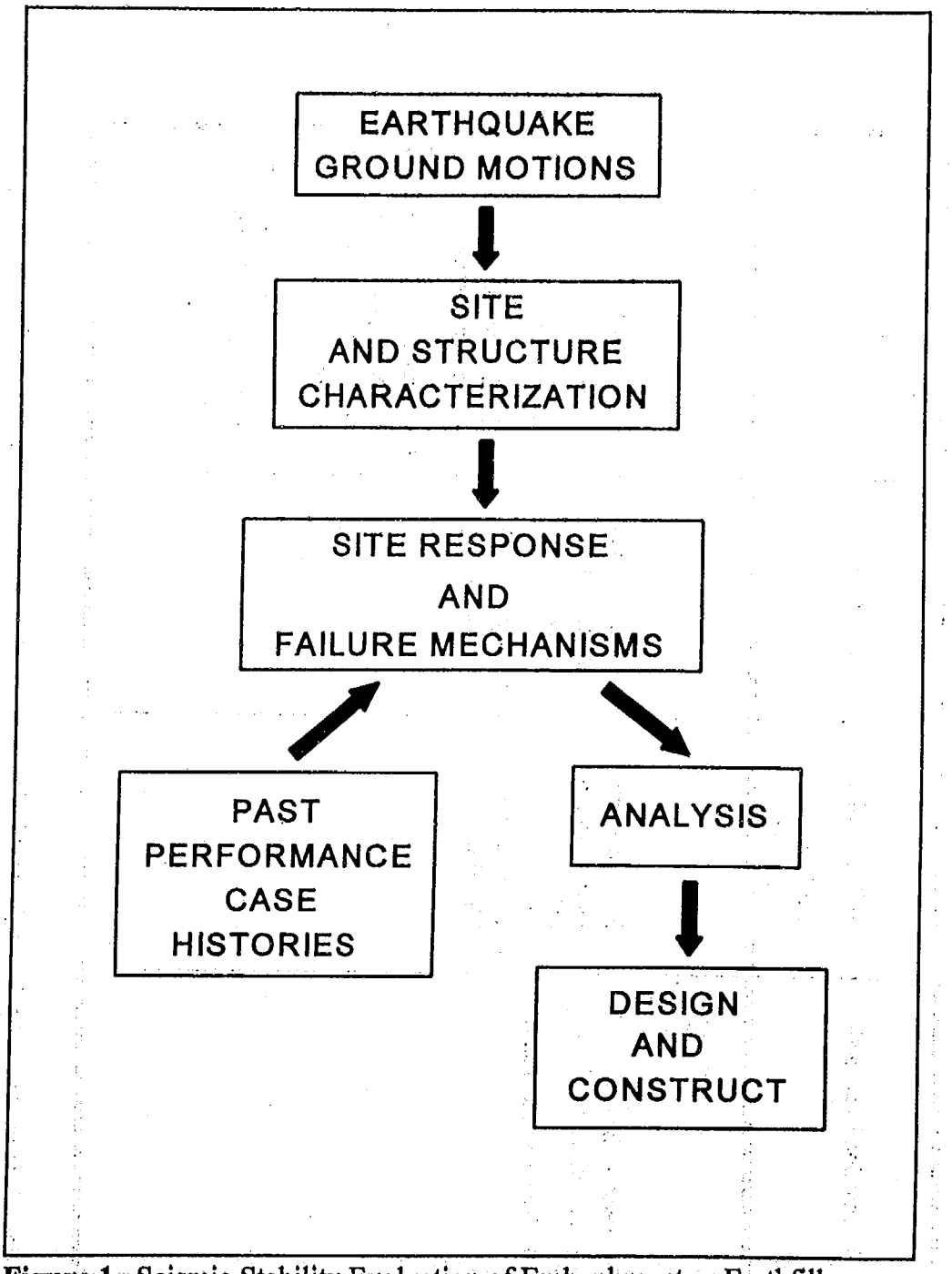


Figure 1. Seismic Stability Evaluation of Embankment or Earthfill Structures

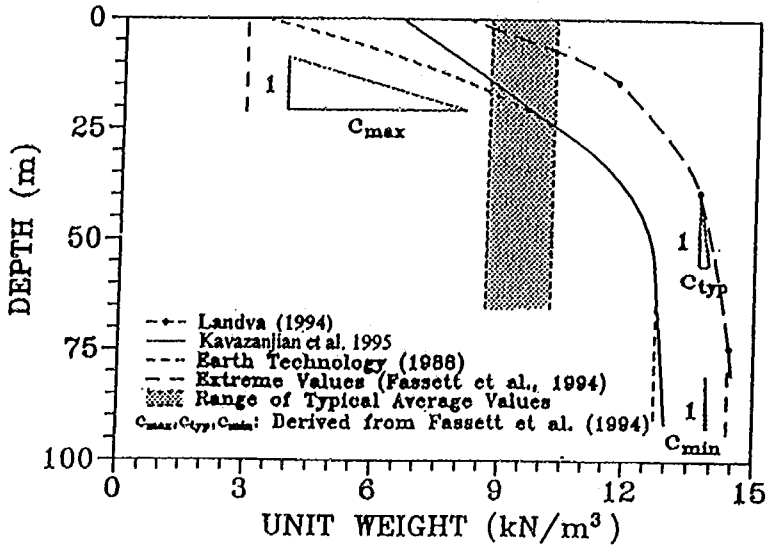


Figure 2. Refuse densities (after Kavazanjian et al. 1995, and Landva 1994)

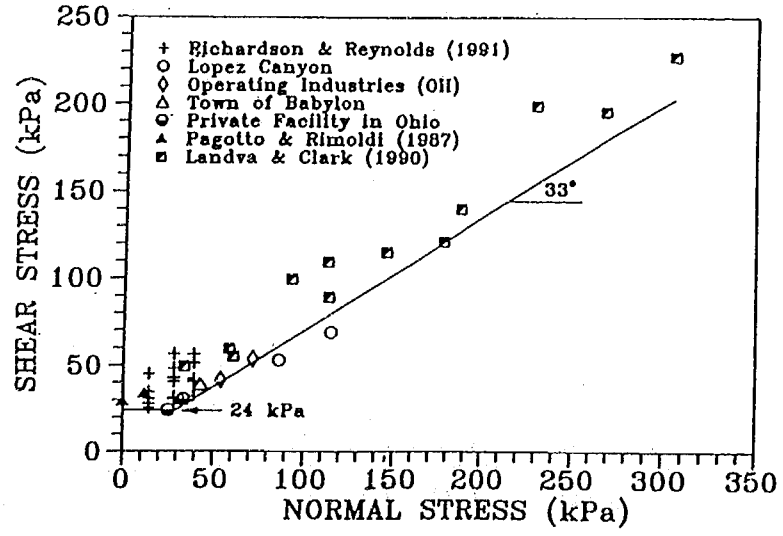


Figure 3. Refuse shear strength (after Kavazanjian et al. 1995)

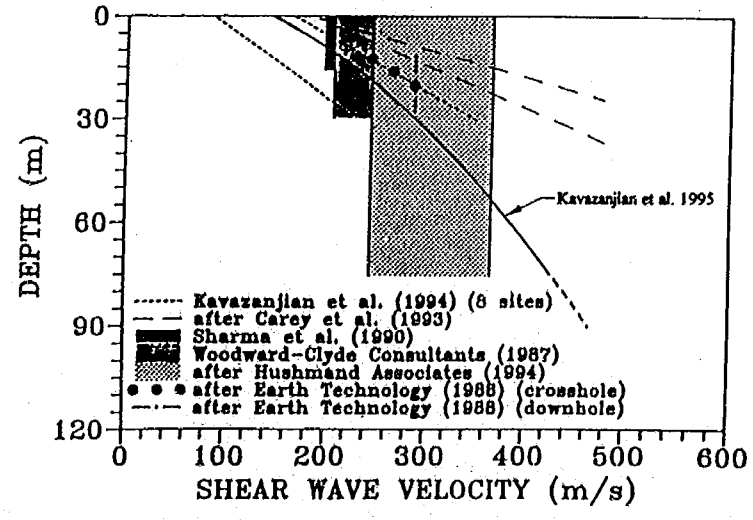
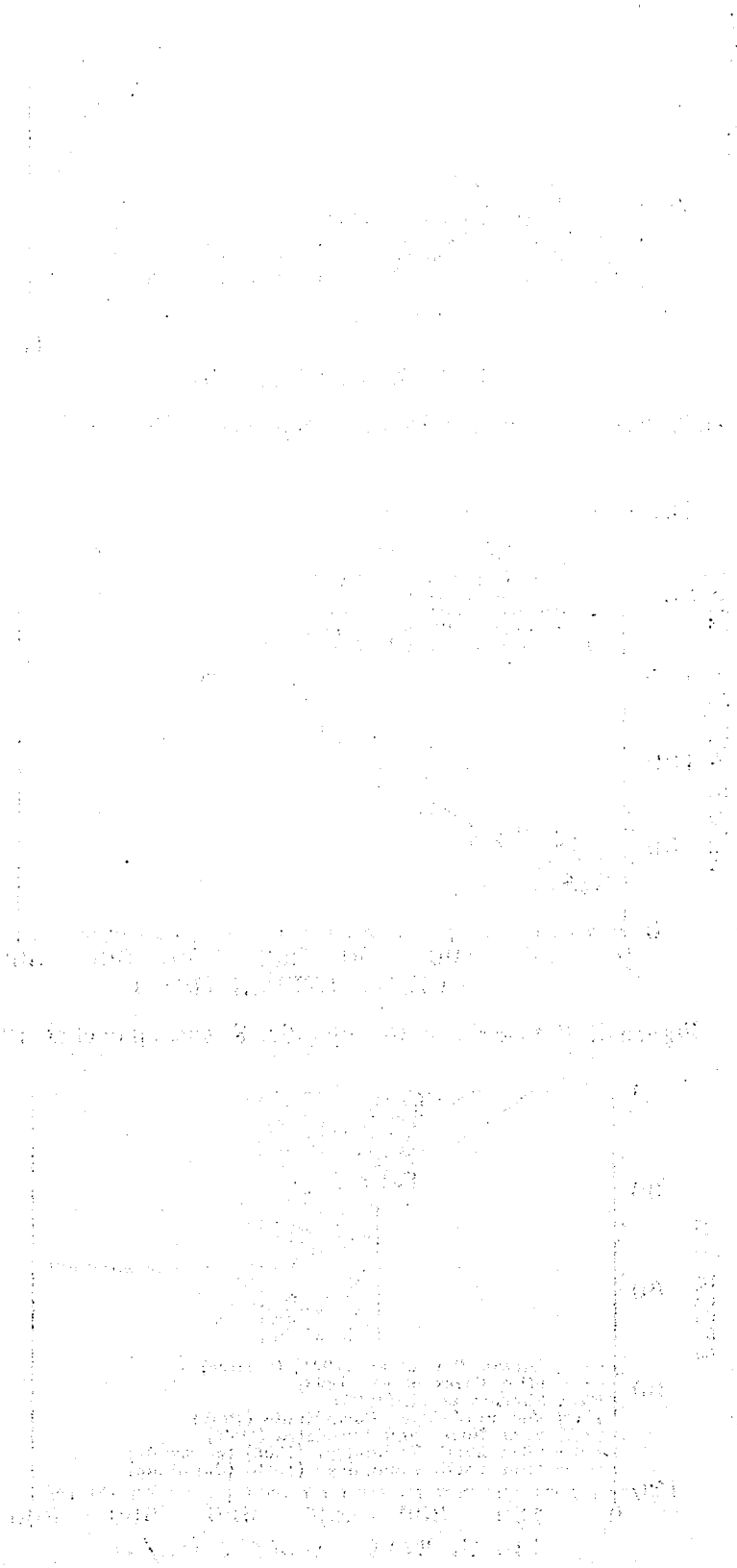


Figure 4. Refuse shear wave velocities (after Kavazanjian et al. 1995)



Evaluation Method of Ground Motion Amplification due to Irregularity of Ground Condition

by
Ryoji Hagiwara[1)]
and
Riki Honda[2)]

ABSTRACT

In the recent studies, it has been said that the ground motion is amplified on the ground which has irregularity in layer configuration or soil properties, causing severer damage on various structures or ground itself than it would on the horizontally layered ground.

In this study, amplification characteristics of ground motion on the various grounds with relatively simple irregularity are investigated through the finite element method analyses (FLUSH) to seize how ground condition's irregularity affects. In order to see the amplification purely due to the irregularity of ground condition, amplification is evaluated by the comparison of the results of the two dimensional analyses by FLUSH and the one dimensional analyses by the multiple reflection method (SHAKE), in which the effect of ground condition irregularity is not considered.

Based on the results of these investigation, method to evaluate the amplification is presented and, to check its applicability, ground motion amplification in several other cases are calculated and compared with the value estimated by the proposed method.

Key Words:Irregular Ground, Ground Motion Amplification, Estimation method.

1. INTRODUCTION

Through the investigation of damage caused by earthquakes, it has been found that on the ground which has geological or topographical irregularity, the seismic ground motion is amplified and causes severer damage. Based on the acceleration records, various studies (1) have been conducted based on the recorded accelerograms to clarify the mechanism how such amplification occurs.

Analytical approach through numerical computations, in which usually ground with simple irregularity are assumed, are also carried out by many researchers(2). Some of these studies have their aims in proposing computational methods for accurate computation of wave deflection, reflection, propagation etc. However, studies conducted from the view point of proposing the method to evaluate the amplification to be considered in practical seismic design of various structures, such as the study by Ejiri and Goto (3), are not so great in number.[1]

It is certainly quite difficult to propose a precise method to estimate such ground motion amplification, because so many factors affects in various ways. The method to estimate the ground motion amplification to be considered in seismic design, however, is necessary, even if it does not give perfectly correct estimation, because, without such method, structures must be designed with unnecessary large safety factors, or insufficient seismic resistance.

2. OBJECTIVE

[1)]Head, Ground Vibration Division, Public Works Research Institute, Ministry of Construction, Japan
[2)]Researcher,ditto

As is mentioned above, it is observed that on the ground with irregularity in topographical or geological condition, the ground motion is amplified and therefore a method to estimate such amplification of seismic waves on the irregular grounds is in urgent need so that such amplification can be taken into consideration in seismic design of various structures.

Considering this, the objective of our study is set to propose a method to evaluate the ground motion amplification to be considered in the seismic design on the irregular grounds.

Our final goal should be proposal of a method that can evaluate the ground motion amplification on any irregular ground with rational accuracy. However, the ground motion amplification is affected by so many factors including the size of the irregularity and the input motion characteristics, and it is almost impossible to carry out analyses that take all possible factors into consideration. Therefore in our study, the ground with rather simple irregularity is considered, as the initial step toward the final goal.

3. CONDITIONS FOR ANALYSIS

3.1 Ground Models Considered

The ground models considered in the two dimensional and one dimensional analyses are shown in Figure 1.

For the two dimensional analyses, ground models are made by changing the three following parameters: the inclination of the hard layer (θ), the thickness of the soft layer (H), and the impedance ratio (Ir). Among the three parameters, θ and H are shown in Figure 1. As the value for the inclination θ, $\tan\theta$=1/2, 1/4, 1/8 are assumed, and as the soft layer thickness, H=10m, 20m, 30m are assumed. The impedance ratio Ir is the ratio of impedance of soft layer to that of hard layer and it is defined as:

$$Ir = \frac{\rho_1 \cdot Vs_1}{\rho_2 \cdot Vs_2}$$

where

ρ_1 :unit weight of soft layer

ρ_2 :unit weight of hard layer

Vs_1 :shear wave velocity of soft layer

Vs_2 :shear wave velocity of hard layer,

and as the value of it, assumed are Ir= 0.31, 0.48, 0.66 (Each corresponds to the shear wave velocity in the surface layer Vs_1=100, 150, 200m/s respectively.).

Changing these three parameters gives 3x3x3=27 types of ground models. One additional model, in which $\tan\theta$=infinity, H=30m and Ir=0.31 are assumed, is also considered. In total, twenty-eight models listed in Table 1 are considered. For all cases, the height of the ground model (H + H2) is 60m.

Soil constants assumed for the soft and the hard layer are shown in Table 2. The non-linearity of soil behavior is considered by equivalent linear method for the soft and the hard layers. As the equivalent linear soil property curve of the soft layer and the hard layer, the curve presented by Iwasaki, Tokita et al.(4) for the alluvial clay and the one presented by Iwasaki, Tatsuoka et al.(5) for the diluvial sand are employed respectively. The equivalent linear soil property curves are shown in Figure 2.

Vertical displacement is fixed to zero for all nodal points on the both side ends and both vertical and horizontal displacement for the points on the bottom are fixed to zero.

In the one dimensional analyses to see the ground motion on the horizontally layered ground, as is shown in the Figure 1, the vertical section of the two dimensional model is employed as the ground model and all conditions such as soil properties, thickness of the soft and the hard layers are set equal to those of corresponding two dimensional ground model. The computation using these one dimensional models gives the ground motion which can be evaluated by the data obtained by vertical boring. Therefore, by comparing the results of the two dimensional analyses with these one dimensional cases, the amplification purely due to the irregularity condition can be

observed.

3.2 Analysis Methods

Two dimensional seismic response analyses of the ground were carried out by FLUSH. One dimensional analyses to see the ground motion on the horizontally layered ground were carried out by SHAKE. Both are based on the equivalent linear method.

3.3 Input Ground Motion

Two incident seismic waves are employed for all ground models. One was recorded in the 1978 Miyagiken-oki Earthquake on the very hard ground near the Kaihoku bridge, and the other was recorded in the 1983 South Ibaraki-ken Earthquake on the relatively hard ground in the Public Works Research Institute. Figure 3 shows their time histories, Fourier spectra and response acceleration spectra for damping ratio of 5%. In the seismic response analysis, both waves multiplied by constants to adjust their maximum acceleration to 100gal, are employed. The input motion is assumed to be spatially uniform along the bottom line of the ground model.

4. AMPLIFICATION DUE TO IRREGULARITY

4.1 Amplified Ground Motion on the Irregular Ground

Ground motion on the irregular ground differs considerably for different models.

Figure 4 shows, as examples, the distribution of the maximum acceleration on the ground model 2, 4 and 23. Tangent of the inclination of the hard layer θ is 1/2, for the model 2 and 4, and 1/4 for the model 23. The thickness of the soft layer H is 10m for the model 2 and 4, and 30m for the model 23. The shear wave velocity in the soft layer of the model 2 and 23 is 100m/s (i.e. Impedance ratio Ir=0.31), and 200m/s (Ir=0.66) for the model 4. In these figures, the area between the two vertical dotted lines corresponds to the area where the hard layer inclines.

As is seen in this figure, the amplification of the ground motion is different for different models. On the model 23, for example, the maximum acceleration reaches 240gal while it is only 120gal on the horizontally layered area such as the left edge of the ground model. On the other hand, it should be also noted that only slight amplification is seen on the model 4.

It is not adequate, therefore, to assume a large seismic design force for every irregular ground. It is required to estimate how much ground motion amplification should be expected, so that it can be considered properly in seismic design.

4.2 Estimation of Amplification

In order to see the amplification purely due to the ground condition irregularity, amplification factor was measured by the ratio of the response acceleration of the ground motion computed by two dimensional analysis, to the response acceleration of that by one dimensional analysis. The latter can be regarded as the acceleration evaluated from the boring data of that site.

The amplification factor R(Sa) is defined in the following manner.

Let $Sa(T,x)_{2D}$ be the 5% damped response acceleration of the linear SDOF system with natural period of T for the ground motion at a certain point x calculated by two dimensional analysis. In the similar manner, let $Sa(T,x)_{1D}$ be defined as the response acceleration of the ground motion calculated by one dimensional analysis conducted on the vertical section of the two dimensional analysis model at the corresponding point x. Here, $Sa(T,x)_{2D}$ is calculated for every node on the ground model surface. But $Sa(T,x)_{1D}$ is calculated for seven vertical models. The thickness H of surface layers in these seven models are

0m, 5m, 10m, 15m, 20m, 25m, 30m. $Sa(T,x)_{1D}$ for the ground which is different in the thickness of layers from these seven models, is linearly interpolated. This does not affect the results so much because the configuration of the ground model is quite simple, consisting of only two layers.

Using these two response acceleration, R(Sa,T) is defined as:

$$R(Sa,T)=Sa(T,x)_{2D}/Sa(T,x)_{1D}.$$

Although R(Sa,T) is the function of x, for simple expression, it is not written explicitly. R(Sa) is the maximum value of R(Sa,T) in the range of natural period T from 0.1 second to 5.0 seconds (frequency = 0.2 to 10Hz). It can be regarded as the coefficient to adjust the seismic design force on the normal ground to the one on the irregular ground.

Two input motions are employed for each ground model and, because the soil property dependent on strain is assumed in the equivalent linear method, different input motion gives different amplification spectra. Tokita et al.(6), shows that the standard deviation of amplification factors for different four input motions, including the two used in this study, is about 10-15%. In this study, therefore, the amplification factor for each ground model is defined as the average of those for two different input motions.

4.3 Effect of Factors Considered

The effect of three factors considered in this study, H, Ir and θ are described below.

The maximum value of R(Sa) over the ground surface is defined as Rmax(Sa). The effect of factors is evaluated by investigating how each factor affects Rmax(Sa).

i) H : Thickness of the soft surface layer

The thickness of the soft layer plays important role in determining the amplification factor at the ground surface. Figure 5 shows the relation of the thickness of the soft layer H and the maximum amplification factor Rmax(Sa) for the cases in which the impedance ratio Ir=0.31 (shear wave velocity in the soft layer is 100m/s) is assumed. It shows clearly that ground motion is amplified largely on the ground with the thick surface layer.

ii) Ir : Impedance ratio

The impedance ratio is also important in determining the amplification factor. The relation of the maximum amplification factor and the impedance ratio for the cases with surface layer thickness H = 30m, is shown in Figure 6, which indicates that the softer the surface layer is, the larger amplification should be expected. The same trend is observed in the cases for which thinner surface layer (H = 10m and 20m) is assumed.

iii) θ : Inclination of the hard layer

The inclination angle θ does not affect the amplification significantly. As is shown in Figure 5 and Figure 6, the amplification factor is almost same for different inclination angle θ.

The same tendency is also observed in the cases with different impedance ratio or different surface layer thickness.

4.4 Method for the Estimation of the Ground Motion Amplification

The results mentioned in the preceding section indicates that the amplification on the ground with the variation of surface layer thickness should be evaluated based on the index which involves the softness of the surface ground and its thickness. Our aim being to present the practical method to evaluate such amplification, the index must be easy to calculate and the data required for the calculation of the index must be easy to obtain. T_G, which is referred to as the traits of the ground in the specification for highway bridge design in Japan(7) satisfies these condition, because it has been used for long in designing to decide the ground type and can be evaluated from the data which is

available from the ground boring data by a simple formula. T_G is defined as :

$$T_G = \sum_{i=1}^{n} \frac{H_i}{V_i}$$

where

n : number of layers above the base.
H_i : thickness of the i-th layer.(m)
V_i : average shear wave velocity of the i-th layer. (m/sec)

T_G represents the fundamental natural period of the ground under the conditions that the displacement is fixed to zero at the upper surface of the underlying base and that the ground behaves elastically. It can be regarded as the fundamental natural period in the small strain range.

First, the maximum value of the amplification factor Rmax(Sa) is estimated based on T_G. ΔT_G is defined as the difference of the T_G at the point with the thickest surface layer and that at the point where no soft layer lies. Figure 7 shows the relation of ΔT_G and Rmax(Sa). There is close correlation among them. Regression analysis of them gives the formula to estimate the maximum amplification factor Rmax(Sa):

$$Rmax(Sa) = 0.885 + 1.481\Delta T_G \quad \cdot\cdot(1)$$

which is also shown in the Figure 7 by a broken line.

Secondly, distribution of the amplification factor is considered. The distance from the origin to the point at which the maximum amplification is observed is referred to as L. The origin is set 100m left from the point at which the underlying hard layer reaches the ground surface, because amplification starts rising near that origin in most cases. Ls is the length of the area in which thickness of the soft layer varies. The definition of L and Ls is shown in Figure 8. The relation of the ratio of L to Ls and Ls is shown in Figure 9. Regression analysis of the data gives the formula to estimate the ratio L/Ls:

$$L/Ls = 116.590/L + 0.778 \quad \cdot\cdot(2)$$

which is also shown in Figure 9 with a broken line.

Thirdly, the spatial variation of the amplification factor is considered. Judging from the results of the twenty-eight ground models, a function of the formula to estimate the amplification factor (R(Sa)) at point x, is assumed as:

$$R(Sa) = A \cdot \left(\frac{x}{\beta}\right)^{\alpha} \cdot \exp\left(1 - \frac{x}{\beta}\right) + 1.0 \quad \cdot\cdot(3)$$

where

A : (Rmax(Sa)-1)/(α^{α}•exp(1-α))
α : constant set to 10.
β : L/α
L : the point which gives the maximum of R(Sa). Given by equation(2).
Rmax(Sa) : Maximum of R(Sa). Given by equation (1).

where α is a constant to determine the sharpness of the distribution form.

In Figure 10, the estimated distribution of the amplification factor (by a rigid line) and the distribution of the calculated R(Sa) (by circles) for the model 2, 20, 23 and 24 are shown. The surface layer thickness H=10m for model 2 and H=30m for model 20, 23 and 24. The inclination of the hard layer tanθ=1/2 for model 2 and tanθ=1/4 for model 23 and 24. The impedance ratio is Ir=0.31 (shear wave velocity in the surface layer is 100m/sec) for model 2 and 4, and Ir=0.48 (shear wave velocity in the surface layer is 150m/sec). The estimated distribution show a reasonable agreement with the distribution of the computed values.

5. APPLICABILITY OF THE PROPOSED METHOD

Amplification factor on eight additional ground models are computed to see the

applicability of the formula (3). In the additional cases, variables such as impedance ratio, shear wave velocity, thickness of the underlying hard layer, are changed from those of the original twenty-eight cases. The ground models analyzed are shown in Table 3 and the soil characteristics additionally assumed are shown listed in Table 4.

Model 29 and 30 are computed to see the effect of the thickness of the hard layer, and model 31 is to see the applicability of the presented method to the ground with the thicker surface layer.

In the analyses of the models 32 to 36, the shear wave velocities in the hard layer are adjusted so that the impedance ratio is equal to the values employed in the preceding twenty-eight cases. These are the cases to verify whether the method can evaluate correctly the effect of shear wave velocity even when the impedance ratio is not changed. In models 32 and 33, the surface layer thickness of 20m is assumed, and in models 34 to 36, the surface layer thickness of 30m is assumed.

For all cases, the inclination of the hard layer is set as $\tan\theta=1/2$, because the preceding investigation indicates that the amplification is almost independent of the inclination angle.

The same soil type (alluvial clay for the surface layer and diluvial clay for the underlying layer), the same equivalent linear soil property curves and the same input motions are employed for these cases.

In Figure 11, the maximum amplification factors Rmax(Sa) for these eight models are plotted with the estimated value indicated by dotted line. Good agreement is seen for most cases, but model 31 is widely apart from the estimated value. This indicates that the amplification on the irregular ground whose soft surface layer is 40m thick or more requires further investigation.

6. CONCLUSION

The practical method to estimate the amplification factor of the response acceleration on the irregular ground which has spatial variation of the surface layer thickness, is presented. The estimation formula is made based on the comparison results of the two dimensional and one dimensional computation conducted for the various ground models. The irregularity of the ground condition is measured by the variation of the traits of the ground T_G, which corresponds to the fundamental natural period in the small strain range. Usage of T_G makes the method more practical, because T_G can be easily calculated from the boring data and has been used in seismic designing. The presented method show good agreement with the twenty-eight cases dealt with in the first part. It also shows reasonable agreement for the additional cases, which are analyzed to see the applicability of the presented method.

Further study, however, is required to investigate the frequency band in which amplification is relatively large. The definition of the irregularly conditioned ground also remains to be determined, because the presented method indicates that the ground motion amplification is independent of the inclination angle of the surface layer, which means the amplification should be always taken into consideration in seismic design no matter how slightly the hard layer may incline. It is also required to investigate the amplification on the ground with the surface layer whose thickness varies in the different (usually more complex) manner.

REFERENCE

1) *for example*, Bard,P-Y et al.: "The Mexico Earthquake of September 19, 1985- A Theoretical Investigation of Large- and Small-scale Amplification Effects in the Mexico City Valley",

Earthquake Spectra, Vol.4, No.3,(1988)
2) Takenaka,H: "Computational Methods for Seismic Wave Propagation in Complex Subsurface Structures", Jishin No.46 (1993) ,(in Japanese)
3) Ejiri,J and Goto,Y: "Introduction of Topographical Effects on Site Response for Design Spectra", J. of Japan Society of Civil Engineers. No.501/I-209 (1994), (in Japanese)
4) Iwasaki,T et al.: "Experimental Study on Dynamic Deformation Characteristics of soils", Report of Public Works Research Institute No.153(1980), (in Japanese)
5) Iwasaki,T et al.: "Dynamic deformation and Strength Characteristics of Alluvial Clay", 15th Japan National Conference on Soil Mechanics and Foundation Engineering (1980), (in Japanese)
6) Tokida,K et al.: "Effects of Geological Irregularities on Ground Motion Characteristics", Proc. of 10th WCEE, (1992)
7) Japan Road Association : "Specifications for Highway Bridges",(1990)

TABLE 1 ANALYSED GROUND MODELS

Model No.	Thickness of soft layer H (m)	Thickness of hard layer H_2 (m)	Inclination angle of hard layer θ tan θ	Shear wave velocity (m/s)		Impedance ratio
				Soft layer	Hard layer	
1	30		∞ (6.0)	100	270	0.31
2	10	50	1/2	100		0.31
3				150		0.48
4				200		0.66
5			1/4	100		0.31
6				150		0.48
7				200		0.66
8			1/8	100		0.31
9				150		0.48
10				200		0.66
11	20	40	1/2	100		0.31
12				150		0.48
13				200		0.66
14			1/4	100		0.31
15				150		0.48
16				200		0.66
17			1/8	100		0.31
18				150		0.48
19				200		0.66
20	30	30	1/2	100		0.31
21				150		0.48
22				200		0.66
23			1/4	100		0.31
24				150		0.48
25				200		0.66
26			1/8	100		0.31
27				150		0.48
28				200		0.66

TABLE 2 SOIL CHARACTERISTICS

	Soft Layer	Stiff Layer
Soil Type	Alluvial Clay	Diluvial Sand
Unit Weight(gf/cm³)	1.55, 1.60, 1.65	1.85
Shear Wave Velocity (m/sec)	100, 150, 200	270
Poisson's Ratio	0.45	0.40
Soil Property	Non−linear *1	Non−linear *2

*1, *2 Nonlinearity of the shear moduls and damping ratio of the soil is accounted for by using the equivalent linear soil properties.

TABLE 3 ADDITIONAL GROUND MODELS

Model No.	Thickness of soft layer H (m)	Thickness of hard layer H_2 (m)	Inclination angle of hard layer θ tan θ	Shear wave velocity (m/s)		Impedance ratio
				Soft layer	Hard layer	
29	20	100	1/2	100	270	0.31
30		200				
31	40	40				
32	20	40		100	180	0.47
33				150	405	0.32
34	30	30		125	270	0.40
35				100	180	0.47
36				150	405	0.32

TABLE 4 SOIL CHARACTERISTICS ASSUMED FOR ADDITIONAL CASES *1

	Soft Layer	Stiff Layer
Soil Type	Alluvial Clay	Diluvial Sand
Unit Weight(gf/cm³)	1.58	1.85
Shear Wave Velocity (m/sec)	125	180, 405
Poisson's Ratio	0.45	0.40
Soil Property	Non−linear *2	Non−linear *3

*1 As for the layer whose shear wave velocity is the same as those listed in Table 2, same condition is assumed.

*2, *3 Nonlinearity of the shear moduls and damping ratio of the soil is accounted for by using the equivalent linear soil properties.

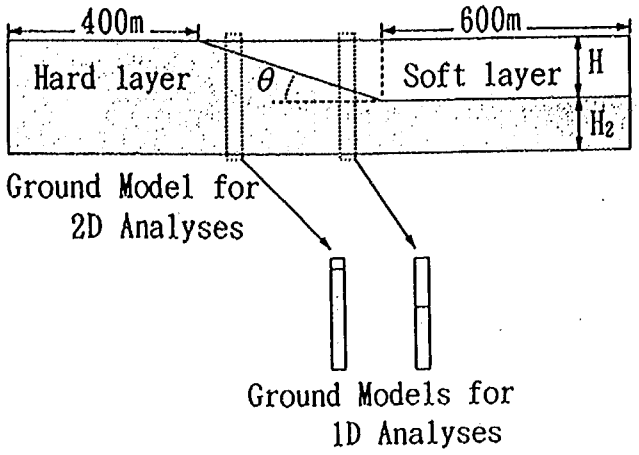


Figure 1 Gound Models for One and Two Dimensional Analyses

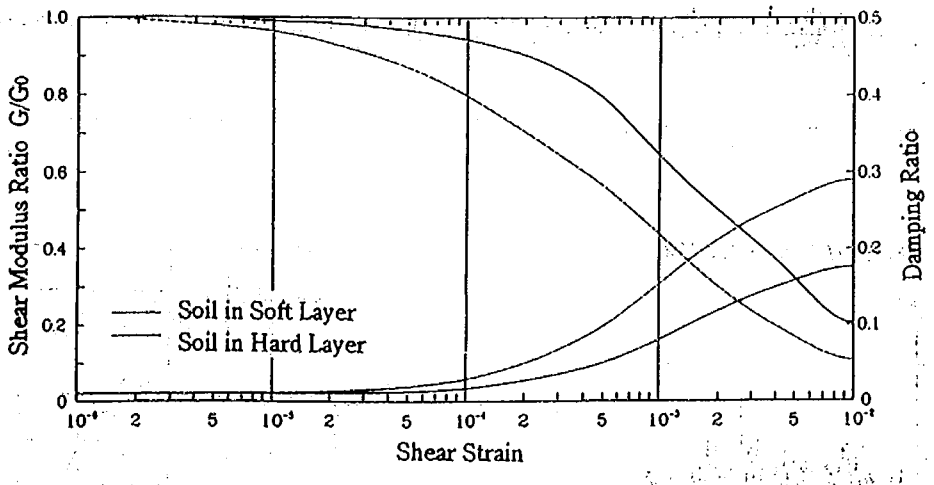
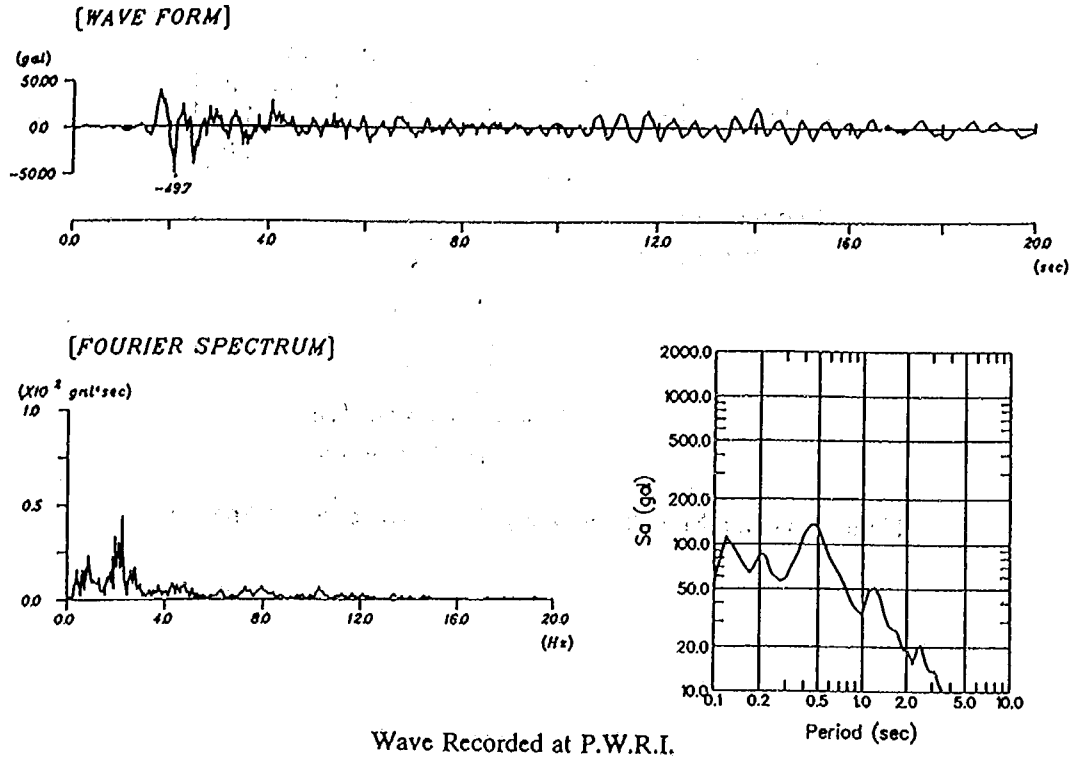
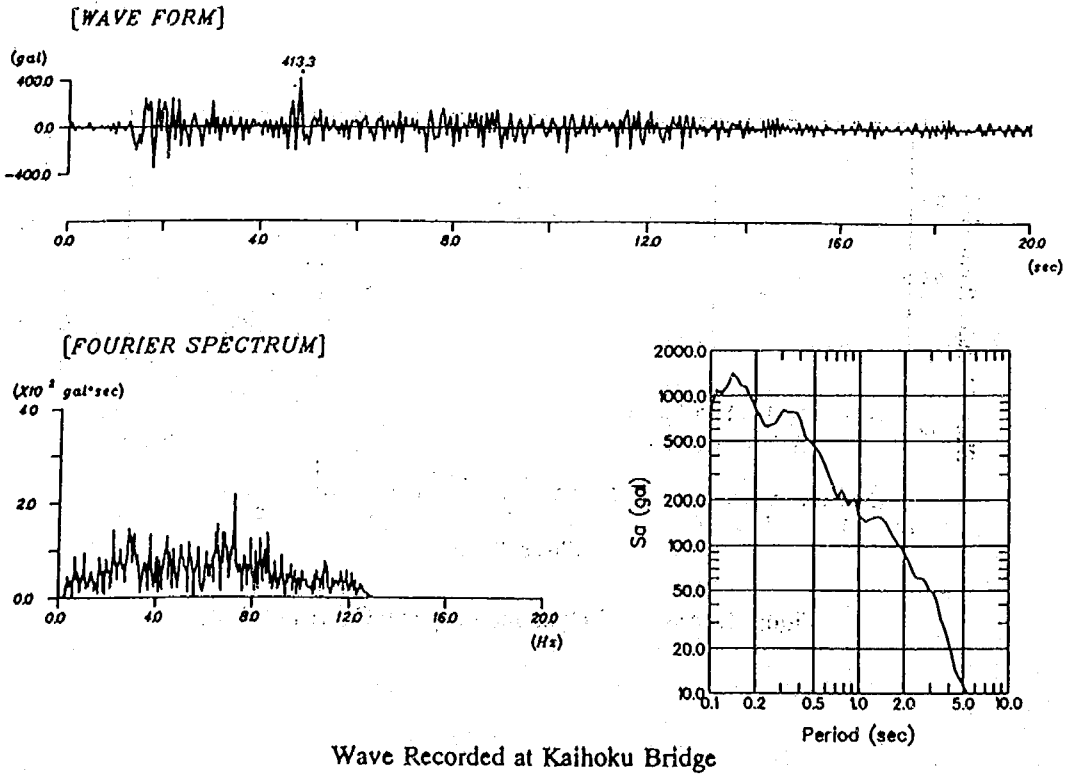


Figure 2 Assumed Dynamic Property Curves of Soils

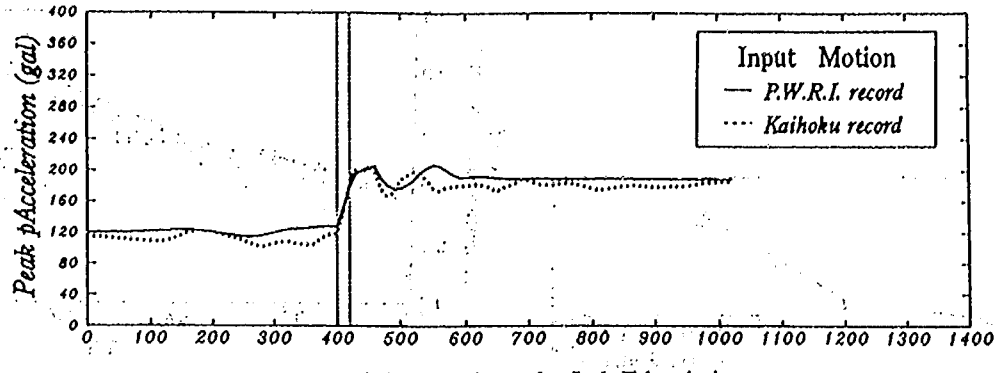


Wave Recorded at P.W.R.I.

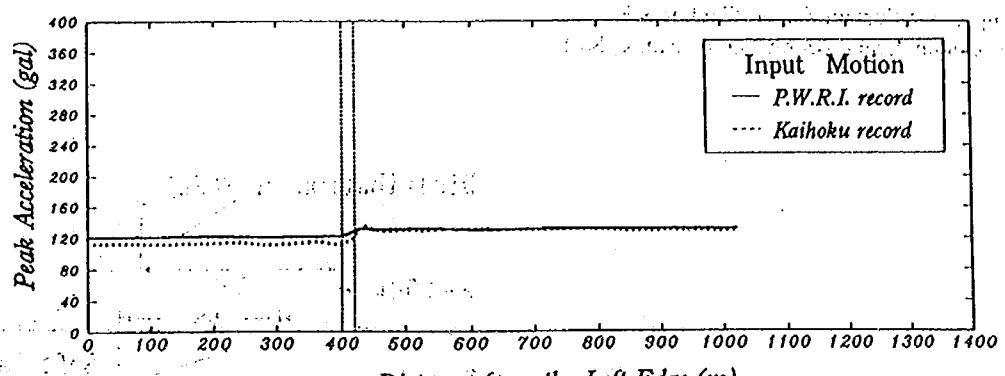


Wave Recorded at Kaihoku Bridge

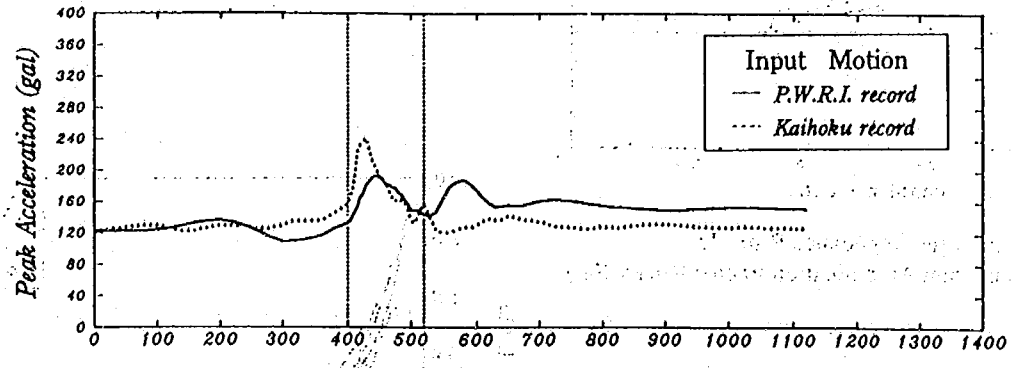
Figure 3 Time history, Fourier Spectra and Acceleration Spectra of Input Motions



(a) Model 2



(b) Model 4



(c) Model 23

Figure 4 Distribution of Peak Acceleration

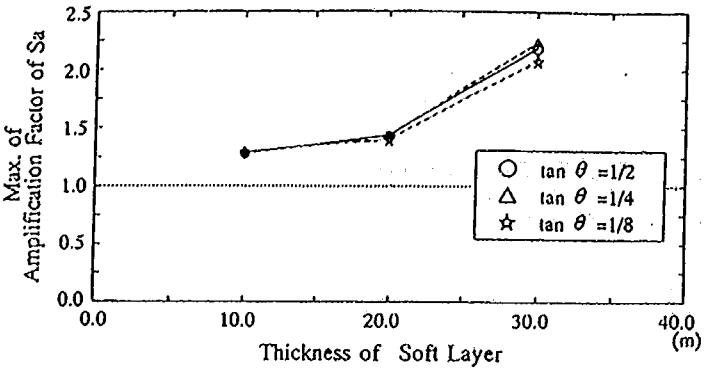


Figure 5 Relationship of the Surface Layer Thickness H and the Maximum Amplification Factor Rmax(Sa)

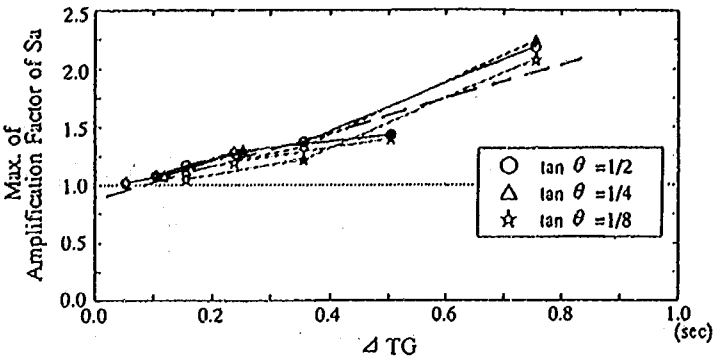


Figure 7 Relationship of the Maximum Amplification Factor Rmax(Sa) and ΔTo

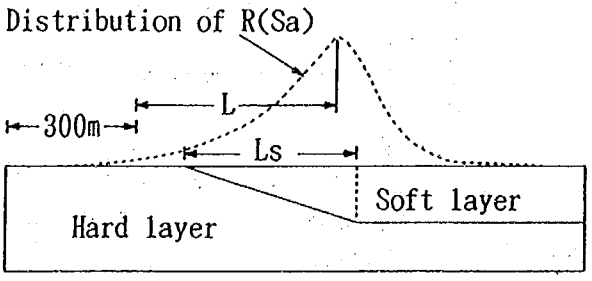


Figure 8 Definition of L and Ls

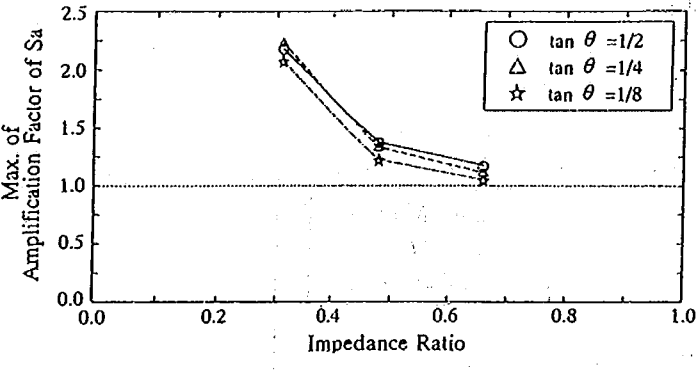


Figure 6 Relationship of the Impedance Ratio Ir and the Maximum Amplification Factor Rmax(Sa)

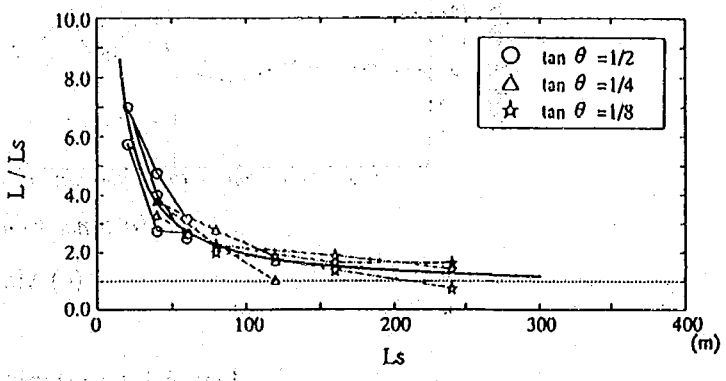
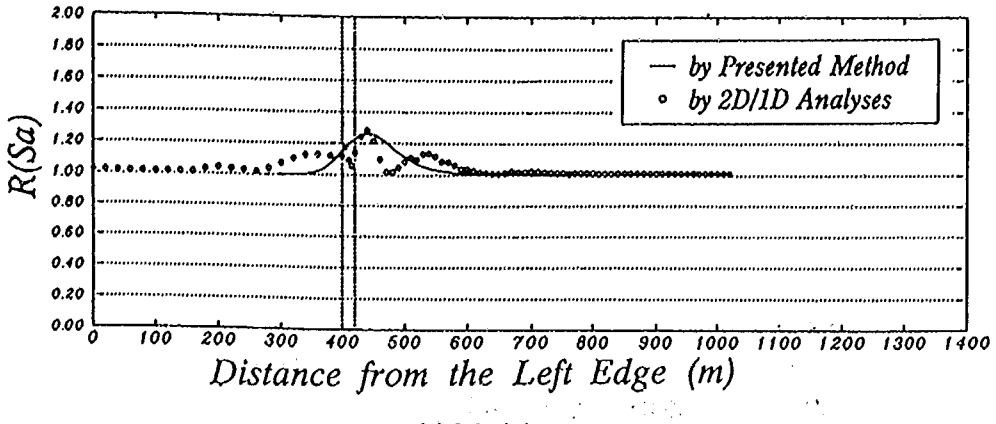
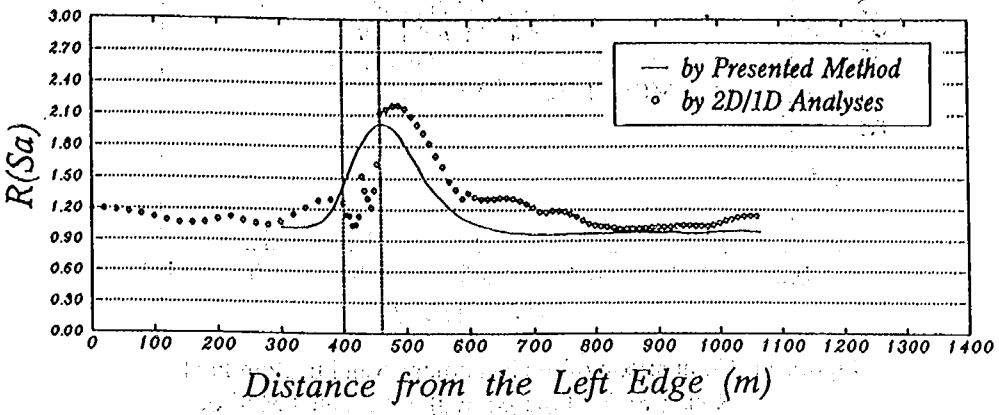


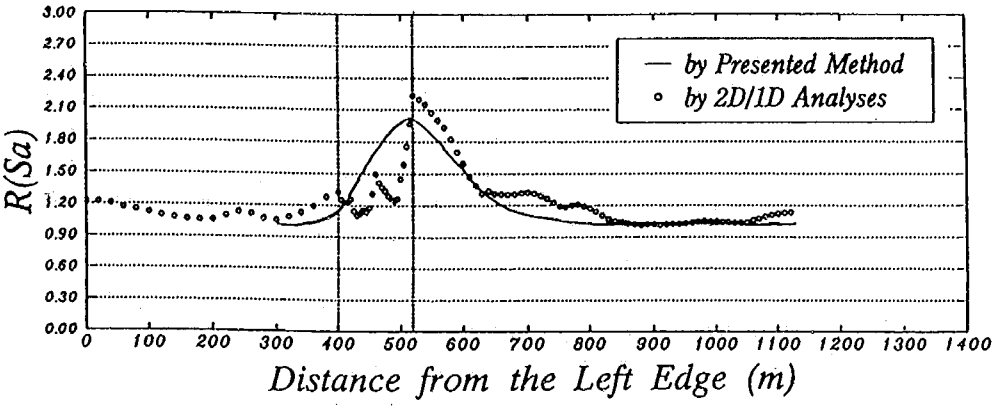
Figure 9 Relationship of L/Ls and Ls



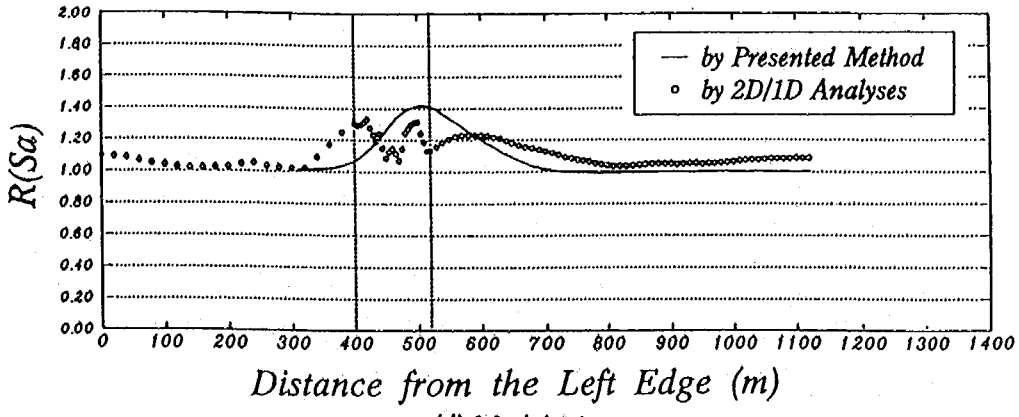
(a) Model 2



(b) Model 20



(c) Model 23



(d) Model 24

Figure 10 Distribution of Amplification Factor R(Sa)

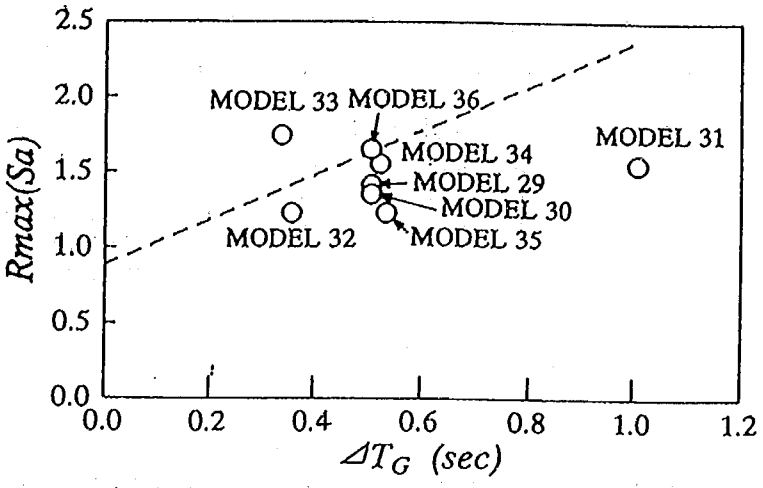


Figure 11 Comparison of the Maximum Amplification Factor Rmax(Sa) estimated by the Presented Method and that by the Analyses of Models 29-36

The Use of Seismic Hazard Maps for Improved Earthquake Risk Reduction

by

Richard J. McCarthy *

and

James E. Slosson**

ABSTRACT

Seismic hazard maps can be an important tool in helping decisionmakers establish levels of "acceptable risk" for structures. The Hoyogo-ken-Nanbu and the Northridge earthquakes have illustrated that much still needs to be done to achieve acceptable risk reduction and building performance. Historically, seismic hazard maps used by California regulatory agencies and local governments depict hazards presented only by fault surface rupture. At present, new seismic hazard maps for California will identify areas of potential amplified ground shaking, seismically induced liquefaction and landsliding, and tsunami inundation. Data recorded during the Northridge earthquake indicate that at some locations, particularly in the near-source area and in areas with unique local geology, shaking exceeded the assumptions underlying design values in the short to mid-period range. This shaking appears to have affected low and mid-rise buildings and caused response in higher modes of vibration for tall buildings. Velocity and displacement-sensitive structures also may have been affected by high velocity pulses. Near-source and local geologic effects must be considered in the design of structures. Therefore, there is a need to develop a new generation of seismic hazard maps depicting potential near-source areas and unique local geologic conditions.

KEYWORDS: fault; hazards; liquefaction; maps; near-source; rupture; tsunami.

1. INTRODUCTION

The damage caused by the 1995 Hyogo-ken Nanbu and the 1994 Northridge earthquakes illustrate that although advances have been made in some areas of earthquake risk reduction, each country still has not reduced earthquake losses to an acceptable level. It is unknown at this time, how California will define "acceptable risk" for the performance of engineered structures. Seismic hazard maps are one valuable tool in helping to identify acceptable seismic risk to buildings, lifelines, dams, bridges, and other man-made structures.

The damage caused Northridge and Kobe are due both to the intensity of shaking and to the natural geologic setting of each city. For example, the Northridge earthquake and its larger aftershocks triggered widespread and abundant slope failures in the region surrounding Simi Valley. An assortment of rock and soil falls from steep cliffs or roadcuts, massive ridgetop fissuring related to large landslides, tossed earth resulting from ridge-top shattering, slumping of loose material into channels or from the banks of rivers and creeks, and innumerable minor cracks along ridgelines were all observed following the Northridge earthquake (CDMG, 1994).

These two moderate earthquakes have demonstrated the need for better land-use planning and improved engineering of structures, including code improvements. One of the tools available to decisionmakers are the wide variety of seismic hazard maps that, if developed with proper science, translated and transferred to users, and applied properly by users, can dramatically reduce earthquake losses and help speed recovery efforts.

2. FAULT RUPTURE ZONES

The Alquist-Priolo Earthquake Fault Zoning Act became law in California in March of 1973. The purpose of this Act was to prohibit the location of most structures for human occupancy across the traces of active faults and to mitigate the hazard of fault-rupture. Under the Act, the State Geologist is required to delineate "earthquake fault zones" along known active faults in California. Cities and counties affected by the zones must regulate certain development "projects" within the zones. They

* Seismic Safety Commission, 1900 K St., Ste. 100, Sacramento, California 95814

** Slosson & Associates, 15500 Erwin St., Ste. 1123, Van Nuys, California 91411

must withhold development permits for sites within the zones until geologic investigations demonstrate that the sites are not threatened by surface displacement for future faulting (CDMG Special Pub 42, 1994).

The Fault Zoning Act defines an "active fault" as one which has had surface displacement within Holocene time (about the last 11,000 years). Earthquake Fault Zones are delineated on U.S. Geological Survey topographic base maps at a scale of 1:24,000. The zone boundaries are straight-line segments defined by turning points. Zone boundaries on early maps were positioned about 660 feet (200 meters) away from the fault traces to accommodate imprecise locations of the faults and possible existence of active branches. The policy since 1977 is to position the Earthquake Fault Zone boundary about 500 feet away from major active faults. As of January 1, 1994, 535 Official Maps of Earthquake Fault Zones have been issued by the California Division of Mines and Geology (CDMG, Special Pub 42, 1994). Figure 1 is an example of an Earthquake Fault Zone.

3. SEISMIC HAZARD ZONES

Lack of geologic and geotechnical information is a particularly acute problem for local governments; state-of-the-art information in many cases is not available to decision makers and planning staffs or is not available in a form they can use in revising general plans, modifying zoning ordinances, or approving subdivision requests. Moreover, a building designer or utility engineer who lacks information on seismic hazards will not take measures to improve building and lifeline performance. Using the knowledge geologists can provide in land use and building decisions will lead to reduced seismic risk.

The Seismic Hazards Mapping Act of 1990 gave promise of greatly improving the extent and quality of geotechnical information available to local governments, building designers, and utilities. The Act directs the State Geologist to prepare maps identifying areas throughout the state that are subject to seismically induced shaking, liquefaction, landslides, ground failure, and other seismic hazards. The California Division of Mines and Geology has begun work on this mapping program, but at the current level of funding, about $1 million per year, it will be decades before maps are complete for most urban areas. Meanwhile, the information available to many local governments to reduce earthquake risks in their communities is not as complete or useful as it should be.

The Federal Emergency Management Agency has awarded a multiyear matching grant to fund preparation of maps in Orange, Los Angeles, and Ventura counties. A request to use the grant money statewide is still pending. The California Division of Mines and Geology proposal is to prepare 66 maps, covering most Los Angeles, Ventura, and Orange counties and the San Francisco Bay Area over a four-year period at a total cost of $20 million.

Although existing planning law does not require periodic revisions of safety elements to incorporate new seismic information, the Seismic Hazards Mapping Act does require published maps to be incorporated in general plans; however, it does not establish deadlines. When the maps and regulations prepared under the Seismic Hazards Mapping Act are published, local agencies will have to require a geologic or geotechnical report before approving a project located in a seismic hazard zone mapped by the State Geologist. Such reports will be prepared by registered civil engineers or certified engineering geologists and will contain site-specific evaluations of the seismic hazards affecting the project, identify portions of the project site containing seismic hazards, identify any known off site seismic hazards that could affect the site in the event of an earthquake, and propose mitigation measures.

Another possible source of information regarding likely damage is a planning scenario. The California Division of Mines and Geology, under contract to the Governor's Office of Emergency Services, has developed seven earthquake planning scenarios intended primarily for emergency response planning. These scenarios depict likely damage patterns in the San Francisco Bay Area, southern California, northwestern California and have been used extensively by emergency response planners, utility companies, and others.

Although these scenarios provide valuable information, they have several limitations for use in developing general plans:

- They are based on the particular characteristics of a certain earthquake; therefore, their application is limited to planning for that event;
- They generally provide only a broad-brush regional perspective, so their usefulness for focused, jurisdiction-specific planning is limited;

- Scenarios have been developed to cover the major urban areas of the state that have experienced the most earthquake damage historically; they are not available for many other areas of California that are susceptible to earthquake damage;

- They focus almost exclusively on public and utility-owned facilities (for example, highways, airports, hospitals, water lines, and electrical transmission lines) for emergency response planning, so they are of limited use in planning for problems associated with damage to private residential, commercial, and industrial facilities.

The background information used to develop the safety element must be thorough and current to serve as a useful basis for decision making. Because collecting original geotechnical information is expensive, most local governments rely heavily on geotechnical information published by the U.S. Geological Survey and the CDMG (Seismic Safety Commission, 1995).

3.1 Liquefaction Hazard Maps

Under the requirements of the Seismic Hazard Mapping Act, the California Division of Mines and Geology is responsible for mapping Liquefaction Hazard Zones. Figure 2 is an example of such a potential liquefaction hazard zone. These zones establish where site-specific geotechnical investigations must be conducted to assess liquefaction potential and, if required, provide technical basis to mitigate the liquefaction hazard. Liquefaction Hazard Zones are geographic areas meeting one or more of the following criteria (CDMG, 1992):

- Areas known to have experienced liquefaction during historic earthquakes. Field studies following past earthquakes indicate liquefaction tends to recur at many sites during successive earthquakes (Youd, 1984);

- All areas of uncompacted fills containing liquefaction susceptible material that are saturated, nearly saturated, or may be expected to become saturated;

- Areas where sufficient existing geotechnical data and analyses indicate that the soils are potentially liquefiable; and

- Areas where existing geotechnical data are insufficient. In areas of limited or no geotechnical data, susceptibility zones may be identified by geologic criteria as follows:

  a. Areas containing soil deposits of late Holocene age, where the M7.5 weighted peak acceleration that has a 10% probability of being exceeded in 50 years is greater than or equal to 0.10g and the water table is less than 40 feet below the ground surface; or

  b. Areas containing soil deposits of late Holocene age (current river channels and their historic flood plains, marshes and estuaries) where the M7.5-weighted peak acceleration that has a 10% probability of being exceeded in 50 years is greater than or equal to 0.20g and the historic high water table is less than or equal to 30 feet below the ground surface; or

  c. Areas containing soil deposits of latest Pleistocene age (between 11,000 years and 15,000 years), where the M7.5-weighted peak acceleration that has a 10% probability of being exceeded in 50 years is greater than or equal to 0.30g and the historic high water table is less than or equal to 20 feet below the ground surface.

4. NEAR-SOURCE HAZARD MAP

The near-source area is the area of the ground surface lying above and adjacent to the fault plane. The most widely used definition is to measure the distance (depth) of the hypocenter (rupture zone) below the epicenter, then use this measurement to draw a radius or distance outward from the epicenter. The area encompassed by this equal distance boundary contour represents the near-source area. In instances where the fault does not break the ground surface, the near-source area also includes the ground surface lying above the extension of the fault plane to the surface. The ground surface in the near-source area generally will be warped permanently by the movement of the fault (Seismic Safety Commission, 1995).

Ground motion in the near-source area is characterized by high accelerations, pulses of large velocity, and permanent tectonic displacement. The

nature of ground motion is related to the direction and mechanics of the fault rupture as well as the path of the seismic wave to the surface. The characteristics of near-source shaking do not follow the "normal" attenuation relationships used to describe shaking at more distant points (Seismic Safety Commission, 1995). Figure 3 shows the approximate near-source area of the Northridge earthquake. This circular pattern represents a typical near-source area for an earthquake caused by a blind or buried thrust fault.

The near-source area in a strike-slip earthquake would have a different shape (generally longer and narrower, extending on both sides of the fault rupture for the length of the rupture), and the nature of the near-source strong motion would also vary, depending on other non-source effects such as local geologic conditions.

Although seismologists have known of the influence of near-source effects on seismic shaking for some time, near-source effects first gained the interest of California engineers following the 1971 San Fernando earthquake. Failure of the Olive view Hospital in 1971 was attributed, in part, to a large, long-period near-source "seismic pulse." Near-source effects have been considered in the design of some critical facilities for a number of years. However, the implications of near-source effects have only recently been studied for use in the design of conventional structures because previous earthquakes have not struck well-instrumented urbanized areas and, therefore, produced few recorded motions from areas close to the source. At present, near-source effects are not explicitly considered in the building codes except for seismically isolated structures.

Near-source effects of engineering interest are related to the direction and mechanics of the fault rupture. The numerous localized, relatively rapid failure of "patches" of the fault surface causes significant high-frequency motion and allows permanent coseismic displacement of the fault and surrounding area. Known as source-effect phenomena, these factors affect the amplitude and frequency content of shaking.

Of critical importance to the design of engineered structures is that near-source effects combined with local geologic effects can adversely alter the seismic performance of a wide range of structures, including high-rise and base-isolated buildings. Data recorded during the Northridge earthquake clearly indicated the need to incorporate measures to mitigate this hazard in building codes. High-velocity pulses in the near-source area are believed by some to be a cause of much of the damage. These pulses were the largest in the northern San Fernando Valley and the Santa Susana Mountains. They were also significant in the southern San Fernando Valley.

The recorded data from the Northridge earthquake associated with alignment of geomorphic features along the southern boundary of the San Fernando Valley are still being evaluated and subject to different interpretations. Strong motion instruments also were not located in many of the areas that suffered the most severe damage. Generally speaking, the motions recorded near the Northridge epicenter were compatible with those used as the basis for the building code, but the motions exceeded those assumed in the code in many cases. At some locations, particularly in the near-source area and in areas with unique local geology, shaking exceeded the assumptions underlying design values in the short-to mid-period range. This shaking appears to have affected low- and mid-rise buildings and caused response in higher modes of vibration for tall buildings. Velocity and displacement-sensitive structures also may have been affected by the velocity pulses described earlier. Near-source and local geologic effects must be considered in the design of structures. There is no compelling evidence that changes to the code force levels are necessary. However, changes are necessary regarding the treatment of the effects of near-source and local geologic conditions (Seismic Safety Commission, 1995).

4.1 Local, Geologically Youthful, Geomorphic/Tectonic Folds

Scattered throughout the region affected by the Northridge earthquake are a wide variety of physical manifestations or evidence of locally intense shaking developed in the ground. These features area called "surface geologic effects." They should not be confused with the much more commonly noticed cracks in pavement, curbs, and walks, references to soft and hard rock, or other aspects of damage to structures.

Superimposed within or on the near-field/near-source area often is a belt of small, youthful, structurally aligned ridges that are often referred to as pressure ridges or Riedel ridges. These ridges and their associated Riedel faults feature left-or right-lateral offset. It is assumed that these geomorphic/structural features are youthful and are undergoing stress and, thus, convey the understanding that the associated fault system is active. Additionally, the San Fernando earthquake

of 1971, Landers earthquake of 1992, Northridge earthquake of 1994, and others occurring in California during the past century have witnessed higher acceleration (or stronger shaking) along the geomorphic expression as compared to other nearby sites. Figure 4 shows some of the major structural and geomorphic features within or near the Northridge earthquake near-source area.

5. TSUNAMI INUNDATION MAPS

Sudden displacement of the seafloor due to fault offset or submarine slumping can generate tsunami waves that can travel vast distances across open ocean and damage coastal communities. Local tsunamis generated by faults located in offshore California waters, the sudden uplift of a large land mass due to faulting, or the downslope displacement of large areas due to slumping in submarine canyons can strike the coastline within less than 10 minutes.

The 1989 Loma Prieta and 1992 Cape Mendocino earthquakes demonstrated the vulnerability of the California coastline to locally generated tsunamis. The 7.1 magnitude Loma Prieta earthquake induced a large submarine slum along the walls of the Monterey Submarine Canyon. A 20-cm-high tsunami struck Moss Landing minutes after the earthquake. The Cape Mendocino earthquake also had a magnitude of 7.1 and created a .5-m-amplitude tsunami at Crescent City and a 20-cm-wave at Eureka, California. The time between the earthquake and the arrival of the tsunami at Eureka was approximately 20 minutes. Fortunately, the tsunami struck Crescent City and Eureka at low tide, and no damage to city or harbor facilities occurred. However, if the wave had arrived during high tide or during a storm when meteorological forcing had created an elevated sea level, damage would have occurred and possibly some loss of life (McCarthy et al., 1993).

The Cape Mendocino earthquake was important to tsunami risk education efforts in California because it demonstrated that local tsunamigenic sources do, in fact, exist off the California coast. After a detailed study of this earthquake, Oppenheimer (et al, 1992) concluded that:

> The Cape Mendocino earthquake sequence provided seismological evidence that the relative motion between the North America and Gorda plates results in significant thrust earthquakes. In addition to the large ground motions generated by such shocks, they can trigger equally hazardous aftershock sequences offshore in the Gorda plate and on the Gorda-Pacific plate boundary. This sequence illustrates how a shallow thrust event, such as the one of moment magnitude (M_W) 8.5 that is forecast for the entire Cascadia subduction zone, could generate a tsunami of greater amplitude than the Cape Mendocino main shock. Not only would this tsunami inundate communities along much of the Pacific Northwest coast within minutes of the main shock, but it would persist for 8 hours at some locales.

The realization that the Cascadia Subduction Zone was tsunamigenic caused the California Seismic Safety Commission to request assistance from the National Oceanic and Atmospheric Administration (NOAA) and the Federal Emergency Management Agency (FEMA). In May, 1992, FEMA hosted an after-action discussion meeting with the scientific community. From these discussions, eight recommendations were formulated, including one to produce tsunami inundation maps for northern California—specifically, Eureka and Crescent City. The tsunami inundation study was ranked number two of the eight and was identified as time-sensitive. NOAA responded to this recommendation by offering to cost-share the study with FEMA. FEMA was to fund the NOAA tsunami inundation study and the California Division of Mines and Geology to examine other effects of a large Cascadia Subduction Zone earthquake such as ground shaking, liquefaction, and landslides. The results of both studies were closely coordinated.

Figure 5 represents a portion of the results of the NOAA (1994) tsunami inundation study and the California Division of Mines and Geology Scenario (1995) based on a magnitude M_W 8.4 earthquake on the Cascadia Subduction Zone. Figure 5 identifies not only the tsunami inundation line but depicts areas adjacent to Humbolt Bay that are likely to experience liquefaction and landslides should the scenario earthquake occur.

The scenario earthquake is assumed to generate a local tsunami that will arrive within a few minutes after the earthquake occurs. The tsunami model for this study was provided by the NOAA 1994 report entitled "Tsunami Inundation Model Study of Eureka and Crescent City, California" by Bernard,

Mader, Curtis, and Satake. That report produced 1:24,000 scale tsunami inundation maps for Eureka and Crescent City, California. The NOAA model assumes an incident wave 10 meters high in water 50 meters deep, based on historical tsunamis generated by earthquakes in the M8 and M9 range (CDMG, 1995).

These maps will serve as prototypes for a larger tsunami inundation program. After a review a comment period, the Seismic Safety Commission will consider whether the next series of inundation maps should focus on the populated coastal areas of southern California.

6. CONCLUSIONS

1. Seismic hazard maps can help decisionmakers determine acceptable levels of risk and performance of structures.

2. Seismic hazard maps are to be used as a general guide for land-use planning and should not preclude information obtained from site specific studies.

3. Data recorded from the Northridge earthquake indicate that at some locations, particularly in the near-source area and in areas with unique local geology, shaking exceeded the assumptions underlying design values in the short to mid-period range.

4. Seismic hazard maps depicting potential near-source areas and areas with unique local geology or geomorphology may be helpful in improving building codes.

5. How the insurance industry will react to the development and use of new generation seismic hazard maps is unknown.

7. REFERENCES

California Division of Mines and Geology, 1992, Guidelines for Delineating Seismic Hazard Zones; May 4, 1992, 10p.

California Division of Mines and Geology, 1995, Planning Scenario in Humbolt and Del Norte Counties, California, for a Great Earthquake on the Cascadia Subduction Zone, Special Publication 115, 151 p.

California Seismic Safety Commission, 1995, Turning Loss to Gain, Executive Order Report to the Governor on the Northridge Earthquake, (in press)

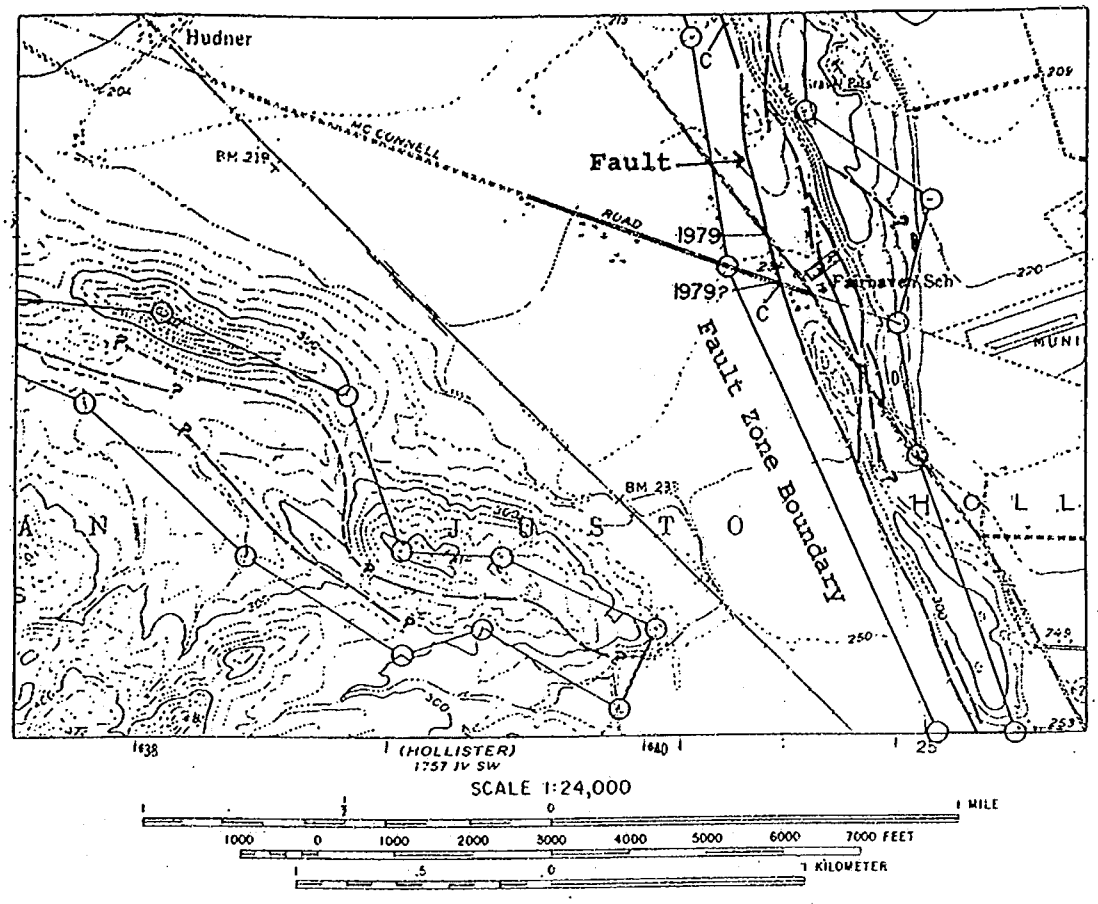
Bernard, E., Mader, C., Curtus, G., and Satake, K., 1994, Tsunami Inundation Model Study of Eureka and Crescent City, California, National Oceanic and Atmospheric Administration Technical Memorandum ERL PMEL-103, 80p.

Heaton, T., 1994, personal communication.

McCarthy, R., Bernard, E., and Legg, M., 1993, The Cape Mendocino Earthquake: a Local Tsunami Wakeup Call? Proceedings of the 8th Symposium on Coastal and Ocean Management, July 19-23, 1993, New Orleans, Louisiana, pp. 2812 to 2828.

Oppenheimer, D., Beroza, G., Carver, G., Denglar, L., Eaton, J., Gee, L., Gonzalez, F. Jayko, A., Li, W., Lisowski, M., Magee, M., Marshall, G., Murray, M., McPherson, R., Romanowicz, B, Satake, K., Simpson, R., Somerville, P., Stein, R., and Valentine, D., 1993, The Cape Mendocino Earthquake Sequence of April 1992, Science, 261, pp. 433-438.

Youd, T.L., 1984, Recurrence of Liquefaction at the Same Site: Proc., Eight World Conf. on Earthquake Engineering, San Francisco, California, V.3, p. 231-238.



Map Identifying Potential Hazard From Fault Surface Rupture
(California Division of Mines and Geology, 1992)

Pros

- A property in an Earthquake Fault Zone must be disclosed to a potential buyer before the sales process is complete.
- Made local governments and public aware of "active faults"
- Reduced damage from fault rupture hazard
- Served as "prototype" for other seismic hazard maps

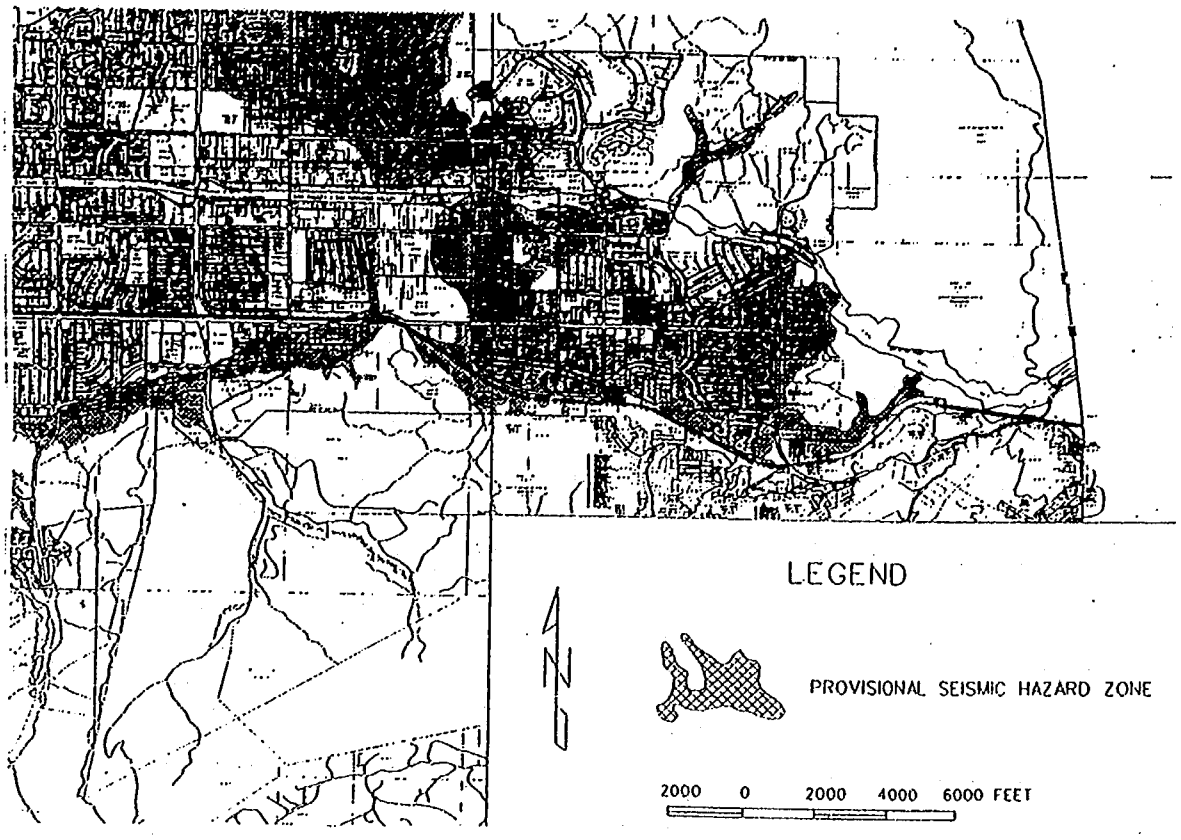
Cons

- Definition of "active fault" confusing to public and decisionmakers
- Some owners of structures that are not located in an Earthquake Fault Zone believe that they have mitigated the seismic risk--even from earthquake shaking.
- Does not apply to lifelines, toxic storage facilities, or land fills.

Recommendations for Improvement

- Use criteria other than fault rupture in "active" definition-such as microseismicity and geomorphic features
- Act should apply to structures other than high occupancy
- Mapping should focus on existing and developing urban areas.

Figure 1



Map Identifying Potential Liquefaction Hazard Zones
(California Division of Mines and Geology, 1994)

Pros

- Useful tool for landuse planners to require liquefaction studies for development planned within zone.
- If properly used, will contribute to a better understanding of the liquefaction hazards within urban areas
- Will enable local governments to require mitigation of the liquefaction hazard in the design of structures during the permit process.

Cons

- Maps should not be perceived as detailed scientific studies are should not take the place of site-specific investigations.
- Based on the results of site-specific studies, hazard zones may change over time; proof of a non-hazardous condition of a site within a zone must also be reflected in the permit process.
- Zones based only on historic water levels may either overestimate or underestimate the liquefaction potential for specific areas.

Recommendations for Improvement

- After several Liquefaction Hazard Zones have been implemented, options to redefine "triggering criteria" should be re-examined.
- Local governments should be given the lead in determining how effective the zoning program is and how it should be improved.

Figure 2

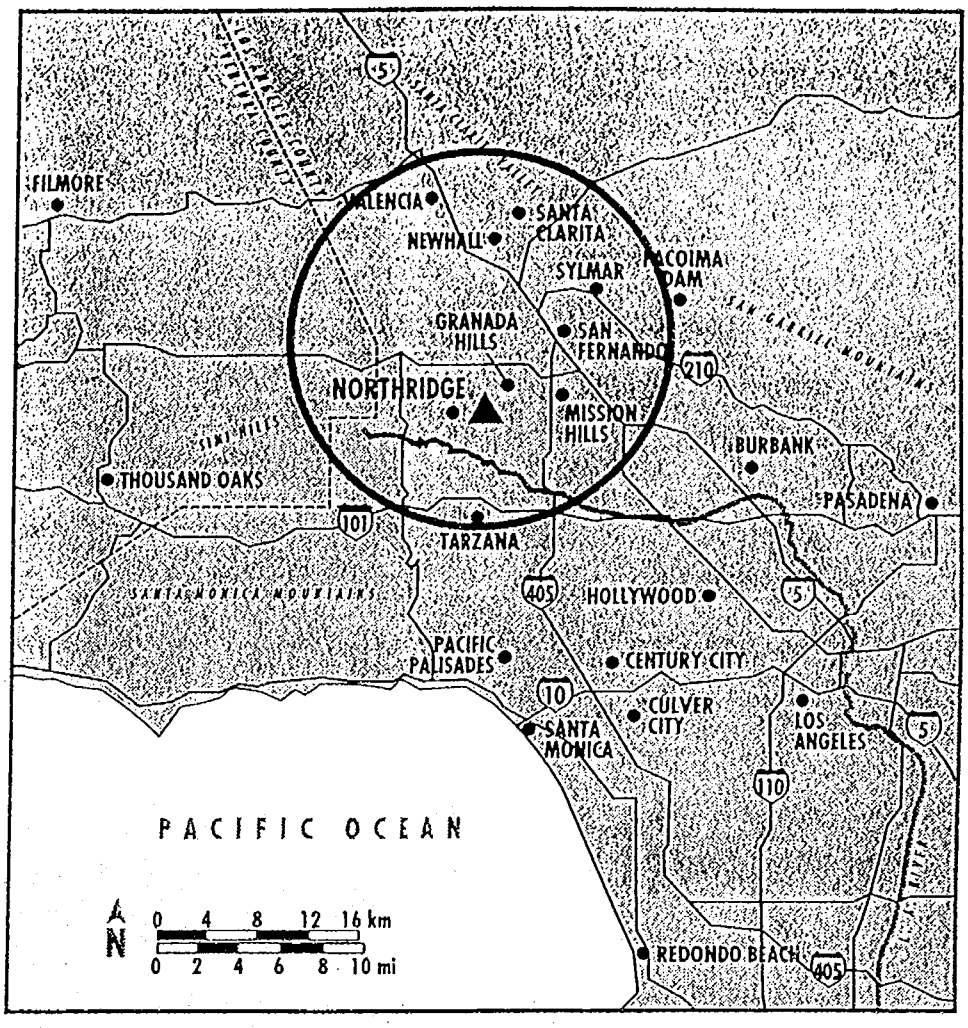


Figure 3

Preliminary "near-source" area map for Northridge earthquake (Heaton, 1994).

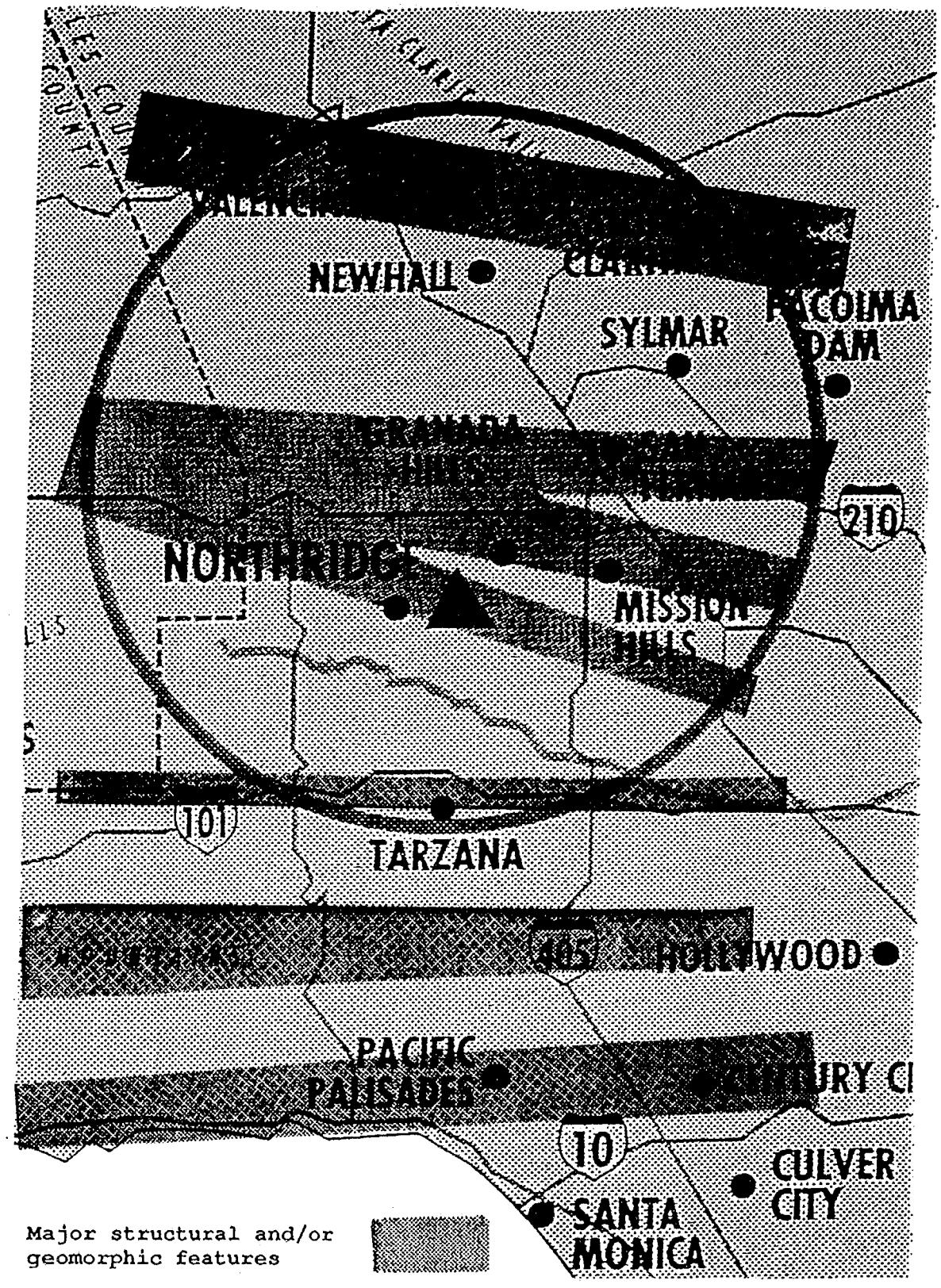


Figure 4 Map of major structural and geomorphic features within or near the Northridge earthquake near-source area (Modified after Heaton, 1994).

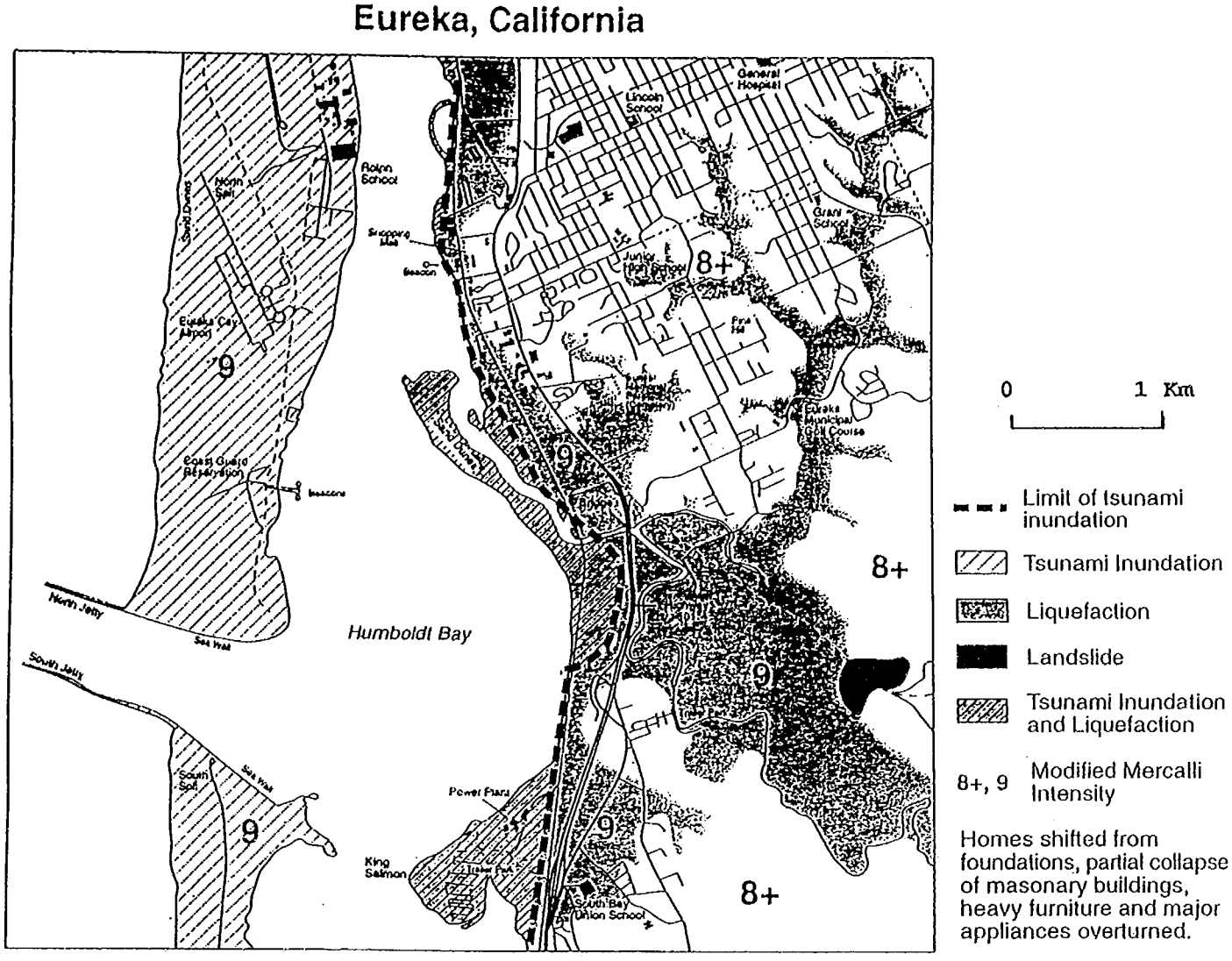


FIGURE 5

Map showing areas subject to tsunami inundation, and seismically induced liquefaction and landsliding from a (M_W) 8.4 earthquake on the Cascadia Subduction Zone (NOAA, 1994; and CDMG, 1995).

Experimental Research on the Use of Viscoelastic Dampers in the Rehabilitation of Lightly Reinforced Concrete Frames

by

John R. Hayes, Jr.*
Pamalee A. Brady*

ABSTRACT

The U.S. military has large numbers of older lightly reinforced concrete frame buildings in its inventory. These buildings were built using detailing practices that have been shown to lead to severe structural deterioration in moderate to high intensity earthquakes. With the growing national emphasis on seismic rehabilitation of older buildings, the U. S. Army Construction Engineering Research Laboratories (USACERL) has undertaken a research program to develop cost-effective methods of seismic rehabilitation of military facilities. Researchers are examining the use of supplemental damping as a means of rehabilitating older buildings. One device under investigation is the viscoelastic damper. This paper outlines the background for and the preliminary results of an analytical and experimental program evaluating viscoelastic damper technology for rehabilitating concrete frame structural systems. The project centers on shaking table tests of scaled replicas of actual U.S. military buildings of the 1950s.

KEYWORDS: buildings, earthquakes, reinforced concrete, supplemental damping, viscoelastic dampers, flat slabs, scaled modeling

1. INTRODUCTION

The U.S. military services have large numbers of concrete frame buildings that were constructed before the seismic provisions of U.S. building codes were upgraded in the 1970s, following the 1971 San Fernando earthquake. Reinforced concrete detailing practices of the earlier era do not provide the strength or ductility required to meet force and displacement demands of moderate to large intensity earthquakes. Common shortcomings of the older structures include the lack of sufficient confining reinforcement in columns, poor reinforcement lap splice location and length in columns, and lack of continuity of slab and/or girder reinforcement in joint regions. Current concrete structure design practice generally precludes using flat slab systems to resist lateral forces. Inadequate shear and moment transfer capacity between slabs and columns leads to punching shear failures of slabs in the column regions when such structures are loaded laterally, especially with high gravity loading present. Researchers at the US Army Construction Engineering Research Laboratories (USACERL) are working on a research program that focuses on improved seismic rehabilitation technologies that address these vulnerabilities. The program examines the use of viscoelastic (VE) damping devices to provide passive energy dissipation in existing lightly reinforced concrete frame structures. Research includes both analytical modeling and experimental testing of scaled model concrete structures on the USACERL shaking table.

USACERL and University of Illinois at Urbana-Champaign (UIUC) jointly conducted a number of one way and flat slab joint subassemblage tests on the USACERL shaking table in 1992 and 1993. The National Center for Earthquake Engineering Research (NCEER), Buffalo, NY, is participating in the project through its support for the work of

* U.S. Army Construction Engineering Research Laboratories (CECER-FLE)
Champaign, IL 61826-9005

researchers at the UIUC. Analysis of the data from those tests is underway. In 1994, USACERL and UIUC tested a one-third scale model of a three-story flat slab frame structure on the USACERL shaking table. This paper focuses on the 1994 testing phase of the project [1].

2. VISCOELASTIC (VE) DAMPER TECHNOLOGY

The rehabilitation technique studied in this project involves adding viscoelastic (VE) dampers in diagonal steel braces to the concrete frame structure. The diagonal struts extend from the bottom of one column to the top of an adjacent column, as shown in Figure 1. Each strut is fabricated from two structural sections with a VE damper device bolted between them. The struts are attached to the reinforced concrete columns using steel collars that are bolted to and around the columns. A typical VE damper is shown in Figure 2. Four layers of VE material are attached to steel plates using epoxy cement. The tensile and compressive strut forces that develop when the structure is subjected to lateral earthquake loading are carried in direct shear by the layers of VE materials.

If the struts did not incorporate dampers, they would only stiffen the structure. This change in structural stiffness would alter the displacement and acceleration responses of the structure to a given earthquake motion. The addition of the VE dampers in the struts not only stiffens the structure but also increases the energy dissipation capacity of the structure, without inducing more structural damage. When the VE layers in the damping devices are sheared, the material heats, converting the input energy into heat energy. This energy dissipation in effect increases the total damping of the structure. Increased damping reduces both displacement and acceleration responses to a given ground motion.

The effects of added stiffness and damping can be seen in the displacement and acceleration response spectra for a single-degree-of-freedom (SDOF) oscillator for the 1940 El Centro earthquake record (Figures 3 and 4). The spectral time scale has been compressed by a factor of $1/\sqrt{3}$ to match that used in the experimental tests. An undamaged reinforced concrete structure under service loads may exhibit an equivalent viscous damping factor of approximately .07. Previous research at both the University of California, Berkeley, and at the State University of New York, Buffalo, indicates that adding VE dampers may result in an equivalent viscous damping factor of .25 for the modified structure. The three-story model tested had a measured fundamental period of approximately .55 seconds without dampers. When the struts with dampers were added, this was reduced to approximately .30 seconds. The acceleration response spectra show that increasing the stiffness without increasing the damping significantly increases the acceleration response; this is illustrated by moving from point A to point B in Figure 4. With the added damping, which is illustrated by moving to point C in the figure, peak acceleration is reduced substantially from that obtained by increasing stiffness without adding damping.

3. PROTOTYPE STRUCTURE

The prototype for the test model is one wing of an H-shaped military barracks building located in the Seattle, WA area. The prototype wing is rectangular in plan, and is approximately 40 feet wide and 117 feet long. It is three stories high, with a structural framing system that is predominately a reinforced concrete flat slab system. Cast-in-place shear walls at the far ends of the length provide lateral force resistance for transverse ground motions, but there are no intermediate shear walls in that direction. Spandrel beams run the length of the building on both longitudinal exterior walls. The spandrels, which are cast monolithically with the floor slabs, support exterior wall and window systems and stiffen the framing. Columns are founded on individual spread footings.

As-built drawings indicate the building was constructed in 1956. The drawings indicate the designers used the Pacific Coast Uniform Building

Code (PCUBC) and the ACI Building Code (ACIBC). All analyses for the project are based on the assumption that the 1955 PCUBC and 1951 ACIBC were used, because they were in effect at the time of construction. The drawings indicate that the structure was designed to PCUBC Seismic Zone III provisions. Structural concrete was designed for a 28-day compressive strength of 3,000 psi; reinforcing steel was designed for a working stress of 20,000 psi.

The drawings show a number of potential problem areas in the structural design, compared with current building code requirements: The structure is a flat slab system. The slab bottom (positive moment) reinforcement is not continuous through interior column regions. Column ties are smaller and spaced further apart than required today. No column reinforcement lap splice details are shown on the drawings, although splice lengths are given. The splice lengths are shorter than would be required today. Splices were assumed to be located in accordance with common practice of that period, directly above each floor level. Stirrups were also widely spaced in the spandrel beams, limiting their flexural steel confinement and torsional capacity. Each of these factors acts to limit the structure's ability to displace laterally without significant damage under the effects of earthquake-induced ground motions.

4. MODEL STRUCTURE

A transverse section near the center of the prototype structure was selected as the basis of the experimental model. This region was considered the most vulnerable area in the structure, as it was a large distance from the perimeter shear walls. The model was constructed at one-third of full scale. Figures 5 and 6 show the overall dimensions and details of the test structure. Reinforcement details in the model were essentially the same as those in the prototype.

The test structure was formed and cast in four levels. The base girder was cast first, followed by the floor and supporting columns in each successively higher story. Ready-mixed concrete with a specified compressive strength of 3,500 psi was used. This strength was chosen to simulate the strength increase with age that would be expected in the prototype. The size of the individual reinforcing bars was also scaled as closely as possible to one-third the size in the prototype by using deformed steel wire from welded wire fabric. The prototype reinforcement was assumed to have a nominal yield stress of 40,000 psi, since the as-built drawings specified a working stress of 20,000 psi. The wire used in the model initially had a yield stress approaching 100,000 psi, so all wire used for longitudinal reinforcement was annealed to match the prototype strength. Column and spandrel transverse reinforcement was not annealed, to save time and expense. The wide tie spacing and the consequent lack of primary steel confinement in the prototype were believed to be more critical than tie strength.

The base girder was cast as a stiff, monolithic unit to accommodate construction of the model structure off the shaking table platform. The model was lifted onto the table for the earthquake simulations, by attaching the crane pickup points directly to the girder. The first-story columns were cast over longitudinal reinforcement that was stubbed out of the base girder.

To simulate gravity load stresses in the various structural elements, and to maintain proper dynamic response characteristics, it was necessary to add lead ingots as floor masses in the model structure. The average total floor load, including the ingots, in the model was approximately 100 psf, which was very close to the total floor load in the prototype structure.

5. REHABILITATION SCHEME

As described earlier, damping devices were added in the column lines of the test structure by adding diagonal struts that included the dampers. The struts were attached to the columns by means of steel collars that were bolted over the columns. Researchers measured the column dimensions and fabricated the collars to provide a snug fit when

they were bolted in place. Before the collars were installed, a thin sand-cement mortar grout was trowelled on the exposed column dimensions. Researchers then bolted the collars in place before the grout set. The collars not only served to transfer the forces that were transmitted by the struts, they also confined the column concrete, thereby increasing the shear and rotational capacities of the columns. In addition, to ensure that the collars did not slip along the column height, an all-thread bolt was placed through each column in the collar region and both sides of the collar. Because of researchers' concern for damaging the scaled model column, the bolt was cast into the column during construction. In a full scale structure, such an attachment would be drilled and grouted in. Figure 1 shows how the damping devices and braces were placed in the test structure, while Figure 7 illustrates a typical detail of an interior column-slab connection.

Structural analyses conducted before the tests indicated that the damper struts would significantly increase shear forces at the bases of the first and second floor outside columns. To minimize the likelihood of a column shear failure, shear transfer capacity was increased at both levels. At the base girder level, the collars were connected to the girder, by means of drilling into the base girder on each side of the column and epoxying in an anchor bolt that was in turn attached to the collar. On the first-story level the researchers drilled and epoxied into the spandrel beam in a similar manner. The overall column flexural strength at the connection to the base girder was increased approximately 25% by using No. 3 bars of 60,000 psi steel, instead of the scaled wire reinforcement with a yield stress of 40,000 psi. Increasing the flexural capacities of these critical columns was assumed to be a likely part of any rehabilitation scheme.

6. TESTING PROGRAM

The model was placed on the USACERL shaking table. Researchers constructed an independent steel safety support structure, added the lead ingots, and installed test instrumentation.

Approximately 75 channels of data were recorded in each test. Instrumentation included longitudinal and lateral accelerations and displacements of the shaking table, base girder, and each floor; damper displacements; damper brace force; damper temperature change (in selected dampers); and reinforcement strains in key column and slab locations.

Earthquake simulation testing was conducted using two different sets of VE dampers, as well as with no dampers in place. 3M engineers fabricated one set of dampers for the desired degree of added damping. They fabricated the second set of dampers with half the volume of damping material of the first set. Prior to the testing, representative samples of the two sizes of dampers sizes were tested in static and cyclic tests, to verify theoretical damper characteristics and ensure sound fabrication. When testing without dampers was conducted, the steel collars remained in place, so that damper effects could be isolated and analyzed.

Before any earthquake simulations, researchers determined the first three modal frequencies and equivalent viscous damping of the undamaged structure in four different states: with no dampers or braces installed, with solid steel braces installed, with the small dampers installed in braces, and with the large dampers installed in braces. White noise tests were conducted to determine the dynamic characteristics of the model. After a white noise test, the table was excited with a sine wave at the model's first mode response frequency. Researchers would then shut the table off and measure the decay of the induced structural motion, from which equivalent viscous damping could be determined, using logarithmic decrement calculations. Measuring the dynamic characteristics became more difficult during the shaking table tests of the model with dampers installed. The high degree of damping in the structure greatly broadened the transfer function bandwidths; peak response frequencies were difficult to identify.

For the earthquake tests with dampers installed in

the model, which were conducted before any earthquake tests without dampers were conducted, two characteristic earthquake records were used: the El Centro site record from the May 18, 1940, Imperial Valley, CA, earthquake, and the Taft site record from the July 21, 1952, Kern County, CA, earthquake. The two records differ significantly, in terms of peak amplitudes and frequency contents. Figures 8 and 9 show the two records with their time scales compressed to $1/\sqrt{3}$ of full scale. To equate the energy contents of the two records for the earthquake simulations, the researchers used the ratio of the spectrum intensities (Housner, 1959) of the two time-scaled records. This process resulted in a need to multiply the Taft motion amplitudes by a factor of 2.1 to approximate the same energy content as the El Centro record. Seismic motions on the shaking table were input through displacement control of the table using the results of double integration of the recorded acceleration records. Earthquake "magnitudes" were varied by increasing input motion displacement amplitudes. Thus, a "100% El Centro" record has motion amplitudes that match the originally recorded motion amplitudes.

Researchers first conducted a series of low level earthquake simulations with the small dampers in place. The simulations were run with base motion amplitudes of 1%, 10%, and 25% of the El Centro record; and at 2.1%, 21%, and 52.5% of the Taft record. Then the structure was tested for the same earthquake records with large dampers installed. After each earthquake simulation, the dynamic characteristics were determined using the previously described white noise and sine decay tests, and the model was checked visually for cracking or other deterioration. The measured dynamic characteristics indicated how the structure was deteriorating under testing.

During the low-level tests, little damage occurred in the model. Larger magnitude earthquake simulations were then conducted using the large dampers. The larger dampers were the original design configuration; their anticipated stiffness and damping characteristics were tuned to the structure. The higher magnitude earthquake simulations were run at motion amplitudes of 10%, 25%, 50%, 75%, 100%, 125%, 150%, 200%, and 250% of the El Centro record; and at amplitudes of 21%, 52.5%, 105%, 157.5%, 210%, 262.5%, 315%,and 420% of the Taft record. Because the higher magnitude El Centro simulations included ground displacements exceeding the peak horizontal displacement capability of the shaking table, the 200% record was run with a .2 hz high pass filter, while the 250% record was run with a .5 hz high pass filter. This filtering of the earthquake record removed the lower frequency, larger displacements in the table motion.

After completing these earthquake simulations, the testing with dampers was terminated. Researchers removed the dampers from the struts. Subsequent tests were then run without dampers; the collars that had been used to attach the dampers to the columns were left in place. Earthquake simulations were then run on the undamped, unbraced structure. The simulations included the same El Centro records that were used in the damper tests. Tests were concluded after the 200% El Centro simulation, when structural failure occurred. No Taft earthquake simulations of the undamped and unbraced structure were included in the test program.

7. INITIAL OBSERVATIONS

Detailed analysis of the experimental data is proceeding. A few initial observations can be made. Initial white noise tests of the structure without struts or dampers showed a first mode frequency of approximately 1.8 hertz (Hz). Based on logarithmic decrement measurements of the acceleration response decay after table shutoff, the baseline structure had an equivalent viscous damping factor of approximately .07 of critical damping. With the large dampers in place, the first mode frequency ranged between 3.05 and 3.56 Hz, for an average of about 3.3 Hz. The equivalent viscous damping based on the logarithmic decrement approached 20% of critical damping.

Preliminary indications are that the model with dampers sustained only minimal damage through the 150% El Centro earthquake simulation (peak ground acceleration, PGA, ≈ .55 g). The white noise tests following this earthquake test showed a first mode frequency that was virtually unchanged from the initial white noise tests. Visual checks of the model showed only minor additional hairline cracking. During the 150% El Centro earthquake test, the largest inter-story drift was measured as .45 inches (1.1%). It occurred in the second story. The total drift at the third floor level was 1.17 inches (1.0%). The maximum base shear experienced during the test was 34.6 kips; the total model weight, neglecting the base girder, was approximately 54.7 kips. Figures 10 and 11 show third floor displacement and base shear response histories, respectively. Tables 1 through 4 show representative tables of data from the tests.

Corresponding El Centro and Taft earthquake tests were run sequentially, so, prior to the 150% El Centro test, the model had sustained the El Centro tests through the 100% level and the Taft tests through the 210% level. Maximum results of the Taft tests performed with the stiff dampers can be found in Tables 5 through 8. Preliminary data review indicates that the model with dampers began to sustain discernable damage in the 200% El Centro earthquake test (PGA ≈ .86 g). The white noise tests following this simulation showed a first mode frequency of approximately 2.88 Hz. Visual checks of the model showed additional hairline cracking had occurred. Most of this cracking was confined to flexural cracking in the floor slabs and minor torsional cracking of the spandrel beams at the interfaces with the columns. During the 200% El Centro simulation, the largest inter-story drift was measured as .88 inches (2.2%), again occurring in the second story. The total drift was 2.04 inches (1.7%). The maximum base shear experienced during the test was 44.2 kips. Figures 10 and 11 show third floor displacement and base shear response histories, respectively. Tables 1 through 4 show representative tables of data from the tests.

For the earthquake tests without dampers, only the El Centro record was used. An initial white noise test showed a first mode frequency of approximately 1.56 Hz, versus the original 1.8 Hz. The model had softened and its measured damping had increased, indicating damage to the structure had accrued during the preceding earthquake simulation tests.
For simulations through the 75% El Centro magnitude, white noise tests (and visual observations) showed little further deterioration of the structure. Following the 100% (PGA ≈ .41g) and 150% El Centro simulation, the fundamental frequency decreased and widened in bandwidth; the average was approximately 1.38 Hz. During the 200% El Centro simulation, the structure failed; it was not catastrophic, but further testing was deemed to be unsafe. Failure occurred when the concrete cover over the reinforcement that extended from the third floor columns into the third floor slab spalled off, substantially softening the joint region. At nearly the same instant, the second and third floor spandrel beams failed in torsion at their interfaces with the columns.

A brief comparison of the 150% El Centro responses with and without dampers (Tables 1-4) shows a trend toward higher base shear forces and lower displacements with dampers installed. Maximum second story drift with the dampers installed was .45 inches, versus 1.21 inches without dampers. Maximum base shear with dampers installed was 34.6 kips, versus 17.0 kips without dampers. The stiffness of the structure had decreased between the two 150% El Centro tests, shifting the response. Significant damage began occurring in the test without dampers in the 150% El Centro test. The 200% El Centro test maxima are also listed in Tables 1-4; note that failure occurred in the unbraced structure at this acceleration amplitude.

Detailed analyses of the test data, including consideration of damper temperatures, displacements, and forces, are underway. Analytical models are also being used to interpret the observed responses. The preliminary results of these experiments indicate that damage can be

controlled or limited in older reinforced concrete structures using supplemental dampers. Although the viscoelastic dampers performed well in the laboratory environment, several design issues must be resolved before implementation in a full-scale seismic rehabilitation program. Key issues to be addressed include damper sizing and placement, ambient temperature control, damper proof testing, and appropriate structural detailing. For further information on these tests, contact Jack Hayes at (217) 373-7248, or Pamalee Brady at (217) 373-7247.

8. ACKNOWLEDGMENTS

The authors express their appreciation to the various organizations that have supported this research: the U.S. Army Corps of Engineers and the National Center for Earthquake Engineering Research for research funding; 3M Corporation for donated engineering expertise and damper devices; and Ivy Wire and Steel for donated steel reinforcement.

9. REFERENCE

1. Hayes, J.R., Jr., Dausman, E.M., Umbright, B.L., Foutch, D.A., Wood, S.L., and Brady, P.A., "Seismic Retrofit of Existing Concrete Frame Structures Using Viscoelastic Damping Devices," DRAFT USACERL Interim Report FM-95, February 1995.

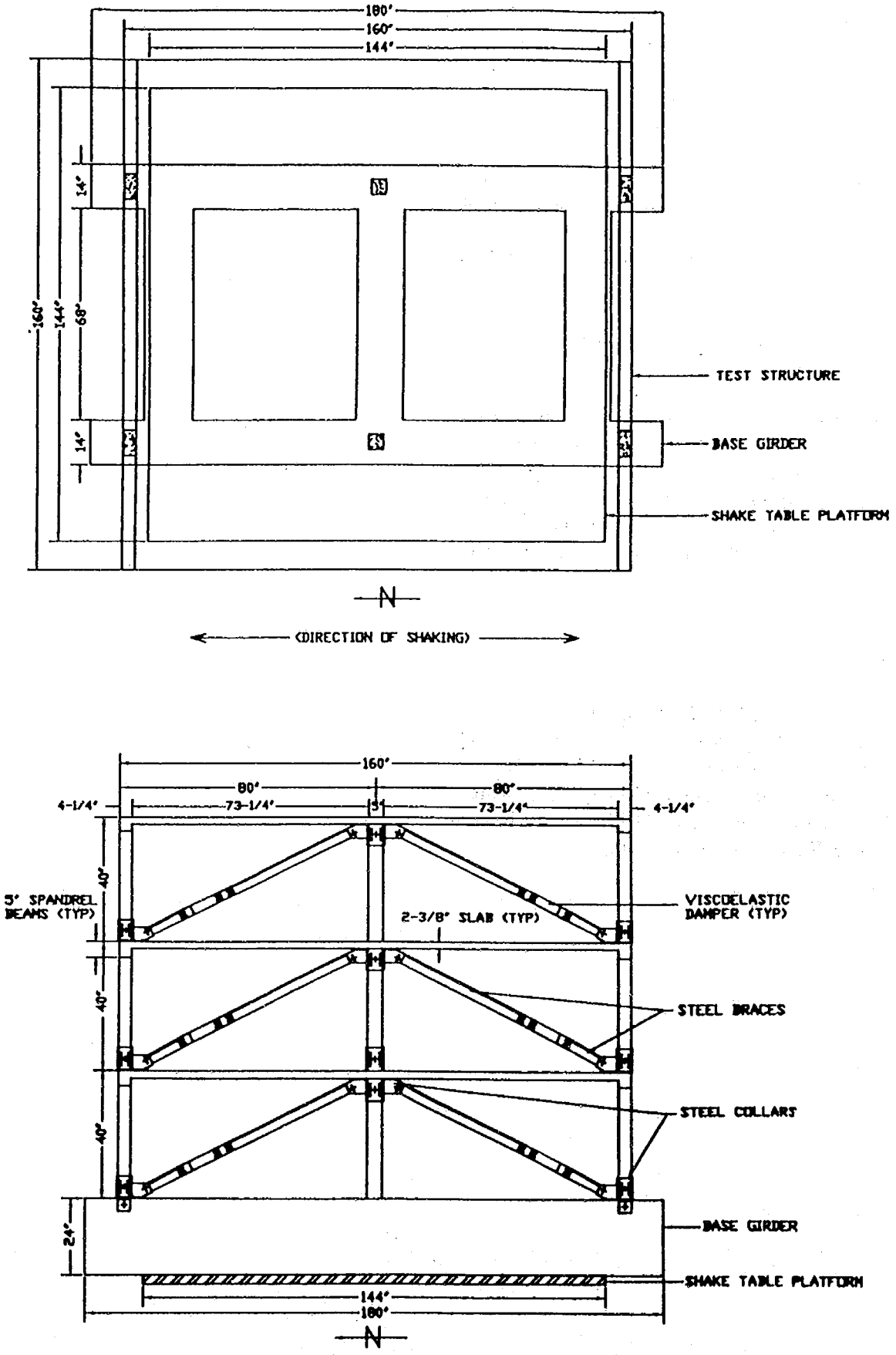


Figure 1. East-West elevation and plan view of structure with dampers and braces in place.

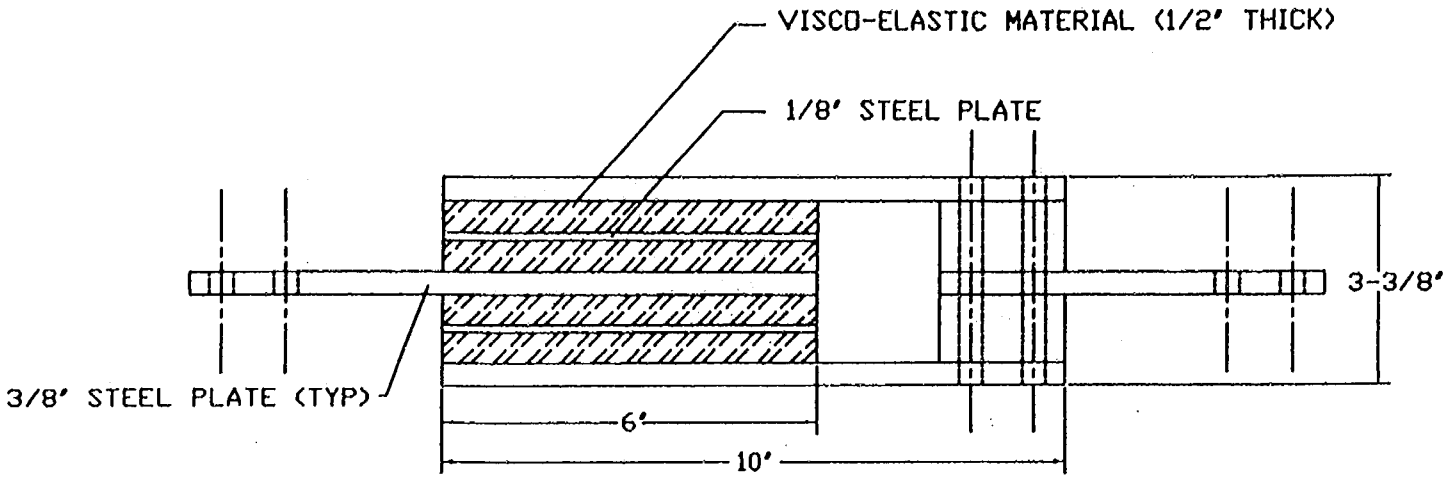


Figure 2.a. Top view of damper.

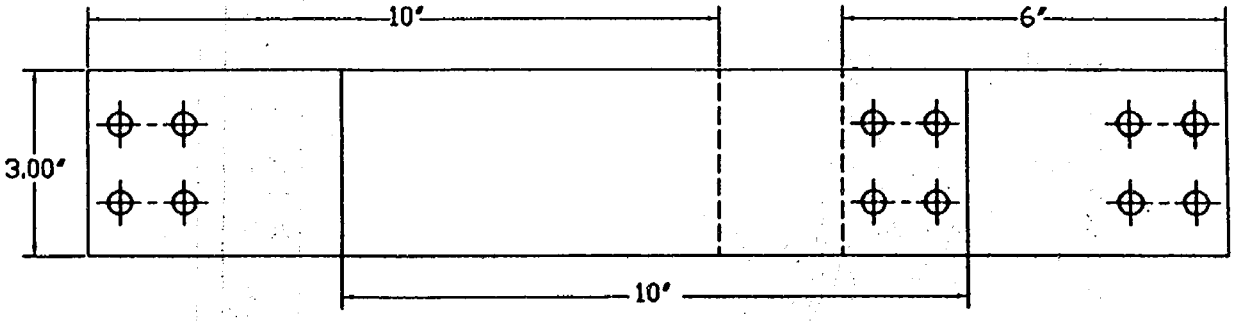


Figure 2.b. Front view of damper.

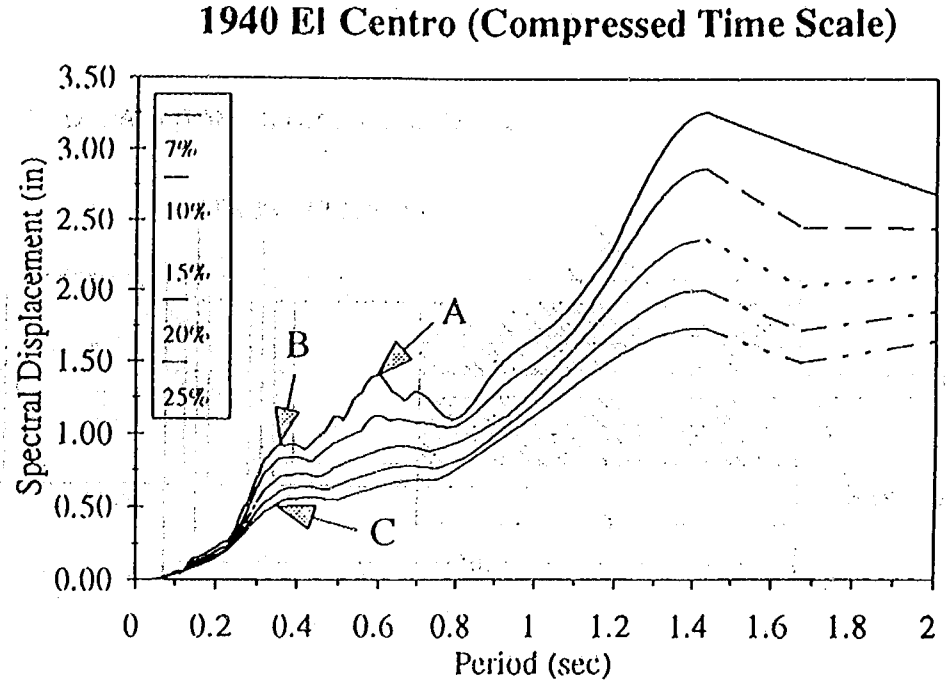


Figure 3. Displacement response spectra.

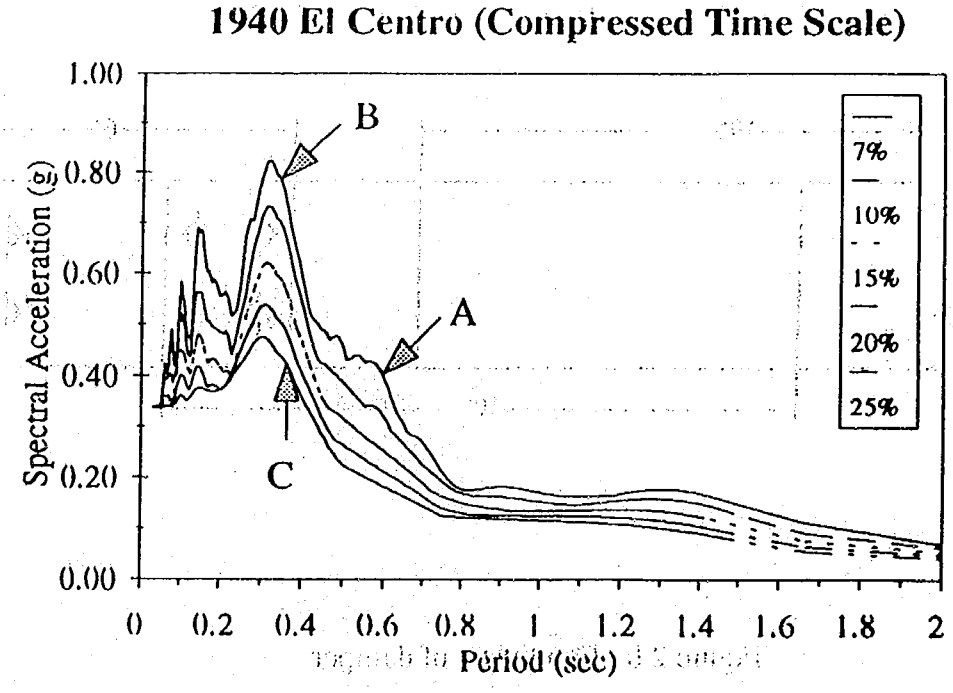


Figure 4. Peak ground acceleration response spectra.

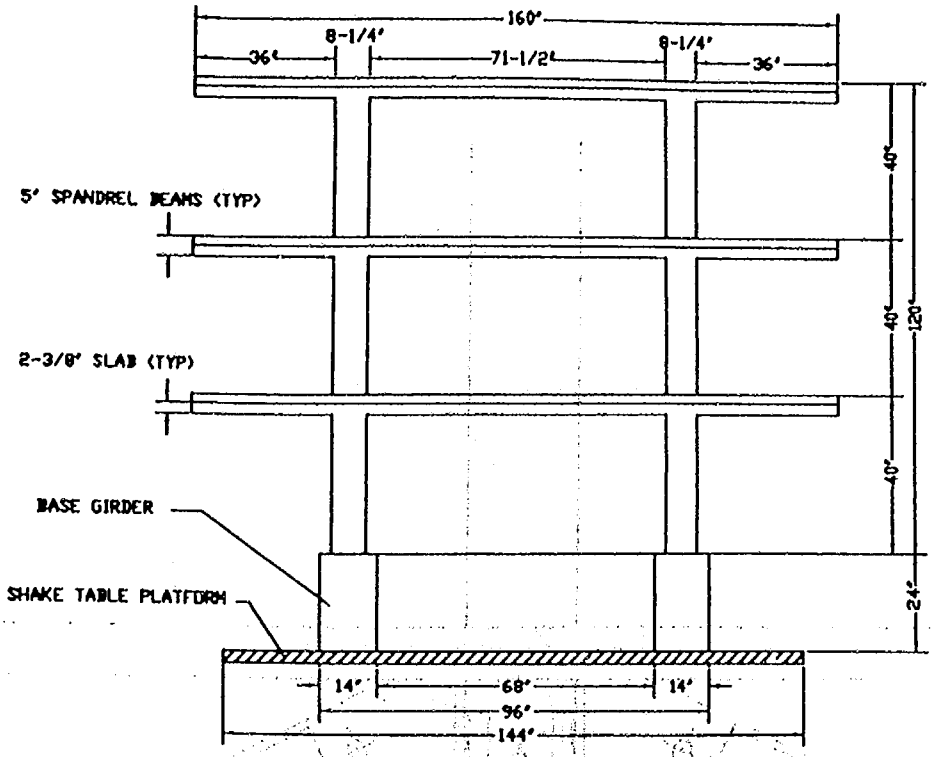


Figure 5. North-South elevation of structure.

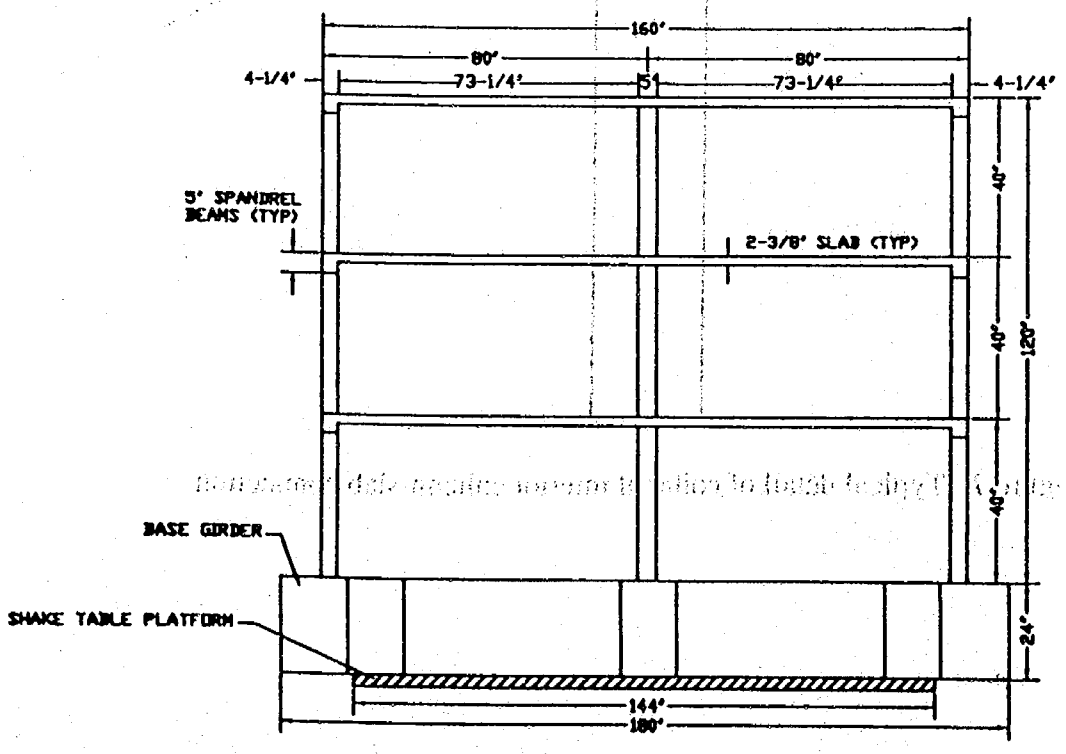


Figure 6. East-West elevation of structure.

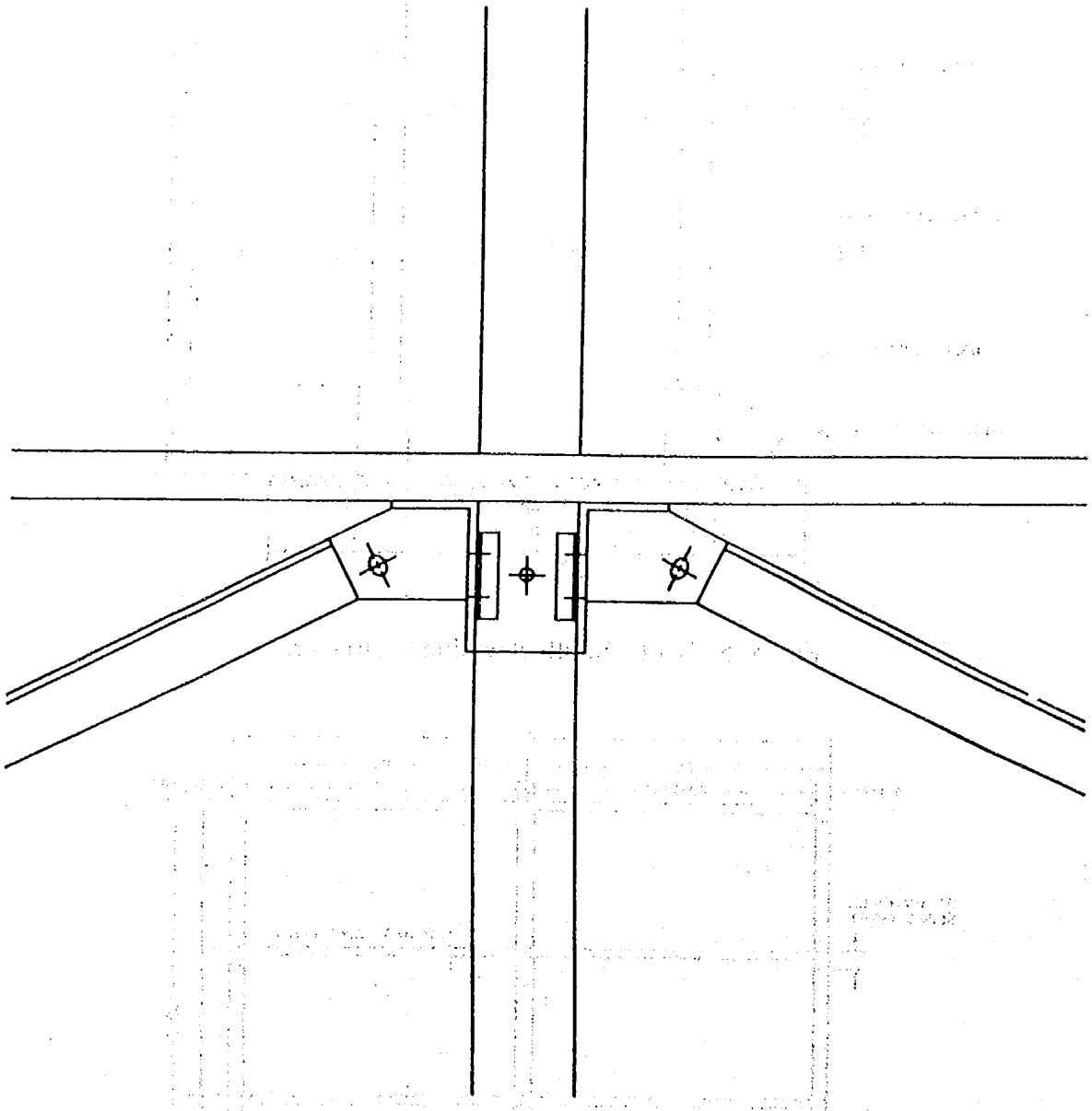


Figure 7. Typical detail of collar at interior column-slab connection.

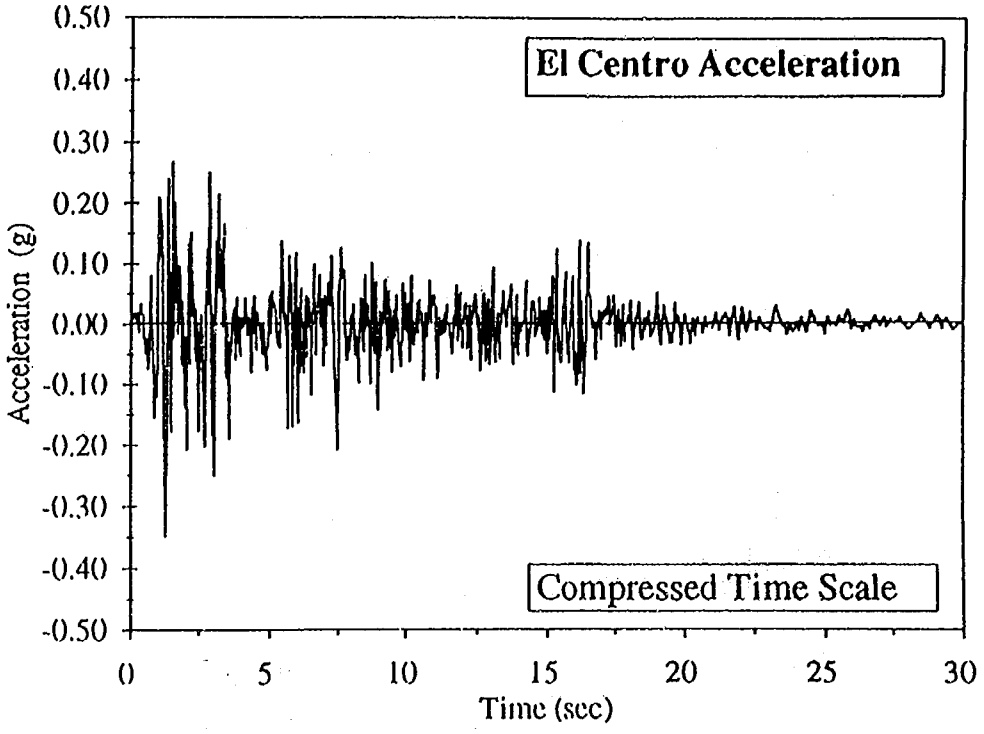


Figure 8. El Centro acceleration input record - time scaled by $1/\sqrt{3}$.

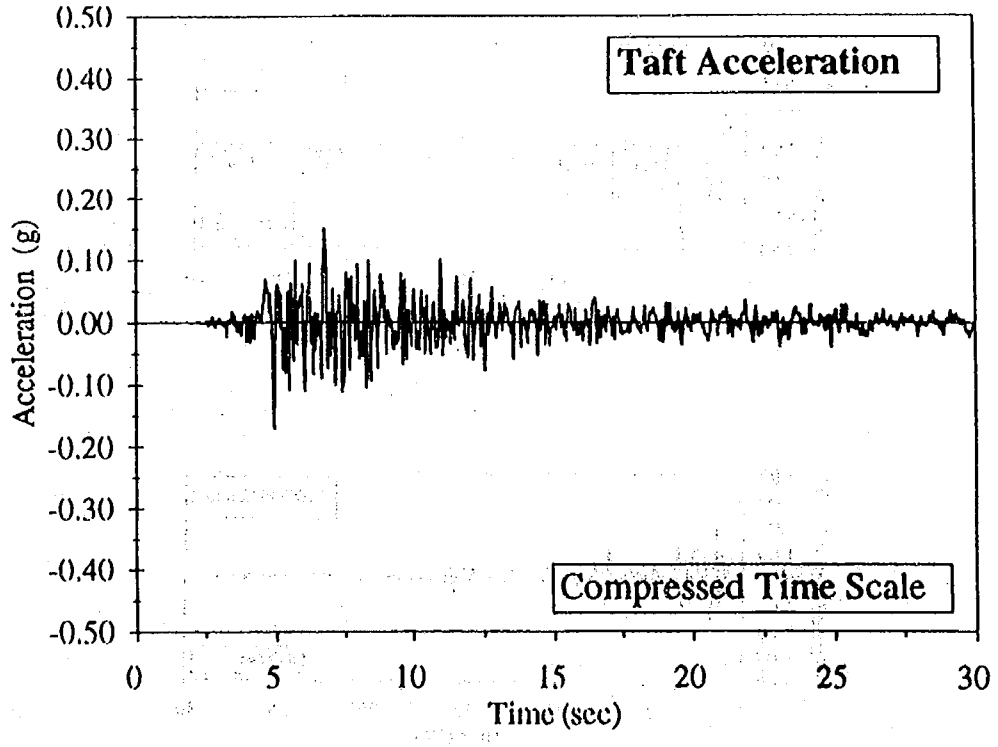
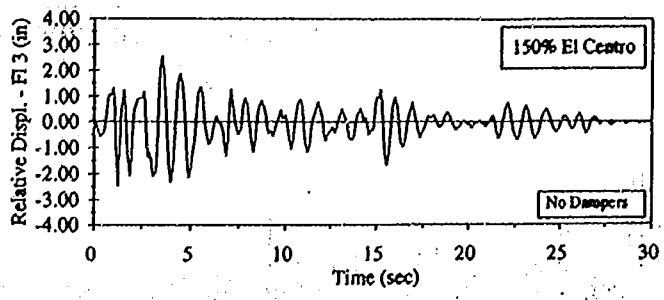
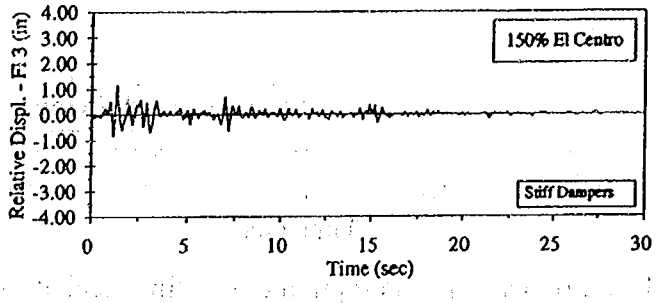
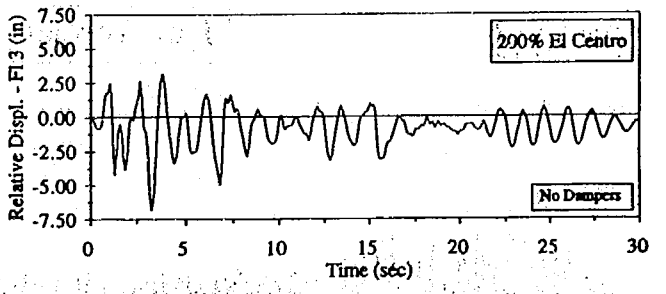


Figure 9. Taft acceleration input record - time scaled by $1/\sqrt{3}$.







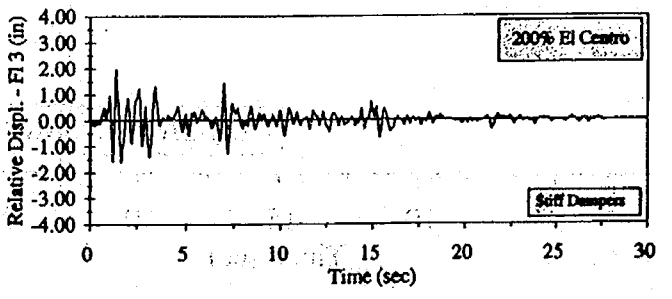


Figure 10. 150% and 200% El Centro third floor relative displacement histories with and without stiff dampers.

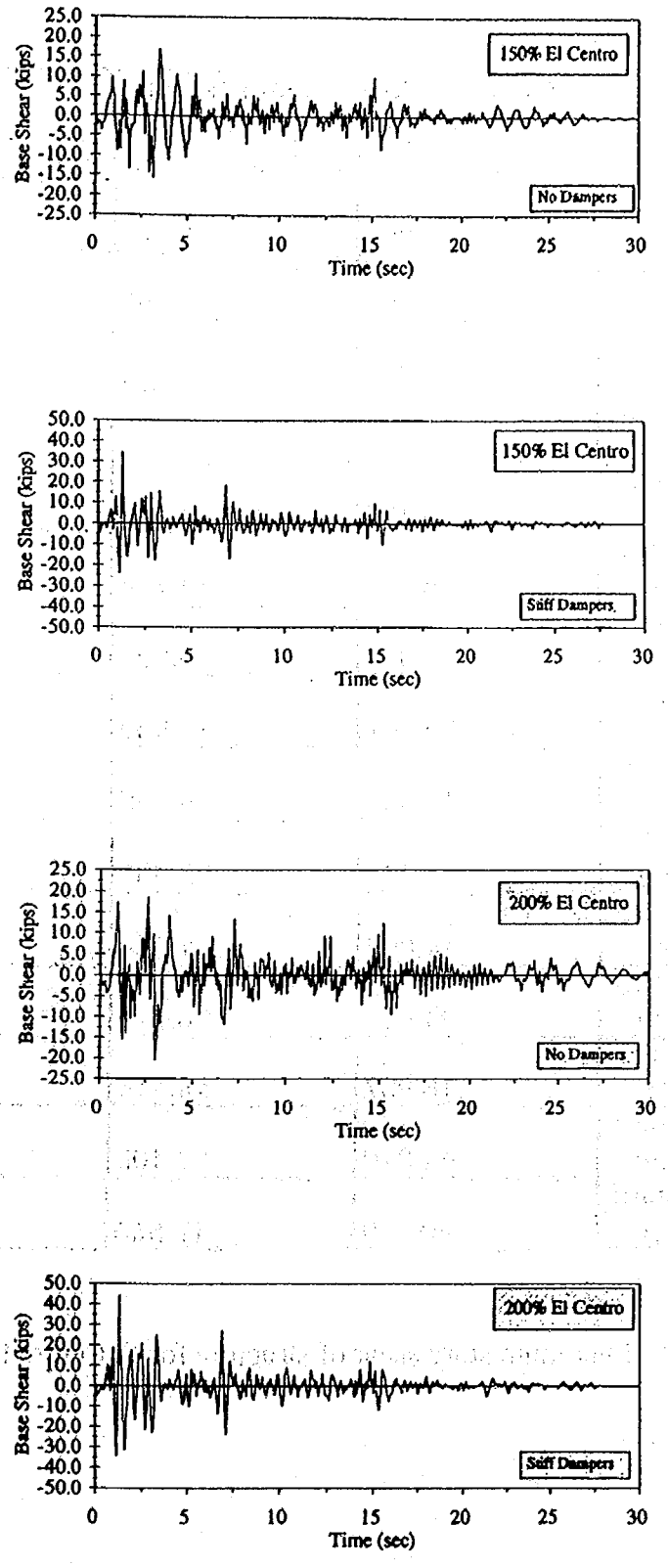


Figure 11. 150% and 200% El Centro base shear time histories with and without stiff dampers.

Maximum Story Shear (kips) (with and without stiff dampers)			
Earthquake Test	*1st Story Shear*	*2nd Story Shear*	*3rd Story Shear*
10% El Centro (with dampers)	2.350	1.674	1.028
25% El Centro (with dampers)	6.054	4.052	2.832
25% El Centro (no dampers)	2.898	2.184	1.569
50% El Centro (with dampers)	13.225	9.717	5.293
50% El Centro (no dampers)	5.180	4.263	3.092
75% El Centro (with dampers)	18.384	14.766	8.304
75% El Centro (no dampers)	8.084	6.925	4.961
100% El Centro (with dampers)	23.707	18.553	10.360
100% El Centro (no dampers)	11.033	9.356	6.968
125% El Centro (with dampers)	27.775	22.350	12.801
125% El Centro (no dampers)	14.092	1.988	8.748
150% El Centro (with dampers)	34.636	26.774	15.007
150% El Centro (no dampers)	16.987	14.414	9.811
200% El Centro (with dampers)	44.219	37.108	21.592
200% El Centro (no dampers)	20.709	17.566	11.694

Table 1. Maximum story shear of structure for El Centro tests.

Maximum Inter-Story Displacement (in) (with and without stiff dampers)			
Earthquake Test	*1st Story Drift*	*2nd Story Drift*	*3rd Story Drift*
10% El Centro (with dampers)	0.029	0.037	0.023
25% El Centro (with dampers)	0.065	0.078	0.049
25% El Centro (no dampers)	0.110	0.185	0.134
50% El Centro (with dampers)	0.124	0.139	0.096
50% El Centro (no dampers)	0.226	0.353	0.257
75% El Centro (with dampers)	0.196	0.228	0.159
75% El Centro (no dampers)	0.348	0.529	0.395
100% El Centro (with dampers)	0.252	0.308	0.219
100% El Centro (no dampers)	0.943	0.710	0.541
125% El Centro (with dampers)	0.343	0.401	0.282
125% El Centro (no dampers)	0.518	0.914	0.706
150% El Centro (with dampers)	0.412	0.453	0.306
150% El Centro (no dampers)	0.687	1.209	0.949
200% El Centro (with dampers)	0.639	0.883	0.522
200% El Centro (no dampers)	0.864	3.076	2.967

Table 2. Maximum inter-story displacement of structure for El Centro tests.

Maximum Absolute Acceleration (g) (with and without stiff dampers)				
Earthquake Test	*Base Girder*	*1st Story*	*2nd Story*	*3rd Story*
10% El Centro (with dampers)	0.049	0.044	0.035	0.059
25% El Centro (with dampers)	0.141	0.141	0.088	0.164
25% El Centro (no dampers)	0.108	0.108	0.114	0.091
50% El Centro (with dampers)	0.228	0.224	0.261	0.306
50% El Centro (no dampers)	0.212	0.213	0.229	0.178
75% El Centro (with dampers)	0.312	0.311	0.384	0.479
75% El Centro (no dampers)	0.304	0.326	0.350	0.286
100% El Centro (with dampers)	0.408	0.397	0.475	0.598
100% El Centro (no dampers)	0.407	0.424	0.493	0.402
125% El Centro (with dampers)	0.467	0.471	0.564	0.739
125% El Centro (no dampers)	0.482	0.539	0.579	0.505
150% El Centro (with dampers)	0.553	0.567	0.690	0.866
150% El Centro (no dampers)	0.563	0.640	0.602	0.472
200% El Centro (with dampers)	0.858	0.779	0.959	1.247
200% El Centro (no dampers)	0.983	0.862	0.798	0.675

Table 3. Maximum absolute acceleration of structure for El Centro tests.

Maximum Relative Displacement (in) (with and without stiff dampers)			
Earthquake Test	*1st Story Displ*	*2nd Story Displ*	*3rd Story Displ*
10% El Centro (with dampers)	0.029	0.060	0.067
25% El Centro (with dampers)	0.065	0.133	0.173
25% El Centro (no dampers)	0.110	0.276	0.382
50% El Centro (with dampers)	0.124	0.255	0.346
50% El Centro (no dampers)	0.226	0.564	0.816
75% El Centro (with dampers)	0.196	0.411	0.566
75% El Centro (no dampers)	0.348	0.861	1.229
100% El Centro (with dampers)	0.252	0.555	0.761
100% El Centro (no dampers)	0.943	1.591	2.033
125% El Centro (with dampers)	0.343	0.724	0.990
125% El Centro (no dampers)	0.518	1.422	2.009
150% El Centro (with dampers)	0.412	0.847	1.134
150% El Centro (no dampers)	0.687	1.838	2.566
200% El Centro (with dampers)	0.640	1.472	1.970
200% El Centro (no dampers)	0.862	3.897	6.814

Table 4. Maximum relative displacement of structure for El Centro tests.

Maximum Absolute Acceleration (g) (with stiff dampers)				
Earthquake Test	*Base Girder*	*1st Story*	*2nd Story*	*3rd Story*
21% Taft (with dampers)	0.046	0.046	0.036	0.051
52.5% Taft (with dampers)	0.099	0.096	0.066	0.128
100% Taft (with dampers)	0.175	0.166	0.203	0.233
157.5% Taft (with dampers)	0.309	0.253	0.305	0.357
210% Taft (with dampers)	0.414	0.348	0.425	0.489
262.5% Taft (with dampers)	0.522	0.436	0.524	0.643
315% Taft (with dampers)	0.628	0.530	0.562	0.722
420% Taft (with dampers)	0.888	0.695	0.770	1.072

Table 7. Maximum absolute acceleration of structure for Taft tests.

Maximum Relative Displacement (in) (with stiff dampers)			
Earthquake Test	*1st Story Displ*	*2nd Story Displ*	*3rd Story Displ*
21% Taft (with dampers)	0.025	0.051	0.076
52.5% Taft (with dampers)	0.057	0.116	0.164
100% Taft (with dampers)	0.120	0.241	0.320
157.5% Taft (with dampers)	0.199	0.397	0.525
210% Taft (with dampers)	0.268	0.575	0.761
262.5% Taft (with dampers)	0.359	0.757	1.002
315% Taft (with dampers)	0.425	0.891	1.172
420% Taft (with dampers)	0.662	1.414	1.844

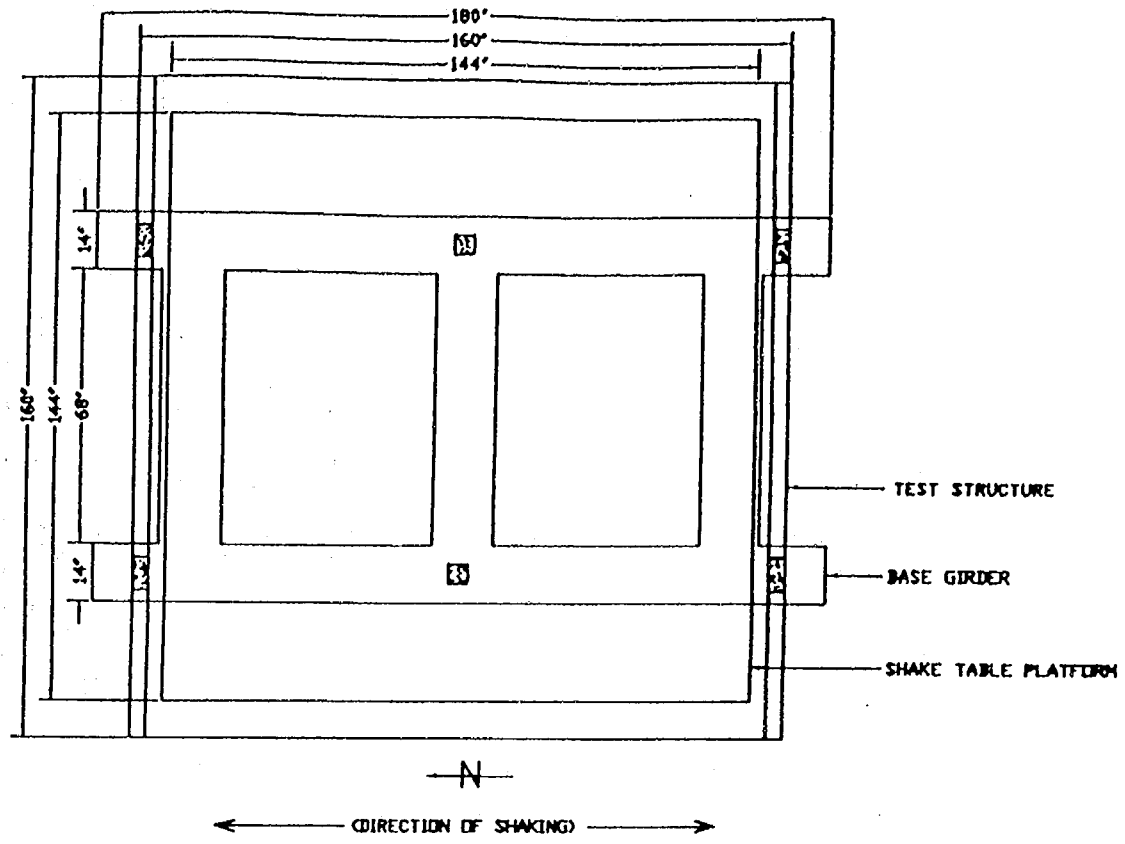
Table 8. Maximum relative displacement of structure for Taft tests.

Maximum Story Shear (kips) (with and without stiff dampers)			
Earthquake Test	*1st Story Shear*	*2nd Story Shear*	*3rd Story Shear*
21% Taft (with dampers)	2.199	1.494	0.886
52.5% Taft (with dampers)	4.869	3.388	2.217
100% Taft (with dampers)	9.544	6.465	2.871
157.5% Taft (with dampers)	15.237	11.671	6.186
210% Taft (with dampers)	19.693	16.368	8.463
262.5% Taft (with dampers)	24.764	20.698	11.135
315% Taft (with dampers)	28.583	22.451	12.509
420% Taft (with dampers)	38.715	31.795	18.568

Table 5. Maximum story shear of structure for Taft tests.

Maximum Inter-Story Displacement (in) (with and without stiff dampers)			
Earthquake Test	*1st Story Drift*	*2nd Story Drift*	*3rd Story Drift*
21% Taft (with dampers)	0.025	0.032	0.028
52.5% Taft (with dampers)	0.057	0.069	0.057
100% Taft (with dampers)	0.120	0.134	0.083
157.5% Taft (with dampers)	0.199	0.219	0.136
210% Taft (with dampers)	0.268	0.336	0.193
262.5% Taft (with dampers)	0.359	0.425	0.256
315% Taft (with dampers)	0.425	0.498	0.288
420% Taft (with dampers)	0.662	0.817	0.448

Table 6. Maximum inter-story displacement of structure for Taft tests.



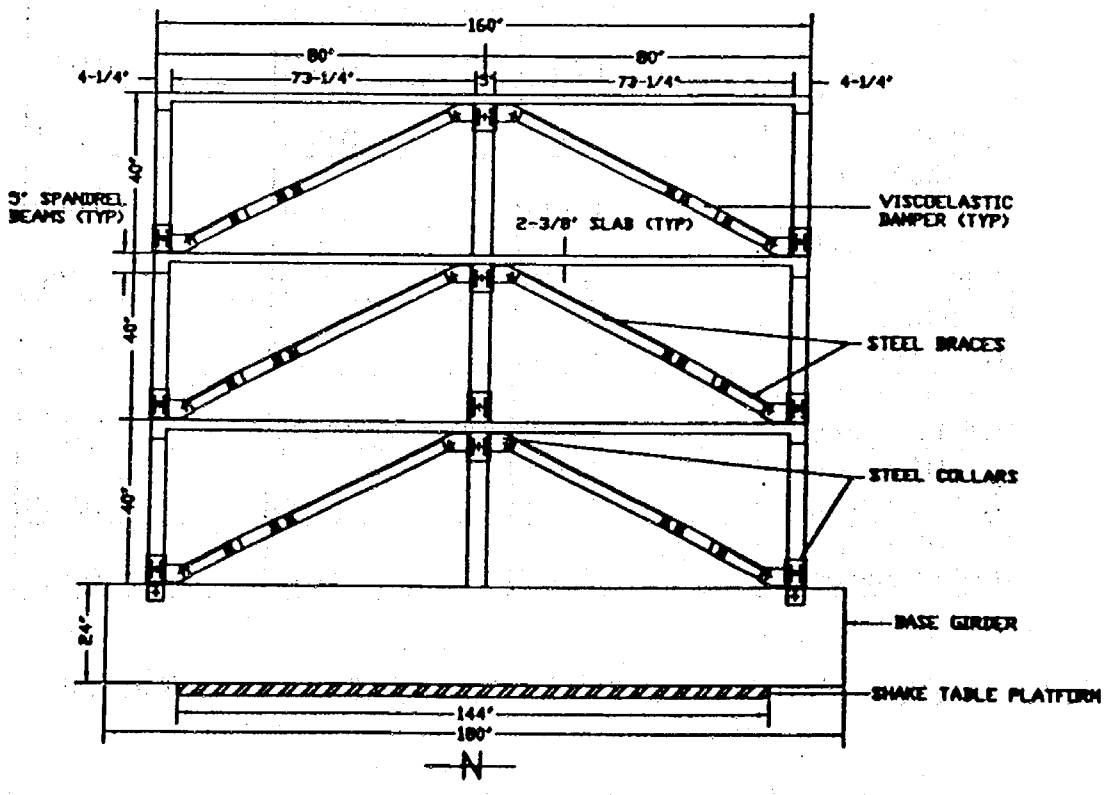


Figure 1. East-West elevation and plan view of structure with dampers and braces in place.

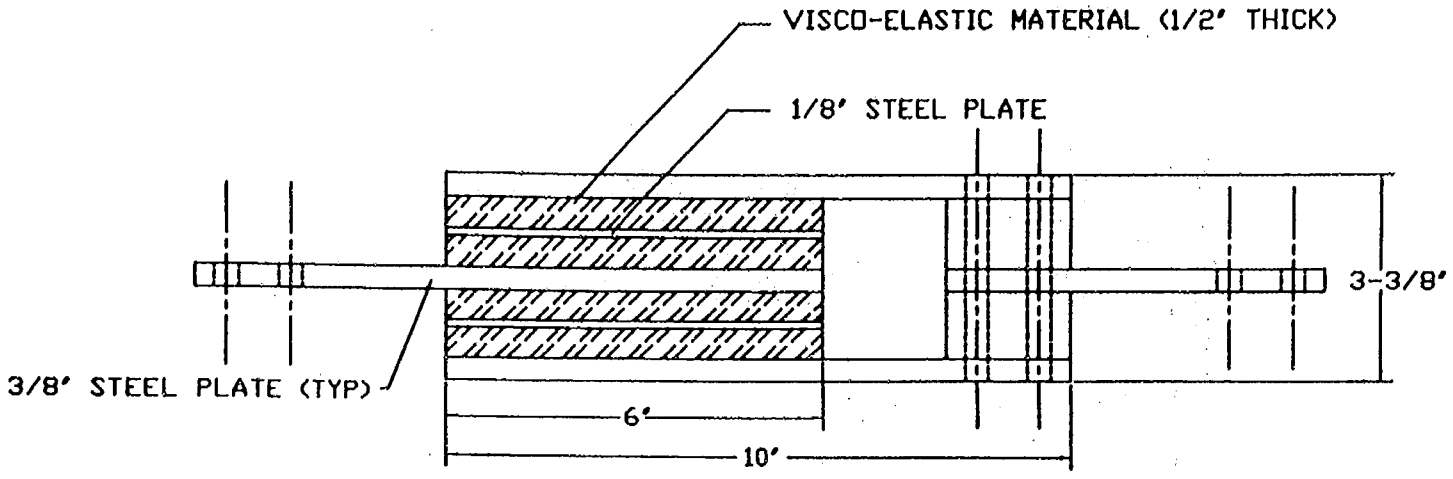


Figure 2.a. Top view of damper.

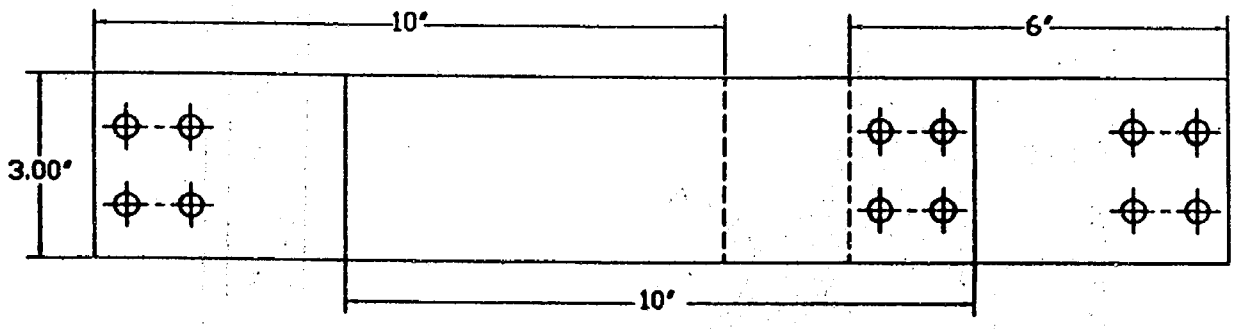


Figure 2.b. Front view of damper.

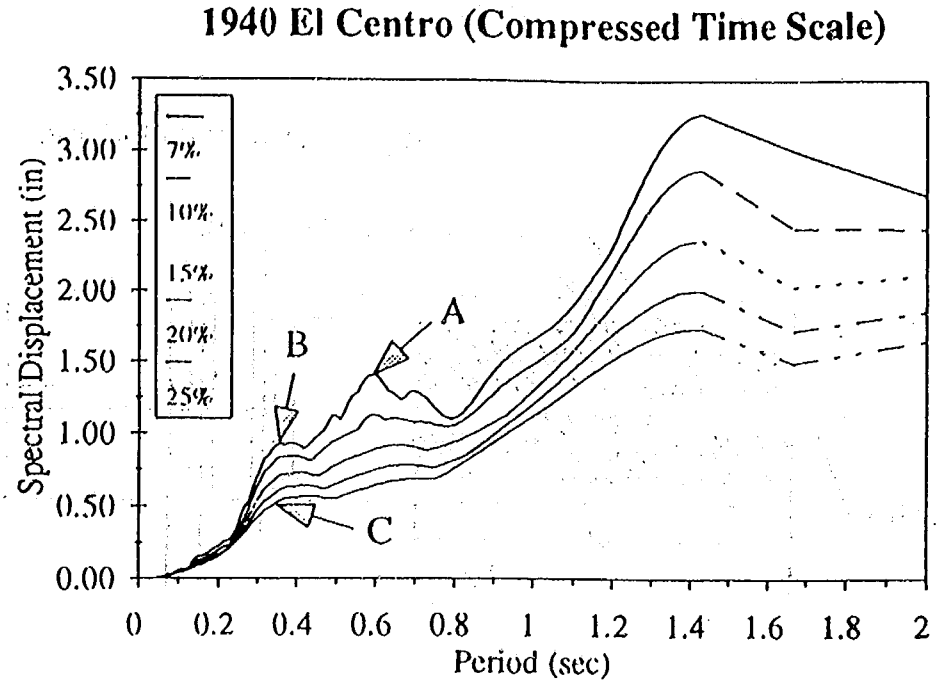


Figure 3. Displacement response spectra.

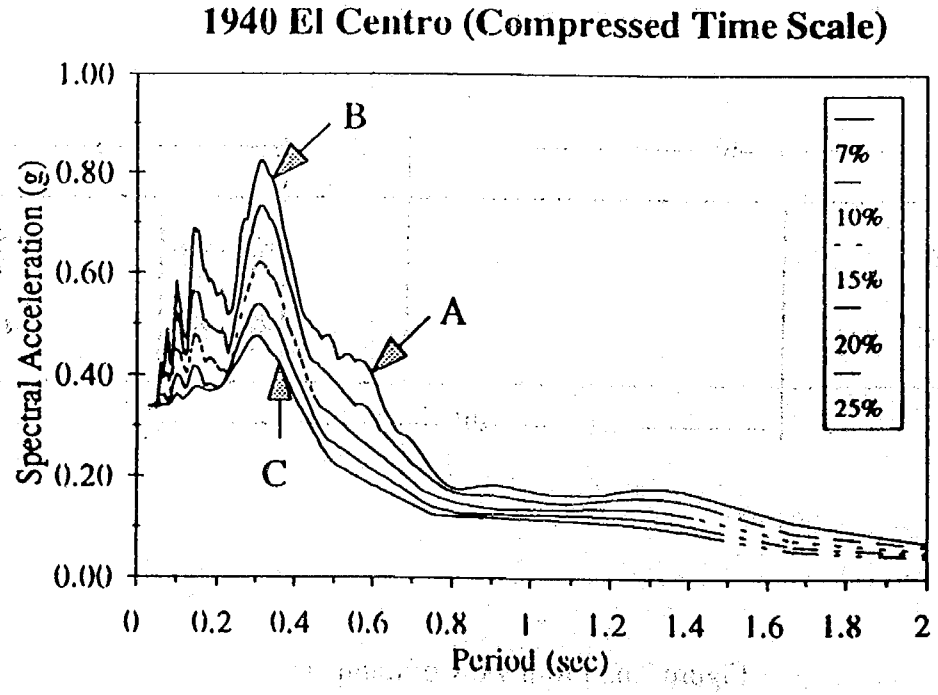


Figure 4. Peak ground acceleration response spectra.

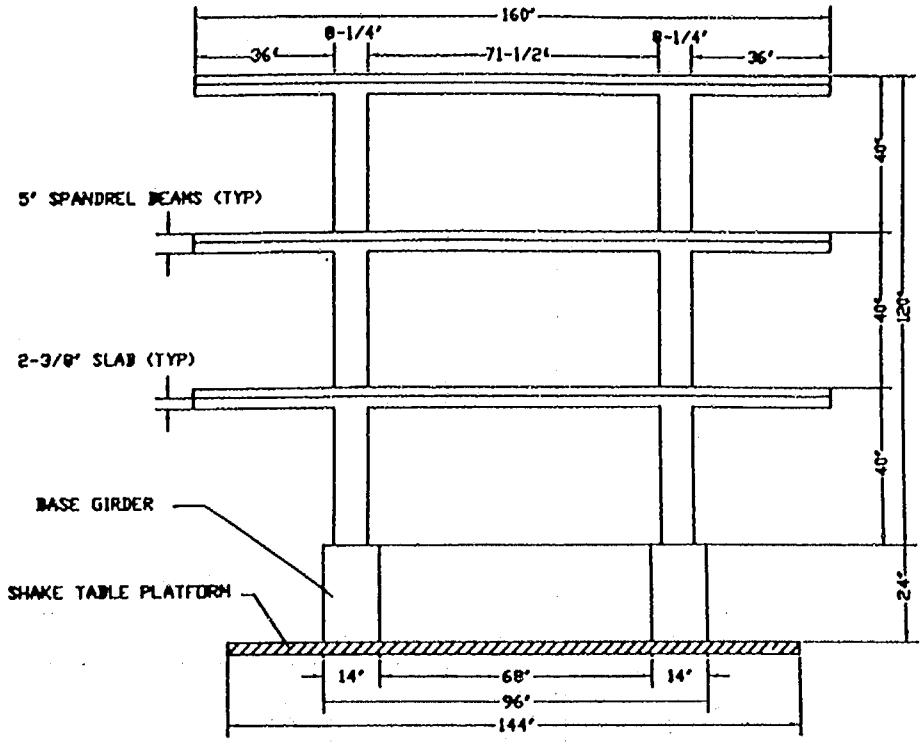


Figure 5. North-South elevation of structure.

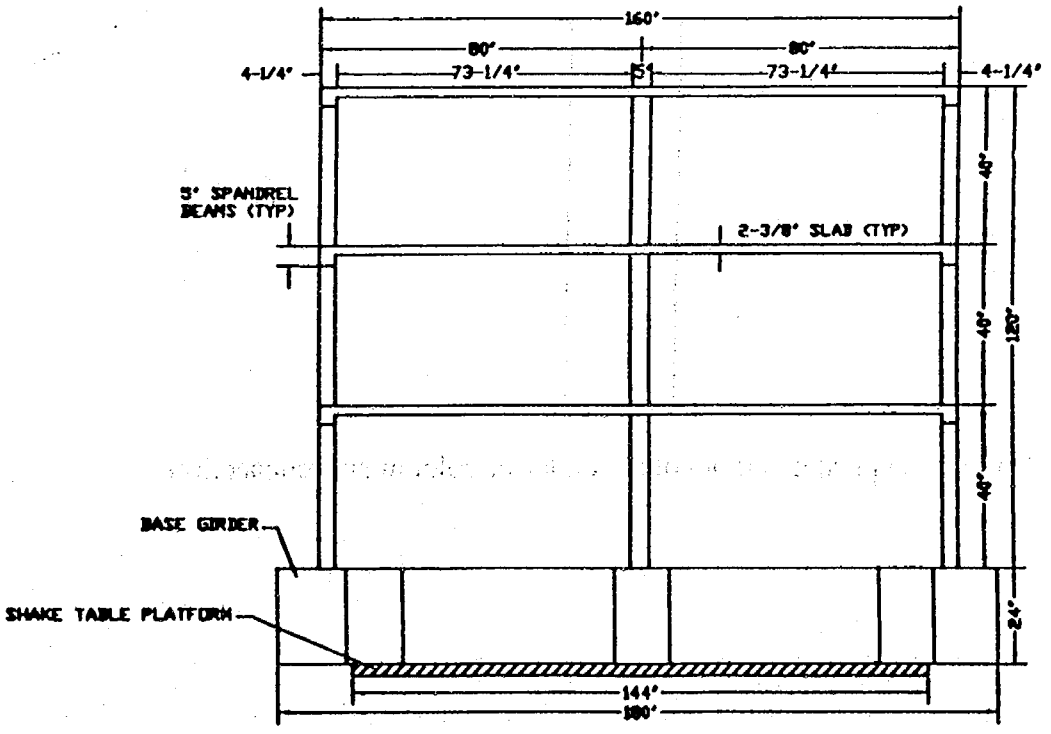


Figure 6. East-West elevation of structure.

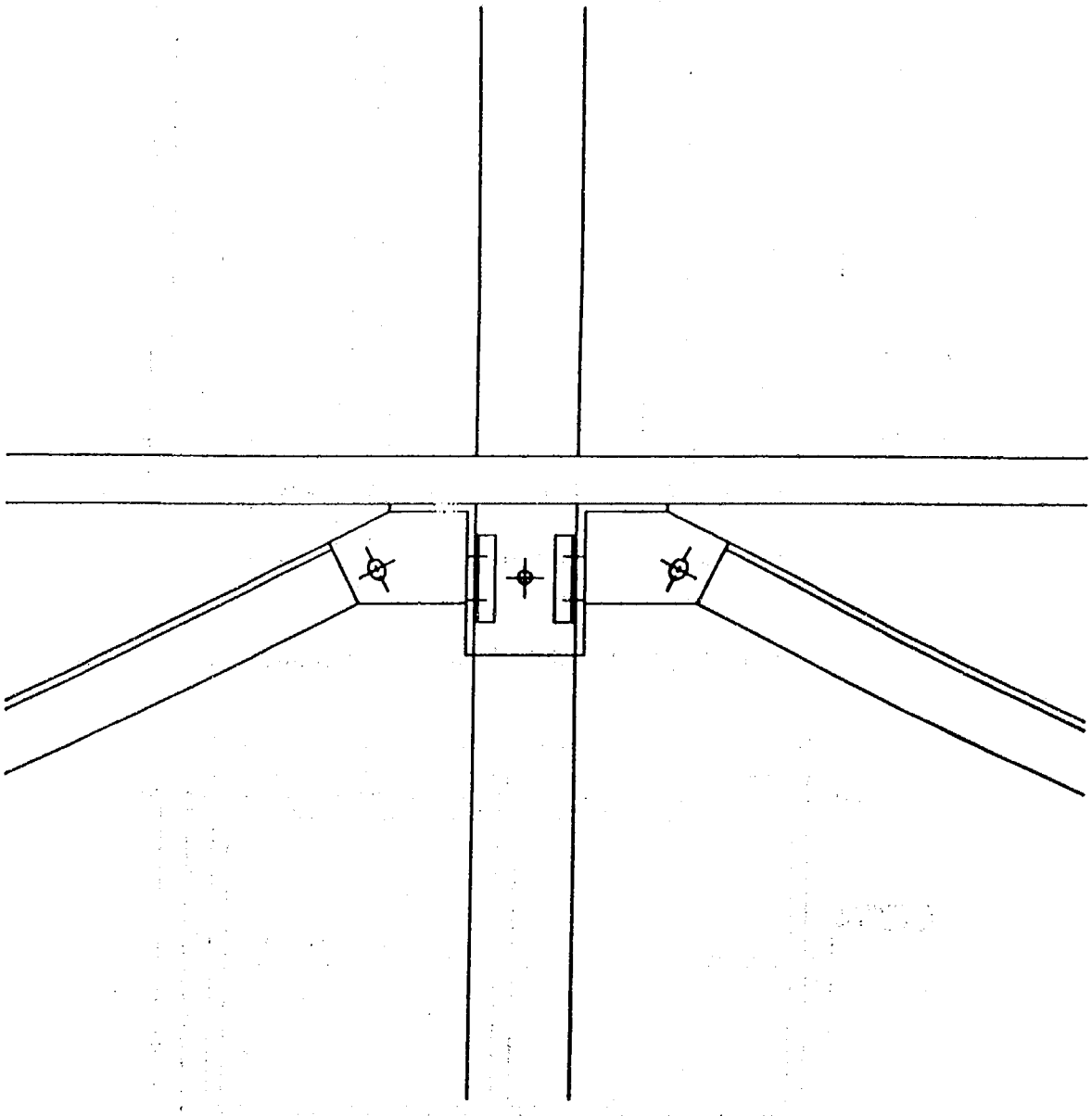


Figure 7. Typical detail of collar at interior column-slab connection.

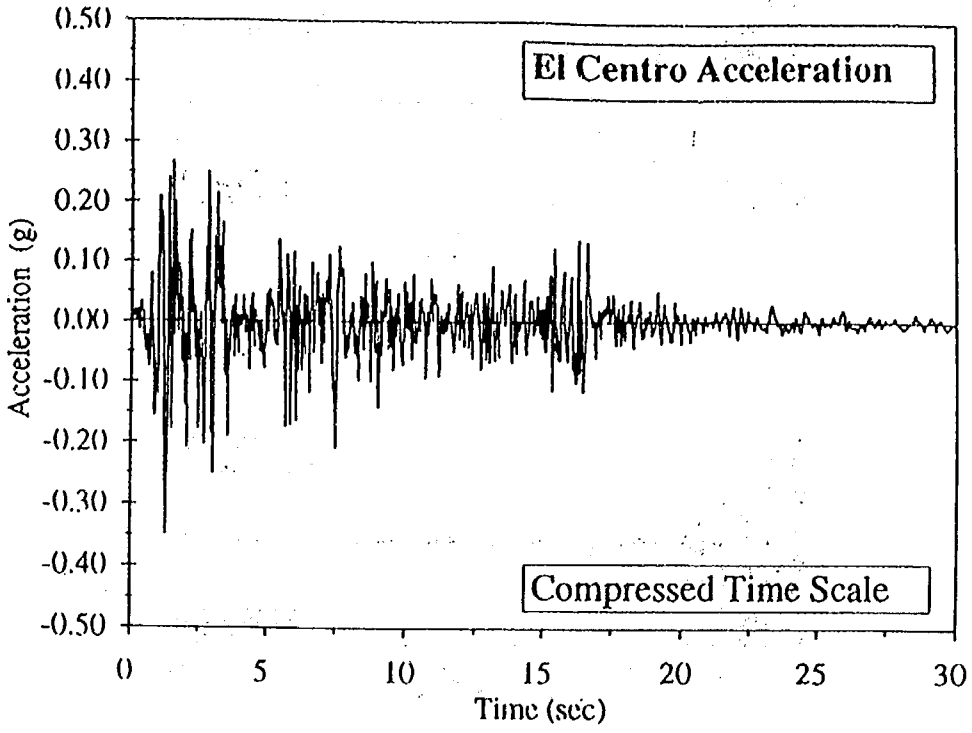


Figure 8. El Centro acceleration input record - time scaled by 1/√3.

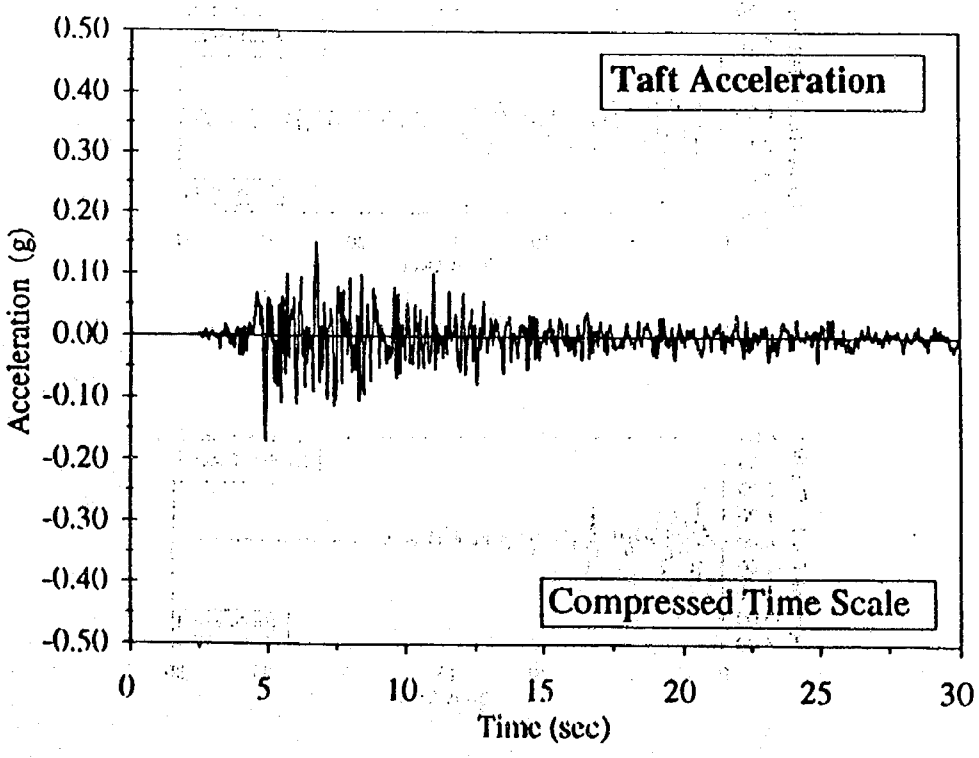
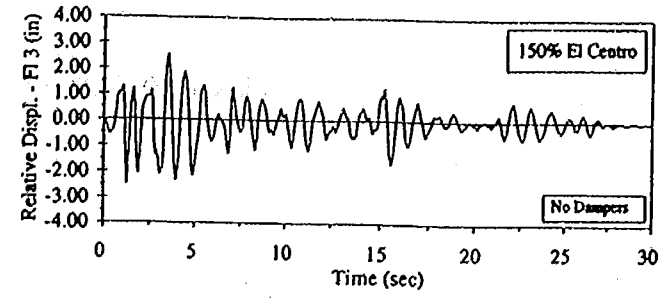
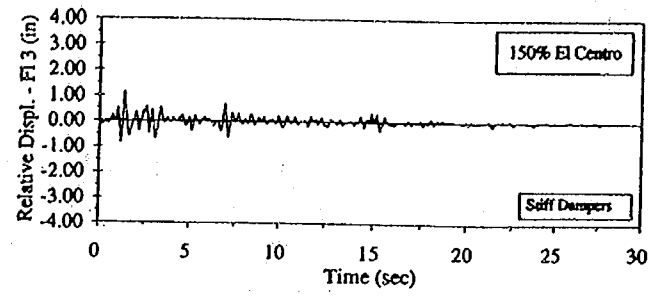
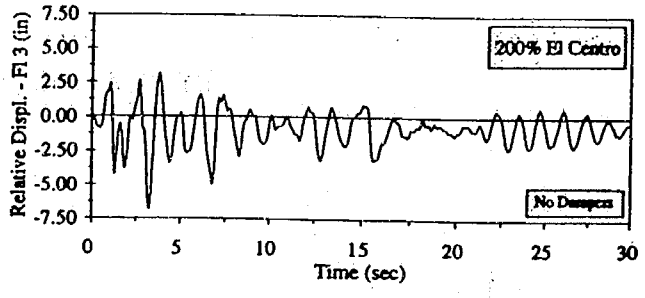


Figure 9. Taft acceleration input record - time scaled by 1/√3.







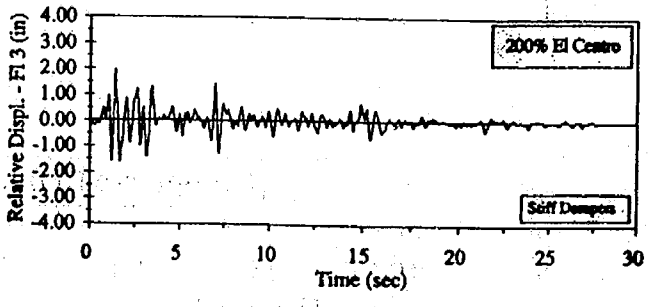


Figure 10. 150% and 200% El Centro third floor relative displacement histories with and without stiff dampers.

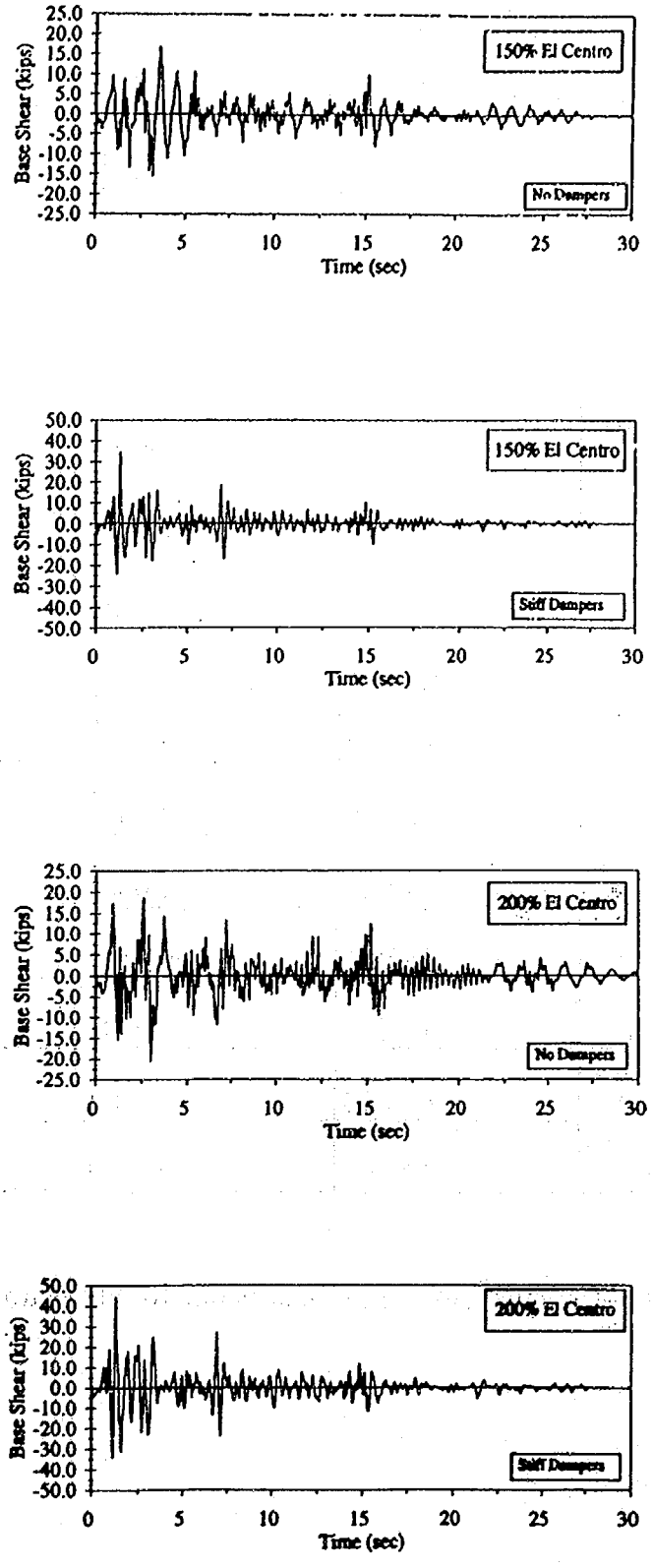


Figure 11. 150% and 200% El Centro base shear time histories with and without stiff dampers.

Maximum Story Shear (kips) (with and without stiff dampers)			
Earthquake Test	*1st Story Shear*	*2nd Story Shear*	*3rd Story Shear*
10% El Centro (with dampers)	2.350	1.674	1.028
25% El Centro (with dampers)	6.054	4.052	2.832
25% El Centro (no dampers)	2.898	2.184	1.569
50% El Centro (with dampers)	13.225	9.717	5.293
50% El Centro (no dampers)	5.180	4.263	3.092
75% El Centro (with dampers)	18.384	14.766	8.304
75% El Centro (no dampers)	8.084	6.925	4.961
100% El Centro (with dampers)	23.707	18.553	10.360
100% El Centro (no dampers)	11.033	9.356	6.968
125% El Centro (with dampers)	27.775	22.350	12.801
125% El Centro (no dampers)	14.092	1.988	8.748
150% El Centro (with dampers)	34.636	26.774	15.007
150% El Centro (no dampers)	16.987	14.414	9.811
200% El Centro (with dampers)	44.219	37.108	21.592
200% El Centro (no dampers)	20.709	17.566	11.694

Table 1. Maximum story shear of structure for El Centro tests.

Maximum Inter-Story Displacement (in) (with and without stiff dampers)			
Earthquake Test	*1st Story Drift*	*2nd Story Drift*	*3rd Story Drift*
10% El Centro (with dampers)	0.029	0.037	0.023
25% El Centro (with dampers)	0.065	0.078	0.049
25% El Centro (no dampers)	0.110	0.185	0.134
50% El Centro (with dampers)	0.124	0.139	0.096
50% El Centro (no dampers)	0.226	0.353	0.257
75% El Centro (with dampers)	0.196	0.228	0.159
75% El Centro (no dampers)	0.348	0.529	0.395
100% El Centro (with dampers)	0.252	0.308	0.219
100% El Centro (no dampers)	0.943	0.710	0.541
125% El Centro (with dampers)	0.343	0.401	0.282
125% El Centro (no dampers)	0.518	0.914	0.706
150% El Centro (with dampers)	0.412	0.453	0.306
150% El Centro (no dampers)	0.687	1.209	0.949
200% El Centro (with dampers)	0.639	0.883	0.522
200% El Centro (no dampers)	0.864	3.076	2.967

Table 2. Maximum inter-story displacement of structure for El Centro tests.

Maximum Absolute Acceleration (g) (with and without stiff dampers)				
Earthquake Test	*Base Girder*	*1st Story*	*2nd Story*	*3rd Story*
10% El Centro (with dampers)	0.049	0.044	0.035	0.059
25% El Centro (with dampers)	0.141	0.141	0.088	0.164
25% El Centro (no dampers)	0.108	0.108	0.114	0.091
50% El Centro (with dampers)	0.228	0.224	0.261	0.306
50% El Centro (no dampers)	0.212	0.213	0.229	0.178
75% El Centro (with dampers)	0.312	0.311	0.384	0.479
75% El Centro (no dampers)	0.304	0.326	0.350	0.286
100% El Centro (with dampers)	0.408	0.397	0.475	0.598
100% El Centro (no dampers)	0.407	0.424	0.493	0.402
125% El Centro (with dampers)	0.467	0.471	0.564	0.739
125% El Centro (no dampers)	0.482	0.539	0.579	0.505
150% El Centro (with dampers)	0.553	0.567	0.690	0.866
150% El Centro (no dampers)	0.563	0.640	0.602	0.472
200% El Centro (with dampers)	0.858	0.779	0.959	1.247
200% El Centro (no dampers)	0.983	0.862	0.798	0.675

Table 3. Maximum absolute acceleration of structure for El Centro tests.

Maximum Relative Displacement (in) (with and without stiff dampers)			
Earthquake Test	*1st Story Displ*	*2nd Story Displ*	*3rd Story Displ*
10% El Centro (with dampers)	0.029	0.060	0.067
25% El Centro (with dampers)	0.065	0.133	0.173
25% El Centro (no dampers)	0.110	0.276	0.382
50% El Centro (with dampers)	0.124	0.255	0.346
50% El Centro (no dampers)	0.226	0.564	0.816
75% El Centro (with dampers)	0.196	0.411	0.566
75% El Centro (no dampers)	0.348	0.861	1.229
100% El Centro (with dampers)	0.252	0.555	0.761
100% El Centro (no dampers)	0.943	1.591	2.033
125% El Centro (with dampers)	0.343	0.724	0.990
125% El Centro (no dampers)	0.518	1.422	2.009
150% El Centro (with dampers)	0.412	0.847	1.134
150% El Centro (no dampers)	0.687	1.838	2.566
200% El Centro (with dampers)	0.640	1.472	1.970
200% El Centro (no dampers)	0.862	3.897	6.814

Table 4. Maximum relative displacement of structure for El Centro tests.

Maximum Story Shear (kips) (with and without stiff dampers)			
Earthquake Test	*1st Story Shear*	*2nd Story Shear*	*3rd Story Shear*
21% Taft (with dampers)	2.199	1.494	0.886
52.5% Taft (with dampers)	4.869	3.388	2.217
100% Taft (with dampers)	9.544	6.465	2.871
157.5% Taft (with dampers)	15.237	11.671	6.186
210% Taft (with dampers)	19.693	16.368	8.463
262.5% Taft (with dampers)	24.764	20.698	11.135
315% Taft (with dampers)	28.583	22.451	12.509
420% Taft (with dampers)	38.715	31.795	18.568

Table 5. Maximum story shear of structure for Taft tests.

Maximum Inter-Story Displacement (in) (with and without stiff dampers)			
Earthquake Test	*1st Story Drift*	*2nd Story Drift*	*3rd Story Drift*
21% Taft (with dampers)	0.025	0.032	0.028
52.5% Taft (with dampers)	0.057	0.069	0.057
100% Taft (with dampers)	0.120	0.134	0.083
157.5% Taft (with dampers)	0.199	0.219	0.136
210% Taft (with dampers)	0.268	0.336	0.193
262.5% Taft (with dampers)	0.359	0.425	0.256
315% Taft (with dampers)	0.425	0.498	0.288
420% Taft (with dampers)	0.662	0.817	0.448

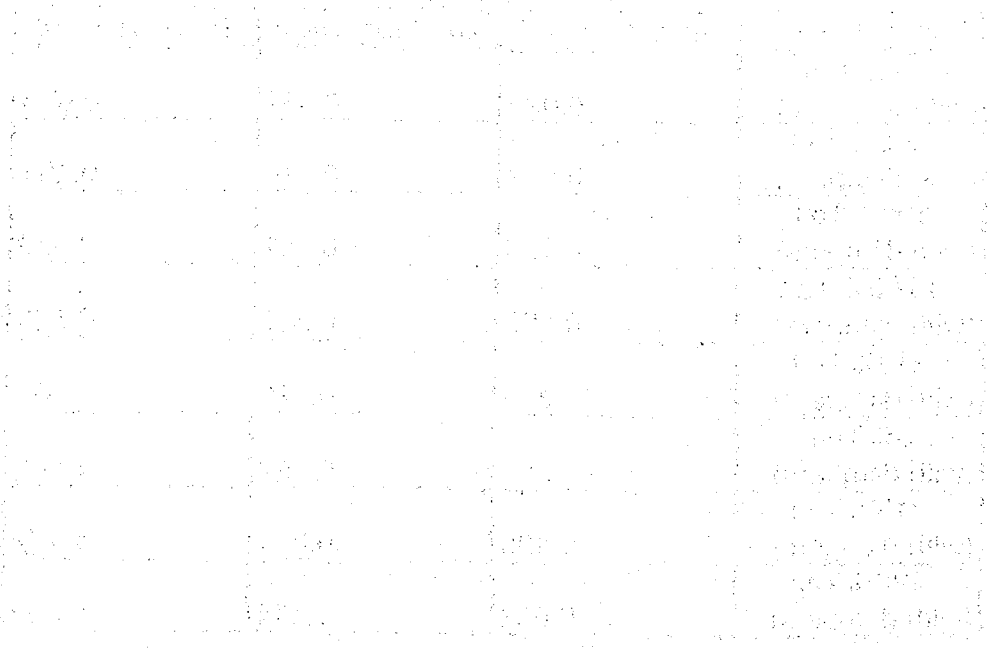
Table 6. Maximum inter-story displacement of structure for Taft tests.

Maximum Absolute Acceleration (g) (with stiff dampers)				
Earthquake Test	*Base Girder*	*1st Story*	*2nd Story*	*3rd Story*
21% Taft (with dampers)	0.046	0.046	0.036	0.051
52.5% Taft (with dampers)	0.099	0.096	0.066	0.128
100% Taft (with dampers)	0.175	0.166	0.203	0.233
157.5% Taft (with dampers)	0.309	0.253	0.305	0.357
210% Taft (with dampers)	0.414	0.348	0.425	0.489
262.5% Taft (with dampers)	0.522	0.436	0.524	0.643
315% Taft (with dampers)	0.628	0.530	0.562	0.722
420% Taft (with dampers)	0.888	0.695	0.770	1.072

Table 7. Maximum absolute acceleration of structure for Taft tests.

Maximum Relative Displacement (in) (with stiff dampers)			
Earthquake Test	*1st Story Displ*	*2nd Story Displ*	*3rd Story Displ*
21% Taft (with dampers)	0.025	0.051	0.076
52.5% Taft (with dampers)	0.057	0.116	0.164
100% Taft (with dampers)	0.120	0.241	0.320
157.5% Taft (with dampers)	0.199	0.397	0.525
210% Taft (with dampers)	0.268	0.575	0.761
262.5% Taft (with dampers)	0.359	0.757	1.002
315% Taft (with dampers)	0.425	0.891	1.172
420% Taft (with dampers)	0.662	1.414	1.844

Table 8. Maximum relative displacement of structure for Taft tests.



A Study on the Deformation Characteristics of Precast hollow Piers during Earthquakes

Masanori Nakano[1], Shigeru Takagi[2], Moriyuki Okoshi[3] PWRI

Abstract

More high piers are likely to be constructed in the future, and construction techniques therefore need to be developed to make effective use of precast technology in order to reduce labor, preserve the natural environment and improve the infrastructure as society develops.

As a part of a fundamental study on the design technology for high piers using precast concrete, we carried out loading tests to determine the factors which affect earthquake resistance, since these are usually difficult to concrete body. In these tests, parameters included the method used to join precast members, the arrangement and shape of reinforcement bars, and the amount of prestress and so forth. We successfully determined the deformation characteristics, sheared gaps between blocks, fracture properties and toughness of the annular (hollow) pier.

1. Introduction

Recently in Japan, the slow progress of construction work, a sharp rise in building costs due to aging and the shortage of laborers have become a serious social problem. In addition, construction conditions are becoming more demanding, for example, bridges requiring high piers in mountainous regions will increasingly be required in the future, while demands for environmental preservation are growing. To solve such problems, studies are underway to reduce the effort and labor involved, and to rationalize construction work. Such measures include the use of precast members for structures, and automated, mechanized construction techniques. This study investigates experimentally the lower structure of bridges, particularly the use of precast piers in above-ground portions.

There have been a number of studies on reinforced concrete piers, yet almost none on hollow prestressed reinforced concrete piers and prestressed concrete piers, and their characteristics remain unclear. We therefore conducted repeated tests on static horizontal positive and negative alternating loading to determine the earthquake resisting properties of precast piers, using parameters such as whether or not there are block joints and shear keys, the amount of prestress and the arrangement and shape of reinforcement bars. This

1)Head, Foundation Engineering Division, Structure and Bridge Department, Ministry of Construction, Tsukuba Science City 305 Japan
2)Research Engineer, ditto
3)Assistant Research Engineer, ditto

study included the following evaluation.

1. Evaluation of (fracture properties,)
2. Evaluation of (range of plastic hinge generation by strain distribution in axial reinforcements,)
3. Evaluation of (restraining effect of hoop tie by its strain distribution,)
4. Evaluation of (proof stress and deformation capacity by load displacement, deformation angle,) etc.
5. Evaluation of (behavior of joints portions by changes in displacement angle, crack width, etc. in joint portions,)
6. Evaluation of energy absorbing power by historical absorbed energy, equivalent viscous damping constant and cumulative absorbed energy,
7. Comparison of amount of slip-out of axial reinforcements obtained by the conventional computation method and our empirical values, and
8. Comparison of ductility factor obtained by the conventional computation method and our empirical values.

2. Outline of Experiments

2.1 Specimens

The structure hypothetically tested in this study consisted of hollow rings piled up one on another, prestressed by PC steel bars and joined as shown in Fig.1. We chose this structure since it is frequently used for the underground base and has established manufacturing and construction methods, and also because we considered it relatively easy to apply to piers.

The specifications of the specimens are listed in Table 1.
Specimens Nos. 2 and 3 are PRC structures using PC steel bars joined by low-level prestressing, their axial reinforcements continuing through the joints from the footing to the upper end of the pier to act ordinarily as tension reinforcements (i. e., not during earthquakes). Specimen No. 4 was also made from precast rings joined by PC steel bars but discontinued reinforcements were used in each block and so only the PC steel bars and prestressing offered resistance to bending tension. Thus, this specimen needed more prestressing than Nos. 2 and 3.

Figure 1 shows the shape and size of the specimens and reinforcement bar arrangement. All specimens were of a similar external shape and size. Specimen No. 1 was a conventional one piece structure of reinforced concrete and was tested for comparison with the others. Specimens Nos. 2, 3 and 4 were precast structures as noted above and no adhesive was applied on their joint surfaces. To prevent shear, shear keys were installed on the joint surfaces of No. 3. The quantities of vertical steel materials were determined so that all the specimens had an equal ultimate proof stress due to bending. For circumferential reinforcements, double, i.e., inner and outer hoop ties per cross section, were placed in specimen Nos. 1 to 4, but the lowermost block of No. 3 was provided with interlaced hoop ties while No. 4 was

provided with U-shape reinforcement bars to restrain the inner and outer axial reinforcements. Hoop ties were placed in all the specimens as required to prevent prior shear failure.

The design reference strength of the concrete was set at 400 kgf/cm2 and commercialise available PC steel bars with a diameter of 9.2 mm (yield strength: 125 kgf/mm3; tensile strength: 140 kgf/mm3) and D10·D6 deformed bars (SD295D) were used.

2.2 Loading Patterns and Loading History

Figure 2 shows of the loading patterns. The strain produced in the primary reinforcement on the outermost edge of the pier was measured. The horizontal displacement (excluding the displacement caused by rotation of the footing) produced on the upper end of the pier when the primary reinforcement yielded at its base was used as the yield displacement (hereafter, δy), positive and negative alternating loading was repeated five times in displacement amplitudes of $n \delta y$ (integral multiples of δy, n= 1, 2, ...).

The displacement due to rotation of the footing was obtained by measuring the angle of rotation using two displacement meters installed on the lower end of the footing and converting it into a horizontal displacement at the upper end of the pier (See Fig. 1). On No. 3, the loading was increased gradually and monotonously by controlling the load until the cracking load was reached. Loading was regarded as complete when it fell to approximately 40% of the maximum load. The height between the pier base and the point of loading (effective height) was 2.6 m and the shear span ratio (ratio of effective height to outside diameter of pier) was 3.25.

3. Test Results

The drawings and tables shown below were prepared by using values obtained when the maximum deformation occurred for the positive load at each δy in each of the fifth cycle.

3.1 Fracture Properties

Figure 3 shows the cracks that were produced. In all the specimens, cracks appear in the positions of the hoop ties (at intervals of 10 cm). In specimen No. 1, cracks are seen across the whole area of the pier whereas cracks are distributed in an area between the base and 1.7 to 2.0 m above it in each of specimens Nos. 2 and 3.

No. 3 has a slightly wider distribution than No. 2, due to dispersion of the shear force owing to the shear keys, dispersion of the plastic hinge range owing to the interlaced reinforcements, and also due to residual prestress. The cracks in No. 4 are concentrated in the base area due to the larger axial prestress. The inside and outside axial reinforcements of specimen No. 1 mostly buckled and broke to the direction of the concrete covers, but the inside axial reinforcements of Nos. 2 and 3 buckled and broke outwardly with respect to the rings.

Table 2 shows the proof stresses and deformation properties.

3.2 Distribution of Strains of Axial Steel Materials

The strains shown in Figs. 4 and 5 do not include initial strain due to prestressing.

(1) Distribution of Strains for Axial Reinforcements

Figure 4 shows the strains of axial reinforcements at 3 δ y in specimens Nos. 1, 2 and 3. (In No. 4, no existence of contiuece axial reinforcement Nos. 1 and 2 had a substantially similar distribution, that is, the reinforcements in their base areas yielded at about 20 cm considering the formation of plastic hinges there. Specimen No. 3 showed that plastic hinges formed in a wider range than the base area and that there was less strain in the base area.

(2) Distribution of Strains for PC Steel Bars

Figure 5 shows distributions and changes of strains of PC reinforcement bars at the similar respective upper end displacements in specimens No. 2, 3 and 4. The PC steel bars have higher yield points than the reinforcement bars and their strain distributions are smoother. Specimen No. 2 tends to have larger strains compared to No. 3. In specimen No. 4, strains of about 5,000 μ were uniformity produced at 1 δ y and above, considering that the grout was cut in all portions.

3.3 Distribution for Strains of Hoop

In this study, hoop were placed between the inside axial reinforcements and the cover concrete in anticipation of reduced toughness of the members due to exfoliation of the concrete, and the effects of the ties were studied. Interlaced hoop ties (No. 3) and U-shape reinforcements (No. 4) were placed and their effects on suppressing buckling of the axial reinforcements were monitored.

Figure 6 shows the strain distributions with the upper end displacement in the respective specimens. In all of them, the inside hoop ties have greater strains. Compared with specimens Nos. 1 and 2, strains in the lowest block of No. 3 are distributed over a smaller area, due to the interlaced reinforcements which restrained the deformation of the axial reinforcements resulting in less strain in the hoop ties. The maximum strains were 534 μ (NO. 1), 455 μ (NO. 2) and 424 μ (NO. 3) respectively in specimen Nos. 1, 2 and 3.

In the distribution of 11 δ y of No. 3, the maximum strain of the inside hoop ties was 814 μ and the strains of the outer ones increased sharply at 12 δ y in the area less than 45 cm from the base and the gauge stopped functioning normally. The strains produced in the interlaced reinforcements corresponded with those of the hoop strain.

In specimen Nos. 1, 2 and 3, the strains in the inside hoop ties remained similar to the positive and negative alternating loads (under

tension and under compression), and the highest strains occurred in the outside hoop ties under compression, which tended to decrease under tension.

3.4 Deformation Capacity

(1) Envelope Line

Figure 7 shows envelope lines which represent the relation between the load and the horizontal displacement. In specimen No. 1, peeling off of the inside and outside concrete started at 9 δ y and major exfoliation and breaking occurred at 11 δ y. In specimen No. 2, the reinforcement bars began to swell at 11 δ y; concrete broke at 12 δ y; and inside concrete conspicuously peeled off at 13 δ y. In specimen No. 3, exfoliation of concrete and breaking of reinforcement bars started at approximately the same value of 16 δ y. As for specimen No. 4, in the tested range of displacements, no clear point of decrease was found although the load began to reduce little by little at 10 δ y. This was believed to be the result of very localized breaking of concrete and the slow progress of exfoliation.

Figure 8 shows envelope lines representing the relation between the load and the displacement angle (δ /2.6m*100). All the specimen reached their ultimate loads at 1% displacement angles and the loads started to reduce at 2%.

3.5 Behavior of Joint Portion

The shear magnitude and width of cracks which developed in joint portions under loading were compared in specimen No. 1, which was a one-piece structure of reinforced concrete, and specimen Nos. 2, 3 and 4, which were precast structures, and the different behaviors of the joint portions were analyzed.

(1) Shearing gaps of Joint Portion

The amount of shearing gaps is obtained by averaging the measurements read from a cantilever type displacement meter and deducting the displacement produced due to bending of the member from the average. Measurements were taken on both sides of each specimen at right angles to the direction of loading.

Figure 9 shows the relation between the amount of shearing gaps and the upper end displacement. The largest shearing gaps were: 0.04 mm in specimen No. 1, 0.17 mm in No. 2, 0.08 mm in No. 3 and 0.2 mm in No. 4. The shearing gaps of No. 3 which was smaller than that of No. 2 is thought to have been due to the shear keys installed in the joint portions. Specimen No. 4 had the largest shear presumably because it had no axial reinforcements piercing through the blocks and the only frictional force was provided by prestressing. Shearing gaps was the largest in the second block from the top in each of specimen Nos. 1 and 2 while the shear was also large in the top block in No. 3. In No. 4, the values for all blocks varied little.

(2) Crack Width

In each joint, the width of cracks

was measured by a π gauge on both sides of the specimen in the direction of loading. Figure 10 shows the relation between crack width and the upper end displacement, both when the load was the maximum and when the load was removed. Comparing the specimens at their maximum deformation, No. 1 had the largest crack width of 1.33 mm and the value was the largest in the lowest block (third from the top). Crack width became narrower as the displacement increases to a certain extent. The amount of displacement starts to decrease approximately when the residual displacement begins to stabilize. The maximum width in specimen No. 2 was 1.06 mm and there is a clear trend similar to No. 1. The amount of residual displacement was also smaller than that of No. 1 probably because of the effect of prestressing. In specimen No. 3, both the lowest and the second lowest blocks had wide cracks, the largest being 1.36 mm. Openings of No. 4 were far narrower compared with those of specimen Nos. 1, 2 and 3.

When there was no load, the crack width in the lowest block of No. 1 started to increase sharply when the upper end displacement was 25 mm, reaching approximately 0.8 mm. In specimen Nos. 2 and 3, the values were similar to or less than those of No. 1. Specimen No. 3 had slightly larger values than No. 2 and residual cracks were scattered in the lowest block and the second block from the top. In No. 4, the residual displacement scarcely increased, indicating the remarkable effect of prestressing.

3.6 Energy Absorbing Power

Figure 11 shows load-displacement curves of the various specimens at 3 δy, 6 δy, 9 δy and the ultimate δy. The ultimate δy of specimen No. 1 had a substantial residual load as the experiment ended with a much smaller displacement compared to the other specimens. The proof stress of specimen No. 4 fell less than Nos. 1, 2 and 3 despite its displacement.

Figure 12 shows the historical absorbed energy, equivalent viscous damping constant and cumulative absorbed energy. Since each specimen had its own 1 δy value, the gradients shown in the respective graphs are different. However, specimen Nos. 1, 2 and 3 begin to show a decrease in historical absorbed energy at almost the same displacement (about 66 mm) and there was no sharp fall before it. On the other hand, the energy absorbed in No. 4 is conspicuously lower than in the others.

The specimens display the same tendency with regard to their equivalent viscous damping constants and cumulative absorbed energy. It is noticeable that the cumulative absorbed energy of specimen No. 1 was slightly higher compared to that of the others. Because of its large displacement per δy, No. 4 was loaded fewer times and thus did not show much difference from the others in the experimental range of this study.

3.7 Computation of Slip-out Length of Axial Reinforcement

To compute the displacement due to slip-out, formulae 1 and 2 given in the Railway Structure Design Standards and Guidelines [Concrete Structures] (hereinafter, "the standards") were used. Values thus obtained were compared with those obtained by integrating the strain distributions of the respective axial reinforcements. In this process, the highest value of strain was set at 2000 μ which was the yield strain.

$$\Delta ly=0.070-0.0054(D/\phi)+0.00017(D/\phi)2$$
$$\Delta lu=0.083-0.0054(D/\phi)+0.00015(D/\phi)2$$

(Formula-1)

Δly: Length of slip-out at yield(cm)
Δlu: Length of slip-out at the end (cm)
D: Distance between the centers of bars (cm)
ϕ: Diameter of bars (cm)

Δly and Δlu obtained from formulae 1 and 2 were 0.511 mm and 0.638 mm respectively. Figure 13 compares these with the empirical values of the specimens. The empirical values when all the specimens yielded were considerably smaller, about 20%, than the computed ones. For the ultimate slip-out, the empirical value of No. 1 was nearly the same as the computed one, whereas specimen Nos. 2 and 3 gave similar values which were smaller than the computed ones.

3.8 Computation of Ductility Factor

The ductility factor of the members was computed by using the following formula given in the Railway Structure Design Standards and was compared with the empirical values.

$$\mu=\delta u/\delta y=(\mu o\cdot\delta yo+\delta ul)/(\delta yo+\delta yl)$$

(Formula-2)

μ: Ductility factor of member,
δu: Ultimate displacement,
δy: Yield displacement,
$\mu 0$: Ductility factor of body,
δyo: Displacement due to body deformation at yielding,
δyl: Displacement due to rotation caused by slipping out of axial reinforcements at yielding,
δul: Displacement due to rotation caused by slipping out of axial reinforcement at the end

μ of specimen Nos. 1, 2 and 3 obtained by using formula 3 was 7.6; which was less than the empirical values.

4. Summary

The main results obtained from this study are summarized as follows:

1. The proof stresses of specimens No. 2 and 3 were approximately equivalent to that of specimen No. 1 RC pier, and computation using the existing formula appears to be valid. Specimen Nos. 2 and 3 were confirmed to have a slightly higher toughness than No. 1.

2. In the specimens reinforced by the arrangement and shape of hoop ties, the inside concrete peeled off less quickly and toughness was increased. Interlaced reinforcement bars thus appear to effectively increase the rigidity of the base.

3. Although prestressed piers absorbed less energy due to the restoring force of the prestressing, the effectiveness of prestressing in suppressing cracks was confirmed.

4. The loading pattern used in this study did not produce conspicuous shear in the joint portions of the PRC piers which had reinforcement bars placed crossways and were not coated with an adhesive, although the specimen with shear keys exhibited a somewhat smaller shear.

These results show that the effects of reducing the shear span ratio and the axial reinforcement ratio, and of increasing or decreasing the amount of prestressing need to be investigated.

References

1) Kawashima, K.: Dynamic Proof Stress and Deformation Capacity of Hollow Circular RC Piers, Civil Engineering Technical Materials 34-10, pp. 34-39, 1992

2) Nakai, M., Shima, H. and Abe, M.: Study on Shear Keys of Post-installation Mortar Filling Type, The 48th annual symposium of the Civil Engineering Society, Section 5, pp. 672-673

3) Japan Road Association: Highway Bridge Specifications V, Earthquake Resistant Design Section, 1993.2

4) Japan Railway Construction Corporation: Railway Structure Design Standards and Guidelines [Concrete Structures]

Table.1 Description of Specimens

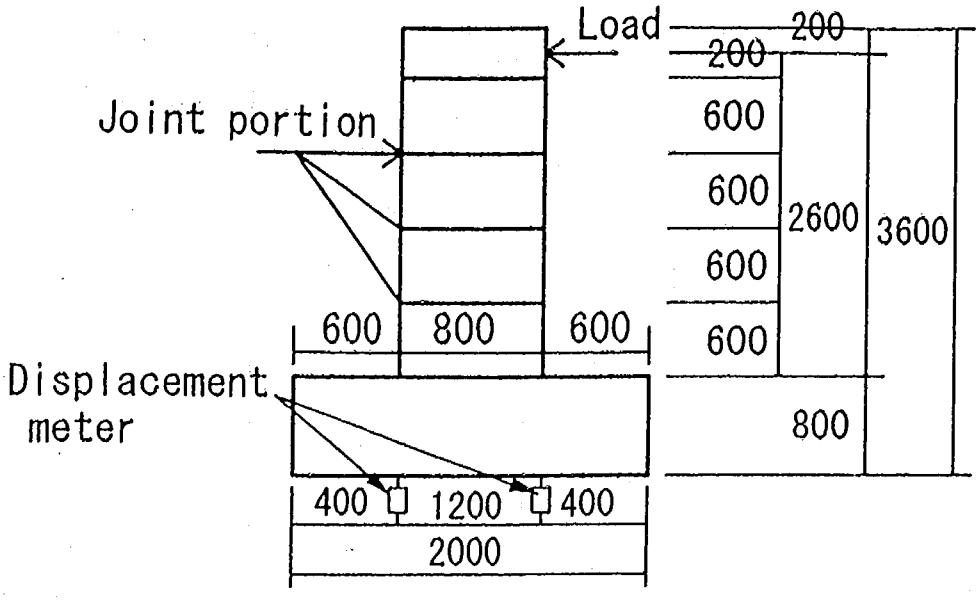
Type of Sample	Structure Type	Sear Key	Axial reinforcement ratio	Traverse reinforcement ratio
NO. 1	RC One piece driving	———	1.9%	0.63%
NO. 2	PRC Without Key	Without	1.4%	0.63%
NO. 3	PRC With Key	With	1.4%	0.63%
NO. 4	PC Without Key	Without	0.58%	0.63%

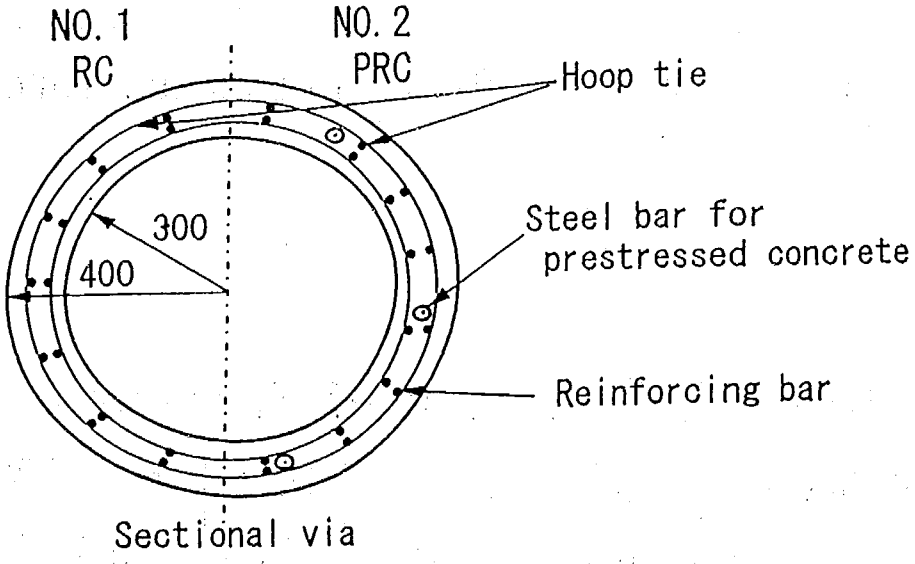
Note: Amount of prestress=Total prestress force÷ Total sectional area

Table.2 Description of Specimens

Name of Sample		NO. 1	NO. 2	NO. 3	NO. 4
Proof stress	Yielding proof stress	12.1	13.4	10.5	14.8
	Maximum proof stress	19.7	20.6	19.6	17.2
	Pm/Py	1.63	1.54	1.87	1.16
Deformation capacity	Yielding displacement	6.0	5.5	4.3	20.0
	Ultimate displacement	72.0	77.0	68.8	160.0
	Ductility factor	12	14	16	8

Note: Horizontal displacement when loading lowered to about 80% of maximum load was regarded as ultimate displacement δu





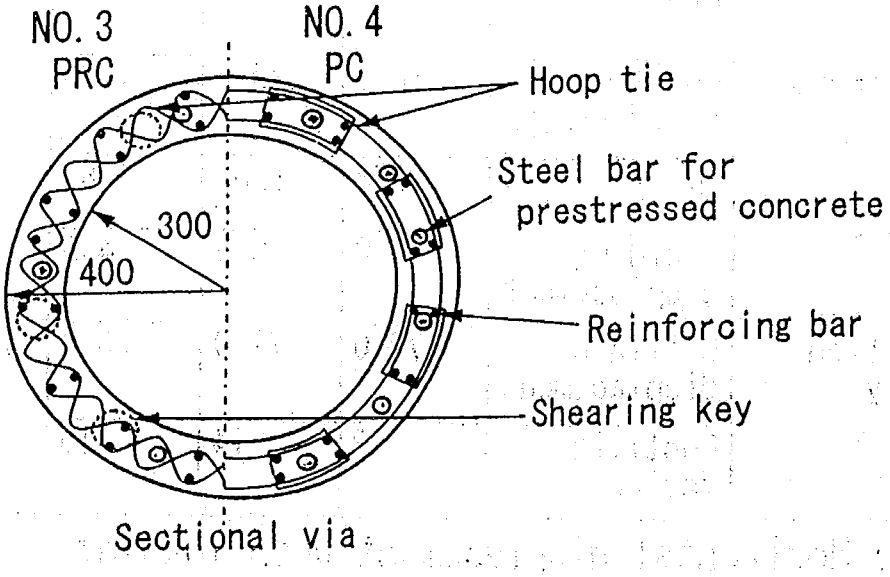


Fig-1 Shape and Size Specimens

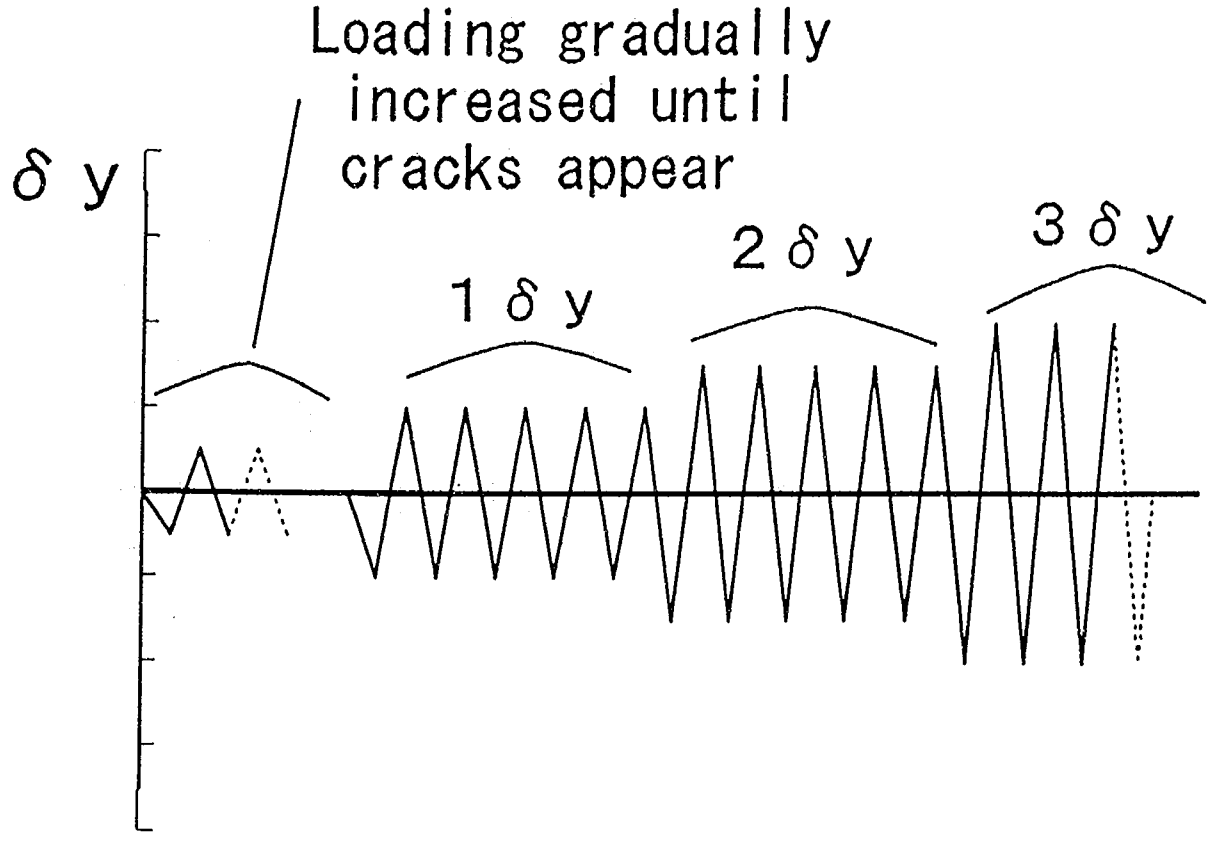
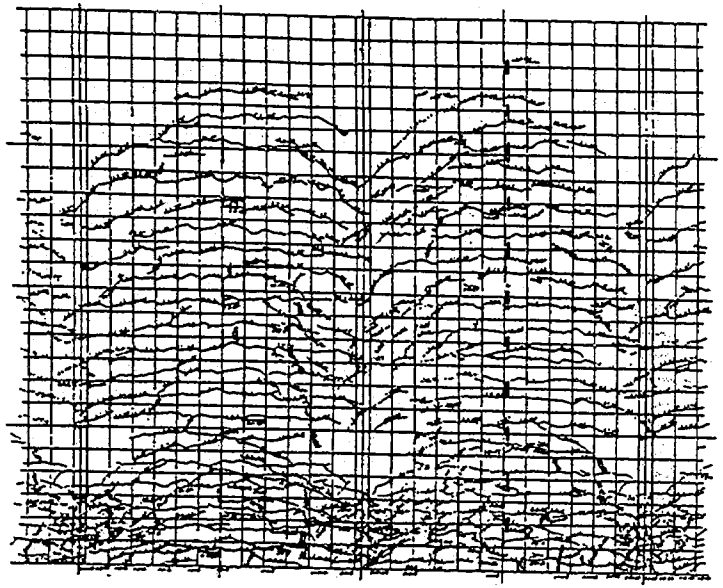
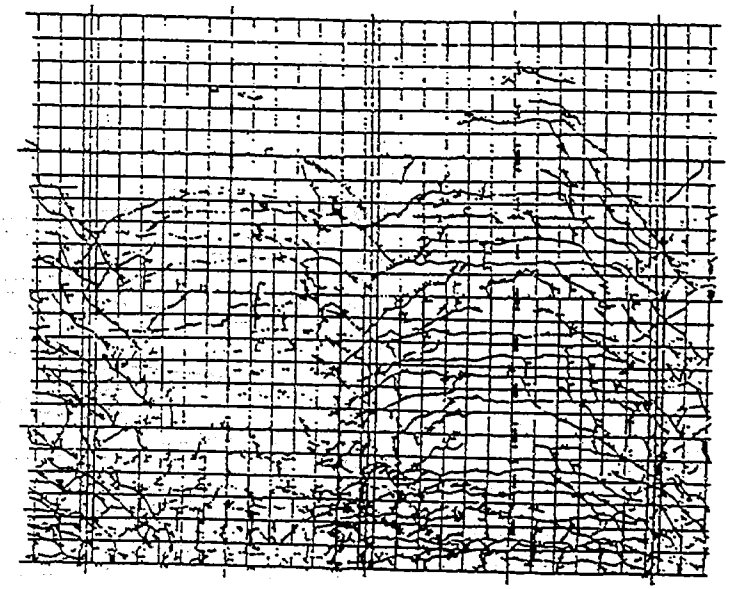


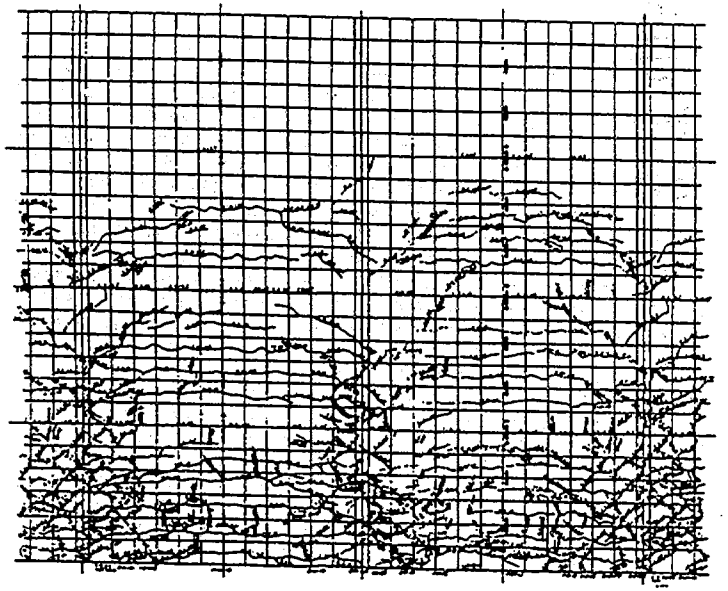
Fig. 2 Type of loading



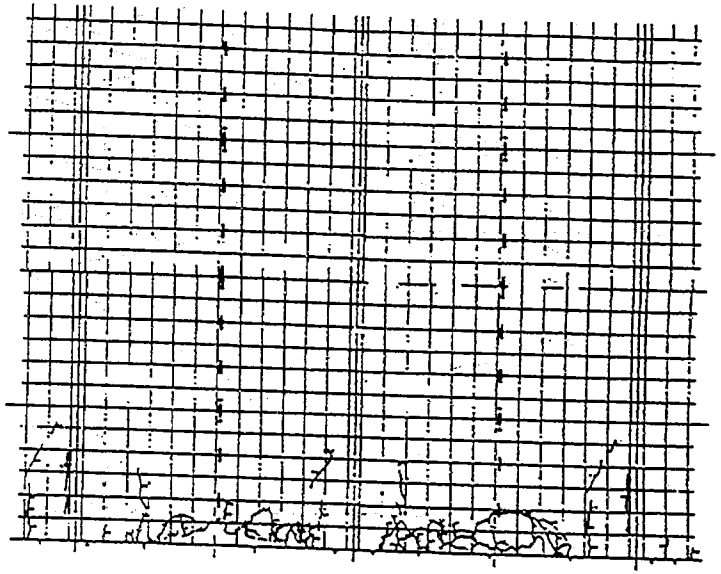
NO. 1



NO. 3

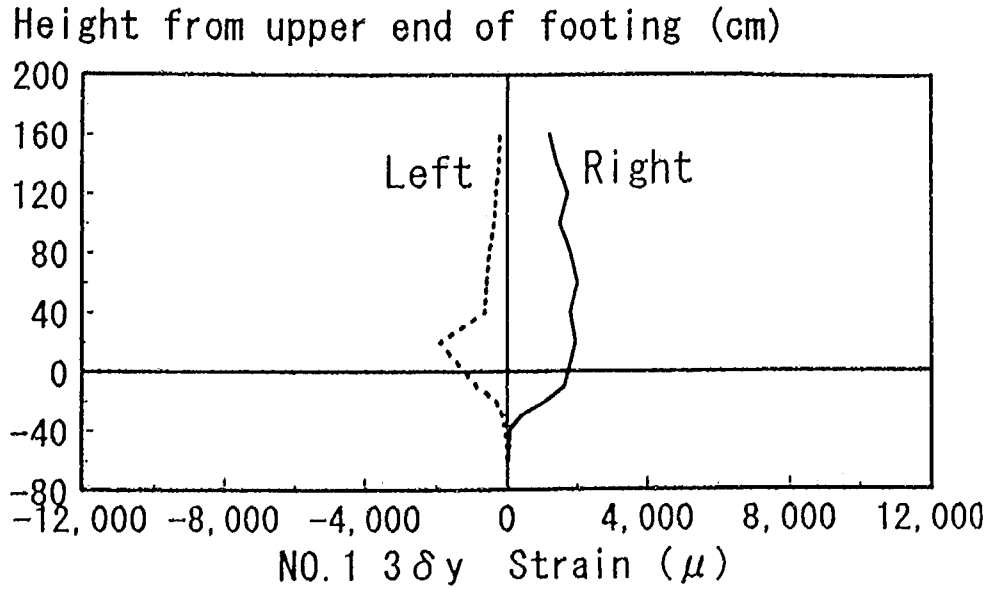


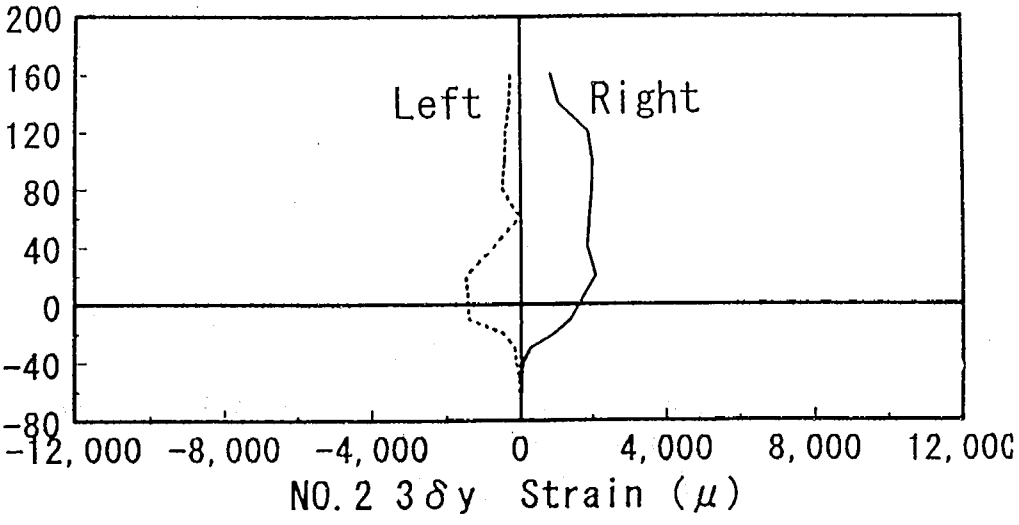
NO. 2



NO. 4

Fig. 3 Cracks





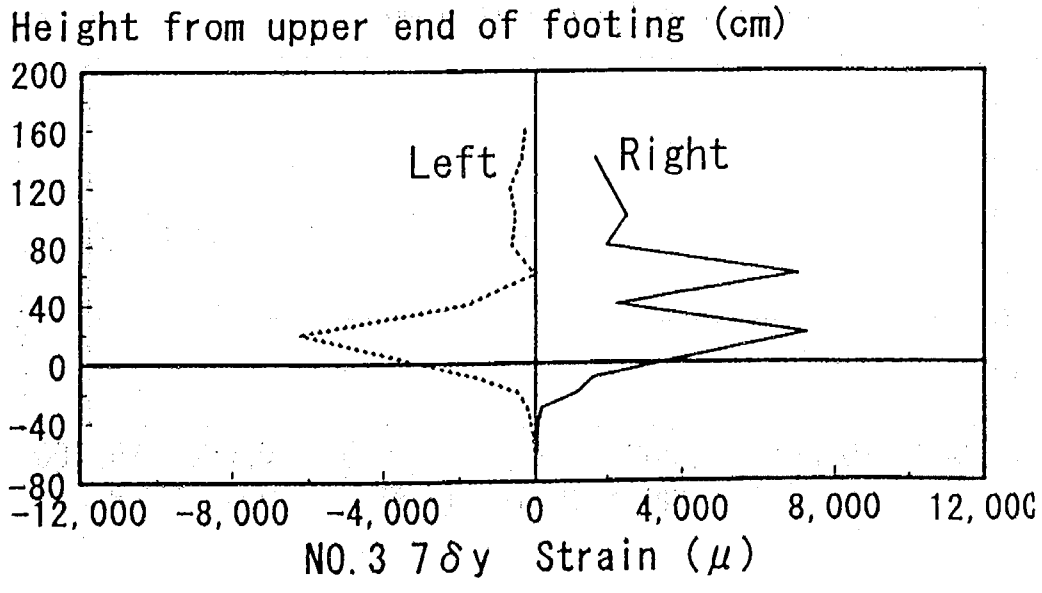
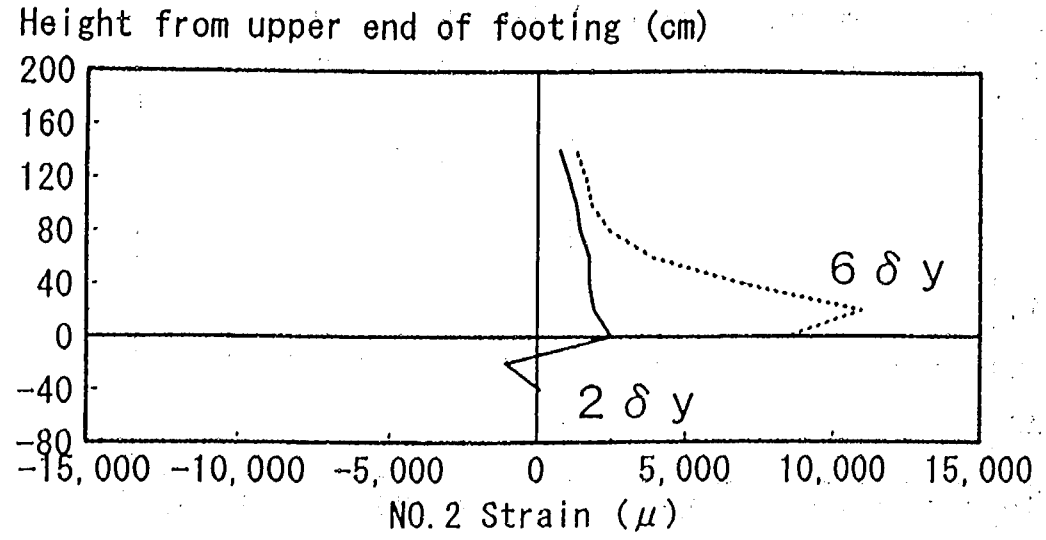
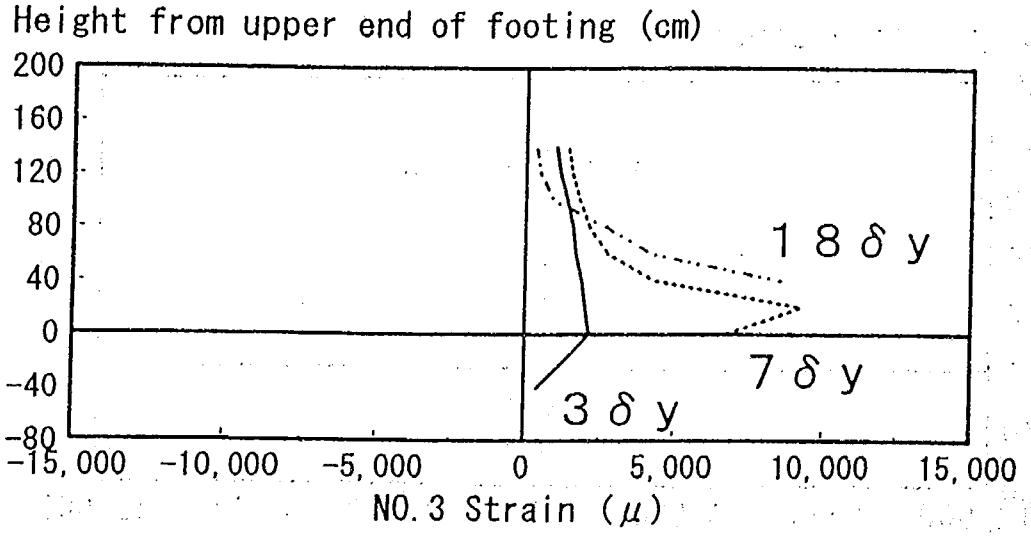


Fig. 4 Strain Distribution of Axial Reinforcement





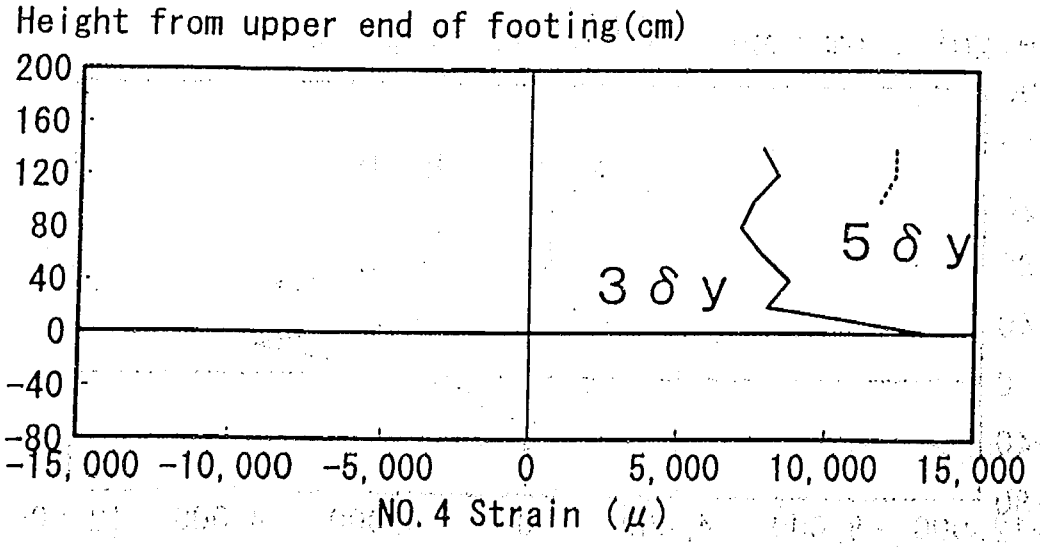
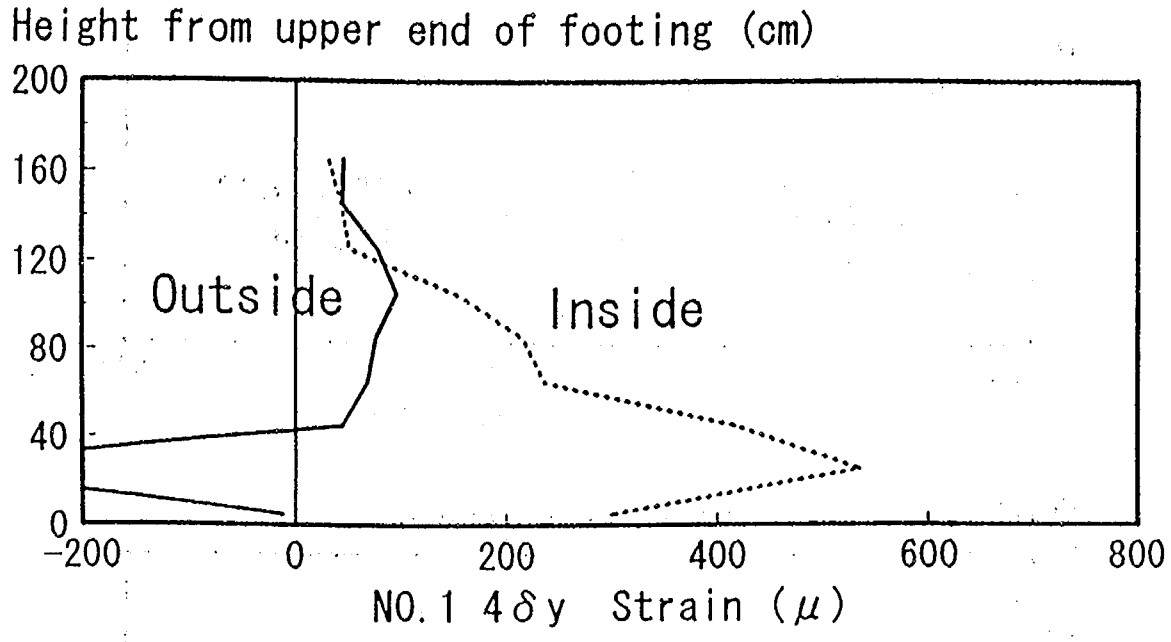


Fig. 5 Strain Distribution of PC Steel Bar



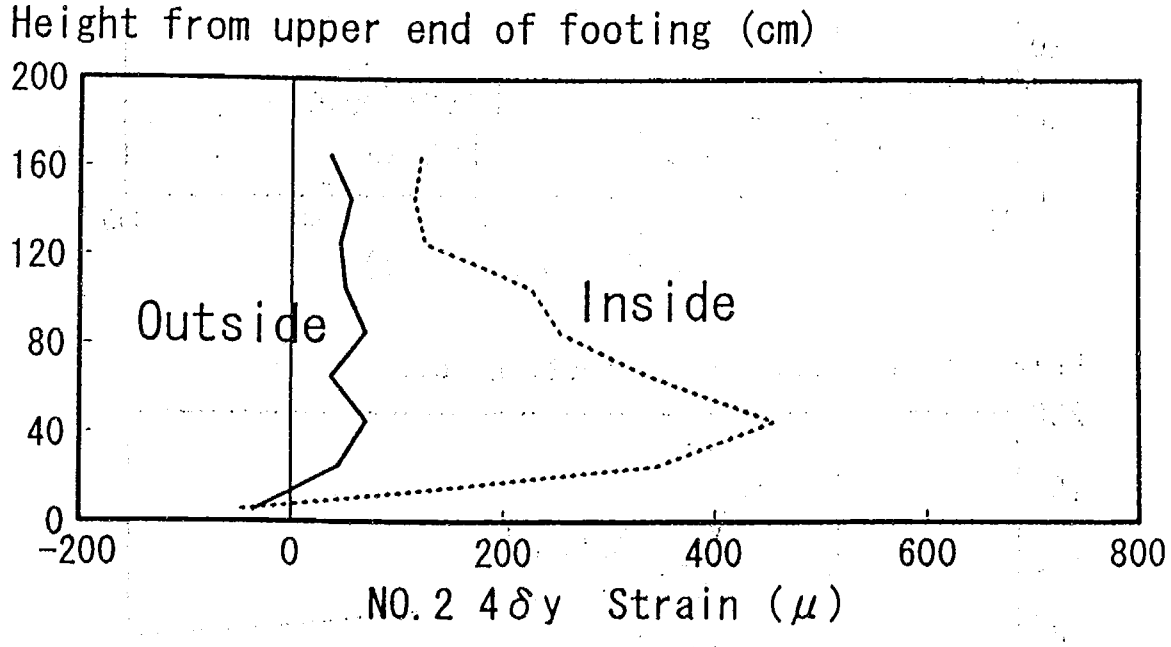
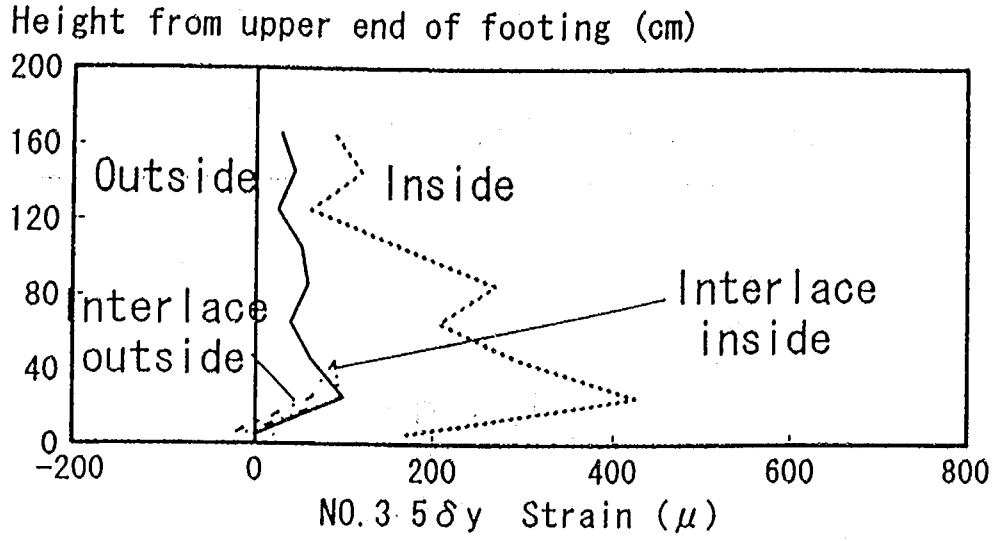
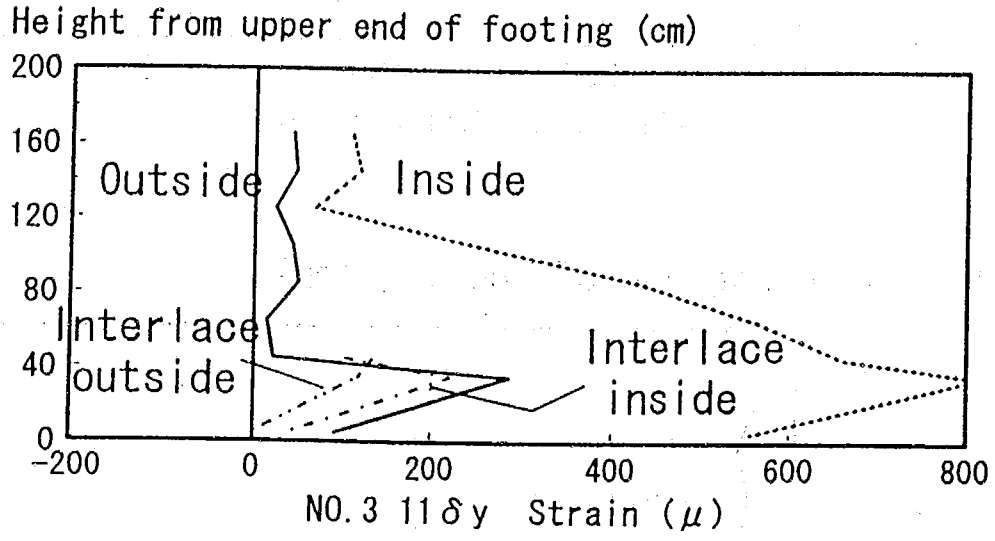


Fig.6 Strain Distribution of Hoop Tie(1)





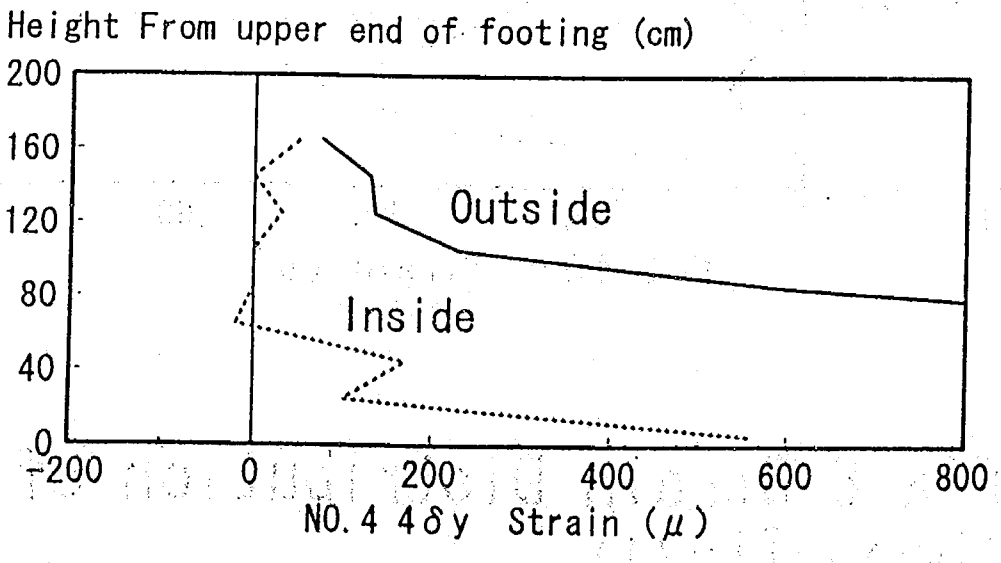


Fig. 6 Strain Distribution of Hoop Tie (2)

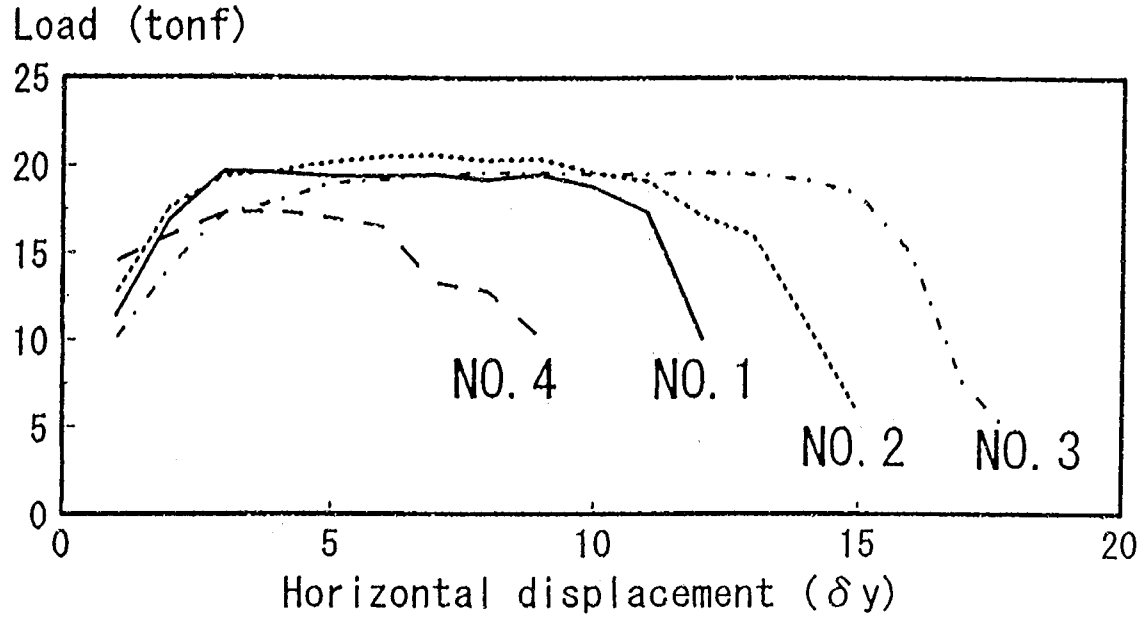


Fig. 7 Load and Horizontal Displacement

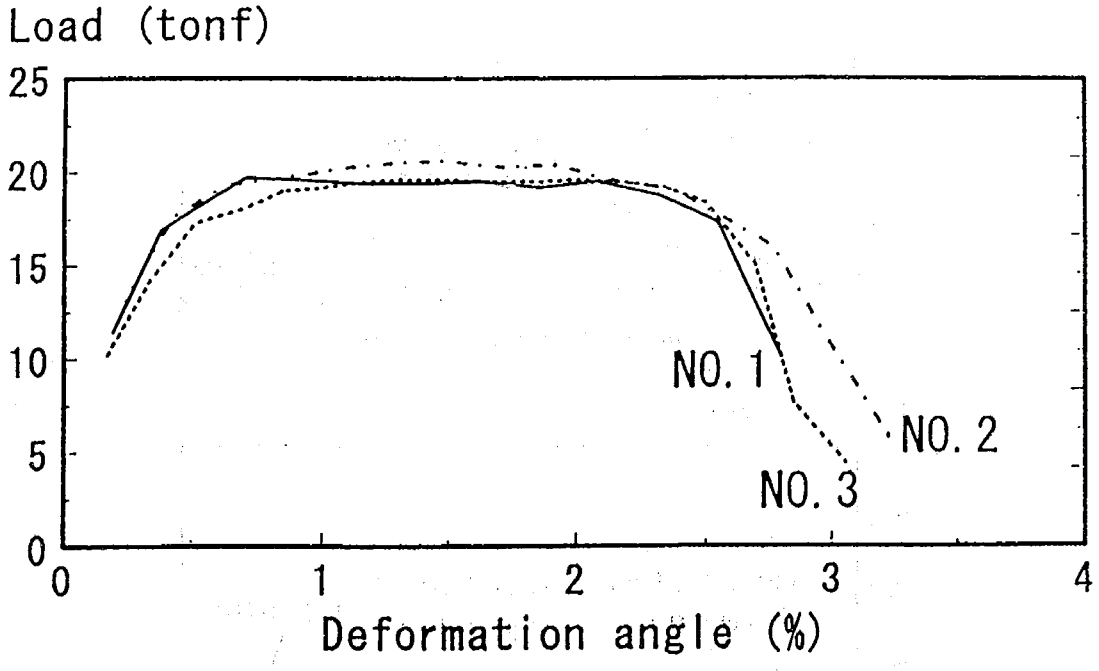


Fig. 8 Load and Deformation Angle

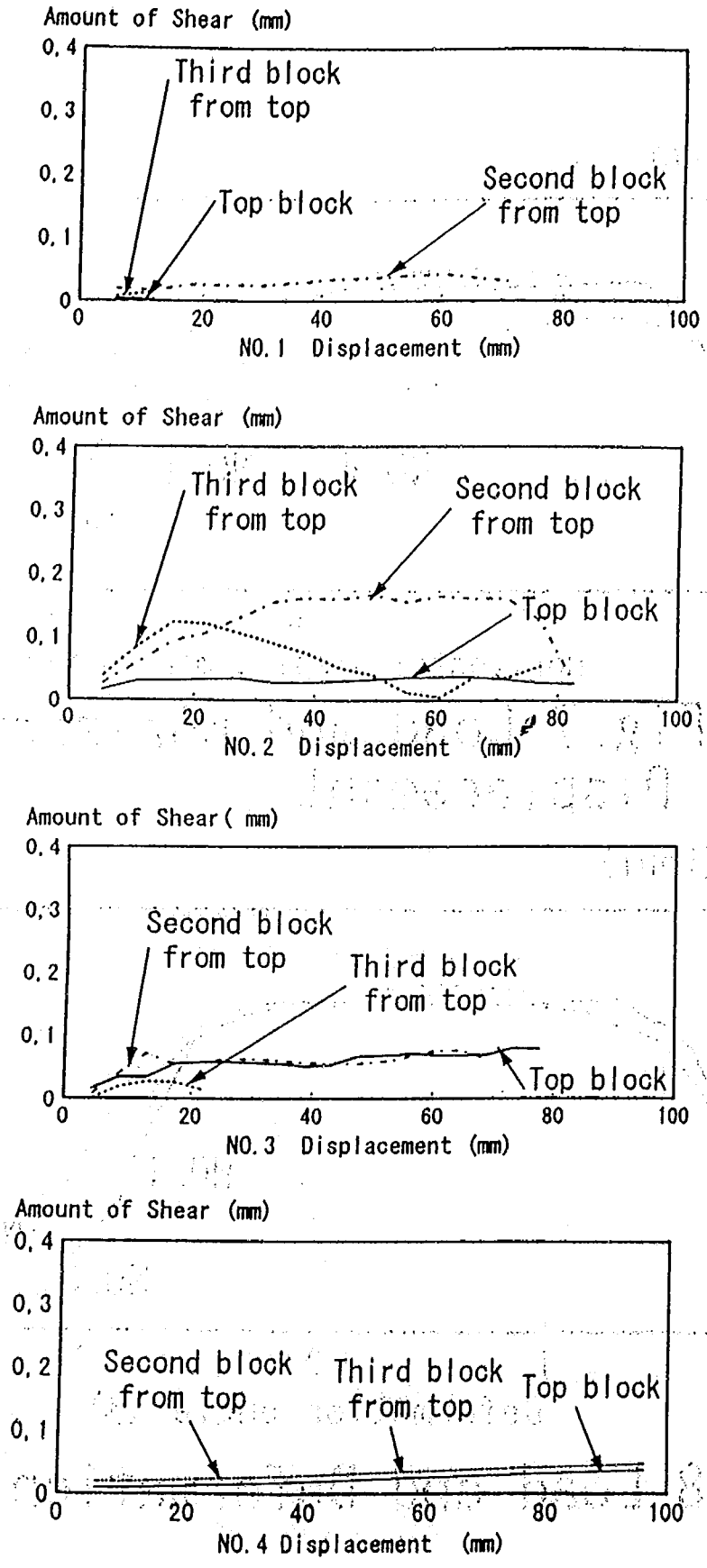


Fig. 9 Amount of Shear in Joint Portion

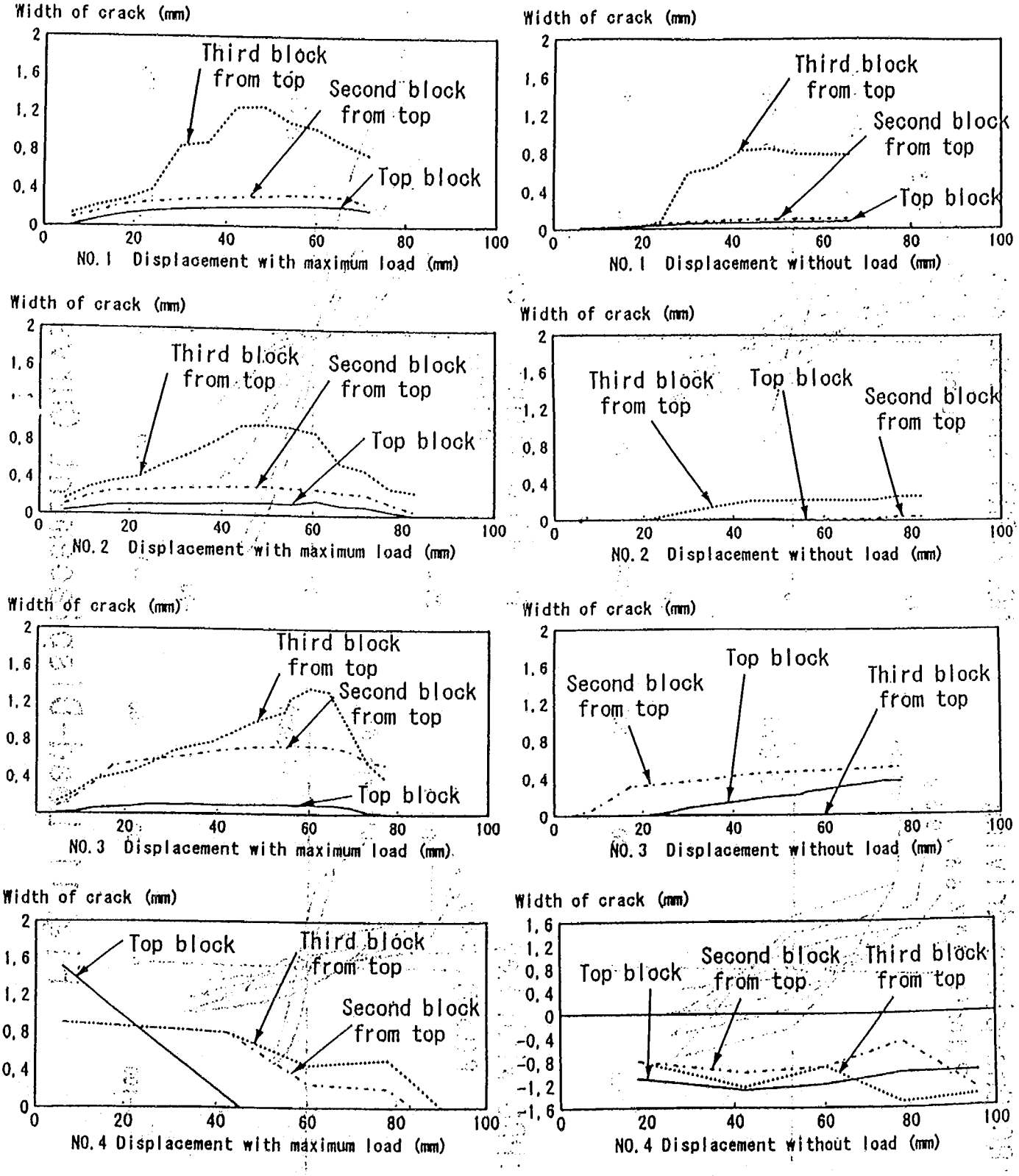


Fig. 10 Width of Crack in Joint Portion

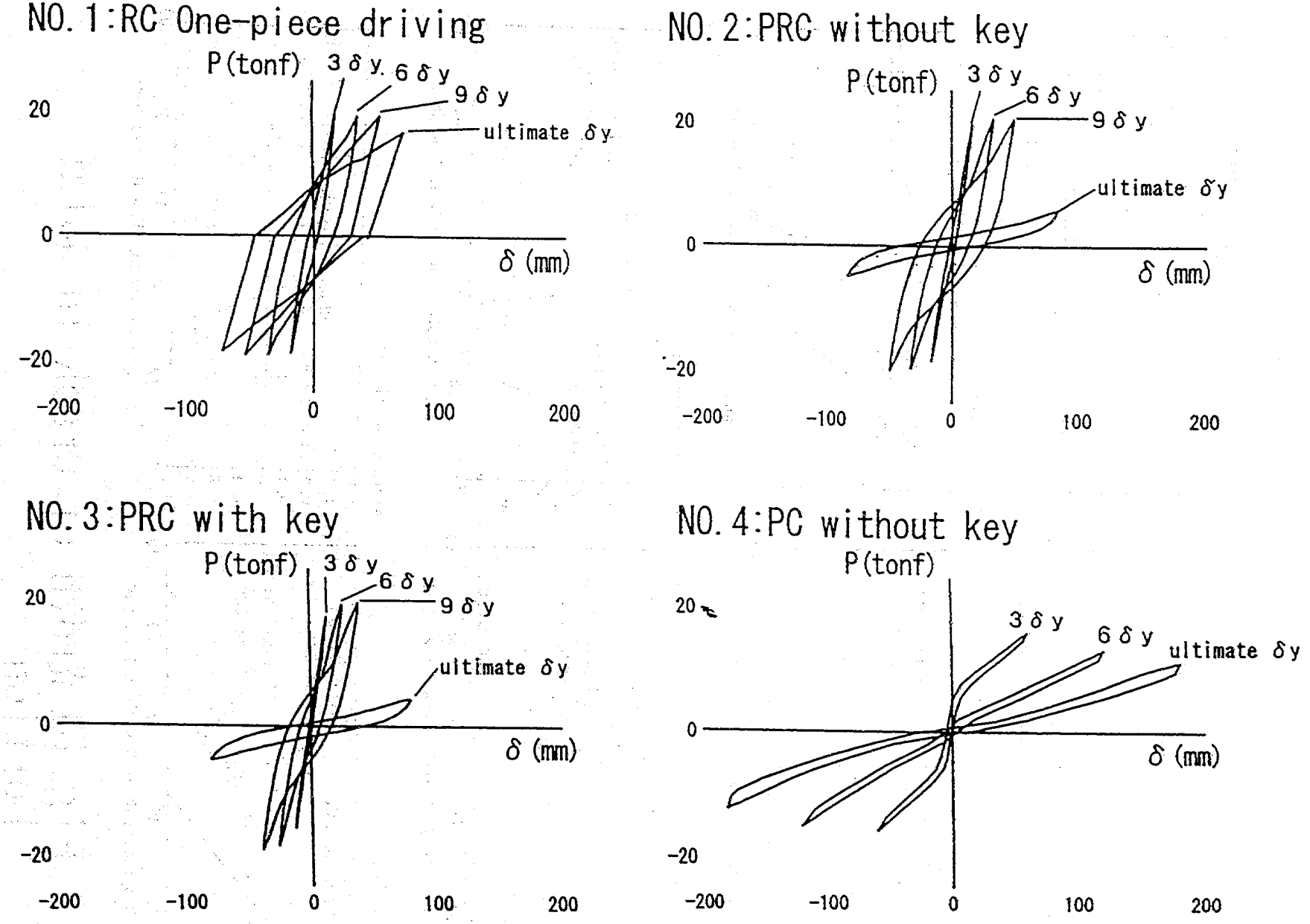


Fig.11 Load-Displacement Curve

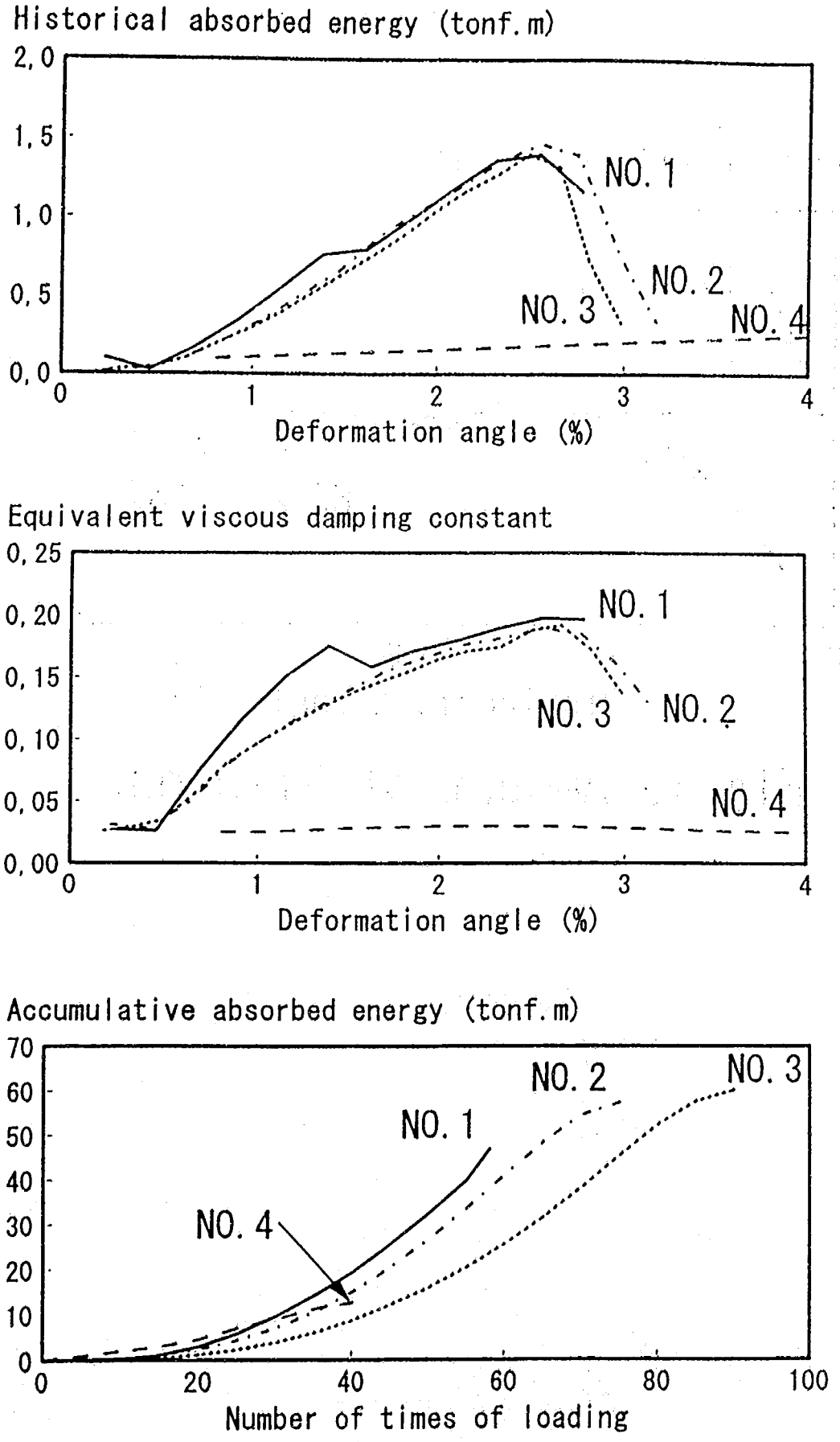


Fig. 12 Energy Absorbing Power

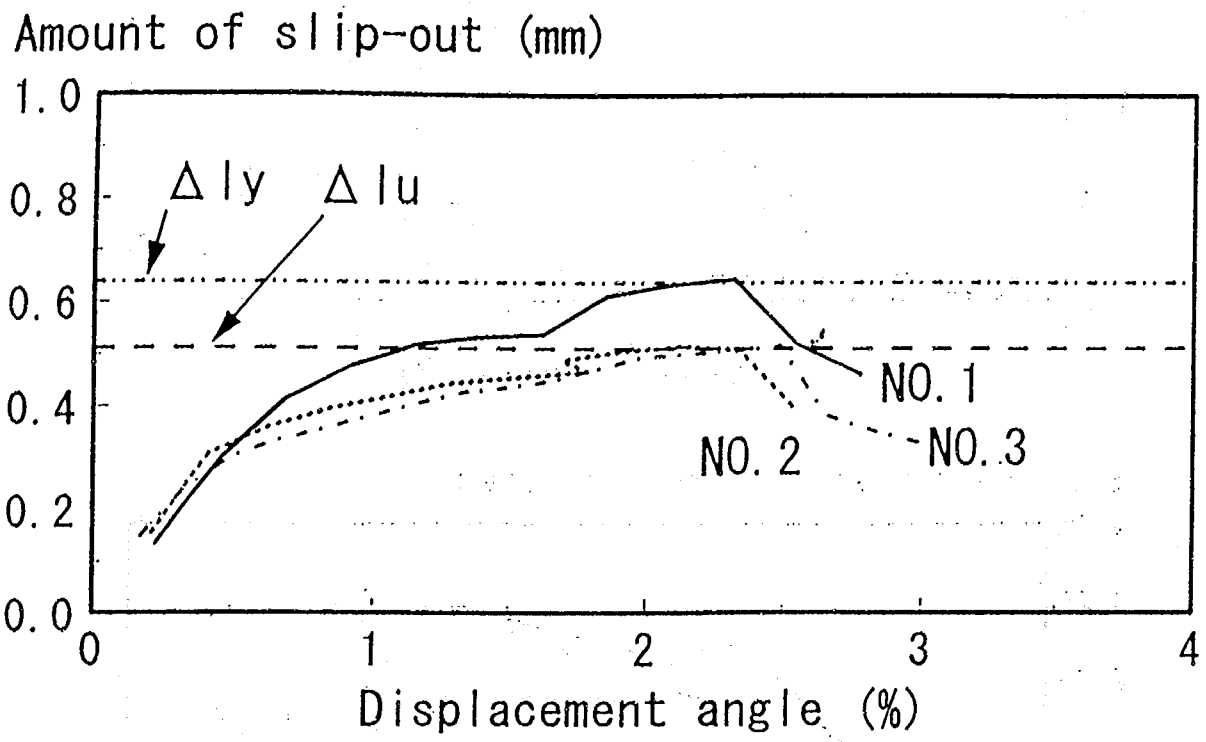


Fig. 13 Amount of Slip-out

Response of On-netoh Bridge during Hokkaido Toho-oki Earthquake of October 1994

by

Masashi SATO[1], Hiroaki NISHI and Atsushi Nishimura[2]

ABSTRACT

The On-netoh bridge is being constructed in the East of Hokkaido to replace the existing bridge, using the Menshin design which employs lead rubber bearings. In October, 1994, the Hokkaido Toho-oki Earthquake with magnitude of 8.1 occurred and strong motion records were obtained from seismographs installed in the bridge. This paper presents the seismic response characteristics of the bridge with a Menshin design during the Hokkaido Toho-oki Earthquake, and the analysis of acceleration records measured at the On-netoh bridge.

Key Words :On-netoh Bridge, seismic response, Menshin design, lead rubber bearing (LRB)

1. INTRODUCTION

The On-netoh bridge is now under construction on national highway No. 44 in Nemuro city, Hokkaido. The Menshin bearings were adopted to one of the side bridges. Strong motion seismographs were installed at the bridge to observe its seismic behavior.

In October, 1994, when the Hokkaido Toho-oki Earthquake occurred acceleration records of the On-netoh bridge were obtained. The seismic response characteristics of the On-netoh bridge have been studied through the analysis of the measured acceleration records.

2. OUTLINE OF THE EARTHQUAKE

The Hokkaido Toho-oki Earthquake occurred at 22:23 hrs.on October 4, 1994. The earthquake registered a magnitude of 8.1 on the Japanese scale and the epicenter was reported as being approximately 180 km off the east coast of Nemuro city at lat. 42° 22′ N. long. 147° 40′ E. The depth of the seismic center was approximately 30 km. **Fig. 1** shows the seismic intensities on the Japanese seven-stage scale for each district of Hokkaido.

The effect of the erthquake was sufficient to examine the seismic behavior of the bridge because the distance from the epicenter to the On-netoh bridge was approximately 200 km and the magnitude was 8.1.

3. ON-NETOH BRIDGE

Fig. 2 shows the On-netoh Bridge which is being constructed by the Hokkaido Development Bureau. The bridge has a total length 456 m and consists of a Nielsen system bridge (main bridge) and three side bridge (one bridge on the Kushiro side and two on the Nemuro side). The side bridge on the Kushiro side are of the Menshin design using lead rubber bearings.

---

1) Head, Structures Section, Structures Division, Civil Engineering Research Institute, Hokkaido Development Bureau, Hiragishi 1-3, Toyohira-ku, Sapporo, 062 Japan

2) Research Engineer, ditto

Photo 1 shows the general view of the bridge. The side bridge has a superstructure of a four-span continuous steel plate girder, a substructure of reinforced concrete and a steel pipe pile foundation (Fig. 2). Rubber bearings are used at the A1 abutment and P4 pier. Lead rubber bearings are used at P1, P2 and P3 piers. The size and materials of lead rubber bearings are: the shear modulus of the rubber (G) is 8.0 kg/cm, plane size is 45 × 45, the thickness of one rubber layer is 1.2 cm, there are 18 rubber layers and there is one lead plug (ϕ 14.5 cm). The stoppers to prevent displacement in a transverse direction were installed at all bearings. **Figs. 4** (a) and (b) show the bearings used for the On-netoh Bridge.

Strong motion seismographs were installed at the girder on the P3 pier, crest of P3 pier and the ground (1.5 m deep) near the abutment of the On-netoh Bridge (**Fig. 3**).

4. ANALYSIS OF THE RESPONSE OF ON-NETOH BRIDGE

4.1 Summary of the Observation Results

Strong motions of the On-netoh bridge during the Toho-oki Earthquake were measured successively by the seismographs. **Fig. 5** shows the peaks of acceleration measured on the girder, the P3 pier and the ground, and **Figs. 6** (a), (b) and (c) show the time histories of the wave forms. Peaks of acceleration of the ground, the P3 pier and the girder were about 316.0 cm/sec^2, 418.3 cm/sec^2 and 354.1 cm/sec^2, respectively.

4.2 Behavior of the Ground

Fig. 7 shows the acceleration response spectrum curves of the strong motion measured in the ground. The predominant period was almost identical to T_G of the ground (2.0cps). The maximum of the acceleration response spectrum curve was about five times the maximum prescribed in the Design Specifications for Highway Bridges. Therefore, for the On-netoh bridge this earthquake seemed to correspond to L2 level (L2 is equivalent to the Great Kanto Earthquake (1923) on the earthquake scale). **Fig. 8** shows the displacement response spectrum curves. The displacement response spectrum values did not change between the time of about 1 second and the long period. This was because the seismic waves at the time of this earthquake had few components of the long period.

4.3 Behavior of the Structure

Fig. 9 shows the Fourier spectrum curves of the girder, and **Fig. 10** shows the transfer characteristics between the girder and the ground. These figures show that the long period of the superstructure produced a decrease in the inertia force (Fig. 5), due to the use of the Menshin bearing.

4.4 Behavior of the Menshin Bearings

In order to find out how the Menshin bearings worked during the earthquake, time histories of lateral force F, and the relative displacement between the superstructure and the substructure δ were calculated (**Fig. 11**). The lateral force F was obtained by multiplying the acceleration time history of the girder by the weight of the girder (per bearing). The relative displacement (δ) is the difference between the integrated values of acceleration records of the superstructure and the substructure with respect to time. Also here, a high cut filter was used to reduce the effect of waves of 2.5 cps and over, as long as it did not influence the max. value of the displacement. **Fig. 12**

show a hysteresis curve of the Menshin bearing. The hysteresis curve dose not complete a loop. The change in lateral force F seems large compared with the displacement.

5. CONSIDERATION

When the measurement results were examined we collected the trends and came to the following conclusions, although there are more subjects to study analytically.

Measured values:

1) According to the acceleration records of each part of the On-netoh Bridge in **Fig. 5** during the Hokkaido Toho-oki Earthquake, there was not much amplification of the ground motion (316 gal) and superstructure motion (354 gal).

2) On the other hand, it seems that the displacement of the Menshin bearings reached about 1.5 cm (**Fig. 11**). This value is supported by the width of the flaw in the Menshin bearing.

The characteristics of the restoring force of the Menshin bearing:

3) The acceleration of 354 cm/sec^2 measured at the girder during the Hokkaido Toho-oki Earthquake produced a lateral force of about 18 tf per bearing.

4) When the characteristics of the restoring force of the Menshin bearing is calculated according to the Manual for Menshin Design of Road Bridges (draft), the maximum relative displacement of the Menshin bearing was 1.31 cm and the reaction force was 16.59 tf. These values were smaller than those measured during the Hokkaido Toho-oki Earthquake.

5) The results of 2), 3) and 4) showed that the displacement of the Menshin bearings installed in the On-netoh bridge was small. However, the effect on the Menshin bearings and the evaluation of the displacement must be further studied.

Comparison with response spectrum based on the ground motion records:

6) The spectrum of the transfer function of the girder/ground in **Fig. 9** has the first predominant frequency at 1.1 cps (0.909 sec) and the second one at 1.7 cps (0.588 sec). To understand the vibration characteristics of the brigde, the natural period of P3 pier, which was modelled a one-mass structure, was calculated.

Assuming that the bearing was fixed,the natural period is 0.37 sec.

Assuming that the Menshin was used and the displacement of the bearing was 1.5 cm, the natural period is 0.64 sec.

The displacement of the Menshin bearing of 1.5 cm and the natural period of 0.64 sec almost corresponds to the second peak of the transfer function. The acceleration response of 0.64 sec. in the ground response spectrum in Fig. 6 was about 600 cm/sec^2, while the acceleration response of 0.37 sec was about 1,000 cm/sec^2, on the assumption that the bearing was fixed. Therefore, we think that the inertia force decreased because the Menshin bearing lengthened the natural period of the bridge.

6. CONCLUSION

From the descriptions above, it was found that the On-netoh bridge showed the desired effects of the decrease of inertia force. At the same time further consideration needs to be given to the design of Menshin bridges.

REFERENCES

1) Heizyurou Ikeda, Naoki Matsumoto and Kouichi Fukuda : The design planning of

the Onnetoh-Oohasi Bridge (in Japanese), Bridge and Foundation, May, 1990

2) Masashi Sato, Hiroaki Nishi, Kazuhiko Kawashima and Shigeki Unjoh : Response of On-netoh Bridge during Kushiro-oki Earthquake of January 1993, Third US-Japan Workshop on Earthquake Protective Systems for Bridges, Jan, 1994

3) Japan Instutute of Construction Engineering : Guidelines for the base-isolated bearing design method for road bridges (draft), March 14, 1989 (in Japanese)

4) Public Works Research Institute : Development of Menshin Design of Highway Bridges, October 1992, Technical Note of Public Works Research Institute, Vol.60

5) Japan Road Association : Part V, Seismic Design of Design Specifications of Highway Bridges,1990

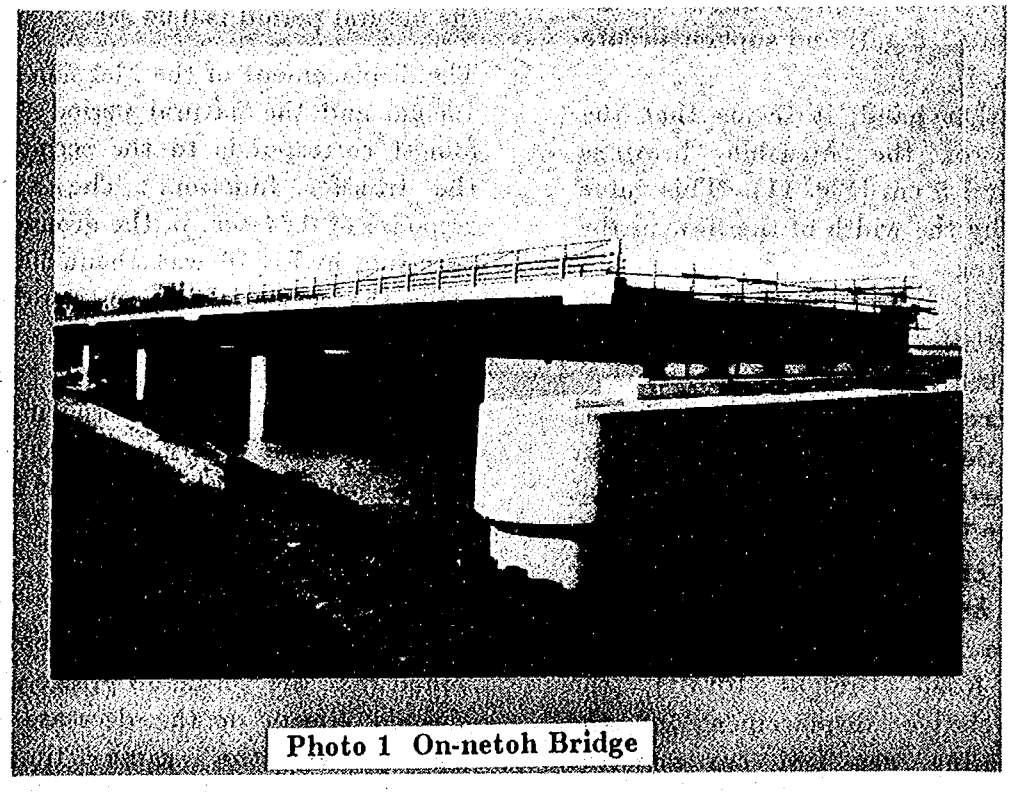


Photo 1 On-netoh Bridge

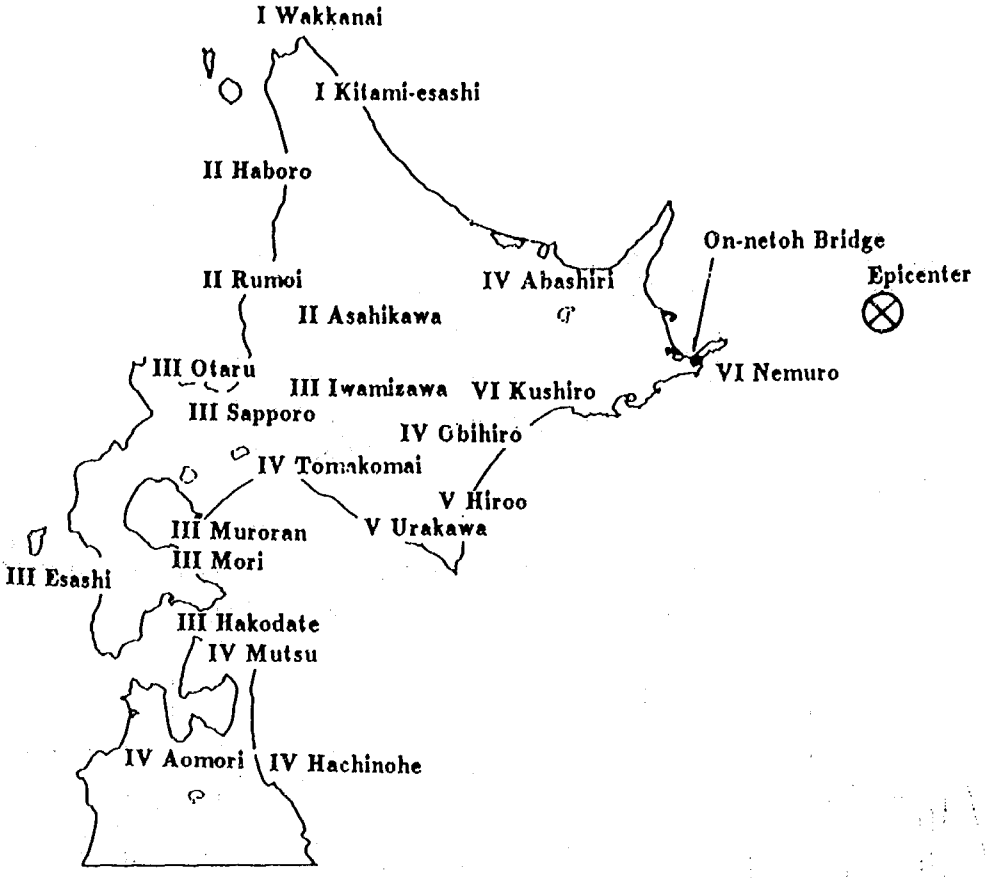


Figure 1 Seismic intensities of each district during the Hokkaido Tôho-oki Earthquake (Japanese seven-stage scale)

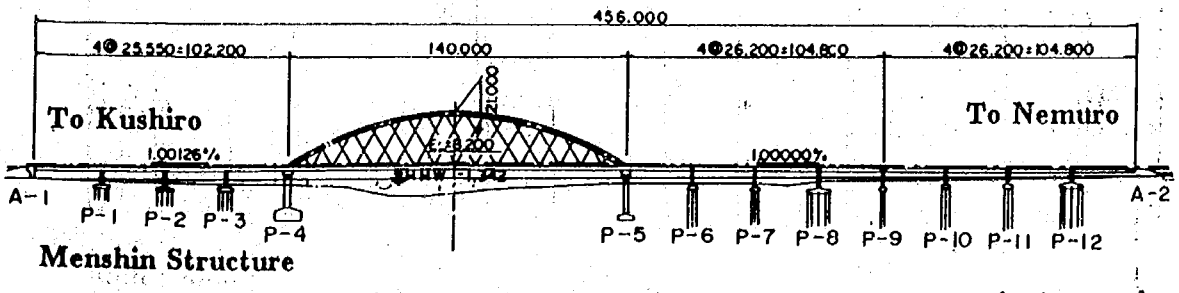


Figure 2 Side View of the On-netoh Bridge [unit : mm]

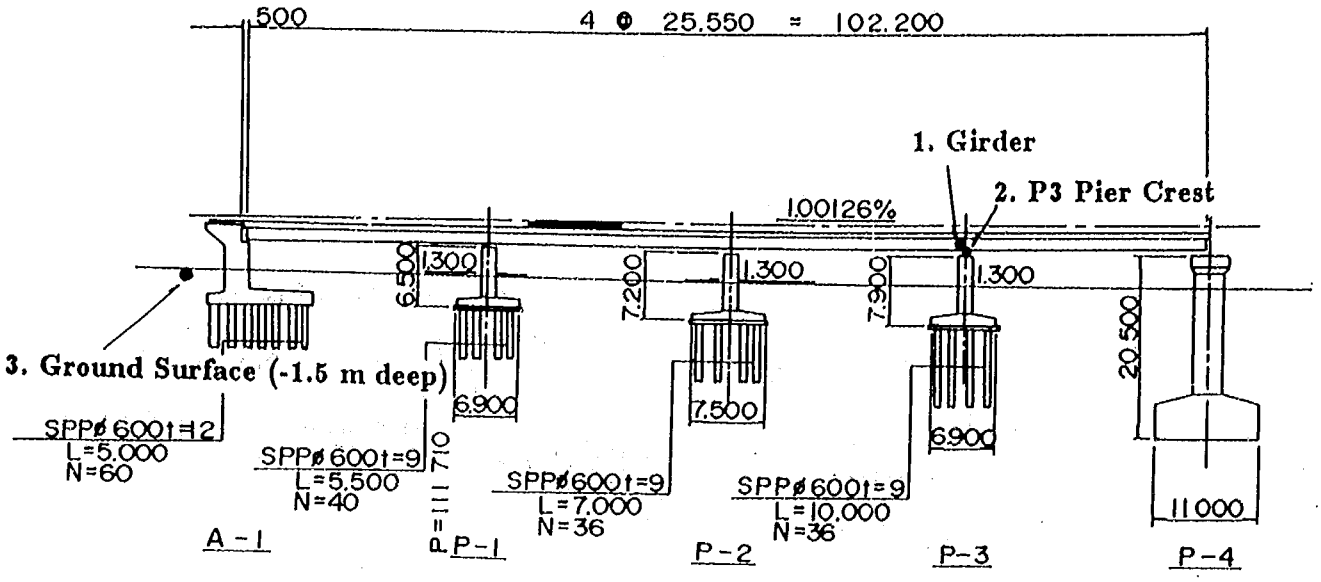
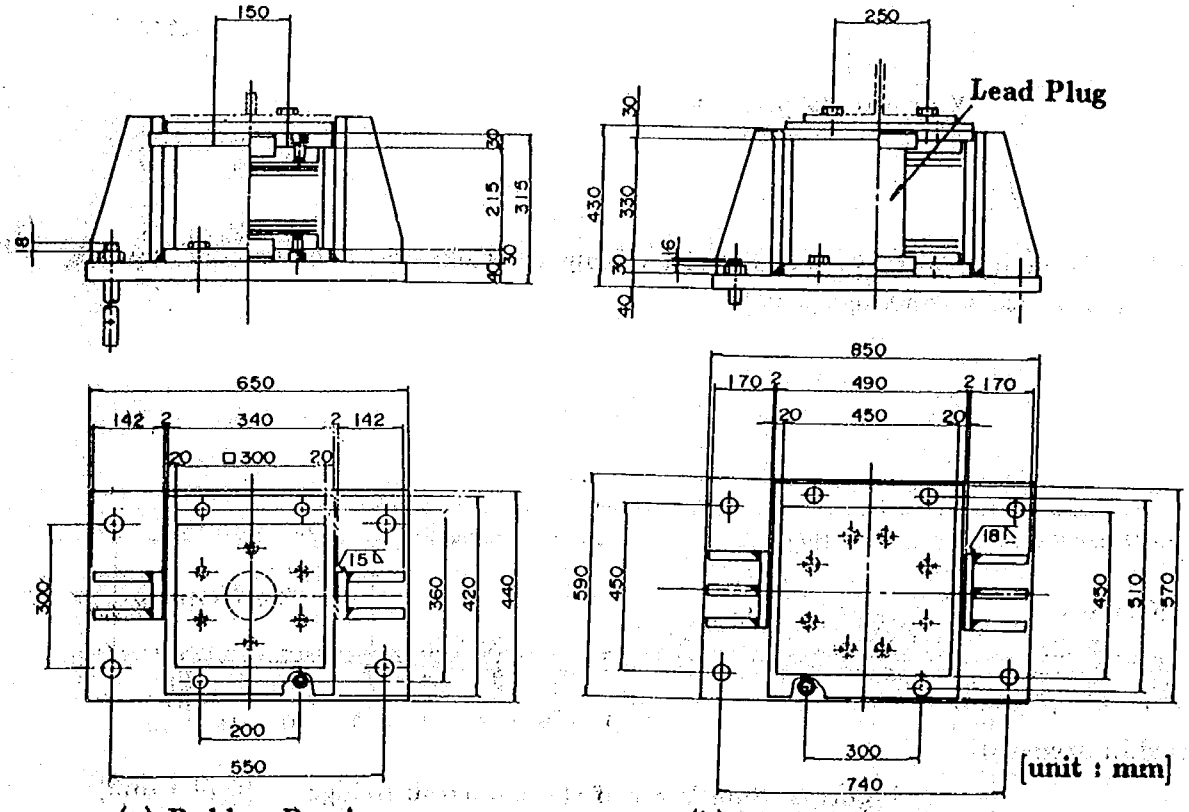


Figure 3 Side View of the Side Bridge (Menshin Designed Bridge)
1.~3.: Location of Strong Motion Acceleregraph



(a) Rubber Bearing (b) Lead Rubber Bearings

Figure 4 Bearings used for the On-netoh Bridge

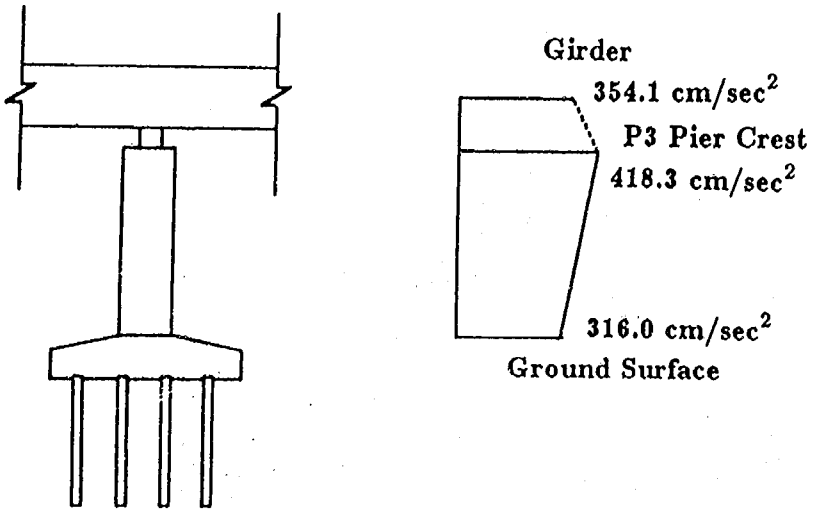
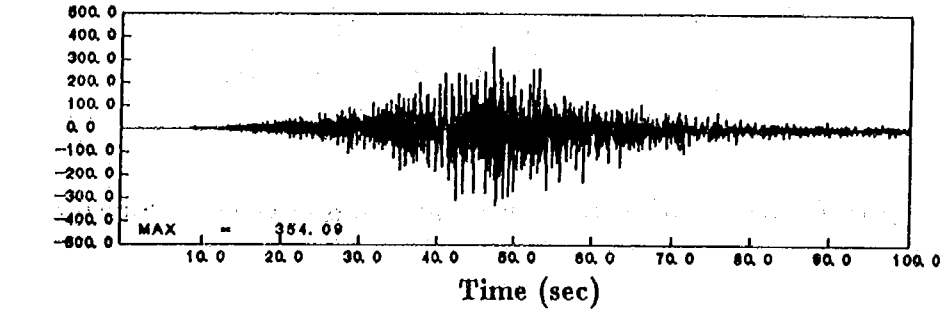
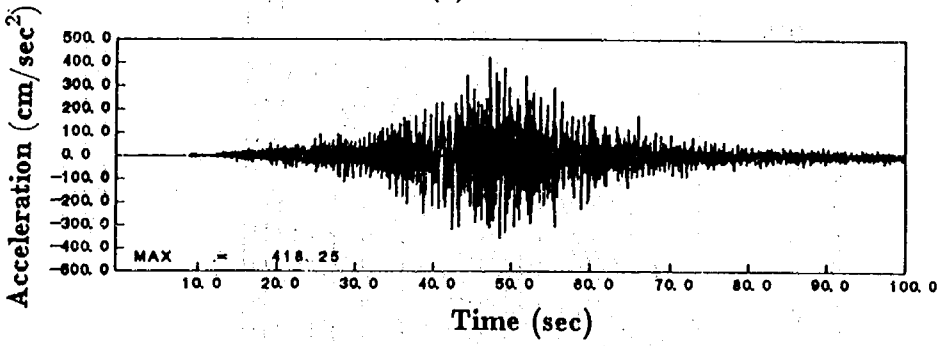


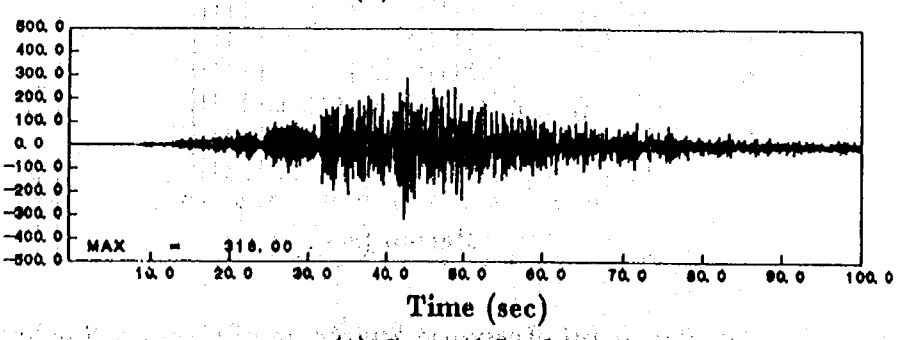
Figure 5 Peak Accelerations



(a) Girder



(b) P3 Pier Crest



(c) Ground Surface

Figure 6 Strong Motion Records

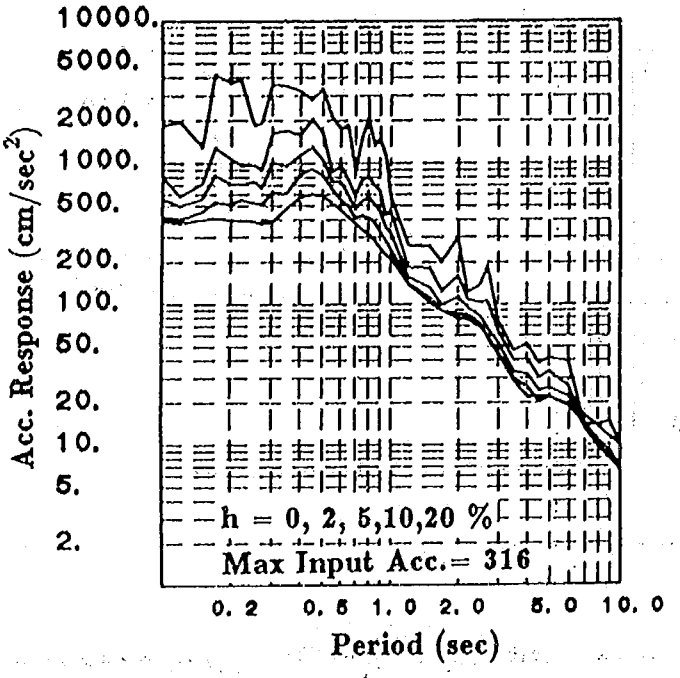


Figure 7 Acceleration Response Spectrum of Ground Surface

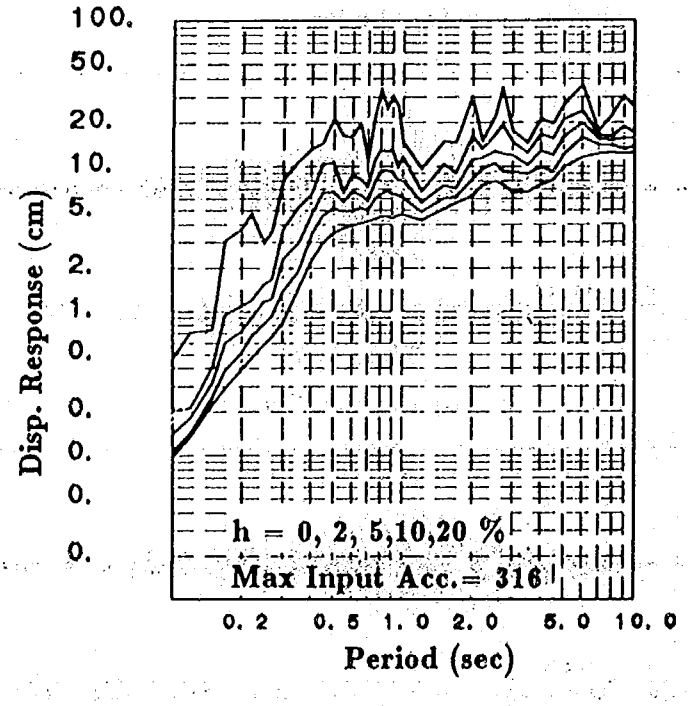


Figure 8 Displacement Response Spectrum of Ground Surface

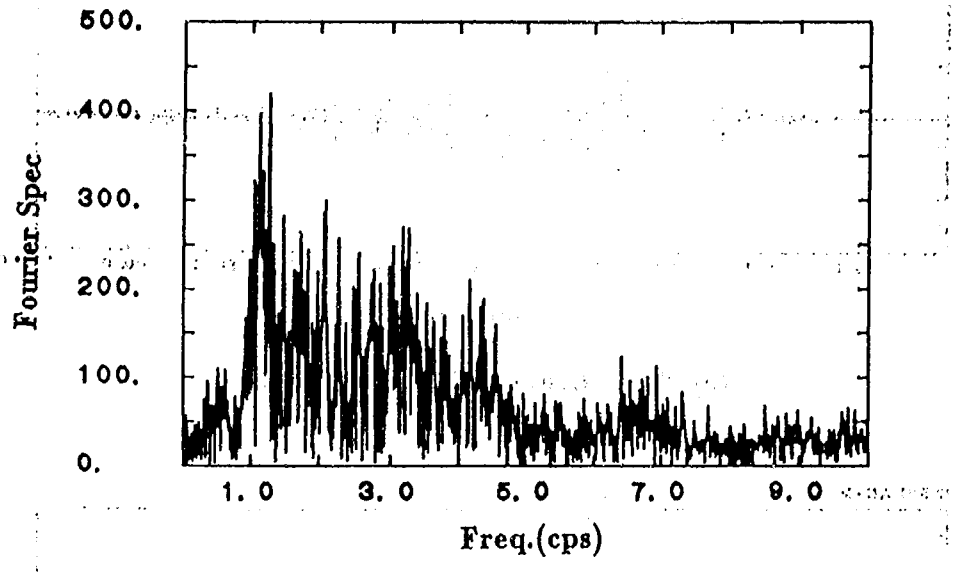


Figure 9 Fourier Spectrum Curve of Girder

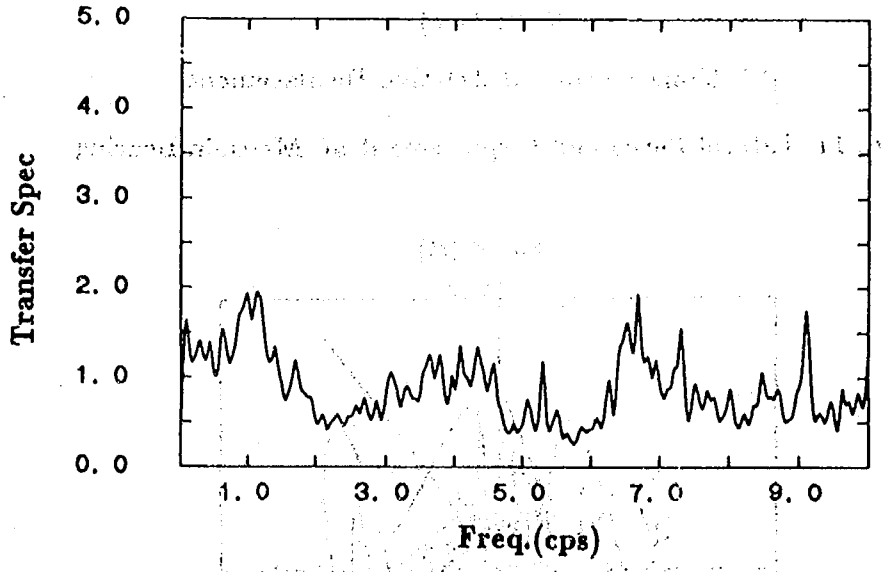
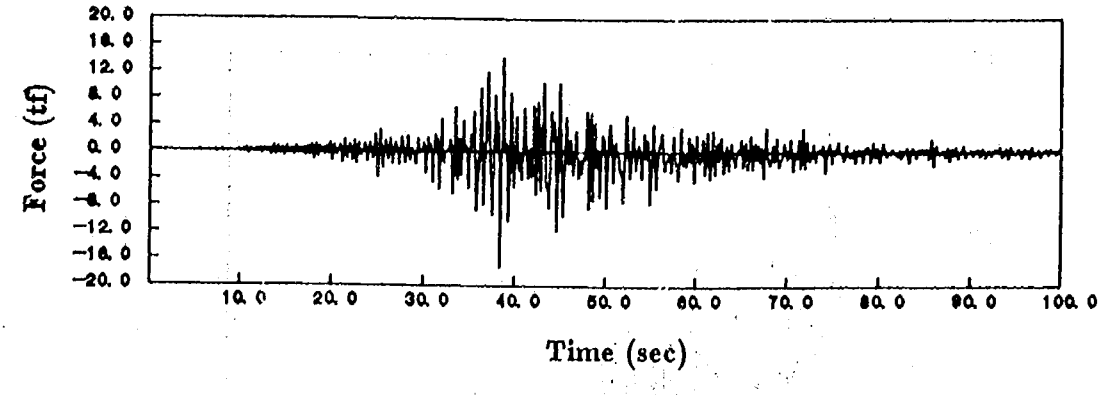
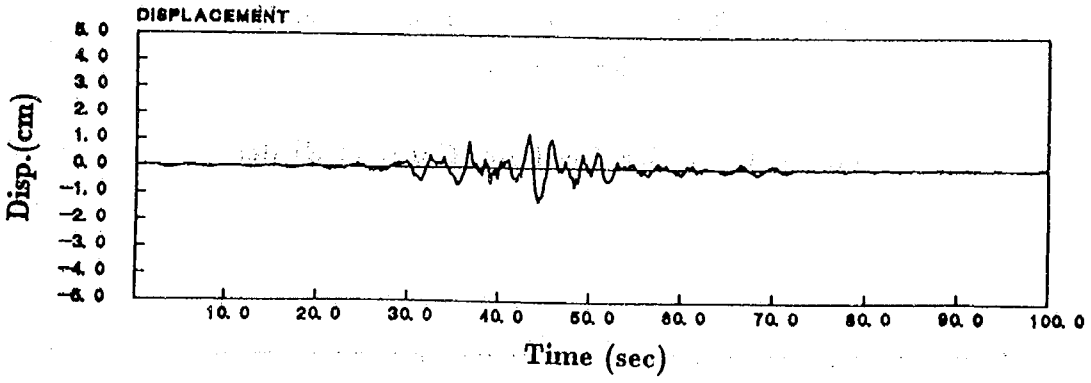


Figure 10 Transfer Characteristics (Girder/Ground Surface)



(a) Time History of Lateral Force



(b) Time History of Relative Displacement

Figure 11 Lateral Force and Displacement of Menshin Bearing

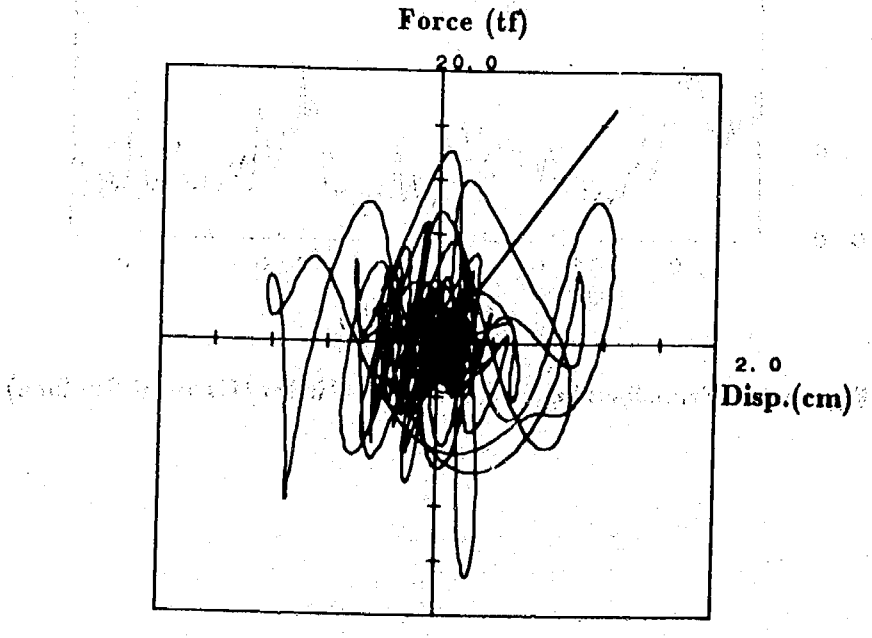


Figure 12 Histeresis curve (Lateral Force ~ Relative Displacement)

Comparison of U.S. and Japanese Highway Bridge Seismic Design Criteria

W. Phillip Yen[1] , James D. Cooper[1] and Ian M. Friedland, P.E.[2]

ABSTRACT

This paper presents comparisons between the philosophy and criteria used for the design of highway bridges as contained in Japanese and United States seismic design specifications. Similarities and differences between the basic design and analysis principles and procedures are discussed, including a comparison of design response spectra and the reduction factors used in the calculation of design forces.

KEYWORDS: Earthquake Engineering, Seismic Design Criteria, Highway Bridges.

1. INTRODUCTION

1.1 Background

Since 1989, a number of relatively large earthquakes have occurred in the United States and Japan. Three earthquakes of significance to bridge engineers are the 1989 Loma Prieta earthquake, the 1994 Northridge earthquake, and the 1995 Hanshin-Awaji earthquake. This is because, in all three earthquakes, there was widespread damage and several catastrophic collapses of highway bridges of various kinds. Most of the collapsed bridges were designed and constructed prior to the implementation of modern seismic codes. However, significant damage also occurred to some bridges built to more recent codes, and these are of special concern to code writing authorities and highway agencies in the two countries.

Japanese bridge design specifications first included seismic design provisions following the 1923 Kanto earthquake. In the United States, earthquake effects on highway bridges were not considered until the 1933 Long Beach earthquake prompted the California State Highway Department (Caltrans) to include provisions for horizontal earthquake forces in its 1940 design specification; these same provisions were then incorporated into nationally-applicable bridge design specifications by the American Association of State Highway Officials (AASHO, now known as AASHTO) in 1941.

Seismic design philosophy and specification provisions in both countries have become more rigorous and rational over time, as subsequent damaging earthquakes have occurred and educated bridge engineers worldwide. It seems that every earthquake provides an opportunity to

[1] Structures Division, Turner-Fairbank Highway Research Center
Federal Highway Administration
McLean, Virginia 22101

[2] National Center for Earthquake Engineering Research
University of New York at Buffalo
Buffalo, New York 14261-0025

improve our understanding of the performance and behavior of structures of all kinds, both through reconnaissance studies and research. In the latter case, observed behavior is often used to calibrate and/or refine our theoretical models, which in turn may lead to changes in construction details and analysis methods.

1.2 Objective

The objective of this paper is to review and present comparisons between the seismic design philosophies for highway bridges as contained in the Japanese and United States' design codes. This review is based on current seismic design specifications being used in the two countries: the newly issued (Spring 1995) Division I-A: Seismic Design of the AASHTO *Standard Specifications for Highway Bridges* and Part V: Seismic Design of the Japan Road Association's (JRA) *Specification for Highway Bridges*, issued in 1990. This review will present the different approaches used for seismic design through a comparison of fundamental design principles and philosophies, design procedures, and dynamic analysis methods recommended in the two specifications.

2. FUNDAMENTAL DESIGN PHILOSOPHIES

In order to understand the application and intent of a design specification, it is important to have an understanding of the underlying philosophy on which the specification is based. In both the United States and Japan, the stated purpose for the two respective highway bridge seismic design codes is to protect against the loss of life and to minimize structural damage due to the effects of earthquakes. However, the implementation of this fundamental philosophy is somewhat different in the codes of the respective countries, and some of these differences are explored in this paper.

The highway bridge design specifications in both countries contain provisions which are intended to prevent collapse in large earthquakes. In small to moderate earthquakes, the intent of the AASHTO code is to resist these loads in the elastic range without significant damage to structural components. The Japanese code is essentially the same; it requires that bridges sustain no damage and continue to be fully functional following the earthquake. In large earthquakes, no span or part of a span shall collapse in either code. However, AASHTO allows that damage is acceptable in these circumstances provided it is limited to flexural hinging in columns and that it occurs above ground in regions that are visible and accessible for inspection and repair.

Forces and displacements for the "design" earthquake as specified in AASHTO are based on a low probability of their being exceeded during the normal life expectancy of a bridge. The AASHTO code specifies probabilistically-based effective peak accelerations throughout the U.S. The JRA code uses a regional seismicity classification map to account for the intensity of design earthquake motions. This map was developed on the basis of statistical analyses from past strong motion data (Kawashima et al, 1989) which were then simplified into three regions so that any discrepancies within a region could be reduced.

A major difference between the two codes is in the way design strengths are specified. The JRA code uses an allowable stress approach, while the AASHTO code is based on an ultimate strength approach. The JRA code provides for an increase in allowable stress by a factor of 1.5 under

seismic forces. Reasons for this difference may be due, in part, to the frequency of occurrence and the type of moderate to large earthquakes that have occurred historically in both countries. In addition, political and cultural issues may be factors here. Table 1 summarizes some of the key fundamental design principles as contained in the highway bridge seismic design specifications of AASHTO and JRA.

3. DESIGN

3.1 Design Procedures

In the seismic design of highway bridges in Japan, design loads are multiplied by a horizontal seismic coefficient. Reinforced concrete elements are then checked against these factored loads, and minimum ductility requirements are imposed. The purpose of the ductility requirement is to ensure that brittle failure of reinforced concrete substructure elements does not occur under seismic loading. For complex superstructures (based on geometry and articulation), a dynamic response analysis is required to be performed. A flow chart demonstrating the JRA design procedure is presented in figure 1. The procedures used for ensuring that reinforced concrete piers have sufficient horizontal strength under the imposed earthquake forces are shown in figure 2.

Under the AASHTO code, bridges are classified into one of four seismic performance categories (SPC). The seismic performance category is defined on the basis of the acceleration coefficient expected for the specific site (A), and the importance classification of the structure (IC). SPCs are shown in table 2. Based on the assignment of these SPCs, minimum analysis and design requirements are then specified by AASHTO. Flow charts demonstrating the AASHTO design procedure are shown in figures 3 and 4. Note that bridges in SPC A are not required by AASHTO to undergo a dynamic analysis. In addition, a dynamic analysis is not required for single-span bridges. However, minimum bearing seat widths must be provided and minimum horizontal connection forces must be satisfied in SPC A and for single span bridges.

3.2 Seismic Design Forces Inertia

The JRA code uses a response spectra to determine the lateral design forces. Design spectra used in Japan are assumed to result in elastic structural response. Seismic loading is then calculated by a seismic coefficient method, as given in equation 1:

$$K_h = c_z \bullet c_G \bullet c_I \bullet c_T \bullet K_{hO} \qquad (1)$$

where K_h is the design horizontal seismic coefficient and should not be less than 1.0; K_{hO} is the standard design horizontal coefficient, typically equal to 0.2; and c_z, c_G, c_I, and c_T are modification coefficients for zone, ground condition, importance, and structural response, respectively. Note that two design force levels are considered in Japan: the allowable stress approach is used to check against small to moderate earthquakes while the ultimate strength of the bridge under lateral loads is checked for large earthquakes (Kawashima, 1994).

The AASHTO code provides the bridge designer the option of using an equivalent elastic analysis method to define the horizontal earthquake load, or a 5-percent damped elastic site-specific response spectrum, which includes the effects of local seismology and site soil conditions.

Based on the elastic seismic response method, the AASHTO code specifies a response coefficient that is to be used with a single mode analysis. This dimensionless coefficient is given in equation 2:

$$C_s = \frac{1.2AS}{T^{2/3}} \qquad (2)$$

where A is the acceleration coefficient, S is a dimensionless coefficient representing the soil profile characteristics at a site, and T is the natural period of the structure. Note that C_s need not exceed a value of $2.5A$ and in certain soil profile cases where $A \geq 0.3$, C_s need not exceed $2.0A$.

Figure 5 shows a comparison between two different response spectra: the JRA spectra for the extreme earthquake event, and the AASHTO spectra which corresponds to a return period of 475 years. Note that the AASHTO spectra is based on a Type II stiff clay site coefficient, S, with 5 percent damping, and an acceleration coefficient of 0.4. The JRA spectra is based on a ground type II, and a seismic coefficient $K_{hO} = 1.0g$. It is important to note that these two spectra are not directly comparable, since the JRA spectra is for an extreme event, while the AASHTO spectra is for what is typically considered to be an "design basis" earthquake; i.e., one that may reasonably occur in the life of the structure. However, the important point that this figure attempts to present is that the response coefficient is much larger in the JRA code than in the AASHTO code in the longer period range.

3.3 Ductility Factors and Response Modification Factors

In the JRA code, ductility checks are only required for reinforced concrete piers with relatively small cross-sections. This provision specifically excludes consideration of multiple-column piers in the transverse direction. The checking process requires the evaluation of the bridge piers and to ensure that they have sufficient capacity to resist the lateral forces caused by large earthquakes; i.e., an ultimate horizontal strength check.

The ductility factor in the JRA code, μ, is a function of a stress-strain model in which $\mu = f(\Delta_u, \Delta_y)$. Note that Δ_u is highly dependent on the confinement of the bridge column section and is based on the specified ultimate concrete strain, ε_{cu}, as it is defined when concrete strain, ε_c, approaches a value of 0.0035. The ultimate horizontal strength coefficient is then reduced by dividing by a factor of $(2\mu - 1)^{1/2}$.

Yielding of the structure is permitted by AASHTO provided the structure does not degrade during cyclic loading. The AASHTO code therefore specifies design details to ensure that minimum confinement, anchorage, and splice requirements are satisfied such that plastic hinging may occur without loss of strength or stability. Such a design strategy permits the elastic forces (obtained from the analysis) to be reduced by substantial factors to obtain design forces in those members permitted to yield. These members are usually the bridge columns and, thus, response modification factors (R-factors) for the columns are specified which range from 3 to 5, depending on the number of columns in each bent. Elements not permitted to yield, such as foundation and connections, have R-factors ranging from 0.8 to 1.0.

The AASHTO R-factors are based on engineering judgement taking into account ductility and redundancy. Generally speaking, however, $R \propto \mu$ and thus, if the AASHTO and JRA reduction factors are to be compared, the result is approximately

that shown in figure 6. It is clear that the higher AASHTO factors lead to greater ductility demands than the JRA designs. It follows, then, that AASHTO bridge columns tend to be more slender than corresponding Japanese columns but contain relatively heavy concentrations of reinforcement which have been detailed for ductile action.

4. ANALYSIS

4.1 Analysis Methods

Four analysis methods are provided in the AASHTO code. The selection of a minimum analysis method is based primarily on the "regularity" of the bridge; note that SPC A bridges do not require a detailed seismic analysis. The four analysis methods are: (1) the uniform load method, (2) the single-mode spectral method, (3) the multimode spectral method, and (4) the time history method. Methods (1) through (3) are response spectra methods of varying levels of complexity. "Regular" bridges can be analyzed according to either methods (1) or (2), while "not regular" bridges must be analyzed in accordance with method (3). A more rigorous analysis, such as method (4), can also be used in lieu of the specified minimum. The AASHTO analysis requires a check of both design forces and displacements.

The JRA design code requires that a dynamic analysis be performed by either a response-spectrum method or by a time-history analysis.

4.2 Dynamic Analysis

Dynamic response analysis is used in Japan to check on the safety of the equivalent static design method. However, this is generally reserved for bridges with complex dynamic behavior or with uncertain response characteristics. For the response spectrum analysis, the acceleration response spectra for modal analysis is determined by equation 3 as follows:

$$S = c_Z \bullet c_I \bullet c_D \bullet S_O \qquad (3)$$

where S is the acceleration response spectrum and is based on the zone modification factor, c_Z, an important modification factor, c_I, the damping ratio modification factor, c_D, and the standard acceleration response spectrum, S_O. The maximum of S_O is 300 gal (approximately $0.3g$) in a zone for ground type III.

The AASHTO design spectrum is used with the analysis methods discussed earlier and is given by equation 2. Time history analysis methods are specified in both codes. Input motions can be either site-specific or spectrum compatible; site-specific records are preferred. Note that if an inelastic time history method is used for analysis, all AASHTO R-factors should be taken as 1.0.

5. SUMMARY

This paper has presented a comparison of the philosophies on which the AASHTO and JRA seismic highway bridge design specifications are based. In comparing design response spectra, it is noted that JRA design forces are much larger than the AASHTO forces in the longer natural periods, and are slightly smaller in the shorter periods. These differences are likely based on the fundamental design philosophies, anticipated soil conditions, return periods, and historical strong motion ground records.

The stated objective of the JRA code for large magnitude earthquakes is to prevent collapse of the bridge. However, in reality, major or important Japanese bridges tend to be designed to higher standards so

that they also can avoid severe damage during large magnitude earthquakes. This same philosophy is also being implemented in the United States for important bridges, as it is assumed that the incremental costs associated with building a stronger bridge will be much less in the long run than the sum of the repair costs and societal costs associated with severe damage or collapse of the bridge.

Japan has had a long, active history of dealing with earthquakes and designing for them since the 1923 Kanto earthquake. Over the years, Japanese design codes have been upgraded in order to address deficiencies found due to damaging earthquakes (Iemura, 1995). This is also the situation for the United States, especially since 1971 (Buckle, 1995). Recent earthquakes, like the 1994 Northridge earthquake, have shown that bridges designed to modern seismic codes perform better, with less susceptibility to collapse, than bridges designed to the older, less rigorous codes.

The Japanese design code and the AASHTO Division I-A specification do not require that earthquake loads be combined with vehicular live loads, but only with other service loads. (Note that the new AASHTO *LRFD Bridge Design Specifications* does require the combination of earthquake loads with one-half the vehicular live load). The lack of live load may underestimate the applied loading (and impact the dynamic behavior) of long or unusually congested highway bridges.

One issue not currently addressed by the codes of either country is the effect of combined vertical and horiontal accelerations on seismic response. High vertical accelerations were recorded in both the Northridge and Kobe earthquakes at some locations. It is likely, therefore, that future generations of the AASHTO and JRA codes will be modified yet again to require minimum allowances for vertical input motions.

ACKNOWLEDGMENT

The authors of this paper would like to acknowledge and thank Dr. Ian G. Buckle for his assistance and suggestions during the preparation of this paper. The authors also like to thank Mr. Junichi Hoshikuma and Mr. Tomofumi Nozaki of PWRI, Japan for providing invaluable information of Japan's seismic design principles of highway bridges.

REFERENCES:

AASHTO, 1995, Interim Revisions to the AASHTO *Standard Specifications for Highway Bridges*, "Division I-A: Seismic Design," American Association of State Highway and Transportation Officials, Washington, DC.

Applied Technology Council, 1994, Meeting notes of the ATC-18 "Seismic Design Criteria Review" project.

Barenberg, M. and Foutch, D., 1988, "Evaluation of Seismic Design Procedures for Highway Bridges," ASCE Journal of Structural Engineering, Vol. 114, No. 7.

Buckle, I., 1995, "Influence of Damaging Earthquakes on Bridge Design in the United States of America," Preprint from the International Bridge Seismic Design Workshop, Tsukuba, Japan.

Iemura, H., 1995, "Damage Characteristics of Bridges," Preprint from the International Bridge Seismic Design Workshop, Tsukuba, Japan.

Japan Road Association, 1990, "Specifications for Highway Bridges," Part V: Seismic Design.

Kawashima, K., 1994, "Seismic Design Force of Bridges," Proceedings of the Second International Workshop on Seismic Design of Bridges, Queenstown, New Zealand.

Kawashima, K., and Hasegawa, K., 1994, "New Design Specification for Highway Bridges in Japan," Earthquake Spectra, Vol. 10, No. 2.

Kawashima, K., Aizawa, K., and Takahashi, K., 1986, "Attenuation of Peak Ground Acceleration, Velocity and Displacement Based on Multiple Regression Analysis of Japanese Strong Ground Motion Records," Earthquake Engineering and Structural Dynamics, Vol. 14, pages 199 - 215.

Table 1. Comparison of AASHTO and JRA Design Principles

PRINCIPLE	AASHTO	JRA
Stated Purpose	To minimize susceptibility of highway bridges to damage from earthquakes	To secure safety of road traffic against earthquakes
Design Strength	Based on ultimate strength	Based on allowable stress; but includes a check for ultimate strength
Small to Moderate Earthquakes	No damage	No damage
Large Earthquakes	No collapse of all or part of the bridge; flexural hinging acceptable	No collapse of all or part of the bridge
Design Earthquake Forces and Displacements	Based on a low probability of exceedance in the lifetime of the bridge	Based on a statistical analysis of past earthquake records

Table 2. AASHTO Seismic Performance Categories (SPCs)

Acceleration Coefficient, A	Seismic Performance Category (SPC)	
	Importance Classification (IC)	
	I	II
$A \leq 0.09$	A	A
$0.09 < A \leq 0.19$	B	B
$0.19 < A \leq 0.29$	C	C
$0.29 < A$	D	C

Note: IC = I is for essential bridges; IC = II is for all other bridges.

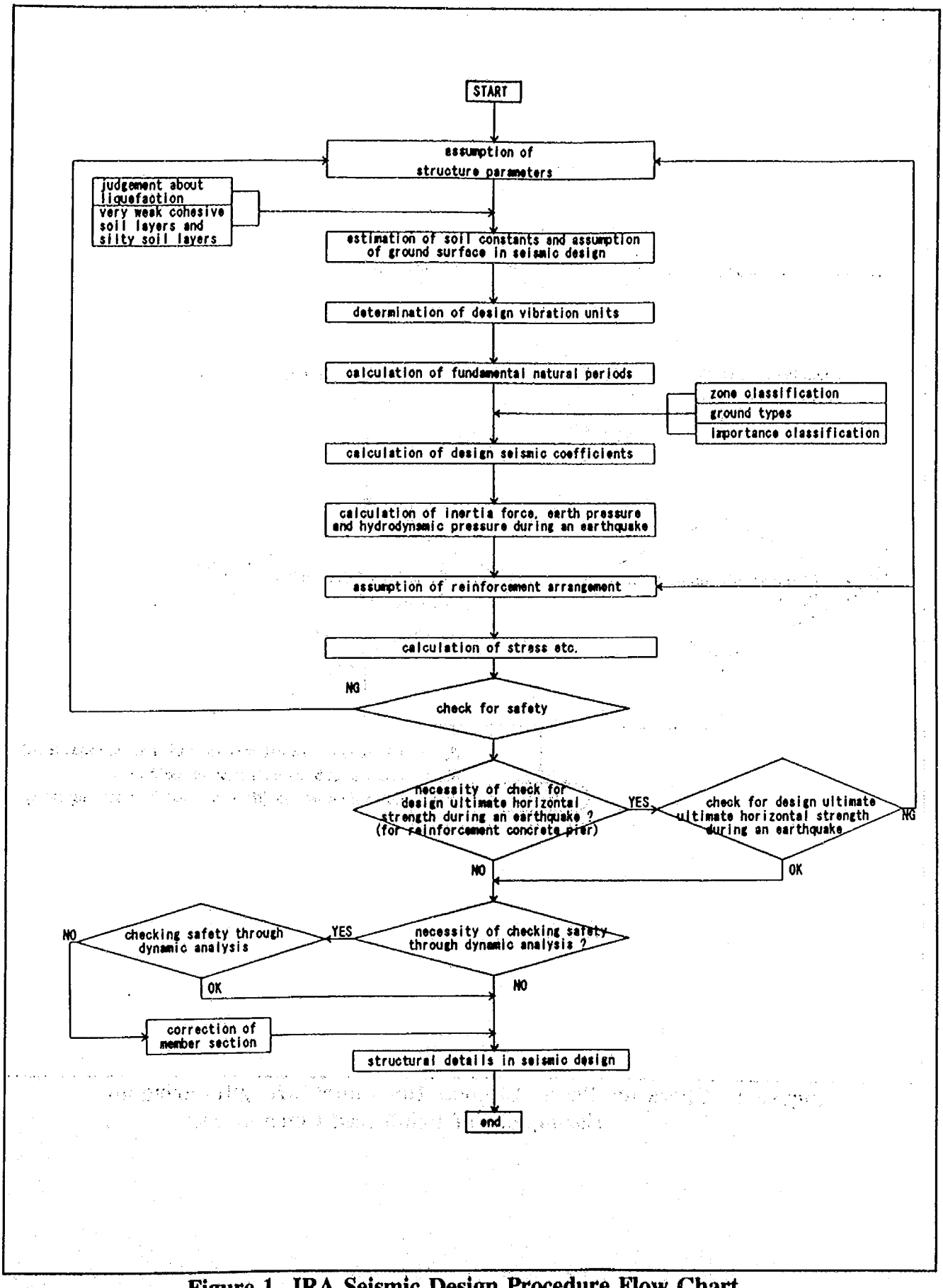


Figure 1. JRA Seismic Design Procedure Flow Chart

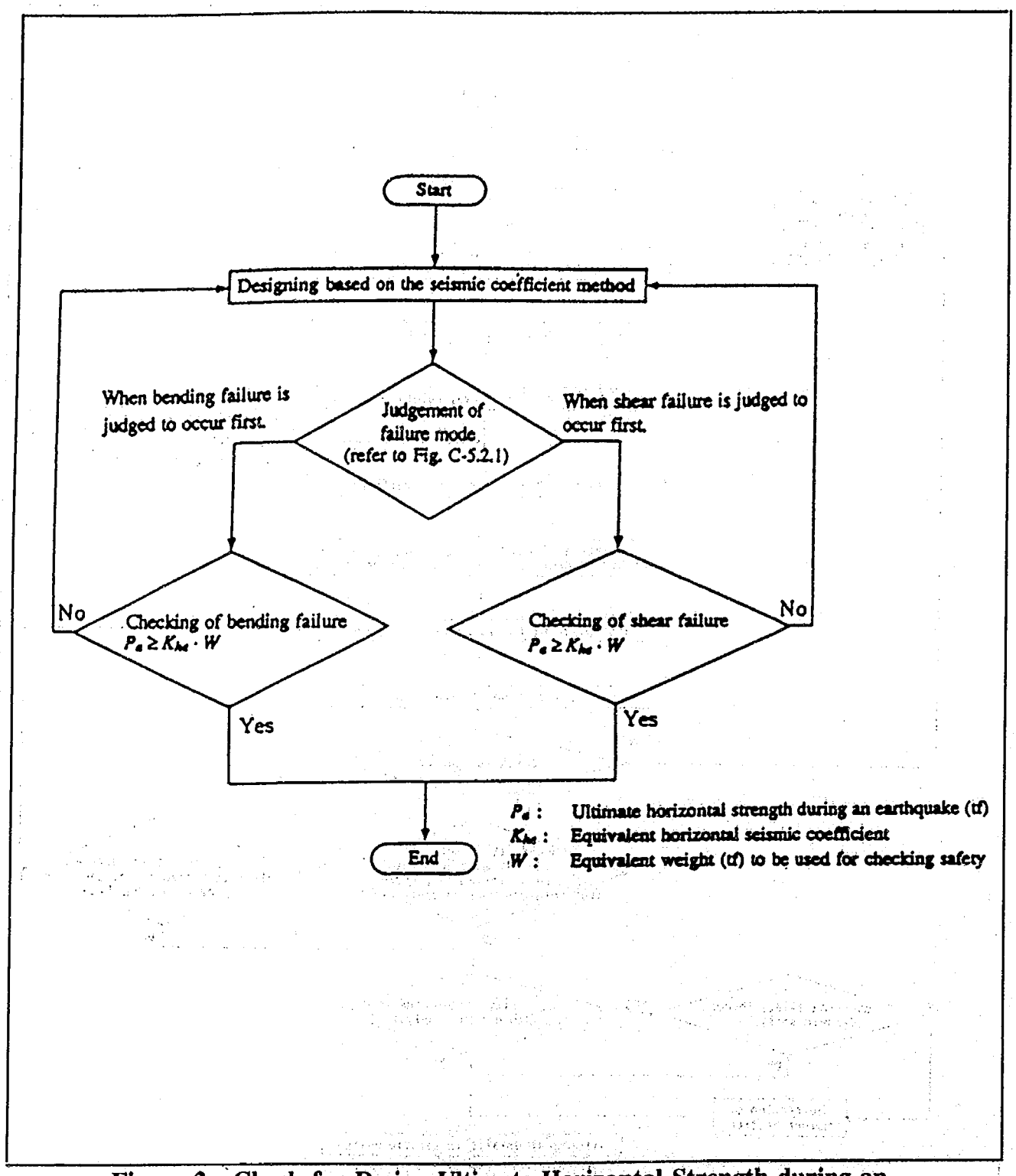


Figure 2. Check for Design Ultimate Horizontal Strength during an Earthquake of Reinforced Concrete Piers

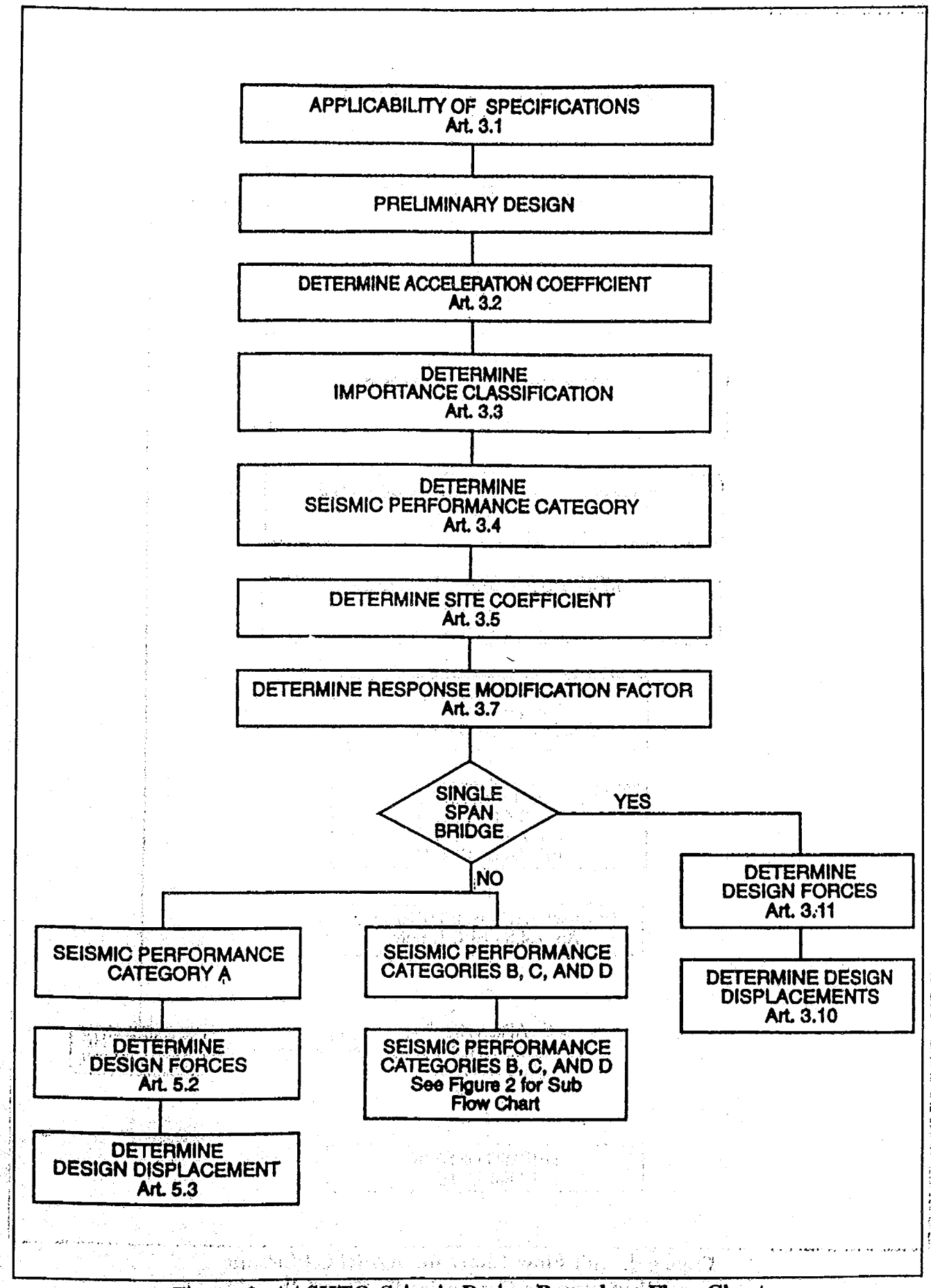


Figure 3. AASHTO Seismic Design Procedure Flow Chart

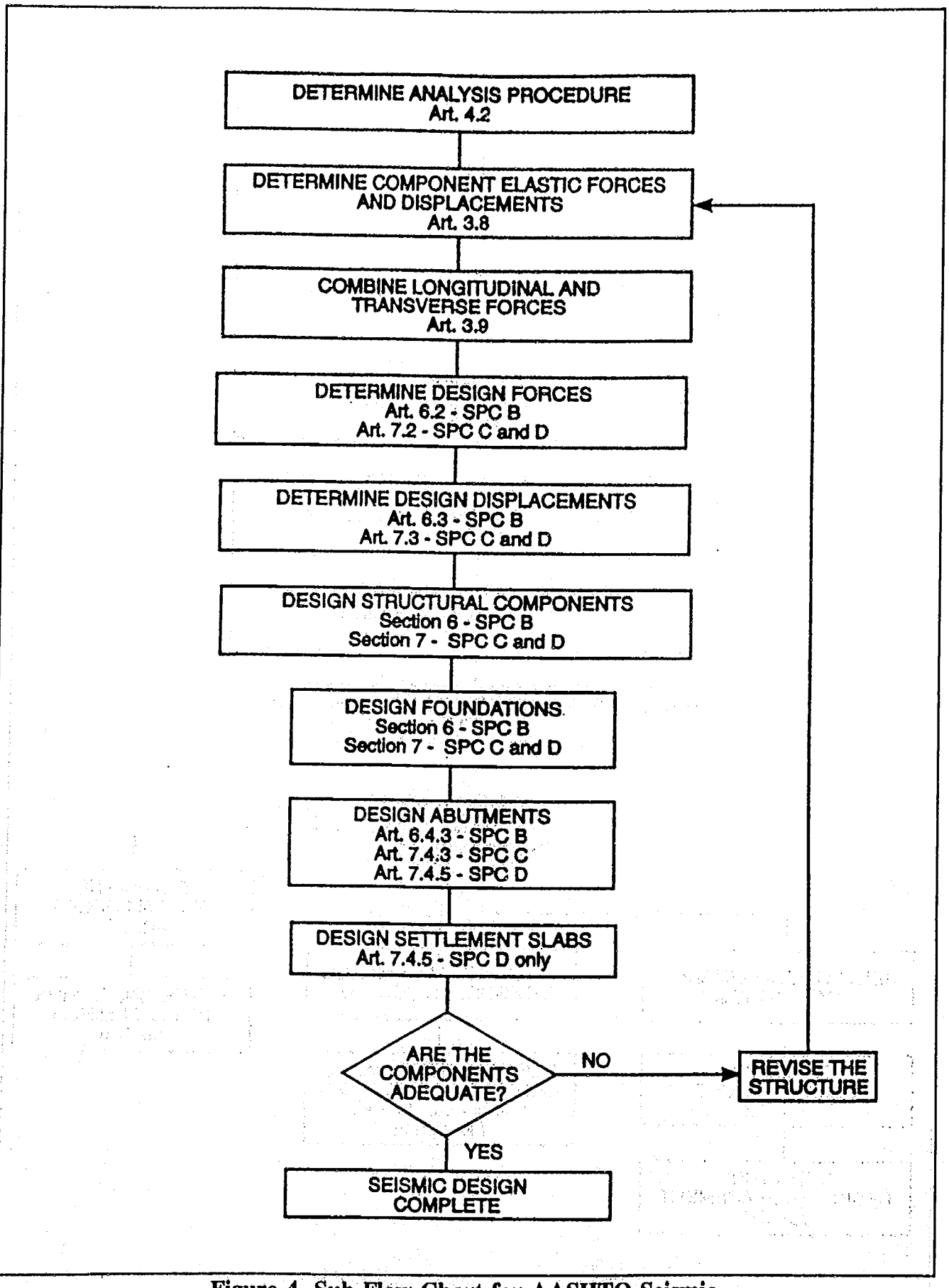


Figure 4. Sub Flow Chart for AASHTO Seismic Performance Categories B, C and D

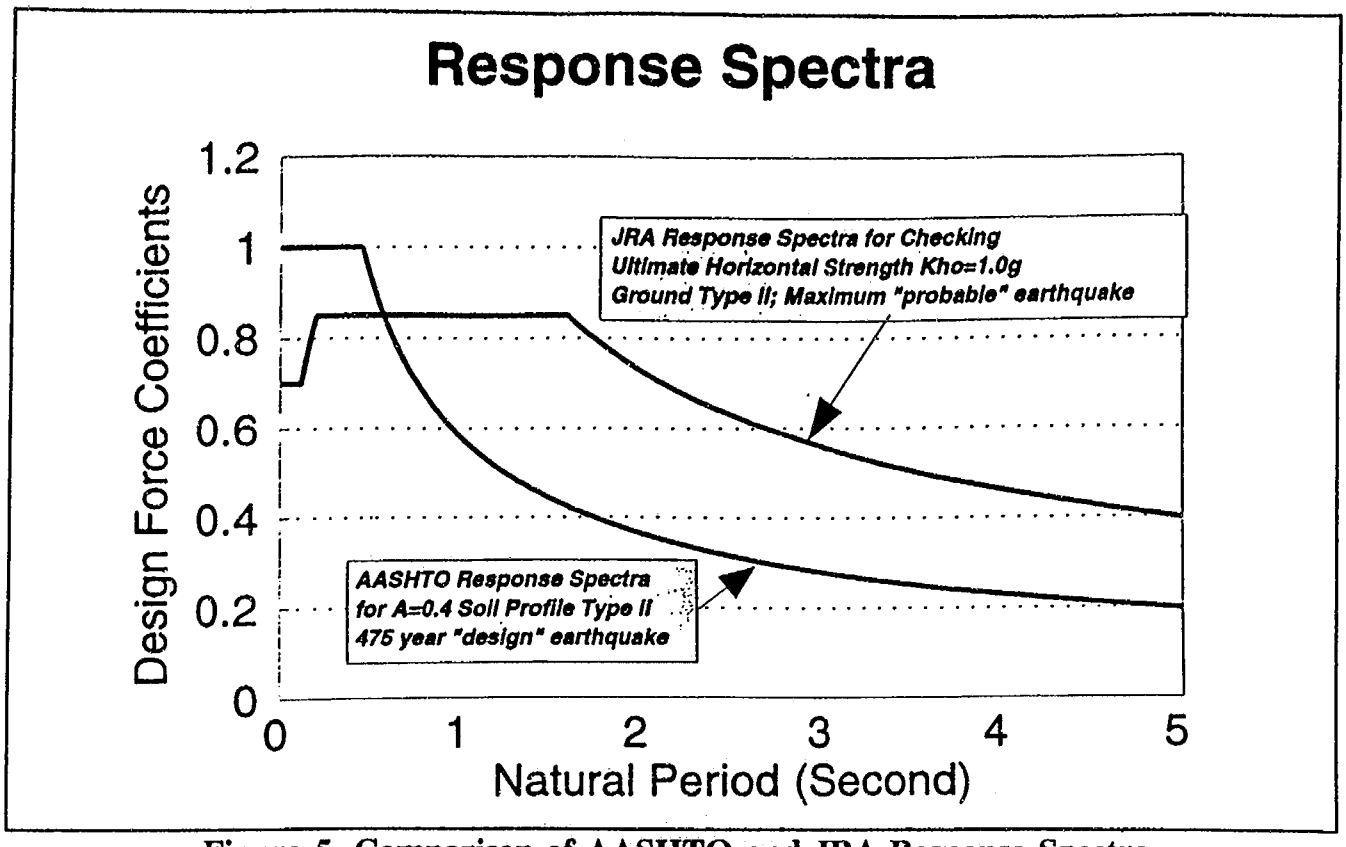


Figure 5. Comparison of AASHTO and JRA Response Spectra

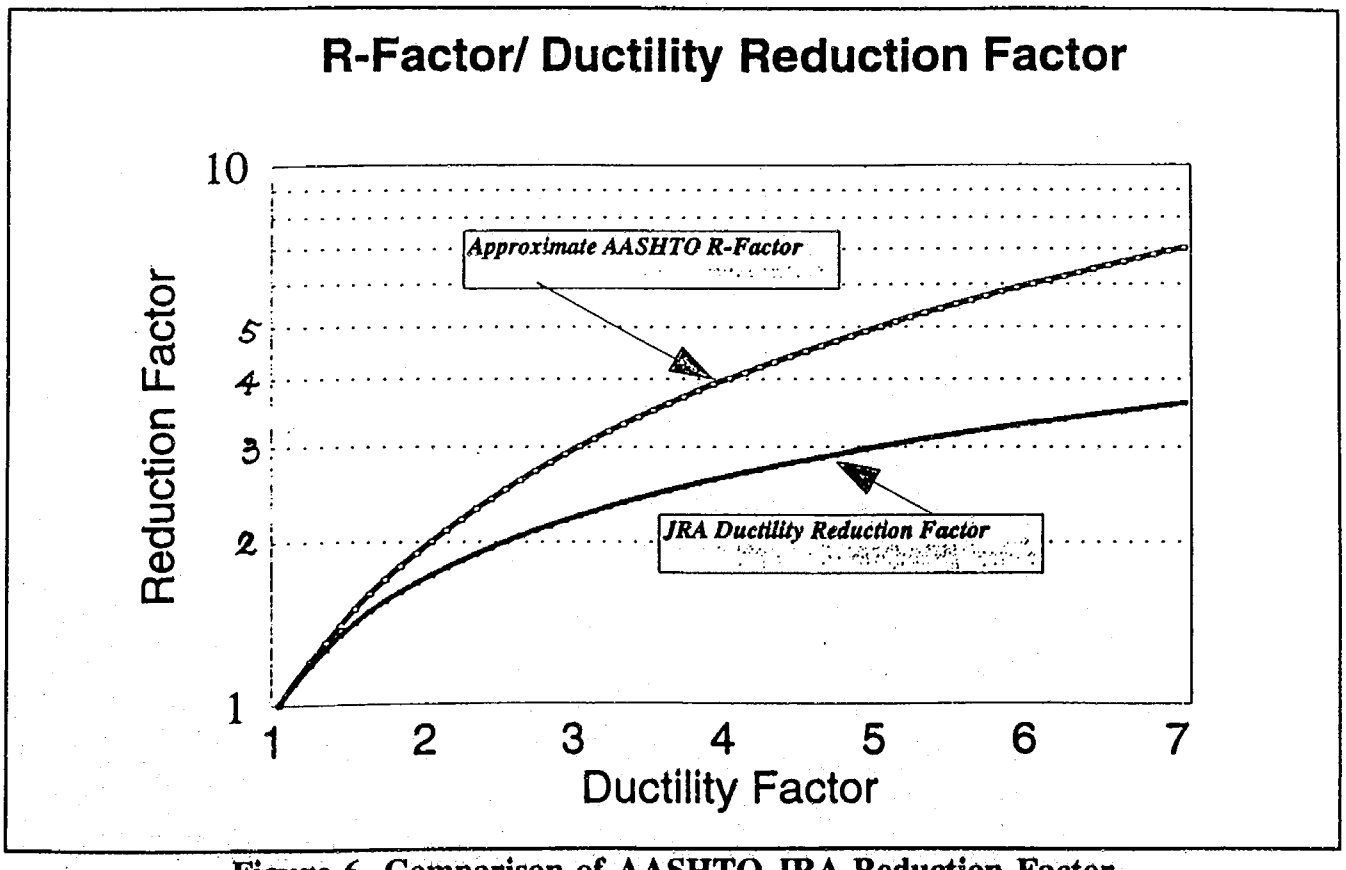


Figure 6. Comparison of AASHTO JRA Reduction Factor

VERIFICATION OF STONE COLUMN CONSTRUCTION USING FIELD INSTRUMENTATION DATA

by

Francis G. McLean[1],
Michael G. Stevens[2]
and Richard H. Kelsic[3]

ABSTRACT

Construction to remedy a seismic deficiency (liquefaction) of the downstream embankment foundation at Mormon Island Auxiliary Dam, part of the Folsom Dam and Reservoir Project near Folsom CA, was accomplished by installing stone columns. This paper presents a brief synopsis of the project and other phases of the repair, then concentrates on the data collection, analysis, and evaluation procedures used to support the decision process applied in assessing adequacy of the stone column construction. The modification area contained approximately 2900 large diameter (1-1.75m) and 4740 small diameter (0.3 m) columns, representing about 160,000 meters of installed columns. The decision process was accomplished in near "real-time" conditions using automated data collection, electronic transmission, and computer-based evaluation techniques. These data also provided the basis for selecting the test locations for the primary density increase verification tool, the Becker Hammer Penetration Test (BPT), and other post-construction field investigations.

KEYWORDS: data collection; foundations; instrumentation; liquefaction; soil improvement; stone columns.

1. INTRODUCTION

The U.S. Army Corps of Engineers (USACE) originally constructed the Folsom Project in the 1950's. Operation and maintenance of the project is done by the U.S. Bureau of Reclamation (Reclamation). Under interagency agreement reached in 1980, the USACE (as the design entity) is responsible for dam safety evaluation. A design team comprised of USACE and Reclamation staff designed, and Reclamation contracted for, the recently completed downstream construction. Of the 11 embankments comprising the project, only Mormon Island Auxiliary Dam (MIAD) was determined to need repair. This was due to the existence of loose materials in the embankment foundation which were the result of dredging operations undertaken for gold recovery.

The seismic studies of the Folsom Project were initiated in 1981 [Hynes-Griffin, 1988; Wahl, 1992], with Phase I construction repairs (dynamic compaction of the upstream foundation and upstream stability berm) for MIAD initiated during a drought period in 1990 [Stevens, 1994]. Construction of the downstream stone columns, Figure 1, began in April, 1993, and was completed in September, 1994. Final evaluation of as-constructed conditions, with respect to adequacy for remedying the liquefaction potential and limiting permanent deformations, is nearing completion.

2. BACKGROUND

MIAD was constructed across a valley which had been repeatedly mined using dredge methods, Figure 2. The central core and inner portions of transition zones were founded on bedrock, while the shells and outer portions of the transitions were constructed on the dredged materials. These materials were irregularly distributed, with localized patterns of inclined and variable "layering" of materials.

Because of the repeated dredging, it was initially difficult to characterize site conditions. However, experience at the site during safety of dams investigations and feasibility test construction of stone columns indicated some general depositional trends (Reclamation, 1993), as depicted on Figure 4, and summarized below:

- Gravel, cobbles and some boulders are present throughout the dredged alluvium. However, there is an overall trend for increased finer grained materials with depth.

[1] Manager, Value Engineering Program (formerly Chief, Geotechnical Engineering and Embankment Dams Branch), USBR, Denver, CO 80225.
[2,3]Civil Engineers, U.S. Bureau of Reclamation, Denver, CO 80225.

- The top 3 to 4.5 m of the deposit, as measured from the downstream embankment toe, consists mainly of coarse sand to cobble sizes. The gravel and cobbles dominate, and determined the response of this zone to remediation efforts.

- A zone of silty-sand, with 15 to 30 percent fines and little or no gravel or cobbles, is present in various thicknesses over the site. This zone was intermittent in a zone between 6.1 and 12.2 m deep. In this zone, the fines content dominated the response to remediation efforts.

- The bottom 3 to 6.1 m of the dredged zone contains a pervasive fine-grained unit. Split-spoon and dry core samples from this zone indicated low to non-plastic fines ranging from 10 to 77 percent and averaging about 30 percent [Reclamation, 1993]. Again, the fines in this unit dominated the response to remediation efforts.

Potentially liquefiable materials were identified in all of the above zones. Evaluation relied on records of original construction, test trenches, borings, SPTs and BPTs, and laboratory testing [Hynes-Griffin, 1988; Wahl, 1992]. Simplified evaluations were used in conjunction with more complex computer-based analyses [Ledbetter, 1991; Nickell, 1994] to determine the extent of the deficiency and evaluate concepts for remedial construction. They are currently being applied to post-construction evaluations of possible permanent deformations.

3. PHASE I CONSTRUCTION

Phase I construction upstream utilized deep dynamic compaction and a stabilizing berm to remedy upstream deficiencies while the reservoir was low during drought conditions. An accelerated design-construction schedule was set, and funds appropriated on an expedited basis. This construction was undertaken first due to the obvious seismic vulnerability and unknown length of conditions favorable for construction. Results of the Phase I dynamic compaction program are well documented [Stevens, 1994; Ledbetter, 1991] and are being combined with downstream treatment results to assess over all dynamic response of the dam during Maximum Credible Earthquake (MCE) loading [Nickell, 1994].

4. COLUMN CONSTRUCTION TEST PROGRAM

Prior to initiation of Phase II downstream designs, uncertainty existed on the adequacy of dynamic compaction to treat the materials to the necessary depths (without extensive dewatering and/or excavation), and whether the construction process was acceptable from a safety standpoint under potentially full reservoir loading conditions. Literature searches and communications with researchers and industry specialists indicated that there was little or no experience using existing technologies to remediate the types of materials present, and to the depths necessary to fully address the identified seismic deficiency. Therefore, a test program was initiated and completed in 1992 to evaluate the construction methods and technical viability of:

- rotary displacement stone columns,
-vibropipe drain stone columns,
-vibrorod compaction,
- bottom feed stone columns, and,
- vibrorod/vibropipe stone columns.

The effectiveness of each method was evaluated based on results of BPTs, SPTs, cross-hole shear wave velocity surveys (Vs), pumped well tests, geophysical logging, material properties tests on SPTs and core samples, piezometric data and sensor data from the construction equipment. Some of the key conclusions from evaluation of the test construction program and collected data are summarized as follows:

- Only the vibropipe method of installing small diameter, continuous, vertically permeable stone columns proved successful in constructing through the Zone 1 embankment shell to the depths necessary to simulate installation of the upstream mini-column zone.

- All methods were successful in achieving installations to the necessary depths at the embankment toe.

- Water and air were required during driving to consistently achieve desired treatment depths. Effects on permeability of installed columns due to flushing fines and fine sand into the placed columns could not be accurately quantified.

- Only the vibratory probe (vibroflot) and rotary displacement methods for constructing large diameter, bottom-feed stone columns produced the desired levels of density increase in materials classified as silty-sands (SM's with 15 to 25 percent fines).

- Density increases for all methods were significantly reduced in the bottom 6.1 m of the deposit. This was attributed to the presence of a zone having a higher fines content. As a result, this zone was targeted for additional effort during final remediation.

- The relative success in achieving density increases with the rotary displacement and bottom feed methods tested, along with concerns about the potential for reduced permeability from using water and air to construct the columns, resulted in a conceptual shift from relying on drainage to obtaining density as the primary design criteria.

- The application and monitoring of air pressure to the vibropipe drain hopper was required to ensure continuous gravel columns of the desired diameter. Only columns constructed by this method could be assumed to be high permeability drainage elements over their entire diameter for preparation of final designs.

5. PHASE II DESIGN

Based on test program results, a final configuration was selected for design, Figures 3, 5, and 6, incorporating the concept of improving foundation density for the majority of the area defined for treatment. Untreated dredged materials outside of the area designated for densification, including a zone under the dam body, were viewed as capable of generating excess pore pressures. The final design provided up- and downstream drainage zones, using closely spaced, small diameter columns (mini-columns) to isolate the densified zone from migrating excess pore pressures. A large portion of the embankment had to be removed prior to remedial construction to accommodate a properly located and adequately sized densification zone to mitigate liquefaction, and resulting deformations, and still optimize overall in situ treatment cost.

The design relied on the use of equipment capable of displacing, and therefore compacting, the soil while gravel backfill was placed at the bottom of the treatment device. It was anticipated that the zones of finer materials in the lower portion of the cross-section would require a somewhat different installation procedure than the more easily treated, overlying, coarser materials. The actual equipment and procedures used successfully during the test construction program were not specified, to allow for flexibility and competition during the bidding process. Instead, minimum column diameters of 1.2 m were specified in the bottom 6.1 m of the deposit, with 0.8 m minimum diameters above this zone. Additionally, spacings of columns were to be no greater than 3 m center to center on a triangular pattern. This allowed flexibility for the contractor to experiment with different procedures, column layouts and equipment in achieving the desired level of density increase. In order to allow the government to assess the effectiveness of the contractor's proposed operations, the contract called for a Demonstration Area to be constructed in Area 14.

The design of the up- and downstream drainage zones, to prevent pore pressure migration into the densified area, used small diameter stone columns. Again, the equipment and procedures used for the test construction program were not specified, to allow for flexibility in completion of the work and competition during the bidding process. A minimum displacement ratio equivalent to that proven successful during the test program was used, i.e., a 0.25 m column on 0.76 m spacing. This minimum column diameter was specified to ensure adequate drainage, and to accommodate displacement which might take place across the columns during seismic loading.

The densification zone was divided into 18 Approval Areas numbered 1 through 18, Figure 5. The total area of treatment in plan was about 275 m by 61 m, resulting in nine 30.5 m by 30.5 m Approval Areas upstream (Areas 1 - 9) and downstream (Areas 10 - 18). Each area contained approximately 140 stone columns, except for Approval Area 14, where the Demonstration Area was located. Areas 1, 10, 17, and 18 overlapped the undredged materials lying along the sides of the valley, and required fewer columns.

This paper will concentrate on methods used to verify the adequacy of the large diameter stone columns used in the central zone where density increases in the foundation materials were desired.

6. CONSTRUCTION OF STONE COLUMNS

The contractor who was awarded the Phase II construction contract elected to use equipment and column spacings similar to that proven successful during the test program. However, during construction of the Demonstration Area, Figure 5, the contractor elected to experiment with a dry method and a second wet method (lower water volumes) of stone column construction, rather then use the wet method proven successful in the test program. Results of post-treatment BPTs indicated that the new procedures were not achieving the

desired density increase, and, hence, not meeting design objectives. After Approval Area 1 and 2 were completed, see below, the contractor chose to proceed with wet method and a 2.7 m triangular spacing for completion of the remainder of the work.

As mentioned, a significant portion of the dam had been removed downstream to expose the foundation area for remediation, Figure 3. The reservoir needed to be back in unrestricted operation for flood control by the late winter rainy season. To prevent further delay, the contractor was allowed to proceed with remediation of Areas 1 - 4, while methods of evaluating actual density increases achieved in the Demonstration Area and Approval Areas 1 - 4, with respect to the original test construction program, could be explored. This led to an intensive review and evaluation of data collected during the construction operation, and, ultimately, to the adopted procedures described herein to monitor and predict the effectiveness of implemented procedures. Because of these construction challenges and scheduling constraints, special effort was expended to collect, process, evaluate and disseminate information obtained by the automated instrumentation system to ensure that adequate treatment was taking place.

Columns were constructed in two passes, primary and secondary, where the primary pass was completed within any given Approval Area prior to beginning the secondary pass, Figure 6. An additional, or tertiary pass, was conducted in select areas where densification objectives and/or procedures were not consistently met or applied. This "additional" work was required for portions of work areas 3, 6, 12, 15, 16, and 17. Depths of primary and secondary columns were generally on the order of 16.7 m to 19.8 m, with the majority of the tertiary columns being installed in the upper 9.1 m of the foundation.

Construction of stone columns started on the upstream half of the modification area, proceeding in Approval Areas 1 to 9 in consecutive order. The downstream portion was accomplished in Approval Areas 18 to 10, in reverse order. Columns within the individual areas were constructed starting from the upstream edge and working downstream.

Developing a reliable method for rapid verification of the foundation densification attained with the contractor's equipment, i.e., two cranes with vibroflot, bottom feed tremie apparatus and related support equipment, and procedures proved to be a key issue in meeting project schedules and design objectives. The purposes of this effort were:

- Identify, during or shortly after the primary column treatment pass, areas within each foundation Approval Area that would probably require additional work effort or special attention during secondary column treatment.

- Use data collected during column construction by the contractor, together with the following information: as-built column location drawings, estimates on the amount of stone used to construct each column, inspector reports, observations of rig performance on site, preconstruction geologic information, to assist with locating BPTs and other post-treatment investigations, thereby ensuring that treatment effectiveness was appropriately represented by the test findings.

- Verify consistency of installation procedures and density achieved within each foundation Approval Area.

- Define the requirements for minimum acceptable tertiary treatment, while meeting the design intent of the remediation plan.

- Implement an efficient communication process between design, construction management (CM) and contractor personnel, so that "real time" response to optimizing site treatment could be implemented.

How the above purposes were achieved constitutes the basis for the remainder of this paper.

7. DATA COLLECTION

The contractor located a Campbell Scientific data logger on each crane. Construction data were collected electronically and transmitted in ASCII format for easy file transfer. Information was collected from a variety of electronic sensors mounted in several locations on various components of the construction equipment. These monitored: amperage output to the vibroflot; water line pressure and volume; the weight of placed material; and, probe depth [Gularte, F. B., 1993]. The sampling rate for these instruments was programmed for every 2 seconds. This interval was governed by the capability of the data logger, and other instrument constraints. The data provided by the contractor consisted of contract specified parameters documenting individual column construction. The contractor successfully obtained

electronic information for over 2,400 stone columns, representing well over 80 percent of the stone columns built. Each raw data file contained over 4,000 lines of information, on the average. Over 1.2 gigabytes of information were collected and transferred to government construction and design personnel by the contractor.

At the end of each working day, memory modules from the data loggers were down loaded to a computer for initial processing and review by contractor personal. The down loaded raw data files were stored on floppy disk and given to government field personnel. In addition to electronic data, for each column the contractor also supplied hard copy Lotus 1-2-3 plots of estimated column diameter, amperage, probe tip depth versus time and manual log sheets documenting similar data, Figure 7. Overall, the data obtained using these sensors formed the basis for evaluating individual columns, forecasting secondary and tertiary pass treatment efforts, and locating post-treatment investigations.

The design team primarily used the sensor data that directly monitored the column construction effort, (i.e., initial insertion of the probe, time, depth of probe, and amperage). The additional information provided by the contractor, including weight of placed material, estimates of column diameter, and measurements of air and water pressures, were not used in the computer data base to directly assess work effort. However, detailed inspection of total stone take was performed as necessary to provide a general indicator of overall treatment effort, and to delineate when some fine grained areas had been treated to the greatest extent practicable with the adopted procedures and equipment.

Reclamation field personnel transmitted the electronic data to the Reclamation Denver Office for analysis. The method of transfer was FTP protocol via the Reclamation WAN. Data were subsequently stored and processed using a HP 9000 computer and Techbase software [MINEsoft, Ltd. 1994] to reduce, analyze, and present the data. This results were returned by WAN to the Government field office using WordPerfect files, or by hard copy using Fax machines. Turnaround time was normally within 24 hours. The field production rate for individual columns was about 1.8 hrs/column, including downtime for repairs and maintenance.

8. ANALYSIS OF COLLECTED DATA

As data were initially collected and evaluated, it became apparent that time, depth and amperage data would be the most useful for further analysis, as they represented the effort expended and reflected changes in required construction effort due to material types or density improvements.

Each data file was sorted and grouped according to its Approval Area and column type (primary, secondary, and tertiary). Each area was divided into nine sub-areas representing approximately the same number of columns. Specific information detailing individual column location (station and offset) was entered into a database. Once the column data were organized by Approval Area and sub-areas, computer programs were developed and used to extract data for use. The process involved identifying the time when the probe was first inserted into the ground for each column, and correlating construction time, current (amperage), and depth values. Every line of data supplied by the contractor was reviewed and pertinent information extracted from each file for further evaluation.

To provide for a rational and consistent interpretation of information, definitions were developed for significant parameters as follows:

Working Depth. This term was defined as the location of the probe tip, and was evaluated by examining the position of the probe to determine if it moved in relation to its previous recorded value. If the probe had moved a minimum of 0.06 m from the previously recorded position, the new position was counted as a valid working depth. The 0.06 m was selected as the best indication that the probe was moving, as values less than that fell within the error of the recording system.

Working Amperages: Working amperage values were established from a range of the amperages recorded, Figure 7, and were evaluated by monitoring the values of amperages applied to the vibrator for the probe system. If the recorded amperage lay within a specified range it was counted as a valid working amperage. Based on site experience, valid working amperages were considered to be within a range of 175 to 300. Values below 175 were an indication that the vibrator was on, but not working the column or surrounding soil. Values above 300 were considered as anomalous spikes.

Working Time: Working time, or column construction time, was defined by the following conditions occurring during the construction of the stone column:

1) The amperage recorded must fall within the working amperage range between 175 and 300 amps, and/or,

2) The depth recorded at the probe must have changed a minimum of 0.06 m from the previous recorded value (working depth).

When either of these conditions were met, the time increment was then considered a valid working time. By using these parameters to define valid working time, unnecessary analysis of data collected during idle or down time was eliminated.

As construction proceeded, the definition of column construction time was further refined to help evaluate the effectiveness of treatment as follows:

Total time - The total time in minutes the contractor spent on a specific stone column including down and idle (non-working) times.

Working time above 9.1 m - The working time in minutes the contractor spent constructing a column above 9.1 m. This depth was selected because it represented the mid depth of the stone columns, and roughly delineated different material zones. Down and idle (non-working) times were not counted.

Normalized time above 9.1 m - The time above 9.1 m divided by 9.1 m. This represents the normalized time in the units of minutes per 0.3 m.

Normalized time below 9.1 m - The working time minus the time above 9.1 m divided by the depth of the stone column below 9.1 m. This represents the normalized time in the units of minutes per 0.3 m.

These parameters were calculated from the data for each stone column. Table 1 is a typical summary table for an Approval Area with time data only. The Table summarizes the time data by sub-area, column type, and number of columns constructed within the sub area. This information aided in identifying anomalous areas within any given Work Area where the contractor may have encountered unusual treatment conditions and/or other procedural implementation difficulties to assist in the locating post-treatment investigations and verification of construction consistency.

Effort factor: This factor related working amperages with working time over specific depth intervals, essentially an energy flux or work effort expended. The effort factor was developed for sub-areas and column type. The depth intervals were at 1.5 m increments to the maximum depth obtained in each sub-area (i.e., 0-1.5 m, 1.5-3 m, etc., to maximum depth). This process involved summing the working time for every column group over the specific depth intervals, then finding the maximum working amperage at every depth interval within the sub-area. The maximum working amperages were then averaged over an area for the depth interval. The final step to obtain the effort factor was dividing the total working time by the average maximum working amperages per depth interval. Analysis of effort factor data was useful in assessing treatment adequacy in the finer grained soils at depth, and identifying as to whether or not enough effort had been applied to treating the intermittent SM zone in the 6.1 m to 12.2 m depth zone.

9. DATA PRESENTATION AND INTERPRETATION

Initially, amperage plots were prepared for Areas 3 and 4, Figures 8 and 9. They showed a difference between the zones, which was important because post-treatment BPT data indicated that Area 4 met design objectives for density, while Area 3 did not. Hence, it became evident that rapid assimilation and display of collected information would play a key role in verifying that the design intent of the specifications was being met. The following describes what was done to effectively evaluate and present collected data, and how it was used to support decisions regarding treatment adequacy.

9.1 Contractor Construction Mode Plots

Review of contractor provided data plots, Figure 7, indicated that the vibroflot was operating at various amperages throughout the depth of any constructed column. In particular, the bottom portion of the treatment zone and the intermittent SM zone were observed to develop much lower amperages than areas containing cleaner materials. Also observed were construction downtimes, or non-working times, of the treatment device, are shown as no amperage or depth fluctuation areas, and times when removal of the probe may have been necessary to unplug the tremie and allow continuous gravel feed. These

general observations led to the development of summary plots of maximum working amperages, as presented on Figures 8 and 9.

9.2 Maximum Working Amperages

As shown, sub-area 3C was treated to a level significantly different in terms of achieved overall amperages than those of sub-area 4A. This was typical in comparing work performed in Area 3 to that of Area 4. An arbitrary amperage level of 200 was identified for use in assessing treatment of Areas 5 - 18, to generally depict relative work effort and/or the occurrence of finer grained materials. These plots were prepared and sent to construction personnel for each of the treatment passes, primary (P), secondary (S), and Tertiary (T). The primary plots and statistics table, Table 1, were used as a general indicator of what work effort had been applied and what might be necessary in each sub-area during subsequent passes to duplicate the results of Area 4. A plot of maximum working amperages for all treatment passes were prepared for overall project documentation.

9.3 Average Maximum Amperages/Column with Depth

It became evident during construction in Areas 5 through 9 that material variability within any given approval area was greater than the sub-area divisions used to present the primary pass maximum working amperage information. Although data and observations indicated that the contractor was proceeding in as diligent and efficient a manner as practicable to treat the high fines content zone at depth, the intermittent SM zone was not receiving the work effort necessary to consistently meet design objectives. Therefore, data for each primary column was processed, as shown on Figure 10, to further enhance "real time" assessment of the primary pass information. Generally, lower amperage data were assumed to be in areas of either high fines content or where less work effort was expended by the contractor. By presenting information in this manner, it was intended to assist the contractor with optimizing work effort during the secondary pass by identifying higher fines zones and/or areas of lower work effort. A typical interpretation of this type of data is provided on Figure 11. Due to contractual limitations, Government interpretation of information in this manner was only performed as a guide for the contractor on how the data might be used to minimize the extent of tertiary treatment. However, the data was processed as described and provided to the contractor without interpretation in an effort to minimize the potential for performing unnecessary tertiary treatment at the expense of the Government.

9.4 Plan Contours of Normalized Working Effort and Effort Factor

To ensure that a consistent construction effort was being exerted within any given area, and/or to identify any anomalous materials conditions, plan drawings of contoured normalized working times were prepared, Figures 13 and 14. These drawings could be quickly evaluated for consistency of applied work effort, above or below 9.1 m, and used to assess overall treatment adequacy. Additionally, this information, along with the statistical data base provided, as in Table 1, were particularly useful when locating post-treatment BPTs so that they were representative of the work and geologic conditions within each treatment area.

Another way of analyzing data was by the computation of an effort factor and plotting it with depth for each sub-area and area, Figure 12. This method of data presentation was used primarily as an overall project documentation tool, and secondarily to confirm that the maximum practicable working effort had been applied in areas having a very high percentage of fines; specifically, for approval of treatment in Areas 9 and 18. Funding limitations prevented pursuing the effort factor analysis approach to the point of identifying what effort factor would be required to remediate different soil types. Also, uncertainties associated with the highly variable conditions at MIAD may have prevented reaching conclusive results without excessive materials exploration, sampling and testing. Evaluation of work effort data, as might be done for each individual BPT using only the data obtained from the columns immediately surrounding the test, may have provided the basis for some general conclusions of this nature.

10. CONCLUSIONS

The methods of developing and evaluating data described herein were used to support decisions of government engineers and CM personnel during the administration of the construction contract. They supplemented the usual construction inspection, monitoring and administration techniques normally used in CM, the key elements of which are interested, observant personnel, cooperative attitudes on the part of involved parties, and open communication.

From the experience gained with instrumentation data on this job we conclude:

1. That the durability and reliability of available sensors and data collection systems make it feasible to monitor and collect real-time data in a harsh construction environment.

2. Transmission of construction data files is feasible, using either hard wire systems (LAN/WAN) or modems via cellar phones.

3. The probe-tremie system used for stone column construction on this job was sensitive enough that collected data reflected material type variations and effectiveness of densification efforts with time. Care should be taken making any extrapolation of data presented herein to other jobs, because each piece of equipment may have unique operational characteristics under differing site conditions.

4. Use of expended energy parameters (amperage, time and depth) allowed a relative assessment of the spatial consistency of the treatment; provided a basis for decisions on re-treatment requirements; assisted with identifying areas where special effort may be required for secondary or tertiary treatment; and allowed reasonable judgement to be made on locating post-treatment investigations to such that they represented the majority of the construction performed.

5. The type of data collected appears to hold the promise of providing more information and understanding of stone column construction and effectiveness, and is worthy of additional research.

6. It is possible that an analysis approach using the "effort factor" might be useful at other sites to identify what effort factors are required to treat different material types by different treatment procedures. Future projects adopting this approach may realize significant cost savings.

In closing, the difficultly encountered in assessing the results of the bottom feed, wet replacement method of stone column construction, as used in the dredged materials at this site, would not have been resolved as rapidly without the data collection and evaluation effort presented. The effects of essentially "homogenizing" the finer grained portions of the foundation with gravel by implementing the adopted procedures could not have been assessed reliably without waiting for a period of time not available because of reservoir refilling and safety considerations. The use of these data and procedures significantly contributed to carrying construction to completion by allowing for procedures to be varied and evaluated in a timely manner, and as necessary to meet design objectives. Additionally, post-treatment testing would have been performed at locations selected on an intuitive basis, and knowledge of spatial variability would have been much less complete.

11. ACKNOWLEDGEMENTS

The team work and spirit of cooperation demonstrated by the many people involved in this job, government, contractor and consultants, made it a challenging and rewarding project.

In particular, recognition is due the system programmers of the Reclamation Structural Behavior and Instrumentation Group, Lee Jacobs, Larry Gilchrist, and Jerry Baab, who diligently worked on developing the programs to analyze and present the data within the limited time available.

Rick Jones, Resident Construction Engineer; Dorothy Frawley, Civil/Geotechnical Engineer; Jimmy Goodwin, Civil Engineer; all from Reclamation's Mid-Pacific Region, and Matt Allen, Civil/Geotechnical Engineer for USACE Sacramento District, are due special recognition for coordinating design and field efforts, and working closely with the contractor, to make the smooth transmittal and evaluation of data possible.

12. REFERENCES

1. Bureau of Reclamation, (1993),"Modifications - Phase II Mormon Island Auxiliary Dam, Folsom Unit - American River Division - Central Valley Project CA", Solicitation No. 3-SI-20-02490, Sacramento CA.

2. Gularte, F. B., (1993), "Letter to Bureau of Reclamation, Subject: One Day Experience and Equipment Submittal, Modification, Phase II, Mormon Island Auxiliary Dam, Folsom CA," Hayward Baker, Inc., Santa Paula CA, June 18.

3. Hynes-Griffin, M.E., (1987), "Seismic Stability Evaluation of Folsom Dam and Reservoir Project, Report 1: Summary Report," Technical Report GL-87-14, U.S. Army Engineer, Waterways Experiment Station, Vicksburg, Mississippi.

4. Hynes-Griffin, M.E., Wahl, R.E., Donaghe, R.T. and Tsuchida, T., (1988), "Seismic Stability

Evaluation of Folsom Dam and Reservoir Project, Report 4: Mormon Island Auxiliary Dam - Phase I," Technical Report GL-87-14, U.S. Army Engineer, Waterways Experiment Station, Vicksburg, Mississippi.

5. Ledbetter, R.H., Finn, W.D. Liam, Nickell, J.S., Wahl, R.E. and Hynes, M.E., 1991, "Liquefaction Induced Behavior and Remediation for Mormon Island Auxiliary Dam," Proceedings from the International Workshop on Remedial Treatment for Liquefiable Soils, U.S. and Japan Panel on Wind and Seismic Effects, Tsukuba, Science City, Japan.

6. MINEsoft, Ltd., "TECHBASE Reference Manual, Version 2.30," vol. 1, Lakewood CO, 1994.

7. Nickell, J.S., Allen, M.G., and Ledbetter, R.H. (1994) - "Seismic Remediation For Liquefiable Gravels: Mormon Island Auxiliary Dam and Others in North California," Proceedings Fourth U.S. - Japan Workshop on Soil Liquefaction: Remedial Treatment of Potentially Liquefiable Soils, Public Works Research Institute, Ministry of Construction, Tsukuba City, Japan.

8. Stevens, M.G., Dise, K., and VonThun, J.L., (1994), "Dynamic Compaction to Remediate Liquefiable Embankment Foundation Soils," Proceedings, Fourth U.S. - Japan Workshop on Soil Liquefaction: Remedial Treatment of Potentially Liquefiable Soils, Public Works Research Institute, Ministry of Construction, Tsukuba City, Japan.

9. Wahl, R.E., Crawforth, S.G., Hynes, M.E., Comes, G.D., and Yule, D.E. (1992). "Seismic Stability Evaluation of Folsom Dam and Reservoir Project, Report 8: Mormon Island Auxiliary Dam - Phase II," Technical Report GL-87-14, U.S. Army Engineer, Waterways Experiment Station, Vicksburg, Mississippi.

Table 1. Typical Working Time Summary of an Approval Area
Mormon Island Stone Column Construction

Approval Area	Type	Working Time	Total Time	Time Above 9.1 meters	Columns in Area
4A		48.0(864.8)	138.3(2489.0)	21.3(383.1)	18
	Pri.	52.9(634.5)	162.8(1953.0)	23.5(281.8)	12
	Sec.	38.4(230.3)	89.3(536.0)	16.9(101.3)	6
4B		60.0(1381.0)	138.5(318S.1)	23.7(544.0)	23
	Pri.	63.7(955.9)	134.9(2023.1)	23.9(358.3)	15
	Sec.	53.1(425.1)	145.2(1162.0)	23.2(185.7)	8
4C		52.0(935.8)	115.8(2085.1)	18.3(328.7)	18
	Pri.	51.9(623.0)	121.5(1458.3)	18.7(224.1)	12
	Sec.	52.1(312.8)	104.5(626.8)	17.4(104.6)	6
4D		52.3(888.7)	127.4(2166.5)	22.9(389.5)	17
	Pri.	58.5(643.8)	129.5(1424.4)	24.9(273.6)	11
	Sec.	40.8(244.9)	123.7(742.1)	19.3(115.9)	6
4E		61.2(1346.1)	124.5(2738.0)	24.3(535.3)	22
	Pri.	70.5(987.6)	138.2()935.2)	26.9(377.0)	14
	Sec.	44.8(358.5)	100.3(802.8)	19.8(158.3)	8
4F		54.8(932.0)	122.9(2089.1)	20.7(351.9)	17
	Pri.	61.4(675.5)	131.5(1446.4)	21.3(233.9)	11
	Sec.	42.8(256.5)	107.1(642.7)	19.7(118.0)	6
4G		50.8(913.7)	115.6(2080.0)	19.7(354.2)	18
	Pri.	54.1(649.0)	120.3(1443.0)	21.4(257.1)	12
	Sec.	44.1(264.7)	106.2(637.0)	16.2(97.1)	6
4H		54.9(1263.0)	114.0(2623.0)	19.6(450.1)	23
	Pri.	57.0(854.5)	114.9(1722.8)	17.6(264.3)	15
	Sec.	51.1(408.5)	112.5(900.2)	23.2(185.8)	8
4I		56.4(1015.4)	113.0(2033.9)	17.8(320.6)	18
	Pri.	62.0(743.4)	118.4(1420.5)	18.4(220.6)	12
	Sec.	45.3(272.0)	102.2(613.4)	16.7(100.0)	6
Totals For Approval Area 4					
		53.3(7245.7)	122.0(16587.5)	20.6(2802.5)	136
	Pri.	58.8(4472.4)	130.6(9924.5)	21.5(1635.8)	76
	Sec.	46.2(2773.3)	111.1(6663.0)	19.4(1166.7)	60

Numbers in parenthesis represent the total sum (in minutes). Numbers to the left of the parenthesis represent the average.

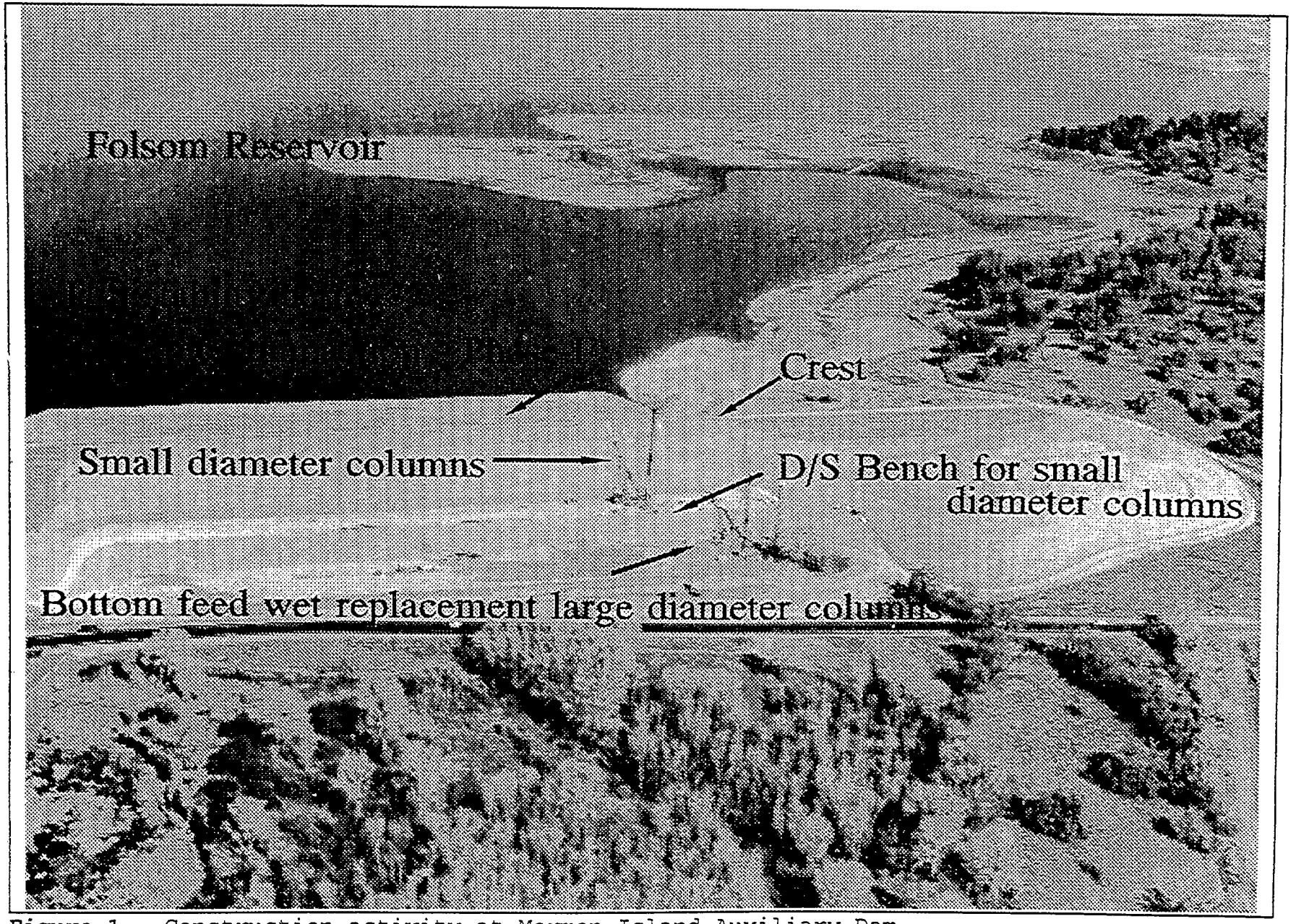


Figure 1 - Construction activity at Mormon Island Auxiliary Dam.

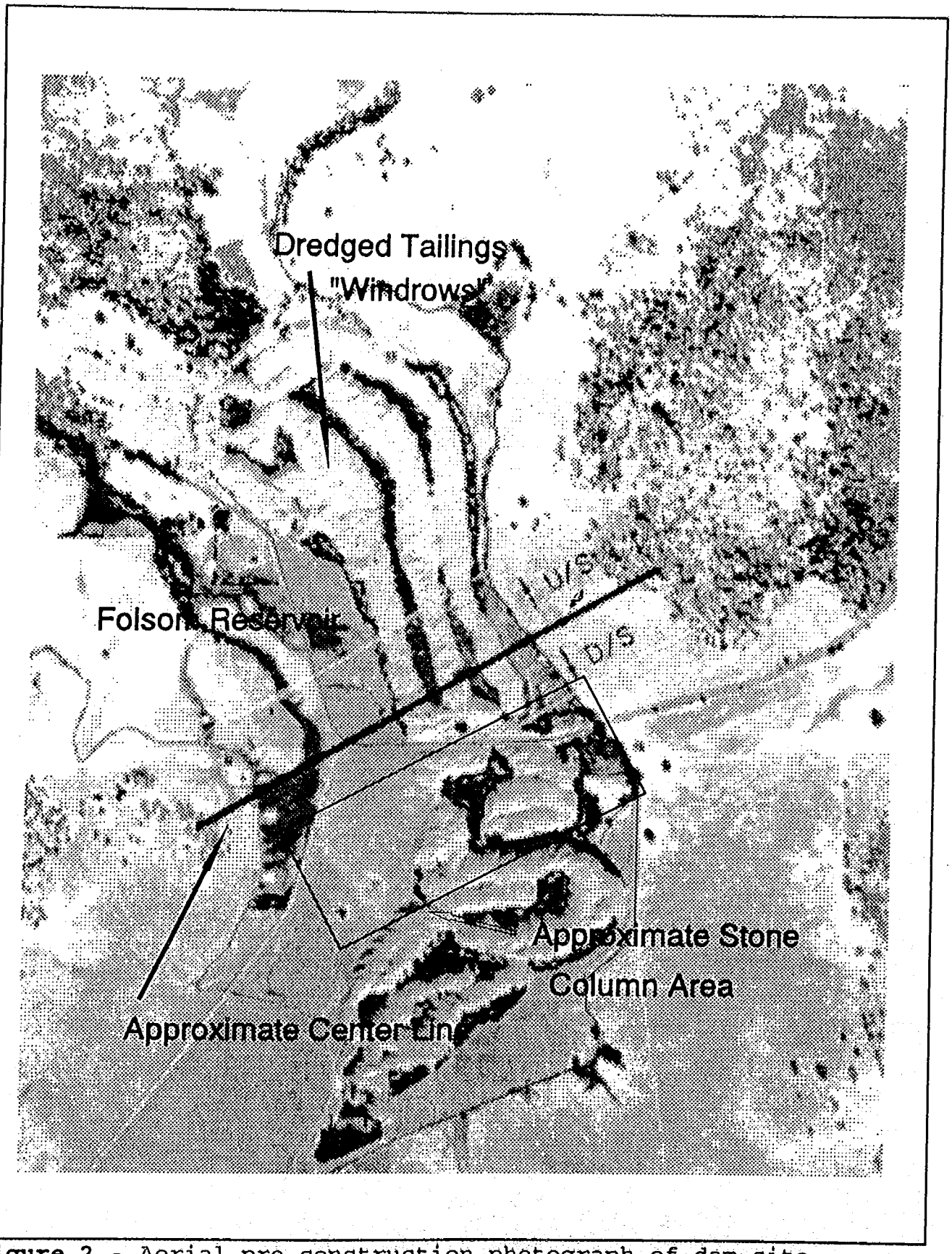


Figure 2 - Aerial pre-construction photograph of dam site.

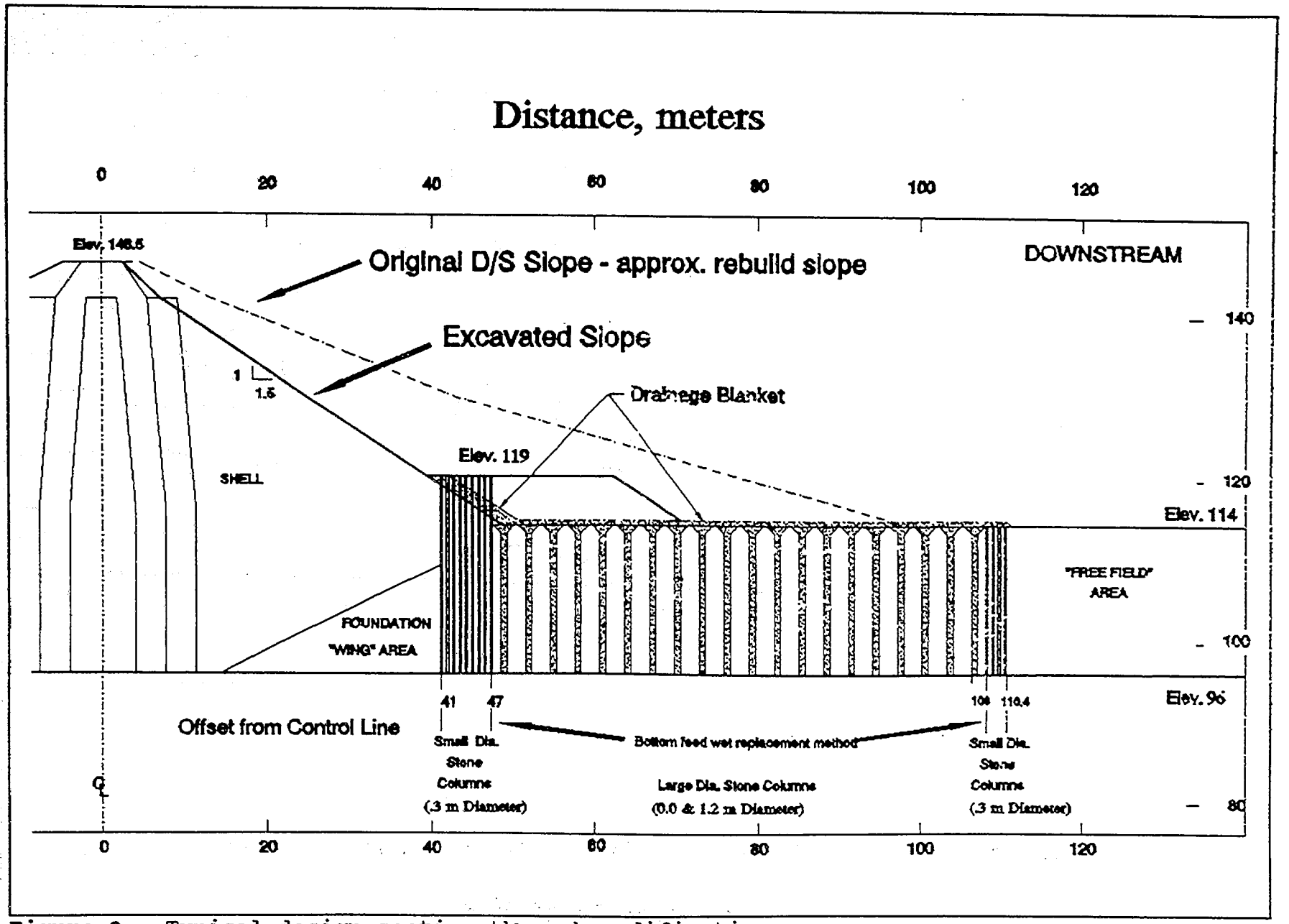


Figure 3 - Typical design section through modification area.

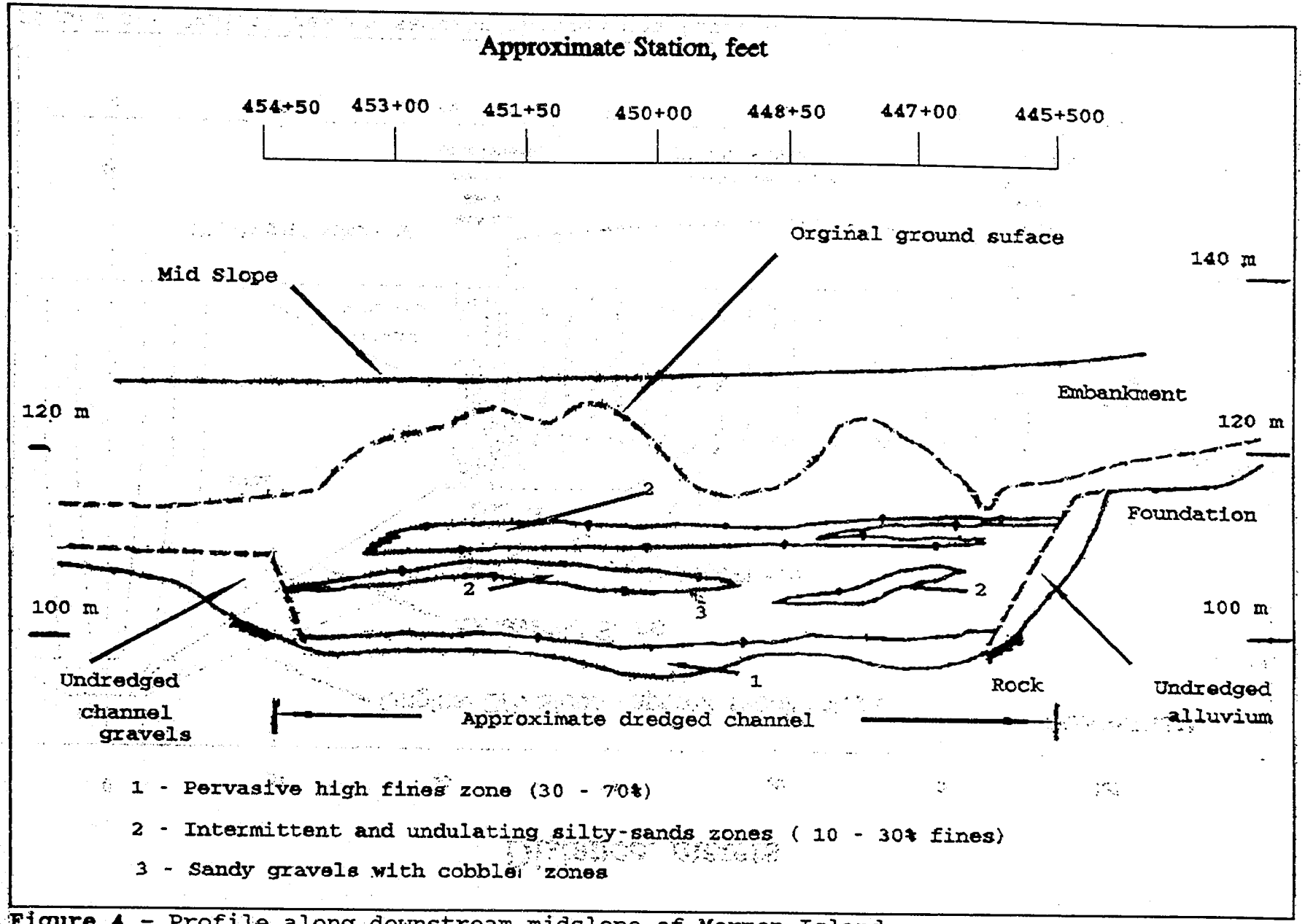


Figure 4 - Profile along downstream midslope of Mormon Island Auxiliary Dam.

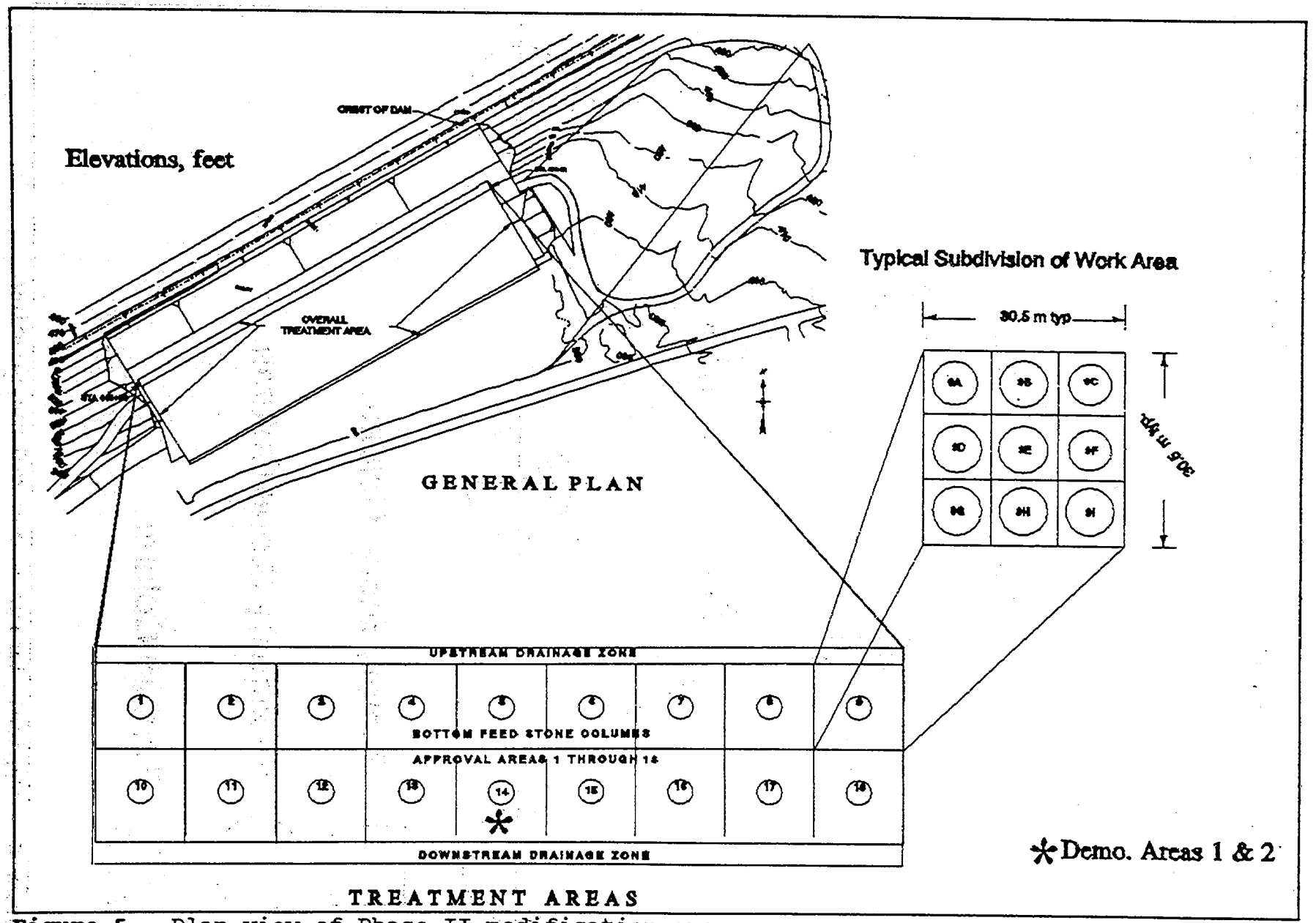


Figure 5 - Plan view of Phase II modification area.

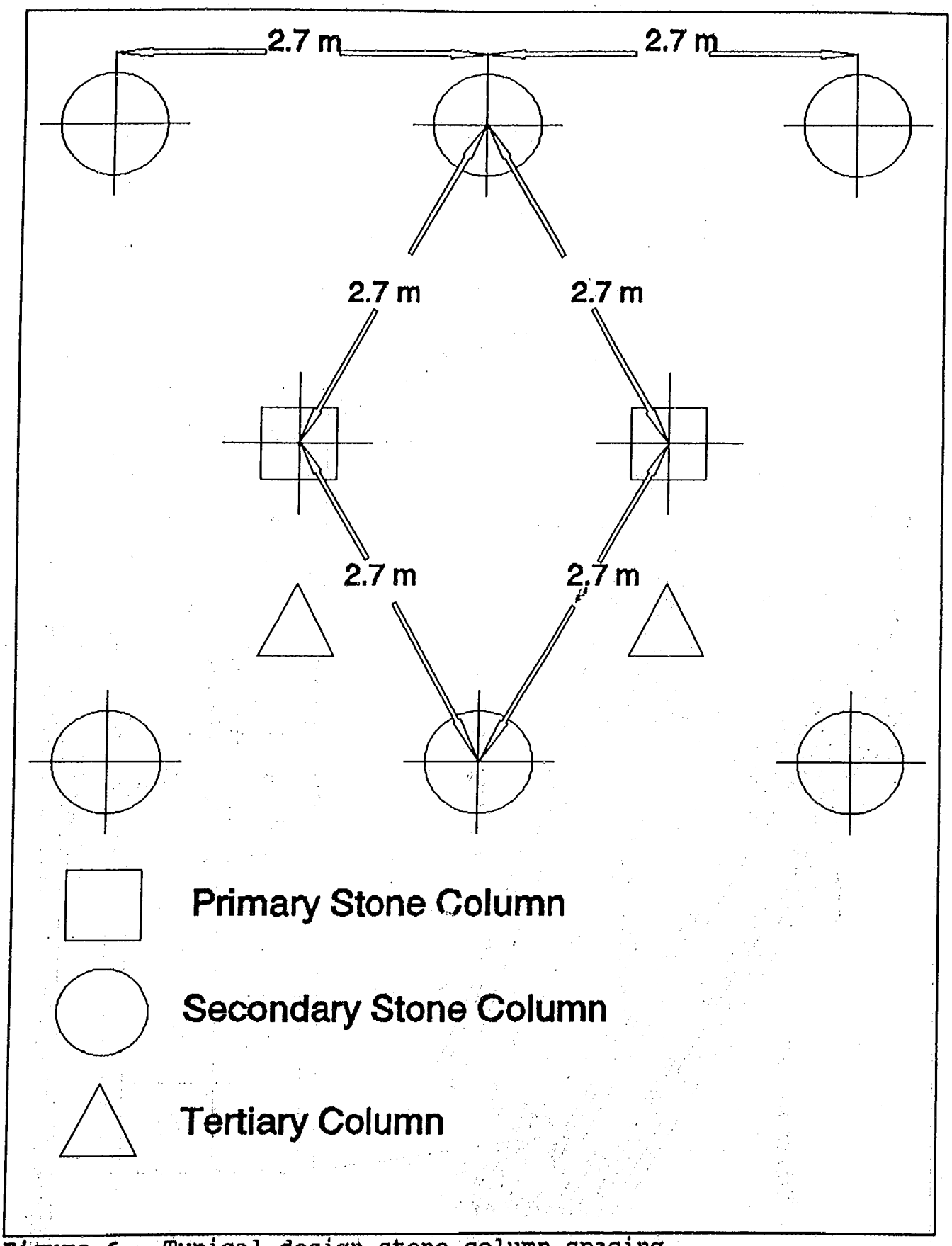


Figure 6 - Typical design stone column spacing.

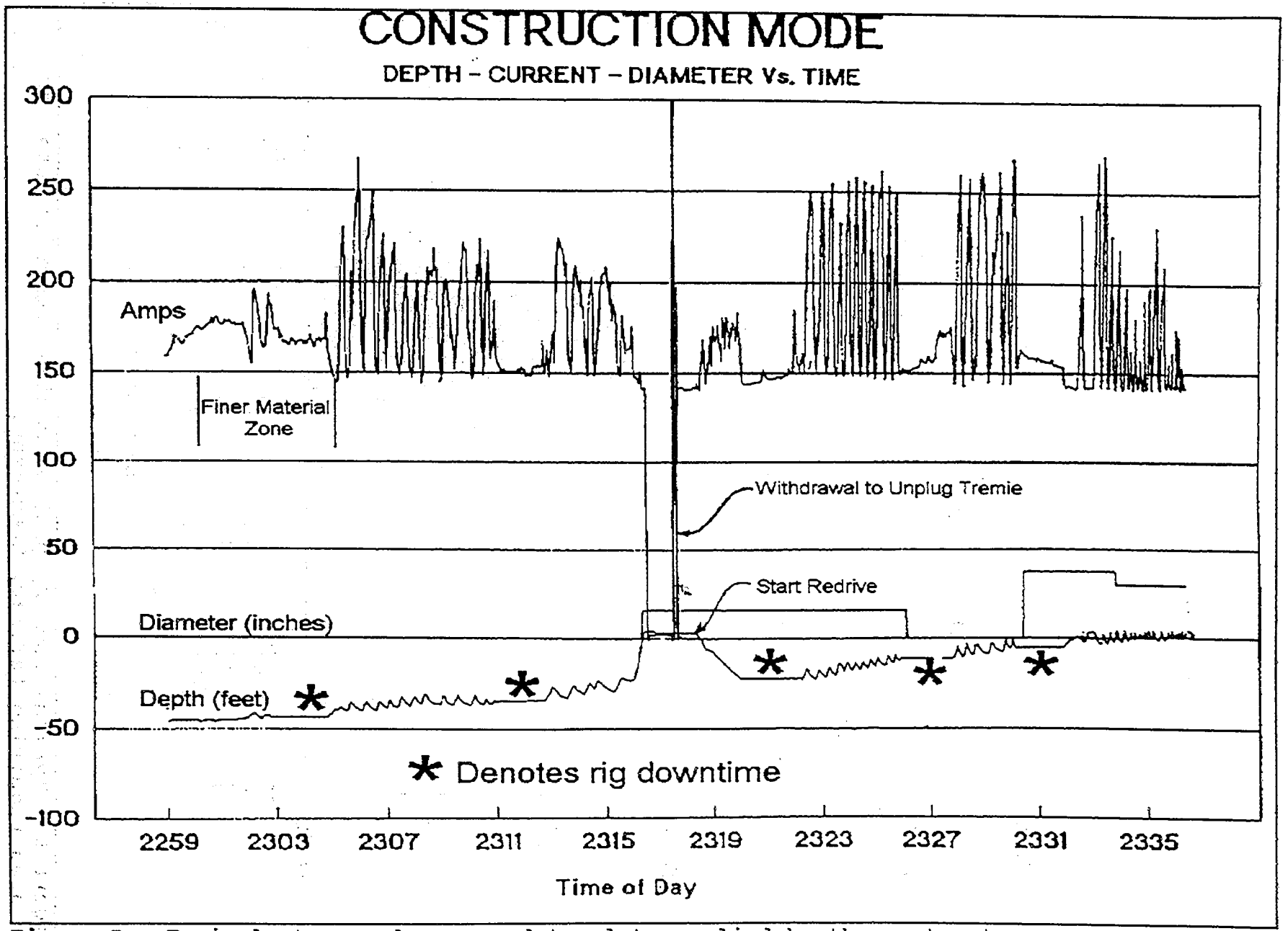


Figure 7 - Typical stone column raw data plot supplied by the contractor.

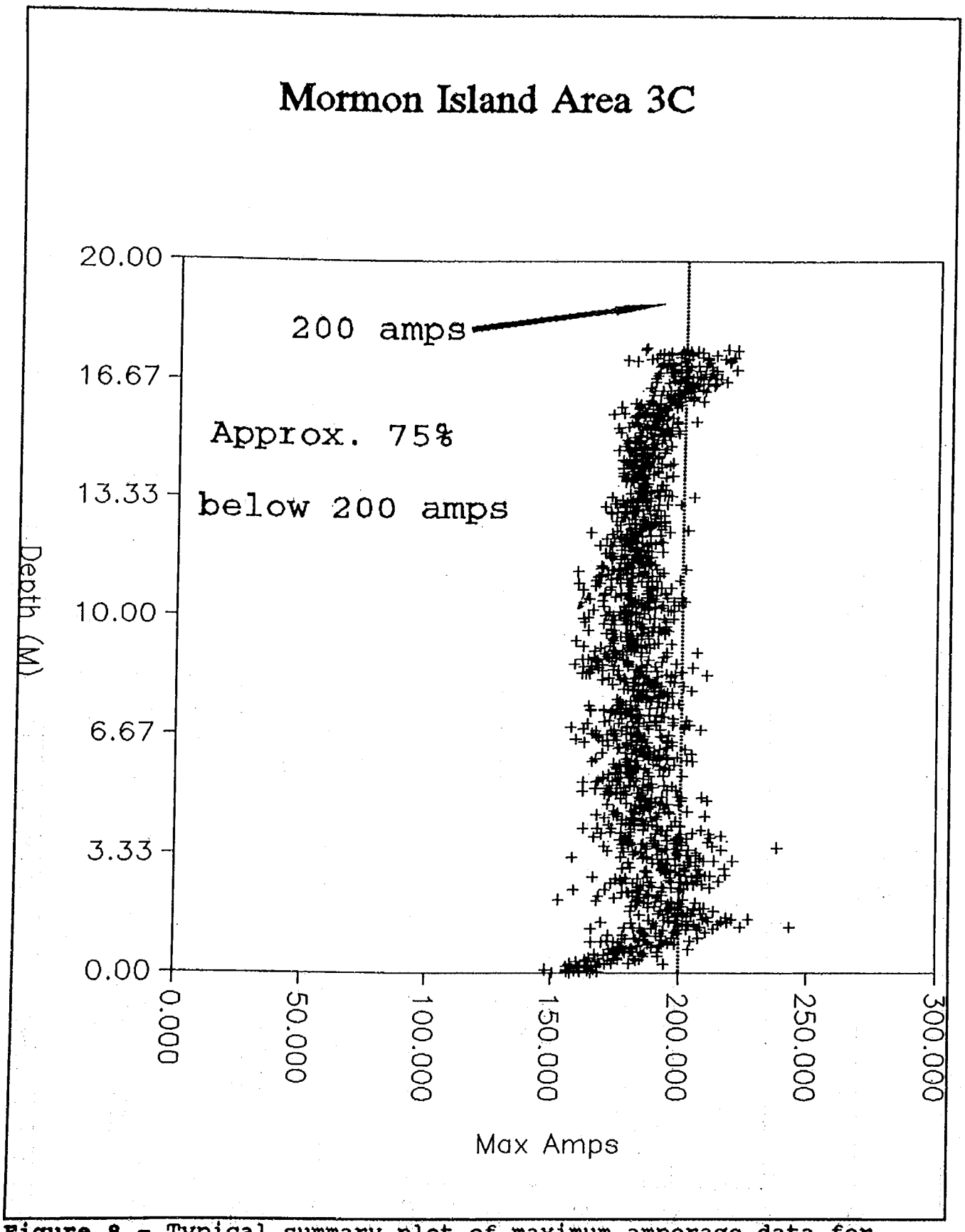


Figure 8 - Typical summary plot of maximum amperage data for an area requiring tertiary treatment.

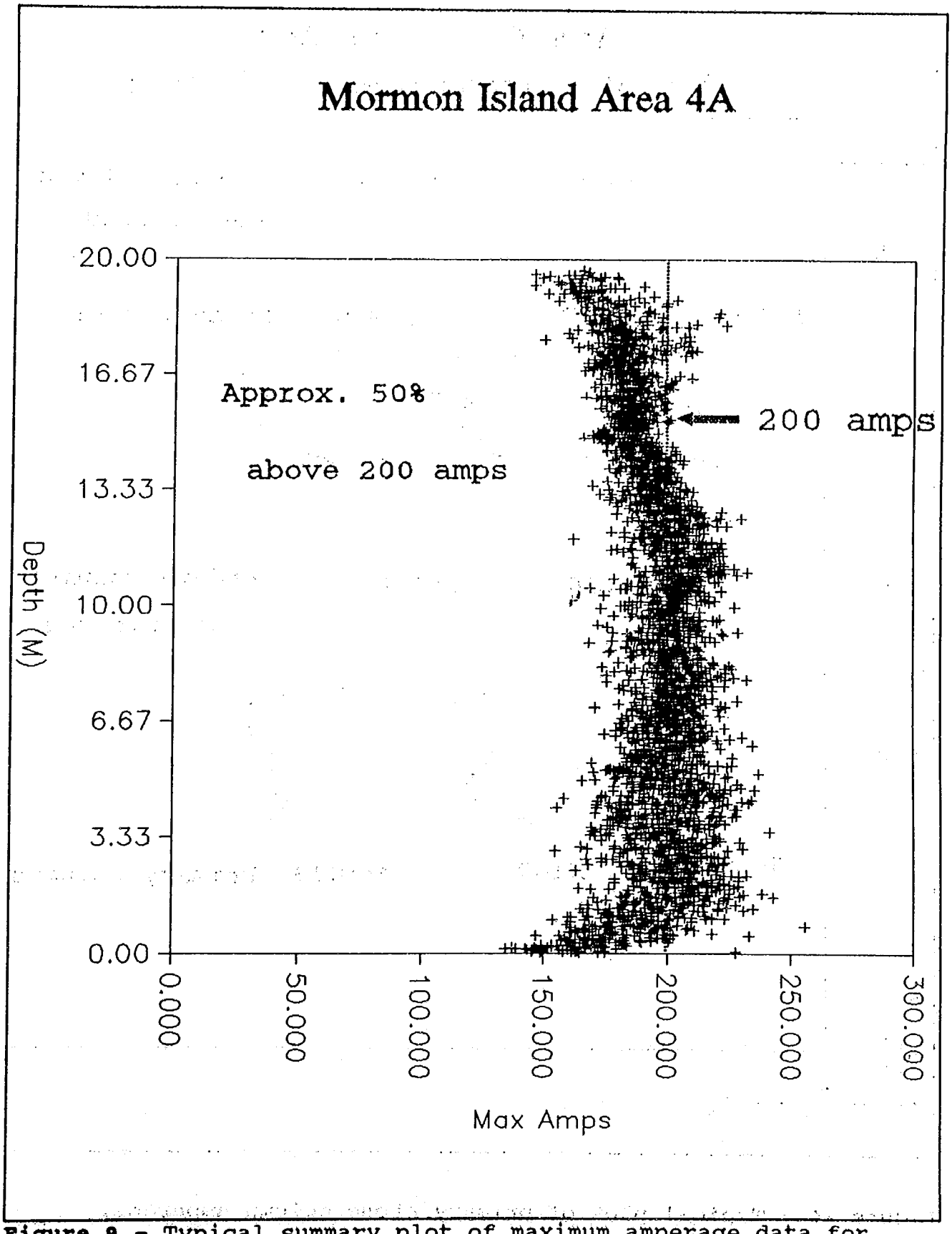


Figure 9 - Typical summary plot of maximum amperage data for an area not requiring tertiary treatment.

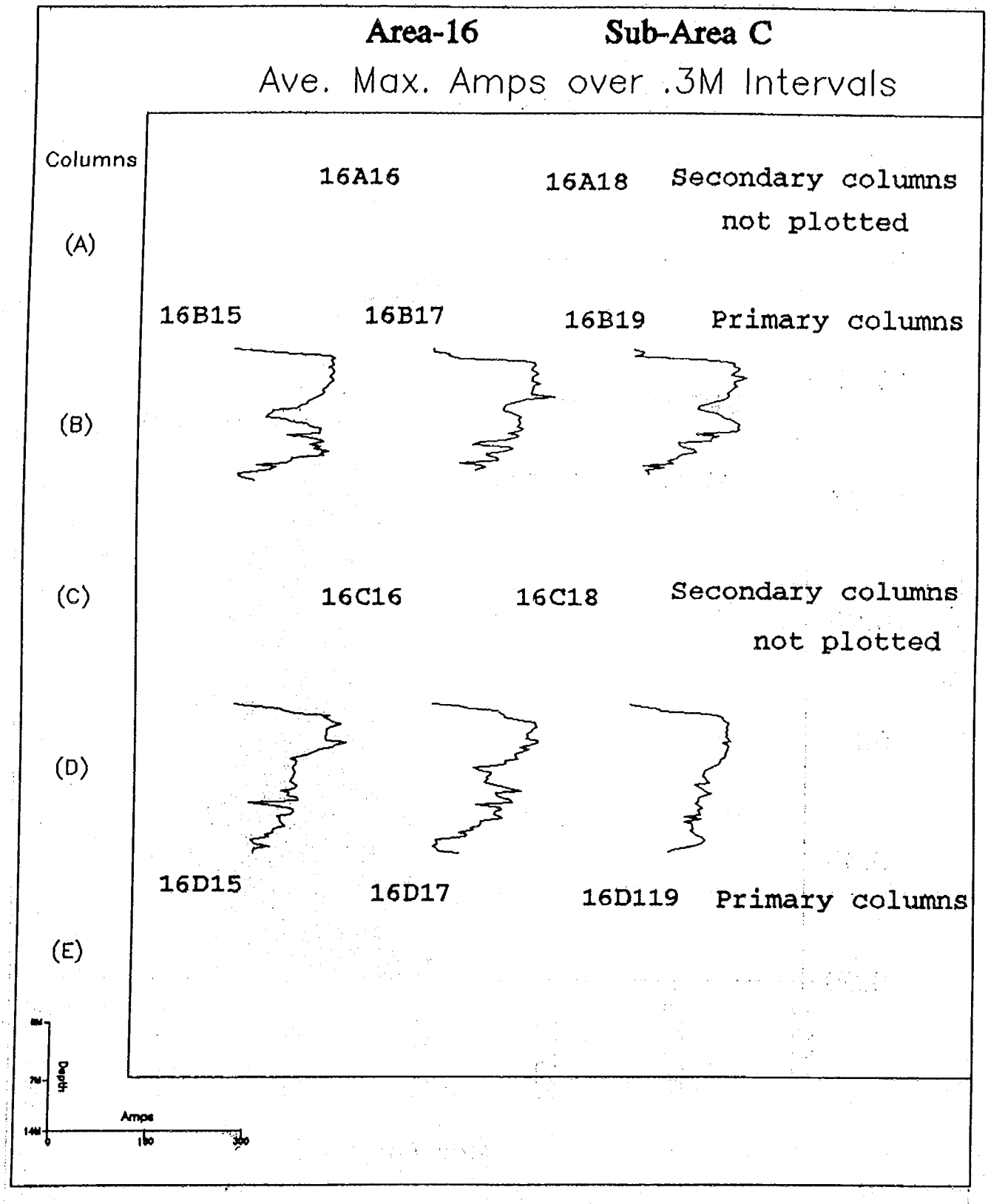


Figure 10 - Typical plot of primary stone column amperage.

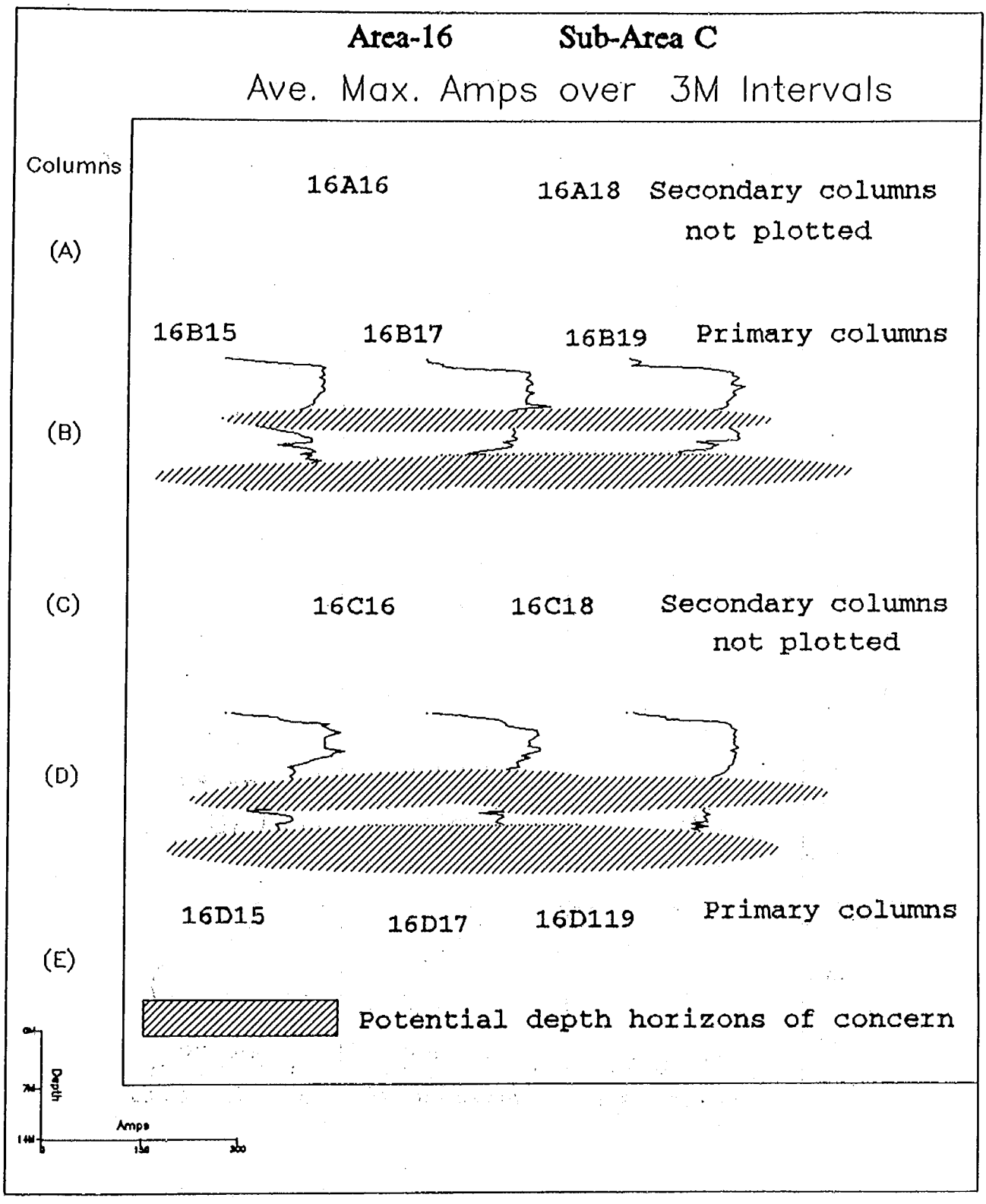


Figure 11 - Typical primary stone column amperage with depth plots identifying areas of concerns.

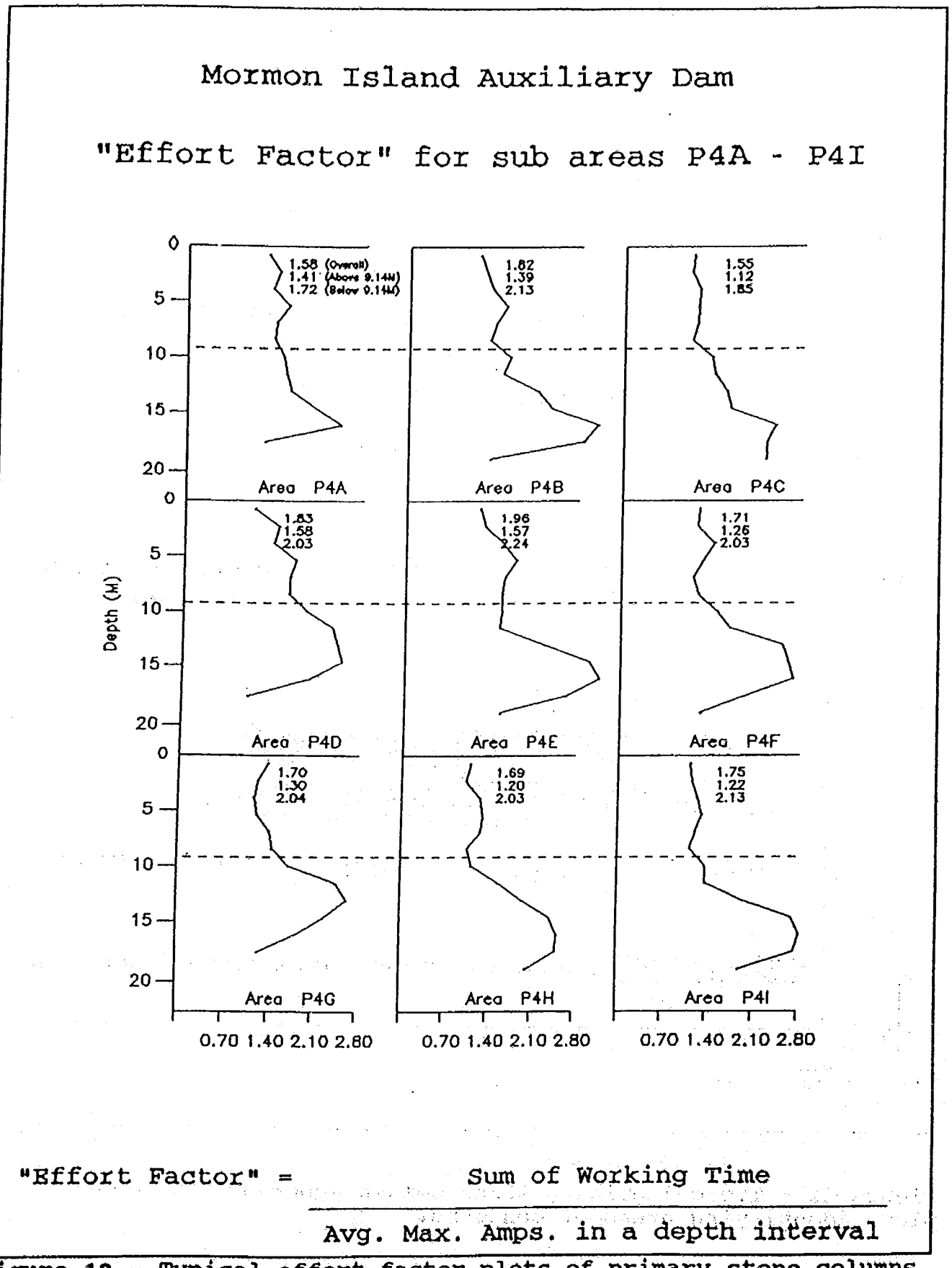


Figure 12 - Typical effort factor plots of primary stone columns.

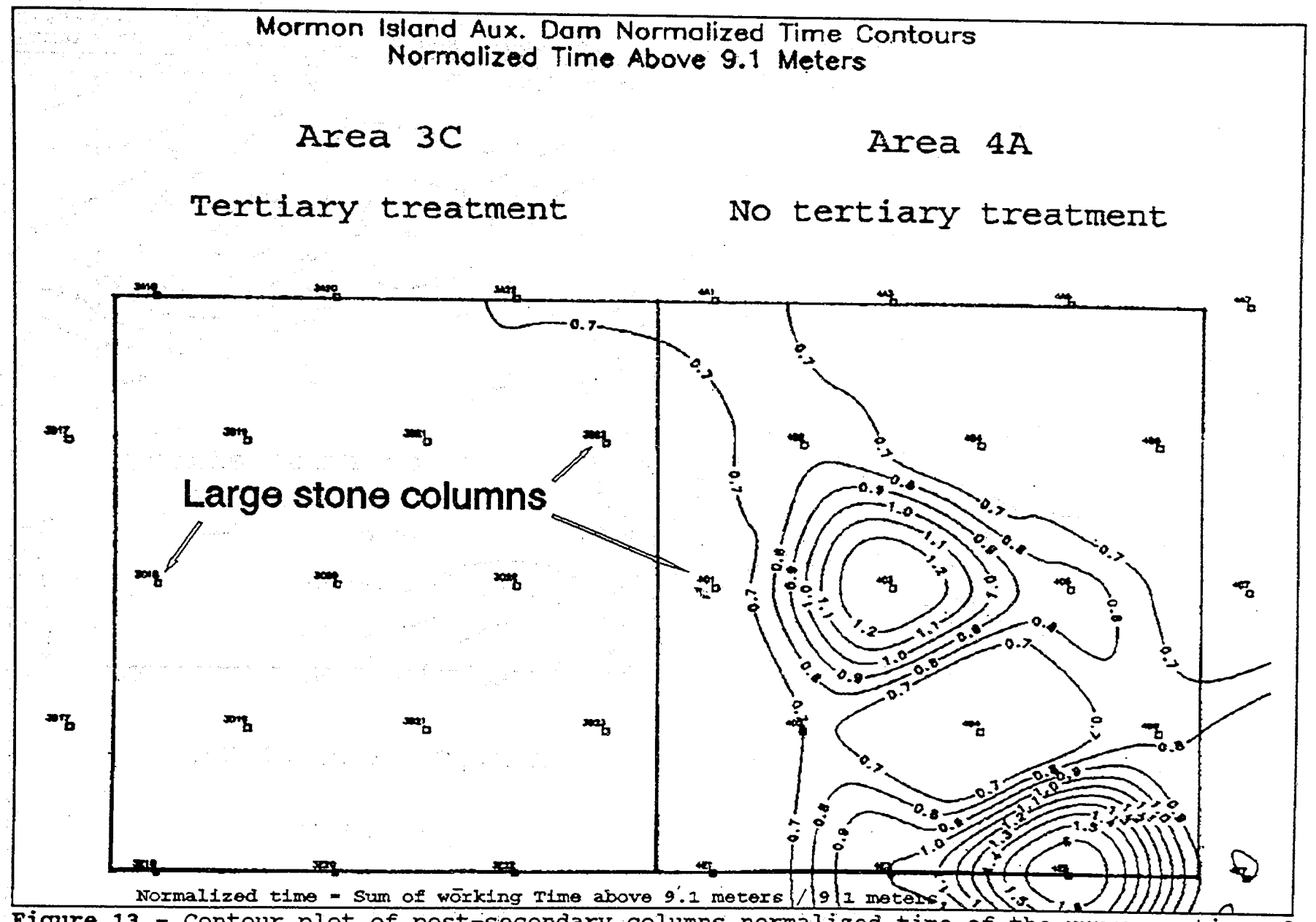


Figure 13 - Contour plot of post-secondary columns normalized time of the upper portion of adjacent areas.

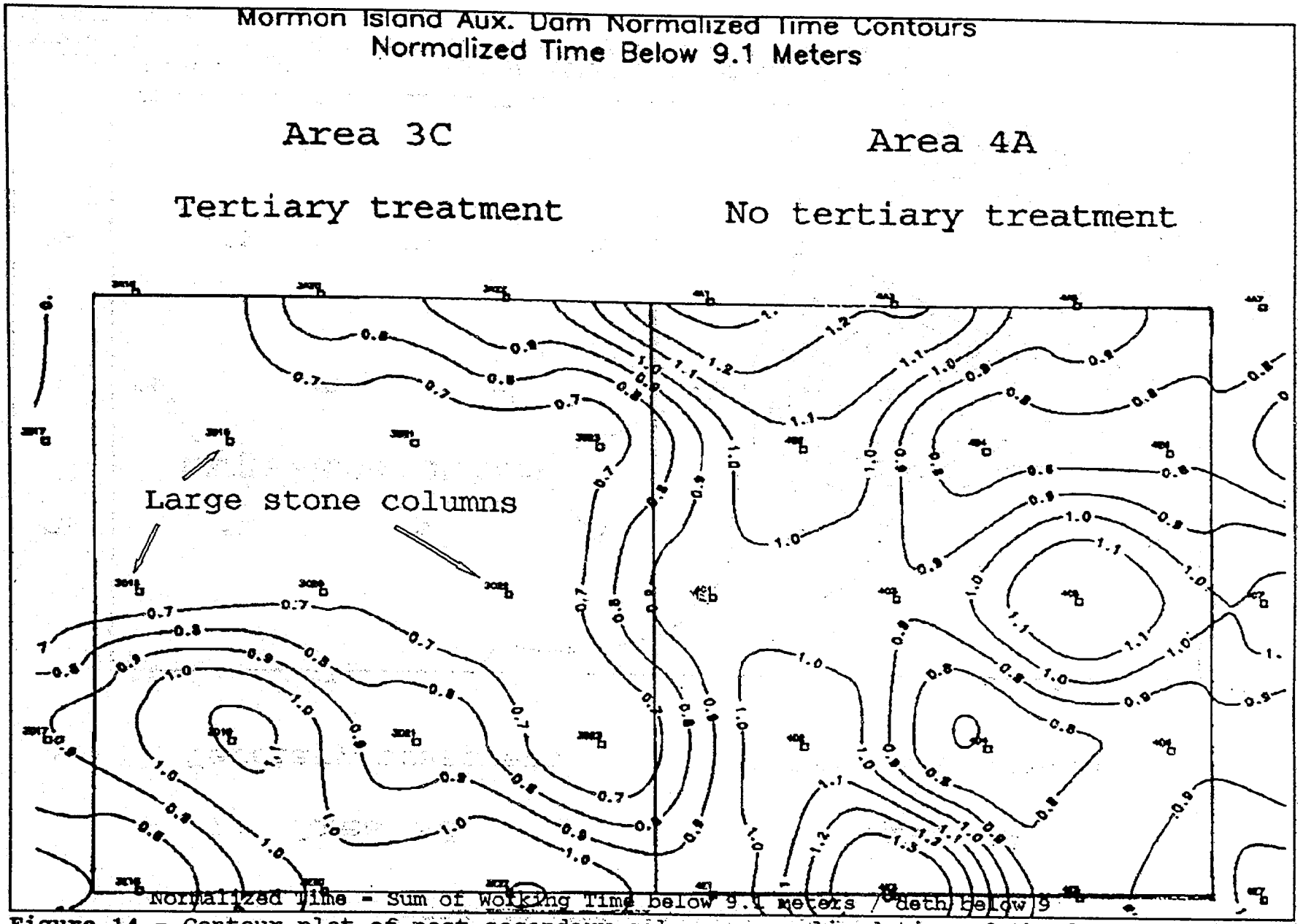


Figure 14 - Contour plot of post-secondary columns normalized time of the lower portion of adjacent areas.

NEW DEVELOPMENTS IN CIVIL INFRASTRUCTURE SYSTEMS

by

K. P. Chong and S. C. Liu
National Science Foundation

ABSTRACT

Solutions to problems in our Civil Infrastructure Systems (CIS) are likely to involve social, economic, environmental, legal, and political issues, as well as technical ones. Some reasons for this are obvious: high and uncertain direct costs; the disruption and costs to neighborhoods and business while work takes places; the impact of completed projects (e.g., a freeway) on familiar environments and valued lifestyles; and the effects on the natural environment. Technology should be better targeted to address these concerns and provide positive rather than negative impacts. For example, micro-tunneling (trenchless technologies) has proven far less disruptive to communities than open excavations for installing utility lines. In this paper CIS research opportunities are described, including unsolicited proposals in four thrust areas; specific competitions on sensors; composite and hybrid structures; and systemic change in urban infrastructure.

KEYWORDS:

Civil infrastructure systems; assessment technologies; deterioration sciences; renewal engineering; institutional effectiveness; productivity; urban systems.

INTRODUCTION

Academic and industrial research in civil infrastructure systems (CIS) over the last decade have spurred numerous advances, e.g., in new materials, structural systems, automated construction, ground improvement, development of underground space, prefabricated assemblies, corrosion inhibition, opto-electronic communication, understanding of public decision, management, location and siting, and public finance. Yet much innovative research remains to be done. New discoveries in areas that cross disciplinary boundaries may offer radically different and valuable ways of improving the infrastructure and providing new infrastructure services.

Investment in civil infrastructure made by public agencies and the private sector involves a major portion of our nation's wealth. Infrastructure systems consist of the constructed physical facilities which support the day-to-day activity of our whole society, and provide the means for distribution of resources and services, for transportation of people and goods, and for communication of information. In the public works arena, these systems have evolved in a piecemeal fashion, with new extensions grafted onto existing systems, and designs often governed by expediency and low construction costs rather than true life-cycle costs. We have inherited a complex network of systems comprised of subsystems with wide variations in age and functionality. How systems interact with other systems is poorly understood. The condition of components within each infrastructure system is often poorly assessed, and maintenance has often been inadequate.

In this country, infrastructure related research has typically been pursued and funded in an

uncoordinated fashion, and few U. S. contractors or owners of infrastructure systems have made significant investment in research and development. In 1987, the Congressional Office of Technology Assessment reported that Japan outspent the U.S. on research and development for public works by a factor of 30. Europe outspent the U.S. in this area by a factor of eight. Furthermore, our civil infrastructure has not benefited much from either U. S. or foreign advances in technology. A combination of the highly competitive nature of the infrastructure construction industry, the difficulty of disseminating new technologies, negative incentives for adopting new technologies, and excessive litigation has impeded technological advances in the industry.

The U. S. has an estimated $20 trillion investment in civil infrastructure systems, including all installations that house, transport, transmit, and distribute people, goods, energy, resources, services, and information. Because of aging, overuse, exposure, misuse, mismanagement, and neglect, many of these systems are deteriorating and becoming more vulnerable to catastrophic failure particularly when earthquakes, hurricanes, and other natural hazards strike. It would be prohibitively costly and disruptive to replace these vast networks. They must instead be renewed in an intelligent manner, which includes the prudent and effective use of our economic, material, and human resources, and which focuses on optimizing the performance of both individual subsystems and of the civil infrastructure systems complex as a whole.

The National Science Foundation (NSF) has long recognized the importance of civil infrastructure to the health and sustainable development of the nation. The Foundation has consistently been the largest single funding source for academic-based civil infrastructure-related basic research in the U.S., providing approximately 70 percent of such expenditures nation-wide. NSF support has provided much of the knowledge base in engineering and science upon which technological developments have been built. Excellent fundamental contributions have been possible but much of the research has been focused on isolated components of systems, and results have often remained in an academic environment, far from application and implementation. Building on this base and consulting with representatives of industry, civil infrastructure-related professional practitioners, and owners, the Foundation in 1994 formally responded to the research community with an integrative research and education program in Civil Infrastructure Systems.

NSF will contribute to the process of intelligent renewal through the support of research focusing on the scientific, engineering, and educational developments needed to sustain civil infrastructure systems. The purpose of this research is to develop new knowledge and innovative approaches and methods through projects involving engineers, economists, and physical, mathematical, materials, and social scientists. New understanding of system performance and guidance in support of resource allocation decisions in CIS investment and management will be sought, rather than improvements in isolated civil infrastructure components. The budget for CIS research, distributed throughout the Foundation in disciplinary programs, is $54.5 million in FY 1995, an approximate $9.0 million increase over the previous fiscal year. The FY1995 CIS budget increase will be allocated to two areas: (1)

for unsolicited proposals through existing programs located in NSFEAs disciplinary research directorates, and (2) for special competitions on integrative research in three specific areas described in detail below.

In cooperation with other government agencies, NSF intends to encourage a vigorous industry-based investment in research and education which is critical to the nation's sustained progress and competitiveness in Civil Infrastructure Systems.

GOALS AND OBJECTIVES

The overall goals of the Foundation's CIS research activity are to advance knowledge and to facilitate knowledge transfer to the communities and agencies responsible for the renewal, design, construction and reconstruction, operation, and maintenance of the nation's civil infrastructure. General objectives include:

a) Expanding the science and engineering knowledge base necessary for ensuring the safety, reliability, functionality, and longevity of infrastructure systems and materials.

b) Understanding civil infrastructure behavior as individual and as interacting systems, and establishing innovative system design and performance optimization methodologies.

c) Understanding the interactions between society and infrastructure systems to determine how the economic and societal needs of communities are served and limited by civil infrastructure, and how infrastructure management interacts with the economic, social, and geographic organization of society.

d) Improving the understanding of interactions between the natural environment and the civil infrastructure, especially in high-risk sites.

e) Promoting dissemination and effective implementation of research results by encouraging active partnerships among university researchers and professional practitioners, contractors, and owners of civil infrastructure components and systems.

f) Providing leadership in the education and training of the scientific and engineering workforce of the future, in its full diversity, by introducing curriculum innovations and by involving graduate and undergraduate students in the research and design processes.

DESCRIPTION OF RESEARCH OPPORTUNITIES

(1) Unsolicited Proposal Program

Intelligent renewal of the infrastructure must begin with integrated research, cutting across traditional disciplines, that will lead to new designs, more durable materials, new integrated network systems with better controls and communications, and improved decision making and management processes. This integration must also focus on approaches for optimizing performance of interacting systems and subsystems. It is also important that this be done so as to facilitate knowledge transfer to the end-user. This integrated approach must involve, for example, the participation of social and behavioral scientists and policy makers, and the development of reliable data bases which specify all aspects of infrastructure renewal and management.

Through consultation with the relevant research and practitioner communities, NSF has identified four important infrastructure research thrust areas: deterioration science, assessment technologies, renewal engineering, and institutional effectiveness and productivity. These interdependent areas comprise the multidisciplinary research efforts needed to advance infrastructure system engineering and management. A brief description of each of the four thrust areas follows:

Deterioration Science is concerned with the mechanisms controlling how materials and systems break down and wear out during normal use and when subjected to natural and technological hazards. Research is needed to improve our understanding of deterioration processes, so that we can design, build, and maintain infrastructure systems that are more durable, safe, and environmentally sound.

Assessment Technology addresses the need to assess the condition of our CIS resources. We need to be able to determine the level of performance, operational safety, reliability, and environmental acceptability of components and systems. The ultimate objective is to develop sensing, monitoring, and controlling systems for the effective management of our infrastructure systems.

Renewal Engineering deals with the development of materials and methods to extend and enhance the useful life of civil infrastructure systems. Research should focus on new approaches for integrated planning, information management, design, construction, installation, maintenance, repair, retrofit, recycling, demolition, and disposal. The research outcome must fit the economics of real-world situations, and must consider the infrastructure lifespan in both normal and hazardous conditions.

Institutional Effectiveness and Productivity pursues effective decision making on civil infrastructure systems. New approaches are needed for decision process and optimization modeling, which involve economists, engineers, mathematical scientists, natural scientists, and social scientists. These models require both qualitative and quantitative input. The impact of civil infrastructure systems investments or regulation on national, regional, and local productivity, and on the economic and social well-being of the public also needs to be evaluated.

Unsolicited proposals will be accepted to conduct fundamental scientific and engineering research which will build upon these thrust areas to support an expanded understanding of infrastructure system design, construction, and performance, of system interactions, and of our policy for intelligent renewal decisions. Proposals involving interdisciplinary teams and investigators with complementary research strengths or facilities are particularly encouraged.

(2) Specific Competitions

(a) Sensors and Sensor Systems

This proposal competition has been established for FY 1995 only, and submission of prerequisite concept papers was required by January 17, 1995. The Sensors and Sensor Systems research initiative is jointly funded by NSF and the Electric Power Research Institute (EPRI). The research activity must be directed toward increasing fundamental knowledge of sensors and sensor systems by cross-disciplinary team efforts in the development of analytical methods and in

laboratory experiments. Proposals may deal with sensing systems, intelligent sensors, optical concepts, materials research for new sensors, adapting existing principles, fundamentally new sensor techniques, information extraction, high temperature chemistry, sensors for transmission and distribution systems, sensors for monitoring the bulk power system, and sensors for monitoring structural integrity in various components and other dispersed civil infrastructure systems, such as highway systems, towers, and liquid and fuel pipelines. Multidisciplinary proposals will receive the highest priority for support.

(b) Composite and Hybrid Structures

Proposals for research on composite and hybrid structures are supported in this program. The aim is to develop new and innovative composite structural elements and hybrid systems using advanced new materials and/or devices, and to develop practical design guidelines (for a unified code development) for typical composite and hybrid structures that are used in current practice.

Four categories of composite structural systems are considered: (1) concrete filled tubes (CFT) column systems; (2) reinforced concrete/steel reinforced concrete (RC/SRC) column systems; (3) reinforced concrete/steel reinforced concrete (RC/SRC) hybrid wall systems; and, (4) new materials, elements, and systems. Proposals may include material and component studies, subassemblage studies, complete structure studies, or design studies. Research proposals for collaboration between U. S. and investigators overseas which take advantage of important research facilities and competencies in other countries are encouraged. Active participation of practicing engineers in all phases of research work is encouraged but is not mandatory.

(c) Systemic Change in Urban Infrastructure

Civil infrastructure systems have evolved in the context of dynamic industrial, economic, and social development. The infrastructure networks are so complex that the need to assess their condition, arrest their deterioration, rebuild, or upgrade them in whole or in part presents a particularly difficult challenge. This is especially problematic in urban areas where productive work can only be done while all parts of the city's civil infrastructure are operating. With an increasing commitment to just-in-time manufacturing operations, and minimized inventory quantity and storage time, efficiency and productivity is increasingly vulnerable to any disruption of urban civil infrastructure systems.

In most of the larger cities in the U. S., traditional approaches have been used for repair, upgrading, and replacement. These approaches are becoming increasingly inappropriate for the aging and rapidly deteriorating civil infrastructure. The problems are exacerbated by the ever-present pressure to provide a short-term fix for the most urgent civil infrastructure problems in the least costly way. Such a posture toward infrastructure planning and maintenance inhibits us from achieving optimally engineered designs, cost-effectiveness, and long-term user satisfaction.

However, decision-making for infrastructure renewal and constructional use must involve the public, and must respond to political realities. In addition, the legal and regulatory environments must be considered in

developing responsive solutions. Many government agencies (federal, state, and local) are involved in civil infrastructure design standards, safety requirements, construction practice, and retrofit and renewal. Thus, public policy issues must be better understood in order to successfully implement innovation in the replacement or renewal of civil infrastructure systems. The importance of public policy issues is addressed in the NSF workshop report "A Public Infrastructure Research Agenda for the Social, Behavioral, and Economic Sciences," available through the CIS Management Team. What is needed now is a new approach that can enable cities to transcend existing local political, fiscal, and environmental constraints, and to identify possibilities for revolutionary advances in civil infrastructure systems. The cities would reap benefits from this approach in the long term. While each city often assumes that its civil infrastructure problems are unique, problems can often be generalized and fundamental understanding can be developed which is pertinent to many locations. Research has produced a wealth of knowledge that is broadly applicable, including not just scientific and engineering advances, but social, behavioral, and economic understanding as well. In order to develop a plan for intelligent renewal, an effective methodology must be developed which converts new and existing scientific, economic, and social knowledge into a framework for life-cycle infrastructure system engineering and management.

Research proposed under the Systemic Change in Urban Infrastructure announcement should develop innovative, interdisciplinary approaches to achieve improved design or redesign, management, and optimized or adaptive performance of the nation's infrastructure systems. Participation of owners, contractors, professional practitioners, and government agencies on research teams is necessary to maintain focus and accelerate the knowledge transfer process, and proposed research must include interactive partnerships between academe and non-academic organizations.

The goal of this research competition is to bring university researchers, infrastructure owners, private industry, and local, state and federal agencies and governments together to plan a strategy for intelligent civil infrastructure renewal and future civil infrastructure development in U. S. cities. It is also essential that the CIS research will provide for training of the technological workforce of the future by involving graduate and undergraduate students in the research process. NSF will fund research and education efforts to stimulate interactions among these stakeholders by promoting and motivating research that will generate future innovations to address the long-term needs, and to build productive sustained partnerships among the city, other federal and state agencies, and industry that will allow implementation of the city's plan.

Proposals are solicited to conduct team research. The proposed research must include the following features:

(1) A cross-disciplinary endeavor addressing the four major CIS research thrust areas of Deterioration Science, Assessment Technologies, Renewal Engineering, and Institutional Effectiveness and Productivity;

(2) A true collaboration among universities, owners, industry, and government (particularly at state and local levels);

(3) A systems integration perspective;

(4) Involvement of both undergraduate and graduate students; and,

(5) An integrated implementation approach to public policy formulation in a politicized environment, including the perspectives of engineers as well as public citizens, owners, and government agencies, and which is contextual to local or regional socio-economic development.

Finally, the intelligent renewal of U. S. infrastructure requires that NSF-sponsored research include, as an integral component, a commitment to work toward a well-educated and diverse workforce which can manage civil infrastructure-related issues in technical, socio-economic, and political arenas. Research proposers are encouraged to include a statement of plans to include under-represented groups as active participants in the research.

CONCLUSIONS

An overview and rationale of the civil infrastructure systems initiative and research opportunities are presented. Authors hope that this paper will act as a catalyst to stimulate innovative research in CIS.

ACKNOWLEDGMENTS AND DISCLAIMER

The authors would like to acknowledge the input from their colleagues and the research community. Views expressed are not necessary those of the NSF.

BIBLIOGRAPHY

NSF 94-91, "Guide to Programs, FY 1995", pp. 5-7.

NSF 93-5, "Civil Infrastructure Systems Research: Strategic Issues".

NSF 94-129, update of "Civil Infrastructure Systems Research: Strategic Issues".

Bordogna, J., "Civil Infrastructure Systems: Ensuring their Civility", Viewpoint, J. of Infrastructure Systems, ASCE, Vol. 1, No. 1, pp.3-5.

Lemer, A. C., Chong, K. P., and Tumay, M. T., "Research as a Means for Improving Infrastructure", J. of Infrastructure Systems, ASCE, Vol. 1, No. 1, pp.6-15.

DEVELOPMENT OF HYBRID SEISMIC RESPONSE CONTROL OF BRIDGES

by

Kazuhiko KAWASHIMA [1], Hisanori OTSUKA [2], Shigeki UNJOH [3] and Hidetoshi MUKAI [4]

ABSTRACT

This paper presents a variable damper using Electro-Rheological (ER) fluid. Two types of experimental model of the variable damper using ER fluid were developed, and thier performance was studied through dynamic loading tests. This paper also briefly summarizes U.S.-Japan cooperative research program on hybrid control of seismic response of bridge structures. In this program, comprehensive research including active and passive control technology have been conducted to develop effective and practical hybrid control technology. Finally, a plan for new research program on development of intelligent seismic structures is described.

Key Words : Seismic Response Control, Bridges, Hybrid Control, Variable Damper, Electro-Rheological Fluid, ER Damper, Variable Stiffness Control, Intelligent Materials

1. INTRODUCTION

Variable damper, in which the damping coefficient is variable dependent on structural response, for structural response control against an earthquake was proposed by the authors in 1989 (Kawashima and Unjoh 1989, Taguchi et al 1990), and various studies have been made at the Public Works Research Institute (Kawashima et al 1991A, 1991B, 1992A, 1992B, 1993, 1994A, 1994D). The effective control algorithm of the variable damper was studied through analytical approach and the effectiveness of the variable damper to control structural response against an earthquake was verified through a series dynamic loading tests and shake table tests of a model bridge.

Electro-Rheological (ER) fluid is an innovative material which has a potential application for a wide range of engineering fields. The viscosity of ER fluid is variable depending on applied electric field strength. Because reliable ER fluid with high applicability for a practical use is recently being developed, various application has been initiated especially in precision mechinery systems (Sasada et al 1975A, Sasada et al 1975B, Ushijima et al 1988, Duclos 1988, Ehrgott and Masri 1992).

The variable damper using ER fluid has several advantages in which the damping characteristics is variable within a quick response (on the order of millseconds) to applied electric field and the mechanical system of the damper can be simplified without complicated valve

1) Professor, Department of Civil Engineering, Tokyo Institute of Technology, O-okayama, Meguro-ku, Tokyo, 152 Japan (Former Research Coordinator for Geospace Use, Planning and Research Administration Department, Public Works Research Institute, Ministry of Construction)
2) Head, Earthquake Engineering Division, Earthquake Disaster Prevention Department, Public Works Research Institute, Ministry of Construction, Tsukuba Science City, 305 Japan
3) Senior Research Engineer, ditto
4) O-taki Dam Construction Office, Kinki Construction Bureau, Ministry of Construction (Former Assistant Research Engineer, ditto)

units. Since the practical application for the structural control is expected, the authors have been studied the applicability of ER fluid for variable dampers (Kawashima et al 1994C).

This paper presents the variable damper using ER fluid. Two types of variable damper using ER fluid were developed and thier performance was studied through dynamic loading tests. This paper also briefly summarizes U.S.-Japan cooperative research program on hybrid control of seismic response of bridge structures. In this program, comprehensive research including active and passive control technology have been conducted to develop effective and practical hybrid control technology. Finally, a plan for new research program on development of intelligent seismic structures is described.

2. DEVELOPMENT OF VARIABLE DAMPER USING ER FLUID

Two types of variable damper using ER fluid (refers as ERVD in the following) as shown in **Fig.1** were developed. They include a cylinder/piston type and a rotation type. The cylinder/piston type ERVD was firstly developed. Based on the dynamic loading tests of an experimental model of the cylinder /piston type ERVD, which will be described later, when the loading velocity exceeds a certain level the damping force developed by fluid viscosity becomes predominant. Therefore, the damping force developed by ER effects is relatively small and the variable range of the damping force is not wide enough to apply for structural control. Based on this experience, therefore, a rotation type ERVD was newly developed in order to improve the variable range of the damping force by ER effects. The rotation type was selected because the area required to develop the designed damping force by ER effects is easily secured and it has the potential applicability to increase the variable range of the damping force by elongating an arm length which connects the damper with a structure, and by adding and integlating several rotation ERVDs as shown in **Fig.1(c)**.

3. DESIGN OF ERVDs

3.1 Cylinder/Piston Type ERVD

The damping force of a cylinder/piston type ERVD with an orifice as shown in **Fig.1(a)** may be given as the sum of the damping force developed by fluid viscosity and ER effects. They may be written as

$$F = F_v + F_\varepsilon \tag{1}$$

$$F_v = \frac{12 \cdot L \cdot A^2 \cdot v}{B \cdot H^3} \eta \tag{2}$$

$$F_\varepsilon = \frac{3 \cdot L \cdot A}{H} \tau_y(E) \tag{3}$$

where,

F : damping force developed by a cylinder/piston type ERVD

F_v :damping force developed by fluid viscosity through an orifice

F_ε : damping force developed by ER effects

A : pressure area of a piston

v : velocity of a piston

L, B, H : length, width and distance of electrodes

η : viscosity of ER fluid

$\tau_y(E)$: shear stress developed by ER effects

E : applied electric field strength

Fig.2 shows an illustration of load-displacement relation by Eq.(1) for a steady state constant displacement loading. The damping force developed by ER effects is frequency independent while the damping force developed by fluid viscosity is frequency dependent. It should be noted in Eq.(3) that only F_ε is variable by controlling the applied electric field strength. Since the shear stress developed by ER effects may be a function of the applied electric field strength between the electrodes, it may be written as

$$\tau_y(E) = \alpha \cdot E^{\beta} \quad (4)$$

where

α , β : coefficients dependent on ER material

According to the dynamic loading tests for ERVD develped, which will be described later, they are written as

$$\alpha = 2.06 \times 10^{-4}$$
$$\beta = 1.7 \quad (5)$$

3.2 Rotation Type ERVD

In a similar way to the cylinder/piston type ERVD, the damping torque of the rotation type ERVD as shown in **Fig.1(b)** may be given as the sum of the damping torque developed by fluid viscosity and ER effects. They may be written as

$$T = T_V + T_\varepsilon \quad (6)$$

$$T_V = \frac{\pi \cdot \omega}{2h} \eta \cdot (R_2^4 - R_1^4) \quad (7)$$

$$T_\varepsilon = R_m \cdot S \cdot \tau_y(E) \quad (8)$$

$$R_m = \frac{2(R_2^3 - R_1^3)}{3(R_2^2 - R_1^2)} \quad (9)$$

where,

T : damping torque developed by a rotation type ERVD

T_V : damping torque developed by fluid viscosity

T_ε : damping torque developed by ER effects

ω : loading frequency of a rotation axis

R_1 , R_2 : outer and inner diameters of a circular electrode

h : distance between electrodes

S : total area of electrodes

The damping torque developed by fluid viscosity is dependent on the loading frequency of a rotation axis and it is changable by a distance between the electrodes. On the other hand, the damping torque developed by ER effects is independent on the loading frequency and loading displacement (rotational angle) and is controlled only by the applied electric field strength.

According to the dynamic loading tests for ERVD developed, the coefficients dependent on ER materials defined in Eq.(4) is written as

$$\alpha = 2.82 \times 10^{-3}$$
$$\beta = 1.6 \quad (10)$$

4. EXPERIMENTAL MODELS OF ERVD AND THIER PERFORMANCE

4.1 Cylinder/Piston Type ERVD

An experimental model of a cylinder/piston type ERVD is developed as shown in **Photo 1** and **Fig.3**. It was designed so that the maximum damping force developed by ER effects and the maximum stroke of the piston be 200N and ± 40mm, respectively. The length of the damper is 521mm, and the length and width of an orifice (electrodes) are 134mm and 3mm, respectively. Pressure area of the piston is 2,089mm^2 . Rubber sleeve is used to enclose the ER fluid. Colloidal solution which includes silicon oil with mixing carbon powder is used as the ER fluid. The initial viscosity of the ER fluid is 0.13Pa•s, and the shear stress at 2kV/mm is 670Pa. The voltage applied between the electrodes is controlled within the range from DC 0kV to 6kV.

The performance of the experimental model of ERVD was studied through dynamic loading tests. Tests were made for the purpose to investigate the displacement, velocity and electric field strength dependency of the damping force. An actuator was attached to the piston and the model was loaded under displacement control.

Fig.4 shows the force vs. displacement hysteresis loops. With the loading displacement being ± 20mm, the loading frequency was varied from 0.5 to 10 Hz. It is seen from **Fig.4(a)** that when the loading velocity was low the rectangular shaped hysteresis loops, which represent a typical friction type hysteresis loop, were obtained. There is a static friction of about 100N between the piston and the cylinder. The damping force increases as increase of the loading velocity, and the shape of hysteresis

loops is gradually changing to an oval shape, which represent a typical damping force developed by the fuild viscosity. It is also seen in Fig.4(a) that there is a phase lag. This may be caused by the compressibility of ER fluid used and deformation of the rubber sleeve. Fig.4(c) shows the hysteresis loops at the applied voltage of 6kV. The damping force increases with increase of applied voltage when the loading frequency is low. However, the damping force by fluid viscosity becomes predominant with increase of the loading frequency.

Fig.5 shows the voltage vs. the damping force relation. The damping force at zero voltage represents the damping force developed by fluid viscosity. The damping force increases as the voltage increases due to ER effects. When the loading frequency is 0.5Hz, the damping force is variable within the range from 100N to 300N. However, as the loading frequency increases the damping force by fluid vioscosity becomes predmonant, therefore the variable range bvecomes smaller.

Fig.6 shows the comparison between the measured and the computed damping forces. The damping force was computed according to Eq.(1), in which the material coefficients to estimate the shear stress developed by ER effects was obtained as Eq.(5). Good agreement was found between the measured and computed damping force. However, the damping force due to ER effects is much smaller than the damping force due to fluid viscosity. An improvement for making ER effects larger is required.

4.2 Rotation Type ERVD

To improve performance of the cylinder/piston type ERVD, an experimental model of a rotation type ERVD was newly developed as shown in Photo 2 and Fig.7. It was designed so that the maximum damping torque developd by ER effects be 500N•cm. The diameter and the thickness of the rotation chamber are 234mm and 76mm, respectively. Outer diameter and inner one of the circular electrode as shown in Photo 3 are 9cm and 3.7cm, respectively. The total area and the distance of the electrodes are 422.9cm ^{2} and 2mm, respectively. The same ER fluid was used as one for the cylinder/piston type ERVD. The measured initial viscosity of the ER fluid is 0.15Pa•s, and the shear stress at 2kV/mm is 660Pa.

The performance of the rotation type ERVD model was also studied through dynamic loading tests. A DC motor was attached to the rotational axis of ERVD and the ERVD was loaded by constant rotation under frequency control as shown in Photo 4.

Figs.8 and 9 show the damping torque developed when the applied voltages are 0kV and 6kV. The loading frequency are assumed as 10rpm, 50rpm, and 100rpm. When the loading frequency is 50rpm and the applied voltagte is 0kV, the damping torque is 12.8N•cm which may be the sum of a friction force and damping force developed by fluid viscosity. When the applied voltage is increased to 6kV, the damping torque is 445N•cm and the increase from the 12.8N•cm is developed by ER effects. The damping torque develped is found to be constant and stable against the loading cycles.

Fig.10 shows the damping torque vs. loading freqeucny relation. The damping torque is almost independent on the loading freqeuncy and the damping torque developed by fluid viscosity is about 20N•cm in the range of the loading frequency from 10rpm to 100rpm.

Fig.11 shows the damping torque vs. applied voltage relation. The computed damping force by Eq.(6) is also shown in the figure. Good agreement was found between the measured and computed damping torque. The damping torque of the model is variable by the applied voltage in the range from 10N•cm to 500N•cm as designed.

5. SUMMARY OF U.S-JAPAN COOPERATIVE RESEARCH PROGRAM ON HYBRID CONTROL

Hybrid control is defined as a combined

approach of active and passive control. Although the active control is an attractive approach, energy required to supply for controlling the seismic response of bridge structures within a desirable level is generally excessive. This obstacle seems quite difficult to solve with use of the current existing technology, in particular in Japan where occurrence of an earthquake with magnitude over 8 has to be taken into account in seismic design.

Based on such considerations, the hybrid control seems more superior than the active control for aiming to reduce structural response of bridges during a significant earthquake. Therefore, research program on hybrid control of seimsic response of bridges was initiated at the Public Works Research Institute from April 1990 as U.S.-Japan cooperative research program through the activities of the Panel on Wind and Seismic Effects, UJNR.

In this research program, comprehensive research including active and passive control technology have been made to develop the effective and practical hybrid control technology.

Effectiveness of the active mass damper to suppress seimsic respponse of bridge structures and the control algorithms were studied through analytical approach (Kawashima et al 1991A).

Variable dampers, in which the damping coefficient can be changed depending on the structural response, was studied (Kawashima et al 1991A, 1991B, 1992A, 1992B, 1993, 1994A, 1994D). The concept of the variable dampers is with the following requirements (refer to **Fig.12**):

1) Damping coefficient is very large during a small deck vibration for preventing the deck vibration due to breaking loads of vehicles and wind effects. It is movable against the low rate motions such as the elongation of deck by temperature change.
2) Against the seismic response with the deck response over a certain value, the damping coefficient is set so as to make energy dissipation maximum.
3) Against excessive deck response during an earthquake, high damping coefficient is required to function as a stopper. Smooth and gradual increase of the damping force may be effective for preventing shocks.

Although various types of the variable damper can be made, the simplest structure may be an piston-cylinder viscous damper as shown in **Fig.13**. A by-pass is installed between the chambers. Damping coefficient of the damper can be controlled by varying an amount of viscous flow of the by-pass. External energy required for such control is generally much smaller than that required for the active control.

For verifying the feasibility of the variable dampers, a prototype variable damper was developed as shown in **Photo 5** (Kawashima st al 1992B). It is a piston-cylinder type viscous damper with the maximum damping force is 200kN and the stroke is $\pm$ 13cm. For verifying the effectiveness of the variable damper, a series of dynamic loading tests and shake table tests was made as shown in **Photo 6**.

The variable stiffness control in which the instantaneous natural period of structures can be changed so that the resonance with the predominant ground motion be avoided, were also studied.

There are various methods to shift the instantaneous natural period of bridges during an earthquake such as change of flexibility of bearings and adoption of active tendons/bracings. The application of the variable dampers were proposed. The variable dampers have various advantage for controlling the instantaneous natural period of bridges because it is more stable for long term use than the active tendons/bracing systems. The energy required is also much less.

Fig.14 shows the algorithm of the variable stiffness control. The instantaneous predominant period of ground motion T^* at time t is computed by the moving window Fourier spectrum. The damping coefficient of variable dampers is varied so that the instantaneous natural period of the bridge T be shifted to prevent the resonance with the ground motion. Effectiveness of the variable stiffness control was

also studied by analytical approach (Kawashima et al 1994A, 1994B).

As discussed in the previous section, the variable damper using electro-rheological (ER) fluid was also developed, and thier performance was studied through dynamic loading tests.

Research results were exchanged through Joint Meetings of the Panel on Wind and Seismic Effects, UJNR, and the workshops sponsored by the task committee under the Panel. Also close research cooparations were successfully made between U.S. and Japan. The analyses using the same model data and the comparison between the proposed control algorithms were made (Yang et al 1994). The shake table test of sliding isolation system developed by the U.S. side was made at the shake table laboratory of the Public Works Research Institute as shown in **Photo 7** (Feng and Okamoto 1994).

6. PLAN FOR NEW RESEARCH PROGRAM ON INTELLIGENT SEISMIC STRUCTURES

Current seismic design methods are based on the strength design concept using the usual materials such as steel bars and concrete. Recently new materials such as high performance/smart/intelligent materials are being remarkably developed and the potential applicability for civil engineering structures is being investgated in various fields.

After a significant earthquake, it takes a great amount of time to investigate and assess the damage of civil strucutres and it is difficult to judge the safety of the damaged strucutres. It also takes a great amount of time and cost to repair and to strengthen the damaged structures even if the damge is not significant. Therefore, it is essential to develop the technology to precisely specify the damage degree and the structures to be easily repaired.

Based on such considerations, this program has been initiated from April 1995 for aiming to develop the intelligent seimsic structures by applying new materials. It includes the following research items :

1) Development of damage asessment technology by using self-diagnosis materials
2) Development of structural components which is easily repairable by using self-repairable materials such as shape memory alloy

7. CONCLUDING REMARKS

To study potential applicability of ER fluid for variable damper, two types of experimental models of ER damper, which included a cylinder/piston type and a rotation type, were developed. The performance were tested through the dynamic loading tests. Although the cylinder/piston type ERVD was developed as designed, it was found that the damping force developed by ER effects is smaller than the damping force developed by fluid viscosity. Thereore, it was required to improve the damping force due to ER effects large enough so that the control by ER effects can be made in a wide range of damping force.

To improve this point, the rotation type ERVD was newly developed. The rotation type was selected because the area required to develop the designed damping force by ER effects is easily secured and it has the potential applicability to increase the variable range of the damping force by elongating the arm length which connect the damper with a structure, and by adding and integlating several rotation type ERVDs. An experimental model of the rotation type ERVD showed that the variable range of the damping torque was improved and high applicability for a practical use to the variable damper was shown.

In the research program on hybrid control, the variable dampers and variable stiffness control were developed at the Public Works Research Institute. Because the variable damper

is a simple extension of the damper stopper technology which has been used in Japan for a long time, it is expected that the variable dampers be implemented in near future.

ACKNOWLEDGMENTS

The research presented herein was made as a part of the U.S.-Japan Cooperative Research Program on Hybrid Control of Seismic Response of Bridge Structures under auspices of the Panel on Wind and Seismic Effects, UJNR. The authors extend their sincere appreciation to the strong support of Dr. S. C. Liu, NSF, Dr. H. S. Lew, NIST, Mr. J. D. Cooper, FHWA, Professor M. Shinozuka, Princeton University, Professor J. N. Yang and Professor M. Feng, University of California at Irvine.

REFERENCES

1) Duclos, T., G. (1988) "Design of devices using electro rheological fluids," SAE Technical Paper No. 881134
2) Ehrgott, R., C. and Masri, S., F. (1992) "Modeling the oscillatory dynamic behavior of electro rheological materials in shear," Smart, Mater. Struct. 1
3) Feng, Q. and Shinozuka, M. (1990) "Use of a variable damper for hybrid control of bridge response under earthquake," U.S. National Workshop on Structural Control Research, University of Southern California, CA.
4) Feng, Q. and Okamoto, S. (1994) "Shaking table tests on base-isolated bridge with sliding system," 3rd U.S.-Japan Workshop on Earthquake Protective Systems for Bridges, Berkeley, CA, Technical Report NCEER-94-0009
5) Kawashima, K. and Unjoh, S. (1989) "Development of hybrid control technology," Civil Engineering Journal, Tokyo, Japan, pp.2-5, Vol.32, No.6 (in Japanese)
6) Kawashima, K., Unjoh, S., Nagashima, H. and Shimizu, H. (1991A). "Current research efforts in Japan for passive and active control of highway bridges against earthquakes," 23rd Joint Meeting, U.S.-Japan Panel on Wind and Seismic Effects, UJNR, Tsukuba, May 1991
7) Kawashima, K., Unjoh, S. and Shimizu, H. (1991B). "Earthquake response control of highway bridges by variable damper," Proc. of Colloquium on Control of Structures, Japan Society of Civil Engineers, Part. B, pp.221-224, July 1991 (in Japanese)
8) Kawashima, K., Unjoh, S. and Shimizu, H. (1992A). "Seismic response control of highway bridges by variable damper," 24th Joint Meeting, U.S.-Japan Panel on Wind and Seismic Effects, UJNR, Gaithersburg, May 1992, NIST Special Publication 843
9) Kawashima, K., Unjoh, S., Iida, H. and Mukai, H. (1992B) "Effectiveness of the variable damper for reducing seismic response of highway bridges," 2nd U.S.-Japan Workshop on Earthquake Protective Systems for Bridges, Tsukuba, Dec. 7-8, 1992, Technical Note of the Public Works Research Institute, No. 3196.
10) Kawashima, K., Unjoh, S. and Mukai, H. (1993). "Seismic response control of highway bridges by variable dampers," 25th Joint Meeting, Panel on Wind and Seismic Effects, UJNR, Tsukuba, May 1993, Technical Note of Public Works Research Institute, No.3217
11) Kawashima, K., Unjoh, S. and Mukai, H. (1994A) "Development of innovative seismic response control of bridges," 26th Joint Meeting, Panel on Wind and Seismic Effects, UJNR, Gaithersburg, May 1994, NIST Special Publication 871
12) Kawashima, K., Unjoh, S. and Mukai, H. (1994B) "Seismic response control of highway bridges by variable stiffness control," 3rd U.S.-Japan Workshop on Earthquake Protective Systems for Bridges,

Berkeley, CA, Technical Report NCEER-94-0009

13) Kawashima, K., Unjoh, S., Suzuki, S. and Endoh, S. (1994C) "Application of electro-rheological fluid for variable damper," 3rd U.S.-Japan Workshop on Earthquake Protective Systems for Bridges, Berkeley, CA, Technical Report NCEER-94-0009

14) Kawashima, K., Unjoh, S. and Mukai, H. (1994D) "Seismic response control of bridges by variable dampers," J. of Structural Engineering, Vol.120, No.9, ASCE, Sep. 1994

15) Sasada, T., Kishi, T. and Kamijo, K. (1975A) "Electro viscous effects of polymer and solid particle solutions," Proc. Japan Society of Mechanical Engineers, Vol.41, No.342

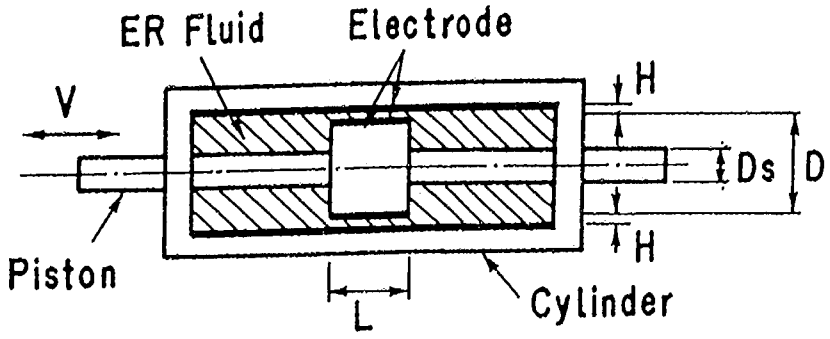
16) Sasada, T., Kamijo, K. and Kishi, T. (1975B) "Electro viscous effects of uni-phase liquid," Proc. Japan Society of Mechanical Engineers, Vol.41, No.343

17) Edited by Scott, D. and Yamagichi, J. (1983) "Solidifying fluid transforms clutches and flow valves," Automotive Engineering, Vol.91, No.11

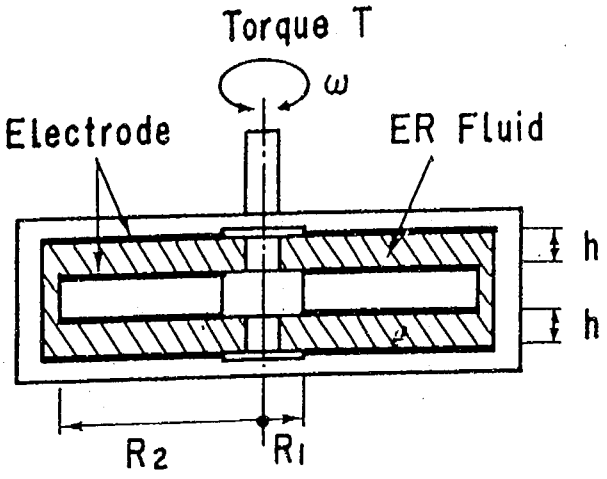
18) Taguchi, J., Iwasaki, T., Adachi, Y., Sasaki, Y. and Kawashima, K. (1990). " U.S.-Japan cooperative research program on hybrid control of seismic response of bridge structures." 22nd Joint Meeting, U.S.-Japan Panel on Wind and Seismic Effects, UJNR, Gaithersburg, Maryland, USA, May, 1990, NIST Special Publication

19) Ushijima, T, Takano, K. and Noguchi, T.(1988) "Rheological characteristics of ER fluids and their application to anti-vibration devices with control mechanism for automobiles," SAE paper No.881787

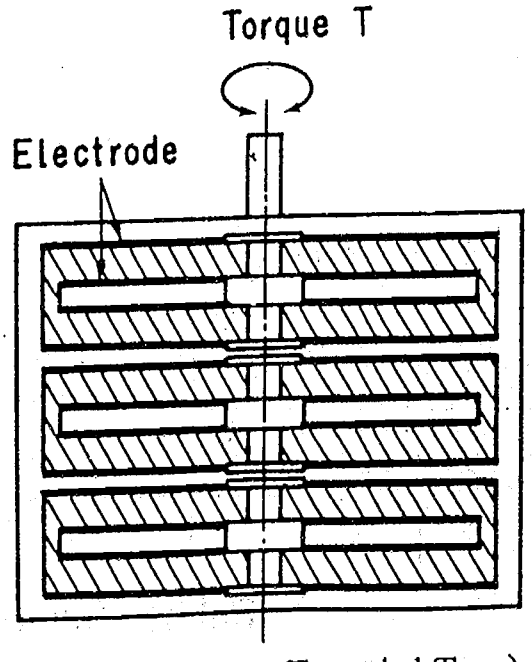
20) Yang, J. N., Li, Z., Wu, J., C., Kawashima, K. and Unjoh, S. (1994) "Hybrid protective systems for seismic-excited bridges," 3rd U.S.-Japan Workshop on Earthquake Protective Systems for Bridges, Berkeley, CA, Technical Report NCEER-94-0009



(a) Cylinder/Piston Type

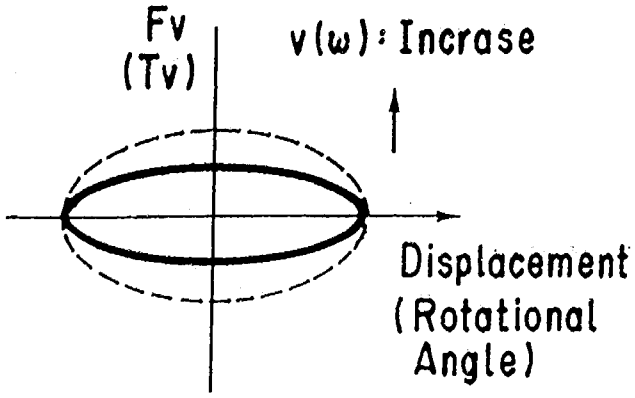


(b) Rotation Type

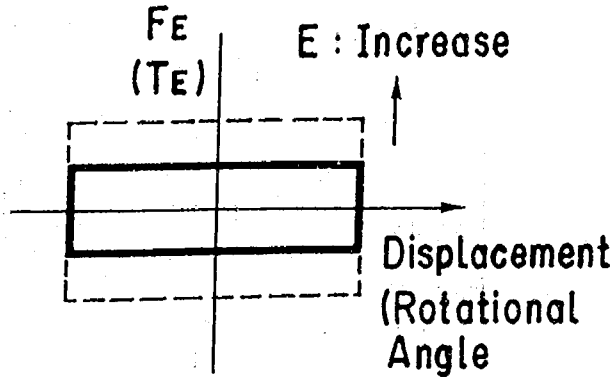


(c) Rotation Type (Extended Type)

Fig.1 Variable Damper using ER Fluid



(a) Damping Force/Torque developed by Fluid Viscosity



(b) Damping Force/Torque developed by ER Effects

Fig.2 Illustration of the Damping Force/Torque developed by ERVD

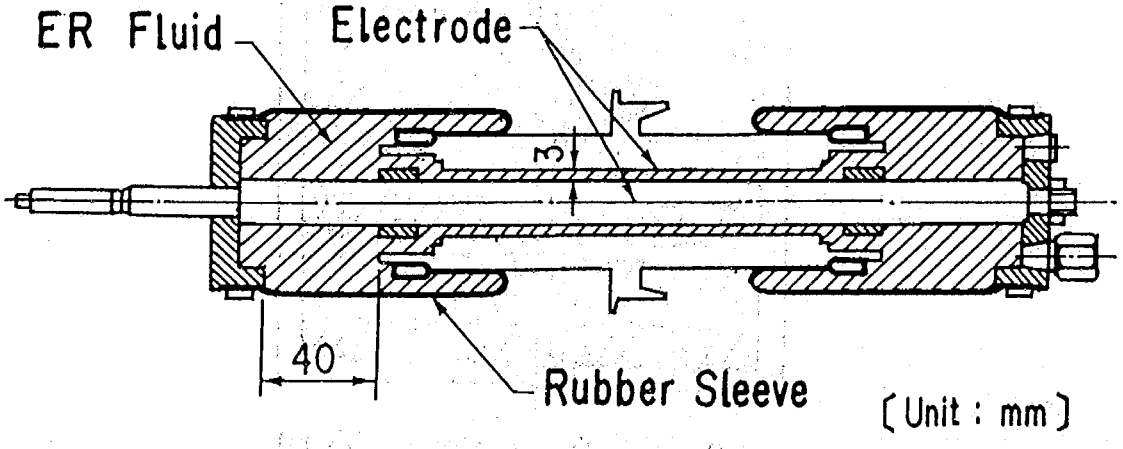
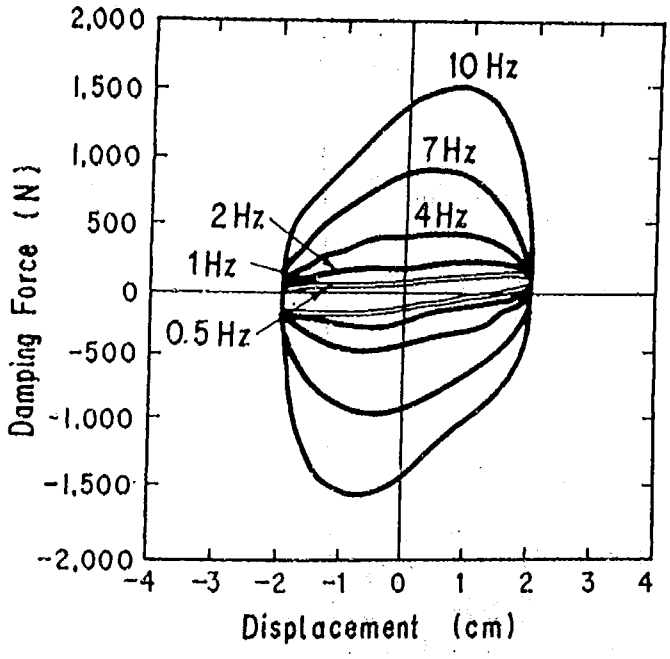
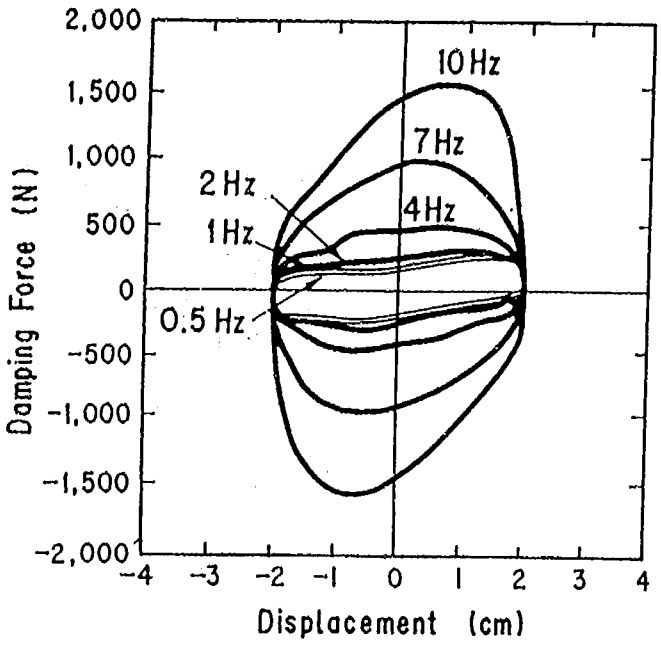


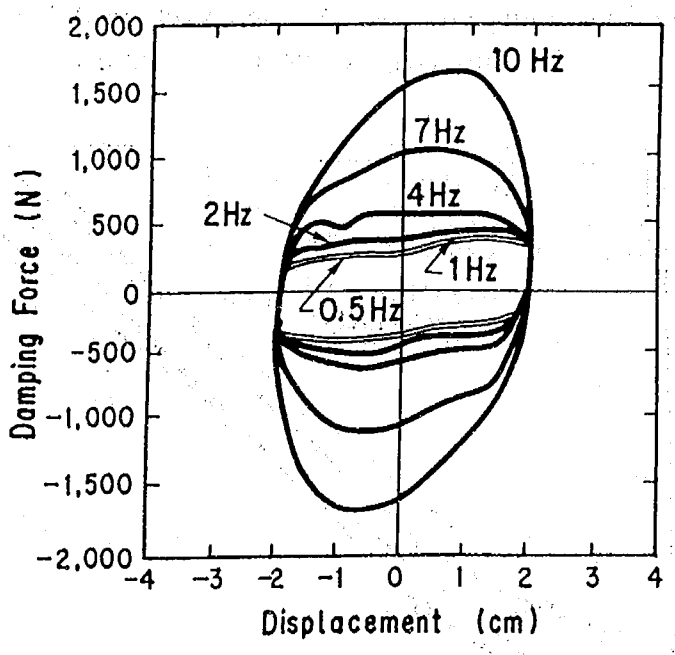
Fig.3 Experimental Model of Cylinder/Piston Type ERVD Developed



(a) Applied Voltage = 0kV



(b) Applied Voltage = 3kV



(c) Applied Voltage = 6kV

Fig.4 Hysteresis Loops of Force-Displacement Relation
(Loading Displacement : ± 20mm)

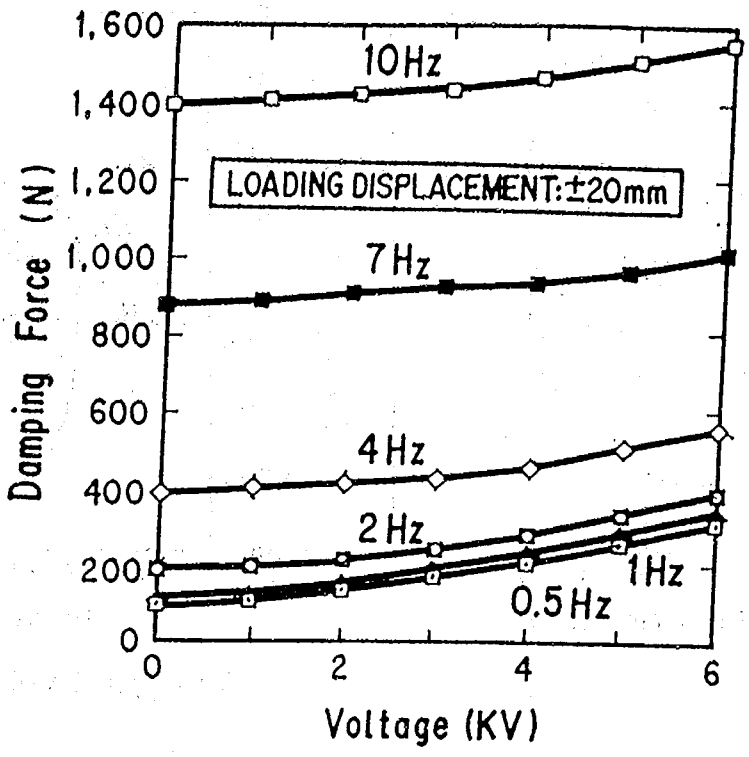


Fig.5 Damping Force vs. Applied Voltage Relation
(Loading Displacement : ± 20mm)

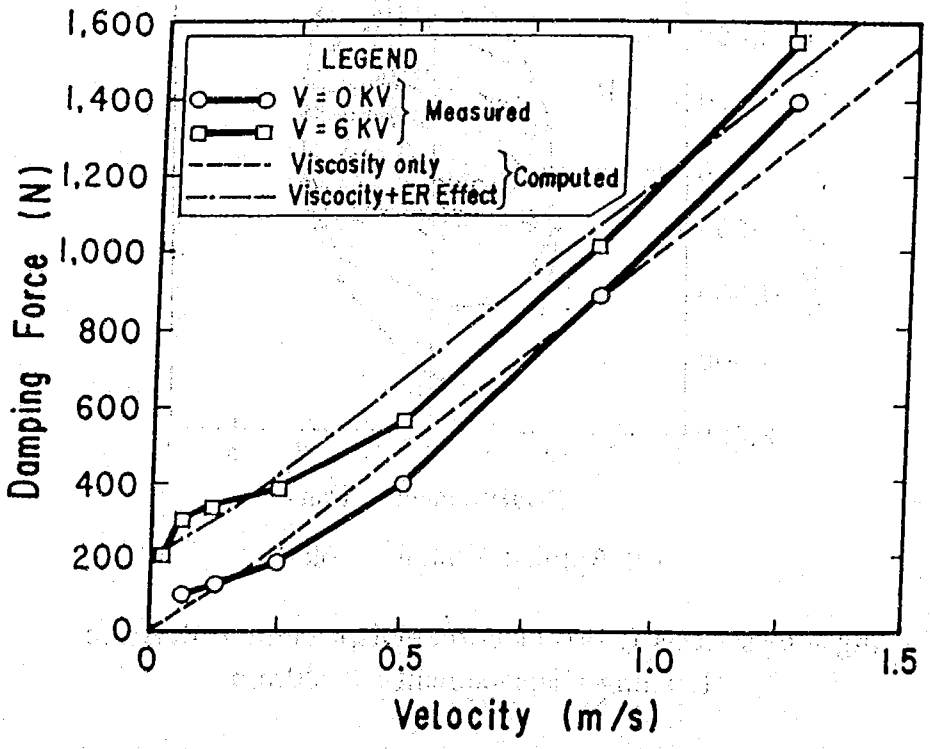


Fig.6 Comparison between Measured and Computed Damping Force
(Loading Displacement : ± 20mm)

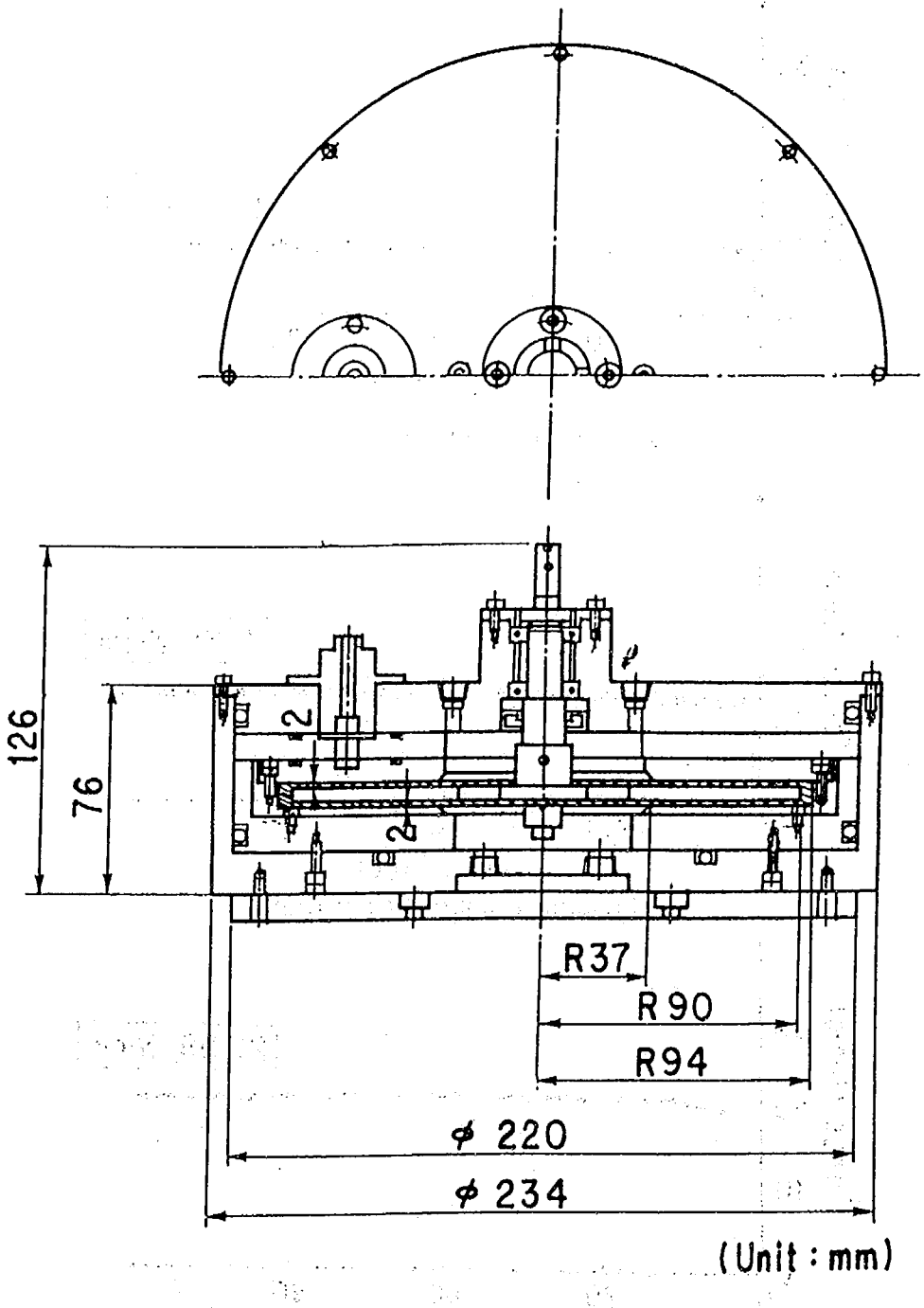
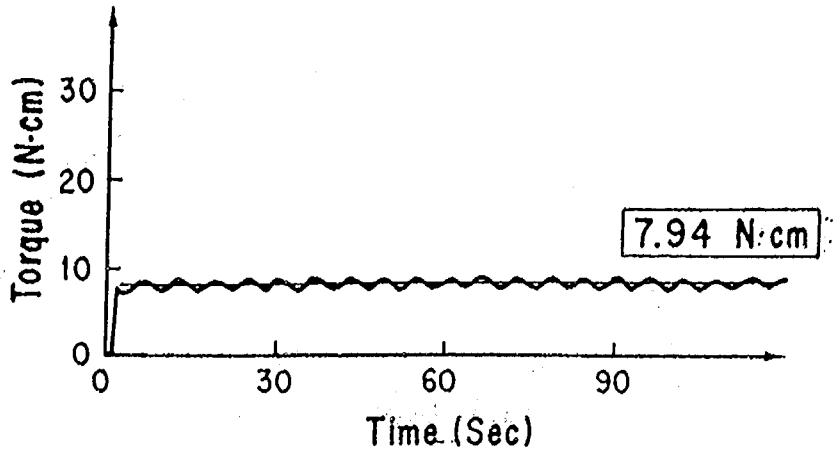
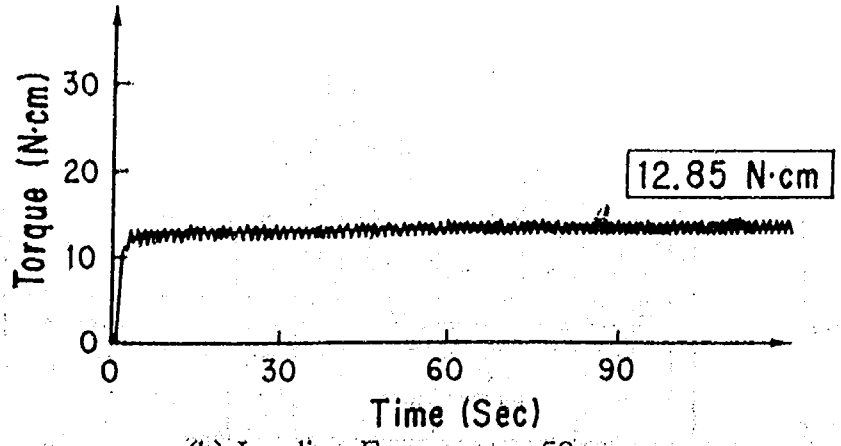


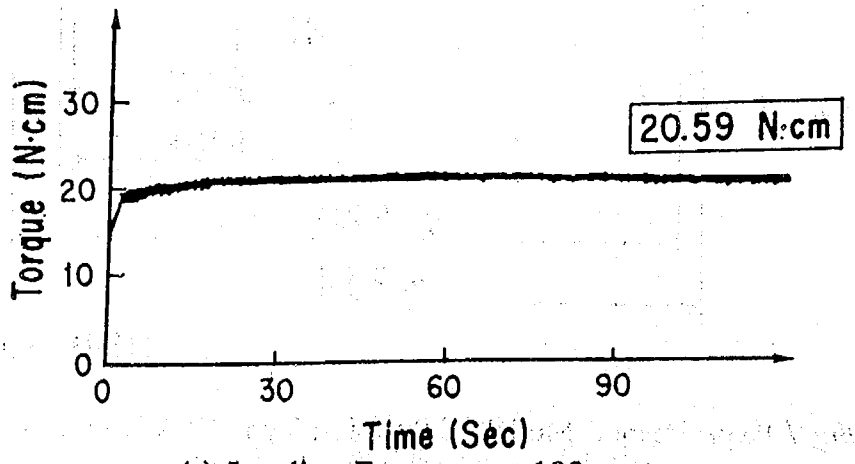
Fig.7 Experimental Model of Rotation Type ERVD Developed



(a) Loading Frequency : 10rpm

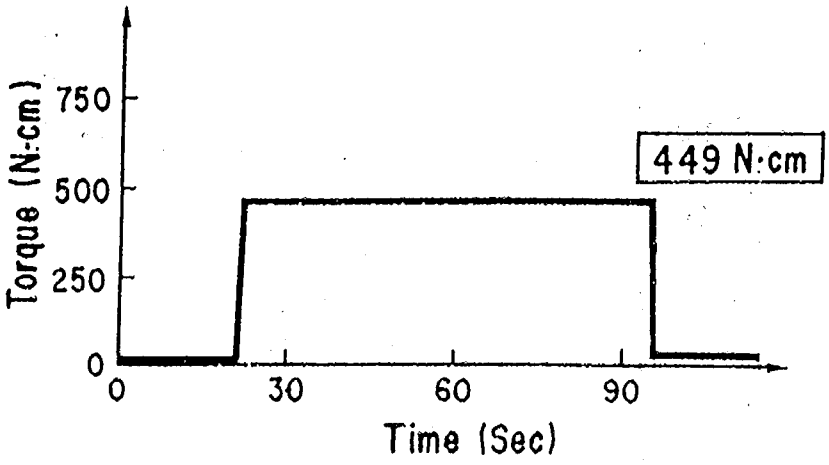


(b) Loading Frequency : 50rpm

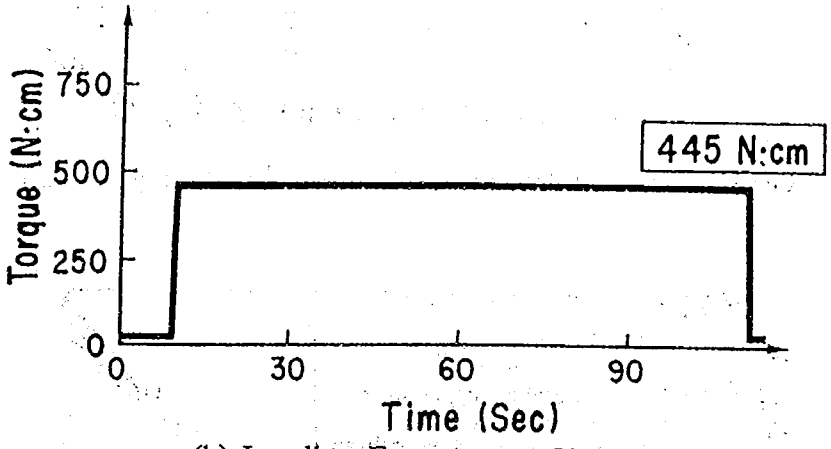


(c) Loading Frequency : 100rpm

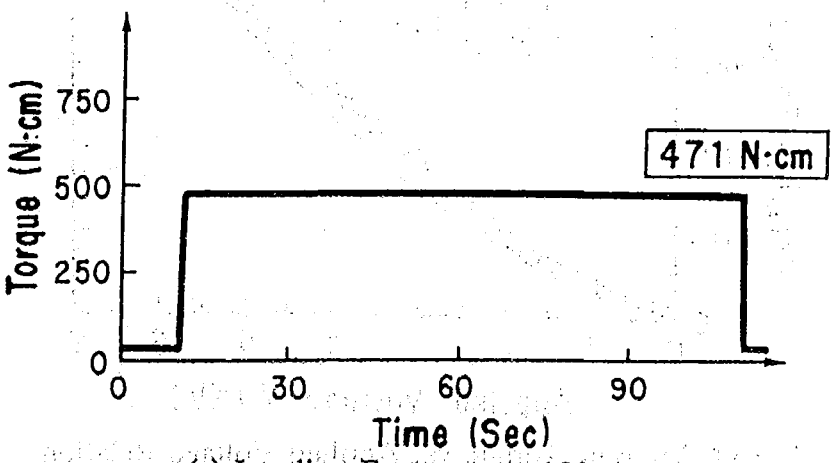
Fig.8 Damping Torque Developed (Applied Voltage = 0kV)



(a) Loading Frequency : 10rpm



(b) Loading Frequency : 50rpm



(c) Loading Frequency : 100rpm

Fig.9 Damping Torque Developed (Applied Voltage = 6kV)

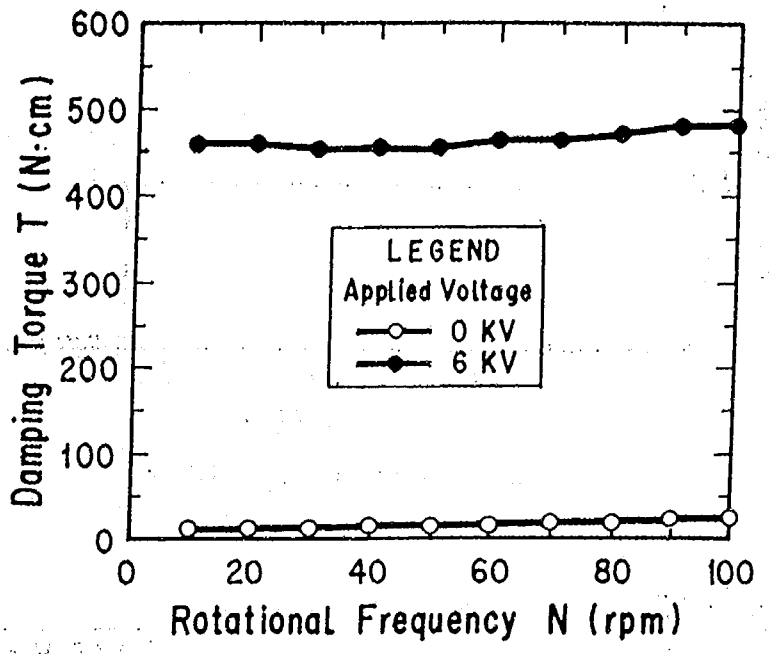


Fig.10 Damping Torque vs. Loading Frequency Relation

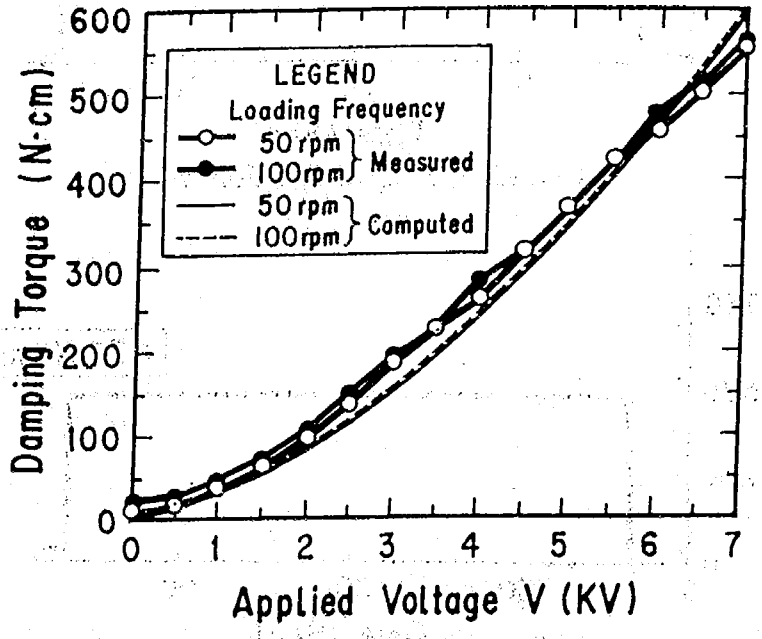


Fig.11 Damping Torque vs. Applied Voltage Relation

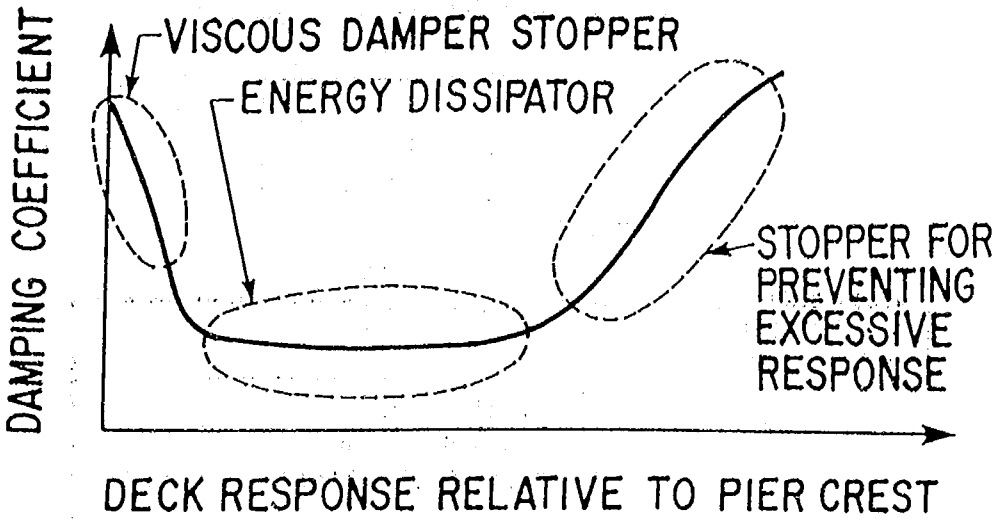


Fig.12 Function of Variable Damper

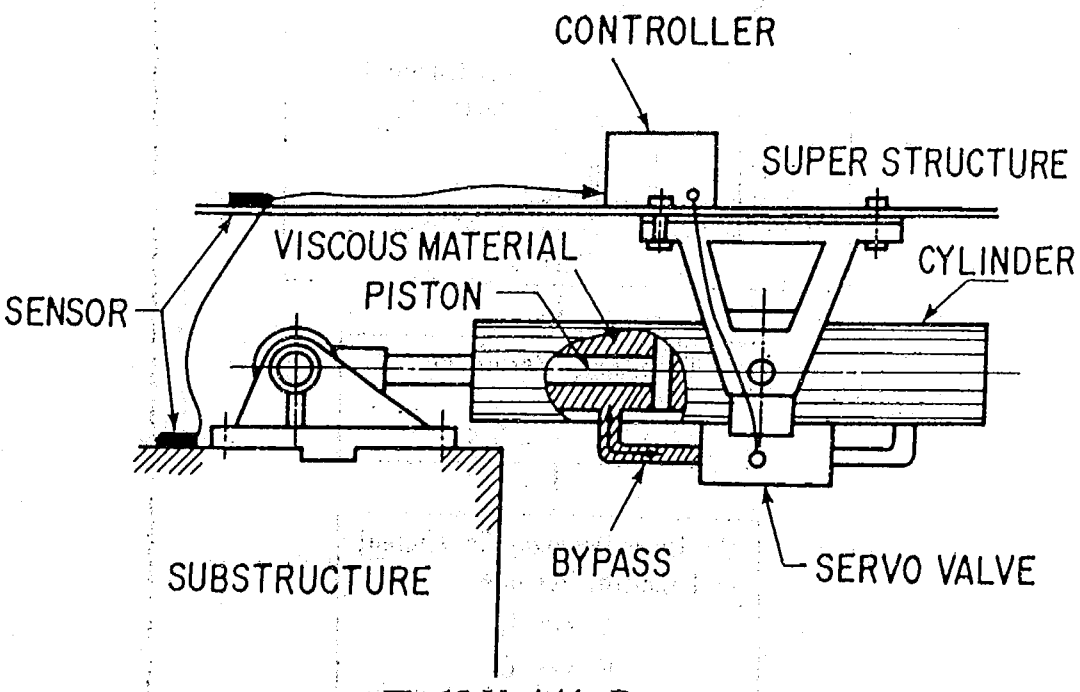


Fig.13 Variable Damper

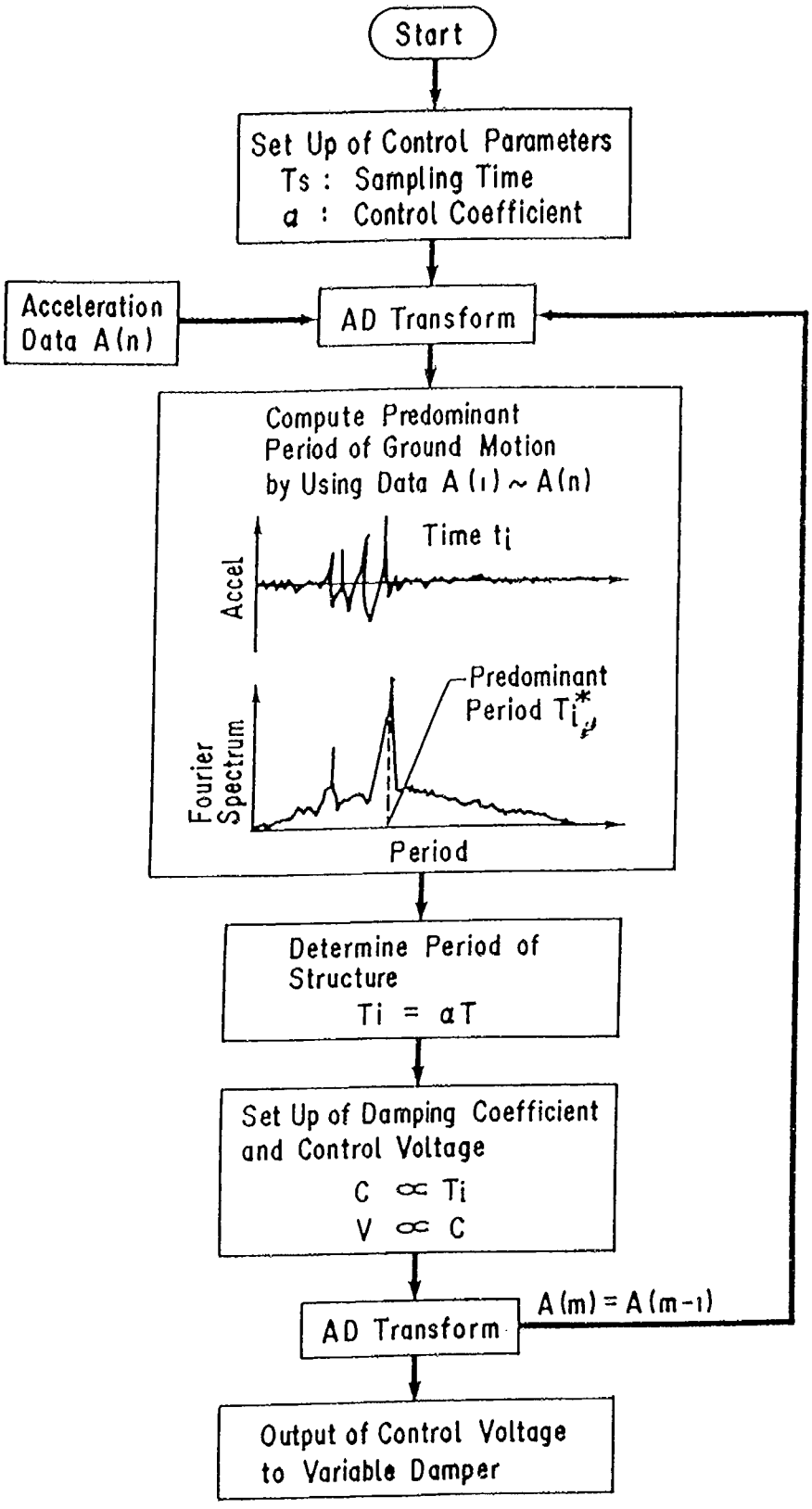


Fig.14 Control Algorithm of Variable Stiffness

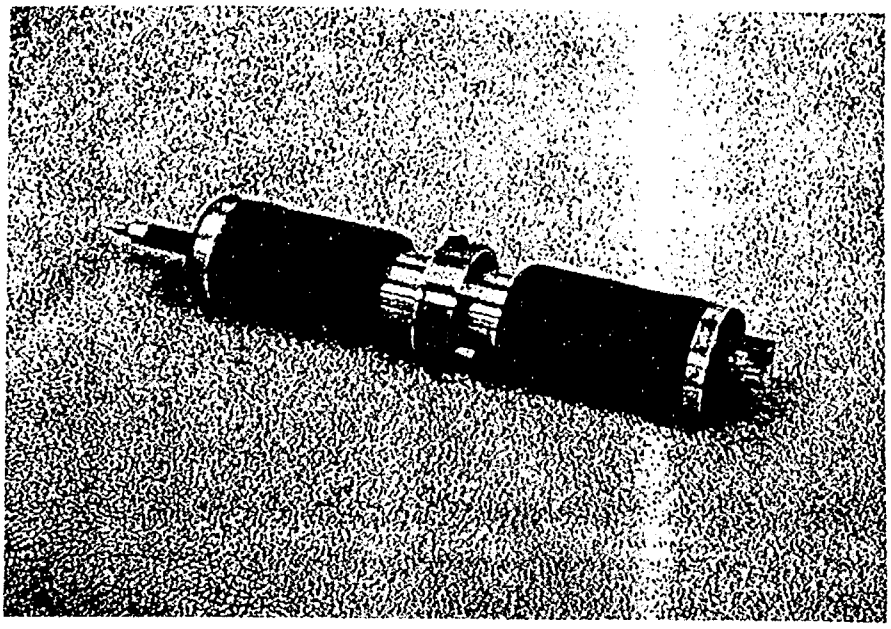


Photo 1 Experimental Model of Cylinder/Piston Type ERVD Developed

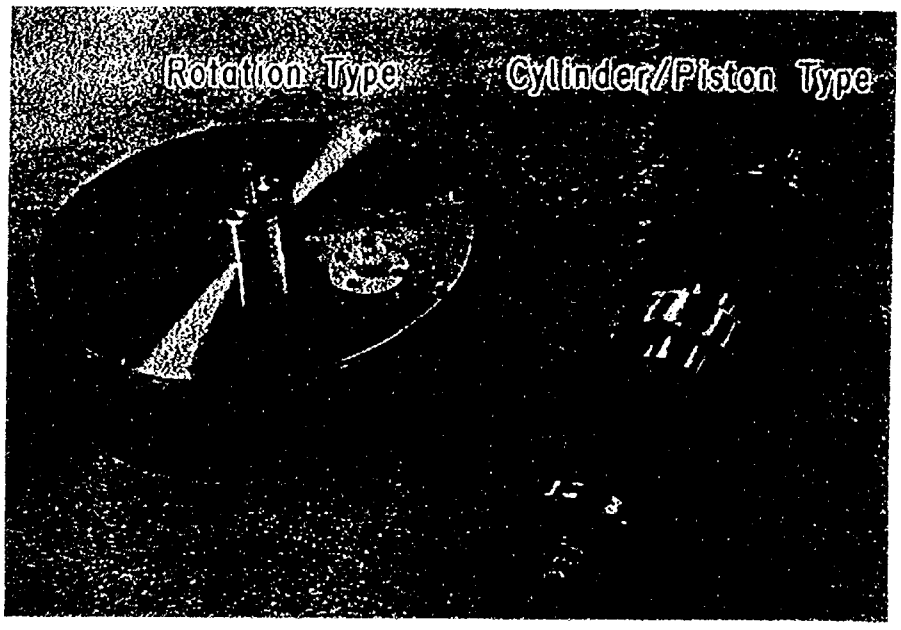


Photo 2 Experimental Model of Rotation Type ERVD Developed

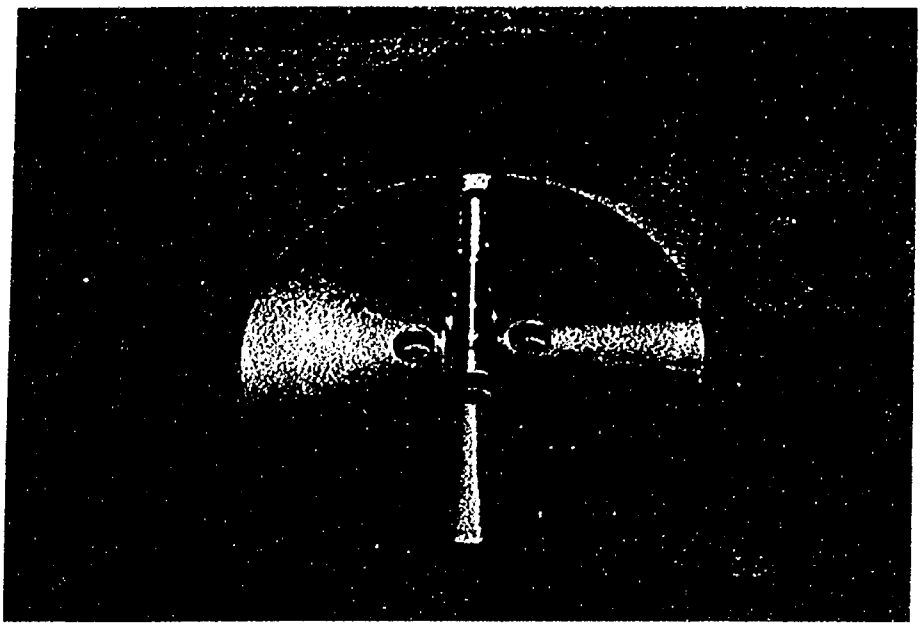


Photo 3 Circular Electrodes of Rotation Type ERVD Developed

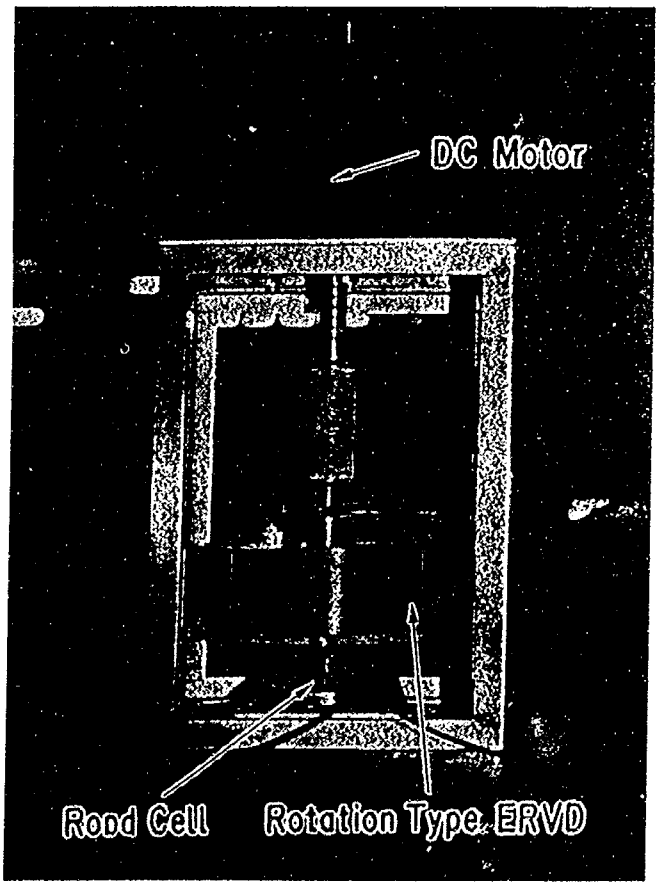


Photo 4 Dynamic Loading Tests of Rotation Type ERVD Developed

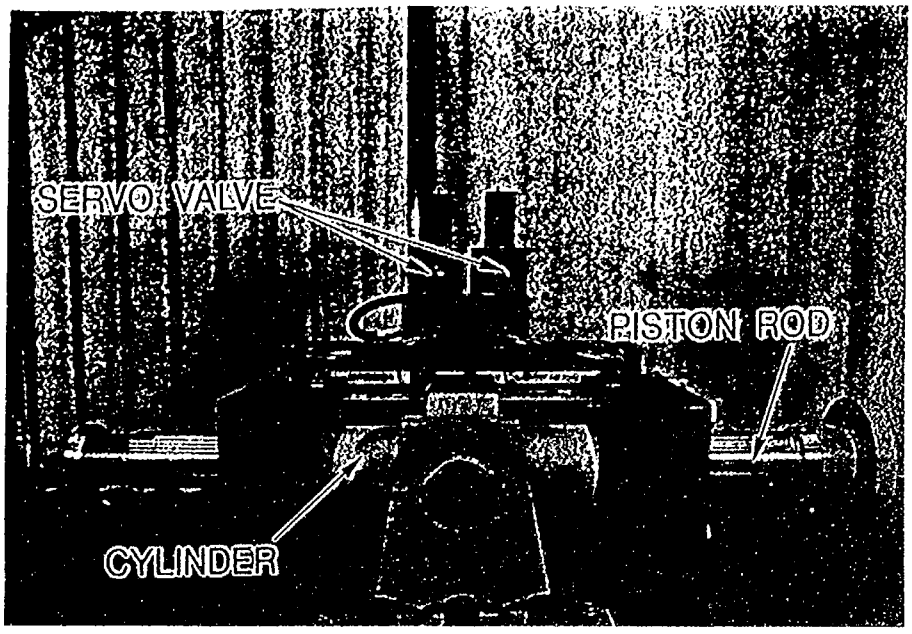


Photo 5 Prototype Model of Variable Damper

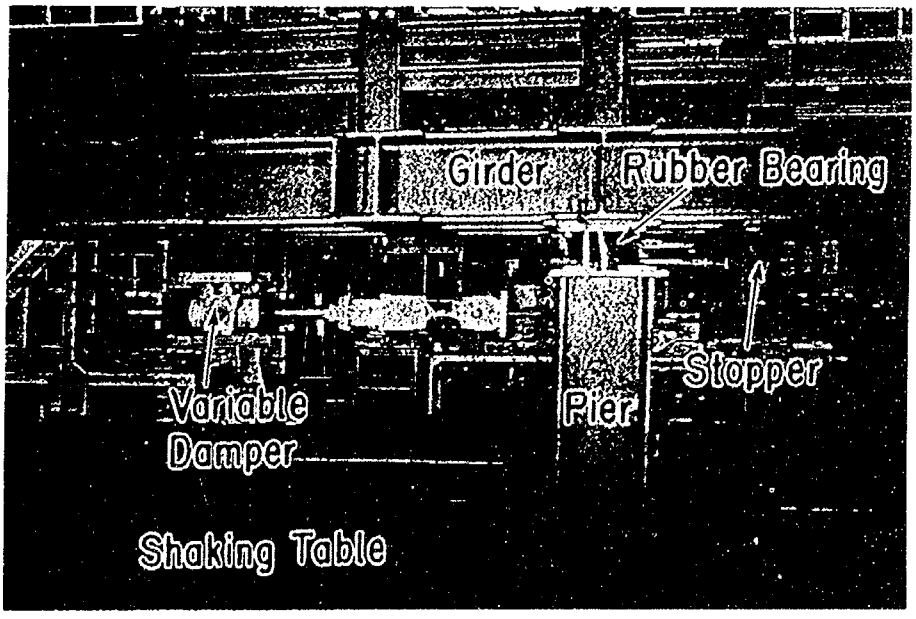


Photo 6 Model Bridge and Prototype Variable Damper Model

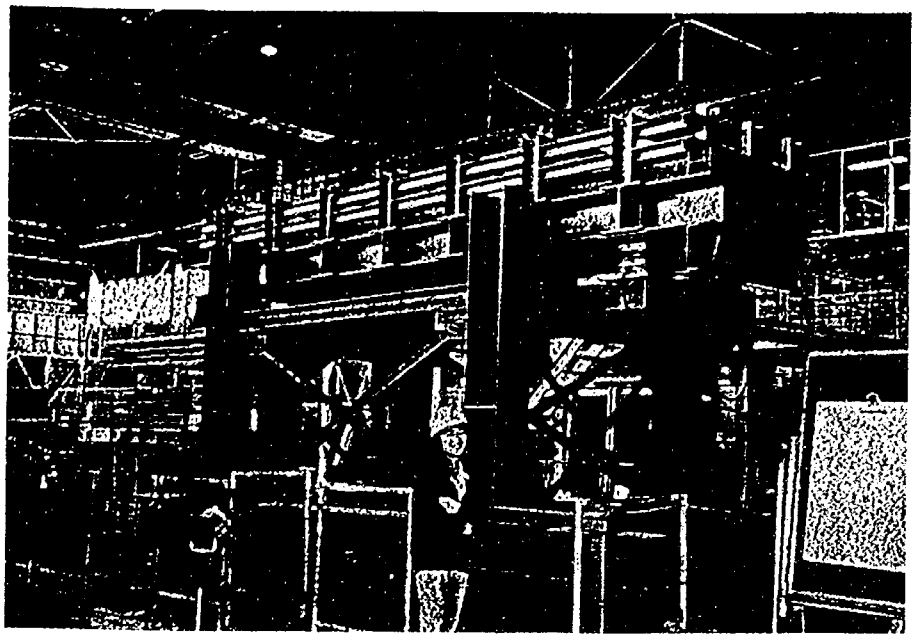


Photo 7 Shake Table Test of Sliding Isolation System

Shape Memory Alloy Dampers For Seismic Rehabilitation of Existing Buildings

by

Steven C. Sweeney[1]
John R. Hayes, Jr.[1]

ABSTRACT

Shape memory alloys (SMAs) represent a class of metallic materials that exhibit very unique structural characteristics. One such characteristic is the ability to elastically deform over very large strains with a nearly infinite fatigue life. One nickel-titanium alloy being studied has an elastic strain capacity of over 6%, more than 30 times that of structural steel. In addition, these materials have very high internal damping. Current research involves experimenting with devices incorporating these materials in dampers which can be installed in new and existing buildings to modify structural behavior under strong lateral loads. Prototype devices have been developed which produce a nearly square hysteresis loop, providing significant energy dissipation capabilities. These devices could be incorporated into existing braces or in braces added to moment frame structures. Tuning the device to the particular force, displacement, and hysteretic characteristics is achieved by altering the cross sectional area, length and configuration of the material or device. Analysis of a typical concrete frame structure incorporating SMA damping devices demonstrates their feasibility.

KEYWORDS: buildings; damping; earthquake; seismic rehabilitation; shape memory alloys.

1. INTRODUCTION

Energy dissipation in conventional structural systems, particularly in large earthquakes, is related to the nonlinear behavior associated with structural damage. In modern frame structures energy dissipation is designed to occur through the formation of plastic hinges in the beams adjacent to the columns. In most instances this damage associated with the hinge formation should be reparable, however in extreme instances the building may have to be closed for an extended period for repairs. A complicating factor is that the lateral load resisting system is the same as the gravity load resisting system, where extreme damage could result in structural collapse. This problem is more significant for structures built prior to modern seismic design codes. Discontinuous reinforcing steel in the joints and insufficient relative strength or stiffness in the columns (resulting in hinges forming in the columns) are common occurrences in structures built prior to the mid 1970's.

A philosophy currently being studied by USACERL and others is to protect a building's gravity load-resisting system through the use of supplemental damping devices. The use of supplemental damping elements to dissipate the earthquake-induced energy in a building is advantageous because energy dissipation can be constrained to occur in the supplemental dampers, therefore limiting damage to elements (supplemental dampers) that can be more easily replaced after an earthquake. The replacement of the supplemental dampers, should it be necessary, will not affect the gravity load-resisting system. The use of supplemental dampers essentially uncouples the gravity and lateral load-resisting systems in a building. Examples of structural dampers include friction damper devices, visco-elastic dampers, and the primary subject of this paper, dampers making use of the super elastic effect of shape memory alloys (SMA).

---

[1] U.S. Army Construction Engineering Research Laboratories, Champaign, IL, 61826-9005

2. SHAPE MEMORY ALLOYS DESCRIPTIVE SUMMARY

Shape-Memory Alloys (SMAs) are a class of alloys that display a characteristic reversible phase transformation as they deform, rather than undergoing intergranular dislocation typical of steel (Figure 1). SMAs therefore have the ability to "yield" repeatedly without sustaining any permanent deformation. The material undergoes a thermoelastic martensitic phase transformation above what is referred to as the transformation temperature range (TTR), which is specific to each alloy. A crystal phase transformation is induced under an applied load, which is reversed when the load is removed or it is heated above the TTR.

2.1 Shape Memory Effect

There are two primary features of SMAs of interest, irrespective of alloy type. The first of these is called the shape memory effect (SME), which occurs if the alloy is strained in shear at a temperature below its TTR. As long as the shear strain is less than a critical strain for the particular alloy, the strain can be accommodated by a twin re-orientation process from an austenitic to a martensitic structure. No dislocation motion or permanent damage occurs at the atomic level. Upon heating the strained structure, each of the twinned elements reverts to the original austenitic crystal structure, and any imposed strain is lost. The material reverts to its pre-strained shape and the shape memory effect is observed. The reversion of the martensite to the austenite is a first-order phase change with a large mechanical force, and only a restraining force large enough to create permanent deformation in the austenitic parent will hinder shape recovery.

Figure 2 shows a typical Nickel-Titanium alloy (NiTi, often referred to as Nitinol) tested at a temperature slightly below the TTR, where it will exhibit the SME. The force-deformation response takes the form of a low flow stress, a long horizontal yield plateau, followed by a significant increase in stiffness. Merely heating the material through its TTR will remove all accumulated strain and return the material to its original form. This is the classical SME.

2.2 Superelastic Effect

The second feature of the SMAs is called the superelastic effect (SEE). This effect is observed when a strain is imposed on an SMA material at a temperature above its TTR. The alloy system can relieve the stress imposed on it by transforming to the thermally unstable martensite and allowing that martensite to strain as it is formed, thus creating a stress-induced martensite. Since this martensite is not thermally stable, as soon as the stress is lowered below the stress level required to create the martensitic form, the material may revert to the austenite and thus eliminate the strain in the stress-induced martensite. The stress at which the martensite undergoes a phase change to austenite is termed the reversion stress.

Figure 3 shows the curve for a typical NiTi tested at a temperature slightly above its TTR, where the alloy exhibits the superelastic effect. The same plateau is seen as in Figure 2, but at a much higher stress. Reduction of the stress at the end of the plateau results in a lower stress at which the material will lose the imposed strain. Different families of SMAs show widely different levels of shape memory strain, have different ultimate ductilities, and show very different responses to cyclic deformation.

3. MATERIALS TESTING RESULTS

Over a dozen alloy families have been shown to exhibit this transformation, and each of these families has many specific compositions, each of which possesses unique mechanical and transformation properties. There are five primary alloy systems of significant interest. These are the NiTi family; two copper-based systems, CuZnAl and CuAlNi; FeMnSi alloys; and some special stainless steel compositions. These alloy systems were chosen based on cost, ease of fabrication, or

optimum mechanical properties. This research program to date has focused exclusively on the NiTi family of alloys because of their superior mechanical properties. The objective of the testing program was to experimentally verify the important characteristics of the superelastic hysteresis of NiTi in tension. Table 3.1 summarizes the test program, consisting of more than 20 tests that evaluated the effects of temperature, strain-rate or frequency, and thermomechanical processing. The results of the materials testing program are discussed below in terms of the implications to the design of structural dampers.

3.1 Hysteretic Energy Dissipation.

The results of Test 4C (Figure 4) demonstrate the high level of energy dissipation available with superelastic hysteresis: more than 2500 in-lb/cubic inch in its elastic range at strains less than 10%.

3.2 Hardening at Large Strains.

Another useful characteristic of superelastic NiTi is that it hardens after its conversion to stress-induced martensite. For the NiTi sample in Test 4C, this effect occurred at approximately 9.5% strain. In Test 4C, strains of up to 10% were recovered; the residual strain of 2% was a result of the preconditioning work treatment of the alloy.

3.3 Thermomechanical Processing.

The influence of thermomechanical processing on the hysteretic response of a NiTi alloy can be seen by comparing the results of Test 2A (Figure 5) and Test 4C (Figure 4). The process for producing the sample for Test 2A was designed to increase the yield, or load stress level, of the alloy. Tests 2A and 4C were conducted at approximately the same temperature. Although the area of the hysteresis loops is similar for both tests, the loading and reversion stresses clearly are influenced by the thermomechanical processes used to produce the alloy.

3.4 Temperature Effects.

Figure 6 illustrates the effects of temperature on superelastic hysteresis: an increase in temperature above the superelastic temperature range (A_f - M_d as shown in Figure 1) produces an increase in both the yield and reversion stresses as well as a reduction in the area of the hysteresis loop. It should be noted that the increase in the yield stress can be useful both for active control purposes and as a complementary effect to viscoelastic behavior in passive composite damping devices and that the total energy dissipated per cycle over a significant range of temperatures remains large.

3.5 Progressive Engagement.

Test 6C (Figure 7) demonstrates the response of a damping device composed of progressively engaged NiTi superelastic elements. The test sample consisted of two groups of NiTi wire loops: the first group of wires was fully engaged over the entire strain range; the second group of wires engaged at 4% strain in the first group of wires. The resulting hysteresis is the sum of the hysteresis of the two wire groups. Such mechanisms provide a useful means of controlling the force-deformation hysteresis of a passive damping device.

4. HYSTERETIC SHAPES

SME and SEE hysteresis can be used with a wide variety of kinematic mechanisms to obtain different hysteresis shapes. Figure 8 shows several of the force-deformation responses (hysteresis) that can be achieved.

The rectangular hysteresis shown schematically in Figure 8c is produced by using pre-stressed superelastic SMA dampers. Figure 9 illustrates the loading cycle of a simple spring element displaying rectangular hysteresis. Upward motion of the crossbar (C) in Figure 9 is assisted by spring A as shown in the schematic stress/strain diagram. Concurrently, this motion is resisted by spring B. Downward motion is entirely symmetric

with the role of the two springs reversed. Thus, the effect of these two prestressed superelastic elements working in opposition to one another is to provide a constant resisting force which is the difference in their respective loading and reversion force levels. Operationally, this schematic device provides a constant resistance force damping element with approximately zero (static) stiffness.

Figure 10 provides a schematic representation of a mechanism which produces the triangular flag hysteresis shown in Figure 8a. Figure 10a shows a prestressed wire W spanning between fixed supports. The displacement of the wire from its initial position at A to B is resisted at a stress SI, that is, the stress at which the phase transformation is induced. Upon reversal of the motion, the wire assists the motion at a stress Sr, the stress at which reversion to parent phase occurs. Thus the device applies both a constant resisting and a constant assisting force over the full range of motion. The triangular force-deformation response shown in Figure 10c is the hysteresis that results from the deformation of this device. The bow tie hysteresis (Figure 8b) can be achieved as the sum of two triangular hysteresis, that is, through the use of two devices.

The force and deformation capacities for all of the hysteretic shapes shown in Figure 8 are essentially unlimited. Higher force levels can be achieved by the addition of more SMA material. Large deformation can be accommodated in relatively compact SMA devices due to the large strain range of the transformation plateau over which stress remains approximately constant.

5. DEVICE TYPES

Because of these unique characteristics of SMAs, simple devices can be developed which are self-centering and which perform repeatedly for a large number of cycles. Several passive damping devices of the major device categories including truss link, joint, constrained layer, mass damping, and shear link types have been developed. Schematic designs for two devices, a truss link device (TLD) and a truss joint device (TJD), both based on simple NiTi wire or tubular components, are presented. Each of these devices can display several types of force-deflection hysteresis, depending on the phase state of the NiTi. On the basis of the material testing results for NiTi wire and for other SMAs, the stability and fatigue characteristics of these devices should be excellent.

5.1 Truss Link Device (TLD)

Figure 11 shows a longitudinal section of a truss link device. The device is comprised of a tubular element sliding within another tubular element. The other tube is slotted to permit the insertion of a pin fixed to the inner tube and sliding in the slot. NiTi wire loop elements connect this sliding pin to two pins fixed in the outer tube as shown.

For the SMA TLD, there is a constant axial resistance in the device in both extension and compression. This results in the pure rectangular hysteresis. The device can be designed to protect against excessive deflection by exploiting the material stiffening which occurs in NiTi at strains in excess of 10%. At strains exceeding 10%, the NiTi device will stiffen and recover excess strain elastically.

5.2 Truss Joint Device (TJD)

Figure 12 shows a section view of a schematic truss joint damping element. This device is composed of a simple bolted connection: the bolt is surrounded by two NiTi annular rings or washers. For this device, the mode of action provides a rectangular flag-shaped force-deformation hysteresis in any direction. This action is the result of the unprestressed superelastic element resisting initially in an elastic manner. At levels of force sufficient to stress-induce martensitic yield, the device will yield and dissipate energy as it cycles through the superelastic hysteresis.

6. ANALYTICAL CASE STUDY

A three-story, non-ductile concrete structure that was designed in 1956 was selected for the analytical study of the use of SMA dampers. The building's footprint is similar to the letter H, with a gross floor area of approximately 51,400 sq. ft. The H-shape is seismically separated into three buildings (wings) by two 2"-wide expansion joints.

The gravity load-resisting system in the building is typically composed of 7-inch reinforced concrete flat plates with shearheads, 18-inch-deep perimeter beams, and reinforced concrete columns. Wind and seismic lateral loads are resisted by reinforced concrete, structural walls, and reinforced concrete, non-ductile, moment frames.

The structure was designed in accordance with the Pacific Coast Uniform Building Code and the ACI Building Code. The design live, wind, and seismic loads specified by the engineers of record, Miller & Ahlson of Seattle, Washington, were:

- live loads: 40 psf to 60 psf typical; 100 psf for stairs
- wind loads: 20 psf on the projected area
- seismic loads: Seismic Zone 3 (1956)

The typical column and beam reinforcement ratios are approximately 1% and 1.25%, respectively, and are substantially less than normal practice in the 1980s and 1990s. Shear reinforcement is typically #3 ties @ 12 inches on center in both the columns and the beams. Shear reinforcement is not provided in the beam-column joints. Typical detailing is shown in Figure 13.

The detailing of the concrete elements in the building is consistent with engineering practice in the 1950s but is inadequate by current standards. The seismic deficiencies in the existing building include no beam-column joint reinforcement, minimal or non-existent splices in column and beam reinforcement, and insufficient beam and slab rebar anchorage in perimeter columns and beams. In a moderate or severe seismic event, these shortcomings will prevent the formation of ductile plastic hinges in the beams and may result in the bottom rebar in the beams pulling out of the beam-column joint as a result of bond failure; buckling of the beam rebar adjacent to the column face due to insufficient lateral restraint; shear fracture of the beam-column joint; or the partial collapse of the building.

6.1 Upgrade Design

There are many issues to be considered for the upgrade of an existing building. These include:

1. the need to protect the existing frame by reducing the lateral displacements such that the plastic hinge formation, bar pull-out, and joint shear failure in the existing frame are precluded,
2. the consequences of increasing the axial force demands in the existing columns,
3. the ease by which the upgrade scheme, including any foundation work, can be implemented,
4. the impact of the upgrade scheme on the aesthetic appeal of the building and on the existing mechanical, electrical, and plumbing services, and
5. the cost-effectiveness of the upgrade scheme.

Of these five issues (and noting that other constraints may apply), only the first two are addressed herein. A complete retrofit of the building was beyond the scope of this study

Two upgrade schemes were developed for the building, based on the use of SMA energy dissipators installed in brace elements. The two principal objectives of the retrofit design were to reduce the interstory displacements to below 0.75 inch (corresponding to a column rotation of approximately 0.006 radians) and to dissipate most of the energy absorbed in the frame in the shape-memory alloy (SMA) dissipators. In both

cases the models were subjected to a moderate level of earthquake shaking considered appropriate for the Fort Lewis site.

Upgrade one (UG1) involved the addition of 12, 6, and 4 energy dissipators in each frame of the wing of the building considered, in the first, second, and third stories of the building, respectively. The position of energy dissipation devices is shown in Figure 14. The SMA energy dissipators are supported by TS4x4x1/2 braces. For these analyses, the SMA dissipators are assumed to have rectangular (rigid-plastic) hysteresis with a yield force of 22.5 kips per damper. The TS4x4 braces were selected so as to ensure that at an interstory drift of 0.5%, less than 10% of the total brace/dissipator axial displacement was in the brace itself, and the buckling strength of the brace was at least 1.5 times the yield force in the SMA dissipator.

Based on the favorable results of the UG1 analysis, upgrade two (UG2) used approximately half the number of dampers, consisting of the addition of 6, 4, and 2 energy dissipators in each frame of the building, in the first, second, and third stories, respectively. The brace layout is shown in Figure 15.

6.2 Analysis Results

Analysis was performed using the DRAIN-2DX program. New non-linear truss-link damper elements were developed as part of this research program. The elements were developed such that they can be easily modified to represent the performance characteristics of many of the devices presented.

Initial stiffness and viscous damping in a linear analysis for both structures initially is essentially the same. Analysis results show the first mode period change from 1.55 seconds for the original structure to 0.20 seconds for an upgrade one. The maximum increase in axial force in any column in the frame can be calculated on the basis of the vertical component of the yield force in the brace, which in this case is 10.3 kips. For the brace layout shown in Figure 15, the maximum change in axial force in any column resulting from the addition of the SMA dissipators is 20.6 kips, or less than 4% of the compression capacity (P_0) of the columns and 20% of the tensile capacity of the columns (T_0). The modified axial forces in the columns in the existing frame for the UG2 upgrade should therefor be acceptable. Both upgrading schemes reduced the displacements in the building to a level whereby the frame suffered no damage when subjected to three moderate earthquake ground motions.

7. PHASE II RESEARCH

This research program is continuing as a Phase II SBIR project. The objectives of the Phase II SBIR are to design, fabricate, and test actual SMA dampers, and to test a large scale model structure with dampers under simulated earthquake loads. As part of this phase, the analytical tools necessary to design and use SMA dampers, and design guidelines will be developed. Sample designs for typical Army structures will also be presented.

8. CONCLUSIONS

The material testing program for the NiTi alloys clearly demonstrates the advantageous properties which can be exploited for use in structural damping. The shape and properties of the hysteresis which can be obtained through material preparation and kinematic devices is virtually unlimited. Application of SMA dampers have been analytically demonstrated to be feasible for the seismic rehabilitation. The results of the nonlinear analyses of the two upgrade schemes presented demonstrates that the addition of the SMA energy dissipators has substantially improved the seismic response of the existing building.

9. ACKNOWLEDGMENTS

The material presented herein is the result of a Phase I Small Business Innovative Research (SBIR) project, performed under contract to the U.S. Army Construction Engineering Research Laboratories by E*SORB Systems, Sunnyvale, California. Principal investigators for E*SORB Systems are Mr. Robert Krumme, Dr. Andrew Whittaker, and Dr. Ian Aiken.

TEST	MATERIAL	DIAMETER (in)	LOOPS	FREQUENCY (Hz)	TEMP (°C)
1A	F4904-2-2	0.015	14	0.2	22
1B	F4903-2B	0.009	22	0.2	22
1C	F00642-1B	0.162	14	0.2	22
1D	F2234-2-2A	0.014	19	0.2	22
2A	F4904-2-2	0.015	14	0.3	22
2B	F4904-2-2	0.015	14	0.3	23
2C	F4904-2-2	0.015	14	1.0	23
2D	F4904-2-2	0.015	14	3.0	23
2E	F4904-2-2	0.015	14	10.0	23
2F	F4903-1B	0.035	5	3.0	23[a]
2G	F4903-1B	0.035	5	3.0	23
3A	F4904-2-2	0.015	14	0.2	40
3B	F4904-2-2	0.015	14	0.2	60
3C	F4904-2-2	0.015	14	0.2	80
3D	F4904-2-2	0.015	14	0.2	0
4A	F00642-1B	0.016	18	0.2	22[b]
4B	F00642-1B	0.016	18	0.1	23
4C	F4903-1B	0.035	6	0.1	23
5A	F4903-2B	0.009	15	0.2	23
6A	F4904-2-2	0.015	14[c]	0.2	23
6B	F4904-2-2	0.015	14[c]	0.2	22[b]
6C	F4904-2B	0.0091	16[d]	0.2	23
6D	F4904-2B	0.0091	16[d]	0.2	23

a. Sample came loose during testing
b. Servo gain too low
c. 6 of 14 loops slack to 2% strain
d. 7 of 14 wires slack to 4% strain
e. 8 of 16 loops slack to 4% strain

Table 1 Details of the Testing Program

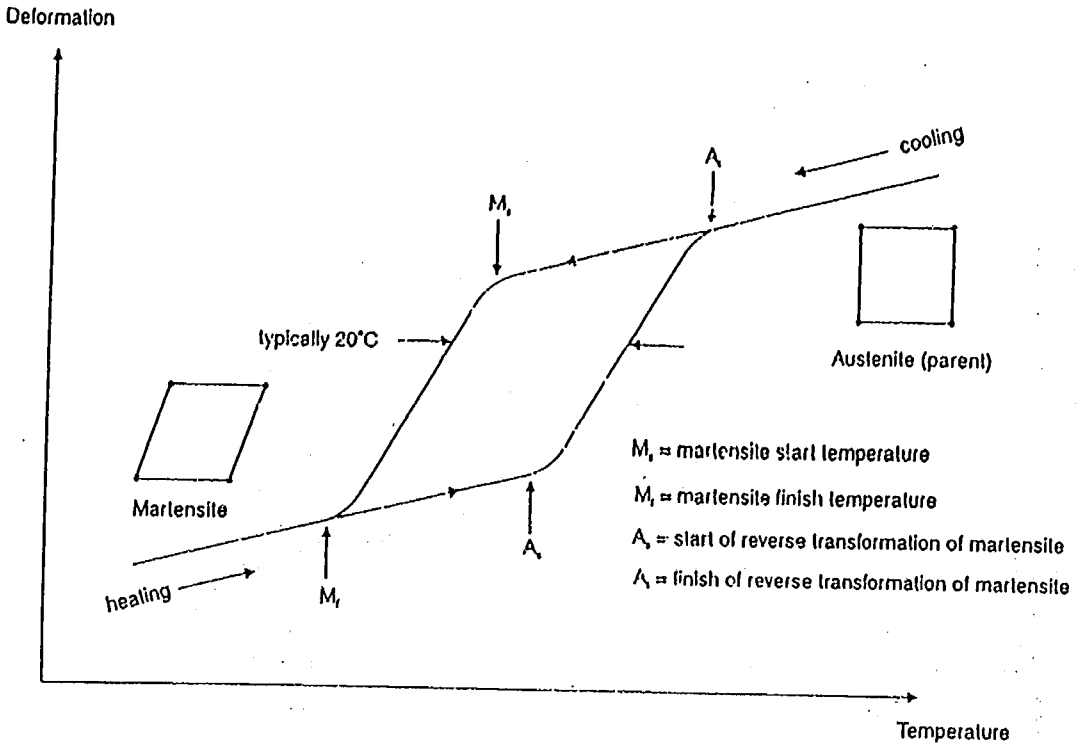


Figure 1 SMA Deformation-Temperature Relationship

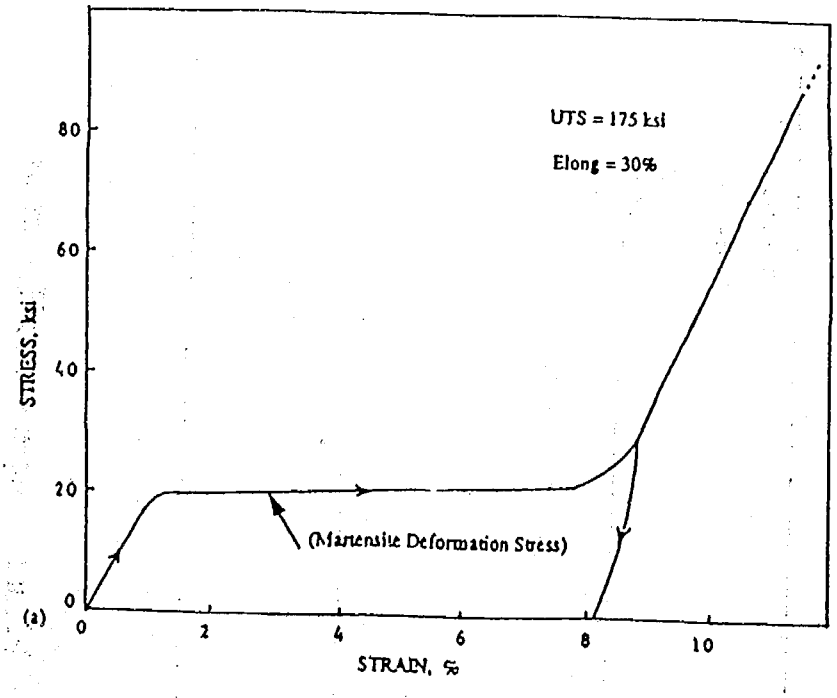


Figure 2 Shape Memory Hysteresis

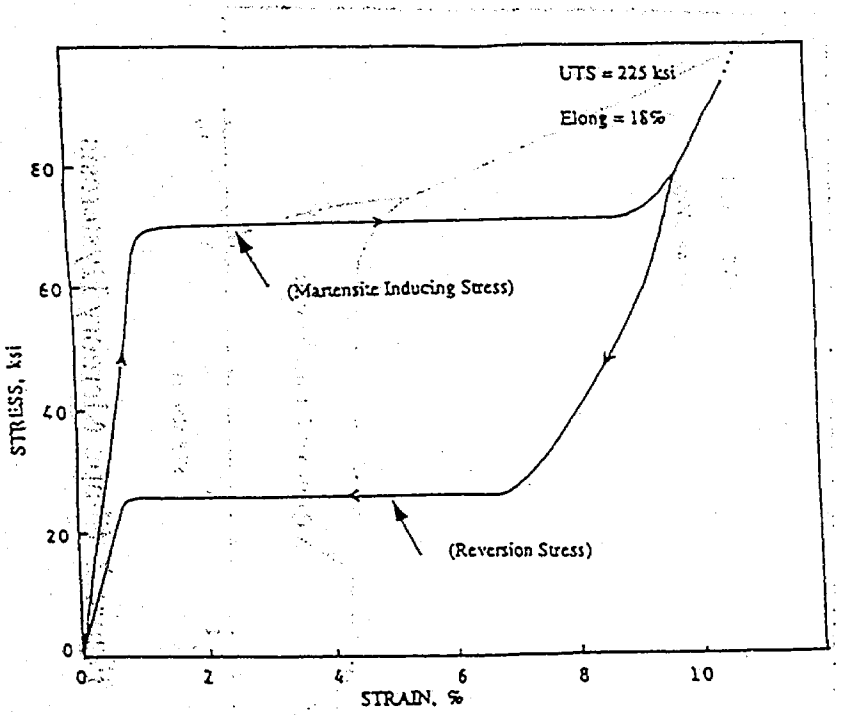


Figure 3 Superelastic Hysteresis

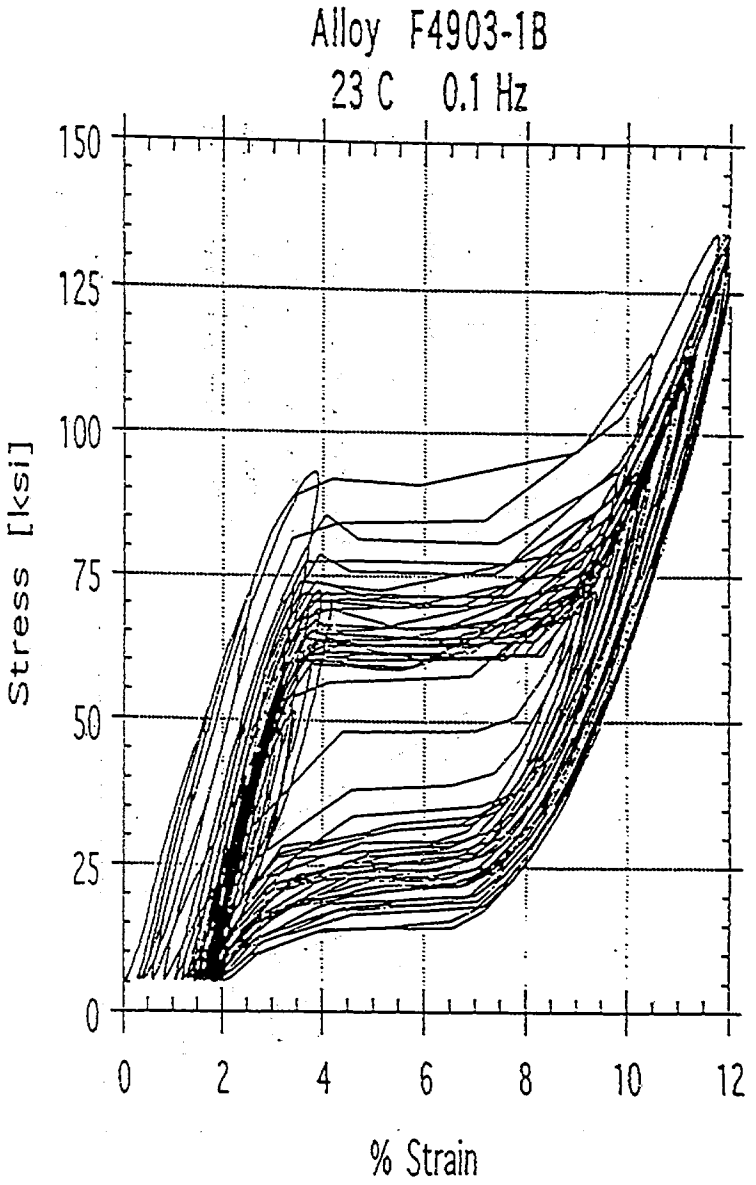


Figure 4 Hysteretic Response: Test 4C

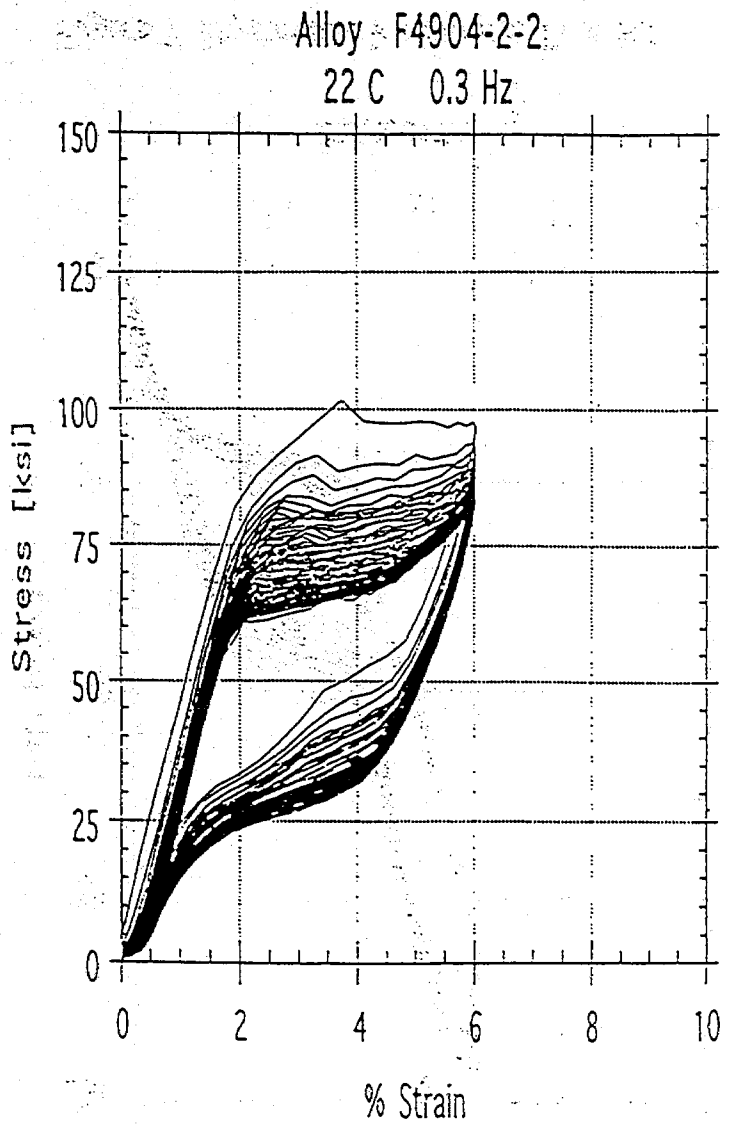


Figure 5 Hysteretic Response: Test 2A

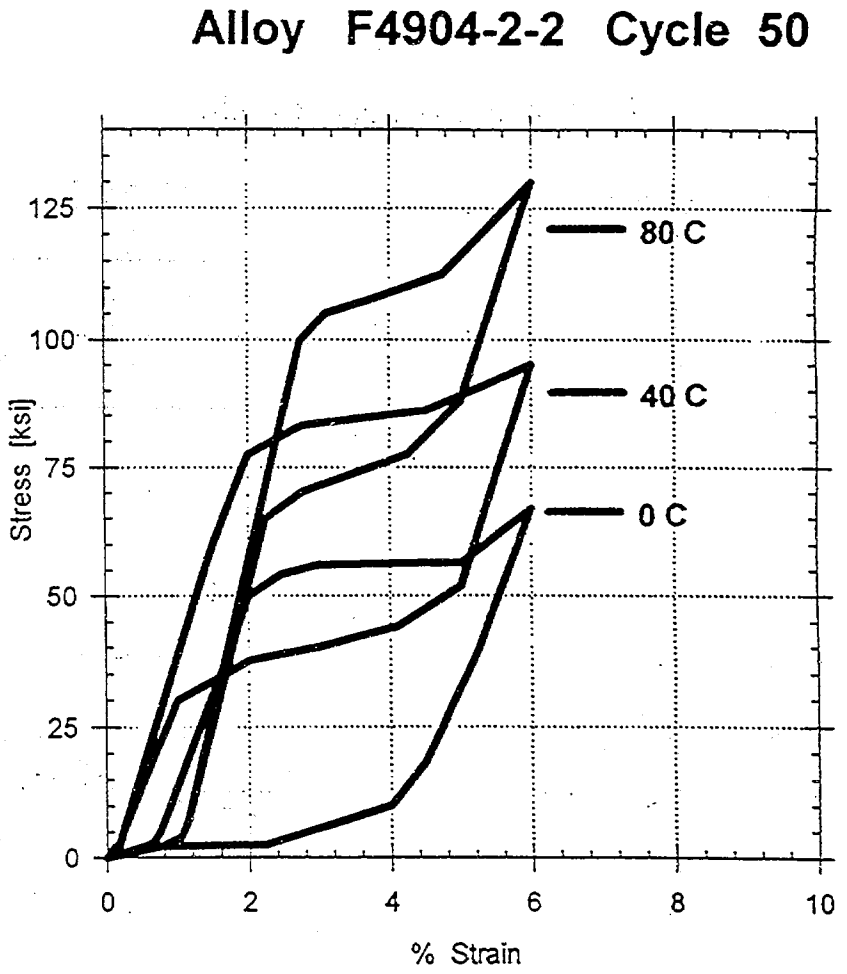


Figure 6 Temperature Dependence of SMA Hysteretic Response

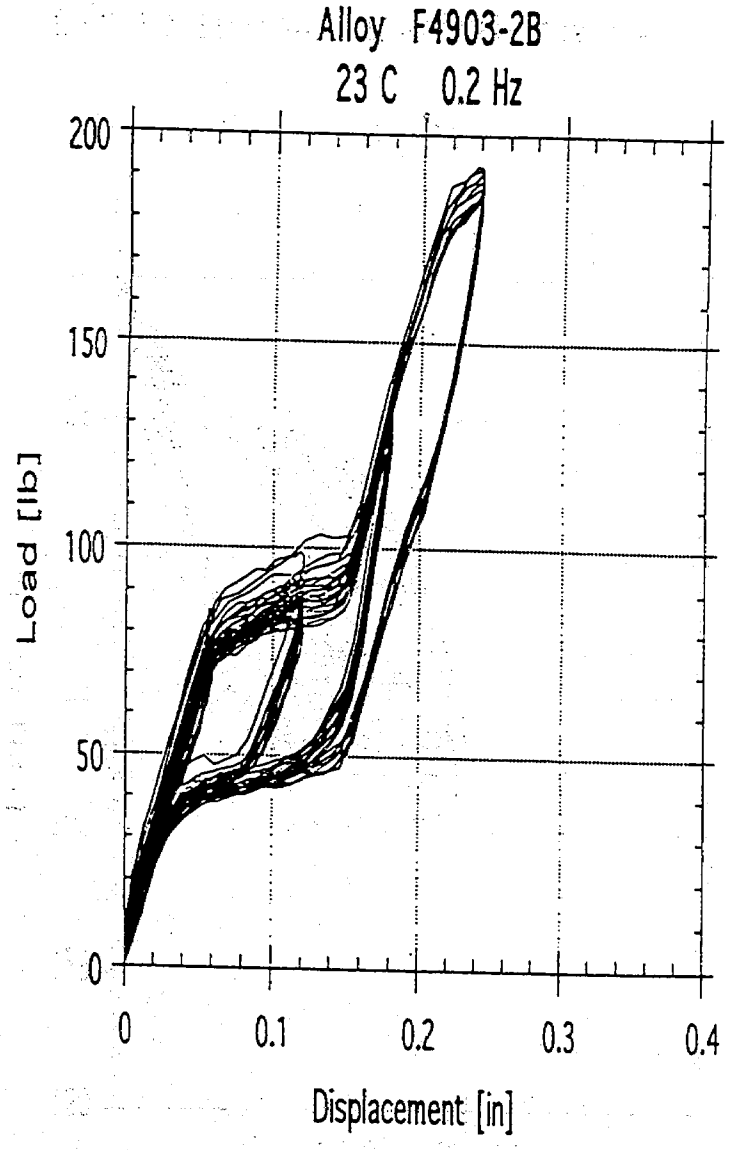


Figure 7 Hysteretic Response: Test 6C

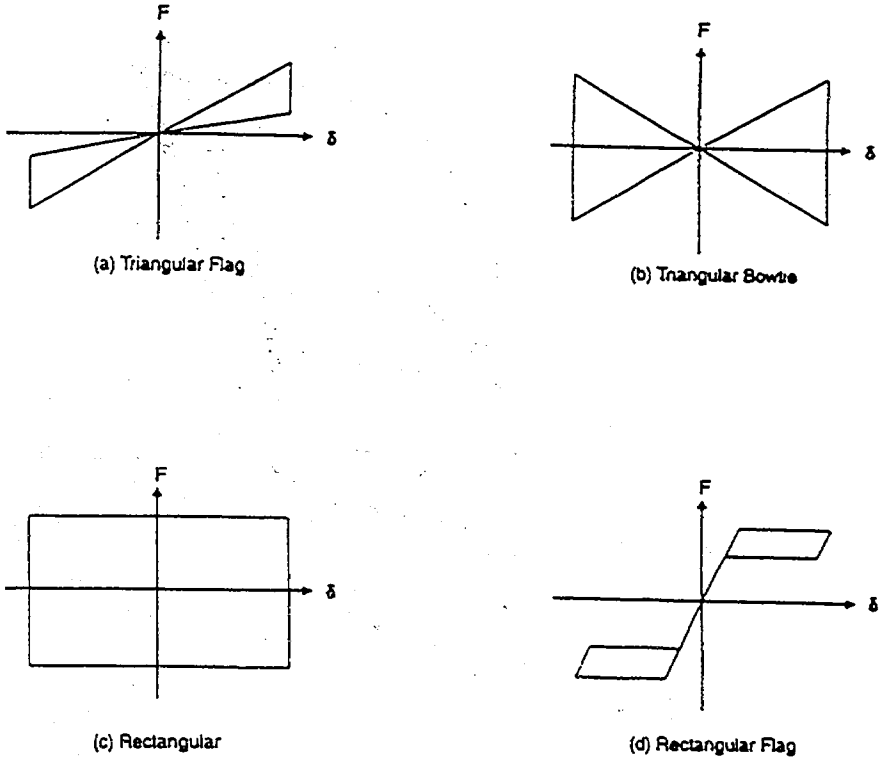
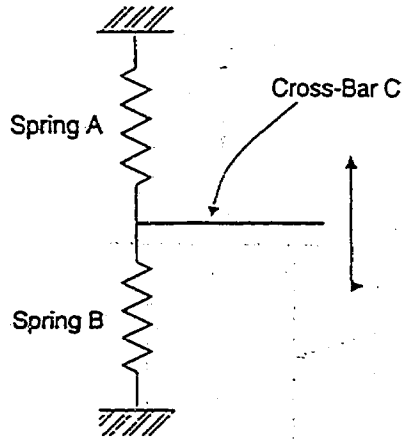
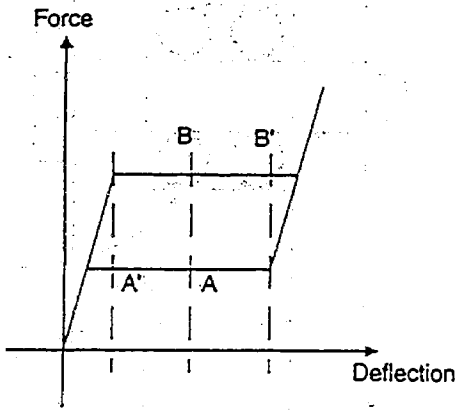


Figure 8 SMA Hysteresis Types

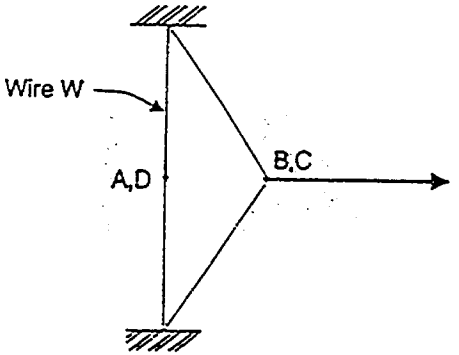


(a) Device Schematic

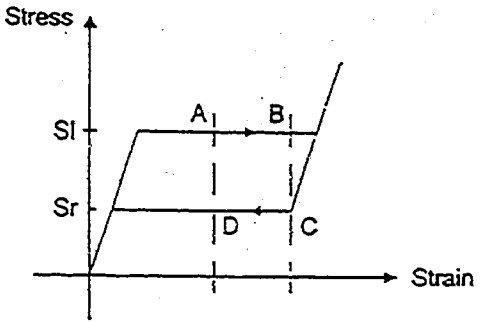


(b) Device Hysteresis

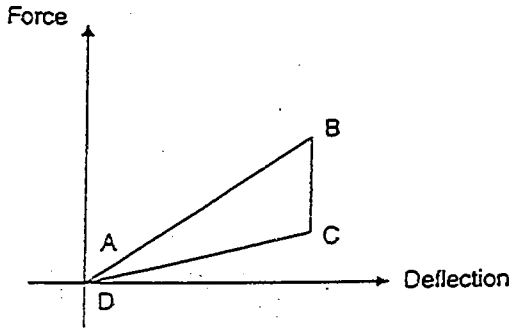
Figure 9 Rectangular SMA Hysteresis



(a) Device Schematic



(b) Stress-Strain Response of NiTi Wire



(c) Device Hysteresis

Figure 10 Triangular Flag Hysteresis

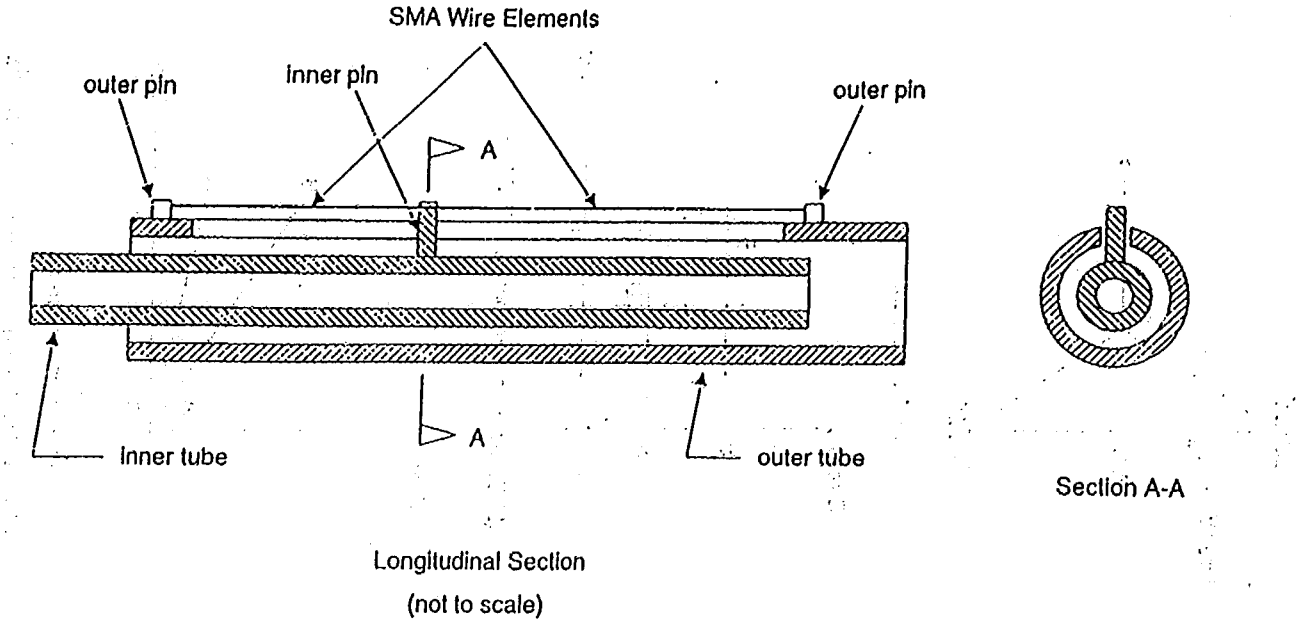


Figure 11 SMA Truss Link Device

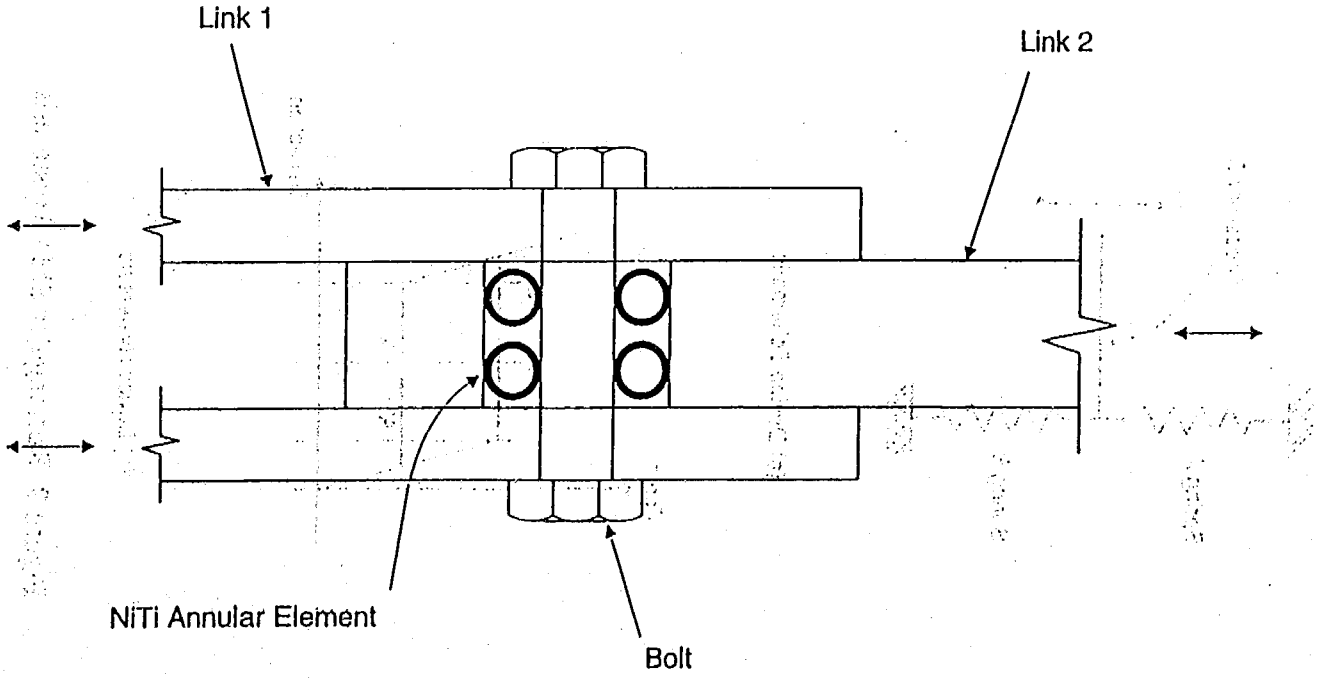


Figure 12 SMA Truss Joint Device

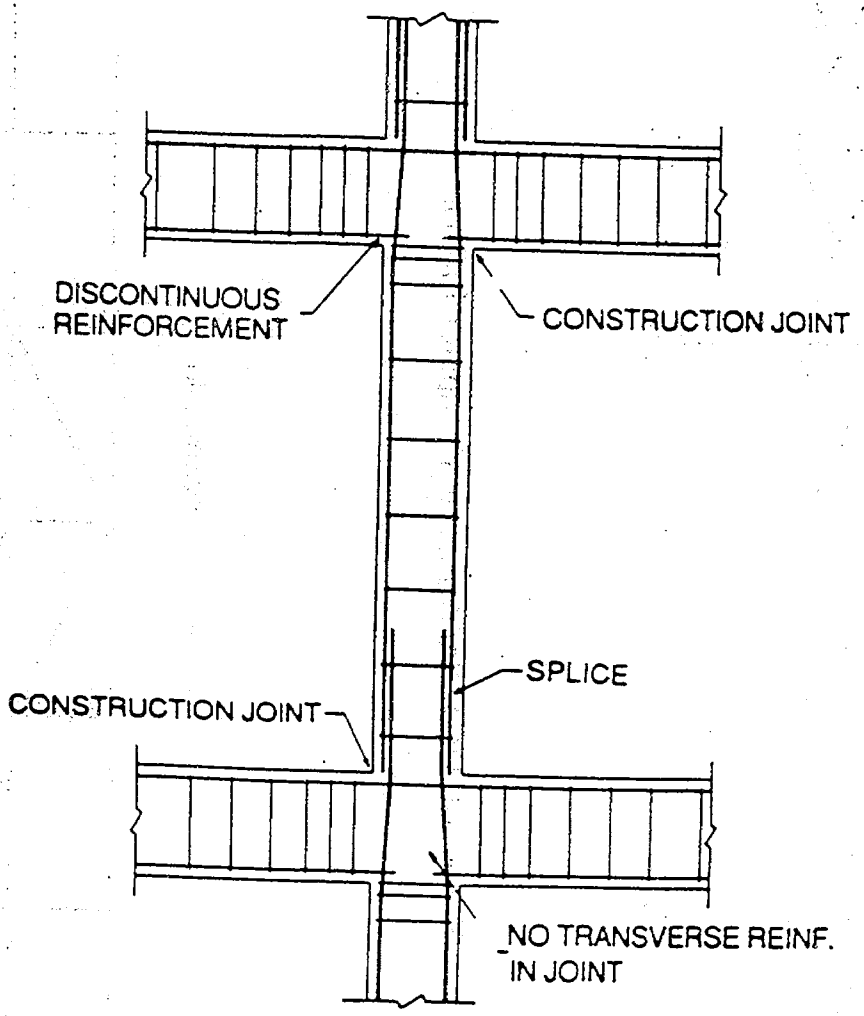


Figure 13 Lightly Reinforced Concrete Frame Detailing

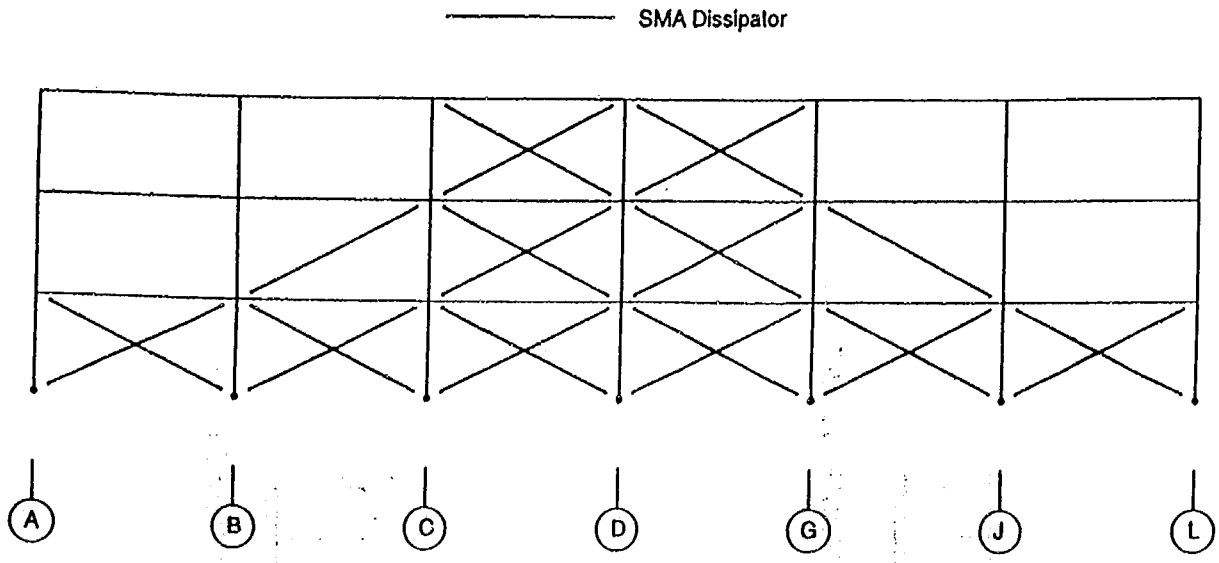


Figure 14 UG1: SMA Energy Dissipator Layout

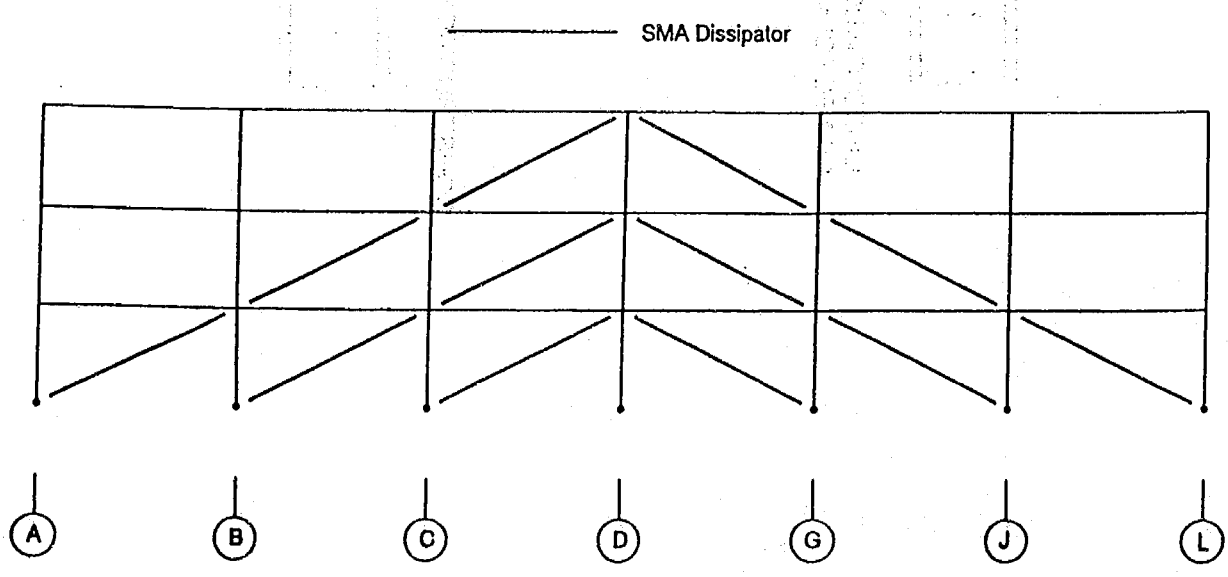


Figure 15 UG2: SMA Energy Dissipator Layout

U.S.-Japan Cooperative Research Program on Composite and Hybrid Structures
- Research Plan and its Progress -

by

Isao Nishiyama [1] and Hiroyuki Yamanouchi [2]

ABSTRACT

The composite and hybrid structural research project [1] is being carried out in Japan and the U.S. cooperatively under the UJNR Panel on Wind and Seismic Effects. In Japan, the research started from 1993 fiscal under the co-sponsorship of the Ministry of Construction and private sectors such as the Building Contractors Society, the Kozai Club, the Building Center of Japan and the Japan Structural Consultants Association, which constitute domestic cooperative research as shown in Figure 1 (Chairman: Prof. H. Aoyama, Nihon Univ., Vice-chairman: Prof. A. Tanaka, Utunomiya Univ.). Meanwhile in the U.S., the National Science Foundation has just started its supports from 1994 fiscal. This report summarizes the Japanese side research plan and its progress.

The project is sub-divided into four research topics; Concrete filled steel tube structure (CFT), reinforced concrete column with steel beam structure (RCS), reinforced concrete core wall with exterior steel frame structure (HWS), and innovative new materials, elements and systems for composite and hybrid structures (RFI).

Key Words:
Concrete Filled Steel Tube,
RC Column with Steel Girder,
Core Wall with Exterior Steel Frame,
New Materials and Systems

1. RESEARCH ON CFT

1.1 Basic Consideration

There are many experimental and analytical studies on CFT systems which are reported in technical journals. First, the strength and ductility of the CFT systems are predicted by processing these data. Secondly, the effectiveness of these predictions will be verified by supplementary experimental studies. As the materials strengths in use are quickly increasing recently, wide range of structural steel strength and concrete strength will be considered to verified the applicability of the predictions.

1.2 Research Items And Its Progress

(1) Experimental Study

The objectives of the experimental study are to evaluate the synergistic effects of structural steel tube and filled concrete and to evaluate stress transfer mechanisms in beam-to-column connections. So as to clarify these problems, the following experiments were planned with several study parameters.

a) Experiments
1) stub-column tests
2) stub-column eccentric loading tests
3) beam-column tests
4) beam-to-column connection tests
5) frame tests

b) Study Parameters
1) tube shapes (circular, rectangular)
2) tube strengths (400, 600, 800 MPa)
3) width-to-thickness ratio
(FA, FC, FD-rank*1)
4) concrete strengths (20, 40, 80 MPa)
5) connection details (diaphragm, etc.)

*1 FA-rank of width-to-thickness ratio means that large member ductility is expected thanks to its compact section. FC-rank means that it can at least assure the yield strength of the member without deterioration. The width-to-thickness ratio of FD-rank is chosen as 1.5 times of that of FC-rank.

---

1) Head, Structural Dynamics Division, Structural Engineering Department, Building Research Institute (BRI), Ministry of Construction (MOC), Tatehara-1, Tsukuba, Ibaraki 305, Japan.
2) Director, Structural Engineering Department, BRI, MOC.

Ninety stub-column tests on circular or square hollow sections were already completed. As the specimen dimensions selected are relatively large, and material strengths of structural steel and concrete are also large, the maximum test strength reached 1,400 tonf. As for the stub-column eccentric loading tests, sixty specimens have been completed. The maximum strengths of the specimens are shown comparing with calculated ones on the moment versus axial force diagrams in Figures 2 and 3.

As for the beam-column tests, 16 rectangular and 12 circular specimens were planned. They are now under fabrication. The constant axial thrust of 40% yield strength will be mainly investigated with varying structural steel strengths (400, 600, 800MPa), concrete strengths (40, 90MPa) and width-to-thickness ratios (FA, FC-rank).

(2) Literature Survey

First, the predictions of the stiffness, strength and ductility of the CFT systems are carried out by literature survey. Then, the validity and limits of the application of these predictions will be verified experimentally.

To facilitate exchange of experimental data, database will be published.

(3) Theme Structure Study

Structural designs of 10, 20 and 40 storied CFT moment frame buildings and CFT dual system buildings were conducted. In the structural design, CFT member strength was calculated based on the simple (generalized) superposing method proposed in the AIJ-SRC standards [2]. The buildings with the same geometry were also designed as pure steel buildings. The total amount of structural steel, which is the index for estimating the economy of buildings, used for CFT buildings was compared with that used for pure steel buildings. In this comparison, CFT showed advantages over pure steel especially for higher buildings. The economical difference in CFT buildings with/without bracings was not large. It was because that the weight of bracings and the weight increase in the braced bay frame compensate with the weight reduction of other frames which carry less horizontal force.

It is also planned in the design implementation study to take into account for the confined effect, which will be verified later in the experiments.

2. RESEARCH ON RCS

2.1 General

In Japan, a great number of beam-to-column sub-assemblage tests on RCS systems have been conducted. However, most of them are just proof tests to verify the performance of the sub-assemblages which were designed as weak beam systems. Therefore, these test results gives us little information on the shear strength and ductility of the beam-to-column joint panels in the ultimate stage.

Therefore, the experimental study in this research is planned to obtain the ultimate strength and ductility of the beam-to-column joint panels by making the specimens to be intentionally weak in panels.

2.2 Research Items And Its Progress

(1) Literature Survey

There are two items. One is to review existing research papers. In the review, classification of the experimental data (details and geometry of specimens) and picking up the design equations for evaluating shear strength of the joint panels are undertaken. This job finished in 1994 fiscal. The report will be summarized in 1995 fiscal.

The other item is to make out of the experimental database. In the database, the information of the load versus displacement relationships will just be included as the turning point information (peak strength and peak displacement etc.) but not as a whole curve. The collection of about 380 test data was completed and the summarization of the database is in its final stage.

(2) Beam-To-Column Connection

a) Through Beam Type Joint Tests

Six exterior beam-to-column connections with through beam type joint details as shown in Figure 4 were tested. In these tests, the effects of transverse beams, band plates, cover plates and face bearing plates are compared each other with the specimens of the same dimensions and the same material strengths.

The prompt results show that the effects of cover plates and band plates are almost identical and feasible of superposing.

The stress transfer from inner concrete panel to outer concrete panel in the through beam type beam-to-column joint panels were also investigated by specially devised specimens.

b) Through Column Type Joint Tests

Ten interior beam-to-column specimens were planned with through column type details. Figure 5 shows the differences in the shape of the specimens schematically. In these tests, the effects of vertical stiffeners and the cover plates will be investigated. About half of the specimens were completed and the results will be soon distributed.

c) FEM Analyses With Basic Tests

Elastic and inelastic characteristics of bond and friction between concrete and steel were investigated by basic experiments. The material model in 3D-FEM is revised taken on account the results.

The six exterior beam-to-column specimens mentioned above were carefully analyzed by 3D-FEM which resulted in good agreements both in the yield strength and the shear stress distribution in the joint panel.

3. RESEARCH ON HWS

3.1 General

The structural system of core wall with exterior steel frame is not common in Japan and its design method is not established yet. So, twelve storied theme structure was first designed and the design problem picked up during the design was investigated. Then, the design implication will be expanded into much higher or lower systems. The rationality of the designed system will be verified through the analytical and experimental studies.

3.2 Research Items And Its Progress

(1) Coupled-Shear Wall Test

One-third scale model of 12 storied coupled-shear wall test is planned as shown in Figure 6. In the test, the forces acting in each member is required to be measured so as to understand the force re-distribution in the coupled-shear walls and boundary beams for design purpose. As a preliminary test for the coupled-shear wall test, test on load cell put into boundary beams in coupled-shear wall has been conducted. It was verified that the load cell accurately picks up shear force and axial force which was transmitted through the boundary beam. The load cell also did not affect the overall behavior of boundary beam at least up to the drift angle of 0.05 radian, which was verified from the tests.

(2) T-Shape Shear Wall Test

So as to understand the stiffness, strength and deformability of 3D-wall is essential for the design implication to HWS systems. Three one-third scale T-shaped shear wall specimens without boundary columns, which represent the walls of the lowest story of the 12 storied prototype HWS system, were conducted. The shear force and flexural moment with different moment-to-shear ratios were applied with varying axial forces. Figure 7 shows the load versus displacement relationships of three specimens.

(3) Literature Survey

About eighty papers on boundary beams and thirty papers on RC wall to steel beam connections were surveyed. As for the inelastic behavior of the boundary beams, the past analytical and experimental information can be considered to be enough for design purpose. On the other hand as for the RC wall to steel beam connections, the isolated joint strength tests can only be found in the reports and no sub-assemblage tests are found. From this viewpoint, some verification test may be necessary for RC wall to steel beam connection. However, as the flexural stiffness of the steel beam with long span is very small and the rotational deformability of the joint itself is not so large, the experiment is not considered at present.

(4) Theme Structure Study

First, twelve story model building was designed on the basis of the general Japanese design concept. The strength of the building is too large to be investigated as the target structure to be developed. Then, the building was revised considering the design concept for the coupled-shear wall in New Zealand [3]. In New Zealand practice, earthquake load is

distributed to each wall according to the overturning moment ratio carried by boundary beams. As the building still has large overstrength, the reinforcements in the core walls are intentionally reduced to reach reasonable strength level, 35 percent of the base shear coefficient. These buildings are investigated whether they perform well or not under the seismic effects through the dynamic inelastic analyses using fish-bone model or frame model.

4. RESEARCH ON RFI

At present, the following two research groups for "Fiber reinforced plastic (FRP) elements" and "High performance concrete (HPC)" are organized. Other themes on, for example, "New type of structural system", "Hinge device system", "Recycle of structural members", "High performance steel" and "Intelligent material" are now being studied on their feasibility as the research themes of RFI.

4.1 FRP Research Plan

The research program on effective utilization of FRP materials for composite and hybrid structures contains three research items as follows. These items were selected through the feasibility study on effective utilization of FRP.

a) Development of the evaluation method for high-performance FRP-RC panels.

b) Development of the effective repair and/or strengthening method by using FRP for existing RC members.

c) Feasibility study on the effective utilization of FRP to the electrical facilities.

The research term is from the fiscal year of 1994 to 1997. Participants on the research group are 20 from industries, 2 from university and 2 from BRI.

4.2 HPC Research Plan

There are few cooperative research between concrete makers and structural designers in Japan. The makers have many technologies but they don't know how to use it. On the other hands, designers have a few information about new technologies of concrete. But they have many hints about the idea of future concrete.

The main objective is to exchange the information of makers and structural designers to discuss about how to use effectively of the concrete materials to the structural members and how will be the future concrete. The research targets will be decided through this discussion. The keywords are as follows.

1) light weight with high strength
2) high tensile strength and ductility
3) stiffness control
4) high energy dissipation
5) intelligent cementicious material

5. SUMMARY

The Japanese research plan and its progress is explained. The research is almost on schedule. The U.S. side research will soon. The problem to be solved at present is how to harmonize the work done by Japan and that will be done in future by both countries.

ACKNOWLEDGMENTS

The authors wish to express their great thanks to the members of Japan TCC (Technical Coordinating Committee) and those of TSC (Technical Sub-Committees) for their useful comments and suggestions.

REFERENCES

[1] "Recommendations for U.S.-Japan Cooperative Research Program - Phase 5 Composite and Hybrid Structures", Report No. UMCEE 92-29, November 1992.
[2] "AIJ Standards for Structural Calculation of Steel Reinforced Concrete Structures (1987)", Architectural Institute of Japan.
[3] T. Paulay and M. J. N. Priestley, "Seismic Design of Reinforced Concrete and Masonry Buildings", John Wiley & Sons, Inc.

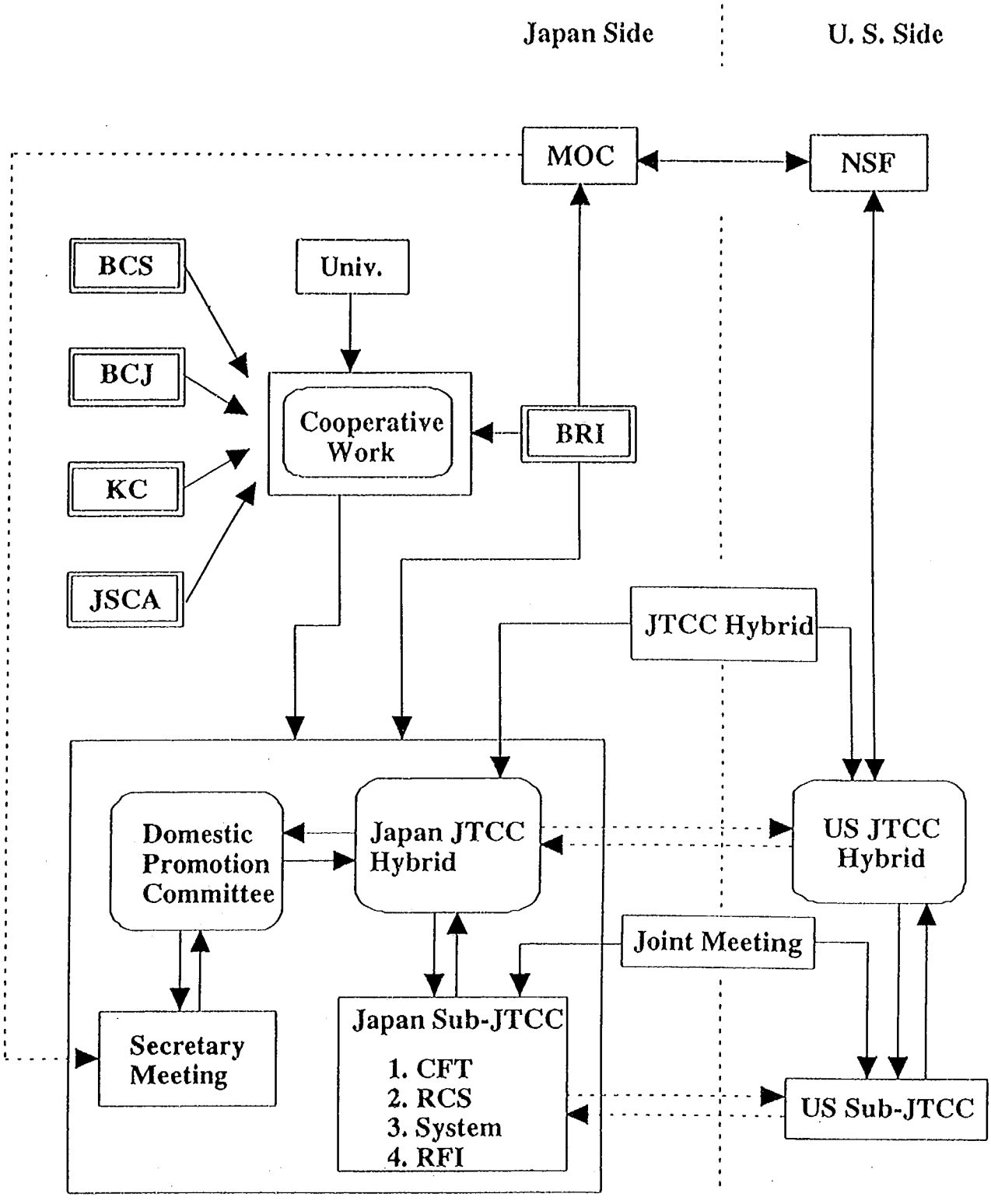


Figure 1 Organization of Cooperative Research

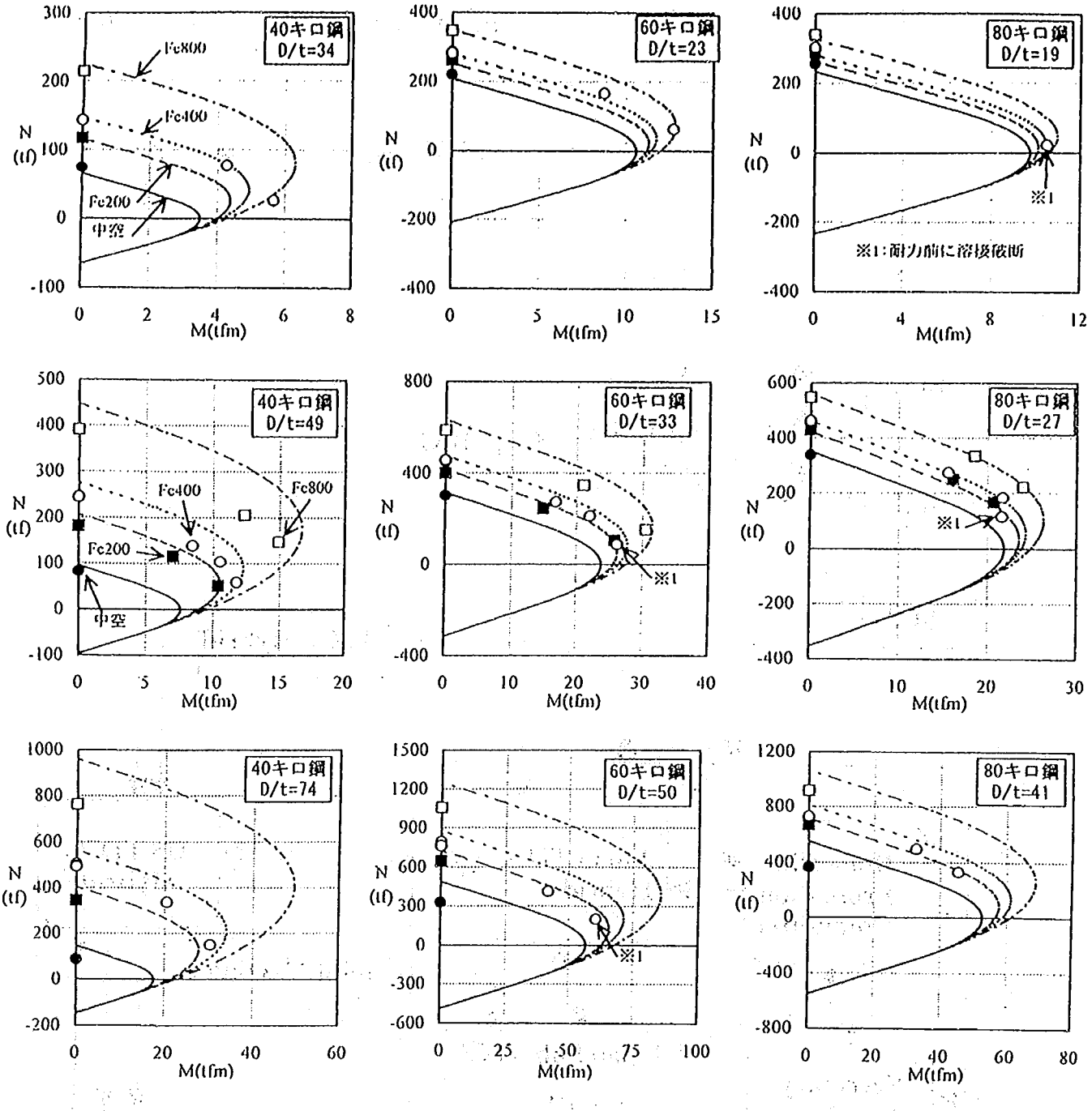


Figure 2 Moment versus Axial Force Diagrams of Concrete Filled Rectangular Tube Sections

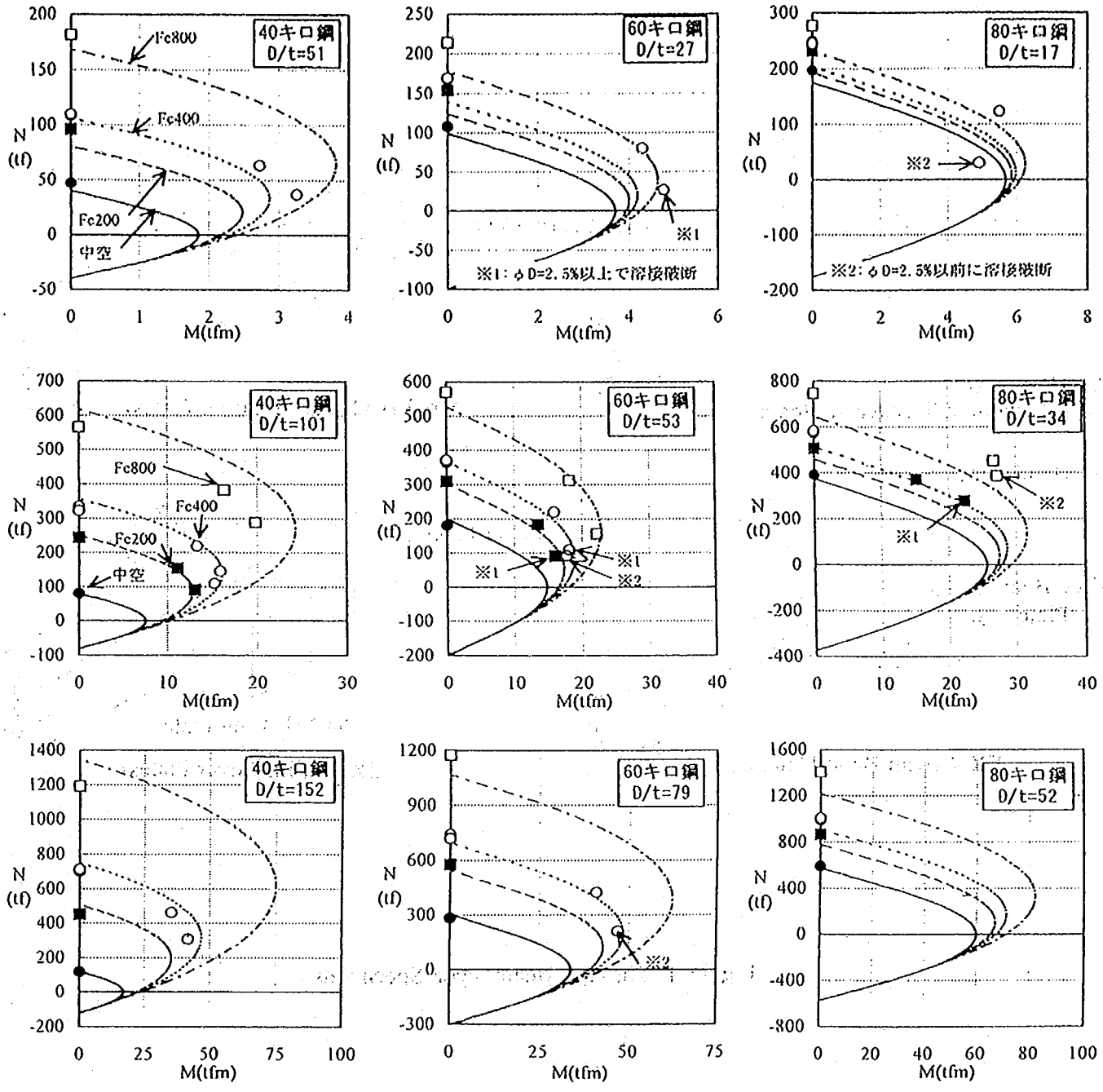


Figure 3 Moment versus Axial Force Diagrams of Concrete Filled Circular Tube Sections

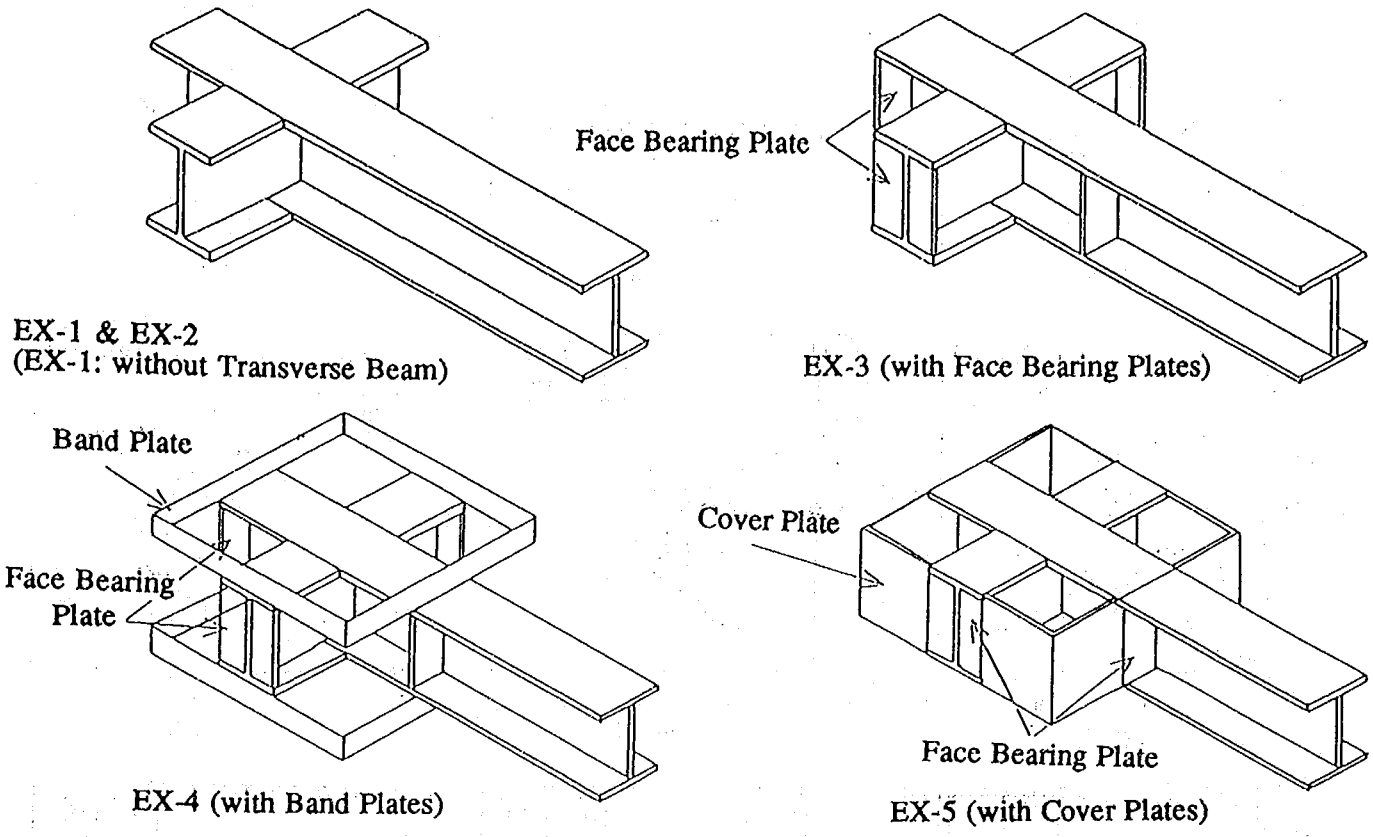


Figure 4 Through Beam Type Specimens

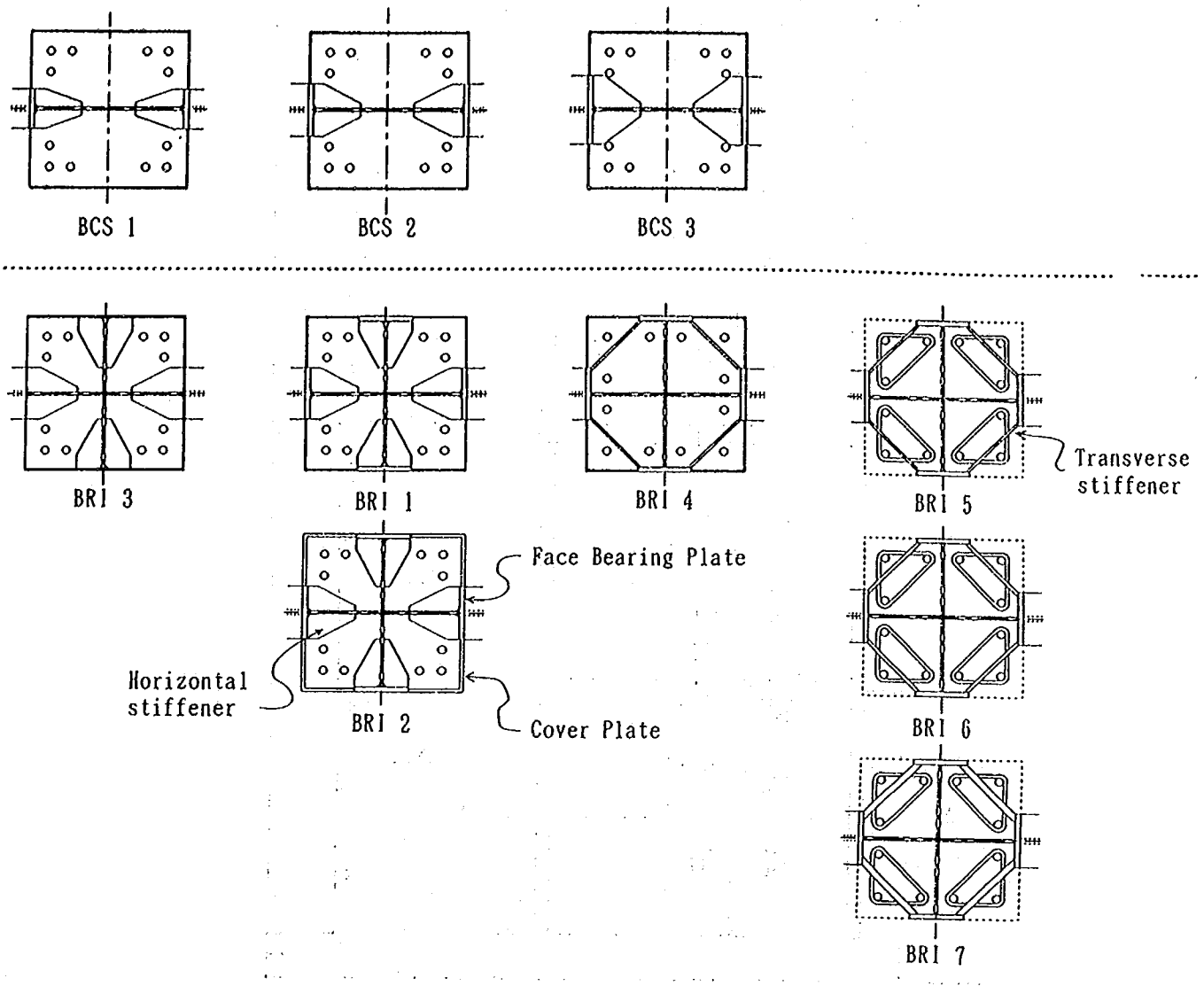


Figure 5 Through Column Type Specimens

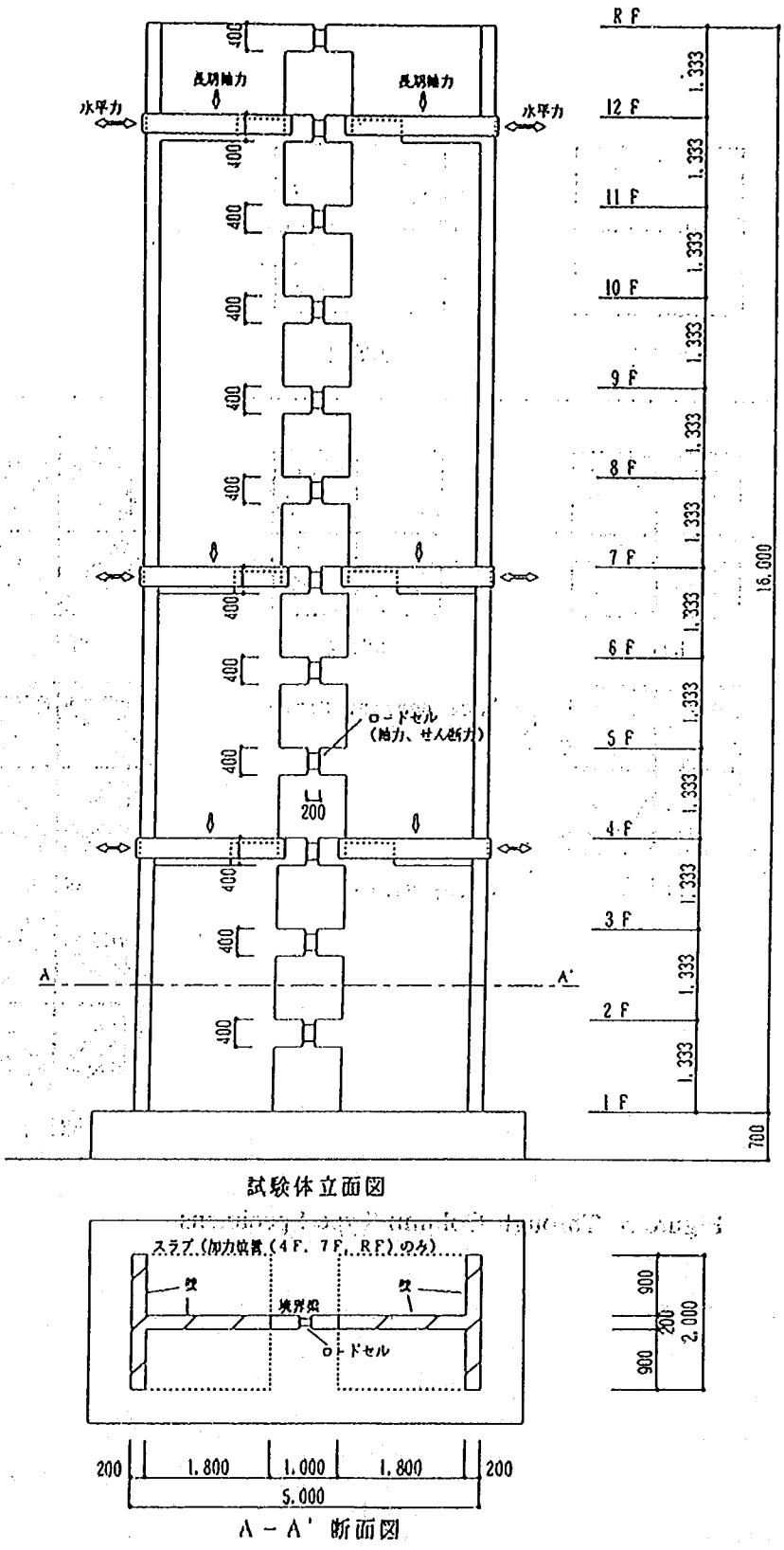


Figure 6 Planned Twelve Storied Coupled Shear Wall Specimen

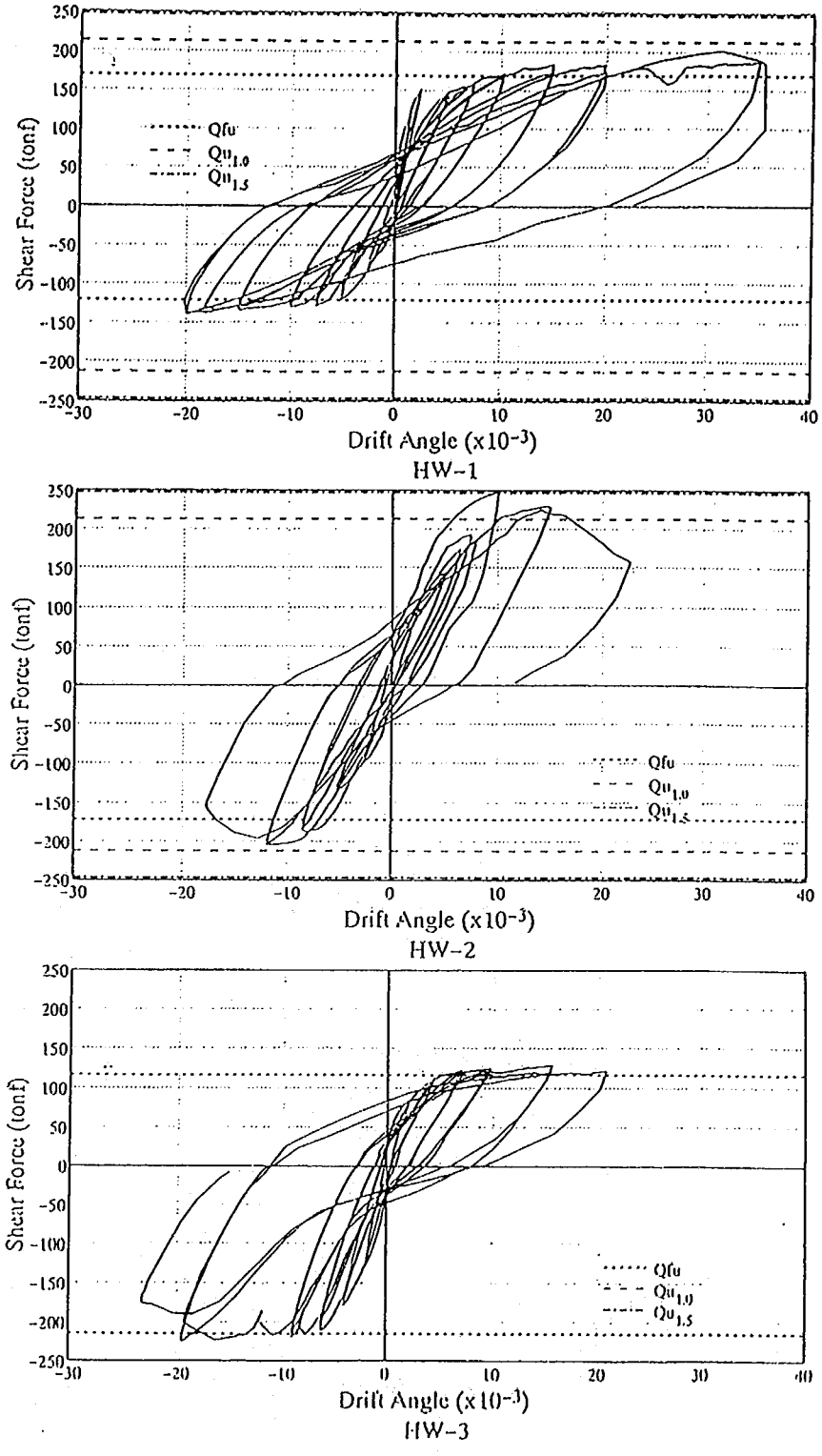


Figure 7 Load versus Displacement Relationships of T-Shaped Walls

Theme 2

Figure 3

Offshore Research Results from Hurricane Andrew

by

Charles E. Smith*

ABSTRACT

As a result of the passage of Hurricane Andrew through the Gulf of Mexico (GOM) on August 26, 1992, extensive damage was suffered by numerous oil and gas facilities located on the Outer Continental Shelf. Because of this damage, specially appropriated funds were provided to the Minerals Management Service (MMS) to investigate damage and to resolve matters affecting the status of safety, pollution prevention, and future regulations. A program known as the Hurricane Andrew OCS Damage Assessment (HAODA) Program was initiated by MMS, comprising joint participation by the oil and gas industry, private engineering companies, academia, and other Government agencies. The program consisted of two essential components: (1) engineering service contracts for assessing damage and evaluating repair techniques and (2) research contracts to gather and analyze engineering data pertaining to the forces on and responses of selected damaged facilities. The purpose of this paper is to provide an overview of the objectives of the HAODA Program initiatives, as well as the key results obtained.

KEYWORDS: Design standards; environmental data; hindcast studies; hurricane damage; offshore pipelines and platforms, research; screening methodologies.

1. INTRODUCTION

Hurricane Andrew was a relatively small but intense hurricane that passed through the Bahamas, cut across the Florida Peninsula, and made its way into the Gulf of Mexico (GOM). Although Hurricane Andrew's maximum-sustained winds were somewhat weaker than the winds associated with the other four major hurricanes which have impacted this region, it was extremely destructive and caused widespread damage to both onshore and offshore facilities. Table 1 provides a comparison between Andrew and the other major hurricanes relative to their minimum central pressures and maximum sustained surface winds.[1]

The damage to platforms and pipelines in the GOM by Hurricane Andrew was extensive and has been classified as the costliest of any storm in the history of offshore oil and gas operations.[2,3] Figure 1 illustrates the general path of the hurricane in respect to the oil and gas production regions of the GOM, and Figure 2 shows the relative density of offshore facilities. Of the 3,269 OCS facilities comprising approximately 4,000 platforms and 20,000 miles of pipelines, over 1,400 facilities were located in a band 50 miles wide to the east and 35 miles to the west of the track of the eye of the storm.

Within this 85 mile-wide path, a total of 55 platforms was destroyed or damaged. Of those, 29 were completely toppled at the time of the storm or were so severely damaged that they were removed later. Another 28 platforms were damaged to the point that they had to be removed from service until repairs could be made. In addition to the damaged platforms, 145 satellites or single-well caissons were damaged or lost to the extent that they had to be removed or repaired.

A total of 496 pipeline segments was also damaged during the storm either as a result of failure of a supporting platform, storm-induced soil movement, or from dragging anchors from drifting mobile offshore drilling units (MODU).

*Research Program Manager
Minerals Management Service
Herndon, Virginia 22070-4817

The largest oil spill, approximately 2,000 barrels, occurred when a MODU, which was moored in a mothball anchorage, broke loose and drifted past a 20-inch oil pipeline where its dragging anchor punctured the pipeline.[4]

Table 2 provides a summary of Hurricane Andrew damage to offshore facilities in the GOM. Considering the loss of oil and gas production, the repair costs for existing facilities, as well as the costs to remove lost or damaged platforms, the total economic impact of the storm may well exceed $2 billion. For comparison, Table 3 shows the number of platform failures in past hurricanes.

2. ASSESSMENT PROGRAM

Hurricane Andrew damage provided a rare opportunity to review and update facility design guidelines and construction standards used by the offshore industry for meeting the requirement of a 100-year, worst-case storm in the GOM.[5] Though Andrew was of storm category 4, it is not considered in most regions of the GOM to be the 100-year design event.

The MMS initiated a program to use this natural disaster to assess the impact of future hurricanes on offshore oil and gas facilities and pipelines. The initiative came to be known as the Hurricane Andrew OCS Damage Assessment Program, and was started with a special appropriation of $1.2 million. However, with the contributions from the oil and gas industry, these funds were leveraged about 3 to 1, and the total program cost was in excess of $3.5 million. The Program was designed to be a joint activity among the oil and gas industry, private engineering companies, academia, and other Government agencies. The HAODA Program was organized as shown in Figure 3 with the following major subsets (1) loss and damage assessments, (2) oceanographer and meteorological forcing functions and hindcast extrapolation to "worst-case" hurricanes, (3) failure modeling and analyses, and (4) design and inspection criteria with report of findings and recommendations.

3. Engineering and Research Projects

With the four subsets as a guide, the Program evolved into a series of 19 engineering and research projects as shown in Table 4. The following is a brief overview of the objectives of the HAODA projects:

- *Post Mortem Platform Failure Evaluation Study*--To use the results of Hurricane Andrew as a means to evaluate engineering methods for predicting potential platform failure or survivability by comparing screening analyses and/or detailed failure analyses against actual field data (i.e. platforms that were exposed to Andrew and either survived, collapsed, or were damaged).

- *Hurricane Andrew Platform Inspection and Analysis*--To provide an independent assessment of platforms subjected to severe storm loads as a result of Hurricane Andrew. The work was also provided to the American Petroleum Institute task group that has been given the charge to develop requalification and reassessment standards for aging facilities.

- *Study of Platform Failures*--To collect information gained from platform failures and survivals during Hurricane Andrew and apply this knowledge to a database for the future management of existing platforms.

- *Underwater Welding Repair Program*--To determine the state of the art of underwater wet welding and how the technology could be advanced by the developmental program for the repair of damaged platforms.

- *Further Evaluation of Offshore Structures Performance in Hurricane Andrew*--To develop separate bias factors for evaluation of pile foundations of GOM offshore steel jackets based upon their performance during Hurricane Andrew. Some similarly limited studies were also performed for caisson structures.

- *Evaluation Methodology for Existing Platforms in Hurricanes*--To develop and demonstrate a two-tier evaluation methodology for determining the adequacy of existing fixed offshore platforms. The first step of this methodology was envisioned to consist of a relatively easy matrix screening system incorporating more important and sensitive design parameters that may impact the actual adequacy of existing platforms. A platform which "passes" such a screening system would be deemed adequate and would not be subject to further evaluation.

- *Assessment of the Performance of Offshore Safety and Pollution Control Devices in the Aftermath of Hurricane Andrew*--To develop a reliability database that will increase the confidence in the methodology used to develop safety systems and pollution-control devices and thereby increase the safety of offshore developments.

- *Evaluation of Securing Procedures for Mobile Drilling Units Subject to Hurricanes*--To investigate failures associated with MODUs during intense GOM hurricanes. The study addressed jack-up units, drillships, drilling barges, and semisubmersible drilling units.

- *Shallow Water Hindcast Study of Waves and Currents Associated with Hurricanes*--To provide a comprehensive and reliable database of environmental data in shallow-water (as well as offshore) areas affected by Hurricane Andrew through the implementation and application of advanced numerical wave and current hindcast models.

- *Workshop on Hurricane Damage to Offshore Pipelines*--To provide a forum where damage to offshore oil and gas pipelines may be discussed. The workshop was intended to facilitate the exchange of information and promote discussions between representatives from oil and gas companies, pipeline operators, design engineers, regulatory agencies, and academic institutions on the integrity of offshore pipelines in the aftermath of severe storms, such as Hurricane Andrew.

- *Verification of Screening Methodologies for Damaged Platforms*--To further develop and verify the variability of Level 1 (qualitative scoring) and Level 2 (simplified quantitative) "screening" methods for the reassessment and requalification of offshore platforms in the GOM. The project utilized platform failure and survival experiences from past hurricanes including Andrew, Betsy, Camille, Carmen, and Hilda to verify and further develop the screening methodologies.

- *Evaluation of Hurricane-Induced Damage to Offshore Pipelines*--To investigate causes for the excessive damage experienced by offshore pipelines during Hurricane Andrew and to develop recommendations or changes to current design and operating procedures that will mitigate damage to pipelines during future hurricanes and minimize the resulting pollution.

- *Development of Damage Criteria for Caisson Structures*--To develop an acceptance criteria for those titled caissons and to develop guidelines for straightening those structures that did not meet the criteria.

- *Hurricane Andrew Effects on Offshore Platforms*--To analyze three platforms in South Timbalier field. Two survived Hurricane Andrew, the other toppled during the hurricane. The intent was to compare analytical predictions with actual field performance, with particular emphasis on individual member and platform system failure.

- *Inspection and Analysis of Three Damaged Platforms and Coordination of Data*--Conduct a physical inspection of three offshore platforms, including the development of inspection reports and subsequent nonlinear structural analysis to determine why the failures occurred and what could be done in the future to prevent failures.

- *Applicability of New Design Standards to Prevent Hurricane Damage to Caissons*--Review and compare API-RP2A 19th and 20th editions criteria specifically applicable to GOM caisson platform design. Assess impact of the 20th edition on a typical design representative of the GOM. Make recommendations commensurate with the findings of the study to prevent failures in hurricanes.

- *Benchmark Test of Design Standards for Hurricanes*--The objective of this task order was to test the methodology included in the draft recommendations prior to the formal issue within API-RP2A. Operators and engineering contractors involved in this test had the opportunity to voice their comments and suggestions regarding the draft recommendations based on "real" experience with their applications.

- *Digitization of Pipeline Locations in the GOM*--To develop a digitized database of all pipeline locations in the entire Federal portion of the GOM. There will be a companion effort to obtain data on pipeline locations in State waters off Louisiana and include these locations as a minimum in the total scope of the proposed effort. Thus, if failures were to occur, as from Hurricane Andrew, specific information on the operator, size, and location of pipelines, etc., would be available to assess damages and plan mitigation measures.

- *Andrew Joint Industry Project, Phase I and II*--To use a load and resistance procedure in the Phase I project to determine platform capacity and was updated based upon results of the Phase I analyses, other related projects, and participant input. These refinements were then incorporated into the existing computer models of the Phase I platforms for use in Phase II. The major effort in the Phase II project was the "tuning" of the recipe to most appropriately match observed field damage. The recipe was adjusted until the analytically predicted damage matched the observed damage as best as possible. The adjusted recipe will then be used as a basis for the analysis of future storm damage to platforms.

4. CONCLUSION

The damage to offshore oil and gas facilities and pipelines as a result of Hurricane Andrew was extensive. The engineering and research projects initiated under the HAODA Program have produced a wealth of data that have greatly increased the profession's knowledge of the integrity of offshore facilities subject to storm-induced loads. Of significance, the platform failures which occurred were predominately on structures installed before 1977 and were the result of wave-in-the-deck loading. In some cases, significant differences were observed between failed members identified by analyses and those observed during field inspections.Additional research is currently being conducted to establish the reasons for these differences. The majority of the pipeline failures can be contributed to the failure of these older structures and to the dragging of anchors from drifting MODUs. The data generated by the HAODA Program will be continually used by both the Government and the oil and gas industry to evaluate reassessment guidelines and design standards to mitigate future hurricane damage to the offshore infrastructure.

5. REFERENCES

1. Breaker, L.C., et al. (1994). "The Impact of Hurricane Andrew on the Near-Surface Marine Environment in the Bahamas and the Gulf of Mexico," Weather and Forecasting, Volume 9, American Meteorological Society.

2. Smith, C.E. (1993). "The Effects of Hurricane Andrew on Offshore Oil and Gas Facilities," Proceedings, International Workshop on Wind and Earthquake Engineering for Offshore and Coastal Facilities, Yokosuka, Japan.

3. Smith, C.E. (1993). "Offshore Platform Damage Assessment in the Aftermath of Hurricane Andrew," Proceedings, 25th Joint Meeting of the UJNR Panel on Wind and Seismic Effects, Tsukuba, Japan.

4. Daniels, G.R. (1993). "Hurricane Andrew's Impact on Natural Gas and Oil Facilities on the Outer Continental Shelf--Interim Report," OCS Report MMS 94-0031, Minerals Management Service, Herndon, Virginia.

5. Bea, R.G., et al. (1995). "Evaluation of Capacities of Template-Type Gulf of Mexico Platforms," Proceedings, 5th International Offshore and Polar Engineering Conference, The Hague, Netherlands.

Table 1 - Basic Characteristics of Major Hurricanes in the Gulf of Mexico

Name	Date	Intensity[a]	Minimum pressure (mb)	Maximum sustained winds ($m\ s^{-1}$)
Audrey	25-28 Jun 1957	4	940[b]	77-93[b]
Carla	3-15 Sep 1961	4	931	90[c]
Camille	5-22 Aug 1969	5	901	90[c]
Gilbert	10-17 Sep 1988	5	888	82
Andrew	16-28 Aug 1992	4	922	75

[a]Saffir/Simpson hurricane intensity scale

[b]Estimated value

[c]Peak value

Table 2 - Summary of Damage in the Gulf of Mexico During Hurricane Andrew

Damages	Number
Platforms Lost*	29
Platforms Damaged**	19
Platforms Minor Damages***	7
Total	55
Satellites Lost*	44
Satellites Damaged**	101
Total	145
Oil Spills Volume - 2,500 Barrels	11
Fires	2
Drifting MODUs	5
Damaged MODUs With Little Drift	5
Pipeline and Flowline Segments Damaged	496

NOTES

* Lost indicates damage so severe that the platform or satellite was completely toppled or was subsequently removed.

** Damaged indicates platform or satellite damaged to the extent that it was taken out of service until repaired.

*** Minor damage indicates considerable damage but the platform wasn't taken out of service.

Table 3 - Past Gulf of Mexico Platform Failures

Year	Number of Platforms* Failed* *	Hurricane
1948	2	Grand Isle
1949	1	Freeport
1957	2	Audrey
1961	4	Carla
1964	15	Hilda
1965	8	Betsy
1969	3	Camille
1985	1	Juan
	36	

* Platforms = Major Drilling (6+ Wells) and/or Production Platforms

** Failed = Collapsed or Rendered Unserviceable and Salvaged

Table 4 - Hurricane Andrew OCS Damage Assessment Program Projects

	Project	Contractor
1.	Post Mortem Platform Failure Evaluation Study	PMB Engineering, Inc.
2.	Hurricane Andrew Platform Inspection and Analysis	W. H. Linden & Associates
3.	Study of Platform Failures	PMB Engineering, Inc.
4.	Underwater Welding Repair Program	Global Divers Contractors
5.	Further Evaluation of Offshore Structure Performance in Hurricane Andrew	PMB Engineering, Inc.
6.	Evaluation Methodology for Existing Platforms in Hurricanes	International Design, Engineering and Analysis, Inc.
7.	Assessment of the Performance of Offshore Safety and Pollution Control Devices in the Aftermath of Hurricane Andrew	J. P. Kenny, Inc.
8.	Evaluation of Securing Procedures for Mobile Drilling Units Subject to Hurricanes	Noble, Denton & Associates
9.	Shallow Water Hindcast Study of Waves and Currents Associated with Hurricanes	Oceanweather, Inc.
10.	Workshop on Hurricane Damage to Offshore Pipelines	Project Consulting Services
11.	Verification of Screening Methodologies for Damaged Platforms	University of California @ Berkeley
12.	Evaluation of Hurricane-Induced Damage to Offshore Pipelines	Southwest Research Institute
13.	Development of Damage Criteria for Caisson Structures	Barnett and Casbarian, Inc
14.	Hurricane Andrew's Effects on Offshore Platforms	PMB Engineering, Inc.
15.	Inspection and Analysis of Three Damaged Platforms and Coordination of Data	PMB Engineering, Inc.
16.	Applicability of New Design Standards to Prevent Hurricane Damage to Caissons	PMB Engineering, Inc.
17.	Benchmark Test of Design Standards for Hurricanes	PMB Engineering, Inc.
18.	Digitization of Pipelines Locations in the Gulf of Mexico	NOLA Computer Services
19.	Andrew Joint Industry Project Phase I & II	PMB Engineering, Inc.

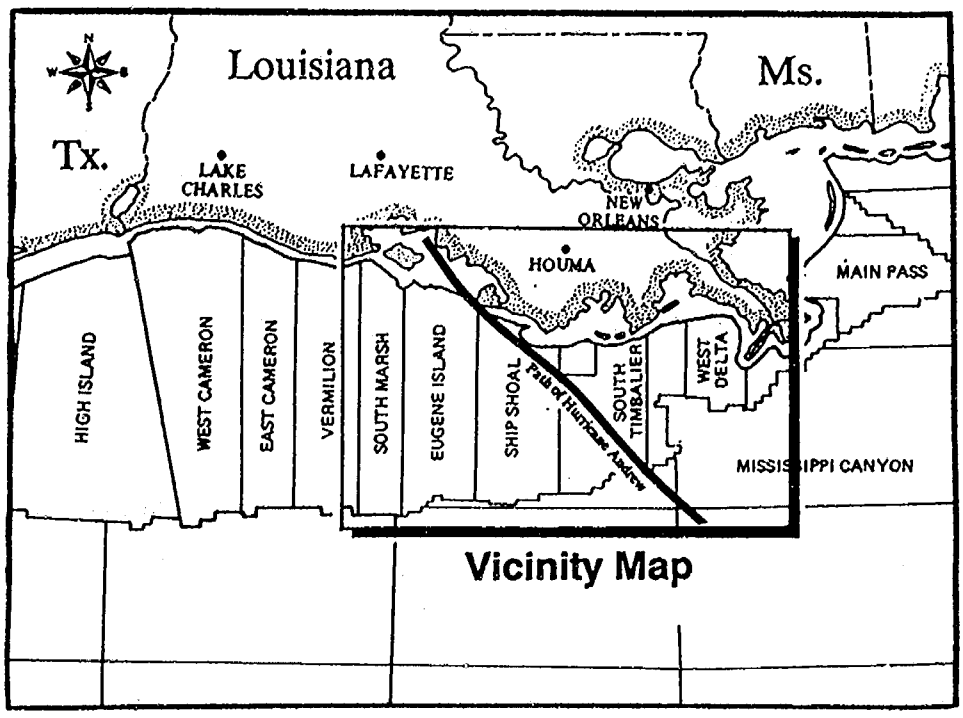


Figure 1. Path of Hurricane Andrew through the Gulf of Mexico

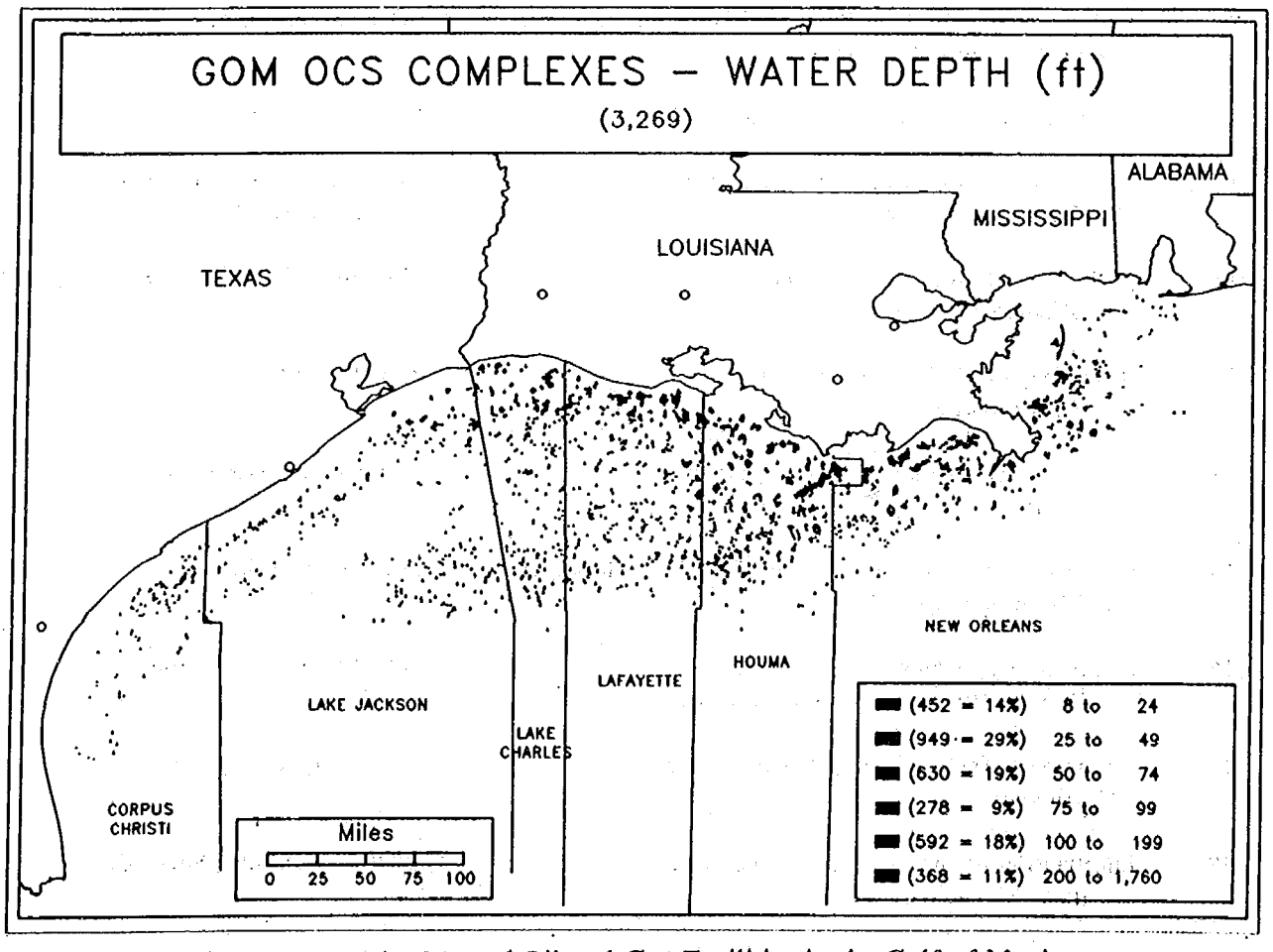


Figure 2. Density Map of Oil and Gas Facilities in the Gulf of Mexico

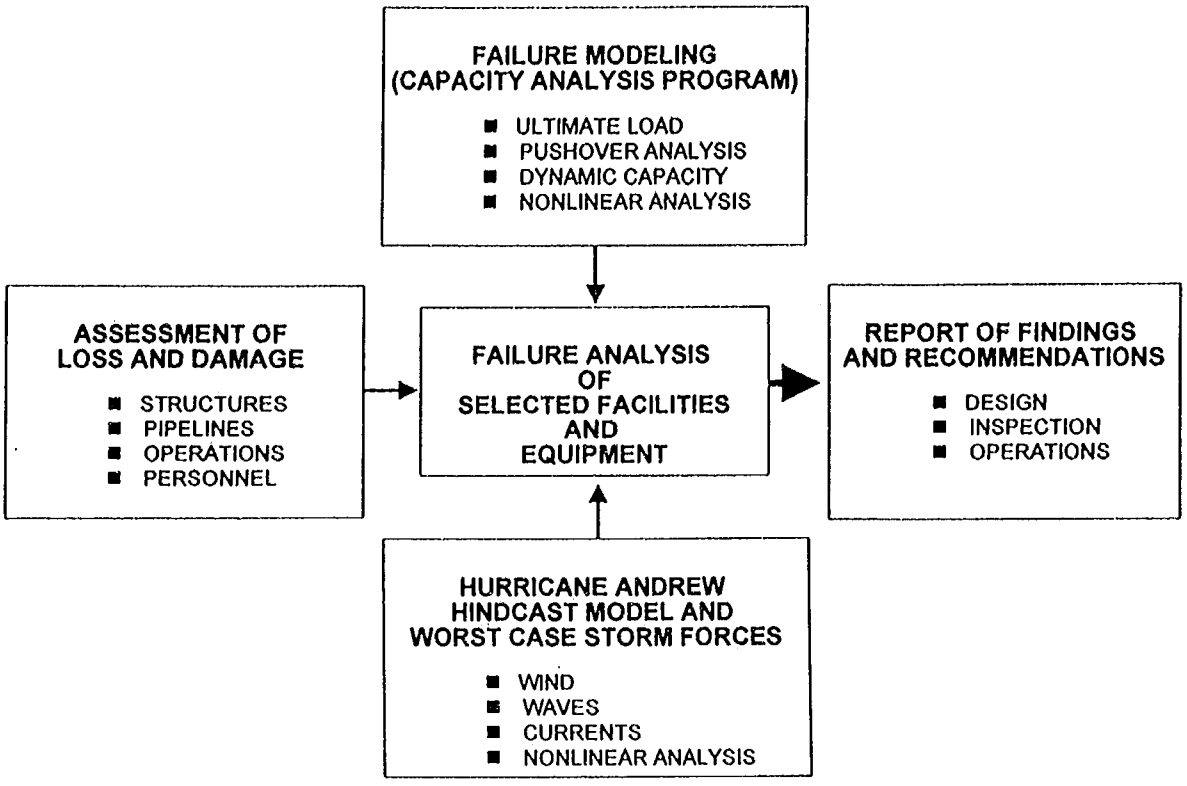


Figure 3. Subsets of the HAODA Program

Wind-Induced Vibrations of a Super Long-Span Cable-Stayed Bridge in Turbulent Flow Generated by Surrounding Islands

by

Hiroshi SATO[1], Makoto KITAGAWA[2], Ryuichi TORIUMI[3] and Hiroshi KATSUCHI[4]

ABSTRACT

Wind-induced vibrations of the Tatara bridge, which is a super long-span cable-stayed bridge whose center span length is 890m, was investigated through wind tunnel test using 1/200 full aeroelastic model in turbulent flow generated by the model of surrounding islands. From the wind tunnel experiment, it was found that the topography increased the gust response significantly when wind direction was 36 degrees clockwise from the north direction normal to bridge axis. The main reasons for the large gust response seem to be high turbulence intensity and high space-wise correlation caused by the surrounding islands.

KEYWORDS

Wind-induced vibrations, Super long-span cable-stayed bridge, Full aeroelastic model, Wind tunnel test, Turbulent flow, Surrounding Islands

1. INTRODUCTION

The Tatara Bridge, which is under construction in Japan, is a super long-span cable-stayed bridge (Fig.1, Photo 1). The center span length of the bridge will be 890m, which is 34m longer than that of the Normandie Bridge in France, the world's longest cable-stayed bridge at present. For such a long span bridge, it is very important to evaluate the aerodynamic stability of the bridge before its construction. Since the main span length of the Tatara bridge is beyond our experience, it was thought that accurate wind tunnel test using a full aeroelastic model should be conducted in the Large Boundary Layer Wind Tunnel in PWRI. The wind tunnel test in smooth flow using 1/70 full aeroelastic model was conducted, and already reported in the previous Joint Panel Meeting (1).

The Tatara bridge will be surrounded by islands as shown in Fig.2. Some of the islands have high mountains up to 400m above the sea level. Therefore, it was considered that topographical effect should be studied using topographical model.

This paper reports the wind tunnel test result in turbulent flow generated by the model of surrounding islands.

2. WIND CHARACTERISTICS AT THE CONSTRUCTION SITE

In order to clarify wind characteristics such as mean wind speed, wind direction, attack angle, and turbulence intensity, an anemometer was installed at the construction site of the Tatara Bridge. Wind tunnel test was also carried out using 1/2000 scale topographical model of the terrain around construction site (See Fig. 2). The measured data at the site was used in order to calibrate the topographical wind tunnel test (See Fig. 3).

Fig. 4 shows the wind flow pattern measured in the wind tunnel test. From the figure, it can be

1)Head, Structure Div., Structure and Bridge Dept., PWRI
2)Manager, First Design Div., Design Dept., Honshu-Shikoku Bridge Authority
3)Deputy Manager, First Design Div., ditto
4)First Design Div., ditto

seen that wind characteristics at the site are very complicated. For example, in the case of wind direction of NNW and SSE, a topographical effect is hardly recognizable. In other words, wind speed and turbulence intensity were scarcely changed by the topography. On the contrary, in the case of wind direction such as NE and W, wind characteristics were changed significantly by the topography. Particularly, in the case of NE direction, the turbulence intensity was considerably increased by the topography, but the wind speed was not remarkably decreased. In the design of the long-span bridge, these wind characteristics were thought to be critical. Therefore, it was thought that the topographical effects on the bridge must be studied in the wind tunnel test with bridge model and topographical model.

3. AEROELASTIC FULL MODEL OF THE TATARA BRIDGE

The scale ratio of the model was determined as to 1/200 considering the size of the wind tunnel, integral scale of turbulence and topographical model to be represented inside the wind tunnel.
Froude number similitude was not adopted to the design of the model, because the wind speed ratio 14 according to Froude number similitude seemed too large to measure wind-induced vibration accurately. The model was fabricated a little stiffer than the Froude number similitude required. The wind speed ratio was about 8.
The model was designed by well known methods, i.e. steel frame was designed to achieve proper stiffness, additional mass was installed to simulate mass and polar moment of inertia, and the frame and additional mass were covered with exterior wooden forms to simulate geometrical shape. Each three cables of the real bridge was represented by one piano wire in the model. Mass of the cables were equally distributed to the tower and the girder.
Fig.5 and Photo 2 show the model of the Tatara bridge in the Large Boundary Layer Wind Tunnel. Free vibration tests in windless condition were carried out to check the dynamic characteristics of the model. Table 1 shows the measured natural frequency and logarithmic damping decrement of the model. The damping of vertical bending mode was a little larger than the target value of 0.02, and the damping of lateral bending mode was a little smaller.

4. WIND TUNNEL EXPERIMENTS OF THE BRIDGE AND TOPOGRAPHY

Wind tunnel experiments were carried out for three cases of wind direction, namely 18, 36 and 180 degrees (See Fig. 4). Wind direction was defined clockwise from the north direction normal to bridge axis. Three directions were chosen because they were thought to be critical from the design point of view. That is, the mean wind speed for 18 and 36 degrees was not noticeably decreased, while turbulence intensity was considerably increased. The wind direction of 180 degrees, normal to the bridge axis, was the prevailing wind at the site. The increase in turbulence intensity due to Hakata Island located in the south of the bridge site was expected to be small.
Wind tunnel experiments were conducted both with and without topographical models. In both cases, approaching flow had slight turbulence generated by spires and roughness blocks.
Fig. 6 shows the rms value of the lateral gust response of the girder at the design wind speed. The experimental results with the topographical models are compared with those without topographical models in these figures. In the case of 18 and 180 degrees, the topographical effect is hardly recognizable because there is little difference in the rms values. On the other hand, in the case of 36 degrees, the topography increased the gust response significantly.
Fig. 7 shows the relationship between the rms value of gust response without the topographical model and mean wind speed along main wind direction at the mid-point of the center span girder. Gust response becomes larger as the wind direction becomes normal to the bridge axis, but this effect is not so remarkable.

Fig. 8 shows the experimental results with the topographical models. The gust response at the yaw angle of 36 degree is much larger than the other two angles.

5. DISCUSSION

According to the quasi-steady theory, aerodynamic force due to approaching turbulence increases with square of mean wind speed and turbulence intensity. Fig. 9 shows the wind characteristics along the bridge axis in the three wind directions. In the case of 36 degrees, a significant increase in turbulence intensity along the bridge axis is recognized. However, the increase in turbulence intensity is associated with decrease in mean wind speed.

Another factor that influences the gust response of long-span bridges is correlation of fluctuating wind speed at different places. Table 2 shows turbulence intensity and integral scale of turbulence at the mid-point of the center span in case of 36 degree. It can be seen that the integral scale as well as intensity was increased very much by the topographical model. Fig. 10 shows co-coherence of fluctuating wind speed at two places on the bridge axis. It can be seen that the correlation is much higher in case of 36 degree than in case of 180 degree.

From these measurements, it seems that the large gust response in case of wind direction 36 degree was caused by high turbulence intensity and high space-wise correlation of the turbulent flow generated by the topographical model.

In order to discuss the topographical effects quantitatively, analytical studies on the gust response are now in progress. The wind resistance of the bridge will be thoroughly evaluated based on the studies.

6. CONCLUSION

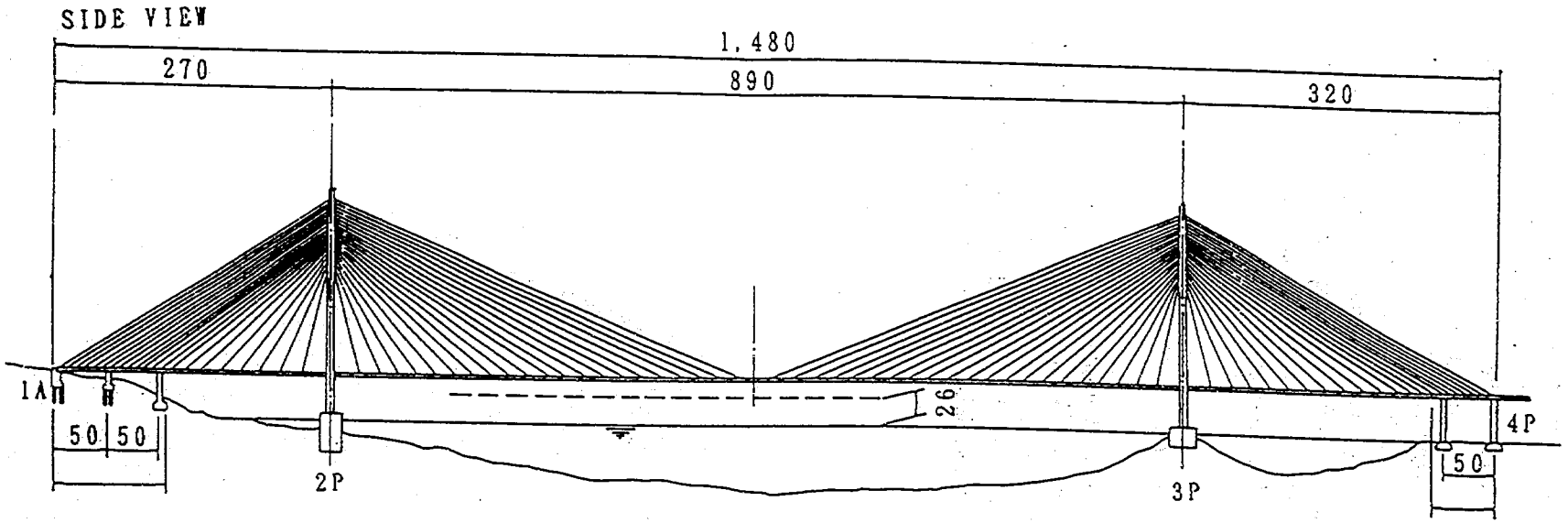
Through wind tunnel test using 1/200 full aeroelastic model in turbulent flow generated by the model of surrounding islands, the gust response of the Tatara bridge was investigated.

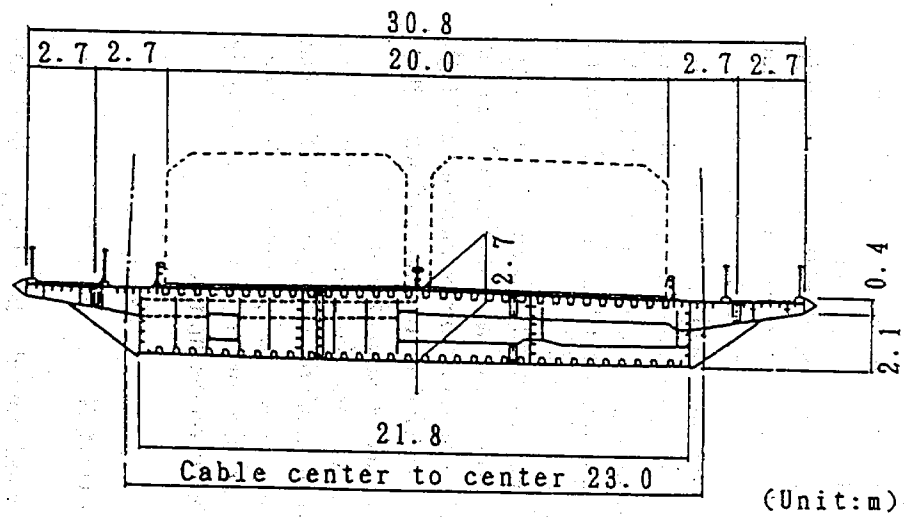
When wind direction was 18 and 180 degrees clockwise from the north direction normal to bridge axis, the topographical effect was hardly recognizable. On the other hand, in the case of 36 degrees, the topography increased the gust response significantly.

The main reasons for the large gust response measured in case of wind direction 36 degree seem to be high turbulence intensity and high space-wise correlation caused by the topographical model.

REFERENCES

1)Sato H., Toriumi R., Kitagawa M. and Katsuchi H, Wind Tunnel Experiment for a Super Long-Span Cable-Stayed Bridge in Smooth Flow, Proc. of 25th Joint Panel Meeting on Wind and Seismic Effects, UJNR, 1993.





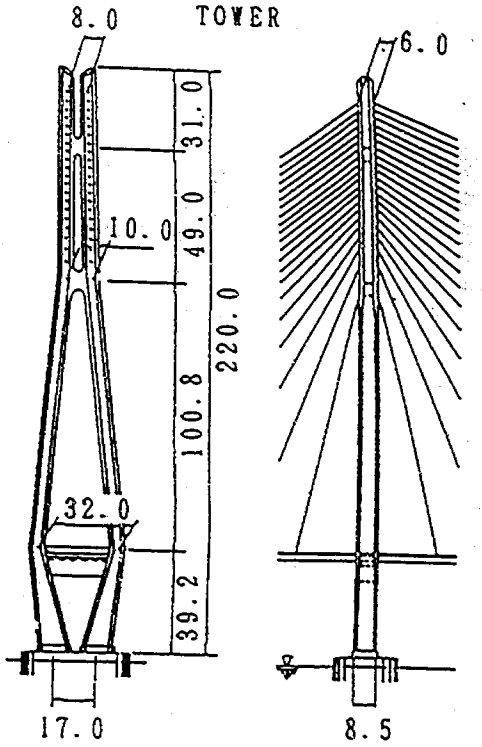


Fig.1 Tatara Bridge

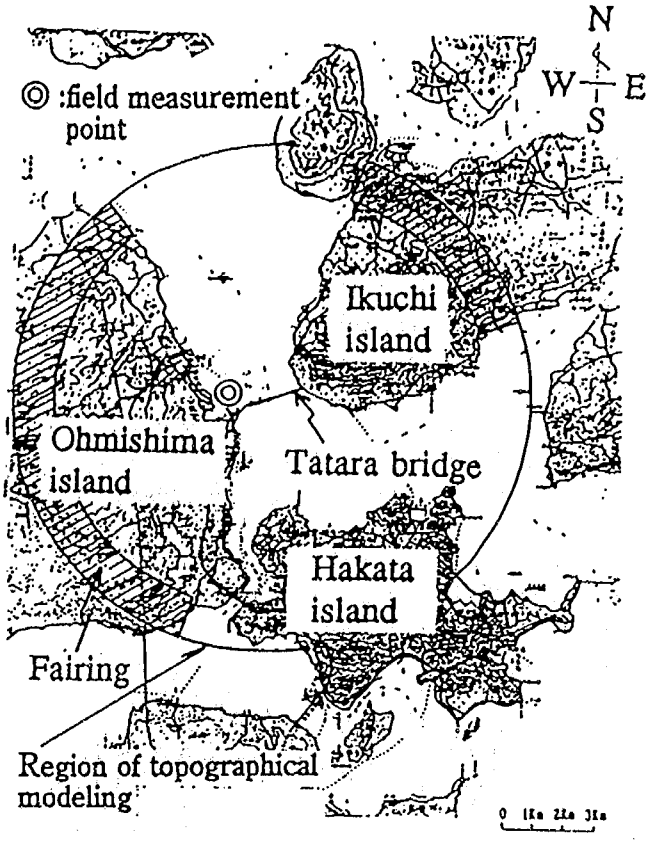


Fig.2 Location of Tatara Bridge and region of topographical modeling

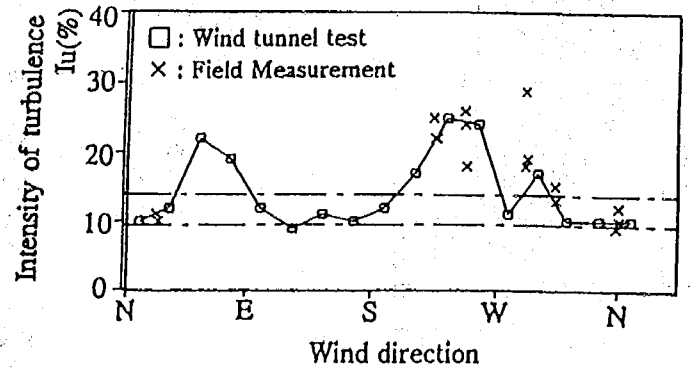


Fig.3 Turbulence intensity at field measurement point

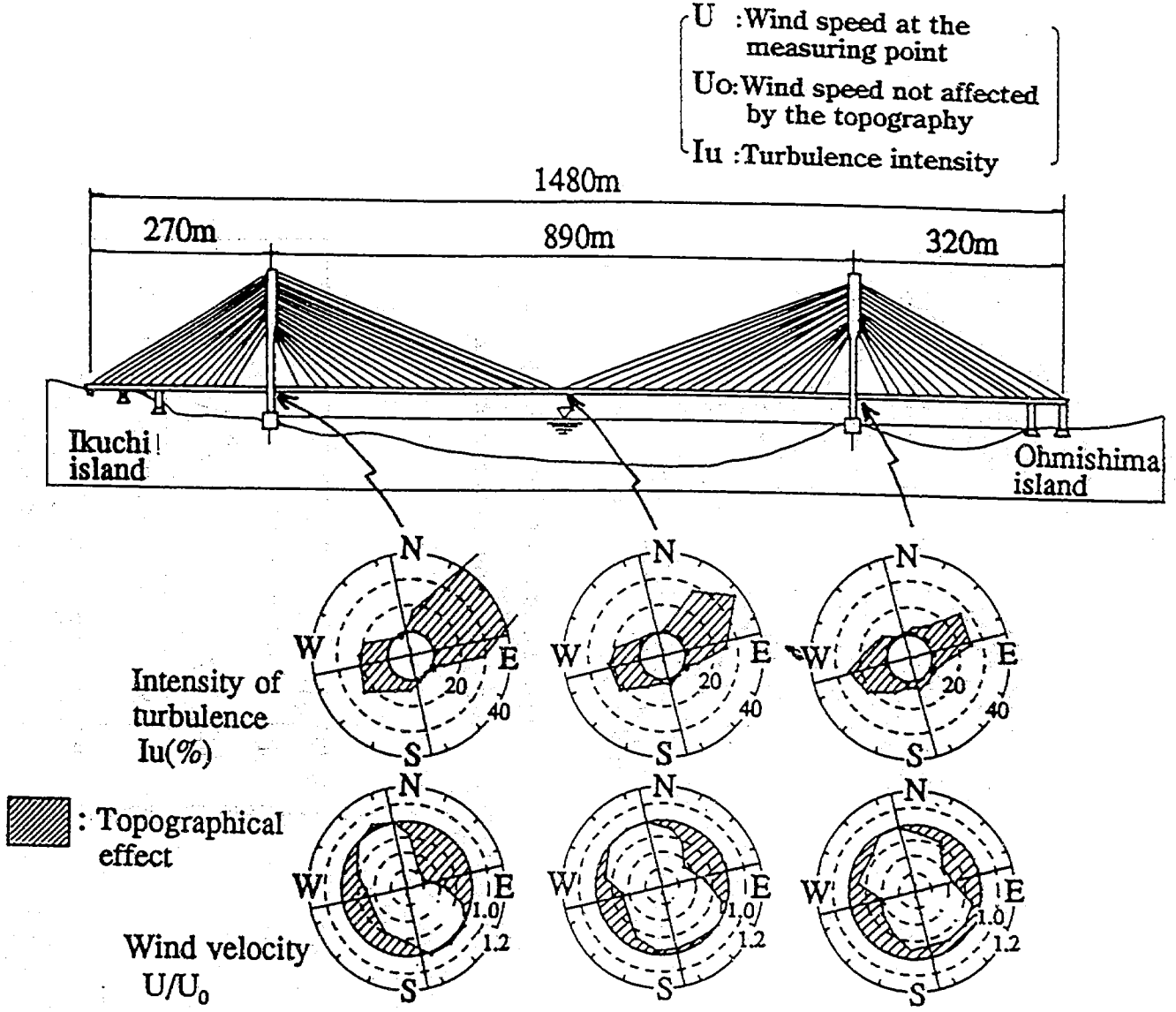


Fig.4 Wind flow pattern at Tatara Bridge construction site

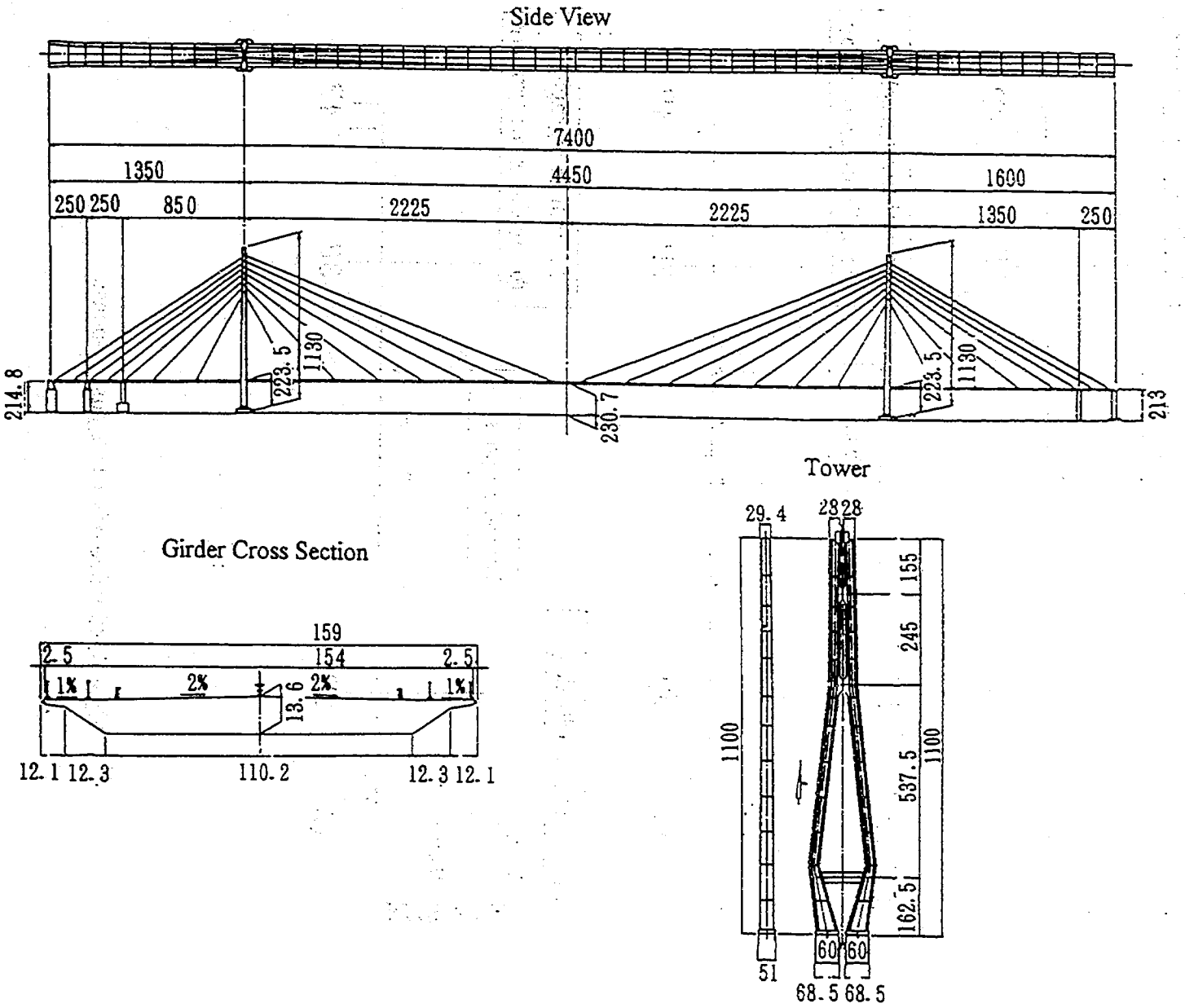


Fig.5 Model of Tatara Bridge

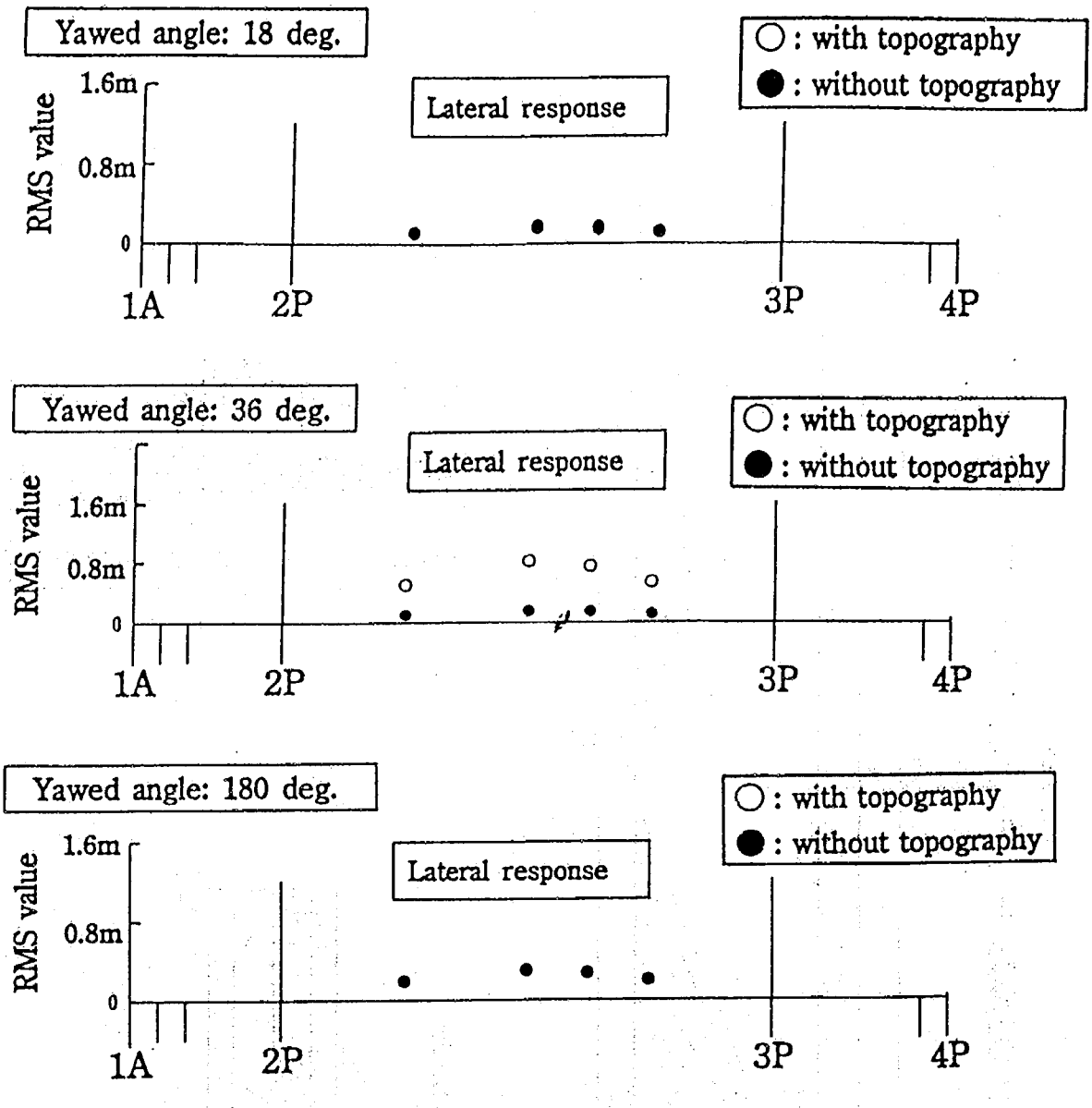


Fig.6 RMS value of girder's gust response

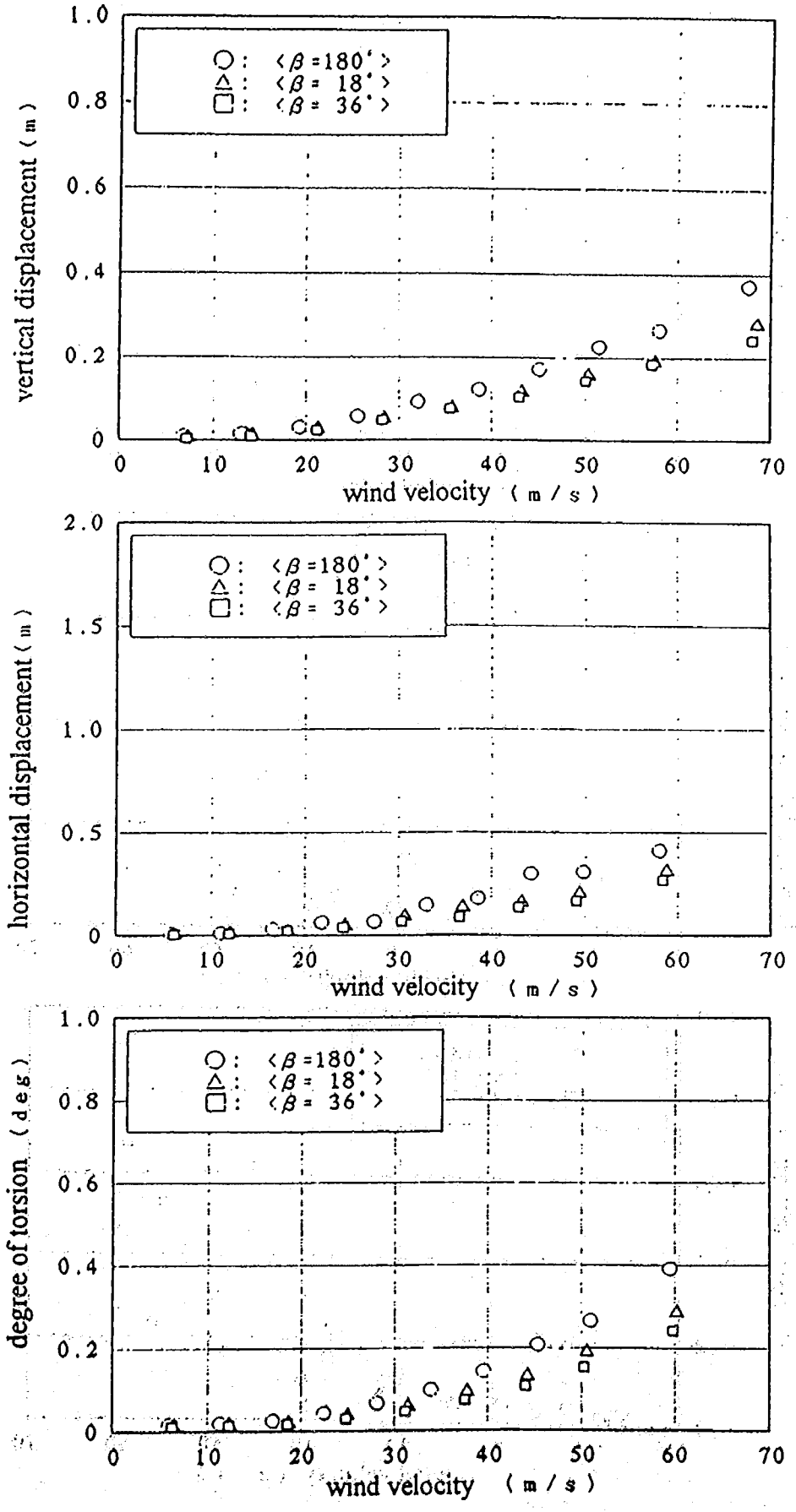


Fig.7 RMS value of gust response without topographical model

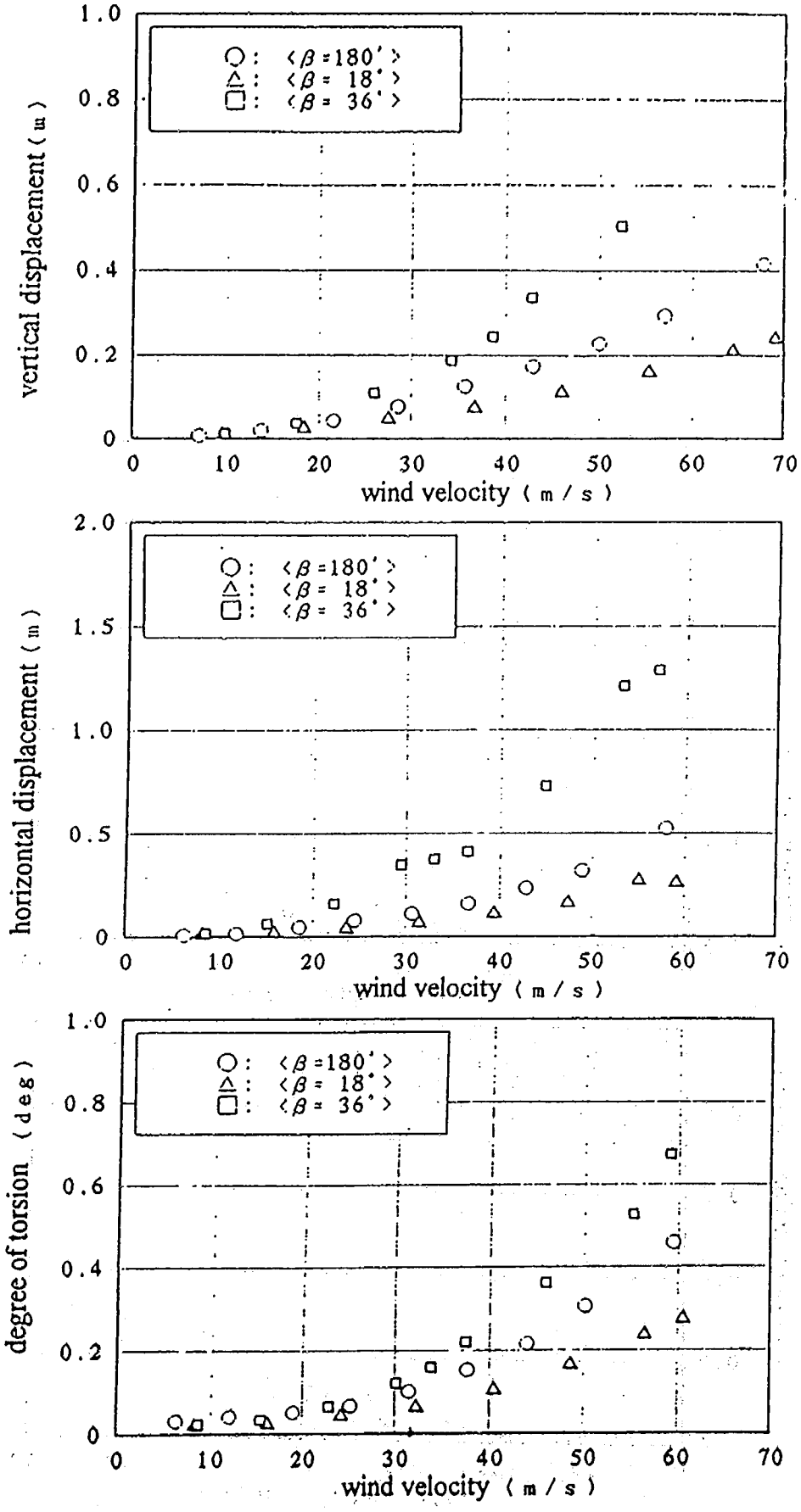


Fig.8 RMS value of gust response with topographical model

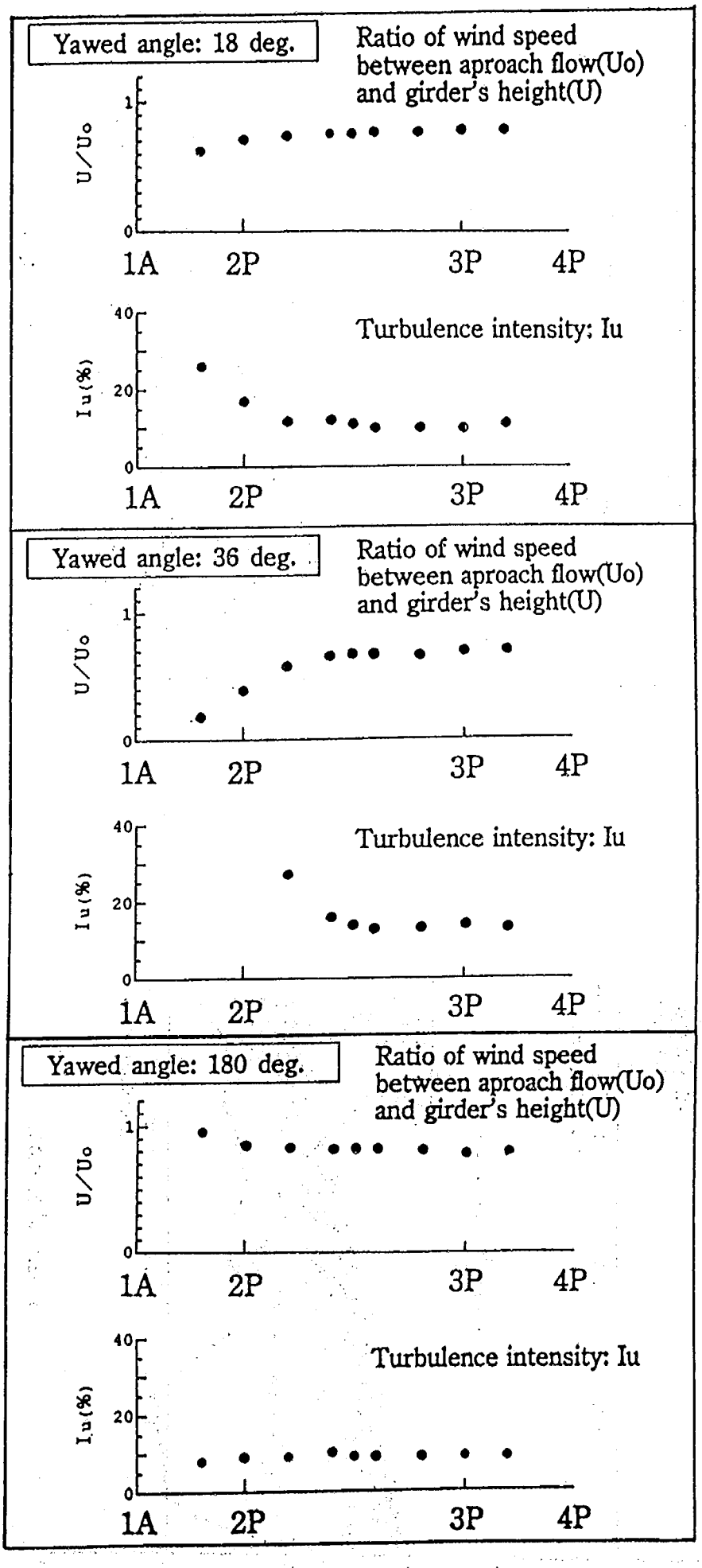
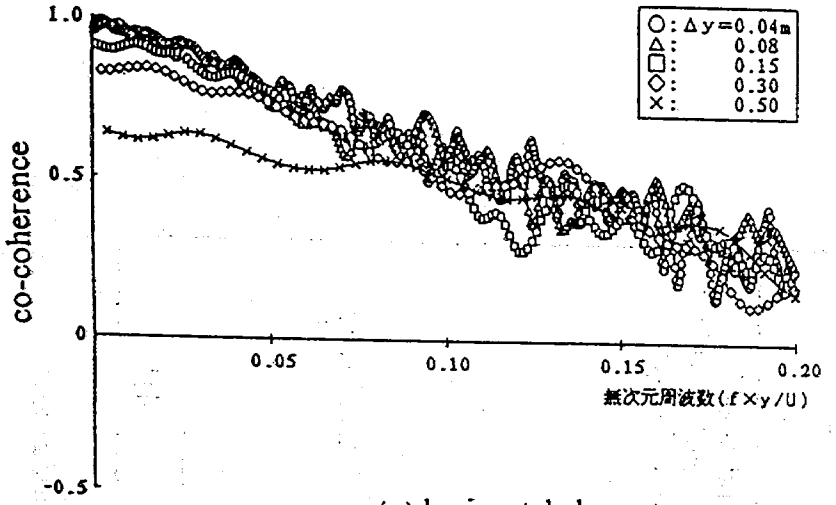
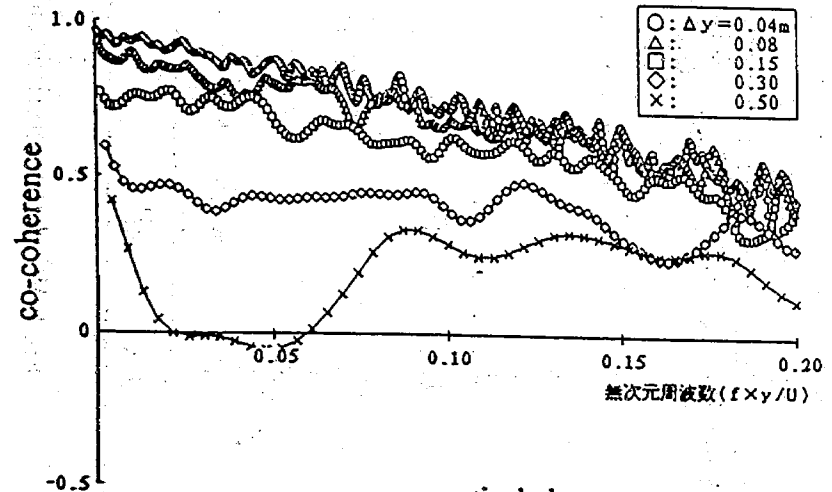


Fig.9 Wind characteristics along bridge axis

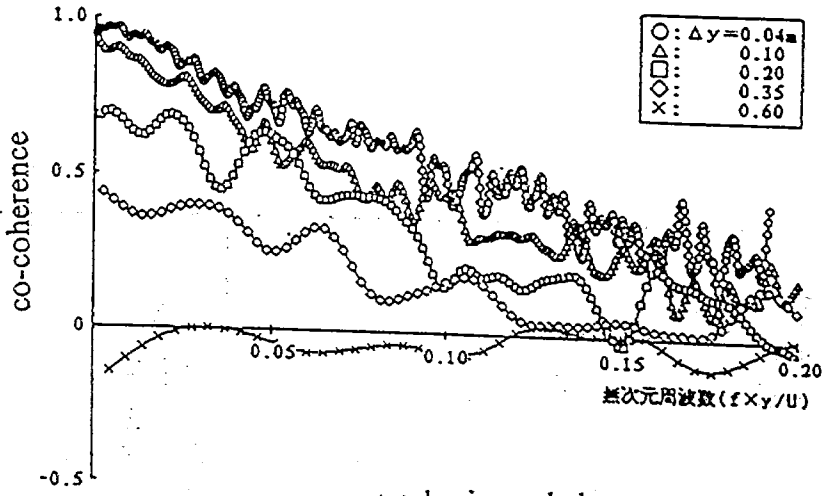


(a) horizontal element

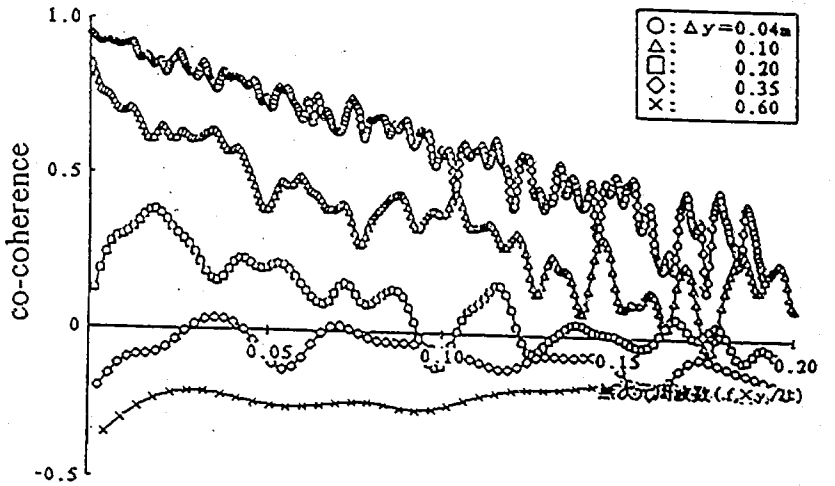


(b) vertical element

(1) $\beta = 36°$



(a) horizontal element



(b) vertical element

(2) $\beta = 180°$

Fig.10 Co-coherence of fluctuating wind speed at two places

△Y:distance form the center of center span, direction is from the center of center span to 2P main tower

Vibration Mode	Natural Frequency (Hz)	Logarithmic Damping Decrement
Vertical		
1st symmetric	4.90 - 5.01	0.028 - 0.045
1st anti-symmetric	5.76 - 6.19	0.025 - 0.043
Torsional		
1st symmetric	12.54 - 12.73	0.013 - 0.033
Horizontal		
1st symmetric	2.14 - 2.29	0.009 - 0.013

Table 1 Natural Frequency and Damping

Wind Characteristics (center of center span)	with topographical model $\beta = 36°$	without topographical model $\beta = 36°$
Turbulence Intensity (%)		
I_u	15.6	9.3
I_w	8.7	5.8
Integral Scale of Turbulence (m)		
L_x^u	1.21 (242)	0.58 (116)
L_x^w	0.25 (50)	0.31 (62)
( ):converted real scale		

Table 2 Turbulence Intensity and Integral Scale of Turbulence

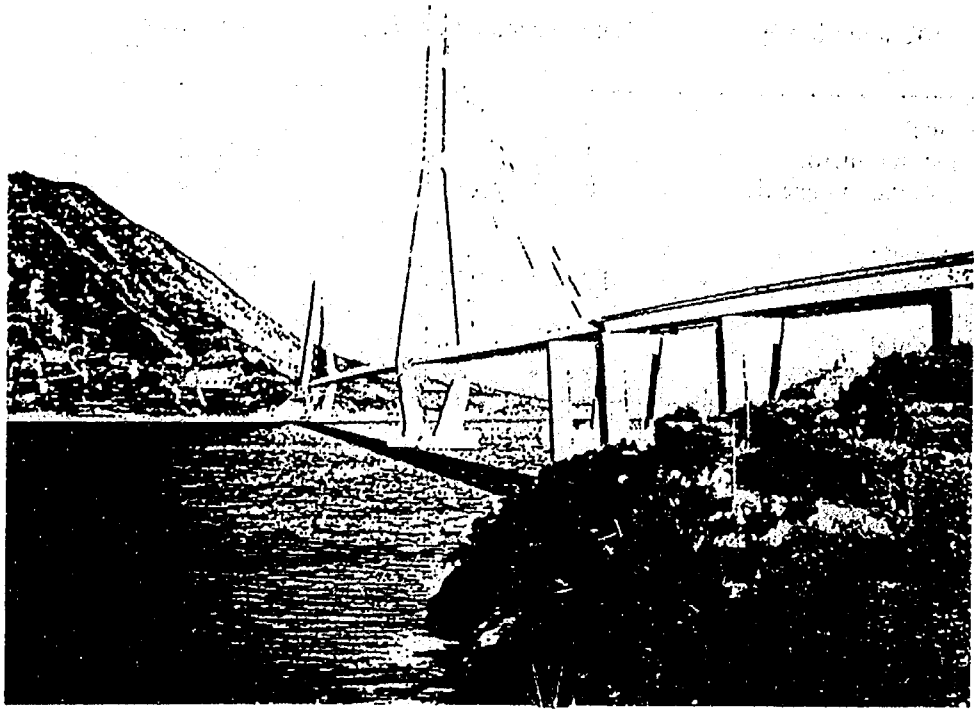


Photo 1 Tatara Bridge

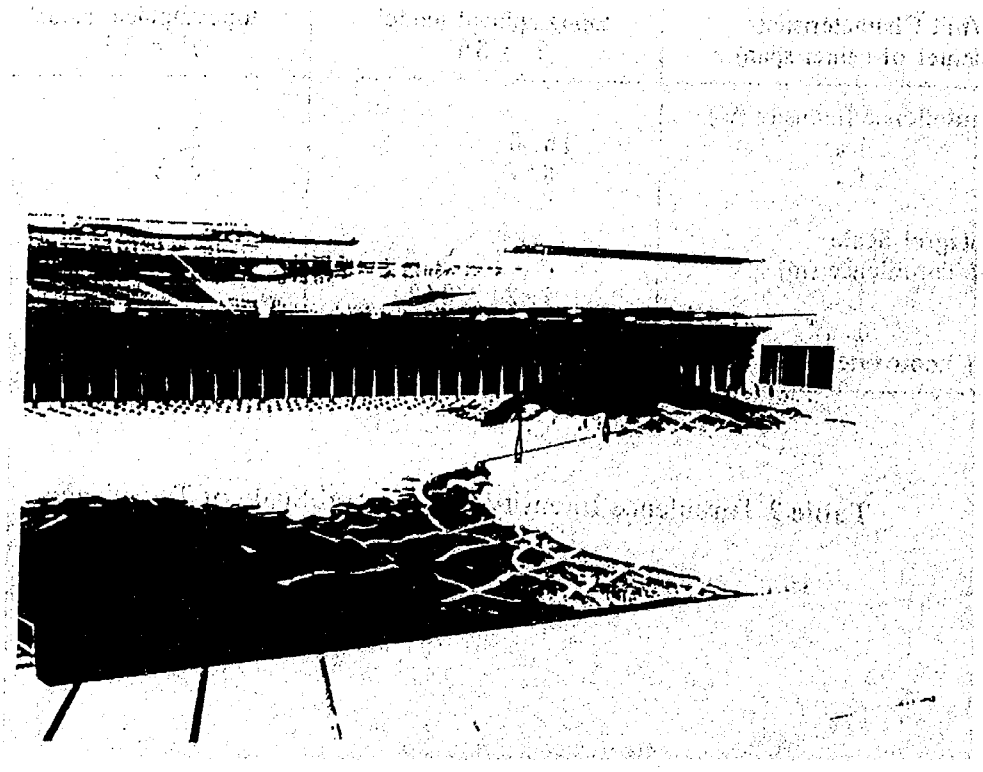


Photo 2 Model of Tatara Bridge

FIRST FIVE YEARS OF NSF'S COLLABORATIVE PROGRAM IN WIND ENGINEERING: RESULTS AND FUTURE ACTIVITIES

by

B. Bienkiewicz*

ABSTRACT

Wind engineering is a multidiscipline area, well suited for cooperative activities. Over the past thirty years it has evolved into a mature field, employing laboratory and field experimental data, analytical and empirical analysis and numerical simulation. One of the focal points of the recent cooperative wind engineering activities in the U.S. has been the CSU/TTU Cooperative Program in Wind Engineering (CPWE). This effort has been established in 1989 with primary funding provided by the U.S. National Science Foundation. The first five-year phase of the program ended in 1994 and the second phase was initiated in January of 1995. This paper is focused on the first phase of CPWE and it is based on a draft Executive Summary Report, currently under preparation by the staff of CPWE. The paper presents an overview of the program, aggregate achievements, the scope of research and research accomplishments. A brief summary of the current activities and future plans for the second phase of the program are also included. In addition, a recently proposed framework aimed towards promotion of international collaborative activities in wind engineering, the International Wind Engineering Forum, is also introduced.

KEYWORDS: buildings; cooperative program; field study; numerical study; wind; wind tunnel modeling.

1. INTRODUCTION

Over the past thirty years, wind engineering has evolved into a mature discipline. Fundamental and applied research resulted in development of powerful tools and methods of analysis, used both by wind engineers and other engineering professionals dealing with wind and its effects on natural and man-made environments. Experience resulting from application of the wind engineering knowledge provided evidence of the value and limitations of the developed techniques and methods of analysis. For the most part, the wind engineering predictions and design guidelines have been validated by field experience. In addition, the engineering community recognized tangible economic benefits resulting from including wind engineering in design and performance evaluations of buildings and structures and in environmental assessments.

The true milestone in the evolution of the discipline of wind engineering has been a recognition of the importance of the effects of the flow shear and turbulence present in the atmospheric boundary layer. This observation and subsequent development of experimental techniques to duplicate such features in wind tunnels initiated a new era in analysis of wind and its effects. Wind tunnel testing, field studies, analytical, empirical and, in recent years, numerical analysis have been utilized in wind engineering. Progress in this area has been affected by emerging new experimental and computational technologies as well as novel methods of analysis and design, developed in the area of wind engineering and other disciplines of science and engineering.

Wind engineering is a multidiscipline area ideally suited for cooperative initiatives involving researchers and practitioners of broad background. Beneficial aspects of such collaborative activities have been demonstrated both in the Unites States and in other countries. A recent example of such a cooperative arrangement is the Colorado State University/Texas Tech University Cooperative Program in Wind Engineering (CPWE) which is the subject of this paper.

---

*Department of Civil Engineering, Colorado State University, Fort Collins, Colorado 80523

Globalization of human activities, also in science and engineering, points to a need for expanding infrastructure promoting such evolution in civil and architectural engineering. A framework aimed towards this goal in wind engineering, the International Wind Engineering Forum (IWEF), has been recently proposed by wind engineers and researchers in Japan and in the U.S. A brief description of this initiative is included in the paper.

The NSF-sponsored CPWE was established in 1989. The first phase of CPWE ended in May of 1994. At the present time CPWE is in its second phase, which was initiated in January of 1995.

This paper is focused on the first phase - "the first five years" - of CPWE. It is based on a draft of the Executive Summary Report, currently under preparation by the CPWE staff. The overview of CPWE is presented in Section 2. Aggregate accomplishments are summarized in Section 3. The scope of research and research achievements are outlined in Section 4. Section 5 contains a brief assessment of impact of CPWE on the U.S. and international wind engineering community. A summary of related U.S.-Japan collaborative activities is also included. Planned activities of the second phase of CPWE are briefly discussed in Section 6. The IWEF is introduced in the Appendix.

2. OVERVIEW OF CPWE

The CPWE has been established to support long-term cooperative research in the area of wind engineering. It involves faculty, staff and students from two universities, Colorado State University (CSU) and Texas Tech University (TTU). The program research has been focused on wind effects on buildings and the surrounding environments. The CPWE employed wind tunnel simulation, field studies, and numerical modeling. As a multi-department, multi-discipline, dual-university program, CPWE involved 16 faculty members, 8 research associates, 49 graduate students, and 64 undergraduates. It allowed to pursue a long-term research addressing a abroad range of wind engineering topics, education, training and technology transfer.

The program, has been supported by the U.S. National Science Foundation and supplementary funding provided by other sources. This cross-university/department effort involved faculty, staff and students from a number of engineering disciplines and atmospheric sciences. Two co-directors, one at CSU and one at TTU, coordinated activities, while overall guidance for the program has been provided by the Technology Assessment and Advisory Council (TAAC). It consisted of nine members representing academia, practicing professionals, and insurance industry.

The CPWE's research program has been conducted through activities of eight tasks headed by co-principal investigators from the two institutions. As shown in Figure 1, the research topics included: (1) Wind Loads on Low-rise Buildings; (2) Studies for Building Ventilation; (3) Building Roofing Studies; (3) Non-boundary Layer Wind Simulation; (5) Structural Glazing Performance; (6) Prediction of Extreme Winds; (7) Numerical Modeling of Air Flow; and (8) Wind Erosion/Sedimentation Transport. These tasks formed the basis for an interdisciplinary wind engineering research and technology transfer.

As shown in Figure 1, the involved in the program co-principal investigators were from Civil Engineering (CE), Mechanical Engineering (ME), Agricultural Engineering (AgE), Chemical Engineering (ChemE) and Atmospheric Sciences (AmSc). The listed primary personnel was assisted by visiting researchers, graduate and undergraduate students. Support for the participation of the undergraduate students was provided through the Research Experience for Undergraduates (REU) program. It has been administered by NSF and designed to get undergraduate students involved in research and to encourage them to pursue graduate study in engineering.

The overall management structure of the CPWE is schematically shown in Figure 2.

3. ACCOMPLISHMENTS

The major goals of the CPWE were to acquire and disseminate knowledge in the field of wind engineering. These goals were addressed through

collaborative research, dissemination of findings, and education and training.

Papers were presented during national U.S. and international conferences, colloquia and symposia on wind engineering. Presentations were also made during annual and specialty conferences organized by professional societies. The CPWE researchers authored or co-authored more than 200 scientific or technical papers that were published or have been accepted for publication.

Over the program duration, members of the CPWE team have presented or attended more than 50 seminars. The co-principal investigators of the CPWE made presentations on the subject of wind engineering and delivered invited lectures to professional and academic audiences. In addition, CPWE staff organized and/or taught 14 short courses on wind engineering. Fifty eight speakers, including 33 lecturers from outside of the U.S., made presentations during wind engineering or wind engineering related seminars organized by CPWE at both the institutions.

Between 1989 and 1994, the first phase of CPWE, 19 undergraduate and 53 graduate courses of relevance to wind engineering were offered at both institutions. Students associated with CPWE were awarded 15 doctoral and 24 master degrees during this period of time. In addition, a significant number of undergraduate students participated in research activities through the REU program.

The CPWE activities resulted in 47 complementary contracts, with 31 funded by private sector, 10 federally funded and 6 funded by state agencies.

4. RESEARCH - SCOPE AND ACHIEVEMENTS

As shown in Figures 1 and 2, eight research topics, denoted as tasks, were addressed by the CPWE personnel. Over the time, the level of funding and the associated activity varied for each task. Overall, Tasks 1 and 3 had been allocated the highest financial support and their research activity was also the highest. In this section a brief description of the scope of research and highlights of the research accomplishments are presented for each task.

4.1 Task 1 - Wind Loads on Low-Rise Buildings

The objective of this task was to measure and compare wind flow near and pressure on low-rise buildings, using the field test building at TTU and small scale models in boundary-layer wind tunnels at CSU. Significant accomplishments of this task include: (1) Assembly of a data base of wind pressure on and wind speed near the TTU test building; (2) Accurate modeling in a boundary-layer wind tunnel the wind flow at the TTU building site; (3) Detailed field and wind tunnel measurement, using 1:100 geometrical scale building model, and comparison of external pressure on building surface; and (4) Measurement of internal pressure caused by porosity or openings in the building.

The developed physical modeling technique allowed to generate in a wind tunnel the surface shear layer of the TTU field building site, Figure 3. Excellent agreement between the field and model external building pressure was found for most of the compared pressure taps. Typical results are shown in Figure 4. The only disagreement was found for the negative peak point pressure and the standard deviation at a few near-roof corner locations, for the cornering wind direction. This situation is illustrated in Figure 5, where the magnitude of the model negative peak and the standard deviation are significantly lower than their full-scale counterparts. Modification of the modeled turbulent flow, pressure sampling and pressure tap geometry improved the agreement, but additional study of the observed discrepancy is needed.

The results of the study of the internal pressure, performed as part of work on this task, are to be incorporated in the 1995 revision of the ASCE-7 Wind Load Standard.

Representative publications describing work on this task are: Cermak and Cochran (1992), Cochran and Cermak (1992), Levitan and Mehta (1992) and Thomas et al (1993).

4.2 Task 2 - Studies for Building Ventilation

The objective of this effort was to enhance the existing capabilities for predicting and assessing

transport of exhaust fumes released on/near low-rise buildings. The study was performed utilizing simplified analytical/empirical models, an existing computational fluid dynamics code and physical modeling in wind tunnel.

Significant accomplishments of this task include: (1) Development of methodology for analysis of building exhaust recirculation and subsequent infiltration into the building interior; (2) Validation of physical modeling as a predictor of plume behavior by direct comparison with filmed releases in the field; (3) Development of criteria for optimal placement of air intake and exhaust vents; and (4) Characterization of the relative effects of building porosity, dominant opening, and gas release location on fume transport and infiltration.

Figure 6 shows geometrical details of the 1:25 geometrical scale model of the TTU building used by this task. Also shown are representative ventilation rates measured during wind tunnel experiments.

Representative publications describing work on this task are: Birdsall and Meroney (1994) and Rege and Tock (1994).

4.3 Task 3 - Building Roofing Studies

This task was focused on the development of basic understanding of wind loading on and performance of loose-laid single-ply, ballasted membrane roofing systems. Specific objectives included: (1) Wind tunnel and field investigation of generic loose-laid roof paver systems; (2) Investigation of the effects of roofing system parameters and building details (e.g. roof parapet) on the system wind loading and performance; and (3) Development and validation of analytical/numerical model to predict the wind uplift for such systems.

Significant accomplishments of this task include: (1) Wind-tunnel measurement of pressure underneath generic loose-laid roofing systems and comparison with field data; (2) Systematic wind-tunnel study of the effects of roofing system parameters on the wind loading. The results of this phase of work were summarized in a data base made available to the wind engineering community; (3) Development and validation of an analytical/numerical model to compute pressure underneath generic loose-laid ballast pavers; and (4) Analytical determination and experimental validation of the main parameter - the ratio of the space between to the space underneath the pavers - governing the net wind loading on the loose-laid ballast pavers without geometric interlock.

Figures 7 through 9 show representative wind tunnel and numerical results for this task. The pressure contours caused by cornering wind on the exterior surface and underneath a generic loose-laid roofing system are depicted in Figure 7. In the figure, the underneath pressure, measured during a wind tunnel experiment, is compared with the pressure computed using the developed computer code. The mathematical model employed in computations is summarized in Figure 8. The effects of the ratio of the space between to the space underneath the ballast roof pavers are illustrated in Figure 9. The data shows that a large value of the ratio is desired to allow for effective pressure equalization, which leads to a reduction in the net wind uplift exerted on the roofing system.

The results of work on this task have been utilized in the development of the design criteria for a number of loose-laid roofing systems employing ballast pavers. This was accomplished through complimentary projects.

Representative publications for this task are: Bienkiewicz and Sun (1992, 1993), Sun and Bienkiewicz (1993), Mehta et al (1992), and McDonald et al (1994).

4.4 Task 4 - Non-boundary Layer Winds

The objective of this task was directed toward a better understanding of the characteristics of high non-boundary layer winds. A major goal was to improve wind tunnel modeling techniques appropriate for simulation of such wind phenomena.

Significant accomplishments of this task include: (1) Development and initial testing of a tornado generator; (2) Development and testing of a large turbulence scale, actively controlled turbulence generator; (3) Collection and analysis of high wind

data for near-ground parametrization; and (4) Formulation of an operational forecast model to predict the onset of strong surface winds due to predominant daytime heating.

Figure 10 shows the concept of the developed tornado generator and representative experimental results, the pressure measured underneath a generated tornado-like vortex.

Representative publications describing work on or related to this task are: Bienkiewicz and Dudhia (1993), and Peterson and Mehta (1994).

4.5 Task 5 - Structural Glazing Performance

The objective of this task was to develop surface pressure wind load histories and to employ them in fatigue testing of cladding components, including structural glazing. Desired were non-Gaussian signals of prescribed spectral characteristics.

Significant accomplishments include: (1) Development of a technique to generate the desired non-Gaussian wind pressure histories; (2) Extension of the simulation technique to multi-point pressures on a building surface; (3) Development of a system capable of applying controlled loading sequences, including non-Gaussian pressure histories, for structural glazing sealants and other cladding components; and (4) Formulation of a cyclic wind pressure spectrum to model hurricane wind force on windows, doors and wall cladding.

Figure 11 shows representative non-Gaussian surface pressure time histories, developed and used by this task.

Representative publications for this task are: Seong and Peterka (1993) and Norville and Sheridan (1993).

4.6 Task 6 - Prediction of Extreme Winds

The objective of this task was to develop a wind speed map for the U.S. contiguous 48 states and Alaska, based on peak gust wind speed measurements.

The above objective has been accomplished. A wind speed map based on 3-second gust speed was adopted for the ASCE-7 Wind Load Standard. The work on this task involved the following items: (1) Development of the concept of superstations for performing wind speed hazard assessments; (2) Comparison of wind pressure based on peak gust and fastest-mile speeds; (3) Investigation of the relationship between peak gust and fastest one-minute monthly wind speeds; and (4) Refinement of wind speeds along the U.S. Gulf Coast and Atlantic Coastline.

The gust speed map proposed for the ASCE-7 Wind Load Standard is depicted in Figure 12.

Representative publications for this task are: Peterka (1992), and Peterka and Mehta (1994).

4.7 Task 7 - Numerical Modeling of Air Flow

The objective of this task was to develop and test numerical models of wind flow around buildings and turbulent flows associated with strong winds passing over arbitrarily shaped bodies.

Significant accomplishments: (1) Modification and utilization of existing computer codes (CSU-RAMS and FLUENT) to simulate extreme wind effects; (2) Large eddy simulation (modified CSU-RAMS) of hurricane landfall, intensification and low-level convergence; and (3) Development of a flow solver, the enhanced panel method, to model fluid flow around three-dimensional geometries.

Representative results illustrating work on this task, performed at CSU, are shown in Figure 13.

Reference publications for this task are: Nicholls et al (1995) and Quasim et al (1992).

4.8 Task 8 - Wind Erosion

The objective of this effort was to predict soil movement by wind. Proposed was an extension of an existing model, to include the prediction of air quality and visibility as influenced by particulate matter of diameter smaller than 10 microns. Work on this task was carried out only at TTU.

Significant accomplishments: (1) Theoretical

resolution of two apparent conflicts in the related data reported in the literature; (2) Development of an isokinetic sampling system for wind tunnel erosion studies and a controlled energy dust generator for air quality studies.

A representative publication for this task is: Gregory et al (1990).

5. IMPACT ON WIND ENGINEERING

The unique value of the CPWE effort, its approach combining field, model and numerical studies, has been recognized by the U.S. and international wind engineering community. A number of researchers and practitioners initiated collaboration with the CPWE personnel at CSU and TTU. In addition, various research groups initiated at their laboratories work related to the CPWE effort.

Researchers from other laboratories also participated in analysis of the CPWE data. A representative example of such an effort is work presented by Letchford et al (1993). Wind engineering laboratories in a number of countries initiated wind tunnel testing of the TTU building model. Examples of such work are studies performed in Canada, Tieleman et al (1993), in New Zealand, Jamieson and Carpenter (1993), and in Australia, Rofail (1994).

Work performed by the CPWE staff had also an impact in Japan. The first wind tunnel modeling of the TTU building performed outside of the U.S., took place in Japan, Okada and Ha (1992). This was followed by other related initiatives undertaken by Japanese researchers independently or though collaborative effort involving research teams in the U.S. A representative example of such a U.S.-Japan effort is work described by Bienkiewicz et al (1993). This effort involved joint planning of the wind tunnel experiments, the experimental work performed in Japan and analysis of the acquired data by researchers both in Japan and in the U.S. This work resulted in a number of joint papers published both in English and in Japanese language.

It has been recognized that a new framework to promote and aid international cooperation in wind engineering, reaching beyond CPWE, might be helpful. This observation and subsequent initiatives by Japanese and U.S. wind engineers and researchers led to the establishment of the International Wind Engineering Forum, described in the Appendix.

The overall impact of CPWE, expressed in terms of a number of published papers, reports, recommendations for wind codes and standards was discussed in Section 3. It is anticipated that as dissemination of the generated knowledge and the data base continues, the CPWE effort will receive even wider recognition.

6. PRESENT AND PLANNED ACTIVITIES

At the present time, CPWE is in its second phase. Current activities of CPWE are focused on planning the near future effort.

It has been proposed to maintain the CPWE's overall administrative structure, developed during the previous phase. However, the number of tasks has been reduced and a new arrangement is being developed to promote closer interaction between co-principal investigators, students and staff at both the universities. A concept of the focus areas, to replace a structure based on separate tasks of the previous phase, has been proposed. Current plans call for four research focus areas: (1) Wind Loads; (2) Wind Engineering Meteorology; (3) Wind Flow around Buildings; and (4) Economic Analysis of Wind Damage. Specific plans for each focus area are currently being formulated. The overall theme is to maintain a close link between field and laboratory experimental investigations and analysis. Equally important aspect is to sustain a balance between fundamental and applied topics of the performed research. A strong emphasis is being placed on continuation and expansion of collaborative activities beyond the CPWE to include both the U.S. and foreign wind engineering researchers and practitioners.

7. CONCLUDING REMARKS

The area of wind engineering has evolved into a mature discipline. At the present time, physical modeling in wind tunnels, numerical simulations, field studies, new methods of analysis and

cooperative, including international, activities play significant role in this field.

The CPWE has been an unique program, providing support for a comprehensive, long-term research in the area of wind engineering. This cross-university, cross-department program involving faculty, graduate and undergraduate students of broad background made a significant impact on wind engineering community. The CPWE research activities have been documented through numerous papers, technical reports, seminars, invited lectures and short course presentations. Educational accomplishments included a significant number of participating and graduating students and related courses taught at both universities at the graduate and undergraduate levels. A significant component of this mission was to get undergraduate students involved in activities of CPWE. It should be pointed out that a number of these students decided to continue their education and enrolled in graduate studies. The technology transfer has been accomplished through short courses, presentations and participation of the CPWE in complementary projects, mainly of applied nature.

It is anticipated that the second phase of the CPWE, currently underway, will allow for strengthening the collaborative spirit of the undertaken research, education and technology transfer. Even stronger participation of the U.S. and international partners will be sought. It is expected that the U.S.-Japan collaboration will be expanded. It is also hoped that the recently established International Wind Engineering Forum will be able to serve as a catalyst in promoting international collaboration within and beyond the CPWE.

8. ACKNOWLEDGMENTS

This paper is based on the draft of the Executive Summary Report, currently under preparation by the staff of CPWE. The author would like to acknowledge contributions made to the report by the the CPWE Co-Directors: Drs. K.C. Mehta and R.N. Meroney, and the Co-Principal Investigators: Drs. J.E. Cermak, J. Gregory, J.R. McDonald, H.S. Norville, S. Parameswaran, J.A. Peterka, R.E. Peterson, R.A. Pielke, and R.W. Tock. Support for the CPWE has been provided by the U.S. National Science Foundation. Active involvement in CPWE of Dr. J.E. Sabadell, Director of the NSF's Natural and Technological Hazards Program, is gratefully acknowledged.

10. APPENDIX - THE INTERNATIONAL WIND ENGINEERING FORUM

10.1 Overview

On March 17, 1994 an Inaugural Meeting of the International Wind Engineering Forum (IWEF) was held in Tokyo. It was attended by over 100 participants representing private and governmental as well as academic entities from Japan, U.S.A. , Korea and Taiwan. The idea for establishing the IWEF, an organization promoting and facilitating collaborative U.S.-Japan activities in wind engineering was first proposed by Japanese side in early Spring of 1993. Since then the organizational structure of the IWEF and the scope of its activities have been discussed during a series of meetings between the U.S. and Japanese representatives, held both in Japan and in the U.S.A. In view of an interest in the IWEF's activities, expressed by wind engineering researchers and practitioners from other countries, it was proposed to expand the geographical scope of the IWEF beyond the two founding countries.

10.2 Purpose and Goals

The purpose of the IWEF is to promote and facilitate collaborative wind engineering research, education and service activities mutually beneficial to Japan, United States and other participating countries. The goals of the IWEF include: (A) Synthesize, exchange and disseminate wind engineering technical information; (B) Facilitate exchange of wind engineering researchers and practitioners; (C) Promote and aid wind engineering knowledge and technology transfer; (D) Offer wind engineering technical expertise; (E) Promote mutually beneficial activities in other related areas of science and engineering.

10.3 Organizational Structure

The IWEF is headed by two Co-Chairmen, one representing the Japanese side and the remaining

one representing the U.S. side. The Co-Chairmen are aided by the Advisory Board, consisting of four Japanese and four U.S. members. The IWEF has two offices, one in the U.S.A., at Colorado State University and one in Tokyo, at the Japan Association for Building Research Promotion.

10.4 Current Activities

Several initiatives have been already undertaken by the IWEF: (A) The IWEF Summer Seminar on Roofing Issues, held in Tokyo, August 1994; (B) Publication of the inaugural issue of the IWEF Newsletter; (C) Tabulation of the surveys distributed during the Inaugural Meeting of the IWEF and during the IWEF Summer Seminar (under way); (D) Development of the data base of recent wind engineering publications by Japanese and U.S. authors (under way).

10.5 Remarks

As already mentioned, the original concept of the IWEF's bilateral U.S.-Japan collaborative wind engineering activities has been amended to include other countries. Wind engineering researchers and practitioners of any interested country are welcome to join the IWEF. Inquiries and input regarding the IWEF are welcome and will be gratefully appreciated.

11. REFERENCES

1. Bienkiewicz, B. and Dudhia, P. (1993). "Physical Modeling of Tornado-Like Flow and Tornado Effects on Building Loading." Proc. 7th U.S. Nat. Conf. on Wind Eng., Los Angeles, CA, 95-104.

2. Bienkiewicz, B. and Sun, Y. (1992). "Wind-Tunnel Study of Wind Loading on Loose-Laid Roofing Systems." J. Wind Eng. Ind. Aerodyn., 43, 1817-1828.

3. Bienkiewicz, B. and Sun, Y. (1993). "Numerical and Experimental Studies of Wind Loading on Loose-laid Roofing Systems." Proc. 7th U.S. Nat. Conf. on Wind Engineering, Los Angeles, CA, Vol. 1, 105-114.

4. Bienkiewicz, B., Tamura, Y., Ham, H.J., Ueda, H., and Hibi, K. (1993). "Proper Orthogonal Decomposition and Reconstruction of Multi-channel Roof Pressure", in Lam, K.M. and Cheung Y.K. (Eds.), Proc. 3rd Asia-Pacific Symposium on Wind Engineering, Hong Kong, Vol. 2, 711-716.

5. Birdsall, J.B. and Meroney, R.N. (1994). "Model Scale and Numerical Evaluation of Tracer Gas Distribution Due to Wind-Forced Natural Ventilation." Proc. 9th Int. Conf. on Wind Eng., New Delhi, India, Wiley Eastern Limited, 1693-1703.

6. Cermak, J.E. and Cochran, L.S. (1992). "Physical Modeling of the Atmospheric Surface Layer." J. Wind Eng. Ind. Aerodyn., 41-44, 935-946.

7. Cochran, L.S. and Cermak, J.E. (1992). "Full- and Model-Scale Cladding Pressures on Texas Tech Experimental Building." J.Wind Eng. Ind. Aerodyn., 41-44, 1589-1600.

8. Gregory, J.M., Borrelli, J. and Fedler, C.B. (1990). "Wind Storm Erosion and Soil Deposition Simulation." J. Wind Eng. and Ind. Aerodyn,. 36, 1415-1424.

9. Jamieson, N.J. and Carpenter, P. (1993). "Wind Tunnel Pressure Measurements on the Texas Tech Building at a Scale of 1:25 and Comparison with Full-Scale." Proc. 7th U.S. Nat. Conf. on Wind Eng., Los Angeles, CA, 303-312.

10. Letchford, C.W., Iverson, R.E. and McDonald, J.R., (1993). "The Application of the Quasi-Steady Theory to Full Scale Measurements on the Texas Tech Building." J. Wind Eng. Ind. Aerodyn., 48, 111-132.

11. Levitan, M.L. and Mehta, K.C. (1992). "Texas Tech Field Experiments for Wind Load. Part I and Part II." J. Wind Eng. Ind. Aerodyn., 43, 1565-1588.

12. McDonald, J.R., Wang, W. and Smith, D.A. (1994). "Field Experiments for Wind Loads on

Pavers." Proc. 9th Int. Conf. on Wind Eng., New Delhi, India, Eastern Wiley Limited, 488-499.

13. Mehta, K.C., Levitan, M.L., Iverson, R.E. and McDonald, J.R. (1992). "Roof Corner Pressures Measured in the Field on Low Buildings." J. Wind Eng. Ind. Aerodyn., 41, 181-192.

14. Nicholls, M.E., Pielke, R.A., Eastman, J.L., Finley, C.A., Lyons, W.A., Tremback, C.J., Walko, R.L. and Cotton, R.W. (1995). "Applications of the RAMS Numerical Model to Dispersion over Urban Areas," in Cermak, J.E., et al (Eds.) "Wind Climate in Cities.", Kluver Academic Publishers, 703-732.

15. Norville, H.S. and Sheridan, D.L. (1993). "Fatigue Behavior of Structural Silicone Sealant." Proc. 7th U.S. Nat. Conf. on Wind Eng., Los Angeles, CA, 483-492.

16. Okada, H. and Ha, Y.-C. (1992). "Comparison of Wind Tunnel and Full-Scale Measurement Tests on the Texas Tech Building." J. Wind Eng. Ind. Aerodyn., 42, 1601-1612.

17. Peterka, J.A. (1992). "Improved Extreme Wind Speed Prediction for the United States." J. Wind Eng. Ind. Aerodyn., 41, 533-541.

18. Peterka, J.A. and Mehta, K.C. (1994). "Proposed Hurricane Wind Speeds for ASCE 7-95." Proc. ASCE Structures Congress '94, Atlanta, GA, 461-466.

19. Peterson, R.E. and Mehta, K.C., (1994). "Mitigation of Hurricane Damage in a Changing Climate of Storm Activity." Proc. 5th Global Warming Int. Conf., San Francisco, CA.

20. Quasim, A., Maxwell, T.T., and Parameswaran, S. (1992). "Computational Predictions of Flow over a 2-D Building." J. Wind Eng. Ind. Aerodyn., 41-44, 2839-2840.

21. Rege, M.A. and Tock, R.W. (1994). "Estimating Hydrogen Sulfide Emissions from Crude Oil Storage Tank Vents in West Texas." Proc. 9h Int. Conf. Wind Eng., New Delhi, India, Eastern Wiley Limited, 1728-1739.

22. Rofail, A.W. (1994) "Full-Scale/Model-Scale Comparisons of Wind Pressures on TTU Building." Proc. 9th Int. Conf. on Wind Eng., New Delhi, India, Eastern Wiley Limited, 1055-1066.

23. Seong, S.H. and Peterka, J.A., (1993). "Computer Simulation of Non-Gaussian Wind Pressure Fluctuations." Proc 7th U.S. Nat. Conf. on Wind Eng., Los Angeles, CA, 623-632.

24. Sun, Y. and Bienkiewicz, B. (1993). "Numerical Simulation of Pressure Distributions Underneath Roofing Paver System." J. Wind Eng. Ind. Aerodyn., 46-47, 517-526.

25. Thomas, G., Cochran, L.C., Cermak, J.E., and Mehta, K.C. (1993) "Comparison of Field and Wind-Tunnel Measured Spectra." Proc. 7th U.S. National Conf. on Wind Engineering, UCLA, Los Angeles, pp. 793-802.

26. Tieleman, H.W., Surry, D., and Mehta, K.C., (1993). "Full/Model Scale Comparison of Surface Pressure on the Texas Tech Experimental Building." Proc. 7th U.S. Nat. Conf. on Wind Eng., Los Angeles, CA, 783-792.

Project Tasks	Co-Principal Investigators	
	Colorado State	Texas Tech
1. Wind Loads on Low-Rise Buildings	J.E. Cermak (CE)	K.C. Mehta (CE)
2. Studies for Building Ventilation	R.N. Meroney (CE)	R.W. Tock (ChemE)
3. Building Roofing Studies	B. Bienkiewicz (CE)	J.R. McDonald (CE)
4. Nonboundary Layer Wind Simulation	B. Bienkiewicz (CE)	R.E. Peterson (AtmSc)
5. Structural Glazing Performance	J.A. Peterka (CE)	H.S. Norville (CE)
6. Prediction of Extreme Winds	J.A. Peterka (CE)	K.C. Mehta (CE)
7. Numerical Modeling of Air Flow	R.A. Pielke (AtmSc)	T.T. Maxwell/ S. Parameswaran (ME)
8. Wind Erosion/Sediment Transport	----------	J. Gregory (AgE)

Figure 1. Tasks and co-principal investigators

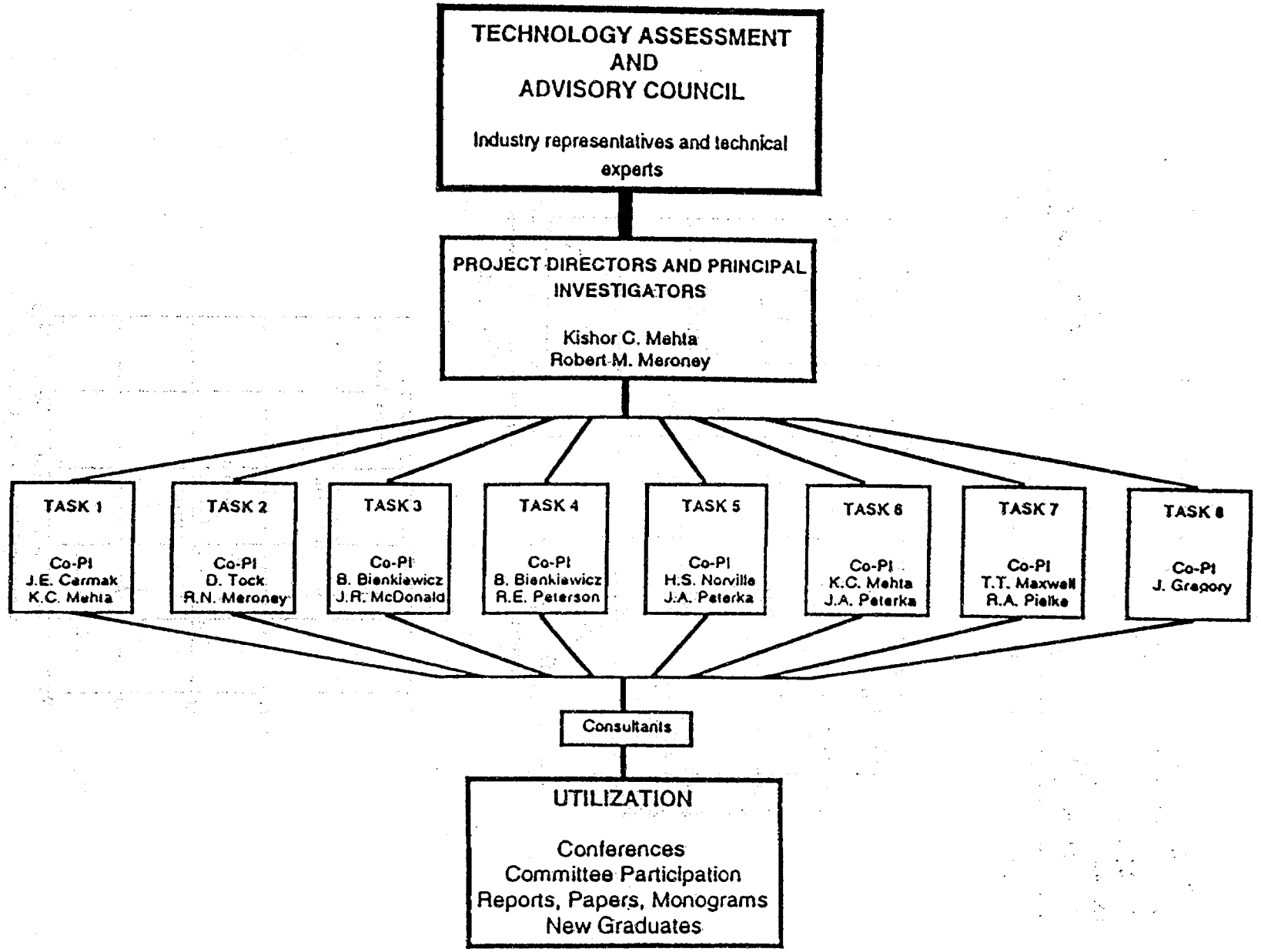


Figure 2. Management structure

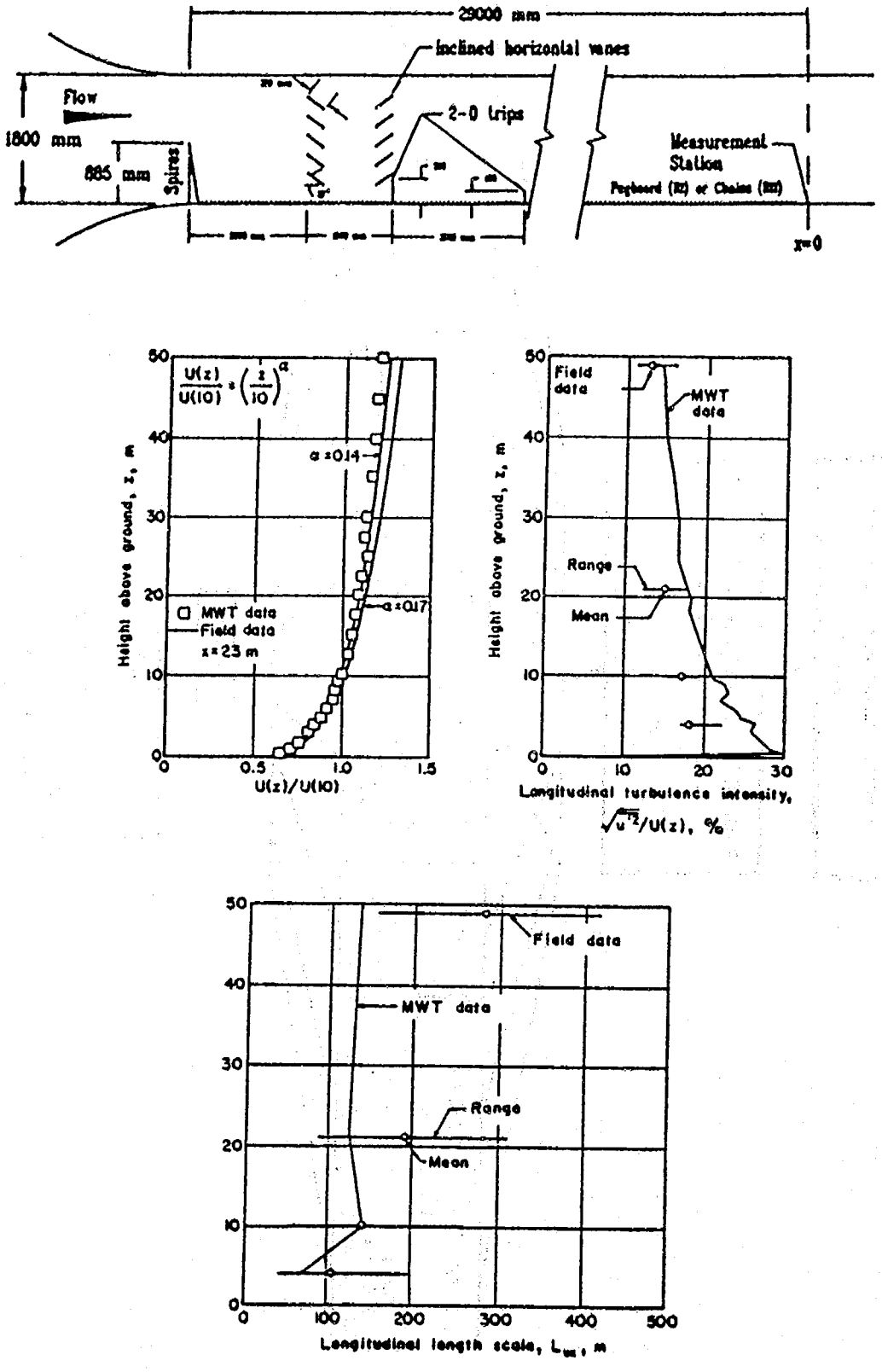


Figure 3. Wind tunnel configuration and generated surface shear layer

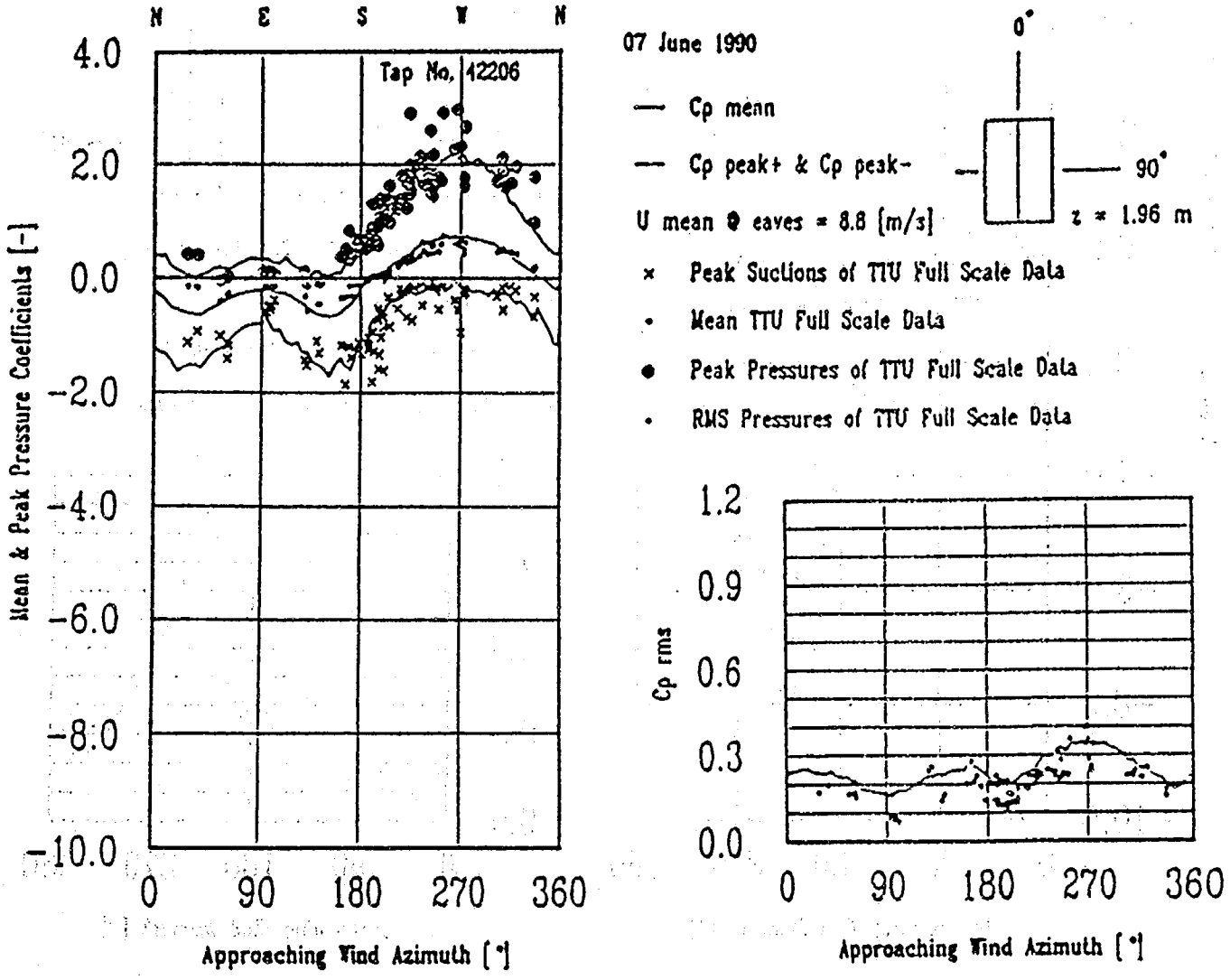


Figure 4. Field and model external pressure on TTU building at tap on western centerline

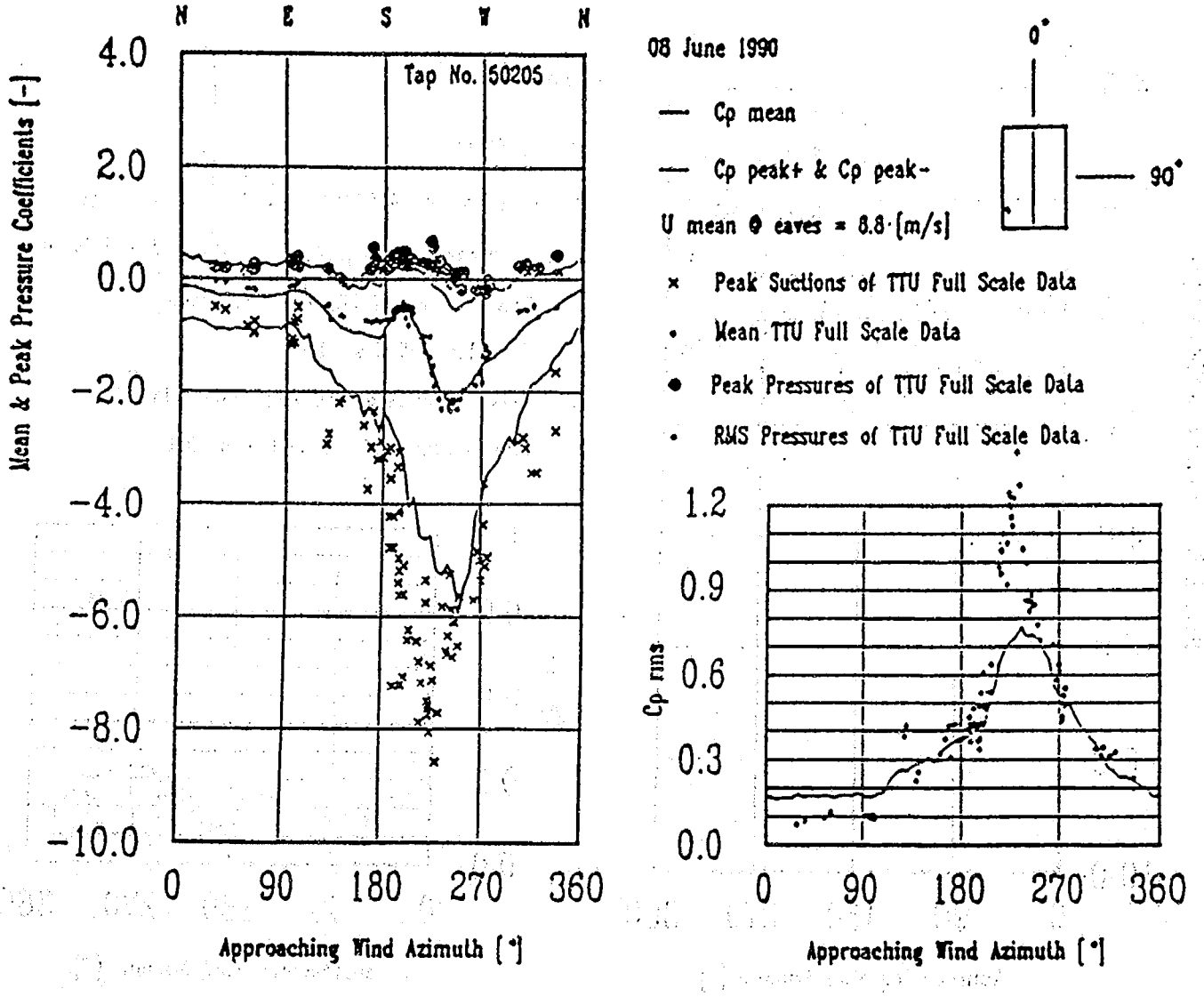
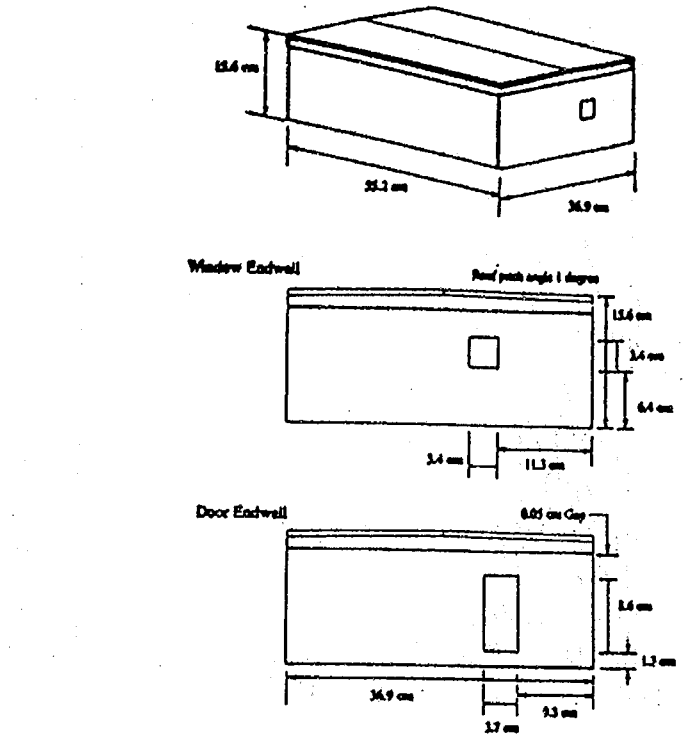


Figure 5. Field and model external pressure on TTU building at marked roof pressure tap



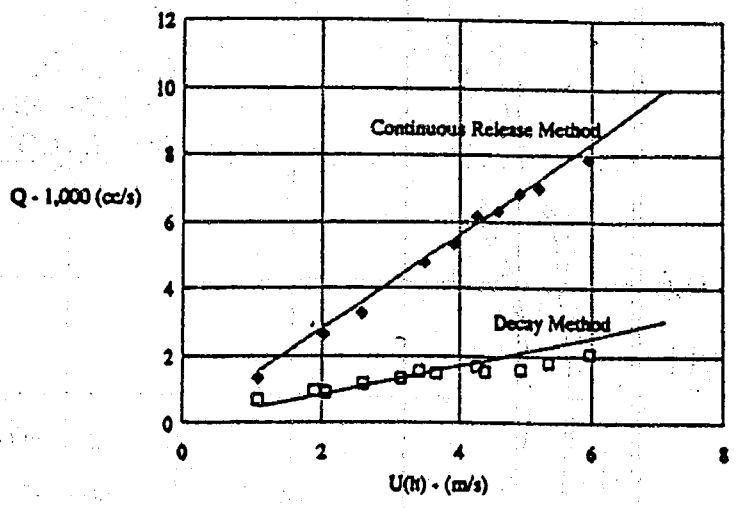


Figure 6. Geometry of 1:25 scale model of TTU building and measured ventilation rates

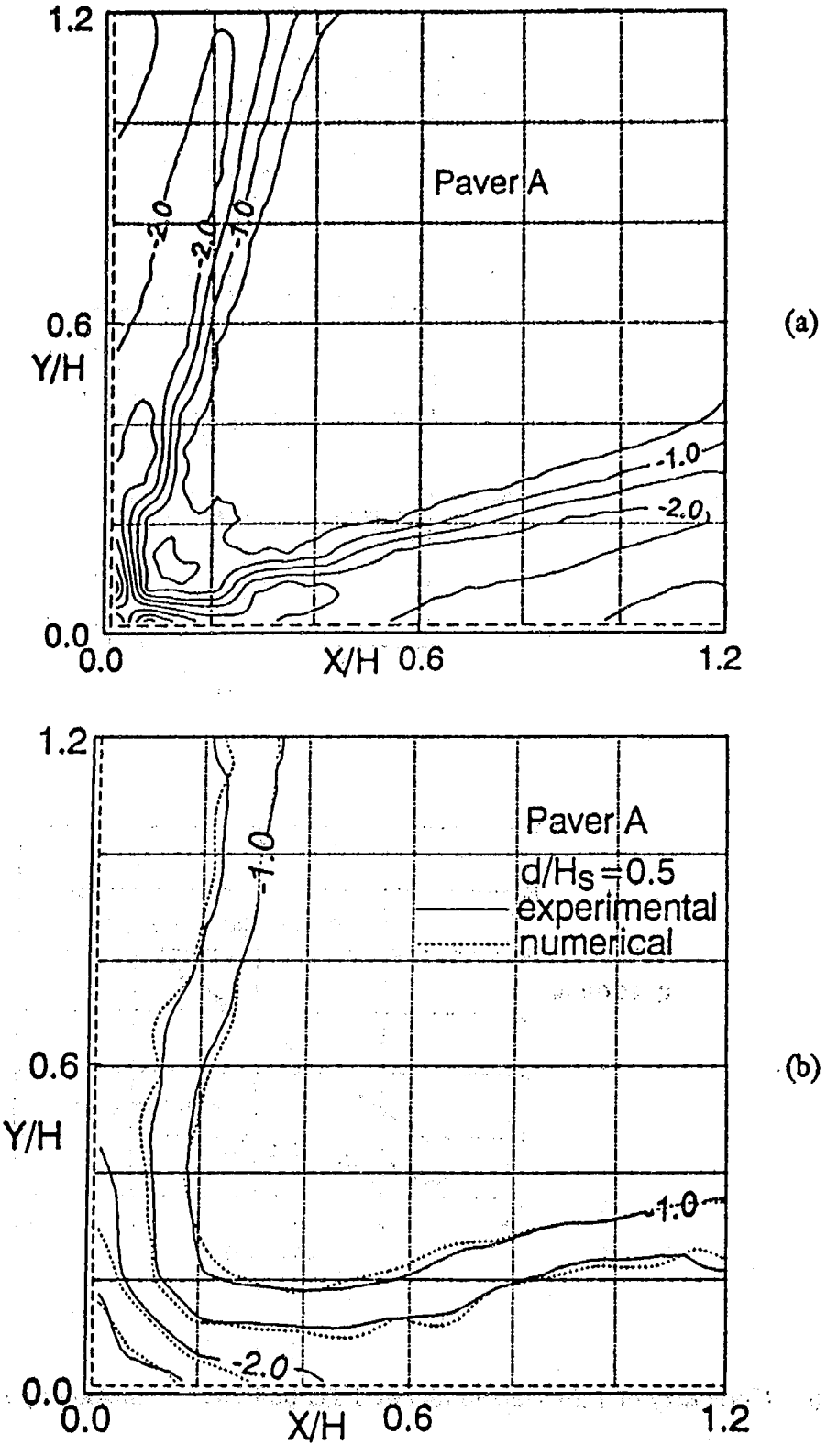


Figure 7. Wind tunnel mean pressure on external surface (a) and underneath loose-laid ballast system (b) on roof of 1:25 scale model of TTU building

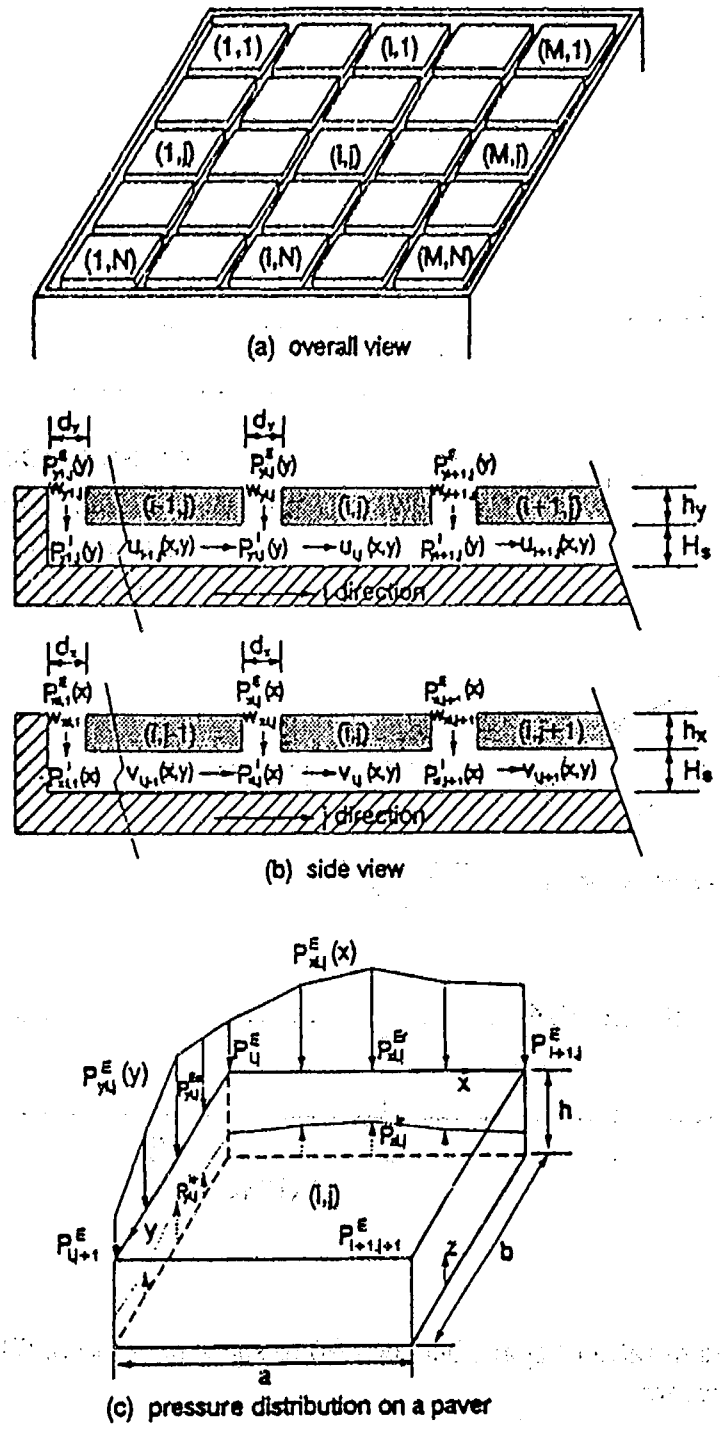


Figure 8. Configuration of generic roofing paver system used to formulate mathematical model

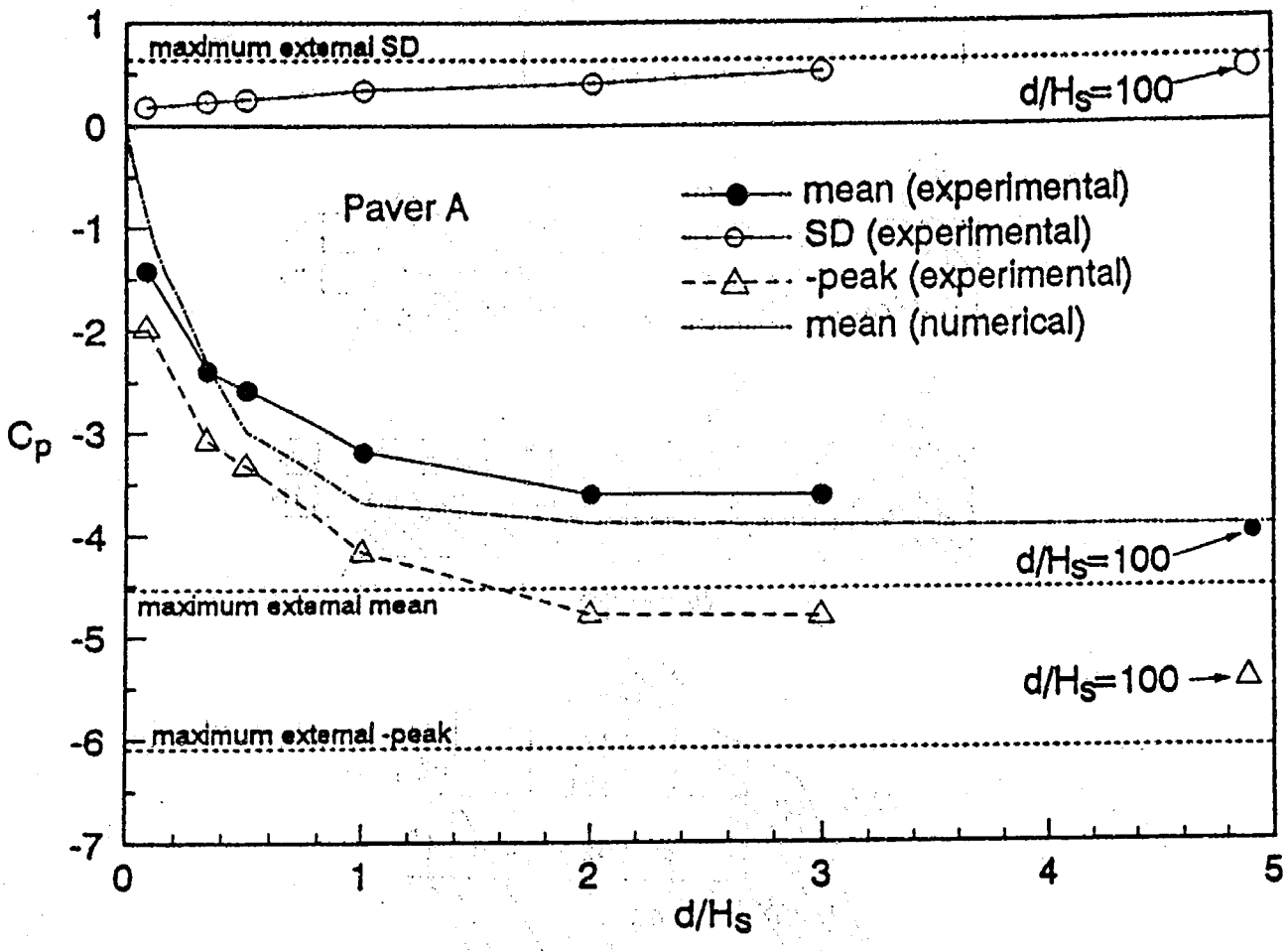


Figure 9. Effects of ratio of space between (d) to space underneath (Hs) loose-laid roofing pavers

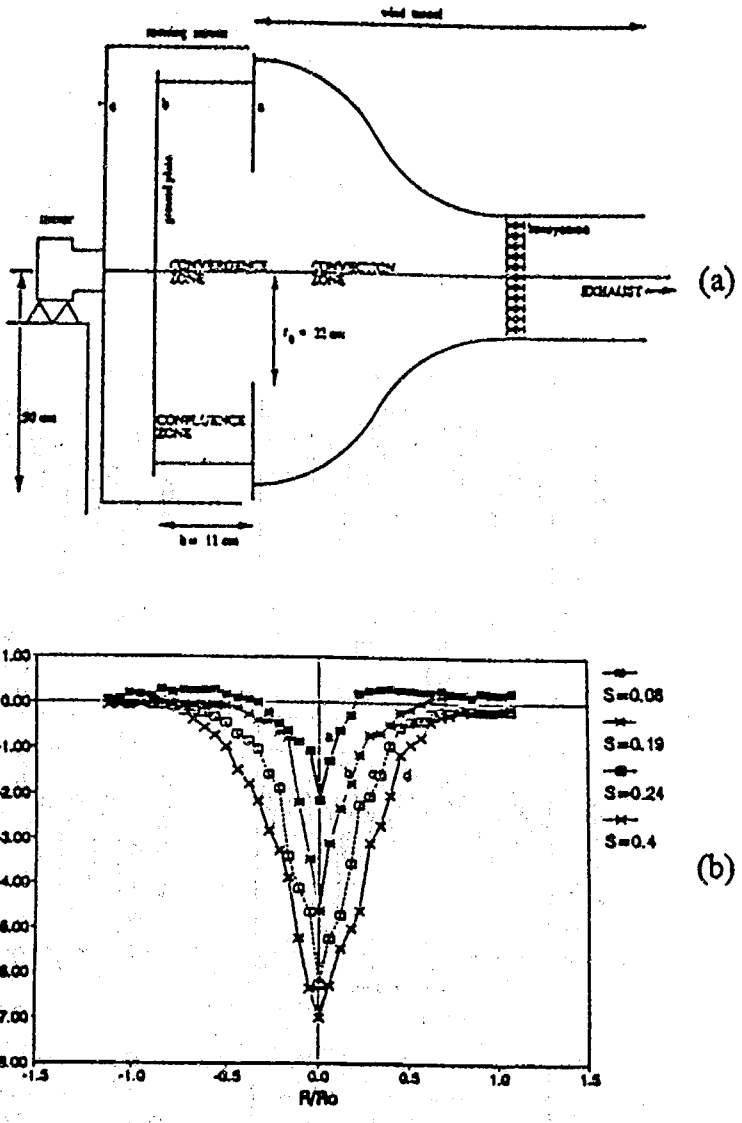


Figure 10. Experimental configuration of tornado generator (a) and mean pressure coefficient underneath tornado-like vortex over rough ground plane, Re = 390,000

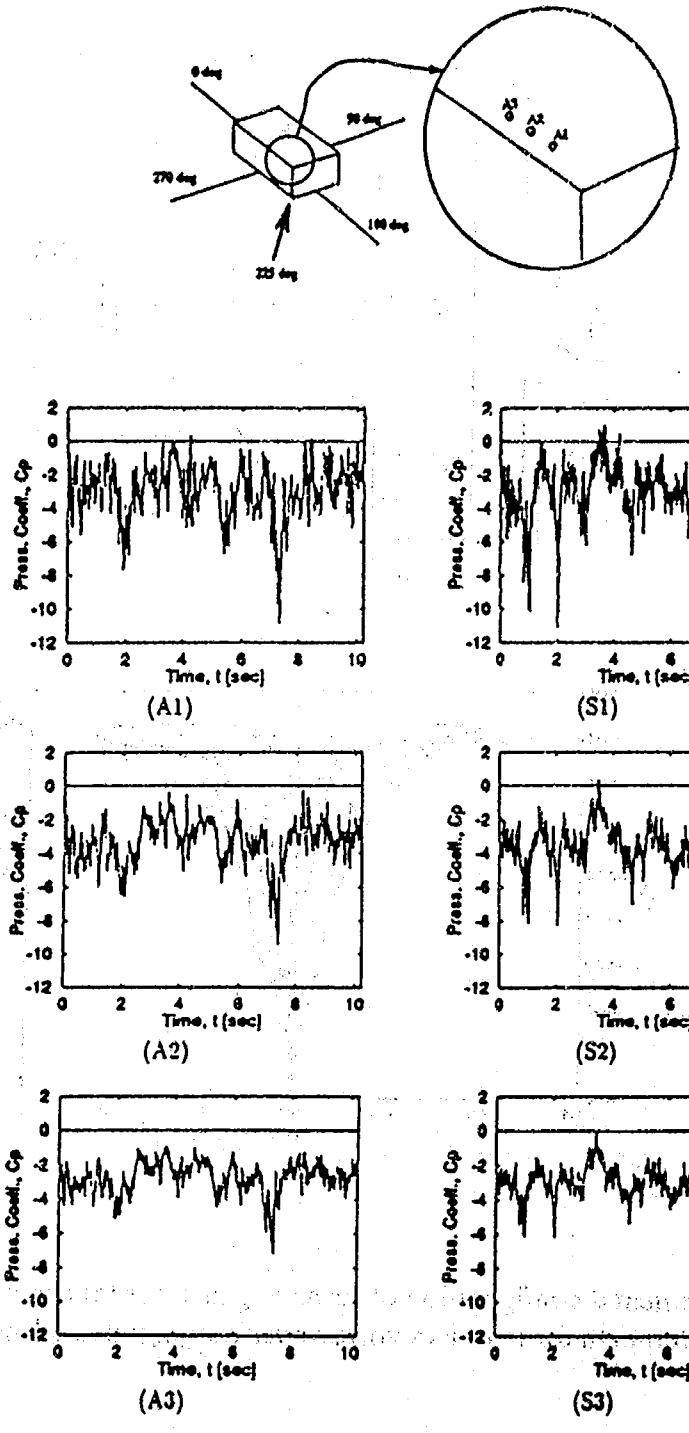


Figure 11. Measured in wind tunnel (A1-A3) and simulated point pressure at taps near roof corner edge

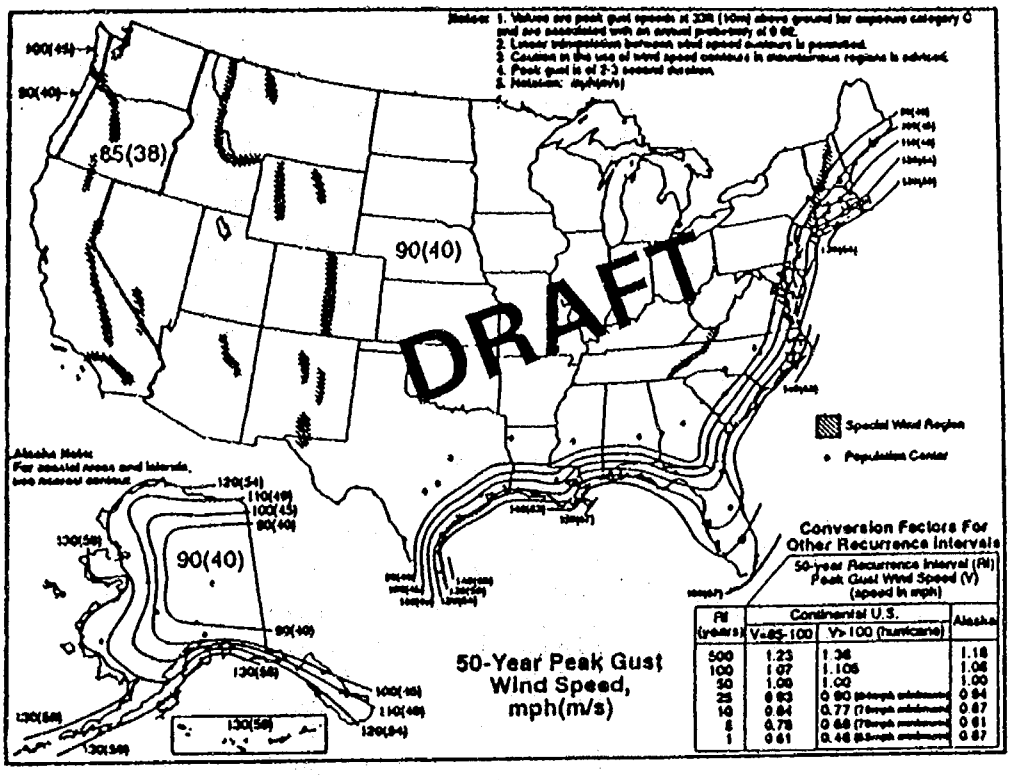
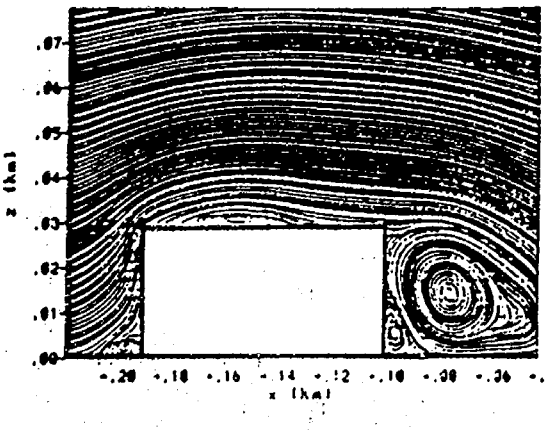
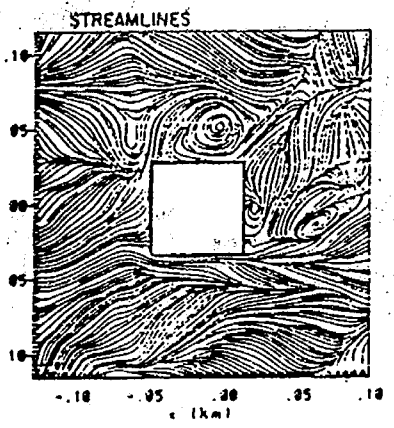


Figure 12. Proposed wind map for ASCE 7-95 Wind Load Standard





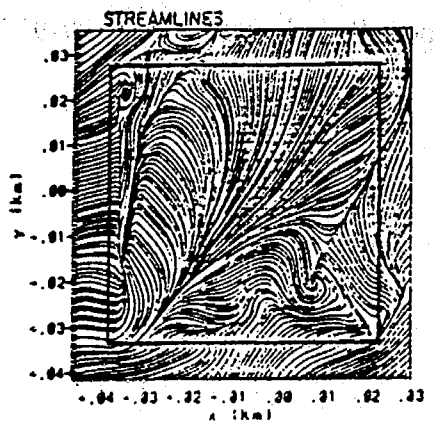


Figure 13. Computed streamlines for two-dimensional building normal to wind and for three-dimensional building exposed to cornering wind

Theme 3

A Preliminary Report on the Hyogo-ken Nanbu Earthquake 1995

by

Hidemi M. Ito[1], Tetsuo Hashimoto[2], Sumio Yoshikawa[1] and Akio Yoshida[2]

ABSTRACT

An earthquake with M7.2 hit Kobe and adjacent cities in western Japan early in the morning of January 17, 1995. This earthquake, named the Hyogo-ken Nanbu earthquake 1995, was the most damaging natural disaster in Japan since the great Kanto earthquake in 1923. As of April 3 the toll had reached 5,500 dead, 2 missing, 36,938 injured, and more than 100,000 houses were completely destroyed. The damage to the supply systems of gas, water and electricity was devastating.

In this report some seismological aspects of the earthquake including its rupture process and aftershock activities will be discussed based on the observation by the Japan Meteorological Agency.

Keywords : Hyogo-ken Nanbu Earthquake,
Aftershock,
Rupture Process

I. MAINSHOCK AND AFTERSHOCKS

The Hyogo-ken Nanbu earthquake occurred at 05h46m of January 17, 1995. Its epicenter is located at 34°34'N, 135°03'E, northern part of Awaji-shima island, and its focal depth is estimated at 14 km.

Some anomalous phenomena prior to the earthquake have been reported. In the focal region where a complex system of active faults exists, a seismic gap was pointed out (Ishikawa 1990). There was a swarm activity including M4.1 earthquake in November 1994 in the vicinity of the focal region of the mainshock. Near the epicenter of the mainshock a foreshock like earthquake with M3.5 occurred in the previous day. Anomalies in electromagnetic field

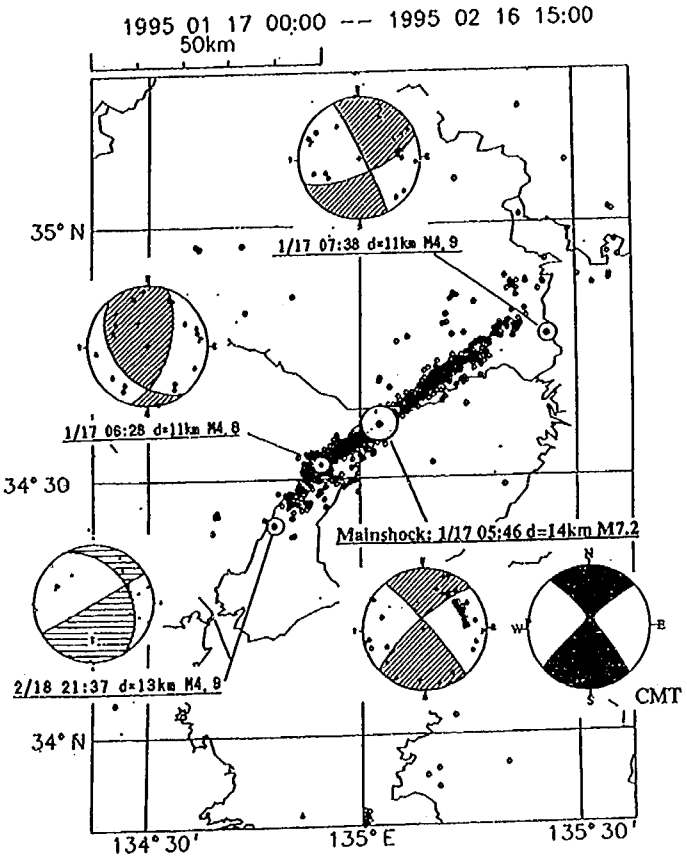


Fig. 1 Epicentral Distribution of Mainshock and Aftershocks

Focal Mechanism diagrams are shown, using the equal-area projection on the lower hemisphere.

1) Seismology and Volcanology Department, Japan Meteorological Agency, Chiyodaku, Otemachi 1-3-4, Tokyo 100, Japan

2) Seismology and Volcanology Department, Meteorological Research Institute, Tsukuba, Ibaraki 305, Japan

were also observed.

Figure 1 shows an epicentral distribution of aftershocks occurring in a month since the mainshock. This figure includes focal mechanisms of the mainshock and major aftershocks. The CMT solution of the mainshock is also given for reference. We see the mainshock has a right-lateral strike-slip mechanism, and its fault stretches as long as about 50km in the direction of SW-NE. This mechanism is compatible with the tectonic environment of east-west shortening of the southwestern Japan.

As will be discussed in the appendix, a waveform inversion analysis of strong ground motion seismograms shows that the total seismic moment is estimated at 2.7 x 10^{19} Nm, and that the rupture continued about 10 seconds.

Figure 2 shows the number of earthquakes every four hours counted at the Kasai station. (See Fig.3 for location). It decreases smoothly, following the modified Omori formula; the hourly number n(t) decays as K/(t+c)p with K=2230, p= 0.97, c=0.0 .

The biggest aftershocks have magnitude M4.9, occurring at 07:38 of January 17 and 21:37 of February 18. Some of the major aftershocks, M4.3 of January 23 and M4.7 of January 25, were preceded by seismic quiescence, which could be a clue to forecasting large aftershocks.

Seismicity in the vicinity of the focal region of the mainshock is feared to be activated. It is worth pointing out the following empirical fact (Yoshida and Ito 1995). We have been hit by 6 shallow inland earthquakes with M≧7.0 other than Hyogo-ken Nanbu Earthquake since 1926 when JMA deployed a nationwide seismic network. All the earthquakes except one were followed by earthquakes with magnitude around 6.5, with distance of 20-60 km and with time lag of 1-8 years. These earthquakes will be called aftershocks in a wider sense. Interestingly, earthquakes with magnitude 4.5 or larger often occurred

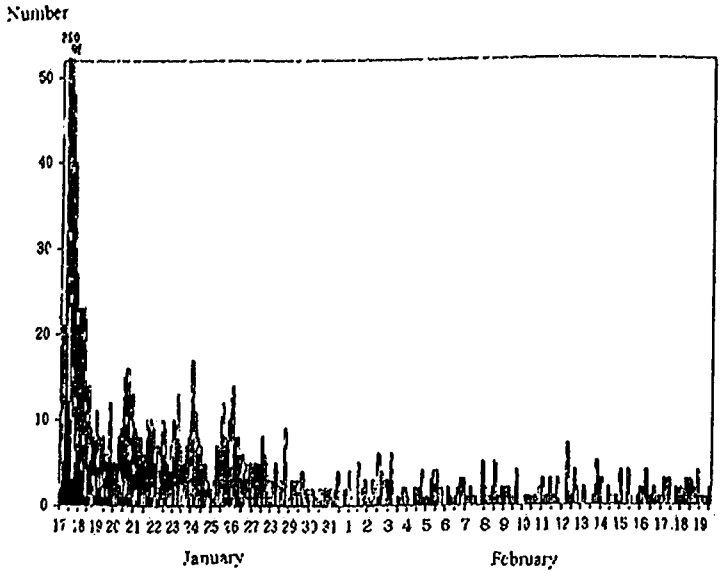


Fig. 2 Time Change of the Number of Aftershocks
■: earthquakes felt at meteorological observatories

in a couple of years later than the M≧7.0 earthquakes near the epicenters of the forthcoming aftershocks in a wider sense.

2. SEISMIC INTENSITY AND GROUND MOTION

Quantities related to earthquake hazard will be discussed in the following .

Figure 3 gives a distribution of seismic intensity of JMA scale measured by intensity meters, which tells the maximum value 6 was recorded at the observations site Kobe and Sumoto, nearest to the epicenter.

A mobile observation team dispatched from JMA immediately after the earthquake found that the seismic intensity had reached as high as 7 in the hatched area along the coast in Fig.4. The highest value 7 was observed for the first time since its introduction to describe the damage by the Fukui earthquake M7.1 in 1948.

One of the interesting features is that the most damaged areas are several kilometers away from the fault system as well as the aftershock region. This will be attributed to the difference in the soil structure.

For reference sake we will give a list of peak

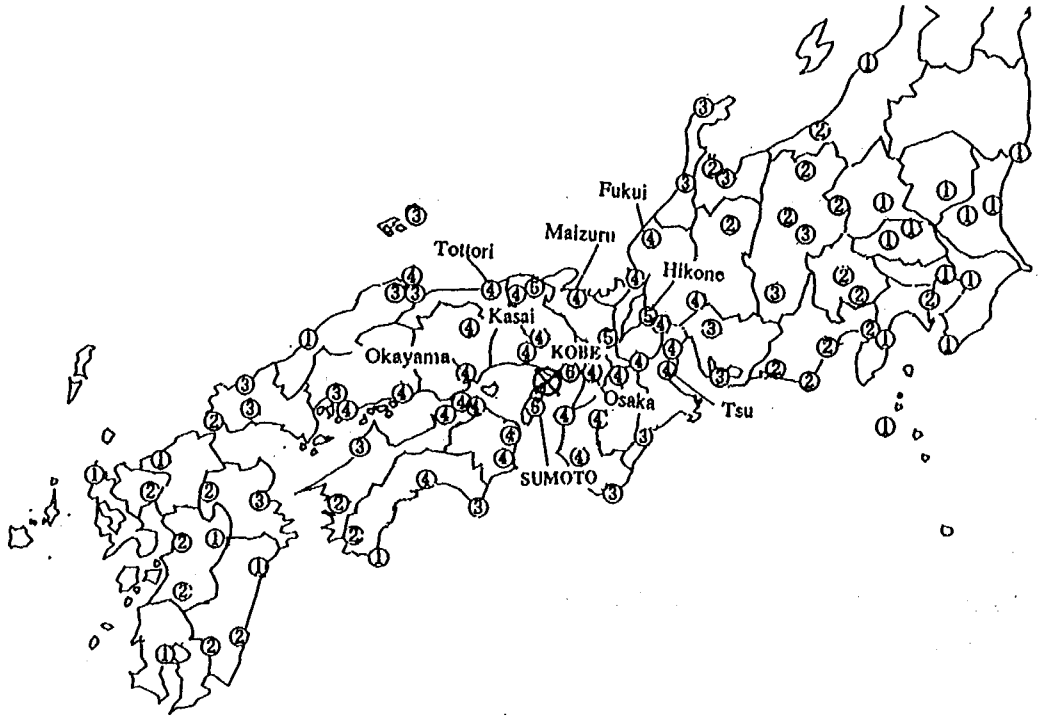


Fig. 3 Seismic Intensity

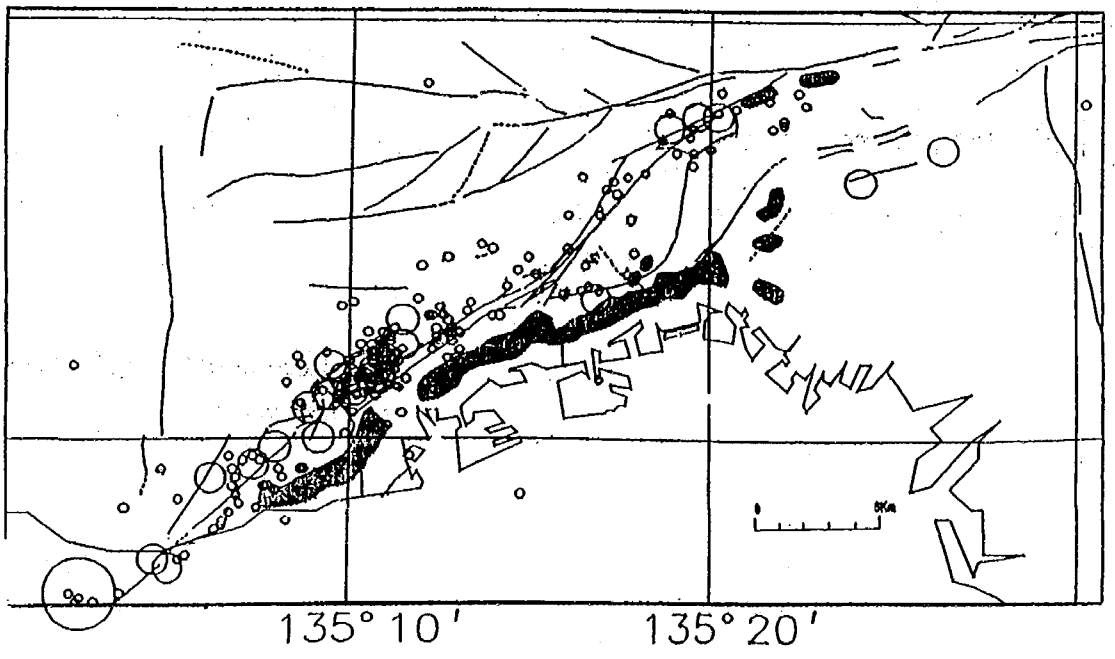
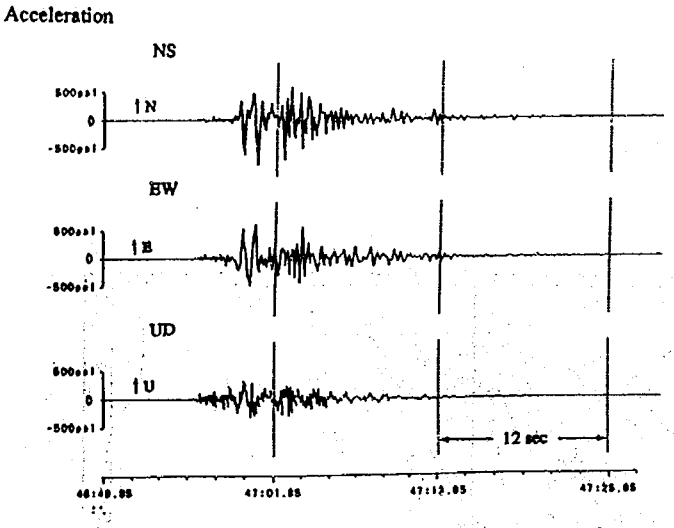
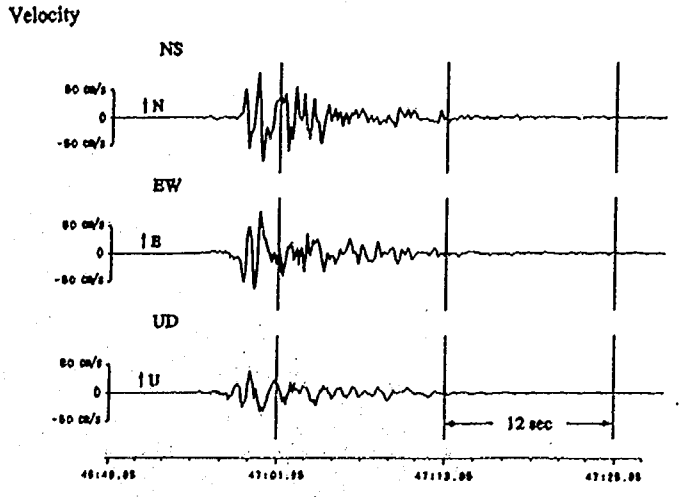


Fig. 4 Areas with Revised Intensity 7 and Active Faults

Location	Peak Acceleration (gal) NS	EW	UD
Kobe	818	617	332
Osaka	81	66	65
Maizuru	67	52	39
Okayama	77	59	36
Tottori	77	74	15
Hikone	137	147	39
Tsu	71	60	26
Fukui	33	42	10

Table 1 Peak Acceleration at Meteorological Observatories





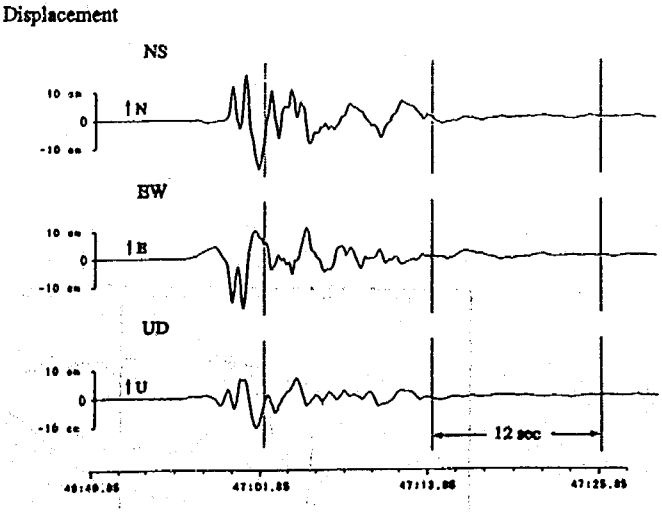


Fig. 5 Records of Strong Seismograph at Kobe Marine Observatory

ground motion acceleration at JMA stations in Table 1 together with a seismogram recorded at Kobe Marine Observatory in Fig. 5.

APPENDIX RUPTURE PROCESS

We will study a rupture process by using the ground motion seismograms of JMA including records of the Kobe Marine Observatory which is located just upon the earthquake fault. The original outputs are three-components digital acceleration records of JMA strong motion seismographs whose amplitude response and phase delay are, respectively, flat and zero shift from DC to 10Hz. Displacement wave forms were used in this study, which were obtained from the original acceleration records with a recursive filter characterizing the motion of a mechanical seismograph (undamped period of the pendulum =20 s, and damping constant =0.5) . The displacement data were resampled with a sampling rate 2.5Hz, viz frequency ranges from 2.5Hz to 0.05Hz in the analysis. Figure 6 indicates the locations of the 7 seismic stations (Kobe, Okayama, Tottori,Maizuru, Kyoto, Osaka and Koyasan) whose data were used.

Such earthquake parameters of the faults as location, dip and shape were so determined as to be consistent with the aftershock distribution, the focal mechanism, the initial motion in Kobe, and the crustal deformation. The fault is divided into two segments: Kobe side and Awaji side. The fault parame-

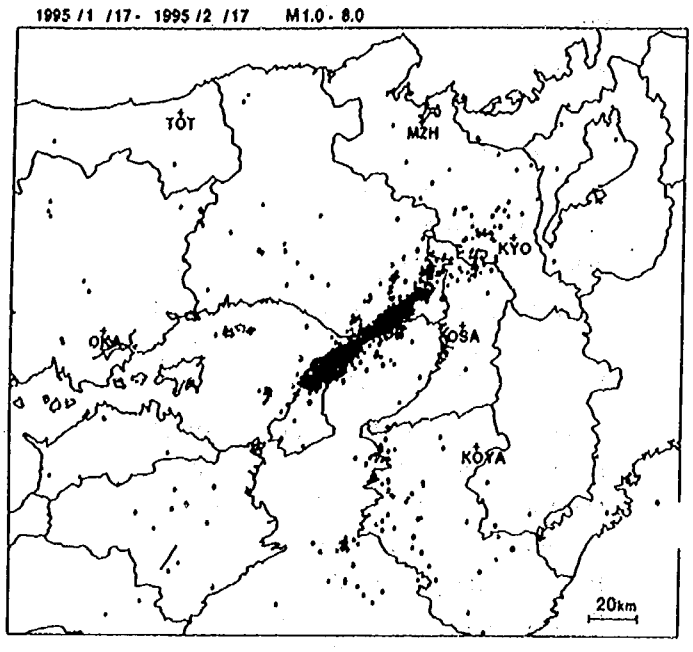


Fig. 6 JMA Stations Used for Analysis

	dip	slip	strike	length	width	top	bottom
northern fault	80	160	233	30 km	15.1 km	0.0 km	15.0 km
southern fault	80	170	53	10 km	15.1 km	0.0 km	15.0 km

Table 2 Parameters of Fault

depth	Vp	Vs	ρ	Qp	Qs
0.0	2.5	1.2	1.9	100	50
0.2	5.5	3.25	2.7	250	100
4.4	6.11	3.61	2.85	350	200
24.0	7.15	4.01	3.25	450	200
34.0	7.81	4.41	3.30	500	250

Table 3 Velocity Structures

ters used are summarized in Table 2. The fault is further divided into 12 subfaults which are regarded as a set of point sources.

Elastic wave field from a point source is calculated by the method by Takeo (1985) which handles the effects of anelasticity represented by a complex velocity in a horizontal layered structure. A velocity structure is given in Table 3 which is modified from the model by Ukawa and Fukao (1981).

The waveform inversion (Takeo 1987) gives a solution of seismic moment release and beginning of rupture on each subfault by assuming the parameters of fault geometry, the slip direction and the rise time. We change the parameters by a trial and error method to get a

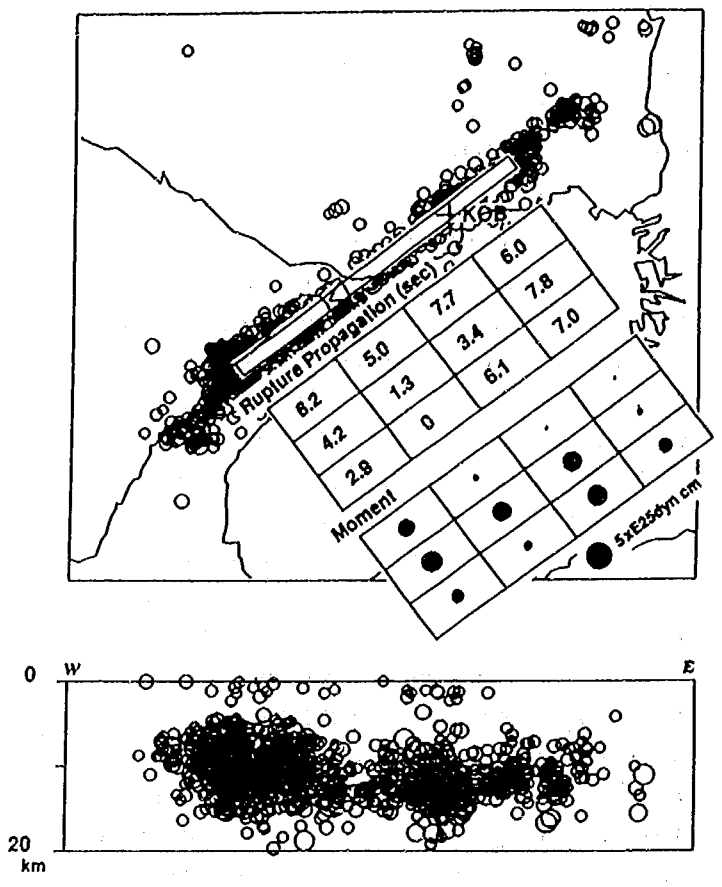


Fig. 8 Rupture Times and Moments
The surface projection of the two fault segments are shown on the mainshock and aftershock distribution. Results shown on the fault subdivided into 10km by 5 km are arranged along the surface projection. Also shown is an EW vertical cross section.

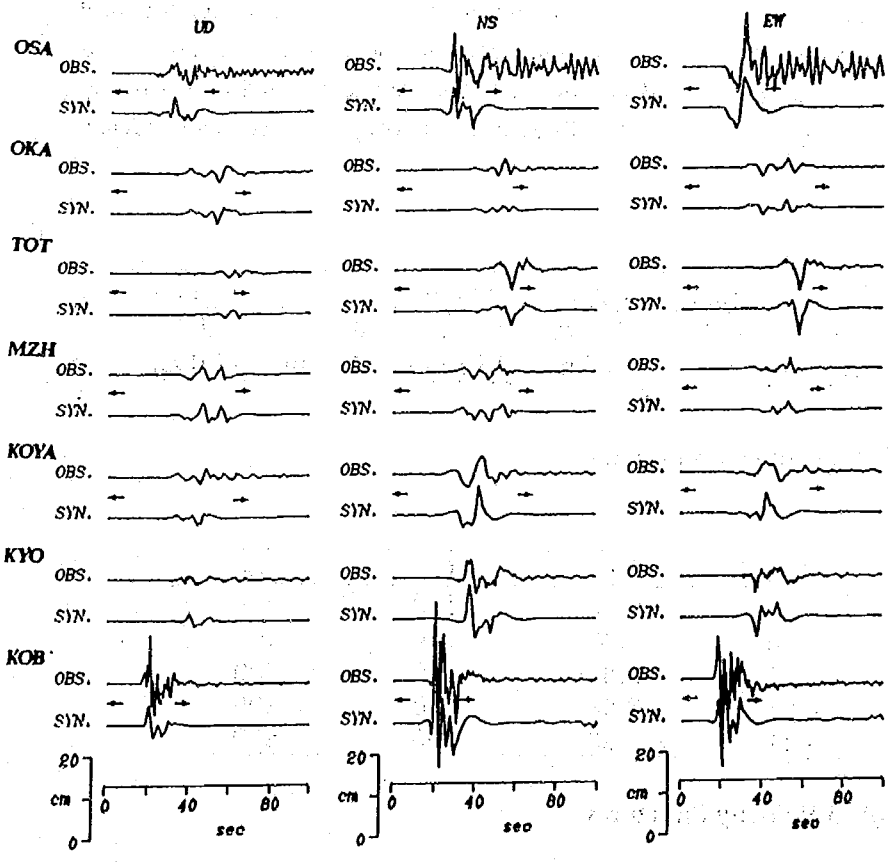


Fig. 7 Observed waveforms and synthetics dsiplayed from 5:46:40, Jan. 17,1995 (JST). The waveform inversion is carried out for the data section indicated by arrows.

better solution with small residuals, non-negative seismic moments and smooth rupture propagation.

Figure 7 displays observed waveforms and synthetics. The waveforms are shown for 100 sec long starting at 05:46:40 (JST). Only the data in between the small arrows were used for the inversion. Released seismic moment and the rupture time on each subfault is given in Fig. 8. The total moment is estimated at 2.7×10^{19} Nm and the rupture propagated in bilateral directions and stopped in about 10sec.

Large amount of moment was released in the shallow part of the Awaji side, showing a contrast to the small moment in the shallow part of Kobe side. This is consistent with the observation of a clear surface rupture of Nojima fault in Awaji island and with no such ones in Kobe side.

ACKNOWLEDGMENT

We used a FORTRAN program of the waveform inversion by Dr. T. Takeo, and SALS of the Univ. of Tokyo. Discussion with Dr. K. Uhira concerning the waveform inversion was very helpful.

REFERENCES

Most of the materials in this paper are taken from preliminary reports by JMA and

Koizumi, T: Hyogoken Nanbu Earthquake, Kisho 4-12, 1995

For contributions from other organizations and researchers, see, for example, the report

Somerville, P: Kobe Earthquake: An Urban Disaster, EOS 76 49-51, 1995

Ishikawa, Y: Seismic Gaps in Japanese Island, Gekkan Chikyu 4 355-361, 1990

Yoshida, A and Ito, H.M : Forerunning Activities for Large Earthquakes Succeed Disastrous Intraplate Earthquakes, submitted to Chigaku Zasshi

Takeo, M: Near Field Synthetic Seismograms Taking into account the Effects of Anelasticity -The Effects of Anelastic Attenuation on Seismograms Caused by a Sedimentary Layer, Pap. Met. Geophys. 36, 245-257, 1985

Takeo, M: An Inversion Method to Analyze the Rupture Processes of Earthquakes Using Near-Field Seismograms, Bull. Seismol. Soc. Am. 77, 490-513, 1987

Ukawa, M and Y. Fukao, Poisson's Ratio of the Upper and Lower Crust and the Submoho Mantle beneath Central Honshu, Japan, Tectno. 77, 233-267, 1981

Relationships between Geomorphologic Condition and Disasters at 1995 Hyogoken-nanbu Earthquake

by

Masaharu Tsuzawa[1], Masakatsu Horino[2], Hidetoshi Nakajima[3]
and GSI Geographic Research Group on Disasters

ABSTRACT

This paper presents tentative summary of our geographical researches for the disaster of 1995 Hyogoken-nanbu Earthquake, well-known as Han-shin Awaji Earthquake Disaster, as of May 1995. We interpreted aerial photos, made field survey and announce the results of the research that the situation and the cause of this disaster. And we confirmed some relationship between geomorphologic condition and the state of calamity at Han-shin area.

Key Words : land condition map
disaster current state map
geomorphologic condition
photographic interpretation
seismic fault

1. INTRODUCTION

In 17 January 1995, Hyogoken-nanbu Earthquake was occurred through northern part of Awajishima island and foot of Mt. Rokko at Hyogo Prefecture, West Honshu, Japan. This Earthquake brought serious damages to Awajishima island and Han-shin area such as Kobe, Ashiya, Nisinomiya. This earthquake is characterized by the epicenter. It is shallow and directly under the megaropolis area. And it had been the worst natural disaster in Japan after World War II.

Geographical Survey Institute (GSI) compiled 1:50,000 topographic base map of damaged area for research and recovery till the night of the day, took and analyze aerial photos, made field survey three times and announce the results of the research many time that the situation and the cause of this disaster.

Follows are tentative summary of our researches for the Disaster as of May 1995.

2. AERIAL PHOTOGRAPHING AND ITS INTERPRETATION

At the day of the occurrence, GSI started the photographing for took information of the situation. GSI Photographic group took aerial photos from Akashi to Osaka (Han-shin megalopolis area) on that day by GSI airplane. These films transferred to GSI immediately and processed and printed through the night. The next day, GSI distributed these photos to administration for disaster and opened to the public (and sold by Japan Map Center).

GSI Photographic group also took photos of Awaji-shima island. Finally, they took aerial photos over 10,000 scenes to 21 January.

We, GSI Geographic Research Group on Disasters researched the existing

1) Head, Third Geographic Division, Geographic Department, Geographical Survey Institute, Ministry of Construction, Tsukuba City, 305 Japan
2) Senior Officer for Planning of Environmental Geographic Information, Geographic Department, GSI
3) Deputy Head, Third Geographic Division, Geographic Department, GSI

circumstances. First we started interpret these photograph. But we couldn't sufficient interpretation of Kobe area first because of smoke of conflagrations. So we use other photo took 20 January in this area.

Next we plotted these results on 1: 10,000 topographic maps.

Items of interpretation are follows:

(1) Collapsed building and house
(2) Burned area
(3) Damaged road and railway
(4) Landslide
(5) Liquefaction of the ground
(6) Damaged pier and embankment

The results were compiled manuscript maps. These were color-separated, processed and printed, then we published it in 26 January as 1:10,000 earthquake disaster current state maps (I).

3. SEISMIC FAULT APPEARED NORTHERN AWAJISHIMA ISLAND

At the day of the occurrence, Dr. T. Nakata of Hiroshima Univ. get the figure of the movement by this earthquake. It was Nojima fault, one of already-known active fault. He announced related organizations including GSI soon.

In 18 January, the next day of the

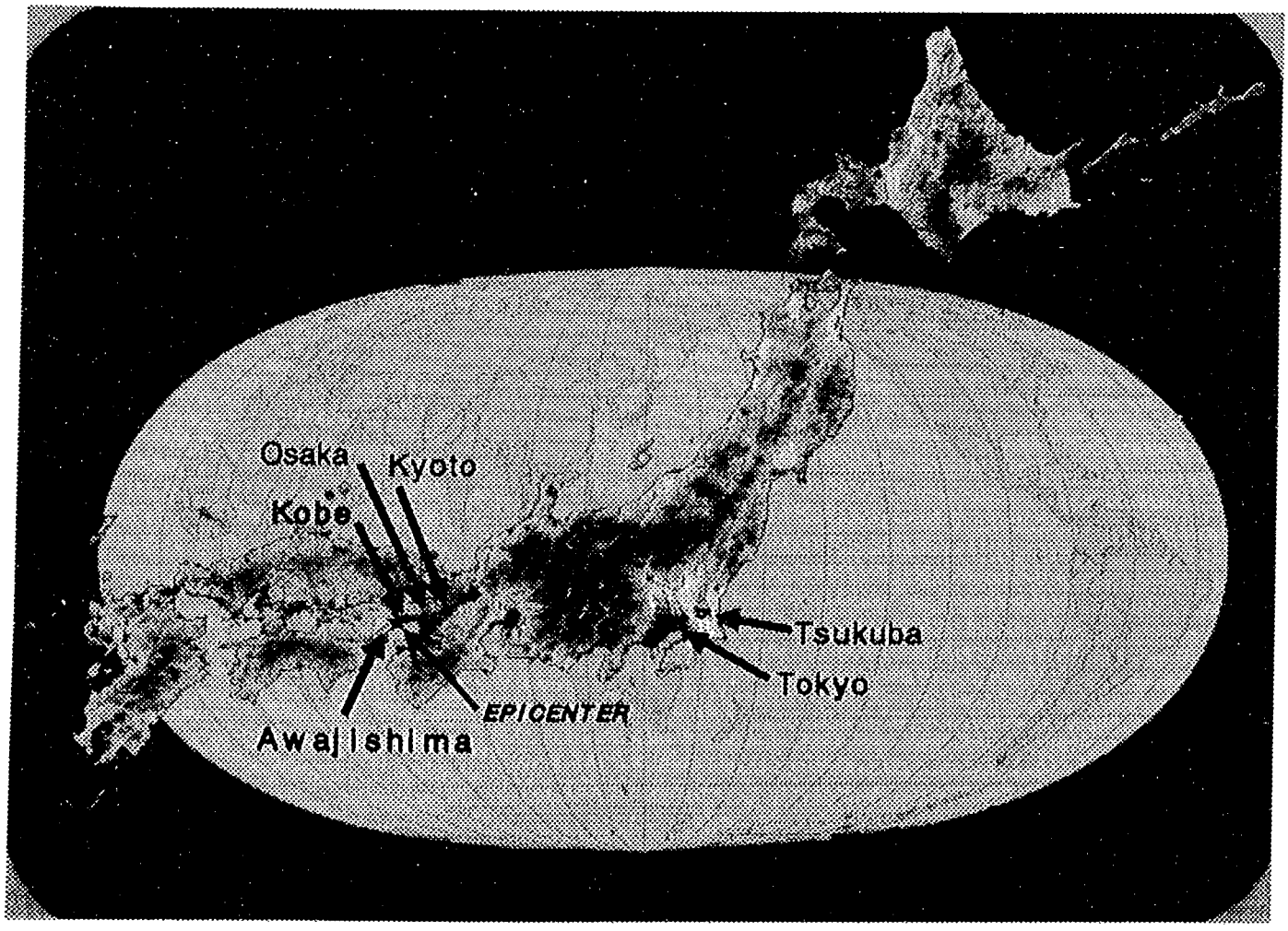


Fig. 1 Location

occurrence, we started to field surveys and researchs by two parties (Han-shin and Awaji). The rest of us interpreted the above-mentioned aerial photograph in office. It could be confirm the location of the seismic fault, we traced it on topographic map and send the results to field survey parties.

According of the interpretation of this fault (by aerial photo only), it had follow feature:

located from the north end of the island to

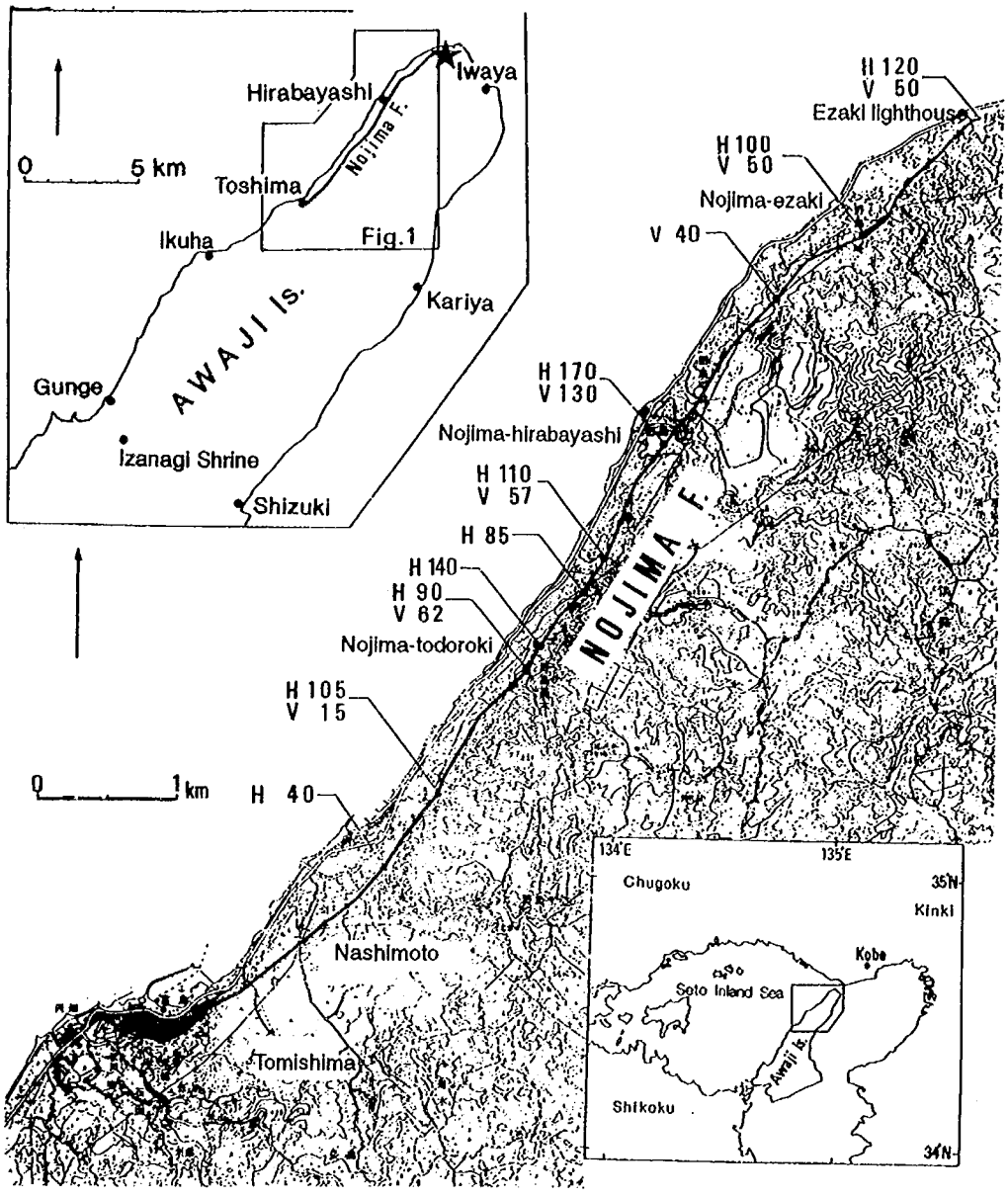


Fig.2 The Location and its Movement of the Seismic Fault

Quote from OTA, HORINO and GSI (1995)

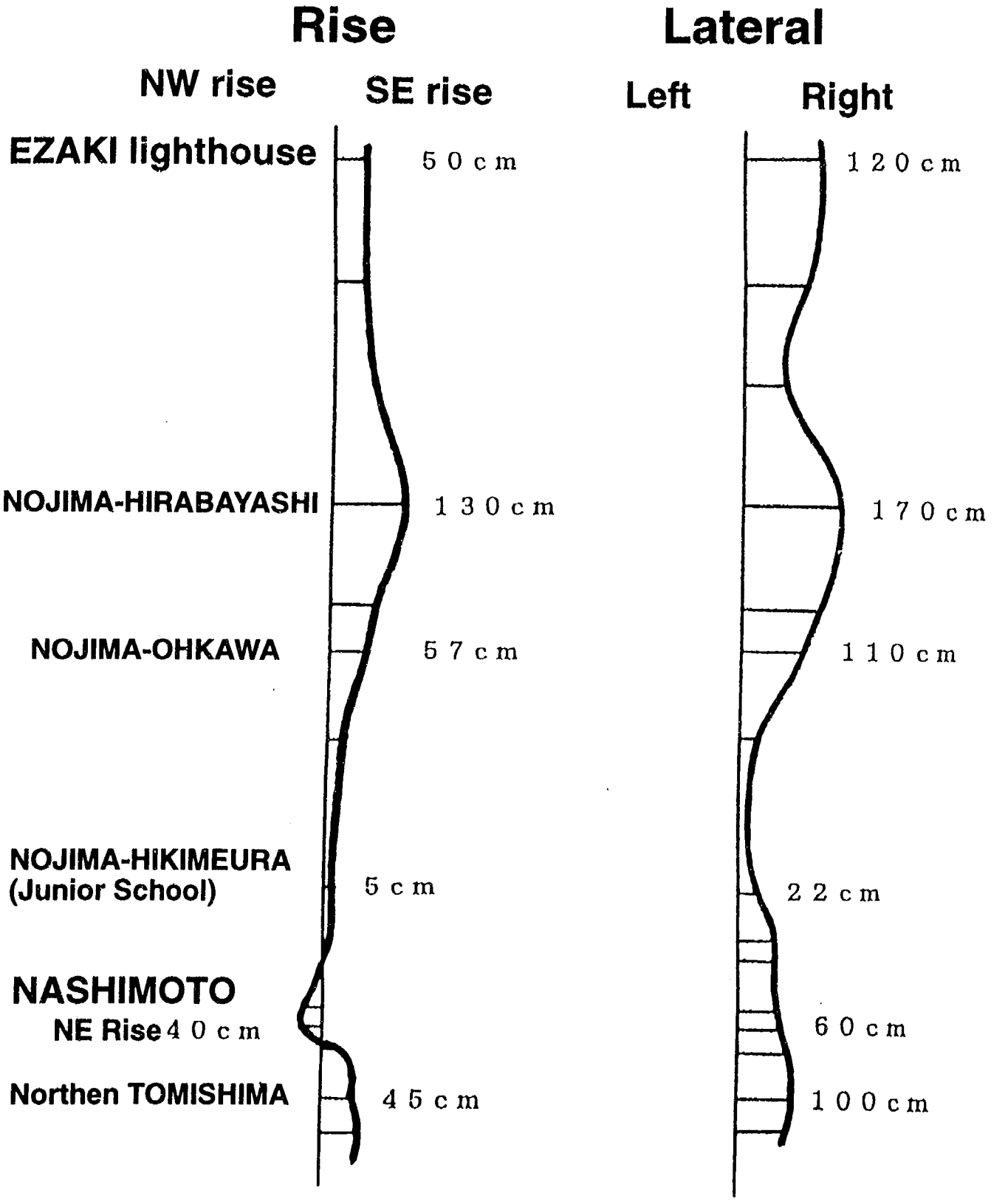


Fig. 3 Movements of Nojima Fault (Seismic Fault)



Pic. 1 Seismic Fault at Nojima-hirabayashi

Tomishima,
along the west coast of the island,
run NE-SW strike, 10km long,
slipped right laterally,
SE rise (partly NW rise).

After received this instruction, field survey party in Awajishima island started to measure the movement of the fault. It had 1.7m right lateral slip and 1.3m SE rise maximum at Nojima-Hirabayashi.

On Han-shin area, we couldn't confirm any seismic fault along an already-known active faults. There were places where the cracks were formed concentrating. But almost of these were the part of local or surface weak spot in the ground or the surface slipped down by gravity. We were not able to find the systematic one that tectonic movement was reflected.

However, a lot of cracks that shown right lateral within 2cm had appeared almost in parallel in the vicinity of the Suma coast. Moreover, we saw right lateral cracks of tens of cm that is not explained easily a little only by the movement of the surface in the central Kobe, so we think that the possibility that the unknown fault lies behind underground.

4. THE DISASTER AND THE GEOMORPHILOGIC CONDITION

By 1965, GSI investigated the land condition and compiled and published the result of the Kobe district to 1:25,000 land condition map.

We executed the investigation of the relation among the geomorphic and the ground condition displayed in the land condition map and the earthquake damage because we had caused remarkable damage in the earthquake according to piedmont of Mt. Rokko.

This area consists of the hill ground and the low ground where the urban area in

the Kobe City and the Ashiya City is long and slenderly recorded between Mt. Rokko and the Osaka bay in the south. This mountain area and low ground area are in contact with active fault. An alluvial fan and a minor terrace, etc. are consecutive according to the the foot of the mountain and the coastal low ground and innings line up on the sea side. Most of all rivers becomes a raised bed river which flow from the mountain, and minute upland in the banks of river continues to the mouth of river.

Our parties surveyed along the investigation route set to cross or to run through different geomorphological features and supplemented with the above-mentioned 1:10,000 earthquake disaster current state map (I) in the locale. The outline of the results are as follows:

(1) In the vicinity of the foot of Mt. Rokko, damage because of the surface slipped down by gravity was seen in the steep slope of the fault-origined cliff along already-known active faults.

(2) The disaster concentrates in the west Han-shin district regardless of the minuteness geomorphological condition.

(3) In the east part district, there were a lot of collapses of the buildings and the structure on gentle frontage of alluvial fan, the edge of lower terraces, shallow valleys and the district where the rice field sign were displayed in the old editioned topographic maps. On the coastal plain, as for the collapse, it was admitted that the tendency limited to supreannuated houses though lots of omissions of the underground things.

(4) At the hill ground, the strangeness of the retaining walls and the destruction of a multistory houses were seen on banking by making smoothly and the former accumulation pond site.

(5) Liquidizings were caused almost completely in innings without a part of Rokko island.

(6) In the shore protections and the quays, the tilt and overhang to the sea side were caused being pushed to liquidized earth and the damage such as harbors facilities were amplified. The erosion by waves has already started in the destroyed quays.

5. CONCLUSIVE REMARKS

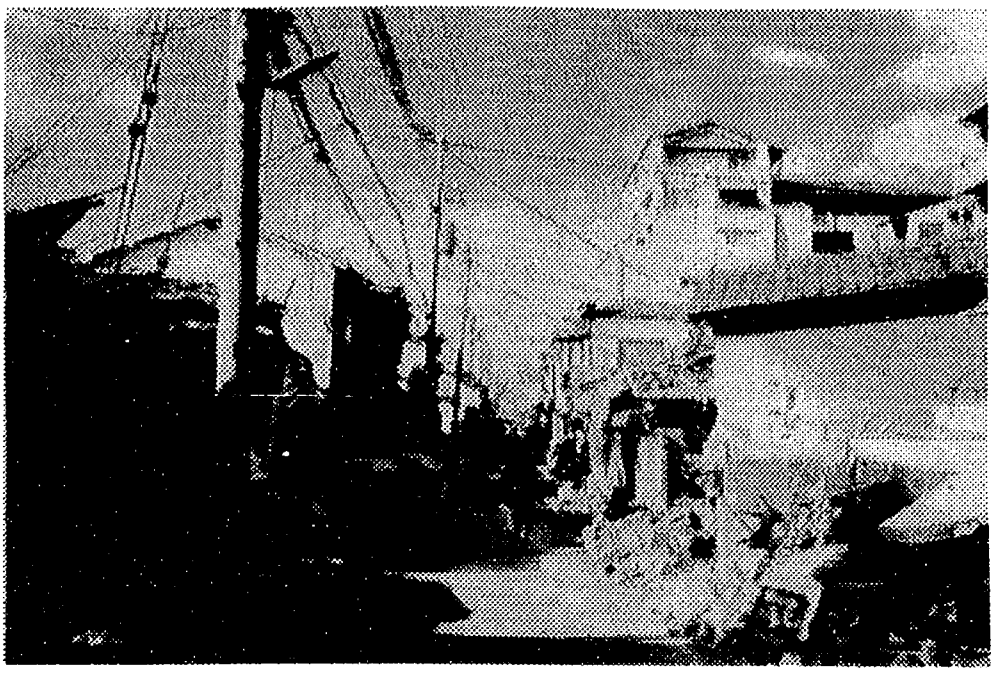
In 2 May, we GSI opened 1:10,000 earthquake disaster current state map (II).

The first edition was the one having made us only from the result of our interpretation of the aerial photograph. But these new maps are compiled of the one that the result of the first edition, future interpretation, our field survey and a lot of the investigation results by many people.

Moreover, we are scheduled to revise the land condition maps of the Han-shin district within this fescal year. We would like to the future research and analysis about the relation to the geomorphologic condition and the earthquake-proof in the ground.

BIBLIOGRAPHY

OTA, HORINO, GSI Survey Group on Disasters (1995): Notes on the Earthquake Fault on Awaji Island, Associated with the 1995 Hyogoken-nanbu Earthquake and Related Disasters, Journal of Geography, **104**, 1, 143-153



Pic. 2 Disasters on Gentle Frontage of Alluvial Fan



Pic 3 View on Coastal Plain

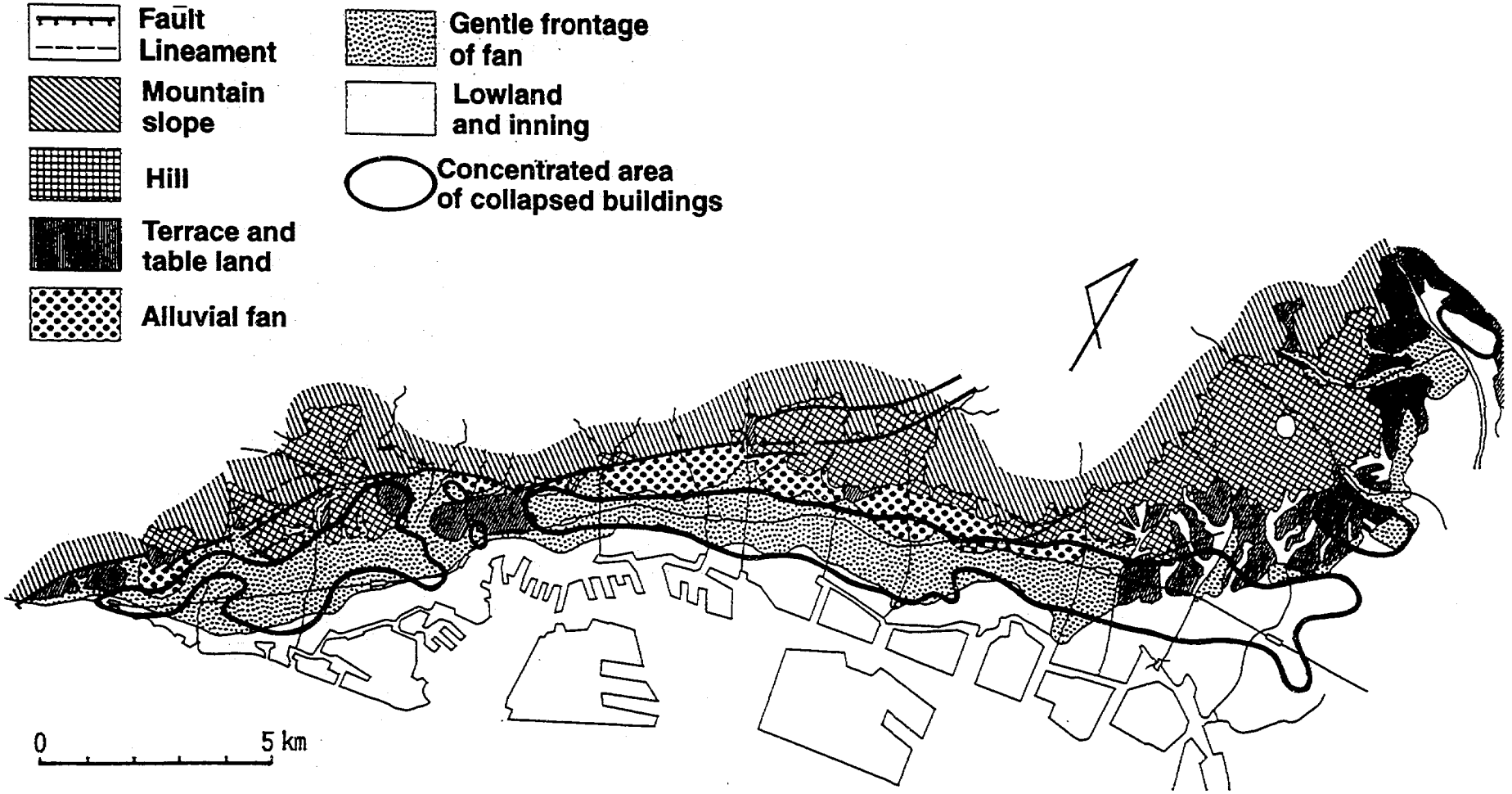


Fig. 4 Geomorphologic Conditions and the State of Calamities of Han-shin Area

Evaluation of Strong Ground Motion in Kobe Area of 1995 Hyogoken Nanbu Earthquake

by

Y.Kitagawa [1], I.Okawa [2], T.Kashima [3], and S.Koyama [4]

Abstract

Hyogoken-Nanbu earthquake left devastating damage to Kobe area. The reconstruction of the city should be based on the understanding of the geological and seismological situations of the city.

Data on earthquake source and geology of the area are being collected at present. Some discussions on the source mechanism, geological features of Kobe and some attempts of aftershock and microtremor measurement are introduced in addition to the properties of strong ground motion during the earthquake.

Key words: Shindo 7, Disaster belt, Rokko Mountains, Aftershock, Microtremor, Overturning of Tombstone

1. Introduction

Hyogoken Nanbu earthquake occurred at 5:46 A.M. JST on 17th of January, 1995. It is worth noting that the earthquake occurred on the same local date with the Northridge earthquake of 1994.

Its epicenter located just north of the Awaji island and at the depth of 14.3 km. The magnitude of the earthquake was determined 7.2 by Japan Meteorological Agency (JMA). The source rupture zone was located close to the central part of Kobe, a densely populated area. Therefore, the damage to the society was so devastating as Japan has never experienced since the Kanto earthquake of 1923.

From the view point of ground motion evaluation, Hyogoken Nanbu earthquake has the following features.

(1) The affected area is so large.
(2) The earthquake source is close to the area.
(3) The geological condition is complicated due to numbers of faults running under Kobe.

Another item making our investigation very difficult is the lack of earthquake preparedness of the society. There has been a misleading recognition of local people that earthquakes would not occur in Kobe in spite of the existence of active faults. Therefore, the strong motion instrumentation was no spontaneously proposed for new construction or to very important structures such as city halls, bridges and skyscrapers etc.

The estimation of ground motion during the earthquake at sites then becomes very difficult due to the lack of strong motion records. Nevertheless, several organizations had installed seismographs around the area and are making these precious records available to date.

Some preliminary efforts for collecting the basic data and evaluating the ground motions of the sites are introduced and some primary outcoming results will be shown in this paper.

2. Overview of the Earthquake

2.1 Shindo (Japanese Seismic Intensity) Map

Japan has unique seismic intensity scaling system, which we call Shindo (or Shindo-kai) system. Shindo scales from 0 to 7, whereas the Modified Mercalli Intensity scale counts from 1 to 12. The definition of Shindo is explained in Table 2.1.1.

The Shindo distribution for this earthquake is shown in Fig.2.1.1 Cities of Kobe and Sumoto were assigned Shindo 6; Cities of Kyoto, Hikone, and Toyooka were assigned Shindo 5, etc. The highest intensity i.e. Shindo 7 in Table 2.1.1 was added after the 1948 Fukui earthquake which caused more than 3700 deaths, in view of the ruinous damage in Fukui city.

1) Director, International Institute of Seismology and Earthquake Engineering (IISEE), Building Research Institute (BRI)
2) Head, Geotechnical Engineering Division, Structural Engineering Department, Building Research Institute
3) Research Staff, IISEE, BRI
4) Research Staff, Production Department, BRI

Table2.1.1 JMA Seismic Intensity Scale and Its Description

Shindo (Intensity)	Description
0	Not felt by people but strong enough to be recorded on a seismometer.
1	Felt only by people remaining still or people sensitive to quakes
2	Felt by most people remaining still or people sensitive to quakes
3	Houses are jolted. Doors and shoji screens rattle. Objects hanging from ceilings, such as light fixtures, swing much. Liquids in containers pitch and roll
4	Houses are jolted strongly, Unstable objects, such as a vase, topple. Liquids spill out of containers. Felt also by people walking. Many people go out of their houses.
5	Walls get cracked. Tombstones fall down. Chimneys and stone fences are damaged
6	Less than 30 percent of houses collapse. Landslides occur. Cracks appear in the ground. Most people cannot stand.
7	30 percent of houses collapse. Landslides occur, the ground cracks or faults are caused by the earthquake.

(The description is taken from Japan Times Special Report, 1995)

After damage reconnaissance survey, JMA reassigned the Shindo 7 for some portions of cities of Kobe, Ashiya, Nishinomiya, and Takarazuka, and portions of the northern part of Awaji island. Shindo 7 was applied for the first time since its enforcement. The reassigned Shindo 7 forms belt-like shape in the area as shown in Fig.2.1.2. We call this linked areas as 'Disaster Belts' for Hyogoken Nanbu earthquake. The causes of the linked damage belts are now discussed among scientists and engineers in Japan. Some insists there are unidentified faults beneath the belts. Some says that the change in geological conditions from outskirts of Rokko Mts. to coastal area formed the limited area of disaster.

2.2. Fault Parameters [3)]

The solution based on the distribution of compression and extension of initial seismic motion is shown together with the CMT solution in Fig.2.2.1. It can be inferred from this figure that the focal mechanism is characterized by a N229E strike, dip equal to 77 degrees, and slip of 173.

Prof. Kikuchi of Yokohama City University reported that a bilateral rupture had occurred with the following characteristics:

Focal mechanism: strike(233 degrees,
dip(85 degrees, slip(165
Seismic Moment:
M_0= 2.5*10^{26}dyne*cm
Fault Area: S=40*10km^2
Relative Displacement: U=2 .1 m
Stress Drop: D=100~200 bar
Duration of Main rupture: T=11 sec

This earthquake was supposed to consist of three sub- events; the parameters for these sub-events are shown in Fig.2.2.2 .

2.3 Activity of Aftershocks [3)]

The distribution of aftershocks as of January 27th is shown in Fig.2.3.1. The surface projection of aftershock activity was along a line approximately 50 km long; this length is slightly longer than the length of 40 km estimated by Prof. Kikuchi for the main shock.

Aftershocks occurred with decreasing frequency after the main shock. As of Jan. 27, eight aftershocks occurred having maximum Shindo 4 or greater; those are identified in Fig.2.3.1. The fourth aftershock, at 7:38 A.M. local time on Jan. 17, occurred at the city of Itami, according to the Disaster Prevention Research Institute of Kyoto University. Itami is located away from the general region of aftershock activity.

3. Geological Aspect

3.1 Geology in Kobe [1), 2)]

The regional distribution of the quaternary geology is shown in Fig.3.1.1.

The Rokko mountains lies to the north of central Kobe, extending east- west direction. Plains exist only along Osaka Bay within a

narrow band of land between the sea and mountains. It is apparent from the slopes of the Rokko and Shin- Kobe tunnels that there is a relatively large difference in elevation between the districts located north and south of Rokko mountains.

The southern side of Rokko mountains is steep and consists of step- like slopes. The border between the southern side and the abutting hills is distinctly marked by a sudden change in slope. The steeper slope constrains the development of the urban areas. The break in slopes coincides with fault line; the steep slope is the fault- scarp. A more complicated topography exists in the region from Egeyama through Nagata, west of Okurayama. Beneath the fault- scarp there are hills, alluvial fans and deltas near the bay, and fed by small rivers draining the steeply sloped portions of the mountains.

3.2 Soil Characteristics [1), 2)]

Urban areas in Kobe have unique geotechnical characteristics stemming from the geological environment. Fig.3.2.1 shows the geology of the central Kobe. The granite bedrock of Rokko mountains is exposed only 3 km from the coastal line; in the urban plains, more that ten rivers flow to Osaka Bay within a distance of 22 km. Thus, the Hanshin plain consists of alluvial fans; most soils are gravel and sands.

Rokko mountains composed primarily of granite, and is fissured by many faults. The southern side has step-like slopes, consistent with downward displacements at the fault scarps relative to the north. Near the ground surface the granite has weathered to become decomposed to granite soil, 'Masado' in Japanese, which is prone to erosion by rain. In the fault area, slope failures occur due to these geological factors combined with creep of the fault fracture zone and the effects of spring water arising from tunnel drilling. Many embankments have been constructed in these soils to control erosion and to redirect the water flows of torrential rains.

Moderate slopes exist at the foot of the mountain, consisting of a series of alluvial fans of decomposed granite soils from Mount Rokko, deposited by landslides and mud flows of sand and stone during floods. For this reason old river beds contain rounded stones and gravely soils; soils in areas away from these rivers consist of sands derived from sedimentary deposits of decomposed granite. Therefore, in this area underground water infiltrates easily.

A flat plain is present in the alluvial low lands between the Jomon Coastal Line (a Holocene coastal line) and the present-day coastal line at Osaka Bay, This low lands area consists of sand bar formed by water currents and a hinterland swamp containing sedimented clays. There are thick alluvial clays at the present coastal line only at the Cape Wadamisaki.

Some areas along the coastline were reclaimed by placement of fill, typically with decomposed granite soils. Examples are East Reclaimed Ground, West Reclaimed Ground, Port Island, and Rokko Island. At Port Island, the thickness of soft clay is 7 meters in the north area and 16 meters in the south area.

3.3 Microtremor Measurement

Microtremor measurement was conducted at two locations. One is for a route connecting Shin-Kobe station and the old Kobe Customhouse building site. The other is for a route along State Route 428 connecting Gion Shrine to Minato primary school near the Harbor Land. The former location has many severely damaged buildings in down to the south of JR Sannomiya station and is included within the disaster belt. However, the latter location has few damaged buildings along, and is outside of the belt.

These measurement sites, shown in Fig.3.3.1, were located at terrace areas and the alluvial plain.

The representative Fourier spectra of the microtremors in the NS and EW directions are shown in Fig.3.3.2, where site R1 to R6 and F1 to F5 is on the diluvial plain, and sites R7 to R12 and F6 to F15 are on the alluvial plain. The peak at long periods, greater than 1.0 sec, reflect the deep ground characteristics, whereas the peaks at short periods, less than 1.0 sec, reflect the shallow subsurface structure.

4. Preliminary Investigation of Strong Motion Characteristics

4.1 Distribution of Peak Ground Acceleration

The distribution of peak amplitudes of strong motion records were prepared by Prof. Kohketsu [5)] and is shown in Fig.4.1.1.

The peak ground accelerations lager than 800 cm/s^2 were recorded during the earthquake. The record of the Kobe Marine Meteorological Observatory was firstly made open to the public. The motion was recorded by the JMA 87 model strong motion accelerograph. The peak accelerations for NS, EW and UD components are 818, 617 and 332 cm/s^2, respectively. It is still the only one that is open to the public. Therefore, the record has become the symbolic one to represent the intensive ground motion of the earthquake. The ground motions are, needless to say, result of source, propagation, and soil amplification. This earthquake occurred close to the affected area and the soil condition in Kobe and surrounding area is not uniform. Therefore, it is not appropriate to make the JMA record represent this earthquake. Several organizations had installed seismographs in affected area and published the records to date. It is not sufficient since the affected area is so large, but they provide data for estimating the ground motion scatter.

The location of earthquake recording sites at the central part is shown in Fig.4.1.2. When we remember the devastation area with assigned JMA intensity of 7, you might find that the recordings were hardly found in the area.

4.2 Vertical Motion

It was reported at the beginning that the great damage was caused by unusual large vertical motion. It is not confirmed yet. However, it seems at present most experts attributes the structural damage to its large horizontal motion as was conventionally pointed out in most of the past earthquakes.

The relationship between horizontal and vertical accs. are shown in Fig.4.2.1.[4] There are sites at which vertical peak acc. exceeds horizontal peak acc.

4.3 Spectral Characteristics

The comparison of the spectral ordinates of records of Hyogoken Nanbu earthquake (JMA Kobe record) with those for past large earthquakes shows its general feature that longer period component of Hyogoken-Nanbu dominates, especially for period longer than 1.0 second (Fig.4.3.1)

5. Damage Distribution and Site Effect

5.1 Damage Distribution based on Overturning of Tombstones

Dr. Takemura [6] and his colleagues investigated the relationship between mapped damage concentrations and ground motion intensities in Kobe, based upon the ratio of the number of overturned tombstones to the total number. He pointed out that the active faults of Suma, Nunobiki, and Gosukebashi coincide with the aftershock areas. The active faults near the center of Kobe are the Suma, Egeyama, Suwayama, and Ashiya faults from west to east. Comparison of the damage map in Kobe with a map of these faults indicates that severe damage occurred south of the fault line of Egeyama- Suwayama-Ashiya, and minor damage occurred north of the fault line. A similar trend was observed at the Koyo fault which exists in Nishinomiya.

Fig.5.1.1 shows a map of damage, the locations of active faults, and geologic boundaries. Dotted lines indicate active faults and dash- dotted lines indicate the boundary between reclaimed land and natural ground and the northern border of deltas.

Fig.5.1.2 (a) shows the proportion, γ, of overturned tombstones to the total number with respect to the shortest distance to the Suma, Nunobiki, and Gosukebashi faults. Fig.5.1.2 (a) shows the same ratio with respect to the shortest distance to the Suma, Egeyama, Suwayama, Ashiya, and Koyo faults, except for the northern extension of the Ashiya fault. I t can be seen from Fig.5.1.2 (a) that there is significant scatter in the values of γ at sites equidistant from a fault and that damage levels do not necessarily depend on distance from a fault. Fig.5.1.2 (b) shows slight scatter in values of γ and the presence of a strongly shaken area approximately 2 km from the fault to the southeast. The intensity of the ground motions decreases rapidly with distance from the strongly shaken area. On the other hand, the decrease in ground motion on the northwest side of the fault in very conspicuous. If the sites of aftershocks are assumed to be the same as the sites of the main shock, the intensity of ground motion during the Hyogoken- Nanbu earthquake should have depended strongly on the topographic north side of this fault line, whereas sedimented deposits are much thicker on the south side and at the location of an alluvial fan.

5.2 Aftershock in Higashinada Ward

Measurements of aftershocks have been conducted by Dr.Kawase[7] and scientists of the Disaster Prevention Research Institute of Kyoto University since January 18. Measurements were made at Kobe Pharmacology College (KMC), Kobe Mercantile Marine College (FKE), Fukuike Primary School in Kobe (FKI), and Seido Primary School in Ashiya City (ASY). Locations of these sites are shown in Fig.5.2.1. Fukuike Primary school in Kobe and Seido Primary School in Ashiya are located within the Shindo7 diaster belt; Kobe Pharmacology College and Kobe Mercantile Marine College are located to the north and south, respectively, of the belt.

A cceleration records of the aftershock EQ29 on January 25 are shown in Fig.5.2.2 for the three points FKE, FKI, ASY. The peak horizontal acceleration at FKI is 1.8 times larger than at FKE. The rations of Fourier spectra at FKE, FKI, ASY to that at KMC are shown in Fig.5.2.3 for 6 aftershocks. F ourier spectra at FKI and ASY, located in inland areas, are about twice as large as for FKE, located inland areas, are about twice as large as for FKE, located near the coastal line.

6. Conclusions

Properties of the strong ground motions recorded during Hyogoken-nanbu earthquake were discussed with some attempts of aftershock and microtremor measurement. The estaimation of regional distribution of ground motion by overturing of tombstones is also introduced.

Acknowledgement

The acceleration data of Kobe JMA Observatory was recorded by JMA 87 model accelerograph.

References

1) City of Kobe, Subsoil of Kobe, 1980
2) The Japanese Society of Soil Mechanics and Foundation Engineering, Kansai Subsoil, 1992
3) Architectural Institute of Japan, Preliminary reconnaissance report of 1995 Hyogoken-Nanbu Earthquake, 1995
4) Shimizu Corporation, Preliminary report of damage reconnaissance of 1995 Hyogo-ken nanbu earthquake, 1995
5) K,Kohketsu, Maximum accelerations and velocities of the 1995 Hyogoken-nambu earthquake, (graph taken through Internet by anonymous ftp of ERI, Univ of Tokyo)
6) M.Takemura, Preliminary report of damage distribution and intensity of ground motion, 1995
7) H.Kawase, Preliminary report of aftershock measurements in Higashinada Ward, 1995

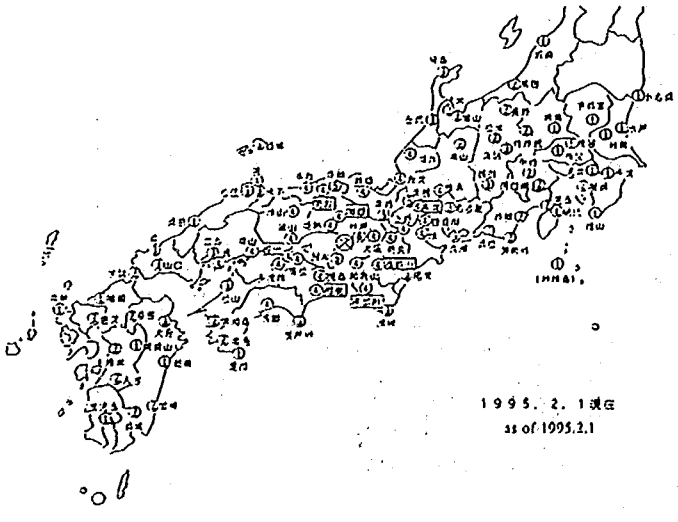


Fig. 2.1.1 Map of JMA Shindo

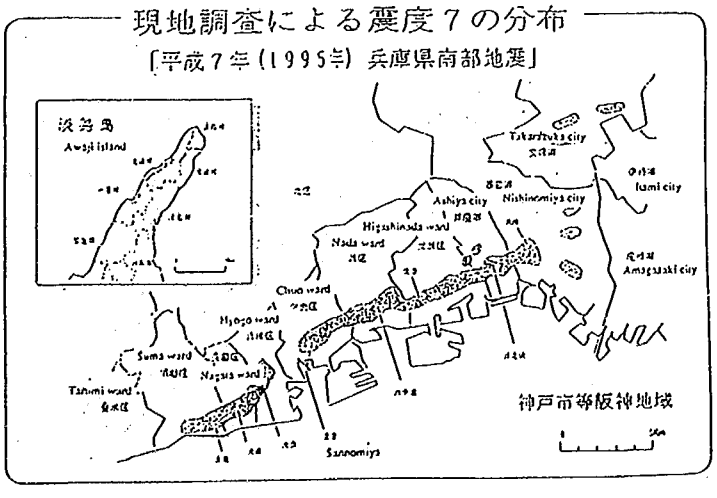


Fig. 2.1.2 Areas of JMA Shindo 7

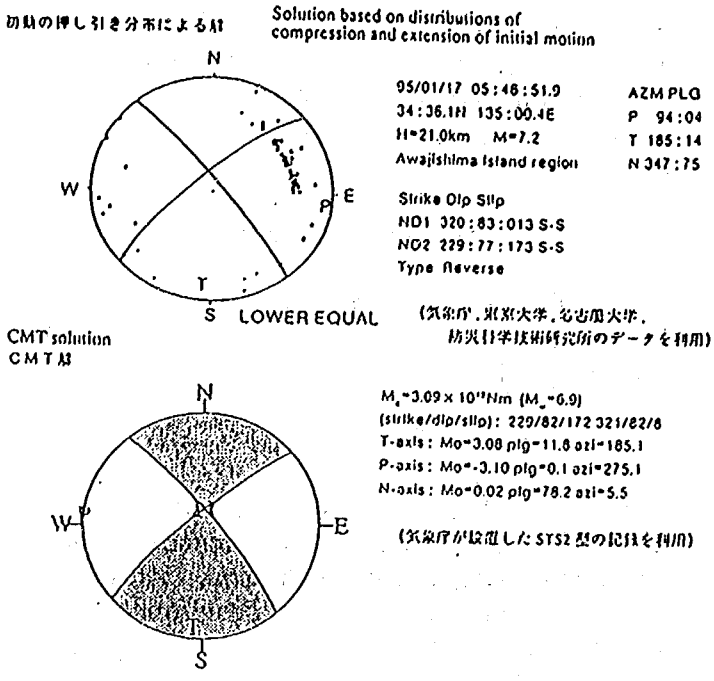


Fig. 2.2.1 Focal Mechanism [3]

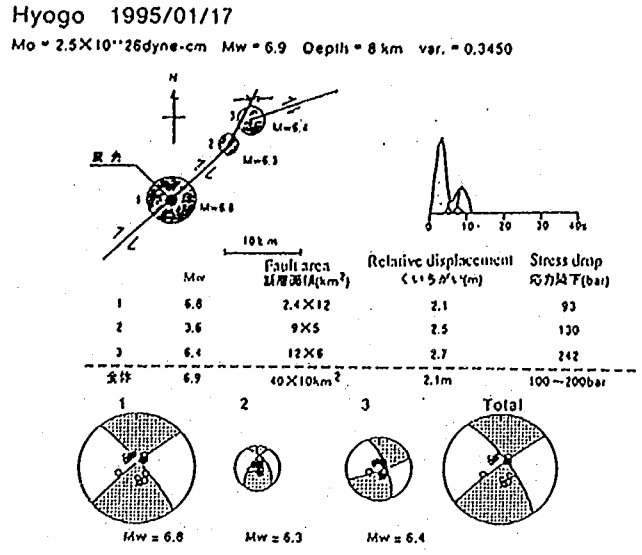


Fig. 2.2.2 Parameters for Sub-events [3]

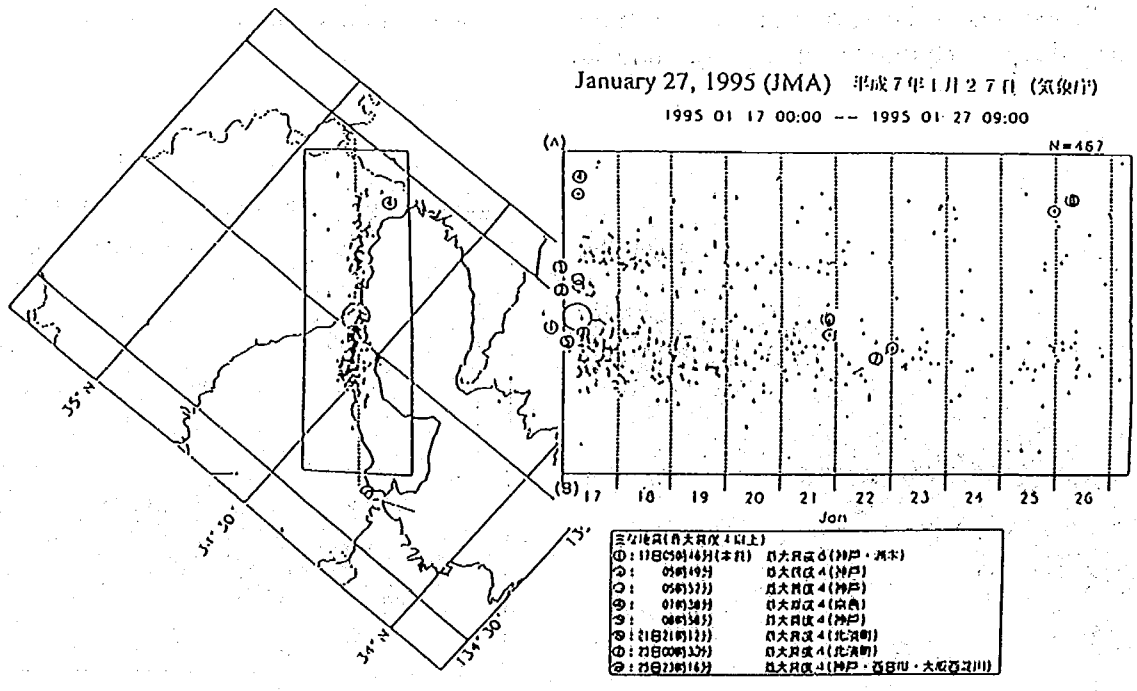


Fig. 2.3.1 Distribution of Epicenter of Aftershocks [3]

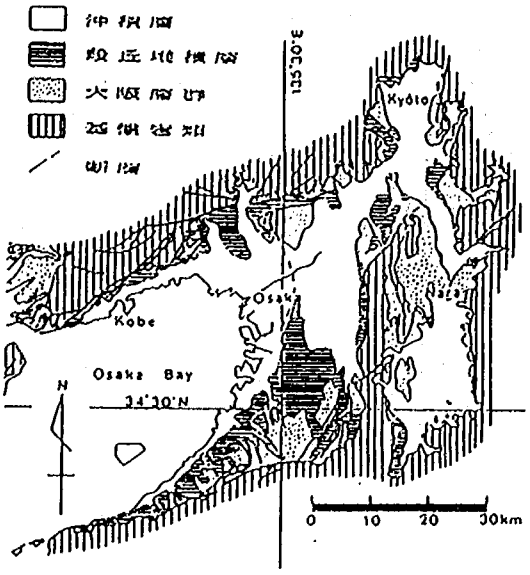


Fig. 3.1.1
Regional Distribution of
Quaternary Geology [2)]

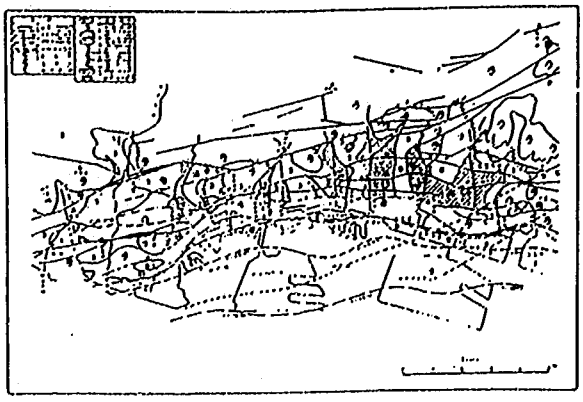


Fig. 3.2.1 Geology of Kobe area [2)]

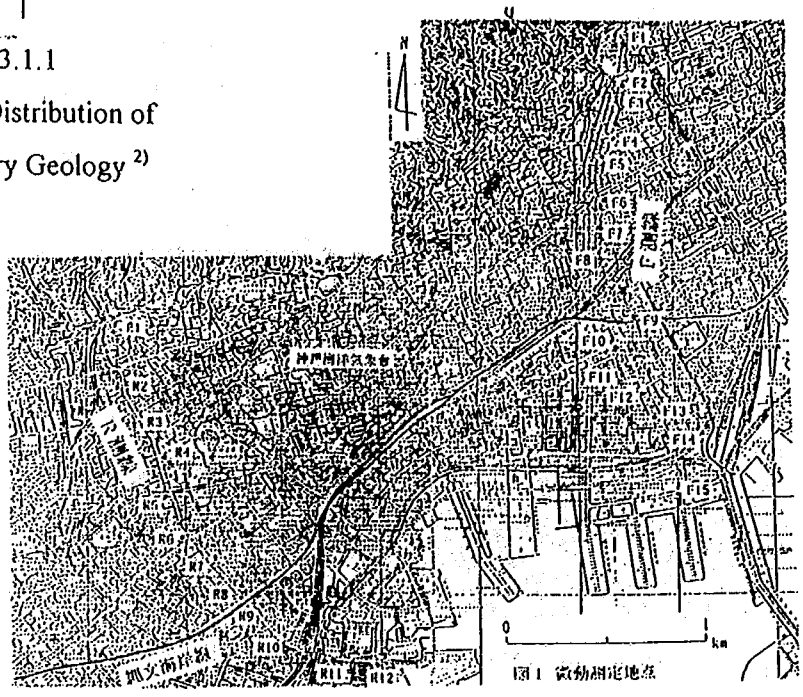


Fig. 3.3.1 Location of Microtremor Measurement Sites

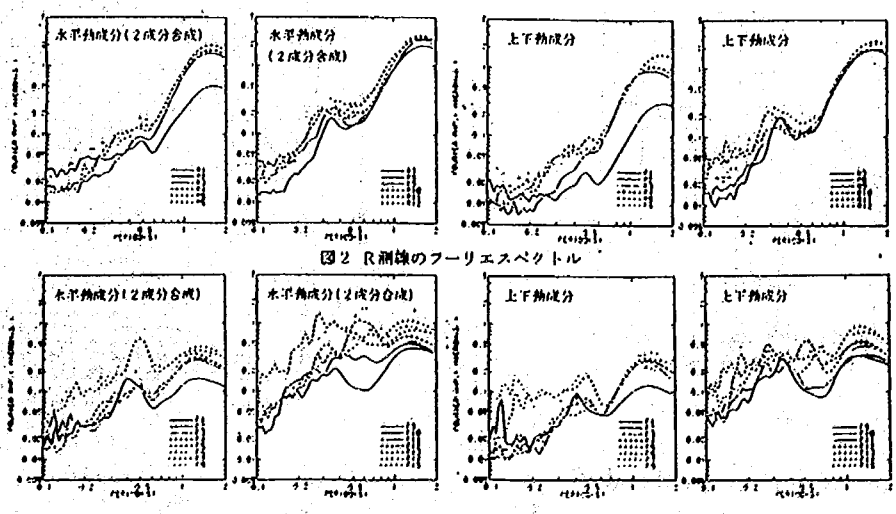


Fig. 3.3.2 Fourier Spectra of Microtremores

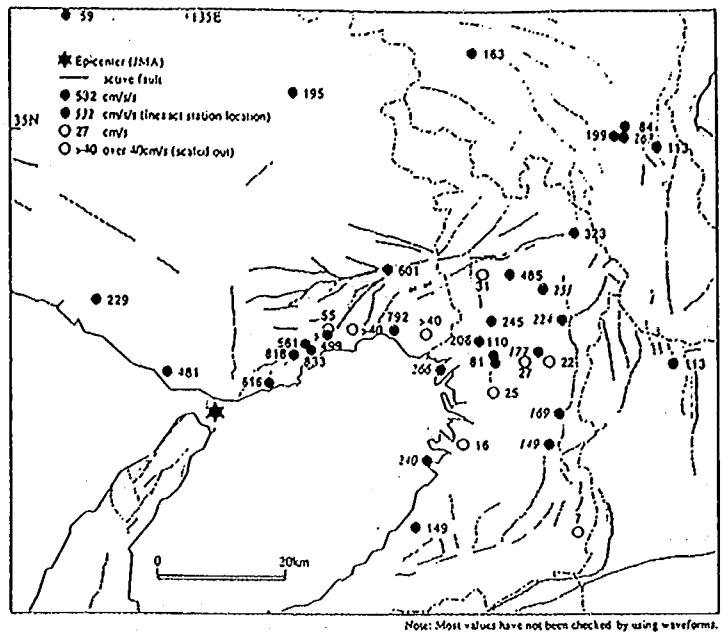


Fig. 4.1.1 Distribution of Maximum Accelerations and Velocities [5]

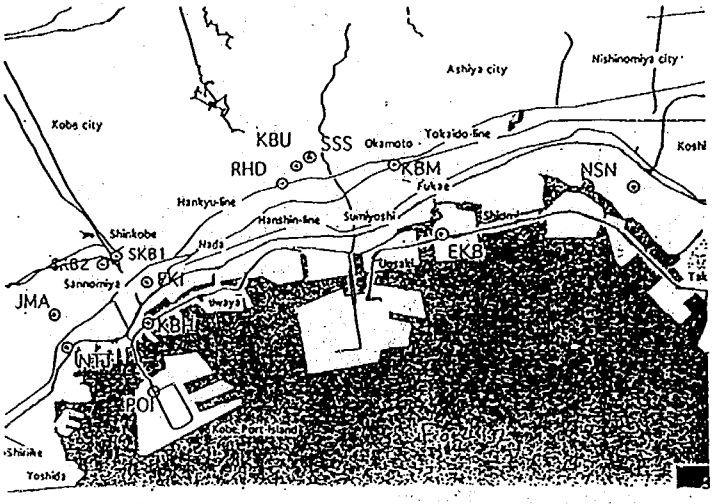


Fig. 4.1.2 Location of Earthquake Recording Sites

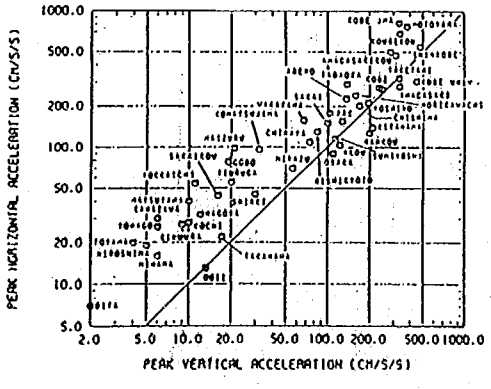
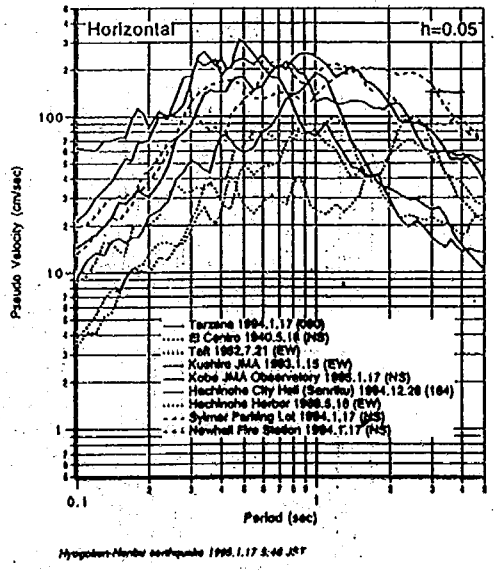


Fig. 4.2.1
Relationship between Horizontal and Vertical Acceleration [4]



Source : PHRI, CSMIP(CDMG), USGS, BRI

Fig. 4.3.1 Response Spectra for Recent Devastating Earthquakes

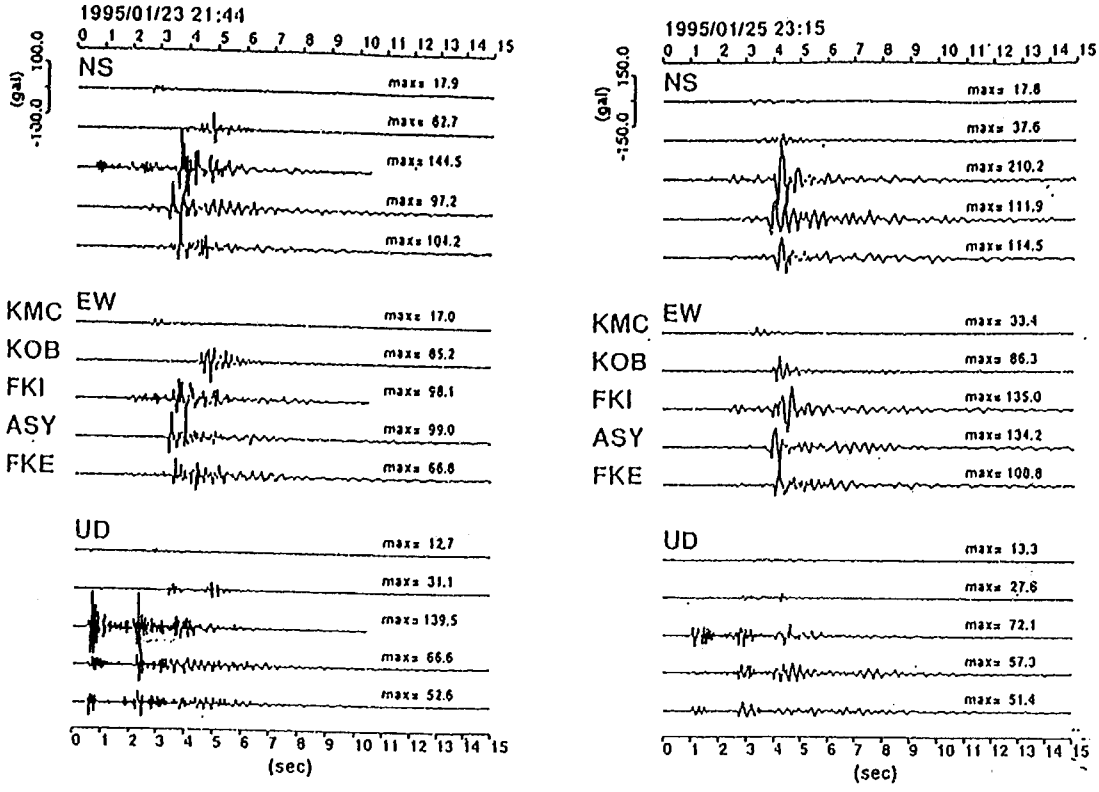


Fig. 5.2.2 Acceleration Records Aftershock [7)]

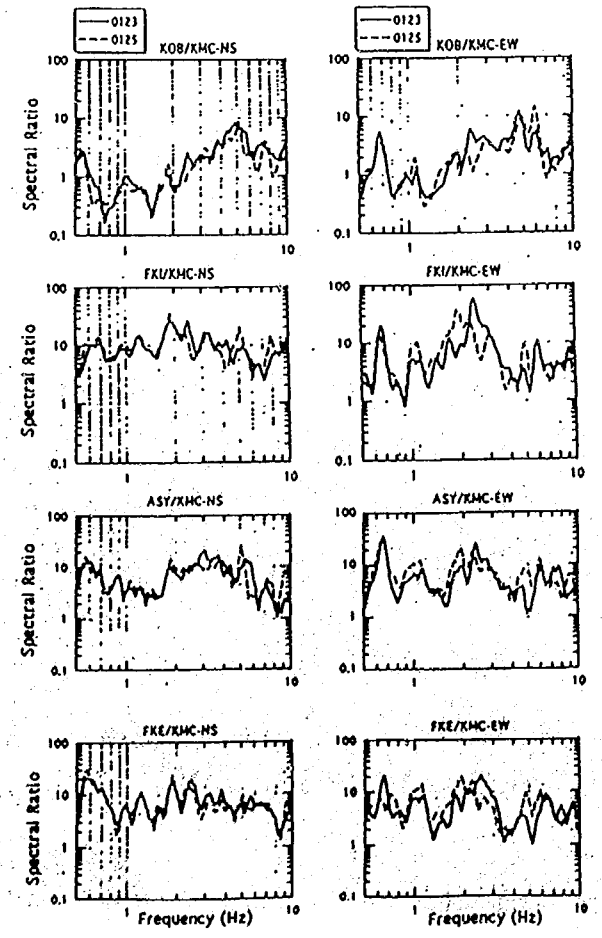


Fig. 5.2.3 Ration of Foaurier Spectra [7)]

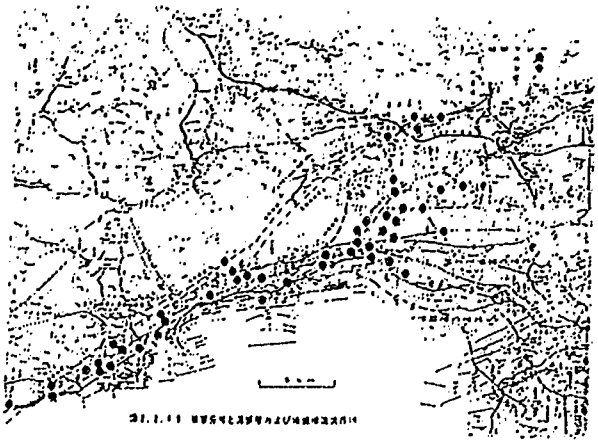


Fig. 5.1.1 Relation of Damage Distribution with Active Faults and Borders of Different Geological Structures [6]

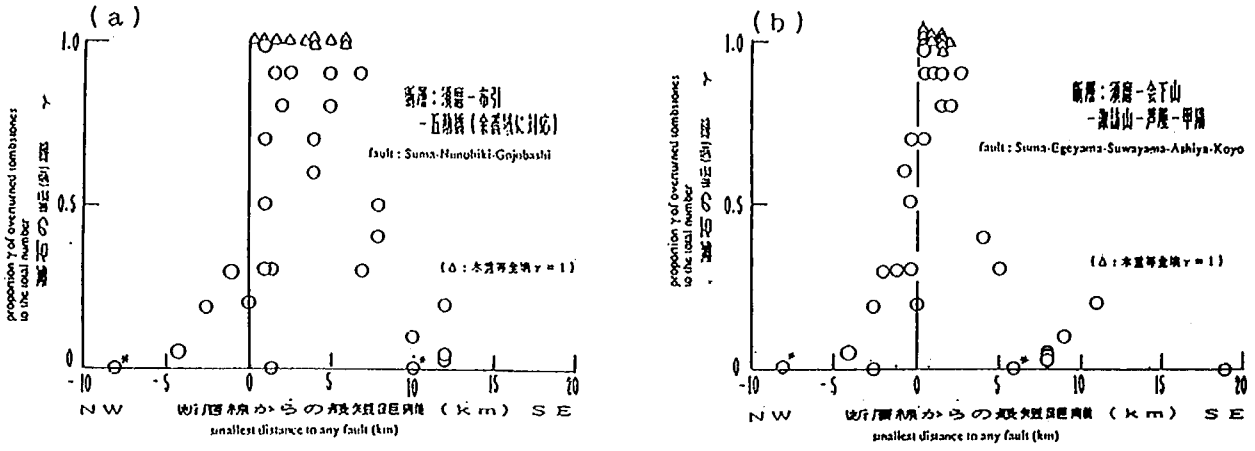


Fig. 5.1.2 Map of Damage [6]

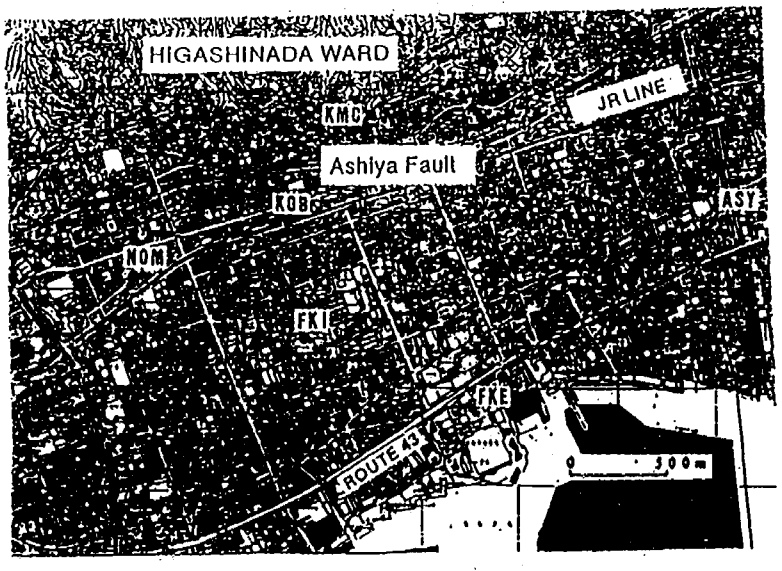


Fig. 5.2.1 Location of Array Observation Stations [7]

INFRASTRUCTURE DAMAGE BY THE 1995 HYOGOKEN NANBU EARTHQUAKE

by

Takashi Iijima[1], Tomonobu Nakaoka[2], Yasuyuki Koga[3]

ABSTRACT

Seismic damage caused by the Hyogoken Nanbu Earthquake of January 17, 1995 is described. Description is given to the damage of highway bridges, slopes, river hydraulic facilities, dams, sewerage facilities, retaining walls and underground structures.

Keywords: *Earthquake damage, Hyogoken Nanbu Earthquake, Highway bridges, Lifeline facilities, Dams, Slope failures, Retaining walls*

1. INTRODUCTION

In the early morning of January 17, 1995, the Hyogoken Nanbu earthquake occurred in the Hanshin area. The magnitude of the earthquake was 7.2 on the JMA scale. Because the epicenter was very close to the highly populated city of Kobe, more than 5,000 fatalities were caused by the earthquake. Extensive damage was developed to various engineering structures and grounds by intense ground motions.

This paper summarizes the quick investigations on the damage, that were conducted by the PWRI reconnaissance teams. The structures covered in this report are : highway bridges, slopes, river hydraulic facilities, dams, sewerage facilities, retaining walls and underground structures.

2. SUMMARY OF THE EARTHQUAKE

2.1 Description of the Earthquake

The Hyogoken Nanbu Earthquake occurred at 5:46 a.m. on January 17, 1995. Its hypocenter was close to the northern tip of Awaji Island (North 34°36', East 135°03'). The Japan Meteorological Agency (JMA) announced that the depth of the hypocenter was 14km and that its magnitude (M) was 7.2. The magnitude is smaller than those of three recent earthquakes near Hokkaido; the Kushiro-oki Earthquake (January 15, 1993, M=7.8), the Hokkaido Nansei-oki Earthquake (July 12, 1993, M=7.8), and the Hokkaido Toho-oki Earthquake (October 4, 1994, M=8.1). However, because its epicenter was closer to an urbanized area than any previous earthquake with similar magnitude, Kobe and other parts of the Kobe-Osaka region and the northern part of Awaji Island were struck by a violent tremor with an intensity of 7 in the JMA seismic intensity scale. This was the first time the JMA had ever declared the intensity of 7.

2.2 Characteristics of the Earthquake Motion

Many acceleration records were obtained in the most seriously damaged area, by the JMA, the Ministry of Construction, Ministry of Transport, the City of Kobe, the Hanshin Expressway Public Corporation, the Committee of Earthquake Observation and Research in the Kansai Area, Japan Railways (JR), Osaka Gas, and others. The acceleration records are still undergoing detailed analysis, and various organizations have announced tentative values for the

1)Director-General, Public Works Research Institute, Ministry of Construction
2)Deputy Director-General, PWRI
3)Director, Earthquake Disaster Prevention Department, PWRI

maximum acceleration, etc. Fig. 2.1 shows the distribution of the maximum acceleration announced by these organizations. During this earthquake, extremely intense earthquake motions were recorded, stronger than any other previously recorded in Japan. The maximum acceleration of the horizontal component exceeded 600gal (cm/s^2) at the Kobe Maritime Meteorological Observatory (JMA), at Takatori (JR), at Fukiai (Osaka Gas), at Takarazuka (JR), and at Nishinomiya (Osaka Gas), which indicates that the maximum acceleration of the ground motion reached extremely high values over a wide area. At the Kobe Maritime Meteorological Observatory in particular, extremely strong ground motion was recorded and its maximum acceleration reached 818gal in the north–south component. The acceleration records are shown in Fig. 2.2. Strong earthquake motion was also observed on soft landfill. On the ground around the Higashi Kobe Bridge on the No.5 Harbor Highway of the Hanshin Expressway, for example, the acceleration records shown in Fig. 2.3 were obtained. Its maximum horizontal acceleration was 327gal. The maximum velocity and maximum displacement of the earthquake motion recorded at the Kobe Maritime Meteorological Observatory were 90cm/sec and 21cm respectively, while the same figures for the ground surface around the Higashi Kobe Bridge were 91cm/sec. and 49cm respectively. They are extremely high values.

Fig. 2.4 presents the response acceleration spectra of the acceleration records of the Kobe Maritime Meteorological Observatory, assuming a damping ratio of 5%. The response acceleration spectrum reached 2G for the natural period between 0.4 second and 1 second, indicating that the ground motion contained large components over an extremely broad frequency range. Fig. 2.5 shows the acceleration response spectrum (damping ratio of 5%) of the acceleration record obtained on the ground near the Higashi Kobe Bridge. At this point, the maximum acceleration was not very high, but the acceleration response spectrum in the wide frequency range was extremely large, and in the wide natural period range, periods of 1 second or greater, it exceeded the response spectrum of the Kobe Maritime Meteorological Observatory record which presents a maximum acceleration of 818gal.

The acceleration response spectrum for the natural period of 2 seconds, for example, reached 724gal for the Higashi Kobe Bridge record, while for the Kobe Maritime Meteorological Observatory record it reached 378gal. This indicates that the ground motion near the Higashi Kobe Bridge contained large components in a frequency range wider than the one recorded at the Kobe Maritime Meteorological Observatory.

The earthquake motion characteristics of the Hyogoken Nanbu Earthquake has been briefly presented in the above, taking as examples, the acceleration records of the Kobe Maritime Meteorological Observatory and the ones registered at the Higashi Kobe Bridge site. These observation records demonstrate that the ground motion during the Hyogoken Nanbu Earthquake was extremely powerful and contained large components over a wide frequency range.

As the natural period of a structure is generally prolonged when it is damaged, earthquake motion with a large response spectrum in the long natural period range has a significant effect on the beaviour of the structure. Such characteristics of the ground motion, as described above, therefore, may be partially the reason for the severe damage by the Hyogoken Nanbu Earthquake.

3. SUMMARY OF THE DAMAGE

The Hyogoken Nanbu Earthquake is not an extremely large earthquake when compared with past large earthquakes in Japan, as long as they are compared in terms of magnitude. However, because this

earthquake had its epicenter closer to an urbanized area than any previous earthquake of the same or larger magnitude, it caused, besides loss in human life, severe damage on numerous structures and a massive financial loss. In this earthquake, 5,497 people lost their lives, 2 people are still missing, 36,820 people were injured, 92,938 buildings totally destroyed, and 86,219 buildings partially destroyed. (As of March 31, 1995, according to National Police Agency and Fire Defense Agency.) As Table 3.1 shows, the cost of the damage to all facilities has reached approximately 9.9 trillion yen. (Estimated figure, as of March 30, 1995.)

4. GEOLOGICAL HAZARDS

4.1 Introduction

The earthquake was a shallow intraplate earthquake with its hypocenter approximately 14km deep in the northern part of Awaji Island. Because the hypocenter was relatively shallow, an earthquake fault appeared in northwest Awaji Island near the hypocenter. This is the major geological hazard produced by this earthquake. Other geological hazards left by the earthquake include liquefaction and subsidence on reclaimed land, cracks, slipped and collapsed slopes, and cracked embankments. These geological hazards are summarized in the below.

4.2 Summary of the Geology of the Disaster Region

Fig. 4.1 presents a summary of the geology of the disaster region. Under Awaji Island, the basement rocks of Quaternary unconsolidated sediments, are Izumi group, Ryoke granites, and unconsolidated sediments including Osaka group, terrace deposits and alluvium. Under Kobe, the basement rocks are Rokko granite, Arima group, and Kobe group. The unconsolidated sediments consist of Osaka group on the mountains, and Osaka group, alluvium, and landfill on the plain. Terrace deposits are found on the boundary between the plain and the mountains.

4.3 Active Faults in the Disaster Region

The active faults in the disaster region are dominated by an active fault (Rokko Fault System) running south–west to north–east from the hypocenter region of Awaji Island to Kobe. The principal part of the earthquake fault which appeared on Awaji Island was revealed at the location of the existing Nojima Active Fault. The hills of Awaji Island rose along the existing Nojima Active Fault, while the sea coast side of the fault has settled. The Nojima Active Fault includes right lateral components. The Rokko Fault System on the Kobe side on the other hand, under the south–east foothills of the Rokko Range, is a dip–slip fault (Rokko mountains rise relatively) and includes right lateral components.

4.4 Relationship of the Geological Hazards with the Topography and Geology

These geological hazards and the damage to structures produced by this earthquake can be related to the topography and geology of the region. The following paragraphs summarize this relationship.

(1) Damage to buildings and geological hazards such as cracked road surfaces occurred most frequently on part of the alluvial plain. Macroscopically, the damage was most severe in, for example, an area extending from the JR Tokaido line to the National Highway No. 43 on a north to south line close to the boundary separating Ashiya City from Higashi Nada Ward in Kobe. The collapse rate of wooden houses was low outside this area on the hilly side and on the alluvial plain along the waterfront. Almost all damage was concentrated in a narrow strip of land parallel to the waterfront: a zone corresponding to the ground which, according

to a February 7, 1995 announcement from the JMA, was subjected to seismic intensity of 7. It is considered that the geological factor of this narrow strip of land is the motion of an unknown active fault (concealed active fault) under the alluvial stratum or soft ground. Future studies will clarify the distribution of the damage on this narrow strip of land.

(2) As already pointed out, the damage on the alluvial plain is concentrated on a narrow strip of land. A precise study of the damage in this area has revealed that it can be broadly categorized into the following four categories.

- No damage to either road surfaces or houses
- Cracking and swelling on road surfaces, but no damage to buildings and other man-made structures
- No damage to road surfaces, but damage to buildings and other man-made structures
- Road surfaces, buildings, and other man-made structures all damaged

There is a strong possibility that the factor accounting for the differences between these types of damage was three-dimensional geology (structure and materials).

(3) The relationship of the topography and geology of the alluvial plain with the damage in the same area is clear from the extensive geological hazards in embankments, around ponds (Photo 4.1), and in reclaimed lands.

(4) The hilly and high terrace districts comprised of pre-Quaternary system were almost completely free of geological hazards and building damage (excluding slope failure on the sides of the Rokko Range), thanks to the high degree of consolidation of the ground, which might have lead earthquake motion weaker than that generated in the unconsolidated sediments of the alluvial stratum.

(5) Within the scope of the survey, neither ground displacement nor earthquake faults considered to have been directly caused by an existing active fault have been identified on the Kobe side. But at the Suma Fault, Gosukebashi Fault, Ashiya Fault, and Uzugamori Fault, various damage trends suggest a relation between the faults and the damage. But because the assumed positions of the faults are along geological and topographical boundaries, it is possible that their proximity to these boundaries was the direct cause of the damage.

(6) Liquefaction occurred in reclaimed areas along the waterfront (Photo 4.2) and in inland landfill areas. The liquefaction produced sand boiling, ground flow, and subsidence. But liquefaction did not occur on all reclaimed land; its occurrence depended upon the landfill materials and the construction method used for the landfill work.

(7) On fault scarps, terrace scarps, and other slopes, some geological hazards were caused by gravitational sliding down of the slope (Photo 4.3). Macroscopically, compressible cracking was distributed linearly at the edge of fault scarps.

5. DAMAGE TO HIGHWAY BRIDGES

5.1 State of the Damage

Fig. 5.1 shows the locations of principal highway bridges damaged by this earthquake. The earthquake caused damage to elevated highway bridges on National Highway No. 2, 43, and 171, the Meishin Expressway, Chugoku Expressway, and the No. 3 Kobe Highway and No. 5 Harbor Highway of the Hanshin Expressway System. This section presents an overview of the principal damage.

(1) National Highways

As Photo 5.1 shows, at the Mondo Elevated Bridge on National Highway No. 171, a simple girder with a skew on the overpass has fallen down. The falling prevention devices connecting the girders was damaged, allowing the girder to fall down. At the Iwaya Elevated Bridge on

National Highway No. 43, reinforced concrete piers and steel piers were damaged. As Photo 5.2 shows, one of the steel piers was damaged and the beams subsided almost to ground level. Photo 5.3 shows the damage inflicted on the No. 2 Hamate Bypass. At the point of contact of a two-span continuous steel box-girder with a three-span continuous steel box-girder, relative displacement of 3.5 m appeared to the transverse direction of the bridge. And as Photo 5.4 shows, steel plate damage was caused by an out-of-plane deformation with a maximum of 5 cm midway between the top and bottom of the pier.

(2) The Meishin Expressway and the Chugoku Expressway

As Photo 5.5 shows, at the Moribe Elevated Bridge between the Nishinomiya Interchange and the Amagasaki Interchange on the Meishin Expressway, a reinforced concrete wall-type pier supporting a five-span continuous reinforced concrete hollow slab was collapsed. And as Photo 5.6 indicates, at the Mukogawa Bridge, a girder fell down from the bearing support, a girder web was damaged, and a device linking the girders to the abutment was collapsed. Reinforced concrete piers were also damaged. And as shown by Photo 5.7 at the Kawaraginishi Elevated Bridge, two spans in a three-span hollow slab bridge with a skew fell down as the locking pier tilted. At the Takarazuka Elevated Bridge on the Chugoku Expressway, the earthquake damaged a three-column type reinforced concrete pier supporting a five-span continuous reinforced concrete hollow slab.

(3) Hanshin Expressway, No. 3 Kobe Line

As Photo 5.8 shows, two connected simple girders fell as result of damage to a reinforced concrete pier at Koshien Takashio-machi in Nishinomiya. At Hamawaki-machi in Nishinomiya, two connected steel simple girder bridges fell down as shown in Photo 5.9 Substantial horizontal movement also appeared in the girders adjacent to the fallen girders. As shown in Photo 5.10, steel piers were damaged and subsided at Ichiniwa-machi in Nishinomiya. Photo 5.11, which was taken at Fukaehonmachi in Higashinada-ku in Kobe, shows damage to an 18-span pilz-deck-type bridge. And as shown in Photo 5.12, on the west side of Fukaehonmachi, a reinforced concrete pier was damaged, which was accompanied by partial damage to a steel box-girder, causing the bridge to sink. Photos 5.13 and 5.14 show damage to a single column type reinforced concrete pier at Hatobacho in Chuo-ku in Kobe. At this pier, the bearings installed under the superstructure crossbeams were directly supported by the column capitals. As shown in Photo 5.15, the base of a rigid frame type steel pier was damaged in Imazufutaba-cho in Nishinomiya. Photo 5.16 shows damaged steel piers of an overpass on the JR Wadamisaki Line. Photo 5.17 shows a damaged reinforced concrete pier in the Minatogawa ramp in Nagata-ku in Kobe. The damage to this pier was accompanied by the partial collapse of a two-span continuous box girder curved bridge shown in Photo 5.18. And as shown in Photo 5.19, on an adjoining ramp, damage to a bearing support displaced a steel box-girder to the transverse direction of the bridge.

(4) Hanshin Expressway, No.5 Harbor Highway

Photo 5.20 shows the collapse of one span of a simple box girder bridge adjoining the east side of the Nishinomiya Bay Bridge at Koshien-hama. On the Higashi Kobe Bridge, steel cable-stayed bridge with 485m central span length, and as Photo 5.21 shows, a pin fell down from a rocker bearing. Photo 5.22 shows damage to the Rokko Island Bridge; the main structure fell from a damaged shoe.

5.2 Characteristics of the Damage of the Bridges

(1) An investigation of the relationship

between damage to reinforced concrete piers and the specifications applied to their design has revealed that on the No.3 Kobe Line of the Hanshin Expressway, 14% of the piers suffered damage rated as class A damage or greater. Piers on the No.3 Kobe Line were designed in accordance with the earthquake resistant design standards of 1964 and 1971. While piers on the No. 5 Habor Highway of the Hanshin Expressway, piers constructed based on the highway bridge specification enacted in and after 1980, were free of damage of this kind.

(2) Most girder damage was found in the part close to the bearing supports. These damage were thought as a result of damage to bearing supports.

(3) There were cases where falling prevention devices failed to prevent the bridge from falling down because of the breakage of either the devices themselves or a girder connected with the devices.

(4) Many steel bearing supports were damaged; their set bolts were broken, the bearing support itself was broken, a roller was knocked out of place, an anchor bolt was broken, and so on. Rubber bearing supports suffered far less damage than steel bearings.

6. DAMAGE TO SLOPES

6.1 Introduction

Many landslides were triggered by the earthquake in the Hanshin Area and the Awaji Island. Field investigation and aerial photo interpretation were conducted for the Rokko Mountains.

6.2 Mountain slope collapses

Most of mountain slope collapses occurred in the eastern part of the Rokko Mountains, in particular, in the basins of the Sumiyoshi River, the Syukugawa River, the Nikawa River, the Sakase River, the Outada River,the Shio River, and the Kan-non River (see Photos 6.1, 6.2 and Fig. 6.1). Besides these, relatively large mountain slope collapses (Photo 6.3) were observed in the Shin-Ikuta River, and the Shin-Minato River. However, most of the mountain slope collapses were surfacial soil landslips with approximately 10-20m wide, about 50-100m long and about 1-2m deep. Most of them were distributed along the Outsuki Fault, the Rokko Fault, the Arima-Takatsuki Tectonic Line (Fig. 6.2). A rock slope collapse with about 50m high, and approximately 40m wide on the right bank and deposition of the collapsed material in the middle reach of the Ashiya River is noteworthy (Photo 6.4). Only a few small mountain collapses were found in the western part of Rokko Mountains. Moreover, crack joints were found on the slopes in the Rokko Mountains. Mountain slope collapses were generated by the earthquake along the Nojima Fault in the northwestern part of the Awaji Island.

None of the erosion control facilities (erosion control dams, channel works , etc.) received a deathblow by this earthquake. In the Rokko Mountains and on the Awaji Island, 27 erosion control facilities were slightly damaged with cracks or slight destruction of revetments.

6.3 Landslides and slope failures

The bedrock in the heavily damaged Rokko Mountains is granite and the geology of the coastal area is composed of diluvium or alluvium of rock wastes. In general, the granites are easily weathered so that steep slopes in the granite area are prone to failure during heavy rainfalls.

From January 22 to 27, 1995, the Ministry of Construction and the local governments investigated about 1,100 slopes of disaster potential, in order to prevent secondary disasters caused by slope movements.

Fig. 6.1 plots 71 slopes rated as slopes of high disaster potential. This shows that the slopes are concentrated in the southern part of the Rokko Mountains, particularly at

the mouths of streams originating from the Rokko Mountains where terraces exist.

The landslide at Nikawa-yurigaoka-cho in Nishinomiya (Photo 6.5) is one of the largest slope movements induced by the earthquake and caused the largest number of casualties: 34 people were buried and killed by the landslide.

The slope facing northeast is located at the right bank of the Nikawa River. The collapsed soil is categorized as Osaka-group which consists of partially cemented silt and sand.

The width and length of the landslide were about 100m each and its volume was about 100,000m^3. The gradient of the slope was about 20 degrees. From houses located under the slopes 18 were destroyed and buried by the collapsed soil. A part of the collapsed soil moved into the channel of the Nikawa River.

Nishi-okamoto area is situated on the left bank of the Sumiyoshi River and residential areas were developed on the terrace (Photo 6.6). A slope failure of about 20m wide, and about 20m long was caused by the earthquake and many cracks were found on the terrace, and it is feared that the slope failure will occur in the future due to rainfall. Considering this condition, inhabitants near the landslide were advised to evacuate from the area. Monitoring equipment such as extensometers, clinometers etc. have been installed.

6.4 Conclusions

34 people were killed by the landslide at the Nikawayurigaoka-cho and 3 more people were killed by steep slope failures in Takarazuka. There was no other casualty due to slope movements during the earthquake. However, many landslides and cracks on slopes were found , and the ground and soil of slopes were loosened by the earthquake. Moreover, a lot of collapsed soils and rocks were deposited in the streams in Rokko Mountains and the Awaji Island. Therefore the probability of the occurrence of debris flows, landslides, and slope failures during rainfall event is increased. Monitoring has to be performed and countermeasures implemented for preventing and mitigating those disasters triggered by heavy rainfalls in the coming rainfall season.

7. DAMAGE TO RIVER DIKES

Flood control river dikes suffered strict failure. The damage of dikes consisted of cracking, settlement, lateral spreading and slumping. In many cases, sand boils were observed at the ground near the dikes. The repair works are now underway. It should be noted that countermeasures against soil liquefaction will be implemented at severely damaged dikes. Typical damage is described in the following.

7.1 Torishima Dike at Yodo River

A total length of 1600 m (kilopost 0.2-1.8km) of the left levee of the Yodo River was severely damaged (Photo 7.1). The Yodo River, flowing through Osaka, is the largest river in the Kansai area. The concrete parapet on the top of the levees tilted and settled. The parapet slided horizontally about 8 m toward the river. Embankment also settled and cracked severely. The average settlement was about 1 to 2 m, with a maximum of 3 m. Sand boils were observed in the ground along the dike. Lateral movements and heaving of the ground occurred in the residential area of the low ground elevation. These facts suggest that soil liquefaction triggered the damage. The existence of sand layer with relatively low SPT N-value of 10 or less was confirmed by soil investigation conducted immediately after the quake.

Treatment of the sandy soil against liquefaction was decided. The deep mixing method will be implemented as a countermeasure.

7.2 Nishijima Dike at Yodo River

An 800 m length (kilopost 1.2–2.0 km) of the right levee was also damaged. Although the structure of the dike was similar to that of Torishima Dike, there was no damage to the parapet. Only the embankment slope failure occurred in the back side slope. A crack developed at the crest with about 20 to 150 cm wide and its slumping amounted to 1 m (Photo 7.2). Sand boils were observed near the back toe of the dike. Implementation of steel sheet piles is underway to prevent slope failure due to liquefaction of the subsurface soil.

7.3 Mogawa Dike

Mogawa River is one of the tributaries of Yodo River. There were three major failures of the dike. Among these, at about 0.4 kilopost point of the right dike, longitudinal and transversal cracking, settlement and lateral spreading were developed for about 1 km (Photo 7.3). Sand boils were also observed at the site. It is interesting to note that the post earthquake survey revealed that the damaged length was almost consistent with the width of old river basin. These facts suggest that the damage was induced by liquefaction of the subsurface soil in the old river basin.

8. EFFECTS ON DAMS

8.1 Emergency Inspection

Emergency inspections were carried out by dam managers at the dams in the river stretch administered under the River Law just after the earthquake. The emergency inspections after the Hyogoken Nanbu Earthquake were conducted at a total of 251 dams. Table 8.1 presents a district breakdown of these dams.

The emergency inspections of all the dams were completed by January 21, and damage requiring emergent protective countermeasures was not reported. Some slight effects on dams – minor cracks in the pavement on the crest of two dams for example – were reported. Seepage increased slightly at nine dams, but the total amount was little and it tended to either decrease or stabilize.

8.2 Dam Investigation by PWRI

The PWRI engineers investigated two groups of dams: those where slight effects were reported by the emergency inspection and the dams located in areas where JMA reported a seismic intensity of 5 or greater. Fig. 8.1 is a map showing the locations of investigated dams. The major results of investigation at each of the dams, listed in Table 8.2, are described in the following.

(1) Tenno Dam

Tenno Dam is a concrete gravity dam, located about 20km from the epicenter. A small collapse occurred above the slope of the right abutment, and another at the right downstream abutment, but the falling rocks did not damage the dam body. It was confirmed that the water level of reservoir had been falling about 2cm/day before the earthquake, but it has been reported that since the earthquake, the water level has been dropping about 10cm/day (equivalent to about 9 liters per second). There was, however, no leakage through the dam body, and the dam and its foundation are now perfectly safe. It is assumed that the water level declined because of an increase in seepage into the ground surrounding the reservoir.

(2) Tokiwa Dam

Tokiwa Dam is a zoned earth fill dam, located about 8 km from the epicenter, it is situated as close as 800 m to the Nojima Fault in the Awaji Island, which was found to be moved by this earthquake. Transverse cracks of 25mm wide and 7m long were observed in the pavement on the end of the crest near both the abutment contacts (Photo 8.1). The slope on the right abutment collapsed slightly, and the concrete shoulder of the access road was cracked. But neither

the upstream nor the downstream slopes of the dam body was damaged.

(3) Kitayama Dam

Located approximately 25km from the epicenter, Kitayama Reservoir is created by five homogeneous earth fill dams – dam No. 1 to dam No. 5. A sliding of about 100 m in longitudinal length occurred on the upstream slope of the dam No.1 (Photo 8.2). The sliding gap of the riprap is approximately one meter at the reservoir level during the earthquake (Photo 8.3). Collapse differences and depressions of the riprap were similarly found on the slope of the road embankment on the reservoir shore. Bore hole exploration to assess the sliding of the dam No.1 is underway.

8.3 Peak Acceleration at the Dam Foundation

The distributions of the peak acceleration observed during the earthquake at the dams foundation or at lower elevation of the dams are shown in Fig. 8.2. The values in this figure are the maximum values among the three component accelerations. These peak accelerations are provisional values; not final values.

8.4 Conclusion

The emergency inspections conducted by each dam manager and the PWRI engineers dam investigations confirmed neither damage to the dams, excluding some slight effects, nor other problems seriously affecting the dams safety or requiring immediate protective countermeasures, except for Kitayama Dam which is out of the river stretch administered under the River Law. But many of the dams were attacked by the earthquake at lower reservoir water level. It will, thus, be necessary to carefully observe the behavior of these dams after the water level rises higher.

9. DAMAGE TO SEWERAGE FACILITIES

9.1 Introduction

Sewerage facilities are generally categorized into sewage treatment plants, pumping stations and sewers which spread to underground in city areas.

It is extremely time-consuming to clarify the extent and nature of earthquake damage to sewerage facilities, particularly damage to sewer pipes, not only because of the vast scale of the sewer pipe system, but because unlike water supply and gas pipes, it is difficult to detect damaged pipes .

9.2 Sewage Treatment Plants and Pumping Stations

A total of 43 treatment plants in Hyogo, Osaka, and Kyoto Prefectures suffered damage by the earthquake. Eight of them, all located in Hyogo Prefecture, were damaged on their treatment functions.

(1) Kobe City

Kobe City has seven treatment plants, three of them were damaged by the earthquake.

Higashi Nada Treatment Plant is located in the old reclaimed land across the Uozaki Canal that has a width of 40 m. At the plant, the sludge collector chains in the final settling tank were knocked out of place (Photo 9.1)and uneven settlement in the area caused many breaks on conduits within the plant (Photo 9.2).

The depressed sewer which crossed the Uozaki Canal was broken, and so, sewages couldn't be pumped into the plant. Because of this, a temporary settling tank consisting in the blocking of a 300 meter long section of the canal was formed by installing sheet piles (Photo 9.3).

The treatment functions at both the Chubu and Seibu Treatment Plants were impaired by the inflow of sea water to the facilities.

(2) Nishinomiya City

At the Edagawa Purification Center, the effluent conduit at the final settling tank was cracked, reducing the plant's treatment capacity by 50%. Because large volumes of sand and groundwater had flowed into the plant through sewers, sewage exceeding the plant's capacity was disinfected and discharged.

At the Koshien Hama Purification Center and Naruo Hama Purification Center, parts of the flights on the sludge collectors were broken and the outlet channels were also broken.

(3) Ashiya City

At the Ashiya Treatment Plant, two force mains were both broken off at their mechanical joints on the treatment side (Photo 9.4), malfunctioning the treatment facility to pump up sewage.

(4) Others

At two treatment plants in Amagasaki City, primary treatment was done to deal with the excess sewage that could not be treated because of the water inflow through cracks.

Damage was also found at the Hyogo Prefecture Regional Sewerage System Treatment Plant and at treatment plants in the City of Osaka.

9.3 Pipe Facilities

(1) Kobe City

In Kobe, primary survey consisting mainly of visual inspections of the ground surface, insides of manholes, and the insides of pipes was completed by January 22, to quickly obtain a clear understanding of the extent of the damage. This inspection revealed approximately 1,400 cases of damage to the city's sewer pipes(Photo 9.5).

A more detailed secondary survey was conducted on 983kmof sanitary sewers and 357km of storm sewers. By February 23, this survey was almost completed, except for locations which could not be surveyed because of collapsed houses.Table 9.1 presents the state of emergency treatment taken to repair damaged pipes as of February 23.

(2) Nishinomiya City

Surveys of unequal subsidence, pipe breakage and other damage with liquefactions of soil had been proceeding in an area of approximately 3,173ha in the south part of the city.

9.4 Damage Survey and Restoration Organization

To assist with damage surveys and disaster recovery activities at sewerage facilities, the Ministry of Construction has set up the Sewerage System Earthquake Measures Liaison Conference on January 19, and opened the On-site Support Head Office in the City of Osaka on January 24.

Furthermore, the Japan Sewage Works Agency and local public bodies have supported with disaster survey activities and disaster assessment surveys to cities affected by the earthquake.

10. DAMAGE TO RETAINING WALLS

10.1 Summary of the Damage

In the damaged area, there are relatively few retaining walls and other earth structures on the plain along the waterfront; such structures are constructed only in embankments for railways, river dikes, and in approaches to bridges crossing the rivers. But many earth structures have been constructed on the foothill slopes of the Rokko Range (called Yamate area). Retaining walls have also been placed along mountain roads. Almost all earth structures constructed as part of river dikes and retaining walls behind residences are masonry retaining walls made of granite, one of the region's most important products.

The earth structures constructed in the continuous embankments for railway, highway bridge approach structures, and mountain roads, are gravity or leaning retaining walls, cantilever retaining walls and

other types of concrete retaining walls, or reinforced earth wall with geotextiles. In the area where the greatest intensity was recorded there were few concrete retaining walls or other retaining structures, which were considered as requiring structural design, but many existed in the Yamate area. The many masonry retaining walls in Yamate area suffered minor damage such as cracks or loosening.

10.2 Damage to Road Retaining Walls

In the waterfront area where the intensity was much higher, however, there were fewer retaining walls and the amount of damage was low. Within the range of this study, the survey team was unable to confirm any deformation that could cause structural problems in any reinforced earth walls: a type whose use has been growing in recent years. Photo 10.1 shows a road retaining wall that suffered particularly severe damage. A counterforted retaining wall constructed at a bridge approach where the Yamate Trunk Line crosses the Ishiya River was deformed forward with rotation for 20 or 30 meters length, and the road behind it subsided about 50 cm.

10.3 Damage to Railway Retaining Walls

Many earth structures for railways in the intensity 7 area are either retaining walls or embankments, and these structures were severely damaged; either collapsing or suffering complete destruction. Photo 10.2 shows damage to a 100 m section of an L-shaped retaining wall with about 6 meters high. The retaining wall has deformed about 20 cm horizontally. In contrast, an adjoining geotextile reinforced earth wall was deformed so slightly that only by examining the joints the damage could be confirmed.

11. DAMAGE TO UNDERGROUND STRUCTURES

11.1 Introduction

Earthquake damage to underground structures has been extremely rare in Japan, and thus it has been generally assumed that such structures show a good performance during an earthquake. However, subways and other kinds of underground structures were seriously damaged by the earthquake.

11.2 Subway Damage

(1) General

Table 11.1 summarizes the damage to subway facilities. Damage (excluding small cracks) was observed at five stations and in approximately 3 km of tunnel. The Kobe Rapid Railway Corporation had reported that the cost of the damage excluding that to elevated structures was approximately 30 billion yen, and that it will cost about 10 billion yen to refrofit the Daikai Station and about 18 billion yen to refrofit the tunnel damage.

(2) Damage to the Kobe Rapid Railway Corporation

Fig. 11.1 illustrates a cross section of the Daikai Station, and Photo 11.1 shows damage to the track level (B2). A total of 31 columns were broken and upper slab collapsed. Spalling-off of concrete and buckling of reinforcement were developed at the haunch, and cracks appeared in four columns. As shown in Photo 11.2, this damage caused subsidence of up to 2.5 m in depth, approximately 90 m in length, and 23 meters in width, to the surface of national road No. 28 located above the subway. The damage, shown in Photos 11.1 and 11.2, occurred in the tunnels near the station. Photo 11.3 shows the damage to the columns of track level (B2) at Nagata Station. Fourteen columns were damaged here; steel reinforcement was deformed in five of them and nine others were cracked.

(3) Damage to the Kobe Municipal Subway

Photos 11.4 and 11.5 show damage to columns in the track level (B2) at Shin-nagata Station and the electricity

supply room (B1) at Kamisawa Station. Fig. 11.2 shows a cross section of damaged locations at Sannomiya Station. At the respective stations, there were 8, 91, and 60 columns with a crack width of 5mm or more. No damage to steel columns was found on the track levels of Sannomiya Station (B2 and B3).

In the tunnel sections, cracks of 5 mm or wider were developed in 64 columns and 27 columns on the east side of Shin-nagata Station (see Fig. 11.3) and on the west side of Kamisawa Station, respectively.

11.3 Damage to Common Utility Ducts and Cable Box (CAB)

Table 11.2 summarizes damage to common utility ducts. A total of approximately 7 km of common utility ducts had been constructed at two areas: one in Kobe city and the other in Amagasaki city. Damage was relatively slight at both sites, and there was no damage which affected the stability and/or the serviceability of the structures themselves.

About 4km of CAB are served in Kobe area. The service for the ground traffic has been a priority since the earthquake, so at the end of February, the CAB had not been excavated to investigate the damage. It has been reported however that indications visible at the surface reveal that the ground subsided around the CAB constructed along National Highway No. 28 and the Municipal Road Ikutamae-sen within the city of Kobe, and that the ground above this CAB has risen up to 10cm.

12. CONCLUDING REMARKS

This paper presented an overview of the earthquake, geological hazards and the damage to various engineering structures. The feature of the earthquake and the damage may be summarized as follows:

(1) The magnitude of the earthquake was 7.2 on the JMA Scale. Although the magnitude was not the largest, the violent ground motion that struck the highly integrated area including Kobe was very destructive, because the epicenter was very close to the area.

(2) The earthquake caused severe damage to human life and property as well as to engineering structures. About 5,500 people were killed. About 180,000 buildings were totally or partially destroyed. The fires that followed the earthquake increased the damage.

(3) The peak ground acceleration as large as 818 gal was recorded. The ground motions recorded in the area may be characterized by their large response acceleration spectra over a broad frequency range, and the large values of velocity and displacement.

(4) An earthquake fault appeared in the Awaji Island near the hypocenter. Although there were active faults in the Kobe area, ground displacement associated with the faults have not been confirmed.

(5) Occurrence of liquefaction was widespread. In reclaimed lands, liquefaction of gravelly granite fill materials was observed and lateral flow of liquefied soils occurred along the coast line.

(6) Elevated highway bridges suffered extensive damage. The damage included collapse of piers, falling off of a simple supported girder, breakage of bearings and/or falling prevention devices. Bridge piers constructed based on the highway bridge specifications enacted in 1980 showed better performance than the older ones.

(7) Many landslides occurred in and around the Rokko Mountains. Among these, three landslides killed 37 people.

(8) River dikes in Yodo River settled as large as 3 m. Extensive sand boils originated by the subsoil liquefaction were observed near the damaged dikes.

(9) A sliding occurred exceptionally on the upstream slope of Kitayama Dam. Neither damage nor other problems seriously affecting dam safety were found.

(10) The sewage treatment plants and pumping stations were damaged, some of which were heavily damaged due to the liquefaction of soils. A vast length of sanitary and storm sewer pipes suffered damages; breakage of pipes and joints, dislodging and pull-out of pipes, etc.
(11) Damage to masonry retaining walls were frequently observed. But there were few serious damage tof gravity and L-shaped retaining walls. Reinforced earth, in particular, showed good performance.
(12) Five subway satations and approximately 3 km of subway tunnel suffered extensive damage. In Daikai Station, a total of 31 reinforced concrete columns were broken and upper concrete slab collapsed.

Immediately after the earthquake, the Ministry of Construction (MOC) conducted urgent investigation of the damage of various structures of which MOC is in charge, and has been doing everything possible to restore the damage.

The technical committees were established to propose the guidelines for restoration and to discuss the seismic design of various facilities, and they have been studying the various aspects of these issues.

As for the highway bridges, for example, "Technical Committee for Highway Bridge Damage in the Hyogoken Nanbu Earthquake" was established on January 24th, which published the specification for restoration on February 27th. The committee also published, on March 30th, the interim report about the mechanism of the damage to the bridges and the issues requiring further research.

Now the restoration based on the specification for restoration is under way.
The Public Works Research Institute started the survey and research of the technical issues which came to light as the urgent problems in the Hyogoken Nanbu Earthquake, from mid- and long-term view points.

ACKNOWLEDGEMENTS

In conducting the post earthquake damage investigation by the PWRI reconnaissance teams, invaluable supports were provided by the organizations: the Hanshin Expressway Public Corporation, the Japan Highway Public Corporation, Water Resources Development Public Corporation, Kobe Rapid Railway Corporation, Hyogo and Osaka Prefectural Government, the City of Kobe, Nishinomiya, Ashiya, Amagasaki, Osaka, and Kinki Regional Construction Bureau, Ministry of Construction. The authors express their sincere appreciation for the supports of the organizations and personnels concerned. A part of the survey was jointly made with the Geographical Survey Institute (MOC) members. Various discussions with the GSI team members were very valuable for the PWRI team. Valuable earthquake records were provided by the Japanese Meteorological Agency, Ministry of Transport, the Committee of Earthquake Observation and Research in the Kansai Area, Japan Railways, and Osaka Gas and many other organizations concerned. A great appreciation is also directed to the PWRI reconnaissance team staffs.

REFERENCES

1)Geological Survey of Japan: Geological Map of Japan, 1: 1,000,000 (3rd Edition), 1992.
2)Edited by research group of active faults : Active faults in Japan, Tokyo-Univ. Publishing Association, 1991.

Table 3.1 Summary of Damage Caused by the Hyogoken Nanbu Earthquake

Items	Estimated Damage (billion yen)
architecture	5,800
railroads	344
highways	550
public facilities (excl. highway)	283
port facilities	1,000
education facilities	335
facilities for agriculture, forestry and fishery	118
medical and welfare facilities	173
facilities for water supply	54
facilities for gas and electricity supply	420
facilities for communication and broadcasting	120
commercial and industrial facilities	630
other facilities	87
total	9,914

Table 8.1 Number of Emergency-inspected Dams in Each District

District	Number of Dams
Kinki District	101
Chubu District	34
Chugoku District	49
Shikoku District	67
Total	251

Table 8.2 Main Effects of the Earthquake on PWRI Investigated Dams
(Include main features of these dams)

Dams in the river stretch administered under the River Law

Name of Dam	Name of river	Type of dams	Height of dams (m)	Depth of reservoir water during the earthquake(m)	Year of completion	Main effects of the earthquake
Yuzuruha	Yuzuruha	concrete gravity dam	42.0	25.1	1974	·slight spalling of mortar on upstream face
Tenno	Tenno	concrete gravity dam	33.8	13.9	1980	·no damage to dam body ·fall of rock at abutment ·drawdown
Tokiwa	Nojima	zoned earth fill dam	33.5	20.9	1974	·transverse cracking on crest near abutment contacts

Dams out of the river stretch administered under the River Law

Name of Dam	Name of river	Type of dams	Height of dams (m)	Depth of reservoir water during earthquake (m)	Year of completion	Main effects of the earthquake
Gohonmatsu	Ikuta	masonry dam	33.3	24.6	1900	·no damage to dam body ·fall of rocks at abutment
Kitayama(No.1)	Syuku	homogeneous earth fill dam	24.5	16.2	1968	·sliding of upstream slope

Table 9.1 Number of Emergency Measures Taken (in Kobe)

As of February 23

	Description	Number of Cases	Percentage(%)
Sanitary Sewage	Pipe Damage	148	2
	Manhole Damage	238	3
	Lateral Damage	427	5
	House Connection Damage	7,602	84
	Blockade	454	5
	Others*	81	1
	Sub-total	8,950	100
Storm Water	Blockade	33	13
	Damage	205	83
	Sediment Accumulation	10	4
	Sub-total	248	100
Total		9,198	———

* "Others" include emergency measures taken to deal with floated up or subsided manholes, and other damages (Source : the City of Kobe) .

Table 11.1 Subway Damage

(1) Kobe Rapid Railway (Source : the Kobe Rapid Railway Co., Ltd.)

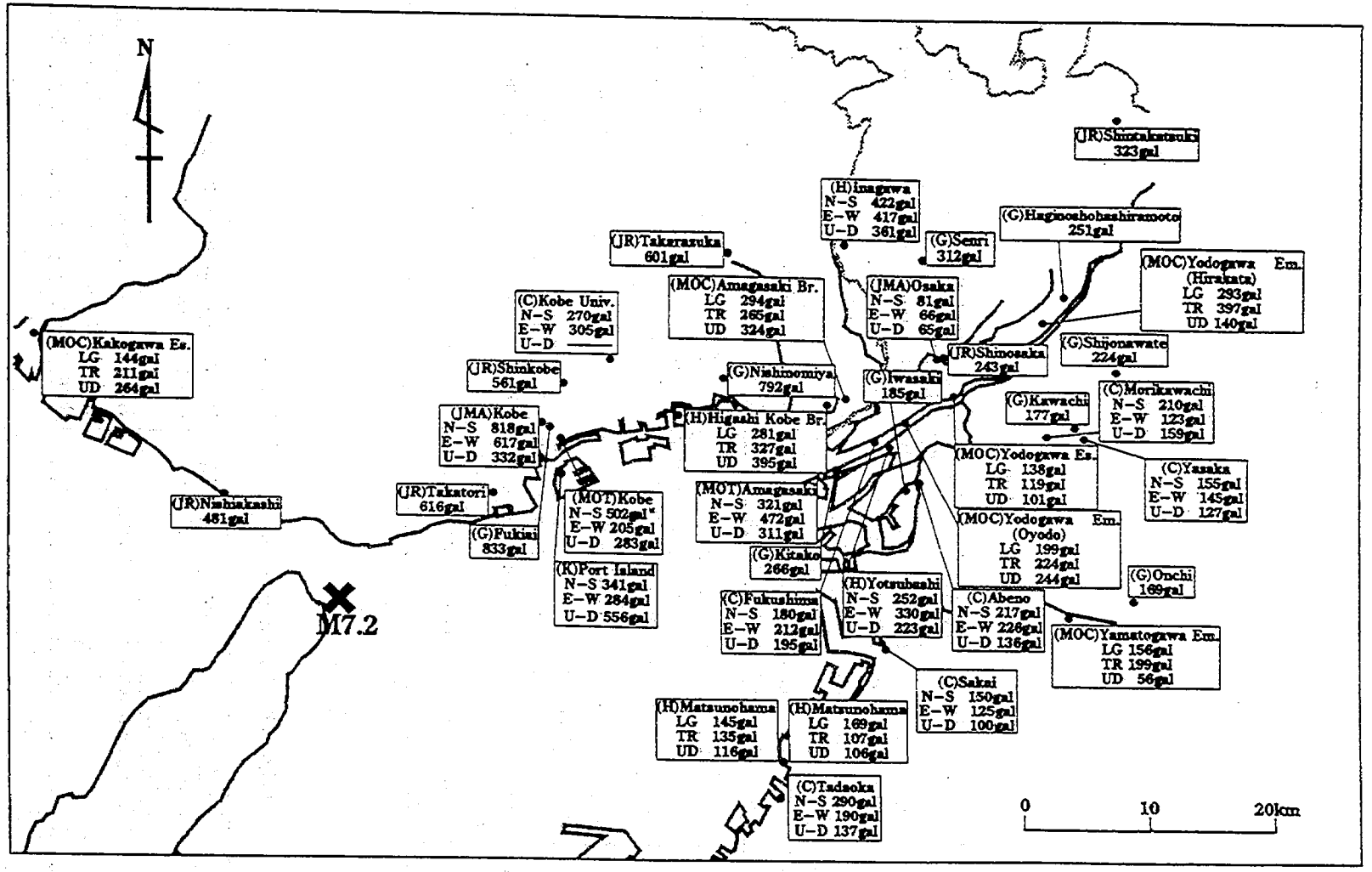
Damage Location	Details of Principal Damage
Daikai Station	Columns at the track level (B2), damage to the top floor slab and haunch on top of the side wall, road surface subsidence above the subway, damage to stairway openings (B1 and B2) and entrances (B1)
Kosoku Nagata Station	Damage to center columns on the track level (B2)
Tunnels Near Daikai St.	Damage to center columns, cracks to the walls, damage to execution joints, leakage (length of damage is approximately 2,380m excluding minute cracks.)

(2) Kobe Municipal Subway (Source : the Kobe Municipal Subway Bureau)

Damage Location	Details of Principal Damage
Shin-nagata Station	Center column damage in the track level (B2), the fire extinguisher pump room (B1).
Sannomiya Station	Center column damage in the ventilation machine room (B1, B2) and the electric room (B2)
Kamisawa Station	Center column damage in the track level (B2) and the electric room (B1)
Tunnels to the West of Kamisawa Station	Center column damage (approximately 500 meters of damage including the stations)
Tunnels to the East of Shin-nagata Station	Center column damage (approximately 480 meters of damage including the stations)

Table 11.2 Damage to Common Utility Ducts

Utility Duct	Location	Service Length	Details of Principal Damage
Kobe Utility Duct (National Road No. 2)	Chuo-ku, Kobe City	1,034m	Cracks in walls and manholes.
Amagasaki Utility Duct (National Road No. 2)	Amagasaki City	6,040m	Breakage and leakage at joints, cracking and leaking on top panels, walls, and floor panels, leakage at ventilation opening



Es. : Estuary Dam
Em. : Embankment
Br. : Bridge

COMPONENTS
L G : Longitudinal comp.
T R : Transversal comp.
U D : Vertical comp.
N-S : North-South comp.
E-W : East-West comp.
U-D : Vertical comp.

ORGANIZATION
JMA : Japan Meteorological Agency
MOC : Ministry of Construction
MOT : Ministry of Transport
JR : Japan Railways
K : City of Kobe
H : Hanshin Expressway Public Corporation
O : Osaka Gas
C : Committee of Earthquake Observation and Research in Kansai Area

Acceleration reported by Japan Railways is the maximum value in the horizontal component.
Acceleration reported by Osaka Gas is measured by maximum acceleration meter.
N-S and E-W components of "(MOT)Kobe" denote the direction of N43E and E43N respectively.
* Scale Out of Range

Fig. 2.1 Maximum Acceleration at Observation Points

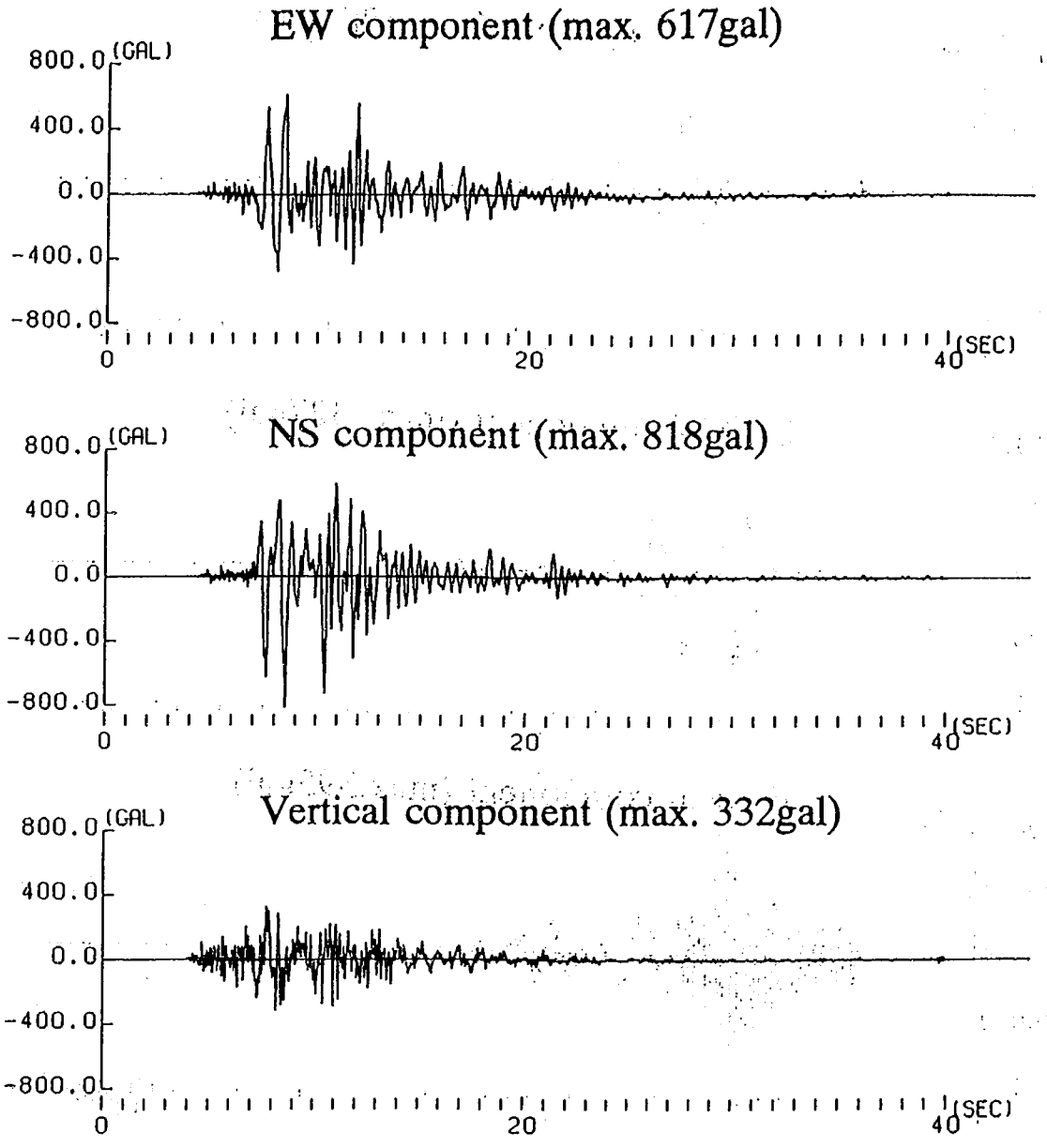


Fig. 2.2 Acceleration Records at the Kobe Maritime Meteorological Observatory

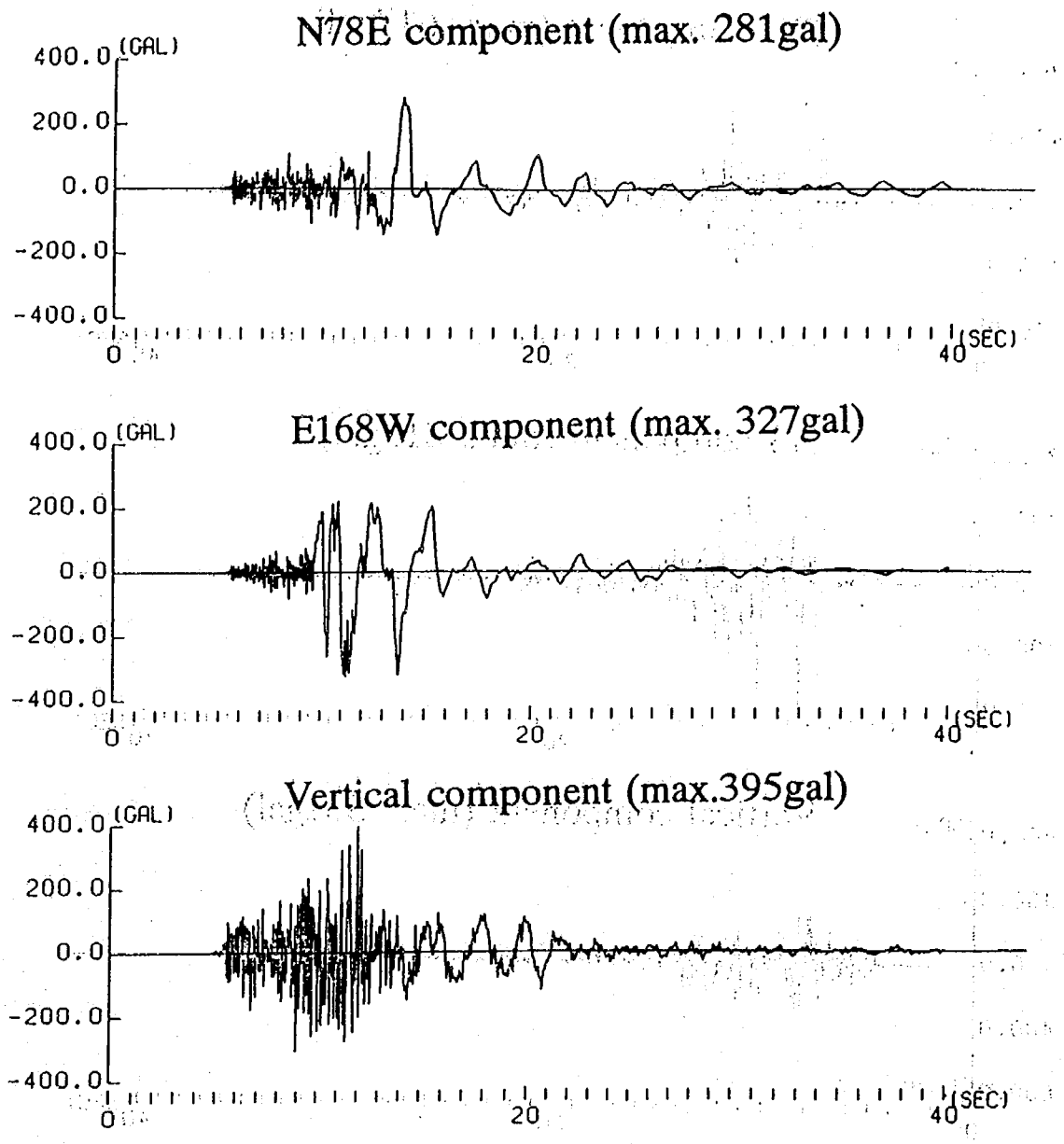


Fig. 2.3 Acceleration Records on the Ground Near the Higashi Kobe Bridge

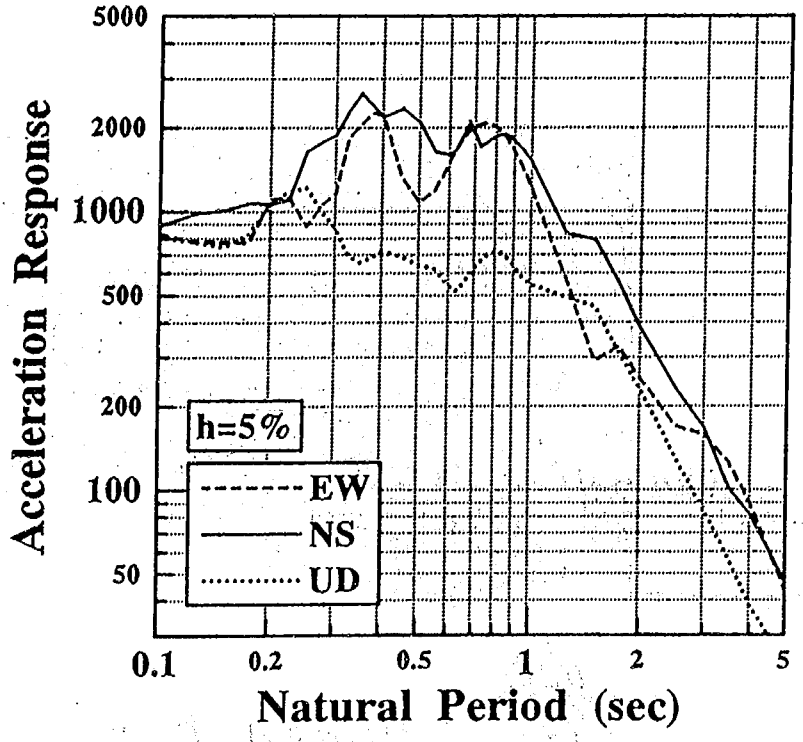


Fig. 2.4 Acceleration Response Spectra of the Ground Motion recorded at the Kobe Maritime Meteorological Observatory

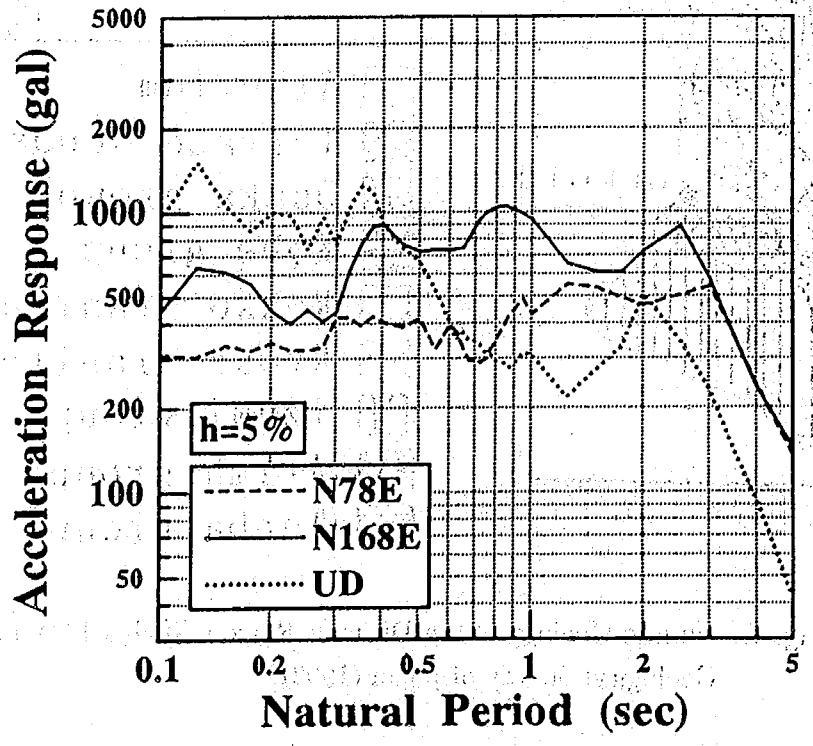


Fig. 2.5 Acceleration Response Spectra of the Ground Motion recorded on the Ground near the Higashi Kobe Bridge

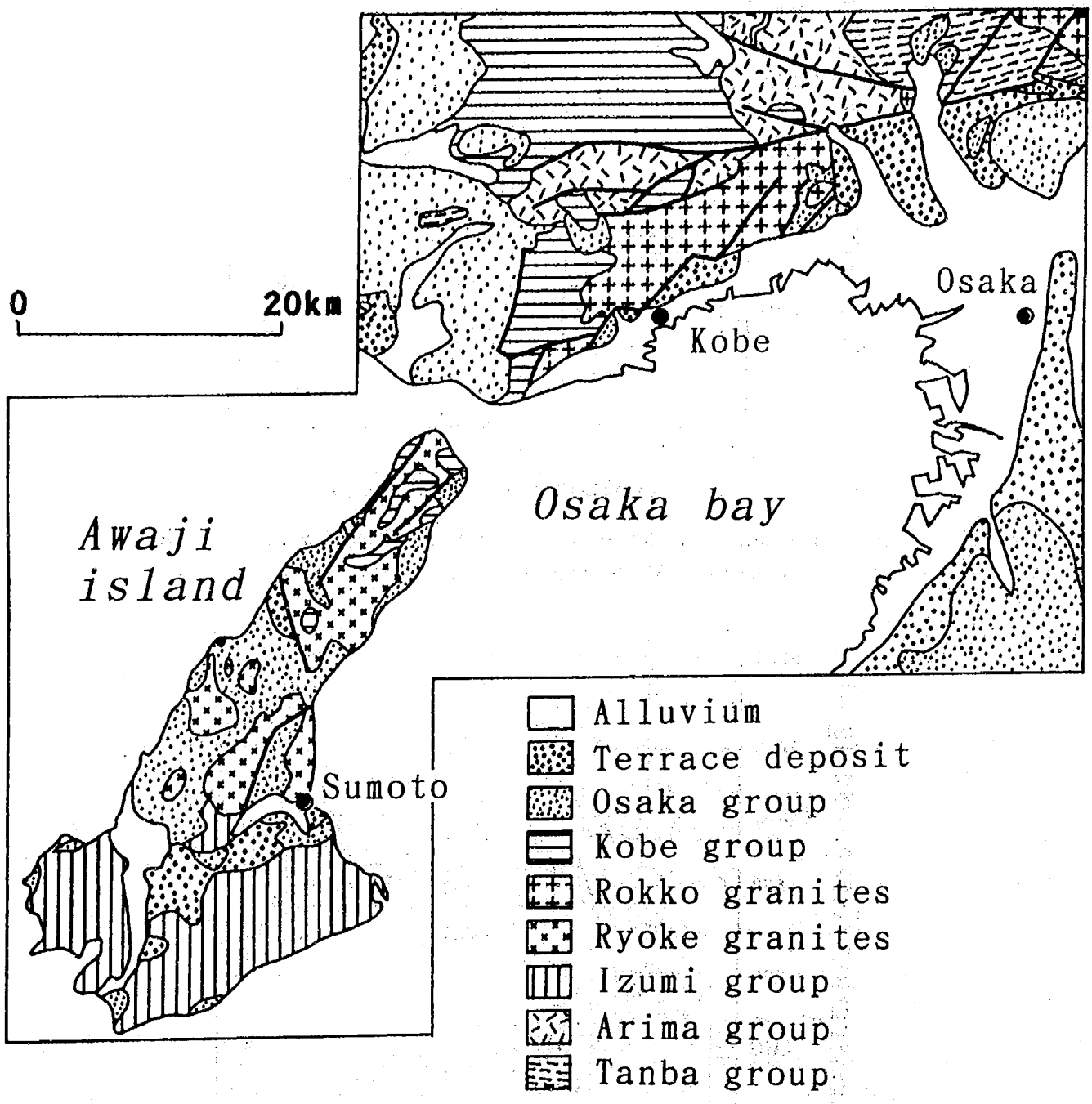


Fig. 4.1 Outline Geology of the Disaster Region, Modified from the Geological Survey of Japan (1992)[1]

No.	Name of Bridge or District	No.	Name of Bridge or District
1	Monto viaduct	13	Nishinomiya,,Ichiniwacho Ebisu
2	Iwaya viaduct	14	Kobe,Fukae−honmachi
3	Hamate bypass	15	Kobe,West of Fukae−honmachi
4	Onishi viaduct	16	Kobe,Hatobacho
5	Moribe viaduct	17	JR Wadamisaki Line
6	Mukogawa bridge	18	Minatogawa ramp
7	Kawaraginishi viaduct	19	Nishinomiya bay bridge
8	Takarazuka viaduct	20	Sin−Shukugawa bridge
9	Nishinomiya,KoshienTakashiocho	21	Sin−Asiyagawa bridge
10	Nishinomiya,Imazufutaba	22	Higashi Kobe bridge
11	Nishinomiya,Hamawakicho	23	Rokkou island bridge
12	Nishinomiya,Ichiniwacho Tateisi		

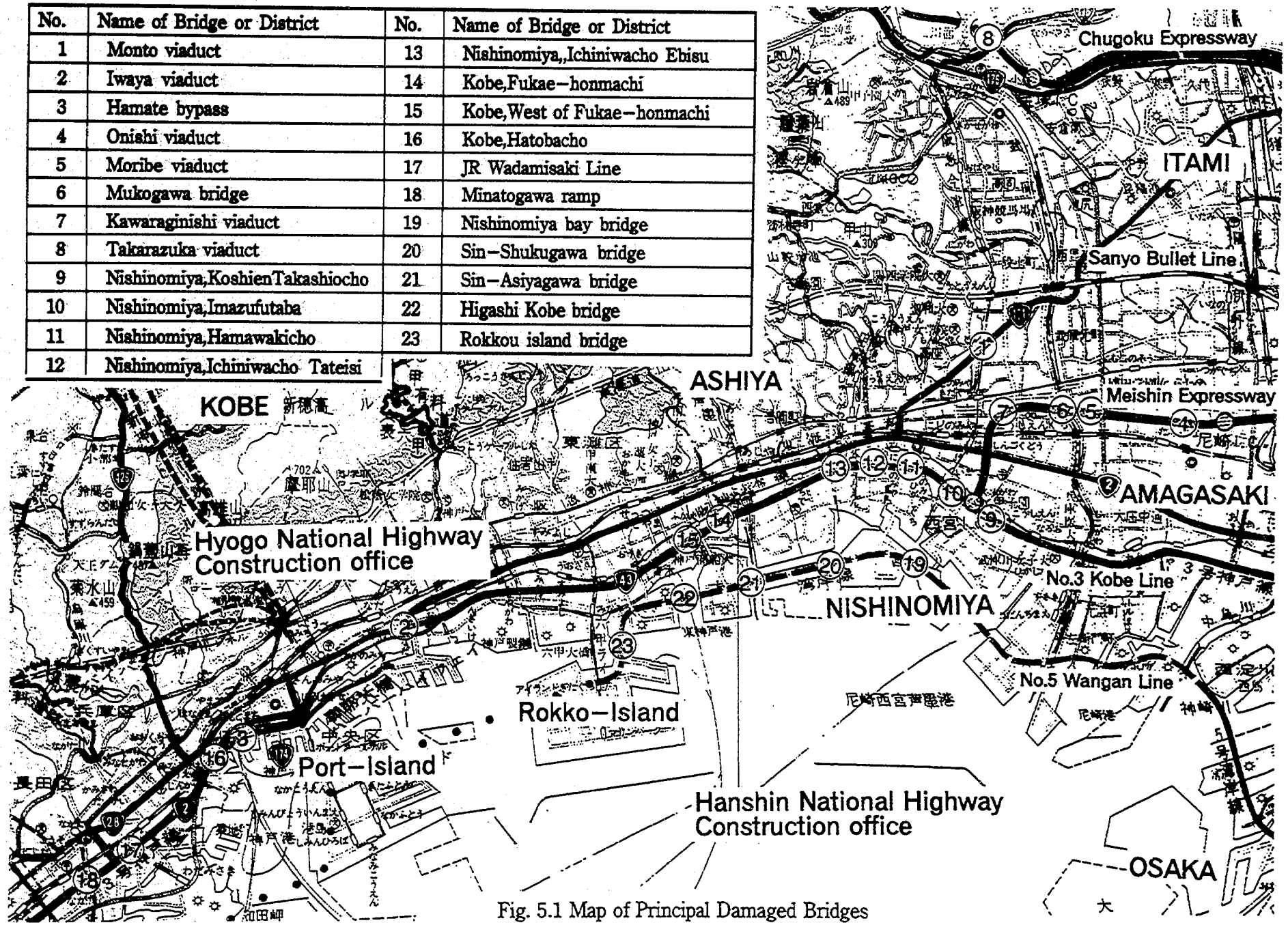


Fig. 5.1 Map of Principal Damaged Bridges

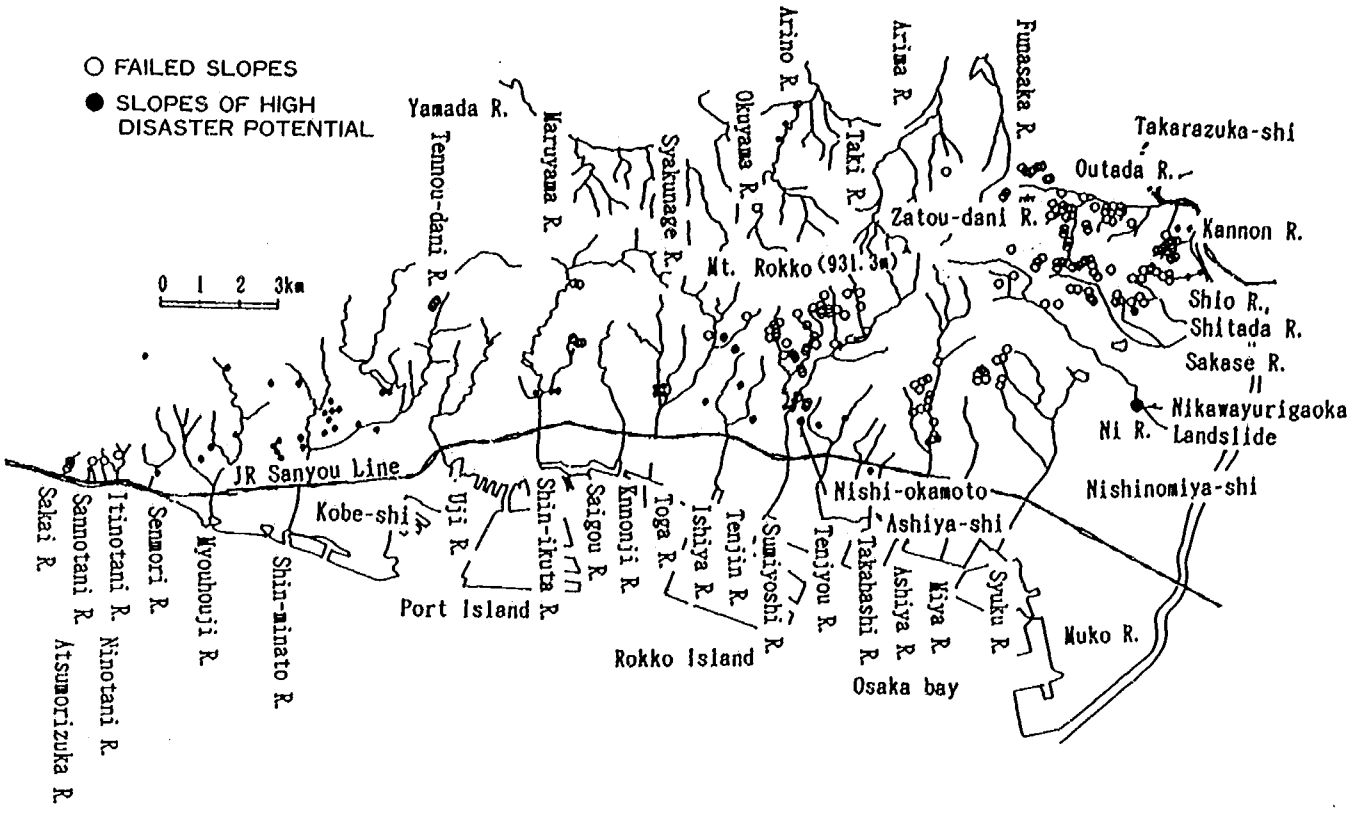


Fig. 6.1 Landslide Slopes by the Earthquake in Rokko Mountains

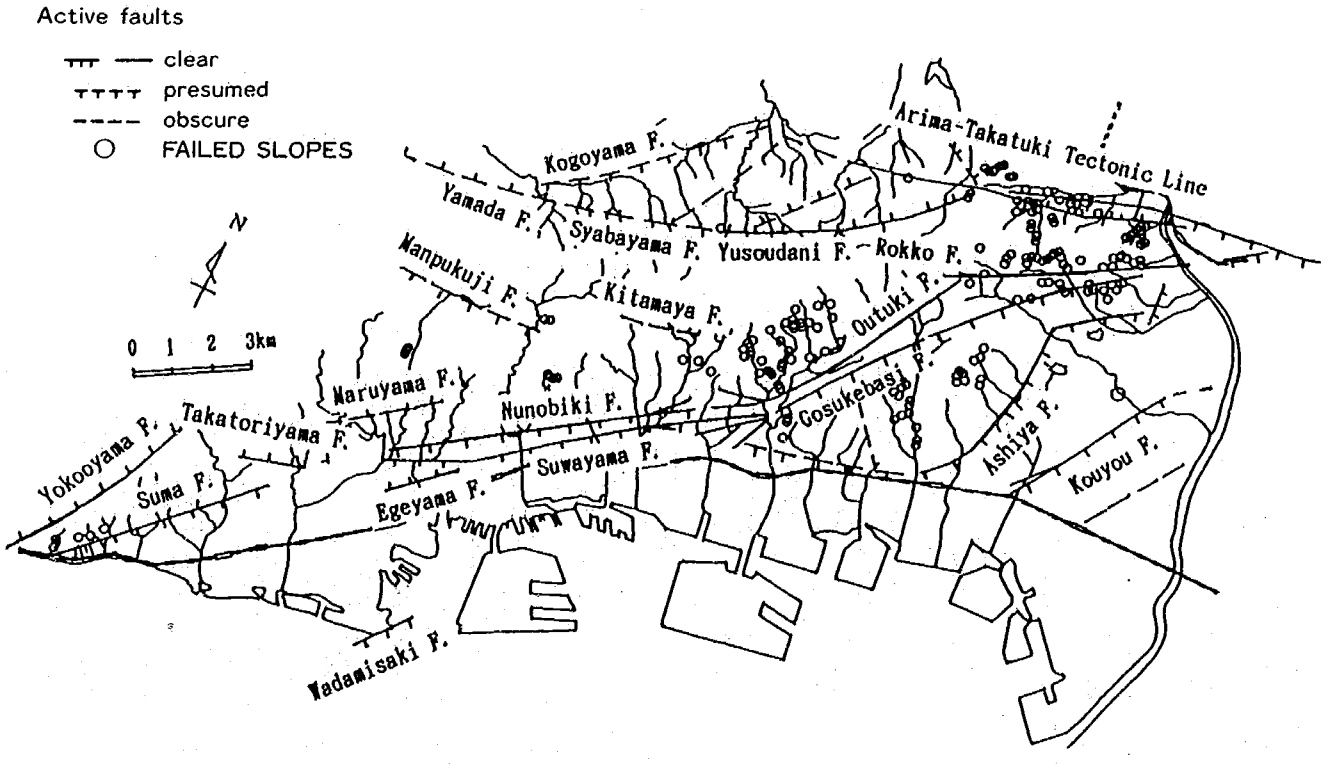


Fig. 6.2 Landslide Slopes and Active Faults in Rokko Mountains[2)]

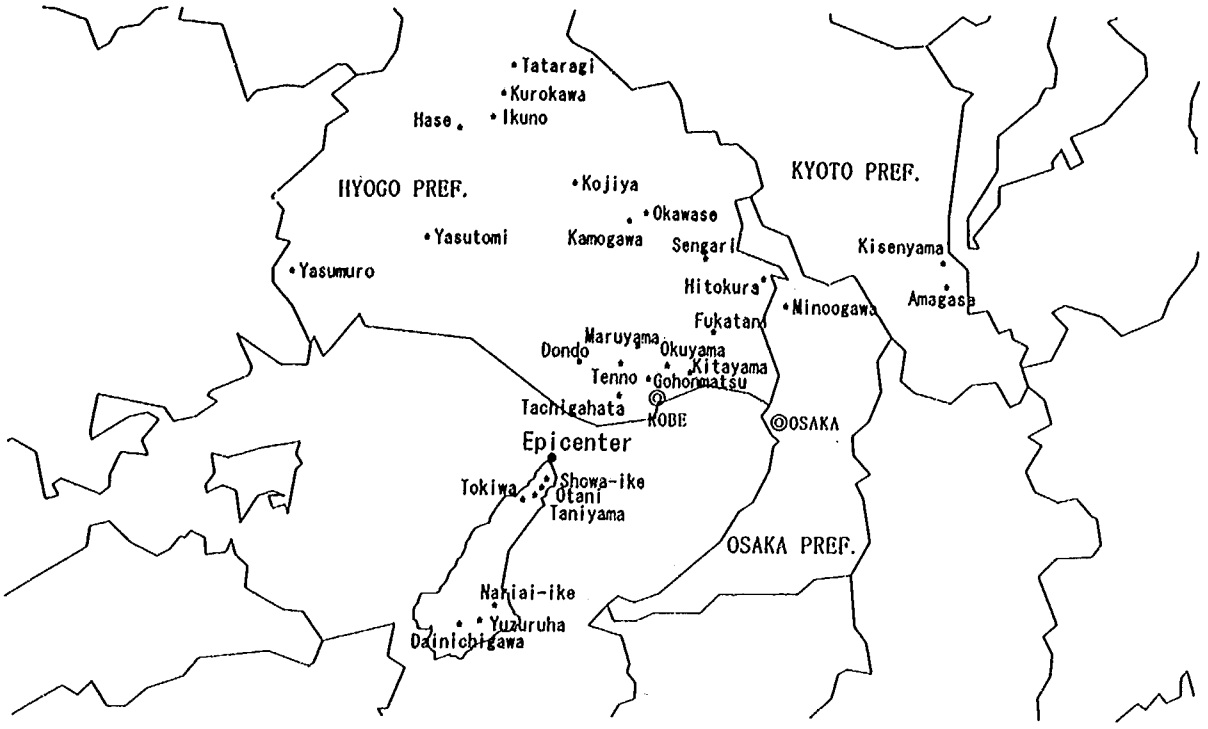


Fig. 8.1 Location Map of the PWRI Investigated Dams

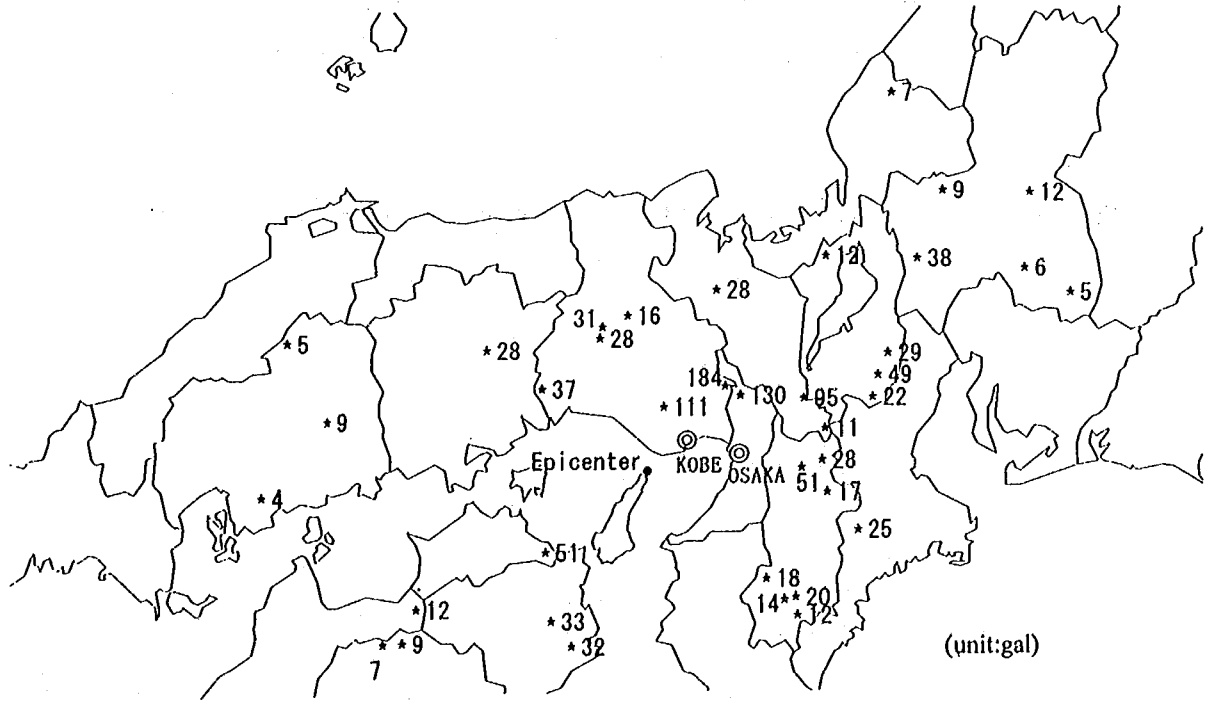


Fig. 8.2 Map of Peak Acceleration at Dam Foundations or Lower Elevation of Dams
(The values are provisional.)

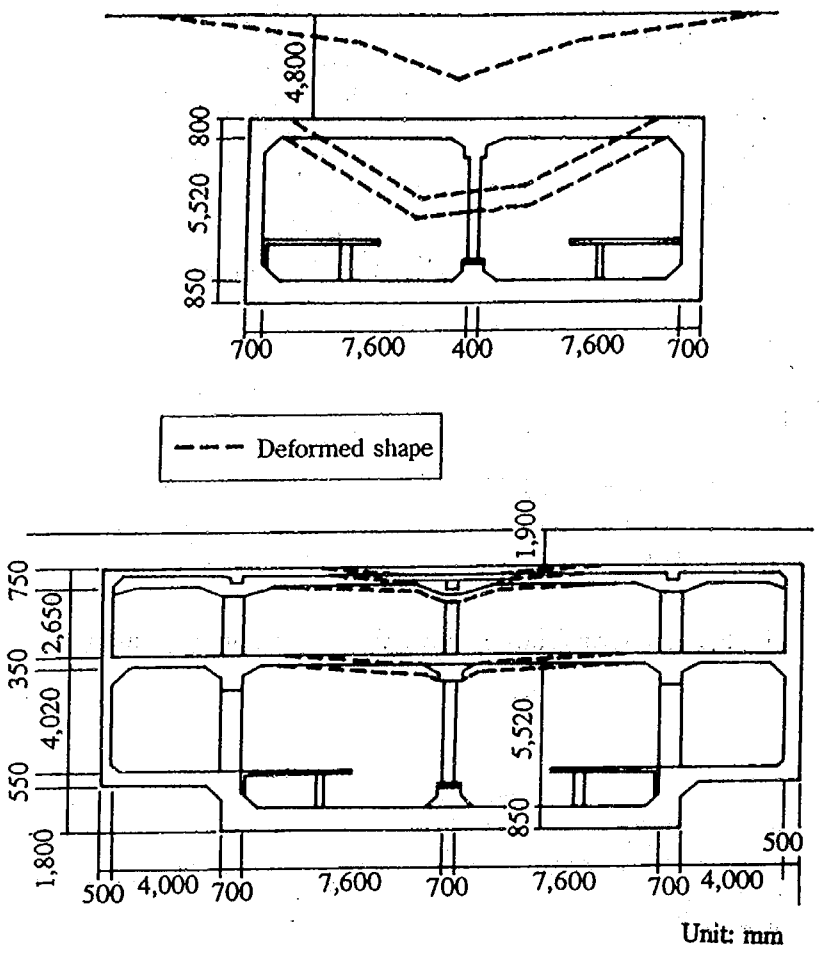


Fig. 11.1 Cross Section of Daikai Station, the Kobe Rapid Railway Corporation.

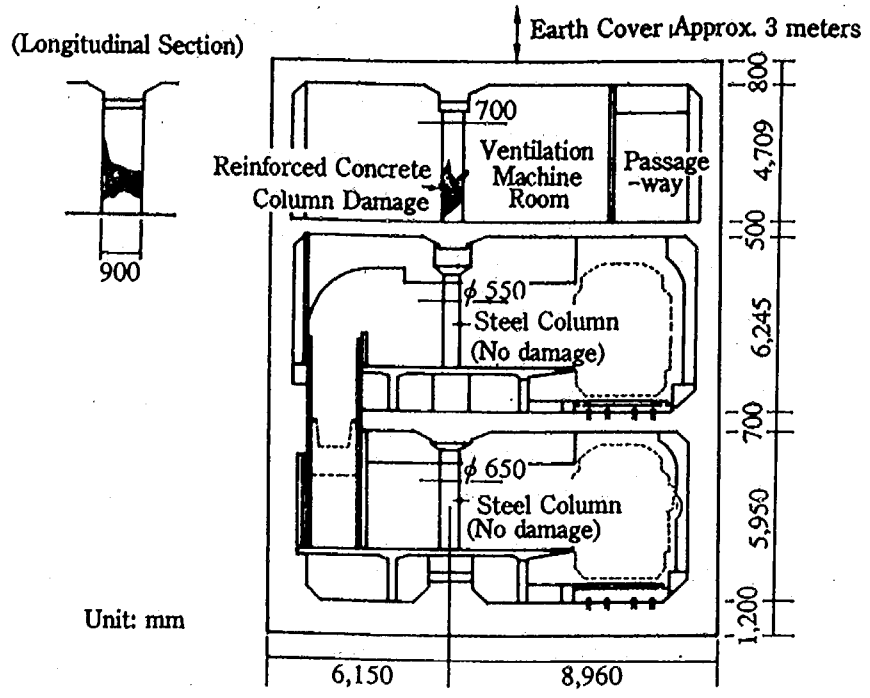


Fig. 11.2 Cross Section of Damaged Locations at Sannomiya Station in the Kobe Municipal Subway

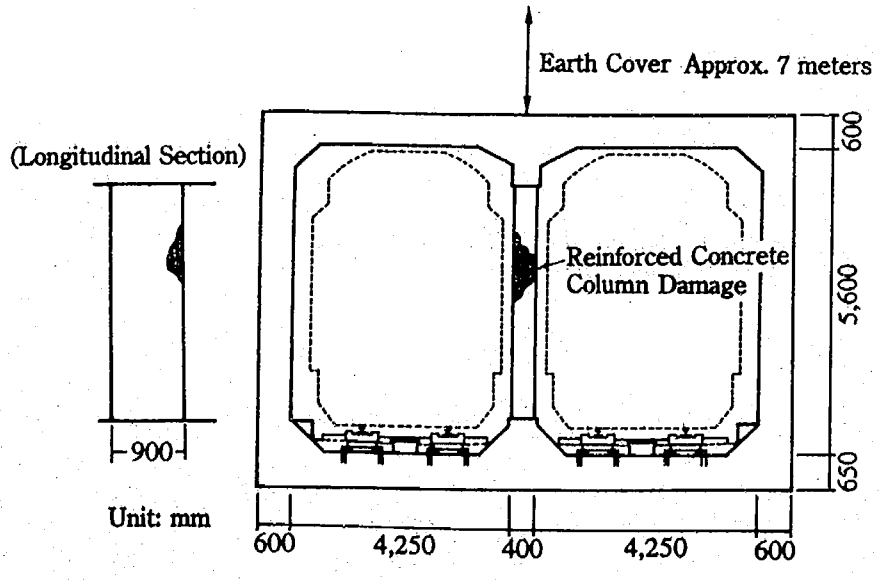


Fig. 11.3 Cross Section of Damaged Locations in Ducts, East of Shinnagata Station, Kobe Municipal Subway

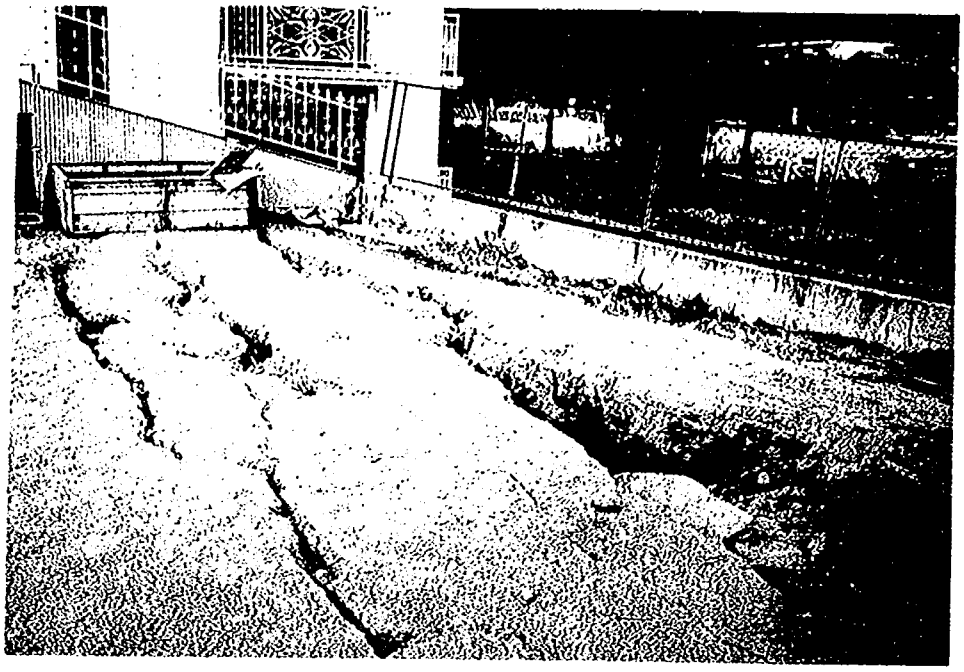


Photo 4.1 Open Cracks Caused by Landslide Towards a Pond. Kobe, Suma-ku, Sumadera-cho.



Photo 4.2 Subsidence near a Quaywall Caused by Liquefaction. Port Island

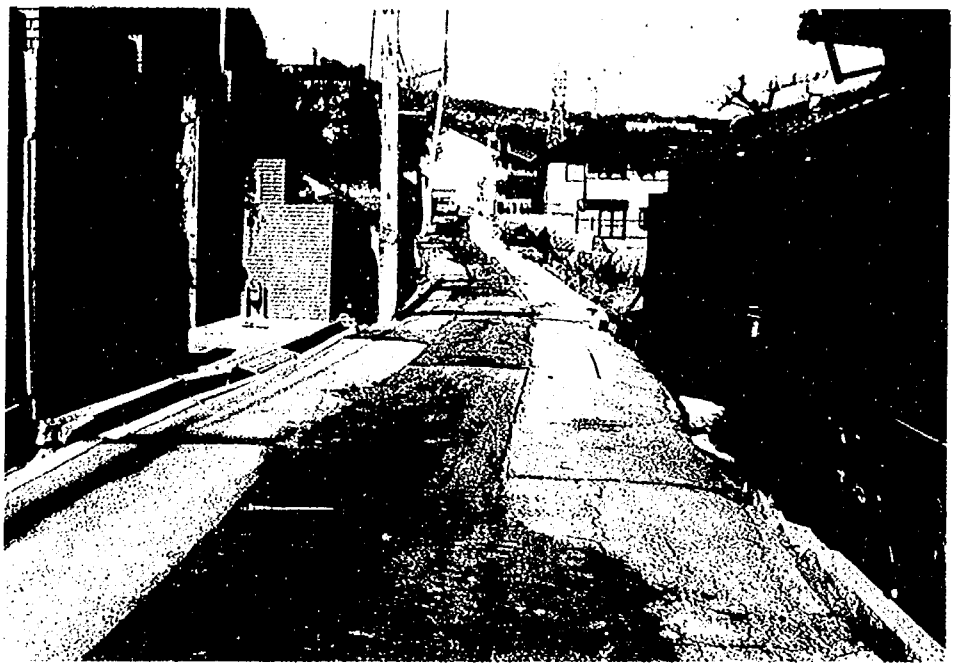


Photo 4.3 Bent Road Caused by Landslide.
This road was straight before the earthquake. Nishinomiya, Kitsuyama−cho



Photo 5.1 National Highway No. 171, Mondo Viaduct Falling of Overpass Bridge

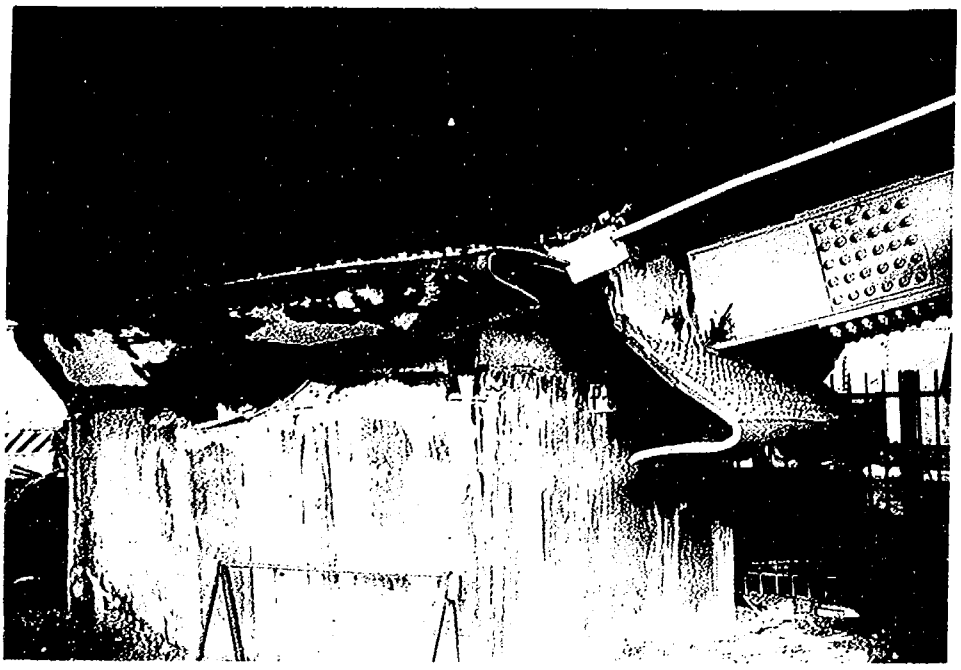


Photo 5.2 National Highway No. 43, Iwaya Viaduct Buckling of Steel Pier

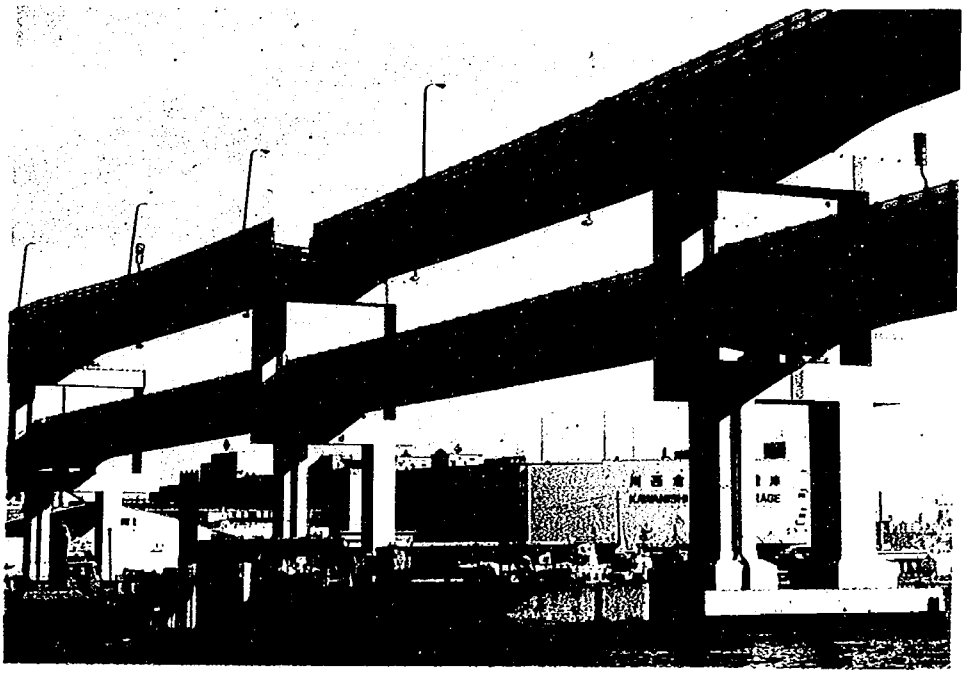


Photo 5.3 National Highway No. 2, Hamate Bypass Movement of Girders

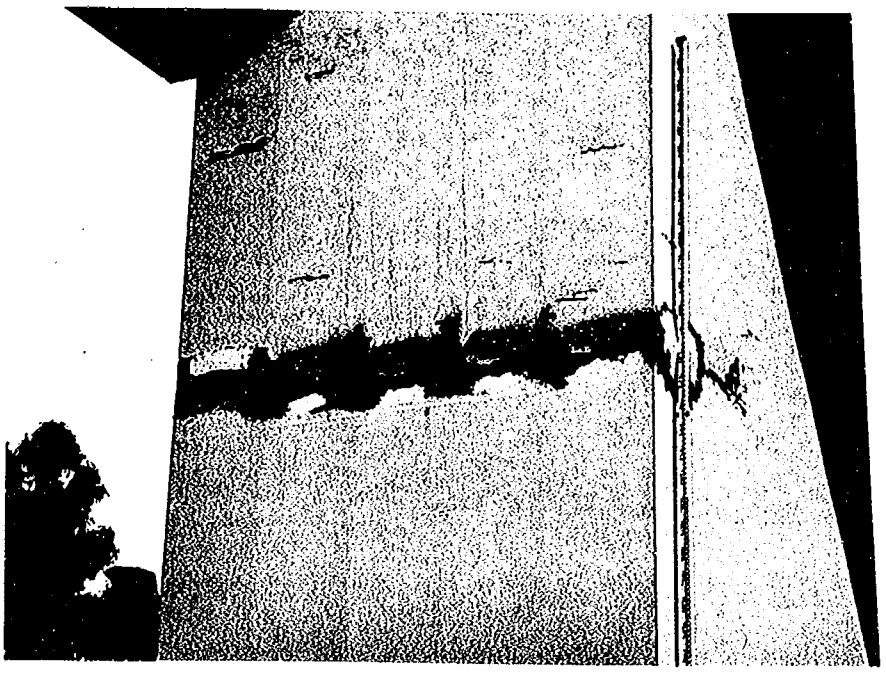


Photo 5.4 National Highway No. 2, Hamate Bypass Local Buckling of Steel Pier

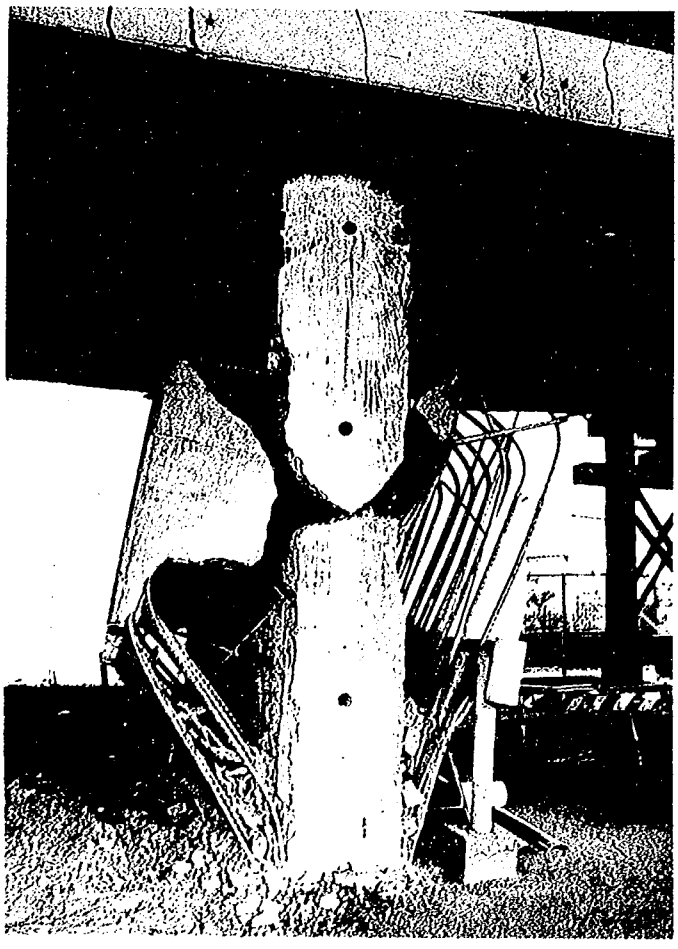


Photo 5.5 Meishin Expressway, Moribe Viaduct Failure of RC Wall Type Pier

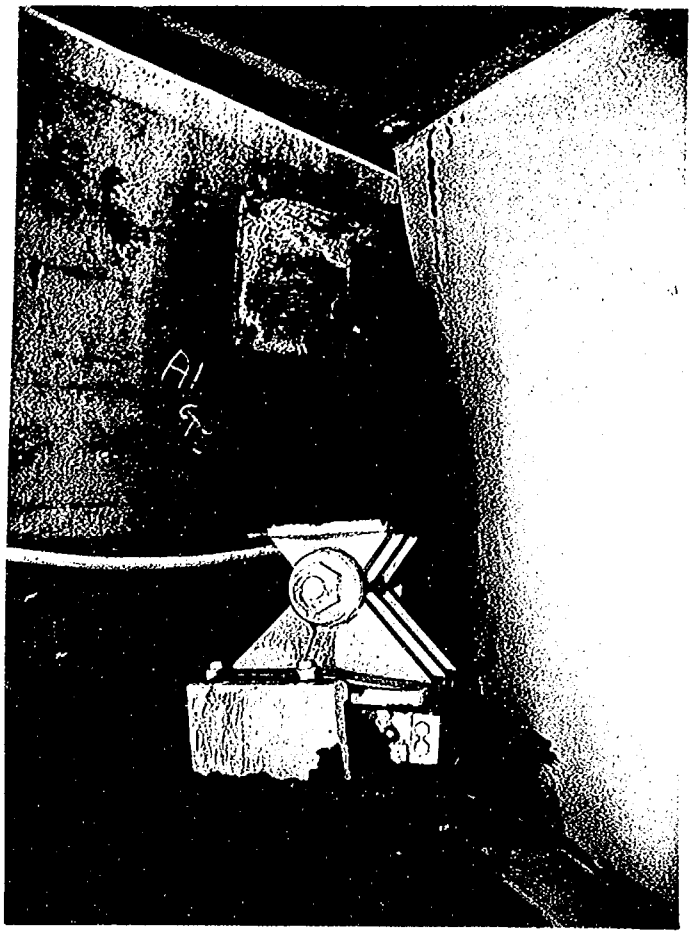


Photo 5.6 Meishin Expressway, Mukogawa Bridge Damage of Bearing and Device Linking the Girder

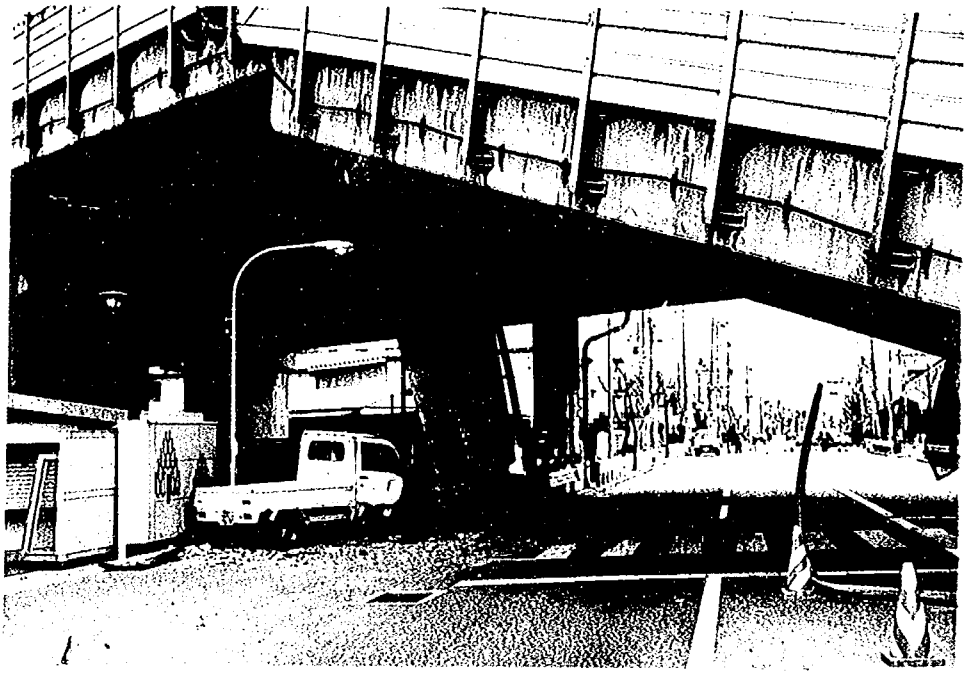


Photo 5.7 Meishin Expressway, Kawaraginishi Viaduct, Falling of Girder

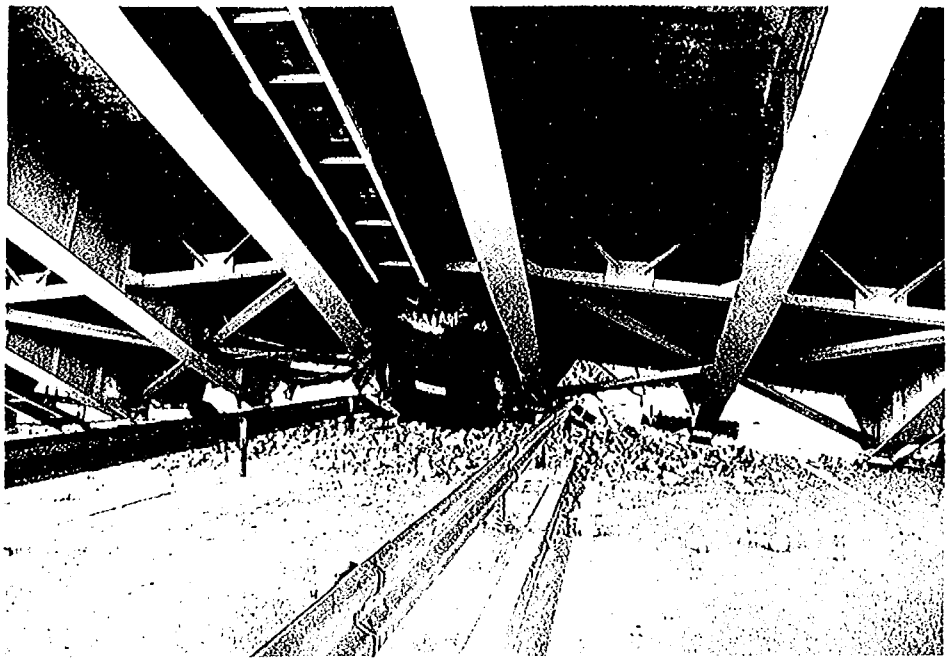


Photo 5.8 No.3 Kobe Line of the Hanshin Expressway, Takashio-machi, Falling of Two Simple Beams as a Result of Damage of RC Pier

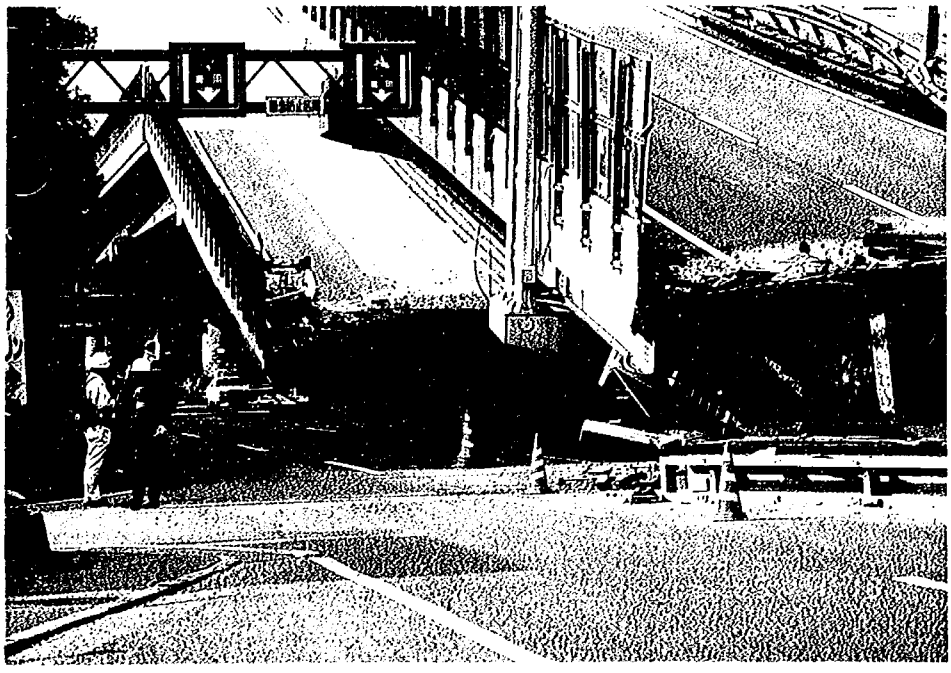


Photo 5.9 No.3 Kobe Line of the Hanshin Expressway Hamawaki-machi, Falling of Simple Beams



Photo 5.10 No.3 Kobe Line of the Hanshin Expressway, Ichiniwa−machi, Damage of Steel Pier

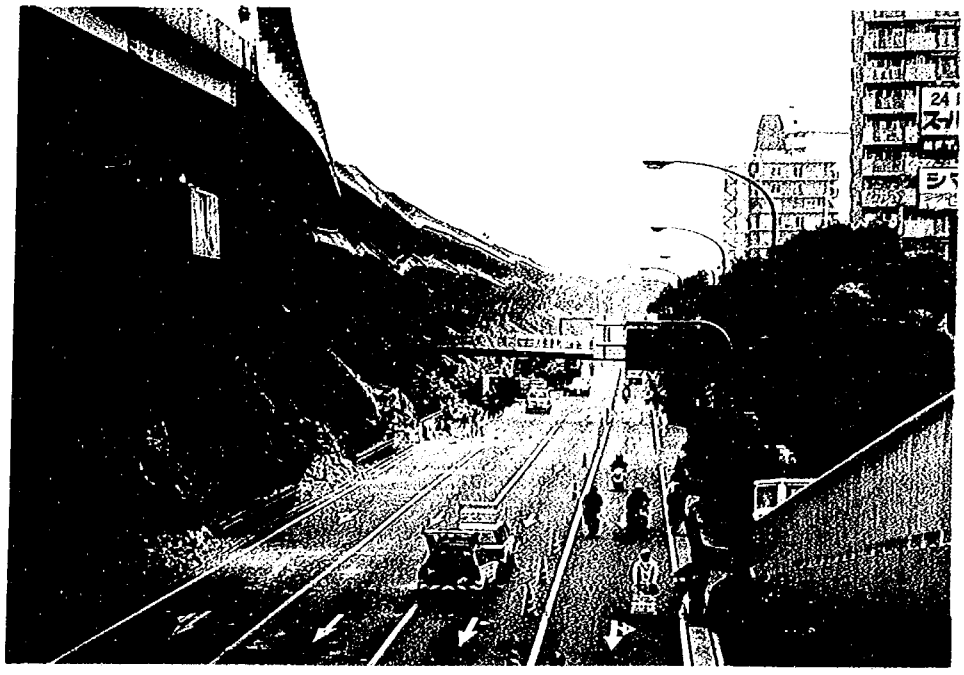


Photo 5.11 No.3 Kobe Line of the Hanshin Expressway Fukae−honmachi, Collapse of Pilz Bridges

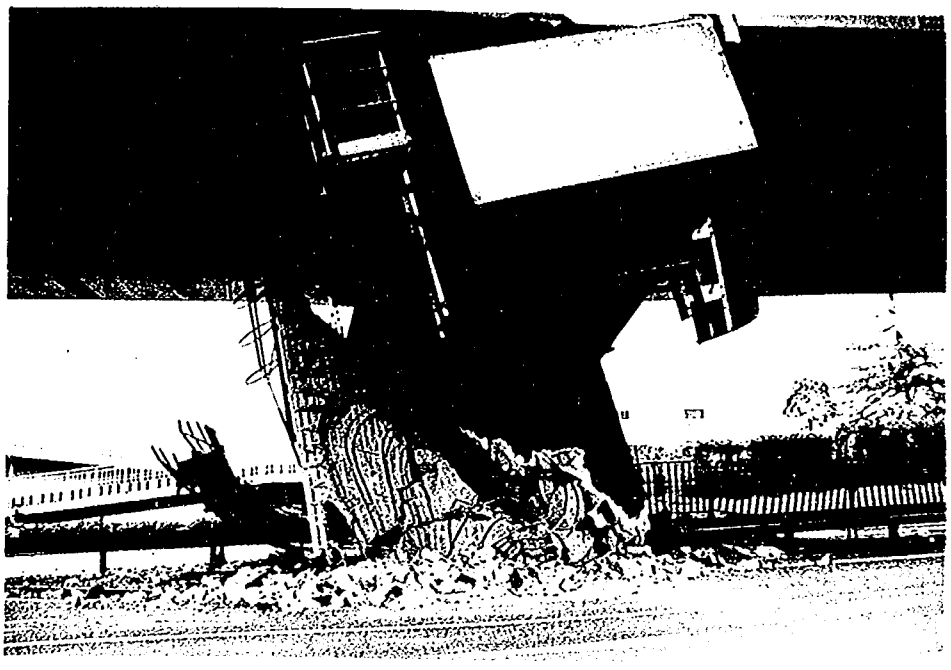


Photo 5.12 No.3 Kobe Line of the Hanshin Expressway West side of Fukae−honmachi, Failure of RC Pier



Photo 5.13 No.3 Kobe Line of the Hanshin Expressway Hatoba−cho, Damages of Bearing and Column Capitals



Photo 5.14 No.3 Kobe Line of the Hanshin Expressway Hatoba-cho, Damage of RC Pier

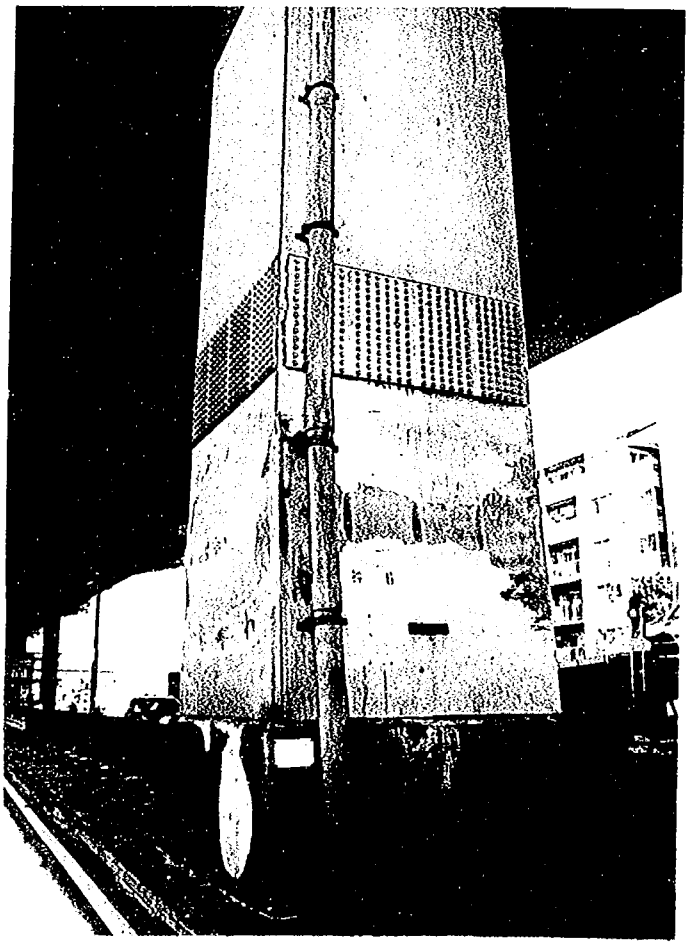


Photo 5.15 No.3 Kobe Line of the Hanshin Expressway Imazufutaba-cho, Buckling of Steel Pier

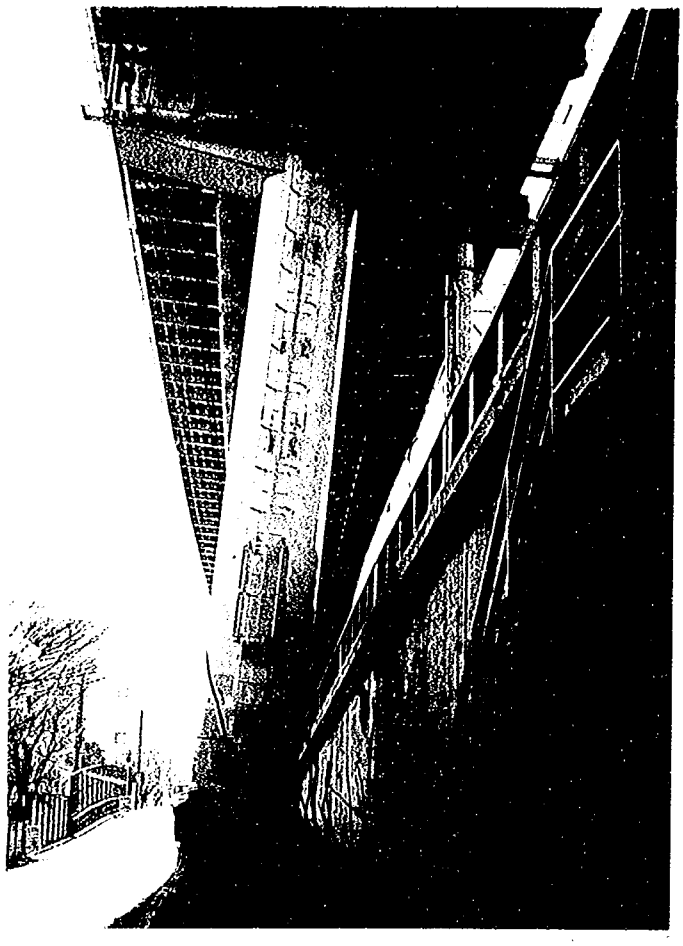


Photo 5.16 No.3 Kobe Line of the Hanshin Expressway Overpass on railway, Damage of Steel Pier

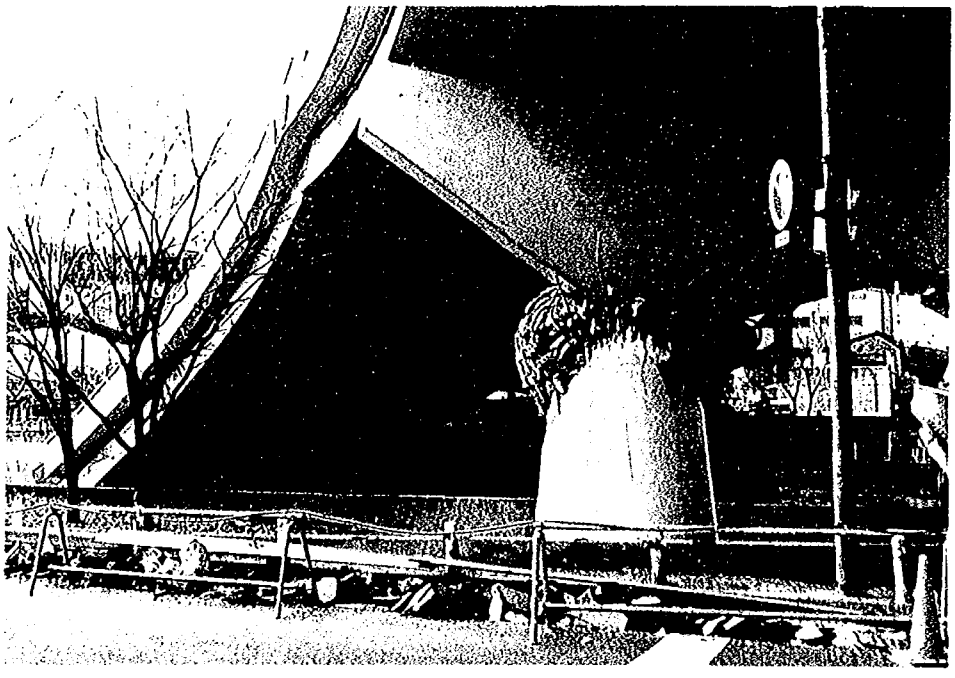


Photo 5.17 No.3 Kobe Line of the Hanshin Expressway Minatogawa Ramp, Damage of RC Pier

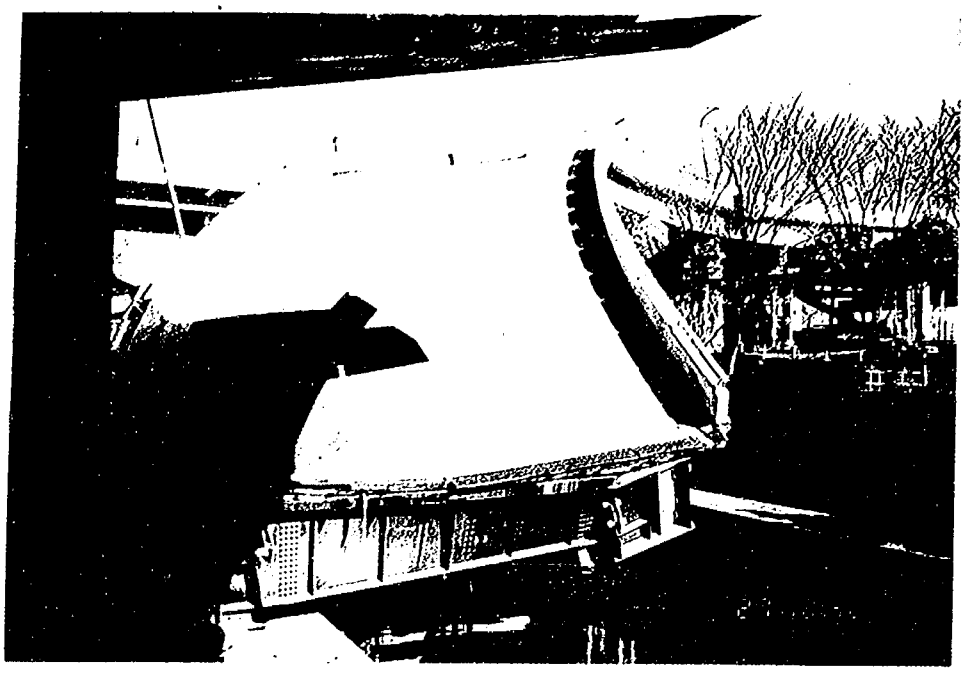


Photo 5.18 No.3 Kobe Line of the Hanshin Expressway Minatogawa Ramp, Falling of Curved Girder

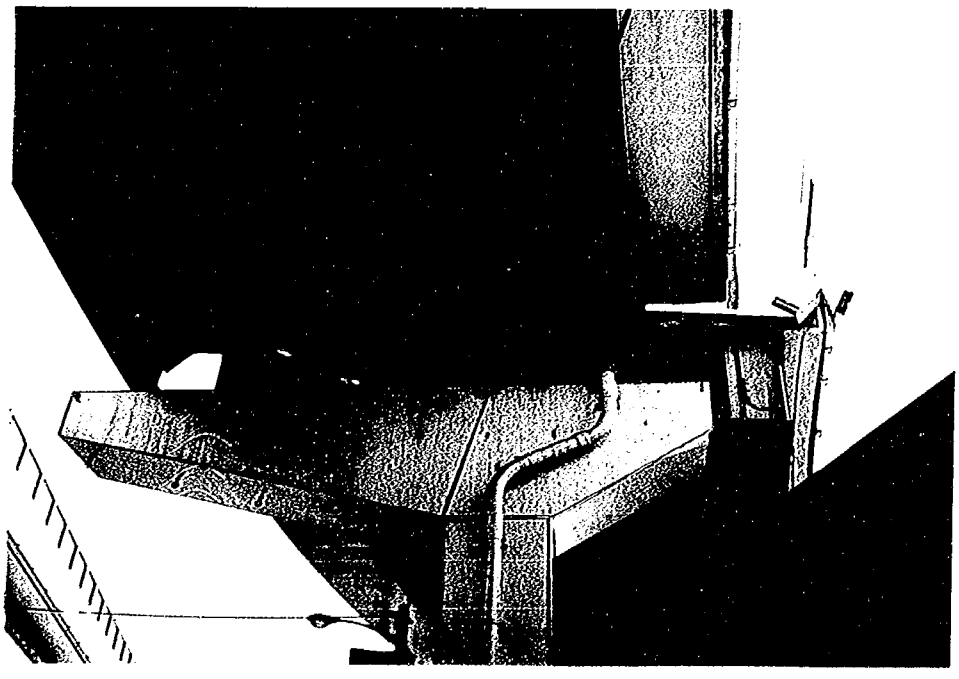


Photo 5.19 No.3 Kobe Line of the Hanshin Expressway Minatogawa Ramp, Movement of Girder

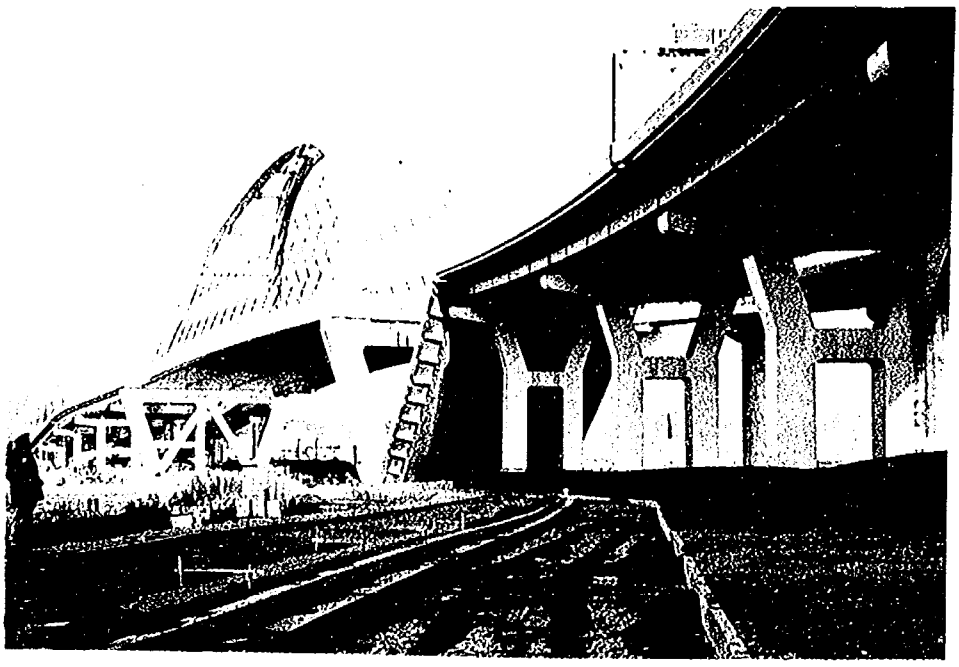


Photo 5.20 No.5 Wangan Line of the Hanshin Expressway Koshien-hama, Falling of Girder

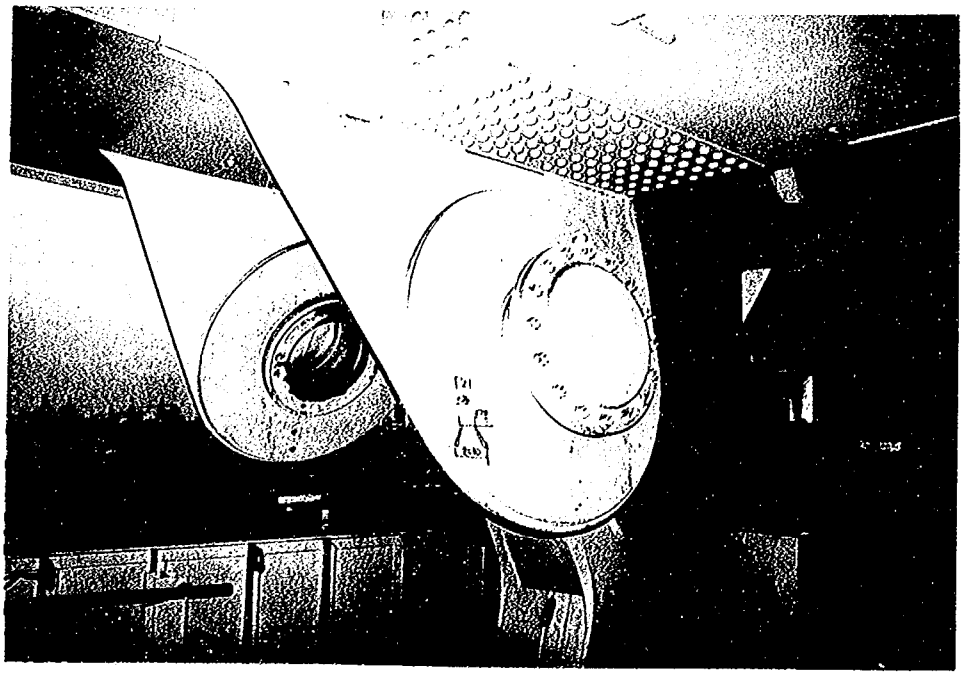


Photo 5.21 No.5 Wangan Line of the Hanshin Expressway, Higashi Kobe Bridge Damage of Pendel Type Bearing

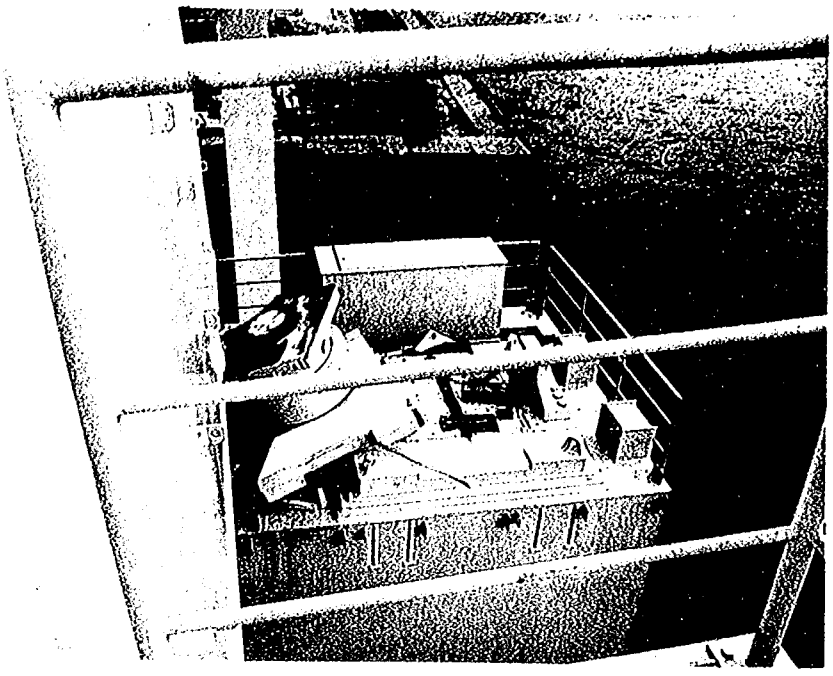


Photo 5.22 No.5 Wangan Line of the Hanshin Expressway,
Rokko Island Bridge Damage of Support Bearing

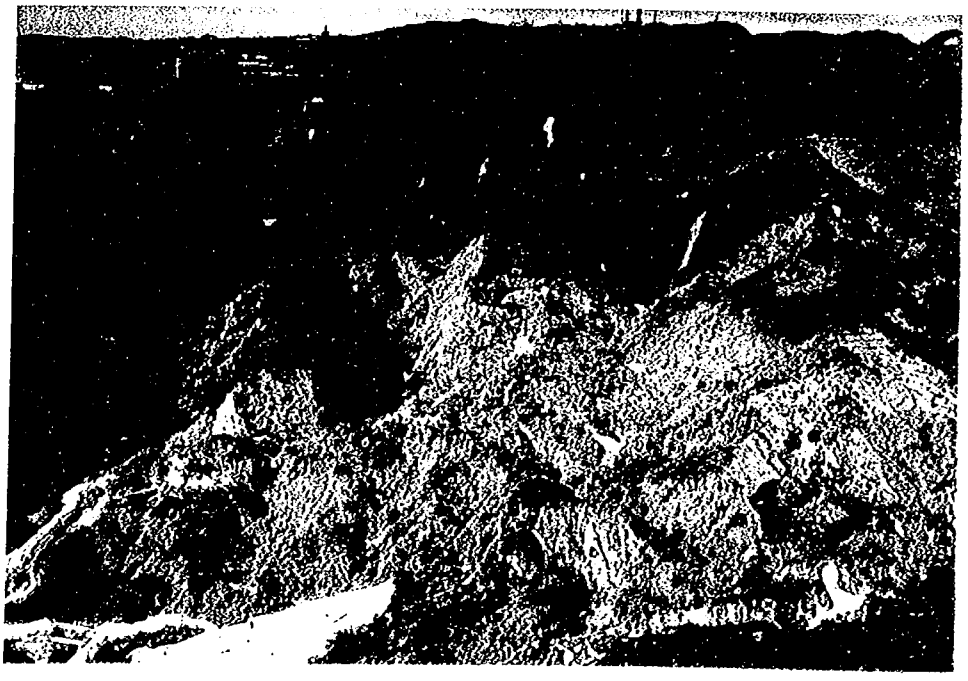


Photo 6.1 Landslides at the Middle Reach of the Sumiyoshi River.

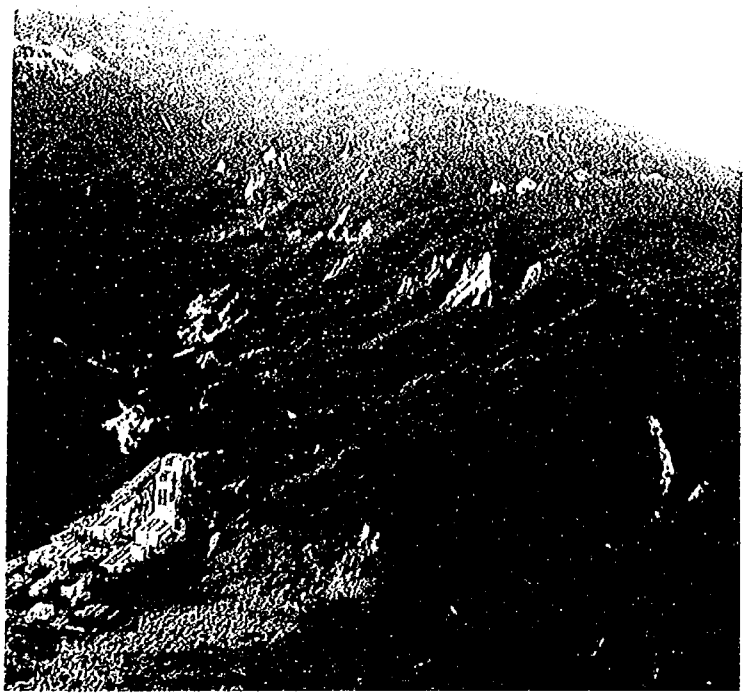


Photo 6.2 Landslides at the Upper Stream of the Sakase River



Photo 6.3 Landslides at the Ukawa River, A Tributary of the Shin−ikuta River



Photo 6.4 Landslide Located near the Channel of the Ashiya River

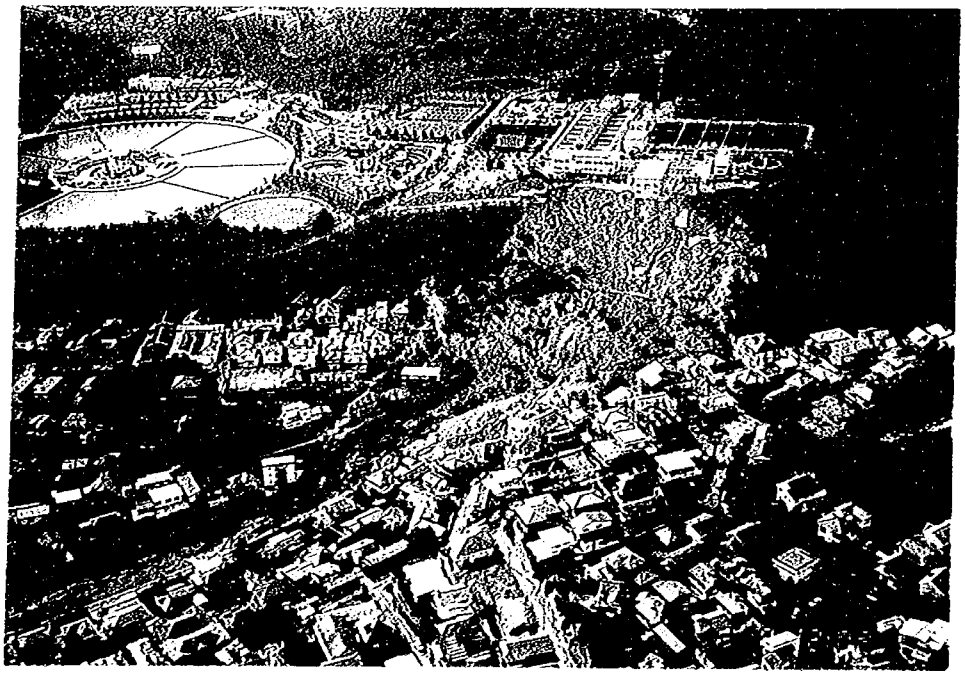


Photo 6.5 Landslide at Nikawa−yurigaoka−cho in Nishinomiya



Photo 6.6 Landslide at Nishi−okamoto Area



Photo 7.1 Torishima Dike at Yodo River



Photo 7.2 Nishijima Dike at Yodo River



Photo 7.3 Mogawa Dike



Photo 8.1 Cracking at the Left Abutment Contact of Tokiwa Dam



Photo 8.2 Sliding of the Upstream Slope of Kitayama Dam

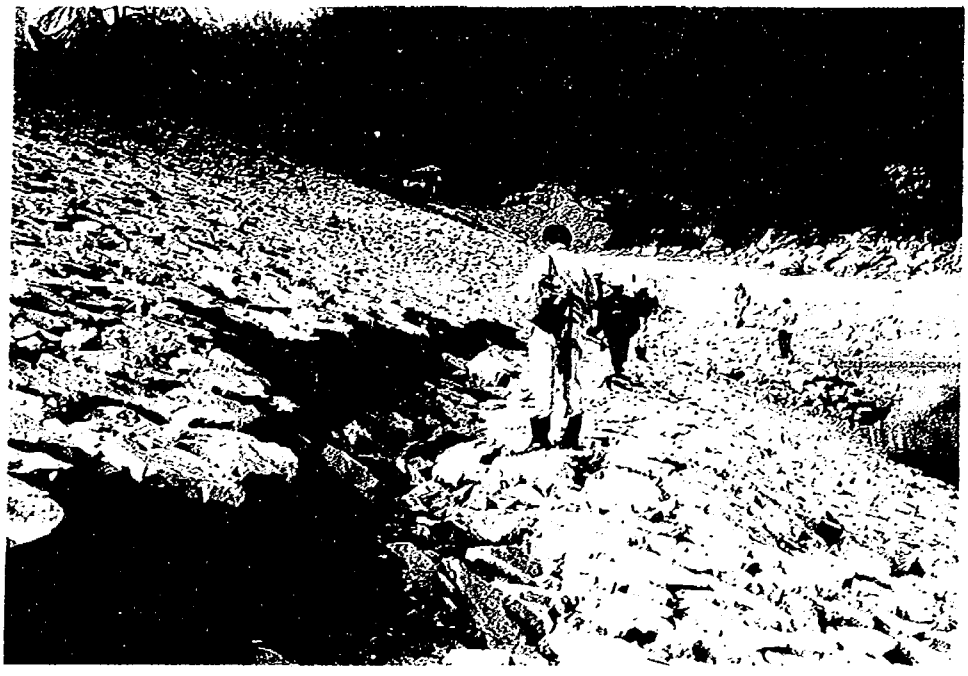


Photo 8.3 Sliding Gap of the Upstream Riprap of Kitayama Dam

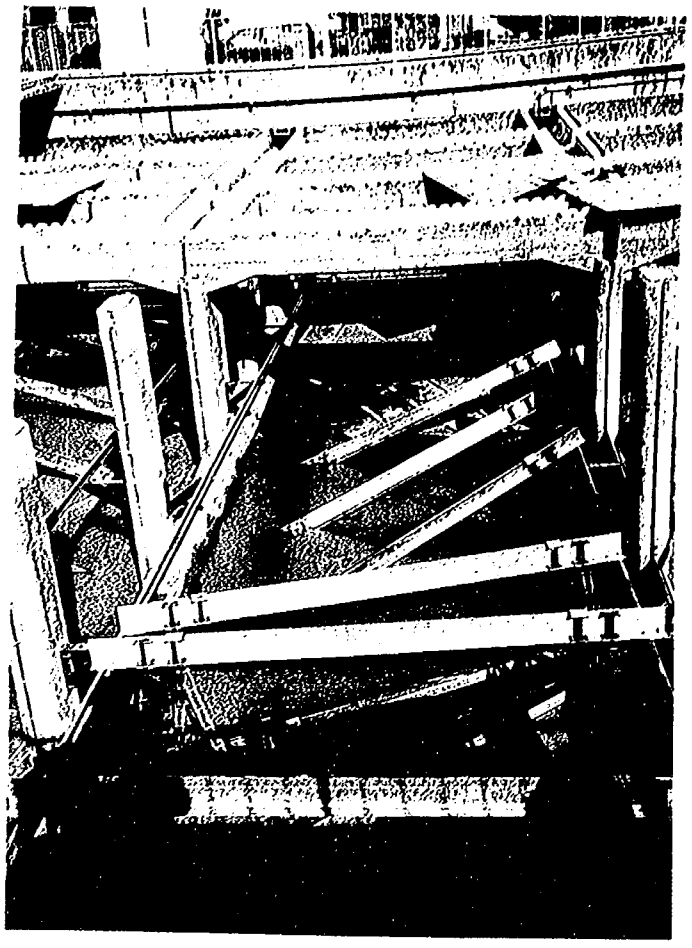


Photo 9.1 The Collapsed Sludge Collector and Straightening Plate in the Final Settling Tank (Kobe, Higashi Nada Treatment Plant)

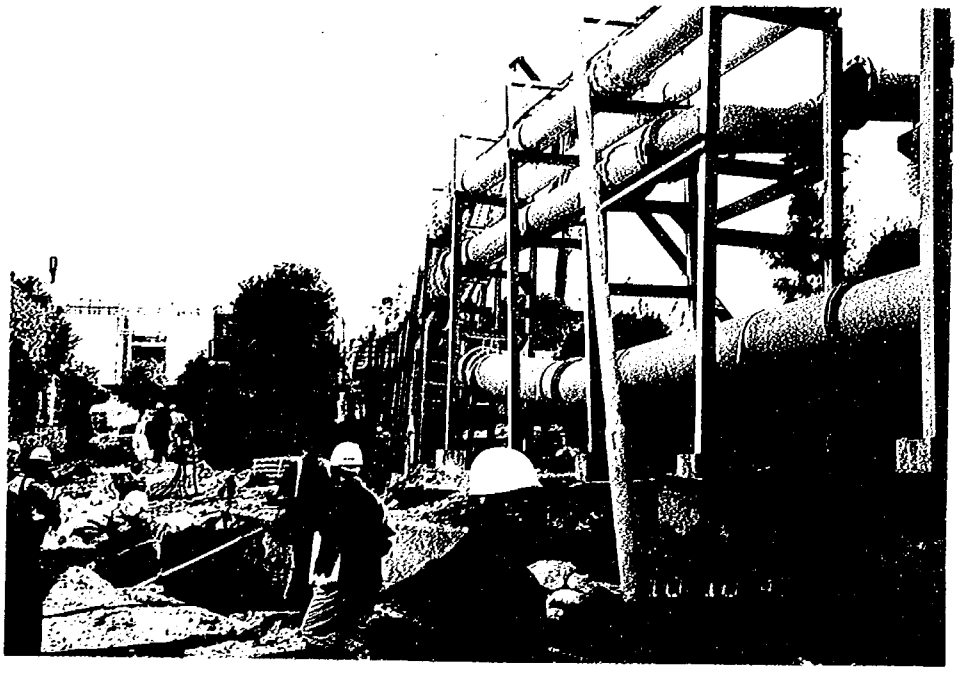


Photo 9.2 Damage to Pressure Pipes and Inflow Culvert Channel (Kobe, Higashi Nada Treatment Plant)

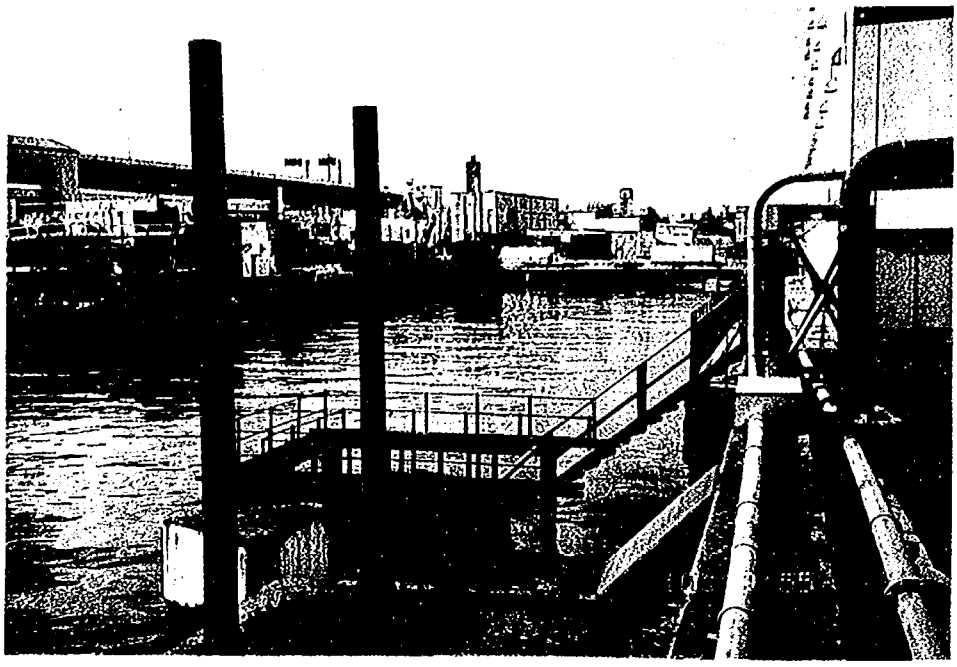


Photo 9.3 Temporary Settling Pond Provided by Blocking the Uozaki Canal with Sheet Piles (Kobe, Higashi Nada Treatment Plant)

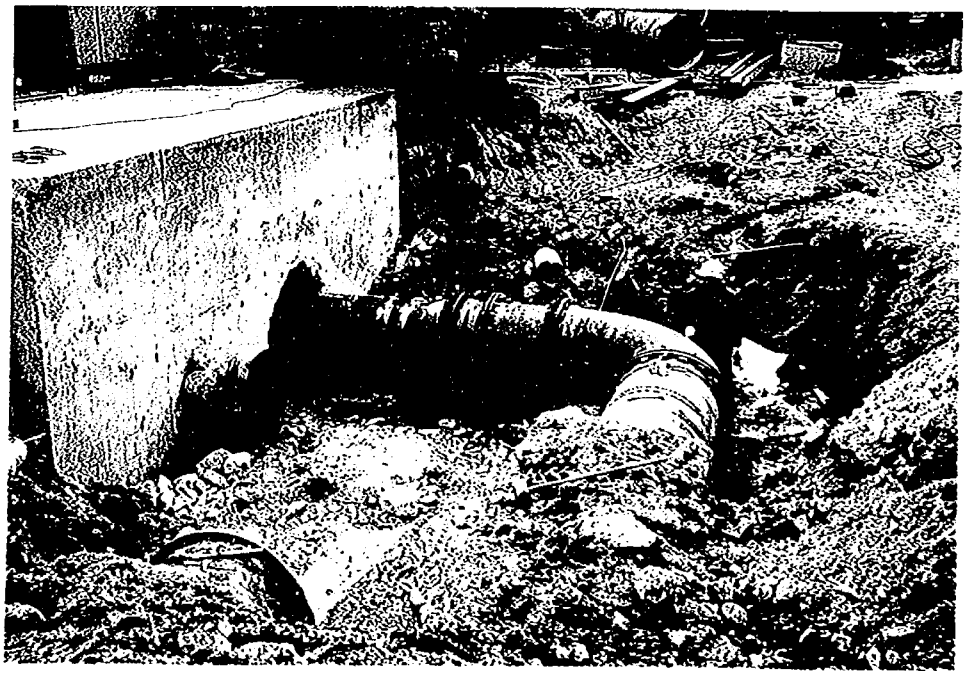


Photo 9.4 Temporary Restoration of a Broken Pressure Pipe by Connecting It with An Emergently Drilled Hole (Ashiya, Ashiya Treatment Plant)

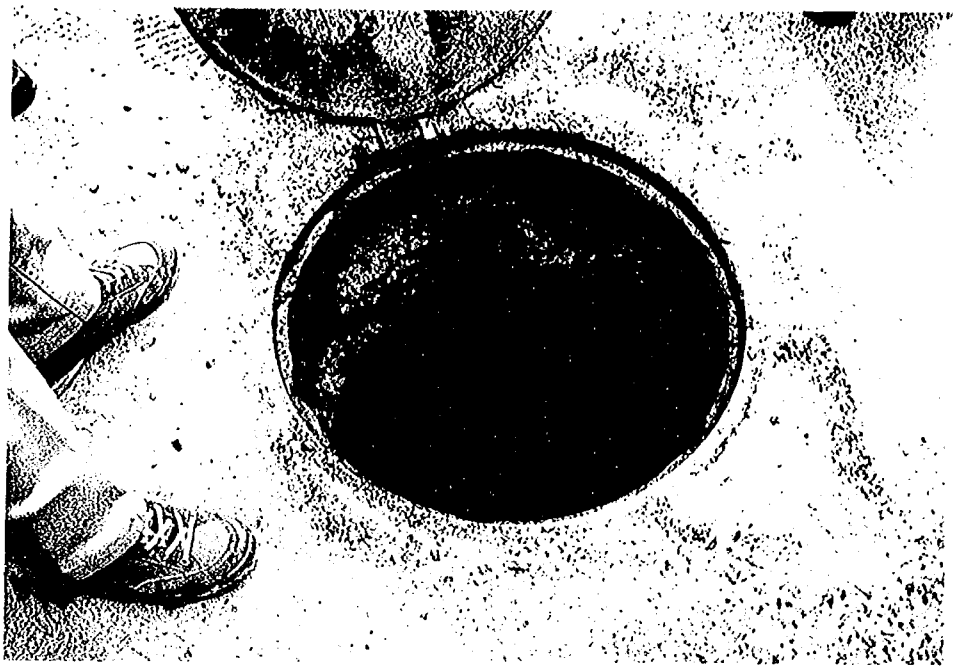


Photo 9.5 Manhole Cover and Pavement Out of Place (Kobe City)

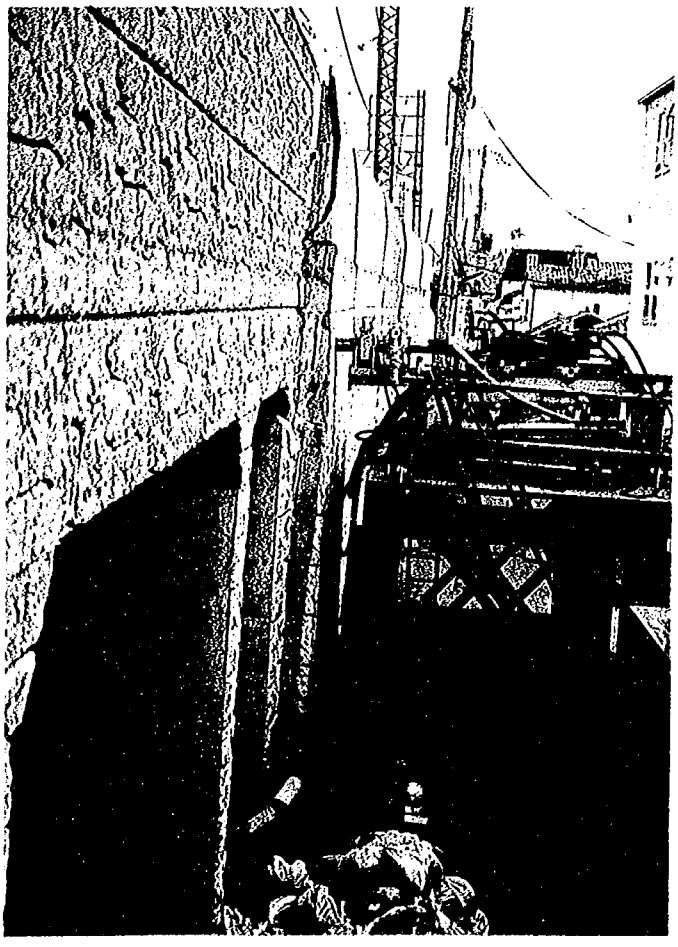


Photo 10.1 Counterforted Retaining Wall at the Ishiya River Approach on the Yamate Trunk Line

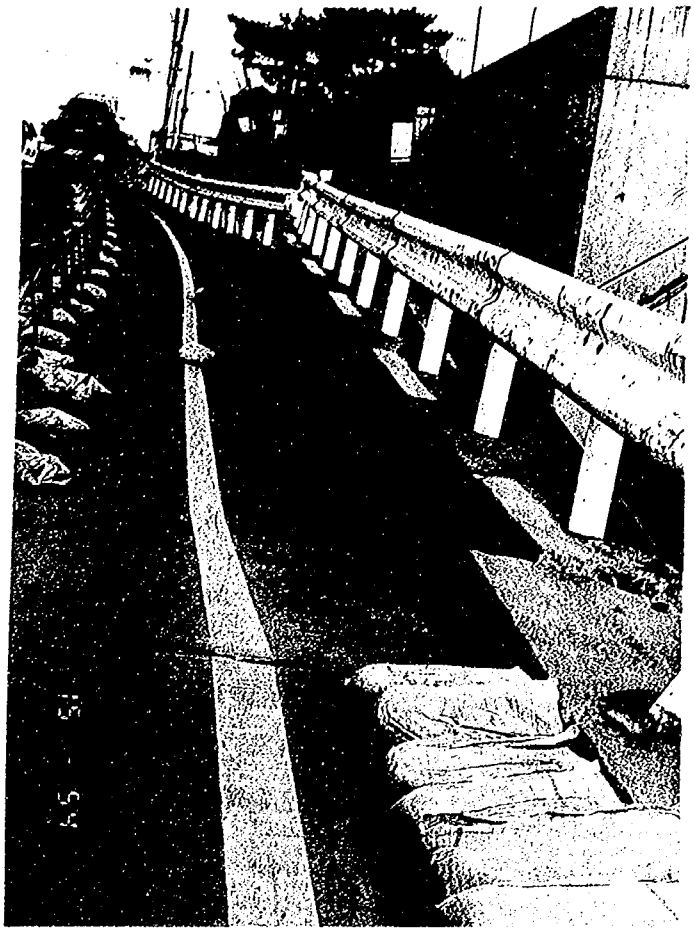


Photo 10.2 L−shaped Retaining Wall for Tokaido Line in the Fukae District, Higashi Nada Ward



Photo 11.1 Damage to Columns in the Duct West of Daikai Station on the Kobe Rapid Railway Corporation.

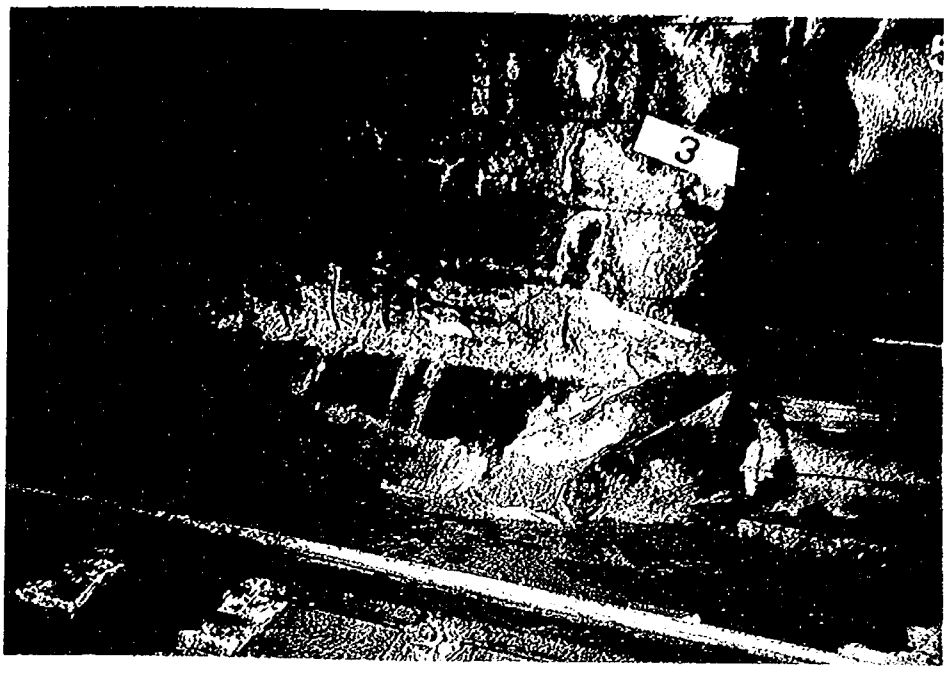


Photo 11.2 Damage to Haunches Under the Side Walls of the Duct to the West of Daikai Station on the Kobe Rapid Railway Corporation.



Photo 11.3 Damage to Columns in the Track Level (B2) of Nagata Station in the Kobe Rapid Railway Corporation.

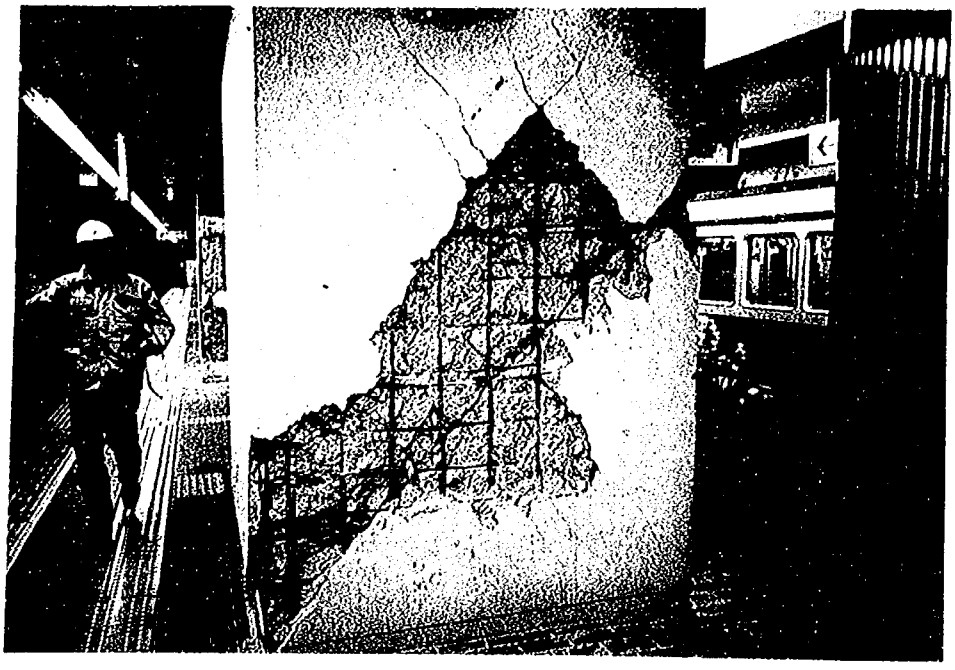


Photo 11.4 Damage to Columns in the Track Level (B2) of Shinnagata Station in the Kobe Municipal Subway

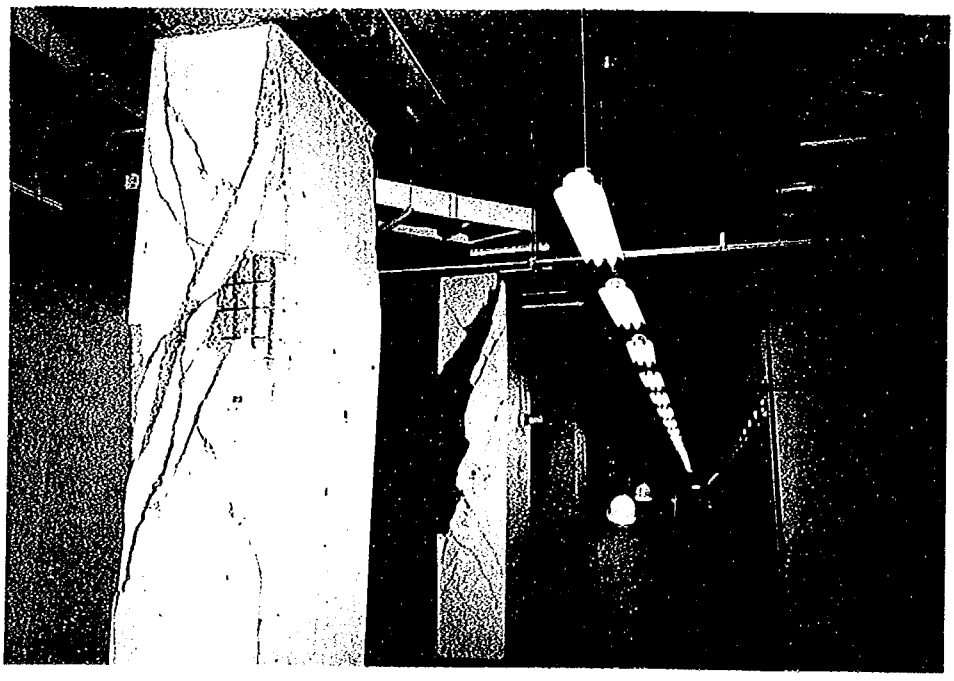


Photo 11.5 Damage to Columns in the Electric Room (B1) of Kamisawa Station in the Kobe Municipal Subway

DAMAGES OF BUILDINGS CAUSED BY THE 1995 HYOGOKEN NANBU EARTHQUAKE

by

Hisahiro Hiraishi [1], Toshibumi Fukuta [2] and Motoi Yasumura [3]

ABSTRACT

An unprecedented numbers of buildings were severely damaged due to the 1995 Hyogoken Nanbu Earthquake, and some of them completely collapsed. This paper describes the outlines of damages to reinforced concrete buildings, steel buildings and wooden buildings. The paper also discusses the major factors of typical damages based on damage investigation and their analysis.

Key Words:
Hyogoken Nanbu Earthquake,
Damage,
Reinforced concrete buildings
Steel buildings,
Wooden buildings

1. DAMAGE OF REINFORCED CONCRETE BUILDINGS

1.1 Outlines of Damages

Reinforced concrete buildings are identified into three groups depending on construction year. First group is the buildings designed in accordance with the older code before 1971. Second group is those in accordance with the former code which were revised at 1971 after great lesson of the severe damage of reinforced concrete buildings due to the 1968 Tokachi-oki earthquake. In this revision, shear design requirement was drastically reinforced so that beams and columns would yield in flexure prior to shear failure, or their allowable shear strength would be about twice that required in the older code. The last group is designed in accordance with the current building code, revised at 1981, in which the ultimate strength of the structure and member ductilities are considered as well as allowable stress design. The damages to buildings belonging to the first group are very severe, and those belonging to the second group are slight. Only some particular structures suffered damage in the buildings belonging to the third group.

The typical damages of reinforced concrete buildings are as follows.

i) Shear failure of columns and shear walls at the first story of low-rise buildings(see Photo.1.1).
Insufficient ultimate shear strength of the first story where the largest shear capacity was required mainly caused this damage.

ii) Torsional failure due to eccentricities of stiffness and mass(see Photo.1.2).

---

1)Associate Director for Composite Structures Research in Structural Engineering Department at Building Research Institute(BRI),Ministry of Construction
2)Head of Large Scale Structure Testing Division at Building Research Institute(BRI),Ministry of Construction
3)Senior Research Officer at Building Research Institute (BRI), Ministry of Construction

This type of failure was typically found in the buildings locating at a corner of streets. Torsional response was arisen because of unbalanced existence of walls.

iii) Shear failure of short columns

Spandrel walls caused this type of brittle failure of columns, which was prominent in the past earthquake damages.

iv) Failure of piloti of the soft first story

v) Collapse of middle story

These two types of damages were discussed in Chapter 1.

vi) Failure of steel-encased reinforced concrete buildings

Tensile fracture of splices of steel plate of the boundary columns of shear walls were observed in steel-encased reinforced concrete buildings(see Photos.1.3 and 1.4). Fracture and buckling of reinforcing steel bars due to pulling out of anchorage bolts of steel base plate was also observed in many medium high-rise buildings.

vii) Others

Damage to beam-column joints, failure of gas-pressure welded splices, damage of non-structural element, shear failure of columns due to collision, etc. which were reported in past earthquake damage were also observed.

1.2 Major Causes of Typical Damages

Two types of destructive damage patterns which might have caused mass loss of human lives were discussed in some detail.

(1) Collapse of middle story

This damage was typically found in the medium high-rise buildings designed by the older code before 1971. Complete collapse of a certain story occurred due to failure of columns(see Photo.1.5). It is possibly considered from the damage inspection that these columns failed in flexure at both ends. If the design shear coefficient is small value as defined in the older code before 1971, amount of longitudinal reinforcement in columns is usually determined by not design shear but minimum requirement of 0.8%. This value of 0.8% of longitudinal reinforcement nearly corresponds to 0.3% of ratio(pt) of longitudinal tensile reinforcement. Based on this assumption, Figure 1.1 shows results of a case study regarding to story shear coefficient of restoring ultimate strength of office buildings designed by older code before 1971. As seen in Fig. 1.1, at both upper and lower stories, minimum longitudinal reinforcement is enough to satisfy current minimum requirement of ultimate strength which is defined mainly based on dynamic behavior of buildings. However at middle stories, strength is not sufficient, and this shortage of strength is more distinctive if pt is increased at lower stories. Moreover, in the Hyogoken Nanbu Earthquake up-down motion might have decreased the axial compression force in columns which gives columns flexural strength corresponding to story shear coefficient of 0.2 to 0.3.

(2) Failure of piloti of the soft first story.

Many residential apartment buildings had reinforced concrete piloti at the first story for open retail space or parking space. These buildings terribly suffered severe damage because of complete collapse of piloti(see Photos.1.6 and 1.7), and some of them felled down. The damage classified as severe or collapse for buildings designed by current design code is mostly this type of failure. In such buildings having the soft first story, most of energy were dissipated in the reinforced concrete piloti of the first story. The lateral reinforcing arrangement which assures the ductile manner to those columns shall be emphasized. However, forces (flexure, shear and axial forces) acting on these columns remarkably change during the earthquake response. It is

recommendable for shear design of these columns to consider the maximum flexural strength at the balanced failure, at both column ends.

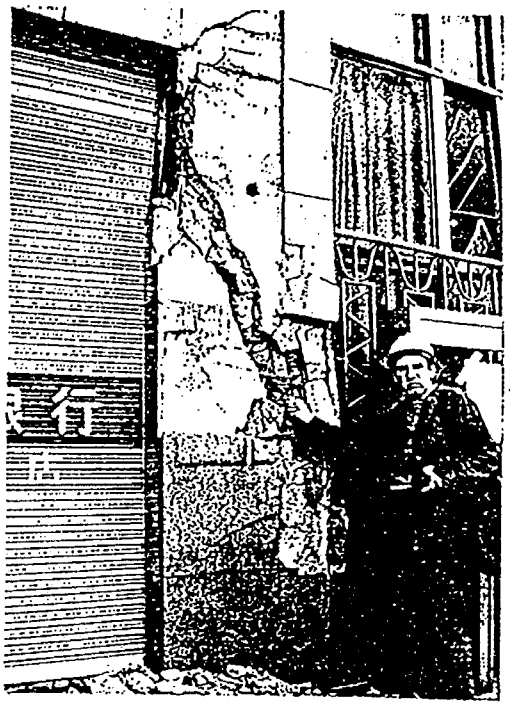


Photo.1.1 Shear failure of column



Photo.1.3 Jointed steel in SRC Column (Fracture of longitudinal bars and the joint plate)



Photo.1.2 Torsional failure due to eccentricities of stiffness and mass



Photo.1.4 Damaged shear wall due to fracture shown in Photo.1.3



Photo. 1.5 Complete collapse of middle story

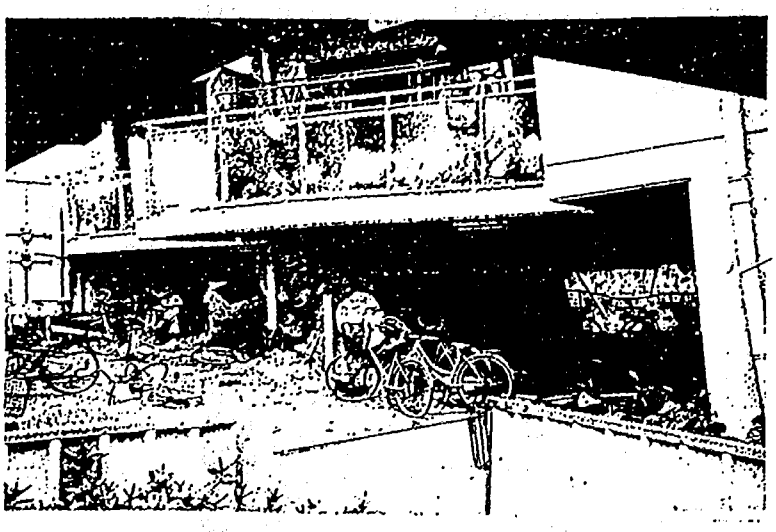


Photo. 1.7 Collapsed first story pilotis

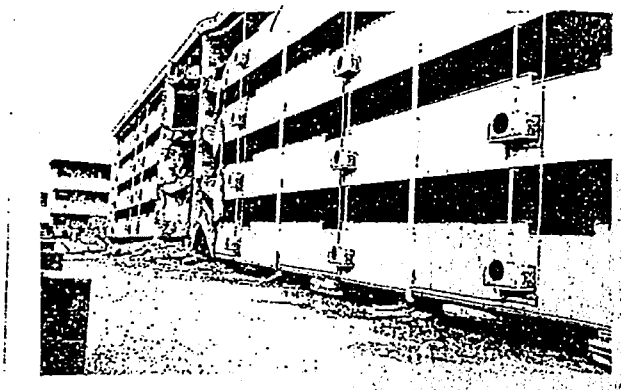


Photo. 1.6 Complete collapse of an apartment house due to failure of piloties of the first story

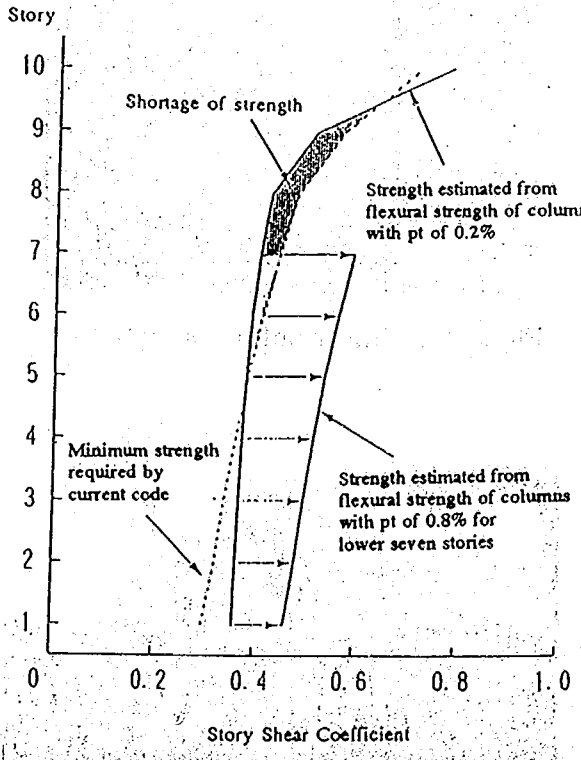


Fig. 1.1 Estimated strength of damaged buildings and minimum strength required by concrete code.
(note: pt is the ratio of gross sectional area of longitudinal tension steel bars to a gross sectironal area of column.)

2. DAMAGES OF STEEL BUILDINGS

2.1 Outlines of Damages

The damages of steel buildings in Kobe city are identified into some patterns. Some of the damages are the same ones as observed in the past earthquakes, such as the buckling or yielding of tension braces, yielding of beams or columns, the collapse of concrete around the base plate of columns, and the fracture of finishing and glasses.

As recorded in seismic observation stations, the intensity of the ground motion during the earthquake was very strong not only in the two horizontal directions but also in the vertical one. The damages described below are the first experiences which have had in the building structures constructed by the modern seismic design process.

(1) Damage of columns with square box

Some buildings which were designed and constructed under the new seismic building standard law, revised in 1981, were damaged in their bases of first story columns, beam-to-column joints and so on. Their columns have square box sections formed in the cold form process, and are welded to the beam-to-column joint at its diaphragm plates. As shown in Photo. 2.1, the welding were completely fractured while the ends of beams and columns did not yield. Therefore the response of the structure was supposed to be brittle under the quake.

Many of these buildings which were damaged in the first story had pin joints of columns with the base plate and anchor bolts. In each joint, a column was fixed to the reinforced concrete foundations by 4 bolts with small size of diameter. These bolts were pulled and elongated, and were cut in the worst case so that the entire structure fell down. The structure in Photo. 2.2 has 4 columns in a story and fell down because of the fracture of the anchor bolts in the tension side columns. The main damages of the building shown in Photo. 2.3 were slipping out of anchor bolts and crack and crush of concrete around the base plate. The slipping out of the bolts from the concrete reached to about 10 cm.

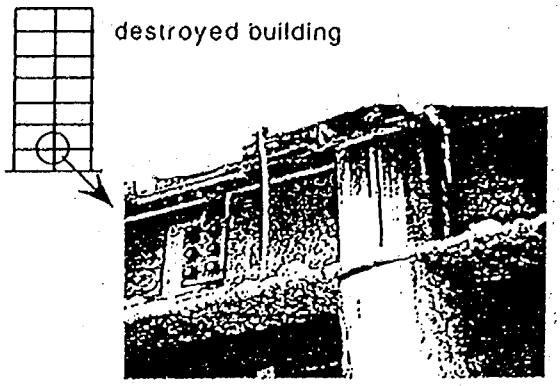


Photo 2.1 Fracture of welding at beam-to-column connections

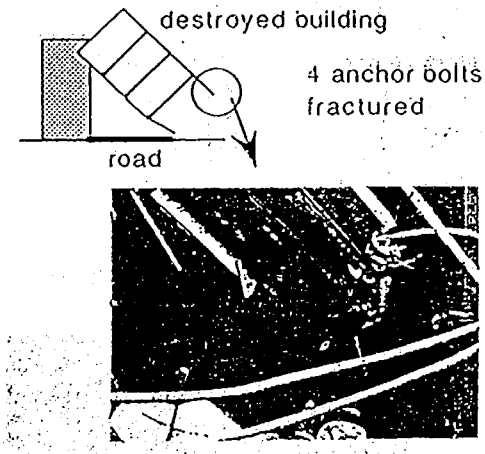


Photo 2.2 Collapse of base & destroyed structure



Photo 2.3 Elongation of anchor bolts and crush of concrete

(2) Damage of mega-structure building

A few high-rise buildings were also damaged in their mega-structures. These buildings are apartment houses located at the seashore. As schematically drawn in Fig. 2.1, residential units with two to six stories made from reinforced concrete walls are supported by the steel main structure. The vertical members in the mega-structure were fractured in tension (Photo 2.4-a). The section height of the member is 50 cm (Ref. 2-1). The fracture surfaces were brittle. But the structures are still standing with almost no inclination. At present, the fractured members of structures have been retrofitted by welding thick stiffeners (Photo 2.4-b).

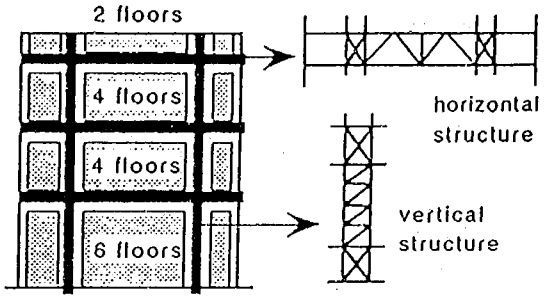
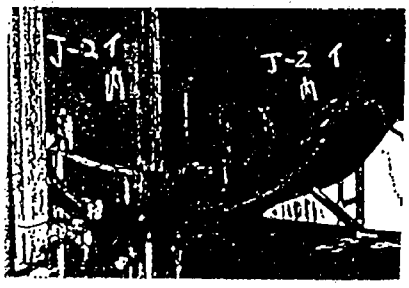


Fig. 2.1 Schematic front view of one of the structures

a) fracture



b) retrofit

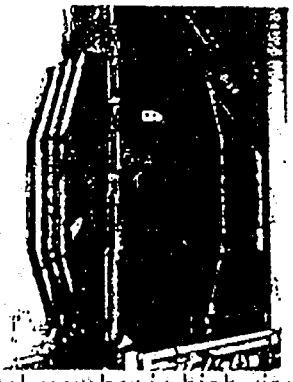


Photo 2.4 Vertical member in high-rise apartment house

(3) Damage of old low-rise buildings

Old steel buildings were severely damaged, some of them were completely collapsed in the first story. They are two to five story structures with small size of H-shapes or channels for columns and beams. The plate elements of these sections are thin. The lower stories of these buildings are used for shops and small restaurants, and the upper stories are for residential use. Therefore the wide openings are required in the both directions for show windows and entrances. The main structure of these buildings are moment resisting frames without any effective bracing or walls. Further more, the members were heavily rusted. The structure in Photo. 2.5 swayed in the first and the second stories. The columns have lost their sectional area because of rust, and buckled in flexure and torsion.

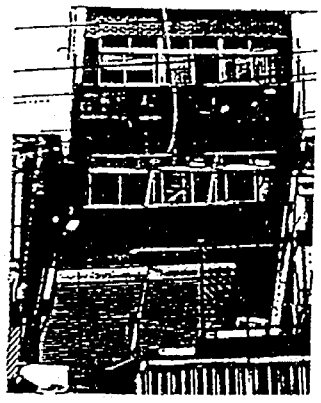


Photo 2.5 Collapse of old low story building with small members

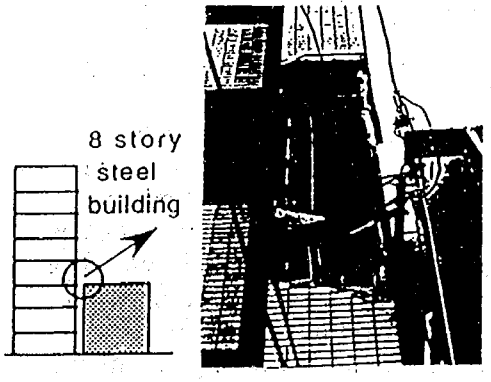


Photo 2.6 Collision

(4) Collision of buildings

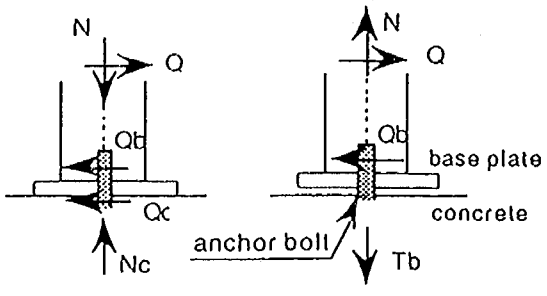
In Photo. 2.6 , the eight story building collided with a low-rise building at the right hand side. The finishing of steel box columns was damaged and fell down partially. In the urban areas, the distance between buildings is very small because of lack of a land space and its extremely high cost.

2.2 Major Causes of Typical Damages

(1) Collapse at base of box columns

There are three types of bases of steel columns: pinned base, basement covered with reinforced concrete, and basement with columns inserted into reinforced concrete foundations. The first one is designed against shear force and axial force. A part of the shear force can be carried by the friction between the steel base plate and concrete. The rest of the lateral shear is transmitted by anchor bolts. When the big tension force in the column is induced by the lateral story shear force and over turning moment, all the lateral shear force apply to the anchor bolts.

In Fig. 2.2 , N and Q are axial force and lateral shear force in the column, respectively. Qb is shear force carried by the anchor bolt. Qc is friction between concrete and base plate. Nc is reaction force of the concrete and Tb is applied by the anchor bolt.



[Q=Qb+Qc, N=Nc] [Q=Qb, N=Tb]

a) N in compression b) N in tension

Fig. 2.2 Stress in pin base of column

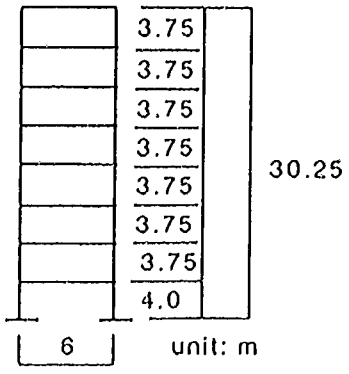


Fig. 2.3 A model Steel Structure

A model steel building with one span and 8 stories as shown in Fig. 2.3 was analyzed by T. Hasegawa in BRI (Ref. 2-2). The input ground motion is the recorded data at Kobe meteorological observatory, its maximum acceleration is 818 gals (recorded by JMA 87 type strong motion seismograph). This type of structures has been constructed in urban areas such as Kobe city, where the land space is narrow but a wide opening at the front side of the building is required by the owner. The structure has only one span along the road, and a few spans in the transverse direction. The building has only a few columns in a story, and the collapse of the base in the tension side columns such as rupture of anchor bolts directly causes the entire structure to fall down.

The maximum response axial forces in the first story column were 24.2 % of yield axial force (Ny) in tension and 53.5 % of Ny in compression. In the analysis, the bases of the columns are assumed to be fixed and maintain a resisting strength even after the yielding of bases. The design axial forces of the columns in the first story are 3.4 % of Ny in tension and 33.1 % of Ny in compression under the seismic loading. The analytical responses of axial forces in the columns are extremely bigger than the design values. Therefore some of this type of buildings collapsed in their bases; yielding, elongating or cutting of anchor bolts, and crack and/or crush of base concrete.

(2) Fracture of beam-to-column joints

Some of the beam-to-column joints in the structures, which had a moment resisting frame with square box columns, were cut at the face of the joints. As schematically shown in Fig. 2.4, the joint panel with a square box is covered with diaphragms by welding, and columns and beams are welded to these diaphragms. The panel zone is a square box with the same dimensions as columns.

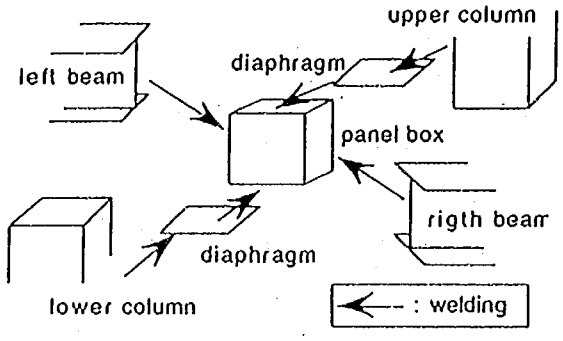


Fig. 2.4 Beam-to-column joint

Many of the fractured connections which were investigated in the extremely damaged area in Kobe city were welded by the fillet welding with small throat depth. The welded sections in the joints did not have sufficient strength, so the columns and/or beams did not behave ductilely.

The present seismic code requires the joints to have enough strength so that the frame would deform well in the post yielding. The design criteria of the joints is

$$Mcr > or = 1.3\ Mp \qquad (2.1)$$

where, Mcr is the maximum bending moment at the welded section of the joint, calculating on the bases of the specified tensile strength of the material, and Mp is the full plastic moment of the column connected to the joint. For example, a member with Box-250x250x8 is used. The minimum size of fillet welding at the joint which satisfies the above mentioned design criteria is 15 mm, i.e., 1.87 times the thickness of the column. The size of the fillet welding used in the fractured connections was far less than the required minimum value. The groove joint is recommended as the welding at the beam-to-column joints in the design code.

(3) Collapse of old low-rise buildings

Many of old low-rise steel buildings were heavily damaged as shown in Photo. 2.5. The structure is one span in X-direction and a several spans in Y-direction. The column is H-shapes with the height of 200 mm and the width of 100 mm, the beam is a small truss constructed with channels of chord members and round bars of web members. The beams and columns are connected by welding or bolts with gusset plates in poor details. In some cases, concrete masonry walls are used as partitions of the housing units in the plane of a moment resisting frame. The weight of the structure is relatively big. This type of the structures was collapsed because of the lack of ultimate strength.

References in Chapter 2

2-1) "Prime Plan in the Competition of the Ashiyahama High-rise Apartment Houses using the Industrialized Construction Technique ASTM", Quarterly Column No. 50 & 51, The Kouzai-Kurabu

2-2) Takashi Hasegawa, et al. "Earthquake Response of Rigid Frames with RHS Columns (Part 7. Earthquake Response against The Hyogoken-nanbu Earthquake)", Annual Meeting of AIJ in 1995 (submitted)

3. DAMAGES OF WOODEN BUILDINGS

3.1 Outlines of Damages

A large number of wooden buildings were collapsed or heavily damaged by this earthquake. Most of these buildings were the dwellings of one or two storey to which the structural calculation was not required. The degree and state of the damages depend on the kinds and the construction method.

Photo. 3.1 shows a typical example of the damaged wooden houses in Nagata district. Whole the building was collapsed completely. This type of damage occurred mainly in old wooden houses constructed before or just after the World War II. Photos. 3.2 to 3.4 show the damages of wooden buildings whose first storey was collapsed. This damage took place generally in wooden houses constructed of the clay wall and heavy tail roof with clay pad, however some newly constructed wooden houses were also collapsed as shown in Photo.3.4. Having a garage in the first floor, this building did not have the sufficient shear walls, but also the shear walls were placed eccentrically. Photos. 3.5 and 3.6 show the damages of the comparatively new wooden houses having a garage of reinforced concrete in first floor. The first level of wooden structure was completely collapse.

Photo. 3.7 shows the damages of a house whose first floor was a shop. This type of buildings have generally a large space in the first floor, and the disposition of the shear walls is eccentric. A number of buildings of this type were heavily damaged. Photos. 3.8 and 3.9 show the damages of the dwellings whose front width was very narrow. This type of buildings have generally very few or no shear walls in front of the building. A number of dwellings of this type were also damaged.

Photo. 3.10 shows the damages of the exterior mortar. The lath-mortar has been used for the exterior in urban area since roughly 40 years ago because of the fire problem. In many houses, the exterior mortar was peeled off because of an inadequate connection between the lath-mortar and sheathing.

Photo. 3.11 shows a non-damaged three-storey house of conventional wooden post and beam structure. These buildings designed by the structural calculation showed in general very few or no damages even in severe earthquake area.

Photo. 3.12 shows the example of the damages of the foundation of wooden building. Although the damages of foundation in wooden building by this earthquake were comparatively small, the foundation of unreinforced concrete was damaged in some wooden buildings.

3.2 Major Causes of Typical Damages

The majority of the collapsed wooden buildings were old houses of post and beam construction consisted of the clay walls and heavy tiled roof with the clay pad. These buildings having no diagonal braces, or very few if any, had comparatively long natural period and insufficient lateral resistance to support the mass of the building. The insufficient reinforcement of the traditional tenon-type joints with steel plats, bolts, etc. is also one of the causes of the collapse. In some old houses, the length of the tenon was not sufficient but also the members were not connected in adequate way.

Some wooden buildings constructed recently were also collapsed or heavily damaged. Most of them were conventional post and beam construction having large openings in the first story. This design appears often in the dwellings whose front width is extremely narrow or those whose first floor is a shop. As the shear stiffness of the floor diaphragm of conventional

construction is generally low, a large horizontal displacement occurs at the front of the building which has very few or no shear walls.

The inadequate application of the diagonal braces is also one of the causes of the damage of wooden buildings. In most cases, braces were connected to the post and horizontal members such as a girder and a sill with only few nails, and the posts and the horizontal members themselves were not connected in an adequate way. These braces do not work sufficiently not only as tension member but also as compressive member.

The second storey of some wooden buildings having a garage of reinforced concrete in the first storey were heavily damaged. It is supposed that the first level of the wooden structure was shaken excessively because of the difference of mass and stiffness between the reinforced concrete and the wooden structure, however further study should be done to verify this fact.

Generally speaking, wooden buildings constructed with the North American Wood Frame Construction Method, Prefabricated panel structure, three storey wooden buildings designed by the structural calculation and well designed conventional wooden post and beam buildings resisted well against the earthquake.

4. CONCLUSIONS

Most reinforced concrete buildings and steel buildings which suffered severed damage were designed in accordance with code before 1981. However some paticular members and buildings such as reinforced concrete piloti and ancharage of steel plate were severely damaged although they were designed by current building code. The damage of wooden buildings depended on structural type. Old houses by Japanese traditional structural system suffered severe damage.



Photo.3.1 Collapse of wooden buildings



Photo.3.2 Collapse of the first storey

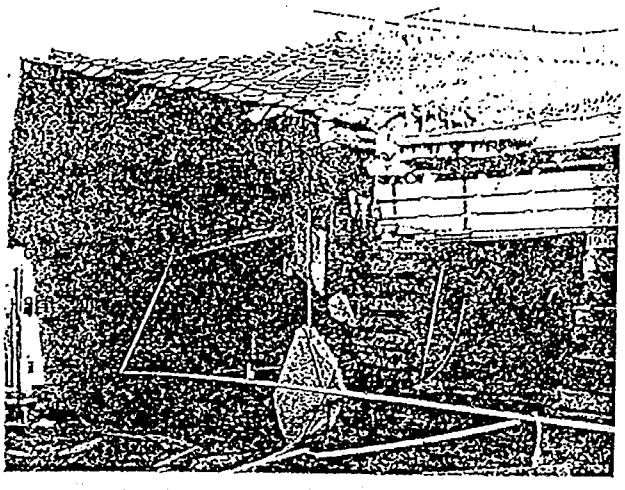


Photo.3.3 Collapse of the first storey



Photo.3.4 Collapse of the first storey

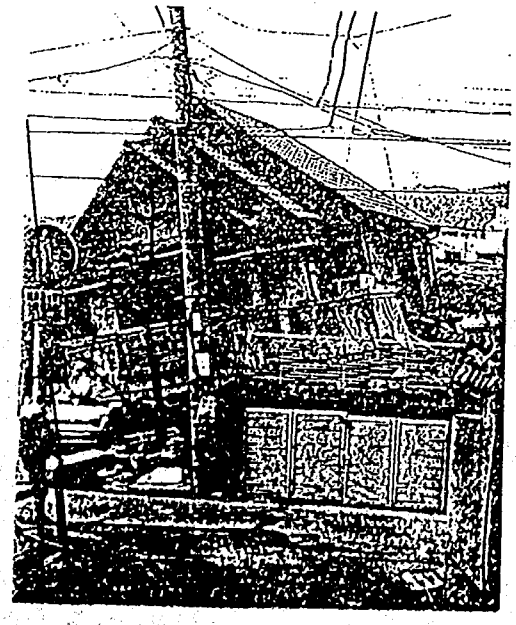


Photo 3.5 Collapse of the second storey
(the first storey in a garage of RC)

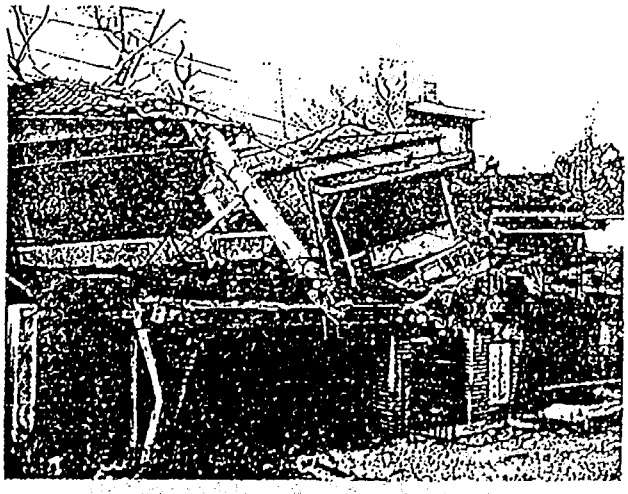


Photo 3.6 Collapse of the second storey
(the first storey in a garage of RC)

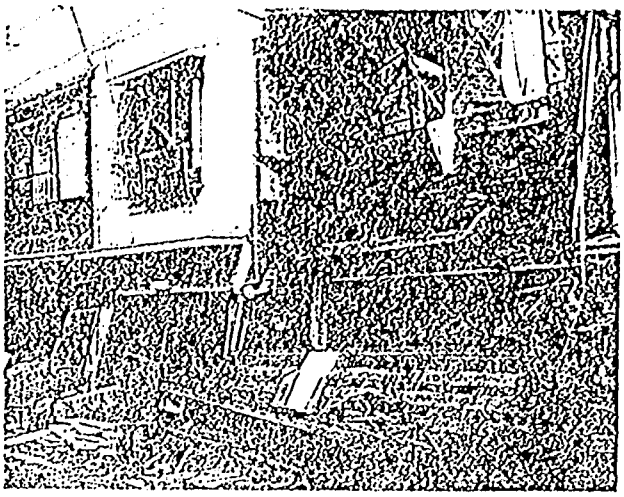


Photo 3.7 Building with large opening



Photo 3.8 Wooden building with a small width

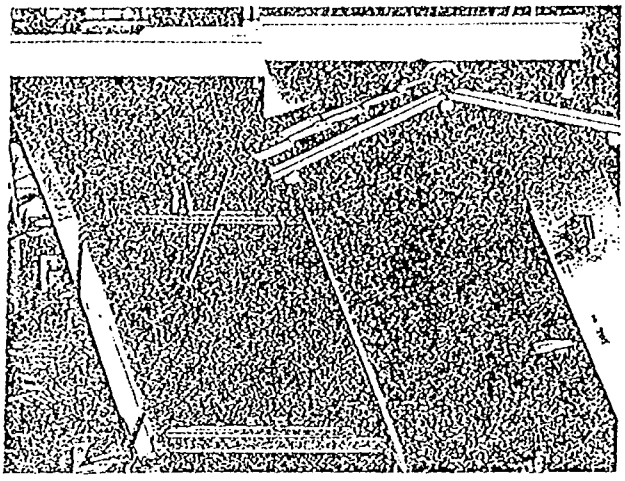


Photo3.9 Wooden building with few shear walls

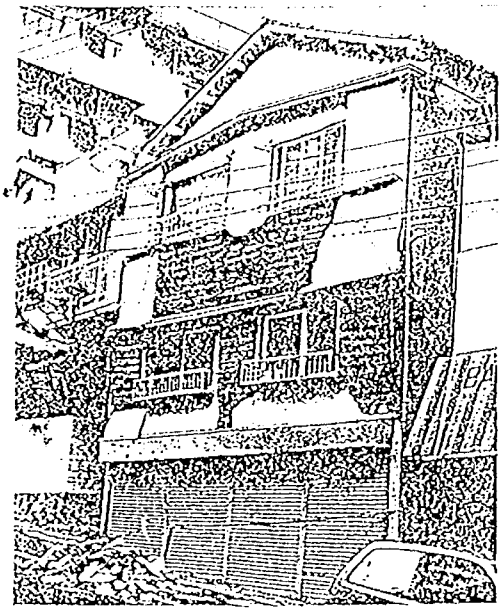


Photo 3.10 Damage of the exterior lath-mortar

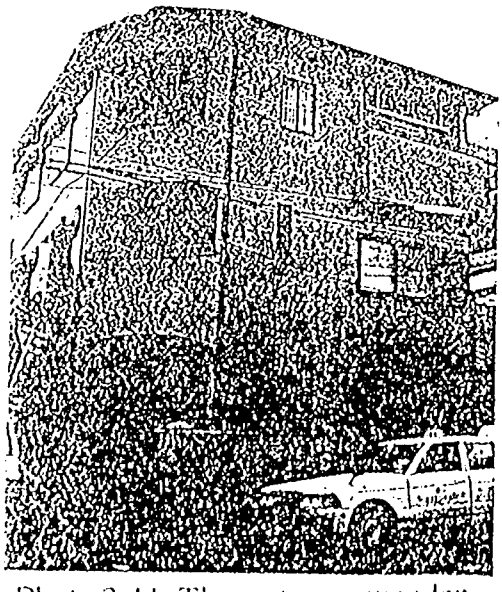


Photo 3.11 Three storey wooden building without damages

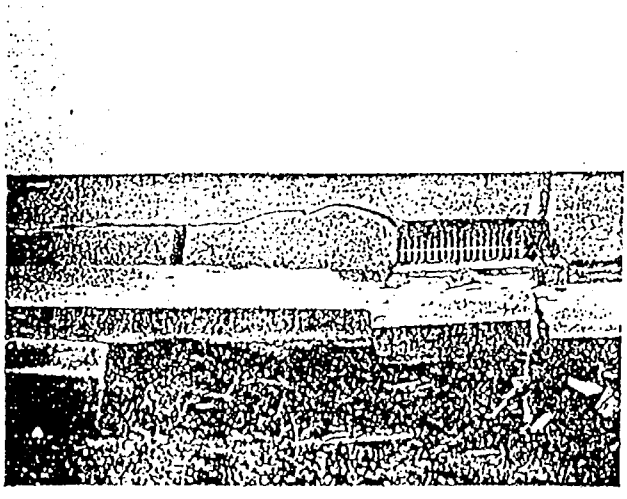


Photo 3.12 Damage of the foundation

Theme 4

Technology Applications by the U.S. Federal Emergency Management Agency in Response, Recovery, and Mitigation Operations Following Natural Disasters

by

Bruce Price[1]
Bob Fox[1]

ABSTRACT

The United States Government has tasked the Federal Emergency Management Agency (FEMA) to coordinate the Federal response to disasters that is beyond the response capabilities of State and local governments. FEMA, in partnership with more than 27 other Federal departments and agencies, is committed to encouraging effective utilization of technology applications to support planning and response to all types of disasters in the United States and its insular areas.

KEY WORDS

Damage Assessment, Emergency Management, Geographic Information System, Internet, Mitigation, Disasters, National Information Infrastructure, Predictive Modeling, Remote Sensing, Response, Recovery, Urban Search and Rescue, Wide Area Network.

1.0 INTRODUCTION

The Federal Emergency Management Agency (FEMA) is responsible for coordinating theUnited States Federal response to catastrophic disasters in the U.S. and its insular areas that are beyond the capability of State and local governments. In accomplishing this goal, FEMA, in conjunction with other Federal agencies, is committed to the most effective utilization of technology applications in planning for, response to, mitigation of, and recovery from catastrophic disasters.
The interrelationship of the Federal, State, and local governments, and volunteer organizations involved in emergency management, requires extensive coordination and communication capabilities. Appropriate planning, including training, mitigation and timely identification of urgent needs to establish relief priorities for the affected population, are the most critical parts of any disaster response. Application of the available and developing technologies is necessary to avoid unnecessary delay, and to maximize management effectiveness.

In the U.S., disasters happen in autonomous States and local communities that are responsible for the protection of the lives and property of their residents. Control of the Federal response ends at the regional level. At the request of the State, FEMA can assist with management and long-term recovery from catastrophic disasters. When required, assistance must be requested by the State(s) involved.

FEMA has divided the U.S. into ten Federal regions, which include its insular areas, as shown in Figure 1. Organizationally, FEMA has seven major Directorates, both at Headquarters and in the regions (Figure 2). Public Law 93-288, as amended (the Stafford Act), provides the basis for FEMA's response to disasters. The Federal Response Plan (FRP), provided for in the Stafford Act, is the primary mechanism for the Federal response to disasters in the U.S. All participating Federal departments and agencies are signatories to the FRP (Figure 3). The FRP is functionally organized into Emergency Support Functions (ESFs). Each ESF is led by a Primary Federal Agency as shown in Figure 4. For this purpose, the American Red Cross, when activated, acts as the Primary Federal Agency

[1]Federal Emergency Management Agency
Washington, D.C. 20472

in charge of mass care (ESF #6). Each ESF has a particular role to fulfill in disaster response and recovery.
Effective and efficient disaster operations require application of a variety of technologies in the following areas:

- Connectivity of federal, state and local emergency managers so that multimedia information on damage projections and impending disasters can be easily interchanged and situation assessment data provided within the first hours of the disaster;

- Preparedness technology tools that are used for simulation, training exercises and other "remote learning" types of training and development;

- Communications and data exchange within and between various responding organizations to improve the management and coordination between all Federal, State and local agencies and volunteer organizations.

2.0 RESPONSE TECHNOLOGIES

2.1 Initial Disaster Response Concept

When disaster strikes somewhere in the country the first priority for FEMA is to estimate the effects of the disaster, primarily deaths, injuries, and the number of homeless. Other key factors that may affect response are the conditions of major transportation routes, power and water systems, and hazardous materials sites. All of these are instrumental in determining the size and nature of the response.

Remote sensing platforms used in the early hours of a disaster help determine the boundaries of the disaster area and certain gross damage effects. Given boundaries, a Geographic Information System (GIS) using national data bases can quickly *estimate* the population and housing that may be affected.

2.2 National Emergency Response Team

When disaster strikes, the FEMA region will deploy an Advance Element of the Emergency Response Team (ERT-A), as soon as possible, to the Emergency Operating Center (EOC) of the affected State(s) and to the disaster area.

At the same time the region will activate an Emergency Response Team (ERT) composed of regional personnel from FEMA and other Federal departments and agencies. If the disaster is catastrophic, preempting a State request for assistance, a National Emergency Response Team (ERT-N) may be dispatched from Washington, DC, to an airport in the vicinity of the disaster site. The plane transporting the ERT-N to the disaster site is designed to provide life support and communications for up to 72 hours for the ERT-N to allow it to function in the area until a Disaster Field Office (DFO) is established and becomes operational with a normal regional ERT.

One of three ERT-Ns can be deployed to catastrophic disaster when the resources of the Regional infrastructure have been, or are expected to be, overwhelmed. While the ERT-N is enroute, the EST operating out of FEMA Headquarters will work with the Regional Operations Center (ROC) to coordinate preparations for the Federal response. The ERT-N, while enroute, has limited communications but can accomplish planning and preparation for operations once on-scene. Once on the ground, the ERT-N works with the ROC to coordination the Federal response, at which time the EST will revert to a support role.

2.3 The National Airborne Operations Center Capabilities

In situations where severe damage either makes access to facilities difficult or infeasible, the National Airborne Operations Center (NAOC) can provide a forward base of operations for up to 40 ERT-N emergency responders until the on-scene DFO is operational. This support capability includes communications, display areas, conference room, limited sleeping

arrangements, food, and security. The NAOC can provide limited connectivity via satellite and Ground Entry Points while enroute. Once on the ground, NAOC can then provide the ERT-N full communications support (satellite, High Frequency radio, landlines, Very High Frequency, and secure voice and FAX).

The NAOC is an E-4B (Boeing 747 type) aircraft weighing approximately 737,000 pounds gross takeoff weight (Figure 5). A minimum runway length of 7,000 feet is required to support NAOC operations. Power and other ground support requirements can be provided by FEMA Mobile Emergency Response Support assets.

2.4 Field Assessment Teams

Three quick-response Field Assessment Teams (FAsT) have been established, covering the Western, Midwestern, and Eastern areas of the United States. They are composed of skilled specialists from FEMA Headquarters, the regions, and personnel from the affected State(s). The FAsT teams are being equipped with laptop computers, satellite phones, video cameras that are linked by serial port to the laptop computers, and specialized software that allows capture and transmission of digitized frames of the video footage. A Global Positioning System (GPS) Receiver chronicles input to geotag each digitized video frame. Thus, the FAsT teams will be able to capture and transmit over satellite phone, digitized images of the damaged area back to the ROC and the EST at FEMA Headquarters to facilitate early damage assessments.

A FAsT may deploy to the disaster area within 12 hours to record and report to various FEMA operating elements actual damage by using mobile computing technology. The ERT-A and FAsT teams can provide sufficient details to enable disaster managers to activate and deploy appropriate mobile assets and Initial Response Resources to the area pending more detailed assessments.

2.5 The Disaster Field Office

The DFO is established near the disaster area within 72 hours to serve as the center for Federal operations in the area. It will provide office space and full communications support for the on-scene ERT composed of Federal staff from multi-agency sources in Washington D.C. and the region in which the disaster has occurred. In a large disaster, the ERT may include hundreds of disaster specialists from up to 28 or more Federal Departments and agencies supplemented by Federalized Disaster Assistance Employees. Within 4-5 days a Local Area Network (LAN) will be operational within the DFO to provide Automatic Data Processing (ADP) support to the ERT. The DFO LAN will be tied into FEMA's LAN/Wide Area Network to provide connectivity to FEMA installations nationwide using the full spectrum of communications media described elsewhere in this paper.

3.0 PLANNING AND MITIGATION TECHNOLOGIES

3.1 Geographic Information System Applications

In its support of *response and recovery* needs, FEMA's Mapping and Analysis Center (MAC) uses two levels of GIS technology. A "high-end" GIS utilizes an ARC/INFO system running on IBM Reduced Instruction Set Computer 6000 UNIX servers and workstations providing high-end GIS support, while "Low-end" PC-based desktop GIS capability is currently provided by MapInfo 3.0 and ArcView 2.

During or prior to a disaster, the MAC executes Damage Assessment Resource Models, incorporates the results of these models into the ARC/INFO GIS, and provides the resulting products to FEMA management, the EST at FEMA Headquarters, the ERT at the DFO, State emergency managers, and officials in other Federal departments and agencies. The MAC also interfaces with data providers, imagery providers, and their

customers, to identify and incorporate the necessary information into the GIS products. This is done on both the ARC/INFO GIS and the desktop GIS depending on the particular data or imagery product required.

The broad areas of GIS support required by the disaster response teams include rapid analysis of the affected area, including basic demographic data giving a socio-economic profile of the population at risk; and updating and refining the earlier general analyses. These analyses can include the distribution of disaster assistance applications and information and data based on aerial reconnaissance photographs, and satellite imagery.

GIS support is provided primarily in the form of hardcopy black and white, and color maps. Maps are also sent to users in digital form so that they can be further refined and enhanced to satisfy their needs.

3.2 Predictive Modeling

FEMA has computer models that use a variety of government and community development data sources. They are capable of estimating the civil resources, infrastructure, and populations at risk from impending hurricanes/typhoons and earthquakes. Those models provide information necessary to prepare and recover from such disasters by providing data to support advance emergency planning, readiness actions, and prepositioning or repositioning of appropriate types and amounts of relief supplies.

3.2.1 Hurricane/Typhoon Modeling

Using an automated, integrated system of models, databases, and Geographical Information System (GIS), estimates of the damage levels and populations at risk are available. FEMA's Hurricane Damage and At-Risk Populations Estimation Module automatically reads the available Maritime Advisory Messages every 6 hours. Current and forecasted hurricane characteristics, including the current and forecast positions of the storm, its maximum wind speed, and the distribution of wind speeds around the storm are part of those messages. Radial profiles of wind speed and dynamic pressure are analyzed and calculated for the current and forecast positions. The Module includes accepted structural response modeling techniques for determining the susceptibility of approximately 20 structure types to the dynamic pressures resulting from hurricane winds. Figure 6 illustrates the relationship between wind overpressures and damage levels to mobile homes.

FEMA bases its predeployment reports and actions on the resulting damage forecasts as well as the identification of sources of required assistance and prepositioning logistical actions. Figure 7 illustrates flooding extents along a coastal area ahead of Hurricane Emily.

Other features of hurricane-related models available to FEMA can provide indications of damage probabilities that arise due to the uncertainty in the forecasts of hurricane tracks. Hurricane storm surges, the abnormal rise of water over and above that caused by astronomical tides, represent another measurable hazard. Surge heights, in terms of the height of water above mean sea level, are indicated by SLOSH (Sea, Lake, and Overland Surges from Hurricanes), a U.S. National Weather Service storm surge model. The elevation of land areas as inducted by the United States Geological Survey (USGS) Digital Elevation Model is subtracted from the surge heights indicated by SLOSH to determine the depth of water over land. The resulting indications of "flood prone" areas assist evacuation and response planners (Figure 8).

These modeling techniques were used as Hurricane Emily approached the United States' Atlantic Coast in 1993. The residential area damage estimates, based upon the forecasts provided by the U.S. National Hurricane Center, proved to be close to real damage assessments.

3.2.2 Earthquake Damage Estimation Model

The motion of the ground due to an earthquake is calculated using a computer model developed by the USGS. The model computes the ground motion throughout the area affected by an earthquake based on the magnitude and location of the event, and the geology of that area. Ground motion is described in terms of Modified Mercalli Intensity (MMI), a numerical index describing the effects of the ground shaking produced by an earthquake on the people and their environment at a given location.

The model input parameters and databases describe the instigating fault rupture and the susceptibility of the local ground to shaking. The specific information required are: latitude and longitude of the center of the fault rupture, strike and depth of the fault rupture, regional attenuation factor, and digital geological database.

Other ground motion parameters, such as Peak Ground Acceleration and Peak Ground Velocity, are derived from the MMI. Low, medium, and high damage levels are assigned according to a specified threshold MMI. The model generates a gridded MMI, Peak Ground Acceleration and Velocity, and damage level data covering the entire area impacted by the earthquake.

The center of the fault rupture is taken as the reported earthquake epicenter. Epicenter and magnitude reports are normally issued by government and academic observatories. The strike of the ruptured fault is generally based on the directions of nearby mapped faults or other major tectonic features. The USGS recommends nominal values for the depth of rupture (always greater than the reported depth) based on the fault type (strike-slip vs thrust). The regional attenuation factor measures the loss of seismic energy with distance from the epicenter. The digital geological database contains the surficial geology and is produced by digitizing the geological map containing the affected area. A database using both the geological database and the spatial relative shaking response throughout the affected area is input to the model.

The GIS work station an extremely valuable tool to the success of disaster response operations. FEMA currently uses Arc/Info GIS software produced by Environmental Systems Research Institute, Inc. The damage levels are displayed to produce maps of areas at risk. Graphical consequence analyses are rapidly constructed by overlaying thematic data layers of interest on top of the map of areas at risk. FEMA's GIS systems are capable of producing highly accurate and detailed decision support products, tailored to the emergency manager's requirements. These maps and graphics are sent electronically over the Internet for their timely dissemination to emergency managers and decision makers. By virtue of its rapid turn-around time and accuracy, the FEMA earthquake simulation and consequence assessment capability is a powerful tool in providing rapid and well-targeted disaster response. Figure 9 displays the predicted levels of damage expected from an earthquake near Carson City, Nevada.

The model simulated the ground motion, in terms of MMI, and predicts damage from the 6.6 magnitude Northridge earthquake that struck the Los Angeles area on 17 January 1994. Considering the tectonics of southern California, it was hypothesized that this earthquake was due to thrusting along a fault immediately south and west of the San Gabriel Mountains. The fault rupture was therefore described as a shallow break striking east-west (this is consistent with post-event USGS analyses). The digital geology used was produced by the USGS from the California geological map. The attenuation factor was found from the USGS attenuation map of the United States.

On the accompanying map of the areas at risk, areas sustaining high, medium, and low damage levels are depicted as shaded areas. The MMI scale consists of twelve values

ranging from I (not felt) to XII (total destruction of engineered structures). *High damage* is assigned to areas where the intensities are IX and above. *Medium damage* is predicted in areas where the intensities are calculated to be VII and VIII, and *low damage* is where the intensities are V and VI. *No damage* is predicted where the intensities are calculated to be below V. In the white areas, intensities are below V and are undamaged.

Generally, the damage bands are oriented east-west, along the assumed strike of the fault rupture (calculated to be nearly 25 km long). These maps of areas at-risk were available within hours after this event. Predicted damage throughout the Los Angeles area from the Northridge earthquake was close to actual damage reports.

3.2.3 Earthquake Loss Estimation

The framework of the methodology embodies each of the components shown in Figure 10: Potential Earth Science Hazards (PESH), Inventory, Direct Physical Damage, Induced Physical Damage, Direct Economic/Social Loss and Indirect Economic Loss. As indicated by the arrows in the figure, the components are interdependent with the output of one module acting as input to another. In general, each of these components will be required for loss estimation. However, the degree of sophistication (and associated cost) will vary greatly by user and application. It is therefore necessary and appropriate that components have multiple levels of detail or precision. Inventorying the damage is probably the most time-consuming and costly aspect of the study, as inventory and other relevant data must be collected and organized for each of the modules shown. Examples of the type of information that the user will need to collect include an inventory of buildings in the region, population census data, soil and geologic conditions and economic data (Figure 11 and 12).

In order to evaluate losses, the user must develop a description of the earthquake and its associated ground motion. In many cases this will take the form of a scenario event of specified size and location. Depending on the size of the event and the local geology, a map of ground motions (in terms of acceleration) will be generated. In addition to ground motion, losses can be a function of ground failure such as landslides, liquefaction, and surface fault rupture. Thus, the PESH module generates estimates of the potential for ground failure in addition to estimates of ground motion. Other earth science hazards that are considered include tsunami and seiche which can result in significant losses.

Once ground motions and ground failures are identified, damage to the built environment can be estimated. In this methodology, damage is estimated for four distinct groups:

(1) general building stock;
(2) essential and high potential loss facilities;
(3) transportation systems; and,
(4) utility systems.

The groups are defined to address distinct inventory and modeling characteristics. General building stock includes residential, commercial, industrial, agricultural, religious, government and educational buildings. Essential facilities include hospitals, police stations, fire stations, emergency operation centers and in some cases, schools. High potential loss facilities are those facilities that are likely to cause heavy earthquake losses if damaged. Examples are nuclear power plants, dams, and military installations. The character of the inventory for general building stock differs from that for essential facilities. While general building stock and essential facilities are both groups of buildings, it is likely that the user will want and will have more detailed information about essential facilities. That is, for general building stock, the inventory is not collected on a building by building basis. Instead it is based upon estimates of building types by census tract, city, or some other designated area. On the other hand, the user will be able to identify the locations of all hospitals, fire stations etc., and may be able to

provide details of these facilities such as their heights and structural types. A similar situation occurs with high potential loss facilities.

Output from the Direct Damage Module will be estimates of damage to each of the groups of facilities described above. Estimates of damage will take the form of probabilities of being in a specific damage state (none, slight, moderate, extensive or complete) given a specified level of ground motion. A probabilistic damage estimate is used to reflect the many uncertainties involved. Lifelines are distinct from buildings in that they usually consist of a network of interdependent components which provide vital . Due to redundancies, damage to an individual component may or may not affect the operation of the system. A damaged system may still be capable of operating at below capacity. A key concern in evaluating lifelines is how long it will take to restore the system to full functionality. Thus damage estimates include restoration times.

Once estimates of direct physical damage are available, losses and induced physical damages are determined. Induced physical damage can be defined as consequences of the earthquake, other than damage due to shaking, that lead to losses. For this methodology, damage estimates include inundation, fire following earthquake, hazardous materials release, and debris generation. Inundation can result from tsunamis, seiches, dam failure, or levee failure. Fire ignitions may occur due to gas pipe breakage, electrical shorts, chemical spills or a number of other causes. The extent of the resulting fire depends on the availability of water and fire-fighting equipment and personnel. The extent of consequences of a hazardous material release (for example, casualties, building damage, pollution) depends on the type and quantity of released material. The quantity of debris generated depends on the types of structures damaged and the extent to which they are damaged. The cost of removing debris can be significant in both monetary and social losses.

Social losses take the form of casualties, short term shelter needs, and long term housing needs. Casualties resulting from damage to buildings and lifelines put a demand on health care facilities and personnel. The ability of health care providers to respond to causalities is dependent upon the degree to which their facilities have been damaged. The loss of functional buildings due to damage or non-functional utilities results in displaced households. These households will need alternative short-term shelter provided by friends, relatives or agencies such as the Red Cross. For units that take a long time to repair, long-term alternative housing must be located. This can be accomplished by using vacant units, importing mobile homes, moving to non-impacted areas or eventually repairing or reconstructing housing.

A final step in estimating earthquake losses are converting damage into monetary losses. Direct economic loss refers to the cost of repair and replacement of damaged structures and systems; structural and non-structural damage and, losses to business inventory are included. Dollar losses that are the direct consequence of building or lifeline loss-of-function are also included as direct economic losses. This includes the broad and long term costs of relocation, income losses, and rental losses.

3.3 Technical Applications in Mitigation

Technology is used to identify hazard areas, through a process of creating mapping products that depict the risks posed by various natural and technological hazards. These maps range from very detailed studies using topographic maps and hydrologic and hydraulic modeling techniques showing flood risks within communities, to statistical maps of wind risks. FEMA's most comprehensive hazard identification program is an effort to map all significant flood risks in the United States at the community level. That effort has resulted in approximately 90,000 flood maps being produced for over 20,000 communities. Technologies used in this program include the use of GIS, Global Positioning System (GPS)

surveys; photogrammetry, including auto-stereo correlation; and computer models.

In the post-disaster environment, technologies are used to assess and inventory damages, establish survey locations and extent, and create decision-making tools for reconstruction and recovery. The objective of these efforts is to facilitate the relocation of structures or communities, the enforcement of enhanced building regulations, and assist in directing recovery in such a manner as to mitigate the impacts of future disasters caused by similar hazards in the area. Technologies used in these mitigation efforts include not only GIS and GPS, but also digital remote sensing; digital photography; and computer networks, including database management systems.

Effective mitigation must be accompanied by laws and regulation that require property owners to build to safety standards in risk areas, and refrain from developing hazardous land parcels. Over the vast areas of the United States, it is difficult to efficiently enforce such laws, particularly where site visits are difficult or impractical and where local laws and planning procedures are restrictive. FEMA is currently prototyping the use of digital remote sensing to detect land use/land cover change in hazardous areas, and the use of distributed data base management techniques to assist with enforcement.

In those areas where Federal disaster assistance has been rendered, FEMA has implemented a Hazard Mitigation Program to track properties where the owners have been paid to move or modify the structure to prevent damage from future flooding. All properties on which Federal compensation has been paid are tracked. Future claims for compensation from property owners in areas included in the Hazard Mitigation Program database will be checked to ensure that a second claim for the mitigated property is not paid in the future.

3.4 Remote Sensing

In conducting analyses of user requirements for data in the immediate and near-immediate periods after a disaster event, post-event imagery of a disaster site is an excellent complement to the baseline maps and GIS spatial data used for response and recovery management. Digital imagery loaded into the GIS environment through direct data-streams or via disk transfer from the imagery analytic element. Adaptation of digitized imagery into the GIS environment allows disaster officials a micro or macro perspective incorporating socio-economic and other pertinent geographic data. By overlaying timely, precise, ground-truth data on a wide array of disaster-pertinent, geographic and demographic data sets, answers can be developed for specific response and recovery issues, such as the extent of flooding by determining how best to use transportation infrastructure or developing a strategy for controlling wide spread fires. Remote sensing may be the only way to get an accurate initial assessment when conventional access routes are impeded and/or there is insufficient time to conduct ground surveys.

Other uses of reconnaissance or remote sensing platforms, in responding to a disaster include identification/assessment of threats or risks to population groups, e.g. damaged chemical factories, weakened dams, pipeline breaks, fire spread etc.; identifying conditions favorable to incidents of disease propagation; studying terrain features/ conditions relevant to disaster causes; and even development of pre-event, mitigation planning portfolios.

Remotely collected data is of great value across the emergency management spectrum. Acquisition of the data however, is arguably the least difficult step in the process. Use of this technology demands rapid exploitation and equally rapid dissemination to field users/requesters. The requirement is to place the data in the hands of the response planners and the field staff as quickly as possible. Therefore, use of remote sensing technology, particularly for the response variable in the emergency management equation, necessitates that the user accomplish significant pre-event

planning, including how and when the data is to be provided to the exploiter from the platform; the time frames in which the exploiter must provide a finished product and what that product is; how the exploiter provides the product to the emergency manager; and, how the product will be handled, including identifying to whom it will be provided to and how will it be disseminated. See Figures 13 and 14 as examples of aerial photos of Mississippi and California flooding.

3.5 Urban Search and Rescue

Urban Search and Rescue (US&R) is the critical capability required for locating, reaching, medically treating and safely extricating survivors deeply entombed in collapsed structures. Victims of this type of entrapment are often critically injured and have unusual medical problems. Crush injuries and airway dust impaction are two of the most common. The process of extrication can markedly accelerate the pathologic processes of the victims and may cause rapid deterioration in a seemingly stable patient who had survived days of entrapment.

US&R is an integral part of the emergency response. The medical team is comprised of two emergency medicine physicians and four experienced paramedics. They are equipped and trained to begin patient evaluation as soon as the victim is reached. Their training emphasized confined-space critical care medicine.

The search component is a multi-disciplinary team that includes search (canine and technical), heavy rescue, emergency medical services, hazardous materials experts, structural engineers, communications specialists, management and other disciplines.

FEMA has developed 25 Urban Search and Rescue Teams sponsored by State and local government across the U.S. See Figure 15. The teams can deploy within 24 hours by military or civilian aircraft to a disaster site.

Presently there are two primary areas where technology assists US&R efforts: damage assessment by the Incident Support Team (IST) and technical search. ISTs are used to support Urban Search and Rescue field operations.

One of the pieces of equipment used by the IST is a computerized mapping/digital camera system. The computerized mapping system incorporates a single CD ROM disk containing detailed street information for the entire U.S. The mapping system coupled with an internal Global Positioning System, allows the user to retrieve mapping information based on their satellite-derived latitude and longitude coordinates. This is of great importance when customary visual references have been destroyed.

A digital camera is used in conjunction with the mapping system. The digital camera allows pictures to be taken of the disaster area. The digital pictures are transmitted via satellite to FEMA Headquarters or other desired locations. These pictures are then downloaded to a computer used in mapping where the images can be enhanced or highlighted to facilitate rapid analysis and to help define priority research areas and approach strategies.

Search cameras using fiber optics, and seismic sensing equipment allow real-time visual inspection of areas too small or dangerous for rescuers to enter without the need for extensive debris removal. These battery operated cameras are either mounted on an extendible pole or on the end of a cable for lowering into voids up to several hundred feet deep.

Seismic sensing equipment uses up to six sensors to detect vibration within a collapsed structure. The sensors are placed on large intact structural members penetrating into the structure. After placement of the sensors, the searcher, using a small public address system, advises trapped victims that a search of the structure is being conducted and directs them to strike a solid object to create vibrations. These vibrations are detected by the sensors, amplified and converted to audio signals which

the technical search specialist is trained to recognize and use in pinpointing the victim's location.

3.6 Automated Construction Estimating System

An innovation which has produced outstanding results and which has streamlined the delivery of aid to those applying for recovery assistance is FEMA's Automated Construction Estimating (ACE) System. The ACE, using custom software developed for hand-held computers, allows field inspectors to conduct home damage inspections which serve as the basis for determining eligibility for disaster assistance. The software allows inspectors to download their assignments when they report to work and upload the results of their inspections directly to the central processing facility at the end of their shift. This significantly increases the number of inspections that can be completed and processed each day. The expedited delivery of assistance to several hundred thousand customers in a politically charged disaster environment has enabled FEMA to focus on its mission and not waste time with administrative detail.

The ACE system, implemented in October 1993, was deployed successfully in the California wildfires, the Northridge earthquake, and most recently in the Georgia, Alabama, and Florida floods. This successful system has resulted in a 20-30 percent improvement in the accuracy of disaster assistance awards, reduced processing time by at least 50 percent, and reduced administrative expenses and paperwork. It is estimated that ACE will save $5.4 million/year in administrative expenses in an average disaster year. Moreover, ACE recouped its development cost in one disaster.

4.0 RECOVERY TECHNOLOGIES

4.1 Information Systems

FEMA has a range of information technology based capabilities, referred to as its Emergency Management Information Systems which includes facilities for data collection and analysis, decision support, response coordination and multimedia communications to support the all aspects of the emergency management function. These systems are available and used at all levels of the federal, state and local government and other disaster responders. While automation and technology cannot replace the need for human intervention and assistance, they can enhance the accurate and timely delivery of assistance.

4.2 Computer Networks

FEMA's 2500 employees are served by computers which are organized into Local Area Networks (LANs) - eight in FEMA Headquarters and 1 or more in each of the ten FEMA regions and other facilities such as the Mt. Weather Emergency Assistance Center. For some years these LANs have all been tied into a nationwide Wide Area Network (WAN) which has been utilizing a static (fixed) routing process. See Figure 16. When disasters occur and DFOs are established, those facilities also must be tied into the WAN to allow connectivity from any FEMA facility, even temporary DFOs, to any other FEMA facility nationwide.

The Agency is in the process of consolidating the headquater LANs from 8 to 1 LAN which will use NETFRAME Computers as file servers, and all regions will have a single LAN system. The new LAN/WAN will need less maintenance because it will have less hardware and software to maintain, which will require fewer support personnel to maintain it.

In upgrading and streamlining the LAN/WAN significant changes are being made to improve, simplify, and speed service, including:

- The network is transitioning from static routing to true dynamic routing of packets so that traffic is routed most efficiently and

alternate routes will be found automatically when traffic is blocked.

- Dynamic Bandwidth Allocation Device multiplexors are being installed to dynamically allocates the minimum bandwidth needed for traffic. This means the bandwidth may be reallocated automatically to other areas where it is needed.

- The LANs are being interconnected with 100 MB/Sec (FDDI) fiber optic cables.

- The LANs are connected to a very robust backbone using mostly T-1 switches with DBAD multiplexors which will provide an adjustable bandwidth for the nodes based on their dynamic need. This will be state-of-the-art architecture. Basically the router system will handle traffic most efficiently based on the dynamic load and the alternatives available.

- Because file servers will be mirrored, there should be no LAN downtime once the system is fully operational.

- NETFRAME file servers for the DFOs will be used in day-to-day operations to ensure they are functioning and their software is up-to-date. This will ensure that when they are deployed to a DFO, they can be brought up on the WAN will be fully operational.

The new system will be very robust so that all users can do their work simultaneously without waiting for a path. It will be much faster than the static routing architecture and will provide significantly higher reliability.

4.3 Internet Connectivity

Internet connectivity for the FEMA LAN/WAN has been temporarily delayed because of security considerations. An Internet security configuration has been devised that will provide a firewall between FEMA's LAN/WANs and the outside as shown in Figure 17. It will allow traffic to flow to a secured gateway where FEMA users can access it. However, it provides protection against hackers accessing the FEMA networks and will provide a reasonable level of protection against viruses. The configuration will be installed and operating this year.

4.4 FEMA Switched Network

On a day-to-day basis, FEMA's voice, data and video requirements are met utilizing a state-of-the-art information technology capability known as the FEMA Switched Network (FSN). The FSN is a multiplexed T-1 network connecting all of FEMA's telephone Private Branch Exchange (PBX) systems; LAN/WAN routers and bridges; video conferencing units; and dedicated point-to-point data terminals. The network hardware and software are FEMA-owned with the T-1 circuits being leased from commercial carriers. The entire network (including the T-1 circuits) are administered, monitored, operated and maintained from a specialized network control center known as the National Network Operations Center (NNOC) located at FEMA's Mt. Weather Emergency Assistance Center about 40 miles west of Washington, D.C.

Beginning with Hurricane Andrew, FEMA inaugurated an effort to extend the full services of the day-to-day FSN into disaster areas to support the disaster response and recovery effort. This initial effort included the use of a KuBand satellite to extend the FSN to mobile units in the disaster area. It also included the use of commercial T-1 circuits to extend a data processing capability into the DFO. These systems remain in place until such time as the disaster recovery is complete. The information technology systems are then returned to a centralized disaster information systems clearing house which stores and prepares them for their next disaster use.

Since Hurricane Andrew, FEMA has continued to build upon its information technology support of disasters to include enhanced call management and data processing centers to

centrally process disaster applications by phone.

4.5 Mobile Communications

FEMA's five Mobile Emergency Response Support (MERS) Detachments are deployed nationally as shown in Figure 18. They have the capability to rapidly respond to a disaster and provide long and short range communications, telephone switchboard systems, and Automated Data Processing (ADP) services for the advance responding elements and the DFO and Disaster Assistance Centers established in or near the disaster. A MERS Detachment of personnel and equipment is completely self sufficient and requires no support from local or State authorities.

Each MERS Detachment's communications capabilities include a Multi-Radio Van (see Figure 19), a REDCOM Switch, an expanded MERLIN switch, Line-of-Sight radios (see Figure 20) and International Marine Satellite (INMARSAT) access capabilities. This KU-band satellite, radio, telephone, broadcast media and other communications technologies are complemented with significant ADP capabilities, including personal and "lap-top" computers, as well as a file server and other LAN/WAN equipment, including printers. In addition to the communications and ADP capabilities each MERS Detachment maintains shelter, vehicles, generators, diesel fuel, water purification and heating, ventilation, and air conditioning capabilities to support emergency responders.

5.0 APPLIED INFORMATION SYSTEMS

5.1 Disaster Channel Operation In Disasters

In major disasters when FEMA establishes a DFO, a media-broadcast Disaster Channel is established as soon as possible in or near the DFO. The Disaster Channel, once up, operates 24 hours a day seven days a week during the early stages of the disaster, at least until it is no longer a media event.

TV and radio stations are able to monitor these broadcasts that include live in-studio and/or remote interviews of disaster officials, government officials and victims; press conferences; and news, information and other broadcasts. Cable TV companies can pick up the feed and distribute it; newspapers reporters can use the feed for print news. The broadcasts are multi-lingual where there is ethnic diversity among the victims.

During the Northridge Earthquake recovery FEMA's satellite broadcast - 'The Recovery Channel" - broadcast 24 hours a day, in several languages, to the news media, cable systems (125 of which retransmitted the broadcast), Disaster Applications Centers, Earthquake Service Centers and members of the general public with satellite receivers. This use of technology greatly facilitated the quick and accurate flow of information to the media and, more importantly, directly to the public about Federal, State, local and voluntary agency services.

5.2 The Internet

FEMA has established an information site on the Internet's World Wide Web (WWW). Over 400 "pages" of FEMA information are available, including photos, fact sheets, bios and news releases. Other services currently available on the site include an electronic Disaster Assistance Employee application form and the opportunity to leave electronic comments or suggestions.

The WWW site can be reached using Mosaic software and a communications line to the Internet. FEMA's Web address is WWW.FEMA.GOV. FEMA press releases are available using "GOPHER." This service provides "text only" files of FEMA press releases.

Other emergency management organizations around the country and some states are also creating Internet information sites. All of these sites are beginning to link up and "point" to each other. This allows users quick access to an enormous range of emergency management and disaster information.

5.3 Teleregistration

FEMA's National Teleregistration Center (NTC) houses a national toll-free telephone bank through which FEMA accepts registrations for disaster assistance. The NTC is equipped to quickly provide guidance and support to disaster victims who wish to register for assistance, express concerns, or who have questions about the various aid programs.

Toll free lines are available 24 hours a day; thus enabling calls to be taken within hours of the President's declaring an area a major disaster. The toll free service is also convenient. There is no need to take time off work, arrange for baby sitters, or stand in lines. Additionally, people living in outlying counties not served by centers physically located nearby, and those registering for aid after those centers have closed, can take advantage of the toll free number.

Further, NTC data processing services include the timely transfer of information obtained from callers to the various providers of disaster aid so that applications can be more expeditiously processed. Electronic data links to the DFO enable the transmission of data within minutes after the call is complete.

The NTC first took calls from disaster victims in October, 1989. Since that time, the Center has been involved with over 100 major disasters, including Hurricane Hugo, the Loma Prieta earthquake near San Francisco, Hurricane Andrew, last summer's flooding in the Midwest and, most recently, the Northridge earthquake in Los Angeles. To date, over 1.6 million calls have been processed using the NTC system.

5.4 Automated Disaster Assistance Management Systems

FEMA's Automated Disaster Assistance Management System (ADAMS) consists of ur Modules: a Human Services Module, Infrastructure Module, Hazard Mitigation Module, and the Operations Support Module. Each Module is designed to track Federal disaster expenditures for their respective programs. ADAMS has been in service for seven years across the FEMA LAN/WAN tracking disaster assistance data in support of FEMA emergency operations. The new system, called RAPID, will incorporate additional user-suggested improvements and features. It will provide additional functionality by expanding the range of data tracked, and automating the data collection and input process.

5.5 Rapid Assistance Programs Information and Delivery System

FEMA's Rapid Assistance Programs Information and Delivery (RAPID) System will be a relational database. It will manage the inspection of damaged facilities, federal grants made to repair these facilities, and various regulatory and administrative actions. Information on the damaged facility will include ownership, flood plain location, type of facility, the estimated cost of repairs, when the facility was inspected, the geographical position of the damaged site, past damage to the facility, and other information from the engineering inspection. Grant information will include information such as when the grant was approved and progress in making repairs. Regulatory and administrative data will include whether the facility has historic value, environmental issues, congressional inquiries and other management information.

RAPID is being designed to accept management data from the State, Geographical Positioning System (GPS) information, digital photographs and inspections made using a laptop computer. It will then export

information to other databases electronically as needed. The RAPID system will not only enhance the State's emergency management of their facilities, but will improve the States' long- term planning to reduce future disaster damages and improve their immediate response to disaster.

6.0 TECHNOLOGIES UNDER STUDY OR BEING IMPLEMENTED

6.1 Trends in Mitigation Measures

In the future, FEMA will incorporate digital orthophotography, a new generation of digital remote sensing satellites of high resolution, and improvements in database management software and network capabilities to make mitigation efforts more efficient.

6.2 Improved Connectivity Among Operations Centers

Communication and connectivity between emergency respondents are critical to the speed and effectiveness of response efforts. A major study is underway to improve automation support in all operations centers of the EST, ERT, ROC, and to improve connectivity to the State Emergency Operating Centers. Software packages in all operations centers will be standardized to ensure compatibility of files transferred; the software will be upgraded to integrate text and images; software packages will utilize Object Linking and Embedding to ensure that changes made in one software package will be promptly reflected in other packages. The upgraded software will be capable of handling and editing GIS images. For more details see the "Automation Support Concept of Operations," Volumes I and II, listed in the Reference section.

6.3 Remote Sensing Trends

FEMA is working with the National Aeronautics and Space Administration (NASA) to develop a refined functional statement of the Essential Elements of Information (EEI) needed in the first 24 hours for initial damage assessment. When the EEIs are clearly defined, a survey of all remote sensing assets available will be undertaken to determine to what degree remote sensing requirements can be met from existing military, government, and commercial sources. If those requirements cannot be met with existing assets, NASA will design and build a prototype remote sensing pod to gather the EEIs that are most critical using state-of-the-art sensors. The prototype will be test flown aboard NASA or other aircraft to refine the design. NASA will then produce a Design Specification that FEMA can use to have the remote sensor pod commercially produced for deployment by contract aircraft. This process will take several years to complete.

6.4 Trends in Public Information

A future goal for the Disaster Channel is to extend availability of the service through a feed to public access channels. Further, there is a need to provide a broader range of multi-lingual services on the channel. In the future the Channel will be made available to a broad audience, including networks, the print media, cable TV networks, and any user that has satellite reception capability.

7.0 INFORMATION MANAGEMENT AND REPORTING

7.1 Situation Reports

ESF-5 (Information and Planning) is streamlining production of Situation Reports (SITREPs) through the use of improved software and distribution techniques. In the future, SITREPs will be distributed to non-Government organizations through the coalition of groups in the National Voluntary Organizations Active in Disaster (NVOAD). Information submitted for the National SITREP is transmitted electronically via the FEMA LAN/WAN. Distribution via the LAN/WAN and through cc:Mail connects

Congress, the White House, and the Federal Departments and agencies.

7.2 Information Integration and Fusion Project

The Response and Recovery Directorate is in the process of building a system called the ***Information Integration and Fusion (IIF)*** **System.** It will eventually have all major FEMA documents in electronic form on a central computer. It will be available initially to EST operations, field elements over Norton/Symantec PC-Anywhere modem link, and to Headquarters personnel over the LAN.

Users will be able to access and search any of the databases, assemble relevant information from sources, and integrate the information into reports, documents, or print it. The system currently has all the SITREPs for Andrew, Iniki, Northridge, and several other major disasters, and emergency plans, procedures and SOPs. The system currently has, or is scheduled to get by mid-1995, all relevant Federal Laws, Executive Orders, Part 44 of the Code of Federal Regulations, Acts, Memoranda of Agreements and Understanding with Federal Departments and agencies, and the States. In addition, the system will serve as a central document repository for all Agency documents including policy memoranda, FEMA Manuals and Instructions, studies, and other day-to-day material that needs to be readily available in a central location. To support emergency operations the system will contain all Plans, Standard Operating Procedures, Manuals, SITREPs, performance reports and recommendations for improvement (such as lessons learned).

A 2-3 page Disaster History Template is used to summarize references for which we have SITREPs. The histories will provide a summary of each disaster. Information such as the size of the FEMA response, how many people, homes, etc., were affected, cost of the disaster, how many Federal agencies and personnel were involved, a chronology of the disaster itself (what happened), significant problems of the response, lessons learned, and recommendations for improving future responses will be included in each disaster summary.

The IIF System will be available agency-wide in the next few years as a single on-line source for all key FEMA documents. They will be available for day-to-day use and for emergency responders in all operating locations.

7.3 U.S. National Information Infrastructure

The U.S. National Information Infrastructure (NII) is a planned system of high-speed telecommunications networks, databases and advanced computer systems. NII will make electronic information more widely available and accessible, even in the most adverse conditions. The NII provides bi-directional high speed networking capabilities that support the needs of the on-the-scene and support emergency personnel. The NII will include a user interface that is multilingual and designed for use by individuals of varying educational levels, skills and abilities.

The NII will improve the training for and mitigation of disasters. Training and public education in planning and reacting to disasters will be improved through more realistic simulations and exercises of emergency response teams. Mitigation and planning efforts improve by the emergency managers' access to greater amounts of pertinent data and better computer models. Further, the NII will have the ability to reach people that may be at risk without those people actively seeking such information. Thus, the public will receive better warnings and be able to take more appropriate action.

The NII's dissemination and availability of information and data will allow for a quantum improvement in the management of disasters and emergency responses in the U.S.

For more information on implementation of the NII see The Information Infrastructure:

Reaching Society's Goals,.... listed in the Reference Section.

8.0 PRIVATE SECTOR TECHNOLOGY INITIATIVES

Private sector organizations are developing systems for international use which will influence how information is shared and exchanged in all countries. *RESPONSE.NET* is a not-for-profit effort sponsored by DeLorme Mapping Company of Freeport, Maine. Response.Net is one example of a system being developed to support governmental and nongovernmental organizations and the United Nations to better plan and execute international relief operations. A map based system using the latest commercial technology, it will rapidly collect and disseminate commonly used disaster information to improve response time.

9.0 REFERENCES

1. Automation Support Concept of Operations, Volume 1 - Concept, and Volume 2 - Capabilities, Requirements, and Analysis, Federal Emergency Management Agency, Information Technology Systems Directorate, October 21, 1994.

2. Code of Federal Regulations, Part 44, "Emergency Management and Assistance," Revised as of October 1, 1994. Published by the Office of the Federal Register, National Archives and Records Administration, United States of America, as a Special Edition of the Federal Register.

3. Emergency Support Team Operations Handbook (draft), Federal Emergency Management Agency, published 1994.

4. Executive Order 12148, "Federal Emergency Management," July 20, 1979.

5. Executive Order 12656, "Assignment of Emergency Preparedness Responsibilities," November 18, 1988.

6. The Federal Response Plan, For Public Law 93-288, as Amended, April 1992.

7. From Red Tape to Results: Creating a Government that Works Better and Costs Less, Report of the National Performance Review, Vice President Al Gore, September 7, 1993.

8. The Information Infrastructure: Reaching Society's Goals, Report of the Information Infrastructure Task Force Committee on Applications and Technology, The Effect of the National Information Infrastructure on Local, State and Federal Emergency Management (Draft for Public Comment), pages 89-105, U.S. Department of Commerce, National Institute of Standards and Technology, 1994.

9. Information and Planning Section: A component of the Federal Response Plan, Federal Emergency Management Agency, April 15, 1994.

10. National Response System: Field Assessment Team Operations Manual (Draft), Federal Emergency Management Agency, published 1994.

11. The Northridge Earthquake One Year Later, Prepared by FEMA in partnership with other Federal departments and agencies who responded to the Northridge Earthquake, January 17, 1995.

12. Principal Threats Facing Communities and Local Emergency Management Coordinators: A Report to the United States Senate Committee on Appropriations, April, 1993.

13. Public Law 93-288, As Amended by Public Law 100-107, "Robert T. Stafford Disaster Relief and Emergency Assistance Act," November 23, 1988.

14. Remote Sensing and Reconnaissance Support: A Component of the Federal Response Plan, Operational System Description and Standard Operating Procedure, Federal Emergency Management Agency, published 1995.

10.0 For Further Information

For further information on any of the topics in this paper, readers may write (in English please) to the following address:

Federal Emergency Management Agency
Attn: Director, Operations Division
Response and Recovery Directorate
500 C. Street, S.W. (FCP 606)
Washington DC 20472

11.0 ACRONYMS

ACE	Automated Construction Estimating (System)
ADAMS	Automated Disaster Assistance Management System
ADP	Automatic Data Processing by computer
DAC	Disaster Application Center
DFO	Disaster Field Office
EEI	Essential Element of Information
EOC	Emergency Operating Center
ERT	Emergency Response Team (composed of *regional* Federal personnel)
ERT-A	Advanced Element of the Emergency Response Team
ERT-N	National Emergency Response Team
ESF	Emergency Support Function
EST	Emergency Support Team (composed of *headquarters* Federal personnel)
FAsT	Field Assessment Team (composed of *Federal* and *State* personnel)
FCO	Federal Coordinating Officer
FEMA	Federal Emergency Management Agency
FRP	Federal Response Plan
FSN	FEMA Switched Network
GIS	Geographic Information System
GPS	Global Positioning System
IIF	Information Integration and Fusion (System)
INMARSAT	International Marine Satellite (portable telephone and data link)
IST	Incident Support Team
LAN	Local Area Network (of computers)
MAC	Mapping and Analysis Center
MERS	Mobile Emergency Response Support (Detachment)
MMI	Modified Mercalli Intensity (Index)
NAOC	National Airborne Operations Center
NASA	U.S. National Aeronautics and Space Administration
NII	National Information Infrastructure
NNOC	National Network Operations Center
NTC	National Teleregistration Center
NVOAD	National Voluntary Organizations Active in Disaster
PBX	Private Branch Telephone Exchange (switchboard)
PC	Personal Computer
PESH	Potential Earth Science Hazards
RAPID	Rapid Assistance Programs Information and Delivery (System)
ROC	Regional Operating Center
SCO	State Coordinating Officer
SITREP	Situation Report
SLOSH	Sea, Lake, and Overland Surges from Hurricanes (Software Program)
US&R	Urban Search and Rescue
USGS	United States Geological Survey, U.S. Department of the Interior
WAN	Wide Area Network (of LANs)
WWW	World Wide Web (Internet network)

Collection and Distribution of Road Information in Disasters
-Kushiro-oki Earthquake, Hokkaido Nansei-oki Earthquake, and Hokkaido Touhou-oki Earthquake-

by

Yasuhiko Kajiya[1], Hideki Abe[2] and Keishi Ishimoto[3]

ABSTRACT

Road network in Hokkaido was damaged by the Kushiro-oki Earthquake and Hokkaido Nansei-oki Earthquake and the Hokkaido Touhou-oki Earthquake. Road is so essential to our daily life, that users demand quick service of its information. We made follow-up survey on the road information collection, distribution in road maintenance offices, and on the information distribution through the media. These surveys proved that there are some problems in emergency communications and information collection, distribution. This report shows these results and recommendations for the future.

Key Words: Road Information, Kushiro-oki Earthquake, Hokkaido Nansei-oki Earthquake, Hokkaido Touhou-oki Earthquake

1. INTRODUCTION

In recent two years, Hokkaido experienced three big earthquakes. The Kushiro-oki Earthquake occurred on Jan.15, 1993, the Hokkaido Nansei-oki Earthquake occurred on Jul.12, 1993, and the Hokkaido Touhou-oki Earthquake occurred on Oct.4, 1994.

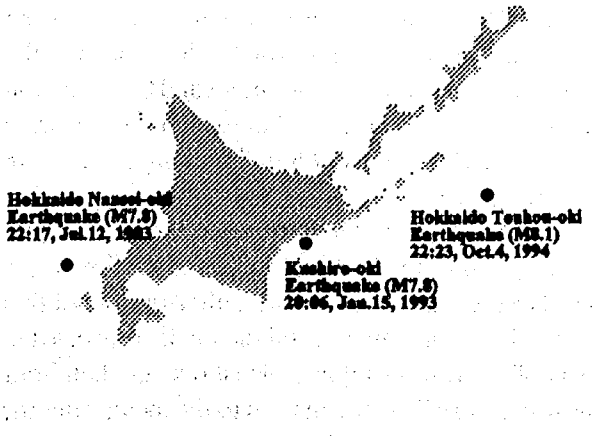


Fig.1 Recent Big Earthquakes in Hokkaido

Hokkaido Development Bureau maintains approximately 6,300 km National Highways which consist of main road network in Hokkaido. These earthquakes made big damages on this network. We made follow-up survey on the road information collection, distribution in road maintenance offices, and on the information distribution through the media.

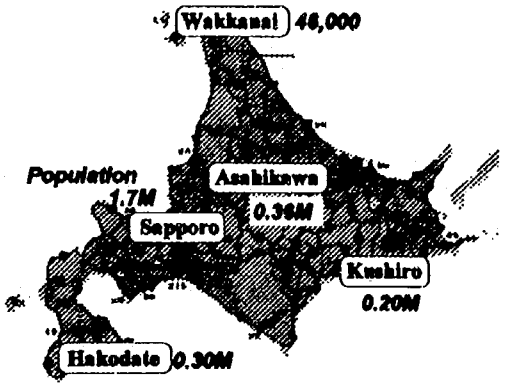


Fig.2 Road Network in Hokkaido

2. The Kushiro-oki and the Hokkaido Nansei-oki Earthquake

As shown on the map following, after the Kushiro-oki Earthquake, eight sections of National Highways and 31 sections of Prefectual Roads were closed. Some area was almost isolated at that time. After the Hokkaido Nansei-oki Earthquake, 5 sections of the National Highways and 31 sections of the Prefectual roads were closed.

We made questionnaire survey on the road information collection and distribution in road maintenance offices after these two earthquakes. The survey

1) Head of Disaster Prevention and Snow Eng. Section, Road Division, Civil Engineering Research Institute, Hokkaido Development Bureau, 1-3 Hiragishi, Toyohira-ku, Sapporo, 062 Japan.
2) Research Engineer, ditto
3) Director of Road Division, ditto

was made in 7 HDB offices and 6 Hokkaido Pref. Gov. offices for the Kushiro-oki Earthquakes, and 10 HDB offices and 10 Hokkaido Pref. Gov. offices for the Hokkaido Nansei-oki Earthquake.

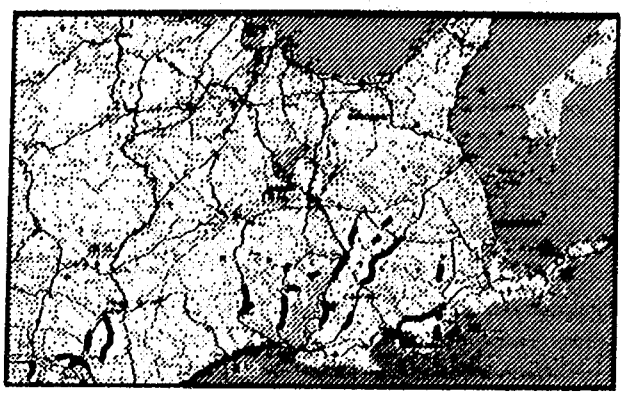


Fig.3 Road Closures by the Kushiro-oki Earthquake

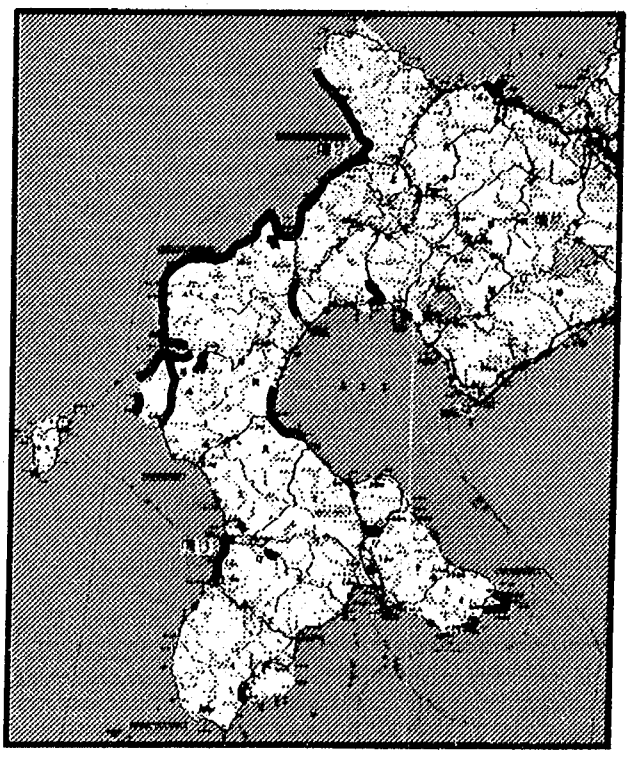


Fig.4 Road Closures by the Hokkaido Nansei-oki Earthquake

Focusing points are, 1)Emergency communications, 2)Staffs gathering, 3)Operation Center, 4)Information come and out, 5)Communication Equipment Damages, 6)Tsunami Information for the Hokkaido Nansei-oki Earthquake instead of 5).

The Kushiro-oki Earthquake occurred on Jan.15, 1993. It was the first day of the three continuous holidays. Some staffs who lived alone in Kushiro went home. There were relatively less staffs in the city than usual. But, almost 20 percents of the staffs came to the office immediately after the earthquake, and at the time of 20:30 when central operation center was established, 24 minutes after the earthquake, half of the staffs voluntary came to the office and began to work. It was almost the same at the Hokkaido Nansei-oki Earthquake.

The Kushiro-oki Earthquake occurred near Kushiro city that many offices and staffs' home were damaged, and emergency communications were not done well. The result of questionnaire shows that about 70 percent offices reported negative answer on this matter. In the case of the Hokkaido Nansei-oki Earthquake, most offices were located in main island of Hokkaido and not damaged by the vibration itself that emergency communications were relatively done well. As reasons, many offices reported 1)Radio-telephone system damage, 2)NTT-telephone lines unconnectable, 3)FAX machines unusable by power failure, 4)Operation center's too busy telephone lines, 5)Take too much time for patrol.

As lessons from the Kushiro-oki and the Hokkaido Nansei-oki Earthquake, we, road authorities should, 1)Improve radio-telephone system's seismic-proof, 2)Use more power back-up equipments, 3)Simplify communication rules, 4)Improve operation center's communication systems, 5)Develop and utilize Highway Disaster Prevention Information Systems.

3. The Hokkaido Touhou-oki Earthquake

As shown on the map following, road network in eastern Hokkaido were greatly damaged also by the Hokkaido Touhou-oki Earthquake. In the area of the Kushiro and Abashiri Development and Construction Department, 4 sections of 3 National highways were closed, and 15 sections of 8 national highways were one-side closed.

Table.1 shows the routes, sections of National Highways closed by the earthquake and the time when road closure started and road authority offered this information to the media, and the media broadcasted it to public. It shows that, at least one and half hour was needed to offer information to the media after the

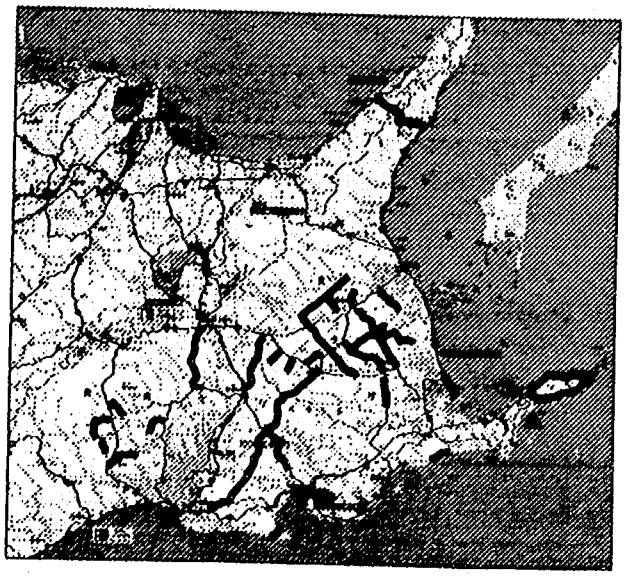


Fig.5 Road Closures by the Hokkaido Touhou-oki Earthquake

road was actually closed. Road patrol should be made much shorter to secure road safety in the future.

On the other hand, the media which was provided information from road authority immediately reported it to public. It took less than one hour, and this means that if road information is immediately and accurately offered by road authority to the media, the media can immediately report it to public.

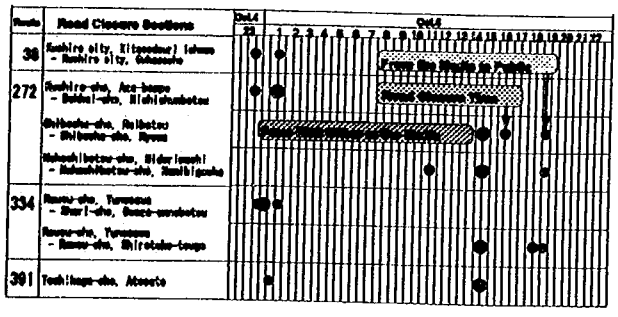


Table.1 Road Information through the Media after the Hokkaido Touhou-oki Earthquake

After the Hokkaido Touhou-oki Earthquake, we recorded NHK-TV for 72 hours, and check off information on National Highways with our bureau's maintenance offices' information. Fig.6 shows that from the earthquake to next morning 7:00 AM, only 20% of the information are OK, 36% of them are not enough, and 44% of them are different.

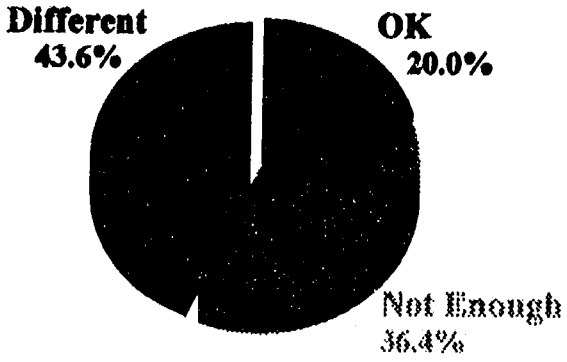


Fig.6 TV Broadcasting Road Information after the Hokkaido Touhou-oki Earthquake (until next morning 7:00 AM)

Major differences between both information were 1)Misunderstanding road closure and one-lane closed, 2)Road closure section name. Why did they occur? The reason must be that 1)media have many information sources, like police, fire department, even restaurants and people along roads, 2)there were so many information which had different time-stamps, that they could not figure out which is the latest one.

As lessons from the Hokkaido Touhou-oki Earthquake, we, road authorities should, 1)make shorter patrol time for road information collection, 5)develop and utilize Highway Disaster Prevention Information Systems, 3)develop and utilize Information Sharing System inside and outside organization, 4)plan more for long-term and train more for short-term disaster prevention. Especially, Hokkaido has less population and one office must maintain relatively long roads, that it is inevitable for us to take much time for road patrol. But, we should develop other way to collect road information, like the system of collecting information from professional bus and track drivers and restaurants and people along the road. In addition, as for Information Sharing Systems, utilizing the INTERNET will be one of the best solution in the future.

4. Conclusions and Recommendations

Based on the experiences of these recent big

earthquakes, the Hokkaido Development Bureau improved emergency communication systems and rules. In addition, the bureau planed to install many small seismic intensity meter on bridges and embankments, and to develop Highway Disaster Prevention Information Systems which can provide immediate information on the earthquake by connecting the meteorological organization's computer and the HDB's Road Weather Information System, and Variable Massage Boards along roads, This is as much important theme as winter road management for us. The HDB will develop it in our own Intelligent Transport Systems Project.

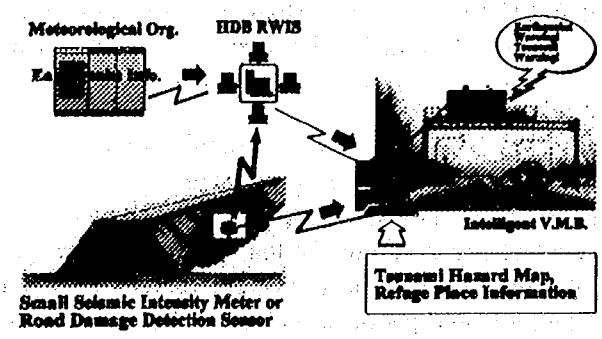


Fig.7 Highway Disaster Prevention Information Systems

ACKNOWLEDGMENT

The authors sincerely appreciate for the cooperation of the Kushiro, Abashiri, Hakodate, and Otaru Development and Construction Department of HDB, and the Department of Public Works of the Hokkaido Prefectual Government.

REFERENCES

1) Yasuhiko Kajiya: Seismic Risk of Road Network, *CERI Report No.100, 1993 Kushiro-oki Earthquake*, pp.49-54, 1993. (in Japanese)
2) Yasuhiko Kajiya: Regional Traffic in Disaster and Seismic Risk of Road Network, *CERI Report No.101, 1993 Hokkaido Nansei-oki Earthquake*, pp.63-68, 1993.(in Japanese)
3) Hideki Abe, Yasuhiko Kajiya: Collection and Supply of Road Information in Disasters, *CERI Monthly Report, No.492*, pp.12-24, 1994.(in Japanese)
4) Yasuhiko Kajiya, Hideki Abe: Seismic Risk of Road Network and Road Information in Disaster, *CERI Report, No.108, 1994 Hokkaido Touhou-oki Earthquake*, pp.33-39, 1994. (in Japanese)

Epidemiologic Methods for Assessing Wind- and Seismic-related Health Effects in Disaster Response

by

Josephine Malilay and Eric Noji*

ABSTRACT

To effect timely and appropriate emergency response and recovery, epidemiology needs to incorporate the expertise from various technological fields. In this paper, we present 1) a definition of epidemiologic methods and a description of their application in disaster settings, with appropriate examples from wind and seismic disasters; 2) a description of the causes of deaths, injuries, and illnesses for each disaster type and the risk factors for those conditions; and 3) an illustration of how these methods are used to evaluate specific response activities. We demonstrate that current results indicate the need for interdisciplinary epidemiologic design and interpretation, particularly from engineering, meteorological, geological, emergency management, public health, and medical sectors. Finally, we recommend directions for the interdisciplinary application of these methods.

KEYWORDS: epidemiology; natural disaster; wind; seismic effects; tropical cyclone; tornado; earthquake

1. INTRODUCTION

Epidemiology, derived from the Greek words *epi*=among, *demos*=people, and *logos*=doctrine, is the study of the occurrence of diseases in human populations (1). Epidemiology addresses disease occurrence by scientifically measuring characteristics of individuals and the relationships of people to their environments. Classically, epidemiology has been applied to infectious diseases in populations, or "epidemics," and investigators have identified microorganisms that cause diseases, determined infectiousness and immunity among humans, and recommended public health measures to thwart the spread of diseases. In recent decades, however, epidemiologic methods have been applied in many health fields, including chronic diseases, environmental health, and injury control.

One recent application of epidemiology is the investigation of the public health and medical consequences of natural disasters, defined as ecological disruptions which typically occur suddenly, exceed the adjustment capacity of the affected community, and call for outside assistance. Known as "disaster epidemiology" or "epidemiology in disaster settings," this discipline developed as scientists realized that the effects of disasters on health are amenable to study by epidemiologic methods (2). Some of the methods involve a comparison of people who were killed or injured with people who were not in order to learn in what ways they differed. Epidemiologists identify risk factors, with the aim of preventing the occurrence of death, illness, or injury. Epidemiologic studies include descriptive studies of the tornado-related injuries, analytic studies of risk factors for deaths due to physical structures in earthquakes, and evaluative studies of external assistance after disasters occur. Results of such research have formed the scientific basis for preventing or reducing disaster-related mortality and morbidity.

2. THE DISASTER SETTING

Of all natural disasters, events involving high winds and seismic activities have the greatest impact on the health and well-being of affected

* Centers for Disease Control and Prevention
Atlanta, Georgia 30341-3724

communities. From 1967 to 1991, high winds and seismic events accounted for 32% of all disasters occurring worldwide (3). Of an estimated 260 million people affected by high winds, tropical storms or cyclones, and earthquakes during this period, approximately 1.6 million were killed and another 1.08 million were injured (3). Although disaster-related mortality is relatively in the United States, enormous sums are spent on relief and recovery from the social and economic effects of natural disasters. In 1989, average losses from Hurricane Hugo and the Loma Prieta earthquake, resulting in 90 deaths, amounted to approximately $60 billion in the United States (4). In 1992, Hurricane Andrew killed 15 people and caused an estimated $25 billion in damage in south Dade County, Florida (5).

3. METHODS FOR EXAMINING HEALTH EFFECTS FROM CLIMATIC ELEMENTS

Historically, the public health impacts of disasters have been examined by disaster type. As shown in Table 1, different disasters tend to produce different health effects (6). For example, earthquakes have caused more deaths and severe injuries requiring medical attention than have other natural disasters. In contrast, disasters with high winds, such as tornados and cyclones, result in relatively few deaths and injuries requiring medical attention. Food scarcity and major population movements are rare following wind or seismic disasters, although they may occur in densely populated urban areas. In both wind and seismic disasters, the risk for increased communicable disease is affected by six conditions: 1) changes in pre-existing levels of disease, 2) ecological changes as a result of the disaster, 3) population displacement, 4) changes in population density, 5) disruption of public utilities and 6) interruption of basic public health services (7). Although few serious epidemics of infectious diseases have been documented to date, the potential for communicable disease exists in situations in which sanitation and hygiene are compromised by environmental changes caused by the disaster.

Since these observations were documented, systematic methods have been developed to identify high-risk subgroups of the population; to determine risk factors for death, illness, or injury; and to evaluate the usefulness of response activities related to wind and seismic events. Initially, epidemiologists conduct descriptive studies for which they collect reports of deaths, illnesses, and injuries from various sources, such as hospital records, death certificates, medical examiners/coroners' reports, disease surveillance systems, and care providers in the disaster site. They then group these data by individual characteristics, place, and time to determine any patterns in mortality and morbidity. Analytic studies may then be conducted to determine the risks for death, injury, or illness among various population subgroups. For analytic studies, epidemiologists use a comparison group from representative or convenience samples of a community exposed to the disaster to help them identify factors -- demographic, biological, chemical, physical, or behavioral -- associated with outcomes of death, illness, or injury.

3.1 High winds

Although the exact mechanism of death during high-wind disasters (i.e., structural collapse or high-velocity projectiles) has yet to be established, deaths, particularly in tornados, are due to severe head trauma, multiple fractures, and arterial lacerations (8). Protective and risk factors for injury or death from tornados are listed in Table 2. Among the protective factors are staying in a basement (odds ratio (OR)=0.2), covering oneself with something (OR=0.2), and staying in a building with one story (OR=0.3) or in a structure whose walls constructed of wood (OR=0.4). Risk factors include staying in an area near glass (OR=2.2), holding onto a part of the building (OR=17.3), and trying to protect oneself under furniture (OR=2.4). Other studies suggest that high-risk groups include the elderly, occupants of mobile homes and vehicles at the moment when a tornado strikes, and occupants of some public buildings

with inadequate warning systems (11).

In tropical cyclones in which winds characteristically exceed 75 miles per hour, 90% of all deaths have been attributed to drowning caused by storm surge (12). Violent winds in Hurricane Andrew in Florida in 1992 may have resulted in structural collapses that led to 11 (73%) of 15 deaths directly attributed to the storm (5). In the same event, two deaths were due to multiple blunt trauma from flying debris. Risks for injury or death associated with occupying structures at 30 feet or higher have yet to be examined in the context of hurricane evacuation safety.

Preparedness and adequate sheltering at individual and community levels are critical for survival. In recent years, improved forecasting technology, better procedures for issuing and disseminating warnings, appropriate sheltering, and the implementation of hazard mitigation have led to a decline in deaths related to wind effects. Much of the epidemiologic research concerning high-wind disasters involves the assessment of warning systems (e.g., passive warning systems such as sirens, alarms, and warning devices that are not dependent on radio or television broadcast media; and active warning systems such as the National Weather Service radios, regular media, and local observer networks).

3.2 Seismic events

Epidemiologic methods for examining earthquakes largely focus on the role of the physical setting, occupants' behavior, and personal characteristics associated with a health outcome, usually death or injury. Typically, epidemiologists examine predictors such as building damage, structural or nonstructural sources of injury, where people are trapped, the details of victim location and extrication, and the delivery of on-site medical care.

The interface between epidemiology and structural engineering has been explored in the context of how building occupants become injured or killed during seismic activity. As shown in Table 3, the data presented are drawn from earthquake-related studies in Armenia in 1988 and in the Philippines in 1990 (13-14). Risk factors for death or injury include being inside a structure (OR=12.2) and remaining there during an earthquake as opposed to running out (OR=4.4) and staying in a building made of concrete or mixed materials versus staying in one made of wood (OR=2.6). Attempts to determine a safe location in terms of floor level have yielded varying results.

Knowledge of protective and risk factors is helpful in planning appropriate search and rescue and relief activities. For instance, knowledge of survival by floor level could be used to guide rescue workers to where they should dig initially--at the top or the bottom of rubble. Similarly, knowledge of the survival rates associated with specific construction materials can be used to determine where survivors are likely to be found. Epidemiologic data can also be useful for rescue workers conducting structural triage (i.e., assess buildings where survivors are likely) during in search and rescue.

4. CONCLUSIONS

Although the health effects from tornados have been investigated in many events over the past few decades, the mechanisms of injury or illness in other wind-related disasters have yet to be elucidated. For example, descriptive studies of the mechanism of wind-related injuries in "dry" tropical cyclones, where storm surge is not a problem, are needed to determine whether or not high winds should be considered environmental threats. Similarly, the mechanisms of building failure and human casualties during earthquakes require further systematic studies in urban and rural areas of high seismic activity worldwide.

We recommend that epidemiologic studies should be designed so as to involve the collaboration of engineers, meteorologists, and emergency management and public health

officials. Each of these disciplines can contribute to the epidemiologic investigation of disasters. For example, understanding building failure requires knowledge of structural engineering, whereas medical and public health expertise is necessary to understand on-site treatment of human injury and to recommend prevention or reduction strategies for emergency managers to implement. Epidemiologic investigations guided by engineering, meteorologic, and emergency management input can best provide the data necessary for planning emergency response activities after wind and seismic disasters.

5. REFERENCES

1. Ahlbom A, Norell S. Introduction to modern epidemiology. Chestnut Hill, MA: Epidemiology Resources Inc., 1984.

2. Lechat MF. The epidemiology of disasters. Proceedings of the Royal Society of Medicine 1976;69:421-6.

3. International Federation of the Red Cross and Red Crescent Societies. World disasters report 1993. Norwell, MA: Kluwer Academic Publishers, 1993.

4. National Research Council. The US national report. Facing the challenge. Washington, DC: National Academy Press, 1994: 78 p.

5. U.S. Department of Commerce, National Oceanic and Atmospheric Administration, National Weather Service. Hurricane Andrew: South Florida and Louisiana, August 23-26, 1992. Natural Disaster Survey Report. Silver Spring, MD: National Weather Service, 1993.

6. Pan American Health Organization (PAHO). Emergency health management after natural disaster. Scientific Publication No. 407. Washington, DC: PAHO, 1981: 67 p.

7. Western KA. Epidemiologic surveillance after natural disaster. Scientific Publication No. 420. Washington, DC: Pan American Health Organization, 1982: 94 p.

8. Brenner SA, Noji EK. Risk factors for death or injury in tornados: an epidemiologic approach. In: Church C, et al., eds. The tornado: its structure, dynamics, prediction, and hazards. Geophysical Monograph 79. Washington, DC: American Geophysical Union, 1993:543-4.

9. Duclos P, Ing R. Injuries and risk factors for injuries from the 29 May 1982 tornado, Marion, Illinois. Int J Epidemiol 1989;18:213-219.

10. Eidson M, Lybarger JA, Parsons JE, MacCormack JN, Freeman JI. Risk factors for tornado injuries. Int J Epidemiol 1990;19:1051-6.

11. Centers for Disease Control and Prevention. Tornado disaster--Illinois, 1990. MMWR 1991;40:33-6.

12. Alexander D. Natural disasters. New York: Chapman & Hall, Inc. 1993.

13. Armenian HK, Noji, EK, Oganesian AP. A case-control study of injuries arising from the earthquake in Armenia, 1988. Bull WHO 1992;70:251-7.

14. Roces MC, White ME, Dayrit MM, Durkin ME. Risk factors for injuries due to the 1990 earthquake in Luzon, Philippines. Bull WHO 1992;70:509-14.

Table 1. Short-term health effects of natural disasters*

Health effects	Earthquakes	Hurricanes / High winds	Volcanic eruptions	Floods	Tidal waves / flash flood
Deaths	many	few	varies	few	many
Severe injuries requiring intensive medical care	overwhelming	moderate	varies	few	few
Increased risk of infectious disease	Potential problem in all major disasters (probability rises with overcrowding and deteriorating sanitation)				
Food scarcity	rare (may occur because of factors other than food shortages)		common	common	common
Major population movements	rare (may occur in heavily damaged urban areas)		common	common	common

* Source: Pan American Health Organization, 1981

Table 2. Protective and risk factors for deaths or injuries caused by tornados (from selected analytic studies related to occupancy of a structure*)

	Odds ratio (p value) [95 % confidence limits]	**Source**
Staying in a basement	0.2 (<0.00001)	Duclos and Ing, 1989
Staying in a single family home (adjusted for floor level)	0.3 (0.0001)	Duclos and Ing, 1989
Holding another person	0.3 (0.0001)	Duclos and Ing, 1989
Covering the body with a blanket or something else while lying down	0.3 (0.01)	Duclos and Ing, 1989
Being covered with something	0.2 [0.0, 1.0]	Eidson et al., 1990
Staying in a building with only one story (adjusted for being in a basement, type of walls, and presence of a glass door nearby)	0.3 (0.08)	Duclos and Ing, 1989
Staying in a building with walls made entirely of wood	0.4 (0.0001)	Duclos and Ing, 1989
Staying in a house with a roof of wood frame and shingle	0.5 (0.0004)	Duclos and Ing, 1989
Lying down (adjusted for protecting the body with something)	0.5 (0.09)	Duclos and Ing, 1989
Being sheltered under something	0.1 [0.0, 0.4]	Eidson et al., 1990
Trying to protect oneself under furniture (adjusted for the room the person was in)	2.4 (0.004)	Duclos and Ing, 1989
Having window glass inside the home	3.5 [1.1, 11.3]	Edison et al., 1990
Staying in an area near glass	2.2 (0.006)	Duclos and Ing, 1989
Holding onto part of the building	17.3 (0.0001)	Duclos and Ing, 1989
Being struck by something while inside the home	9.2 [3.1, 27.4]	Eidson et al., 1990
Age 60+ years	3.9 [1.6, 9.7]	Eidson et al., 1990
Age 5-14 years	0.2 [0.2, 0.8]	Eidson et al., 1990
Having gone to a particular room for protection	0.3 [0.1, 0.9]	Eidson et al., 1990

* Protective factors are indicated by odds ratios < 1.0; risk factors are indicated by odds ratios > 1.0.

Table 3. Protective and risk factors for deaths or injuries caused by earthquakes (from selected analytic studies related to occupancy of a structure*)

	Odds ratio (p value) [95 % confidence limits]	**Source**
Being inside a building at the time of an earthquake vs being outside	12.2 [3.6, 63.8]	Armenian et al. 1992
Leaving a building during an earthquake vs staying inside	0.3 [0.2, 0.8]	Roces et al., 1992
Staying indoors vs running or jumping out	4.4 [2.2, 8.7]	Armenian et al. 1992
Staying in a building made of concrete or mixed materials vs staying in one made of wood	2.6 [1.7, 4.1]	Roces et al., 1992
Staying at floor level: top vs ground	1.9 [1.3, 2.9]	Roces et al., 1992
Staying at floor level: middle vs ground	3.4 [2.2, 5.5]	Roces et al., 1992
Staying in a building with ≥ 5 floors vs staying in one with < 5 floors	3.6 [2.1, 6.3]	Armenian et al. 1992
Staying on floor 2-4 vs staying on floor 1	2.6 [1.42, 4.7]	Armenian et al., 1992
Staying on floor 5 vs staying on floor 1	4.0 [2.1, 14.9]	Armenian et al., 1992

* Protective factors are indicated by odds ratios < 1.0; risk factors are indicated by odds ratios > 1.0.

Theme 5

Virtual Reality Expression System for Tsunami Prevention

by

Hironao TAKAHASHI [1] ,Kouji SAKAI [1] ,Testsuya HIRAISHI [2] and Toshihiko NAGAI [2]

ABSTRACT

A computer graphic system of tsunami propagation and runup are newly developed. The main merits of the system are the change ability of location and height of view point, the wide view angle with five screens each 70inch wide, and the real time expression. The paper introduces some example images for the 1946 Nankai Earthquake Tsunami.

Key Words; Computer graphic,
Disaster prevention plan,
Virtual reality image,
Tsunami simulation

1.INTRODUCTION

Computer graphic is widely applied to present the results from numerical simulation. It becomes one of the most effective methods to make a design of landscape. Tsunami propagation simulated in the numerical models is able to be expressed in the computer graphics. Some effective graphics to show the attack of the 1993 Hokkaido Nansei-oki Earthquake Tsunami were presented in the 41st Conference of Japanese Coastal Engineering (1994). The computer graphic is effective to design of the tsunami prevention facilities like breakwaters and sea walls. It is also useful to planning of the refuge route and alarm system.

The view point in the computer graphics is, however, fixed to a single point. The bird's eye view system is normally employed to determine the view point. It is important to get the total information like the arrival time of tsunami wave and the distribution of the tsunami runup heights. However, the human's view point system is necessary to make the refuge planning and to establish the alarm system. It is also very important to give an visual alarm to the local residents. The virtual observer should take any position and move to any space to get the detail information of tsunami attack. Therefore, a new computer graphic technic has to be developed for the human conscious prevention.

Meanwhile, a ship maneuvering simulator system has been developed in some research institutes(Hayafuji,1990). The ship maneuvering simulator system is for the discipline of vessel navigation in a port. An examiner can get a virtual scene around his vessel according to his position in the port. When he advances the vessel forward, the imaginary scene on the screen may be gradually changed. The Port and Harbour Research Institute has developed a navigation simulator with five wide screen each 70inch wide. An examiner is able to get a virtual reality image with port facilities.

This paper describes a newly developed computer graphic system for tsunami propagation and runup in a port. The ship maneuvering simulator is applied to express the simulation results. The virtual reality image of tsunami attack is observed in the system. The characteristics of the system are as follows;

1) The observation point is removable.
2) The view angle is wide.
3) The time in the graphic is changeable

1)Planning and Design Standard Division, Port and Harbour Research Institute, Ministry of Transport, Nagase 3-1-1, Yokosuka, Japan 239
2)Hydraulic Engineering Division, ditto

Table 1 Hardware of graphic system

EWS : Onyx Reality Engine2 (Sylicon Graphics)
CPU 85 MIPS x 2 CPU clock : Outer clock 50MHz Inner clock 100MHz Graphics texture memory : 4MB Z - buffer : 32bit Color : full
Operation software :
operation system: IRIXTM ver5.2 language :X-Window, C
Screen :
rear projector system size : 70inch x 5 view angle : 225°

(Real time expression is available).

2.REAL TIME 3D GRAPHIC SYSTEM

Table 1 shows the system hardware. **Figure 1** shows the arrangement of the screens. Each screen is 70inch wide. The total view angle with the five screens is 225°. The observer in front of the screens is able to have a real time image of tsunami propagation, runup and attack in the field. The presented graphic images can expressed in what is called 'virtual reality'.

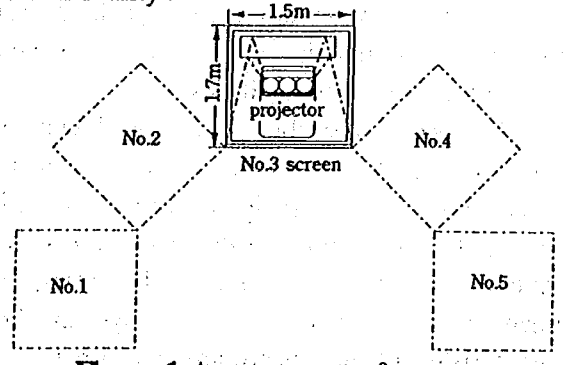


Figure 1 Arrangement of screen

For the expression of tsunami propagation, the background like houses, mountains and port facilities should be kept in the computer hard disk in advance. The software 'MultiGen' by Software System Co. are applied to complete the background image data. The photographs of buildings and houses are able to be overlapped on the image data on the screen. The software 'IRIS Performer' by Silicon Graphics Co. are employed to form the three dimensional graphics of the tsunami attack and background. This system has the following functions;

(i)Data Curling Function:The graphic image data beyond the view angle is not calculated to reduce the CPU time.

(ii)Level of Detail Function : The detail level of graphic image is changed according to the distance of the object from the observer.

In the tsunami simulation, the water level and flow velocity in the two components are output at each time step. In the graphics system, only the water level data are expressed on the screen. The flow velocity is one of the important factors which show the intensity of tsunami. However, the system presents only the water surface elevation change because the CPU size and memory size are not so large to include the flow velocity data.

For the computer graphics of three dimensional objects, the following three models are available;

(i) Wire Frame model : A three dimensional object is expressed in wires (line). The memory size necessary to the model is the smallest, so the high speed graphic is available.

(ii) Surface model: A plate is set on the space surrounded by wires in the wire frame model. In this model, a large number of two dimensional planes are employed to express the three dimensional figure. The plane is called 'Polygon'.

(iii)Solid model: The internal information of an object is added on the plane in the Surface model.

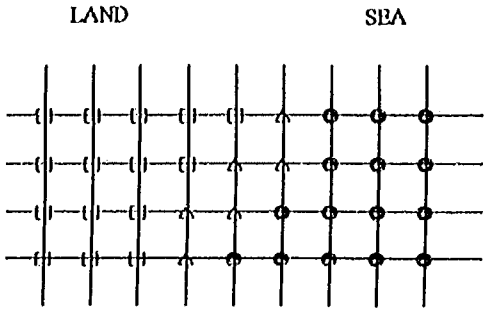
For the tsunami propagation graphic, the surface model is employed. **Figure 2** shows the arrangement of computation grids. The computed water surface elevation is given on

the corresponding grid. The grid in the land is allocated the value of -99m as dummy. The vertical wall may be formed on the sea-land boundary without any modification. To protect the formation of vertical walls, we give an averaged water level to the land grid one mesh inside of the boundary. The averaged water level is calculated employing the water levels on the surrounding grids. The moving boundary of shore line is computed as the cross line of the sea polygons and the land polygons. The height data of land is derived from the 'Numerical Map (250m mesh)' published by the Geographical Survey Institute, Ministry of Construction.

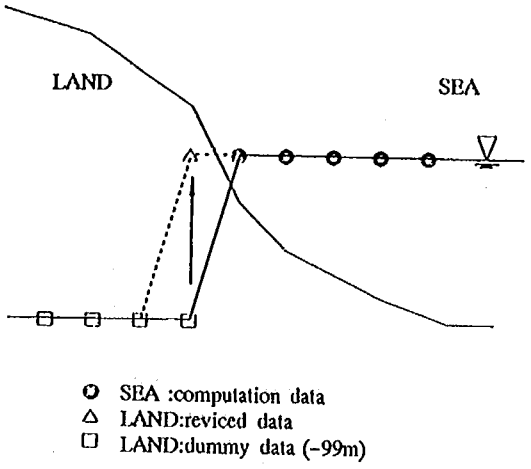
3.TSUNAMI SIMULATION

In the tsunami simulation, the initial distribution of water surface elevation is assumed to be same to the sea bed rise by an earthquake. The sea bed rise by earthquake is computed from the land fault corresponding to the specified earthquake by using the elastic body model(Manshinha and Smylie, 1971).

The Nankai Earthquake Tsunami is adopted as the model tsunami in the computer graphic. The Nankai Earthquake Tsunami occurred in 1946 and caused the heavy damages to the south-west Japan. Especially,



(1) Arrangement of computer grid



(2)Imaginary water leven at sea-land boundary

Figure 2 Computation grid

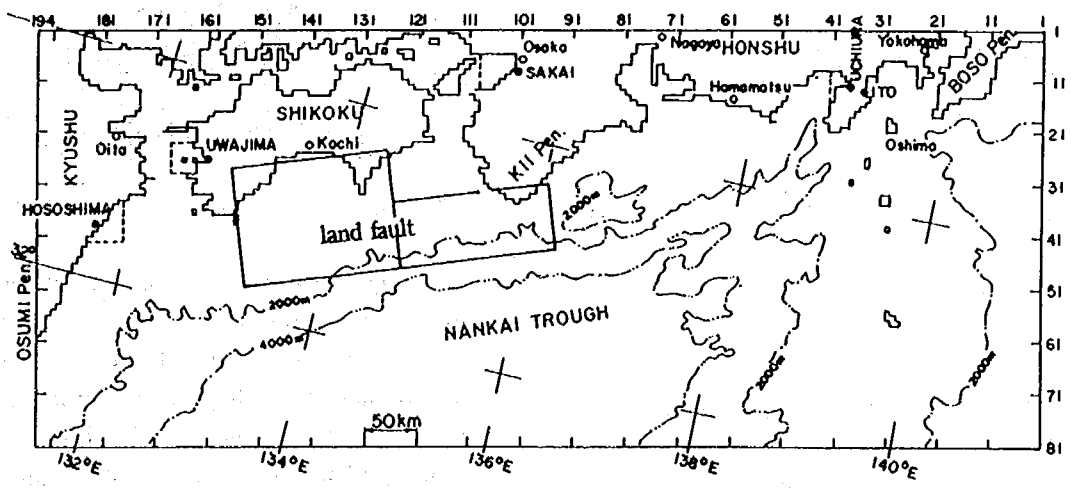


Figure 3 Failure of 1946 Nankaido Earthquake Tsunami

Kochi-prefecture in Shikoku island heavily suffered from the tsunami. About 1000 people were killed by the tsunami attack in Kochi-prefecture(Takayama and Hiraishi, 1986). Another Nankai earthquake occurred in 1854. Therefore, the return period of the Nankai earthquake is considered to be about 100 ~ 150year. A big tsunami may be generated again in near future in the offshore area of the south-west Japan.

A tsunami breakwater is under construction at the Suzaki port to protect the tsunami attack. The disaster prevention planning is seriously discussed to complete the hard and soft ware to protect the port. In the computer graphic, we reproduce the 1946 Nankai Earthquake Tsunami in the Suzaki port to make an image information for the disaster preven tion planning.

Figure 3 shows the location of land fault of 1946 Nankai Earthquake proposed by Aida(Aida,1981). Tsunami propagation is computed by resolving the finite difference expression for the continuous and momentum equations. The continuous and momentum equations of non-linear long wave are given by(Goto,1993),

Continuous equation

$$\frac{\partial \eta}{\partial t}+\frac{\partial M}{\partial x}+\frac{\partial N}{\partial y}=0 \qquad (1)$$

Momentum equation

$$\frac{\partial M}{\partial t}+\frac{\partial}{\partial x}\left(\frac{M^2}{D}\right)+\frac{\partial}{\partial y}\left(\frac{MN}{D}\right)+gD\frac{\partial \eta}{\partial x}+\frac{f}{D^2}MQ=0 \qquad (2)$$

$$\frac{\partial M}{\partial t}+\frac{\partial}{\partial x}\left(\frac{MN}{D}\right)+\frac{\partial}{\partial y}\left(\frac{N^2}{D}\right)+gD\frac{\partial \eta}{\partial y}+\frac{f}{D^2}MQ=0 \qquad (3)$$

where,

(x,y) : spatial coordinates on mean sea level
t : time
η : water surface elevation
h : water depth under mean sea level
D : total water depth (η +h)
g : gravity acceleration
M : flow flux in x coordinate axis
N : flow flux in y coordinate axis
Q : total flux M2 + N2
f : composed coefficient of energy loss and sea bed friction

The above fundamental equations are approximated in the Leap-frog finite difference method(Goto, 1993). The sea and land computation area is expressed by the grid topography in the finite difference method. The water surface elevation and flow flux on the computation grids are simulated with a specified time interval. The tsunami runup boundary is computed in Iwasaki and Mano model(Iwasaki and Mano,1979). **Figure 4** shows the computation area for the Suzaki-port. The grid distance in the port computation area is 50m and the time interval is 1s. The tidal level in computation is T.P.(Tokyo Bay mean sea level) +0.80m.

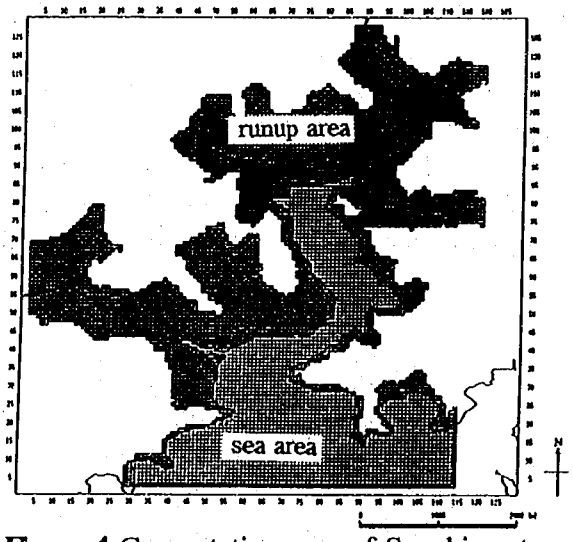


Figure 4 Computation area of Suzaki port

Figure 5 shows the simulated tsunami profile at the mouth of Suzaki port. The period of Nankai Earthquake Tsunami is about 40 ~ 60min, and it is longer than the tsunami like the 1983 Nihonkai-Chubu Earthquake Tsunami(Tanimoto et.al.1983) and the 1993 Hokkaido Nansei-oki Earthquake Tsunami (Takayama et.al.,1994) which are caused in the

Japan-sea. The maximum tsunami height at the mouth of Suzaki port is 2.30m.

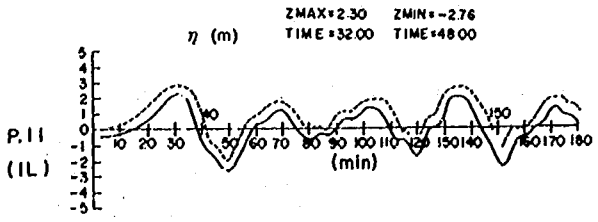


Figure 5 Tsunami profile at port entrance

4.GRAPHIC IMAGE

One of the characteristics of the developed computer graphic system is that the location and height of the observer's view point is changeable any time. The virtual image is observed only at the front of the wide screens. In the report we introduce some copies of the virtual reality images of the tsunami presented on a screen. **Figure 6** shows the observation points in the Suzaki port. **Point 2** is located in the most urban place in the city. The main buildings like the city office are concentrated in the vicinity of **Point 2**. **Point 1** shows the construction site of the tsunami breakwater. **Point 3** and **4** are located in the innermost part of the port where the tsunami height may become the highest. The wide agriculture field is spreading behind **Point 4**. Therefore, the height above sea level at **Point 4** is low and the tsunami overtopping sea walls may flood into the wide area.

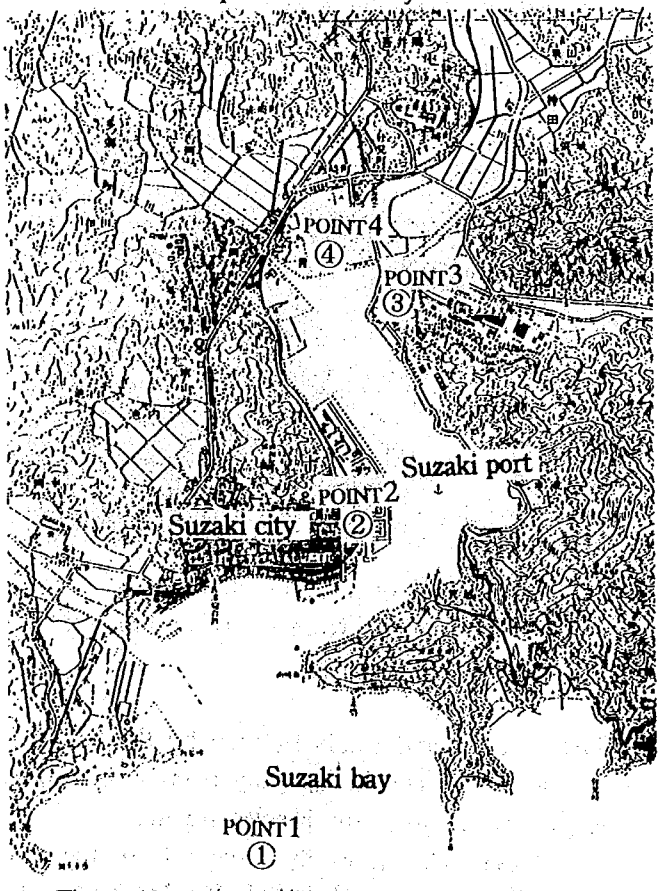


Figure 6 Observation point in Suzaki-port

Figure 7 shows the bird's eye view image from **Point 1**. The height above sea level of the view point is 500m. The time is about 40min after the earthquake shaking. The east part of the city area is flooded by the first wave of the tsunami.

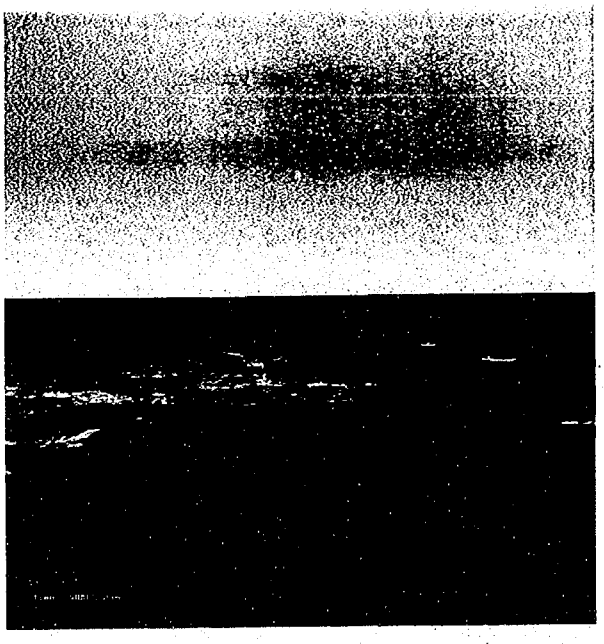
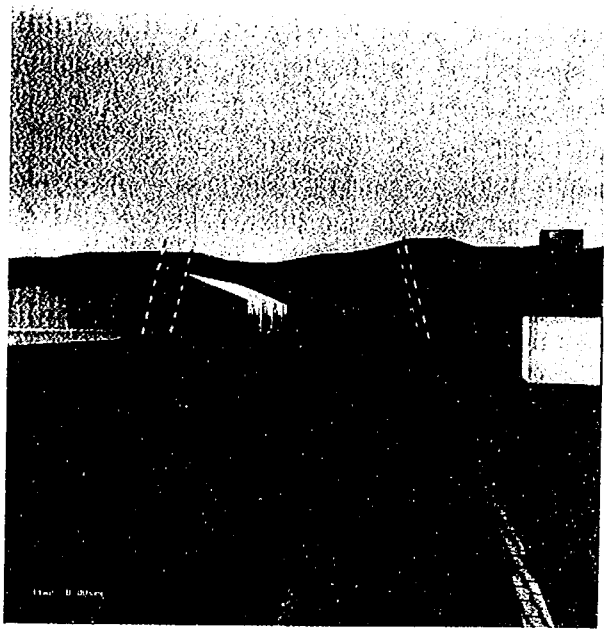
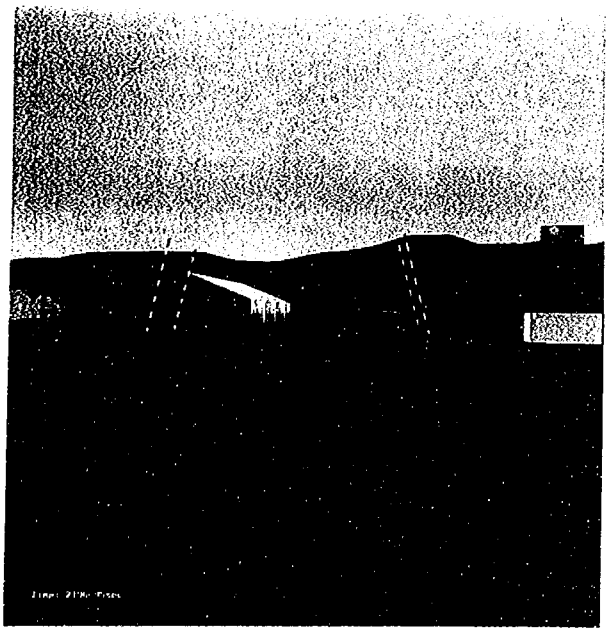


Figure 7 Bird's eye view from Point1

Figure 8 shows the virtual reality image of an observer standing on a road near **Point 2**. **Fig.8(1)** shows the image before the earthquake. He is looking at the dry road, a monument at the right, a crossing forward and so on. **Fig.8(2)** shows the observed scenery 35min after the shaking. The road is perfectly flooded by the runup tsunami and the lower part of the storehouse and monument are under water level. The image is effective to expect



(1) before earthquake



(2) on tsunami flood

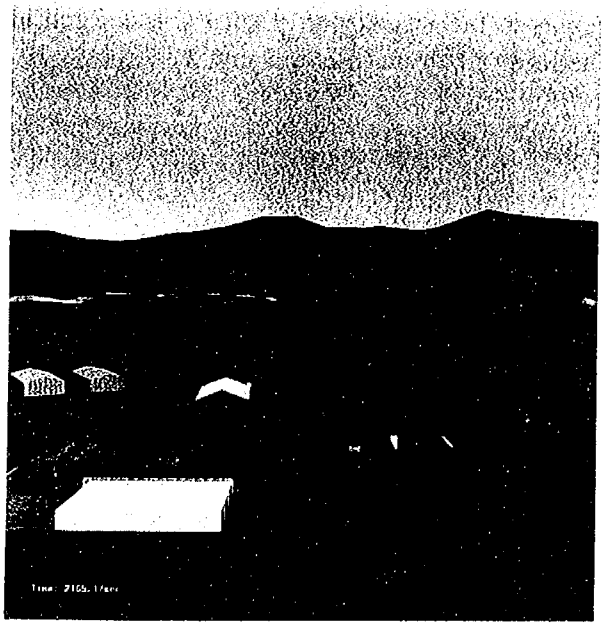
Figure 8 Image on a road of Point2

the damage by the tsunami runup.

Figure 9 shows the image from the observer on the top floor of a city hall at **Point 2** with height of 50m. **Fig.9(1)** and **(2)** is corresponding to the image of the urban area before and after tsunami attack respectively.



(1) before earthquake



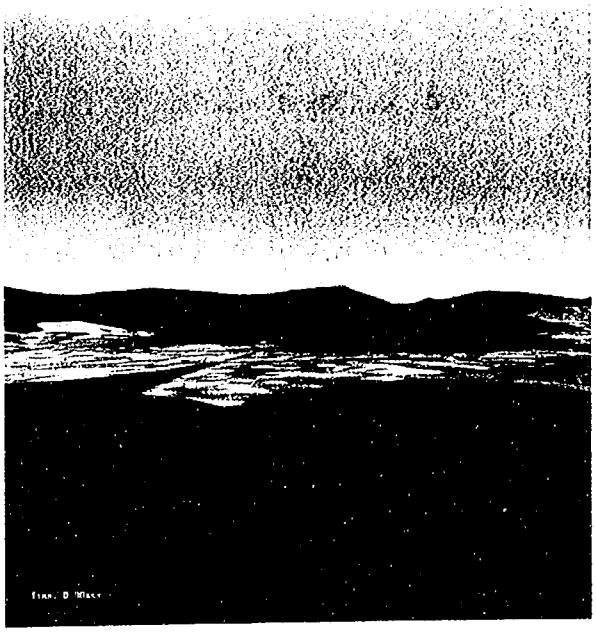
(2) on tsunami flood

Figure 9 Image from top of building at Point2

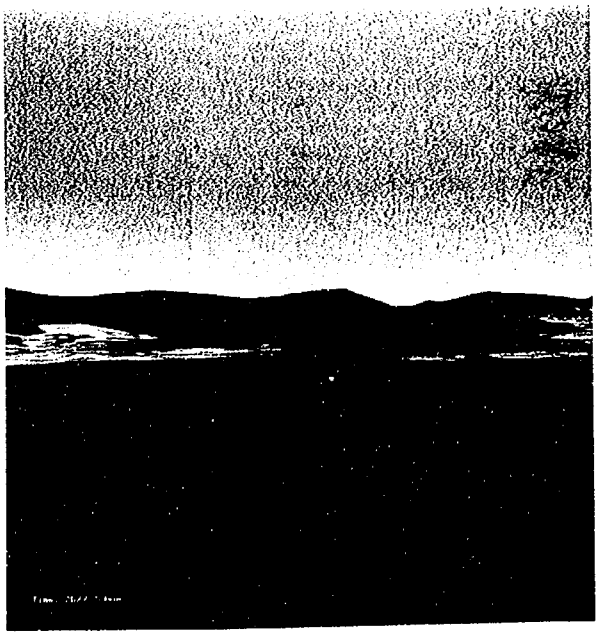
The grounds and roads flooded by the tsunami are observed. The image may become effective to give an alarm to the local residents.

Figure 10 shows the image from the top of a hill located at **Point 3**. **Fig.10(1)** and **(2)**

shows the image of the agriculture field before shaking and after tsunami invasion. We are able to understand that the wide area behind the low sea wall may be invaded by the overtopping tsunami. **Figure 11** shows the image from the observer standing on the low field at **Point 4**. He is facing to the port and watching the tsunami propagation at **Fig.11(1)**. When the water level becomes high, the height of his view point may become lower than the tsunami height. **Fig.11(2)** shows the image from the view point under water. Therefore, we are able to exam the tsunami damage and behavior in a port from any angles by applying

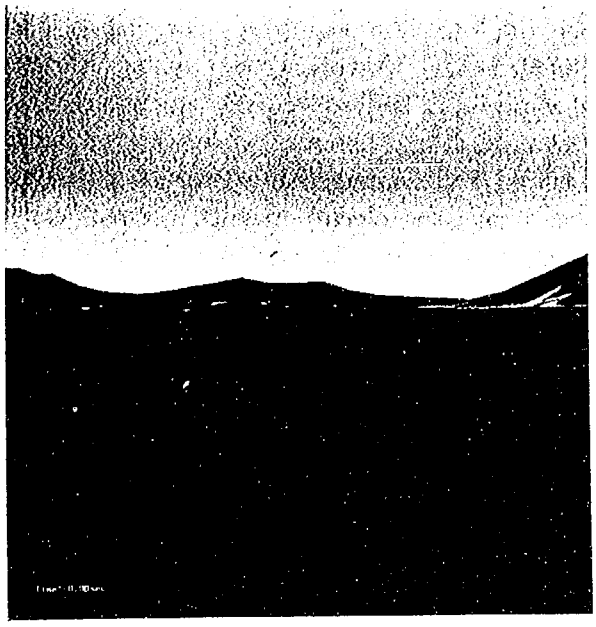


(1) before earthquake

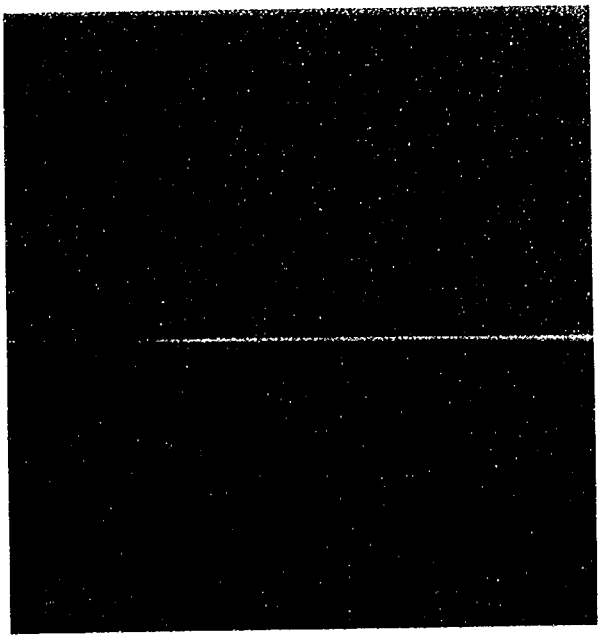


(2) on tsunami flood

Figure 10 Image of field from Point3



(1) facing Suzaki port before tsunami attack



(2) after tsunami attack

Figure 11 Image from Point4

the virtual reality image graphic system.

5.OBSERVATION OF TSUNAMI

For preservation of the tsunami disaster, it is important to investigate the behavior of real tsunamis.The Port Bureau, Ministry of Transport is applying the NOWPHAS (Sugawara, Nagai et.al.1994) wave observation network to the tsunami observation. In NOWPHAS network, the water surface elevation and current velocity are observed as real time data at about 50 points around Japan islands. The combination sensor of ultrasonic wave gage and electro-magnetic current meter is employed to get the wave data.

Figure 12 shows the tsunami profile observed at Kobe port in the Hyogo-ken Nanbu Earthquake this year. The change of water level by tsunami is clearly observed in the wave gage. **Figure 13** shows the tidal level observed at the Kansai international airport island on Jan.17. The spike noise on 5:46 may be caused by the earthquake. The observed amplitudes of tsunami are 2~3cm. The continuous observation is inevitable to get the detail information of tsunami propagation in the sea.

6.CONCLUSIONS

The newly developed computer graphic system is effective to the following items;

(i)Total image of tsunami damage in a specified port.

(ii)Flood condition by tsunami in a town area

(iii)Estimation of invasion condition of tsunami in a low ground.

REFERENCES

Aida,I.(1981):Numerical experiments for the tsunami generated off the coast of the Nankaido district, *Bull. of Earthquake Research Institute*, Vol.56,pp.731-740.

Goto,C and K.Sato(1993):Development of tsunami numerical simulation system for Sanriku Coast in Japan, *Report of Port and Harbour Research Institute*, Vol.32, No.2, pp.4-44.

Hayafuji,Y. et.al.(1990):An application of ship maneuvering simulator to port and harbor planning, *Technical Note of P.H.R.I.*, No.686, 41p.

Iwasaki,T. and A.Mano(1979):Numerical simulation of two-dimensional tsunami runup by Euler's coordinates, *Proc. of 26th Conference of Japanese Coastal Engineering*, pp.70-74.

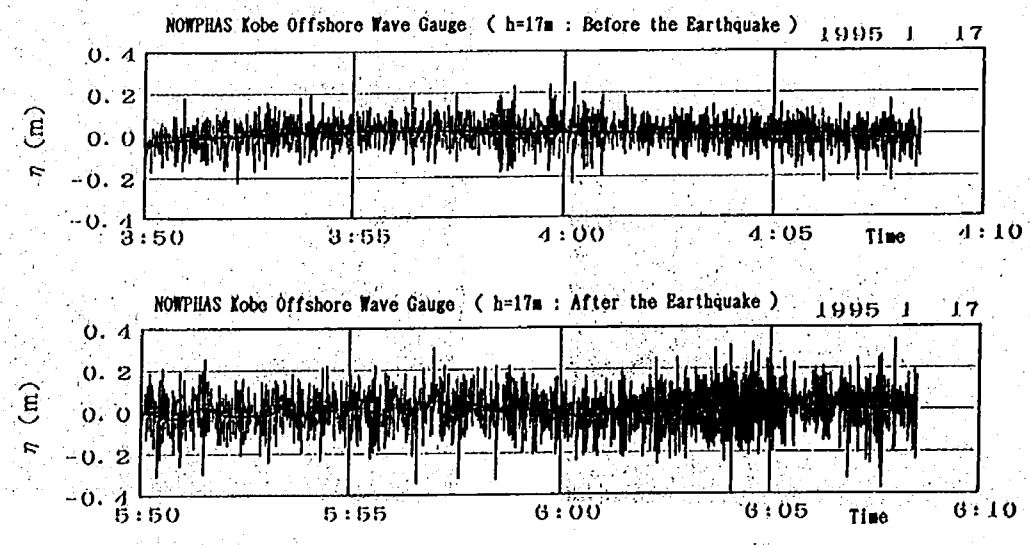


Figure 12 Tsunami profile observed in Kode(Jan.17,1995)

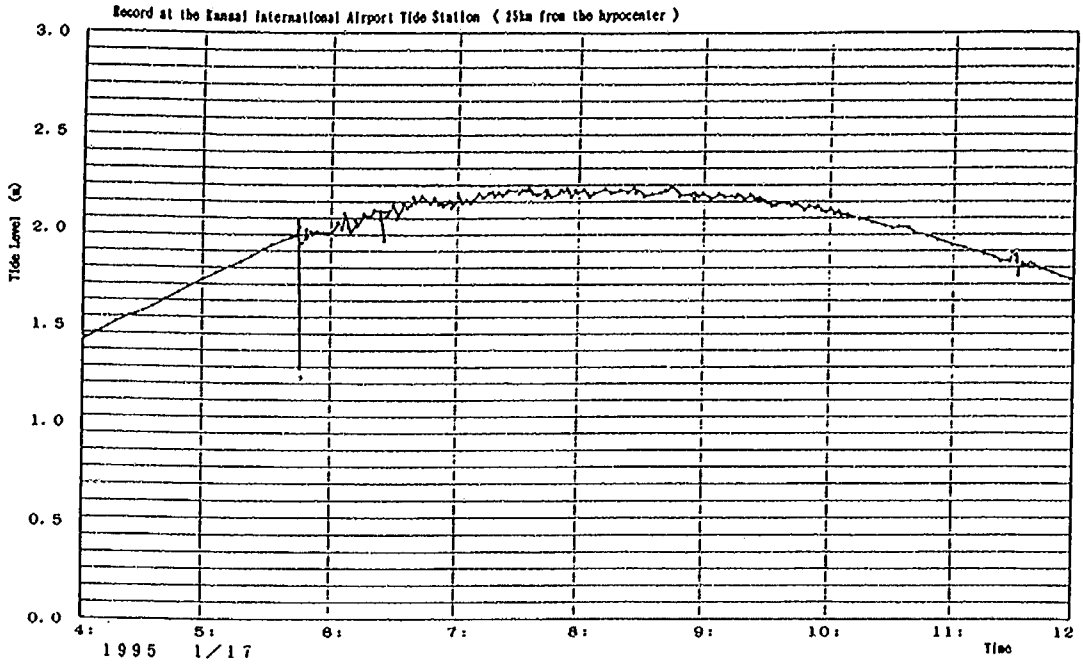


Figure 13 Change of tidal level observed at Kansai International Airport

Manshinha,L. and D.E.Smylie(1971):The displacement field of inclined faults, *Bull. of the Seismological Soc. of America*, Vol.61, No.5, pp.1433–1440.

Sugawara,K.,T.Nagai,N.Hashimoto and K.Shimizu(1994):Summary of the NOWPHAS wave observation facilities, *Technical Note of P.H.R.I.*,No.782,326p.

Takayama,T. and T.Hiraishi(1986):Hydraulic model tests on tsunami at Suzaki-port, *Technical Note of P.H.R.I.*,No.549,131p.

Takayama,T. et.al.(1994):Field investigation of the tsunami caused by 1993 Hokkaido Nansei-oki Earthquake,*Technical Note of P.H.R.I.*,No.775,225p.

Tanimoto,K.et.al.(1993):Field and laboratory investigation of the tsunami caused by 1983 Nihonkai Chubu Earthquake, *Technical Note of P.H.R.I.*,No.470,299p.

TSUNAMI RECONNAISSANCE PROCEDURES

by

Harry Yeh

ABSTRACT

Recent tsunami surveys were conducted by multi-national tsunami reconnaissance teams mainly consisting of Japanese, U.S. and the local scientists. The organization and arrangement of the survey team have been made in a very informal manner. The survey procedures that took place and some typical results based on the surveyed data are discussed. Based on the experience, some improvements of the survey procedures are proposed, emphasizing on multi-national cooperation with multi-disciplanary personnel.

KEYWORDS: Tsunami, Survey, Runup, Reconnaissance, Measurement.

1. INTRODUCTION

There have been six major tsunami disasters within the last three years: first in Nicaragua (1992), then Flores Island, Indonesia (1992), Okushiri Island, Japan (1993), East Java, Indonesia (1994), the South Kuril Islands (1994), and most recently in Mindoro Island, Philippines (1994). All events were surveyed and documented by multi-national tsunami reconnaissance teams, e.g. Abe (1993) and Satake et al. (1993) for Nicaragua, Tsuji (1993) and Yeh et al. (1993) for Flores, Shuto (1994) and Hokkaido Tsunami Survey Group (1993) for Okushiri, Yeh et al. (1995) for Shikotan. This frequent occurrence of major tsunamis in such a short time is remarkable, especially considering the fact that before the Nicaragua tsunami, there had not been a major tsunami for more than nine years: the last major tsunami event was the 1983 Nihonkai-Chubu tsunamis. In the case of the 1983 Nihonkai-Chubu tsunamis, the tsunami survey was conducted by the Japanese scientists alone, although the US reconnaissance team was sent a few months later (Hwang and Hammack, 1984). Korean coasts and Russian (then, USSR) coasts were surveyed independently by the scientists of each country.

The first international cooperative tsunami survey team was formed in a rather informal manner immediately after the 1992 Nicaragua tsunami. Since then, the five subsequent tsunamis were surveyed with international team cooperative efforts. Increasing trends of international cooperation must be the result of the recent advancement of world-wide communication systems, especially the development of the INTERnet system, improvement of transportation, and global political stabilization. Even if an earthquake occurred in a remote area, recent advancement of instrumentation and communication permit us to obtain fairly accurate information within a few hours (perhaps even minutes) through the INTERnet e-mail system. If the civil war had still existed in Nicaragua, the tsunami survey would have not been possible. Since the end of the US-USSR Cold War, more areas that used to be inaccessible can now be entered by scientists to conduct tsunami surveys, e.g. the South-Kuril Islands. Note that the tsunami effects of the 1983 Nihonkai-Chubu tsunamis on the Far-East-Region (USSR) coasts were very sketchy at that time and, due to military-security reasons, no quantitative data were presented by the Soviet scientists during the Tsunami Symposium that was held in Victoria, Canada in 1984.

This paper presents the recent tsunami survey results describing what we measured, observed and accomplished. Based on that experience, some improvements of the survey procedure are proposed, with an emphasis on international cooperative practice.

Professor
Department of Civil Engineering
University of Washington
Seattle, WA 98195
U.S.A.

2. INTERNATIONAL TSUNAMI SURVEY

THE 1992 NICARAGUA TSUNAMIS (MS 7.2):

This was the first major tsunami to cause substantial damage and casualties since 1983 when the Nihonkai-Chubu Tsunami struck the west coast of Honshu, Japan. As a result, in a very informal way, an ad hoc international tsunami survey team was formed for the first time. First, Japanese scientists, with leader Dr. Kuniaki Ade, formed their own team consisting of seismologists, tsunami specialists, and geophysicists. Meanwhile, the United States government agencies attempted to organize a U.S. team. Without clear jurisdiction and funding structures, this attempt did not materialized except for sending three scientists from the U.S. Geological Survey. Several U.S. scientists in academia approached the Japanese colleagues directly for a possible cooperative survey. Interestingly, this was also done independently by two separate groups of U.S. scientists; one group contacted Dr. Katsuyuki Abe of the University of Tokyo and the other group contacted Dr. Shuto of Tohoku University. In the end, four U.S. scientists from academia joined the Japanese scientists, thus forming the first "international" survey team.

A pre-survey meeting with the local agency, INETER (Instituto Nicaraguense de Estudios Territoriales), was arranged by the Japanese team. All the parties, including those from the U.S. government agencies, attended this meeting which essentially became the Nicaragua-Japan-U.S. "international" pre-tsunami-survey meeting.

The actual tsunami survey was conducted by the international team consisting of six Japanese, two Nicaraguan, and four U.S. scientists. At the same time, three scientists from the U.S. Geological Survey mainly surveyed seismological strong motion effects and building damage. One scientist from the U.S. National Oceanic and Atmospheric Administration (NOAA) conducted an aerial tsunami survey and one independent scientist from the U.S. examined tsunami damage and social effects. Six months later, another survey party consisting of two U.S. and one Canadian scientists visited the tsunami sites for further runup survey. Since then, the U.S. geologist who had been a member of the "international" survey team returned to the sites twice to examine the effects of tsunami sediment deposits in conjunction with the paleo-tsunami evidence elsewhere. Another U.S. scientist, also a member of the "international" team, returned to the sites for a detailed bathymetry survey. After this event, NOAA established an e-mail bulletin board called 'Tsu-Nica' to exchange tsunami-related information. Later on, the name of the bulletin board was changed to the more generic name: the 'Tsunami' Bulletin Board. This Nicaragua event is now considered to be the corner stone of tsunami survey practice in terms of the international cooperation and establishment of the e-mail bulletin board.

THE 1992 FLORES ISLAND TSUNAMIS (MS 7.5):

The international survey team was formed in a very informal manner, just like the team for the Nicaragua tsunamis. First, the Japanese officially formed a survey team under leader Dr. Y. Tsuji. Three U.S. scientists in academia contacted Dr. Tsuji and the local agency (National Meteorology and Geophysics Agency or MGA) in Jakarta. Most of the communications were made through fax, although the e-mail 'Tsu-Nica' Bulletin Board was also used between Japan and the United States. Another attempt was made to form an official U.S. survey team but this never materialized. However, four Indonesian, one British, one Korean and three U.S. scientists joined the Japanese team to form a truly international (five nations) survey team. Because of strong economical and political ties between Japan and Indonesia, prior to the tsunami survey, an immediate reconnaissance was made by the Japanese Government special team that was formed to provide humanitarian aid.

Over a year later, the tsunami attack sites were revisited by the U.S. team, mainly to investigate submarine landslide effects. A few months after this U.S. team visit, the Japan-U.K. international team members also revisited the sites to investigate tsunami sediment deposits.

THE 1993 OKUSHIRI TSUNAMIS (MS 7.8) :

An official U.S.-Japan cooperative survey team was formed based on the UJNR program. It consisted of three U.S. and two Japanese members. Besides this UJNR team, other Japanese teams conducted tsunami surveys on Okushiri Island and in Hokkaido. They were the Tohoku University team, the University of Tokyo team, the Public Works Research Institute team, the Port and Harbor Research Institute team, the Hokkaido Development Bureau team, and the Japan Meteorological Agency team. Evidently, the survey of this event was very intense, and many valuable data were obtained. Important information were conveyed through the e-mail 'Tsunami' Bulletin Board: note that the name of the bulletin board was changed from 'Tsu-Nica' to 'Tsunami' in the fall of 1993.

THE 1994 JAVA TSUNAMIS (MS 7.2) :

The formation of the international survey team, with the leader Dr. Tsuji, was very informal, consisting of twenty-one Indonesian, five Japanese, two U.S., one Thai, and three Italian scientists. Prior to the participation of the International survey team, Indonesian and three U.S. scientists conducted a preliminary survey, reported through the e-mail Tsunami Bulletin Board.

THE 1994 SHIKOTAN TSUNAMIS (MS 8.1) :

This was the only event in which the Japanese team did not participate. The team was formed with fifteen Russian scientists and two scientists from the U.S. Many communications were made via e-mail Tsunami Bulletin Board. The actual tsunami survey plan was made at the Institute of Marine Geophysics and Geology (IMGG), Sakhalin, Russia. Some locations could not be surveyed due to lack of transportation. The preliminary survey results were posted on the e-mail Tsunami Bulletin Board immediately after the survey.

THE 1994 MINDORO TSUNAMIS (MS. 7.0) :

Again, an informal international tsunami survey team was formed with the aid of the e-mail Tsunami Bulletin Board. The team consisted of three members from the Philippines, two from the U.S., two from Thailand, two from Japan, and one from Korea.

3. SURVEY PROCEDURE

Although case-by-case details were different in the aforementioned six tsunami surveys, the following general procedure was taken for all the surveys.

Pre-Survey Data Collections and Preliminary Modellings:

Prior to the survey, preliminary information on tsunami damage and data were collected utilizing all available means. This data gathering included compiling the information provided by local agencies and local and international news media (e.g. NHK, BBC, Reuters). Immediate preliminary surveys were often made by local scientists and the information was disseminated through the e-mail Tsunami Bulletin Board: e.g. in the case of the Java tsunamis, a survey was conducted by scientists from the National Meteorology and Geophysics Agency (MGA) in Jakarta. In the case of the Flores tsunamis, an emergent team for humanitarian aid was dispatched by the Japanese Government. For the Shikotan tsunamis, the scientists from the Institute of Marine Geophysics and Geology reported the preliminary runup data. Meanwhile, based on preliminary seismic data (e.g. earthquake magnitude, fault parameters, aftershock distributions, rigidity of the earth crust), numerical simulations were performed. Numerical models used for this purpose were typically based on the linearized shallow-water-wave theory without modelling detailed runup on dry beaches. Instead the model assuming the presence of fictitious vertical walls offshore, typically along the 10 m deep contour. Based on the preliminary numerical simulations and reports from news media and local agencies, the hardest hit areas and the coverage of the planned tsunami survey were identified.

Pre-Survey Meeting:

For the final planning, a pre-survey meeting was normally held at the local agency, for example, at INETER (Managua, Nicaragua) for the 1992 Nicaragua tsunamis, at MGA (Jakarta, Indonesia) for the 1992 Flores tsunamis and the

1994 Java tsunamis, and at IMGG (Yuzhuno-Sakhalinsk, Russia) for the 1994 Shikotan tsunamis. The main purposes of the surveys were to measure tsunami runup distributions, to observe tsunami effects on natural and manmade environments and structures, to collect any instrumental measurements such as tide gages, to interview local residents for tsunami attack conditions including its arrival time and socio-economical impacts to the community, and to examine the effectiveness of any existing tsunami warning systems and preparedness efforts. It is important to keep in mind that a primary survey purpose is to learn from the disasters in order to mitigate future tsunami events.

Transportation:

It is sometimes formidable to reach the tsunami affected sites. Most of the time, automobiles with four-wheel drives are sufficient means for transportation. However, boats, special military ground vehicles (Fig. 1) and helicopters (Fig. 2) are often needed and the cooperation of government military agencies are often critical to the survey.

Tsunami Runup Survey:

Tsunami runup heights and distances were measured with simple surveying hand-levels, stuffs, and tapes. Vertical heights of runup marks were measured from the mean sea level at the time of the measurements by noting the measurement time and location (Fig. 3). After the survey, the measured runup heights were converted to the values of runup at the time of tsunami attack: this conversion was made based on the tide levels at the time of measurement and at the time of tsunami attack. The measurement locations were recorded with the portable Global Positioning System (GPS) together with the topography map. Because of the many uncertainties involved in measured data, an approximate 25 cm error in runup heights is acceptable. Tsunami runup marks were identified by the following conditions. Flooding water marks on a structural wall are considered to be reliable evidence of runup height. Accumulated marine-origin objects are considered to be another type of reliable runup marks(Fig. 4). Other types of runup marks are scratch marks on tree trunks caused by the collision of water-born objects (Fig. 5), and marine-origin vegetation (e.g. seaweed) on tree branches (Fig. 6). The runup distances from the shoreline were usually measured with a surveying tape (100 m long). Again, this type of survey does not require high accuracy. In addition to the runup marks, flow directions for both runup and rundown processes were inferred from the direction of tree falls (Fig. 7) and patterns of debris accumulations.

Interviews:

Interview procedure and a systematic questionnaire were developed and has been improved by Dr. Tsuji of Tokyo University and Dr. Kawata of Kyoto University. None the less, further improvement in this area would evolve by including input from other scientists.

Post-Survey Briefing:

After the survey, the results and recommendations were presented at the local host agency. This meeting is important for the local government who attempts to mitigate future tsunami disasters by learning lessons from the present event. The information and data reported by the scientists immediately after the event are reliable and valuable for the damage assessment.

4. POST-SURVEY ANALYSES

A wide variety of data analyses were performed based on the collected data and information. The following are some examples that might be useful to consider when the next tsunami survey is planned.

Measured runup height distributions and flow patterns are essential information to understand tsunami phenomena. By utilizing numerical simulation models, the initial source pattern can be identified by matching the measured runup distribution. (This practice is considered to be the inverse problem of tsunami runup: i.e. given the runup distribution, the initial condition of tsunami generation is computed.) With the identified initial source pattern, the earthquake mechanism is often clarified. This type of exercise was conducted for almost all tsunami events by the Tohoku University group and the

U.S. group at the University of Southern California. For example, the deformations of sea bottom associated with the 1983 Nihonkai Chubu earthquake and the 1993 Okushiri earthquake are now understood to have very complex patterns (Shuto, 1991; Takahashi et al., 1994). The 1992 Nicaragua earthquake was identified as a so-called tsunami earthquake (Kanamori and Kikuchi, 1993).

Detailed runup distribution patterns often reveal the tsunami characteristics. For example, locally high anomalous runup in Flores Island led us to suspect the occurrence of massive submarine landslides that generated waves. Later on, this conjecture was verified by a bathymetry survey (Plafker, 1995). Fairly uniform runup heights along the south side of Shikotan Island and much smaller runup along the north side led to the estimation that the tsunamis of the 1994 Shikotan earthquake had their wave periods of approximately 20 minutes (Yeh, et al., 1995).

The disaster on Babi Island (the 1992 Flores tsunamis) received special attention and, in fact, was discussed prior to the survey. Observations of the topography maps and bathymetry charts showed its unique location and simple island shape: the island has a cone shape with a steep beach surrounding it. Early reports to the speculation that the cause of disaster was 1) tsunami focusing of the reflected waves from Flores Island, as seen in Fig. 8, or 2) trapping wave energy around the island. It is well known that a conical-shaped island is capable of trapping quasi-steady oscillatory waves around an island due to wave refraction and that trapping occurs when the wavelength is comparable to the island dimension, although the behavior of transient waves like tsunamis were unknown at that time. Based on the runup measurements, subsequent detailed numerical simulations for a cone-shaped island and large-scale laboratory experiments, the cause of total disaster, where 263 people were killed by the tsunamis, can now be explained (Yeh, et al., 1994). When the tsunami hit the island, the tsunami split in two. The split tsunami wrapped around the island and joined to create a new, larger wave that crashed into the wave-shadow side of the island (Fig. 8).

Another anomalous runup which was identified by the survey at Hamatsumae on Okushiri Island is explained from the results of numerical and laboratory experiments (Tanaka et al., 1995). Not only wave refraction but also the effects of wave dispersion were found to have enhanced the tsunami runup heights near Hamatsumae. The wave dispersion could have been triggered when the tsunami propagated around the southern tip of Okushiri Island, where the water is shallow.

In addition to obtaining the data for the tsunami runup heights and flow patterns, tsunami surveys provided us with many important information that might be useful for future disaster mitigation. Figure 9a and b show the contrast of houses along the beach of El Popoyo, Nicaragua. Almost all beach houses were destroyed and washed way by 5 m high tsunamis, as shown in Fig. 9b. Because there was no strong ground shaking, all damage was due solely to tsunamis. Two quite dissimilar structures (Fig. 9a) survived: one made of very rigid concrete blocks, and the other made of wood supported with extremely flexible slender columns. Evidently, slender columns are capable of withstanding tsunami flows. This appeared to hold true in many cases. For example, trees often remained standing while nearby houses were totally destroyed in El Transito, Nicaragua.

Scouring effects of tsunamis were often observed. Figure 10 shows the approximately 1.6 m step formation on the beach due to tsunami scour at Rajekwesi, East Java, during the 1995 Java tsunami survey. Similar beach scouring effects were found in Aonae, Okushiri Island (Fig. 11).

Tsunamis are also often capable of transporting rocks and boulders, as well as sediments. Figures 12a, b, and c show that, respectively, a beach rock was transported at El Popoyo, Nicaragua, large corals were transported at Riangkroko, Flores (for a scale reference, note a person standing at lower left corner in Fig. 12b), and another large beach rock was transported near Monai, Okushiri Island. These types of information and data are important not only for future prevention of beach scouring and structure damages, but also for the assessment of geological evidence of prehistoric tsunami events.

Another remarkable tsunami/earthquake effect was discovered in the 1992 Flores tsunami survey. Several extremely large subaqueous slumps were observed, as shown in Fig. 13, and tsunami runup heights measured in the vicinity of slumping were much higher than those measured several kilometers away. As mentioned earlier, this observation led us to conjecture that the high tsunami runup was caused by the waves generated by the slumping. Also this gave us a typical example of the fact that significant geomorphologic changes are often caused by extreme events.

Observations of land uplift and/or subsidence were often made during the survey. Such data collected in Flores Island and Okushiri Island gave important information to determine the mechanisms of the earthquakes. Collection and retrieval of tsunami records such as tide gage records are also an important task for the tsunami survey. Figure 14a shows the tide gage record in the Malokurilskaya Bay, Shikotan Island. The data after removing astronomical tides are shown in Fig. 14b which displays the evident mean water-level shift of 53 cm after the earthquake. The data presented in Fig. 14b are considered to be a rare quantitative recording of the land subsidence with the tide gage.

5. Closing Remarks

Based on my experience, the following comments with regard to tsunami survey procedure are made:

1. When a tsunamigenic earthquake occurs, the decision must be made whether or not a tsunami survey is necessary, especially one with international cooperative efforts. Considering the limited resources, the decision must be made prudently and correctly based upon all the available information of the event. In spite of some evidence of measurable tsunamis, tsunami effects associated with the 1993 Guam earthquake were not surveyed: perhaps because the event occurred immediately after the 1993 Okushiri event that caused significantly greater tsunami damage, hence the Guam tsunamis were simply overlooked.

2. For given seismic parameters, a quick numerical simulation should be made. The results will be used for the decision making for the tsunami survey discussed in item 1, as well as for the determination of the hardest hit areas, tsunami magnitudes, and the extent of affected areas. Both Japanese and U.S. scientists should make this type of simulation independently for the comparison purpose.

3. All the available information from local and international media must be analyzed prior to the survey. In the past tsunami surveys, the news media, in particular NHK and Reuters, contributed significantly to our scientific tsunami survey plans. Establishment of formal cooperative procedures between scientific community and news media is desirable. It is also preferable that local scientists commence their preliminary survey immediately after the earthquake with the preliminary survey results disseminated immediately, perhaps through the e-mail Tsunami Bulletin Board: the preliminary surveys done by the local scientists in the past have been extremely useful for planning the subsequent international tsunami survey.

4. Should a tsunami survey be performed with multi-national cooperation or by local scientists alone? Probably so, not only because scientists from abroad (in particular, Japanese scientists) have better technological facilities and are more experienced at carrying out the survey more effectively and efficiently than local scientists, but also, unlike other natural disasters (e.g. earthquake, hurricanes, tornadoes, droughts, floods), tsunamis can affect broader areas. The 1960 Chile tsunamis caused substantial damage in Hawaii and Japan; the 1964 Alaskan tsunamis greatly affected Hawaii and California. More recently, after the 1994 Shikotan tsunamis, Pacific wide tsunami warnings were issued and consequently large-scale evacuations from coastal zones in Hawaii and the U.S. west coasts were enforced, although the effects of tsunamis were minimal. Consequently, substantial economical damage resulted indirectly from the South-Kuril tsunamis. Tsunamis are not only the local problem but also potential problems for many distant countries. From this view point,

tsunami survey by a multi-national team is not only justified, but critical.

5. Financial supports for tsunami surveys must be identified. The past surveys described above were funded by Japan Monbusho, the U.S. National Science Foundation (NSF), Russian Fund of Basic Research, and others. All the U.S. NSF funds had not been allocated for the survey but the principle investigators of an existing NSF funded research were allowed to use monies for the emergent surveys: the monies had originally been allocated for their tsunami-related research purpose but not for the survey. This funding structure was only a temporary measure and will not be available in the future. For this reason, it is essential to identify the agencies willing to be responsive to the international tsunami survey supports. As a first step for the long-term survey plan, perhaps, the U.S. and Japan should establish a protocol for the international survey procedure and should identify the U.S. and Japanese agencies for the survey support.

6. The survey is not only for the maximum runup distribution measurements but also for other important observations: sediment transport, erosion effects, tsunami flow effects on man-made structures and natural geomorphologic features, social impacts, identifications of all salient features for the use of future mitigation. For this reason, the survey should be conducted by multi-disciplanary personnel including civil engineers with surveying experience, applied mathematicians, geologists, sedimentologists, seismologists, physical oceanographers, hydrodynamists, disaster-mitigation planners, and sociologists. The survey team should consist of a mixture of well-experienced scientists and those without tsunami-survey experience. Simple-but-important tsunami survey technique must be taught to as many tsunami-related scientists as possible to cope with quick response to future tsunami events. It is emphasized that a quick dispatching capability is crucial for the tsunami survey, in order to capture as much information as possible. Tsunami runup marks, destruction patterns, and other detailed tsunami-affected features can be disappear within a few weeks. For this reason, it is preferable that the survey be conducted within a month of the earthquake.

Assumption has been that once a major tsunami occurred, no large event would happened for a long time based on its probability based concept. Every time, I participated in the past tsunami survey, I thought that that was the last event for a long time. Because of this, the survey organization had been done in a temporary manner, anticipating to establish better survey procedures in later time. Apparently this assumption was wrong: six major tsunami events occurred in a little over three years. There is evidently no time for us to wait; serious discussions and actions for the survey procedures are urgently needed.

REFERENCES

Abe, K. (1993) *Research on the 1992 Nicaragua earthquake and tsunamis*. Report, 106 pp.

Hwang, L.-S. and Hammack, J. (1984) *The Japan Sea Central Region Tsunami of May 26, 1983: A Reconnaissance Report,* National Academy Press.

Hokkaido Tsunami Survey Group (1993) *Tsunami devastates Japanese coastal region,* EOS, 74, 417 & 432.

Kanamori, H. and Kikuchi, M. (1993) *The 1992 Nicaragua earthquake: a slow tsunami earthquake associated with subducted sediments*. Nature, 361, 714-716.

Plafker, G. (1995) personal communication.

Satake, K., Bourgeois, J., Abe, K., Tsuji, Y., Imamura, F., Iio, Y., Katao, H., Noguera, E., and Estrada, F. (1993) *Tsunami field survey of the 1992 Nicaragua earthquake,* EOS, 74, 145, 156-157.

Shuto, N. (1991) Tsunami Engineering Technical Report No. 8, 55 - 81.

Shuto, N. (1994) *Survey Data,* Tsunami Engineering Technical Report No. 11., 1 - 120.

Takahashi, T., Shuto, N., Ortiz, M., and Imamura, F. (1994) *The 1993 Hokkaido Nanse-Oki earthquake tsunami*, Proc. International Symposium: Waves - Physical and Numerical Modelling, Univ. of British Columbia, Canada, 456 - 465.

Tanaka, S., Sato, S., and Noguchi, K. (1995) *Propagation of Hokkaido-Nansei-Oki earthquake tsunami around Cape Aonae*, Second International Workshop on Wind and Earthquake Engineering for Offshore and Coastal Facilities, University of California at Berkeley.

Tsuji, Y. (1993) The Report of the Field Survey of the Flores Island Earthquake-Tsunami of December 12, 1992.

Yeh, H., Imamura, F., Synolakis, C., Tsuji, Y., Liu, P., and Shi, S. (1993) *The Flores Island tsunamis*, EOS, 74, 369, 371-373.

Yeh, H., Liu, P., Briggs, M., and Synolakis, C. (1994) *Propagation and amplification of tsunamis at coastal boundaries*, Nature, Vol. 372, 353-355.

Yeh,H., Titov, V., Gusiakov, V., Pelinovsky, E., Khramushin, V., and Kaistrenko, V. (1995) *The 1994 Shikotan Earthquake Tsunamis*, Pure and Applied Geophysics, (in press).

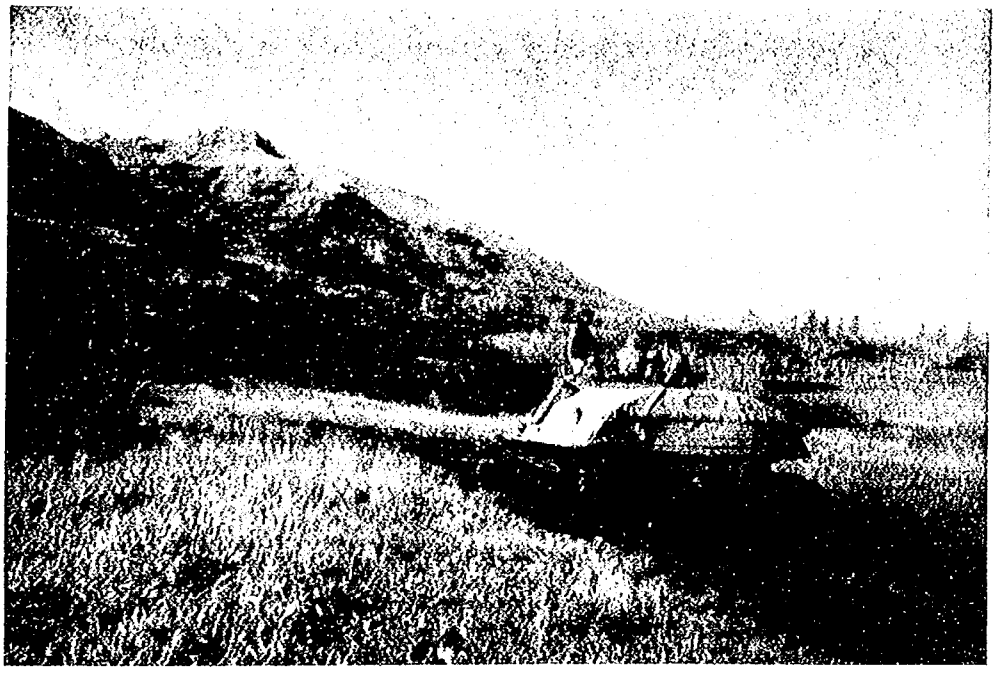


Figure 1. A Russian Army tank used for the 1994 Shikotan tsunami survey.

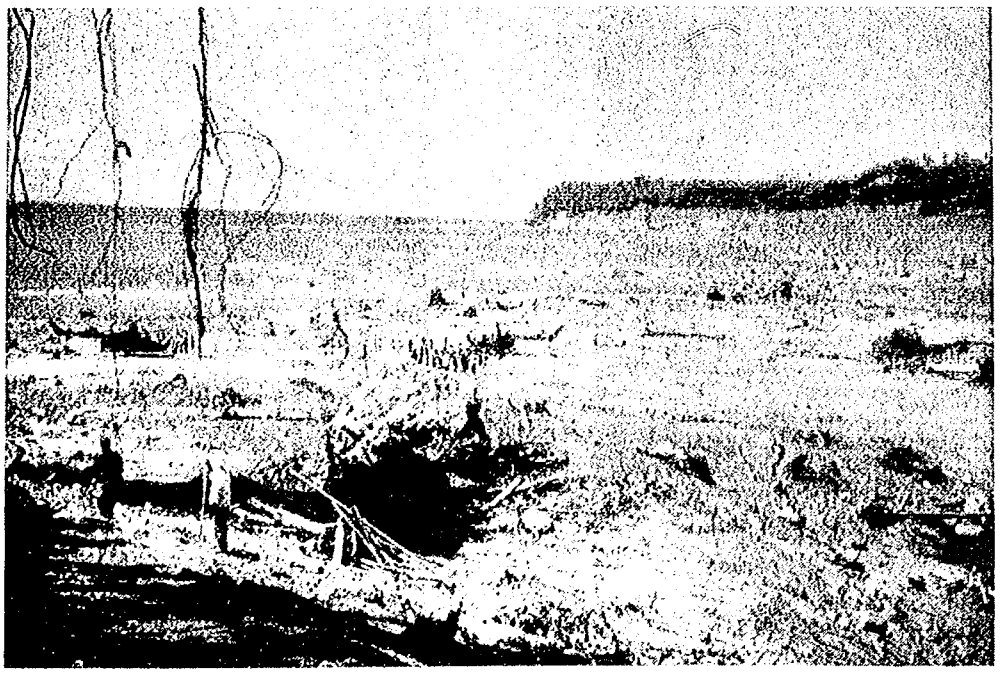


Figure 2. Indonesian military helicopters used for the 1992 Flores tsunami survey: the photo was taken at Riangkroko.

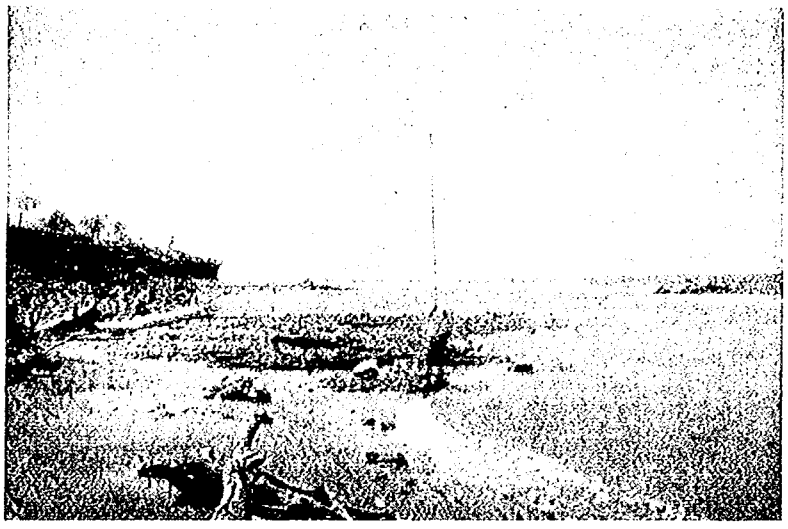


Figure 3. Tsunami runup heights were measured from the local mean sea level (Riangkroko, Flores Island).



Figure 4. Tsunami runup mark -- accumulated marine-origin objects (Babi Island, Flores).



Figure 5. Tsunami runup mark -- scratch marks on tree trunks caused by the collision of water-born objects (El Transito, Nicaragua).



Figure 6. Tsunami runup mark -- marine-origin vegetation (e.g. seaweed) on tree branches (Shikotan Island).



Figure 7. Flow directions were inferred from the direction of tree falls (Babi Island, Flores).

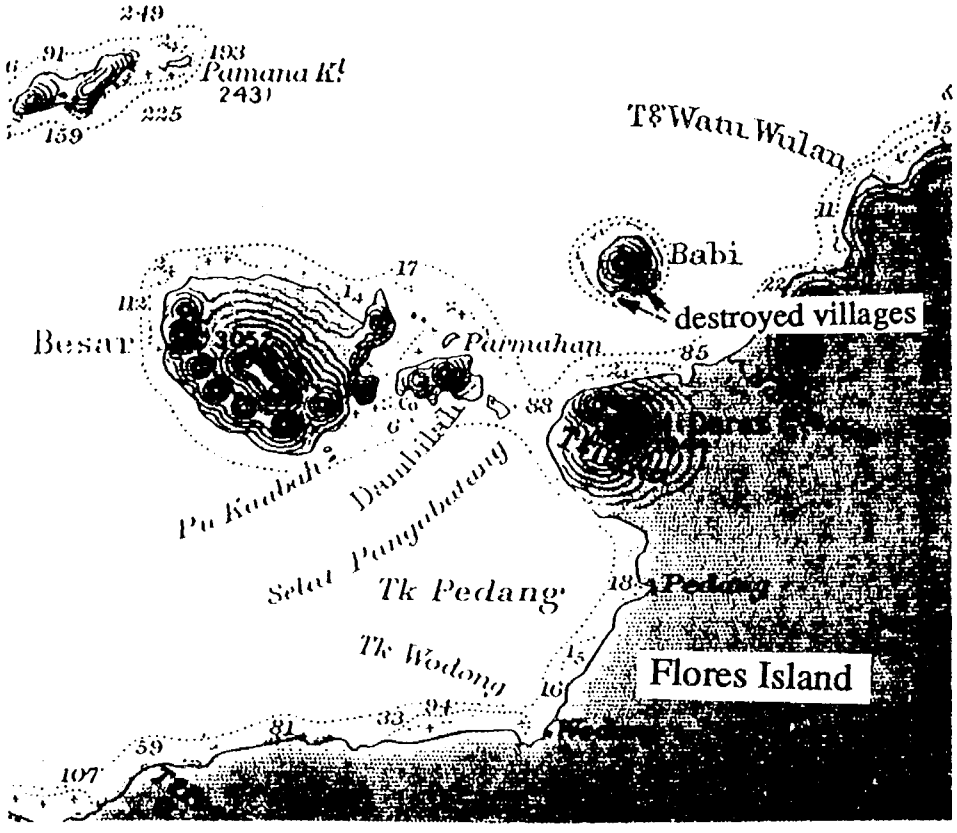
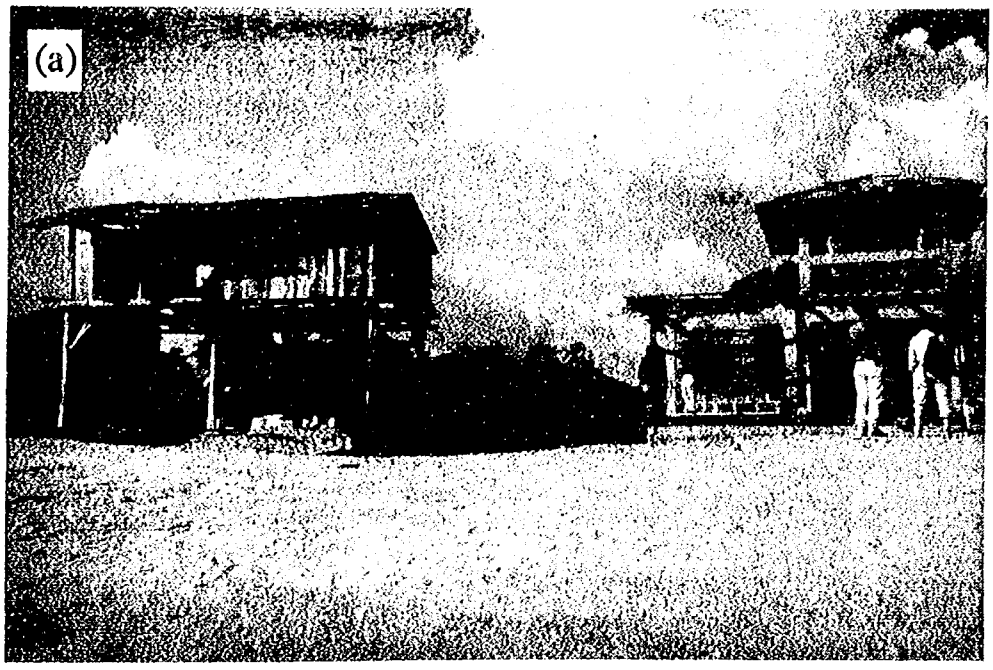


Figure 8. A map of Babi Island.



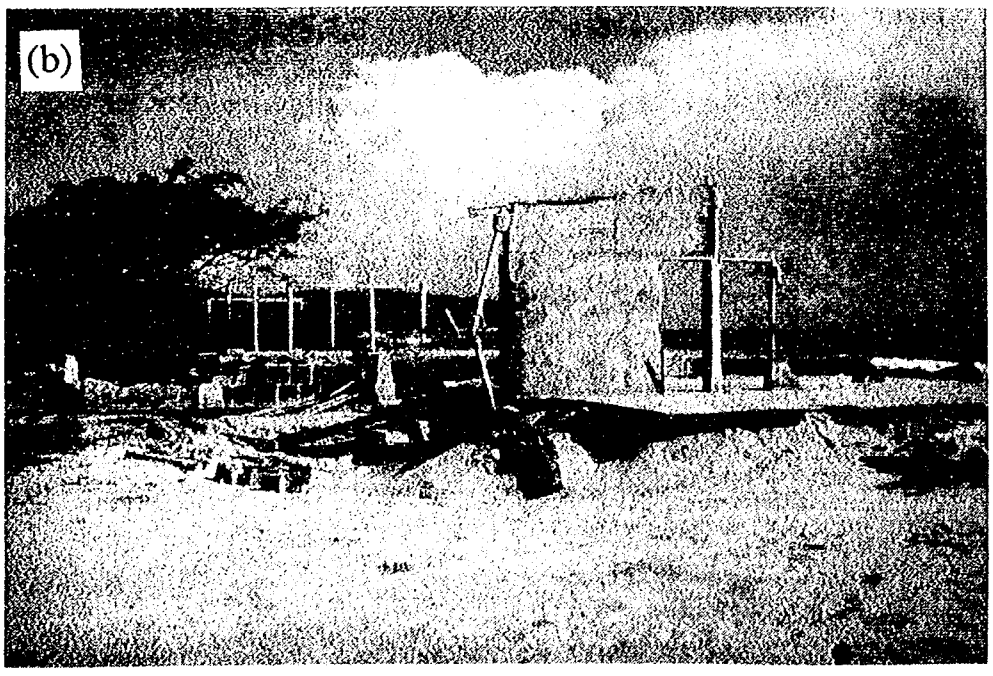


Figure 9. Beach houses in El Popoyo, Nicaragua: a) two dissimilar houses survived from the tsunami attack; b) a typical tsunami damage.



Figure 10. Beach face scour found in Rajekwesi, East Java.



Figure 11. Beach scour in Aonae, Okushiri Island.

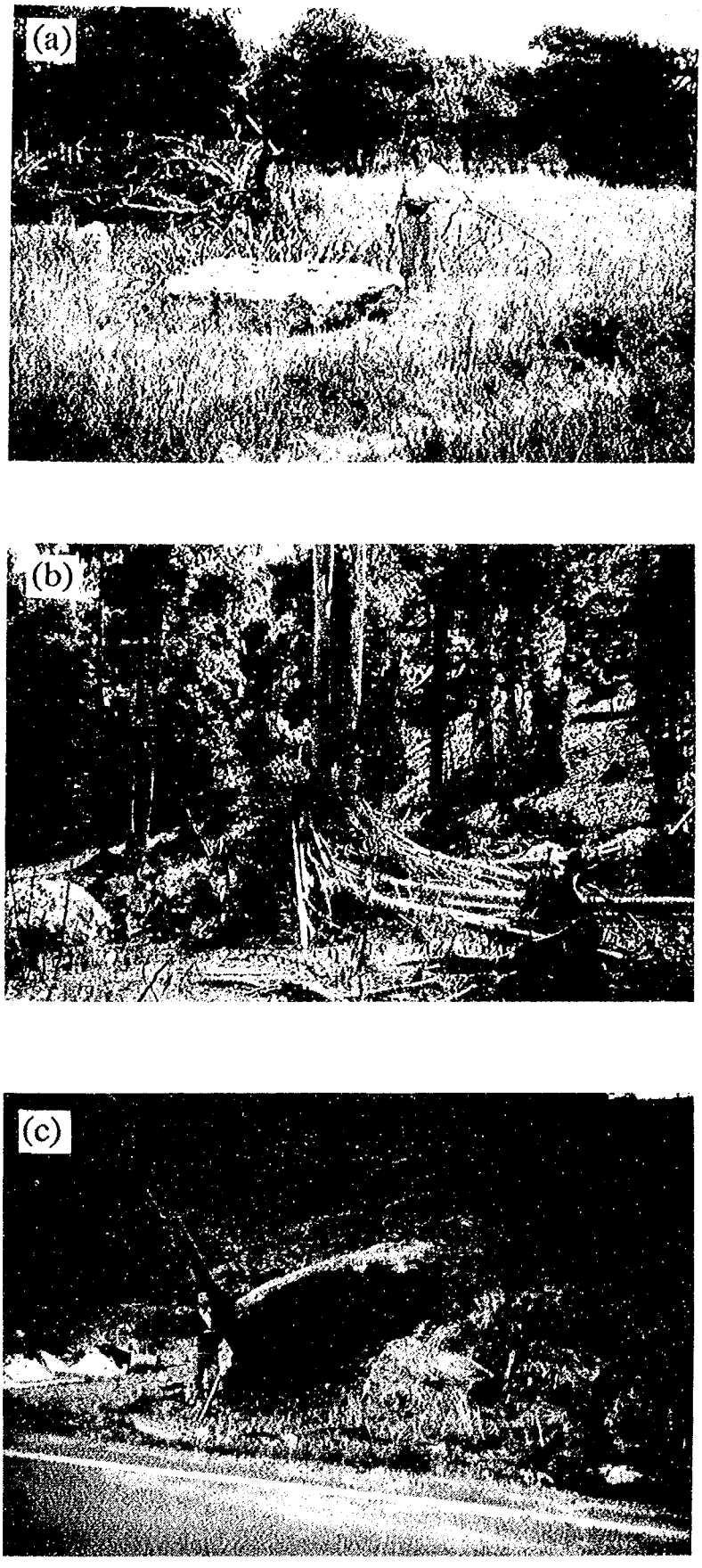


Figure 12. Rocks transported by tsunamis: a) beach rock at El Popoyo, Nicaragua; b) corals at Riangkroko, Flores; c) beach rock at Monai, Okushiri.



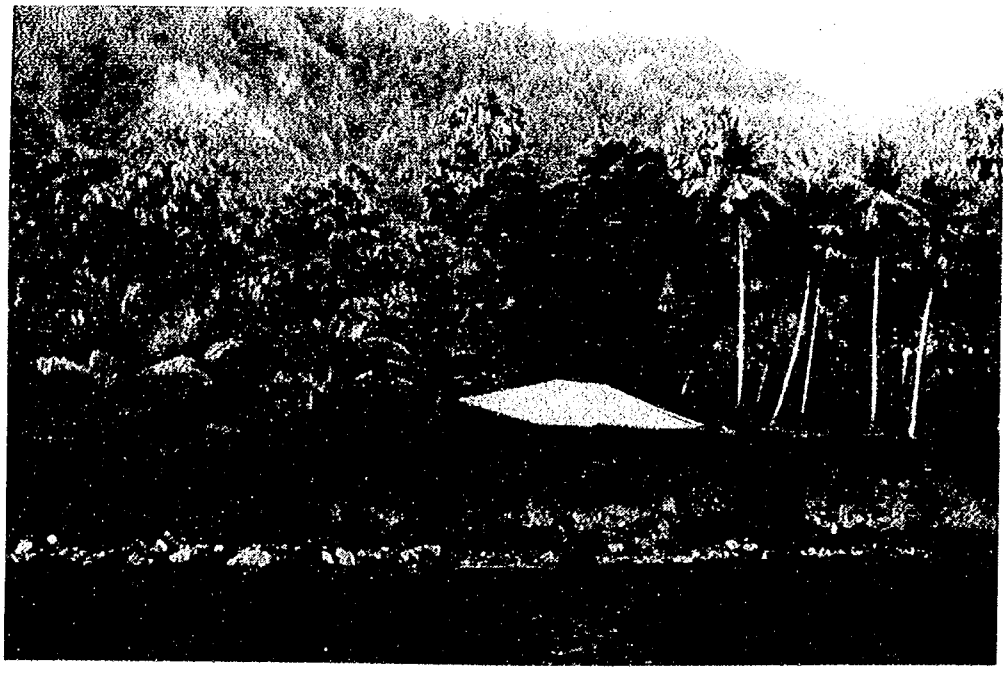


Figure 13. Subaqueous slump that is approximately 2 km long at Leworahang, Flores.

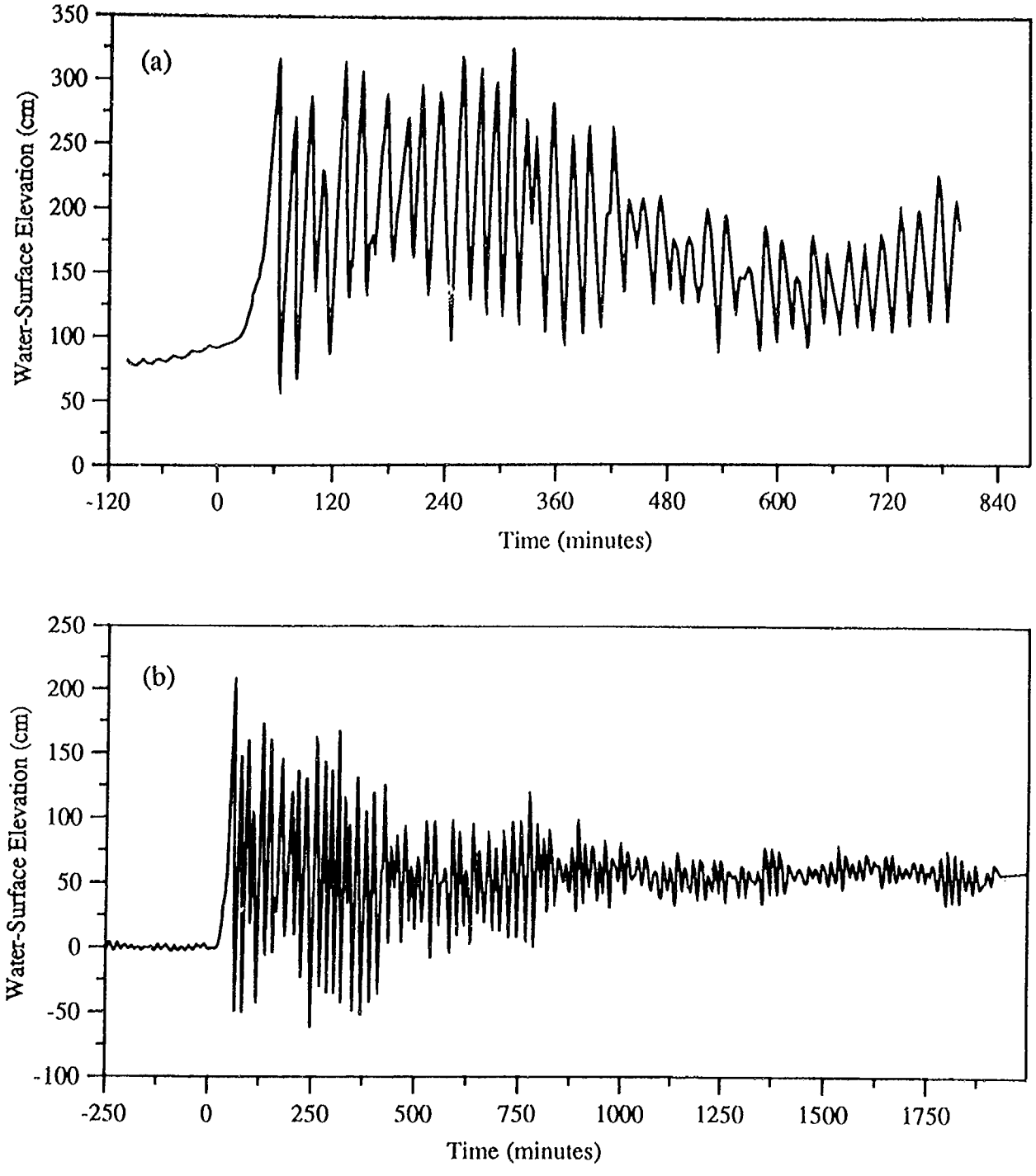


Figure 14. The tide-gage record in Malokurilskaya Bay: a) raw data, b) after removal of the astronomical tides.

CIVE 472 -- Introduction to Hydraulics in Water Resources

Environmental Hydraulics

(3 units - 1 design credit)
MWF 130-220

Instructor: Harry Yeh

Tentative Course Outline

1. The Oceans and Atmosphere

    a. Earth's gravitational effects
    b. ocean basin characteristics
    c. radiative equilibrium and the Greenhouse effect
    d. large-scale circulation of oceans and atmosphere
    e. the hydrological cycle

2. Properties of Fluids and Their Vertical Distributions

    a. salinity
    b. temperature: in situ, potential, adiabatic lapse rate
    c. density: "sigma tee", potential, baroclinic and barotropic stratification, buoyancy, Brunt-Väisälä frequency, vertical stability
    d. the ST relation: water masses, diffusion processes and the diffusion coefficient, mixing of water masses, caballing and conservation of vertical stability

3. Fluid Mixing

    a. molecular diffusion
    b. turbulence
    c. dispersion

4. Forces Affecting Environmental Fluids

    a. gravitation and buoyancy
    b. pressure
    c. Coriolis
    d. friction
    e. turbulence and Reynolds stresses

5. Two-Layer Flow Hydraulics

    a. internal waves
    b. gravity currents
    c. hydraulic jump

6. Scaling and Approximation -- will be taught by Prof. Petroff

7. Diffuser Design -- will be taught by Prof. Nece

8. Mixing in Estuaries and Lakes

Propagation of Hokkaido Nan-sei Oki Earthquake Tsunami around Cape Aonae
- nonlinear propagation of tsunami in shallow water -

by
Kenji Noguchi[1], Shinji Sato[2] and Shigenobu Tanaka[3]

Abstract

In Okushiri island on July 12, 1993, by the tsunami generated by Hokkaido Nan-sei-oki earthquake, a district Hamatsumae shelterd by cape from tsunami source area had peculiar large inundation heights. Physical model tests were performed to investigate the tsunami propagation. It is considered that the tsunami experienced breaking and dispersion. The crest line of head of the tsunami formed a caustic with large wave height by refraction. The maximum inundation height is not accomplished by head of the tsunami but by 2nd or later waves. Results of physical model tests can reasonably explain the distribution of inundation heights obtained by the field survey.

Key Words : Tsunami propagation, Physical model, Refraction, Inundation

1. Introduction

A huge disaster occurred in Okushiri island on July 12, 1993, by the tsunami generated by Hokkaido Nan-sei oki earthquake. The inundation heights over 10 m were found in three districts, which are Inaho located on the west side of north end, along the southwest coast and Hamatsumae district located on the southeast part. One of these areas with higher tsunami run up , Hamatsumae district was of particular interest since it is located in a sheltered area by Cape Aonae from tsunami source area. In addition, this Hamatsumae district is not bay or not inlet rather outlet. It is not manifest that the mechanisms of higher inundation height in Hamatsumae. It is remained to solve.

Numerical simulations reproduce outline of propagation and inundation (for example, Takahashi et al.; 1994). But these simulation can not reproduce the peculiar inundation height around Hamatsumae. The reason is that numerical simulations demand additional mechanisms. In this study, physical model tests were performed to investigate the mechanism of tsunami transformation in this area in detail.

1) Researcher, Coastal Engineering Division, River Department, Public Works Research Institute, Ministry of Construction, Tsukuba City, 305, Japan
2) Senior Researcher, ditto
3) Head, ditto

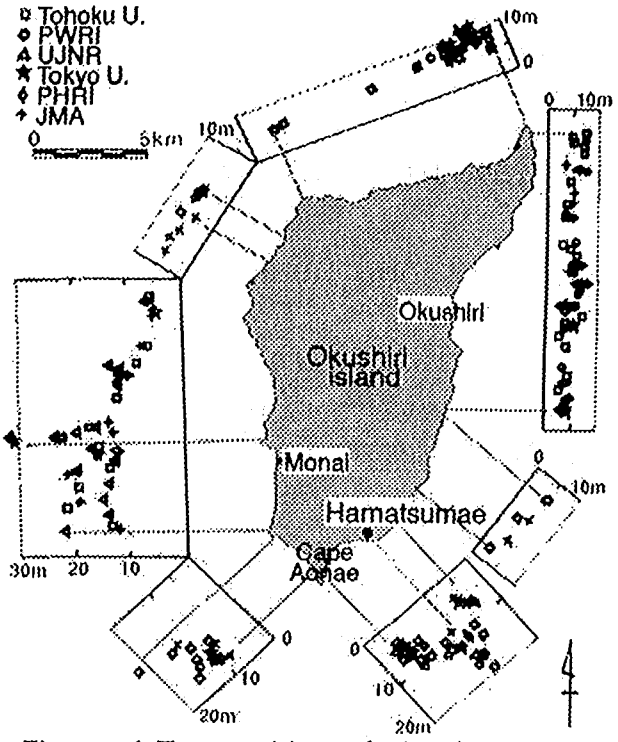


Figure. 1 Tsunami inundation hieght (after Bernard and Gonzáles)

2. Tsunami inundation height in Okushiri island

Several groups of tsunami researchers measured tsunami runup height immediately after the tsunami. These data were summarized by Bernard and González (1993, Figure 1). According to this Figure, the runup heights over 20 m were recorded along the southwest coast of the island and southeast Hamatsumae district located on the southeast part. Monai on the southwest coast recorded 31.7 m inundation height.

The source area of the tsunami was about 10 km to the west of Okushiri island. Monai is located direct incident side and nearer place to tsunami source area. But, the main

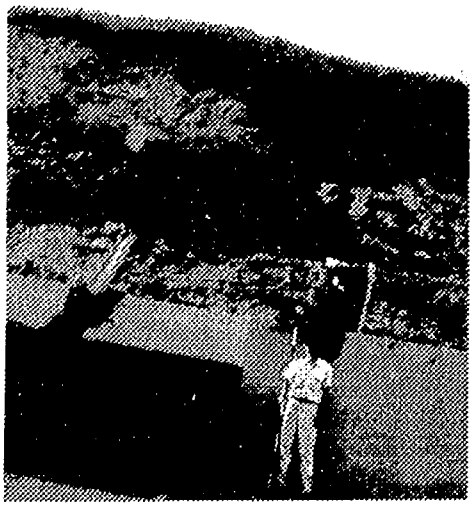


Photo. 1 Road parapet overturned to seaward

reason of the largest inundation is Monai is situated pocket beach and v-shape valley. The other hand, Hamatsumae district is located in a sheltered area by Cape Aonae and is convex to the sea. It is then unusual that the inundation height was much larger than several incident front side.

As for structure disaster, road parapet in the southwest was overturned to mountain side, but one in the northeast of Hamatsumae was overturned to sea side (Photo. 1). These would be caused by different phenomenon each other.

Around Cape Aonae, there is shallow sea where small fishery boat hits ground. So, at the peak of Cape Aonae, it is capable to watch that the small wave are just usually breaking. Information of breaking the tsunami was few, since it came in midnight at 10:17pm and immediately after the earthquake. Then, breaking of the tsunami should be also observed in physi-

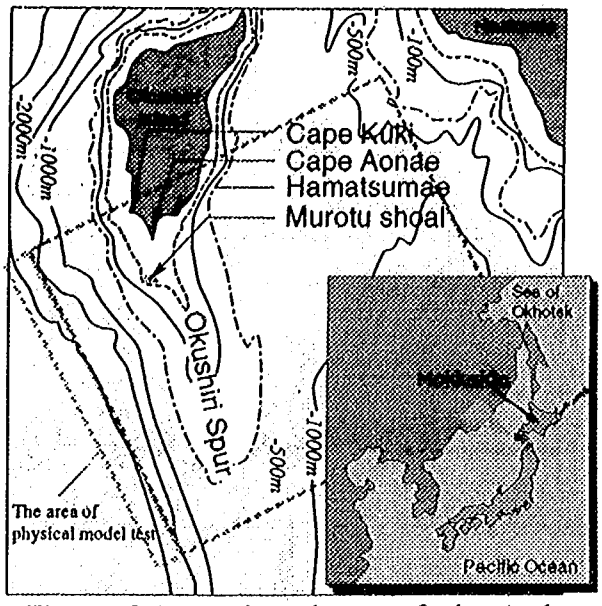


Figure 2 Reproduced area of physical model test

cal model test.

3. Implementation of physical model tests

It is considered that the tsunami propagation was influenced by the complex bottom topography on the Okushiri Spur, especially in the shallow sea area surrounded by Cape Aonae, Murotsu rock islands and Hamatsumae. The area which was selected was a rectangular area shown in Figure 2. The area was selected on the basis of numerical simulation of tsunami refraction so that it contained the whole source area which might affect tsunami transformation around the southern part of the Island. The experimental basin has 35m length, 30m width and 0.6m depth. The physical model reproduced topographies from 500 m beneath the sea level to 20 m above the sea level with non-distorted 1/1100 scale.

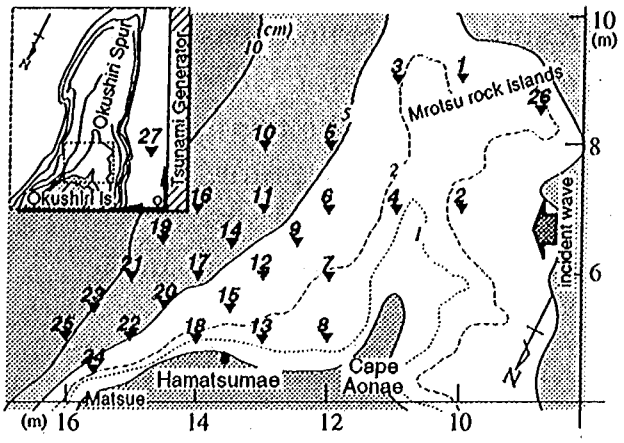


Figure 3 Measuring points

The pneumatic tsunami generator is structured three main parts that are air chamber, a suction valve and release valve. The water in the chamber joining with experimental basin, will suck up and make potential unbalance in water level between basin and chamber. If the release valves open, the water in the chamber will fall down immediately. A tsunami will occur on experimental basin.

There exists a broad shallow sea, called Okushiri Spur, in front of the coast between Cape Aonae and Hamatsumae with gently slope for southeast. Murotsu rock island is located in this area.

The physical model tests were performed for 8 cases with incident tsunami height ranging between 2.7 and 7.8 mm. The wave heights were measured by capacitance-type wave gages. At the same time, video pictures from three angles were taken. Their snapshots are (1) the whole propagation from right over to down, (2) fo-

cus to swash motion around Hamatsumae and (3) from northeast Hamatsumae on the coast for Murotsu island. In the Figure 3, the triangle symbol denotes measuring point. Measuring points are intensively situated in the shallow area around Hamatsumae.

4. Results of a test

4.1. Tsunami wave profiles and propagation

The propagation of tsunami with 3.9 mm of incident wave height will be described in detail since it reproduced the initial water elevation in the tsunami source area estimated by fault model. The incident wave profile of this case is shown in Figure 4. The time 't' is the elapsed time from the initiation of data sampling.

Tsunamis may be dispersed into several short waves while traveling to shallower water. In the Nihonkai Chubu earthquake tsunami in 1983, the dispersion affect to wave absorbing works. The blocks of wave absorbing works were scattered in large area. In this test, the tsunami dispersed after it passed over the Okushiri Spur.

Figure 5 shows dispersion states, which are selected among offshore measuring points. On the point 4, the wave profile does not show dispersion. Profiles of eastern than point 5 and point 6 show dispersed waves. Point 6 might be located crossing point of refracted waves from slope A and slope

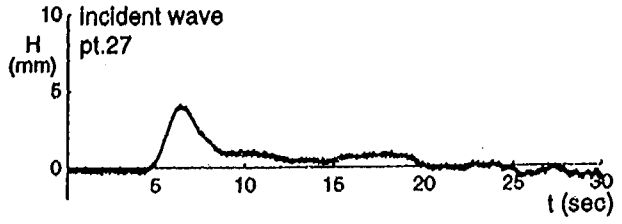


Figure 4 Incident wave profile

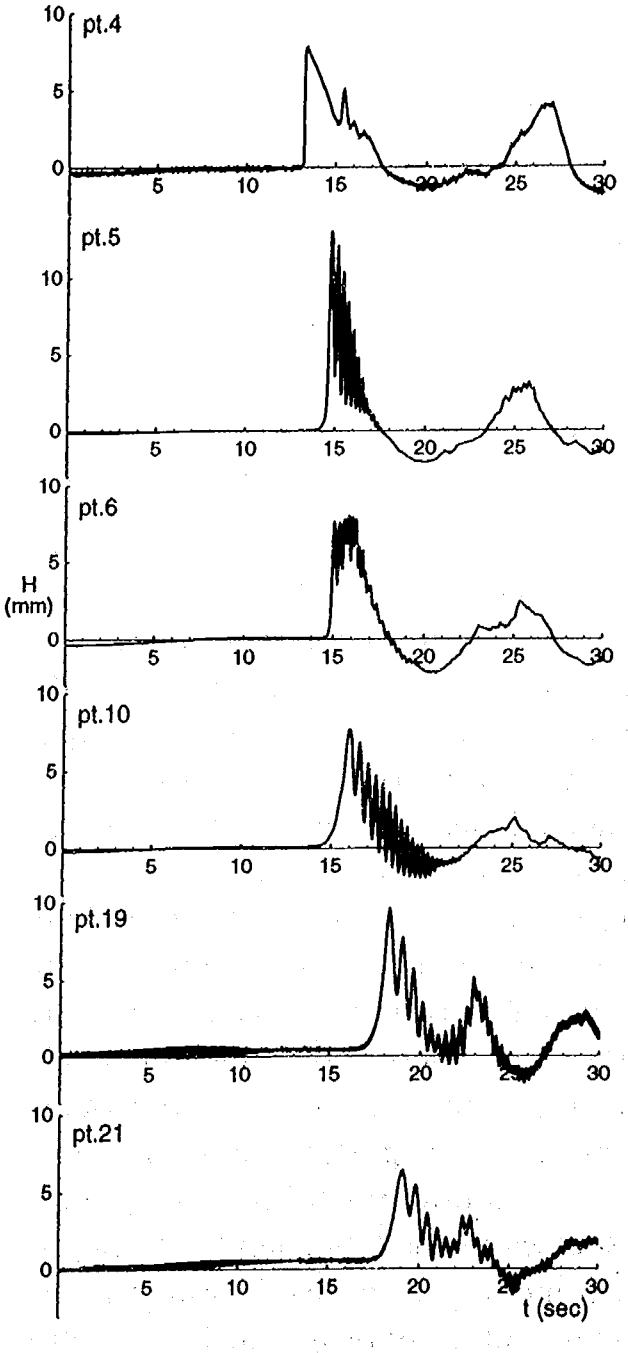


Figure 5 Wave profiles for dispersion in offshore

B. These waves have different direction but very tiny. Non-linear interaction was carried out at this crossing point. It showed unusual propagation in profile of point 6. Breaking of tsunami was occurred on the ridge between Murotsu island and Cape Aonae over the Okushiri Spur. The tsunami dispersed after breaking around Cape Aonae. In this paper, the each waves on dispersed wave are called individual wave. The distance of individual waves are narrow, since point 5 is near the beginning of dispersion. Each individual waves have different each velocity. Some later passed, they makes longer distance than before. Profile of point 10 shows that small waves were late. At point 19 and point 21, the distance of individual waves are stretched more than that of point 5. Much smaller individual waves were born and late.

Figure 6 shows profiles along shoreline to investigate the tsunami status along the coast. Point 8 is the nearest to Cape Aonae. Point 8 is quite sheltered by the cape. Point 13 locates westward of Hamatsumae. Difference of point 13 and point 18 is which side of convex part. Point 18 recorded the highest wave height. Then it shows that the inundation height would be given in coast around point 18. These four profiles have remarkable two peeks. According to video movie analysis, the second hill is due to reflected wave from land.

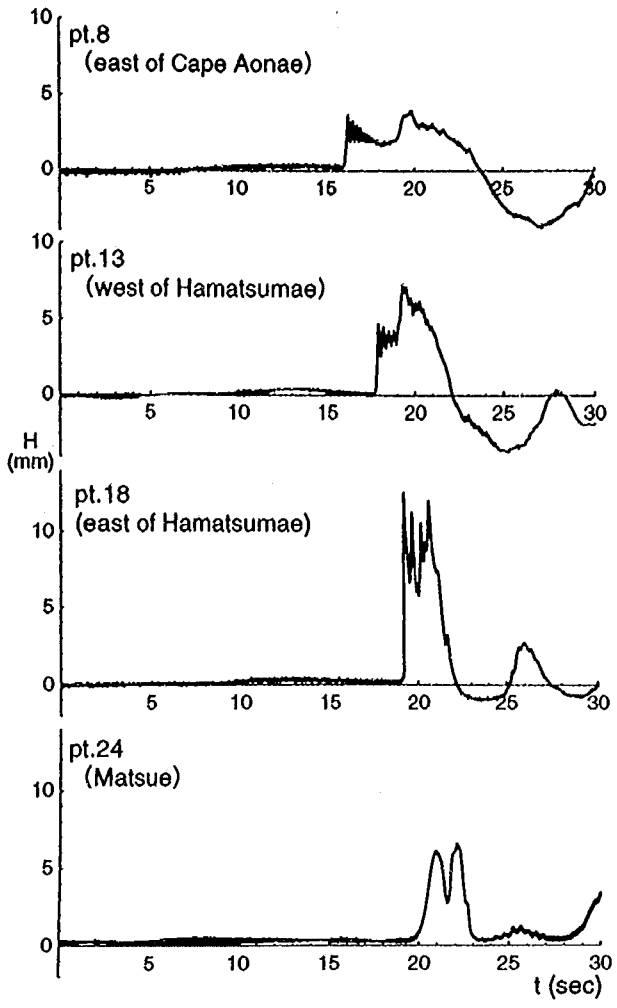


Figure 6 Wave profiles along shoreline

4.2. Amplified wave height at a concave part in crest line

Video pictures were captured to detect the maximum height along the shoreline in point 18. There is a part of higher among the crest line of first individual wave. It moved from east of point 7 to Hamatsumae district with refraction. Four snapshots of video movie are shown in Photo. 2 (1) to (4). Photo. (1) (t=14.02s.) shows a scene immediately after breaking over the

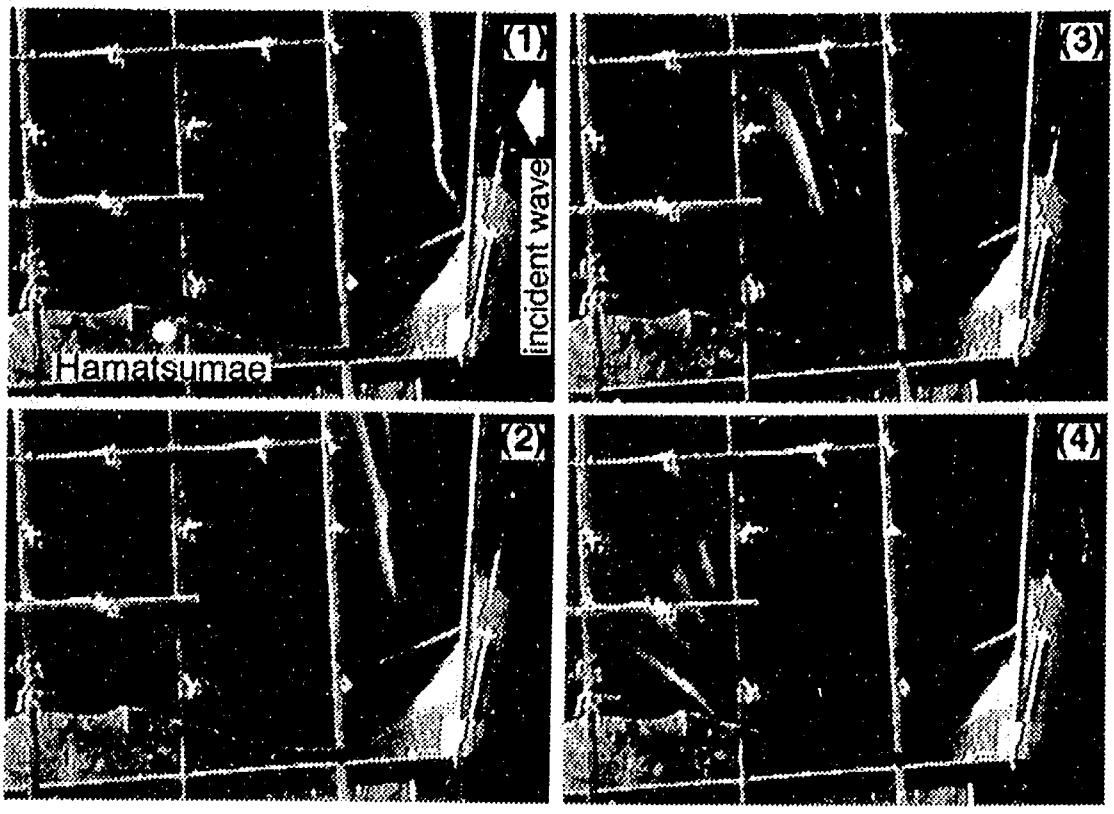


Photo. 2 Snapshots of tsunami propagation
(1)t=14.20s, (2)t=14.26, (3) t=16.20s, (4) t=18.60s

Okushiri Spur. In photo. 2 (2), the crest line of the first individual wave made a caustic due to refraction and created a concave part. Wave height of this caustic part became higher than those on both sides. This part increased its celerity, since a higher wave height on the long wave gives a larger celerity. In photo. 2 (3), this delayed but higher part would advance of both sides. When the part advanced, it made a new concave part on the crest line. The new part was amplified the wave height and speed in similar motion. At last, in photo. 2 (4), the higher part reached the east of Hamatsumae with refraction.

4.3. Observation of swash motion

Swash motions around Hamatsumae were detected from video movie snapshots. The dispersion occurred on shallow sea in southeast of Okushiri island. The dispersion also affect the swash motion. It is complex in the swash motion that each individual waves of dispersed tsunami run up in succession.

The maximum inundation lines are illustrated in Figure 10 with various line types depending on which wave gives the maximum inundation height. The thin breaking line is meaning uncertain of which wave second or later, because the sight was too far from camera to separate the each

waves. It shows that the maximum inundation height is not produced by the first wave, but by the second or the following wave.

Tohoku university surveyed the inundation heights around Hamatsumae in detail. Their data are shown in Figure8. The area surrounded by broken line indicates the area shown in the Figure7. Inundation height eastward of convex part to sea got more than 16 m. 16 m is scaled to 14.5 mm in this test. In west of Hamatsumae village, it got about 10 m that is also scaled to 9.1 mm. It is noticed that the physical model tests reproduced the large inundation heights observed around Hamatsumae.

5. Conclusion

1) It is considered that the tsunami generated by Hokkaido Nan-sei-oki earthquake experienced breaking and dispersion over shallow sea around Cape Aonae.

2) The crest line of the first individual wave formed a caustic with large wave height. The caustic part advanced gradually than those on both sides.

3) Tsunami is refracted to Hamatsumae influenced by 1) and 2).

4) The maximum inundation height is accomplished by the second or the following dispersed wave of tsunami, not by the first wave.

5) Results of physical model tests can reasonably explain the distribution of inundation heights obtained by the field survey.

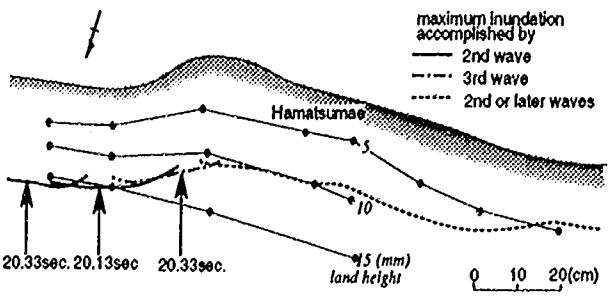


Figure 7 Distribution of maximun inunafation height in this test

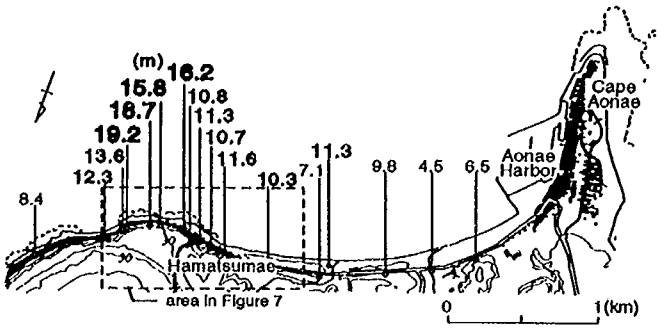


Figure 8 Inundation height around Hamatsumae by Tohoku Univ.

Reference

Bernard, E. and F. I. González (1993):Tsunami Devastates Japanese Coastal Region, EOS, Transactions, American Geophysical Union, Vol.74, No.37, Sep., 14, pp.417,432.

Takahashi, T., N. Shuto, F. Imamura and H. Matsutomi (1994): The measured and computed Hokkaido Nansei-Oki Earthquake tsunami of 1993, 24th ICCE abstracts, pp.126,127.

BREAKWATER ARMOR DESIGN ADVANCES

by

William E. Roper[1], Ph.D., PE

ABSTRACT

This paper summarizes the importance of breakwaters and other shore protective structures to reduce the impacts from tsunamis and storm surge wave attack. A new concrete armor unit called CORE-LOC™ designed to provide shoreline structural protection in high wave energy envirnments is described, testing results are presented including structural and hydraulic analysis, and three dimensional stability assessment. The CORE-LOC™ armor unit is compared to other commonly used concrete armor units for static and dynamic performance and for armor layer volume requirements. Based on the success of laboratory and analytical studies CORE-LOC™ is a superior armor unit and is planned for application in several U.S. structures.

TSUNAMIS INTERACTION WITH SHORE PROTECTION STRUCTURES

Breakwaters and seawalls have historically provided protection from tsunamis. Breakwaters may decrease the volume of water flowing into a harbor and onto the coastline, and a high seawall or dike may prevent flooding of backshore areas. Proper placement of breakwaters may also decrease wave heights by changing the natural period of an inlet.

A tsunami may damage shore protection structures; therefore, care must be exercised in the design of the structures. Numerous instances of tsunamis damaging or destroying protective structures have been recorded. Types of damage include movement of stones from rubble structures; erosion of dunes, embankments, and earthen dikes; scouring of backfill behind bulkheads; scouring of the seaward base of a revetment or seawall; and overturning and sliding of structures such as caissons.

The 1946 tsunami overtopped and breached the breakwater at Hilo, Hawaii, removing 7.25 metric ton stones to a depth of about one meter below the water surface along nine sections of the breakwater crest with a total length of over 1,800 meters (Camfield, 1994).

There are numerous other examples of tsunamis and storm surge wave damage to coastal structures. This underscores the importance of well designed breakwaters and other protective structures to withstand the surge, drag, buoyant, hydrostatic and impact forces of wave attack. To accomplish this in an economically efficient manner is a significant technological challenge.

CONCRETE ARMOR DESIGN IMPROVEMENTS

Concrete armor units are commonly used to protect coastal rubble structures. The units are individually placed on the breakwater in a regular pattern or quasi-random matrix. Concrete armor units come in a variety of

[1] Director, Civil Works Research and Development, U.S. Army Corps of Engineers, Washington, DC, U.S.A.

shapes and sizes, and some have several recommended placement configurations. Figure 1 shows an example of random dolos and tribar layers, and a pattern-placed single layer of tribars on the Nawiliwili breakwater in Hawaii. Concrete armor units are used on structures when stone of a sufficient size to resist wave action is not available or uneconomical.

In the past, the choice of armor unit shape and method of application have largely relied on engineering judgment, partly because no optimal armor unit existed. Figure 2 shows several of the more commonly used armor shapes. These units span ranges of hydraulic stability and structural capacity. When placed in an armor layer they exhibit various porosities. Most existing armor units require rather shallow structure slopes to maintain hydraulic stability, but present design trends are pushing toward steeper slopes.

Optimal Armor Characteristics

The Waterways Experiment Station, Coastal Engineering Research Center has an ongoing research effort to develop improved concrete armor unit shapes for both new coastal construction and repair of existing coastal concrete-armored rubble structures (Turk and Melby, 1995). This research stems from the engineering need to protect navigation structures in high wave-energy environments, such as on the U.S. west coast and the Hawaiian Islands. Because of the very difficult construction, in-service conditions, and repair needs associated with these environments, the basic development program has focused on randomly placed armor units.

One of the goals of this effort has been to develop optimal concrete armor unit shapes that can be used for both new construction and repair of existing rubble structures. This development requires incorporating all of the best engineering features from the various existing armor shapes into a single unit while eliminating the major weaknesses. The optimal armor engineering characteristics are summarized as follows:

- High single-unit-thickness hydraulic stability at any slope angle.
- Reserve stability for wave conditions beyond design event.
- No tendency for units to rock on the slope.
- Continued stability when broken or following renesting.
- Efficient combination of porosity and slope roughness to dissipate the maximum wave energy.
- Maximum performance with a minimum concrete armor layer volume.
- Hydraulically stable when placed as a repair with other shapes.
- Low internal stresses, so no reinforcement is required.
- Easy to cast.
- Easy construction placement of armor layer, even in low visibility water.
- Uses minimal casting yard or barge space.
- Utilizes conventional construction materials and techniques.

Most existing armor units have been successfully applied, but all have weaknesses in one or more of these engineering performance characteristics. For instance, block shapes, are often uneconomical because the armor layers require larger units and more concrete than layers of slender armor. Pattern-placed blocks, (Wilkenson and Allsop, 1983; de Rouck et al.,

1994; Brown, 1983), have improved economies over solid blocks, but require idyllic construction conditions to assure the armor layer transitions will not be mobile.

Existing unit shapes such as the dolos and tribar have slender central sections and long legs, producing very high stresses in the central sections of the units. This results in units which break into pieces having must less mass than the original unit. The broken units have little stability and may contribute to the breaking of adjacent units.

Tetrapods exhibit even lower stability than dolosse. Their legs extend a shorter distance from the centroid so interlocking is less, and their rounded sections promote rocking on slopes and when destabilized.

CORE-LOC™ Concrete Armor Unit

A new series of coastal rubble structure concrete armor units called CORE-LOC™ and illustrated in Figure 3 has been developed by the Corps of Engineers that attempts to incorporate all of the aforementioned optimal features (Melby and Turk, 1995). The CORE-LOC™ units have been designed to be placed in a single-unit-thickness layer on steep or shallow slopes. The CORE-LOC™ shape has been optimized to maximize hydraulic stability, unreinforced strength, and reserve stability, but minimize casting yard space. The primary intent of this shape optimization is to have a very stable armor layer, with good wave energy dissipation characteristics, and yet have stresses low enough that regular strength unreinforced concrete can be used with little or no armor breakage occurring during the life of the structure. Table 1 summarizes the engineering characteristics of the CORE-LOC™ unit and its basic parameters.

Many breakwater concrete armor layers built between 1950 and 1985 in the U.S. have lasted less than 10 years between rehabilitations, primarily due to armor breakage (Melby and Turk, 1994). The CORE-LOC™ strength has been maximized, through optimization of the unit shape, to minimize armor unit breakage. During the last few years of research on the structural response of dolos units it was found that very high flexural and torsional stresses occurred in the slender central cross sections on the dolos units (Melby and Howell, 1989; Melby and Turk, 1992). The CORE-LOC™ units were designed to eliminate the slender central section. The CORE-LOC™ design was also specifically designed to interlock well with dolosse so it could be used as a repair unit. When CORE-LOCs™ are placed on a slope with dolosse they have a superior interlocking affinity. Figure 4 illustrates an armor matrix composed of both CORE-LOCs™ and dolosse. The two units are almost indistinguishable from each other.

Structural Analysis

Structural analyses have been done using the finite element method (FEM) to compare the structural response of dolosse, tribars, and accropodes with CORE-LOCs™ for several static loading modes. The properties of the finite element models are shown in Table 2. The FEM grids for the four units modeled are shown in Figure 5 along with loading and boundary conditions for a torsional load case. While the four units have diverse shapes, the weights of each were set at an arbitrary 10 tons. Similar loads and boundary condition constraints were applied to each. The units were loaded in flexure, torsion, and a combination of these. Figure 6a shows a CORE-LOC™ loaded in flexure with a 10-ton point load applied to one fluke end and the other fluke fixed. Figure 6b shows another flexural load condition with a

10-ton load applied to the center of the fluke. Figure 6c shows a loading condition where 10-ton flexural and torsional loads were applied to one fluke tip with the opposing fluke fixed rigidly along the outside surface.

The FEM results are summarized in Table 2 in terms of maximum tensile stresses. All load cases were analyzed for the dolos and CORE-LOC™ but only the pure torsion and pure flexure with tip load were analyzed for the accropode and tribar. As illustrated, for equivalent weight units, the CORE-LOC™ maximum tensile stress for static loads ranged from 34 percent to 62 percent that of dolos., was 74 percent that of accropode for both torsion and flexure, and was only 38 percent for torsion and 33 percent for flexure that of the tribar. These results are graphically depicted in Figure 6.

The significance of these stress reductions can be better understood by examining an actual design case. For the Crescent City, CA breakwater 42-ton dolosse unit, the design tensile stress level corresponding to a 2-percent exceedance was approximately 696 psi. This structure is performing reasonably well with 2-percent breakage since the 1986 rehabilitation. The strict concrete specification for Crescent City produced a high-strength, expensive concrete with a 28-day splitting tensile strength of 725 psi. For the same size CORE-LOCs™, the maximum design stress could be reduced to 62 percent of this value, which is approximately 430 psi. This stress is below the 28-day splitting tensile strength met on most Corps concrete armor projects. Lower strength requirements of CORE-LOC™ would result in significant cost savings for the concrete needed for larger armor units.

Hydraulic Evaluation

Over the past 1-1/2 years, a large number of CORE-LOC™ hydraulic stability tests have been conducted under a variety of situations. Figure 8 shows a CORE-LOC™ slope under wave attack in an early test series. The research on CORE-LOC™ stability is still ongoing (Carver and Wright, 1994). The tests completed to date show that the CORE-LOC™ armor layer is two-dimensionally stable for wave heights far exceeding those causing damage to most other armor shapes. During the testing, researchers noted that the units showed very little movement on the slope, including in-place rocking. No-damage Hudson stability coefficients have exceeded 150 in several instances, and for many tests, the wave generation capacity of the flume was reached before damage to the armor layer occurred.

A conservative armor-layer design would never specify armor using very high stability coefficients. Regardless of the armor type, designs should not vary drastically from the noninterlocked armor stability because of the many uncertainties involved with breakwater design which add to the risk of failure. Therefore, these tests indicated that, when designed conservatively for two-dimensional situations (such as for use on a revetment) the CORE-LOC™ armor will have considerable reserve stability beyond the design wave or repeated subjection to the design wave.

It is recommended that $K_D = 16$ be used for trunk sections and $K_D = 13$ be used for head sections, for both breaking and nonbreaking waves, where K_D = the Hudson stability coefficient. Also, the reflection coefficients from the slope were almost indistinguishable from those of dolosse, indicating that existing dolos reflection and runup design information could be used for preliminary estimation of reflection and runup on CORE-LOC™ slopes. As always, physical model tests should be used to validate this preliminary design guidance.

Repair of Dolosse Structures

A series of two-dimensional stability tests were conducted to determine the stability of a dolos slope repaired with CORE-LOCs™. The tests were done in shallow water with a 1.5-m-wide fronting *reef* in the 0.6-m-wide flume. A very high wave height-to-depth ratio occurred at the structure because the fronting reef was narrow relative to the wavelength; therefore, the wave height was not stabilizing before it hit the structure. Where placed in groups, the CORE-LOCs™ had interlocked and stabilized the original damaged regions on the slope. The displaced CORE-LOCs™ were lone repair units placed near the cap and were never interlocked. For an actual repair, the existing dolosse in and near the repair region would be removed from the slope so the CORE-LOCs™ could be interlocked with these units as they were placed. These tests showed that the CORE-LOC™-repaired areas were qualitatively more stable than the original dolos slope, and considering the higher structural strength of the CORE-LOC™, further justify its use as a repair unit for dolos slopes.

Testing of the CORE-LOC™ as a repair unit for dolosse has moved from the first *proof of concept* phase to a three dimensional physical model investigation. For a range of wave periods, dolosse slopes were damaged by wave action then subsequently successfully repaired with CORE-LOC™. Finite element structural analysis conducted show stresses in CORE-LOC™ to be approximately 62 percent of dolosse, therefore CORE-LOC™ should prove to be the repair method of choice for all future dolosse rehabilitation.

Armor Volume Efficiency

The cost of an armor layer depends primarily on the volume of concrete on the slope, number of units, unit material cost, and unit construction costs. The unit construction costs include casting yard, transport, and placement costs. Yard costs include construction of formwork; concrete placement, storage, and handling; and cost of equipment necessary to handle the units. But the total armor material volume dominates the armor layer cost and therefore should be minimized by maximizing the porosity and minimizing the armor layer thickness.

Because of CORE-LOC's™ high stability, high porosity, and single-unit-thickness layer, building an armor layer from CORE-LOCs™ requires less concrete than other commonly used armor units. A graphical comparison with other armor units is shown in Figure 9. When designing for breaking waves on a 1V:1.5H trunk section, accropodes require 51 percent more concrete than CORE-LOCs™; dolosse, 53 percent more; randomly placed tribars, 110 percent more; and tetrapods, 159 percent more (Melby and Turk, 1994). Similar savings can be achieved with the use of CORE-LOCs™ when designing for head sections and other slope configurations.

Future Plans

The patent-pending CORE-LOC armor unit has been successfully tested as primary armoring and as a repair unit for existing structures. It will be first used at the Kodiak, Alaska Breakwater, instead of natural quarry stone, resulting in savings of over $1,000,000. The Noyo, California Offshore Breakwater, in planning stages for 20 years, now with CORE-LOC can meet the required benefit-to-cost ratio, and is slated for construction in 1998. The Kaumalapau Breakwater in Hawaii will save almost $3,000,000 over the least cost alternative by using CORE-LOC. Consideration is being given to using CORE-LOC on the Ouzinkie, Alaska Breakwater; Maalaea, Hawaii Breakwater; Grays Harbor, Washington Jetty; and Manasquan, New Jersey Jetties.

Research plans include large-scale testing of the CORE-LOC™ at the Oregon State University

large wave flume is this year, and a Cooperative Research and Development Agreement is being negotiated to conduct prototype drop tests of both 1.5- and 20-ton CORE-LOCs™.

In addition, a U.S. patent is pending, and foreign patents in most industrialized countries are being filed. Licensing of these patents will be advertised in the Federal Register.

SUMMARY

CORE-LOC is intended primarily for the protection of coastal and shoreline structures in high wave energy applications. The CORE-LOC™ units interlock in a random matrix to form a highly stable, highly porous armor layer. Hydraulic stability tests are described which show the CORE-LOC™ to be one of the most stable randomly-placed armor units ever tested. Flume tests showed that the CORE-LOC™ was stable for breaking wave heights 5 to 7 times the maximum dimension of the unit on slopes of 3V:4H and 1V:5H. The maximum no-rocking no-damage stability numbers for these tests were consistently over 7, corresponding to Hudson stability coefficients over 150. Initial hydraulic stability tests of CORE-LOC™-repaired dolos layers showed the CORE-LOC™ to be an effective repair unit without the inherent structural weakness of dolosse. No rocking, no-damage design Hudson stability coefficients for CORE-LOCs™ are preliminary and conservatively suggested to be 16 for trunk sections and 13 for head sections, based on H_s. There is no need for structural steel reinforcement in CORE-LOCs™ as structural numerical simulations show the maximum tensile stresses in the CORE-LOC™ to be well below those in dolosse and tribars and similar those in accropode. Finally, the required armor layer volume is shown to be less than that required for other commonly-used armor units.

REFERENCES

F. E. Camfield, "Tsunami Effects on Coastal Structures," Journal of Coastal Research Special Issue No. 12: Coastal Hazards, pp 177-187, 1994.

R. D. Carver; B. J. Wright, "Stability of CORE-LOC™ Armored, Rubble-Mound Breakwater Trunks," Progress Report, U.S. Army Engineer Waterways Experiment Station, Vicksburg, MS, 1994.

C. T. Brown, "Seabees in Service," *Proc. Coastal Structures '83*, ASCE, NY, NY, 235-258, 1983

J. de Rouck; P. Hyde; L. van Damme; F. Wens, "Basic Characteristics of the HARO®, A Massive Hollow Armour Unit," *PIANC Bulletin No. 82*, 5-19, 1994.

J. A. Melby; G. L. Howell, "Incorporation of Prototype Dolos Static Response in a Dolos Design Procedure," *Proc. Int. Assoc. Hyd. Res. XXIII Congress*, IAHR, C391-C398, 1989.

J. A. Melby; G. F. Turk, "The CORE-LOC™: Optimized Concrete Armor," in publication, *Proc. 24th Int. Conf. on Coast. Engr.*, American Society of Civil Engineers, New York, 1995.

J. A. Melby; G. F. Turk, "Concrete Armor Unit Performance in Light of Recent Research Results," *ASCE/WPCO Sem. on Case Histories of Design, Constr., and Maint. of Rubble Mound Struc.*, ASCE, in publication, 1994.

J. A. Melby; G. F. Turk, "Dolos Design Using Reliability Methods," *Proc. 23rd Int. Conf. Coast. Engrg.*, ASCE, 1385-1399, 1992.

G. F. Turk; J. A. Melby, "CORE-LOC™: A Major Development in Concrete Armor," The REMR Bulletin, U.S. Army Engineer Waterways Experiment Station, Vicksburg, MS, p. 1-5, 1995.

A. R. Wilkenson; N. W. H. Allsop, "Hollow Block Breakwater Armour Units," *Proc Coastal Structures '83*, ASCE, NY, NY, 208-221, 1983.

Table 1
Engineering Characteristics of the CORE-LOC™

Unit	Volume V	Number of Layers[1] n	Porosity P as %	Layer Coefficient k_Δ	Packing Density ϕ	Typical Slope cotα	Number of Units[2] N_1/C^2
CORE-LOC™	$0.2240C^3$	1	66	1.6	0.54	1.5	1.46
Dolos	$0.1561C^3$	2	56	0.94	0.83	2.0	2.86

Footnotes
1. The two dolos armor layers are always constructed as a single layer but n = 2 corresponds to k_Δ = 0.94 in equations 2 and 3.
2. Here the number of units is given per square armor unit dimension.

Table 2
FEM Static Stress Comparison

Load Case	Tensile Stress, psi (Mpa)			
	CORE-LOC™	Dolos	Accropode	Tribar
Torsion	162 (1.12)	302 (2.08)	220 (1.52)	432 (2.98)
Flexure - fluke tip load	162 (1.12)	349 (2.41)	220 (2.52)	487 (3.36)
Flexure - fluke center load	305 (2.10)	496 (3.42)	NA[1]	NA
Combined flexure and torsion	277 (1.91)	555 (3.83)	NA	NA

[1]NA = not applicable.

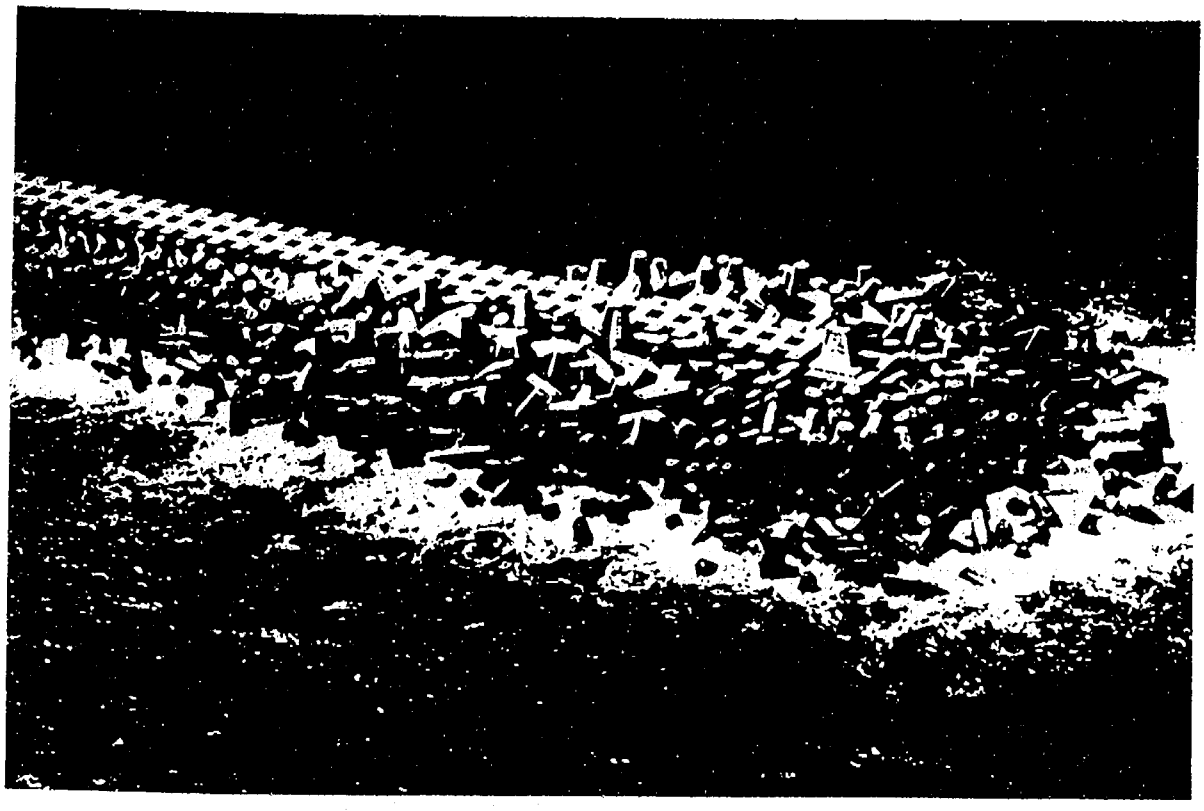


Figure 1. Dolosse and Tribar on the Nawiliwili Breakwater in Hawaii

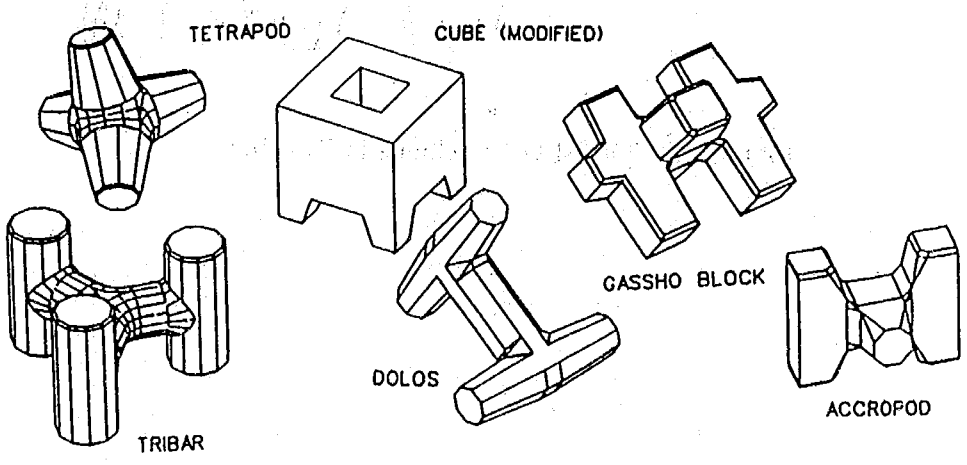


Figure 2. Various Concrete Armor Shapes

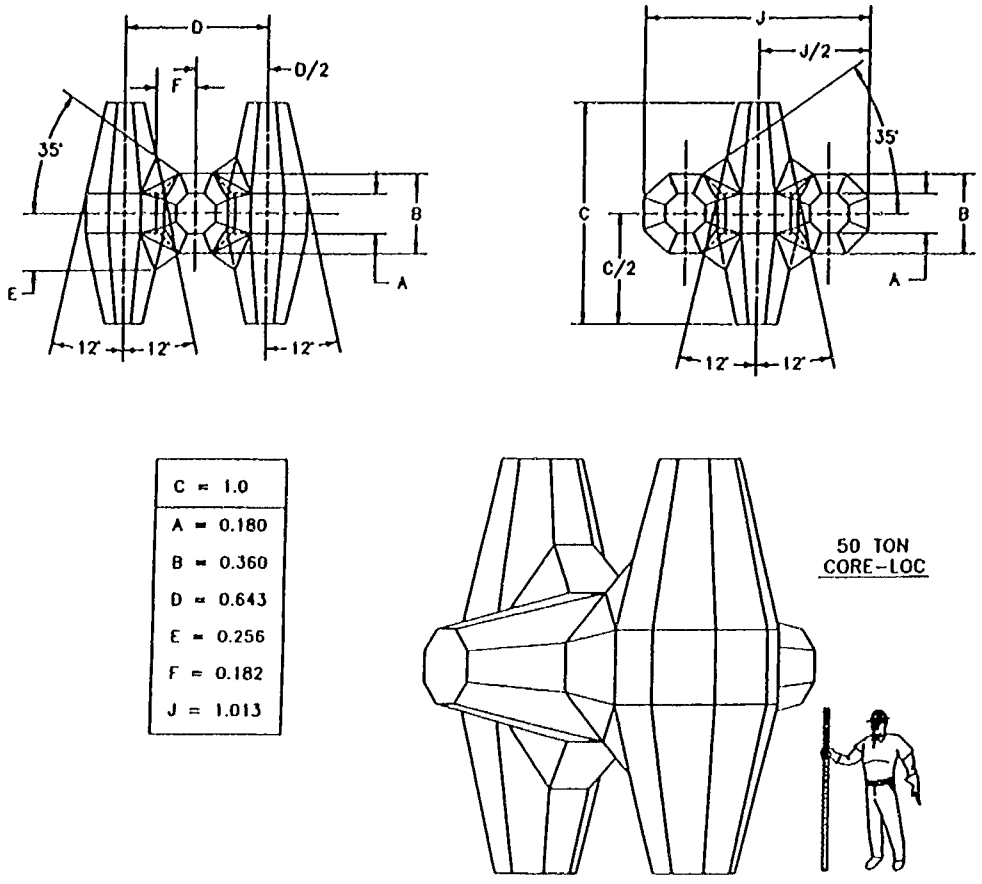


Figure 3. CORE-LOC™ Schematic Drawing

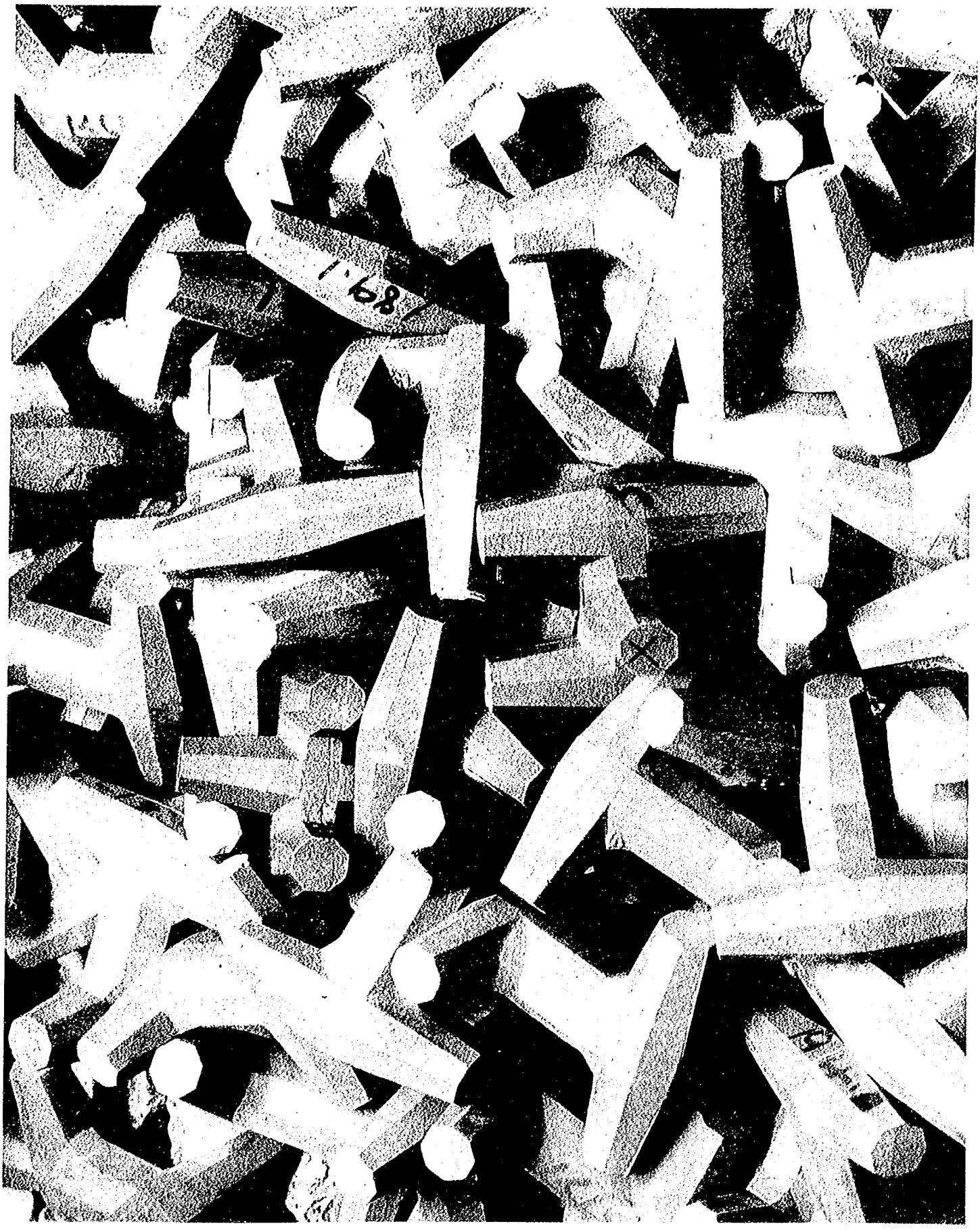


Figure 4. CORE-LOC™ and Dolos Armor Matrix

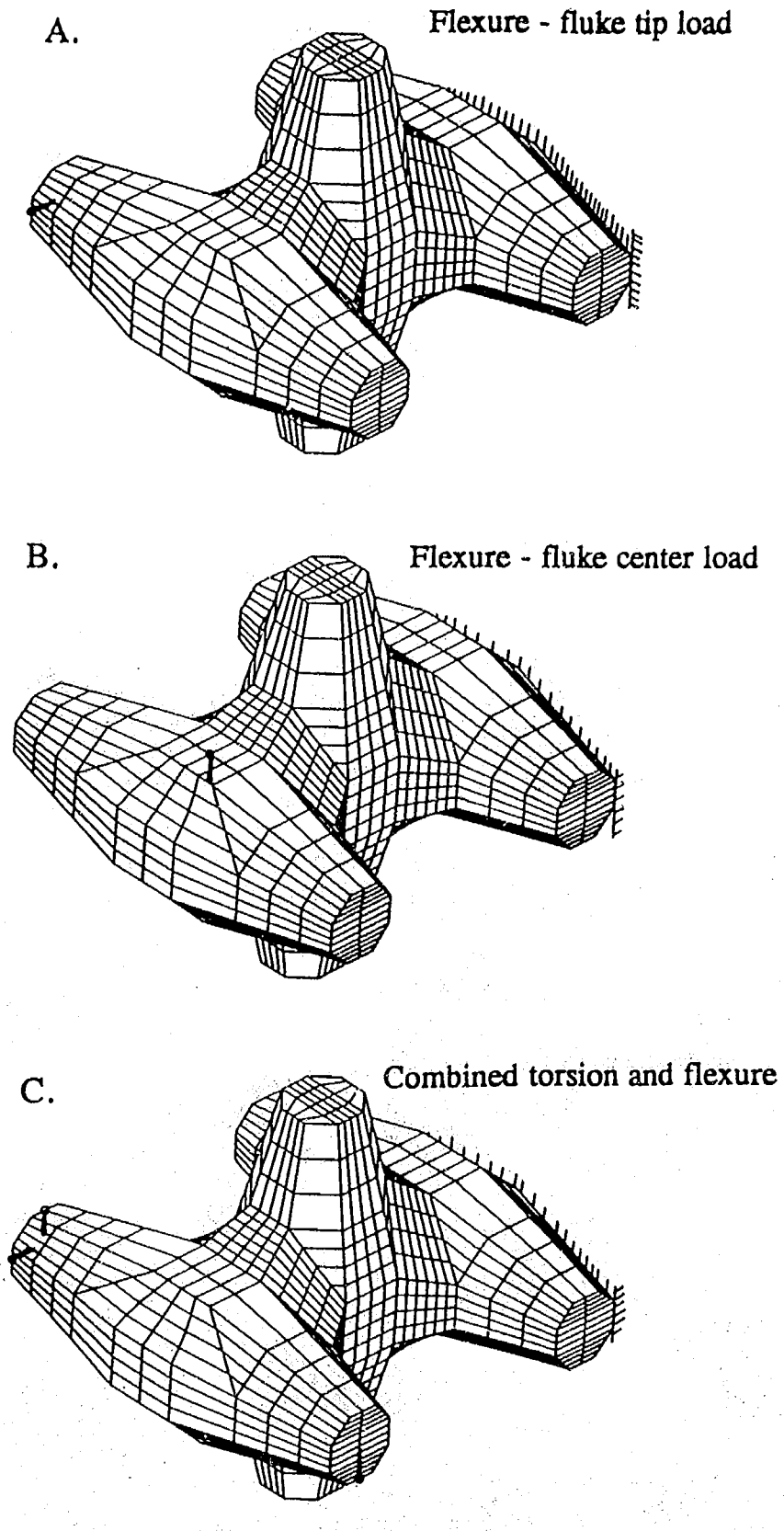


Figure 6. Loading and Boundary Conditions for Other Load Cases

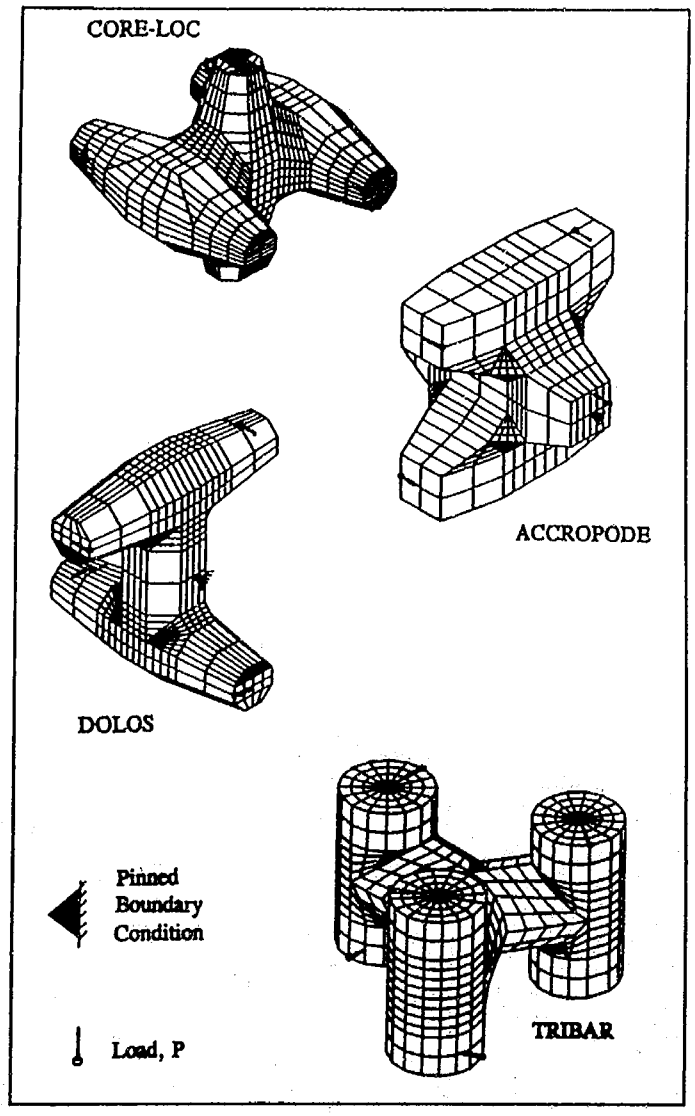


Figure 5. FEM Grids for CORE-LOC™, Accropode, Dolos, and Tribar

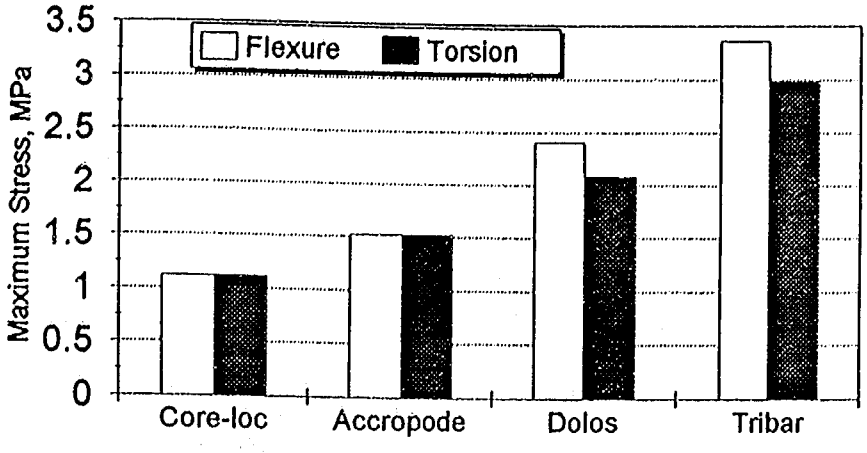


Figure 7. Finite Element Structural Response Comparison



Figure 8. CORE-LOC™ Under Wave Attack During Early Testing

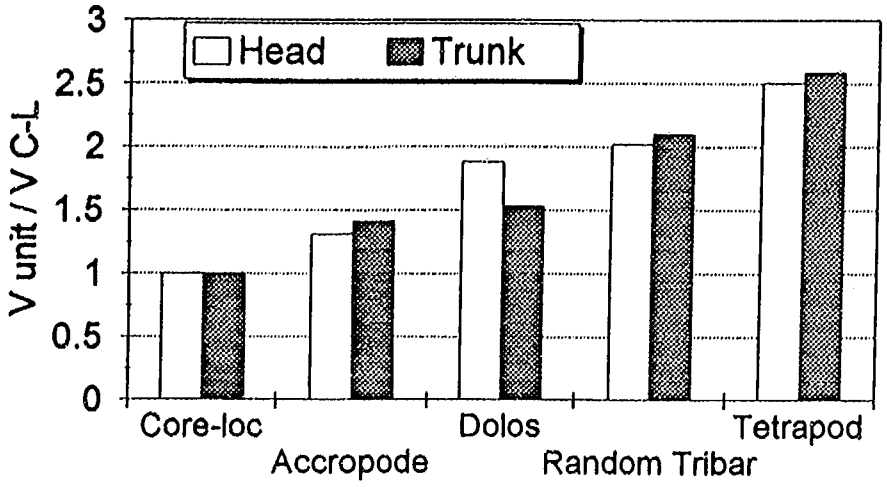


Figure 9. Concrete Armor Volume Comparison

Manuscripts Authored for Panel Meeting But not Presented Orally

A Review of Wind Research Currently Underway in the Vincent Aerodynamics Laboratory

by

Harold R. Bosch* and Dryver R. Huston**

ABSTRACT

This paper presents an overview of the ongoing research and engineering activities of the U.S. Federal Highway Administration's (FHWA) Aerodynamics Laboratory. The activities include: wind tunnel studies of generic structural sections, cylinders, tapered cylinders, and bridge deck sections; field studies of the aerodynamic performance of 2 long-span bridges - including the recently fairing-retrofitted Deer Isle bridge; the development of numerical modeling techniques that are specifically-designed for problems related to the aerodynamic and aeroelastic performance of highway structures; and climatological studies, with a focus on the Deer Isle bridge site.

KEYWORDS: aerodynamics; bridges; damage; highways; structures; wind engineering.

1. INTRODUCTION

The FHWA Vincent Aerodynamics Laboratory is the center of the FHWA's wind engineering research and design activities. The laboratory is engaged in a broad range of activities related to understanding and improving the aerodynamic performance of highway structures. These activities include: the operation of a wind tunnel for scaled model and fundamental aerodynamic and aeroelastic studies; the measurement of the wind environment and the resulting performance of highway structures in the field; the development of numerical methods for structural, aerodynamic and aeroelastic simulations; and the integration of wind tunnel and numerical simulations to predict prototype behavior. Historically the bulk of these activities have focused on the problems related to the aeroelastic response of long span bridges. However, other highway structures such as signs, appurtenances, and long slender beams are also subject to wind effects and are an ongoing point of study.

2. WIND TUNNEL STUDIES

The FHWA Vincent Aerodynamics Laboratory contains a low-speed open jet wind tunnel, the G.S. Vincent Wind Tunnel, that is specifically designed for the testing of bridge sections. The tunnel has a speed range of 0 to 15 m/s. The flow is nominally very laminar, with intensities less than 0.5%. The test section is 1.5 m by 1.5 m. The wind tunnel is equipped with a variety of force balances, aeroelastic balances, anemometry, data acquisition systems and turbulence generators.

2.1 Cylinder Tests

Cylinders of various shapes are primary components of many highway structural systems such as signs and appurtenances. The FHWA is engaged in a study to catalog the aerodynamic behavior of cylinders with both uniform and tapered cross-sections (Bosch, 1994). The cylinders under study have circular, hexagonal, octagonal and actual prototype cross-sections. The uniform cross-section cylinders are a set of circular, hexagonal, and octagonal forms, each with diameters of 2, 3, 4, 5, and 6 in. (51, 76, 102, 127, and 152 mm). The tapered circular, hexagonal, and octagonal cylinders are sets with equivalent diameters of 3, 4, and 5 in (51, 76, and 102 mm), and taper ratios of 0.05, 0.10, 0.14, 0.20, 0.25, and 0.30 in/ft (8.33, 11.7, 16.7,20.8, 25 mm/m). These models are fabricated mostly out of wood to be rigid and lightweight. The surfaces of the models are sanded and varnished smooth. The corners on the polygonal sections are cut sharp so as to produce a repeatable flow separation. In addition, two cylinders cut out of actual prototype sign structural members are included in the test set. One of the prototype cylinders has a circular cross-section with a diameter of 5.0 in

*Federal Highway Admin., McLean, VA 22101
**Univ. of Vermont, Burlington, VT 05405

(127 mm) and a taper ratio of 0.26 in/ft. (21.7 mm/m). The second prototype section is octagonal with a taper ratio of 0.134 in/ft (11.1 mm/m).

The test configuration involves placing the axis of the cylinder horizontal and perpendicular to the flow. The cylinder is rotated about its axis and then fixed at an angle so that either the flat faces of the polygons or the corners are oriented directly into the flow. Additional configurations involved testing at rotation angles that ranged to +/-15 degrees, in one degree increments, from the initial orientation. The test protocol is to collect drag, lift and moment forces from the cylinders, at 31 different wind speeds, with a full repeat, for at least 90 seconds with a 100 Hz/channel sampling rate. Figure 1 shows a typical result of the drag force that was measured on a hexagonal tapered cylinder at two different angles of incidence.

The future course of this research will be to measure the Strouhal numbers for all of the cylinders, and possibly the tendency to some other aeroelastic behaviors such as galloping or flutter. It is anticipated to extend this work to cylinders with cross-sections that mimic very closely that which is used in various highway sign posts, e.g. welded boxes with short overlapping flanges or extruded boxes with rounded corners.

2.2 Structural Section Tests

In addition to the cylinder tests, a variety of generic box and H-shaped sections are being tested in the wind tunnel for static force and moment characteristics, vortex shedding properties, and flutter proclivities. The box sections include 12 rectangular shapes, and 12 H-shaped sections with height to width ratios (H/W) of 0.1 to 1.0,. Ten of the H/W ratios for rectangular and H-shaped sections run from 0.1 to 1.0, in increasing increments of 0.1. A repeat section with a 17% smaller width was added for the H/W ratio of 0.5. Additional sections with H/W ratios of 0.25 were included. The reason for adding sections with H/W ratios of 0.25 to the test sets is that the aerodynamic behavior of these sections seem to undergo a dramatic change in this range, and because the original Tacoma Narrows bridge had an H-shaped plate girder section with a height to width ratio in this critical range. In addition to the generic sections providing a catalog of aerodynamic behaviors, they also serve the purpose of forming a calibration standard for determining the repeatability of wind tunnel results in different wind tunnel facilities (Huston, 1987).

2.3 Bridge Tests

The Deer Isle bridge continues to be a subject of study in the Vincent tunnel. One issue of interest is to obtain a very detailed understanding of the performance of the fairing system that has been installed as a retrofit on the prototype structure. Some of the detailed studies include an examination of the effects of curb venting and partial fairing coverage. Since the bridge is situated in a northern climate, the curb vents and sidewalk grates are often clogged with snow and ice. Various combinations of open and closed grates and vents on both the upstream and downstream sides of the deck are being examined. Another item of interest is the effect of partial fairing coverage on the aerodynamic performance of the bridge. The prototype structure has been fitted with fairings across the full span. However, dead weight and construction concerns raise the possibility of partial fairing coverage as a configuration worth examining. A preliminary wind tunnel study of partial fairing coverage was conducted on the Deer Isle bridge using crude cardboard fairing prototypes (Huston et al. 1988). The next phase, which is mostly complete, is to conduct a study of the effects of partial fairing coverage using fairings that are modeled faithfully to that which has been installed in the field. Of particular concern is to test the validity of the commonly-used assumption of strip theory aerodynamics that permits the superposition of the aerodynamic behavior of the faired and unfaired section of the bridge.

Preliminary plans are underway to attempt to test a 3-D model of the Deer Isle bridge. A characteristic feature of the Deer Isle bridge is that it has a very large camber, i.e. grades of 6.5% on the side spans. The camber may introduce 3-D aerodynamic effects that cannot be captured with a simple 2-D section model, particularly those that may arise due to a wind that approaches the deck at an oblique angle. This is also of interest because anecdotal remarks of the bridge maintenance personnel indicate that quartering winds seem to cause the largest deck motions. The 1.5 m by 1.5 m cross

section of the Vincent tunnel makes it awkward to conduct a traditional 3-D aeroelastic model test. However, the use of a 3D aeroelastic model in a quartering geometry, or a hybrid cambered section model, or a partial taut strip model, may make such a test feasible.

In addition to the above Deer Isle bridge studies, there are several studies of bridge aerodynamics that are in the longer term scheduling plans of the wind tunnel. These include the testing of the aerodynamic performance of the large library of bridge sections that the Vincent wind tunnel has accumulated, as well as 5 streamlined box shapes that are reminiscent of various streamlined box girder bridge decks. Most of these sections have not been tested using the modern methods, such as flutter derivative extraction. Other long term studies are the use of active turbulence generators and forced vibration section model motions in more fundamental studies of bluff body aerodynamics.

3. FULL SCALE MEASUREMENTS

Since the ultimate goal of the activities of the FHWA Vincent aerodynamics laboratory is to improve the aerodynamic performance of actual highway structures, the laboratory maintains an active program of taking full scale prototype measurements. These full-scale studies are intended to establish wind environments and the resulting bridge behaviors through the measurement of wind speeds and bridge motions. The long intervals between interesting events requires a long term testing strategy that includes the use of automated data acquisition equipment for remote control and event-triggered measurements, the acquisition of continuous weather chart data, and the development of special testing procedures.

3.1 Deer Isle-Sedgwick Suspension Bridge

The Deer Isle-Sedgwick bridge has been the subject of an extensive aeroelastic performance monitoring study since 1981. The Deer Isle bridge was constructed in 1938. The original deck section of the bridge was an H-shaped plate girder that is quite similar to that of the original Tacoma Narrows bridge. As a result the Deer Isle bridge is prone to wind-induced motions. These motions have been large enough to cause localized damage and traffic disruption. In an attempt to reduce the wind-induced motions and to prevent the occurrence of a Tacoma Narrows-type catastrophe, the bridge structure was stiffened on several occasions through the use of diagonal stays and deck-cable binding blocks, Figure 2. Nonetheless, the fundamental aerodynamic instability persisted. An aerodynamic modification to the bridge in the form of triangular-shaped fairings that were added to the full length of the bridge was completed in 1994, Figure 3. The bridge is now being monitored after the fairing modification to determine the effectiveness of the fairings on the aerodynamic performance of the bridge. The field instrumentation consists of 15 accelerometers, 6 tri-axis anemometers with a relatively high-frequency response, two low-frequency sky-vane anemometers, three thermometers, and various voltage reference channels (Bosch and Miklofsky, 1993). In all, 44 channels of data are collected simultaneously in digital form and stored on site. The data acquisition system is queried and controlled via telephone communications with the FHWA Vincent lab in McLean, VA. Figures 4 and 5 shown a typical time history and the corresponding spectrum for an accelerometer that was attached to the deck.

3.2 Luling-Destrehan Cable-Stayed Bridge

The Luling-Destrehan bridge spans the Mississippi River near New Orleans. It is one of the first cable-stayed bridges in North America to be built with a streamlined deck and to be placed in a hurricane-prone setting. As a result, the Luling bridge is also being monitored for wind-induced vibrations. To date no hurricanes have crossed the bridge site, in spite of some close calls. Therefore, the wind and vibration data measured at the site has been rather uneventful. In general, the bridge has performed well, as predicted in the wind tunnel. However, there have been several occasions where the stay cables have been reported to vibrate. In an effort to observe the stay cable vibrations, accelerometers have been deployed on a limited number of cable stays. Unfortunately, the stay cable vibrations, that have been reported, have occurred in the quadrants of the bridge that were not instrumented. One of the top priorities of the Luling monitoring project is to enhance the transducer coverage of the bridge so as to be able to capture these vibrations in the future.

3.3 Analysis of Field Data

The data sets gathered at the field sites are quite large. The processing, managing, archiving and interpreting of the data is a formidable full-time task that requires judicious use of computer processing techniques. The data are initially stored in digital form onsite on cassette magnetic media. The cassettes are manually retrieved and mailed to the FHWA lab for processing. The first step in the processing is to perform a cursory catalog and summary of the data by scanning the time histories and calculating means, RMS's, and peak values. This initial summary process serves as an initial check on the validity of the data as well as identifying interesting events for detailed analysis. Next, the data are processed more in detail with the calculation of wind spectra, acceleration spectra, modal motions and other statistical parameters. Automated software processing has been developed so that for each 50-70 MB data tape, a 3 cm thick notebook, binder of statistical analysis and plots is produced, reviewed, and stored. The storage of the data on magnetic media poses problems due the relatively short shelf life of the media and the rate at which the tape drives become obsolete. Therefore, the original field data are copied and archived onto optical media. It is believed that the optical media will be much more robust for long term storage.

Of course the big question related to the data processing is the interpretation of the data and using it for engineering research and design purposes. The item on the top of the field data interpretation agenda is: What effect do the fairings produce on the behavior of the Deer Isle bridge? The data sets gathered since the completion of the fairing modification are at present rather minimal. However, very preliminary and cursory observations of the post-retrofit data indicate that the fairings have indeed significantly reduced the aerodynamic actions of the bridge.

4. NUMERICAL MODELING

The goal of the numerical modeling efforts of the lab are to create a set of tools so that the aerodynamic and aeroelastic performance of various highway structures can be analyzed and designed effectively and efficiently with the aid of a computer. The effort has focused on: the adaptation of finite element codes to the peculiarities of long-span bridge aeroelasticity, the application of computational fluid dynamics techniques to bridge deck bluff-body aerodynamics, and stochastic fatigue modeling of highway support structures.

4.1 Finite Element Methods

The mechanics of suspension, cable-stayed and other cable supported bridges under wind loading are quite complex and somewhat different than that of more traditional structures. The distinguishing characteristics of these cable-supported bridges are that the cable forces and reactions can be nonlinear, and that the aerodynamics often involves flow patterns with highly-separated turbulent wakes. While modeling tools are available for the analysis of cable-supported structures and likewise the for the analysis of the aeroelasticity of bluff sections, there are no readily-available numerical models that are capable of incorporating all of these effects. Therefore, a development effort has been underway to create a set of numerical, i.e. finite element-based, procedures that can be used to predict the responses of bridge structures to wind loads and ultimately be used in an optimal structural design process.

Aeroelastic modeling requires the complementary modeling of structural and aerodynamic forces. The modeling of the structural forces in cable-supported bridges requires accounting for the geometric nonlinearities associated with cable forces. Fortunately, if the bridge motions are relatively small, then the dynamic cable forces are linear, and it is only the static cable forces that must be modeled with nonlinear methods. Finite element techniques have been developed that can model the dynamics of cable-supported bridges by first performing a nonlinear static analysis and then a linear dynamic analysis about a position of static equilibrium. This method has been applied to both the Deer Isle and the Luling bridges (Cai, 1993). During the course of analyzing the Deer Isle bridge, it became apparent that a knowledge of the nominal bridge properties was insufficient for accurate analysis, since the presence of a number of diagonal stays produced a highly-indeterminate pretensioned structure. The magnitudes of the pretensions in the diagonal stay cables can significantly affect the dynamics of the bridge. Since the pretensions were

unknown, certain ad hoc assumptions had to be made in the modeling. However, with the addition of fairings to the Deer Isle bridge in 1994, the cable tensions were all measured and reset to accommodate the added dead load. The retensioning of the stays presents an excellent opportunity to redo and verify the structural analysis.

The state of the art of modeling the aerodynamics of bluff structures, such as bridge decks, is to employ a semi-empirical approach where the observed behavior is classified as being one of a few distinct phenomena, i.e. flutter, buffeting, vortex shedding and possibly galloping. Simple mathematical models are then used to describe the aeroelastic interactions (Scanlan and Tomko, 1971). One of the major portions of the numerical modeling efforts has been to extend the simple bluff-body aeroelastic models, via an assumption of strip-theory aerodynamics, to full scale 3-D structural models by combining the aeroelastic models with the finite element method (Cai, 1993 and Cai and Bosch, 1993). This aeroelastic finite element technique has been successfully completed for flutter, buffeting, and vortex-shedding. Different variations of the flutter and buffeting formulations have been implemented so as to incorporate the effect of turbulence in the flutter derivatives and to incorporate the parametric excitation models of Lin (1979). An example of the capabilities of this software are shown in Figure 6 where the buffeting response of the Deer Isle bridge for different partial faring coverages and diagonal stay configurations are calculated. The future plans for this research effort are to verify a recently-developed vortex-shedding finite element model, apply these techniques to model the fatigue of highway support structures, and to develop finite element-based aeroelastic models of many of the major bridges that have been studied in the Vincent laboratory.

4.2 Computational Fluid Dynamics

A long term and ongoing research activity of the Vincent Laboratory is to develop and adapt computational fluid dynamics (CFD)methods to the particular requirements of highway structures analysis. The bluffness of highway structures, e.g. bridge decks or members, results in wind flow patterns that are characterized by separated and turbulent wakes. A detailed 3-D modeling of the aerodynamics and aeroelasticity of bluff structures is very difficult and pushes the limit of present CFD techniques. Nonetheless, the attractiveness of creating realistic simulations on the computer for design and analysis purposes certainly justifies what will be a long-term undertaking. A major effort along these lines was carried out by Onyemelukwe (1993) where the flow around generic bridge deck sections was calculated by a finite difference procedure. The calculations were performed on a 386-PC and a Unix workstation. The results were definitely promising in that reasonable-looking flows with vortex-shedding around the bluff sections were created. However, the amount of the calculation required limited the length of the simulated time histories to a couple of vortices. The calculated lift and drag coefficients, as well as surface pressures, were usually within 30% of the experimentally-measured values. Figure 4. shows a typical set of simulated velocity contours from the Chesapeake Bay Bridge.

Planned future extensions of the CFD research include: 1. Considering other algorithms, such as vortex-based methods; 2. Porting the existing finite difference algorithms to bigger and faster computers for more extensive computation; 3. The introduction of turbulence into the upstream air; and 4. The introduction of section motions, i.e. make the system aeroelastic.

4.3 Reliability Modeling of Highway Support Structures

Highway support structures such as signals and luminaries are also subjected to wind effects, in particular the action of fatigue. Since the wind-induced fatigue failure of highway support structures is a rare, but observed, phenomenon, a research program is underway to develop methods of predicting the fatigue response of these structures. The research is aimed at developing rational stochastic-based models. The main issue of concern is how to model the effects of vortex-shedding, wind gusting, and truck turbulence on the fatigue life of support structures. The inherent randomness of wind loads, and relatively large spreads that are observed in the fatigue life of structures under random loadings, suggest that a stochastic-based model of highway support fatigue would be a rational approach. Namini and Bosch (1995) use such methods to compare the ASCE wind load provisions, the AASHTO specifications, and rational stochastic models that include wind

gusting. The results of this methodology are that the gust response in the form of RMS stresses can be calculated for support structures, but that it would be best to include detailed local climatological information.

5. CLIMATOLOGICAL STUDIES

The rational aerodynamic design of highway structures, particularly long-span bridges, requires the use of estimates of the speed, direction, and duration of the winds which will attack a structure during its lifetime. One of the best methods of establishing the design wind environment is to use historical wind data as a basis. The United States has an extensive log of wind data from weather stations that are distributed throughout the country. Unfortunately, this data set consists of a patchwork of different formats, none of which are precisely suited to the task of formulating design wind speeds for bridges, and most of which are collected at locations that are near to, but not at, the bridge site. An effort is currently underway to begin to remedy the situation by examining the climatological data at or near a particular bridge site, and adapting the data to the standard design formats (Zhang, 1995).

6. INFORMATION DISSEMINATION

The ultimate success of the research conducted by the Vincent Laboratory and by other wind engineering centers is the extent to which procedures and practices developed as part of the research program are implemented in the field, and the resulting performance of these procedures and practices. A large impediment to having these new techniques adopted is that practicing engineers are not readily exposed to the information. As a result, the Vincent Laboratory is in the process of developing educational and promotional literature that supplements the usual papers, reports and technical presentations. The educational literature will be in the form of newsletters, technical guides, technical booklets, and case studies on wind engineering practice, particularly as it pertains to highway structures. This literature will then be distributed to practicing engineers.

7. CONCLUSIONS

The FHWA Vincent Aerodynamics Laboratory has ongoing research activities that span the broad topics related to the wind engineering of highway structures including wind tunnel studies, field measurements, computer simulations, design practice development and information dissemination.

8. REFERENCES

Bosch, H.R., and Miklofsky, H.A. (1993) "Monitoring the Aerodynamic Performance of a Suspension Bridge," Paper presented at the Seventh United States National Conference on Wind Engineering, Los Angeles, CA.

Bosch, H.R. (1994) "Wind Tunnel Tests on Tapered Cylinders for Highway Support Structures," Paper presented at 26th Joint Meeting UJNR, Panel on Wind and Seismic Effects, Gaithersburg, MD.

Cai, C.S., (1993) "Prediction of Long-Span Bridge Response to Turbulent Wind," Ph.D. dissertation, University of Maryland, College Park, MD.

Cai, C., and Bosch, H.R., (1993) "Improved Analytical Procedure for Predicting Flutter Response of Long-Span Bridges," Paper presented at the 25th Joint Meeting UJNR, Panel on Wind and Seismic Effects," Tsukuba, Japan.

Huston, D.R., (1987) "Flutter Derivatives Extracted from Fourteen Generic Deck Sections," Bridges and Transmission Line Structures, L. Tall ed., pp. 281-291, Proc. ASCE Structures Congress, Orlando, Florida, August 1987.

Huston, D. R., Bosch, H. R., and Scanlan, R. H., "The Effects of Fairings and of Turbulence on the Flutter Derivatives of a Notably Unstable Bridge Deck," Journal of Wind Engineering and Industrial Aerodynamics, 29 (1988) 339-349.

Onyemelukwe, O, (1993) "Computer Simulation of Wind Effects on Bridges and Other Bluff Bodies," Ph.D. dissertation, Department of Civil Engineering, University of Pittsburgh, Pittsburgh, PA.

Lin, Y.K., (1979) "Motion of Suspension Bridges in Turbulent Winds," Jnl. of Eng. Mech., ASCE 105(6), 921-932.

Namini, A., and Bosch, H.R. (1995) "Stochastic-Based Model of Wind-Induced Highway Support Fatigue Response," ICASP7, 7th International Conf. on Applications of Statistics and Probability, Paris, July 1995.

Scanlan, R.H., and Tomko, J.J. (1971) "Airfoil and Bridge Deck Flutter Derivatives," Jnl. Eng. Mech., ASCE 97(6), 1717-1737.

Zhang, X., (1995) "The Climatology and Wind Environment of the Deer Isle Bridge Site," M.S. thesis, Dept. of Civil Engineering, University of Vermont, (pending).

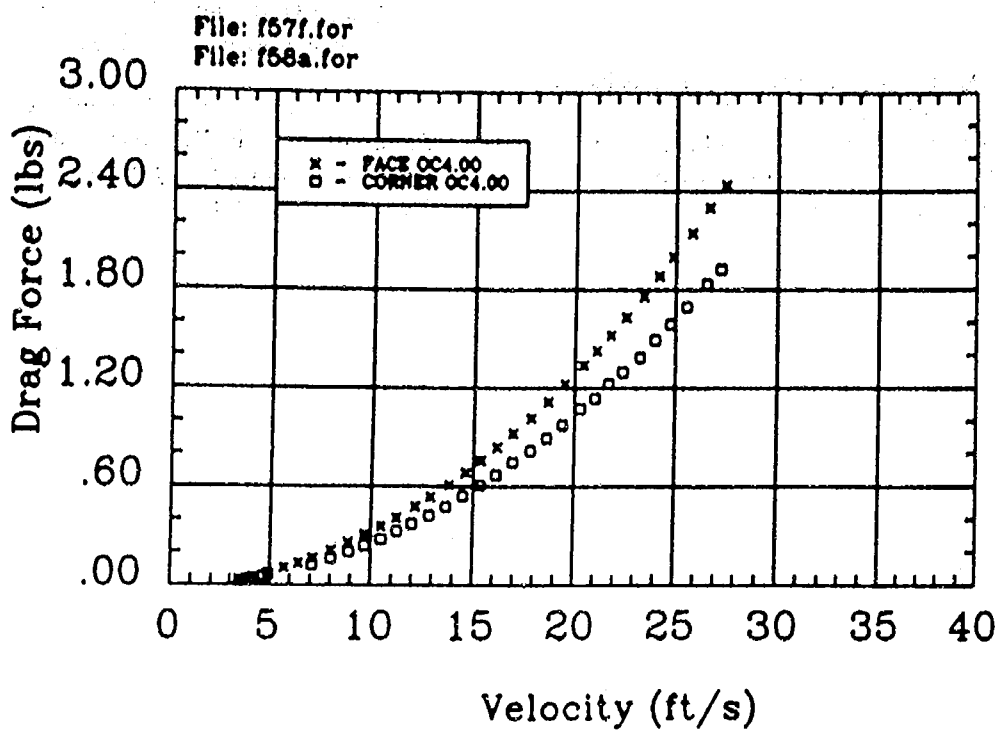


Figure 1. Typical drag force coefficients measured on an octagonal cylinder for a face-on and an angle-in orientation.

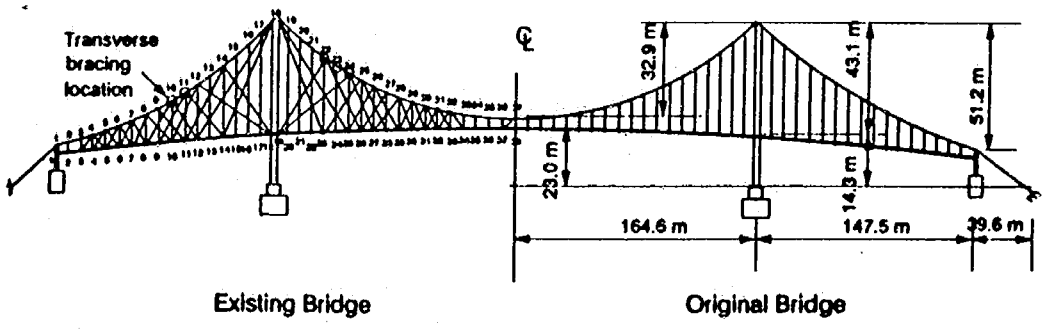


Figure 2. Side view of the Deer Isle bridge showing the original cable configuration and the addition of diagonal stays.

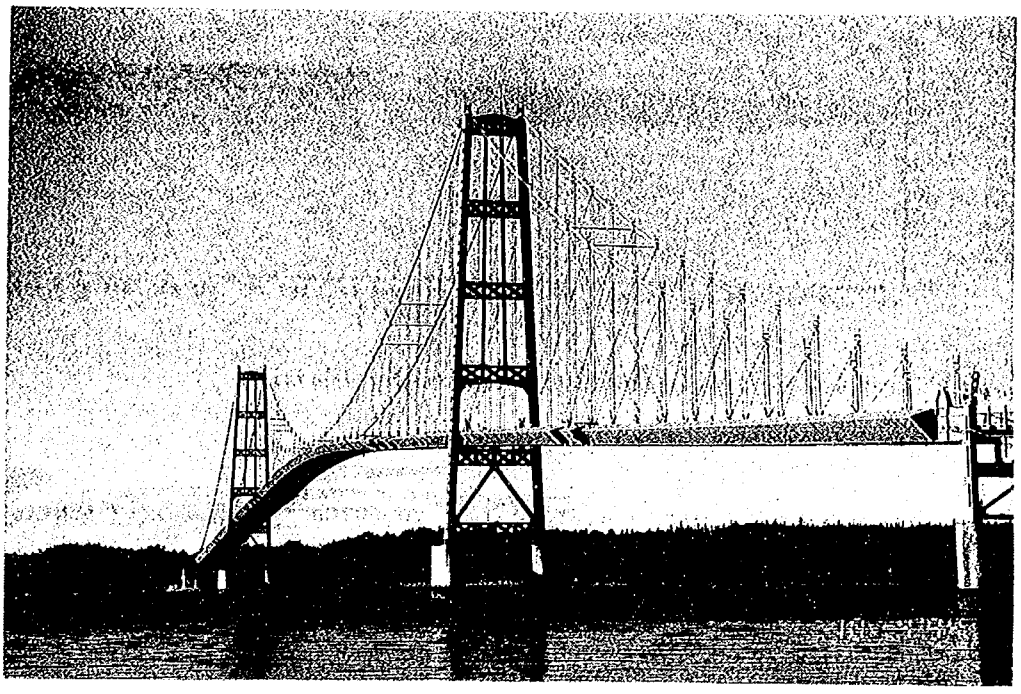


Figure 3. Deer Isle bridge with fairings attached to the deck.

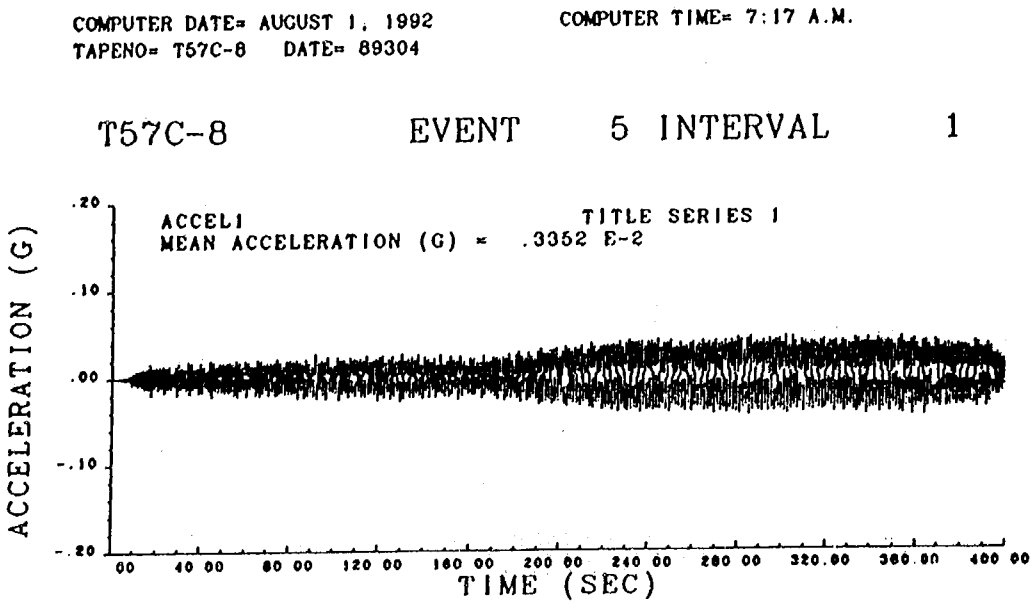


Figure 4. Typical deck acceleration time history from the Deer Isle bridge.

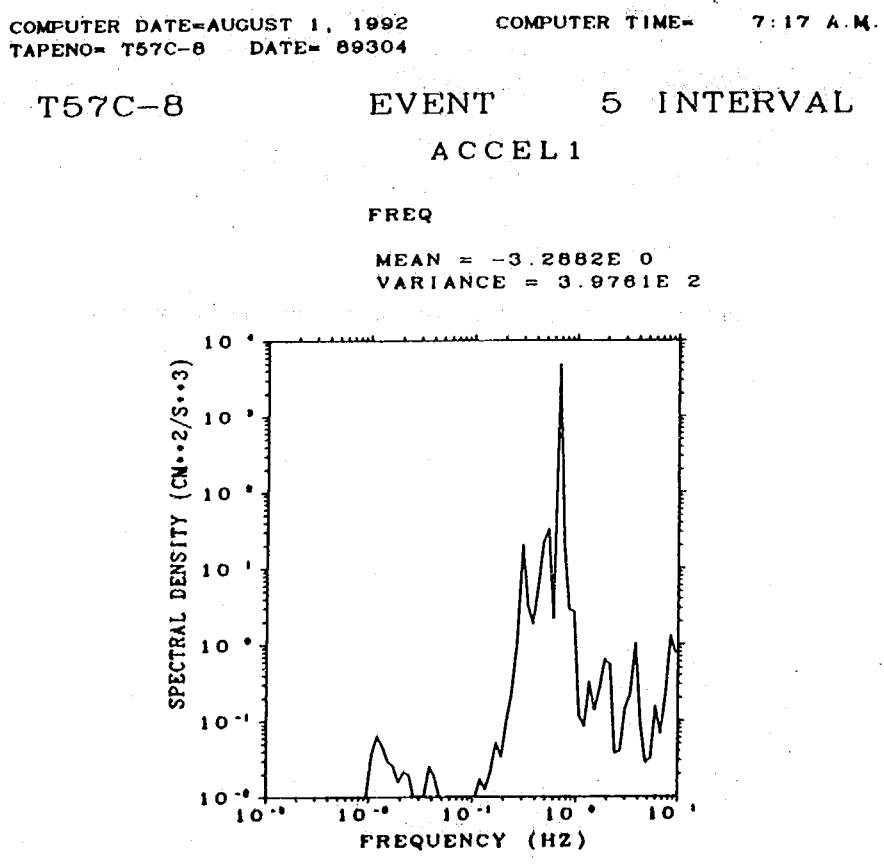


Figure 5. Spectrum of deck acceleration from Deer Isle bridge corresponding to Figure 4.

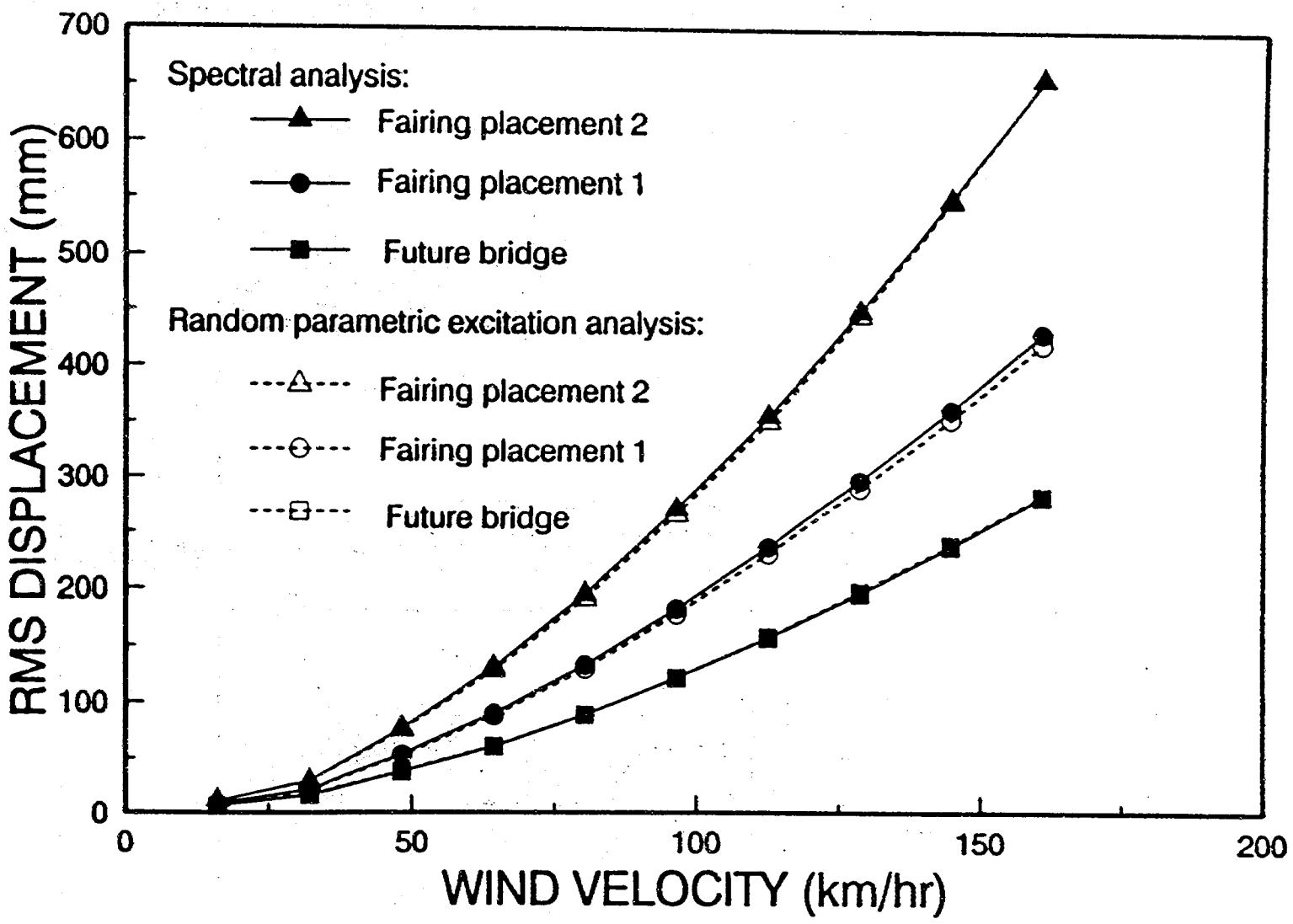


Figure 6. Buffeting response calculations for the Deer Isle bridge with different fairing coverage and a configuration (labeled future) without diagonal stays using both the spectral and parametric models (Cai, 1993).

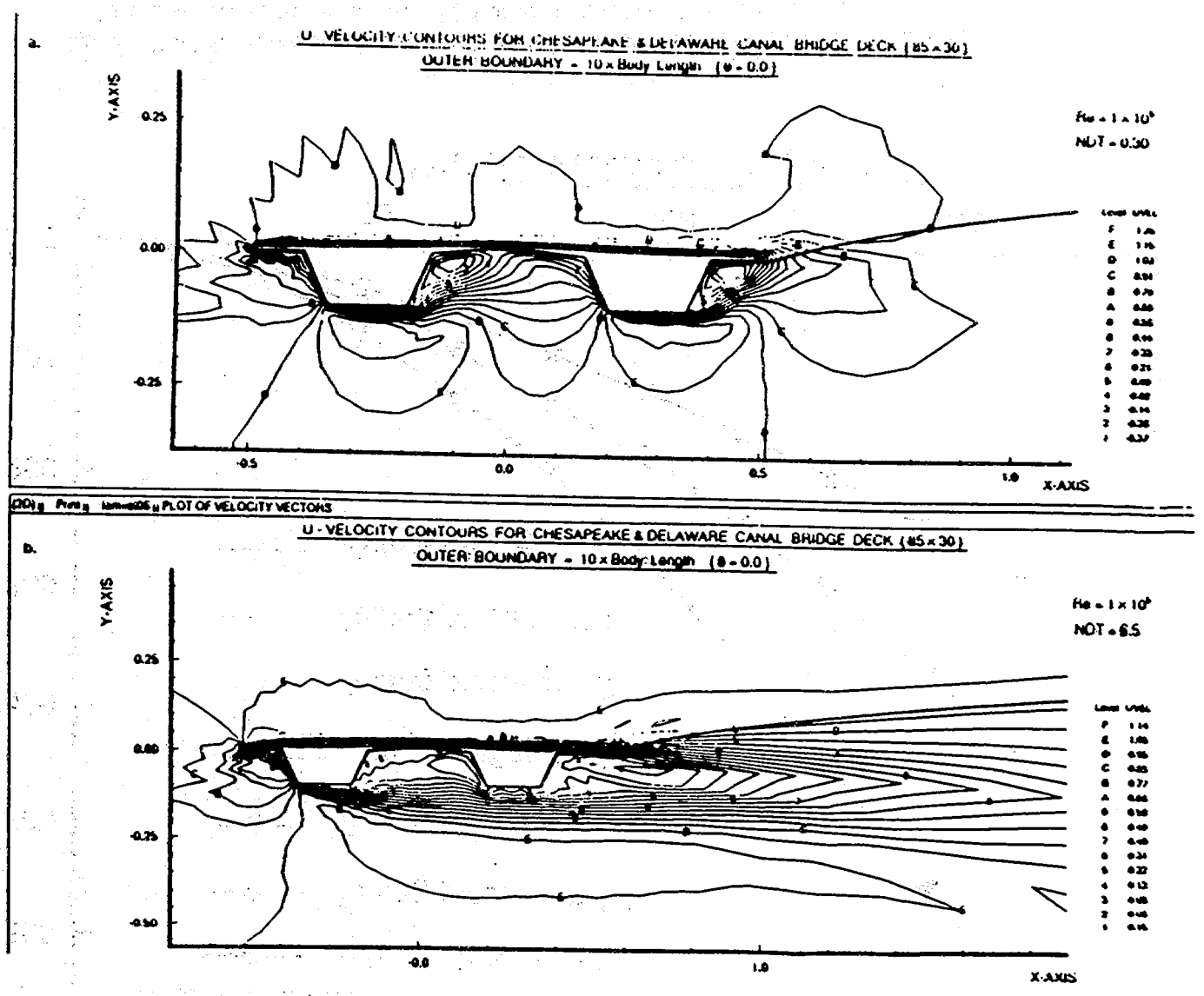


Figure 7. Velocity contours calculated for the Chesapeake & Delaware Canal bridge deck for a laminar oncoming flow and Re = 10^5 (Onyemelukwe, 1993)

EARTHQUAKE ENGINEERING RESEARCH FOR RESERVOIR DAMS

by

William E. Roper[1], Ph.D., PE

ABSTRACT

The U.S. Army Corps of Engineers initiated a sever year Earthquake Engineering Research Program in 1995 focused on providing design procedures, assessment tools, and criteria for assuring the seismic safety of civil works reservoir dam projects. The research programs background is outlined and the program structure in the two major areas of geotechnical and structural research are presented. Accomplishments during the past year are summarized. The preliminary findings of a specific research effort to mea sure reservoir-bottom reflection coefficient indicate current design practice maybe overly conservative. The paper concludes with future research plans focusing on the 1996 program.

INTRODUCTION

The Earthquake Engineering Program (EQEN) is an applied research program whose purpose is to provide design procedures, assessment tools, and criteria for assuring the seismic safety of the Corps' unique civil works facilities, namely dams, locks and levees. The primary emphasis is on reservoir dam projects since these are the Corps' most critical structures in terms of public safety. The Corps is responsible for more than 200 reservoir dam projects located throughout the United States in areas of significant seismic shaking potential shown in Figure 1.

The EQEN cooperates with and draws from the basic and applied research elements provided by other Corps R&D efforts, other federal agencies, and academic and professional experts, and extends and integrates these elements with in house work to fully address Corps seismic safety issues. EQEN is formulated to contain a balance of short-term work units designed to address immediate questions related to currently used methods of analysis, and longer-term efforts to provide better methods with stronger theoretical foundations and greater validation. The program was developed by a combination of input from field offices, Headquarters Technical Monitors Headquarters National Research Program Mangers and Laboratory earthquake engineering researchers.

This program is designed to develop better estimates of the earthquake ground

[1]Director, Civil Works Research and Development, U.S. Army Corps of Engineers, Washington, DC, U.S.A.

motions for use in design and to predict more accurately and quantitatively the amount of deformation and damage these ground motions will cause to our facilities. If remediation is found necessary, to provide more effective and efficient options to select from and practical tools to design and implement a remedial action.

The elements required to do this are developed from a solution process that includes: 1) evaluation of the seismic hazard, 2) site characterization and conceptualization, 3) modeling the material behavior and computing the expected damage (see Figure 2). The development of effective, economical remedial measures puts even greater demands on steps 2 and 3, since the materials are now complex composites, possibly requiring a three dimensional analysis to evaluate. It is the underlying plan of this research program to provide practical products from each research focus effort that work together to achieve the advancement in the state-of-the-art we seek.

RESEARCH PROGRAM STRUCTURE

The EQEN Program currently has sixteen focus efforts which are organized into two major seismic research areas: 1) Geotechnical Research, and 2) Structural Research.

Geotechnical Research

The geotechnical research address the steps involved in solving a seismic problem for embankment dams: earthquake ground motions, site characterization, liquefaction-deformation-damage assessment, and remedial measures.

Earthquake Ground Motions

Knowledge of the behavior of ground motions advances with each new earthquake and breakthroughs in basic research by seismologists. The ground motion focus efforts will maintain cognizance of these advances and translate the aspects important for engineering analysis into usable tools to provide ground motion input for analysis in the form needed as computational ability advances. These focus efforts are thus closely coordinated with the development of structural and geotechnical numerical models.

Site Characterization

Present methods of site characterization rely mainly on individual borings to provide key information about stratigraphy, velocities and penetration resistance. The research in this area will be focused on 1) developing improved geophysical techniques to link together borehole information, and to directly measure soil parameters needed for analysis, and 2) resolving the present controversy regarding interpretation of Becker Hammer measurements widely used in liquefaction evaluation of gravelly soils, and possibly develop a new in situ testing tool that is more amenable to direct analysis, so that the translation of field information to inputs needed in numerical analysis is as seamless as possible.

Liquefaction-Deformation-Damage

The present procedures for assessing liquefaction potential and post earthquake stability rely almost exclusively on empirical correlations between penetration resistance and cyclic and

residual strength. These procedures do not provide a basis for quantitatively predicting deformations and assessing damage. Advances have been made in developing more fundamental constitutive models and numerical dynamic analysis codes that can solve large-deformation problems. To advance beyond present procedures it is proposed to perform a combination of physical and numerical modeling research to:

1) Critically examine the shortcomings of existing Seed procedures through two focused series of centrifuge experiments which will provide direct observation of underlying mechanisms of behavior of liquefying materials and the deformations that result. These tests will provide quantitative measurement of residual strength and poorly understood "correction factors" such as K_{sigma} and K_{alpha}; simplified guidance for controlling foundation features necessary to experience large deformations; an improved method of interpreting more traditional laboratory test results; measurement of the actual damage that deformations cause to internal structures such as filter and core zones; and a full-scale performance data base against which various numerical models can be tested.

2) Critically examine the present state of development of fundamental constitutive models and large deformation numerical dynamic analysis codes to provide guidance for choosing among them in the short term, and to select the most promising for development, verification and simplification for practical use in the long term. To resolve remediation problems, this effort must work towards a three-dimensional analysis capability.

Remediation

Efforts to advance remediation guidelines have been slowed by the cost of full scale field testing and the difficulty in generalizing results since remedial actions are very site specific. The centrifuge provides the opportunity to perform these full scale tests on a wide variety of r-emediation geometries to test our ability to compute their effectiveness. A series of centrifuge tests will be conducted including tests to examine the actual state-of-stress and density field that exists in remediated soils, since this stress history plays a major role in the future cyclic behavior of the

soil. These efforts, combined with lessons learned from actual remediated sites should provide a basis for improved guidance so remediation is used only where it is actually needed.

Structural Research

The structures research is designed to develop the necessary analytical tools and corresponding guidance to predict the dynamic response of concrete dams and outlet works from elastic behavior to the development of failure mechanisms. The understanding of the dynamics of the structural response will allow the determination of the ultimate capacity of these critical structures. The research necessary to develop these products is divided into the areas of concrete dams, outlet works, and earthquake analysis tools.

Concrete Dams

This research will focus on determining dynamic ultimate capacity of conventionally placed and roller-compacted concrete dams. The research will address the nonlinear behavior and failure mechanisms of the different types of dams as well as include component tests, scale model tests, and tests of existing structures.

Outlet Works

This work will focus on determining the ultimate capacity of intake towers and the ductility of other than lightly reinforced concrete members. One major work unit will determine the ductility of lightly reinforced structures. The other efforts will focus on different aspects of nonlinear behavior and failure mechanisms of these reinforced concrete structures.

Computational Tools

This research will develop numerical tools to support the dams and outlet works areas. It will produce time-domain numerical analysis tools compatible with the nonlinear materials models, and postprocessing tools to aid in the interpretation and understanding of output from time-history and response spectrum analyses. Other research will support the appurtenant structures to the outlet works and dams. These efforts will address dynamic earth pressures on walls and the dynamic response of piles.

ACCOMPLISHMENTS

The EQEN Program was initiated this year, although planning had been underway since 1993. There were fifteen development efforts accomplished this year. A selected member of these are summarized by major research area below (Hynes, 1995):

Geotechnical Research Summary

- Completed conceptual design of comprehensive ground motion analysis system and user interface module. Acquired USGS three-dimensional, elastic, finite difference, full waveform, wave propagation code and developed software for graphical portrayal of results.

- Held workshop to clarify requirements for integration of acoustic impedance and seismic crosshole tomography

techniques and to select test sites for establishing correlations of these geophysical measurements to liquefaction potential.

- Established limiting gravel content criteria for interpretation of Standard Penetration test results in gravelly soils. Completed energy and friction correction study for Becker Penetration tests performed at Success Dam, CA. Designed field tests to be performed in FY 1996.

- Completed design of centrifuge tests to determine overburden corrections for liquefaction susceptibility analyses. Acquired some of the materials and instrumentation necessary to conduct these tests in FY 1996.

- Completed comparison of Newmark-sliding-block analysis results with collection of field cast histories. Provided guidance for calibration of analysis results with actual field performance and limits of applicability for a range of field conditions.

Structural Research Summary

- Completed critical evaluation of existing nonlinear constitutive models that include crack initiation and propagation for conventionally placed concrete materials. Selected the best features of the existing models and formulated improved model for incorporation in numerical code.

- Completed and reported survey of existing intake towers including key features of their design and past performance during earthquakes. Completed pre-test analysis for physical testing of key components of intake towers.

- Evaluated current methods for determining ductility of outlet works structures and surveyed remediation techniques in use for other types of structures.

- Completed post-processors for finite element time history analyses, developed a modal stress calculation procedure, encoded it, and prepared user manual.

Example Project: Reservoir-Bottom Reflection Coefficient

Background

One of the research efforts in the EQEN Program this year addressed measurement of reservoir-bottom reflection coefficients. The work performed under a grant by Yusof Ghanaat and Bruce B. Redpath of Quest Structures, Emeryivlle, CA show some promising preliminary results.

The reflection coefficient known as "α", which is the ratio of the reflected to incident wave amplitude of a pressure wave impinging on the bottom of a reservoir is

used to represent pressure wave absorption by alluvium and fine-grained bottom sediments. This absorption effect can significantly reduce dam response to earthquake loading (Hall and Chopra 1980, Fenves and Chopra 1984).

In practice, the value of α is deliberately set close to unity to ensure that the predicted earthquake response of the dam is conservative. Alternatively, a lower value of α may be employed, if the sensitivity analyses performed for several values of α would indicate the earthquake response of the dam is less sensitive to the value of α. In either case, the estimation of α is very difficult and cannot be fully justified without field measurements.

The arbitrary values of α currently used in the practical analyses are generally high and may result in more expensive design of new dams or unnecessary strengthening of the existing dams. To determine appropriate values of the reflection coefficient for the lake-bottom materials, two procedures for measuring α in the field were recently investigated in an experiment conducted in China (Ghanaat, et al., 1993). This experiment demonstrated that the actual values of α for the reservoir-bottom material can now be measured in the field, indicating that arbitrary estimates of α are no longer necessary.

The ability to measure in-situ values of α will permit more realistic calculations to be made of hydrodynamic forces, which are known to have significant effects on the response of dams to earthquake loading. Such measurements are especially applicable to the existing dams built in regions of high seismicity, and would enable more realistic evaluation of the dam safety.

Measure Techniques

This study employed two independent approaches to determine the reflection coefficient α, defined as the ratio of reflected to incident wave amplitude of a pressure wave striking the reservoir bottom or sides. The seismic reflection and refraction techniques employed were those developed in our previous field measurements (Ghanaat, et. al., 1993).

The seismic reflection approach was an attempt to measure α directly by recording incident and reflected sound pulses generated by a blasting cap on the bottom of the reservoir. The ratio of the reflected and incident amplitudes, corrected for wavefront spreading, is the reflection coefficient. As depicted in Figures 3 and 4, the reflection technique used a vertical array of 12 hydrophones suspended in the water. A blasting cap was used as source of energy and a multi-channel exploration seismograph was employed to record the signals. All measurement operations were conducted from two boats.

The seismic refraction test program was based directly on a technique developed by Hunter and Pullan (1990) of the Geological Survey of Canada. The method was originally developed for conducting sub-bottom surveys from ice floes in the Canadian Arctic. The technique employs a vertical array of hydrophones suspended above the lake bottom and an impulsive energy source located on the bottom at one or more distances away from the array. A schematic of the source/hydrophone configuration is shown in Figure 5.

Investigation Design

The study effort collected data and a measured the values of reservoir-bottom reflection coefficient at the seven concrete dam sites of Hoover, Pine Flat, Glen Canyon, Folsom, Monticello, Narrow Point, and Crystal. At each dam fathometer surveys, temperature and sound velocity profiles, refraction surveys, and reflection surveys were conducted. A sample of survey products for Hoover Dam are shown in Figures 6-12 and Table 1 and 2.

Preliminary Results

The average values of α for the reservoir-bottom materials measured directly by recording incident and reflected sound pulses are given in Table 3. The results show that at these dam sites the value of α varies over a range of -0.55 to 0.66, significantly different than the customary use of α values close to unity in practical analyses. In fact, except for $\alpha=0$ used for research purposes, no α value of less than 0.5 or negative values have ever been considered previously. In this study three out of seven dams tested had negative α values, a fourth one (Glen Canyon) has a very low α of 0.15, and none of the remaining three dams has an α of greater than 0.66.

The α values determined on the basis of the propagation velocity and density of the bottom sediments are summarized in Table 4. The propagation velocities were measured only at the sites for which the refracted arrivals through the bottom sediments could be observed. For other sites, propagation velocities were estimated in view of α values obtained from the reflection surveys and the fact that the acoustic impedances of the bottom sediments were less than that of water. In all cases, appropriate values were assumed for density of the bottom sediments. Table 4 shows that the resulting α values compare favorably with those obtained in the reflection surveys (Table 1), except that the propagation velocities at Pine Flat and Folsom which are low.

FUTURE RESEARCH PROGRAM ACTIVITIES

For next year the EQEN Program will expand and build on the research projects stated in 1995. Current plans by the two major research areas are as follows:

Geotechnical Research

- Development of improved understanding of earthquake ground motions and their impact on the design of new and remediation of existing water resource facilities: This involves a continuing effort to incorporate the latest advances in seismology and geology in procedures for assessing appropriate ground motions for engineering analyses and construction of a comprehensive ground motion analysis system to prepare the ground motion input for engineering analyses. FY 1996 efforts will focus on basis response altered by irregular boundary effects and construction of accelerogram and response spectra data base modules and accelerogram processes tools.

- Development of improved

methods to determine site characteristics relevant to seismic performance: This effort focuses on geophysical and penetration testing techniques. In the geophysical area, FY 1996 activities will include completing the integrating of seismic impedance and crosshole tomography capabilities and performing the first series of field tests. There will also be a continuing effort to update the seismic velocity data base with new data, as available. In the penetration testing effort, FY 1996 activities will include two series of field tests to examine and verify Standard Penetration and Becker Penetration Test correlations and energy and friction corrections for interpretation of test measurements.

- Development of improved methods to predict material behavior under seismic stresses: This effort involves a combination of physical testing to establish actual seismic material behavior and development of constitutive models for representation of this behavior in numerical dynamic codes. In FY 1996 laboratory tests will be completed to establish the complete stress-strain relationships for soil materials as they approach the liquefied state, liquefy, and then restabilize at large strain levels. A series of centrifuge tests will be performed to examine the validity of currently used overburden corrections to cyclic strength of soils. The centrifuge and laboratory test results will be used to evaluate and calibrate the constitutive model selected from the FY 1995 activities.

- Development of improved capability to predict seismically-induced deformations: This effort involves a combination of centrifuge tests and numerical dynamic code development. The centrifuge tests provide a data base of the seismic response and deformation of full-scale equivalent, complex geotechnical systems. In FY 1996, the centrifuge tests will be designed and an initial series of tests will be performed to examine and quantify controlling stratigraphic features that can lead to damaging levels of seismically-induced deformations. Work will also progress in the development/modification of a two- and three-dimensional numerical wave-propagation code that can be used to calculate large deformations. The centrifuge test results will be used to evaluate the modifications to the code.

Structural Research

- Development of improved understanding of seismic

response of concrete dams and development of constitutive models criteria for design of new and rehabilitation of existing concrete dams: This research will complete development/ modification of nonlinear constitutive models for conventionally-placed and roller compacted concrete materials and begin coding for insertion to numerical dynamic code.

- Development of improved understanding of the effect of earthquakes on reservoir outlet works and development of models and criteria for the design of new and rehabilitation of existing outlet works: Work will report the results of physical tests of key components typical of Corps-designed intake towers. The design and physical tests will be performed to investigate reinforcing details typical of Corps-designed intake towers. Design and physical tests will be conducted to investigate bridge-tower interaction under seismic loads, and the design and physical tests on key components of other outlet works structures will be completed.

- Development of specialized computer tools for seismic analysis of concrete dams and outlet works. Post-processing computer tools to screen finite element analysis results for extent and duration of seismically-induced stress excursions beyond acceptable thresholds will be continued. An interface to graphically portray these results with the existing plotting package will be completed. Verification of the modal stress calculation procedure developed in FY 1995 against example problems will be completed and a user manual prepared. Complete validation of two-dimensional numerical code with improved constitutive model including crack initiation, propagation and joint opening will be completed. Development and validation of the structure-reservoir-foundation interaction features of the numerical code will be started.

SUMMARY

In spite of major advances over the last 25 years, serious gaps in our knowledge base still exist in the areas of earthquake hazard predictions, site characterization for seismically sensitive parameters, constitutive behavior and material properties of rock, soils, and composite (reinforced) materials under seismic loads, and the stress and deformation responses of site and facilities to seismic loading. Economical remediation and defensive design techniques are needed in addition to careful calibration of fast advancing numerical methods to actual field performance. Through this combination of research improved methods will be developed to predict appropriate ground motions for input to analyses, to investigate our sites more economically and more thoroughly, to improve our analytical

ability to predict the amount of damage that the design level earthquakes cause to out critical Civil Works structures, and to provide better guidance as to how to remediate structures if needed.

REFERENCES

Fenves, G., and A.K. Chopra, 1984. "*Earthquake analysis and response of concrete gravity dams*," Earthquake Engineering Research Center, University of California, Berkeley, Report No. UCB/EERC-84/10, August 1984.

Ghanaat, Y., H.-Q Chen, B.B. Redpath, and R.W. Clough, 1993. "*Experimental study of Dongjiang Dam for dam-water-foundation interaction*," Report submitted to the National Science Foundation on research conducted under the US-China Protocol for scientific and technical cooperation in earthquake studies. Report No. QS93-03, QUEST Structures, Emeryville, CA, July 1993.

Hall, J.F., and A.K. Chopra, 1980. "Dynamic Response of Embankment Concrete-Gravity and Arch Dams including Hydrodynamic Interaction," Earthquake Engineering Research Center, University of California, Berkeley, Report No. UCB/EERC-80/93, October 1980.

Hynes, M.E., 1995. "Earthquake Engineering Program Review," U.S. Army Waterways Experiment Station, Vicksburg, MS., March 1995.

Table 1. Reflection coefficient estimated from refraction surveys

Hoover Dam	Assumed unit weight $lb/ft^3(N/m^3$	Sound velocity ft/sec (m/s)	α
Water	62.5 (10,000)	4,770 (1454)	--
Bottom surficial material	62.5 (10,000)	4,600 (1400)	-0.02
Bottom surficial material	68.75 (11,000)	3,936 (1200)	-0.05

Table 2. Reflection coefficient obtained from reflection surveys

Hoover Dam	No. of Data	Averaged measured α	Standard Deviation (σ)
Bottom surficial material	8	-0.09	0.08
Cofferdam	12	0.41	0.14
Concrete dam	36	0.68	0.30
Canyon rock walls	12	0.77	0.21

Table 3. Reflection coefficient of bottom sediments obtained from reflection surveys

Dam	No. of Data	Averaged α	Standard Deviation (σ)
Monticello	29	+0.63	0.15
Pine Flat	60	-0.45	0.11
Hoover	8	-0.09	0.08
Glen Canyon	16	+0.15	0.04
Morrow point	51	+0.45	0.13
Crystal	11	+0.66	0.15
Folsom	72	-0.55	0.13

Table 4. Reflection coefficient of bottom sediments estimated from refraction surveys

Bottom Sediments	Assumed unit weight $lb/ft^3(N/m^3)$	Measured (M) and derived (D) sound velocity ft/sec (m/sec)		α
Monticello (sediment)	125 (20,000)	M	6,148 (1874.5)	0.44
Monticello (rock)	140 (22,400)	M	10,486 (3197.0)	0.66
Pine Flat	68.75 (10,000)	D	1,673 (510)	-0.45
Hoover	68.75 (11,000)	D	3,936 (1200)	-0.05
Glen Canyon (sediment)	87.5 (14,000)	D	4,600 (1400)	0.15
Glen Canyon (rock)	140 (22,400)	M	6,134 (1400)	0.49
Morrow Point (rock)	140 (16,000)	M	7,150 (2180)	0.55
Crystal (rock)	156 (22,400)	M	6,153 (1876)	0.53
Folsom	62.5 (10,000)	D	1,270 (387)	-0.55

Seismic Hazard Map

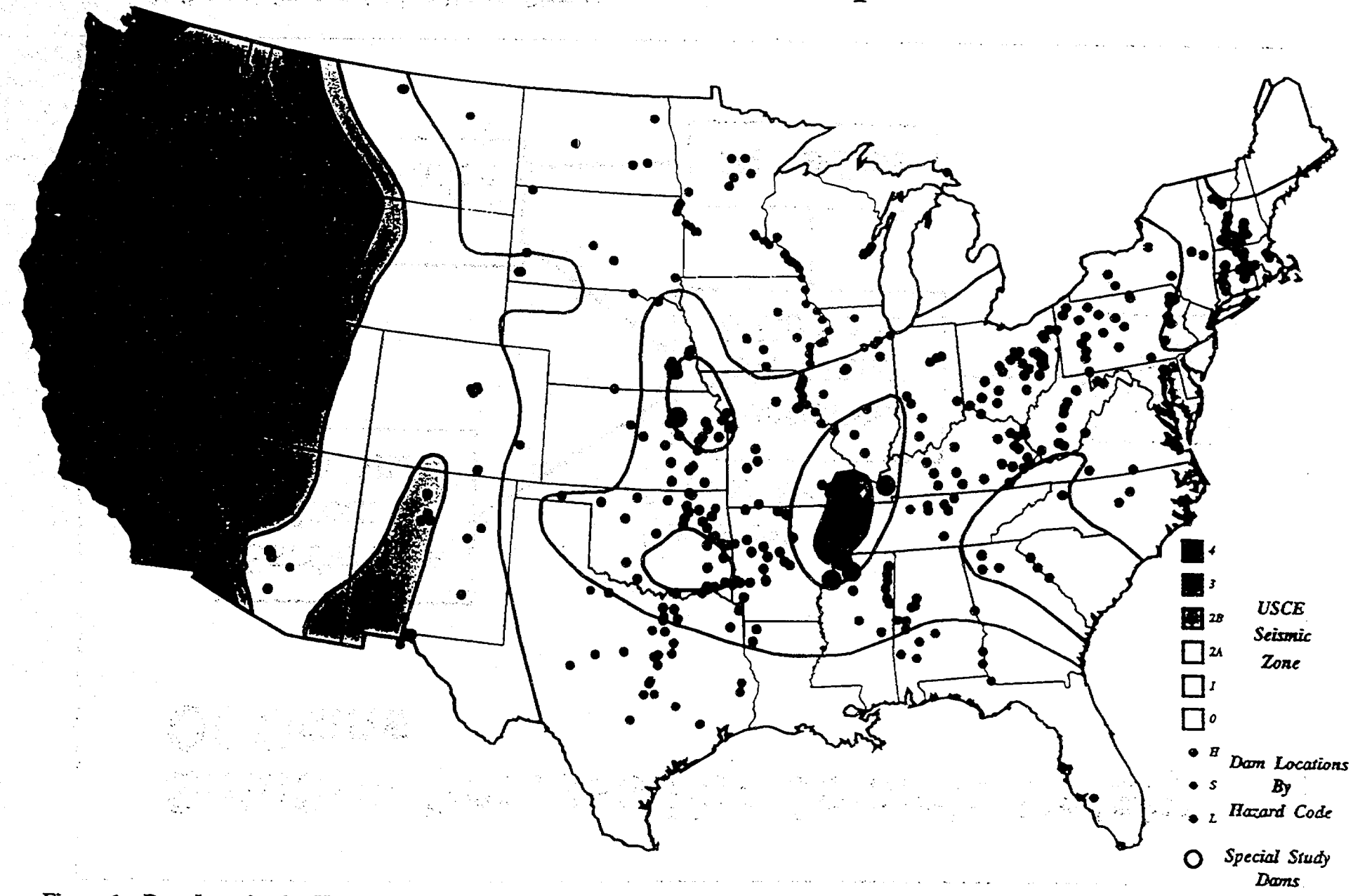


Figure 1. Dam Location by Hazard Zone

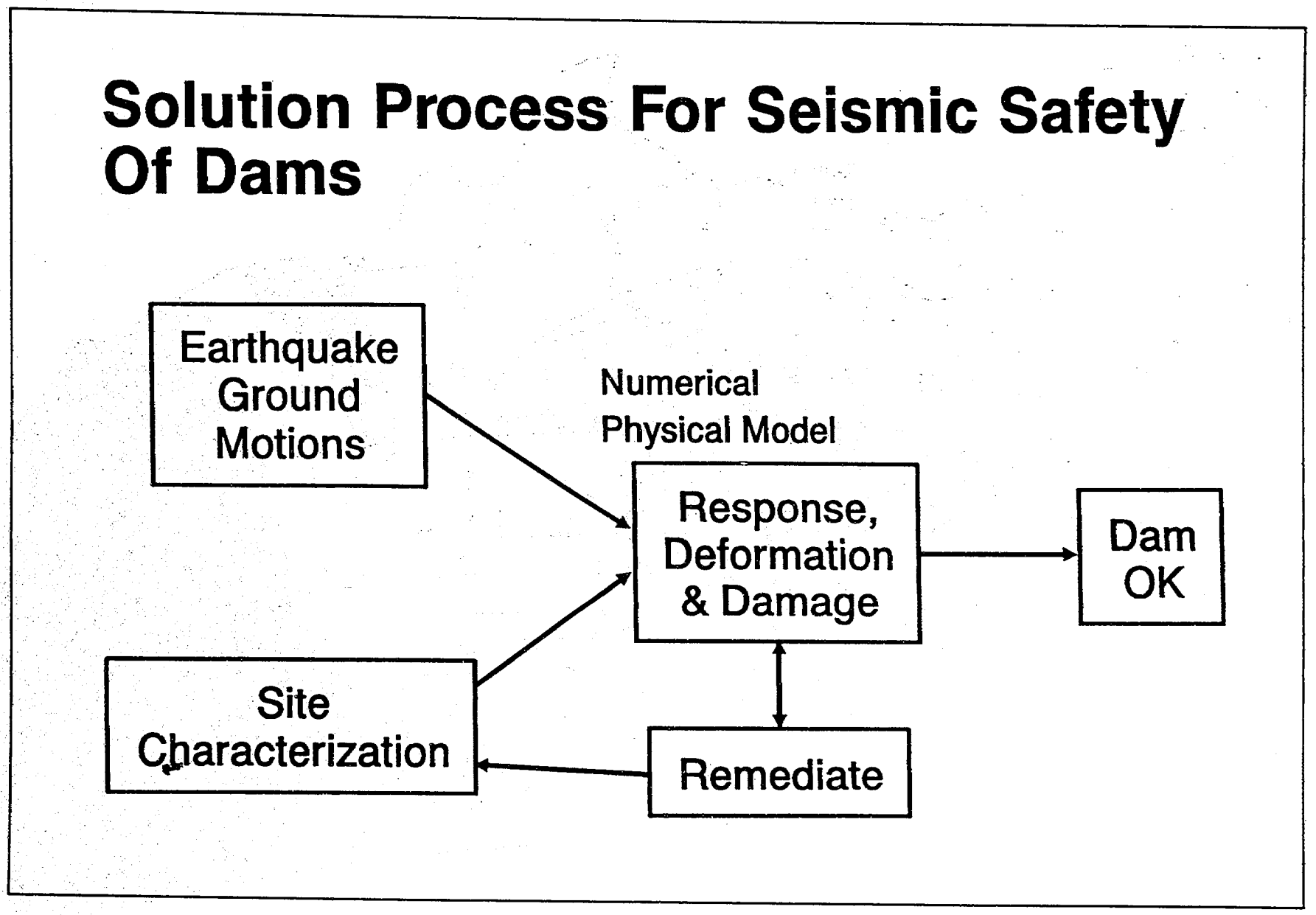


Figure 2. Research Program Solution Process Diagram

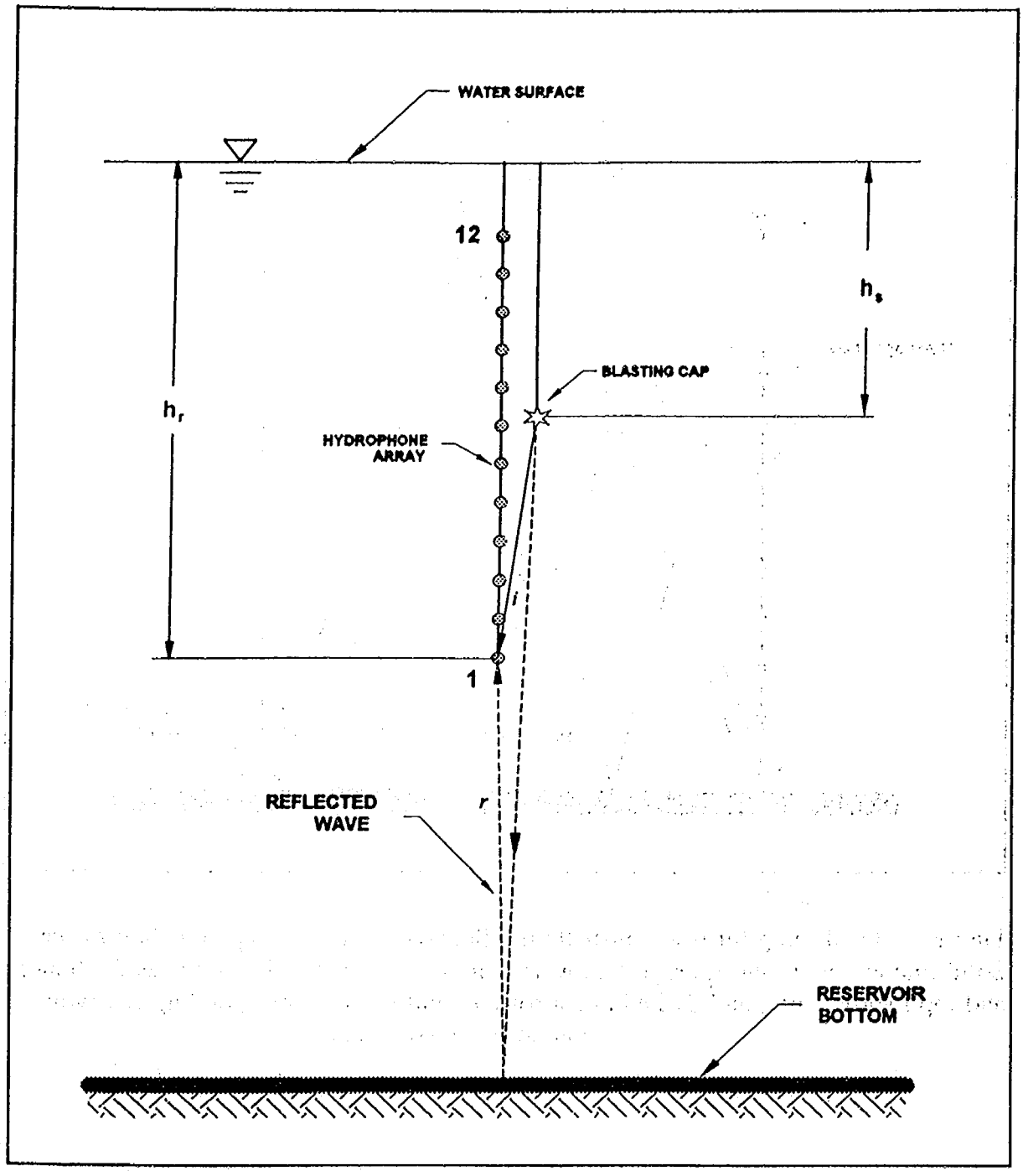


Figure 3. Field setup for reservoir-bottom reflection survey in deep water. Solid line arrow *i* represents direct incident wave, and dashed-line arrow *r* is reservoir-bottom reflected wave

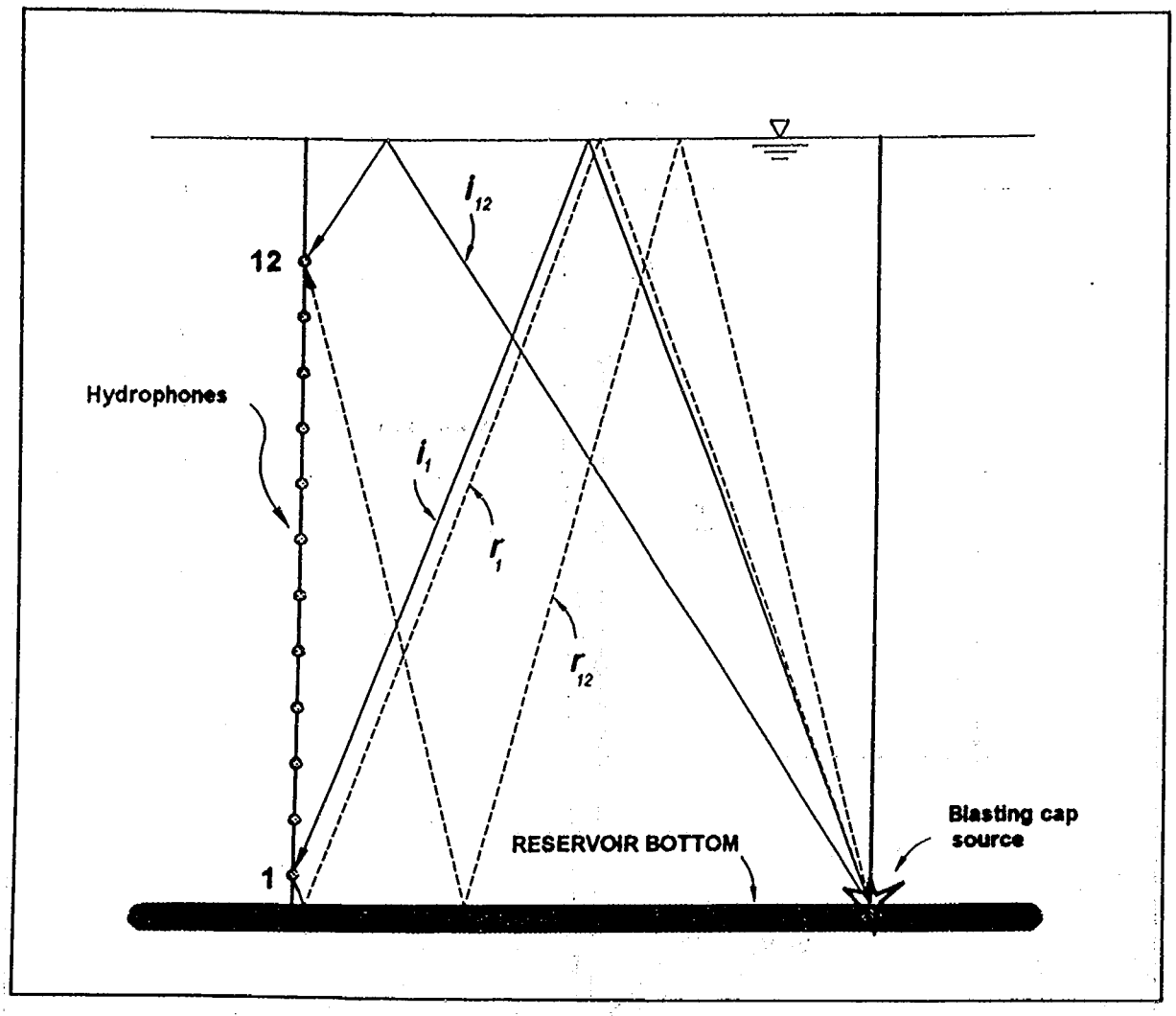


Figure 4. Field setup for reservoir-bottom reflection survey in deep and shallow water. Solid line arrows i_1 and i_{12} represent water surface-reflected incident waves for bottom and top hydrophones, and dashed-line arrows r_1 and r_{12} are corresponding reservoir-bottom reflected waves

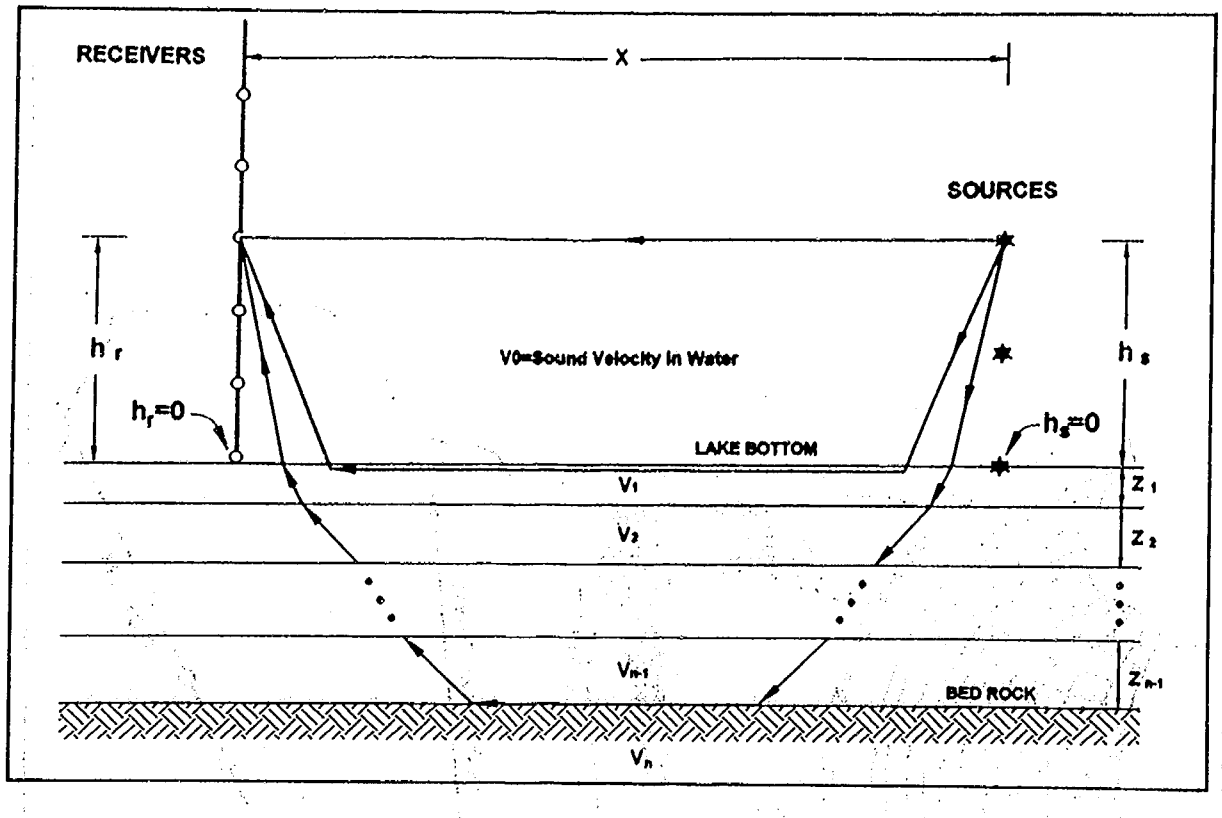


Figure 5. Geometry of a vertical refraction experiment assuming flat-lying subbottom refractors (adapted from Hunter and Pullan, 1990)

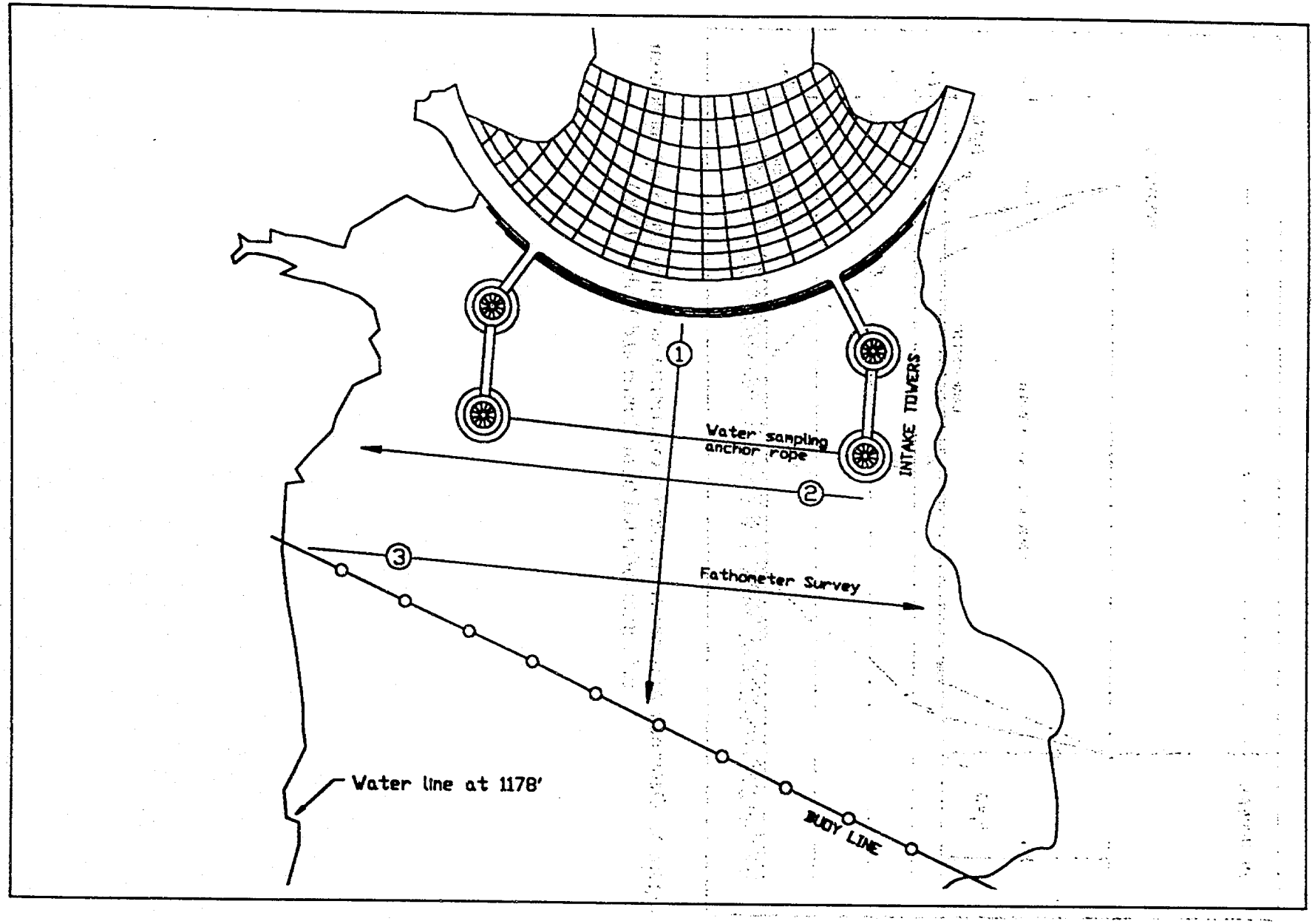


Figure 6. Plan view of acoustic survey (fathometer) lines for measuring reservoir-bottom profiles at Hoover Dam

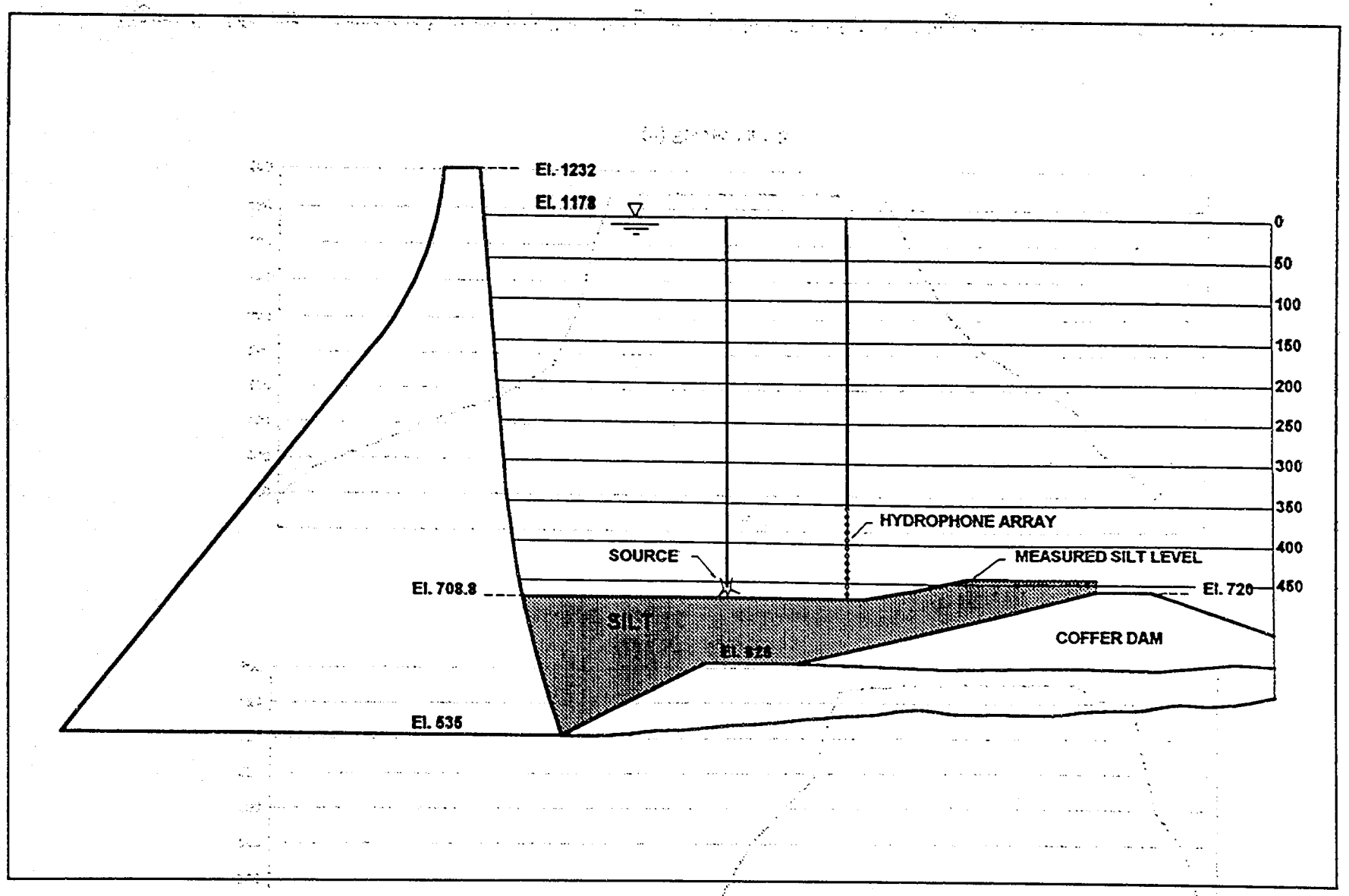
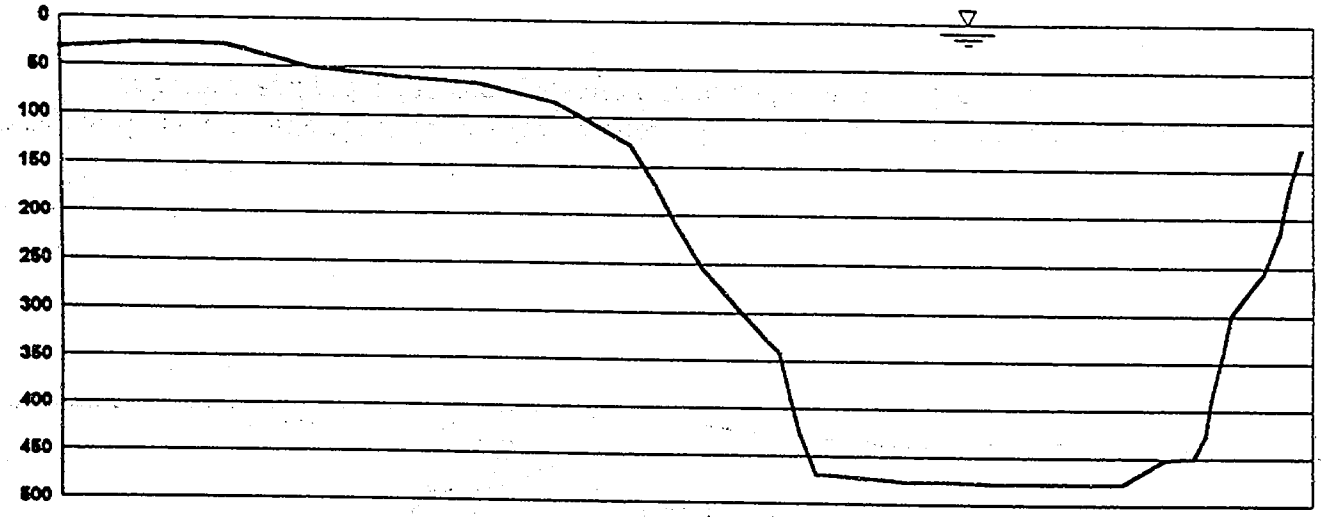
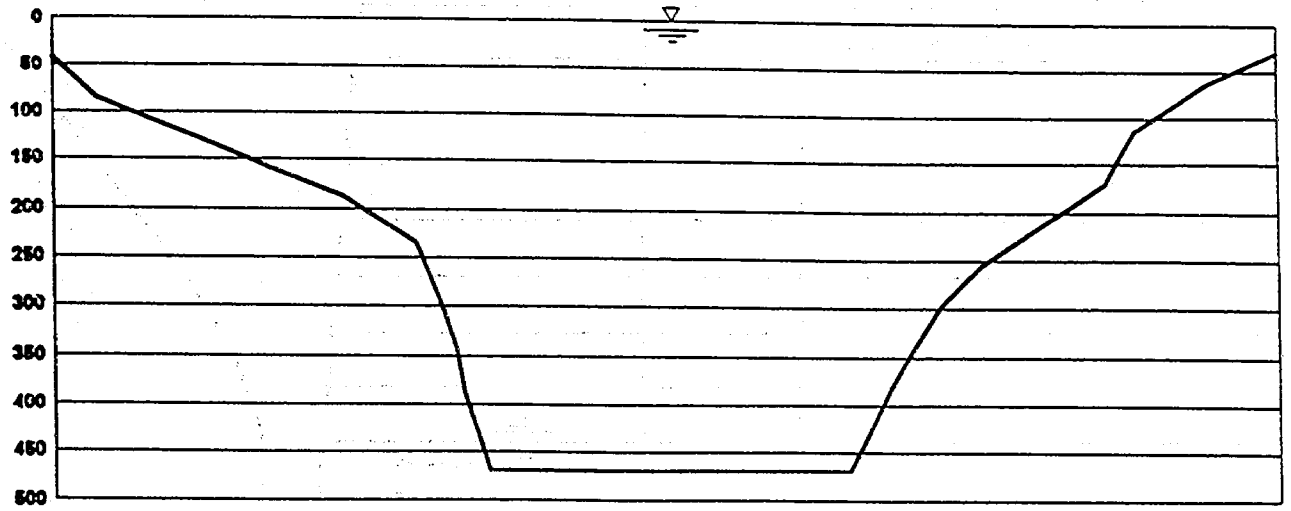


Figure 7. Measured reservoir-bottom profile along Line 1 (see Figure 6-1) at Hoover Dam showing accumulated silt, location of refraction and reflection surveys, coffer dam, and crown section of dam



(a) Survey Line 2



(b) Survey Line 3

Figure 8. Measured reservoir-bottom profiles along survey Lines 2 and 3 (looking downstream) at Hoover Dam

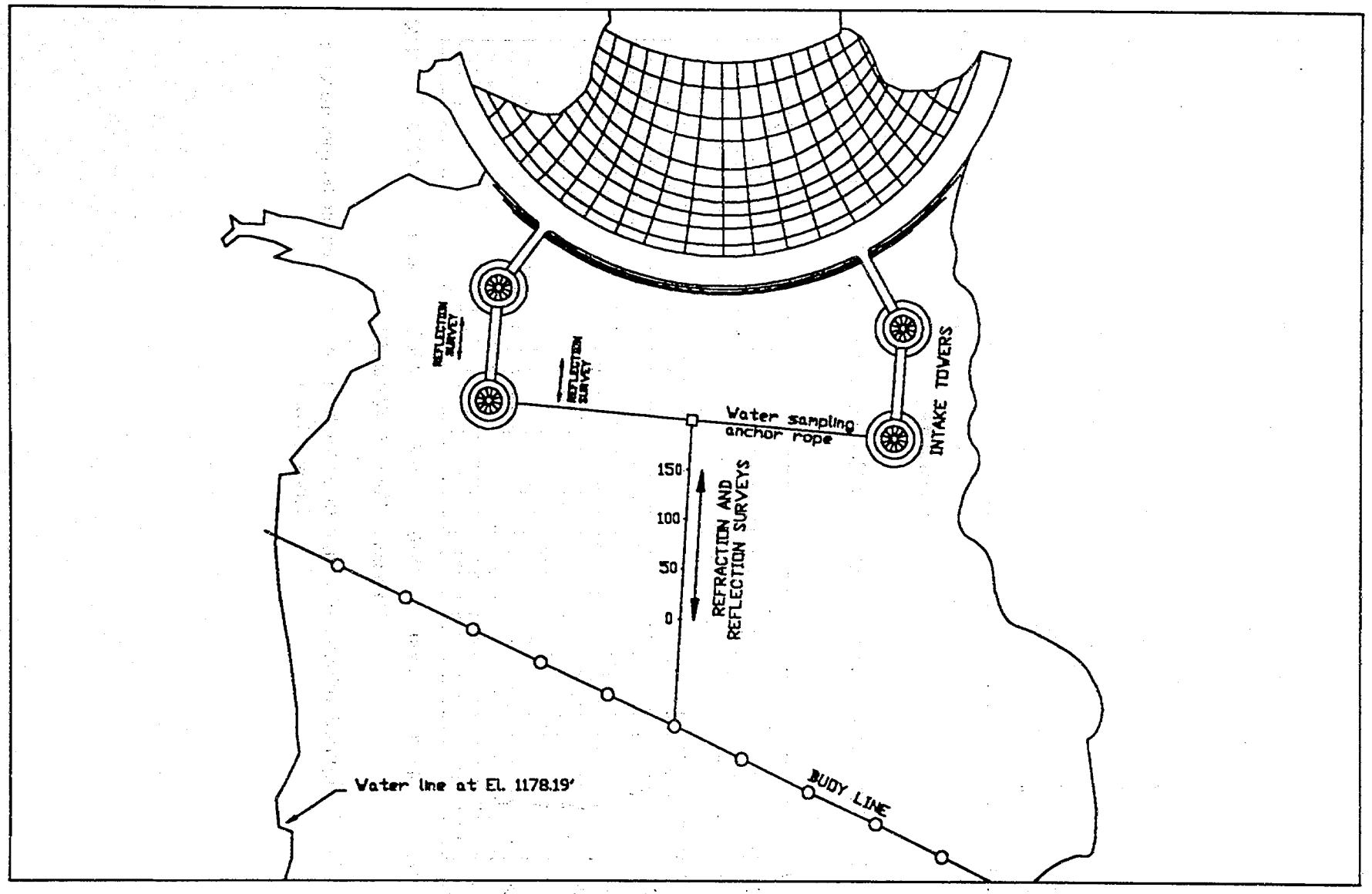


Figure 9. Plan view showing buoy line, support ropes, and location of refraction and reflection surveys at Hoover Dam

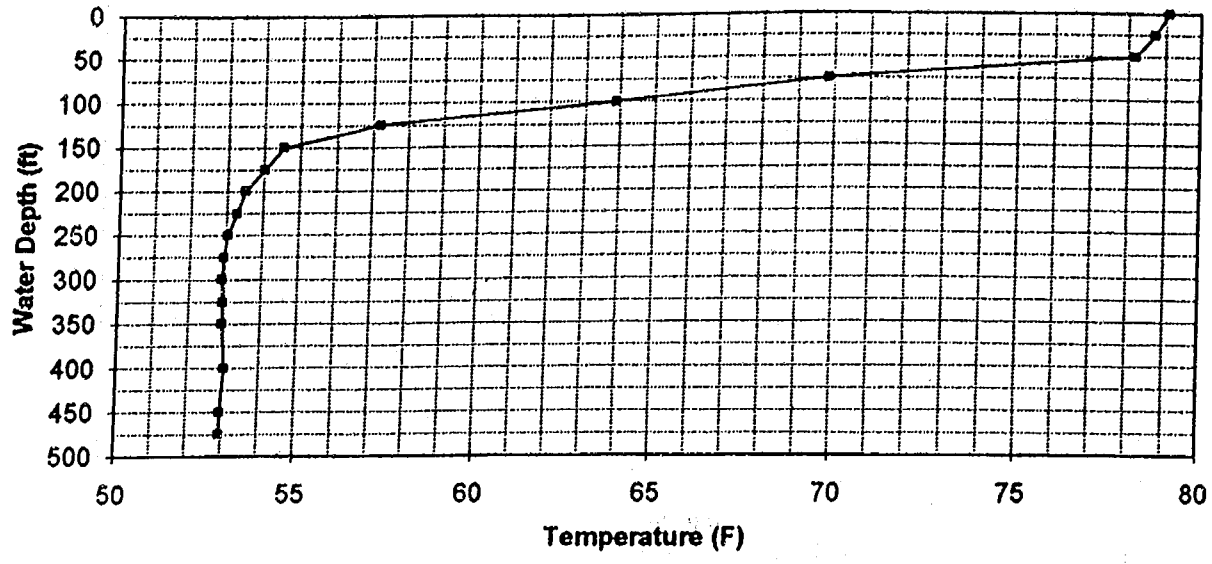


Figure 10. Measured water temperatures at Hoover Reservoir (Lake Mead)

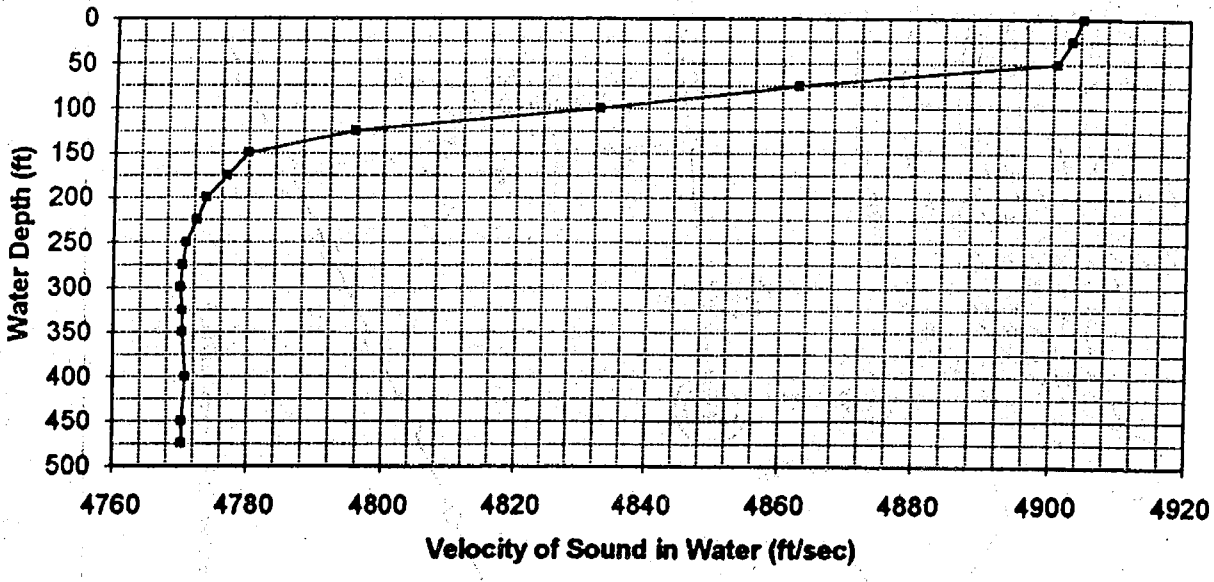


Figure 11. Computed velocity of sound in water from measured water temperatures at Hoover Dam

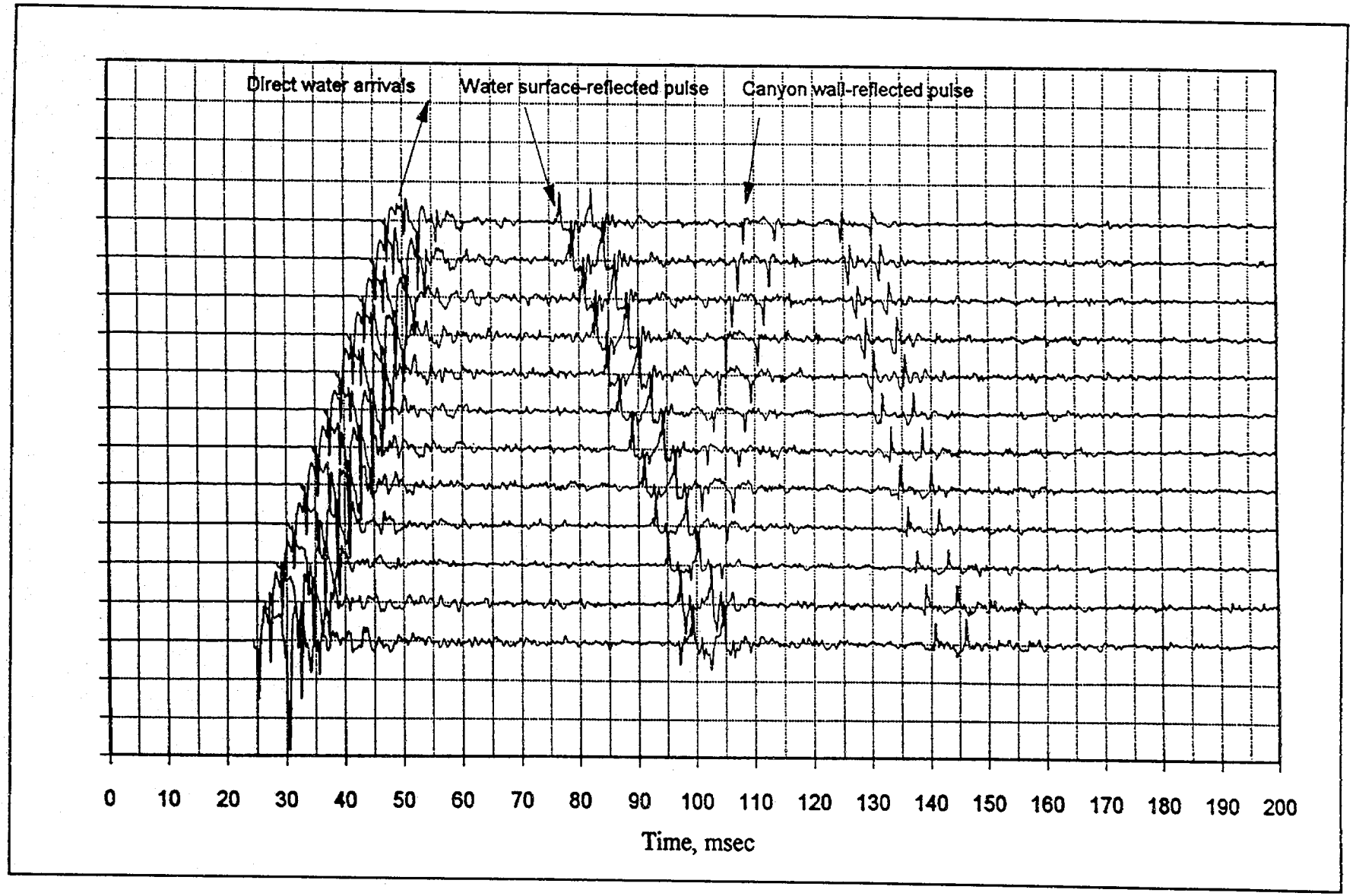


Figure 12. Seismic reflection signals for canyon walls at Hoover Dam with depth of bottom hydrophone at 180.4 ft below water surface, energy source at bottom (300 ft below water surface), and offset x = 25 ft

Durability of Structural Retrofit with Carbon Fiber Reinforced Plastics (CFRPs).

by:

L.C. Muszynski [1]
R.L. Sierakowski [2]

ABSTRACT

The current research effort was initiated to evaluate the effect of environmental conditioning on the performance of concrete members strengthened by externally-bonded advanced composite materials. Test specimens were fabricated and cured following standard procedures, and CFRP external reinforcement strips were attached to the specimens using a high-performance epoxy adhesive. Control samples were tested prior to exposure to different environmental conditions. The externally-reinforced concrete samples were tested to determine the effects of freeze-thaw cycling, hot water immersion, and exposure to ultraviolet light/condensation following ASTM test standards.

KEYWORDS: carbon fiber; composites; environmental effects; concrete; NDT.

1. INTRODUCTION

The use of advanced composite materials, characterized by their lightweight, high stiffness, excellent fatigue properties, and outstanding corrosion resistance, have been used in the aircraft and space industry with great success. Bonding thin steel plates, to critical areas of concrete subjected to tensile loading, has been shown to be an effective strengthening method (Swamy, 1987 and Jones, 1988). The outstanding properties of advanced composite materials, such as carbon fiber reinforced plastics (CFRPs), make these new materials suitable candidates for strengthening structural concrete members. Previous work in this area compared reinforced plastic (RP) plates made of glass, aramid and carbon to those of mild steel. The results demonstrated the feasibility of using RP plates for upgrading the strength and stiffness of a reinforced concrete beam (Ritchie, 1991; Sharif, 1994 and Chajes, 1994).

Over the last two years, there has been a concerted research effort by the Wright Laboratory Airbase Survivability Section (WL/FIVCS) to explore the strengthening effect of CFRP strips applied to both reinforced and non-reinforced concrete beams, both in the tensile and shear areas of the beam. The load-carrying capacity of concrete beams was increased dramatically when using CFRP strengthening tapes.

The objective of this effort was to test and evaluate the effect of environmental conditions on the performance of concrete members strengthened by externally-bonded advanced composite materials. Testing was performed by both non-destructive (NDT) and destructive methods.

2. TEST PROGRAM

2.1 Description of materials:

Portland cement concrete beams were prepared in the usual manner and moist cured for 28 days. The 50 mm by 50 mm by 300 mm beams were cast from a mix design referred to as "G-mix." Its composition is given in Table 1.

1 Applied Research Associates, Inc.
Tyndall AFB, FL 32403
2 Ohio State University
Columbus, OH 43210

The G-Mix water to cement + fly ash ratio was 0.6 and had a 28-day compressive strength of 29 MPa. The calculated flexural strength and static modulus of elasticity are 3.4 Mpa and 25,000 MPa respectively. One side of each beam was prepared by in a like manner by surface scarification. The prepared surfaces were primed with a low viscosity two-part epoxy primer. The bonding of the 50 mm wide, 2-ply CFRP strips was performed using a two-part epoxy adhesive having a paste-like consistency. Curing time was 7-days at ambient temperature. The properties of the 2-ply CFRP are given in Table 2.

2.2 Test Conditions

The test specimens were divided into four groups. Group 1, control samples were externally reinforced concrete beams that were conditioned in a laboratory environment at ambient temperature. Group 2 samples were exposed to QUV according to ASTM G-53, "Operating Light and Water Exposure Apparatus for Exposure of Nonmetallic Materials."
This method is intended to simulate deterioration caused by moisture as rain or dew and the ultraviolet energy in sunlight. Test specimens were exposed to test conditions consisting of 8 hours of UV at 60 degrees C. and 4 hours of condensation at 40 degrees C. for a total combined time of 1000 hours. The samples were oriented in such a way that only the externally bonded CFRP reinforcement was exposed to the effects of UV light and condensation. Group 3 samples were exposed to conditions of freezing and thawing according to ASTM C-884, "Thermal Compatibility between Concrete and an Epoxy Resin." The method is intended to evaluate whether or not delamination or the presence of horizontal cracks near the bonded composite-concrete interface has occurred when exposed to 5 cycles of freezing in air and thawing in air. Each cycle consisted of freezing in air for 24 hours at -18°C. and thawing in air for 24 hours at 25°C. Group 4 samples were exposed the effects of moisture and temperature according to ASTM D-1151, "Effect of Moisture and Temperature on Adhesive Bonds." This test method is used to determine a materials' performance, exposed to a variety of moisture and temperature conditions, based on the ratio of strength retained after exposure to the original strength. The test specimens were exposed to 7 days of water immersion at 60 degrees C. followed by 7 days of drying and ambient temperature.

2.3 Test Methods

2.3.1 Pulse Velocity

Two test methods were used in this study to evaluate the effect of the environmental conditions described previously on the quality of externally bonded CFRP to portland cement concrete (PCC). The first method, ASTM 597, "Pulse Velocity Through Concrete," covers the determination of the pulse velocity of propagation of compressional waves in concrete (ASTM 4.02:284). Pulses of compressional waves are generated by an electro-acoustical transducer that is in contact with one surface of a material, and received and converted into electrical energy by a second transducer located at a distance "x" from the transmitting transducer. The velocity of the pulse traveling longitudinally in an elastic solid is directly proportional to the elastic modulus of elasticity of that solid, which is directly related to the strength of that material. This non-destructive test method is used to assess the uniformity and relative quality of concrete and other materials, and to estimate the severity of deterioration or cracking.

In this study the arrangement of transmitting and receiving transducers is shown in Figure 1. This method is often referred to as the "surface indirect method" for determining cracking and/or delamination at the reinforcing material/concrete interface. As the receiving transducer is moved to different distances x1, x2, x3, and x4, a plot of pulse time versus distance is generated. A straight line function indicates that the interfacial area is free of cracks and delaminations; and on the other hand, a sharp increase in time (reduced pulse velocity) would indicate the presence of a

crack or delamination at a given distance from the transmitting transducer.

2.3.2 Flexural Toughness

The second method, ASTM C-1018, "Flexural Toughness and First-Crack Strength of FRC (Using Beam with Third-Point Loading)," was implemented to evaluate the flexural toughness of the externally bonded CFRP-PCC composites (ASTM 4.02:491). This method provides for the determination of toughness indices that identify the pattern of material behavior up to a selected deflection criteria. Toughness indices are determined in terms of areas under the load-deflection curve to a specific deflection. Toughness is an indication of the energy absorption capability of a particular test specimen. The test also provides for the determination of the first-crack flexural strength using the load corresponding to the point on the load-deflection curve defined as first-crack. The first-crack strength characterizes the behavior of the composite material up to the onset of cracking in the matrix, while the toughness indices characterize the behavior thereafter.

Toughness is also measured by a Japanese standard JCI-SF4, that determines the area under the load-deflection curve up to a deflection corresponding to the span of the test beam divided by 150. In this method, the flexural strength is defined with reference to the maximum load sustained by the test specimen, and measures the area under the load-deflection curve to a greater deflection than the ASTM standard.

Both methods of determining flexural toughness utilize a beam type specimen having a span equal to three times its depth, loaded by third-point loading according to ASTM C-78, and a mid-span deflection controlled at a rate of 0.05 to 0.1 mm/min, according to Figure 2.

3. RESULTS

The results of the non-destructive pulse velocity test are given in Table 3. Samples Group 1A and 1B represent control samples. Group 2A and 2B samples were exposed to 1000 hours of QUV, according to the following cyclic exposure: 8 hours of UV at 60°C. and 4 hours of condensation at 40°C. Group 3A and 3B samples were exposed to 5 cycles of freezing in air at -18°C. and thawing in air at 25°C., and Group 4A and 4B samples were exposed to immersion in 60°C. water for 7 days.

According to Table 3, Group 2 CFRP-PCC composite samples appeared to be slightly altered by the environmental exposure of 1000 hours of QUV. The pulse velocity was slightly reduced, thus reducing the dynamic pulse modulus of elasticity of the composite material by less than 15 percent. The exposure to freeze-thaw cycling and hot water immersion did not appear to deleteriously effect the CFRP-PCC composite materials determined by NDT.

The CFRP-PCC composite samples were then destructively tested according to ASTM C-1018, "Flexural Toughness and First-Crack Strength of FRC (Using Beam with Third-Point Loading)," Figure 3. Toughness indices that identified the pattern of material behavior up to a selected deflection criteria were determined from these curves, and are given in Table 4. Toughness indices are determined in terms of areas under the load-deflection curve to a specific deflection..

Toughness and flexural strength or Modulus of Rupture, MOR, were also measured by the Japanese standard JCI-SF4 (Nemegeer, 1989). The flexural strength is defined with reference to the maximum load sustained by the test specimen, and toughness as the area under the load-deflection curve up to a deflection corresponding to the span of the test beam divided by 150. These results are also given in Table 4.

The results in Table 4 indicate no significant reduction in mechanical properties for Group 2, 3 or 4 samples based on the ASTM C-1018 criteria for first-crack strength and toughness indices. First-crack toughness, I(c), is represented by the area under the load-deflection curve up to first-

crack deflection (δ). This area represents the behavior of the CFRP-PCC material to the point where the CFRP begins to actively contribute. The other toughness indices I(5), I(10), and I(30) correspond to areas under the load-deflection curves up to deflections of 3δ, 5.5δ, and 15.5δ respectively. Values of toughness indices of 5.0, 10.0, and 30.0 for I(5), I(10), and (30) correspond to linear elastic material behavior up to first-crack and perfectly plastic behavior thereafter. Values of 1.0 for I(5), I(10), or I(30) correspond to plain, unreinforced concrete.
The flexural strength and area under the load deflection curve of the Group 2 CFRP-PCC samples appears to be somewhat less than control CFRP-PCC samples. The Group 2 samples, that were exposed to 1000 hours of QUV, failed prior to reaching a deflection corresponding to 1/150 of the span of the sample as specified in JCI-SF4. This premature failure may be responsible for the 23 percent reduction in toughness. The Group 2 samples also had a correspondingly 17 percent reduction in flexural strength, or MOR.

4. CONCLUSIONS

Based on the experimental investigation reported herein, the following conclusions can be made.

1. Exposure to UV CON, freeze-thaw and hot water immersion did not deleteriously effect the performance of concrete beams externally reinforced with CFRP laminates.

2. External Reinforcement of concrete by CFRP laminates increased the first-crack strength by approximately a factor of two, and the maximum flexural strength by a factor of six.

3. The energy absorbing capacity of PCC externally reinforced with the CFRP laminates was increased by a factor of 50 as determined by the ASTM toughness index, I(30).

4. Pulse velocity (Indirect Method) testing appears to be a viable NDT method for determining the integrity of the bond interface between the CFRP and concrete substrate.

5. The energy absorbing capacity and maximum flexural strength of externally reinforced concrete beams were best determined in this study using the method described in JCI-SF4.

5. REFERENCES

1. ASTM, 1988. 4.02:284-286.

2. ASTM, 1988. 4.02:491-496.

3. Chajes, M. J., T. A. Thomson Jr., T. F. Januszka, and W. W. Finch Jr. 1994. Construction and Building Materials, 8(3):191-201.

4. Jones, R., R. N. Swamy, and A. Charif. 1988. Structural Engineer (London), 66(5):85-94.

5. Nemegeer, D., 1989. Fibre Reinforced Cement and Concretes-Recent Developments, Elsevier Applied Science, pp.401-410.

6. Ritchie, P. A., D. A. Thomas, L. Lu, and G. M. Connelly. 1991. ACI Structural Journal, 88(4):490-500.

7. Sharif, A., G. J. Al-Sulaimani, I. A. Basunbul, M. H. Baluch, and B. N. Ghaleb. 1994. ACI Structural Journal, 91(2):160-168.

8. Swamy, R. N., R. Jones, and J. W. Bloxham. 1987. Structural Engineer (London), Part A., 65a(2):59-68.

Table 1. Composition of "G-mix" Portland Cement Concrete.

Component	Wt. in Kg/cubic meter
Type 1 portland cement	224
Limestone aggregate (10mm max.)	1005
Concrete sand (FM. of 2.1)	800
Fly ash (Class F)	145
Water	217

Table 2. CFRP Composite Properties.

Material	0° Tensile Strength, MPa	0° Tensile Modulus, MPa	Fiber Volume %	Cured 2-Ply Thickness, mm
AS4/1919	2200	138,000	60	3

Table 3. Results of NDT Testing.

Sample	Avg. width mm	Avg. depth mm	Weight Kg	Unit Wt. Kg/cu.m	Pulse Vel. m/sec	E(p) MPa
Group 1A	51.05	51.56	1.73	2293.88	4165.79	39655.17
Group 1B	51.31	51.82	1.73	2293.71	4180.62	39931.03
Group 2A	51.56	51.82	1.75	2295.80	4107.52	38551.72
Group 2B	51.82	51.82	1.75	2287.45	4210.59	40413.79
Group 2A-UV	51.56	51.82	1.69	2212.88	3878.97	33172.41
Group 2B-UV	51.82	51.82	1.69	2203.07	3914.40	33655.17
Group 3A	51.56	51.82	1.89	2320.55	3968.76	36413.79
Group 3B	51.31	52.07	1.89	2317.50	3941.38	35862.07
Group 3A-F/T	51.56	51.82	1.87	2295.16	3987.22	36344.83
Group 3B-F/T	51.31	52.07	1.86	2291.95	3941.38	35448.28
Group 4A	51.56	52.07	1.88	2304.96	4111.53	38827.59
Group 4B	51.31	51.82	1.86	2304.80	4062.81	37931.03
Group 4A-HW	51.56	52.07	1.89	2307.54	4275.57	42000.00
Group 4B-HW	51.31	51.82	1.87	2312.52	4191.95	40482.76

Table 4. Results of Flexural Strengths and Toughness Indices.

Sample	1st Crack Load N	1st Crack Strength MPa	I(5)	I(10)	I(30)	JCI area, Kg-m	Max load, N	Maximum Strength MPa
Group 1	4185.94	7.30	6.10	13.50	51.00	12.38	12726.87	22.20
Group 2	3603.20	6.28	7.80	18.00	71.00	9.60	10578.29	18.45
Group 3	3781.14	6.59	6.90	17.40	69.30	15.05	15311.39	26.71
Group 4	4893.24	8.53	6.20	14.80	57.60	11.54	14003.56	24.42

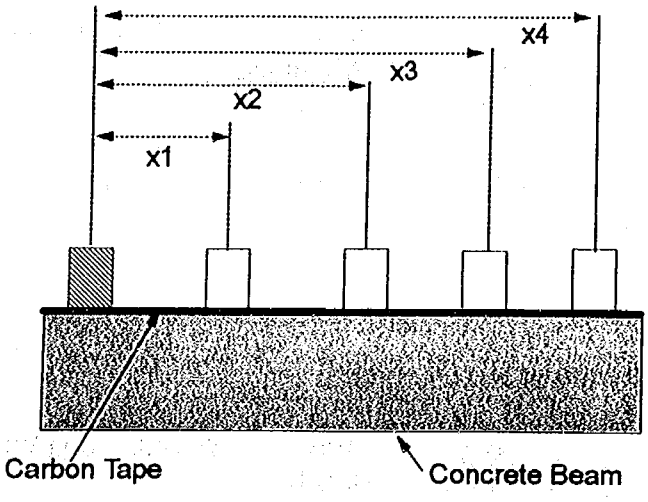


Figure 1. Pulse Velocity Determination on Externally Bonded CFRP - PCC Composites.

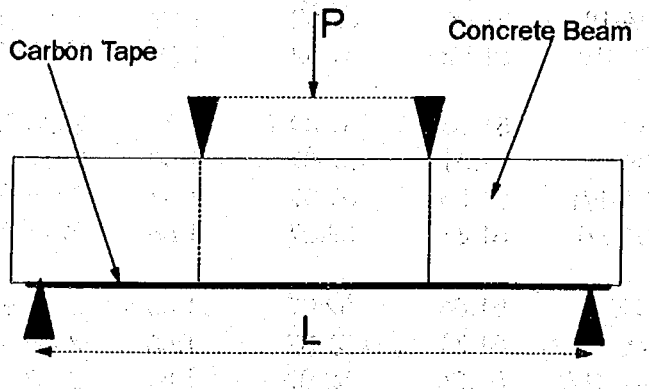


Figure 2. Test Setup for Third-Point Loading of CFRP-PCC Beam Specimens.

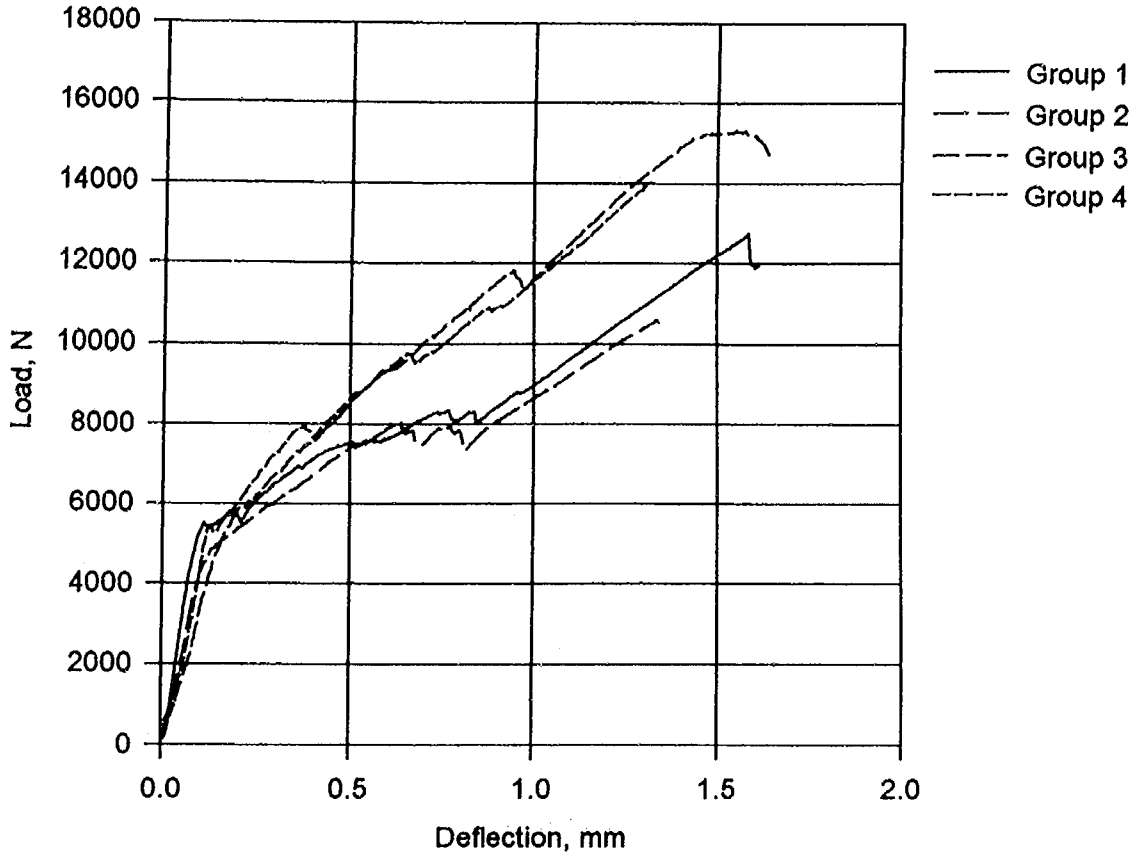
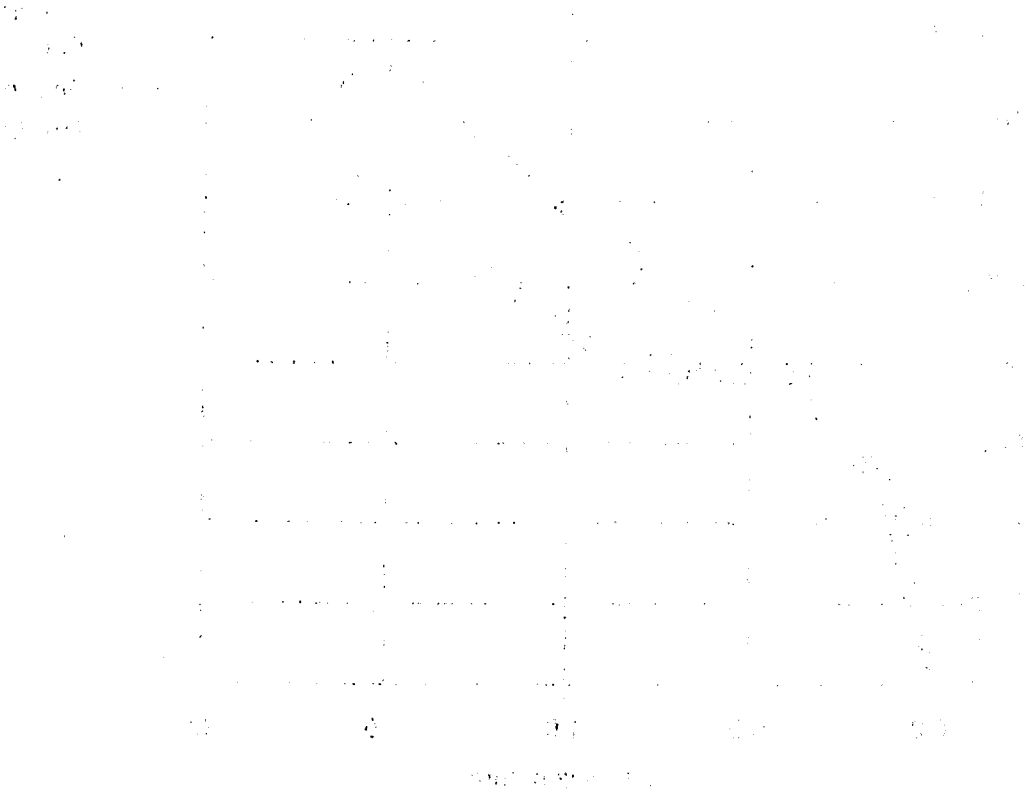


Figure 3. Load-Deflection Curves for CFRP-PCC Composites.



Concrete Beams and Aerospace Composite Material

C. A. Ross[1]
M. L. Hughes[2]
R. L. Sierakowski[3]
J. W. Tedesco[4]
W. C. Naylor[5]

Abstract

Concrete beams with externally bonded advanced aerospace composite panels offers significant enhancement beyond that of the traditional base line materials. Carbon fiber reinforced plastic (CFRP) panels externally bonded to conventional steel reinforced concrete (RC) beams can significantly increase the flexural load carrying capacity of the beam. Third-point static flexural bend tests of 0.2m x 0.2m x 2.8m (8 x 8 x 108 in) RC beams with CFRP have been accomplished and test results are presented. A strength of materials approach based on RC beam analysis was developed to include the CFRP panels. The analysis results in a piecewise linear load-displacement curve which agreed very well with the static experimental results. CFRP delamination occurred for beams whose steel reinforcement ratios were less than 1.0 percent. Compressive concrete failure in the beam upper surface occurred for beams whose steel reinforcement ratios are greater than 1.0 percent.

[1]Professor, Graduate Engineering Research Center, University of Florida, P O Box 1918, Eglin AFB, FL 32542-0918

[2]Research Structural Engineer, Wright Laboratory, WL/FIVCO, 139 Barnes Drive, Suite 2, Tyndall AFB, FL 32403-5323

[3]Professor, Dept. of Civil Engineering, Ohio State University, Columbus, OH 43120-1275

[4]Professor, Dept. of Civil Engineering, Auburn University, Auburn, AL 36849-5337

[5]Instrumentation Mechanic, Wright Laboratory, WL/FIVCO, 139 Barnes Drive, Suite 2, Tyndall AFB, FL 32403-5323

Introduction

Application of aerospace type filamtary composite material to reinforced concrete structures has been described by Meier et al. [1], Meier [2], Kaiser [3], and Triantafillou et al. [4]. More recent studies are presented by Sharif et al. [5] and Chajes et al. [6].

A series of small beam experiments of plain concrete with externally bonded carbon fiber reinforced concrete (CFRP) and larger steel reinforced conrete (RC) beams with CFRP were tested statically and reported on by Sierakowksi et al. [7]. RC beams 8 in x 8 in x 9 ft (0.2m x 0.2m x 2.8m) with external tensile CFRP and varying tensile steel content were tested statically by Wright Laboratory Flight Dynamics Directorate (WL/FIVCS), Tyndall AFB, FL. The CFRP panels were made from aerospce composite material AS4C/1919 graphite /epoxy and furnished by the Wright Laboratory Material Directorate, (WL/MCBC) Wright-Patterson AFB, OH. The CFRP was 60 percent graphite fiber by volume with a room temperature 0^0 fiber direction tensile strength of 320 ksi (2.413 GPa) and a 0^0 fiber direction tensile modulus of 20 Msi (138 Gpa). Structural analyses of the beams were supported by Wright Laboratory Armament Directorate (WL/MNSA) Eglin AFB, FL and is described in detail by Ross et al. [8]. Additional details of these tests and analytical results are described by Ross et al. [9].

CFRP Beam Fabrication

A general schematic of the CFRP beams is shown in Figure 1. Concrete beams of 7.95 ksi (54.8 MPa) compressive strength and reinforced with 60 ksi (0.41 GPa) steel were cast in metal molds and air cured for approximately 60 days. A three ply uniaxial CFRP panel was cemented to three beams of each tensile steel reinforcement ratio as shown in Figure 1. A control beam of each steel reinforcement was tested without CFRP. Most all CFRP panels were cemented using Sikadur® 32 adhesive, but for a few CFRP panels Dexter Hysol® cement was used.

Test Results and Analysis

All beams were tested statically using third-point bending of Figure 2. Detailed test results and analyses are reported in References [8]. An enhancement ratio, defined as the peak load of CFRP/beam peak load control beam, was calculated for each beam test and these results are shown in Figure 3.

Ten. Steel Table

Beam Series No.	Ten. Steel No.*
3A,B,C,D**	3
4A,B,C,D	4
5A,B,C,D	5
6A,B,C,D	6
7A,B,C,D	7
8A,B,C,D	8

*Nominal Rod Diameter In 1/8s Of An Inch

**All Suffix A Beams Tested Without CFRP

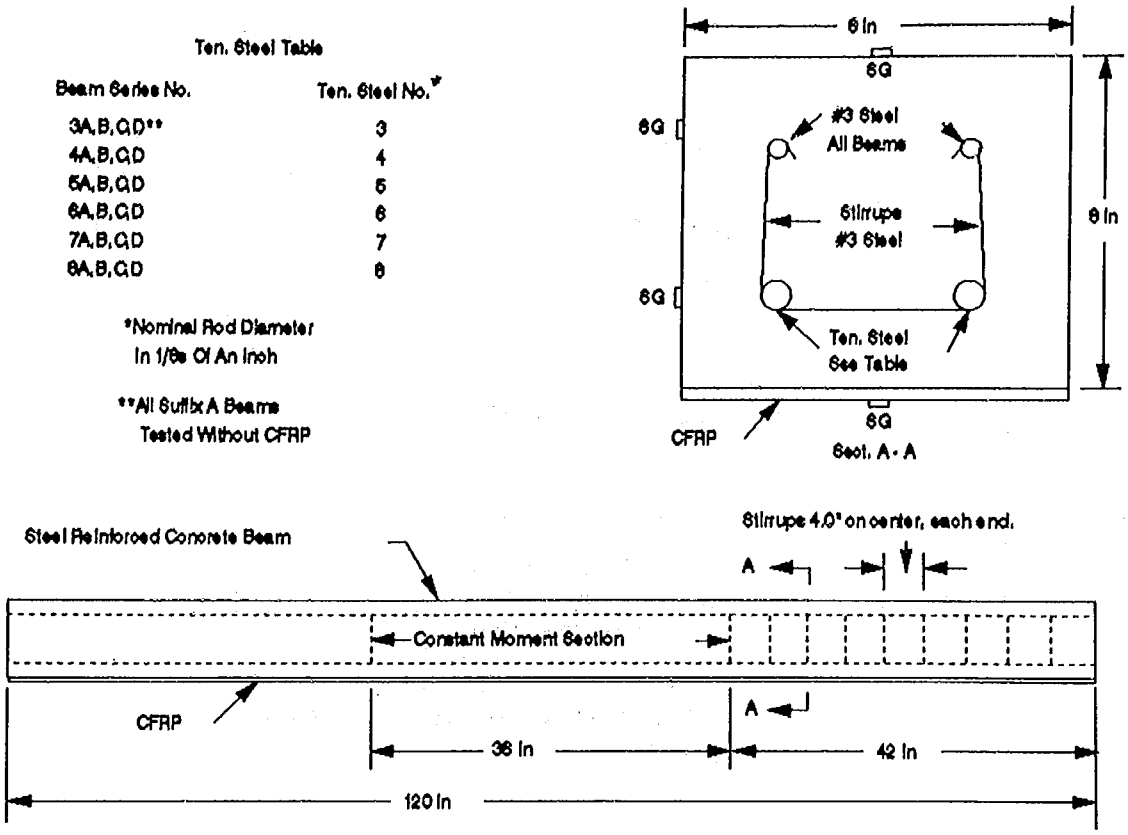


Figure 1. Schematic of test beams.

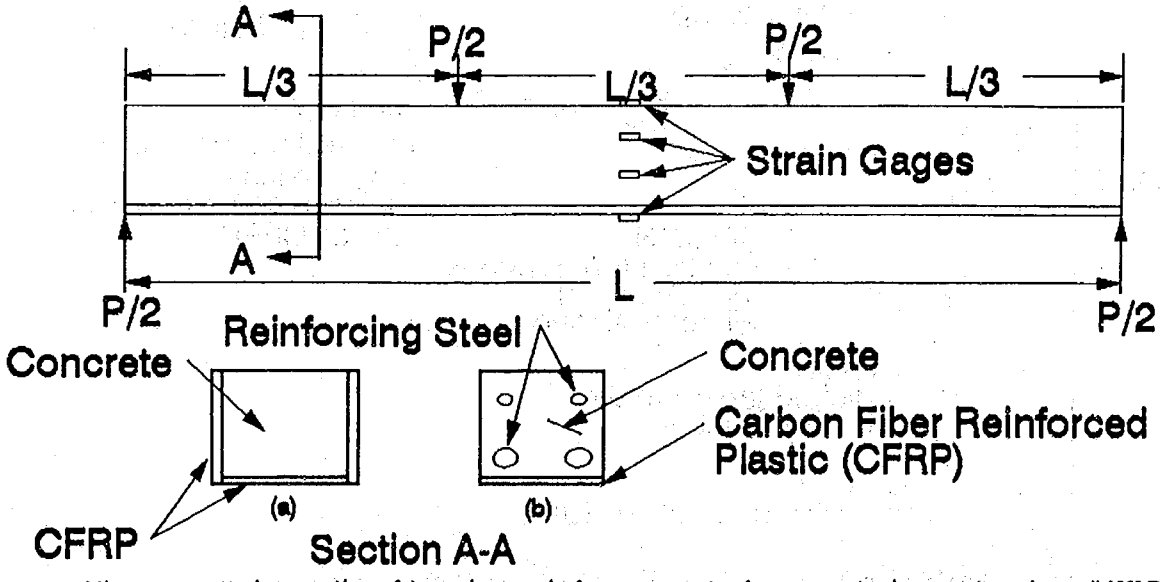


Figure 2. Schematic of tension reinforcement of concrete beams using CFRP and beam test arrangement.

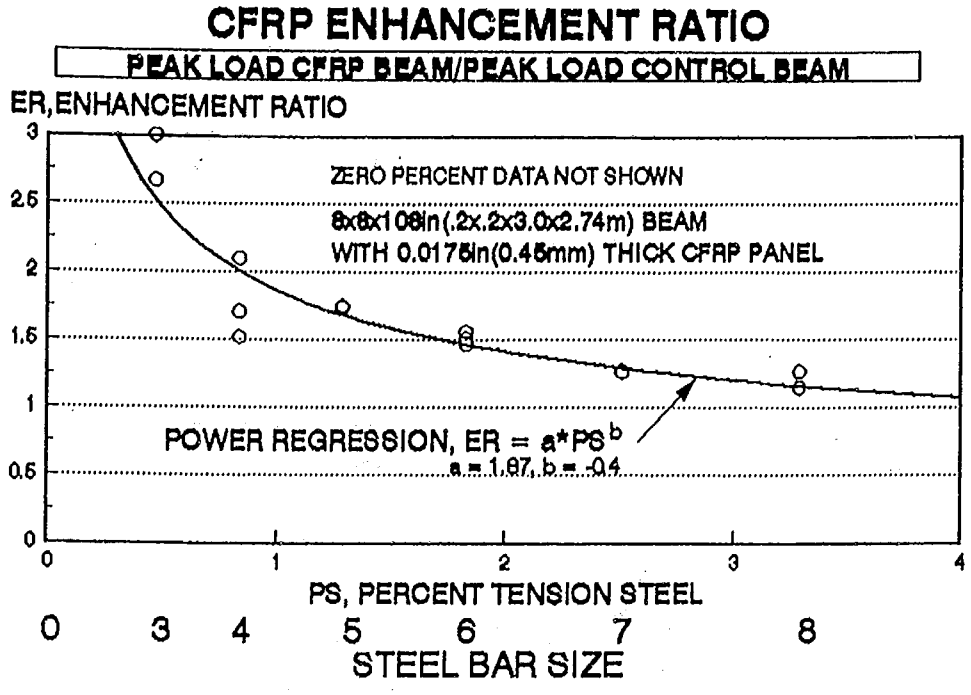


Figure 3. Enhancement ratios for RC beams with CFRP externally bonded to the bottom of the beam.

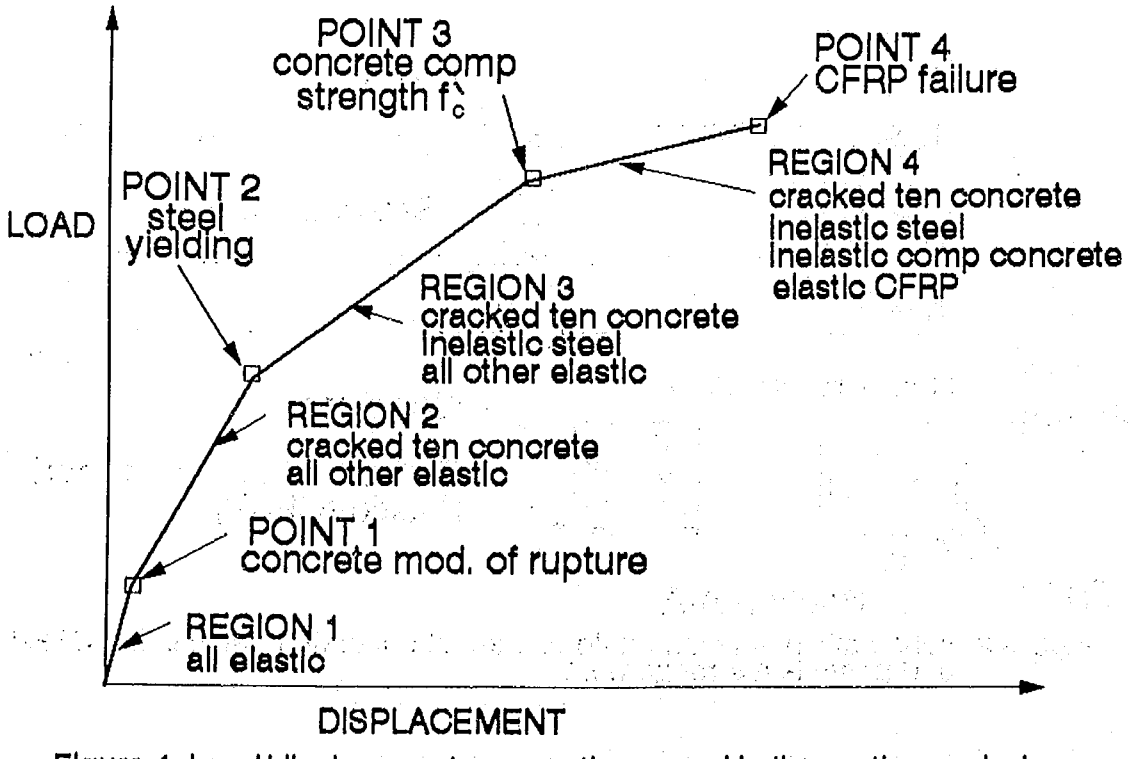


Figure 4. Load/displacement assumptions used in the section analysis.

A section analysis based on assumptions shown in Figure 4, was used to calculate load displacement curves for each series of beams. Examples of the section analysis and finite element method (FEM) analyses [8,9,] compared to experimental results, are shown in Figures 5 and 6.

For beams with the lower tensile steel reinforcement the failure mode was delamination of the CFRP between the CFRP and the adhesive. For the higher tensile steel ratio beams, failure occurred by crushing of the upper compression concrete accompanied by horizontal cracking of concrete at midspan near the position of the tensile steel. These two failure modes are shown schematically in Figure 7.

Conclusions and Recommendations

The addition of the aerospace composite material to RC beams shows considerable strength enhancement over plain RC beams in bending. Preliminary analyses show that the strength enhancement is strongly dependent on the CFRP stiffness rather than strength. The high strength of the CFRP was not fully utilized due to the delamination of the CFRP panels. A basic study on bond strength and mechanics is recommended to produce improvements in strength enhancement.

References

1. Meier, U., Deuring, M., Meier, H., and Schwegler, G., Strengthening of Structures with CFRP Laminates: Research and Applications in Switzerland. K. W. Neale and P. Labossiere, Eds., Canadian Society for Civil Eng., 1992, pp. 243 - 251.

2. Meier, U., "Bridge Repair with High Performance Composite Materials," Material und Tichnik, V. 4, 1987, pp. 125 - 128
(in German).

3. Kaiser, H., "Strengthening of Reinforced Concrete with Epoxy-Bonded Carbon-Fiber Panels," Doctoral Dissertation, ETH, 1989 (in German).

4. Triantafillou, T. C., Deskovic, N., and Deuring, M., "Strengthening of Concrete Structures with Prestressed Fiber Reinforced Plastic Sheets," ACI Structural Journal, V. 89, No. 3, May - June 1992, pp. 235 - 244.

5. Sharif, A., Al-Sulaimani, G. J., Basunbul, I. A., Baluch, M. H. and Ghaleb, "Strengthening of Initially Loaded Reinforced Concrete Beams Using FRP Plates," ACI Structural Journal, March/April 1994, pp. 160-168.

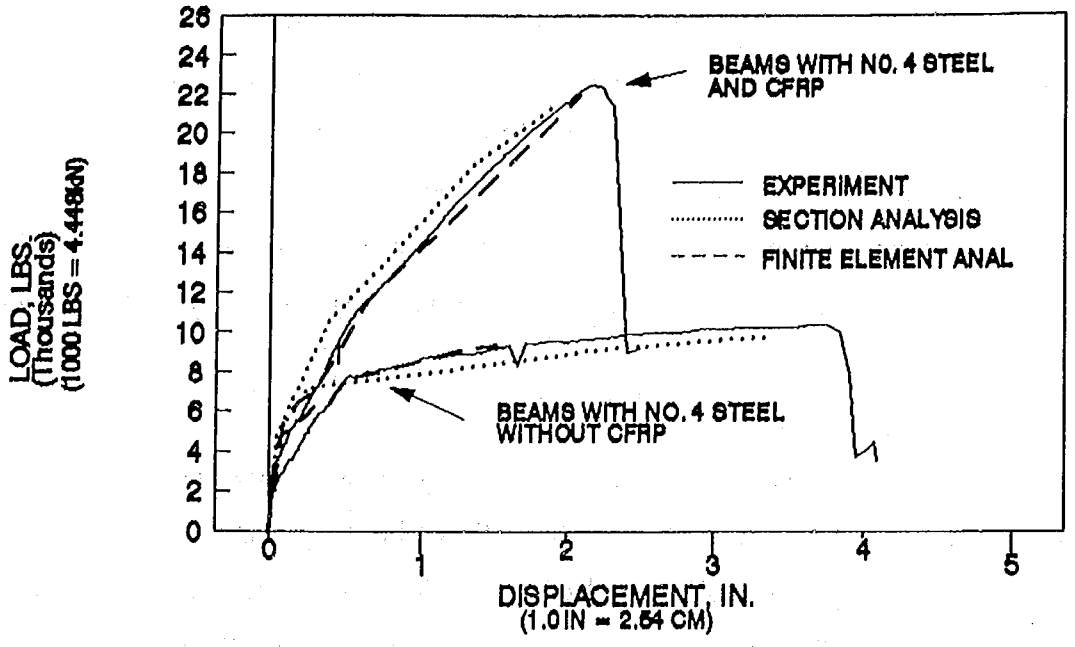


Figure 5. Comparison of calculated and experimental curves for CFRP beams with No. 4 tensile steel.

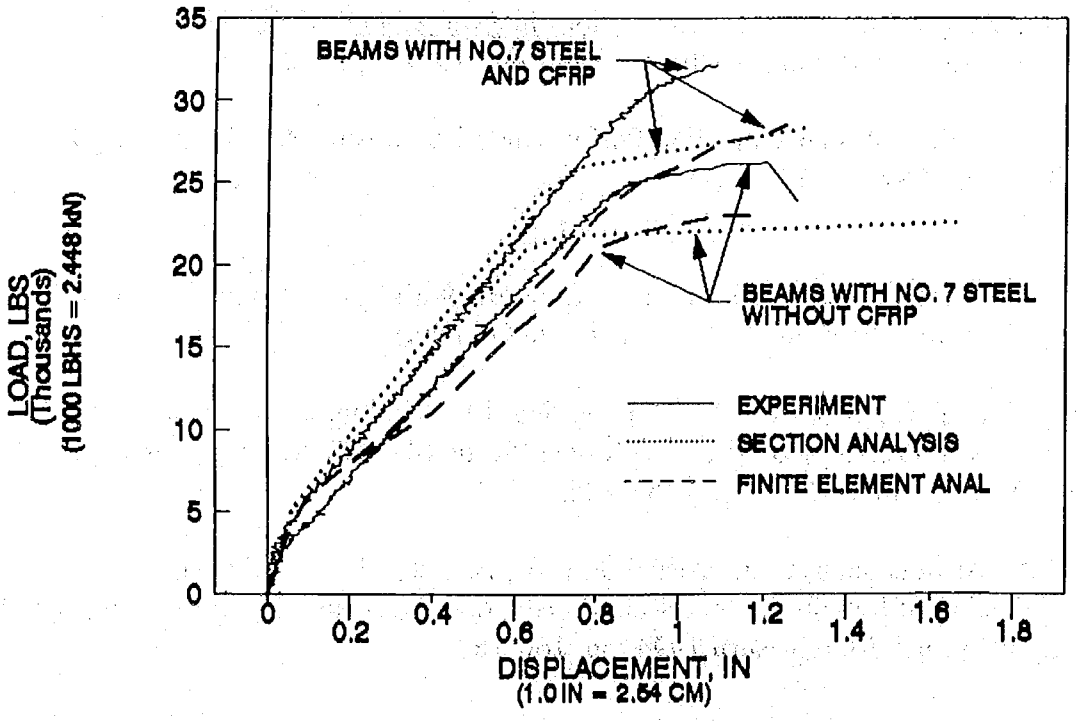


Figure 6. Comparison of calculated and experimental curves for CFRP beams with No. 7 tensile steel.

6. Chajes, M. J., Thomson, T. A. Jr., Januszka, T. F., and Finch, W. W. Jr., "Flexural Strengthening of Concrete Beams Using Externally Bonded Composite Materials," Construction and Building Materials, Vol. 8, No. 3, 1994, pp. 191-201.

7. Sierakowski, R. L., Ross, C. A., Tedesco, J. W., and Hughes, M. L., "Concrete Beams with Externally Bonded Carbon Fiber Reinforced (CFRP) Strips," Proceedings of ASCE 3rd Materials Engineering Conference: Infrastructure, San Diego, CA, Nov. 1994, pp. 139 - 146.

8. Ross, C. A., Jerome, D. M., and Hughes, M. L., Hardening and Rehabilitation of Concrete Structures Using Carbon Fiber Reinforced Plastics (CFRP), WL-TR-94-7100, Wright Laboratory Armament Directorate, Eglin AFB, FL, Dec. 1994.

9. Ross, C. A., Jerome, D. M., Hughes, M. L. , Schmidt, M. J., Sierakowski, R. L., and Tedesco, J. W., "Concrete Beams with External Carbon Fiber Reinforced Plastic Panels," Seventh Int. Symp. on Interaction of Nonnuclear Munitions with Structures, Mannheim Germany, April 1995.

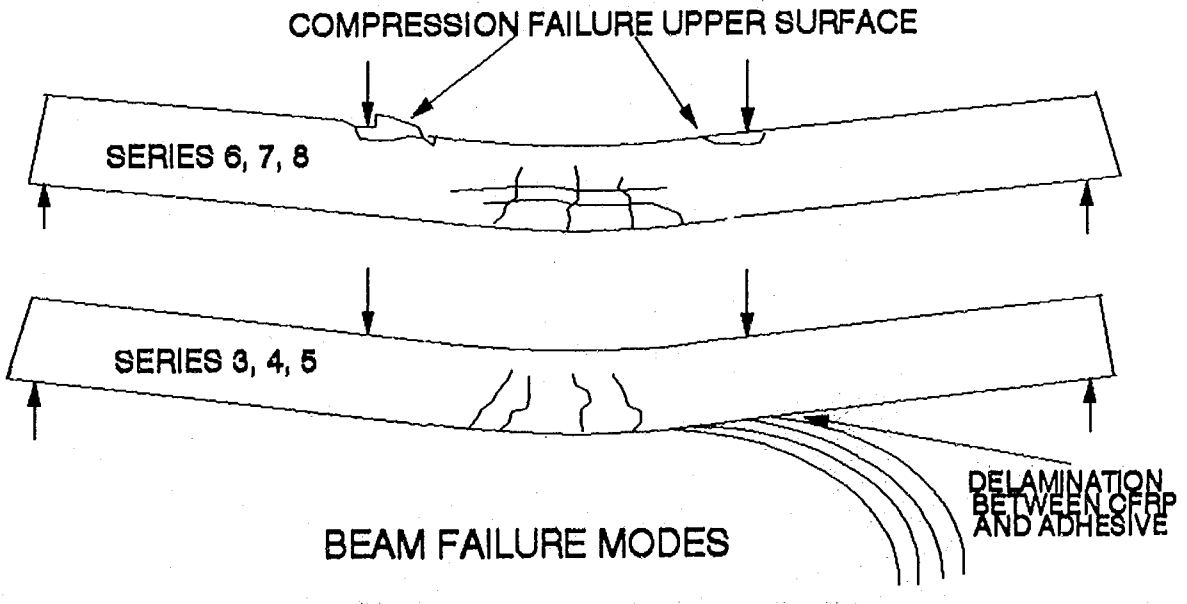


Figure 7. Failure modes for CFRP concrete beams.

Probabilistic Assessment of Soil Liquefaction

by

Nikolaos Simos*
Carl J. Costantino*
Morris Reich*
Thomas McSpadden**

ABSTRACT

A probabilistic model is formulated to assess liquefaction potential of soils during earthquakes. The model is introduced to substitute for deterministic methods which estimate susceptibility of soil to liquefaction for a single seismic event. Further, the probabilistic approach in this study will allow for the calculation of continuous probabilities of soil liquefaction for a given site. The basis for the proposed probabilistic model are the statistical properties of the earthquake and the uncertainties associated with the characterization of the soil.

Earthquakes are are assumed realizations of a random process, expressed in the form of a power spectral density, that characterizes the region. Uncertainties in the soil resistance to liquefaction are also introduced with probability density functions around *in-situ* measurements of parameters associated with the soil strength. The liquefaction probabilities are computed using Monte Carlo simulations along with transfer functions of the soil model response.

KEYWORDS: Probability, damage, liquefaction, effective stress, pore pressure

1.0 INTRODUCTION

During an earthquake event of considerable duration and intensity an earthen dam can experience partial or total failure that stems from either loss of soil strength due to liquefaction or reduction of the inherent resistance to sliding along a potential failure surface. In trying to assess the potential to failure in either mode, one has to essentially incorporate two types of probabilities. One that is associated with the occurrence of an earthquake in the proximity of the structure and the other with the state of the soil and its tendency to liquefy or fail in shear.

The coupling of the two essential components (excitation and soil state) with inherent statistical properties can only be achieved through response analyses that allow for the combined statistics to participate. A promising approach is the one involving the Unit Response of the domain that can eventually provide the system response resulting from a seismic event which in turn represents a stochastic process. Such procedure, however, implies that the domain exhibits linear behavior. While in typical soils this is only true in small strains, the benefits of the Unit Response approach compensate for the lack of nonlinear considerations.

The constitutive response of the granular soil skeleton and its coupling with the fluid phase is formulated around the Biot dynamic equations of motion. The finite element analysis utilized in the evaluation of the dynamic response is a linear in character but it treats the soil as a two-phase medium. While the drawback of linearity is somewhat compensated with the equivalent hysteretic damping, it is the two-dimensional pore water/soil skeleton interaction that provides a realistic description of the behavior of the soil in a dynamic mode. The solution takes place in the frequency domain and the resulting harmonic response, inverted with the use of Fast Fourier Transform techniques, provides the intergrannular stress as well as the pore water pressure fluctuation during the seismic event.

The probability of liquefaction failure is evaluated by incorporating the *in-situ* strength conditions, which exhibit a random behavior around soil strength properties, and seismically induced random dynamic stresses at various potentially liquefiable locations within the cross section of the dam. The driving random forces in such process are the dynamic (cyclic) shear stress that is generated in the soil layers and the buildup of pore pressures.

---

* Brookhaven National Laboratory, USA
** US Department of Energy (EH)

A limit state function that contains the failure criterion is established as a cumulative effect for the duration of the random earthquake and it is an indicator of the pore pressure build-up. It should be noted that while a linear analysis can only predict the buildup of pore pressures only heuristically, it can provide the level of shearing at low strains that the soil experiences during the seismic event. Since most probabilistic models of soil liquefaction provide *deterministic* answers (probability can only take the values of one for liquefaction occurrence or zero when no liquefaction occurs), the present model through Monte Carlo simulations both in the earthquake and in the soil strength, expressed as function of a single field parameter (SPT N-values or relative density D_r), results in a continuous probability between 0 and 1.

For the sake of numerical implementation of the procedures discussed in the paper, a sample problem is analyzed. The selected soil structure consists of a three-layer deposit in a narrow valley saturated almost to the surface and surrounded by the bedrock. The model is subjected to horizontal accelerations on the bedrock which in turn are realizations of a random statistical process expressed in the form of a Kanai-Tajimi power spectrum. At the end of the numerical computations cumulative liquefaction probabilities as well as limit state are estimated for the three distinct soil layers.

2. GOVERNING EQUATIONS

In a saturated state of soil deposits the pore pressure of the water trapped in the soil skeleton will fluctuate during an earthquake and impact on the intergrannular soil stresses. Since the strength of the soil is tied to the intergrannular stresses, it is vital that the dynamic pore pressure be captured. The coupled behavior of pore water and soil skeleton requires that the medium must be treated as a two-phase one with governing equations that reflect the coupling.

Further, the ability of the soil to resist liquefaction is one hand dependent on its initial stress state (effective stress) and on the other hand on the intensity of the dynamic shear stress. The shear stress variation at different locations in the embankment and the foundation as well as the number of stress cycles during the earthquake event determine whether the soil is susceptible to such failure.

Therefore, to effectively analyze the system, the employed theoretical/computational model must enable;

a. The description of the domain as a two-phase medium.
b. The implementation of actual or representative earthquake input.
c. The evaluation of the time variation of stresses resulting from the seismic input.

In order to perform the dynamic analysis, which satisfies the above requirements, the POROSLAM code is employed. The code is a two-dimensional finite element representation of Biot's dynamic equations for both soil and fluid phases. Biot's equations are a linear description of the response of the soil skeleton and of the pore water in the form,

$$\frac{\vartheta \tau_{xx}}{\vartheta x} + \frac{\vartheta \tau_{xy}}{\vartheta y} = \varrho \ddot{u}_x + \varrho_f \ddot{w}_x$$

$$\frac{\vartheta \tau_{yx}}{\vartheta x} + \frac{\vartheta \tau_{yy}}{\vartheta y} = \varrho \ddot{u}_y + \varrho_f \ddot{w}_y$$

and

$$-\frac{\vartheta p_f}{\vartheta x} = \varrho_f \ddot{u}_x + \frac{1}{f}\varrho_f \ddot{w}_x + \frac{\eta}{k}\dot{w}_x$$

$$-\frac{\vartheta p_f}{\vartheta y} = \varrho_f \ddot{u}_y + \frac{1}{f}\varrho_f \ddot{w}_y + \frac{\eta}{k}\dot{w}_y \qquad (1)$$

where,

$[\sigma_{xx}, \sigma_{yy}, \sigma_{xy}]$ = intergrannular stresses

p_f = pore pressure

$[u_x, u_y]$ = displacements of soil skeleton

$[w_x, w_y]$ = displacements of pore water

$$\{\tau\} = \{\sigma_{xx} - \alpha p_f, \sigma_{yy} - \alpha p_f, \sigma_{xy}\}^T$$

while, f = porosity, ϱ = total mass density, ϱ_f = fluid mass density, α = compressibility of solid, M = compressibility of the fluid, η = fluid viscosity and k = soil permeability.

The resultant equations that expresses the total stress vector and pore pressure in terms of the displacement vector is discretized and adopted to the finite element scheme. Explicit definition of the above equations can be found in [5].

3. RANDOM EXCITATION

For the probabilistic mode the input seismic excitation is expressed in terms of the complex input

$$X(\omega_k) = e^{i\omega_k t}$$

Evaluation of the response at the frequencies ω_k leads to the complex frequency response $H(\omega)$.

The Fourier coefficients of a response quantity $Y(\omega)$ (displacement or stress) from a synthetic input with coefficients $X(\omega)$ can be obtained through the relation

$$Y(\omega) = H(\omega) X(\omega) \qquad (2)$$

Within the Monte Carlo scheme (multiple evaluation of the response at the same intensity level but with random distribution of peaks), the simulated earthquakes are assumed belong to a certain family. Such family can be characterized by either a **response spectrum** or a **power spectrum**. Earthquake records can be synthesized on the basis of either spectrum. By assuming that an earthquake family is described by the **Kanai-Tajimi** power spectrum

$$S_x(\omega, \lambda) = S_0 \frac{\left(1 + 4\zeta_g^2 \alpha_0^2\right)}{\left(1 - \alpha_0^2\right)^2 + 4\zeta_g^2 \alpha_0^2} \qquad (3)$$

where, $\alpha_0 = \frac{\omega}{\omega_g}$, $\lambda = [\zeta_g, \omega_g, S_0]^T$
synthetic acceleration time histories are deduced according to the relation

$$g(t) = 2\zeta(t) \sum_{i=1}^{N} \sqrt{S_x(\omega_i)\, \Delta\omega} cos(\omega_i t + \phi_i) \qquad (4)$$

Each synthetic record is a realization of the process described by the power spectrum. $\zeta(t)$ accommodates for the non-stationary part of the ground excitation, ϕ_i is a vector of random phase angles (uniformly distributed between 0 and 2π and $w_i = i\Delta\omega \quad \Delta\omega = \frac{\omega_{upper}}{N}$.

4. PROBABILISTIC LIQUEFACTION

As it has been previously mentioned, the assessment of the probability of liquefaction failure at a given site given that an earthquake has occurred is typically deterministic or in other words the probability takes the value of 1 for liquefaction occurrence or the value 0 for no liquefaction. In this study a procedure through which a continuous probability between 0 and 1 can be established will be adopted.

In assessing the likelihood of liquefaction one has to keep in mind that several sources of uncertainty exist. Uncertainties emanate from the definition of the earthquake and from the characterization of the particular site. There are various *vectors* of parameters that can characterize both the earthquake and the site. A typical set of parameters for an earthquake are the peak ground acceleration and the duration or the magnitude. The equivalent vector for the site indicating resistance to liquefaction could consist of the corrected standard penetration resistance or the relative density and the percent fines content. The two independent uncertainty sources will be addressed separately but the *limit state function* that reflects the failure criterion will incorporate both uncertainties.

Consider the following limit state function,

$$g(\chi, \psi) = (SF)_{LIQ} - 1$$

$$= \frac{Strength(\chi)}{Induced\ Stress(\psi)} - 1 = 0 \qquad (5)$$

where χ = the parameter vector of the site and $\psi = \psi(pga, T)$ is the earthquake load vector. The probability that $g(\chi, \psi) < 0$ conditional to the occurrence of an earthquake and a given vector of site soil parameters $\chi = \overline{\chi}$ is

$$P\left[g(\overline{\chi}, \psi) < 0|_{quake}\right] = \int_{\psi} P\left[g(\overline{\chi}, \overline{\psi}) < 0\right] d\Psi \qquad (6)$$

where $\Psi(\psi)$ the probability distribution of the parameters in the earthquake characterization vector. Quantities with a bar over them are considered to be known. To reduce the complexities, the parameter indicating the earthquake duration is no longer considered random (tendency to only incorporate the strong motion portion of the record which in turn can be defined by an average value). Hence, the conditional probability can be written

$$P\left[g(\overline{\chi}, \psi) < 0|_{quake}\right] = \int_{\alpha} P\left[g(\overline{\chi}, \alpha) < 0\right] d\Psi \qquad (7)$$

where α is the random peak acceleration of the earthquake. If one estimates the earthquake occurrence rate λ per year for the particular site from appropriate hazard curves then the probability of liquefaction failure per year at the site and at a specific location characterized by the vector $\overline{\chi} = \overline{\chi}(\overline{N}, \overline{D_r}, etc)$ can be deduced from
$P[g(\overline{\chi}, \alpha) < 0|_{year}] =$

$$1 - exp\{-\lambda \int_{\alpha} P\left[g(\overline{\chi}, \alpha) < 0\right] d\Psi(\alpha)\} \qquad (8)$$

In order to incorporate the uncertainties of the site characterization into the probability measure, the randomness of the vector parameters in $\overline{\chi} = \overline{\chi}(\overline{N}, \overline{D_r}, etc)$ must be established. The elements of the above vector are indicative of the soil liquefaction resistance. If, for the sake of simplicity, one can deduce a single parameter that can fairly represent the soil, then the randomness of the selected parameter will characterize the uncertainties of the site. The SPT blow count N values can play that role.

To establish its statistics for a particular site one has to consider the following: It is not realistic to accept a distribution of N-values for a site as a function merely of the depth and the type of soil unless one considers the soil medium perfectly homogeneous. If such is the case, then for a given site and type of soil the N-values can be estimated based on the effective overburden stress (not random) and the relative density of the soil which in turn can be considered as the random variable. In most applications, however, one has available a profile of the SPT N-value with depth from actual *in-situ* testing. It is expected that variability of the N-value at any depth exists along with the variability with depth. Rather than attempting to establish a distribution for the entire medium, randomness to the value of N at a given location can be assumed. If a good size sample is available (very rare) for every location, the statistical properties can then be established (mean, variance etc.) as well as the distribution type.

If (as in most cases) a single value of N is available for the location, a distribution can be assumed about the value which can represent the mean. The random nature of the members of the assumed distribution will provide the uncertainty in the liquefaction resistance.

Denoting the probability distribution about the SPT N-value at a location h as $\Xi(N)\,|_h$ then the probability of a liquefaction failure at the specified site and this particular location within a time period T *years* can be estimated through the expression

$$P\left[g<0|_T\right] = \int_N \left[1 - exp\{-\lambda T \int_\alpha P\left[g\left(\overline{\chi},\alpha\right)<0\right] d\Psi\}\right] d\Xi \qquad (9)$$

The integrals $\int_N$ and $\int_\alpha$ are evaluated between the range of expected minima and maxima for the site (i.e. $\int_\alpha = \int_{\alpha_{min}}^{\alpha_{max}}$ and $\int_N = \int_{-n\sigma}^{+n\sigma}$).

For the process to be complete an explicit definition of the limit state function $g(\chi,\psi)-1=0$ must be established. There are several ways in defining soil strength or resistance to liquefaction and seismically induced action. Specifically, the vulnerability of the soil to liquefaction is determined by the level of stress or strain that develops during a dynamic event or by the build-up of pore pressure in the saturated soil. In addition, one must keep in mind that the failure criterion it is not an instantaneous event but rather the result of an accumulated effect for the span of the earthquake and can be estimated based on the induced cycles of the soil straining. For a shear stress or strain failure type the developed stress or strain in the soil must exceed a threshold value for failure to occur. Typically, an equivalent stress ratio $r_{equiv} = \frac{\tau_{equiv}}{\sigma_0'}$ and an equivalent number of cycles N_{equiv} is estimated from the shear stress response at a particular location and the resistance to liquefaction is determined as the ratio of $\frac{\tau|N_{equiv}}{\tau_{equiv}}$ from appropriate $\frac{\tau}{\sigma_0'}$ *vs.* N curves. For complex stress state, however, where the impinging seismic waves cause more than shear action, it is suggested that strength curves be developed (from laboratory tests) reflecting the strength of the soil as a function of the stress invariant $\sqrt{J_2'}$.

An alternative definition of the limit state function is the evaluation of the resistance to liquefaction based on the generated pore pressures. With this approach liquefaction occurs at zero effective stress. Since the state of failure is reached progressively, a cumulative damage index is evaluated as the earthquake passes by and it has the form

$$D(t) = \sum_{induced\ cycles} \frac{1}{N_{liq}} \qquad (10)$$

N_{liq} represents the number of uniform cycles required to induce liquefaction at the shear stress level of one of the actual stress cycles the soil is subjected to.

The shear stress ratio r_τ can be related to N_{liq} through empirical formulae of the type

$$N_{liq} = \xi\ tan\left[\frac{\pi\left(r_0\left(D_r\right) - r_\tau\right)}{2\left(r_0\left(D_r\right) - r_\infty\right)}\right] \qquad (11)$$

In the above expression r_τ is the shear stress ratio for an induced cycle, $r_0(D_r)$ and r_∞ are shear stress ratios associated with the strength of the soil with variation in the relative density D_r (see

Figure 11) and ξ is a curve fitting parameter. The last expression actually ties both the induced effect and the soil resistance. Thus, given the shear stress history at a particular location (generated randomly) and for a randomly selected SPT N-value, the corresponding relative density D_r can be deduced from the appropriate for the soil relation of Figure 10.

With a given D_r at the location (conditional to the value N) the N_{liq} *vs.* r_r relationship is established. At the same time, by continuously tracking the time history of the randomly induced stress at the same location for the entirety of the random earthquake, the limit state function is established and can be implemented in the probability integrals. For any synthetic earthquake the damage index is evaluated and related to the pore pressure ratio $r_{p_f} = \frac{p_f}{\sigma_0'}$ with the simple relation $r_{p_f} = D(t)$. Liquefaction occurs when the pore pressure and the effective stress are equal or $r_{p_f} = 1$. Thus the limit state function is defined as

$$g(\chi, \psi) = r_{p_f} - 1 = 0$$

4.1 Probability Distribution Functions

Equations 6 through 12 incorporate the probability distribution functions Ψ and Ξ of the two parameter vectors ψ and χ. It has been assumed that the earthquake vector $\psi = \psi(\alpha)$ has uncertainty only in the peak ground acceleration. If for a given site one accepts that there exists a low PGA value α_0 below which the earthquakes for the site are insignificant and that the occurring earthquakes constitute a Poisson process with an average rate λ_0 per year, for a time interval $(0, T)$ (where T could be the lifetime of the structure) the significant earthquakes can be deduced from

$$P(N_T = n) = \frac{(\lambda_0 T)^n}{n!} e^{-\lambda_0 T} \qquad (12)$$

The distribution of the peak accelerations of Eqn (12) can take the following exponential form

$$\Psi_{PGA}(\alpha) = 1 - e^{-\beta(\alpha - \alpha_0)} \qquad \alpha \geq \alpha_0$$

$$= 0 \qquad \alpha < \alpha_0$$

The parameter β is site specific and it ranges between 1.5 and 2.3. The smaller the value of β the higher the frequency of larger earthquakes.

The uncertainty in the soil strength vector is summarized in the SPT N-value for the specific depth where liquefaction susceptibility is sought. On the basis of *in-situ* SPT testing certain distribution functions can be deduced. For a given site where n borings have been performed with variability of blow counts in the depth as well as variability between their individual profiles the following assumptions can be made: (a) there exists a normal distribution with mean and variance approaching that of all the data in the n-borings and it represents the entire site. (b) at different depths h a normal distribution about the mean value of $\overline{m}_N(h)$ also exists along with a standard deviation $\sigma_N(h)$. Given that there exists great variability of the soil profile in actual sites, it will be a hopeless task to attempt and deduce a continuous probability distribution as a function of depth. Instead, the distribution and its properties mentioned above (formed from actual boring test data) will represent the particular depth. If one is interested in the probability of liquefaction failure at a specific depth where no data are available, the distribution of the entire site can be used. Thus, the random N value at the selected location will be a member of the normal distribution with an expected mean and standard deviation.

4.2 Monte Carlo Simulations

Through this approach a continuous probability of liquefaction failure will be deduced by relying on *deterministic* assessment for any individual realization of the involved stochastic processes (randomness of the induced ground acceleration at any level of peak acceleration and randomness of the soil strength parameter N).

The methodology that will lead to the evaluation of the probability integrals (Eqns 5,9) is presented below. The ultimate goal is to determine the probability that the site will liquefy at any depth during its lifetime. In the process, however, the annual probability of liquefaction at any depth conditional to the occurrence of an earthquake as well as the probability of liquefaction at various depths as a function of peak ground acceleration can be estimated.

Prior to entering a double loop in which the soil strength parameter and the earthquake temporal variation are randomly selected, the effective overburden stress σ_0', the unit response of the soil domain $H(\omega)$ and the distribution parameters $\overline{N}(h_i)$ and $\sigma_N(h_i)$ are evaluated. With this information at hand the flow chart of the process will be

as follows:

External Loop

- The range of depth h_i of interest starting from h_0 and extending to h_{max} such that $h_i = i\Delta h$ is selected.
- At each increment characterized by $\overline{N}(h_i)$ and $\sigma(h_i)$ n values of **N** are randomly selected from the governing normal distribution. This is achieved by generating random normal (Gaussian) deviates from a distribution with zero mean and unit variance. When the deviate (multiplied by $\sigma_n(h_i)$) is superimposed on the mean $\overline{N}(h_i)$ a random soil strength parameter is N^* deduced and with this value the inner loop is entered.

Inner Loop

- The loop is performed over the range of peak acceleration anticipated for the site (a_0 to a_{max}) with increments of Δa. At each increment the probability distribution $\Psi(a_j)$ is computed ($a_j = j\Delta a$). The peak acceleration a_j will reflect on the **power spectral density** function of Eqn (3).

- With a power spectrum $S(\omega, \overline{\lambda})$ but for **M** realizations of the random phase angle ϕ_i, **M** synthetic histories of the form in Eqn (4) are deduced and through Eqn (2) the response of the domain is calculated. For each synthetic history of peak acceleration a_j the temporal variation of the induced shear stress and the liquefaction damage index are evaluated. The criterion for failure during any such simulated event is that the damage index is greater than 1.0.

- The probability of failure at any α_i, conditional to a strength value $N^*(h_i)$ can be computed in the following sense

$$P\left[SF(h_i) < 0 \| N = N^* \| pga = \alpha\right] = \frac{M_f}{M} \quad (13)$$

where, M_f are the number of simulated earthquakes at $pga = \alpha$ that induced failure and M is the total number of simulations.

- Repetition of the process for the selected PGA range ($\alpha_0 ..... \alpha_{max}$) a fragility curve can be developed reflecting the susceptibility of the soil to liquefaction provided that the strength of the soil is $N^*(h_i)$. The probability that $SF_{LQF}(h_i, \|N^*) < 0$, conditional to the occurrence of an earthquake is

$$P\left[SF_{LQF}(h_i, \|N^*) < 0 \| quake\right] =$$

$$\int_{a_0}^{a_{max}} P\left[SF_{LQF}(h_i, N^*) < 0 \| \alpha\right] d\Psi(\alpha)$$

The probability of failure for the lifetime T of the dam

$$P_T(h_i, N^*) =$$

$$1 - exp\left(-\lambda_0 T\, P\left[SF(h_i, N^*) < 0 \| quake\right]\right)$$

- The probability of liquefaction failure at depth h_i at which the strength parameter is normally distributed about the mean $\overline{N}(h_i)$ and with $\sigma_N(h_i)$ can be written

$$P\left[g < 0 \|_h = h_i\right] =$$

$$\sum_n P\left[g(N, \alpha) < 0 \|_{N=N^*}\right] \Xi\left(N^*, \overline{N}, \sigma\right)$$

where Ξ is the normal distribution density function of N at depth h_i.

- Since we have discretized the distribution function of the soil strength parameter with the depth and since, for this stage, no other strength parameter that has a depth-dependent distribution is involved, the probability of liquefaction failure in the soil under consideration is simply the maximum of the probabilities calculated at each depth, hence

$$P\left[g < 0\right] = max\left(P\left[g < 0 \|_{h=h_i}\right]\right)$$

5. ANALYSIS OF SAMPLE CASE

The configuration shown in Figure 1 has been analyzed in order to address the particularities of the overall procedure that involves the dynamic response of the soil system to random earthquakes and its susceptibility to liquefaction. Specifically, a narrow valley is considered with three distinct layers of soil deposit making up the cross section. The bottom layer is assumed to be clean sand with $D_r = 60\%$ and shear wave velocity $V_s = 1300 ft/sec$. The clean sand is followed by a thin layer of silt with $V_s = 990 ft/sec$ while the rest of the deposit consists of a sand layer with properties $D_r = 40\%$ and $V_s = 560 ft/sec$. As shown in Figure 1 the soil deposit is resting on the surrounding bedrock. The silt layer has been assumed much less permeable than the two sand layers. This consideration is expected to induce

higher pore pressure in the clean sand below. The water table has been placed at 9 ft below the ground level.

The domain of interest is discretized into the finite element mesh shown in Figure 2. The resulted model is analyzed statically first in order to compute the initial effective stresses. The horizontal Unit Response of the model is computed by imposing the acceleration $a_h = e^{i\omega t}$ along the entire interface of soil and bedrock. Figures 3 through 5 depict the normalized Fourier spectra of the acceleration at selected locations in the three different soils. By utilizing the Kanai-Tajimi power spectrum of Eqn (3) a series of simulated earthquakes are generated for different values of peak acceleration. The peak acceleration defines the value of S_0 in the power spectrum expression while arbitrary seed numbers introduce the random phase angles in the input acceleration expression. Figure 6 represents a time history of a simulated acceleration that has duration $T = 20\ secs$ and $PGA = 0.20(g)$. The resulting dynamic shear stresses in the three distinct zones are shown in Figures 7 through 9.

It should be noted that since the selection of the model is arbitrary, no variation of the soil strength, as it is expressed in terms of the normalized penetration blow count, is introduced. Instead, it has been assumed that appropriate curves of *stress ratio vs. cycles to liquefaction*, Figure 11, describe the susceptibility of the involved soils explicitly. With that assumption the external loop in the probabilistic computation is discarded.

For an arbitrary selection of (a) the range of peak ground acceleration α expected for the site and (b) the distribution of these peak accelerations $\Psi_{pga}(\alpha)$ a fragility curve, Figure 12, has been deduced. Further, liquefaction probability values are computed for the three locations conditional to the occurrence of an earthquake with peak acceleration within the selected range. It is clearly shown that the saturated part of the top layer, which consists of sand with low relative density $D_r = 40\%$ and is under lower initial effective stress, is more susceptible to liquefaction. The silt layer in the middle is more resistant to liquefaction due to the fact that in cyclic tests higher stress ratios $(\frac{\tau}{\sigma_o'})$ are required to induce liquefaction.

4. REFERENCES

1. *Probabilistic Theory of Structural Dynamics*, Y.K. Lin, Kriger, 1976.
2. *Dynamics of Structures*, R.W. Clough, McGraw Hill, 1975.
3. *Probabilistic Evaluation of Liquefaction Potential*, H.H.M. Hwang and C.S. Lee, Technical Report NCEER-91-0025, 1991
4. *Evaluation of Potential for Liquefaction of a Soil Deposit Using Random Vibration Procedures*, N. C. Donovan, 1974.
5. *Seismic Risk Assessment of Small Earthdams*, C.J. Costantino, N. Simos, Y.T. Gu, Technical Report NCEER-91, Earthquake Research Center, City University of New York.
6. *POROSLAM. Two-Dimensional Dynamic Solution of Elastic Saturated Porous Media*, N. Simos, C.J. Costantino, C. Miller, Earthquake Research center, City Univ. of New York.
7. *Liquefaction of Soils During Earthquakes*,Committee on Earthquake Engineering *et al*, National Academy Press, 1985.
8. *A simplified Procedure for Evaluating Soil Liquefaction Potential*, H.B. Seed, I.M. Idriss, Report No. EERC 70-9, 1970.
9. *Evaluation of Soil Liquefaction Potential for Level Ground During Earthquakes*, NUREG-0026, 1976.
10. *Cyclic Stress Conditions Causing Liquefaction of Sands*, K.L. Lee, H.B. Seed, Journal of Soil Mechanics and Found. Div., No. SM1, pp.47-70, 1967.
11. *Comparison of Dynamic Analyses for Saturated Sands*, W.D.L. Finn, G.R. Martin, M.K.W. Lee, Proc. of the ASCE Geotech. Div., Vol.1, pp. 472-491, 1978.
12. *An Engineering Approach to the Analysis of VELACS centrifuge Tests*, W.H. Roth and S. Inel, Verification of Numerical Procedures for the Analysis of Soil Liquefaction Problems, Volume 1, pp. 1209-1229.

Acknowledgments

This work was performed under the auspices of DOE

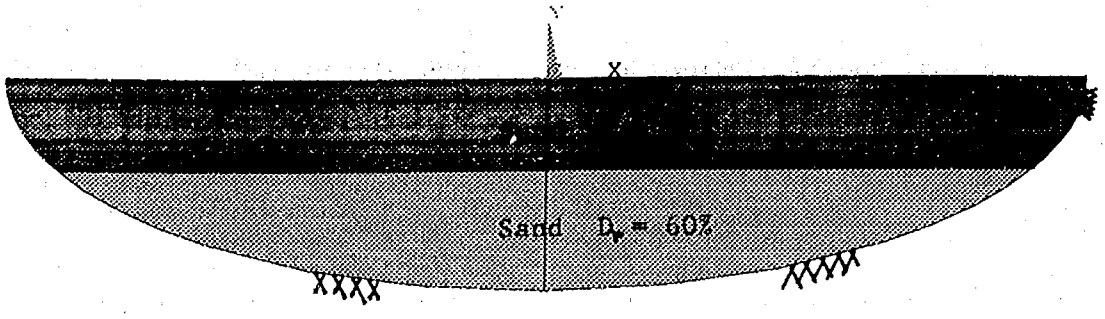


Figure 1. Problem Configuration

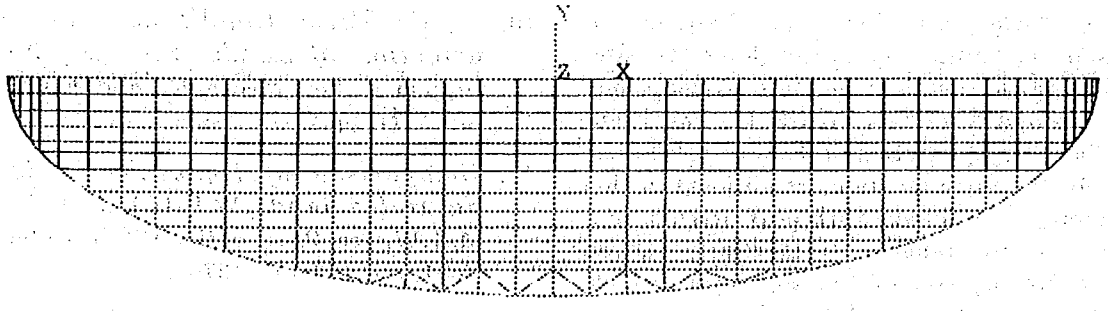


Figure 2. Finite Element Discretization

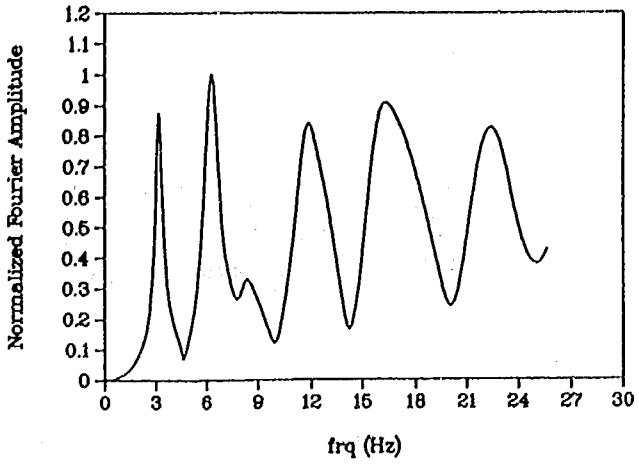


Figure 3 Normalized Acceleration Fourier Spectra in Lower Layer

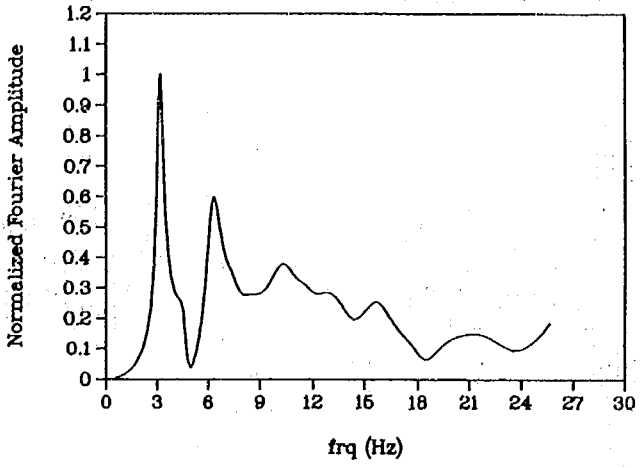


Figure 4 Normalized Acceleration Fourier Spectra in Middle Layer

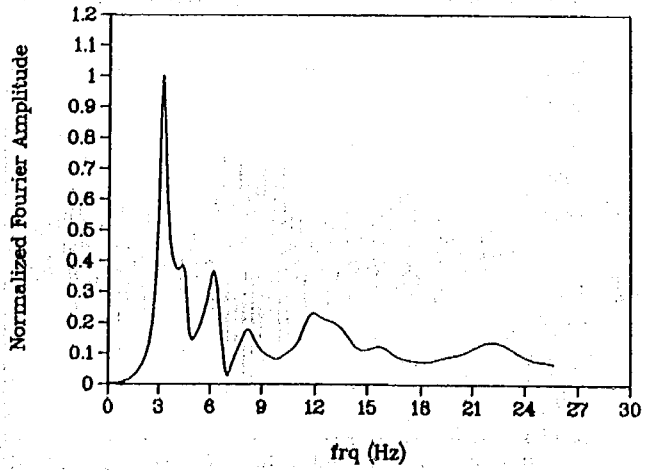


Figure 5. Normalized Acceleration Fourier Spectra in Top Layer

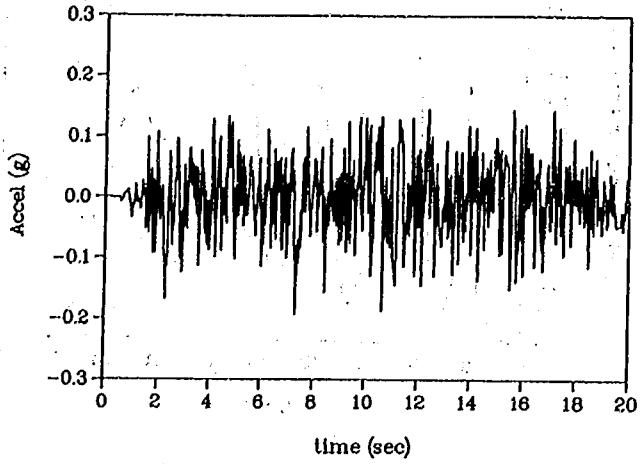


Figure 6. Generated Artificial Bedrock Acceleration

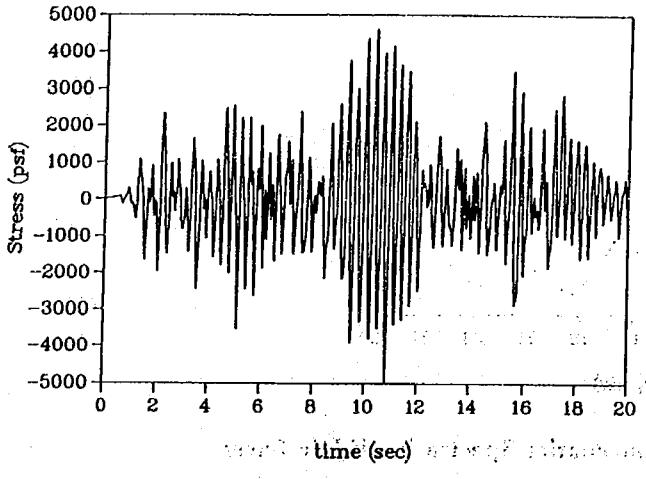


Figure 7. Shear Stress in Lower Layer

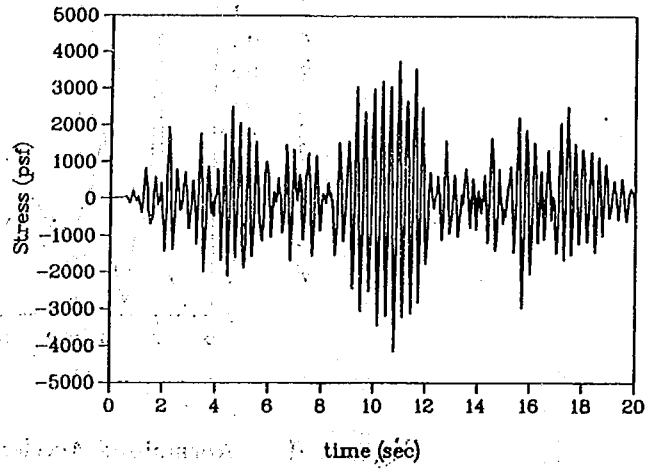


Figure 8. Shear Stress in Middle Layer

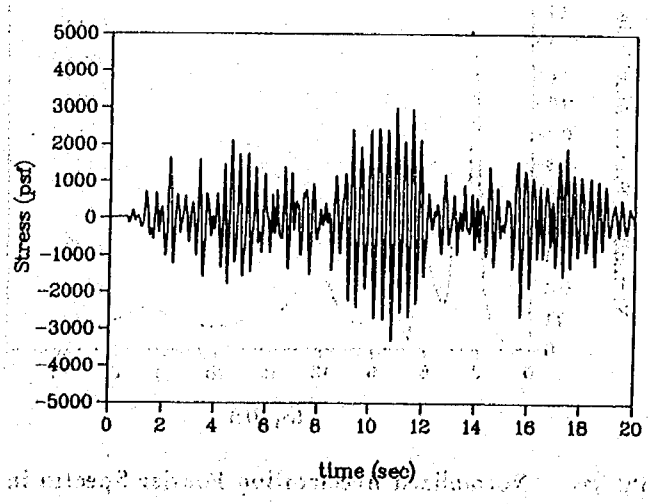


Figure 9. Dynamic Shear Stress in Top Layer

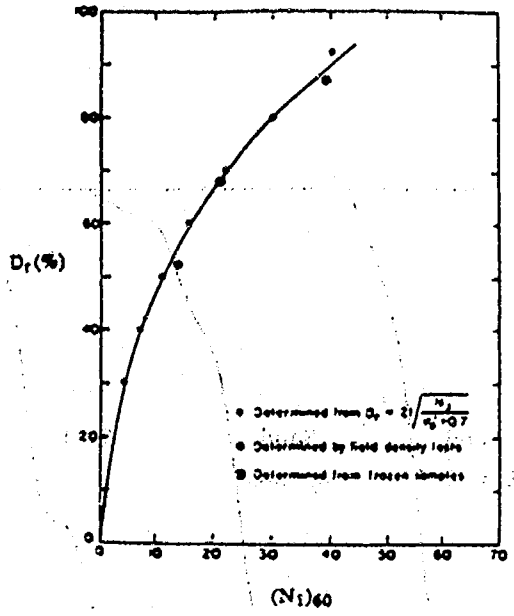


Figure 10. Relative Density D_r vs. $(N_1)_{60}$

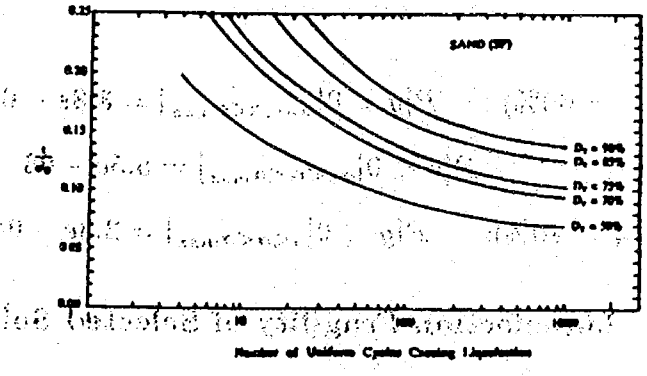
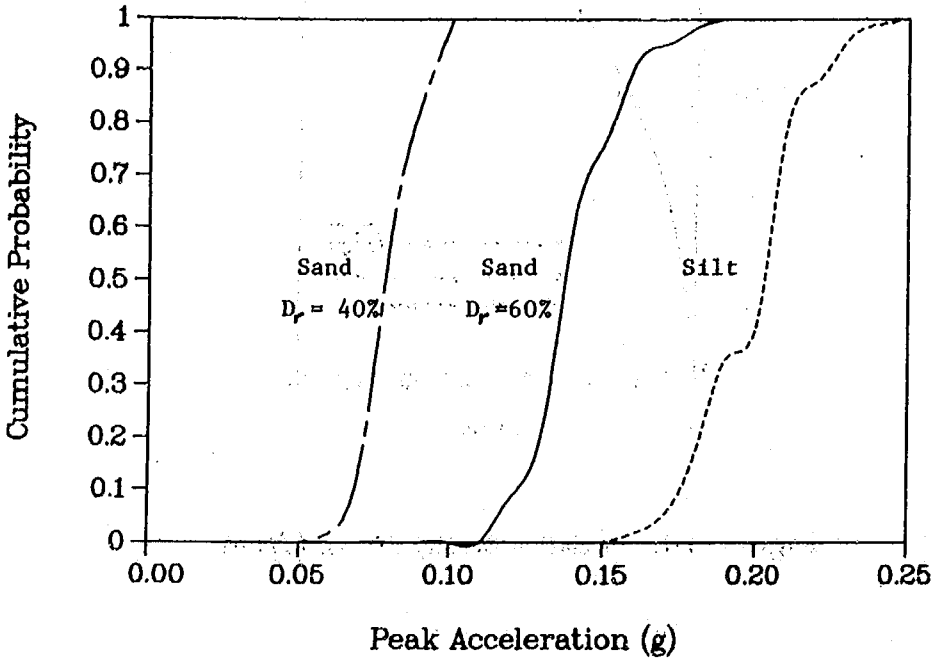


Figure 11. Cyclic Test Data for Sands



Sand ($D_r = 60\%$): $P[g < 0|_{\alpha_o<\alpha<\alpha_{max}}] = 3.8e-05$

Silt: $P[g < 0|_{\alpha_o<\alpha<\alpha_{max}}] = 5.5e-06$

Sand ($D_r = 40\%$): $P[g < 0|_{o<\alpha<\alpha_{max}}] = 2.8e-04$

Figure 12. Liquefaction Fragility of Selected Soil Layers

Impedance Functions of Footings Embedded in Saturated Strata

by

A.J. Philippacopoulos*
Nikolaos Simos*
Thomas McSpadden**

ABSTRACT

Impedance functions associated with the vibration of rigid massless strip foundations embedded in a fluid saturated poroviscoelastic stratum are evaluated using finite element procedures. The foundation medium is treated as a two-phase material behaving according to Biot's classical theory of wave propagation in fluid saturated porous media. A set of parametric studies were performed to verify that the adopted finite element procedures yield reasonable correlations with known solutions of foundation-soil interaction problems. Vertical impedance functions are presented for various *embedment depth/layer thickness* configurations. It is shown that saturation influences the foundation impedances especially their imaginary parts. This can be reasonably explained as being the result of additional dissipation in the system associated with the motion of pore fluid relative to the soil skeleton.

KEYWORDS: Foundations, saturation, vibrations, embedment, impedances.

1. INTRODUCTION

Recently, the dynamic response of foundations associated with saturated media has drawn attention primarily because of the effects of the pore fluid on the response parameters. This study particularly focuses on such effects as they are related to foundation impedances. Specifically, the system treated involves a rigid footing embedded in a saturated stratum. The case of a strip footing is analyzed.

The approach used is based on finite element procedures which take into account the two-phase nature of the underlying medium. Solution procedures have been implemented into the computer code POROSLAM (Ref. 5) the formulation of which is based on a discretization of Biot's 2-D coupled equations of motion under plane strain conditions. Both the solid and the fluid displacements are discretized in the near field while the far field is simulated with transmitting boundaries. Such formulation is consistent with acceptable techniques used to simulate infinite media for dry foundation conditions. The additional factor is the inclusion of the fluid motion and its associated pore pressure field which characterizes the saturated medium.

Impedance functions for such media, but limited to surface type foundations, have been obtained in previous studies with POROSLAM. These studies are extended here to include embedment effects which could be of significant interest in engineering applications of soil structure interaction to seismic problems.

The problem and the parameters of interest are described first, followed by a set of studies which demonstrate correlations of POROSLAM results with analytic solutions. Specifically, a series of numerical evaluations were made for surface foundations resting on dry half spaces and the results are compared with corresponding analytical solutions (Ref. 1). In addition, analytic solutions for 1-D wave propagation problems in saturated porous media are compared with corresponding solutions resulting from discrete models through POROSLAM. It is shown that POROSLAM produced results which are in good agreement with analytic solutions for both types of problems considered.

This is followed by the description of a series of solutions for vertical impedance functions of embedded foundations on saturated media. The main trend observed in these results is a relative increase in the imaginary part of the impedance functions which is attributed to the additional damping caused by the relative motion of the pore fluid with respect to the soil skeleton.

* Brookhaven National Laboratory, USA
** US Department of Energy (EH)

2. PROBLEM STATEMENT

The system analyzed is shown in Figure 1. The foundation has width **2b**, embedment depth **D** and is considered to be massless, rigid and impervious. The stratum has depth **H** and it is saturated up to the surface ($y = 0$).

With respect to a cartesian coordinate system $x - y$ and under plane strain conditions:

$[u_x, u_y]$ = solid displacements
$[w_x, w_y]$ = fluid displacements
$[\sigma_{xx}, \sigma_{yy}, \sigma_{xy}]$ = intergrannular stresses
p_f = pore fluid pressure

The total stresses are:

$$\{\tau\} = \{\sigma_{xx} - \alpha p_f, \sigma_{yy} - \alpha p_f, \sigma_{xy}\}^T$$

The governing equations of motion are:

$$\frac{\vartheta \tau_{xx}}{\vartheta x} + \frac{\vartheta \tau_{xy}}{\vartheta y} = \varrho \ddot{u}_x + \varrho_f \ddot{w}_x$$

$$\frac{\vartheta \tau_{yx}}{\vartheta x} + \frac{\vartheta \tau_{yy}}{\vartheta y} = \varrho \ddot{u}_y + \varrho_f \ddot{w}_y$$

and

$$-\frac{\vartheta p_f}{\vartheta x} = \varrho_f \ddot{u}_x + \frac{1}{f}\varrho_f \ddot{w}_x + \frac{\eta}{k}\dot{w}_x$$

$$-\frac{\vartheta p_f}{\vartheta y} = \varrho_f \ddot{u}_y + \frac{1}{f}\varrho_f \ddot{w}_y + \frac{\eta}{k}\dot{w}_y \qquad (1)$$

where,

f = porosity, ϱ = total mass density, ϱ_f = fluid mass density, α = compressibility of solid, M = compressibility of the fluid, η = fluid viscosity, and k = permeability.

2.1 Boundary Conditions

The following boundary conditions are considered ($x - y$ plane):

$y = 0$(surface) & $|x| > b$:

$$\sigma_{yy} = \sigma_{xy} = p_f = 0$$

along footing-stratum interface:

$$u_y = \Delta_y e^{i\omega t} \qquad u_x = 0$$

also

$$|x| \le b \text{ and } y = D \quad : \quad w_y = 0$$

and

$$|x| = b \text{ and } 0 \le y \le D \quad : \quad w_x = 0$$

At $y = H$ (bottom of stratum)

$$u_x = u_y = w_y = 0$$

Note that for the case where half-space is simulated, then in addition to continuity in displacements along the line $y = H$, also continuity in σ_{yy}, τ_{xy} and p_f is satisfied.

3. FE IMPLEMENTATION

The discretized form of the coupled equations (1) adopted in the finite element formulation is expressed as

$$\{\tau\} = E_c \left([D_1] \{[D_0] + [D_3] \frac{\vartheta}{\vartheta t}\} \right) \{u_x, u_y\}^T + \alpha^2 M [D_2] \{u_x, u_y\}^T + \alpha M [D_2] \{w_x, w_y\}^T \qquad (2)$$

where,

$$[D_0] = \begin{bmatrix} 1 & \frac{\nu}{1-\nu} & 0 \\ \frac{\nu}{1-\nu} & 1 & 0 \\ 0 & 0 & \frac{1-2\nu}{2(1-\nu)} \end{bmatrix}$$

$$[D_3] = \begin{bmatrix} \xi_c & \frac{\xi_c \nu}{1-\nu} & 0 \\ \frac{\xi_c \nu}{1-\nu} & \xi_c & 0 \\ 0 & 0 & \frac{\xi_s (1-2\nu)}{2(1-\nu)} \end{bmatrix}$$

$$[D_1] = \begin{bmatrix} \frac{\vartheta}{\vartheta x} & 0 \\ 0 & \frac{\vartheta}{\vartheta y} \\ \frac{\vartheta}{\vartheta y} & \frac{\vartheta}{\vartheta x} \end{bmatrix} \qquad [D_2] = \begin{bmatrix} \frac{\vartheta}{\vartheta x} & \frac{\vartheta}{\vartheta y} \\ \frac{\vartheta}{\vartheta x} & \frac{\vartheta}{\vartheta y} \\ 0 & 0 \end{bmatrix}$$

$$p_f = -\alpha M (e_{xx} + e_{yy}) - M \left(\frac{\vartheta w_x}{\vartheta x} + \frac{\vartheta w_y}{\vartheta y} \right)$$

ξ_c is the hysteretic damping ratio associated with hydrostatic compression while ξ_s represents the damping ratio associated with shear strains and $E_c = \frac{(1-\nu)E}{(1+\nu)(1-2\nu)}$.

The finite element implementation of the problem described above is subjected to the following computational aspects:

a. Simulation of radiating conditions at the sides of the finite element mesh with the use of transmitting boundaries. Similarly, when half-space solutions are sought then the bottom boundary is also subjected to similar transmitting boundaries.

b. The fineness of the mesh that will allow transmission of the frequencies used for the computation of impedance functions. Typically, element sizes of $1/6$ of the wavelength of interest were used. The dimensionless frequencies considered were up to $\alpha_o = 5.0$.

c. The finess of the mesh along the interface between the footing and the surrounding medium such that the summation of resultant forces representing the impedance functions are reasonably obtained.

$$F_y = \int_c \tau_{ij} ds \quad ; \; i = 1, 2$$

c = footing/medium interface

τ_{ij} = bulk stress defined in Eqn. 1.

3.1 Verification of FE Approach

3.1.1 Solution Comparison for Dry Half Space

POROSLAM was used to obtain solutions for vertical impedances of strip footings resting on a dry half space. In this case, to simulate the infinite medium transmitting boundaries of the conventional one phase material were used at the bottom of the FE mesh (Figure 2). The depth of the mesh was selected such that no reflections from the bottom boundary were seen on the solution within the frequency range of interest. Comparisons of vertical compliances between POROSLAM and Luco's analytical solution (Ref. 1) are shown in Figures 3a,b for Poisson's ratio $\nu = \frac{1}{4}$ and $\nu = \frac{1}{3}$ respectively. For consistency, in both cases the compliances have been normalized to $\frac{\pi G}{b}$. As expected, the difference between the results is greater at very low frequencies where the solution becomes singular.

3.1.2 Solution Comparison for Saturated Soil Column

A set of 1-D wave propagation problems for fluid saturated media were considered to further validate the accuracy of the FE procedures, implemented in POROSLAM. The discrete model used in the FE analysis is shown in Figure 4. Note that the transmitting boundary in this case has been formulated so that it allows continuity of pore pressure as well as intergrannular stresses (Ref. 5). Analytic solutions of the corresponding 1-D saturated problem were also obtained according to the conditions shown in Figure 4a. Amplitude comparisons for solid displacements, fluid displacements and pore pressure are shown in Figures 5a,b,c respectively. The agreement shown between the two results is excellent.

3.2 Impedance Functions

In determining the vertical impedances for the rigid strip footing embedded into a saturated stratum two geometrical considerations were given i.e. the ratio of width to depth of the embedment (b/D) and of the stratum thickness to the embedment width (H/b). This resulted in four (4) different FE models which are shown in Figures 6a through 6d. Hysteretic damping was assumed at 5% and the Poisson's ratio at $\nu = \frac{1}{3}$. In addition, the porosity of the stratum was taken as 30%, the permeability at 0.001 ft/sec and the viscosity was selected such that $\frac{\eta}{k} = 1000 \frac{lbf-sec}{ft}$. The pore fluid was treated as incompressible. Impedances were computed up to the dimensionless frequency $\alpha_0 = \frac{\omega b}{V_s} = 5.0$.

Figures 7, 8 and 9 show variations of impedance functions with frequency for $H/b = 2, H/b = 3$ and $H/b = \infty$ (half space) respectively. Each of the latter figures displays the real and the associated imaginary part of the impedance functions for foundation width to embedment depth ratios $b/D = 1$ and $b/D = 2$ respectively. Note that the impedance function has been assumed to have the form

$$K_{vv} = k_{vv} + i\alpha_0 c_{vv}$$

where k_{vv} and c_{vv} are the values which are plotted in Figures 7 through 9. Finally, Figures 10, 11 and 12 show variations of impedance functions for the dry cases corresponding to $H/b = 2, H/b = 3$ and $H/b = \infty$ (half space) respectively.

4. CONCLUSIONS

Impédance functions for rigid massless foundations embedded in a fluid saturated poroviscoelastic stratum where presented using finite element numerical solutions. From the results obtained it appears that the pore fluid influences the foundation impedances with a relative increase in their imaginary parts, perhaps due to additional damping resulting from the motion of the pore fluid relative to the solid matrix material. Similarly, for the cases studied some differences in system frequencies were also observed which signify differences in wave speeds between the saturated and corresponding dry media. In general, such differences are judged to be of no primary significance for typical soil-structure interaction applications.

5. REFERENCES

[1] J.E. Luco, R.A. Westmann, *Dynamic Response of a Rigid Footing Bonded to an Elastic Half Space*, Journal of Applied Mechanics, Paper No. 71-APMW-15, 1972.

[2] C.J. Costantino and A.J. Philippacopoulos, *Influence of Ground Water on Soil-Structure Interaction*, NUREG/CR-4784, 1987.

[3] A. Pais and E. Kausel, *Stochastic Response of Foundations*, Department of Civil Engineering, MIT, Research Report R86-6, 1985.

[4] J.J. Johnson, *Soil-Structure Interaction: The Status of Current Analysis Methods and Research*, NUREG/CR-1780, 1981

[5] N.Simos, C.J. Costantino and C. Miller, *POROSLAM. Two-Dimensional Dynamic Solution of Elastic Saturated Porous Media*, Earthquake Research Center, City University of New York, 1988.

[6] R.H. Lung, *Seismic Analysis of Structures Embedded in Saturated Soils*, Ph.D. Thesis, Department of Civil Engineering, City University of New York, 1980.

[7] N. Simos, M. Reich, *Seismic Analysis of the PAR POND DAM, Study of Slope Failure and Liquefaction*, Technical Report BNL-52450, 1994.

[8] ANSYS Engineering Analysis Systems. Swanson Analysis Systems Inc., 1989.

Acknowledgments

This work was performed under the auspices of US DOE

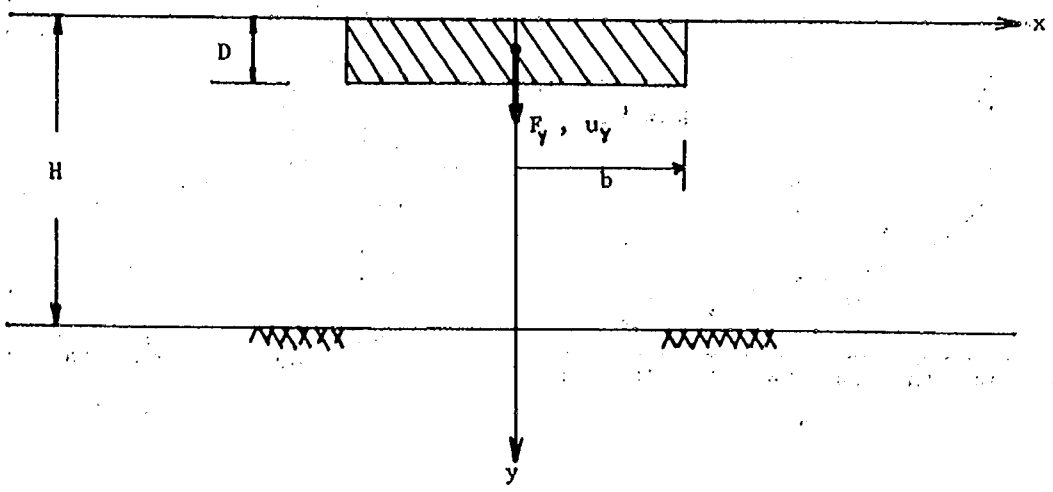


Figure 1. Problem Description

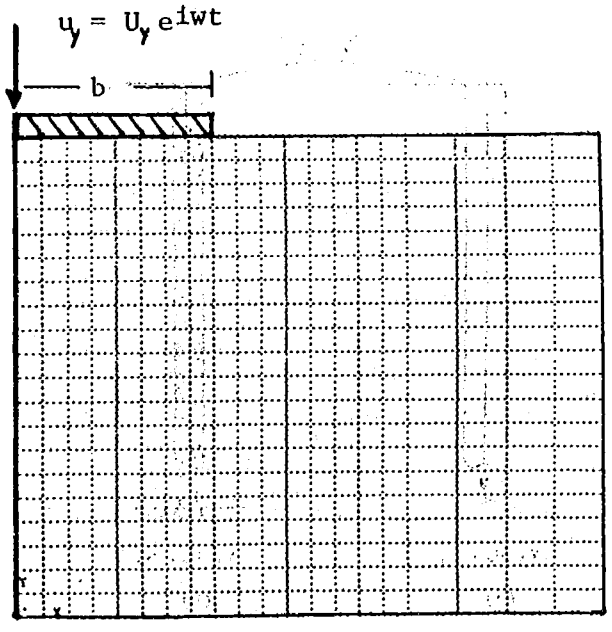


Figure 2. Finite Element Mesh for *Dry* Half Space

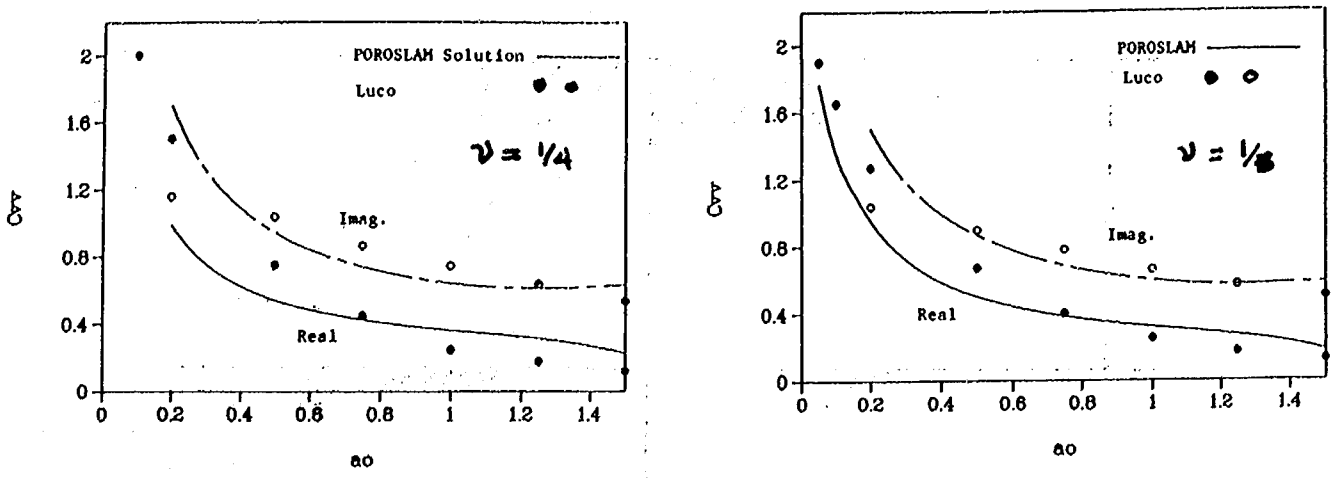


Figure 3. Compliance Comparisons for *Dry* Half Space

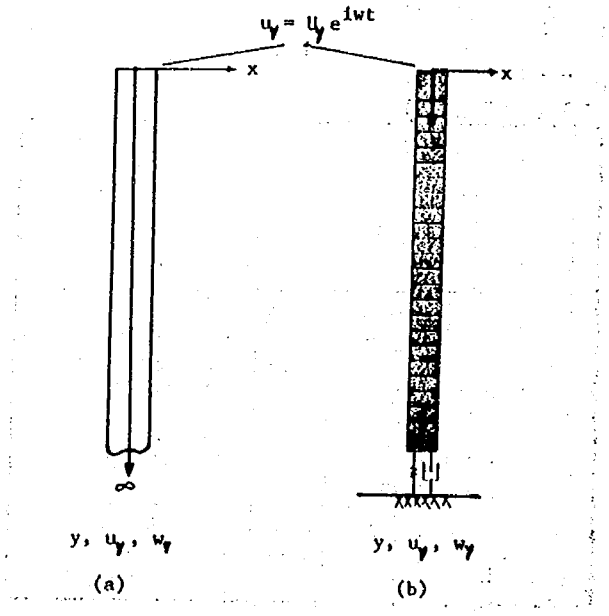


Figure 4. Modeling of Saturated Soil Column

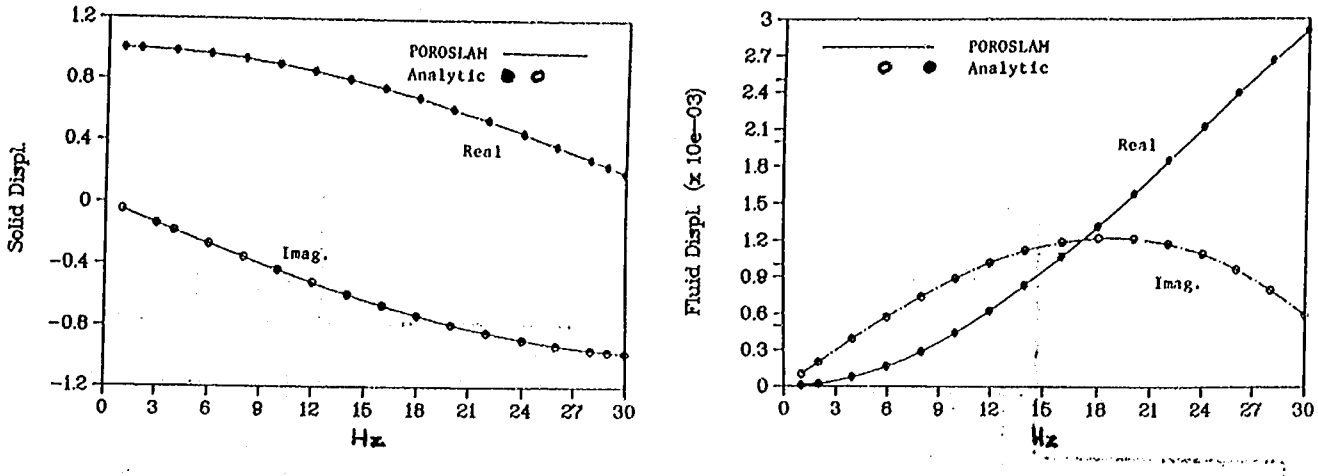


Figure 5a,b. Displacement Comparisons in Saturated Soil Column
(a: solid ; b: fluid)

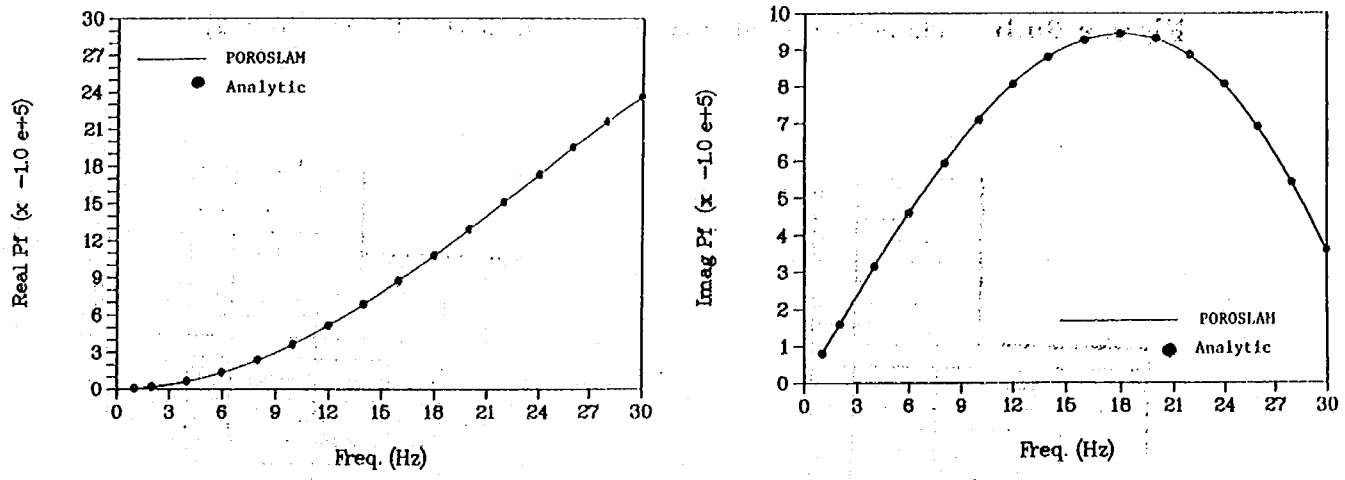


Figure 5c. Pore Pressure Comparisons in Saturated Soil Column

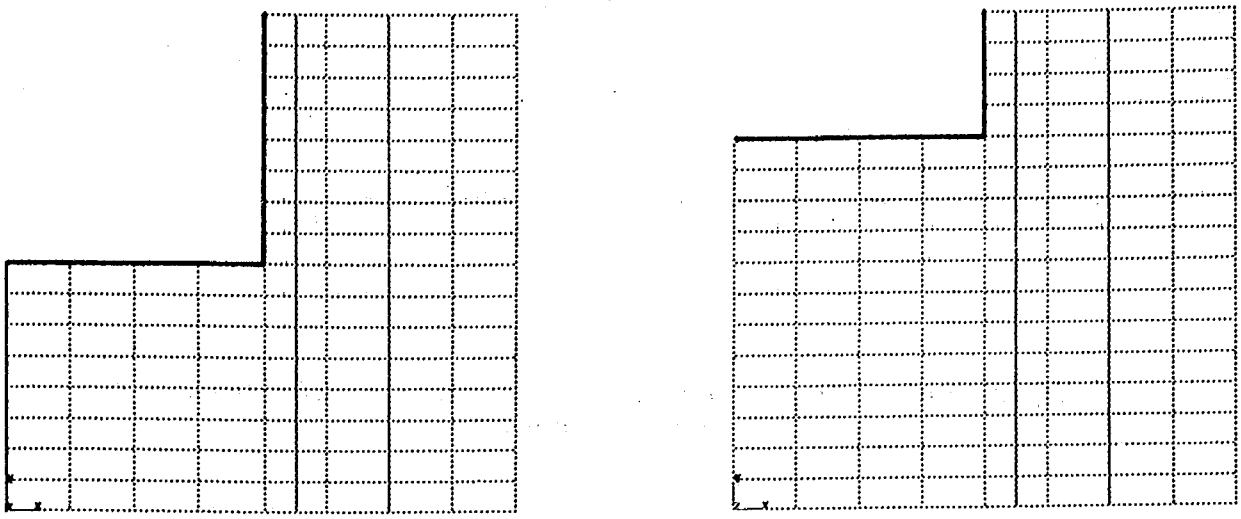


Figure 6a,b. Finite Element Models (H/b = 2 a: b/D = 1 b: b/D = 2)

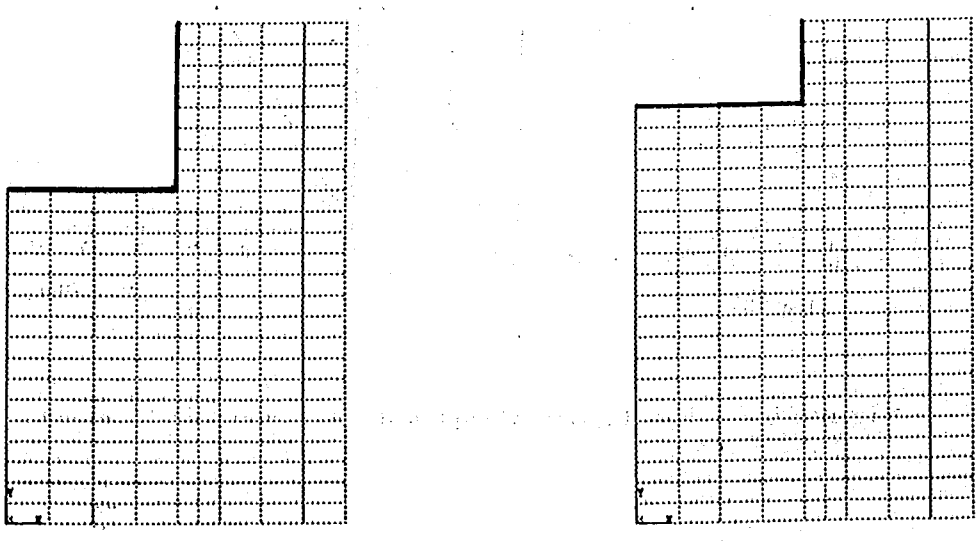


Figure 6c,d. Finite Element Models (H/b = 3 c: b/D = 1 d: b/D = 2)

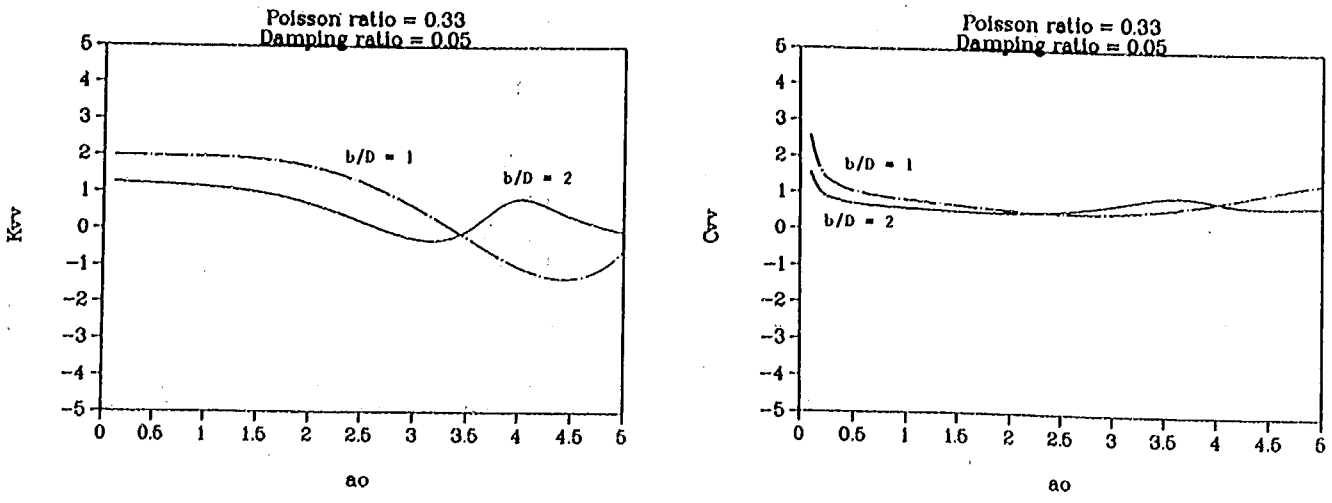


Figure 7. Impedance Functions. Case: H/b = 2 Saturated Stratum

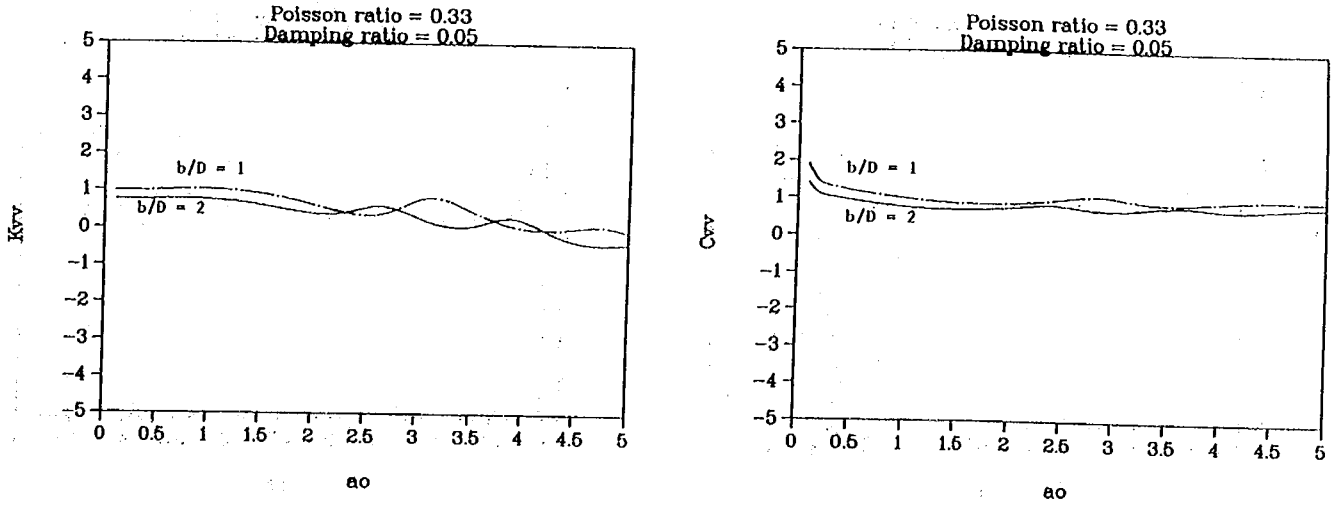


Figure 8. Impedance Functions. Case: H/b = 3 Saturated Stratum

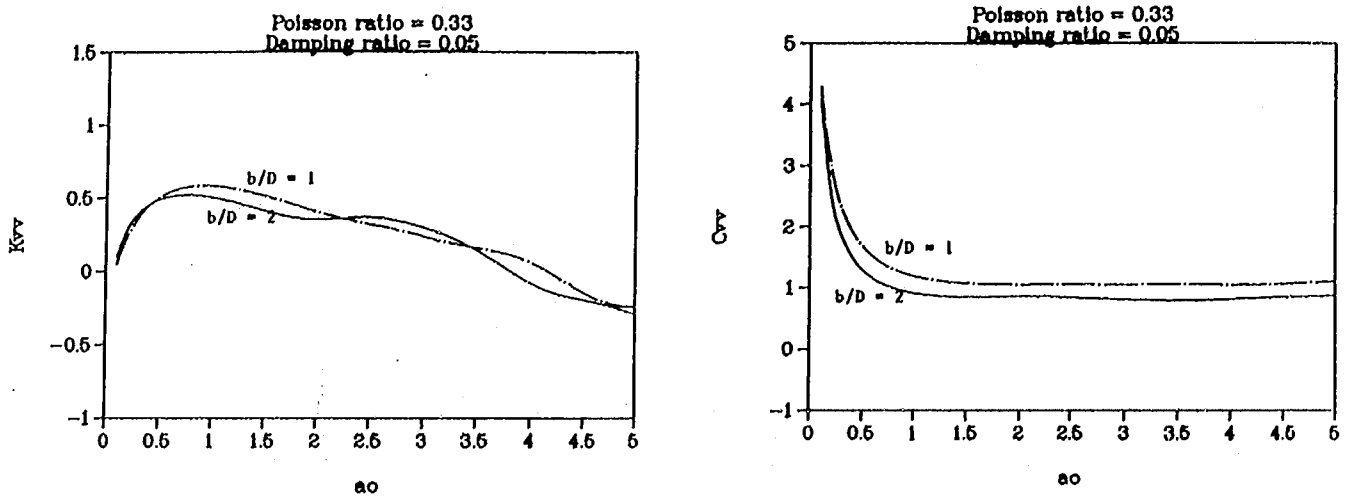


Figure 9. Impedance Functions. Case: $H/b = \infty$ Saturated Stratum

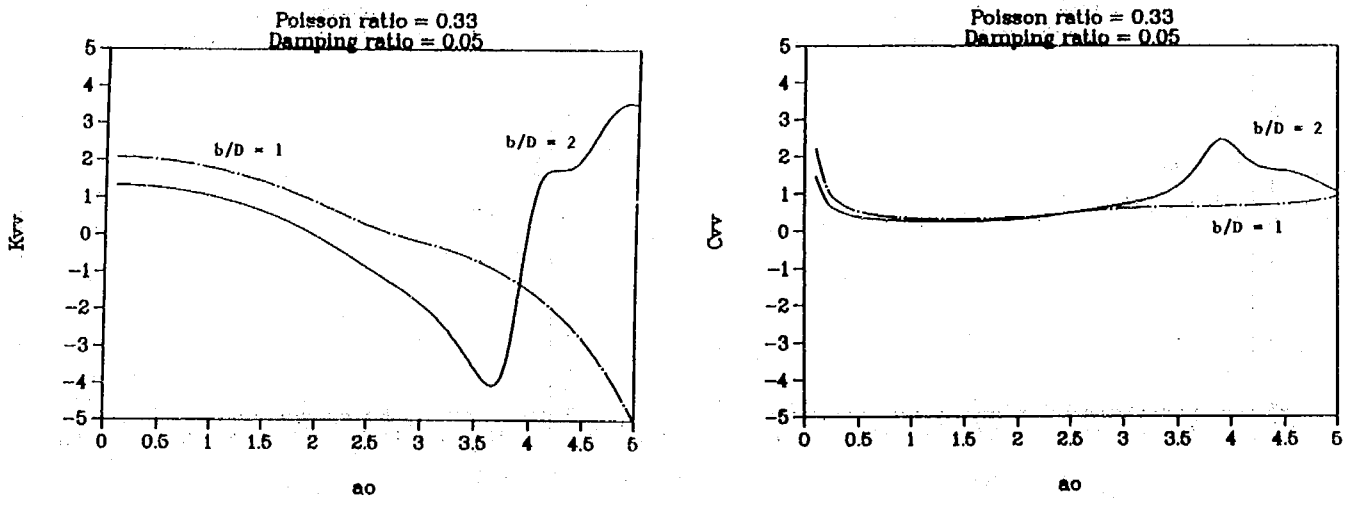


Figure 10. Impedance Functions. Case: $H/b = 2$ Dry Stratum

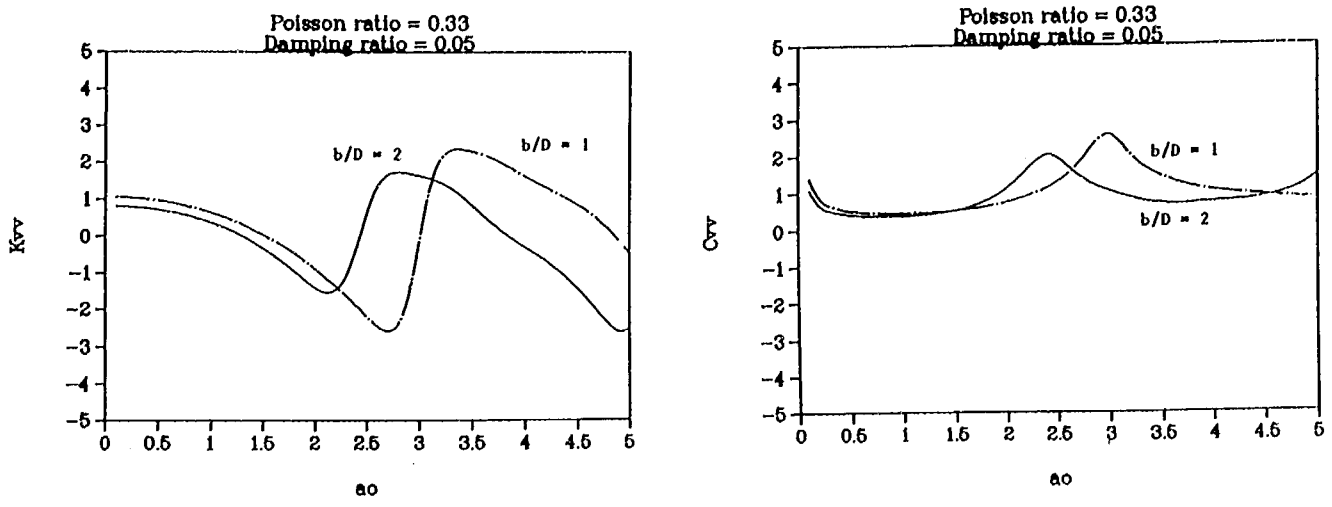


Figure 11. Impedance Functions. Case: H/b = 3 Dry Stratum

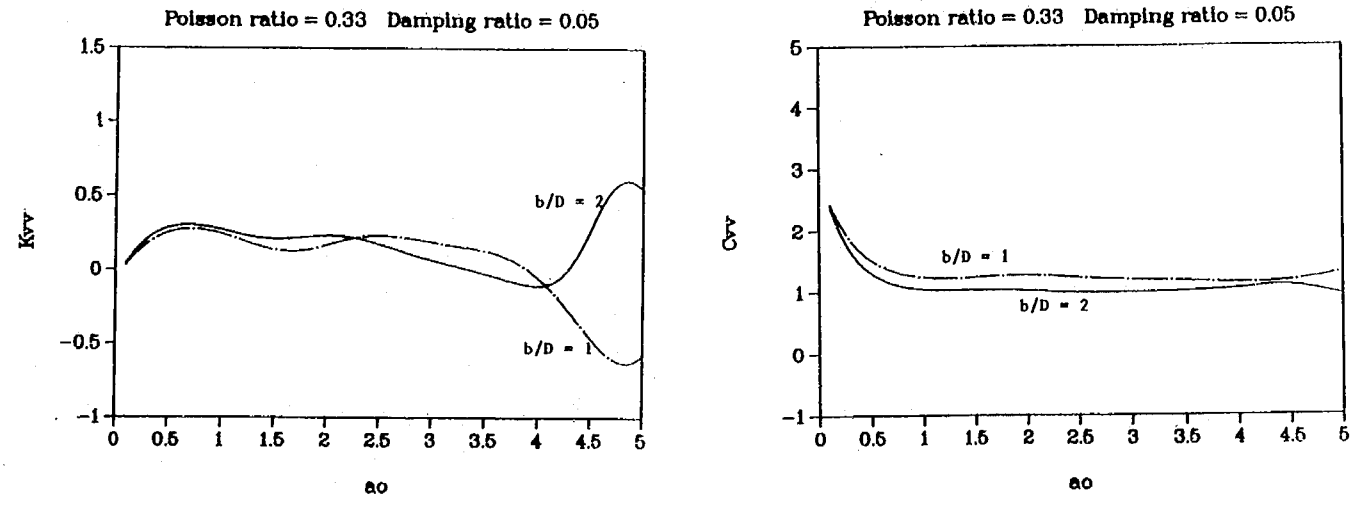
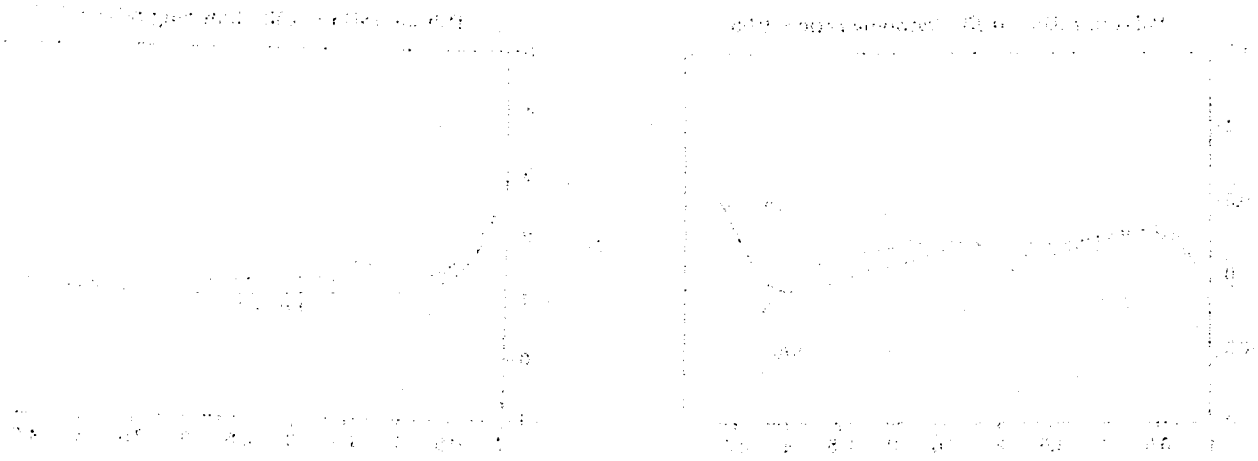


Figure 12. Impedance Functions. Case: H/b = ∞ Dry Stratum



Performance of Multi-Unit Residential Buildings During the 17 January 1994 Northridge Earthquake

by

Diana Todd* and Riley Chung*

ABSTRACT

The January 17, 1994 Northridge Earthquake (surface-wave magnitude 6.8) was centered under the densely populated San Fernando Valley northeast of Los Angeles, California. At the request of the Department of Housing and Urban Development (HUD), the Building and Fire Research Laboratory (BFRL) of the National Institute of Standards and Technology (NIST) conducted field observations of multi-family residences three stories or more in height in the affected area for the purposes of identifying common damage states in residential construction. Sixty-nine HUD-affiliated sites, totalling 464 buildings and over 10,000 living units, were visually examined from the exterior and interior. By collecting information primarily on damaged structures, it was possible to identify typical types and degrees of damage to residential buildings. Only a few HUD-affiliated buildings were severely damaged. By and large the damage observed was minor and cosmetic, consisting largely of cracks to interior and exterior wall surfaces. Nevertheless, this type of damage is costly to repair.

KEYWORDS: building technology; damage; earthquake; earthquake damage; multi-family; residential buildings; seismic.

1. INTRODUCTION

A surface-wave magnitude 6.8 earthquake centered under the community of Northridge in the San Fernando Valley shook the entire Los Angeles area at 4:31 a.m. local time on Monday, January 17, 1994. January 17 was a Federal holiday (Martin Luther King's Birthday) and, because of this and the early morning hour, most non-residential buildings were empty and traffic was light. This fortuitous circumstance helped limit the number of deaths and injuries.

The Northridge earthquake was unique in the history of the United States in that it was centered under a heavily populated area. More buildings of varying ages and structural types were severely shaken by the Northridge earthquake than in any previous seismic event in this country. Spectacular damage was limited to the collapse of a handful of concrete commercial buildings and to a number of three-story apartment buildings in the epicentral area. Less spectacular but nevertheless disruptive and costly damage was widespread.

Following the Northridge earthquake, the Department of Housing and Urban Development (HUD) entered into an agreement with the Building and Fire Research Laboratory (BFRL) of the National Institute of Standards and Technology (NIST) to document damage in residential buildings of three stories or more in height.

2. SCOPE

Usually, the focus of immediate post-earthquake reconnaissance activities is on documenting cases of spectacular or unusual damage to structures. The HUD/BFRL study was intended to identify common, rather than spectacular, damage in multi-family residential construction. No restrictions were placed on the age or structural type of the buildings to be examined; a goal was established to investigate a broad spectrum of building construction types.

* National Institute of Standards and Technology, Gaithersburg, MD 20899.

The group of buildings inspected in this study was not a statistically random sample of multi-family residences in the affected area. The study was not designed to provide estimates of the extent or probability of damage. Rather, the study was intended to serve as documentation of building performance in damaged multi-family residential buildings. Therefore, only qualitative conclusions can be drawn from this sample about the likelihood of damage to certain classes of construction in future earthquakes.

Building performance was documented on data-collection forms during on-site inspections. Where available, building plans were examined to verify data on structural types, configuration, dimensions and other parameters. Engineering analyses of the buildings were not performed.

3. METHODOLOGY

Sites for study were selected from about 200 HUD-affiliated earthquake-damaged properties. Some sites contained a single building, others had multiple buildings. The sites were screened by reviewing HUD damage reports and performing drive-by inspections. Buildings with very minor or no damage were eliminated from the list. At the suggestion of the national HUD office, several public housing projects, selected by local public housing authorities, were included in the study. A total of 69 sites were included in the study. The sites collectively contained 425 buildings and a total of over 10,000 living units.

A data-collection form designed and used by the Applied Technology Council (ATC) was selected for use in this project, to ensure uniformity of data-collection by the BFRL investigation teams. The data-collection form divides building components into structural, nonstructural, and equipment categories, defined as follows:

- Structural components and systems are those elements of a building, such as beams, columns, and diaphragms, that resist the gravity and lateral loads.
- Nonstructural elements and systems are not designed to be part of the load resisting system. Nonstructural elements can be exterior cladding, interior non-loadbearing partitions, and other functional or decorative building components such as ceilings, parapets, porches, and so on.
- Equipment includes heating, cooling, plumbing, electrical and similar systems.

Overall damage states for structural elements, nonstructural elements, equipment, and contents are recorded. Damage states range from 1 for no damage (0 percent) to 7 for total damage (100 percent), and are shown in Table A.

Table A: ATC-13 Damage Scale Used in this Study

Damage Rating	Relative Amount of Damage	
1	None	0%
2	Slight	0%-1%
3	Light	1%-10%
4	Moderate	10%-30%
5	Heavy	30%-60%
6	Major	60%-100%
7	Destroyed	100%

Prior to departure for the Los Angeles area, all team members jointly reviewed methods for identifying building types and interpreting damage, and familiarized themselves with the data collection form. Slides of damaged buildings that had been taken by BFRL personnel in the days immediately following the earthquake were used in exercises to familiarize all personnel with the data collection method, and to establish a common understanding of damage levels.

In the field, inspections were performed by teams of at least two people. Evening meetings were held each day at which teams reported on their observations, using instant photographs to illustrate key points. These daily reviews allowed the investigators to adjust their rating of damage states to conform to a uniform scale, to acquire additional insight into particularly interesting or challenging technical issues, and to share suggestions on dealing with non-technical issues. The pairings of investigators were regularly rotated to maximize the consistency of the evaluations between the teams.

Inspections were scheduled with a request that a building manager, engineer, or other knowledgeable person be available to escort the investigation team. The building was examined from the exterior and interior, and all known damage sites were documented. At sites consisting of a large number of living units and/or additional undamaged buildings, not all units/buildings were inspected. Non-living space, such as basements, attics, utility rooms, and stairwells, received particular attention. These spaces, when they lack architectural finishes such as ceilings and wall paneling, allow investigators to directly view the structure of the building. In instances where building plans were available, these were reviewed to verify observations about structural types, dimensions, and other items of interest.

4. OBSERVATIONS AND ASSESSMENTS

Five of the sites selected by public housing authorities for inspection by the BFRL team did not show evidence of having been damaged by the earthquake. These sites were removed from the sample prior to analysis. Thus, although the field inspections covered 69 sites with 464 buildings and 10,893 living units, the data analyses covered only 64 sites, which consisted of 211 buildings containing a total of 9,430 living units.

Techniques used in the attempt to identify trends included production of sorted data tables, generation of scatter plots, and regression analysis. The parameters selected for study included: structural system, number of stories, age, and distance from epicenter. These parameters were compared to numerical ratings of damage to structural systems, nonstructural systems, and equipment. Table B presents the distribution in the sample of structural systems, by site and by number of living units.

Table B: Distribution of Structural Types

Structural System	Percent of total sites	Percent of total units
Wood frame	50%	58%
Concrete	17%	24%
Precast concrete	13%	13%
Unrein. masonry	17%	3%
Reinforced masonry	3%	2%

A regression analysis was performed for each of the pairs of parameters that were examined except for comparisons involving structural type. A correlation coefficient was calculated to determine if there was any statistically valid correlation between the parameters. Because structural type is a qualitative rather than a quantitative variable, regression analysis is not possible for that parameter. For these comparisons, averages of damage states for each of the structural types were calculated and compared. These analyses evaluate the influence of only a single variable at a time (e.g. age or number of stories). The number of data points in the sample did not justify multi-variable analysis (considering the combined effects of parameters in attempting to identify trends).

No strong correlation was found between any of the possible pairs of parameters selected for study. This finding likely reflects both the sparsity of the data and the wide variability in

building behavior that is documented after every earthquake. General observations on the types and severity of damage in the sample can nevertheless provide some insight into the performance of multi-family residences subjected to strong ground shaking.

Typical characteristics of multi-family residential buildings are multiple interior partitions and frequent openings in walls. The massive amount of wall surface such systems create is vulnerable to cosmetic, but nonetheless expensive-to-repair, damage. Rectilinear door and window openings create stress concentrations at each corner, making these locations particularly vulnerable to cracking (fig. 1). The damaged multi-family residences observed by the BFRL team following the Northridge earthquake typically had cracks in plaster or gypsum board interior wall surfaces, especially at the corners of door and window openings and along vertical and horizontal joints in wall sheathing (fig. 2). Less common was damage to the structural system.

Damage to equipment, such as water heaters or air conditioning units, occurred at slightly more than half the sites. The damage was usually minor, such as equipment shifting off supports. Occasionally, these movements led to collateral damage, such as gas or water leaks from ruptured pipelines. An example occurred at Fickett Towers, a 12-story concrete shear wall building about 8 km from the epicenter. A 130,000 liter (35,000 gallon) water tank on the roof shifted, severing the attached water pipes (fig. 3). The resulting discharge of the tank contents caused water damage to walls, ceiling, and carpet at all levels.

Of the over 200 buildings in the sample at the 64 damage sites, only two buildings were damaged by fire. These both occurred at Granada Gardens, a complex of wood-frame two-story apartment buildings located about 6.5 km from the epicenter. The fires were reportedly caused by ruptured gas lines. Most of the 51 buildings at this particular site were heavily damaged. The buildings featured large stretches of open first stories for parking, with apartments above. The vulnerability of this configuration to earthquake ground shaking was vividly demonstrated in many collapsed and damaged apartment buildings near the epicenter [1] which were not a part of this study.

Buildings at 8 of the 64 sites in the sample were permanently or temporarily unusable because of damage. (Buildings which were vacated for only a few hours or days pending inspection are not included in this number.) Two of the uninhabitable sites, labeled Vadehra IV and Vadehra Vb, each consisted of a single unreinforced masonry building about 70 years old that had been condemned due to earthquake damage and was under demolition at the time of the inspection (fig. 4). A third unreinforced masonry building of the same vintage, Uptown Manor, suffered damage to a few of the top-story units, which had been evacuated (fig. 5). The majority of the 60 living units in the building remained usable. A fourth unreinforced masonry building, Vadehra IVb, had been yellow tagged by the city, meaning that the building was judged to be potentially hazardous and should not be occupied until a more detailed analysis showed the building was safe or the damage was repaired. About four percent of the 285 living units in Westminster Towers, a concrete frame building about 20 km from the epicenter, were unusable due to damage. One site with a single wood frame building, Sherman Park Apartments, suffered damage requiring 10 out of 135 living units to be evacuated for one week while repairs were made. At another site with a single wood frame building, Sunset E, the city had yellow tagged the building, requiring evacuation of all 18 units pending more thorough evaluation (fig. 6). By far the largest number of unusable units in the survey occurred at Granada Gardens where 120 of the 169 living units had to be evacuated due to structural damage.

In total, approximately 300 of the over 9,000 living units at damage sites, or about three percent of the total, were rendered unusable due

to damage. Note that this percentage relates to the number of units that were uninhabitable at *sites with damage*. It is not a measure of the percent of total available living units that became uninhabitable. Note that 97 percent of damaged living units remained inhabitable.

Systematic collection of information on injuries was not included in the scope of this project, but investigators noted anecdotal information when it was available. The BFRL team found that only two fatalities were associated with the buildings in the sample, both heart attacks, one at Castle Argyle Apartments and one at Sherman Park Apartments. At no site were the investigators told of major injuries. However, many residents told of being temporarily trapped in their apartments by jammed doors (fig. 7). Broken glass and fallen contents produced hazards in many buildings. The physical hazards produced by these impediments were exacerbated by the lack of illumination due to the loss of electricity.

Two of the buildings in the sample were instrumented with strong motion recorders that were reported to have been activated by the earthquake. This provides an opportunity for future in-depth study of the behavior of these buildings. The instrument at 16-story Cathay Manor, about 33 km from the epicenter, was installed and maintained by Kinemetrics Inc. of Pasadena, California. The instrument at 10-story Pacific Manor, about 21.5 km from the epicenter, is part of the California Strong Motion Instrumentation Program, and is identified as CSMIP Station No. 24385.

Almost all of the unreinforced masonry buildings in the sample were observed to have been rehabilitated prior to the earthquake using bolts, outfitted with steel plate washers, that pierced the masonry at the lines of the floors and roof. Parapet bracing was also observed. The City of Los Angeles has a mandatory seismic rehabilitation ordinance for unreinforced masonry buildings constructed prior to 1934 that applies to apartment buildings that have five or more living units. Surrounding jurisdictions do not have similar mandatory requirements. In some instances the Los Angeles ordinance, known colloquially as Division 88, requires the addition of new cross walls, supplementary vertical supports, and other strengthening actions in addition to the commonly required through-bolts and parapet bracing. While the BFRL investigators did note the presence of through-bolts and parapet bracing, they did not determine whether the rehabilitation effort conformed with the requirements of Division 88. Of the buildings that were constructed of materials other than unreinforced masonry, investigators found none that clearly had been rehabilitated prior to the earthquake.

Only two of the damaged buildings were reinforced masonry. However, the dearth of examples of damaged buildings with steel or reinforced masonry systems in the sample does not necessarily imply that these types of structural systems performed particularly well during the quake. Because a reliable estimate of numbers of damaged and undamaged buildings is not available partitioned into structural type, it is impossible to determine whether the small number of damaged buildings with these structural systems indicates good performance by these type of buildings, or whether it merely reflects a small number of buildings in the housing inventory with these systems.

There were no steel frame buildings in the candidate group of damaged multi-family residential buildings.

V. CONCLUSIONS

The study examined earthquake-damaged multi-family residences three-stories or more in height affiliated with HUD programs. Approximately three percent of the 9,430 living units located in 211 buildings at 64 sites *at which damage occurred* were rendered uninhabitable by the Northridge earthquake. At sites where damage occurred, 97 percent of the living units remained useable.

Damage almost always included cracks in plaster and gypsum surfaces of interior nonstructural partitions, usually at corners of door and window openings and along vertical and horizontal joints. Damage to structural systems was generally less severe.

The level of damage to building equipment, such as water distribution and air handling systems, was generally lower than the level of nonstructural damage and about the same as the level of structural damage. Occasionally, collateral damage occurred due to water or gas leaks. Only two buildings in the sample were damaged by fire.

A large variation in performance, even among apparently identical buildings at a single site, was observed in this study. This finding is not an unusual feature of the Northridge earthquake; wide variations in performance have been typically observed following earthquakes.

Poor performance of wood frame buildings with open first-stories used for parking was observed in some of the buildings in this sample and in other non-HUD-affiliated buildings. Based on this observed behavior, buildings with this type of vertical configuration can be identified as potentially vulnerable to earthquake damage.

Among the residential facilities observed in this study, no particularly vulnerable aspects of structural systems could be identified in concrete, precast concrete, and reinforced masonry buildings. Vulnerable nonstructural components common to most types of residential buildings included gypsum board and plaster coverings on non-bearing walls and exterior stucco, which often cracked at corners of door and window openings and along horizontal and vertical joints.

A complete report on this study can be found in *Performance of HUD-Affiliated Properties During the January 17, 1994 Northridge Earthquake*, by Diana Todd et al. [2].

5. REFERENCES

1. Hall, John F., Editor (1994). *Northridge Earthquake January 17, 1994, Preliminary Reconnaissance Report*, EERI 94-01, Earthquake Engineering Research Institute, Oakland, CA.

2. Todd, Diana et al. (1994). *Performance of HUD-Affiliated Properties During the January 17, 1994 Northridge Earthquake*, NISTIR 5488, National Institute of Standards and Technology, Gaithersburg, MD.

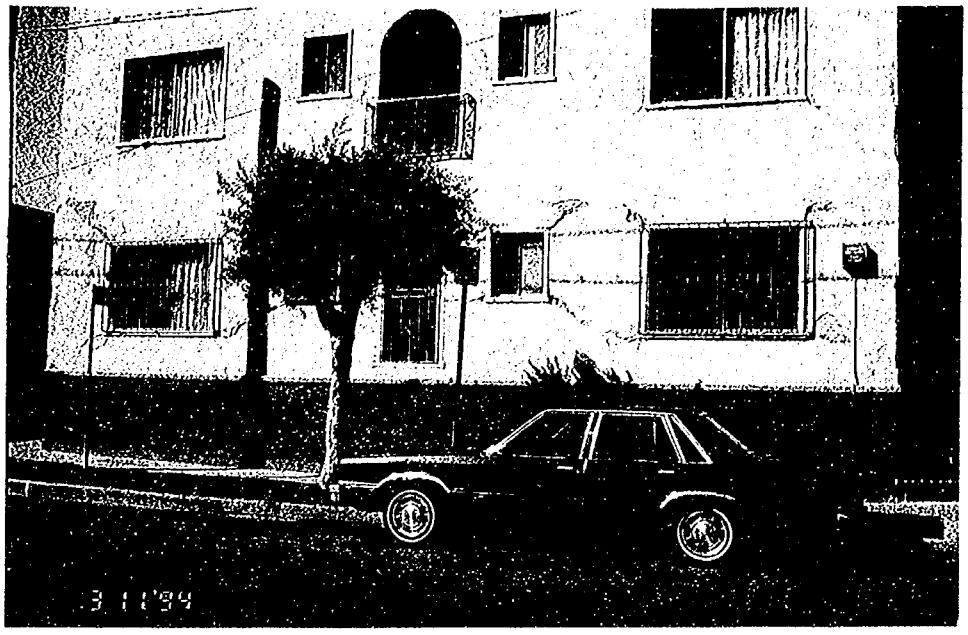


Figure 1 *Residential construction is characterized by multiple door and window openings. The corners of these rectilinear openings create stress concentrations, making these locations particularly vulnerable to cracking.*



Figure 2 *Typical nonstructural damage in residential buildings caused by the Northridge earthquake included cracks in interior partition walls, such as these horizontal and vertical cracks at the edges of the gypsum wallboard panels.*

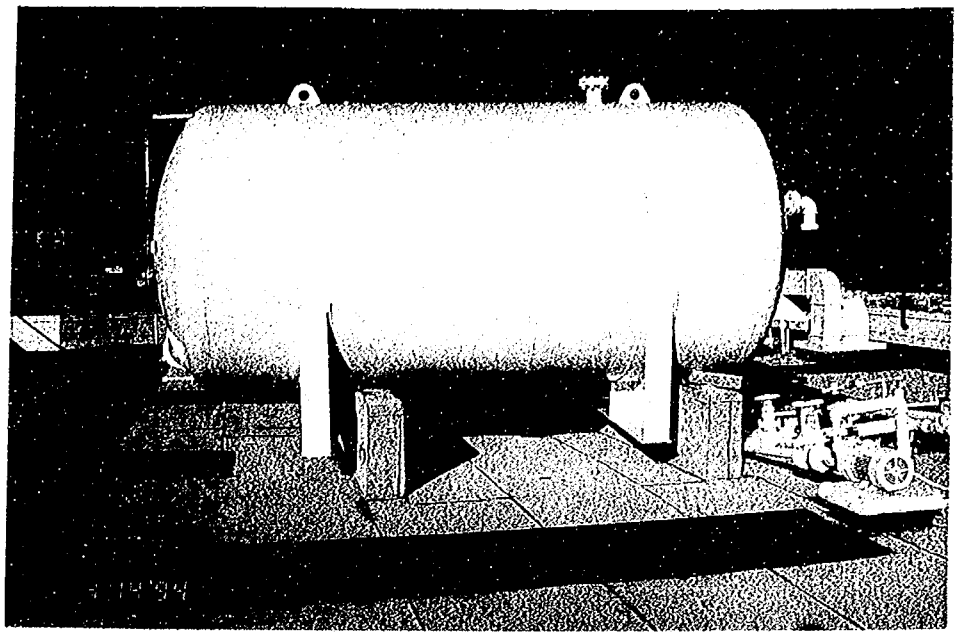


Figure 3 *Movement of equipment, such as this 130,000 liter rooftop water tank at Fickett Towers, caused collateral damage in some cases. When this tank dropped from its supports, rupturing a water pipe, water damage to the building interior resulted.*



Figure 4 *Vadehra IV, an unreinforced masonry building, was condemned because of extensive earthquake damage. When this photograph was taken, the top story had already been removed by the demolition team.*



Figure 5 *Loss of portions of the parapet and wall at Uptown Manor, an unreinforced masonry building, caused several living units to be declared unsafe by city inspectors.*



Figure 6 *Sunset Apartments E, a three-story wood-frame building, was declared by city inspectors to be potentially unsafe. Note the horizontal crack in the stucco at the foundation line, the vertical crack to the right of the window, and the diagonal crack and bulging stucco at the lower corner of the window.*



Figure 7 *Buckled door frames occurred in several buildings.*

Strength Of Concrete Frames With Masonry Infill

by

Steven C. Sweeney[1]
Ghassan Al-chaar[1]

ABSTRACT

Many buildings used by the U.S. Army are reinforced concrete frames with masonry infill walls. There is therefore a need to develop reliable analysis tools to predict the real strength and the dynamic response of such infilled frames. For that reason, a comprehensive multi-year study was undertaken by the U.S. Army Construction Engineering Research Laboratories (USACERL). In that study, several half-scale specimens consisting of reinforced concrete frames (bare and with masonry infill), were subjected to simulated earthquake motions using the Biaxial Shock Test Machine (BSTM), a large shaking table. The experimental data obtained by USACERL was used by researchers at the University of Texas, Austin, to evaluate the behavior of infilled frames. Load-displacement characteristics were obtained; and maximum loads, deflections and internal strains were measured and assessed. Dynamic response was predicted analytically, using various mathematical idealizations. Finally, simplified analytical idealizations were developed to predict the strength and stiffness of infilled frames.

KEYWORDS: buildings, dynamic testing, infill, masonry, strength

1. INTRODUCTION

Two and three story concrete frame structures are a predominant structural type in the U.S. Army's building inventory. Most of these structures were built prior to the 1970's, and nearly all of them to some degree are infilled with masonry. In attempt to better determine the seismic vulnerability of the Army's building inventory, USACERL performed a series of earthquake simulated dynamic tests on small scale reinforced concrete frames infilled with masonry panels. The test data was analyzed by researchers at the University of Texas, Austin, who made recommendations for simplified analysis procedures for these buildings. This paper summarizes the results of the strength analysis for these tests.

2. TEST SPECIMENS

One set of test specimens, referred to from now on as weak frames, was intended to represent buildings designed by the 1956 ACI Code and old construction practices. A second set of specimens, referred to as "strong frames," was designed by the 1989 ACI Code, and was intended to represent modern buildings. The specimens were half scale models of bare and infilled reinforced concrete frames. Each specimen consisted of two parallel one story, one bay frames, connected at their top levels by a stiff concrete slab. The slab was attached to the top beams by transverse steel rods. The frame columns were founded on massive beams that were rigidly connected to the shake table floor. Figures1, 2 and 3 show the layout and dimensions of the frames and the structural elements. Infills, with a height to thickness ratio of 18, were made of half scale clay brick laid with a Type N mortar. The measured masonry prism compressive strength was 5000 psi (35 MPa).

To simulate the effects of the vertical gravity loads generated by overlying stories, post tensioning cables were threaded through each column in order to increase their axial load. In addition, masses of 8.0 kips (36 kN) and 6.0 kips

[1] U.S. Army Construction Engineering Research Laboratories, Champaign, IL, 61826-9005

(27 kN) were added to the slab of the strong and weak frame specimens respectively. These masses were intended to simulate the lateral inertial forces generated in the full scale prototype under base excitation.

3. TESTING PROCEDURE

The overall experimental program is summarized in Table 1. As shown in Table 1, the experimental program consisted of tests on eight models. Each model consisted of a combination of strong or weak frame, strong or weak infill, damaged or undamaged infill, and tested in-plane or out-of-plane. Ground accelerations were input to the specimens using the USACERL BSTM. All seismic tests were performed by subjecting each specimen to a series of earthquake records scaled from the North South component of the El Centro 1940 ground motion. In some cases, high pass filters with cut off frequencies ranging from 2.0 to 4.0 Hz were used to remove the low frequency components of the shake table input, permitting the application of higher maximum shake table accelerations without exceeding the table's velocity or displacement limits. For each one of these models two random vibration tests were performed, one before and after conducting the seismic tests series, to measure their dynamic properties.

Test specimens were instrumented to record accelerations, displacements and strains. Absolute displacements (measured with respect to a fixed datum on the laboratory floor) and relative displacements (between the infill and frame) were both recorded. Beams and columns were instrumented to record internal strains.

3.1 Strong Frame

The first series of tests of interest in this paper, performed on strong frame specimens, comprised Models #1 and #2. The bare frame specimen (Model #1) was subjected to a series of in plane ground motions until cracks appeared in the structural elements. Infills were then added to the frames, and the specimen was renamed Model #2. A new series of gradually increasing in plane ground motions was applied to this model until the infills cracked.

3.2 Weak Frame

The series of tests of interest performed on weak frame specimens consisted of models #6 and #7, followed a sequence similar to that of the first series of tests. Model #6 was a bare frame specimen, tested in plane. It was then infilled with masonry, and renamed Model #7. This Model was tested in-plane until its infills cracked.

4. EXPERIMENTAL RESULTS

4.1 Bare Frames

In-plane, bare-frame tests involving very low levels of base acceleration (under 0.5g) clearly show load-displacement characteristics that are inconsistent with each other, and not useful for evaluating specimen behavior. These poor load-displacement patterns are apparently due to the precision of the instruments. Seismic tests with higher levels of ground input acceleration were useful. The average in-plane stiffness for these tests was about 130 kips/inch (23 kN/mm) in the case of the strong-frame specimen, and about 50 kips/inch (9 kN/mm) for the weak-frame specimen. The maximum base shear in both cases was about 20 kips (89 kN).

The values of stiffness for the strong frame, obtained from the results of random tests, varied from 150 kips/inch (26 kN/mm) to 80 kips/inch (14 kN/mm). The values of stiffness for the weak frame, obtained from the results of random tests, varied from 120 kips/inch (21 kN/mm) to 40 kips/inch (7 kN/mm).

4.2 Infilled Frames

Again in this case, tests involving low levels of base acceleration (under 2.0g) show poor load-displacement characteristics. Seismic tests with higher levels of ground input acceleration were useful. An initial stiffness of about 300 kips/inch

(53 kN/mm) was measured for the weak infilled frame. For subsequent tests, a degraded stiffness of less than 200 kips/inch (35 kN/mm) was measured. Maximum base shear was about 60 kips (267 kN). For the strong infilled frame, inconsistencies in measured displacements made it difficult to estimate the stiffness with confidence. Maximum base shear was about 50 kips (220 kN).

The results of random tests were used to estimate the in-plane stiffness of the infilled frames. In the case of the weak infilled frame, the initial stiffness is about 1180 kips/inch (207 kN/mm) while the final stiffness is about 360 kips/inch (63 kN/mm). From these results, it can be concluded that after a series of moderate ground motions, the in-plane stiffness of the infilled frame was reduced to less than one third of its initial value. The initial and final values of stiffness for the strong infilled frame, obtained from the results of random tests, were 590 kips/inch (103 kN/mm) and 120 kips/inch (21 kN/mm), respectively. These values of stiffness are inconsistent with those obtained for the weak infilled frame and therefore, they are not believed to represent the actual levels of stiffness of this specimen.

Table 2 summarizes the maximum strains measured in the longitudinal bars of beam and columns of Model #1 for Seismic Tests #9, #10 and #11. No yielding was recorded in any bars for these tests. Table 3 summarizes the maximum tensile and compressive strains measured in the longitudinal bars of beam and columns of Model #2. In this case yielding was barely reached, since the maximum strain of 2250 $\mu\epsilon$ at Gage S1 in Seismic Test #19 is very close to the yield strain of 2110 $\mu\epsilon$.

Table 4 summarizes the maximum strains measured in the longitudinal bars of beam and columns of Model #6. For Seismic Test #47 considerable yielding occurred in several locations. Table 5 summarizes the maximum strains measured in the longitudinal bars of beam and columns of Model #7. Again, in this case yielding was observed at several strain gages.

In summary for the strong frame model, cracking began in the bare frame and yielding occurred after it was infilled. For the weak frame model, yielding occurred in the bare frame and again in the infilled frame.

5. ANALYTICAL IDEALIZATIONS

The half-scale in-plane specimens were analyzed with the help of four computer programs. The programs RCCOLA (Mahin 1977, Farahany 1983) and DRAIN-2DX (Kanaan 1975) were used to idealize the bare frames. The programs FEM/I (Ewing 1987) and LPM/I (Kariotis 1992) were used to idealize the infilled frames. RCCOLA was used to calculate the moment-curvature behavior of beams and columns for subsequent input into DRAIN-2DX. DRAIN-2DX was used to analyze the response of the weak and strong bare frames, excited with the ground accelerations obtained from the shake table data. FEM/I was used to calculate the response of the infilled concrete frame, in a static push-over analysis (Figure 4). LPM/I was used to analyze the response of the weak and strong infilled frames, excited by the ground accelerations obtained from the shake table data.

5.1 Bare Frames

Computer idealizations using DRAIN-2DX give acceptable predictions of the load-displacement behavior of the bare frames. The computer idealizations predict backbone stiffness and maximum base shear within 10% of the values obtained experimentally. Values for maximum tip displacement are less accurate, and can be 30% higher than the values obtained experimentally. The computer idealization exaggerates the effect of spikes in the ground acceleration, especially if the structure is yielding. Predicted displacements and base shears resulting from spikes were generally about 20% higher than those measured. Spikes in excitation while the structure was yielding caused tip displacement to be over estimated by about 50%. Still, analysis assuming no bond slip or anchorage failure is apparently reasonable for prediction of base frame shear and

displacement maximum. Also, developing elements which can idealize strength and stiffness degradation will give more accurate results.

5.2 Infilled Frames

The programs FEM/I (Ewing 1987) and LPM/I (Kariotis 1992) were used to idealize Model #2. The finite element program FEM/I was used to calculate the response of a single infilled frame in a static push over analysis. In this analysis, finite elements were used to represent the masonry infill and the reinforced concrete frame. The finite element model assumes that tension cracks are distributed (smeared) around the integration points of each element. It includes compressive strength reduction after tensile cracking occurs in orthogonal directions, but does not incorporate any stiffness degradation. Results of the finite element idealization are shown in Figure 4.

The program LPM/I was used for the dynamic analysis of Model #2. The infilled frame was idealized using Element 11 of LPM/I. Element 11 is a nonlinear, hysteretic, degrading envelope spring element. The characteristics of this element are described by force-deformation relations based on analysis and observation of cyclic experiments of reinforced masonry walls. The values of the spring parameters were obtained from the output of the push-over analysis performed by FEM/I. Figure 5 shows the force-displacement characteristics of Element 11, and how it relates to the FEM/I output.

The idealization had a calculated initial fundamental period of 0.023 seconds and an average lateral stiffness of 1820 kips/inch (320.3 kN/mm). Calculated histories of base shear versus tip displacement (in response to the shake table input) are shown in Figure 6. Calculated responses were compared with those observed experimentally. The analytical idealization predicted no significant yielding or energy dissipation, and the load-displacement pattern was almost linear elastic. One exaggerated loop was noticed, with almost twice the average tip displacement and base shear, resulting from a spike in the ground acceleration. Corresponding diagrams plotted using the actual test data showed wider loops, implying more energy dissipation. The same exaggerated loop existed in these recorded diagrams. The maximum predicted base shear was close to that obtained from the actual test data (37.5 kips, or 167 kN versus 40 kips, or 178 kN). However, the predicted maximum tip displacement was much lower than that obtained from the test data (0.025 inch, or 0.64 mm versus 4 inch, or 101 mm). Because the experimental value for the maximum tip displacement is unreasonable for an infilled frame (0.7 inch), and because the experimental load-displacement pattern is irregular, implying some problems with the displacement gages (which reached the end of their travel), the displacement values obtained experimentally are believed to be inaccurate in this test, and the predicted lateral stiffness cannot be compared to that obtained experimentally.

6. SIMPLIFIED ANALYTICAL METHODS

Studies of the behavior and strength of masonry infills excited in-plane have been of interest to researchers for the last several decades. Previous experimental and analytical research has led to the development of several methods for predicting the lateral stiffness and strength of infilled frames. The in-plane structural action of an infilled frame may be idealized in two ways; as a shear wall, and as an equivalent diagonal strut.

In a shear wall idealization, the infilled frame may be viewed as an isolated shear wall whose in plane strength is due to vertical diaphragm action. However, this idealization neglects the interaction between the infill panel and the frame, and greatly underestimates the infilled frame strength and stiffness (Thomas, 1990). Previous research (Thomas, 1990) showed that the lateral stiffness and strength of an infilled frame is greater than the sum of the contributions of the frame and the infill, because of the difference between the flexural deformation pattern of the frame, and the shearing deformation pattern of the infill (Figure 7).

In the equivalent strut idealization, the infilled frame is viewed as a frame braced by a compression diagonal (Stafford Smith, 1966). The equivalent strut idealization of the infilled frame can be justified as follows: Lateral deflection of the infilled frame causes a separation between the frame and the infill panel over part of their contact interface (Figure 7). Therefore, contact is maintained only at opposite corners, at the ends of a compression diagonal that forms through the infill panel. The infill panel acts like an equivalent strut, oriented along the infill panel's compression diagonal.

However, the equivalent strut idealization simplifies the load transfer between the frame and the infill panel (Stafford Smith, 1962). Load transfer actually takes place over an extended contact length, not just at one point at the corners of the infill panel. In spite of this, application of the equivalent strut theory is still justifiable. In most practical structures, the frame is very flexible compared to the infill panel, and any discrepancy caused by this simplification is insignificant (Stafford Smith, 1962).

The effect of this equivalent strut simplification was investigated by constructing three different finite element idealizations for the infilled frame. In the first idealization, the actual properties of masonry were used to represent the whole infill. In the second idealization, finite elements were used to idealize the masonry forming a diagonal strut between the corners of the frame only, to show the effect of the equivalent strut idealization. In the third idealization, the tensile strength of the elements representing masonry units at the boundary of the infill was specified to be 10% of the actual masonry tensile strength, to show the effect of separation at the interface between the infill and the confining frame. Figure 8 shows that the results from the push over analysis for the three idealizations are almost identical. This indicates that the equivalent strut idealization accurately represents the behavior of infilled frames.

6.1 Simplified Methods For Stiffness of Infilled Frames

Based on criteria of accuracy, consistency and simplicity, previous research (Thomas, 1990) recommended the use of Stafford Smith' s equivalent strut method (Stafford Smith, 1966) for the prediction of the lateral stiffness of infilled frames. Furthermore, Stafford Smith's second strut method was preferred because of its simplicity and the availability of design graphs for it. Recent research (Angel, 1994) suggested the use of Holmes (Holmes 1961, 1963) equivalent strut method for the prediction of the lateral stiffness. Although not the subject of this paper, both of Stafford Smith's methods and Holmes method were compared to results from finite element analysis for both the strong and weak infilled frames as part of the analysis. Table 6 compares the simplified methods with the finite element idealization secant stiffness at half the lateral capacity of the infilled frames.

The finite element model stiffness was matched closely by SS2, and by Holmes method. Of these, SS2 is recommended, because it considers the relative stiffness of the frame and the infill in estimating the contact length between them, giving a more accurate value for the effective width of the equivalent strut. In contrast, Holmes method uses a constant value for the width of the equivalent strut, which may lead to inaccurate results in some special cases. One additional note on stiffness of infilled frames; previous research shows that the stiffness of infilled frames exposed to cyclic loads eventually degrades to about half this initial value (Angel, 1994).

6.2 Simplified Methods For Strength of Infilled Frames

Previous research (Thomas, 1990) recommended the use of Liauw and Kwan's (Liauw, 1982, 1983a, 1983b, 1985) method for determining the lateral strength of the infilled frames. The predictions of this method were rather conservative (low) in some cases, but they were also very consistent (Thomas, 1990). Liauw and

Kwan's method, and also an older method proposed by Holmes (Holmes, 1963) were compared to results from the push over analyses performed using the finite element idealizations, for both the strong and weak infilled frames. The predicted lateral strength will not be compared to results from the dynamic tests, as the infilled frames tested in plane were not excited up to ultimate lateral strength.

6.2.1 Liauw and Kwan's Method for Predicting the in-Plane Strength of Infilled Frames

Liauw and Kwan combined plastic theory with nonlinear finite element analysis to arrive at collapse loads for infilled frames. They addressed concerns that they maintained had been ignored in previous studies by Wood (Wood, 1978). These included multi story design and the distinction between integral and non integral infill panels.

According to Liauw and Kwan, Wood's failure to differentiate between integral and non integral frames led to wide discrepancies between his theoretical predictions and experimental results (Liauw, 1983). Integral infilled frames have mechanical connectors between the frame and infill. Non Integral infilled frames have no such connectors. Wood did include a penalty factor to lower the effective crushing stress of the infill panel to account for its lack of plasticity (Wood, 1978). According to Liauw and Kwan, Wood's over estimation of the collapse shear is due to the assumption of excessive friction at the interface between the infill panel and the frame, and to neglect of separation between infill panel and frame in the composite shear mode.

Liauw and Kwan felt friction has an insignificant effect, and should be considered only as reserve strength. Therefore, only three failure modes exist for the non integral infilled frame, as shown in Figure 9: 1) corner crushing with failure in columns, b) corner crushing with failure in beams, and 3) diagonal crushing. The collapse shears for each failure mode in single story, non integral infilled frames are:

Mode 1: $$H_u = \sigma_c t h \sqrt{\frac{2(M_{pj} + M_{pc})}{\sigma_c t h^2}}$$

Mode 2: $$H_u = \frac{\sigma_c t h}{\tan\theta} \sqrt{\frac{2(M_{pj} + M_{pc})}{\sigma_c t h^2}}$$

Mode 3: $$H_u = \frac{4M_{pj}}{h} + \frac{\sigma_c t h}{6}$$

where

H_u = in-plane design strength of infill (kips)
h = story height
t = infill thickness
M_{pb} = plastic moment of the beam (in-kips)
M_{pc} = plastic moment of the column (in-kips)
M_{pj} = the smaller of M_{pb} and M_{pc}
σ_c = crushing stress of panel material

The collapse shear is the minimum value from the above three equations.

Plastic theory can be applied to multi-story infilled frames as well as single story ones, because the collapse modes for both are basically the same. However, many different possible combinations of failure modes are possible, and the evaluation of ultimate load can become quite complex. A simplified procedure was developed by Liauw and Kwan for the story by story design of multi story infilled frames. Equations for predicting the collapse shears for lower stories (that is, all stories except the top one) in integral and non-integral infilled frames are given by the equations:

Mode 1: $$H_u = \sigma_c t h \sqrt{\frac{4M_{pc}}{\sigma_c t h^2}}$$

Mode 2: $$H_u = \frac{\sigma_c t h}{\tan\theta} \sqrt{\frac{4M_{pb}}{\sigma_c t h^2}}$$

Mode 3: $$H_u = \frac{4M_{pj}}{h} + \frac{\sigma_c t h}{6}$$

The lateral strength of both the strong and the weak infilled frames were calculated using Liauw's methods for both single and multi story frames, and were compared with the results from the finite element idealization (Table 7). As expected, the predictions of this method were low.

6.2.2 Holmes Method for Predicting the in-Plane Strength of Infilled Frames

This method is based on the analysis of the results of small scale and full scale tests of steel infilled frames, performed by Holmes (Holmes, 1963). As in Holmes stiffness method, the infill has been replaced by an equivalent strut leaving the frame itself to carry the forces, as shown in Figure 7. By equating the change in the length of the diagonal AC of the frame to the shortening of the equivalent strut, the load causing failure is given by:

$$H = \frac{24 E I_c \varepsilon_c' d}{h^3 \left[1 + \left(\frac{I_c}{I_b}\right) \cot\theta\right]} \cos\theta + \frac{t d f_c' \cos\theta}{3}$$

where

- E = elastic modulus of the frame (ksi)
- I_c = column moment of inertia (in^4)
- I_b = beam moment of inertia (in^4)
- d = diagonal length of infill panel (in)
- θ = angle between diagonal and the horizontal (degrees)
- ϵ_c = strain in infill at failure
- h = height of frame (inches)
- A = equivalent strut cross-sectional area (in^2)
- f'_c = diagonal compressive strength of the infill panel (ksi)
- t = thickness of infill

The first term on the right hand side of the above equation represents the load carried by the frame alone, calculated on an elastic basis. However, this value should be limited by the peak strength of the bare frame, which is given by the lesser of:

$$\frac{4M_{pc}}{h}$$

or

$$\frac{4M_{pb}}{h}$$

where M_{pc} and M_{pc} are the fully plastic moments of the columns and the beams respectively, and h is the height of the frame. The value of the lateral strength obtained by this method, shown in Table 7, is much higher than that predicted by the finite element idealization.

The main reason for the high value of the estimated collapse load for the infilled frame under study in Holmes method is that the area of the equivalent strut is exaggerated. In Holmes method, the width of the equivalent diagonal strut is fixed to one third the length of the infill diagonal, irrespective of the relative stiffness of the frame and the infill in the estimation of the contact length between them. An expression based on Holmes method, and modified for the effect of relative frame infill stiffness on the width of the equivalent diagonal strut, is:

$$H = \frac{24 E I_c \varepsilon_c' d}{h^3 \left[1 + \left(\frac{I_c}{I_b}\right) \cot\theta\right]} \cos\theta + A f_c' \cos\theta$$

where A is the area of the diagonal strut obtained using the curves proposed by Stafford Smith (Method SS2), shown in Figure 10. This method will be referred to here as the CERL method. As shown in Table 7, predictions of this method are very close to those obtained by the finite element idealization,. The use of the new expression (CERL Method) is recommended for the estimation of the lateral strength of the infilled frames.

7. CONCLUSIONS

Infilled frames under in-plane excitation were not excited up to failure; however, some damage was induced in them. Test data was limited to verifying the structural response of the finite element models, however ultimate strength must still be approximated.

Nonlinear response predictions using FEM v. 109 followed by the LPM/I computer idealizations had a similar pattern to experimental test data. Maximum predicted base shear was close to that obtained experimentally (within 10%). Computer idealization predicts the effects of spikes of shake table acceleration on the response accurately (within 15%). Energy dissipation was predicted fairly well in one case, but not in another.

The stiffness of the confining frame significantly affects the response of the infilled frames. Finite element analysis showed that the infill in the strong frame would crack at higher lateral loads than the infill in the weak frame, because the contact length between the frame and the infill is higher for the strong frame than for the weak one.

The lateral strength of infilled frames excited in-plane, based on the finite element analysis and support by the test data, is most accurately predicted using the CERL method.

8 ACKNOWLEDGEMENTS

The analysis of the test data was performed at the University of Texas at Austin by graduate students Terek Bashandy and Nestor R. Rubiano, under the supervision of Dr. Richard E. Klingner. Their contribution to this research effort is greatly appreciated.

9 REFERENCES

1. Allahabadi, R. and Powell, G. H. (1988), "DRAIN-2DX User Guide," EERC Report No. 88/06, University of California, Berkeley.

2. Angel, R., Abrams, D., Shapiro, D., Uzarski, J. and Webster, M. (1994), "Behavior of Reinforced Concrete Frames with Masonry Infills," Civil Engineering Studies, Structural Research Report No. 589, University of Illinois, Urbana, March 1994.

3. Ewing, R. D., El-Mustapha, A., and Kariotis, J. C. (1987), "FEM/I: A Finite Element Computer Program for the Nonlinear Static Analysis of Reinforced Masonry Building Components," Report No. 2.2-1 EKEH (Revised 1990).

4. Farahany, M. M. (1983), "Computer Analysis of Reinforced Concrete Cross-Sections," Master's Thesis, The University of Texas at Austin, December 1983.

5. Holmes, M. (1961), "Steel Frames With Brickwork and Concrete Infilling," Proceedings of the Institution of Civil Engineers, Vol. 19, No. 6501, August 1961, pp. 473-475.

6. Holmes, M. (1963), "Combined Loading on Infilled Frames," Proceedings of the Institution of Civil Engineers (25), pp. 31-38.

7. Kanaan, A. E. and Powell, G. H. (1975), "DRAIN-2D," EERC Report No. 73-6 and 3-22, University of California, Berkeley.

8. Kariotis, J. C., Rahman, A. M. D., Wafqi, O. M., and Ewing, R. D, (1992), "LPM/I Version 1.03 A, Computer Program for the Nonlinear, Dynamic Analysis of Lumped Parameter Models," Report No. 2.3-4, EKEH.

9. Liauw, T. C. and Kwan, K. H (1982), "Nonlinear Analysis of Multistory Infilled Frames," Proceedings of the Institution of Civil Engineers, Part 2, No. 73, pp. 441-454.

10. Liauw, T. C. and Kwan, K. H (1983a), "Plastic Theory of Non-Integral Infilled Frames," Proceedings of the Institution of Civil Engineers, Vol. 75, September, pp. 707-723.

11. Liauw, T. C. and Kwan, K. H (1983b), "Plastic Theory of Infilled Frames with Finite

Interface Shear Strength," Proceedings of the Institution of Civil Engineers, Vol. 75, December , pp. 707-723.

12. Liauw, T. C. and Kwan, K. H (1985), "Unified Plastic Analysis of Infilled Frames," Journal of Structural Engineering, ASCE, Vol. 111, No. 7, July 1985.

13. Mahin, S. A. and Bertero, V. V. (1977), "RCCOLA: A Computer Program for Reinforced Concrete Column Analysis, User's Manual and Documentation," Department of Civil Engineering, University of California, Berkeley, August 1977.

14. Stafford Smith, B. (1962), "Lateral Stiffness of Infilled Frames," Proceedings of the Institution of Civil Engineers, Vol. 88, No. 3355, December 1962, pp. 183-199.

15. Stafford Smith, B. (1966), "Behavior of Square Infilled Frames," Journal of the Structural Division, ASCE, Vol. 92, No. ST1, February 1966, pp. 381-403.

16. Thomas, R. D. and Klingner, R. E. (1990), "Behavior of Infilled Frames," Chapter 4 in Limit States of Masonry. The Masonry Society, Boulder, Colorado.

17. Wood, R. H., (1978), "Plasticity, Composite Action, and Collapse Design of Unreinforced Shear Wall Panels in Frames," Proceedings of the Institution of Civil Engineers, Vol. 65, June, 1978, pp. 381-411.

Frame Type	In-Plane Seismic Tests		Out-of-Plane Seismic Tests	
	Bare Frame	Infilled Frame	Unrepaired	Repaired
Strong Frame	Model #1	Model #2	Model #3 Model #5 (virgin)	Model #4
Weak Frame	Model #6	Model #7	Model #8	Not Tested

Table 1. Overall Experimental Program Summary of Tests

Gage	Seismic Test #9		Seismic Test #10		Seismic Test #11	
	Tension	Compression	Tension	Compression	Tension	Compression
S1	408	-215	728	-287	1072	-387
S2	206	-131	463	-241	1007	-336
S3	333	-161	663	-245	998	-404
S4	153	-98	364	-190	787	-317
S5	152	-90	294	-162	546	-292
S6	274	-60	492	-146	816	-284
S7	225	-160	454	-234	938	-351
S8	266	-81	587	-138	915	-238
S9	151	-154	411	-282	1323	-462
S10	137	-91	127	-141	375	-219
S11	290	-253	507	-441	1171	-576
S12	281	-143	693	-224	1114	-448
S13	220	-162	446	-278	1130	-401
S14	303	-165	678	-262	1108	-475
S15	184	-191	434	-329	1074	-465
S16	305	-144	644	-240	1076	-410

Table 2. Maximum Strains in Longitudinal Reinforcement, Model #1 (micro-strain)

Gage	Seismic Test #18		Seismic Test #19	
	Tension	Compression	Tension	Compression
S1	218	-154	2250	-2147
S2	129	-34	998	-52
S3	337	-26	1391	-180
S4	126	-36	843	-90
S5	58	-56	538	-79
S6	508	-45	1565	-36
S7	178	-88	192	-854
S8	37	-478	27	-1467
S9	267	-1553	275	-1532
S10	90	-177	334	-497
S11	87	-75	216	-967
S12	73	-116	462	-759
S13	133	-119	426	-910
S14	29	-296	202	-1339
S15	202	-63	496	-719
S16	28	-343	109	-1245

Table 3. Maximum Strains in Longitudinal Reinforcement, Model #2 (micro-strain)

Gage	Seismic Test #45		Seismic Test #46		Seismic Test #47	
	Tension	Compression	Tension	Compression	Tension	Compression
S1	0	0	1568	-431	3272	-180
S2	218	-104	915	-628	3649	-425
S5	136	-74	1011	-349	1579	-482
S6	146	-67	802	-323	3584	-208
S9	33	-36	97	-182	468	-257
S11	21	-21	298	-20	500	-71
S15	21	-29	57	-62	48	-114
S17	14	-12	479	-13	582	-201
S14	11	-25	31	-57	29	-96

Table 4. Maximum Strains in Longitudinal Reinforcement, Model #6 (micro-strain)

Gage	Seismic Test #51		Seismic Test #52	
	Tension	Compression	Tension	Compression
S1	0	0	0	0
S2	2495	-473	2664	-801
S5	976	-45	3362	-801
S6	18	-48	15	-29
S9	292	-83	389	-211
S11	199	-51	347	-24
S15	30	-38	35	-102
S16	479	-87	1218	-228
S14	89	-28	134	-14

Table 5. Maximum Strains in Longitudinal Reinforcement, Model #7 (micro-strain)

Model	Predicted Stiffness			
	Finite element	Simplified Methods		
		SS1	SS2	Holmes
Strong frame	1486	776	1380	1268
Weak frame	1306	670	1160	1234

Table 6. Predicted Specimen Stiffness, kips/in.

Model	Predicted Strength			
	Finite Element	Simplified Methods		
		Liauw	Holmes	CERL
Strong Frame	192	128	311	196
Weak Frame	164	97	30.5	162

Table 7. Predicted Specimen Strength, kips/in.

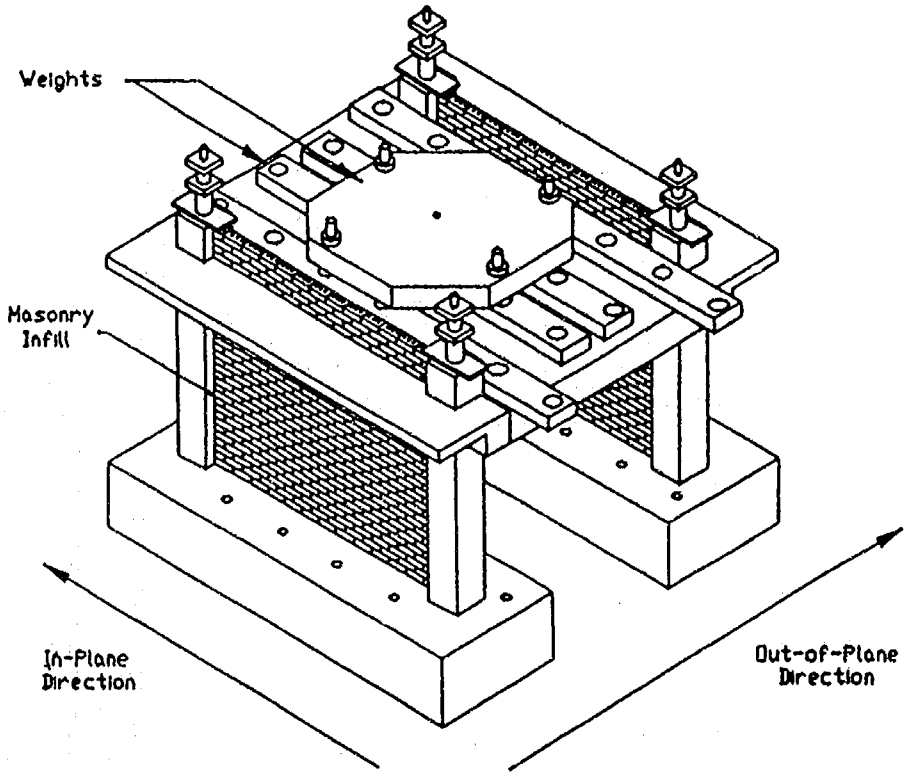


Figure 1. Experimental Model

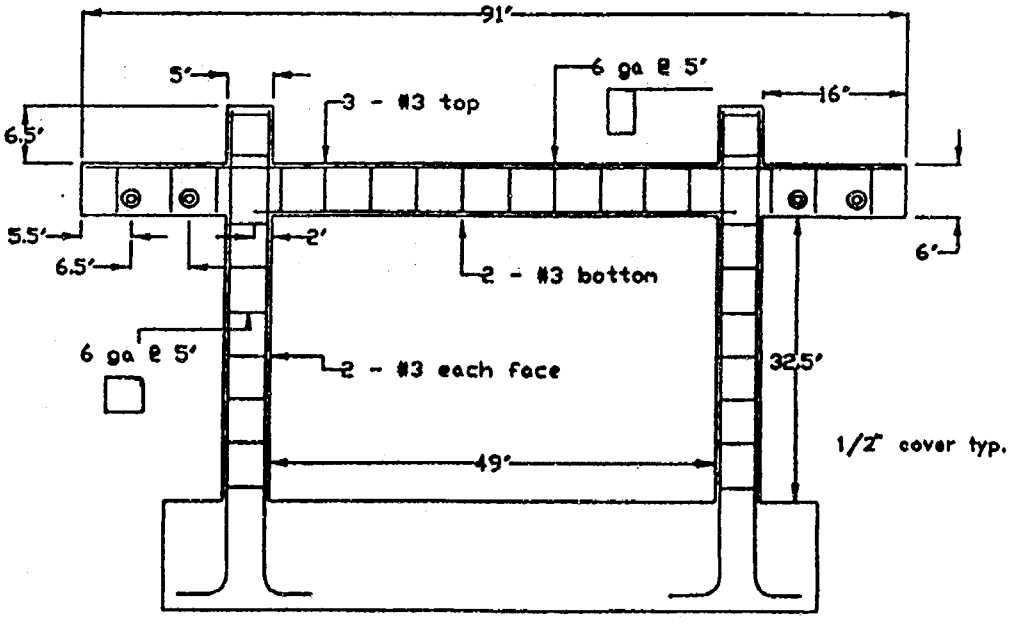
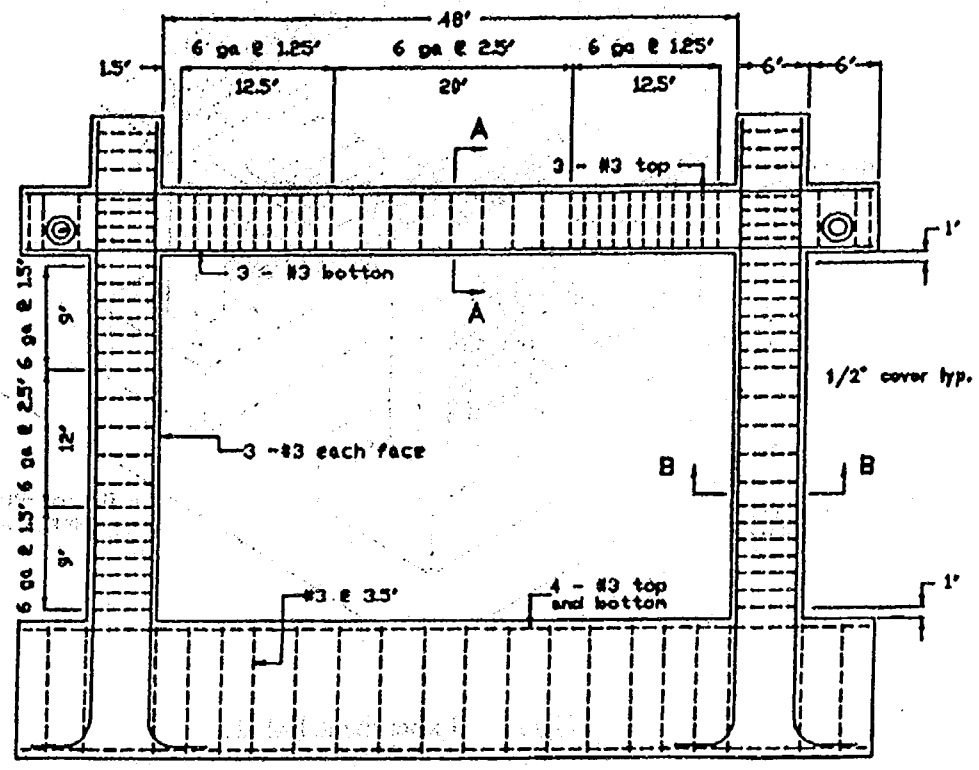


Figure 2. Details of Weak Frame



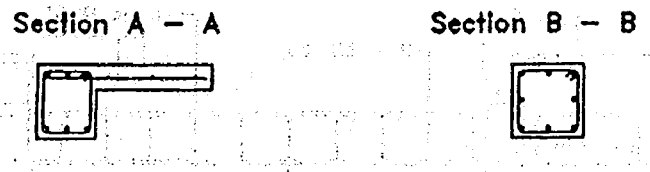
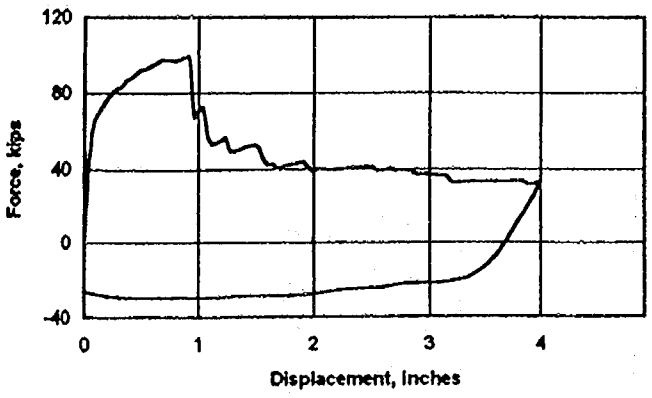
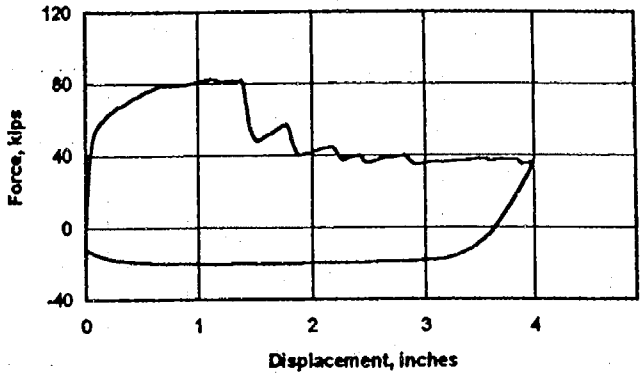


Figure 3. Details of Strong Frame



(a) Strong Infilled Frame (Model #2)



(b) Weak Infilled Frame (Model #7)

Figure 4. Results of FEM Pushover Analysis

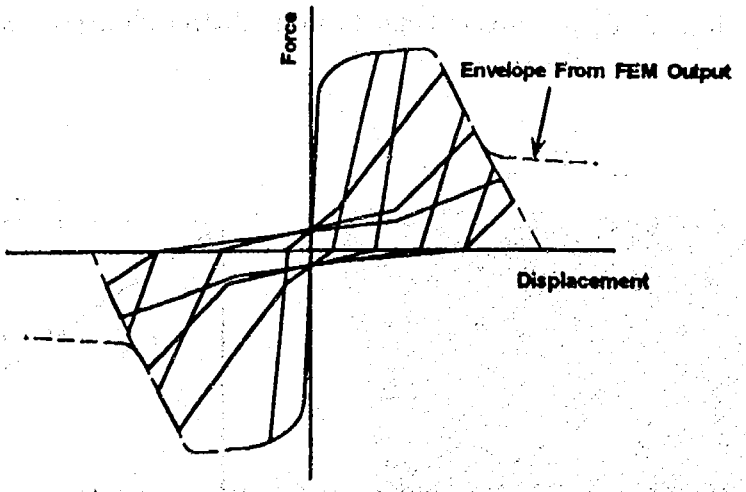
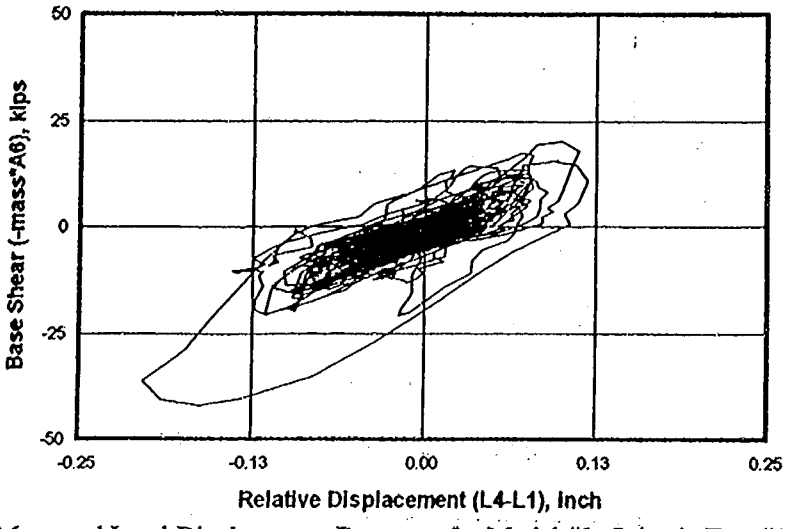
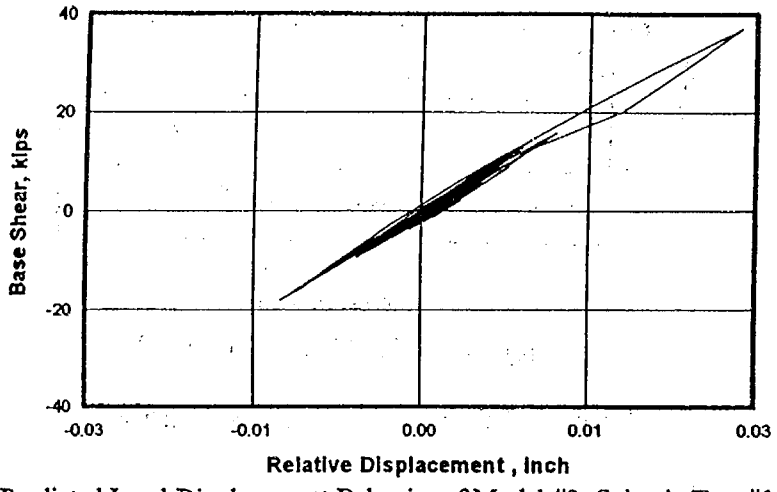


Figure 5. Hysteretic Model, LPM/I Element 11, Based on Pushover Analysis



(a) Measured Load-Displacement Response for Model #2, Seismic Test #18



(b) Predicted Load-Displacement Behavior of Model #2, Seismic Test #18

Figure 6. Comparison of Finite Element Model with Experimental Data

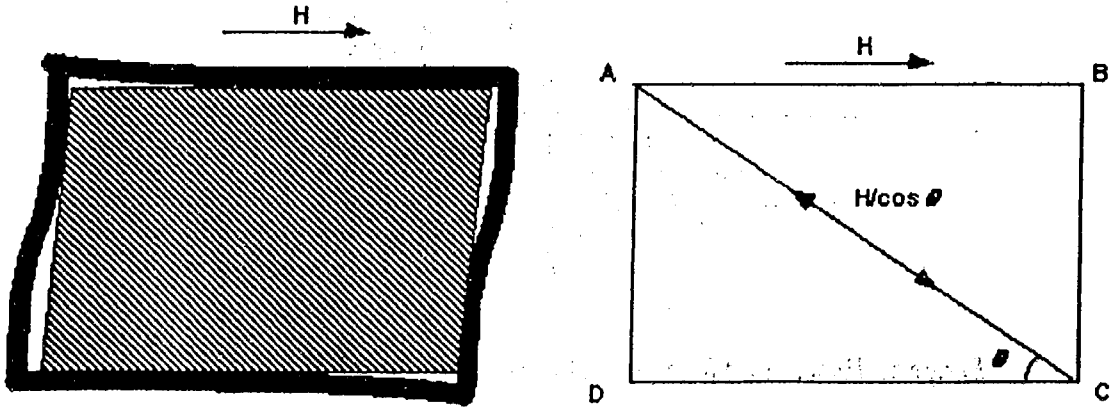


Figure 7. Structural Action of Infilled Frame With Lateral Force H

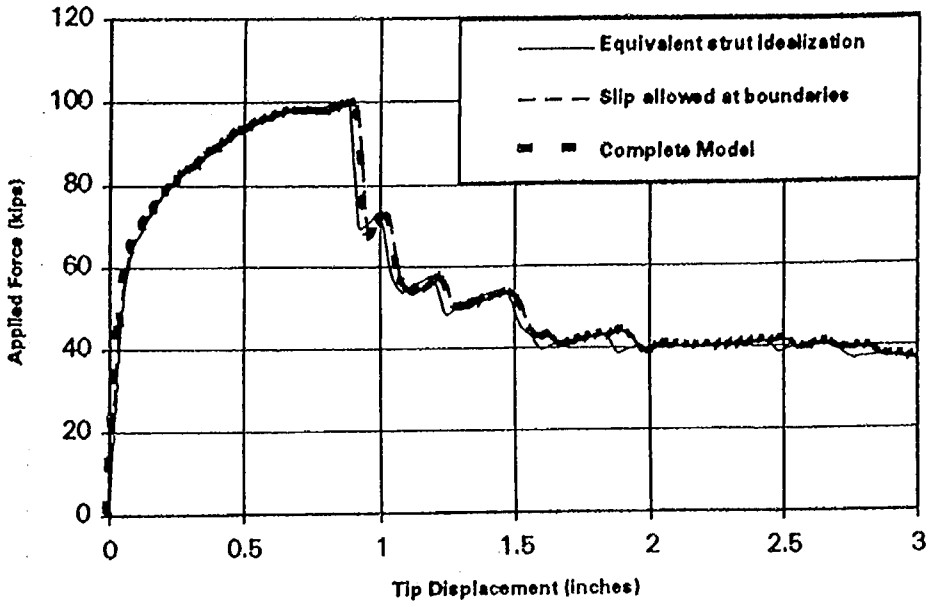


Figure 8. Effect of Different Equivalent Strut Methods on Finite Element Analysis Results

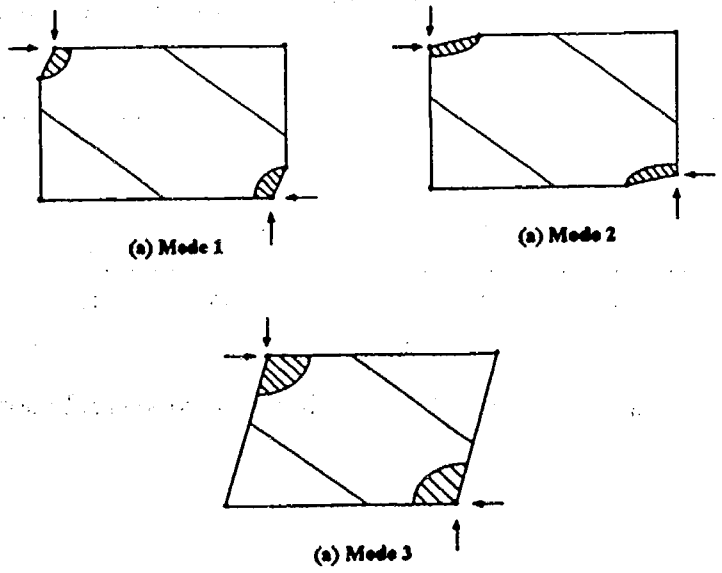


Figure 9. Liauw and Kwan Collapse Methods for Infilled Frames

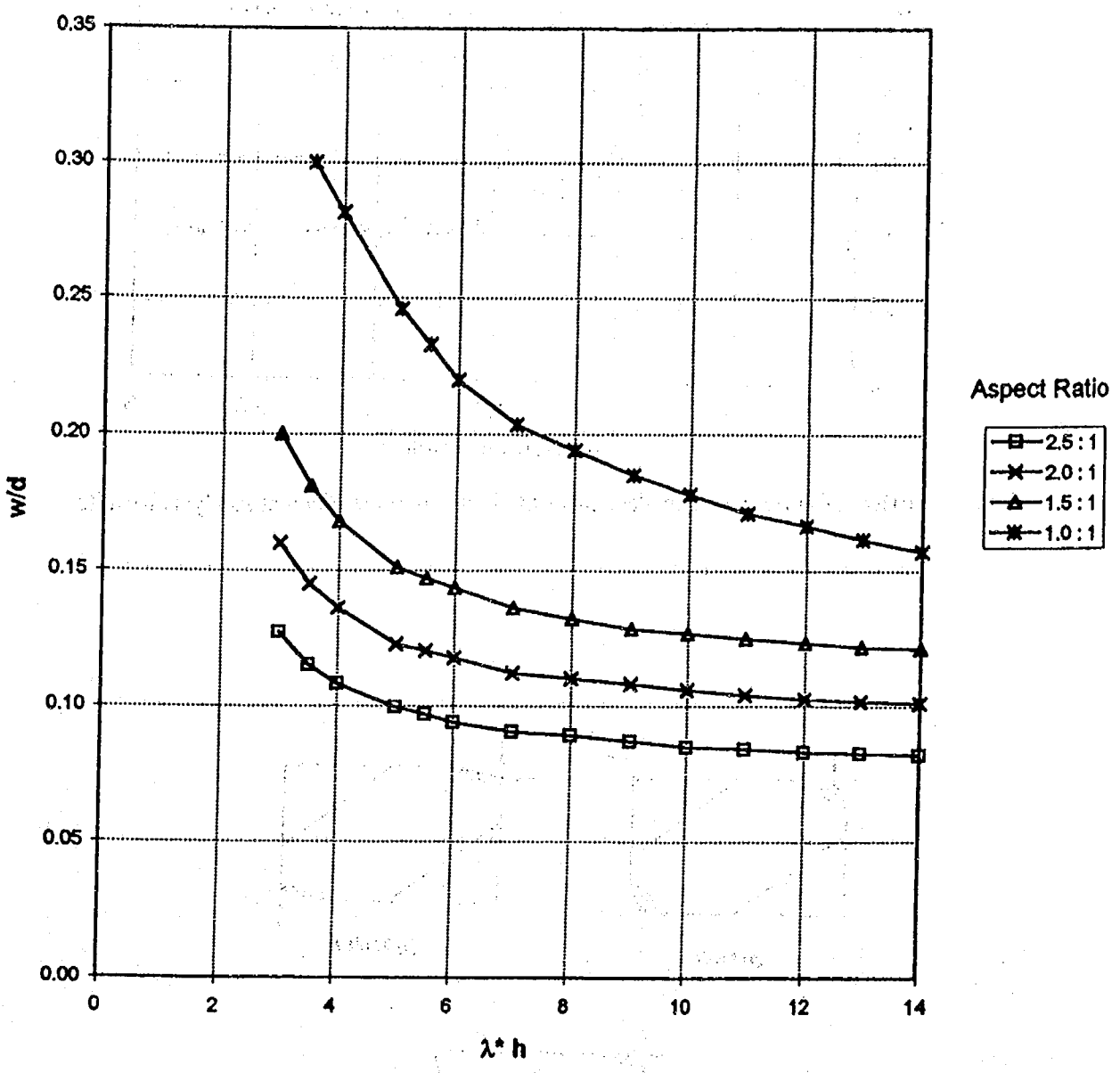


Figure 10. w/d vs. λ*h For Calculating Area of Strut With Respect to Aspect Ratios (Stafford Smith 1966)

Use of Experience Data for Seismic Evaluations at Department of Energy Facilities

by

James R. Hill*, Dan J. Guzy*, Jeffrey K. Kimball*
and Robert C. Murray**

ABSTRACT

Seismic evaluations of essential systems and components at Department of Energy (DOE) facilities will be conducted over the next several years. For many of these systems and components, few, if any, seismic requirements applied to the original design, procurement, installation, and maintenance process. Thus the verification of the seismic adequacy of existing systems and components presents a challenge.

DOE has undertaken development of the criteria and procedures for equipment seismic evaluations that can be used in a timely and cost effective manner. As demonstrated in previous applications at DOE facilities and by the experience from the commercial nuclear power industry, use of experience data for these evaluations is the only viable option for most existing systems and components. This paper describes seismic experience data, the needs at DOE facilities, the precedent of application of nuclear power plants and DOE facilities, and the program being put in place for the qualification of equipment in existing facilities.

1. INTRODUCTION

Seismic experience data are the documented performance of systems and components that were subject to earthquake motion. It includes items in commercial and industrial facilities that were in the strong motion regions of major earthquakes, and items that underwent shake table tests.

Over the past several years, the Seismic Qualification Utility Group (SQUG) and the Electric Power Research Institute (EPRI) have developed a seismic experience data base that includes the response of systems and components in about 100 industrial facilities located in the areas of strong ground motion from 20 past earthquakes. The earthquakes have Richter magnitudes in the range of 5.2 to 8.1, with peak ground accelerations from 0.10g to 0.85g, for about 3 to about 50 seconds duration. Soil conditions, building structure types, and location of equipment vary considerably within the data base.

The facilities surveyed and documented contain a large number of mechanical and electrical equipment, and control and distribution systems identical or very similar to those found in DOE facilities. Information sources consist of interviews with facility management and operating personnel, walkdown inspections of facilities, photographs and performance data records of systems and components, facility operating logs, and the facility's inspection reports. Available design criteria and specifications, component data books, and design drawings were collected. The experience database represents diversity in equipment design, size, configuration, age, application, operating conditions, manufacturer, and quality of construction and maintenance.

The earthquake experience data are useful for determining common sources of seismic damage or adverse effects on equipment and facilities, thresholds of seismic motion corresponding to various types of seismic performance, and qualification of equipment construction and installation to ensure the ability to withstand anticipated seismic loads.

As an expansion of the earthquake experience data, EPRI and SQUG also collected data on shake-table qualification tests from utilities, manufacturers, and test laboratories. Results were compiled from about 300 shake table tests of equipment components, covering 15 generic classes of equipment which are representative of much of the equipment found in DOE facilities.

* U.S. Department of Energy
Washington, D.C. 20585
** Lawrence Livermore National Laboratory
Livermore, California 94550

The objective was to compile the information by class, and to obtain generic insights, if any, by class, that could be used to assist utilities in evaluating these equipment classes in their plants. These generic equipment ruggedness data represent substantially higher levels of seismic motion than the earthquake experience data, but in most cases are applicable to a narrower range of equipment parameters. EPRI and SQUG also obtained available electro-mechanical relay chatter shake table tests and performed additional tests for other relays. The relay test experience data base provides capacities for about 150 specific models of relays.

Another important element of seismic experience data is the design of anchor bolts that are commonly used in many DOE facilities to attach systems and components to the supporting building structure. EPRI and SQUG have summarized capacity information for expansion anchor bolts, covering about 1200 ultimate capacity tension and shear tests. Capacity data have also been compiled for other anchor types including welded attachments, cast-in-place bolts and headed studs, grouted-in-place anchors, and cast-in-place J-hooks.

2. FACILITY NEEDS

DOE facilities need to have adequate measures of ensuring hazardous material confinement for protection of the public health and safety, on-site worker life safety, and investment protection in the event of natural phenomena hazards including earthquakes. Due to the evolutionary nature of design and operating requirements, and developments in engineering technology, existing DOE facilities embody a broad spectrum of design features for earthquake resistance. The earliest facilities often have the least seismic design documentation, yet potentially exhibit the greatest difference between their design basis and what DOE would require today for seismic design criteria for new facilities.

Compliance with the recent DOE Order 5480.28 (Reference 1) for the seismic evaluation of systems and components leads to consideration of the following alternatives:

Seismic qualification by testing.
Seismic qualification by analysis.
Verification of seismic adequacy using experience data.

As was concluded in the nuclear power industry (Reference 2 to 4), the first two alternatives, testing or analysis are most often not viable (removal, decontamination, shipment of equipment for testing; access and potential damage for in-situ testing, etc.) As demonstrated in previous applications at DOE facilities and by the experience from the commercial nuclear power industry use of experience data for these evaluations is the only viable option for most existing systems and components.

3. PRECEDENTS

3.1 Application to Nuclear Power Plants

In the late 1970s, the U.S. Nuclear Regulatory Commission (NRC) expressed the concern that nuclear equipment seismically qualified to standards preceding IEEE-344-1974 may not provide sufficient assurance of seismic adequacy. This concern was reinforced through field inspections of earlier nuclear power plants where equipment lacked adequate anchorage. This NRC concern resulted in the issue of Unresolved Safety Issue (USI) A-46, "Seismic Qualification of Mechanical and Electrical Equipment in Operating Nuclear Power Plants" (Reference 2). The NRC pursued several options for resolution of USI A-46, including use of shake table testing, in situ testing, deterministic and probabilistic analytical methods, and seismic experience data. Most options proved not to be viable because of the unavailability of older model components for testing, high costs of component replacements, and complications of testing radiologically contaminated equipment.

The NRC concluded, based on research by the national laboratories, that use of experience data could provide a reasonable alternative of resolution of USI A-46 (Reference 4). The NRC also endorsed the methodology developed by SQUG, EPRI and the Senior Seismic Review and Advisory Panel (SSRAP) (Reference 5). In 1987, NRC Generic Letter (GL) 87-02 required utilities to respond to USI A-46, and encouraged participation in generic resolution by using the SQUG approach, documented in the Generic Implementation Procedure (GIP) (Reference 6). NRC has accepted the SQUG GIP by a generic safety evaluation report (Reference 7), taking a few exceptions, which have since been resolved and are being incorporated into Revision 3 of the GIP.

The SQUG GIP consists of four sets of criteria:

1) the experience based capacity spectrum must bound the plant seismic demand spectrum, (See Figure 1)
2) the equipment item must be reviewed against certain inclusion rules and caveats,
3) the component anchorage must be evaluated, and
4) any potentially significant seismic systems interaction concerns that may adversely affect component safe shutdown function must be addressed.

These SQUG criteria are in the form of screening evaluation guidelines. Items not passing the screen are not necessarily inadequate, but other seismic engineering methods must be used to evaluate these items further.

An important element of the SQUG GIP is its application by the use of specially trained and experienced seismic review teams who must exercise considerable judgment while performing the in-plant screening evaluations. Besides establishing strict qualification requirements for review team engineers, SQUG and EPRI provide a training course in the use of the implementation guidelines and procedures.

The seismic evaluation method based on experience data has become a key element in the ongoing earthquake evaluations for commercial nuclear power plants. The experience based evaluation methods address most plant components needed for safe shutdown in the event of a design basis earthquake, including 22 classes of electrical and mechanical equipment, cable trays and conduit systems, relays, anchorage capacity, tanks and heat exchangers. See Table 1.

3.2 Application to DOE Facilities

The SQUG experience-based seismic evaluation approach has already been used at a few DOE facilities. The most extensive application was at the Savannah River Site (SRS). The SRS reactors were built in the 1950s when seismic qualification requirements were in their infancy. SRS became a member of SQUG in 1988, and used the GIP at its nuclear reactors to evaluate the seismic adequacy of selected safety systems for their design basis earthquake. The SRS reactor program included definition of the system scope requiring review, development of SRS plant specific procedures, use of seismic screening evaluation walkdowns and calculations, and identification, resolution, and upgrading of outliers. This application at SRS has been reviewed and accepted by internal DOE oversight.

The SRS seismic evaluation program represents an expansion of the SQUG GIP in several areas. Programmatic changes were incorporated to enhance engineering assurance. Several technical changes were added to address unique needs at SRS such as additional steps for expansion anchor verification, development of capacity for lead cinch anchors, implementation of consistent guidelines for HVAC ducting, and use of experience based screening guidelines for piping.

The SRS seismic evaluation program was a major success. Roughly 60 percent of the items were verified to be seismically adequate as-is. For the others, about 11 percent were resolved by additional evaluation; the remainder were resolved by upgrade. The typical upgrades consisted of anchorage enhancement and elimination of seismic interaction concerns by providing restraint or removal of the interaction source. The use of the experience based evaluation approach enabled efficient identification of realistic seismic concerns at SRS. Maximum safety enhancement was achieved with reasonable engineering effort. This seismic experience based approach is currently being used at SRS to evaluate non-reactor facilities.

Similar benefits from use of experience data were realized at the High Flux Isotope Reactor (HFIR) at Oak Ridge National Laboratory (ORNL). Prior to plant restart, seismic verification of essential systems and components had to be demonstrated. Experience based in-plant screening evaluations were used as a key part of the seismic evaluation and upgrade program. Several items were determined to be acceptable in their as-installed configuration. Backfit modifications were installed to increase seismic adequacy as needed. This included providing anchorage for some components, additional restraint for items were deflection considerations were governing capacity, and correction of potential seismic systems interaction hazards.

Other successful applications of experience data for seismic design issues at DOE facilities

include the Princeton Plasma Physics Laboratory and the Idaho Chemical Processing Plant (ICPP). At Princeton, active electrical and mechanical equipment, fluid pressure boundary components, and seismic interaction effects were evaluated and resolved by use of experience based methods. At ICPP, seismic adequacy of critical fire protection components was verified using the experience based approach.

The example application at SRS, HFIR, Princeton, and ICPP have proven the viability of the experience data base approach for DOE facilities. These evaluations have withstood strict scrutiny during technical audits, peer reviews, quality control audits, and other independent reviews. Given the experience from the nuclear power industry, coupled with previous applications at DOE sites, the controlled and proceduralized application of experience data provides DOE sites with an efficient tool for determining the necessary seismic evaluations.

Currently, the SQUG methodology is being used for evaluations at the SRS Canyons, LLNL's Plutonium Facility, and may soon be applied at Rocky Flats' Building 371.

4. PROGRAM

The DOE facility evaluations can take direct advantage of the experience data base compilations and guidelines developments by SQUG and EPRI. Through special agreement the SQUG and EPRI reference documents (References 6, 8, and 9 through 20) for use of experience data are available to DOE for the facility reviews. Two orientation workshops and a 5-day training course have already been conducted to provide facility personnel with an overview of the SQUG and EPRI reference materials and detailed training on its application. The attendance at the training course is currently a mandatory step for any site wishing to obtain the documents. A training program will be continued to permit use of these documents for safety basis evaluations.

Because the systems and components in DOE facilities are so diverse, other experience based tools are needed for the DOE efforts beyond those currently included in the EPRI/SQUG data base. Additional needs include other equipment groups beyond the 22 SQUG classes of equipment. A questionnaire was used to help determine the types of safety systems and equipment components that will require seismic evaluation. A list of 20 DOE additional classes of equipment has been developed and is shown in Table 2.*

In contrast to the SQUG deterministic criteria, DOE facilities are required to demonstrate the ability to achieve probabilistic performance goals (Reference 21). The larger the potential risk, the stricter the performance requirements. DOE and its contractors are therefore assessing the probabilistic performance goals achieved when seismic experience based screening evaluation methods are used. This effort is complete and documented in Reference 22.

4.1 Overview of Program Plan

DOE has implemented a program for the development of seismic evaluation guidelines for systems and components at existing facilities. The program plan intends to maximize the use of past experience, in conjunction with a walkdown screening evaluation process.

The program will provide walkdown guidelines such that systems and components can be identified, assessed, and remedied as needed in an efficient manner. The program will also provide screening guidelines whereby systems and components that have demonstrated ability to withstand known levels of seismic motion, based on past experience, can be verified as meeting applicable requirements without needing additional analysis or testing. Guidelines will be developed for analysis or testing of systems and components that do not meet the screening criteria. Documentation requirements will be developed to streamline evaluation process yet still provide sufficient traceability and accountability for the reviews.

Implementation of these procedures will require experienced, well trained engineers applying sound engineering judgment. As a result, the program will provide for the transfer of the necessary technology to DOE sites and the training of engineers to conduct evaluations. In addition, peer review requirements will be established to provide an independent verification of the judgments made during the screening evaluations.

---

* Screening criteria for piping (including fire protection and masonry walls equipment classes are being developed.

DOE facility management and operations personnel will play an important role in the development and review of the guidelines. A Steering Group of selected individuals from the operating contractors will ensure that appropriate priorities are established from the facility operations perspective. The Steering Group has also chartered a team of industry experts for technical review of the implementation guidelines. The Technical Review Team determines the adequacy of the technical content of the screening evaluation guidelines, including the safety margins that will result from implementation of the criteria. The steering group has met seven times since December 1992 to guide the overall program.

4.2 Progress to Date

The first phase of the program was to obtain a DOE license for use of the EPRI/SQUG Seismic Evaluation Material (References 8 through 20) at DOE facilities. This was followed by orientation and training on the use of this material within the DOE complex. This seismic assessment material was arranged into 8 volumes and 100 sets were distributed throughout the DOE. Procedures are being developed for current SQUG certificate holders to obtain DOE certificates of training.

A Walkthrough Field Guide (Reference 22) was developed to assist in identifying major deficiencies at DOE facilities. The document was developed based on walkdown experience at nuclear power plants and then tested and revised by applying it to walkdowns at selected DOE facilities. This document was also distributed throughout DOE as part of the training course.

Piping systems was identified early in the program. A team of industry experts was lead by WSRC to develop practical screens over the last year. This effort has been reviewed by the Technical Review Team and documented in Reference 23. Training on the use of this screening criteria is currently under development.

Development of screening criteria for seismically evaluating unreinforced masonry walls was begun in mid 1994 and is nearing completion. The draft document will then be reviewed by the Technical Review Team.

DOE's seismic criteria is performance based and uses a graded approach, therefore every structure, system, and component is placed into a Performance Category (PC). These range from PC 0 with no requirements, to PC 1 and 2 which are like conventional building code criteria, to PC 4 which approaches commercial nuclear power plant criteria. A study has been completed which quantifies the performance of structures, systems, and components whose seismic capacity is defined using experience data. This study proposes experience data factors to scale Structure Response Spectra which need to be bounded by experience data results such as the Reference Spectrum, GERS Spectra, or Qualification Test Results.

4.3 Planned Work

The primary emphasis will be to develop the DOE Implementation Plan for the SQUG 22 classes of equipment. This will be followed by developing screening tools for the DOE unique items along with the associated training.

The Steering Group plans to monitor applications at DOE sites during the initial implementation phase which will take place in 1996.

Lessons learned from the Northridge and Kobe Earthquakes are also being assembled jointly with EPRI and NRC. Part of this effort may include detailed study of DOE's Energy Technology Engineering Center (ETEC) located a few miles from the epicenter. This will expand the experience data base of equipment located at DOE facilities.

The use of experience data is being extended to qualification of components of electric transmission systems. Application of seismic experience and testing data to other lifeline systems is expected to reduce system vulnerability to earthquake damage.

5. REFERENCES

1. Natural Phenomena Hazards Mitigation for Department of Energy (DOE) Owned Facilities, DOE Order 5480.28, January 15, 1993.

2. Nuclear Regulatory Commission, NUREG 1030, "Seismic Qualification of Equipment in Operating Nuclear Power Plants, USI-A46," February 1987.

3. Nuclear Regulatory Commission, NUREG 1018, "Seismic Qualification of Equipment in Operating Nuclear Power

Plants, A Status Report on USI-A46," September 1983.

4. Nuclear Regulatory Commission, NUREG 1211, "Regulatory Analysis for Resolution of Unresolved Safety Issue A-46, Seismic Qualification of Equipment in Operating Plants," February 1987.

5. Senior Seismic Review and Advisor Panel (SSRAP). February 28, 1991. "Use of Seismic Experience Data to Show Ruggedness of Equipment in Nuclear Power Plants." Revision 4.

6.* Winston and Strawn; EQE Incorporated; MPR Associates, Inc., Stevenson & Associates; and URS Corporation. February 1992. "Generic Implementation Procedure (GIP) for Seismic Verification of Nuclear Plant Equipment." Revision 2, Corrected February 14, 1992.

7. U.S. Nuclear Regulatory Commission. May 1992. "Supplemental Safety Evaluation Report No. 2 on Seismic Qualification Utility Group's Generic Implementation Procedure, Revision 2, Corrected February 14, 1992 for Implementation of LG 87-02 (USI A-46), Verification of Seismic Adequacy of Equipment in Older Operating Nuclear Plants." Attachment to Supplemental No. 1 to Generic Letter (GL) 97-02.

8.* NTS Engineering and RPK Consulting. July 1991. "A Methodology for Assessment of Nuclear Power Plant Seismic Margin." Revision 1. EPRI Report NP-6041. Prepared for Electric Power Research Institute, Palo Alto, Long Beach, and Yorba Linda, CA.

9.* EQE Engineering. March 1991. "Summary of the Seismic Adequacy of Twenty Classes of Equipment Required for Safe Shutdown of Nuclear Plants." EPRI Report NP-7149. Prepared for Electric Power Research Institute, Palo Alto, CA.

10.* ANCO Engineers, Inc. February 1991. "Generic Seismic Ruggedness of Power Plant Equipment in Nuclear Power Plants." Revision 1. EPRI Report NP-5223. Prepared for Electric Power Research Institute, Palo Alto, CA.

11.* URS Corporation/John A. Blume & Associates, Engineers. June 1991. "Seismic Verification of Nuclear Plant Equipment Anchorage." Volumes 1, 2, and 3. Revision 1. EPRI Report NP-5228. Prepared for Electric Power Research Institute, Palo Alto, CA.

12.* URS Corporation/John A. Blume & Associates. June 1991. "Seismic Verification of Nuclear Plant Equipment Anchorage." Volume 4. "Guidelines for Tanks and Heat Exchangers." Revision 1. EPRI Report NP-5228. Prepared for Electric Power Research Institute, Palo Alto, CA.

13.* MPR Associates, Inc. December 1990. "Procedures for Evaluating Nuclear Power Plant Relay Functionality." EPRI Report NP-7148. Prepared for Electric Power Research Institute, Palo Alto, CA.

14.* ANCO Engineers, Inc. February 1991. "Seismic Ruggedness of Relays." EPRI Report NP-7147. Prepared for Electric Power Research Institute, Palo Alto, CA.

15.* Stevenson & Associates. December 1990. "Development of In-Cabinet Amplified Response Spectra for Electrical Benchboards and Panels." EPRI Report NP-7146. Prepared for Electric Power Research Institute, Palo Alto, CA.

16. Senior Seismic Review and Advisor Panel (SSARP). March 1, 1991. "Review Procedure to Asses Seismic Ruggedness of Cantilever Bracket Cable Tray Supports." Revision 3.

17.* EQE Engineering. March 1991. "Cable Tray and Conduit System Seismic Evaluation Guidelines." EPRI Report NP-7151. Prepared for Electric Power Research Institute, Palo Alto, CA.

18.* EQE Engineering. March 1991. "The Performance of Raceway Systems in Strong Motion Earthquakes." EPRI Report NP-7150. Prepared for Electric Power Research Institute, Palo Alto, CA.

19.* EQE Engineering. March 1991. "Longitudinal Load Resistance in Seismic Experience Data Base Raceway Systems." EPRI Report NP-7153. Prepared for

Electric Power Research Institute, Palo Alto, CA.

20.* EQE Engineering. March 1991. "Seismic Evaluation of Rod Hanger Supports for Electrical Raceway System." EPRI Report NP-7152. Prepared for Electric Power Research Institute, Palo Alto, CA.

21. Kennedy, Robert P., et al. April 1994, Natural Phenomena Hazards Design and Evaluation for DOE Facilities." DOE-STD-1020-94.

22. Eder, Stephen J. et al., November 1993, "Walkthrough Screening Evaluation Field Guide," UCRL-ID-115714 Rev. 2.

23. Westinghouse Savannah River Company, July 1994, "Procedure for the Seismic Evaluation of Piping Systems Using Screening Criteria," WSRC-TR-94-0343 Rev. B.

24. Salmon, Michael W. and Robert P. Kennedy, December 1994, "Meeting Performance Goals by the Use of Experience Data," in printing.

* Available through license.

Table 1. EPRI/SQUG Classes of Equipment

Motor Control Centers	Air Compressors
Low Voltage Switchgear	Motor-Generators
Medium Voltage Switchgear	Distribution Panels
Transformers	Batteries on Racks
Horizontal Pumps	Battery Chargers and Inverters
Vertical Pumps	Engine-Generators
Fluid-operated Valves	Instruments on Racks
Motor-operated Valves	Temperature Sensors
Fans	Instrumentation and Control Panels and Cabinets
Air Handlers	Electrical Raceways
Chillers	Tank and Heat Exchangers
and Relays , Anchorage Capacity	

Table 2. Additional Classes of Equipment Identified by DOE

Gloveboxes	Gas Bottles
HEPA Filters (and Compartment)	Other Instrumentation
HVAC Ducting (Exhaust and Fume Hood)	Communications Equipment (Emergency)
Conveyors (of material)	Computer Data/Storage
Dampers	Security Systems
Fire Suppression Systems	Architectural Items
Piping	Elevators
Tubing (for I & C)	Switchyards
Bus Ducts	Maintenance Shop Equipment
Other Tanks	Underground Conduit

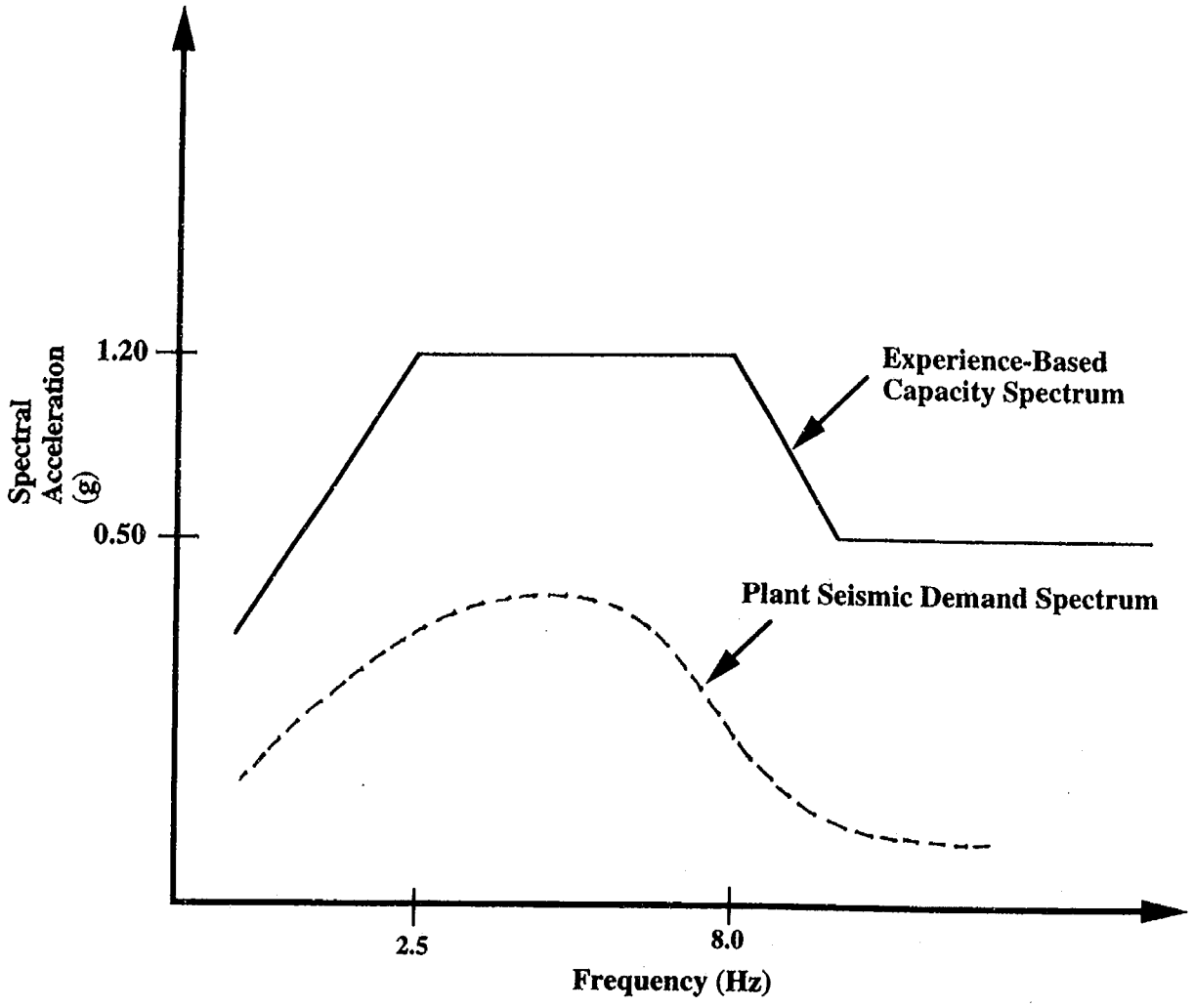
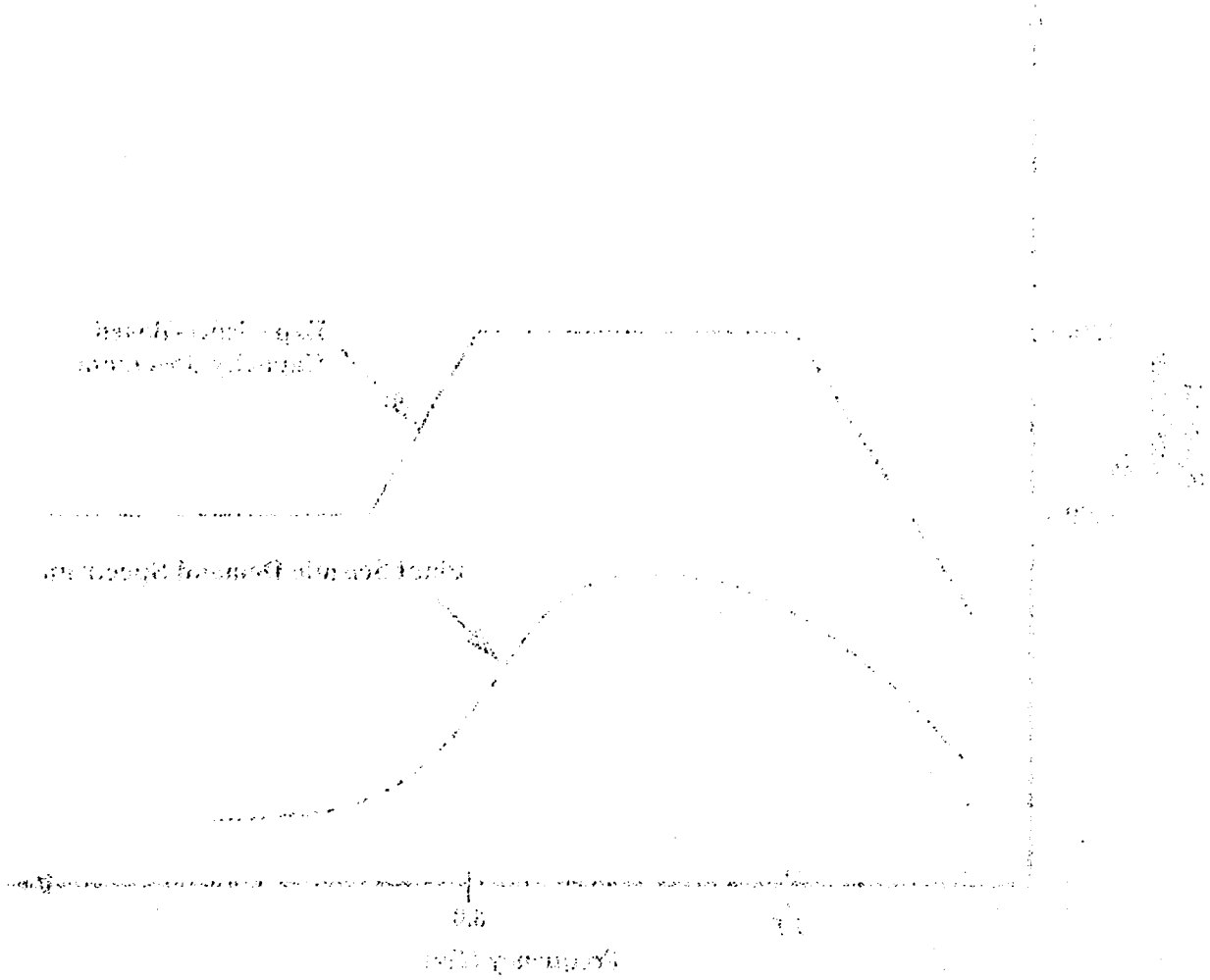


Figure 1. Demand Versus Capacity



Triaxial Upgrade of USACERL Shaking Table

by

John R. Hayes, Jr.*
and
James B. Gambill*

ABSTRACT

The U.S. Army Construction Engineering Research Laboratories (USACERL) have operated a unique biaxial shaking table, the Biaxial Shock Test Machine (BSTM), since 1972. The BSTM was originally used largely for creating high frequency and high acceleration motions that replicated weapons effect-induced ground motions for large test articles. As interest in seismic safety within the U.S. Department of Defense has increased, the use of the BSTM to perform seismic simulations for civil engineering models has grown. This paper outlines ongoing efforts to upgrade the shaking table by adding a third degree of translational capability and updating the table's electronic control and data acquisition systems.

KEYWORDS: earthquake simulation, seismic simulation, shaking table.

1. INTRODUCTION

The U.S. Army Corps of Engineers Construction Engineering Research Laboratories (USACERL) are upgrading the USACERL shaking table, the Biaxial Shock Test Machine (BSTM), from its original biaxial motion capability to a dual-capable biaxial and full triaxial earthquake simulation system, with translational capabilities in three orthogonal directions, accompanied by appropriate rotations. This paper briefly discusses the need for such research capability in the U.S., presents an overview of the events leading to the upgrade, and describes the ongoing facility development, which is planned for completion in June-July 1995.

2. REQUIREMENTS FOR EXPERIMENTAL TRIAXIAL SEISMIC SIMULATION

The primary reason for providing triaxial ground motion simulation, with independent controlled translations along and rotations about three orthogonal axes, is that seismic event observations have shown that seismic motions are random, with no definite correlation among measured orthogonal axes of motion. There frequently is not a single preferred direction for significant components of ground motion at a given site. Often accompanying the random nature of the direction and magnitude of the measured motions is randomness in the phasing and frequency of motions in different orthogonal directions. In the U.S., there has been no large or medium shaking table platform capable of producing controlled independent orthogonal motions that can faithfully reproduce the random nature of ground motions for testing structural models. Experimental efforts to simulate actual earthquake ground motions have generally centered on performing biaxial (ie translations and rotations involving the vertical axis and one orthogonal horizontal axis) tests in one of two ways: performing separate biaxial tests, one for each of two orthogonal horizontal axes of a test structure, or performing single biaxial tests in which structural models are oriented at some angle that is neither perpendicular nor parallel to the primary horizontal axis of table motion. Both procedures have shortcomings. Since construction economy dictates allowing inelastic structural behavior

* U.S. Army Construction Engineering Research Laboratories (CECER-FLE)
Champaign, IL 61826-9005

with large intensity earthquake ground motion input, the (elastic) principle of superposition does not apply. One cannot simply assume the results of separate tests conducted about a test structure's primary orthogonal axes are directly additive. Also, if a test specimen is oriented at an odd angle with respect to the table motion, while it receives motions input at angles other than one of its two primary axes, it still experiences motion input corresponding to a single axis. There is no meaningful duplication of the observed random ground motions in actual seismic events.

While rapid advances in computer hardware and software have occurred, current analytical capabilities still have serious shortcomings. Advances in nonlinear dynamic structural analysis techniques have made computer modeling more realistic and viable. However, the complexity of modeling simultaneously in the nonlinear and dynamic regimes still presents major obstacles in producing practical, design-oriented tools that can provide significant insight into post-elastic structural response to earthquake motions. Dr. Mete Sozen notes (Reference 1): "observation is still the essential ingredient in dealing systematically and confidently with materials and structural types having poorly understood behavior. Unlike forces related to gravity, earthquake forces act on structures very infrequently. While errors made in relation to gravity forces are almost immediately tested before accumulating a large inventory of vulnerable structures, errors made in relation to earthquake forces can be repeated hundreds or even thousands of times before experience reveals the error."

In Reference 1, Professor Sozen provided several noteworthy examples of structural failures in North American earthquakes that were attributed to limitations of engineers' knowledge of three-dimensional structural response to earthquake ground motions. Torsional effects were cited as primary contributions to failure of the JC Penney Department Store Building in the 1964 Anchorage, AK, earthquake, and in the Pino Suarez Building in the 1985 Mexico City earthquake. The famous "soft-story" failure of the Olive View Medical Center in the 1971 San Fernando, CA, earthquake prompted extensive post-failure analyses. The analyses did not resolve completely the reasons for the large lateral displacements associated with the failure. Subsequent thought among researchers has been that the lack of good theoretical or analytical models that consider three-dimensional response was the major reason that the analyses were inconclusive. In the 1979 Imperial County, CA, earthquake, the Imperial County Services Building in El Centro, CA, was severely damaged. It was coincidentally well-instrumented, so good estimates of actual lateral and vertical forces were available. The calculated building resistance did not correlate well with the observed failure mechanisms. As Professor Sozen has wryly pointed out, if the building had not failed, the same analyses could have been used to explain why the structure did not fail!

Such questions about fundamental knowledge continue to arise. In the 1994 Northridge, CA, earthquake, strong orthogonal ground motion components were observed, also with a strong vertical motion component. Similarly, in the 1995 Hanshin-Awaji earthquake, strong orthogonal ground motion components were observed. In both events, numerous collapses of engineered buildings occurred, leading to questions about torsional behavior of structures and the relationships among significant orthogonal ground motion components and associated structural response.

As a result of the lack of understanding about three-dimensional motion phenomena, earthquake-resistant structural design is negatively impacted in two ways. First, unexpected catastrophic failures can occur, as occurred in the 1994 and 1995 earthquakes. Second, when the poorly understood failures occur, code developers, designers, and builders adopt highly conservative construction philosophies, raising construction costs and reducing architectural and functional innovation in building design.

There is already international recognition of the need to study triaxial earthquake motion phenomena. Three-dimensional shaking tables are being operated around the world today. There are at least fourteen such facilities in Japan, the People's Republic of China, Russia, the Federal Republic of Germany, Greece, Italy, Romania, and South Korea. Japan is the international leader in this field, with several large triaxial shaking tables within its borders. Within the US research community, there is widespread conviction about the need for three-dimensional earthquake simulation, but no such capability is yet available. The University of California, Berkeley, is upgrading its shaking table to full triaxial capability at the same time that USACERL is performing its upgrade. By 1996, there will therefore be two U.S. national triaxial shaking tables. In addition, the U.S. Congress has mandated further study of the needs for large U.S. shaking table systems. The study is to be led by the National Institute of Standards and Technology.

3. A BRIEF HISTORY OF THE USACERL UPGRADE INITIATIVE

USACERL is among several laboratory organizations within the U.S. Army Corps of Engineers (USACE). Sister laboratory organizations include the U.S. Army Waterways Experiment Station (USAWES) and the U.S. Army Cold Regions Research Laboratory. USACERL performs infrastructure and environment-related research that directly supports the design, construction, maintenance and repair of conventional U.S. military facilities worldwide. Among other research mission areas, USACERL performs structural and seismic engineering research on conventional building facilities (USAWES performs seismic structural research in support of the USACE Civil Works mission).

The USACERL Biaxial Shock Test Machine (BSTM) was designed and constructed by MTS Systems Corporation in 1971. The BSTM was developed to perform shock testing of equipment intended for use in the SAFEGUARD antiballistic missile program. This dictated a number of the unique features found in the original BSTM. They provided advantages over other shaking tables for simulating the weapons effect-induced ground motion environment that was postulated for threats to the SAFEGUARD system, but there were also some limitations imposed on the system capabilities insofar as earthquake ground motion simulation was concerned. The BSTM has relatively high frequency and high acceleration capabilities for large payloads, but these were somewhat offset in the seismic environment by relatively small displacement ("stroke") capabilities and associated velocity limitations. In recent years, the emphasis on weapons effect research has lessened, while there has been growing concern within the U.S. government over the potential vulnerabilities of federal and other facilities to the effects of major earthquakes. In December 1994, for example, President Clinton signed a federal Executive Order mandating that all federal agencies assess seismic vulnerabilities in their existing buildings and develop cost estimates for mitigating the vulnerabilities. For the past five years, USACERL has had an Army-funded research program to study the seismic vulnerabilities of, and possible rehabilitation techniques for, existing military facilities. The majority of these facilities are very "conventional" in their construction details; they closely resemble their non-military counterparts. As engineers at USACERL became more aware of this, it became obvious that the Army research program could benefit immensely from close cooperation with other federal research agencies (principally NIST), the U.S. university research community, especially the University of Illinois at Urbana-Champaign (UIUC), and, to a lesser extent, the private sector. USACERL was originally sited in Champaign largely because of its close proximity to the UIUC and its world-renowned civil engineering research talents.

USACERL engineers began discussing renewed seismic research cooperation with UIUC researchers in 1988; there had been close cooperation in the 1970's. It was clear that

USACERL could gain much from close partnership with UIUC in this area; UIUC researchers were in turn interested in the applied perspective of the USACERL program and the mutual development of the BSTM, with associated research programs. Professors Mete Sozen (now at Purdue University) and William Hall supported the partnership concept and were involved in subsequent initiatives. Professor Sozen had initially proposed an upgrade of the BSTM to a three-dimensional "Earthquake Simulation System" in 1986. With the renewed interest in research cooperation, USACERL hosted a workshop in 1990 to address the use and possible upgrade of the BSTM. The workshop involved federal engineers from various agencies (eg National Science Foundation, National Institute of Standards and Technology), university researchers (including the National Center for Earthquake Engineering Research), and a small number of engineers from the US private sector. The workshop panelists made a number of recommendations concerning the BSTM (Reference 2). There were two key recommendations. First, USACERL should pursue a general upgrade of BSTM system capabilities and specifically pursue upgrading the BSTM to a triaxial configuration, without sacrificing any of the original BSTM high frequency, high acceleration capabilities. Second, USACERL should develop closer partnerships with other research organizations, particularly the UIUC and other members of the university community.

In January 1991, USACERL hosted another workshop, a meeting of researchers from UIUC, the University of Michigan, the University of Minnesota, and the University of Texas at Austin, to discuss forming a consortium of institutions located in regions of generally low to moderate seismic risk; the consortium would focus primarily upon experimental seismic structural engineering research. These institutions all had active experimental research programs, with common concerns about the need for research addressing the needs of regions where large magnitude earthquakes are known to be infrequent, hence resulting in less stringent building code requirements than for more active regions. All of the university representatives at the initial and subsequent meetings endorsed the consortium concept and, in parallel, a pursuit of a triaxial upgrade for the BSTM, with future joint usage in cooperative research projects. Since then, four additional institutions, Purdue University, Memphis State University the University of Washington and the University of Toronto, have joined; the consortium is now informally known as the Mid-America Consortium for Earthquake Hazard Reduction (MACEHR). It is important for the reader to note that MACEHR is an informal collective of engineers with common interests and research goals. It is not a formal organization, and "members" do not currently plan to formalize the organization or exclude others who may wish to "join." The general thought has been that the consortium will become active with the opening of the upgraded USACERL shaking table facility.

USACERL also pursued the first recommendation, that of upgrading the BSTM to a true six degree-of-freedom triaxial configuration. USACERL submitted a proposal to the US Army for funding of a proposed upgrade for the BSTM. The Army funded the upgrade in 1993. USACERL issued a competitive request for contractor proposals for performing the upgrade in early 1993. In September 1993, after its engineers reviewed the contractor proposals that were submitted, USACERL awarded a contract for the upgrade project to MTS Systems Corporation. In the contract solicitation, USACERL set a number of key performance requirements and allowed the contractors to propose specific technical configurations for meeting the performance requirements. The required performance characteristics for the upgraded shaking table were developed cooperatively by USACERL and the initial MACEHR members; the characteristics represented a consensus of practical modifications that could be implemented without severe cost penalties.

4. ORIGINAL BSTM CAPABILITIES

A brief description of the original facility will establish a baseline for detailing the upgrade. References 2 and 3 provide detailed overviews of the original operating characteristics, which are summarized here. When the upgrade project is completed, the basic dynamic characteristics of the original system will become the "BSTM Mode" of the upgraded system.

Figures 1 and 2 present traditional log-log "tripartite" plots of the performance envelopes of the BSTM. Figure 1 shows vertical performance, while Figure 2 shows performance for the one original horizontal axis of motion. Maximum velocity for both axes of motion is 30 inches per second (76 cm/sec). For a nominal 12,000 pound (5,450 kg) payload, the maximum rated vertical acceleration is 30 g, while the maximum rated horizontal acceleration is 20 g. The table is capable of testing larger payloads at corresponding lower peak accelerations. The 60,000 pound (27,240 kg) payload acceleration plotted is not the table payload limit; it is the largest payload tested to date. For smaller payloads, the BSTM has proven to be controllable over a frequency range of 0-600 hz.

The test platform is a twelve foot (3.66 m) square aluminum weldment with an internal cellular construction; the platform combines light weight with high stiffness. It weighs approximately 12,000 pounds (5,450 kg) and has a first natural frequency near 200 hz. A total of 15 electrohydraulic actuators is used to drive the table in the BSTM mode. Nine vertical actuators provide a total force of 810,000 pounds (367,700 kg); six horizontal actuators provide a total force of 450,000 pounds (204,300 kg). Vertical stroke range is 2.75 inches (7 cm), while horizontal stroke range is 5.5 inches (14 cm), measured peak-to-peak. Separate vertical and horizontal concrete reaction masses are used, with a combined weight of about 4,000,000 pounds (1,816,000 kg).

The original BSTM was controlled by a predominately analog system. It controlled each actuator individually with a separate closed-loop control circuit consisting of three integrated feedback loops. By interconnecting the control loops of the 15 actuators, five degrees of freedom were controlled: vertical translation, horizontal translation, roll, pitch, and yaw. Lateral displacement was passively restrained by spherical hydraulic bearings attached to the horizontal reaction mass. The analog system also controlled several other parameters: force balancing, overshoot and ringing, stabilization, model center of gravity effects, and actuator cross-coupling.

A minicomputer-based digital system was used to generate test time-history waveforms. While antiquated by today's standards, It was flexible and could be used to generate shock, seismic, random vibration, sine sweep, and a variety of other waveforms. The original data acquisition system was a 60 channel modular signal conditioning system which recorded to a 70 channel magnetic tape recorder. USACERL acquired 64 channels of microcomputer-based digital data acquisition and has access to 64 more such channels at the UIUC. The digital system has served as the primary data acquisition system for the past several years.

5. TRIAXIAL UPGRADE PROJECT

During the original discussions among the engineers involved in the proposed upgrade, two overriding philosophies prevailed. First, given budgetary constraints, building a new triaxial test facility was not considered possible; modifying the existing facility was seen as the only realistic option. Second, while the goal was to develop a capable triaxial earthquake simulation system, USACERL engineers had to maintain the existing BSTM-mode capabilities. As mentioned above, the first upgrade proposal was developed in 1986. In that proposal, for the "Triaxial Earthquake Simulation System (TESS)," the envisioned triaxial configuration had two alternatives, based on a 60,000 pound (27,240 kg) payload: 1.7 g peak acceleration, or 3.4 g peak acceleration, in

each of the two horizontal axes. The existing biaxial performance envelopes would have been maintained, but manual switching of system valving would have been required in changing from biaxial to triaxial test configurations.

USACERL and other MACEHR engineers developed a new consensus performance requirement for the triaxial upgrade that balances performance and economy. The upgrade will provide a triaxial capability as shown in the tripartite plot of Figure 3. The existing BSTM-mode capability will be maintained, and it will be transparently run through the new system control software and hardware. In the Triaxial Earthquake Simulation (TES) mode, both axes of motion will have peak acceleration capabilities of 2.0 g, for a 120,000 pound (54,480 kg) specimen; the existing horizontal axis will still have a 5.5 inch (14 cm) stroke, while the new horizontal axis will have a twelve inch (30.5 cm) stroke, measured peak-to-peak. Detailed performance requirements are shown in Table 1 (Reference 5). Figure 4 (Reference 5) presents a plan view of the proposed new configuration.

Key features of the proposed upgrade are discussed in References 4 and 5. A number of preliminary analyses were performed to validate the conceptual framework of the features. Several of the more significant factors involved in the upgrade are listed briefly below.

To balance economy with functionality, blowdown accumulators will provide peak forces for table motion. A study of the sustained pumping capacity needed to provide the peak performance indicated that both the initial acquisition cost and the operating cost would be high. MACEHR engineers arrived at a 10 second requirement for peak force capability; for such a time period, accumulators provide an economical alternate solution (this is consistent with the current operational concept for the BSTM). Both 48 new high pressure accumulators and some of the original accumulators are being used to develop the required dynamic forces.

The new axis of motion necessitates a number of major modifications to the existing table, mechanical system, and foundation. A single new horizontal actuator is being added on each appropriate side of the table (see Figure 4). The table itself will require slight structural modification; the existing slide bearing mounting plates will be used to accommodate attachment points for the new actuators. A finite element analysis of the original table in its new configuration, with emphasis on the lateral actuator mounting areas and specimen tiedown insert regions, was performed to ensure that the new forces would not pose problems for the structure. In addition, MTS engineers performed a nondestructive evaluation of the platform's condition using visual, penetrant, and ultrasonic testing; this evaluation showed no fatigue problems in either the base metal (aluminum alloy 5083-0) or the welds.

The table is essentially surrounded at surface level by the horizontal reaction mass. This reaction mass is reinforced with both deformed bars and post-tensioning rods. Creating access boxes for the new horizontal actuators has required cutting some of the existing bars, but not the rods. The reinforcement was originally configured primarily to prevent fatigue failure of the concrete, not to accommodate high service stresses. Detailed finite element analyses of the original reaction masses as modified to accommodate the new system indicate reinforcing the mass to offset the loss of the bar continuities was needed but not difficult to accomplish. Large steel reinforcements are being installed around the perimeters of the access box cutouts. The swivels on all 15 existing actuators are being replaced with new swivels that can accommodate the more substantial angular movement that will be associated with the added translation.

Complete new analog-digital controls and digital data acquisition systems are being installed. The shaking table system will be driven by an MTS 469 six degree-of-freedom, three variable analog control system. The required total digital sampling throughput rates for both the BSTM

(204-306 kHz) and the TES (20.4-30.6 kHz) were too large to be accommodated by today's direct digital control architectures, necessitating the use of the analog system. An MTS 468 digital-analog, analog-digital interface system will link Digital Equipment Corporation (DEC) minicomputers to the 469 system, so that the user will "see" a digital control system that is clear and straightforward. Two DEC minicomputers will be used on the front end. A DEC VAXserver 4000 will serve as the digital controller, with a VAXstation 4000 graphics workstation used as the direct user interface. The MTS Seismic Test Execution (STEX) software package will be used for creating and executing test profiles, performing data acquisition, and performing data analysis. The STEX software is being modified by MTS to accommodate both the BSTM and TES operating modes. The initial integrated data acquisition capability will accommodate 128 channels of instrumentation; anti-aliasing filters and analog-digital converters are being provided. The data acquisition system will be expandable to as many as 512 channels for potential future expansion. Total throughput to disk will be 50,000 samples per second for the basic 128 channel system. This electronic system is quite similar to the system that MTS installed on the Kumagai-Gumi Corporation shaking table in Ibaraki-ken, Japan, in 1988.

Before the start of the upgrade project, several dynamic tests were conducted with the BSTM to analyze critical performance characteristics associated with the triaxial configuration. The tests focused upon the friction in the actuation and restraint systems, oil column resonant frequencies, friction and resonance effects on the acceleration waveforms, overturning moment restraint stiffness and capacity, and foundation response to dynamic input. A stringent series of post-installation performance tests will be conducted by USACERL and MTS engineers to ensure that all dynamic performance criteria are met, for both operating modes.

Paralleling the shaking table improvements, USACERL has enlarged the shaking table test high bay building by 50% over its 1972 size and has provided air-conditioning. Both of these improvements were undertaken to improve test specimen fabrication capabilities and experimental control. Office space is being set aside for guest researchers to use.

As was mentioned above, USACERL initially awarded the upgrade contract to MTS in September 1993. MTS engineers disassembled the old BSTM system in April and May 1994. MTS engineers are now installing the new system components. All new pumps and accumulators are installed as of this writing, as are many of the new hydraulic hard line components. With system installation proceeding rapidly, USACERL expects the upgraded system to be operational in the summer of 1995.

7. PROPOSED FUTURE ACTIVITIES

Predominant thought within the MACEHR consortium is that the upgraded capability will lend itself best to proof testing of scaled models of structures and their components. USACERL and partner consortium members have considered a number of initial research thrusts for the proposed facility. USACERL's current primary focus is in the rehabilitation of existing reinforced concrete and masonry structures. The U.S. military has an abundance of existing "nonductile" structures that likely will require seismic rehabilitation in response to the recently signed Executive Order, so Army-sponsored research is likely to continue in this area. This is consistent with other MACEHR members' desires to study reinforced concrete frame-wall structures. They cite (Reference 1) recent joint US-Japan studies on a seven-story structure at Tsukuba Research Laboratory. Predicted and measured base shears in the structure differed significantly. Subsequent small-scale model tests of the same configuration at the University of California, Berkeley, and at UIUC, raised many questions about dynamic behavior of the structure under imposed biaxial horizontal and vertical motions. Therefore, a probable early test series might involve a replica of the Tsukuba structure at approximately 1/5

scale. Complementing such a model structure test series would be a number of component tests to study fundamental behavior. In particular, the behavior of columns under imposed biaxial horizontal motion would be a significant test initiative; both bending hysterisis and shear would be studied.

MACEHR members also propose (Reference 1) to study torsional-translational behavior of braced steel moment frames; the results of using irregularly-shaped framing systems in regions of low to moderate seismicity; torsional effects due to structural and mass eccentricities in composite steel-concrete systems; out of plane response of masonry systems, particularly unreinforced masonry in regions of low to moderate seismicity; diaphragm action in steel joist roof systems used in regions of low to moderate seismicity; connection details in precast and prestressed concrete structures, and both passive and active structural control systems.

USACERL tentatively plans to initiate a four year study of earthquake-induced triaxial and torsional effects in building structures in 1996. USACERL engineers will be seeking partnerships with other research institutions as this work commences. USACERL engineers and NIST engineers are also studying means by which they can enhance their research cooperation.

USACERL is a U.S. federal research institution. The new shaking table facility is available for use on a cost-reimbursable basis by anyone in the U.S., within minor limitations imposed by the US Army. Plans outlined herein involve MACEHR member institutions because of the common interests shared by all. The USACERL staff will welcome the opportunity to work with other institutions as well.

8. REFERENCES

1. Sozen, MA (1992), "Three-Dimensional Earthquake Simulator."

2. Hayes, JR, Gambill, JB, Wilcoski, J, Brady, PA, and Al-Chaar (1991), G, "Use and Upgrade of the USACERL Biaxial Shock Test Machine: Workshop Summary," USACERL Special Report M-91/20.

3. Fisher, WE, and Gambill, JB (1983), "Vibration Table Shakes Flaws from Equipment," Industrial Research & Development..

4. MTS Systems Corporation (1993), "A Proposal for the Triaxial Upgrade of the USACERL Biaxial Shock Test Machine (BSTM)."

5. Wood, SL (1992), "Biaxial Shock Test Machine Upgrade Design Study," University of Illinois.

6. MTS Systems Corporation (1994), "Existing Welded Aluminum Shaking Table Platform: Lateral Modification Analyses, Design Calculations, Test Results, and Shop Drawings for the USACERL Contract."

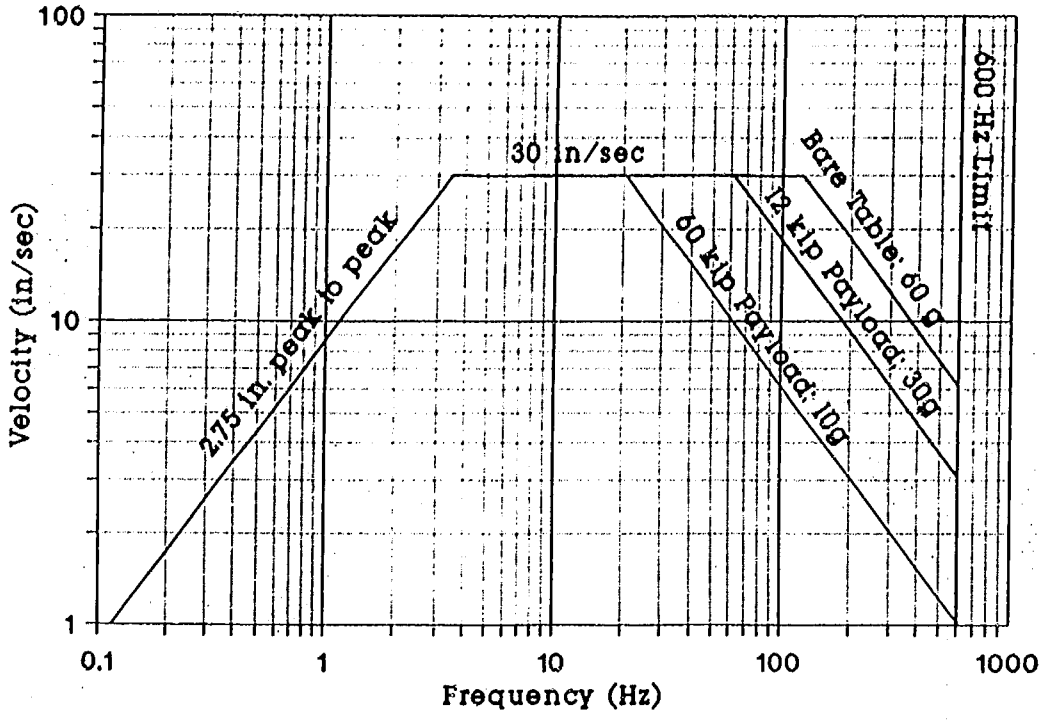


Figure 1. USACERL BSTM - Existing Vertical Performance

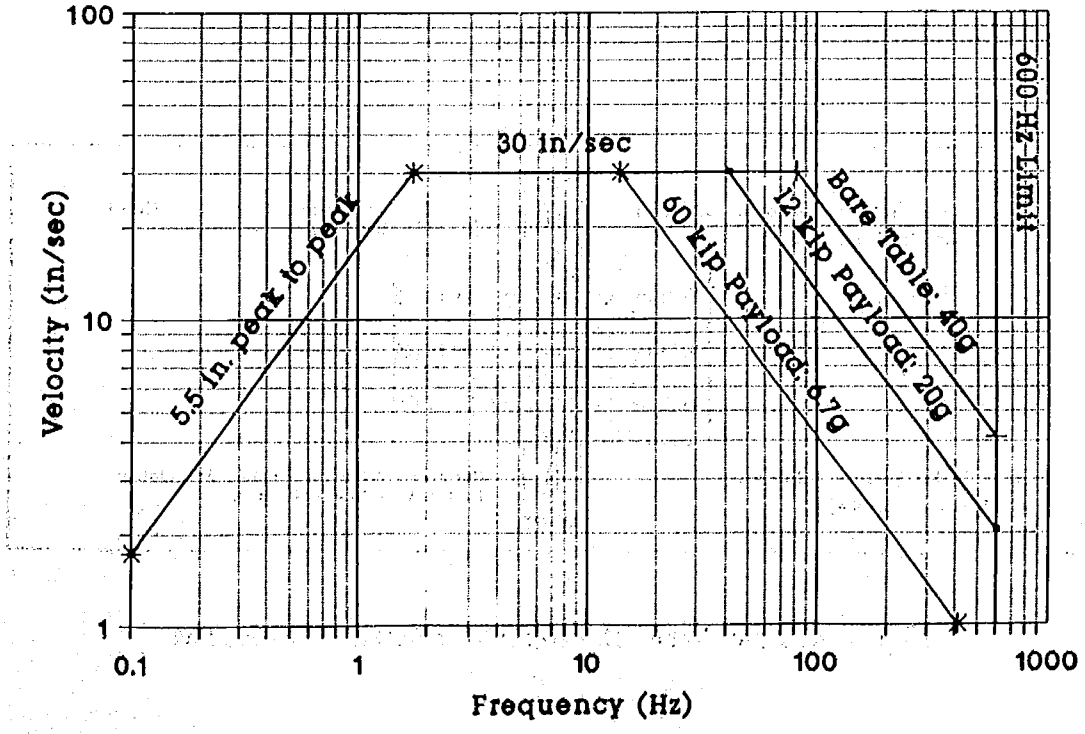


Figure 2. USACERL BSTM - Existing Horizontal Performance

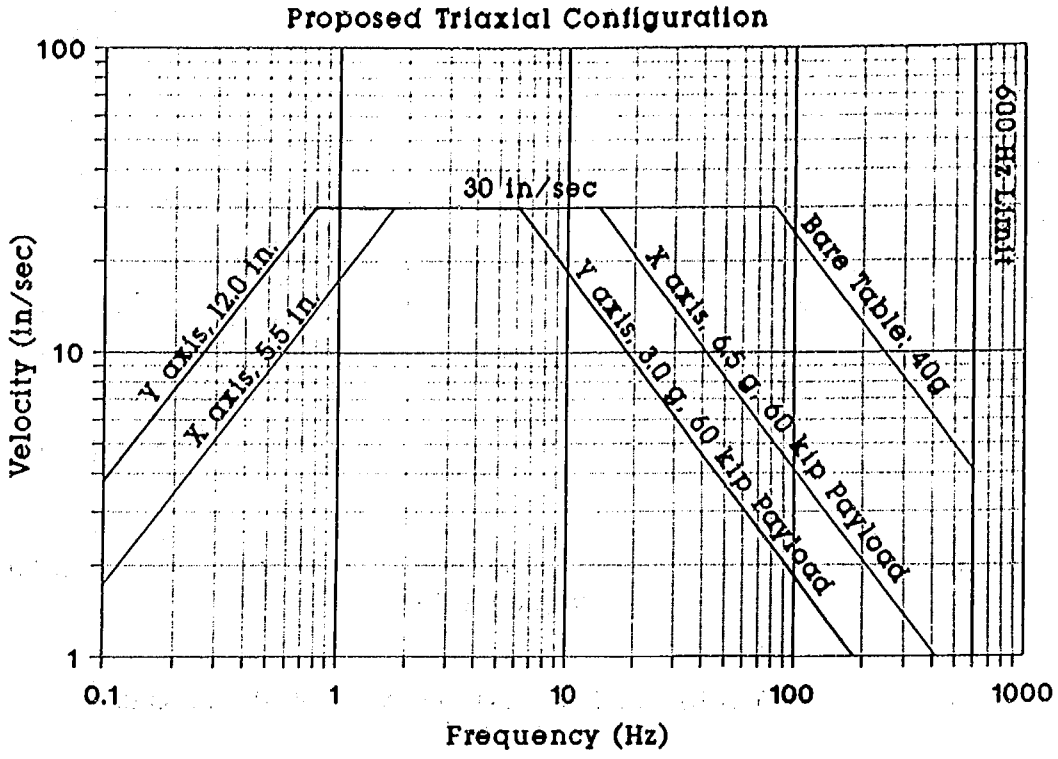


Figure 3. USACERL BSTM Upgrade - Horizontal Performance

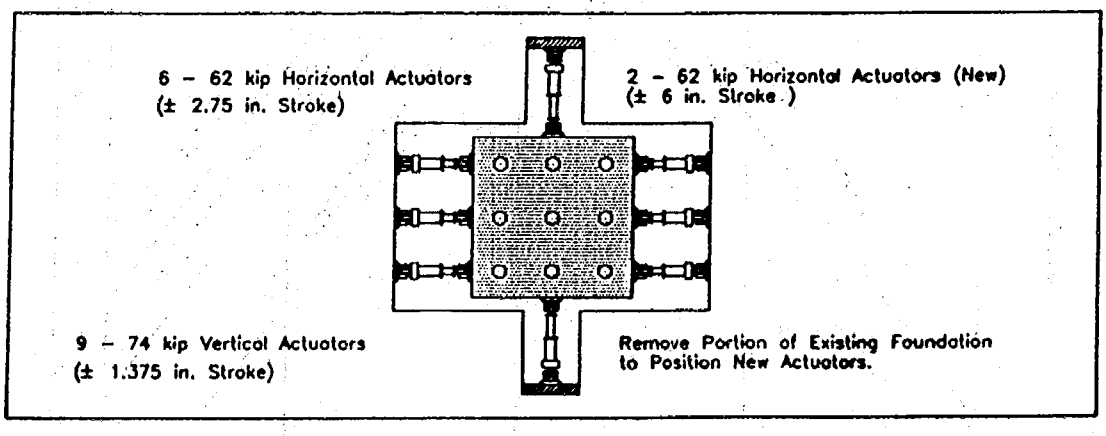
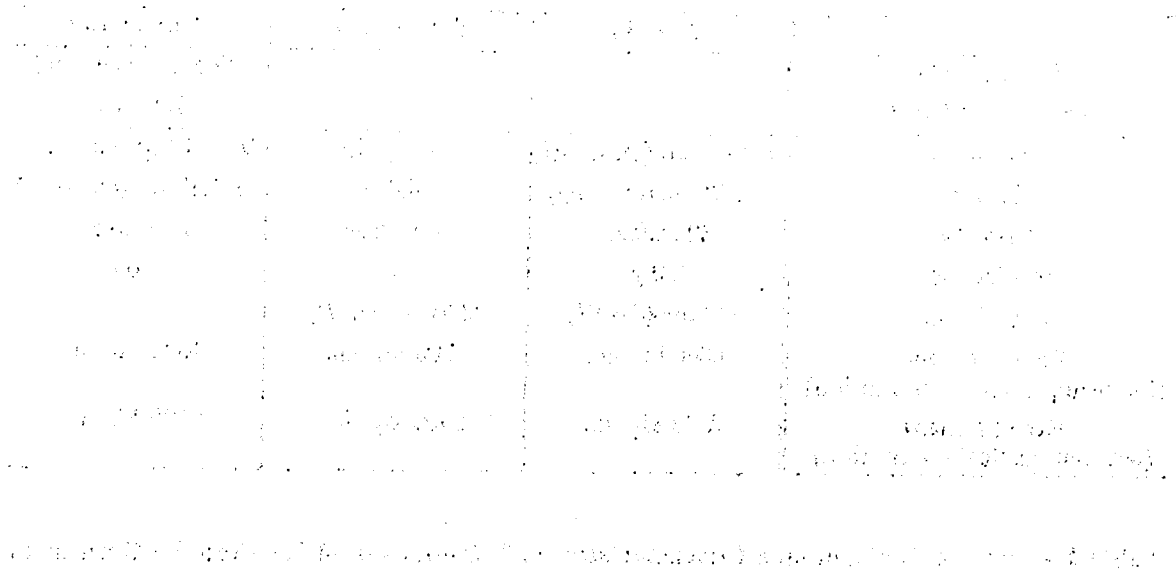


Figure 4. Plan View of Proposed Revisions to BSTM

	X direction	Y direction	Z direction
Table Weight			12 kips (existing)
Specimen Weight			120 kips
Actuators	6 – 62 kip (existing)	2 – 62 kip	9 – 74 kip (existing)
Stroke	± 2.75 in. (existing)	± 6.0 in.	± 1.38 in. (existing)
Velocity	30 in./sec	30 in./sec	20 in./sec
Acceleration	2.0 g	2.0 g	1.0 g
Base Shear	72 kips (0.6 W)	72 kips (0.6 W)	
Base Moment (including vertical eq. motion)	6000 kip–in.	6000 kip–in.	4000 kip–in.
Base Moment (without vertical eq. motion)	8500 kip–in.	8500 kip–in.	6000 kip–in.

Table 1 – Desired Performance Characteristics of 3–Dimensional Earthquake Simulator



Seismic Response Properties of Concrete Gravity dam with Interaction of Dam and Foundation Rock

by

Isao NAGAYAMA[1], Takashi SASAKI[2]

ABSTRACT

The dynamic response of a dam and foundation system to earthquakes is computed by the modal analysis technique. The following response properties of a dam are obtained from the analysis.

(1) Resonant frequency of a dam decreases when the elastic modulus of foundation rock decreases.

(2) The acceleration at the crest of a dam decreases when the elastic modulus of the foundation rock decreases.

(3) The vertical stress of the heal of a dam due to earthquake is not so influenced by the interaction of a dam and foundation.

Key Word : Concrete Gravity Dam, Dam- Foundation Interaction, Resonant Frequency

1. INTRODUCTION

Seismic design of dams in Japan is based on the seismic coefficient method. The earthquake resistance of the dams designed by this method is reliable because dams have never been severely damaged by earthquakes. But the uniform distribution of acceleration in a dam body which is assumed by the seismic coefficient method differs remarkably from the observation records of actual dams during earthquakes and it is therefore necessary to establish a more reasonable seismic design method to confirm the dam safety during earthquakes.

To compensate for such defects in the seismic coefficient method, the dynamic analysis is conducted in the large and important dams. The dynamic analysis is believed the best way to assess the earthquake resistance of the dam. But because of its complex procedures, it is not a suitable way to determine the economical cross- section of a dam in its design. Consequently, the simplified seismic design method that can account for the dynamic response properties of a dam should be developed.

The modified seismic coefficient method is one of the rational seismic design methods, where the distribution of the seismic coefficient of a dam is defined in accordance with the dynamic response properties of a dam. The authors have already proposed the modified seismic coefficient method of concrete gravity dams (Nagayama, 1988). The authors have also conducted a study of the dynamic response of a concrete gravity dam accounting for the interaction between a dam and its reservoir (Nagayama et al, 1991). But in these cases, foundation rock was assumed a rigid body. Consequently, the dynamic analysis of a concrete gravity dam which accounts for the deformability of foundation rock is performed in this paper.

2. METHOD OF ANALYSIS

2.1 Model Dam and Boundary Condition of Foundation Rock

The 150m high concrete gravity dam with a vertical upstream slope and a downstream slope of 0.8 to 1 on 150m thick rock stratum is used in the analysis as shown Figure 1. The rock stratum is assumed uniform and homogeneous elastic body.

---

1) Head, Dam Structure Division, Dam Department, Public Works Research Institute, Ministry of Construction, Tsukuba Science City, 305 Japan

2) Research Engineer, ditto

In the analysis using the Finite Element Method, two models are used. One is a finite rock mass model with horizontally free and vertically fixed boundaries at the both sides and the other is an infinite rock mass model with transmission boundaries (Lysmer and Drake 1972). Figure 2 shows the concept of these two models with a conventional model without foundation.

Firstly, the results of the response properties of the dam by earthquakes for these two model was analyzed, and then stress response in the dam with deformable foundation was analyzed using the finite rock mass model. The effect of a reservoir was not included in this analysis because it had been already studied in the former paper (Nagayama et al, 1991).

2.2 Vibration Equation

The vibration equation of a dam-foundation system is expressed as follows:

$$[M]\{\ddot{u}\}+[C]\{\dot{u}\}+[K]\{u\} = -[M]\{i\}a(t)+\{p(t)\} \quad (1)$$

where, $\{u(t)\}$ is the relative displacement of the dam and the foundation, $a(t)$ is acceleration at the base of foundation, $\{i\}$ is the direction vector of the earthquake motion, $[M]$, $[C]$ and $[K]$ are the mass, damping and stiffness matrices respectively, and $\{p(t)\}$ is the virtual force acting on transmission boundaries. In the case of the modal analysis, transmission boundary technique cannot be used and $\{p(t)\}$ becomes 0.

2.3 Frequency Response Function of Displacement, Acceleration and Stress

When the input acceleration $a(t)$ is the harmonic vibration $a_0\exp(j\omega t)$, the solution of Equation (1) in the case $\{p(t)\}=0$ is expressed by

$$\{u(t)\}=\{Yu(\omega)\}a_0\exp(j\omega t) \quad (2)$$

where $\{Yu(\omega)\}$ is called the frequency response function of the relative displacement.

Then, the dynamic response of the absolute acceleration $\{z(t)\}$ and the stress $\{\sigma(t)\}$ in the dam are expressed by

$$\{z(t)\}=(\{i\}-\omega^2\{Yu(\omega)\})a_0\exp(j\omega t) \quad (3)$$

$$\{\sigma(t)\}=[E][B]\{Yu(\omega)\}\,a_0\exp(j\omega t) \quad (4)$$

where $[E]$ and $[B]$ are the strain-stress conversion matrix and the displacement-strain conversion matrix respectively. From Equation (3) and Equation (4), the frequency response function of the absolute acceleration $\{Ya(\omega)\}$ and the frequency response function of the stress $\{Y\sigma(\omega)\}$ can be defined as follows:

$$\{Ya(\omega)\}=\{i\}-\omega^2\{Yu(\omega)\} \quad (5)$$

$$\{Y\sigma(\omega)\}=[E][B]\{Yu(\omega)\} \quad (6)$$

2.4 Modal Analysis Technique

According to the modal analysis technique, the relative displacement $\{u(t)\}$ can be expressed as the superposition of vibration modes of relative displacement $\{us\}$, that is,

$$\{u(t)\}=\sum_s \beta si\{us\}\,\phi s(t) \quad (7)$$

$\{us\}$ is the eigen vector derived from the following equation.

$$[K]\{u\}=\omega^2[M]\{u\} \quad (8)$$

And βsi is expressed by the following equation and is called the s-th modal participation factor.

$$\beta si = \frac{\{us\}^T[M]\{i\}}{\{us\}^T[M]\{us\}} \quad (9)$$

Then $\phi s(t)$ is the solution of the following equation and is called the s-th normal coordinate.

$$Ms\,\ddot{\phi}+Cs\,\dot{\phi}+Ks\,\phi = -Ms\,a(t) \quad (10)$$

where

$$\left.\begin{aligned} Ms&=\{us\}^T[M]\{us\}\\ Cs&=\{us\}^T[C]\{us\}=2h(\omega s^2/\omega)Ms\\ Ks&=\{us\}^T[K]\{us\}=\omega s^2 Ms \end{aligned}\right\} \quad (11)$$

In Equation (11), ωs is the eigen value of Equation (8) and is called the s-th natural circular frequency and h is called the hysteresis damping constant.

Then, the relative displacement expressed by Equation (2) can be rewritten by

$$\{u(t)\}=\sum_{s}\beta si\{us\}Rs(\omega)a_0\exp(j\omega t) \quad (12)$$

where $Rs(\omega)$ is called the s-th frequency response function of the relative displacement and is expressed by

$$Rs=\frac{-1}{\omega s^2-\omega^2+2jh\omega s^2} \quad (13)$$

As the result, the frequency response functions of the relative displacement, the absolute acceleration and the stress are expressed as follows:

$$\{Yu(\omega)\}=\sum_{s}\beta si\{us\}Rs(\omega) \quad (14)$$

$$\{Ya(\omega)\}=\{i\}-\omega^2\sum_{s}\beta si\{us\}Rs(\omega) \quad (15)$$

$$\{Y\sigma(\omega)\}=\sum_{s}\beta si\{\sigma s\}Rs(\omega) \quad (16)$$

In Equation (16), $\{\sigma s\}$ is defined as the s-th vibration mode of stress in this paper, and is obtained by

$$\{\sigma s\}=[E][B]\{us\} \quad (17)$$

2.5 Solution for Model with Transmission Boundaries

In Figure 2(b), the rock mass under the dam is called Internal Domain I, and left and right side ares of this rock mass is called External Domain L and External Domain R respectively.

Considering the apparent nodal force $\{p_L(t)\}$ and $\{p_R(t)\}$ acting on the interface between Domain I and Domain L / R respectively, the vibration equation is expressed as follows (Lysmer and Drake 1972, Shimizu et al. 1975):

$$[M]_I\{\ddot{u}\}_I+[C]_I\{\dot{u}\}_I+([K]_I+[L]_L+[R]_R)\{u\}_I=-[M]_I\{i\}a(t)+([L]_L-[D]_L)\{u\}_L+([R]_R-[D]_R)\{u\}_R \quad (18)$$

The first term of the right side of equation expresses the force produced by the acceleration from the base of Domain I, the second and third terms express the apparent forces transmitted from Domain L and Domain R. And $[L]_L$ and $[R]_R$ are the dynamic boundary stiffness matrices and $[D]_L$ and $[D]_R$ is the static boundary stiffness matrices, and $\{u\}_L$ and $\{u\}_R$ are the displacement solution for the External Domain L and External Domain R obtained from

$$[M]_L\{\ddot{u}\}_L+[C]_L\{\dot{u}\}_L+[K]_L\{u\}_L=-[M]_L\{i\}a(t) \quad (19)$$

$$[M]_R\{\ddot{u}\}_R+[C]_R\{\dot{u}\}_R+[K]_R\{u\}_R=-[M]_R\{i\}a(t) \quad (20)$$

3. COMPARISON OF RESULTS OF ANALYSIS BETWEEN TWO ROCK MASS MODEL

3.1 Analytical Condition

Firstly, the results of the analysis of two rock mass models (that is, the finite rock mass model and the infinite rock mass model with transmission boundaries) are shown.

The horizontal harmonic vibration is inputted at the base of the rock mass and the absolute acceleration of the crest of the dam and the stress at the heel of the dam are compared.

The physical properties used in the analysis is shown in Table 1. The hysteresis damping constant was assumed 10%.

Table 2 shows the analytical technique and the boundary condition used for each model. The first 10 vibration mode are included in the modal analysis.

3.2 Results from Finite Rock Mass Model

Figure 3 shows the first 6 vibration modes of the relative displacement obtained from the modal analysis for the finite rock mass model. Here, the relative displacement is normalized so that the maximum displacement becomes 1. The participation factor for each mode βsx (Index "x" expresses the horizontal direction. The positive direction is the downstream direction.) also shows in the figure. It is evident that

the effect of the 1st and 2nd vibration modes is predominant. It is considered from the figure that the 1st mode conforms basically to the vibration of the dam and that the 2nd mode conforms the combination of the vibration of the dam and the rock mass. The benefit of modal analysis is that the features of the vibration of the structure system is easily visible in this way.

Figure 4 shows the response spectrum of the vertical stress at the heel of the dam. The figure shows the response of stress for the first 2 vibration modes and the superimposed stress response of 10 vibration modes. It is evident that the influence of the first 2 vibration modes is predominant and that the two peaks of the superimposed response spectrum is almost the same as that of the 1st and 2nd vibration modes respectively.

3.3 Comparison of Results of Two Rock Mass Models

a) Response Spectra of Absolute Acceleration and Stress

Figure 5 shows the response spectrum of the absolute horizontal acceleration at the crest of the dam. Figure 6 also shows the response spectrum of the vertical stress at the heel of the dam. The solid line shows the result from finite rock mass model and the dotted line shows the result from the infinite rock mass model. It can be said that two spectra have relatively good correspondence, but that the peaks of the spectrum at the first 2 resonant frequencies for the finite rock mass model is smaller than those of the infinite rock mass model.

b) Response Properties for Acceleration of Dam Base

It is difficult to know the actual acceleration of the base of the rock mass and the available data is generally at the surface of the rock mass or the base of the dam. Then, the results of Figure 5 and Figure 6 has been reviewed from this point. That is, the basis point of acceleration is adopted at the upstream edge of the interface between the dam and the rock mass, and Figure 5 and Figure 6 are replotted as the response spectra to the acceleration at this basis point. In this case, the response spectrum is defined by

$$Xa(\omega) = \frac{Ya(\omega)c}{Ya(\omega)b} \tag{21}$$

$$X\sigma(\omega) = \frac{Y\sigma(\omega)c}{Ya(\omega)b} \tag{22}$$

where, th index "c" expresses the point of concern and the index "b" expresses the basis point (the upstream edge of the interface between the dam and rock mass). The results are shown in Figure 7 and Figure 8. After these processes, the response spectrum for the infinite rock mass model and the response spectrum for the finite rock mass shows good coincidence. It is therefore justified that the modal analysis of the dam with finite rock mass is utilized in the evaluation of effect of the deformability of the rock mass on the dynamic response of the dam during earthquakes.

It should be noted that the frequency which provides the peak of response spectrum in Figure 7 and Figure 8 is different from that of Figure 5 and Figure 6. Therefore, the frequency for the peak response in the following discussion is called as the "peak frequency".

4. CHANGE IN DYNAMIC RESPONSE OF DAM DURING EARTHQUAKES CAUSED BY DEFORMABILITY OF ROCK MASS

4.1 Analytical Cases

In view of aforementioned conclusion, the modal analysis technique is used in the following analysis. The response spectrum is plotted for the acceleration at the heel of the dam in the analysis.

Table 3 shows the analysis cases which are conducted in this study. The ratio of elastic moduli of rock mass and concrete of the dam is selected as ∞, 1/1, 1/5 and 1/10. It was revealed that the influence of the high vibration modes become larger as the elastic modulus of the rock mass become lower, and then the higher vibration modes were included in such a case (see Table 3).

4.2 Response of Absolute Acceleration at Crest of Dam

Figure 9 (a) shows the magnitude of the response spectrum of the absolute horizontal acceleration at the crest of the dam, and Figure 9 (b) shows the phase delay of the acceleration at the crest of the dam for the acceleration at the heal of the dam. It is evident in the figure that the peak frequency and peak value of the response spectrum decrease when the elastic modulus of the rock mass decreases (It should be noted that the decrease of peak of response spectrum is numerically equivalent to the increase of the damping constant). It is also revealed that the delay of phase is almost 90° when the response acceleration is the maximum.

It should be also added that the first peak frequency is located between the 1st and 2nd resonant frequencies.

4.3 Response of Vertical Stress at Heel of Dam

Figure 10 (a) shows the magnitude of the response spectrum of the vertical stress at the heel of the dam. Figure 10 (b) shows the phase delay of vibration of stress for the acceleration at the heal of the dam. The peak frequency for the maximum response of vertical stress is the same as that for maximum response of acceleration at the crest of the dam. The phase delay of vibration when the maximum stress response is - 90° (90° ahead). It means that the vertical stress becomes the maximum when the acceleration at the crest of the dam becomes the maximum to the upstream direction (the deformation become the maximum to the downstream direction).

It is also evident in the figure that the maximum response of the vertical stress is almost the same level although the ratio of the elastic moduli of rock mass and concrete varies from infinite to 1/10. It is also evident that the higher vibration modes have only slight effect on the vertical stress at the heel of the dam.

5. CONCLUSION

The dam and foundation interaction during earthquakes was analyzed in this paper. Firstly, the structure model with the infinite rock mass and the structure model with the finite rock mass were compared. Then, the effect of deformability of foundation rock is evaluated for the structure model with the finite rock mass using the modal analysis technique.

The following are concluded from the analysis.

(1) The response spectra of the acceleration at the crest of the dam and the vertical stress at the heel of the dam of the two model have relatively good correspondence, although the peak value of the spectrum for the model with the finite rock mass is less than the model with the infinite rock mass.

(2) The response spectra of the acceleration at the crest of the dam and the vertical stress at the heel of the dam of the two model have good coincidence when these response spectra are plotted for the acceleration of the base of the dam.

(3) The peak frequency and peak value of the response spectrum of the absolute acceleration at the crest of the dam decrease, when the elastic modulus of the rock mass decreases.

(4) The delay of phase is almost 90° when the response of the acceleration at the crest of the dam is the maximum.

(5) The maximum response of the vertical

stress is almost the same level, although the ratio of the elastic moduli of the rock mass and concrete varies from infinite to 1/10.

(6) In the evaluation of the tensile stress in the dam, which is the main concern in the seismic resistance design of concrete dam, the effect of the deformability of rock mass is not so important.

(7) The higher mode of vibration has only a slight effect on the vertical stress in the dam.

References

Nagayama, I.: Simplified Seismic Design Methods for Concrete Gravity Dams, Engineering for Dams, Japan dam Engineering Center, No. 25, pp. 15 to 23, 1988. (in Japanese)

Nagayama, I., T. Sasaki and T. Hiratsuka: Effects of Hydrodynamic Pressure on a Concrete Gravity Dam During an Earthquake, Engineering for Dams, Japan dam Engineering Center, No. 58, pp. 30 to 41, 1991.(in japanese)

Chopra, A.K. and S. Gupta: Hydrodynamic and Foundation Interaction Effects in frequency Response Functions for Concrete Gravity Dams, Earthq. Eng. Struct. Dyn., 10, pp. 89 to 106. 1982.

Shiojiri, H. and S. Aoyanagi: Earthquake Response Analysis of Concrete Gravity Dams Including Dam- Reservoir-Foundation Interaction Effects, Reports of the Central Research Institute of the Electric Power Industry, No. 381041, 1982.

Lysmer, J. and L.A. Drake: A Finite Element Method for Seismology, Methods in Computational Physics, B. Alder, S. Fernback and B.A. Bolt, eds, vol. 11, pp. 181 to 216, Academic Press, 1972.

Shimizu, N., H. Tajimi, S. Yamamoto, E. Kawata and Y. Koori: Earthquake Response Analysis of Nuclear Reactor Building Embedded in a Ground by the Thin Layer Element Method, Proc. Fourth Japan Earthquake Engineering Symposium- 1975, pp. 297 to 304, 1975. (in Japanese)

Chopra, A.K., P. Chakrabarti and S. Gupta: Earthquake Response of Concrete Gravity Dams Including Hydrodynamic and Foundation Interaction Effects, Earthquake Engineering Research Center, Univ. California, Berkeley, UCB/EERC- 80/01, 1980.

Table 1 Physical Properties of Materials

	Concrete	Rock Mass
Elastic Modulus (kgf/cm^2)	$Ed=3.0\times10^5$	$Ef=3.0\times10^5$
Poisson's Ratio	$\nu d=0.2$	$\nu f=1/3$
Density (g/cm^3)	$\rho d=2.3$	$\rho f=2.6$
Damping Constant	hd=10%	hf=10%

Table 2 Analytical Cases and Boundary Condition of Rock Mass

Case	Boundary Condition of Rock Mass		Analytical Method
	Both Sides	Base	
CASE A (finite rock mass model)	horizontal : free vertical : fixed	Fixed	modal analysis (up to the 10th mode)
CASE B (infinite rock mass model)	transmission boundary	Fixed	direct integral

Table 3 Analytical Cases and Elastic Modulus of Rock Mass

Case	Elastic Modulus (kgf/cm^2)		Ef/Ed	Number of Modes Included
	Dam [Ed]	Rock Mass [Ef]		
CASE 1	3.0×10^5	——	∞	10 modes
CASE 2	3.0×10^5	3.0×10^5	1 /1	10 modes
CASE 3	3.0×10^5	6.0×10^4	1 /5	50 modes
CASE 4	3.0×10^5	3.0×10^4	1 /10	100 modes

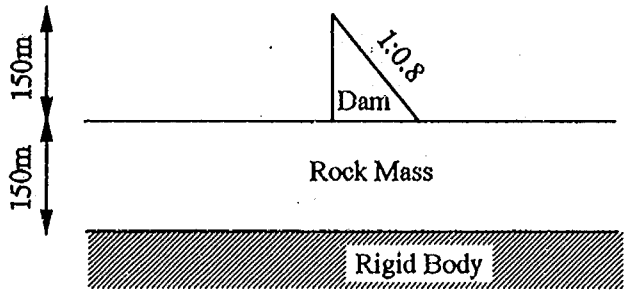


Figure 1 Dam and Rock Mass Model

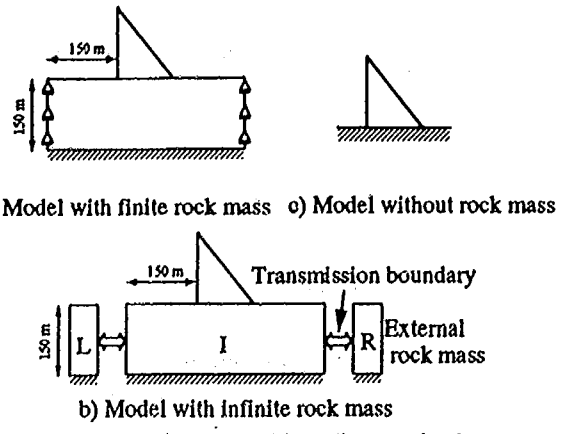
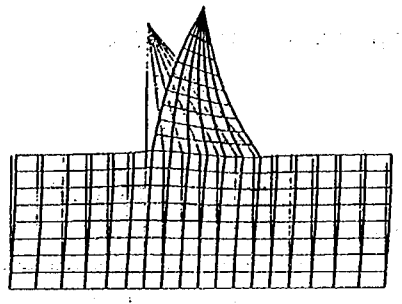
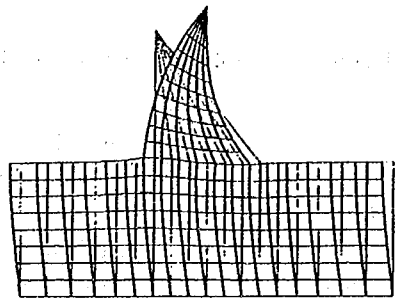


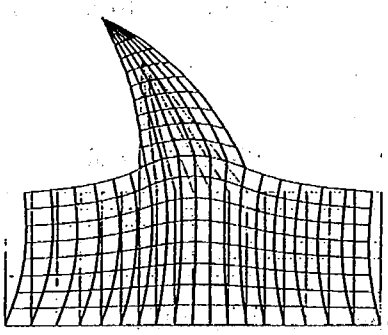
Figure 2 Concept of Each Analytical Model



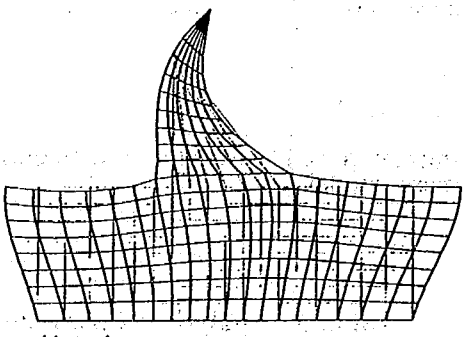
1st mode
resonant frequency : 2.44Hz
participation factor : 3.99



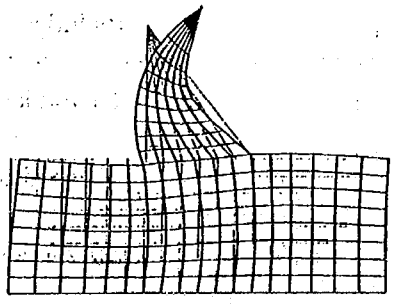
2nd mode
resonant frequency : 3.47Hz
participation factor : 3.99



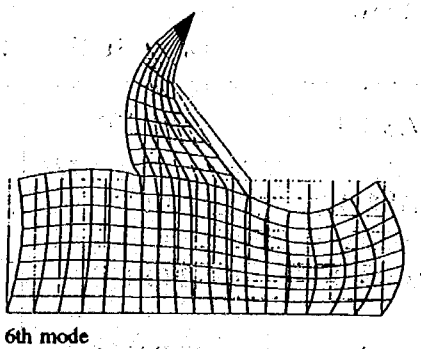
3rd mode
resonant frequency : 4.65Hz
participation factor : 0.17



4th mode
resonant frequency : 5.95Hz
participation factor : 0.15

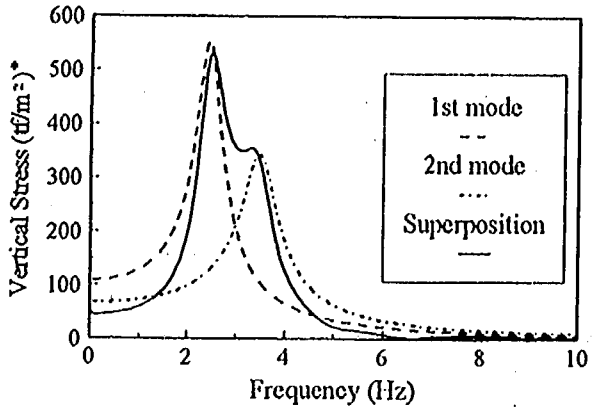


5th mode
resonant frequency : 6.21Hz
participation factor : 1.05



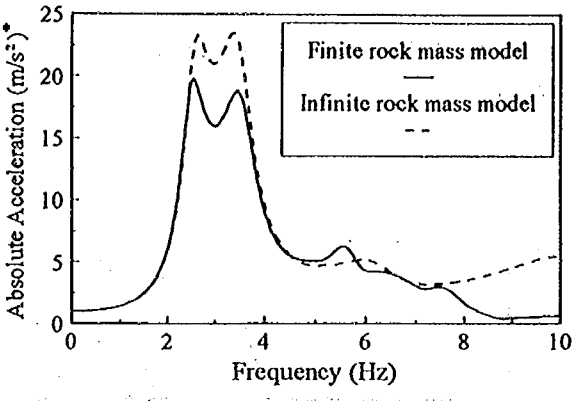
6th mode
resonant frequency : 7.21Hz
participation factor : 0.35

Figure 3 Vibration Modes of Relative Displacement



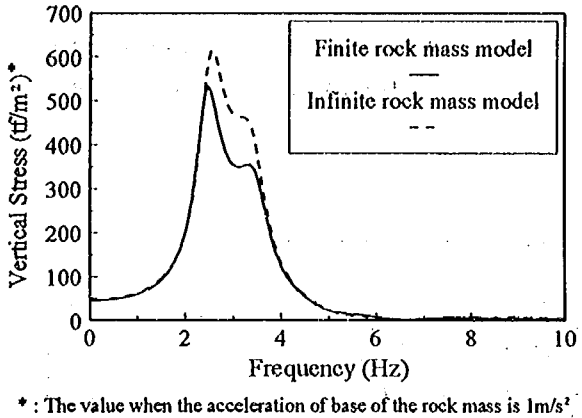
* : The value when the acceleration of base of the rock mass is 1m/s²

Figure 4 Response Spectrum of Vertical Stress at the Heel of the Dam



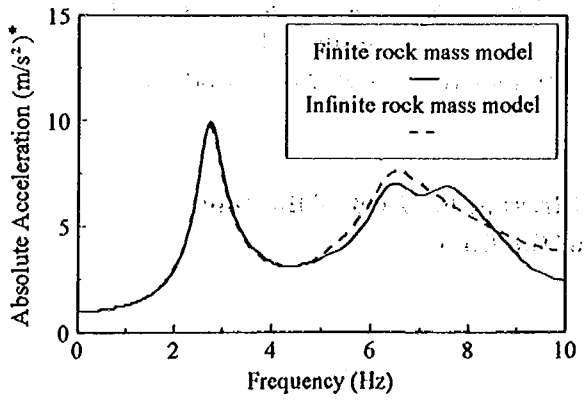
* : The value when the acceleration of base of the rock mass is 1m/s²

Figure 5 Response Spectrum of Absolute Acceleration at the Crest of the Dam



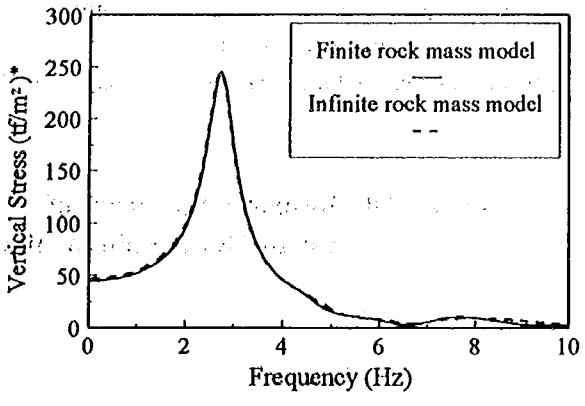
* : The value when the acceleration of base of the rock mass is 1m/s²

Figure 6 Response Spectrum of Vertical Stress at the Heel of the Dam



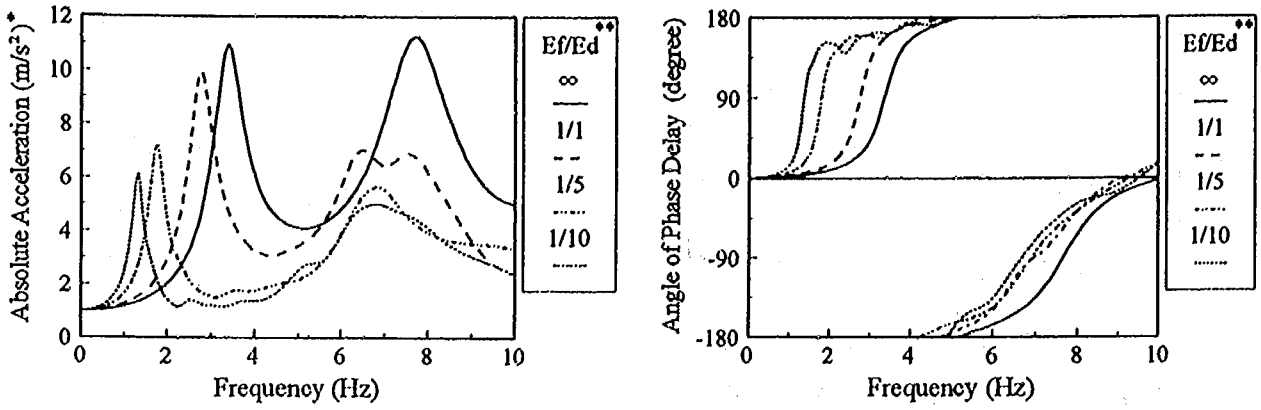
* : The value when the acceleration of heel of the rock mass is 1m/s²

Figure 7 Response Spectrum of Absolute Acceleration at the Crest of the Dam for the Basis Point at the Heel of the Dam



* : The value when the acceleration of heel of the rock mass is 1m/s²

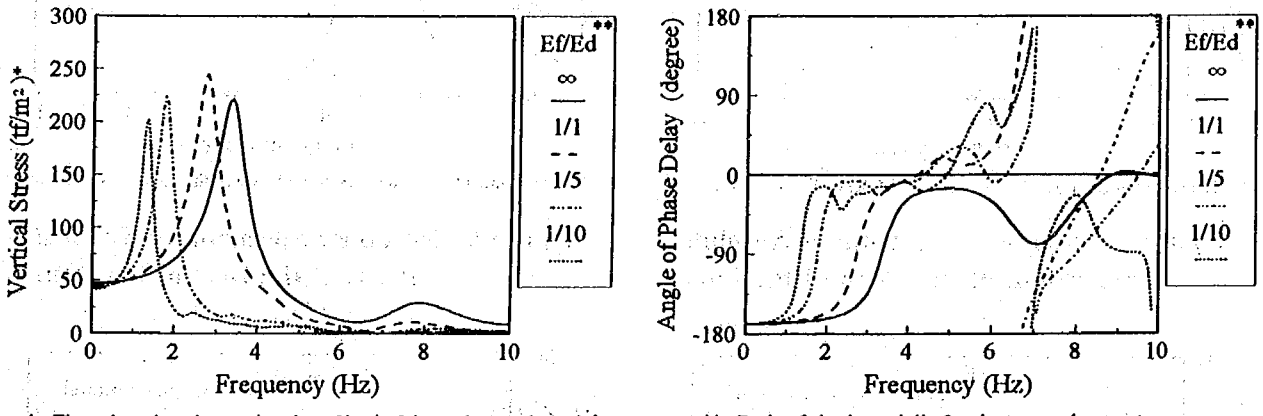
Figure 8 Response Spectrum of Vertical Stress at the Heel of the Dam for the Basis Point at the Heel of the Dam



* : The value when the acceleration of heel of the rock mass is 1m/s²

** : Ratio of elastic moduli of rock mass and concrete

Figure 9 Response Spectrum of Absolute Acceleration at the Crest of the Dam for the Basis Point at the Heel of the Dam



* : The value when the acceleration of heel of the rock mass is 1m/s²

** : Ratio of elastic moduli of rock mass and concrete

Figure 10 Response Spectrum of Vertical Stress at the Heel of the Dam for the Basis Point at the Heel of the Dam

River Embankment Damage Caused by the 1993 Hokkaido Kushiro-oki and Hokkaido Nansei-oki Earthquakes and Their Restoration Methods

by

Akihiro YAMAKOSHI[1], Yasuro IDE[2], and Masahide KAJI[3]

ABSTRACT

In 1993 two great earthquakes, the Kushiro-oki Earthquake in January and the Hokkaido Nansei-oki Earthquake in July, hit Hokkaido. Both of them registered magnitude 7.8. As is well known, they caused a great deal of damage to Hokkaido. Amongst other damage, the damage to the river embankments by the two earthquakes was enormous. The number of rivers with damaged embankments reached as many as seven: Kushiro river, Ombetsu river, Watembetsu river, Shibetsu river and Tokachi river, which were hit by the Kushiro-oki Earthquake; Shiribeshi-toshibetsu river and Shiribetsu river, which were hit by the Hokkaido Nansei-oki Earthquake.

Immediately after they occurred, we carried out an investigation into the damaged areas, carried out emergency work to prevent secondary disasters, and then conducted full-scale restoration work.

It became generally known that in both earthquakes the liquefaction of sandy soil played a crucial part in causing great damage to the embankments. Also, it became clear that there was a great difference between the two earthquakes in how the embankments suffered damage; the damaged parts of the embankments, which were built on peat ground and affected by the Kushiro-oki Earthquake, shows some aspects greatly different from those shown by the damaged parts of the embankments built on sandy ground affected by the Hokkaido Nansei-oki Earthquake.

Here we describe details of the damaged embankments and their restoration plan.

1. OUTLINE OF THE EARTHQUAKES

(1) Kushiro-oki Earthquake (1993)

This earthquake occurred at 20:06 on January 15, 1993 (JST). Its hypocenter was off the coast of Kushiro, 107 *km* under sea level. In Kushiro, the nearest town to the hypocenter, it registered the 6th grade (disastrous earthquake) on the Japanese seismic intensity scale. It was the first 6th grade earthquake in Hokkaido in 11 years since Urakawa (Hokkaido) was hit by the Urakawa-oki Earthquake (magnitude 7.1) in 1982. It also registered 5th grade in Obihiro, Hiroo, Urakawa and Hachinohe. It was felt not only in Hokkaido, but in all areas of Tohoku, Kanto and Koshinetsu districts.

Fortunately, there were no tsunamis, since the hypocenter was 107 *km* under sea level. (As was evident from past earthquakes, earthquakes whose hypocenter is more than 80 *km* under sea level do not cause tsunamis.)

(2) Hokkaido Nansei-oki Earthquake (1993)

This earthquake occurred at 22:17 on July 12th, 1993 (JST). Its hypocenter was in the Japan Sea, to the west of Oshima Peninsula. It registered the 5th grade (strong earthquake) in Suttsu, Esashi, Otaru and Fukaura, and was also felt in Tohoku and some parts of Koshinetsu districts. Since the hypocenter

[1] Takikawa Construction Office
Hokkaido Development Bureau

[2],[3] Civil Engineering Research Institute
Hokkaido Development Bureau

Table 1.1.1. FACTORS RELATED TO THE EARTHQUAKES AND AN OUTLINE OF THE DAMAGED EMBANKMENTS

Name of the earthquake / Items	Kushiro-oki Earthquake		Hokkaido Nansei-oki Earthquake		Remarks
Time of occurrence	20:06 on Jan. 15, 1993		22:17 on Jul. 12, 1993		
Hypocenter	lat. 42° 51'N long. east 144° 23'E		lat. 42° 47'N long. east 139° 12'E		
Depth	107km		34km		
Magnitude	7.8		7.8		
River embankments	Kushiro river	Tokachi river	Shiribeshi-toshibetsu river	Shiribetsu river	
Distance from the hypocenter	25km	70km	67km	95km	Distance between the hypocenter and the river mouth
Seismic intensity scale	Kushiro: 6	Obihiro: 5	Esashi: 5	Suttsu: 5	
Tsunami	Nil	Nil	The wave height was 5-6m in the Ofunato area. The wave ran 2-3km up the river.	The wave height was 3m in Arito port. The wave ran 2km up the river.	
Number and length of damaged embankments	26 places 10.1km	20 places 9.2km	28 places 5.6km	6 places 2.3km	Only those embankments under the governance of Hokkaido Development Bureau.

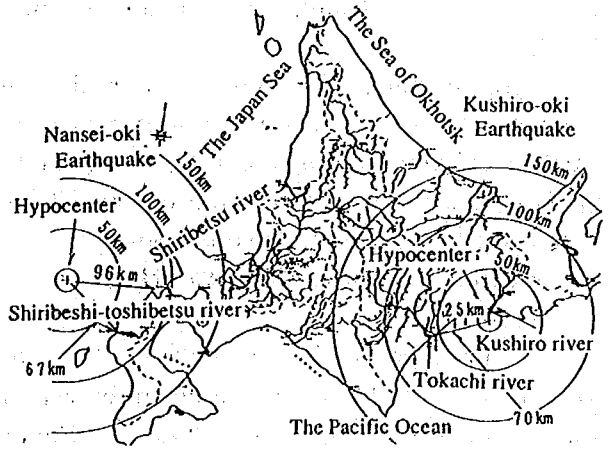


Figure 1.1.1. The location of the hypocenter and damaged embankments

was only 34 km deep, tsunamis occurred almost simultaneously with the earthquake. It took no time in sweeping along the coast of Oshima Peninsula and Okushiri Island.

Some places were hit by waves of more than 10 m in height. The loss of lives and goods was more serious than in the Kushiro-oki Earthquake.

Table 1.1.1 shows factors related to the earthquakes and outlines the damage. Figure 1.1.1 shows the location of both the hypocenters and the rivers with damaged embankments. From the figure, it is evident that the embankments damaged by the earthquakes are those situated within a radius of 100 km of the hypocenter.

2. DAMAGE TO THE RIVER EMBANKMENTS

2.1 Outline

The number of damaged embankments due to the earthquakes reached seven.

Figure 2.1.1(4page) shows typical damage after the earthquake. The following is a summary of the damage observed with the naked eye when we carried out an on-site investigation immediately after the earthquake:

Embankments damaged by the Kushiro-oki Earthquake: settlement occurred around the crown and humps of the slope surface.

Embankments damaged by Nansei-oki Earthquake: there were no remarkable humps on the slope surface, and only the settling and sinking of the ground around the crown were noticeable.

There was no deformation of the ground on both the river and land sides of the embankments caused by Kushiro-oki Earthquake.

There were many cracks and sand boils both on the river and land sides around the embankments caused by Nansei-oki Earthquake.

2.2 Kushiro river

(1) Outline of the river

The Kushiro river has its source in Lake Kussharo and has a drainage basin of 2,510 square km. The trunk stream of 154 km long flows south through the Kushiro marshland into the Pacific Ocean in downtown Kushiro. Most of lower course of the river runs through lowland composed of peat of the Kushiro marshland. In 1920 the city of Kushiro suffered great damage from a disastrous flood, and a new watercourse of about 10 km long, the lowermost course of the river, was excavated to protect the city from flooding. The Kushiro marshland is strictly preserved as a national park special conservation area and a registered wetland under the Ramsar Convention (Convention on Wetlands of International Importance especially as Waterfowl Habitat). In the Kushiro river, the upstream Kushiro marshland, from a cross-embankment about 8 km from the mouth, has the form of a retarding basin. In this area embankments on the left bank along the new watercourse and on the right bank, extending from the new watercourse like a fan, were constructed to surround the southernmost part of the marshy plain.

The Kushiro area is known for frequent earthquakes. One of the earthquakes that damaged embankments on the Kushiro river was the Tokachi-oki Earthquake in 1952. As shown in Figure 2.2.1, embankments at that time were smaller than the present ones. The Tokachi-oki Earthquake, like the recent Kushiro-oki Earthquake, caused extensive damage, mainly to the embankments within the retarding basin.

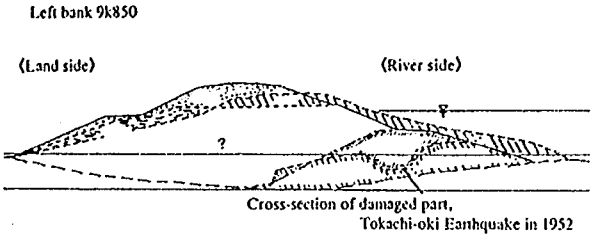


Figure 2.2.1 An example of the history of embankment construction on Kushiro river

(2) Extent of damage

Figure 2.2.2 shows a geological longitudinal section along the Kushiro river. Damage from the earthquake was caused in the peaty soils that form the downstream marshy plain. Over 90 percent of the stricken sites were centered on the embankments of the retarding basin and its lower course (Figure 2.2.3).

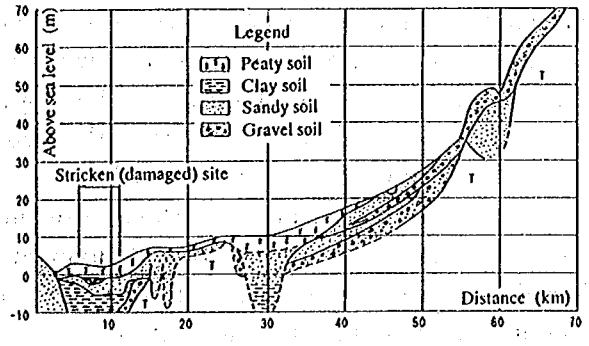
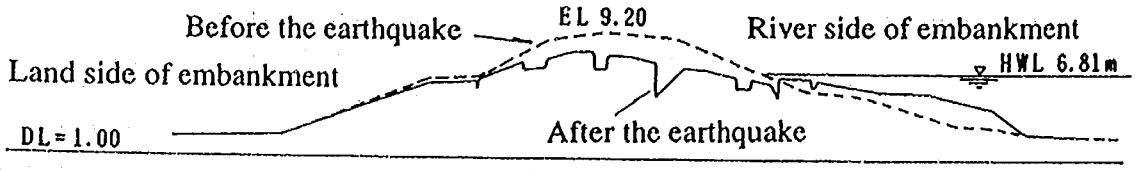


Figure 2.2.2 Geological longitudinal section along the Kushiro river

Kushiro-oki Earthquake
Kushiro river

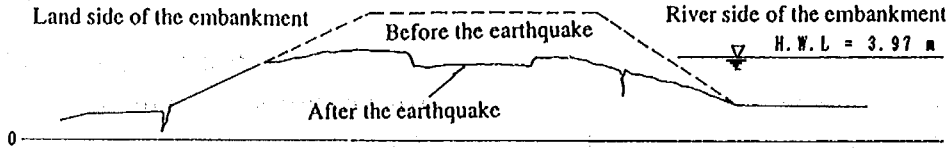
Cross-section of the damaged embankments
The left bank of a retarding basin(the left bank KP 9.85)



Notable features of the damages embankments
- The crown was vertically cracked with its maximum difference in level up to 2 m.
- Many vertical cracks were seen from the crown to the river side of the slope.
- Both the left and the right embankments had collapsed toward the river.
- There was some humps on the river side of the slope.
- Deformations of ground were observed around the heel of the river side of the slope, such as humps or uplifts.
- In some places, the soil of the embankment flowed out onto the land on the river side of the embankment.
- There were no cracks and sand boils on both the land and river sides of the embankment.

Hokkaido Nansei-oki Earthquake
Shiribeshi-toshibetsu river

Cross-section of the damaged embankments
Kabutonochisaki(the left bank KP 0.865)



Notable features of the damaged embankments
- The crown settlement was 2 m at the maximum.
- There were many cracks on the crown and on both the river side and back slopes of the embankment.
- There were cracks, sinking and sand boils on the ground around the toe of the back slope.
- There were many cracks and sand boils on the flood plan.
- There were cracks, sinking and sand boils in fields on the land side of the embankment.

Figure 2.1.1. Details of the damaged river embankments

The embankments on either bank were seriously deformed from the crown to the river side of the slope, and the maximum crown settlement exceeded 2 m. Humps of the slope face were great and the banquettes also protruded. Deformations of the ground, such as humps and uplifts, occurred at the foot of the slope. At some places the soil of embankments flowed out onto the marshy plain on the river side of embankments (Picture 2.2.1).

Disturbances, such as cracks and sand boils, were not found on ground close to embankments. By the use of a water level observation well set at the foot of the slope facing the land side of the left bank of the retarding basin, it was observed that, at the time of the earthquake, ground water rose 50 - 60 centimeters, which in time fell to the initial level (6page,Figure 2.2.4). As this observation well is used to measure the water level of the sandy stratum directly under the peat stratum, the observations indicate that fluctuations in water level were due to liquefaction during the earthquake.

On the day when the earthquake occurred, the daily mean temperature was below

-5 ℃, and the embankment surface and the ground close by were frozen. The layer of the frozen ground of the embankment surface was about 50 cm thick; the unconfined compressive strength of the frozen ground was about 70 kgf/cm^2. Therefore it seems that at the stricken sites, the cracks caused the embankment surface to split in the form of a plank, and not to collapse in fragments.

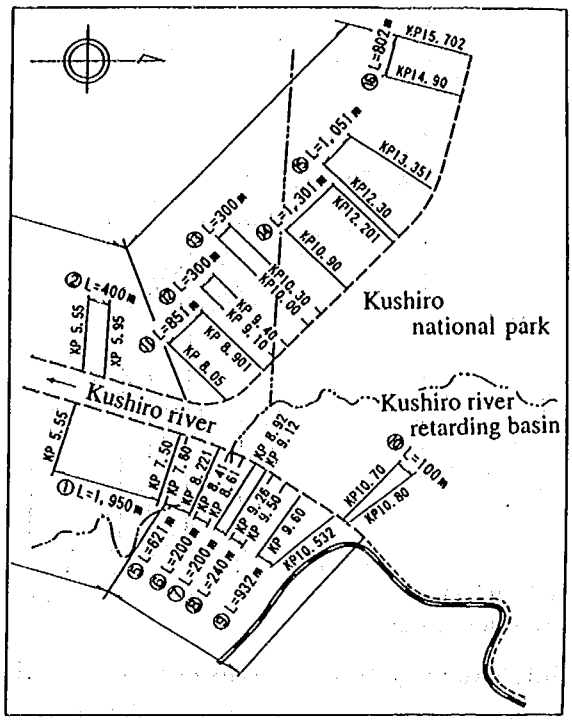


Figure 2.2.3 Stricken sites of the embankments at the retarding basin of Kushiro river caused by the Kushiro-oki Earthquake

2.3 Shiribeshi-toshibetsu river

(1) Outline of the river

The Shiribeshi-toshibetsu river originates in Mt. Oshamambe (972m above sea level) and flows for 80km to the Japan Sea, with a drainage basin of 720km^2. The upper stream of the river flows in the mountains, while the mid and lower streams flow through an alluvial plain formed by flooding of the river and its tributaries. The lower course used to have a large number of meanders.

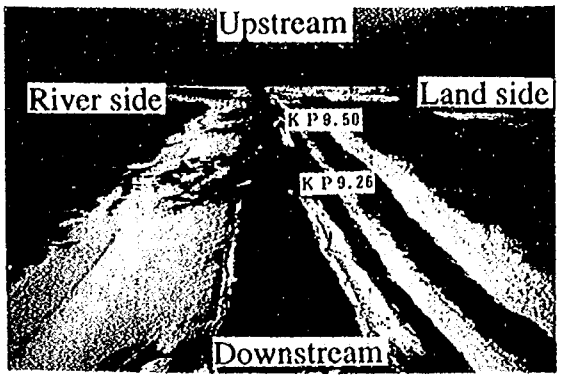


Photo 2.2.1 Outflow of the soil of embankment onto the river side of the embankment (left bank at the retarding basin)

This river was improved over two different periods to provide a straight course and embankments having a cross-section shown in Figure 2.3.1. The downstream basin is dotted with watercourses and ponds which are remnants of the old channel left behind by the river improvement.

At some parts of the downstream plain, peat is found, but the plain is composed mainly of sandy soil. The basin of the Shiribeshi-toshibetsu river had not suffered any damage from the earthquakes until the recent Nansei-oki Earthquake.

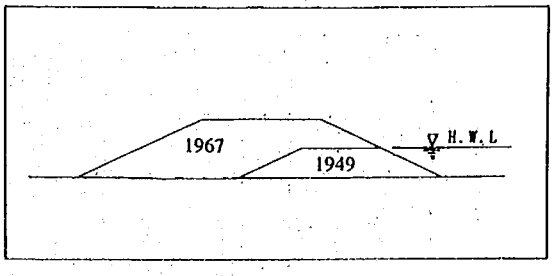


Figure 2.3.1 Standard cross-section of the embankment on the Shiribeshi-toshibetsu river

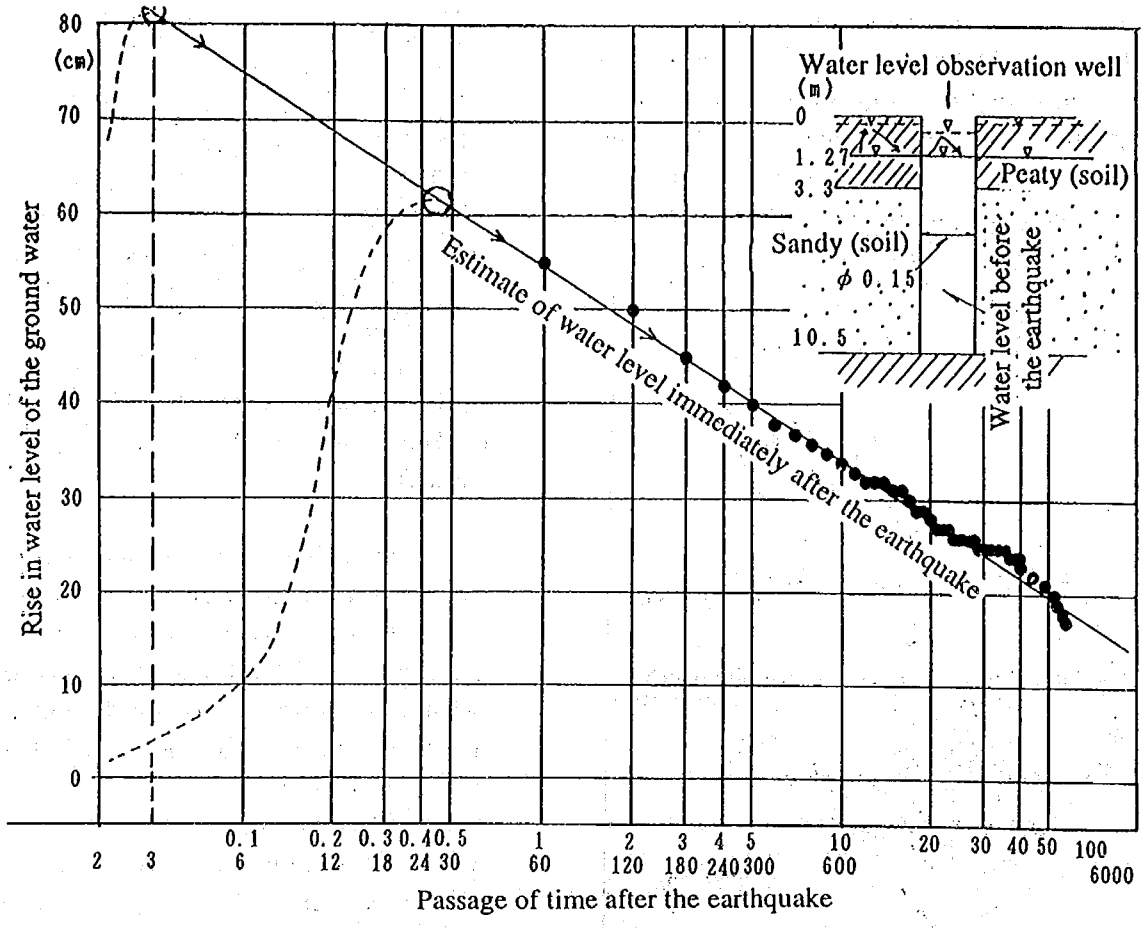


Figure 2.2.4 Changes in water level which raised when eartquake occurred

left bank of the Shiribeshi-toshibetsu river

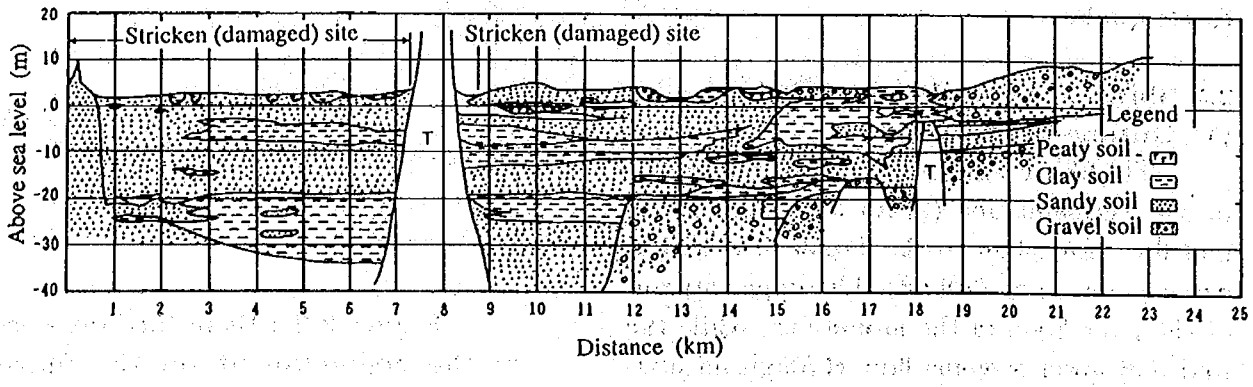


Figure 2.3.2 Geological longitudinal section along the downstream of the Shiribeshi-toshibetsu river

(2) Extent of damage

Figure 2.3.2 shows a geological longitudinal section of the lower course of the Shiribeshi-toshibetsu river. Stricken sites were found generally where the geological structure is made up mainly of sandy soil, and Figure 2.3.3 shows the stricken sites and the location of the old river channel. Many of these sites were in the vicinity of the old channel. Furthermore, the sites where damage was serious tended to correspond to the old channel.

On the left bank of Kabutono embankment, which was damaged most seriously (near kp 9.85), considerable cracks extending for 100 m and longer and settlement occurred. The maximum settlement reached over 2 m. Caveins of the crown was almost equal in degree to those of the Kushiro river and the Tokachi river, while humps on the slope face were not so conspicuous (Picture 2.3.1).



Photo 2.3.1 Damaged embankment on the Shiribeshi-toshibetsu river

There were also several sand boils and open cracks in the flood plain. Furthermore, from the toe of the land side of the embankment slope to the paddy fields and meadows in the protected lowland, cracks and sand boils were also found, and unevenness appeared in streaks. From the aerial photos taken after the damage was caused, it seems that streaky disturbances on the landside are related to changes in the old river channel.

In the Shiribeshi-toshibetsu river, the tsunamis ran upstream after the earthquake. The flood plain was flooded from the lower course to the vicinity of kp 2.4km. The water overtopped the embankment on the right bank downstream between kp 0.2 and 0.4. In addition, the stream flowed in reverse from some sluiceways onto the land side area. Damage to the embankment and river structures due to the tsunamis has not been confirmed.

3. CAUSES AND FEATURES OF THE DAMAGE

Investigations made at the four major rivers which suffered from both earthquakes showed that the damage to these rivers can be classified, in most cases, into two types: (1) Kushiro-oki Earthquake-type and (2) Nansei-oki Earthquake-type because of the difference of ground condition, not from difference of earthquake motion or form of embankment. The investigations by type are as follows:

3.1 Kushiro-oki Earthquake-type (Kushiro river, Tokachi river)

Figure 3.3.1 (a) shows a geological section of the left bank at the retarding basin of the Kushiro river as a typical stricken site. The stricken sites of the Kushiro and Tokachi rivers were constructed largely on peaty ground. The peat of the Kushiro river has a thickness of between 3m and 5m. The moisture content of peat is between 300% and 1000%. The height of the embankment is about 5m. Directly under the crown, the consolidation settlement of the peat stratum occurred with the construction of the embankment. This settlement reduced the initial thickness of the stratum by 2/3 to 1/2, giving the appearance of the embankment soil sinking into the old ground surface. On the left bank of the Kushiro river, the sandy soil, with a distribution of about 5m, is below the peat stratum.

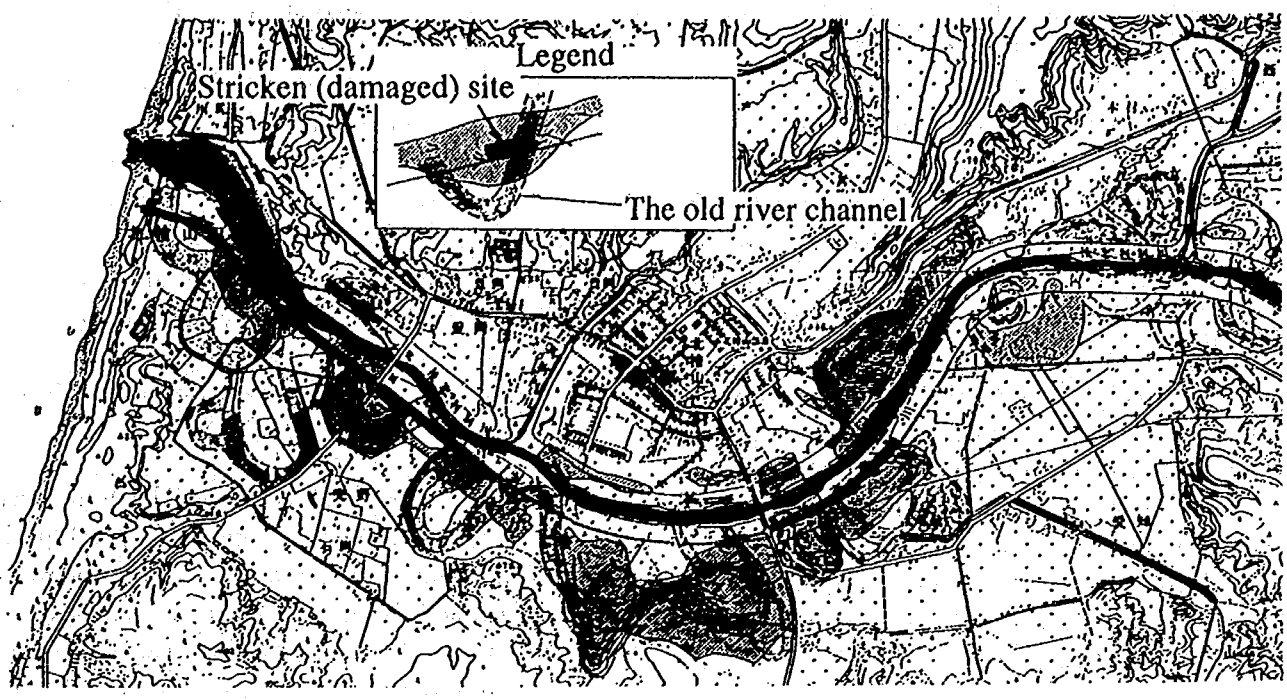


Figure 2.3.3 Stricken (damaged) sites of the embankments on the Shiribeshi-toshibetsu river due to the Nansei-oki Earthquake

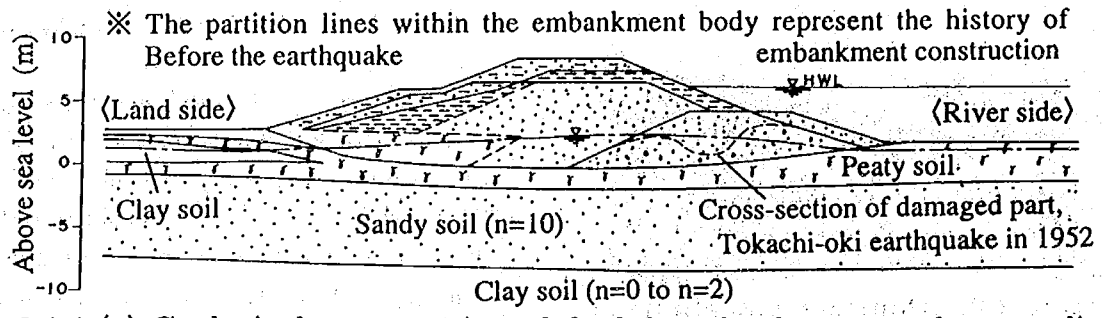


Figure 3.1.1 (a) Geological cross-section of the left embankment at the retarding basin of the Kushiro river 9K850)

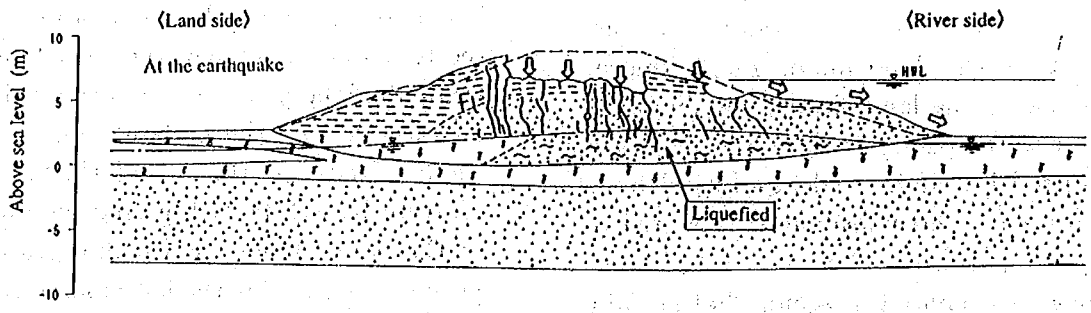


Figure 3.1.1 (b) Mechanism of the embankment collapse due to the Kushiro-oki Earthquake

The soil of the embankment is mainly sandy soil of grain size distribution shown in Figure 3.1.2., and is loose with an N-value of under 5 from the standard penetration test. Also, the water level inside the embankment was a little higher compared with that of the ground close by. There were many sites where the level was the same as the old ground surface, or higher at about 1 m. Such a rise in water level seems to be a phreatic surface formed by rainwater infiltration from the embankment surface. Thus the lower part of the soil of the embankment, composed mainly of loose sandy soil, became a zone that was lenticularly saturated with ground water.

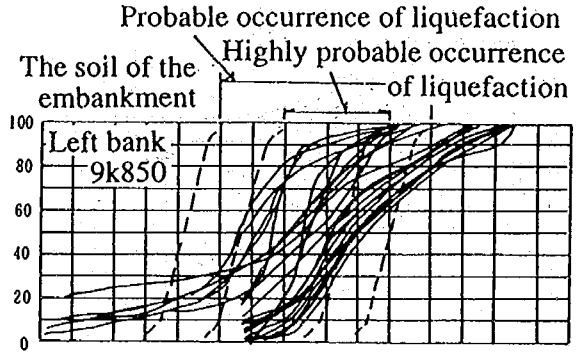


Figure 3.1.2 Grain size accumulation curve of the soil of the embankment (left bank at the retarding basin of the Kushiro river 9K850)

Observations of the inside of an embankment by open-cut investigation showed that directly under the crown, longitudinal open cracks appeared to a considerable degree, part of the crown had broken into several blocks and had settled, which gave rise to stepped dislocations. At the lower ends of the deep cracks reaching to the lower part of the embankment, a vein of sand that had intruded from far down the excavation, was observed. It seems that liquefied sand rose upwards.

From the above descriptions, damage from the Kushiro-oki Earthquake was caused by the liquefaction of the embankment soil made up of saturated sandy soil that distributes lenticularly under the embankment. Figure 3.1.1 (b) shows a mechanism of the collapse at the time of the earthquake.

Liquefaction seems to have occurred in the left embankment on the Kushiro river because the water level of the sandy stratum underlying the peat stratum rose at the time of the earthquake. However, as the sandy stratum is covered with the peat stratum, it is not fully understood to what extent the sandy stratum had an effect on the damage to the embankment.

3. 2 Nansei-oki Earthquake-type (which caused damage to Shiribeshi-toshibetsu river and Shiribetsu river)

Figure 3.2.1 (a) is a cross-section of the left bank of Shiribeshi-toshibestu river in the Kabutono area, which is a typical example of a damaged embankment. The damaged sites of the embankments of both rivers are made up mainly of sandy soil. In particular, the upper layer of the sandy soil with a thickness of 5m - 10m is not dense and shows an N-value below 10 from the standard penetration test. Some parts of the surface have a thin viscous soil stratum, but this kind of ground condition differs from the embankments of the Kushiro river and Tokachi river where the consolidation settlements are greater. The height of the banks of both Shiribeshi-toshibetsu river and Shiribetsu river is about 5m.

It was obvious from an open-cut investigation that because of the occurrence of the cracks in both shoulders of the crown, the embankment was divided into three parts — that is, the masses of earth in the crown, on the land side, and on the river side. The mass of earth in the crown sank about 2m, appearing as if it sank into sandy soil. With this sinking, the mass of earth on the river side was

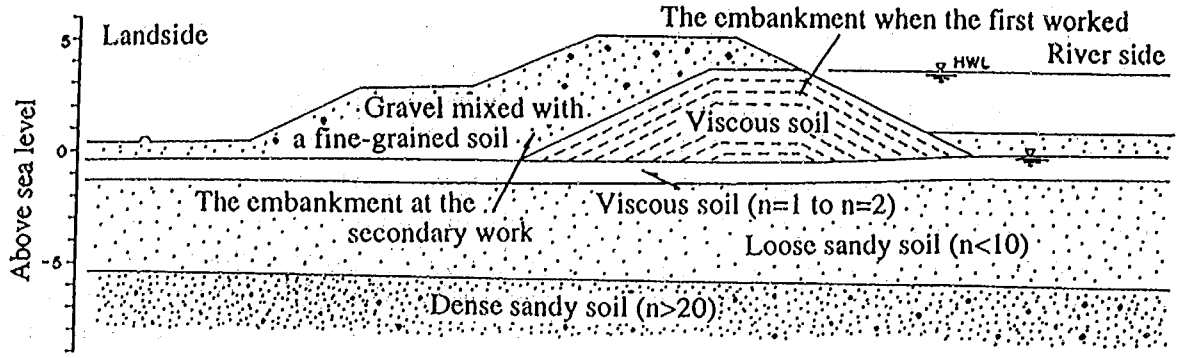


Figure 3.2.1 (a) Cross-section of the left bank of Shiribeshi-toshibetsu river in the Kabutono area

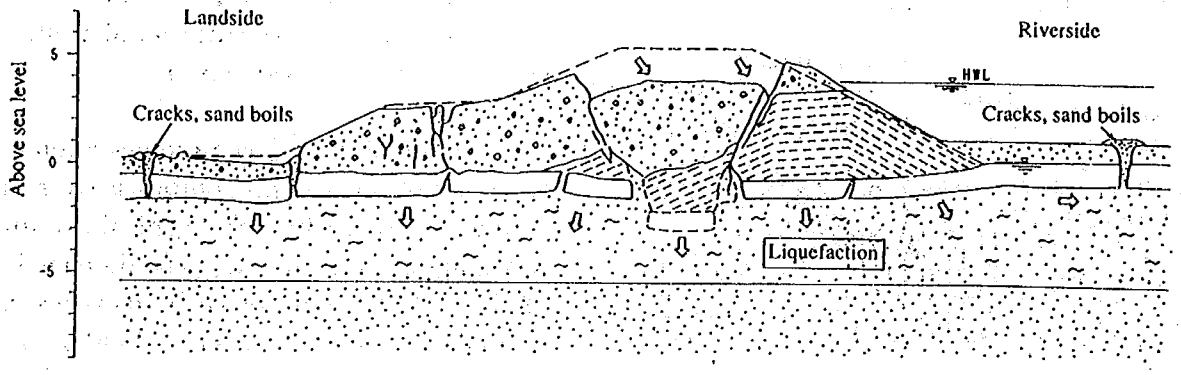


Figure 3.2.1 (b) Damage mechanism on the left bank of Shiribeshi-toshibetsu river in the Kabutono area

assumed to have moved toward the river as if it was pushed out. On the lower part of the cracks which divide the masses of earth, we observed a sand vein rising along the cracks.

Many cracks, and the sand boils which gushed out from them, were observed on the flood plan. The paddy rice fields of the land side of the embankment had cracks and sand boils. Much unevenness on the surface of the ground stretched from the paddy fields to the toe of the land side of the slope.

From these findings, we can outline the damage mechanism (Figure 3.2.1 (b)). Liquefaction occurred in a wide area of the ground around the embankment as well as directly beneath the embankment, and a great decrease in bearing capacity of the foundation ground caused collapses of the earth of the crown. Compared with the total amount of the sunken soil of the embankment, the humps of the ground were not remarkable because the humps were absorbed by a widespread outflow of the liquefied layers.

4. RESTORATION METHODS

4. 1 Outline of the emergency and restoration work

The emergency work was conducted at the damaged sites of the embankments promptly in order to restore their function and to avert the occurrence of a secondary disaster until

the restoration work began. As a fundamental purpose of the restoration work, damaged sites, including areas where cracks had spread, were cut and filled, and then compacted by rolling. This was carried out by the methods in Table 4.1.1 based on the level of damage.

Components considered essential for rest oration work are shown below:

(1) The differences in the restoration methods between the Kushiro-oki Earthquake and Nansei-oki Earthquake

The restoration procedures between the Kushiro-oki Earthquake and Nansei-oki Earthquake demonstrated in Table 4.1.1. are classified primarily according to weather conditions. The restoration work of the damage below the height of HWL (high water level) was generally done by partial cutting immediately, but since the Kushiro-oki Earthquake occurred in mid-winter, compaction by rolling was difficult, so emergency work was improvised up to the spring.

Also, the Nansei-oki Earthquake took place in a period when flooding was often caused by typhoons. Therefore, approaching typhoons was of the biggest concern. At areas where the damage reached the height of HWL, a double-wall cofferdam was installed using steel sheet piles at the stage of emergency work. Also, in some areas of the Shiribetsu river, where the level of damage was relatively low and there was enough space, the embankment was widened on the land side instead of compacted by rolling.

(2) Method to determine the cross-section to be cut and filled

After testing the area of the damage by cutting open the embankment to confirm the spread of cracks inside, the cross-section to be cut was determined. Lime water was poured when emergency work was conducted to recognize the cracks easily during the restoration work. In addition, a method of injecting grout (a mixture of cement and bentonite) by boring was attempted in the Kushiro river. Depending on the soil of the embankment, pouring lime water made the cracks difficult to recognize, and so pouring grout was the method used as it was more effective.

(3) Consideration of the environment

The land on the river side of the embankment of the Kushiro river retarding basin is protected as a national park and a registered wetland of the Ramsar Convention. Therefore we conducted restoration work, paying much attention to the preservation of the environment of the wetland. The details are:

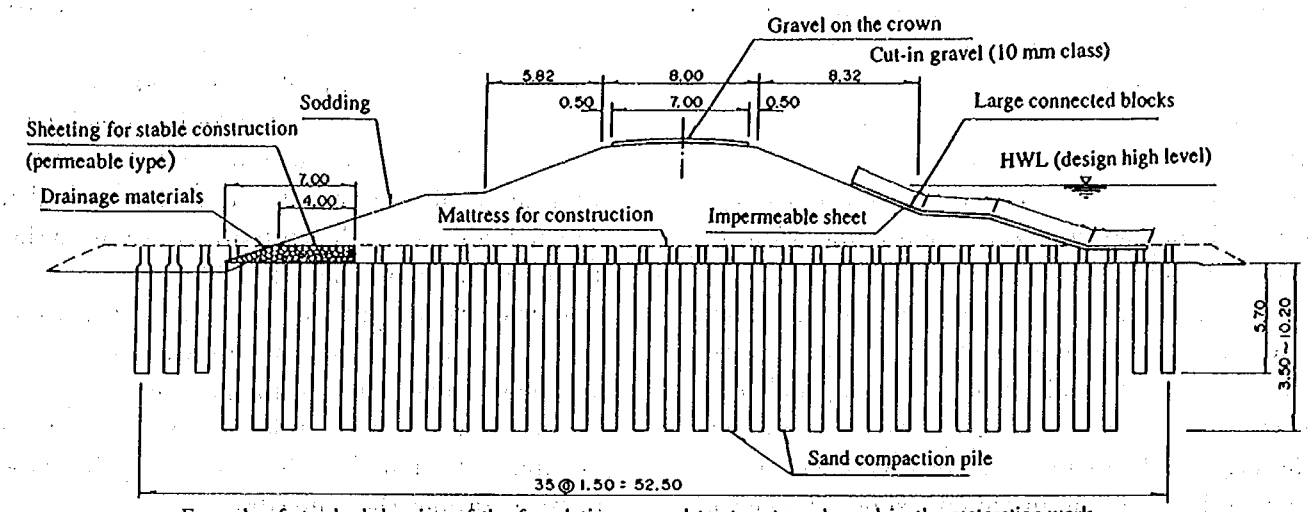
- work to prevent the outflow of soil onto the wetland, water pollution, dust etc.
- there is a colony of Salamandrella keyserlingii (a species of salamander special to Hokkaido) located in the embankment adjustment area. Sheet pile cofferdams were installed on the land side of the embankment where the salamander colony was located.
- prior to the restoration work, the salamander and their eggs were moved to where no harm would come from the work.
- perforated sheet piles were used where ground water may be affected during the work from installing the cofferdams.
- conducting surveys on the current situation of the animals, vegetation, vibration noise, water quality, etc.
- using environmental advisors.

4. 2 Foundation ground treatment methods

Where there was serious damage which required whole embankments to be cut down, it was considered that the foundation grounds were greatly disturbed and their strength reliability had decreased, and so safe, speedy work in cutting and filling was considered. The survey of such places was given high priority and it became clearly known that the safety factors required for embankments were no longer

Table 4.2.1. FOUNDATION GROUND TREATMENT METHOD APPLIED TO EACH EMBANKMENT

Name of river	Method applied	Sites where applied	Application
Kushiro river	Sand compaction method	4 sites, 1601 m	Improvement of damaged peat stratum and sandy stratum
Tokachi river	Sand compaction method	1 site, 600 m	The same as above
	Pile net method	1 site, 100 m	Insufficient space for sand compaction.
Shiribeshi-toshibetsu river	Sand compaction method	1 site, 130 m	Improvement of damaged viscous stratum and sandy stratum
	Heavy hub compaction method	1 site, 70 m	Applied to the site where the work does not cause much destruction on the environment
	Geotextile method	2 sites, 320 m	Applied as a supplementary method to crowns which are also used as roads.



Example of standard drawing of the foundation ground treatment work used in the restoration work

Figure 4.2.1 Cross-section of site where sand compaction method was applied

satisfactory.

Therefore, we compared and examined methods from the aspects of soil characteristics, the effects on the environment, cost, procedure, and depth of foundation ground. We decided on the sand compaction method as the major foundation ground treatment method for the restoration work of the Kushiro river, Tokachi river and Shiribeshi-toshibetsu river (Table 4.2.1).

The purpose of the foundation ground treatment at this time was to obtain necessary ground strength for the restoration work. As a result, the relative density between the embankment soil and sandy stratum was increased by pressing-in sand piles which also had the effect of improving the resistance against liquefaction.

Figure 4.2.1 shows an example of a cross-section where the sand compaction method was applied for the restoration work. Crushed stones used for temporary work were placed at the top of the land side of the slope of the embankment as a top of the slope drainage

method which makes the level of water retention in the embankment lower and strengthens the embankment.

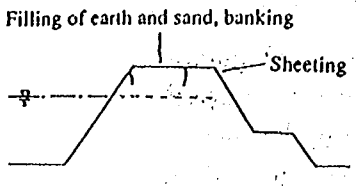
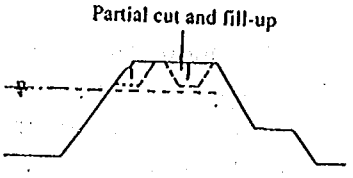
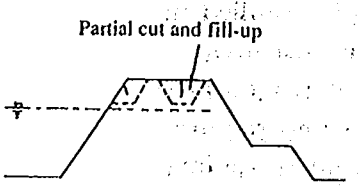
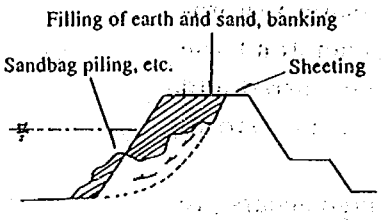
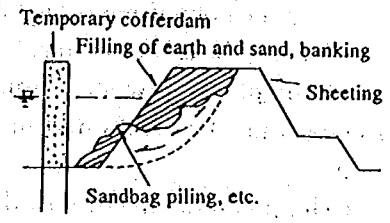
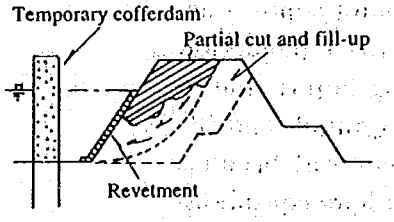
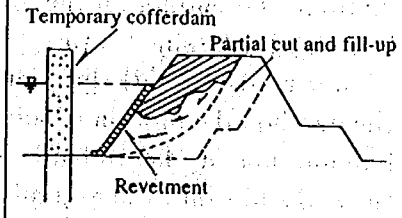
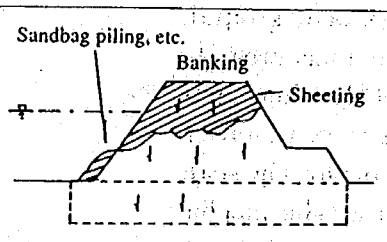
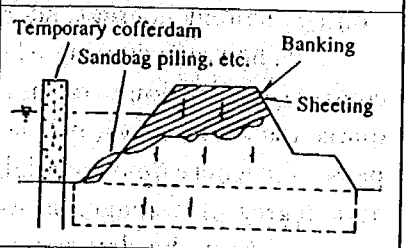
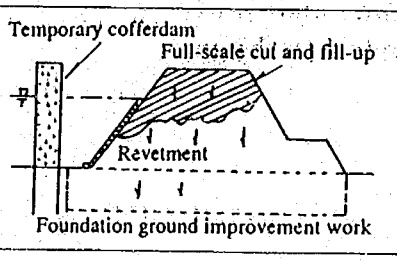
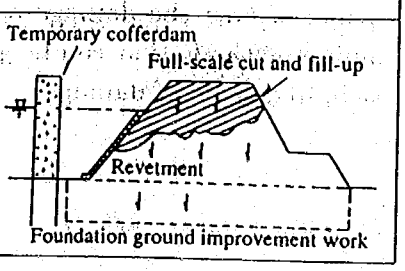
5. CONCLUSION

Hokkaido experienced two earthquakes within six months which had hardly occurred in the past. We experienced and learned a lot from the process of the restoration work of river embankments after the damage due to the earthquakes which needs to be applied in the future as disaster prevention measures:

- once an earthquake occurs, it results in a serious disaster to a large extent and requires a huge amount of work to prevent secondary disasters and to restore former conditions.
- to conduct safe and quick disaster restoration work, it is necessary to understand the mechanisms of how the damage occurred and to examine the issues and methods of restoration.
- the mechanisms of how damage occurs are different depending on the ground conditions. Damage is classified into: (1) the liquefaction of sandy ground, (2) the sliding failure due to the earthquake motion of soft ground, and (3) liquefaction of the embankment soil because the soil sinks into the ground where consolidation settlement is great, such as peat ground.

When considering these measures, to conduct restoration work smoothly when earthquake disasters occur, it is necessary to anticipate sites where damage might occur, the scale and degree of damage, as well as the mechanisms of how the damage occurs, and to examine methods that can be applied to the anticipated scale of damage.

Table 4.1.1 RESTORATION WORK OF THE DAMEGED EMBANKMENT

Degree of damage	Type of work	Kushiro-oki Earthquake	Hokkaido Nansei-oki Earthquake
Damage below H.W.L Application rate for each river Kushiro river: 0.3 % Tokachi river: 4.1 % Shiribeshi-toshibetsu river: 30.4 % Shiribetsu river: 20.5 %	Emergency work		
	Restoration work		Emergency work =Restoration work
Damage above H.W.L Application rate for each river Kushiro river: 83.9 % Tokachi river: 88.3 % Shiribeshi-toshibetsu river: 61.7 % Shiribetsu river: 79.5 %	Emergency work		
	Restoration work		
Great damage to the foundation ground Application rate for each river Kushiro river: 15.8 % Tokachi river: 7.6 % Shiribeshi-toshibetsu river: 7.9 % Shiribetsu river: 0.0 %	Emergency work		
	Restoration work		

Strong Motion Records of Hokkaido Toho-oki Earthquake in 1994

by

SATO Masashi[1], SHIMADA Takeshi [2]and KANEKO Manabu[3]

ABSTRACT

Presented are the results of an investibation in which collected strong-motion records on the Hokkaido Toho-oki Earthquake were digitized and wave analyses including power spectram, acceleration response spectrum and so on were performed.

On roads, there was little damage to bridges except bridges with poor substructure, but much damage to earth works in cuts and embankments.

we consider that from all the records of the earthquake that the Toho-oki Earthquake did not depend on the natural period of the ground. Further analysis and investigation of records of analogue strong motion seismographs are necessary as well.

Key Words: Hokkaido Toho-oki Earthquake; strong-motion record; strong-motion seismograph;

1. INTRODUCTION

A large earthquake (magnitude 8.1 on the Japanese scale) hit Hokkaido with its hypocenter 180km off the coast of Nemuro City at around 10:23 pm, October 4, in 1994 when two large-scale earthquakes, the Kushiro-oki Earthquake (M7.8) and the Hokkaido Nansei-oki (M7.8) Earthquake, were still fresh in our memory. Named "1994 Hokkaido Toho-oki Earthquake" by the Meteorological Agency, the earthquake was recorded as a disastrous earthquake (seismic intensity VI on the Japanese scale) in Kushiro and Akkeshi close to the hypocenter, and caused much damage to road facilities. This earthquake also caused tsunami (tidal waves) along the eastern coast of Hokkaido and the Pacific coast of Honshu, recording a maximum wave height of 173cm in Hanasaki Port.

Since the installation of a SMAC-type strong motion seismograph at Chiyoda Bridge in 1966, the Hokkaido Development Bureau (Structures Section, Structures Division, Civil Engineering Institute) has been setting up strong motion seismographs at 29 bridges in Hokkaido to form an observation network. Ten of these bridges have had installed an on-line digital-type strong motion seismograph ("digital strong motion seismograph" in the following) which has been designed to immediately retrieve and analyze strong motion records by the section.

In Hokkaido Toho-oki Earthquake, valuable strong motion records were registered at 17 bridges installed with strong motion seismographs by the section. Here we have gathered strong motion records which could be retrieved instantly and analyzed.

2. GENERAL FEATURES OF THE EARTHQUAKE

Table 1 illustrates general features of Hokkaido Toho-oki Earthquake in 1994. Table 2 shows a list of major earthquakes in Japan since World War II.

It is conceivable that the scale of the earthquake exceeded both the Kushiro-oki Earthquake and the Nansei-oki Earthquake of 1993 and had the strongest intensity of all major earthquakes in Japan, except for the Tokachi-oki Earthquake in 1952. The seismic intensities on the Japanese scale for the main districts were registered as: IV (disastrous earthquake) in Kushiro and Akkeshi near the hypocenter and V

1) Head,Structures Section,Structures Division, Civil Engineering Research Institute,Hokkaido Development Bureau,hiragishi 1-3, Toyohira-ku,Sapporo,062 japan

2) Research Engineer, ditto

(strong earthquake) in Nemuro, Hiroo and

Urakawa for the Toho-oki Earthquake (1994). Apart from the Kushiro-oki and the Nansei-oki Earthquakes, no other earthquake that occurred in the Hokkaido area had registered an intensity of VI after the Urakawa-oki Earthquake in 1982. It is therefore unprecedented that a large-scale earthquake recording an intensity of VI has hit Hokkaido during only two years since 1993.

3. OBSERVATION STATIONS AND STRONG MOTION RECORDS

Fig. 1 shows the stations that produced strong motion records from the earthquake. ◎ indicates a digital strong motion seismograph while ○ represents a analogue strong motion seismograph. The records registered at respective bridges provided with a digital strong motion seismograph, as well as the ground classifications and distances from epicenter, are shown in Table 3. LG (Longitude) indicates the bridge axis direction while TR (Transverse) and UD indicate the right angle direction of the main axis and vertical direction, respectively.

The records from Onneto Bridge, the nearest to the epicenter (177.94km) of all bridges, show that vertical shocks produced a greater maximum acceleration than for LG and TR direction motions which are horizontal.

Fig. 2 illustrates the regression lines when only the distance from the epicenter is taken as the explanatory variable and the maximum acceleration obtained from Toho-oki, Nansei-oki and Kushiro-oki Earthquakes is a vertical line. Also shown are the curves of distance damped equation introduced by the Civil Engineering Institute of the Construction Ministry from previous data.

Three different cases are shown as follows: when records obtained from Toho-oki Earthquake only is valid; when records from both Nansei-oki and Kushiro-oki Earthquakes are valid; when all records from Toho-oki, Nansei-oki and Kushiro-oki Earthquakes are valid. Compared with the second case, the first case demonstrates that acceleration does not damp at places some distance from the epicenter and that acceleration remains great. In the second case, however, there is a tendency that acceleration rapidly damps at 200km from the epicenter. The third case, the results from the second case and the first case combined, indicates that the acceleration was affected by the results of the Toho-oki Earthquake and remains relatively great even at a place distant from the epicenter. Consequently, one of the characteristics of the Toho-oki Earthquake was the lack of any sign of a damping of acceleration even when the distance from he epicenter was great, which was quite different from the other two earthquakes.

4. RESULTS OF SPECTRUM ANALYSIS

Figures 3-4 illustrate wave forms of strong motion records by components obtained from strong motion seismographs installed on the ground of Shichiho Bridge and Onneto Bridge as examples of strong motion records registered at the observation stations shown in Table 3.

Spectrum analyses of the strong motion records were made. Figures 5-6 and Figure 7, respectively, indicate power spectra and acceleration response spectra of Shichiho Bridge and Onneto Bridge shown in Figures 3-4. Each graph of acceleration response spectra shows a solid line representing the average value on the condition that the response of respective cycle component makes a normal standard distribution, as well as the dotted line being 95% probability.

With Shichiho Bridge, there is no predominant frequency common to LG, TR and UD directions. It is remarkable that most of the frequencies remain between 1Hz and 3Hz. Acceleration response spectra shows that there is no particular predominant frequency in the LG direction wave, horizontal component, and the various kinds of frequencies were recorded.

With Onneto Bridge, LG and TR directions, horizontal components, have a predominant frequency of approximately 2Hz in common. We assume that, however, many frequencies exceed 5Hz in the UD direction. We found that the acceleration response spectra of LG and TR indicate that frequencies extend slightly

over a wider area than those of Shichiho Bridge.

Although not indicated in this paper, we consider that from all the records of the earthquake that the Toho-oki Earthquake did not depend on the natural period of the ground. Further analysis and investigation of records of analogue strong motion seismographs are necessary as well.

5. CONCLUSION

Three big earthquakes struck Hokkaido in the last two years. It is highly fortunate that there were no dead or missing people recorded in the Hokkaido Toho-oki Earthquake in 1994. Further examination of the earthquake countermeasures in Hokkaido is indispensable in the future.

<References>

1) NAKANO Osamu, KANEKO Manabu, ONO Yuji, SATO Kei, Analysis of strong-motion records of Kushiro-oki Earthquake; the 48th annual conference of the Civil Engineering Society. September, 1993

2) Report on Hokkaido Toho-oki Earthquake in 1994 (flash); Structures Section, Structures Division, Civil Engineering Research Institute, November 1994

3) Science Chronological Table 1994: Compiled by National Astronomical Observatory, the 67th volume, November 1993

4) Handbook of aseismic design of roads; Japan Road Association, February 1988

Table 1 General features of the Hokkaido Toho-oki Earthquake

Data/Time		22:23 October4, 1994
Mabnitude	(JMA)	8.1
Hypocenter	Latitude north	43 22
	Longitude east	147 40
	depth	30km
Damage section		Damage
Human casualties	Dead	0
	Missing	0
	Injured	435
Residential damage	Completely/partially	421
	Partially damaged	7154
Non-residential damage	Public buildings	1
	Others	6
Damage to traffic network	Road	1762
	Bridges	31
Port damage	Port	7
	Fishing port	28
Rivers affcted		110
Damage to agricultural facilities		2346

Table 2 General features of major earthquakes after World War II

Date	Earthquake	M	D
December 21, 1946	Nankai Earthquake	8.0	-
June 28, 1948	Fukui Earthquake	7.1	-
March 4, 1952	Tokachi-oki Earthquake	8.2	0
November 26, 1953	Boso-oki Earthquake	7.4	-
Augast 12, 1961	Kushiro-oki Earthquake	7.2	80
June 16, 1964	Nigata-oki Earthquake	7.5	40
April 1, 1968	Hyuganada Earthquake	7.5	30
December 4, 1972	Hachijojima-toho-oki Earthquake	7.2	50
June 17, 1973	Nemurohanto-oki Earthquake	7.4	40
June 12, 1978	Miyagiken-oki Earthquake	7.4	40
March 21, 1982	Urakawa-oki Earthquake	7.1	40
May 26, 1983	Nihonkai-chubu Earthquake	7.7	14
January 15, 1993	Kushiro-oki Earthquake	7.8	107
July 12, 1993	Nansei-oki Earthquake	7.8	34

Table 3 Observation station of strong temblors,epicenter and maximum acceleration

Observation station name	Ground classification	Distance from epicenter(km)	Instalation Location		Installation Direction	Maximum acceleration		
			Latitude	longitude		LG	TR	UD
Chiyoda Bridge	Ⅲ	352.14	42° 55′ 11″	143° 23′ 21″	N 53° 45′ E	205.69	232.28	76.66
Otanoshike Bridge	Ⅱ	280.73	43° 00′ 33″	144° 15′ 16″	N 42° 47′ W	155.91	107.75	101.94
Shinishikari Bridge	Ⅲ	500.55	43° 08′ 15″	141° 31′ 15″	N 45° 15′ E	47.91	40.47	15.66
Shitoho Bridge	Ⅰ	647.43	41° 35′ 40″	140° 10′ 50″	N 65° 30′ E	9.56	12.25	5.63
Ishikarikako Bridge	Ⅲ	513.45	43° 13′ 20″	141° 21′ 10″	N 42° 42′ E	26.34	25.75	8.84
Shari Bridge	Ⅲ	251.29	43° 54′ 05″	144° 38′ 50″	N 78° 53′ E	298.00	328.00	
Sizunai Bridge	Ⅲ	448.81	42° 19′ 10″	142° 22′ 30″	N 03° 00′ W	16.14	16.01	
Shizunai Bridge	Ⅱ	510.58	42° 36′ 15″	141° 30′ 15″	N 61° 40′ E	51.06	47.09	28.66
Onneto Bridge	Ⅲ	177.94	43° 15′ 00″	145° 29′ 00″	N 87° 10′ E	316.00	352.94	378.44
Hiroo Bridge	Ⅰ	376.95	42° 16′ 00″	143° 19′ 00″	N 23° 00′ W	159.51	144.00	36.58
Sapporo IC Overhead Bridge	Ⅲ	509.76	43° 04′ 00″	141° 25′ 00″	N 09° 43′ W	53.50	66.91	24.94
Hakutyou Bridge	Ⅲ	561.29	42° 20′ 42″	140° 57′ 11″	N 08° 08′ E	83.35		42.91
Shinhamaazuma Bridge	Ⅲ	483.24	42° 36′ 41″	141° 50′ 31″	N 09° 40′ W	72.21	95.30	26.08
Tokachikakou Bridge	Ⅲ	338.29	42° 42′ 07″	143° 37′ 26″	N 08° 50′ W	234.00	183.00	144.00
Tokachi Bridge	Ⅱ	367.16	42° 56′ 00″	143° 12′ 00″		121.66	140.75	95.19
Laboratory		514.21	43° 02′ 00″	141° 22′ 00″		14.63	6.97	11.72
Tyoshiro Embankment		475.07	42° 35′ 00″	141° 57′ 07″	N 65° 00′ E	62.00	59.00	27.00
Kakou-ugann Embankment		472.18	42° 30′ 12″	142° 00′ 48″	N 75° 30′ E	57.00	51.00	20.00
Ootu Embankment		337.53	42° 41′ 05″	143° 38′ 22″	N 00° 25′ E	216.00	206.00	118.00
Toitokki Embankment		338.79	42° 43′ 35″	143° 36′ 34″	N 00° 26′ E	184.00	191.00	104.00
Tbikorai Embankment		341.41	42° 45′ 11″	143° 34′ 05″	N 00° 28′ E	149.00	182.00	96.00
Horooka Embankment		341.96	42° 46′ 53″	143° 33′ 09″	N 00° 28′ E	264.00	207.00	155.00
Reisakubetu Embankment		346.72	42° 50′ 00″	143° 28′ 42″	N 00° 31′ E	276.00	301.00	166.00
Tounai Embankment		349.53	42° 53′ 21″	143° 25′ 44″	N 00° 34′ E	365.00	453.00	124.00
Usyubetu Embankment		348.77	42° 47′ 20″	143° 27′ 55″	N 00° 32′ E	214.00	197.00	142.00
Higashiinaho Embankment		337.25	42° 47′ 06″	143° 36′ 37″	N 00° 26′ E	487.00	223.00	167.00
Kushiro Shigai		267.65	43° 03′ 20″	144° 24′ 24″	N 25° 01′ E	351.00	380.00	252.00

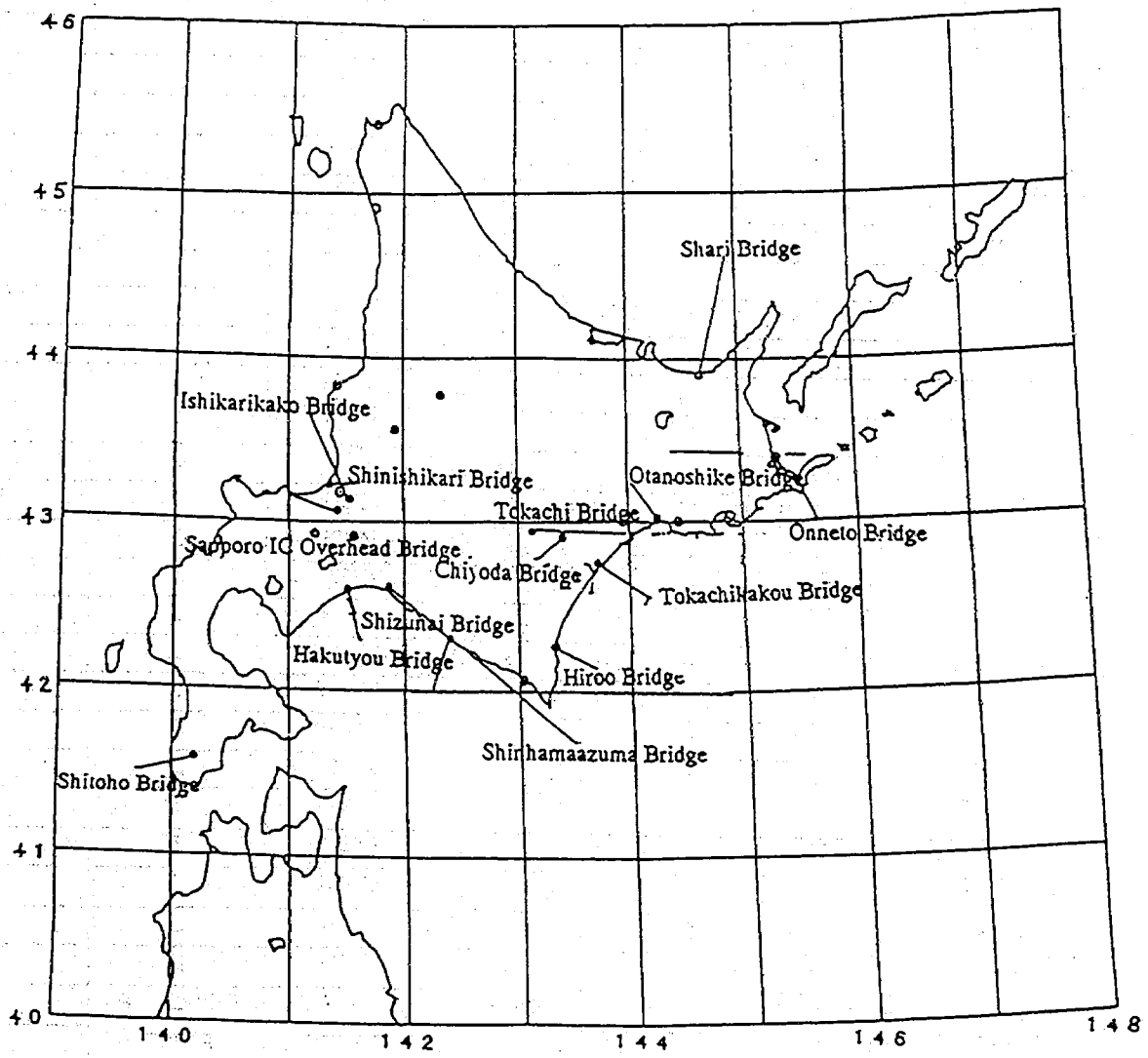
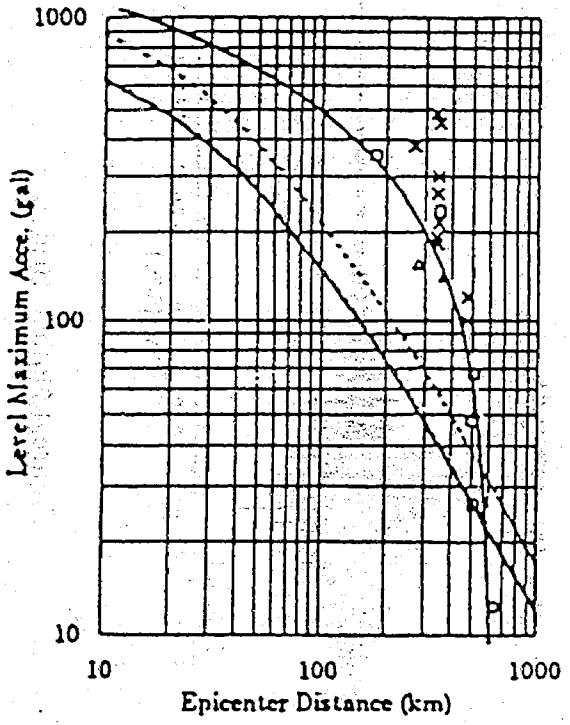
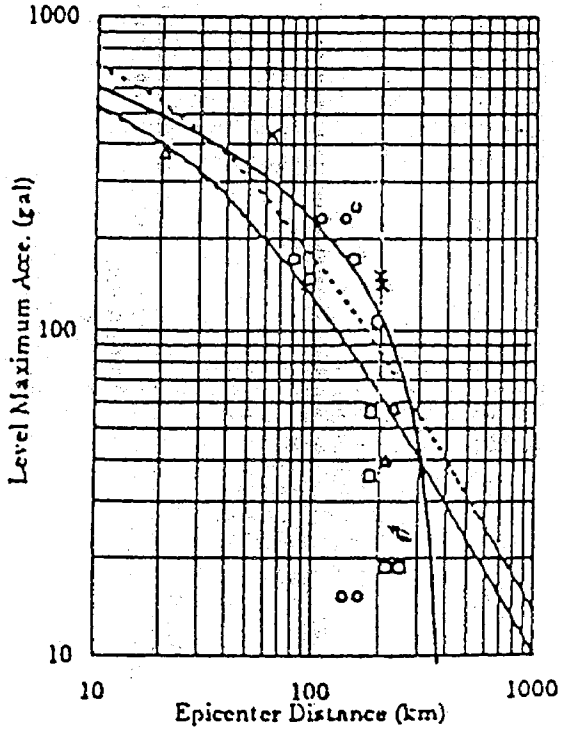


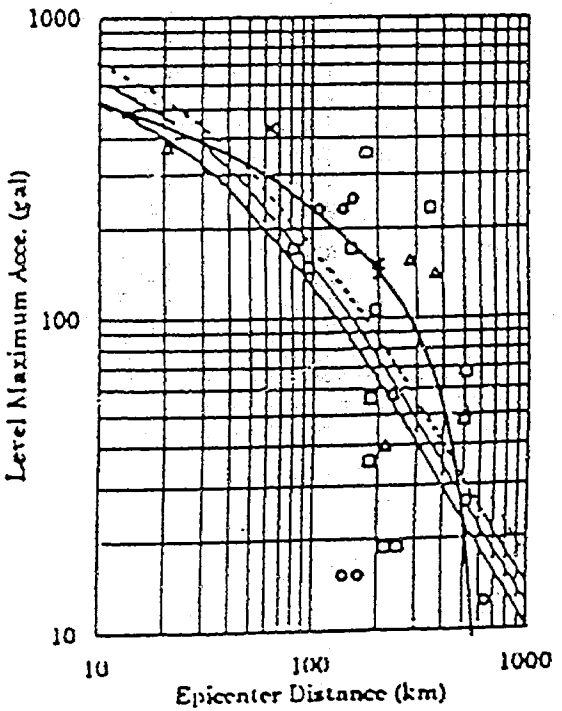
Figure.1 Epicenter and observation stations of strong temblors



Toho-oki Earthquake

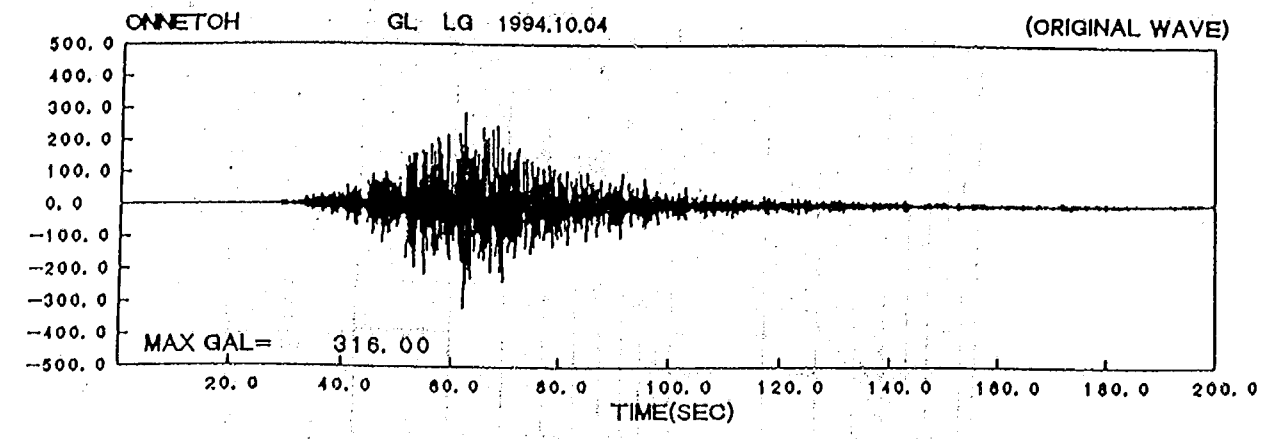


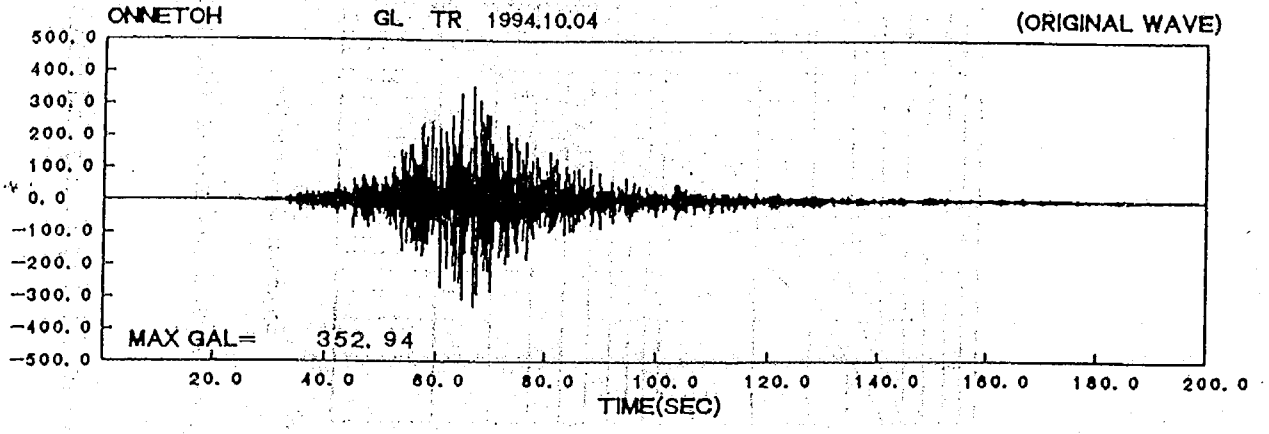
Nansei-oki and kushiro-oki Earthquakes



Touhou-oki,Nansei-oki and
Kushiro-oki Earthquakes

Figure .2 Distance from epicenter and maximum acceleration





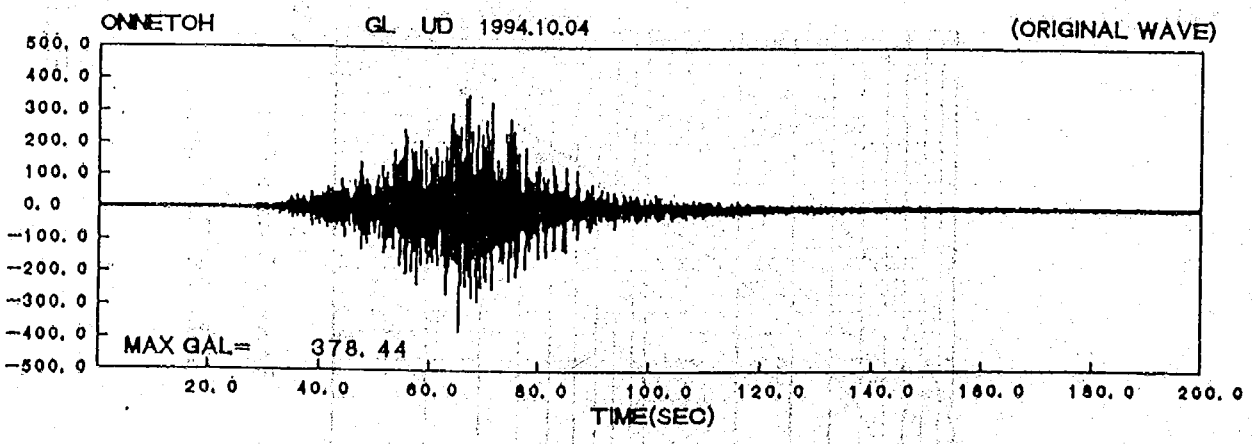
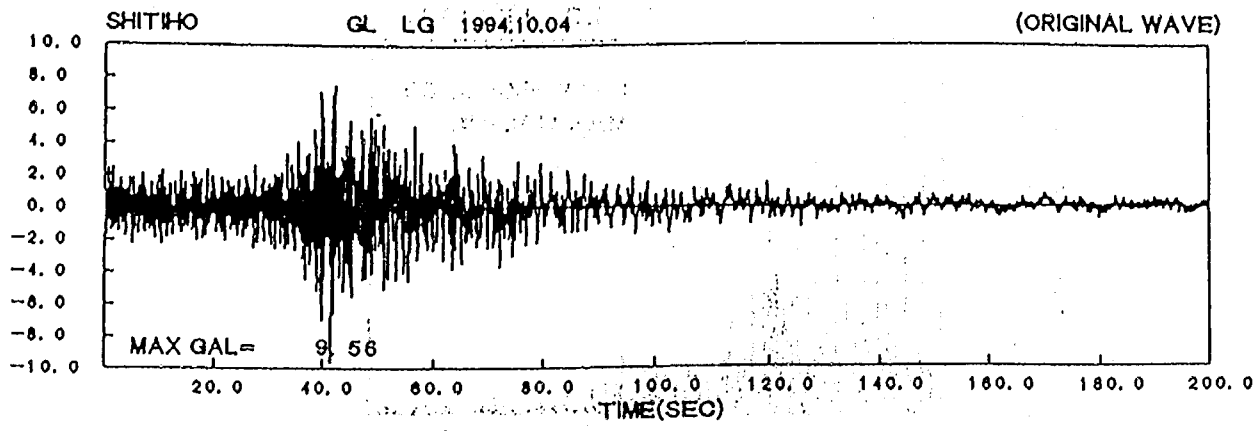
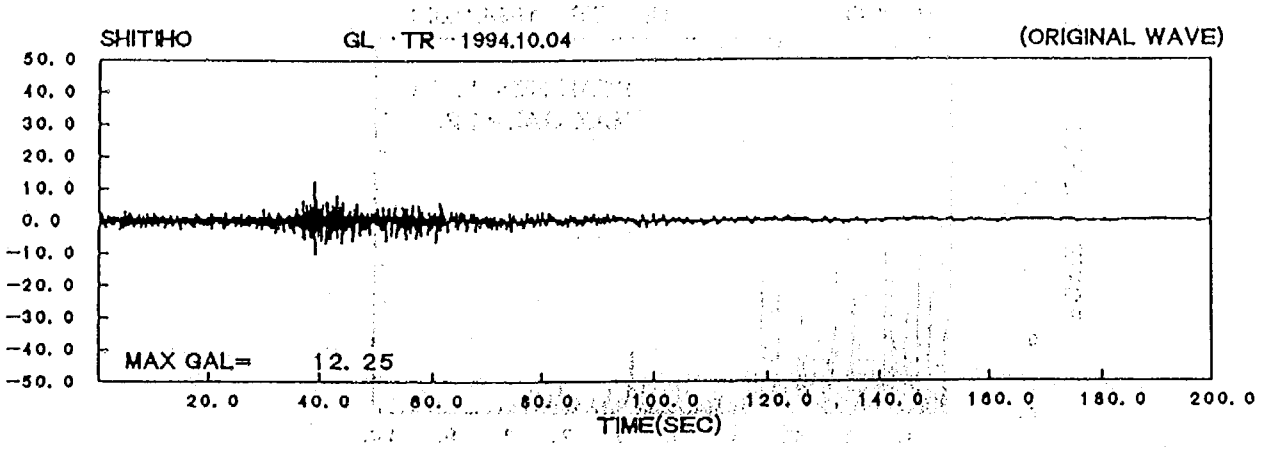


Figure.4 Onneto Bridge





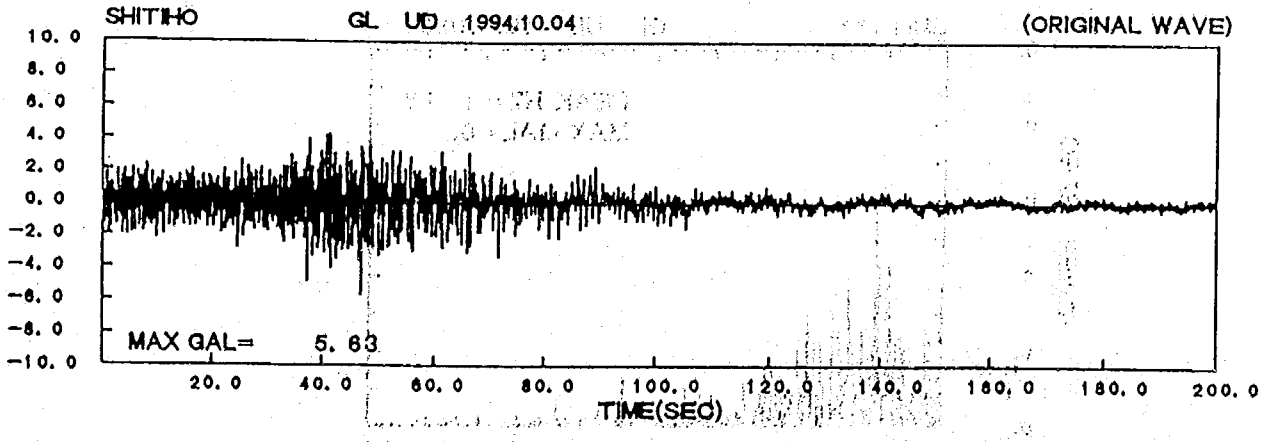
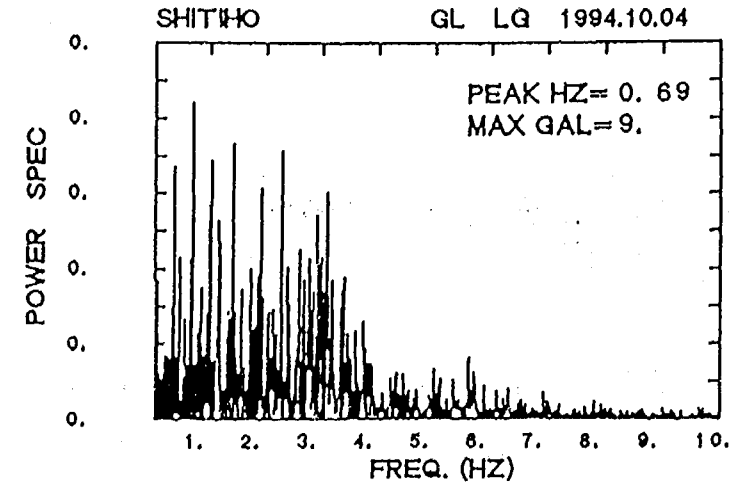
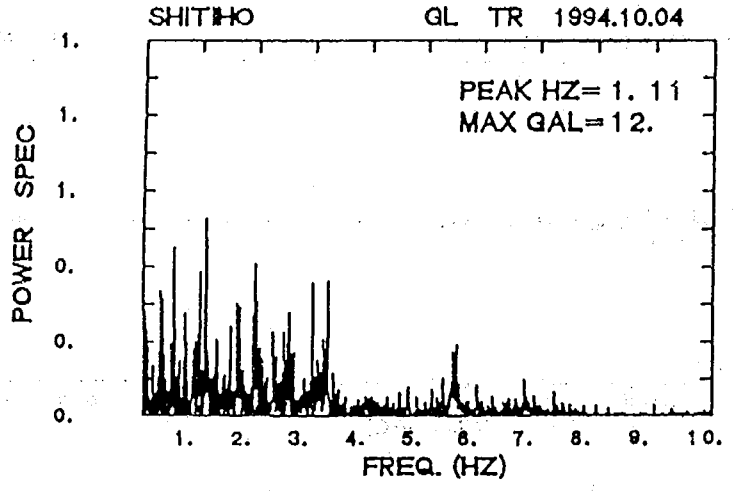


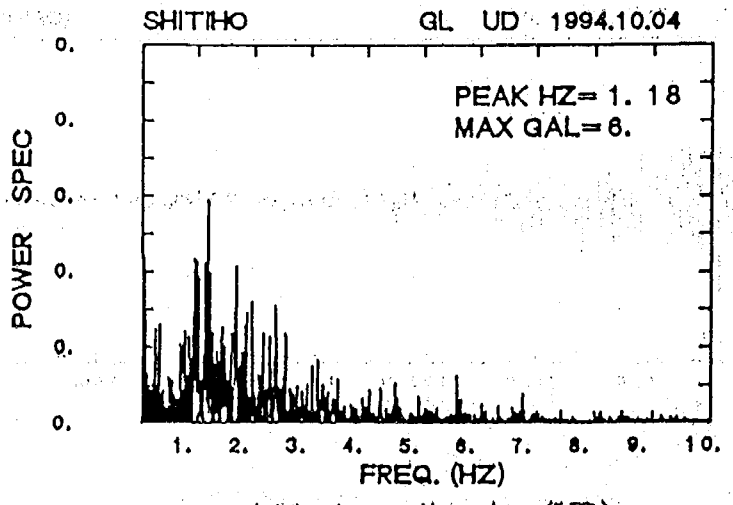
Figure.3 Shichiho Bridge



a) Longitude direction (LG)

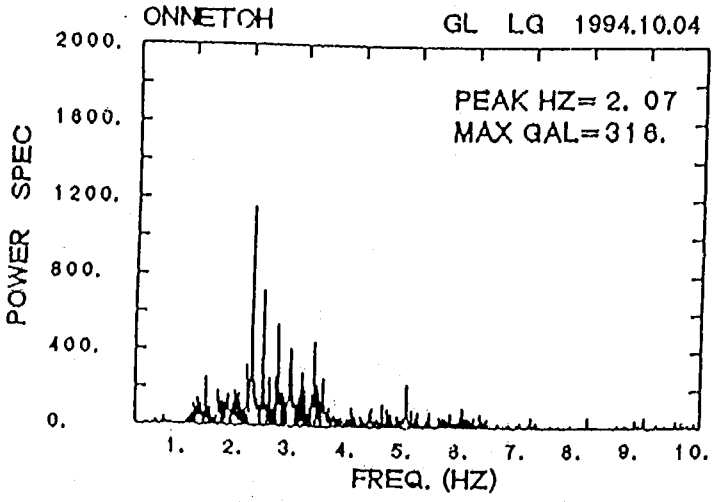


b)Transverse direction (TR)

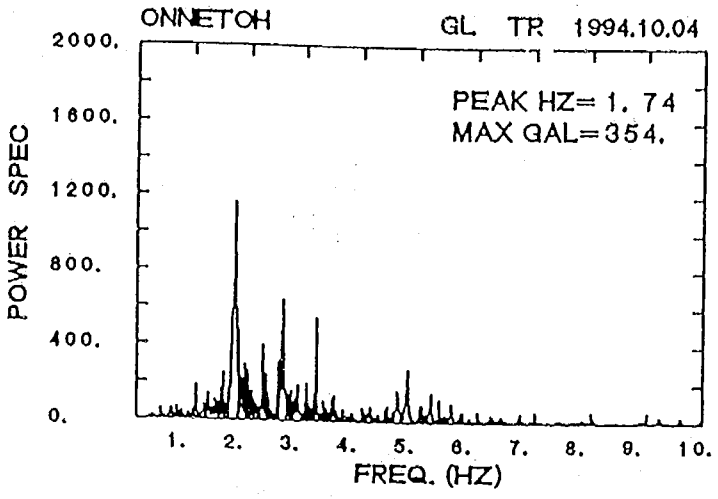


c) Up-down direction (UD)

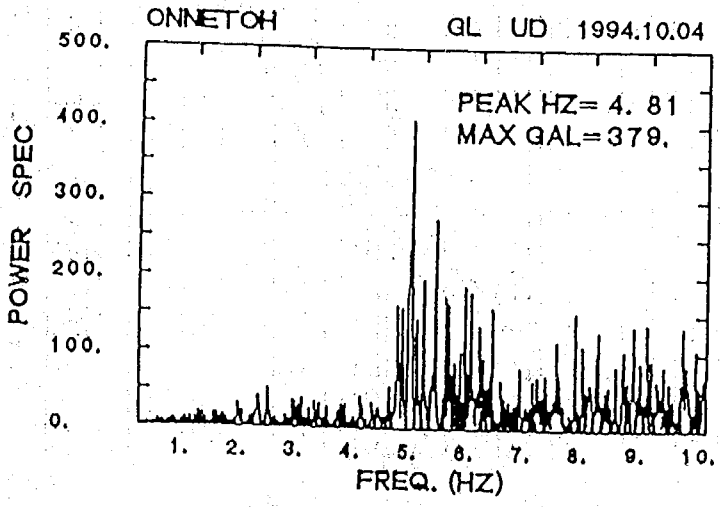
Figure.5 Power spectra of Shichiho Bridge



a) Longitude direction (LG)

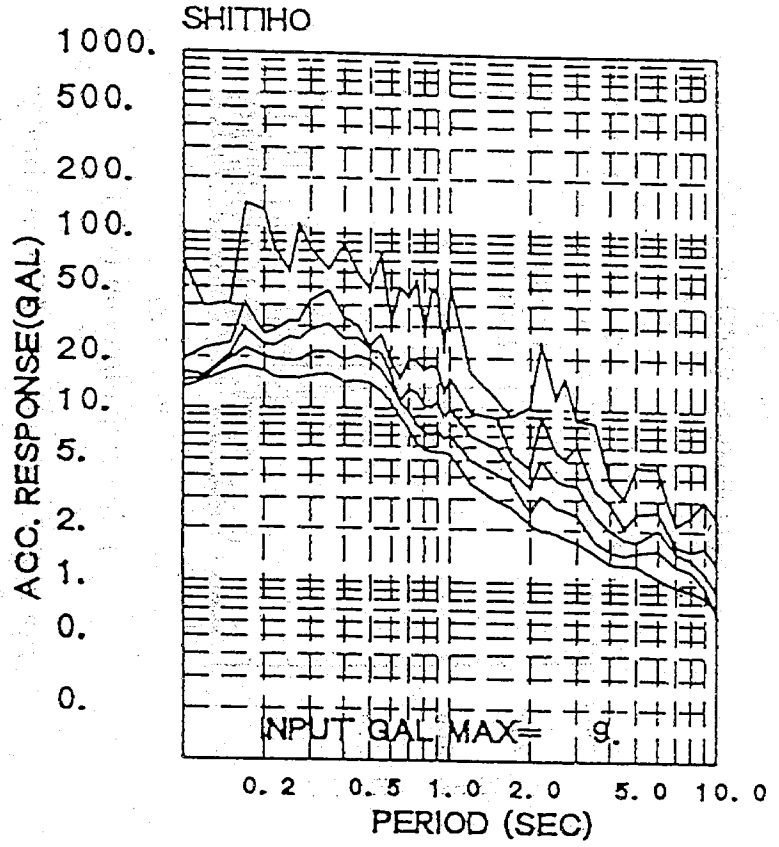


b)Transverse direction (TR)

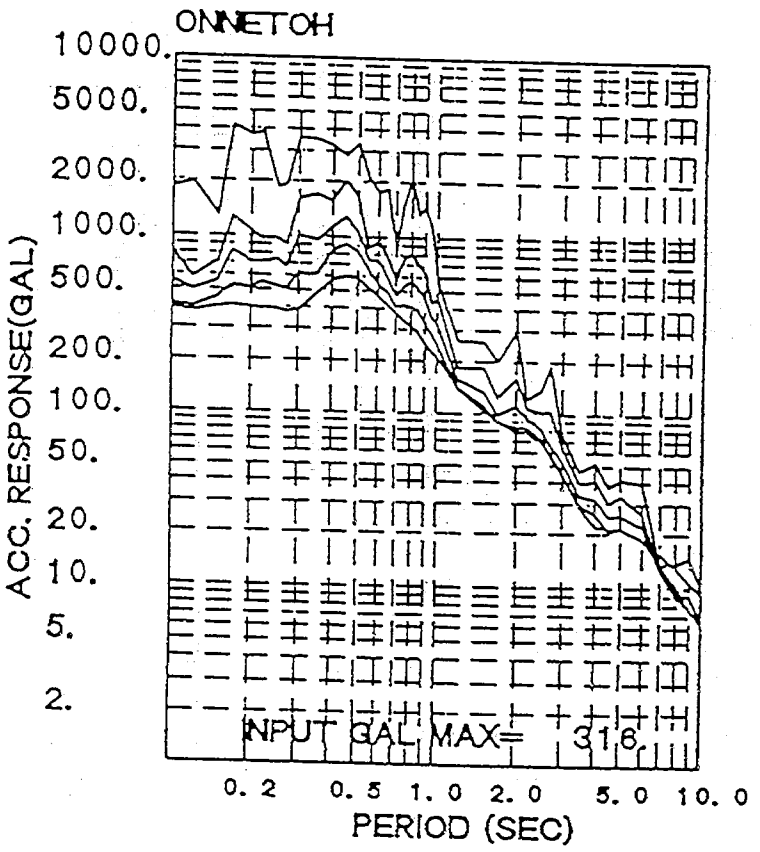


c) Up-down direction (UD)

Figure.6 Power spectra of Onneto Bridge



a) Shichiho Bridge



b) Onneto Bridge

Figure.7 Acceleration spectra in the direction of LG

Features of Damages to Road Embankments by Recent Earthquakes in Hokkaido,Japan

by
Jun'ichi Nishikawa [1] and Yasuaki Matsuda [2]

ABSTRACT

Three big earthquakes hit Hokkaido in 1993 and 1994. They caused many damages to embankments of national highway. Failures or deformations of road embankment in each earthquake had some variety, resulting from geology and topography in damaged area and types of embankment. Examining the above features, high embankments, embankments on catchment topography, embankments on soft ground and approach embankments to bridges have rather high potential damage by a big earthquake. It is needed to asses the possibility of failure of the above embankments by a future big earthquake and to examine reinforcement work of road embankments.

Key Words : Earthquake,
Road Embankment,
Failure
Earthquake-resistant Fill

1.INTRODUCTION

Hokkaido was hit by the Kushiro-Oki Earthquake in January 1993, the Hokkaido Nansei-Oki Earthquake in July 1993 and the Hokkaido Toho-Oki Earthquake in October 1994 in succession(Fig.1). Damaged area of the first two earthquake were the eastern part of Hokkaido, while the southwestern part of Hokkaido for the latter one.

Road embankments of national highway of the above area were damaged much by the three earthquakes. This paper reports the features of those embankment failures and examines types of high potential failures of road embankment in a big earthquake.

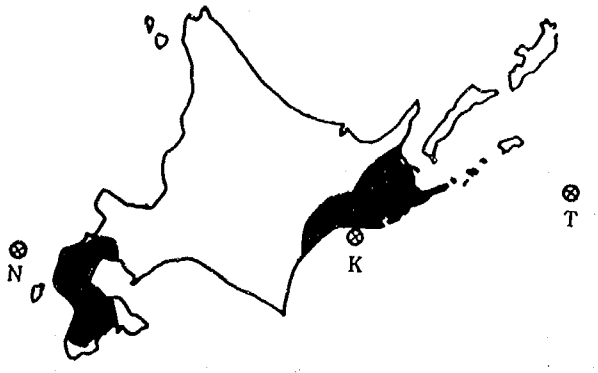


Fig.1 The epicenters of the three big earthquakes occurred in Hokkaido in 1993 & 194 and damaged area (shaded) of national highway
K:Kushiro-Oki,
N:Hokkaido Nansei-Oki
T:Hokkaido Toho-Oki

2.THE KUSHIRO-OKI EARTHQUAKE

This earthquake occurred on January 15,1993 with magnitude 7.8 of Richter-Japan Meteorological Agency(JMA) scale. The epicenter was 15km south of Kushiro city, and the focal depth was 107km.

Embankments of national highway in Obihiro and Kushiro area, where are in the eastern Hokkaido, were damaged much (Nishikawa,1993). Failures of embankment, cracks and settlement of pavements and settlement of approach embankment to bridges are main damages to national highway. They are more than hundreds, while approximate 30 big damages which needed careful rehabilitation. Most of large failure was observed at transverse

1) Head, Geotechnical Section, Structures Division, Civil Engineering Research Institute, Hokkaido Development Bureau, 1-3 Hiragishi, Toyohira-Ku, Sapporo, 062 Japan
2) Research Engineer, ditto

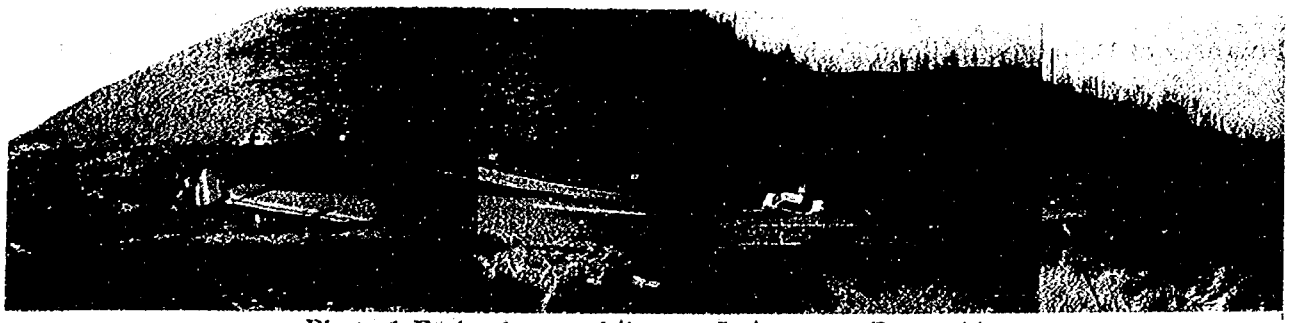


Photo.1 Embankment failure at Itoizawa on Route 44

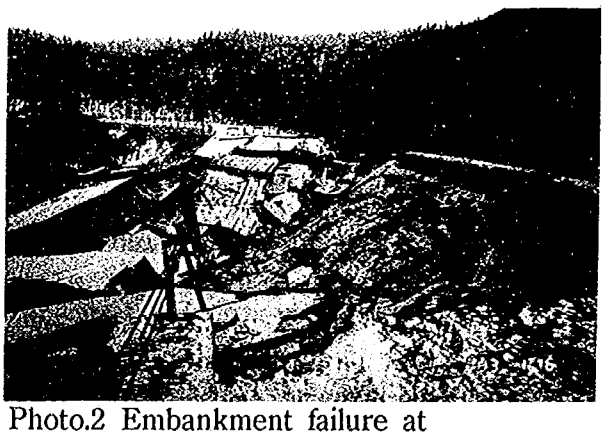


Photo.2 Embankment failure at Higashiarekinai on Route 272

embankment on small valley. The four cases, which were Pashikuru in Shiranuka Town on Route 38, Itoizawa (Photo.1) in Akkeshi Town on Route 44, Higashiarekinai (Photo.2) in Shibecha Town on Route 272 and Toritohshi in Kushiro Town on Route 391, were typical of such failures.

The section of the failure at Itoizawa is shown in Fig.2. The embankment failure was 68m long and about 3m deep. This was a half bank and half cut site where natural slope of alternating beds of sandstone and conglomerate was cut and the cut soil was filled. Peaty swamp was widely distributed in front of the slope. Colluvial deposit reached 35 to 45m from side of the road with remaining shape of the surface of embankment slope. Water which appeared from slip surface was observed. Although it is not distinct whether this water was derive from inside of alternating beds of sandstone and comglomerate or from neighboring stream, some part of embankment were estimated to be high on water ratio.

Failure at Higashiarekinai on Route 272 was occurred at the site where slope of volcanic sand was cut and the cut soil was filled(Fig.3). Remained slope had two streams , and surface water and ground water were easy to concentrate to fills. Water was sprung from slip surface. Groundwater level before failure was estimated to be in half height of embankment.

The common features of four big failures in national highway are as follows;

① Groundwater is easy to concentrate into embankment fills.

② Some of fills or slopes had possibility to be saturated with water and to be weakened in strength. Frozen surface of embankment had possibility to disturb drainage of groundwater from fills.

③ Moving distance of every colluvial deposit is rather great compared to height of embankment.

④ Material of fills is sand or sandy soil. Ground water level was estimated to be high at the earthquake.

Some of the above may suggest that excess pour-water pressure occurred in fills at the earthquake and that shear strength of fills was strongly weakened. However, sand boil was not observed.

Distributions of failures and deformation of embankment in national highway are not always reflected to distance from the epicenter. They depend on geology, topography ,and shape and size of

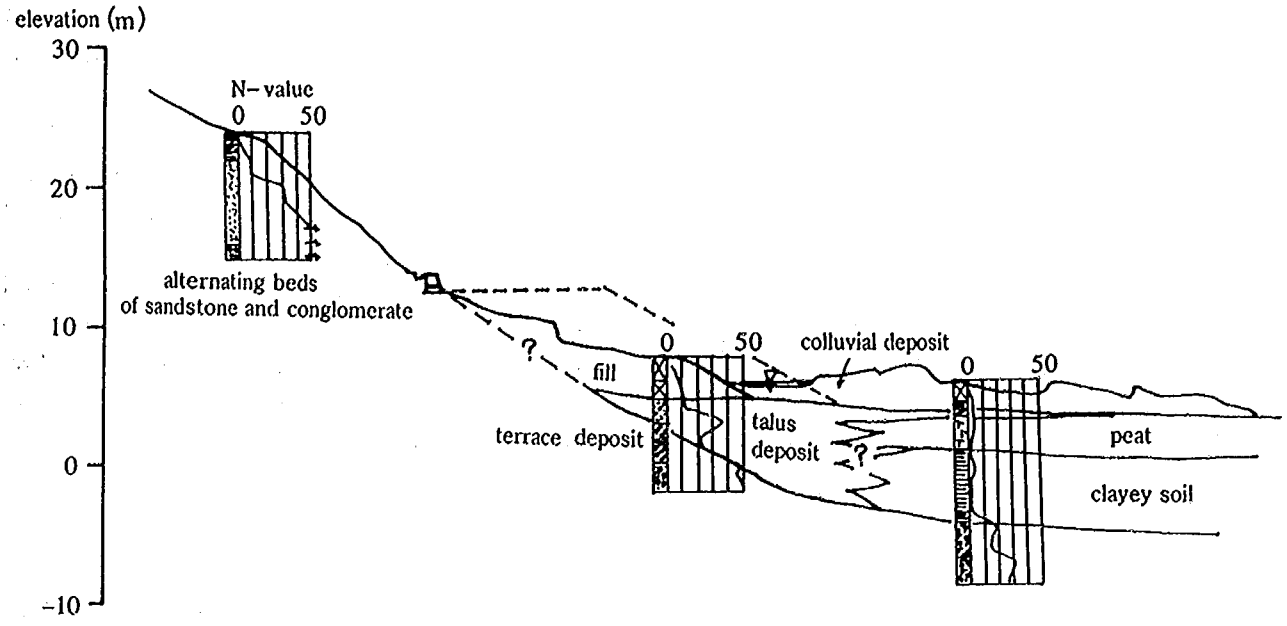


Fig.2 The cross section of the failure site at Itoizawa

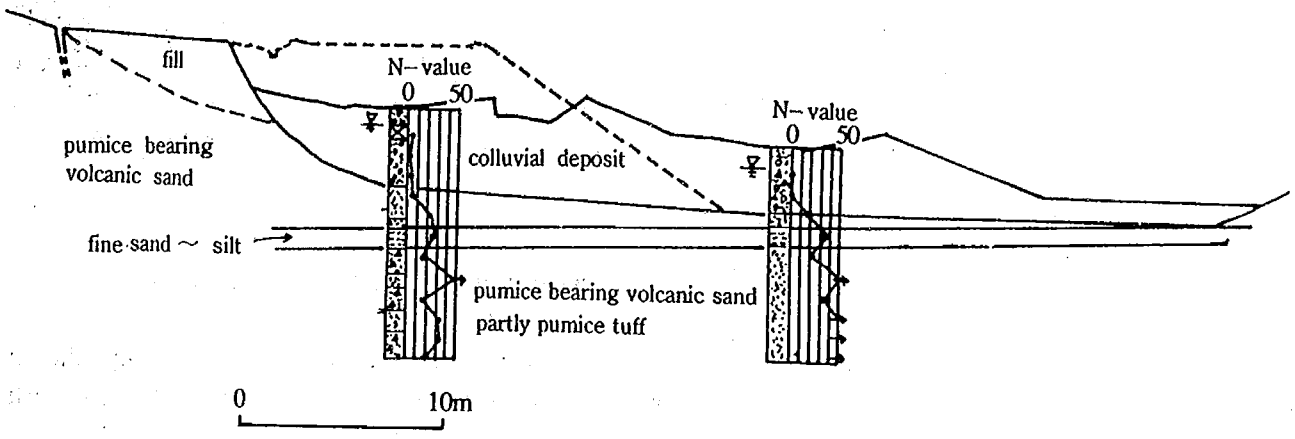


Fig.3 The cross section of the failure site at Higashiarekinai

embankment fills. Many damage such like cracks and deformation occurred in low embankment fills on peaty soft grounds.

3.THE HOKKAIDO NANSEI-OKI EARTHQUAKE

This earthquake occurred on July 12,1993 with magnitude 7.8 of Richter-JMA scale. The epicenter was approximate 100km of southwestern Hokkaido, and focal depth was 34km. A great number of damage was caused by this earthquake especially in Okushiri Island and the southwestern part of Hokkaido.

National highway of the southwestern Hokkaido was damaged much (Nishikawa, 1994). This area, Oshima Peninsula, is generally mountainous. National highway leads along the coastline and across the peninsula. As mountains of western side are close to the Sea of Japan, national highway in these area runs along rock slopes. Rock slope failure and rock fall were occurred much in these section at this earthquake. Settlement of approach embankment to bridges was often occurred even in these rocky section.

A big failure of embankment occurred at Chirai in Oshamanbe Town on Route 5

(Photo.3). The size of failure was 100m wide, 50m long and 6 to 8m deep. No other failure of embankment like this volume was not found in this earthquake.

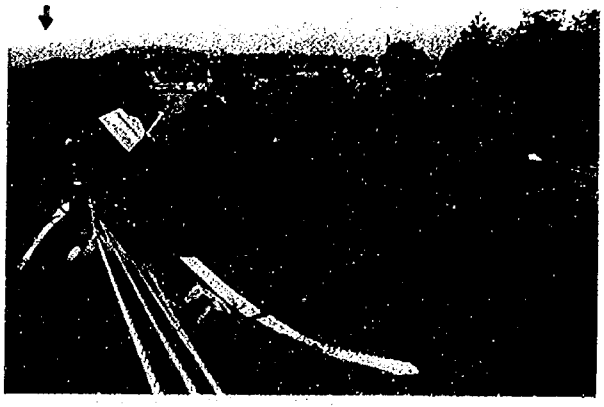


Photo.3 Embankment failure at chirai on Route 5 in the Hokkaido Nansei-Oki Earthquake

The embankment was filled on the section between hill and flats. Alluvial organic soil overlying lignite-bearing diluvium clay with conglomerate is distributed in mountain side and alluvial clay with peat,clay and peat unconformably overlie on diluvium in river side(Fig.4). Peaty swamp between national highway and railroad is very soft and water level there is high. Materials of fill is clayey soil and fill itself was seemed to be compacted regularly. Mechanism of this failure is estimated as follows. Soft ground of peat and clayey soil near toe of slope began to move laterally and embankment fills which lost support followed to move.

Route 5 runs on low shore terrace along Uchiura Bay. Collapse of shoulder, settlement of curb stone, cracks and wavy settlement of pavement occurred in these section(Photo.4). Sand boil was observed with the above phenomena. This was also observed in surrounding area such like grassland, housing sites and school ground. This suggests that these road deformation were formed by liquefaction of grounds.

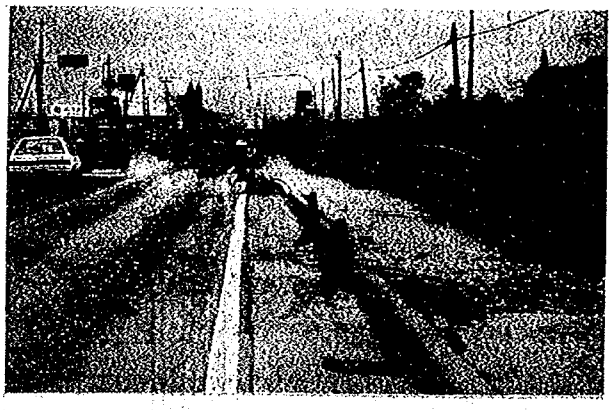


Photo.4 Wavy settlement caused by liquefaction

Two sites on foot of Mt. Komagatake of Route 5 were found to be deformed with volcanic ash boil.

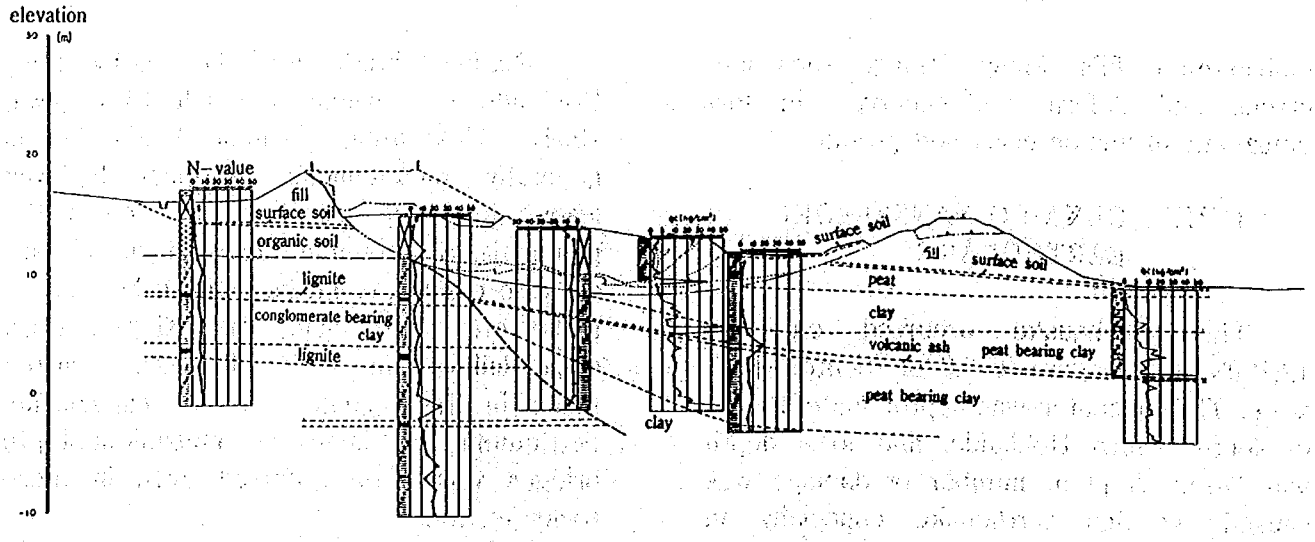


Fig.4 The cross section of the failure at Chirai

Road embankment damage in the Hokkaido Nansei-Oki Earthquake was characterized as settlement of approach embankment to bridges, failure of embankment near soft ground and wavy settlement of fills caused by ground liquefaction.

4.THE HOKKAIDO TOHO-OKI EARTHQUAKE

The Hokkaido Toho-Oki Earthquake occurred on October 4,1994 with magnitude 8.1 of Richter-JMA scale. The epicenter was 180km east of Nemuro city, and the focal depth was 30km.

Damaged area of this earthquake spreads on the east side of that of the 1993 Kushiro-Oki Earthquake with some overlap. Approximate 200 damages of national highway were counted with 13 great damages. They are almost related to embankment fills. Damages in road embankment are cracks and settlement at shoulders of one or both sides of embankment, slides of slope surface, deep slides of slope including pavement, and failure and settlement of approach embankment to bridges.

The failure of embankment at Nakachanbetsu of Sibecha Town on Route 272 was one of the typical example of failure of high embankment in this earthquake. This site is 100m long embankment section of which height is 8m. Two big slope failure of 40m long occurred with deep longitudinal cracks in the center of the road(Photo.5). Shoulder of reverse slope had longitudinal cracks and its slope was deformed much. Cutting embankment at restoration works, it is found that groundwater seeped into fills. It is estimated that drainage of groundwater was not sufficient and strength of embankment was weakened.



Photo.5 Embankment failure at Nakachanbetsu on Route 272

Approach embankment of the Toyooka Bridge of Nakashibetsu Town on Route 272 was settled 30 to 50cm and its slope was deformed much(Photo.6). Approach embankment of this bridge, of which height is 6m, was also deformed such like slope failure ,crack at shoulder and settlement of pavement.

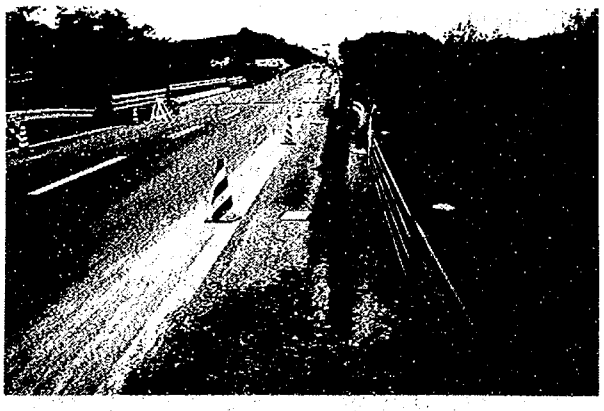


Photo.6 Settlement and deformation of approach embankment to the toyooka bridge

The damaged area of this earthquake is gently hilly topography covered by volcanic ash. Rivers cut this area from west to east with forming terrace. Marsh is distributed in lower reaches in these rivers. National highway which runs from north to south has more chance to cross rivers, while national highway which runs from east to west has less chance. Damages to embankment this time are found among embankments in hills, approach embankments to bridges, and low embankments on soft ground. National

highway transverse south and north had more damaged sites than those of east and west. This reflects different embankment which is derived from different topography.

5.POTENTIAL DAMAGES TO ROAD EMBANKMENTS BY EARTHQUAKES

The occurrence of damages to road embankments by the three earthquakes, which were mentioned before, suggests that ground shaking of intensity of more than 5 or 6(JMA stage) causes them. Not every road embankment fail in such ground shaking of course. It is important to check road embankment which has potential to be failed largely and to interfere traffic. Investigating examples of damages by recent three big earthquakes in Hokkaido, it is pointed out the followings as high potential damages to embankments by big earthquake.

① embankments of which height is more than 5 or 10m
② embankment on sloping ground
③ embankment on catchment topography
④ approach embankment to bridge
⑤ embankment on soft ground
⑥ embankment on sandy ground with high water table

6.EARTHQUAKE-RESISTANT ROAD EMBANKMENT

Japanese guidelines for embankment fills (Japan Road Association,1986) does not consider earthquake resistance for road embankments except special cases, for road embankment which are filled properly stand an earthquake of moderate intensity. However, as the occurrence in the above earthquakes show, some road embankments fail at earthquakes of intensity of more than 5. It is needed to assess potential damage to road embankments and to reinforce them if necessary This work is important to maintain traffic of national highway at intense earthquakes.

7.CONCLUSIONS

Investigations on damages to road embankments by recent three big earthquakes, which are the Kushiro-Oki Earthquake in 1993, the Hokkaido Nansei-Oki Earthquake in 1993 and the Hokkaido Toho-Oki earthquake in 1994, revealed that high embankment, embankment on catchment topography etc. have potential damage by intense earthquakes. Further assessment of embankments like the above and necessary reinforcement of high potential damage of embankment by intense earthquakes are important in order to maintain traffic of national highway.

REFERENCES

Japan Road Association(1986),Road Earth Work-Slope Work Guidelines,P.434.(in Japanese)

Nishikawa,J.(1993),Road Embankment, Damage to Highway and its Countermeasure, In Report on Investigation of Damages caused by "Kushiro-Oki Earthquake in 1993". *Rep.Civil Eng.Res.Ins.*,100,pp.33-40,(in Japanese)

Nishikawa,J.(1993),Road Embankment, Damage to Highway and its Countermeasure, In Report on Investigation of Damages caused by "Hokkaido Nansei-Oki Earthquake in 1993". *Rep.Civil Eng. Res. Ins.*, 101, pp.33-40,(in Japanese)

Nishikawa,J. et al.(1993),Road Embankment, Damage to Highway and its Countermeasure, In Report on Investigation of Damages caused by "Hokkaido Toho-Oki Earthquake in 1994". *Rep.Civil Eng.Res.Ins.*,108, pp.17-24,(in Japanese)

Damage and soil liquefaction caused by the 1994 Hokkaido Tohooki earthquake

Katsuyoshi SUZUKI*, Yoshitaka YAMADA*

ABSTRACT

The earthquake of magnitude 8.1 occurred off the eastern coast of the Hokkaido district on the 4th of October in 1994. It induced heavy damage to ports, roads, railways, bridges and lifelines in the areas of Kushiro and Nemuro districts.

The authors investigated damaged areas to clarify characteristics of various kinds of damage and the relationships between landforms and the damage for 5 days from the 7th to 12th of October.

They made sure that soil liquefaction was caused in former river courses, valley floor plains, alluvial lowlands, interlevee lowlands in sand dune area, reclaimed land by landfill and wetland. And this time, the sandblow was interbedded with pumice in Shibetcha town and peaty material in Shibetsu town. And soil liquefaction was caused at coastal landfill sites.

The Kushiro east fishery harbour was damaged by soil liquefaction. But the scale and intensity of the damage were more slightly than the ones by the Kushirooki earthquake in 1993. They also made sure that the difference of soil liquefaction between 1993 Kushirooki earthquake and 1994 Hokkaido tohooki earthquake was caused by the difference of the countermeasures against earthquake damage between 1993 earthquake and 1994 earthquake.

Key Words: Hokkaido Tohooki Earthquake, Disaster, Liquefaction, Landform

1. Introduction

On the 4th of October in 1994, an earthquakes of magnitude 8.1 hit the

---

*Geographic Department, Geographical Survey Institute, Ministry of Construction.

eastern part of the Hokkaido district. The epicenter of the earthquake was located at 35° 21' N, 147 ° 29' E, 30 km in depth (Japan Meteorological Agency (JMA): 1994). This earthquake was named the 1994 Hokkaido Tohooki Earthquake. It induced various kinds of damage in the eastern part of the Hokkaido district.

The authors investigated the areas of Kushiro and Nemuro cities, Shibecha, Nakashibetu, Shibetu, Bekkai towns. They clarified characcteristics of damage and the relationships between landforms and soil liquefaction. The authors will report the result of the investigation.

2.Earthquake

2.1 Earthquake

Fig.1 is a map showing the distribution of the seismic intensity by the main shock (Japan Meteorological Agency: 1994). The earthquake caused the seismic intensity VI in the areas of Kushiro city and Akkeshi town, and V in the areas of Nemuro city, Hiroo and Urakawa towns(JMA scale). It quaked broad areas including the Tohoku, Kanto and Chubu districts.

The Kushiro area was also hit by the 1993 earthquake with seismic intensity VI. This time, the earthquake in 1994 was caused by the rupture of the inside of the plate (JMA:1994). According to the department of technology, Hokkaido University, the hypocentral region was located 30km below the sea level, and it was distributed about 130km long in a major axis from northwest to southeast in the inside of the plate (Fig.2).

2.2 Records of strong motion at Kushiro observatory

Records of accelerograph in Kushiro observatory were shown in Fig. 3 (JMA:1994). The maximum accel-eration by the Hokkaido Tohooki Earthquake was 473 gal for a pretty long time. The maximum acceler-ation of the 1993 Kushirooki Earth-quake was 919 gal in a shorter time.

3. Physical Settings

The geological base of the area consists of Cretaceous system and Paleogene system. And Diluvium, Kushiro formations cover these old base in these area. The north-western margins of the Nemuro and Kushiro sub prefectures consist of volcanic mountains called Mts. Shiretoko, and Kussharo-and-Akan crater lakes.

Nemuro and Kushiro areas are characterized by the Konsen

tableland with many small rivers rising from itself. The Konsen tableland consists of two terraces called the Nemuro and Kushiro terraces, and their ground levels are 70-140m and 30-60m. There are many wetlands and lakes in the small river valleys. The areal extent of the Kushiro wetland, is about 29.1km^2.

It is distributed in the lower drainage basin of the Kushiro river. This largest wetland in Japan, including lagoons such as Tatsukobu marsh, Touro lake and Shirarutoro marsh. There are a few coastal dunes between the coast and the the Kushiro wetland(Fig. 4).

4. Outline of damage

The earthquake induced various types of damage in the areas covering the Kushiro and Nemuro cities, Kushirocho and Nakashibetu towns. In Kushiro city and its vicinities, soil liquefaction was caused in many sites in reclaimed lands by landfill in the coastal lowland. It was accompanied by spouting water with sand and sticking out of manholes with subsidence of ground surface.

Many buildings and houses were destroyed partially in Nakashibetu, Bekkai and Shibetu towns. Gas pipes and water supply pipes were damaged. But electric power lines were damaged little. This time, the intensity of the damage of lifelines was not so severe as the one by 1993 Kushirooki earthquake. And landslides and failures were caused in hilly areas. Land subsidence was caused in reclaimed lands by landfill (photo.1). Casualties were no death and 436 injuries (Table.1).

5. Soil Liquefaction

The outline of soil liquefaction by the 1994 Hokkaido Tohooki Earthquake is shown in the followings:(Table.2)

a)Kushiro wetland:

Soil liquefaction was seen in landfill. Sandboils came out through cracks at the edges of roads or the electric light poles at Ashino in Kushiro city (Photo. 2). Some irrigation canals were ruptured by the earthquake shock, and soil liquefaction stuck out pipes about 30cm from ground surface and spouted water with sand to form sandboils at Mutsumi in Kushiro town (Photo. 3). The damage of houses at landfill wetlands in the 1994 Hokkaido Tohooki Earthquake are more slightly than the one by the 1993 Kushirooki Earthquake.

b) Area along the coastline

Piers and relating facilities were intensively damaged repeate-

dly by both 1993 and 1994 Earthquakes in Kushiro port. In spite of the same seismic intensity between these two earthquakes, the damage in 1994 was more slightly than the one in 1993 at the same places. At landfill, hard soil layer covers soft ground and for the reason soil liquefaction can be easily caused when the soft ground(with specified grain size sand layer) is saturated with water (Photo. 4,5). Such cases were seen at landfill areas near the coast.
c) Sandboils were seen at a gravel road at a residential area. Slight damage was seen in many sites in the Shibecha town (Photo. 6).
d)Unequal land subsidence:

Soil liquefaction was caused at Shibetsu high school and Shibetu kindergarten which are located at landfill in peaty backmarsh in Shibetu town (Photo.7). It caused the land subsidence and step like differ-ence of the ground level with about 10 to 15cm in relative height (MINOWA, etc.:1995).
e)Landfill in the interlevee lowland:

Soil liquefaction was seen at landfill in the interlevee lowlands of Otanoshike area along the Kushiro-kaido route (main road) and in the lowermost drainage basin of the Shibetsu river. It was with spout of water, cracks and unequal land subsidence in the Kushiro wetland and in the lowermost basin of the Shibetu river.

6.Discussion
(1)Sites of soil liquefaction:

Most of soil liquefaction was caused at landfill where soft ground is covered by hard soil layer. Soil liquefaction was seen in the following areas: a)The landfill in the Kushiro marshy land. (Kushiro city, Kushiro town), b)The reclaimed land along the coastline. (Kushiro port, Kushiro city, and Hanasaki fishing port, Nemuro city), c)The landfill in the former river courses (the Shibecha river, Shibecha town), d)The landfill in the marshy lowland (Shibetu kindergarten, Shibetu town), e)The landfill in the lowland interdunes (Otanoshike, Kushiro city).

As for soil liquefaction at former river courses, it was made sure that soil liquefaction was caused in the inside of the soft ground, because pumice was found among spouting materials. It shows that the pumice came out through the landfill covering soft ground layer. because the landfill consisted of only gravels and sand without pumice. This was found at Shibecha town by the authors themselves.

According to MINOWA et al, they made sure that soil liquefaction was caused in the inside of peat layer at

Shibetu town. This is very rare case.

These cases show that soil liquefaction may be caused easily at soft ground including peat layer and at the sites where popular landfill are seen.

(2) Comparison of damage with 1993 and 1994:

This time, soil liquefaction was caused at almost the same sites as sites where the 1993 Earthquake caused. But the total damage by the 1994 earthquake was one fourth of that by the 1993 Earthquake. It was caused by the differences of the distance from the hypocenter and of the duration of the earthquake.

Especially the damage by soil liquefaction was one fifth at the Kushiro west fishery pier and its surroundings Soil liquefaction sites, were distributed in specific landforms in lowlands. Most damage concentrated in artificial landfilled areas.

(3) Foundation improvement works:

As we mentioned in (1) and (2), soil liquefaction and subsequent damage were caused in specific artificial microlandforms in marshy lowlands. But, in Kushiro city, there are the grounds of some construction lots of which foundation were improved after the 1993 earthquake damage. Little damage was caused in such sites.

7. CONCLUSION

Both the 1993 and 1994 earth-quakes caused various kinds of damage in common areas. Damage by the 1994 earthquake was one fifth of that by the 1993 earthquake.

Most of damage are related to characteristics of ground. Especially, they correspond to microlandforms in lowlands. Most of geomorphological change was caused by soil liquefaction. Urbanized areas are usually formed in artificial landfill onto soft ground in lowlands and most of soil liquefaction was caused in such areas.

Slope failures were caused at roadbeds in many sites. But they were not so intensive except a few sites. These were also caused in the thickly banked area onto a soft ground which had once been marshyland in the alluvial lowlands.

Thus, the authors concluded that this time the the damage in lowlands were caused in landfill and banked sites onto soft ground. And small damages also were caused in the borders of terraces and landfill sites at the end of terraces. There is very evident relationships between microlandforms and various kinds of damages by the earthquake.

ACKNOWLEDGMENTS

The authors are full of gratitude to many organizations and people. They helped the authors to clarify actual conditions of the Hokkaido Toho oki earthquake as shown in the followings: Kushiro Development Department of the Hokkaido Development Agency, Kushiro branch office, Nemuro branch office, Kushiro city, Nemuro city, Kushiro-machi town, Shibecha town, Naka-shibetu town, Shibetu town, Bekkai town, Shin Gijutu Consultants Co. and Kokusai Kogyo Co.. Mr.Kiyoshi MIMURA gave a chance of the research.

REFERENCES

The followings are in Japanese.

1)Shozo KAJIKAWA and Shinji TAKAZAWA (1993): Damage Researching Report of Kushirooki Earthquake. Bull. of the Geographical Survey Institute Vol.78. p28-40

2)Measurement Committee on Soil Liquefaction, National Land Agency (1993): Soil Liquefaction Map and Engineering Method of Measurement. p11-20

3)Yoshio OKAZAKI, Shigeru SATO and Haruo NAGAHAMA (1966): OTANOSHIKE, Explanatory Text of the Geological Map of Japan (scale 1;50,000). Hokkaido Development Agency. p90

4)Yoshio OKAZAKI (1993): Damage by Kushirooki Earthquake. Jour. Geol. Soc. Japan. Vol.99 , No.7, photo. 16 (frontispiece with descriptions), Nov. 1993.

5)Japan Meteorological Agency (1993): Disaster Earthquake Kushirooki Earthquake of October in 1993 Disasters, No1. p18

6)Japan Meteorological Agency(1994): Disaster Earthquake. Hokkaido Tohooki Earthquake in 1994 Disasters, No2. p27

7)Documentary Record of Kushiro oki Earthquake, Record Commission, Kushiro City(1993):The Report of the 1993 Kushirooki Earthquake. pp377

8)Research Group on the Quaternary of Japan. Quaternary in Hokkaido (1969): Quaternary System of Hokkaido, Hokkaido Group Monograph15, p1-35,

9)Chikahiro MINOWA, Takashi INOKUCHI, Makoto MIYAMOTO, Takaaki KAGAWA and Akio ABE (1994): Report on the Disaster Caused by the East off Hokkaido Earthquake on October 4, 1994. The National Research Institute for Science and Disaster Prevention, Science and Technology Agency, Japan. No.33 p153

Table. 1, General Aspect of Damage(Made up as of February 22th, 1995. Fire and Disater Prevetion Division of Hokkaido)

Class		Amount of damage
Casualties	Dead	0
	Injured	436
Houses	Complete Destruction	39
	Partial Destruction (half collapsed)	382
	Partial Destruction (slightly damaged)	7,154

Table. 2, Geomorphological Condition for Soil Liquefactionand damaged places in liquefied aras

Geomorphological Condition	Damaged Place
present river courses, former river courses	Shibecha, Shibecha town
landfilled area in an alluvial lowland	Shibetsu town
lowland in a coastal dune peaty and marshy lowland	Otanoshike, Kushiro city Ashino and Busa, Kushiro city Mutsumi and Kokuyo, Kushiro town
reclaimed land in a coastline reclaimed land in a port	Tatsukobu, Kushiro town Kushiro port, Kushiro city. Nemuro port, Nemuro city. Kiritappu fishing port, Hamanaka town

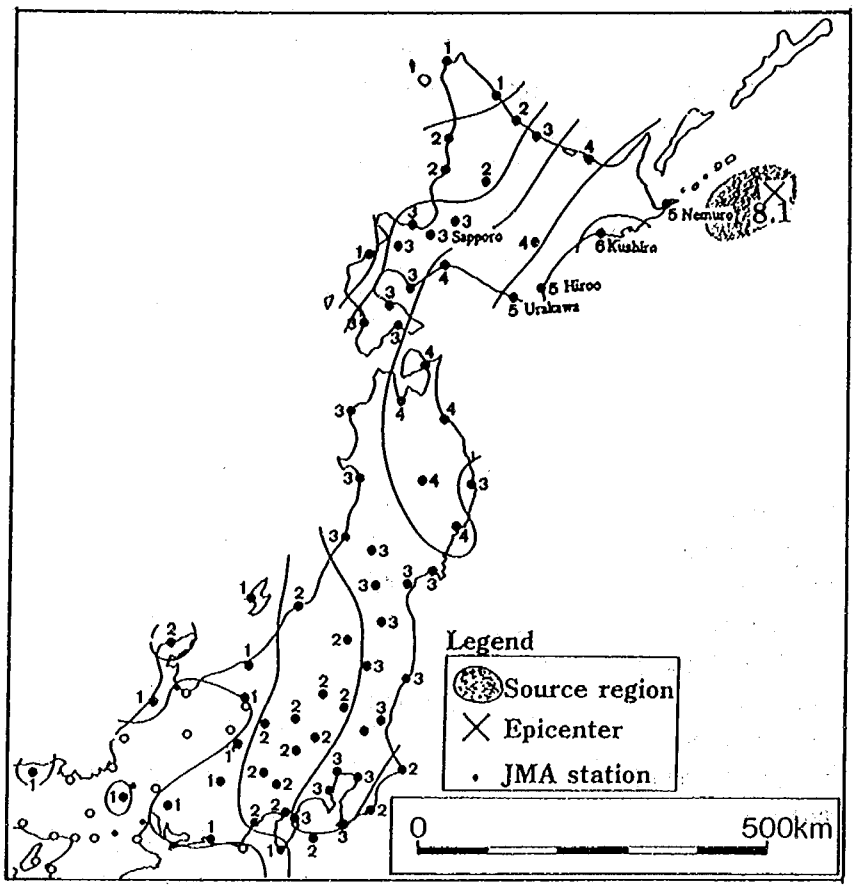


Fig. 1
Distribution of seismic intensities on Japan Meteorological Agency Scale by the Hokkaido Toho-oki Earthquake in 1994.

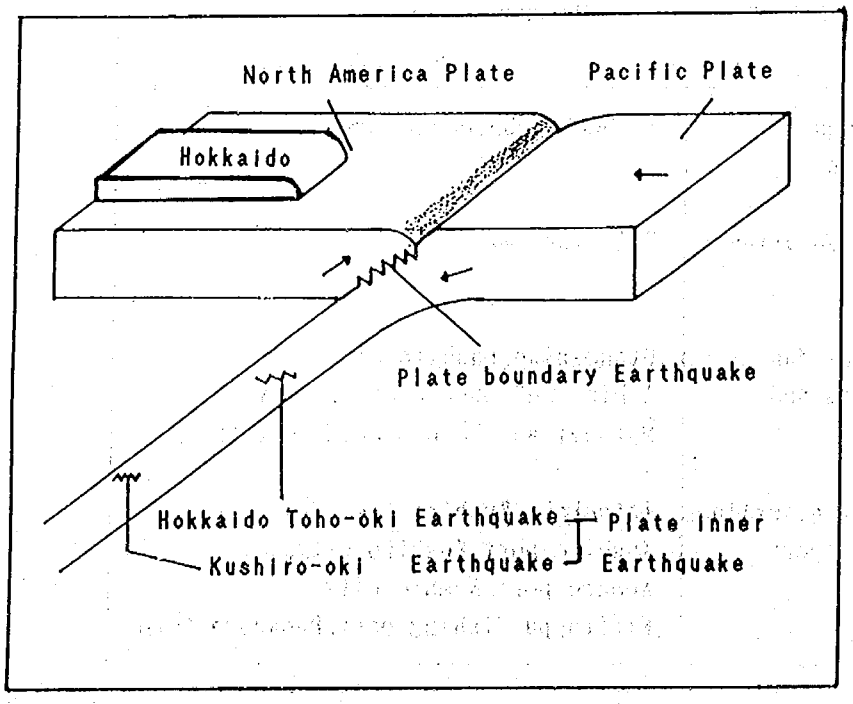


Fig. 2
Schematic illustration explaining the relation of deep and shallow earthquakes near Hokkaido

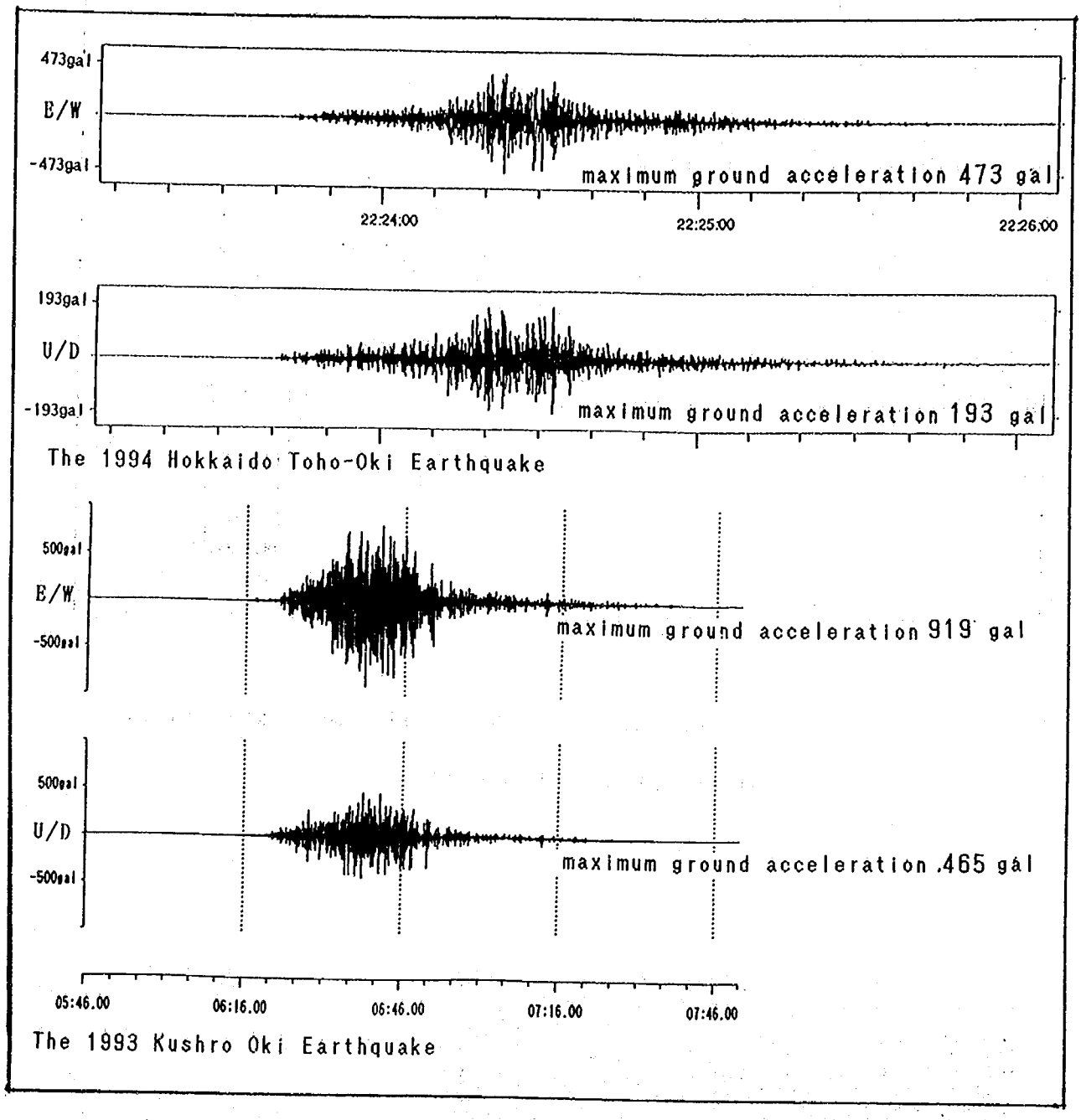


Fig. 3 The strong motions(, E/W, U/D) recorded at Kushiro (Accelero gram of Japan Meteorological Agency station (J.M.A, 1993.1994))

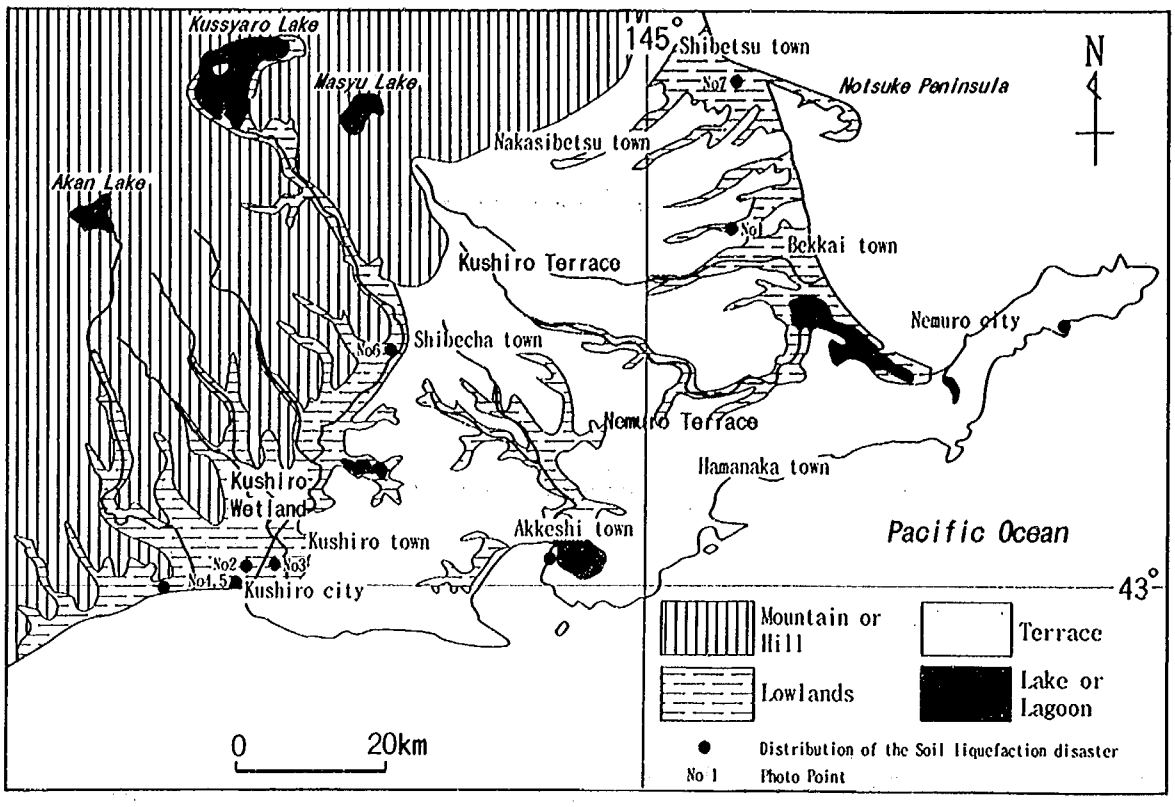


Fig.4 Index map of the Kushiro and Nemuro area in the eastern part of Hokkaido.

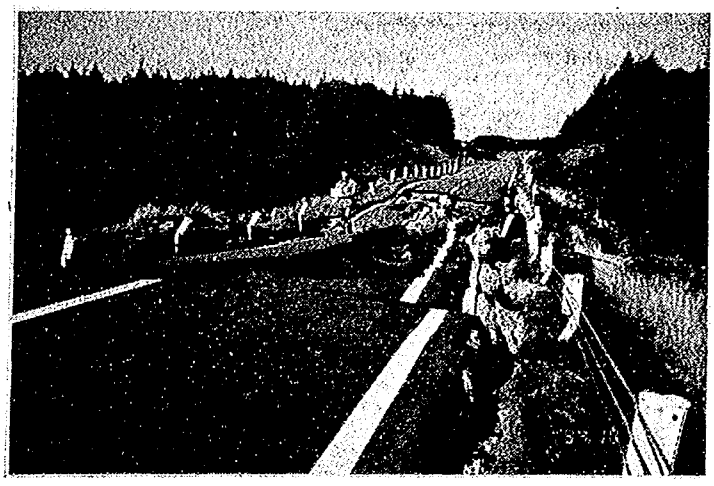


Photo.1
Collapse of banked-up road at Mihara, Bekkai town.



Photo.2
Sand blow between the road curve at Ashino, Kushiro City.



Photo.3
Sand blow through cracks around the manhole at m-utsumi, Kushiro town.

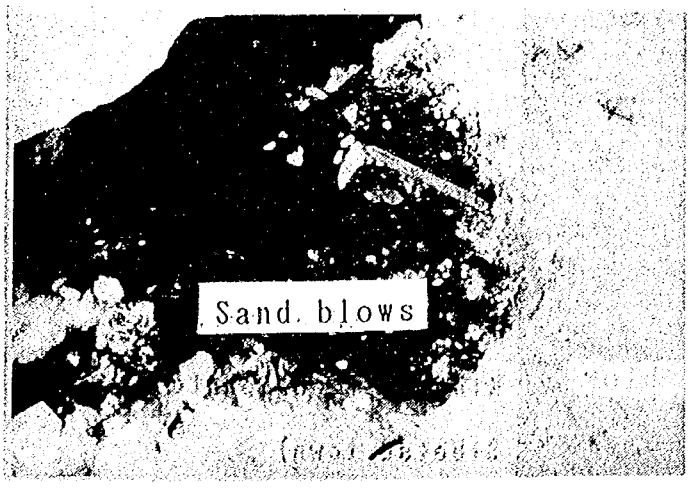


Photo.4
Sand blows in the Kushiro-higashi Fishing Pier by the 1993 Kushiro-oki Earthquake. (shown in the Aerial photo,2)

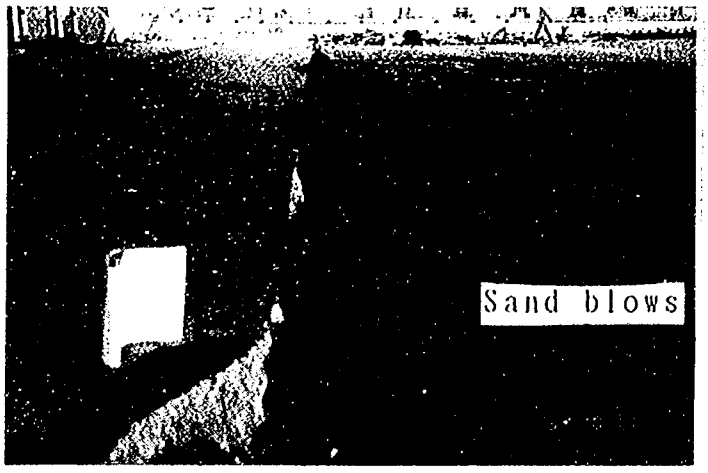


Photo.5
Sand blows at the same place by the 1994 Hokkaido toho-oki Earthquake. (shown in the Aerial photo,1)



Photo.6
Sand blows from cracks on town road in Shibecha town (photo by Shibecha town)

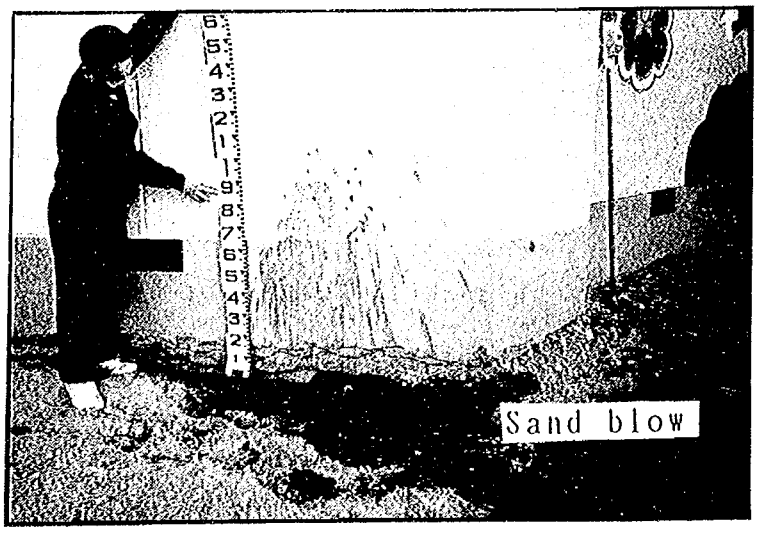
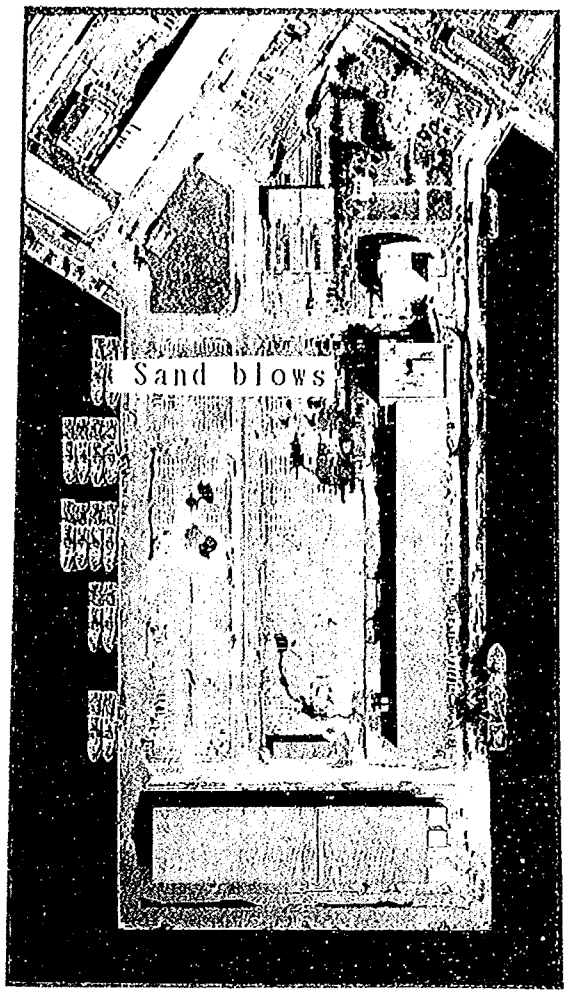
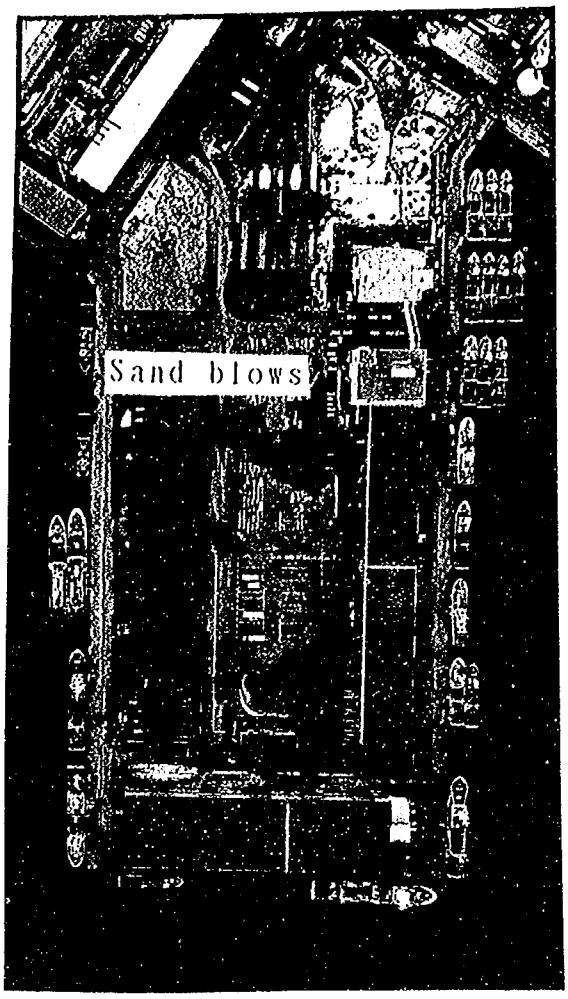


Photo.7
Sand blows from cracks in the ground of Sibetsu Kindergarten. (photo by Sibetsu town)



Aerial Photo,1
The 1994 Hokkaido Toho-Oki Earthquake(Taken at 6th of Oct. in1994,Fishery port of Kushro sity)



Aerial Photo,2
The 1993 Kushro Oki Earthquake(Taken at 16th of Jan. in1993,Fishery port of Kushro sity)

(Dark part of each photograph is identified as extruded sandy sediment.)

The relationships between Physical Conditions and Various Damage Caused by the 1994 Sanriku-haruka-oki Earthquake

Masakatu HORINO, Seiji ICHIKAWA, Yasushi ONO

Abstract

The 1994 Sanriku-Haruka-Oki Earthquake hit the eastern part of Aomori Prefecture. It caused various kinds of damage in Hachinohe city and its vicinities, which is located in the southeastern part of Aomori prefecture in the north edge of the Tohoku district in Honshu. The authors researched actual conditions of these damage after the earthquake. And they clarified characteristics of these damage and the relationships between physical conditions and the damage.

The damage consist of the destruction of constructions in artificially changed hilly slopes, the destruction of con-structions in shallow valleys on the surface of terraces and damage of lifelines along the foot of terrace escarpments and soil liquefaction and relating phenomena in the lowlands.

The authors concluded that there are clear relationships between damage and artificially changed landforms.

Key words: 1994 Sanriku-haru-Oki Earthquake, physical conditions, edge of terrace, artificial changed landform, soil liquefaction

1.Introduction

The Sanriku-Haruka-Oki Earthquake hit the area facing the Pacific Ocean. And its epicenter was about 200km east to Hachinohe city in the eastern part of Aomori Prefecture in the northern part of Japan on the 28th in December in 1994.

Geographical Survey Institute (GSI) used to send a researchers' team at every intensive natural disaster including flood damage, volcanic hazard and earthquake. GSI sent a research team to the damaged area urgently from the 6th.to 10th of January. The authors researched actual conditions of these damage and tried to clarify the relationships between physical conditions and the damage. And this research was sponsored by Science and Technology Agency (STA).

2.Characteristics of the Earthquake

The main shock of the earthquake was caused at 21:19 on the 28th of December in 1994. The epicenter was approximately 200km far to the east of Hachinohe city. Magnitude of the earthquake was 7.5. The maximum aftershock (M6.9) was caused about 80km off the coast of Hachinohe city on the 7th of January in 1995. Fig.1 shows study area.

This earthquake was caused at a site in Japan trench. The epicenters of the earthquake were located at a shallow site near the border between the Pacific plate and Northern American plate. The Japan trench is located in the deep sea to the east of the northern part of Honshu.

The eastern part of Aomori Prefecture facing the Pacific ocean were repeatedly hit by intensive earthquakes through the history. In 1968, the Daini Tokachi-Oki Earthquake (Daini: Second) hit the area and including intensive damage. The hypocentral region of the 1994 earthquake superimposed partially in the south area of the hypocentral region of the earthquake 1968. It is shown in Fig.2.

And the hypocentral region of the 1994 earthquake including the main shock and after-shocks was distributed from east to west. And the epicenters gradually moved westward. The maximum aftershock was caused at the west end of the hypocentral region of

Geographical Survey Institute

the aftershocks (Fig.3).

The seismic intensity of this earthquake in 1994 was shown in the followings: main shock: VI:Hachinohe and Misawa, V:Aomori and Mutsu. Maximum aftershock: V:Hachinohe, IV: Misawa (seismic intensity: Japan Meteorological Agency Scale, Fig.4).

Horizontal crustal displacement was caused by this earthquake. The maximum value was about 9 cm toward the epicenter at Kuji. This was observed using GPS of GSI(Fig.5).

This earthquake was observed by the observation well for ground water level at GSI in Tsukuba. The ampiitude of the change of groundwater level was 3.1cm and the groundwater level kept lower level than the one in normal condition for several hours after the earthquake (Fig.6).

Tsunami was also caused by the earthquake. The maximum was 55 cm at Miyako(Fig.7).

3.General Descriptions of Landforms

Hachinohe city is the second largest city of which population is about 240,000 in Aomori prefecture. It is located at the coast facing the Pacific ocean (Fig.9). Recent years the urban has rapidly developed in the surroundings of the existing city area.

The area consists of well developed marine and fluvial terraces, valley floor plains, flood plains, coastal plain and artificially changed landforms in hilly land and lowlands geomorphologically.

Terraces develop well :the highest terrace is about 200m from mean sea level and it decreases its height from inland toward the coast. Terraces consist of 5 to 6 terraces whose period is different to each other tephrachronologically. The oldest one was formed about 500,000 years ago. The youngest one was formed about 30,000 years ago except Holocene terraces.

These terraces are covered by 5 to 20m of volcanic ash, which had come from Lake Towada (crater lake in the present). Hachinohe volcanic ash layer was suppiled about 13,000 years ago and covers the top of older volcanic ash. Older terraces have been being dissected more intensively than younger ones. Subsequently these have been changed into hill slopes.

Shallow valleys with gentle cross section of valley slopes have been being formed on the surface of the young terrace. These shallow valleys join dissected valleys.

Valleys have dissected terrace areas and shallow valleys are distributed at the upper basins of small valleys. Small valley floors and edge of terraces are artificially banked areas. At the end of terraces, geomorphological boundaries are not clear because of gentle slopes without clear break lines. Deposit consists of soft soil of Hachinohe volcanic ash at the shallow valley. There are landfills at small valleys which are distributed at the end of terraces.

Floodplains develop well in the lower drainage basins of the Mabechi and the Niida rivers. There are many former river courses and well developed natural levees there. Most of them were changed artificially for the farmland consolidation of paddy fields. Back marshes are also seen in hinterlow-lands of natural levees. Valley floor plains have been formed in the valleys rising from terraces. Coastal lowlands are seen along the coastline. And beach ridges, bars and dunes had been seen along the coastline.

It is defined temporarily in this report that terrace end gentle slope consists of slope below about 10° at the end of terrace or at terrace cliff. Recent years, artificially changed landforms are seen remarkably in this areas of terrace-ends and shallow valley floors in the terrace areas. There are many new houses on the landfill at terrace-cliffs which consist of terrace end gentle slopes. (Fig. 9)

4.Characteristics of earthquake damage

Loss of people : 2 death, 606 injuries by the main shock, and 23 injuries by the maximum aftershock.

Damage of houses and buildings: Damage by the main shock: complete destruction of houses,46. partially destruction of houses, 295. Damage by the maximum aftershock: complete destruction of houses, 15 in the eastern part of Hachinohe city and partial destruction of house, 48 in the city urban.

There are about 8,000 houses in the damaged area. Ratio of complete destruction of houses is about 0.8%, partial destruction houses is about 4.3%. Only 7% of houses was never damaged at all. Damage of a pachinco center (a kind of Japanese popular game center) was broken at the first floor of the building by the buckling of main concrete columns (photo 1).

As for public facilities, wall fell down by the buckling of concrete pillars and many window glasses were broken at the older building among Hachinohe city hall buildings(photo 3).

At the first floor of the Hachinohe-higashi senior high school, pillars were sheared and frames of many windows bended like "L" character. At the school buildings (photo 2) of Chiba Gakuen Senior high school, joint parts between new and older buildings were damaged into gaps horizontally and vertically, diagonal beams of the Hall bended like "S" character, and same kinds of damage of windows were also seen at Negishi primary school, too.

Hachinohe branch office NTT(Japan Telecommunication and Telephone co.) was damaged : gaps were caused at joint bridge between new and older buildings, and land subsidence of the edge of artificial landfill which the office was located at the terrace end gentle slope and the falling-down of wall at the older offices. Damage is very similar to the past earthquake damage, which was caused repeated earthquakes.

Landslides were caused at the end of the hills in Matsugaoka hill housing area with the scale of about 150m long and 5m high (relative height)(photo 4). The site is about 5km far from the city urban. Large and small cracks were caused at the backward of landslide cliff. Roadbed was displaced toward the valley floor. Small landslides and roadbed were collapsed, and subsequently a car running fell down into the crack of roadbed. The details is shown in fig.8.

Small failures were seen at a banked site of the terrace end at Choujayama hill with several cracks in its surroundings. Those cracks may show the border between initial hill and banked area.

In the lowland, the thickly banked railway on the roadbed of JR (Japan Railway Company, Tohoku line) was collapsed completely about fifty meters long and the earth hit a house. The roadbed was banked about 15 meters.

Soil liquefaction and rapid land subsidence of landfilled area: Soil liquefaction and subsidence of landfilled area were caused in the coastal area. Subsidence of landfill at the quarries of iron sand are located at sand dune area with interdune lowland and at the pier of the ports. Soil liquefaction was caused at the inside of the caisson of the pier at the port. This soil liquefaction was also caused by the maximum aftershock (photo 5).

5. The Relationships between Damage and Landforms with surface Materials

It is possible to consider as shown in the followings based on the comparison with landforms-and-surface materials and earthquake damage.

1) Damage in the shallow valley on the terraces

The pachinco game center, Hachinohe higashi senior high school, and

Chiba Gakuen senior high school were damaged as above mentioned and these are distributed in landform of a shallow valley on the terraces.

Characteristics of shallow valley is that the relative heights of terrace surface and valley floor is about several meters and the boundaries between valley floor and valley slopes is very gentle and not evidently.

Deposit material at the valley is black soil originated from Hachinohe volcanic ash and very soft with much water. Houses in these shallow valleys were damaged more intensively than the surrounding houses on the terrace.

The authors presumed that soft ground in shallow valley amplituded earthquake motion.

2) Landfill damage at the edge of a terrace

One of NTT Hachinohe offic-es (older) is located on the landfill at the terrace slope. Another office (new) is located in the lowland. The second floor of the older office was connected with third floor of the new one using a bridge. Landfill was warned by a retaining wall with about 3 meters in relative height. This landfill was subsided behind the retaining wall with cracks. This behavior of landfill cut the bridge apart from the office building. This is an example which the deformation of landfill caused damage of the office building.

Terrace cliffs at Chojayama hill and Hachitaro tunnel were deformed into flat by landfill with the the depth of 0.6 to 2.0 meters. And the ends of the landfill were failured with cracks. Subsequently separated block by cracks was subsided about several cm.

These are very simple examples of geomorphological landform change. The authors presumed that the cracks were distributed at approximate border between a terrace and landfill, and this kind of cracks were easily caused by the earthquake motion in such former geomorphological border.

3) Landfill damage at small valley floor and its surroundings

Older office building of Hachinohe city hall and failured sites at Matsugaoka hill housing area were located at artificially changed zones. These flat zones were formed by cut of hill tops and by landfill in the former dissected small valley floors.

The damage of the older office building of Hachinohe city hall is an example which was damaged remarkably without any geomorphological change in its surroundings.

Cracks were caused behind the failure of landfill with 1.6 meter in relative height at Matsugaoka hill housing area. The directions of cracks were distributed in specified linear zones, which are the former borders of geomorphological units between the valley slopes and landfill. Cracks and damage of houses were seen along the borders, but not so intensively.

4)Damage in the lowlands

Banked roadbed of the railway of the Tohoku line (JR) is located in the marshy lowland. The lowland consists of extremely weak ground which had been formed at where a small river rising from the terrace was dammed up by a natural levee. The earthquake motion was stronger than the shearing strength of the roadbed in the marshy lowland and subsequently the roadbed was collapsed completely about 50 meters long in the marshy lowland.

The road near the Hachitaro tunnel was constructed on the banking on landfill at a pond, which was formed at interlevee lowland. This part was suspended by the subsidence by the earthquake motion.

Negishi primary school is located at the foot of a steep cliff of a terrace. The site consists of very weak ground where a backmarsh had been formed behind a natural levee. Damage of the

school building was intensively without geo-morphological change.

These cases which are building damage and roadbed damage were caused by the amplitude of the earthquake motion in marshy lowland.

5) Soil liquefaction and damage at landfill and banked sites along the coastline

Along the coastline, quarr-ies of iron sand had been mined for a long time and such sites had been landfilled. These former quarry sites were sub-sided by the earthquake motion. And the inside of caissons were liquefied with subsidence and spouting water and sand.

Soil liquefaction was caused in many sites in small scales only in the reclaimed land by landfill and banked areas along the coastline. And the authors presumed the reason that there was no soil liquefaction site as follows based on geomorphological characteri-stics and subsoil, boring data and relating references. The sand layer above ground water level was not enough thick to be able to cause soil liquefaction.

6) Damage of people's houses

There are about 8,000 houses in the damaged area. Ratio of complete destruction of houses is about 0.8%, partial destruction houses is about 4.3%. Only 7% of houses was never damaged at all.

The example of photo-6 shows the feature that the retaining wall was deformed and a house was separated from the foundation. 70% of the complete destruction are located at landfills in the gentle slope of terrace ends and its surroundings and shallow valleys. These artificial landforms are weaker than the flat terrace surfaces against earthquake motion(tab.1).

7) Damage of lifelines

Damage of lifelines are character—ized as follows. The main routes of water supply pipes and gas pipe lines were damaged remarkably at the roads along the foot of the terrace cliff and shallow valleys. Branches and end lines to homes were damaged by the reason that the compaction of the refilling after the con-struction work for setting pipes to each home.

6.Conclusion

The authors researched actual conditions of damage by the 1994 Sanriku-Haruka-Oki earthquake and tried to clarify characteristics of damage and the relationships between landforms and damage.

It was clarified that various dam-age were caused at landfills on the gentle slopes in the fringe of terra-ces, at landfills in small valleys, at edges of terraces, in shallow valleys, in back marshes and in reclaimed land by landfill.

Based on these, it can be said that there are close relationships between physical settings (mainly geomor-phology) and various damage. Fig.9 shows the distribution of landforms and damage.

As the city area has been spreading rapidly, housing areas are expanding into gentle slopes of terrace-ends, fringes of terraces, back marshes, which were not used for housing areas in 1970s.

The Sanriku-Haruka-Oki Earth-quakes was caused in a trough of the Japan trench in the Pacific ocean. And earthquake damage were influenced by landforms with surface materials in common.

As above mentioned, there are evident relationships between physical settings(mainly landforms with surface materials) and earthquake damage. Always the aspects of landform dis-tribution vary, but it is possible for people to predict the earthquake damage based on these information of physical settings. Especially, it is possible to estimate the damage areas depending on

specified geomorphological units.

It is very important for planners to analyze earthquake damage previously based on characteristics of physical settings for the countermeasures against earthquake disasters.

Acknowledgement

The authors are full of gratitude to many people and government organizations as shown in the followings: Prof. Toshikazu TAMURA, Tohoku univ., prof. Susumu YASUDA, Tokyo electrical univ. of electric technology, prof. Housei HOTTA, Hachinohe institute of technology who helped them in the field, Aomori Prefectural gov., Hachinohe city, Aomori construction office and Takase river con-struction office of Ministry of construction and Tohoku branch office of GSI. Mr.Takahito KUROKI, researcher of planning division of geographic department, GSI, helped us to compile this report. Mr.Kiyoshi MIMURA, Head of the Geographic Department, gave a chance to authors to research this earthquake damage and landforms.

References

1):Housei HOTTA, Osamu MIURA, Toshikazu TAMURA(1968):Landslides in Southern Part of Aomori Prefecture on 1968 Tokachi-oki Earthquake, Annals of Tohoku-Geographical Assosiation, Vol. 20, No.4, 202-205

2):Takahiro MIYAUCHI(1985) : Teracce in Kamikita Plain and Quaternary tectonics, Geographical Review of Japan, Vol.58 No.8, 492～515

3):Takahiro MIYAUCHI(1988): Correlation and Chronology of the Late Pleistocene Marine Terraces in Northern Northeast Japan.Geogr.rev. of Japan vol.61 No.5 p404-422

4):Hiroshi MIZUNO・Housei HOTTA (1968): Damage in Aomori Prefecture on 1968 Tokachi-oki Earthquake, thern Northeast Japan. Gegr.rev. of Japan Vol 61.No.5 p404-422 Annals of Tohoku-Geographical Assosiation, Vol. 20, No. 4, 187-194

5):Kasuke NISHIMURA, Hideyoshi SEGAWA, Hiroshi MIZUNO, Housei HOTTA, Osamu MIURA, Toshikazu TAMURA, Takekazu AKAGIRI (1968): Geomorphorogical Disaster on 1968 Tokachi-oki Earthquake, Annals of Tohoku Geographical Assosiation, Vol. 20, No.3, 157-163

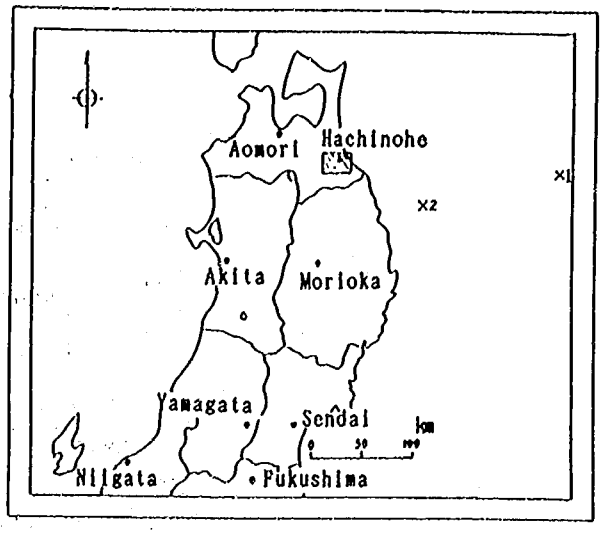


Fig.1 Sutdy area (hatced area is Hachinohe City)
(×1: Main epicenter, ×2: maximum aftershock epicenter)

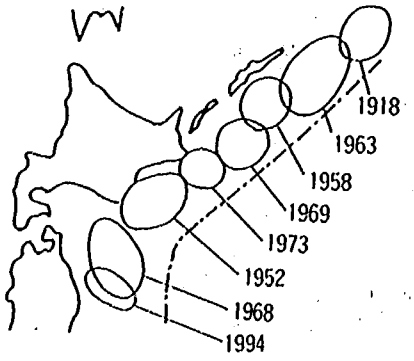


Fig.2 Distribution of main large earthquakes along the northern Japan trench
(The 1994 is Sanriku-Haruka-Oki earthqake)

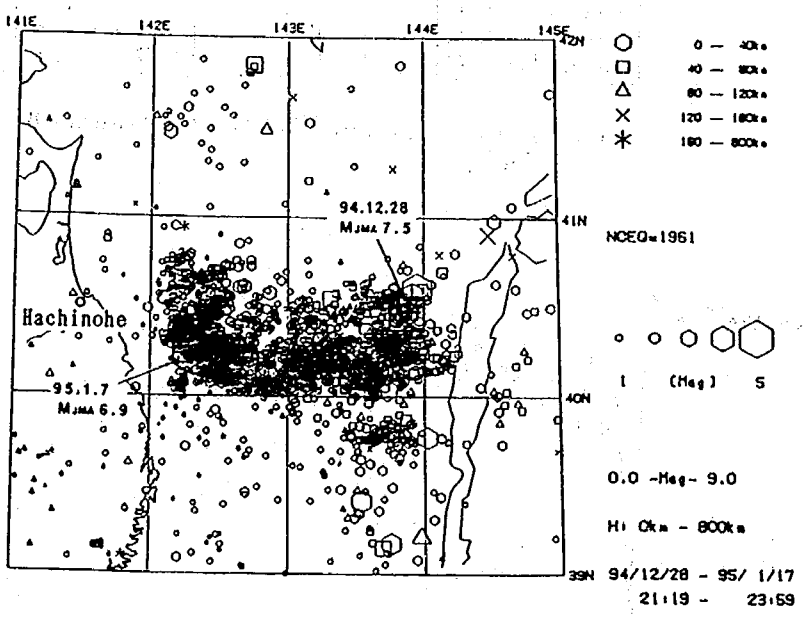


Fig.3 Distribution of aftershocks
(by the Meteorological Agency)
(Des.28th, 1994~ Jun.17th, 1995)

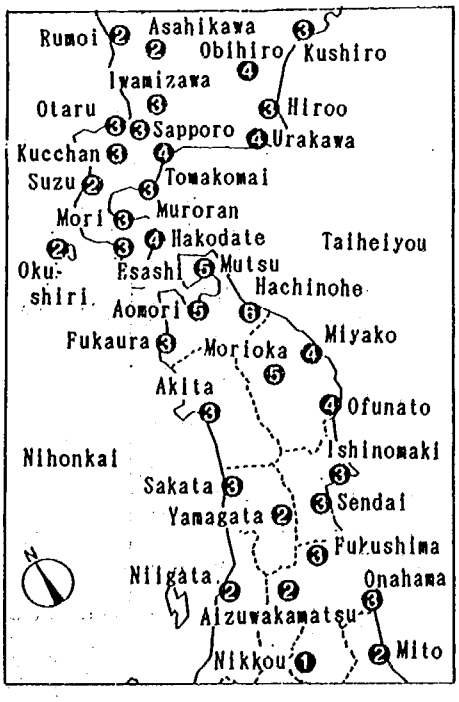


Fig.4 Distribution of the 1994 Sanriku-Haruka-Oki Earthquake intensity on the Japanese scale

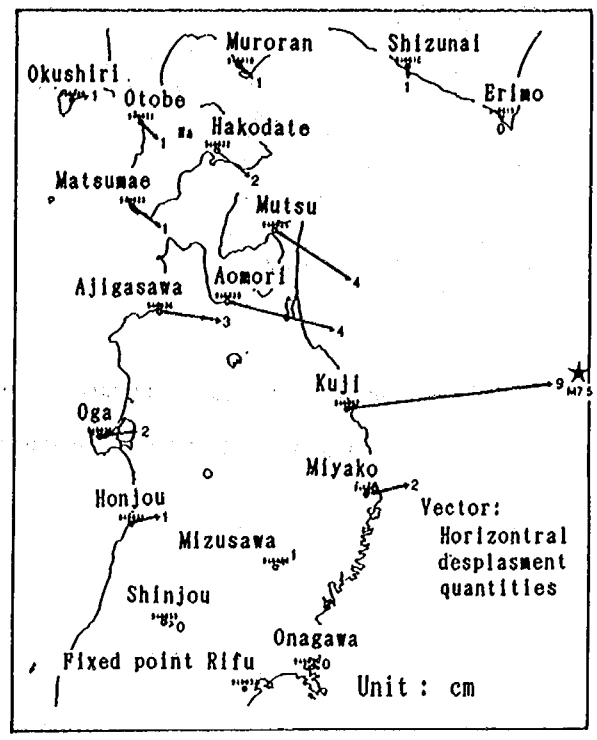
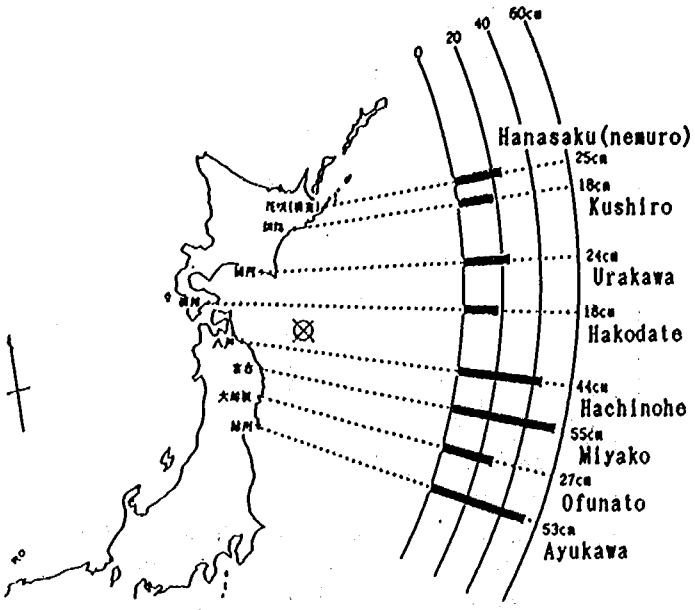


Fig.5 Horizontal displacement(vector) caused by the 1994 Sanriku-Haruka-Oki Earthquake (Obseaved by GPS stations)



Observation point	First wave		Maximum height of Tsunami	
	Arrived time d h m	Push (+) Pull (-)	Appeared time d h m	height
Hachinohe	28 21 55	(+) 41cm	28 23 02	44cm
Miyako	28 21 45	(+) 51cm	28 22 12	55cm
Urakawa	28 21 58	(+) 14cm	28 22 56	24cm
Ofunato	28 21 59	(+) 27cm	28 22 02	27cm
Ayukawa	28 22 10	(+) 30cm	28 22 33	53cm
Kushiro	28 22 10	(+) 16cm	28 22 56	18cm
Hanasaku	28 22 19	(+) 19cm	28 22 40	25cm
Hakodate	28 22 23	(+) 18cm	28 22 46	18cm

Fig.7 Tsunami caused by 1994 Sanriku-Haruka-Oki Earthquake

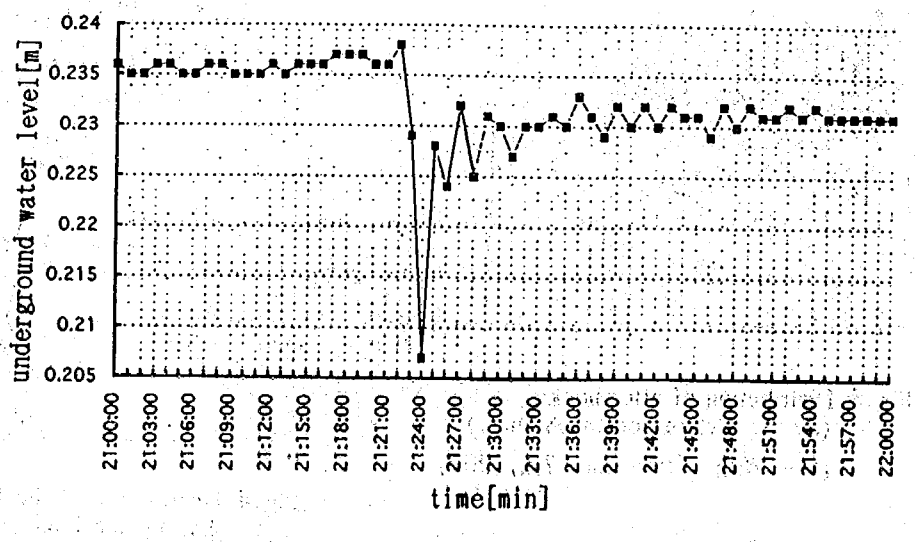


Fig.6 displacement of underground water level at GSI by 1994 Sanriku-Haruka-Oki Earthquake

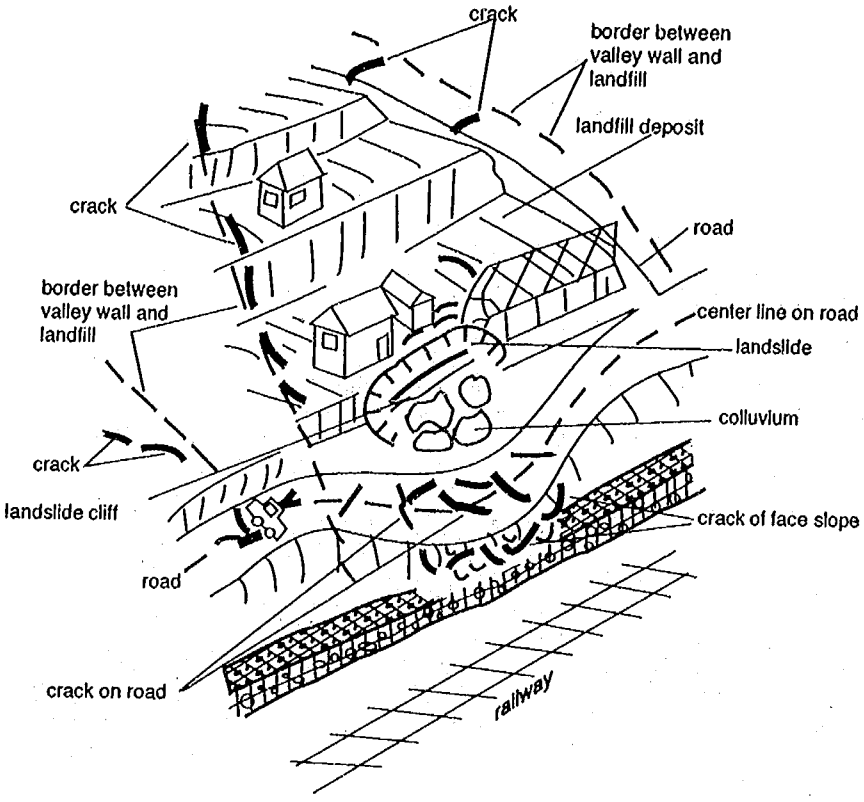


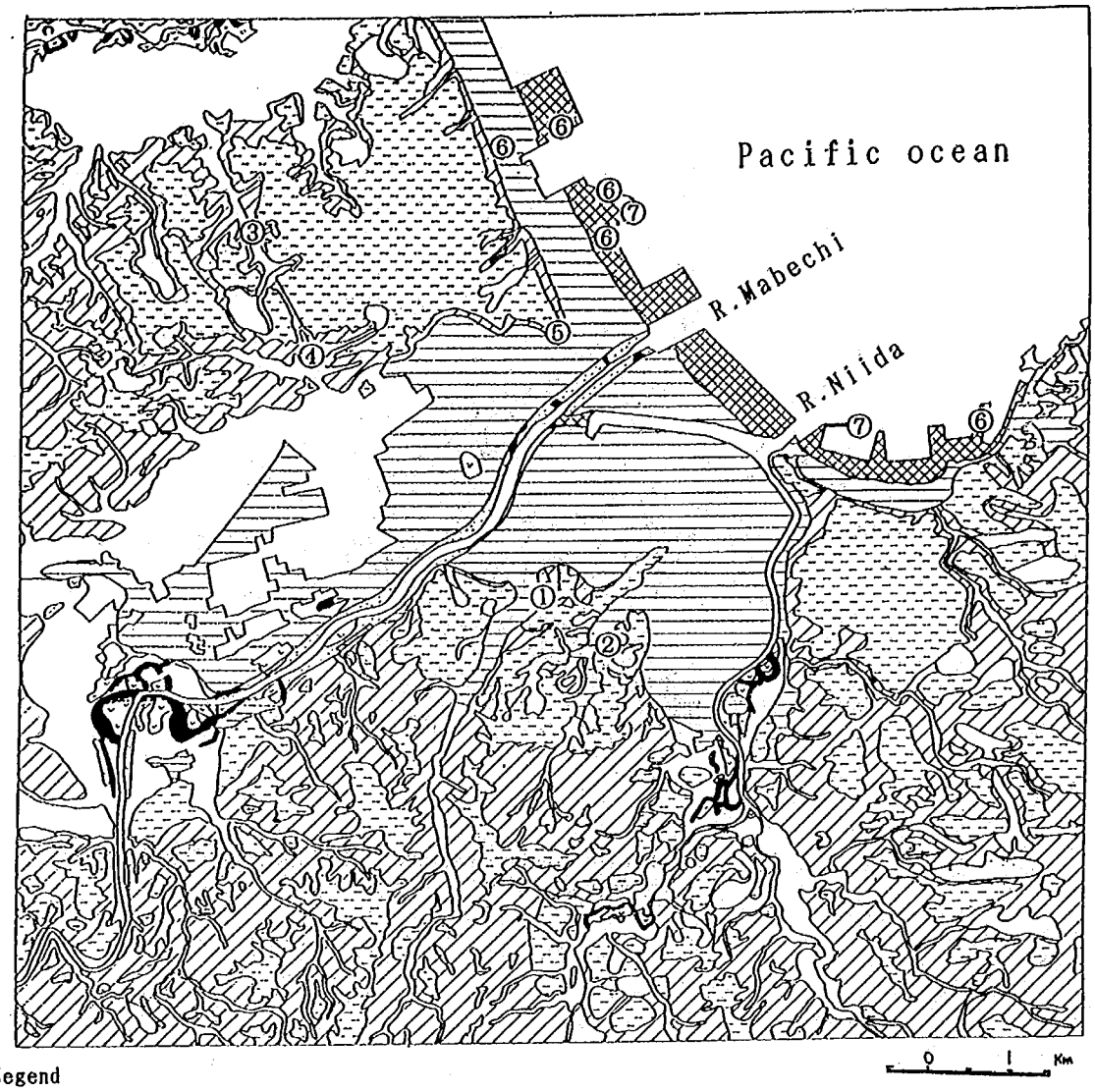
Fig.8 Schematic picture Landslide at Matsugaoka hill housing area

Table 1 Ratio of relationships beteen landforms and damaged houses

Landform	Gross number of houses in damaged area	Commpletely destroyed houses	Ratio(%)
Flat of top on terraces	1,200	9	0.08 (15)
Gentle slope of terraces criff	1,300	28	0.22 (46)
Shallow valleys	800	15	0.19 (24)
Flood plain	4,700	9	0.02 (15)
Total	8,000	61	

( ) is ratio within completely houses in each landform

Fig.9 Outline of geomorphological classification and damage



Legend

Flat of top on terraces | Hilly slope | Shallow valley | Natural levee | Former river bed

Allubual plane, valley | Recraimed land | Alltificially area

① Older building of Hachinohe city hall
② Hachinohe-higashi senior high school
③ Landslide at Matsugaoka hill housing area
④ Landslide of large landfill at Tohoku railway(rail hung)
⑤ Subsidence of roadbed on landfill side of tunnel
⑥ Subsidence at reclaimed land
⑦ Sand boil for soil liquefaction at reclaimed land

Fig. 8 Outline of geomorphological classification and damages



Photo.1
Pachinnko game center, crushed the first floor



Photo.2
Pillar of school buld. sheared at
the Hachinohe-higasi senier high scholl

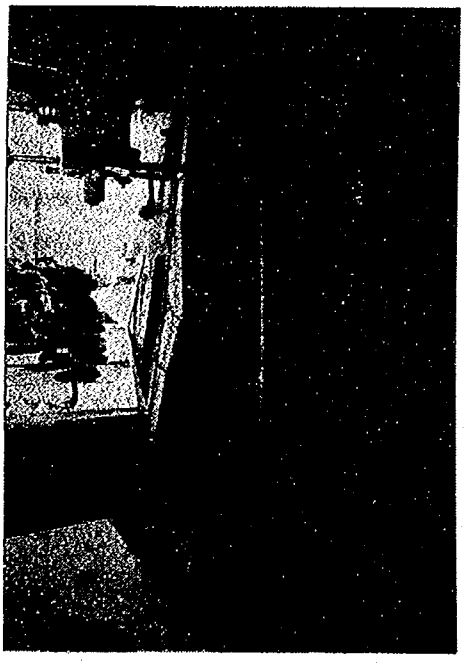


Photo.3
Crushed pillars by shearing in older
building of Hachinohe city Hall

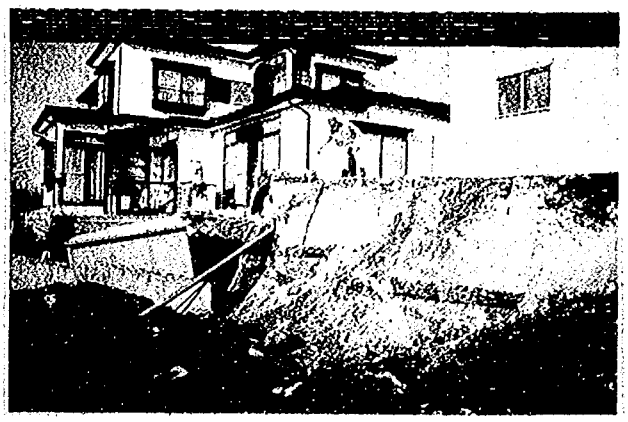


Photo.4
Landslide at Matsugaoka hill housing area

Photo.5
Sand boil phenomonum by soil liquifuction
(At time of maximun aftershock)



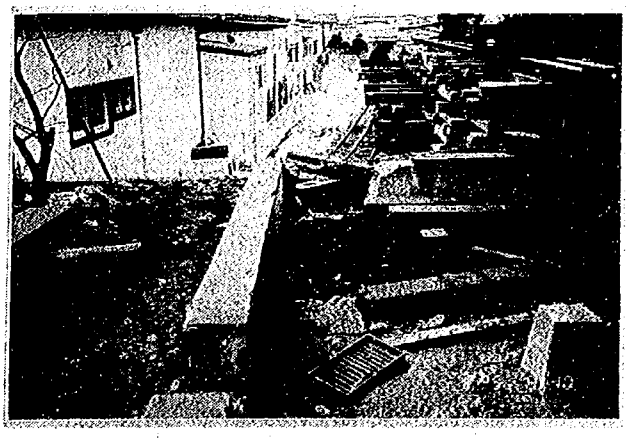


Photo.6
Destoryed revetment by deformetion of landifills

Characteristics of Water Level in Rivers Before the 1993 Hokkaido Nansei-okiEarthquake

by
Masashi SATO [1], Tadayuki SHIRONO [2], Takashi SATO [3]

ABSTRACT

In this study, multiple analyses were made on the wave profiles of water levels before and after the Hokkaido Nansei-oki Earthquake from the viewpoint of fractal and auto-correlation, based on the observation data of water levels in rivers which are usually used for observing precipitation. The effects of changes in the tide level on the water levels in rivers at the time of an earthquake are also examined by comparing the water levels in rivers and tide levels in the harbors in the vicinity.

Key Words : fractal dimension
Hokkaido Nansei-oki Earthquake
spectrum analysis
tide levels in the harbors
water levels in rivers

1. INTRODUCTION

At 22:17 on July 12, 1993, a big earthquake occurred in and around the southwestern part of Hokkaido causing tremendous damage to Okushiri Island in Hiyama subprefecture and to many other places in the southern part of Hokkaido. It was reported that the epicenter was about 100 km off the southwestern coast of Hokkaido (Lat. 42° 47′ N and Long. 139° 12′ E), the depth of the hypocenter was 34 km and that the earthquake registered magnitude 7.8 on the Japanese scale. The seismic intensity on the Japanese scale at various places was estimated at 6 (a violent earthquake) in Okushiri Island near to the epicenter, 5 (a severe earthquake) in Esashi, Suttsu, Otaru and Fukaura, and 4 (a medium earthquake) in Hakodate, Muroran, Kutchan, Aomori and Mutsu.

One of the greatest features of this earthquake was a gigantic tsunami, and a warning for big tsunamis was given to the coastal areas of Hokkaido and Tohoku regions 5 minutes and 8 minutes after the earthquake, respectively. A tsunami struck Okushiri Island soon after the earthquake, and then within ten minutes a tsunami struck the coastal area in the western part of Oshima peninsula in Hiyama subprefecture. The first tsunami to be confirmed at a tidal observation point of the Meteorological Agency arrived at Fukaura in Aomori prefecture at 22:40, and the greatest wave, 37 cm high, was observed in Wakkanai at 04:45 on the 13th [1]

2. OUTLINE OF HYDROLOGICAL OBSERVATION

(1) The location of observation points

The data on the water level in rivers used in this study were obtained at

1)Head,StructuresSection,CivilEngineering Research Institute
2)ex-Research Engineer,ditto
3)Research Engineer,ditto

two observation points shown in Table 1. Kaiun bridge observation point is located 22.60 km from the mouth of the Sarobetsu river, downstream of the Teshio river system, and Koitoi bridge observation point is 0.50 km from the mouth of the Koitoi river, the Koitoi river system [2]. The locations of these two observation points are shown in Figure 1.

(2) Outline of the device for observation

The water gauge installed at the two observation points was a W-021 Suiken 62 type, long-term self-recording water gauge, which is designed for recording changes in the water level at low and high tides in rivers, dams and harbors for a long period of time. Vertical movement of a float caused by changes in the water level is transmitted to a recording pen through pulley and gear. The range of measurement is 0～10 m, the precision is ± 1 cm, and the speed of feeding paper is 6 mm/h or 18 mm/h. The power source for feeding the paper is an N-010 quartz clock, and recording is continuous for 3 months or 1 month[3].The external dimensions of the water gauge and the location of the installation are shown in Figures 2 and 3, respectively.

3. OUTLINE OF THE ANALYSIS

(1) Purpose of the analysis

The analysis was to examine the characteristics of the wave profiles of the water level occurring at the time of an earthquake obtained at the observation points. Although spectrum analysis is usually used to understand the features of seismic waves and tsunami, very few studies have been done with this analysis on the wave profiles of water levels in rivers. In order to analyze the wave profiles of water levels in rivers before and after the Hokkaido Nansei-oki Earthquake in our study, analog data and digital data were used to examine the geometrical features and the prominence of frequency component by the spectrum, respectively. Additionally, the data of tides obtained in the three harbors nearby are analyzed and the effects given to the water level in rivers by tidal change are examined.

(2) Procedure of analysis

First, the analog to digital conversion was made with records from the two observation points on the wave profiles of the water level for one month, including the time of the earthquake. The resulting digital data per every two minutes was stored on disc in the form of an ASCII text file. The wave profile data was made into graphic, and it was read by an image scanner to make it into wave profile data for each day whose criterion was the time of the earthquake. Because the resolution of the data was 126 dpi, the reading resolution applied this time, 200 dpi, seemed to be sufficient as a minimum grid size. Then the data was stored as image data by existing graphic processing software. In order to clarify the geometric features of the wave profiles, the fractal dimension (an index of complexity) was computed by means of the box-counting method(4, 5).

The text file of wave profiles, as in the case of the image data, was used to make a data file per day whose criterion was the time of the earthquake, and a variety of spectrum analyses were made

on it to examine the changes in the characteristics of the wave profiles of the water level by day. Auto-correlation coefficients were calculated to examine the correlation between separateddata within one series of data. In addition, a spectrum analysis which is generally employed in the analysis of seismic waves and tide levels was applied to obtain the Fourier amplitude, Fourier spectrum and power spectrum.

4. THE RESULTS OF THE ANALYSIS

(1) Fractal dimension

Figure 4 shows the data on wave profiles for 4 days before and after the earthquake, in which the effect of tsunami on the wave profiles was noticed 6 hours after the earthquake. Figure 5 shows the change by day of the fractal dimension without fine image processing. Apparent prominence occurred on the day of the earthquake. The value at Koitoi bridge observation point was fairly high on the day before the earthquake compared with other days, but the data from Kaiun bridge observation point showed the opposite tendency. Table 2 shows the climatic conditions on and around the day of the earthquake. At both observation points, it was fine or cloudy on the day of the earthquake and the previous day, and so the effect of rainfall was negligible.

(2) Auto-correlation coefficient

The auto-correlation coefficient is calculated to detect the periodicity inherent in certain functional values, and the correlogram showing the relationship between auto-correlation coefficients and time lag is considered to be a kind of spectrum. Thus a peak in the correlogram means that the periodic wave corresponding to the time lag of the peak is included in the original wave profiles as a component [6]

According to our analysis, however, no conspicuous peaks were recognized at both observation points, while several peaks were found only on the day of the earthquake. With regard to the two observation points, correlograms for the previous day and day of the earthquake are shown in Figures 6 (a) and (b), respectively, in which the vertical line represents auto-correlation coefficients and the horizontal line represents sample numbers.

(3) Comparison with the characteristics of the tide level

In order to examine the effect of changes in the tide level in the nearby harbors on the water level in rivers, data from the tide gauges in the harbors of Haboro, Iwanai and Rumoi were used for spectrum analysis. The period of tide level data was 18 days in Haboro harbor, shorter than for the water level data in rivers, because the data available there were discontinuous. Data for the harbors of Rumoi and Iwanai taken before and after the earthquake were used for reference. Figures 7 show the wave profiles of the tide level in Haboro harbor before and after the earthquake.Figure 8 shows the power spectrum which is smoothed by the band range of 0.40, together with the data from the water level observation points on the rivers. Figure 8 shows that frequency was prominent around 1 cph at all three observation points, and that the

characteristics of vibration were almost identical between Haboro harbor and Koitoi bridge at 2 cph and 4 cph. Figures 9 shows the running spectrum of the Haboro harbor , Kaiun bridge observation point, and Koitoi bridge observation point, respectively.The running spectrum was obtained by using the wave data in which the frequencies of 0.13cph and under were eliminated by filtering in order to avoid the regular changes in the tide level were included as an element. Figure 7 indicates that the amplitude was prominent at the frequency of 0.2 and 0.4 cph at 3 observation point before the earthquake. Two days before of the earthquake at Kaiun bridge observation point, and one day before of the earthquake at Koitoi bridge observation point and Haboro harbor, the amplitude became prominent at the frequency of 0.3 cph only. After the earthquake, prominent point gradually got back to normal point at Kaiun bridge observation point. And the amplitude was also prominent at the frequency of 4.5 cph at 3 observation point. In addition, at Koitoi bridge observation point another prominent point was observed at the frequency of 2.7 cph fromthe day before the earthquake. From these characterisities, it is conceivable that the frequency characterisities of the both obserbation points are similar to those of the Haboro harbor. Also, it is possible to estimate that the water levels of rivers are influenced by the tidal levels. But it is difficult to find out the influencial factors to the frequency characterisities, and we will leave it to the future study.

Figure 10 shows the wave profiles of the tide level before and after the earthquake in Iwanai harbor and Rumoi harbor, and Figure 11 shows the Fourier amplitude on the day of the earthquake. These data are given as a reference because the data is limited. But in Iwanai harbor where the data is comparatively large, a peak is noticeable at 1.0 cph, as in the case of Rumoi harbor .

5. CONCLUSION

The effects of tsunami on the tide levels can be attributed to the generating mechanism of tsunami in the wave source area, transformation, dispersion and refraction which occur during the spread of tsunami, reflection and refraction in the sea area shallower than the continental shelf, and natural vibration of the sea area [8] . Additionally, the tide level in a harbor depends not only upon tsunami, ebbs and tides, but also upon the seiche in the harbor. The seiche is influenced by wind, swells, atmospheric pressure and interaction between wave motions with different periods. It is clear, however, that the tidal wave, which is ordinarily the major source of subvibration, is not such a great factor as to influence the sea conditions in a bay, because the difference in the level between ebb and flow in the Ishikari Bay, for example, is only 35 cm at maximum [9]

The analysis clarified that particular frequencies become prominent in the water level in rivers as well as in the tide level when an earthquake occurs, and that the characteristics of the tide level in a bay affect the water level in relatively distant rivers. At Koitoi bridge observation point, values of fractal

dimension and spectrum on the day before the earthquake were different from those of ordinary days. This fact has to be examined further in the future. The difference in these two values was less conspicuous at Kaiun bridge observation point than Koitoi bridge. This is possibly because Kaiun bridge is located far away from a river mouth and the river is a tributary of the Teshio river leading to the Sea of Japan, and so the characteristics of the river are more dominant than those of an earthquake and tsunami.

The data on the water level we used in the analyses were for every 2 minutes and were much coarser than data on seismic waves for spectrum analysis. The data were collected from half a month before the earthquake to half a month after it. This period was rather short for identifying the characteristics of the water level in rivers which change greatly every year. In addition, the analyses of the data from only two observation points are not sufficient for determining whether the features of the wave profiles specific to the Nansei-oki Earthquake are universal or not. In fact, in the process of the spread of seismic and tsunami characteristics from the hypocenter to a tide level observation point and then to an observation point of the water level in a river, a great many factors, including geographic conditions, hydrological conditions, weather and other natural conditions, affect the data on the water level.

We will therefore continue to analyze in a variety of ways the characteristics of water levels in rivers and tide levels in the case of the Kushiro-oki Earthquake and the Hokkaido Toho-oki Earthquake based on the present data.

REFERENCES

1)KOKEN Engineering Co., Ltd.; TECHNICAL REPORT, After one year from the 1993 Hokkaido Nansei-oki Earthquake, July 1994.

2)Hokkaido Development Bureau; The Present State of the Hydrological Observation Station, April 1994.

3)YOKOGAWA Weazac Co., Ltd.; Instructions on the use of Suiken 62 type long-term self-recording water gauge, January 1994.

4)Tadayuki Shirono, Manabu Kaneko, Yuji Ono, Osamu Nakano; On the quantification of bedrock crack in the Tanno tunnel, Proc. for the 48th Annual Conference of the Civil Engineering Society, pp. 284 - 285, September 1993.

5)Tadayuki Shirono; Characterization of Jointed Rock with Fractal Dimension, FORMA Special Issue: Fractal Analyses in Geology and Civil Engineering, Volume 9 Number 2, pp. 113 - 123, 1994.

6)Mitsuhiko Osaki; Introduction to spectrum analysis of earthquake motion, Kashima Publishing Company, May 1988.

7)Mikio Hino; Spectrum Analysis, Asakura Publishing Company, October 1980.

8)Masaru Takahashi; The Characteristics of Tsunami in the Tsugaru Straits and Uchiura Bay, Proc. for the 23rd Conference on Coastal Engineering, pp. 459 - 463, 1976.

9)Masaru Takahashi; Tsunami and subvibration in the Ishikari Bay, Research Report No. 130 of the Faculty of Engineering,Hokkaido University, 1986.

Table 1. Details of the water level observation points

Observation points		
River system	Downstream of Teshio river	Koitoi river
Name of the river	Sarobetsu river	Koitoi river
Name of the point	Kaiun bridge	Koitoi bridge
Data on the points		
T.P.m	0.00	0.00
Distance from the river mouth	22.60 km	0.50 km
Gradient of the rive	1/8000	1/3000
Basin of the river	369.60 km ^{2}	244.20 km ^{2}
Address		
City / County	Teshio County	Wakkanai City
Town / Village	Toyotomi Town	--------
Section	Toyotoku	Koitoi

Table. 2 Weather before, on the day of and after the earthquake

Date	Time	Kaiun bridge	Koitoi bridge
July 11	6:00	rainy	rainy
	18:00	rainy	cloudy
12	6:00	cloudy	fair
	18:00	fair	fair
13	6:00	cloudy	fair
	18:00	cloudy	rainy
14	6:00	cloudy	fair
	18:00	cloudy	cloudy
15	6:00	cloudy	rainy
	18:00	cloudy	cloudy

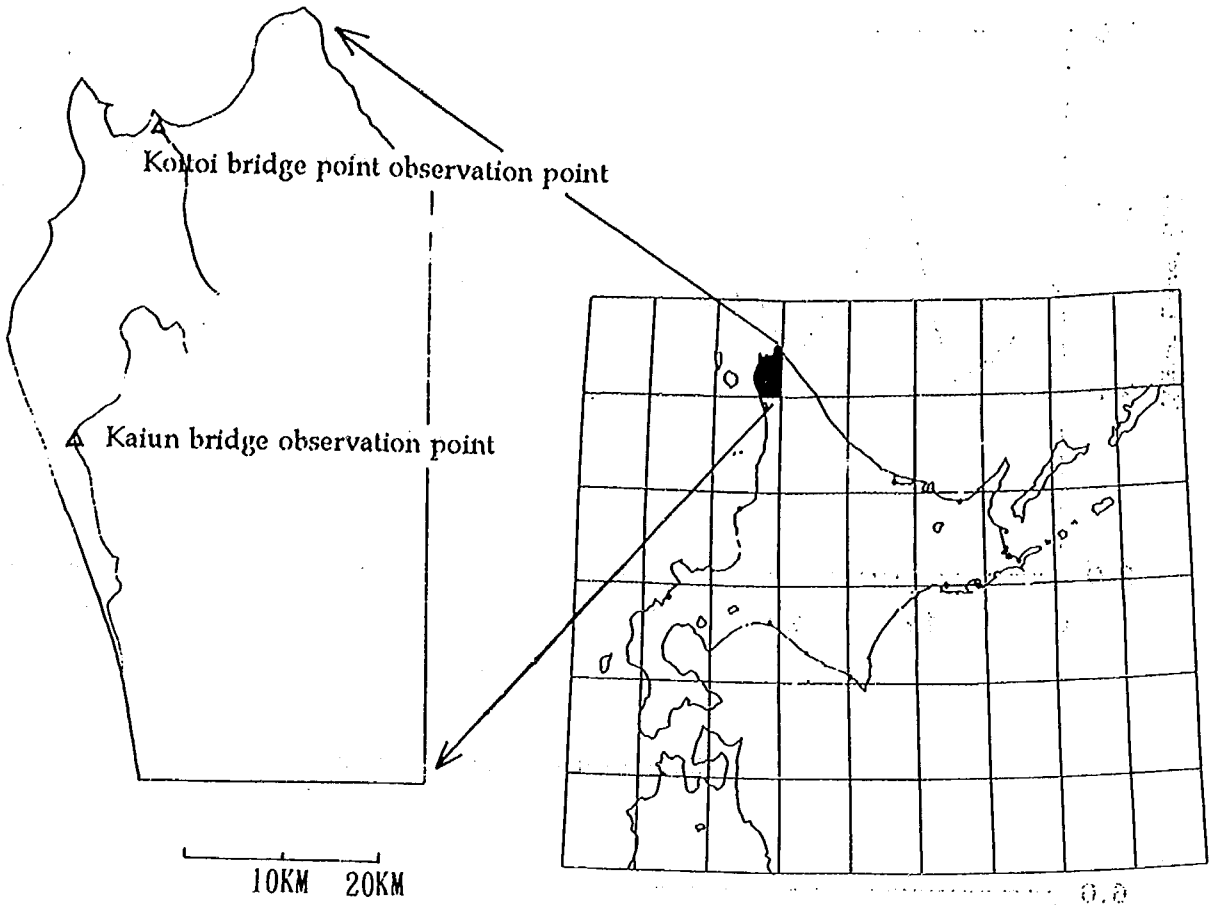


Figure 1. Location of the water level observation points

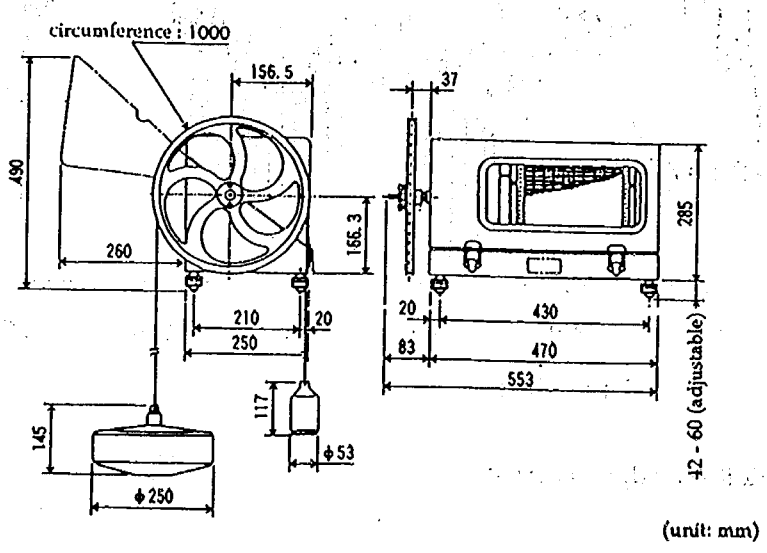


Figure 2 External dimensions of the water gauge

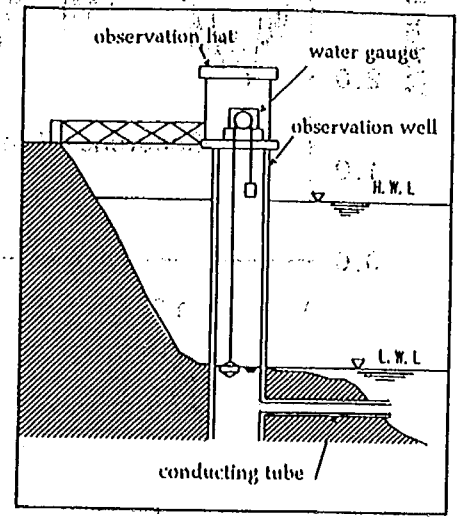
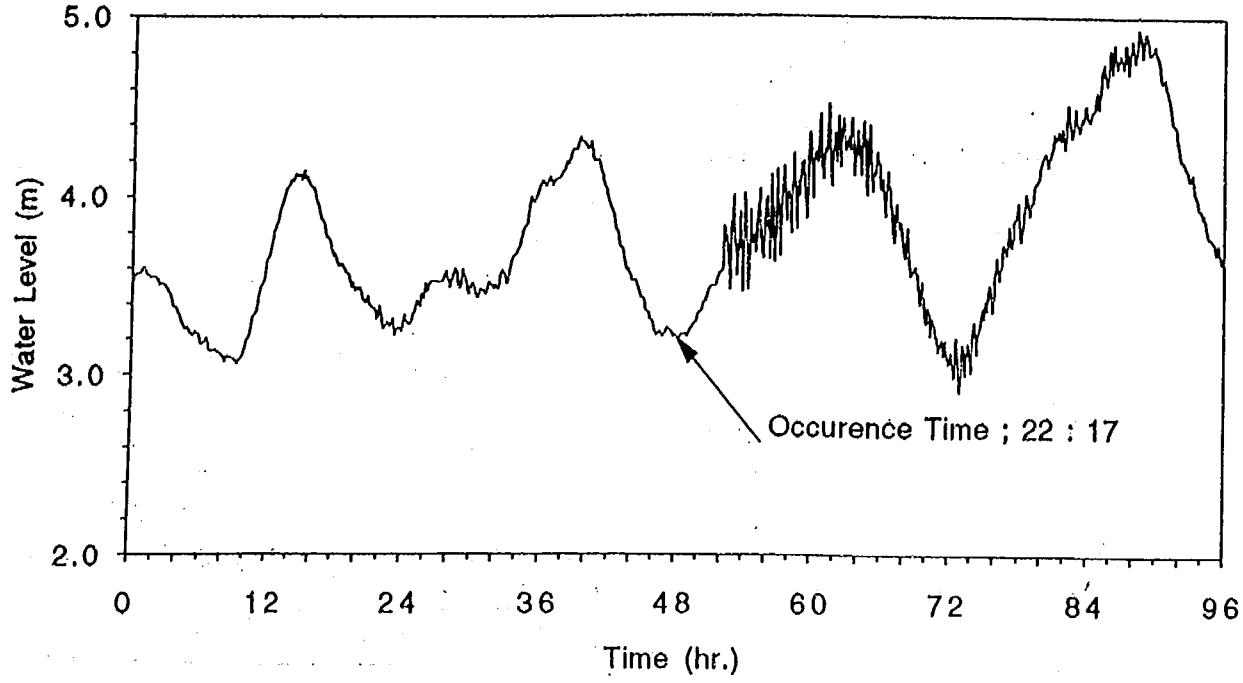
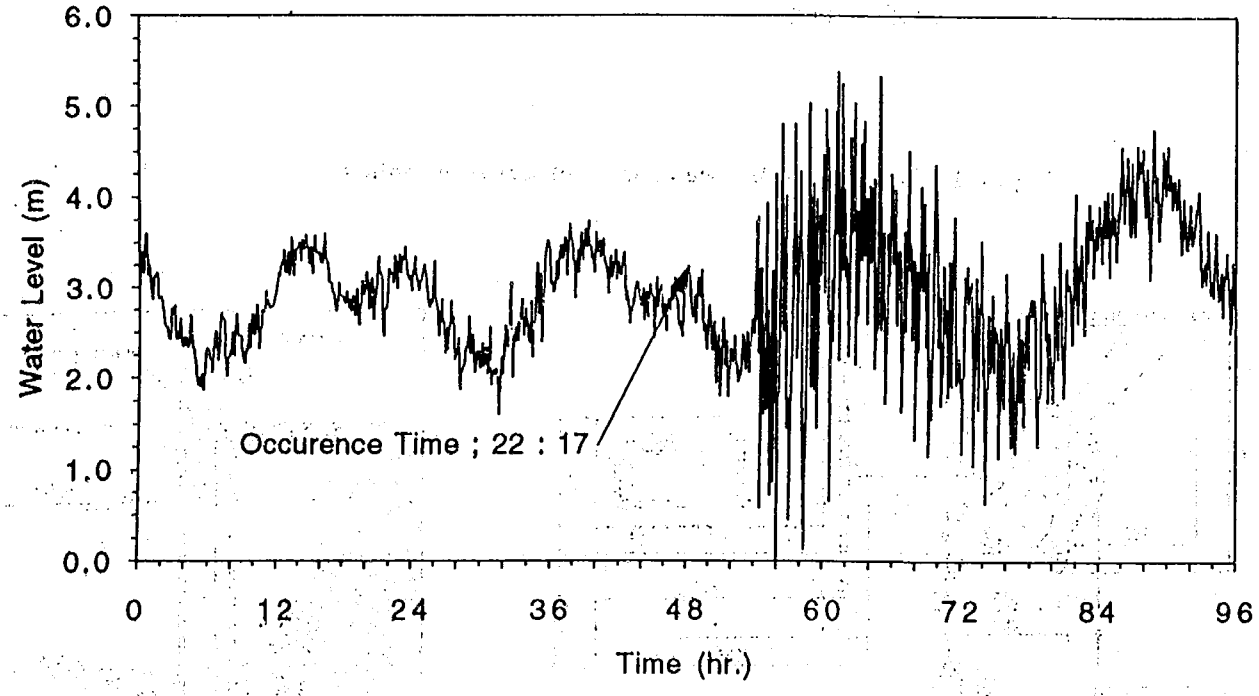


Figure 3 Location of installation

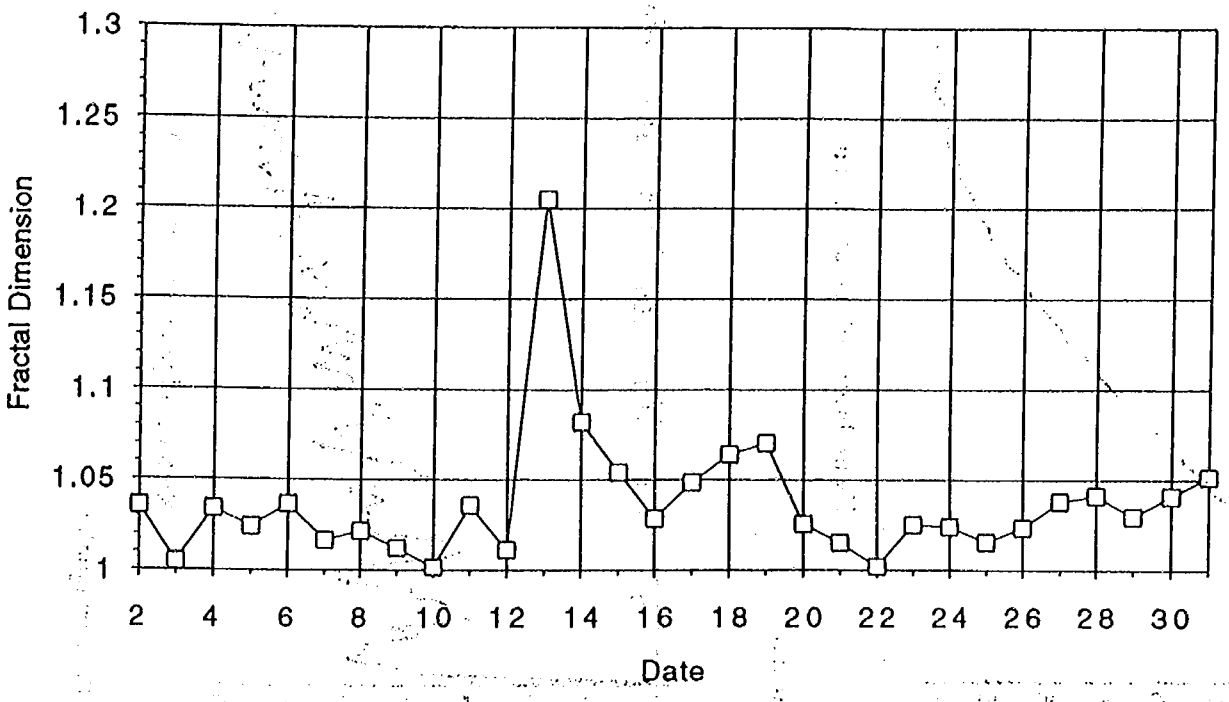


Kaiun bridge observation point

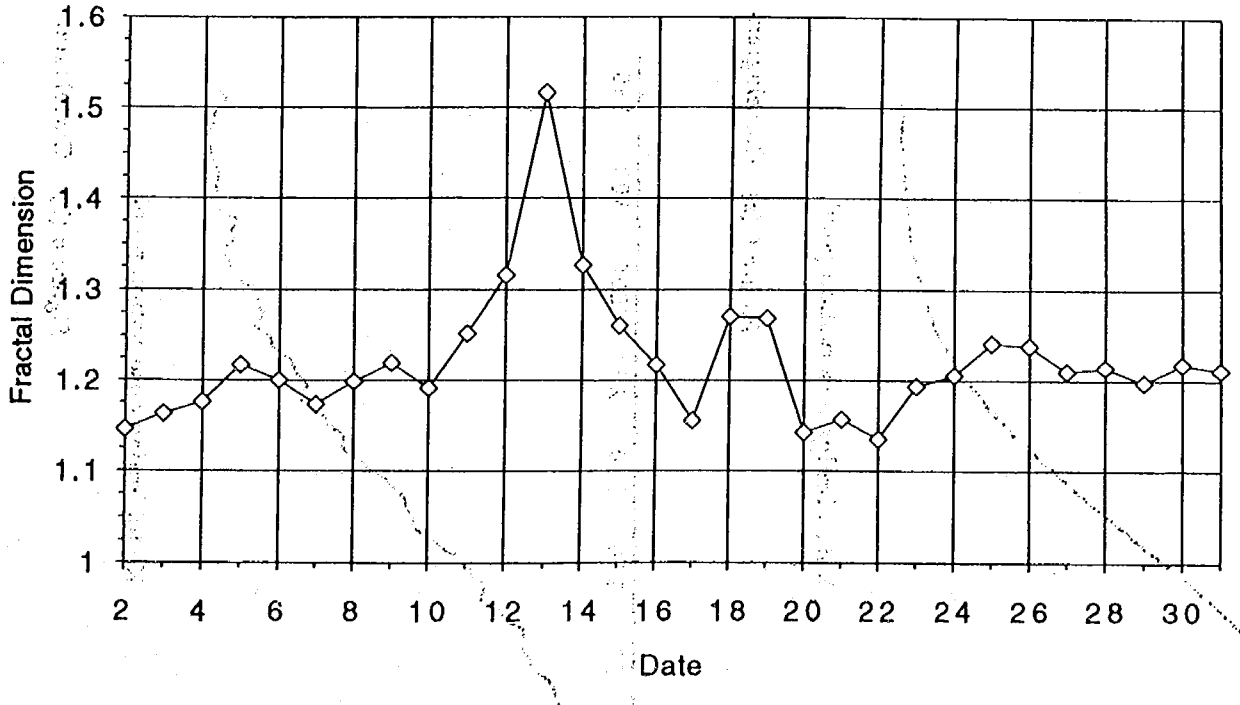


Koitoi bridge observation point

Figure 4 Wave profiles of the water level before and after the earthquake

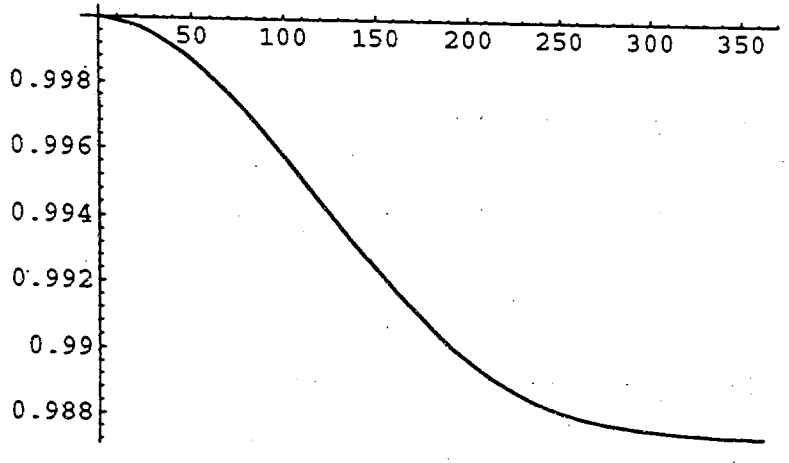


Kaiun bridge observation point

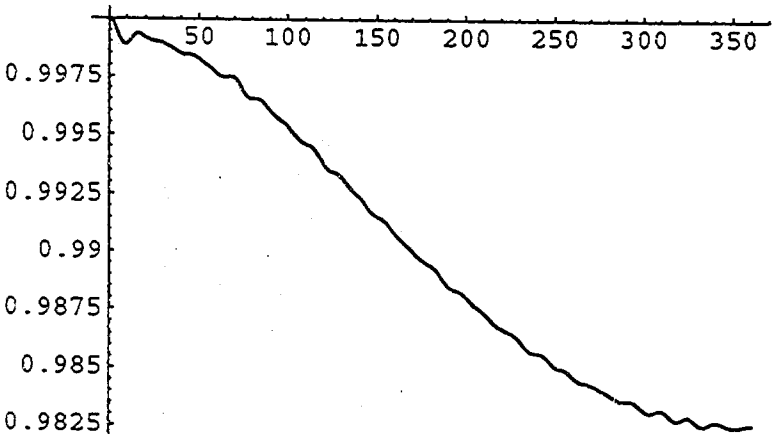


Koitoi bridge observation point

Figure 5 Changes by day of fractal dimension

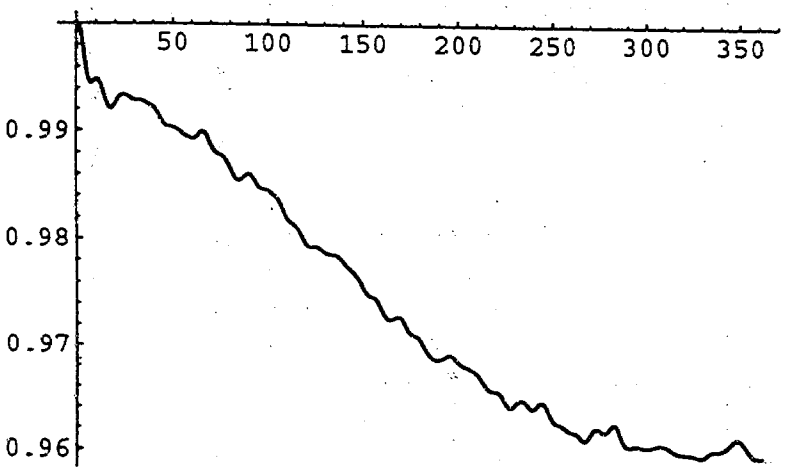


Kaiun bridge observation point

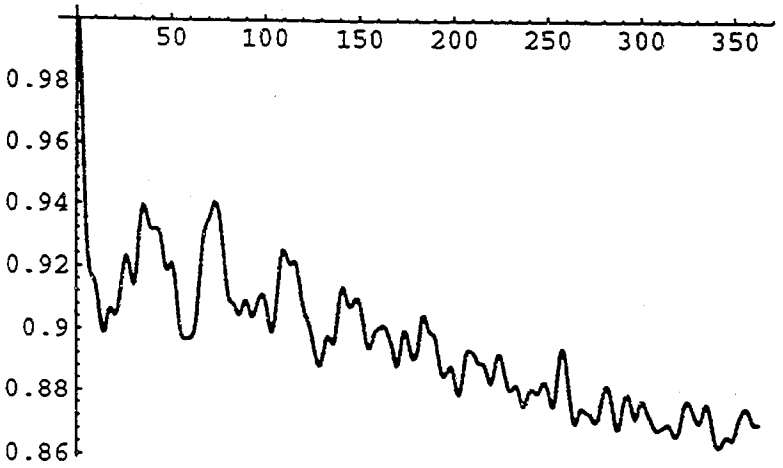


Kaiun bridge observation point

Figure 6 (a) Correlogram for the previous day



Koitoi bridge observation point



Koitoi bridge observation point

Figure 6 (b) Correlogram for the day of the earthquake

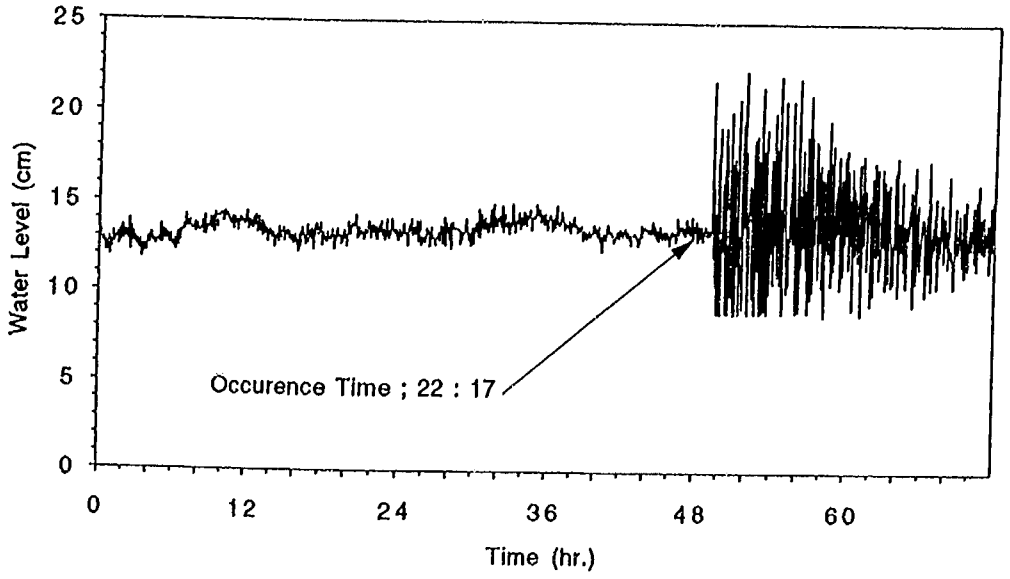
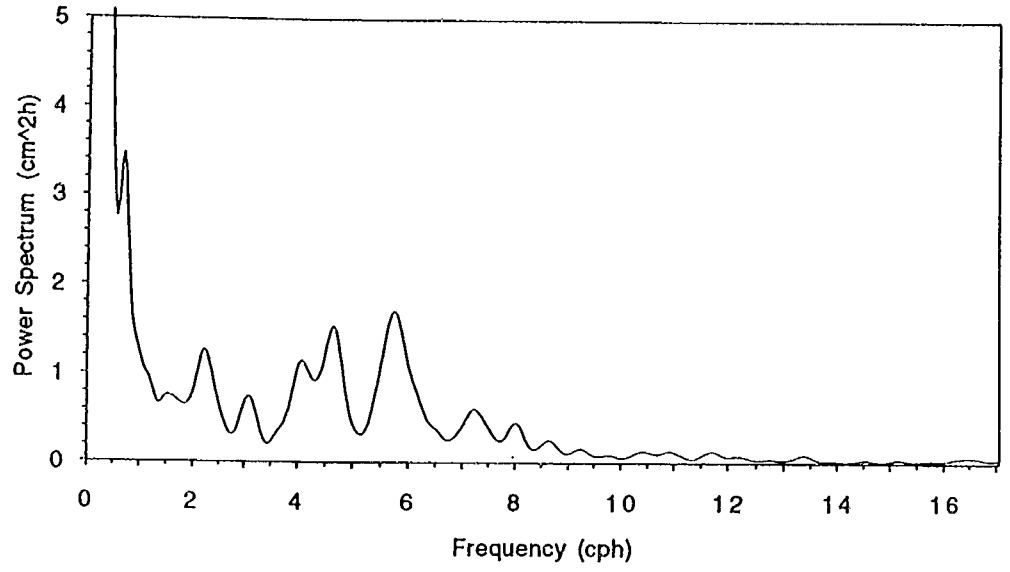
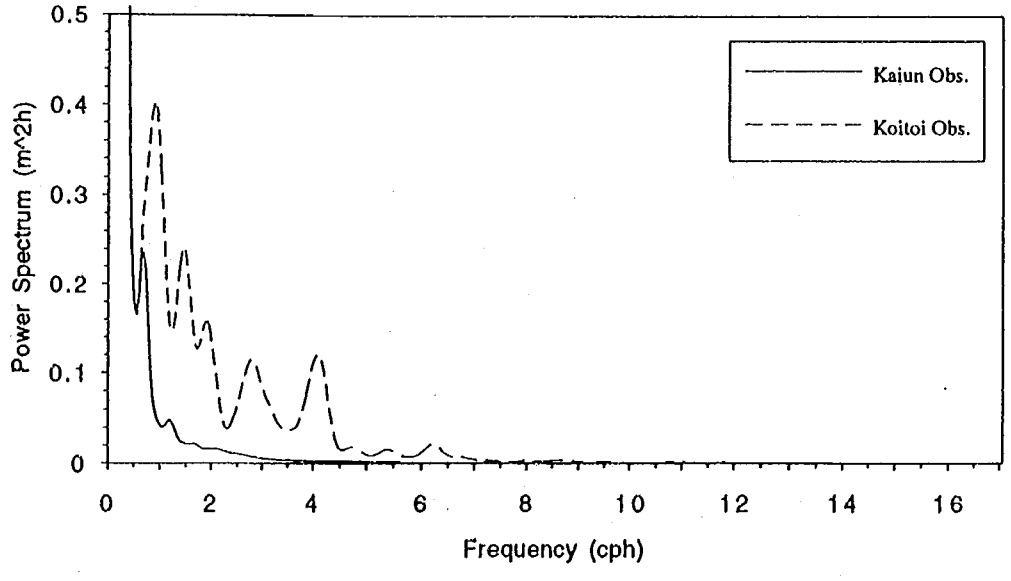


Figure 7 Wave profiles of the tide level in Haboro harbor before and after the earthquake



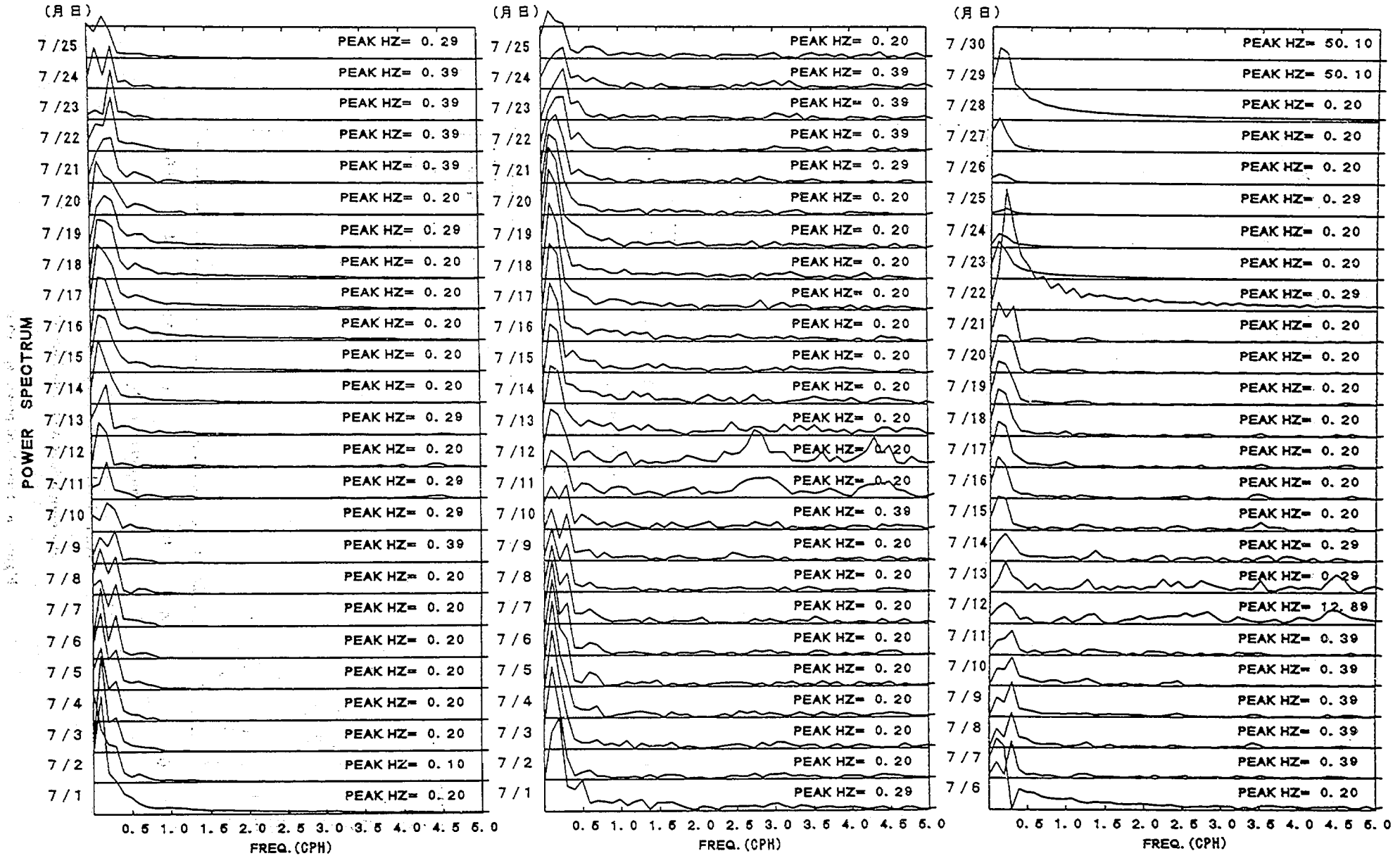
Haboro harbor



Water level observation points

at Kaiun bridge and Koitoi bridge

Figure 8 Smoothed power spectrum

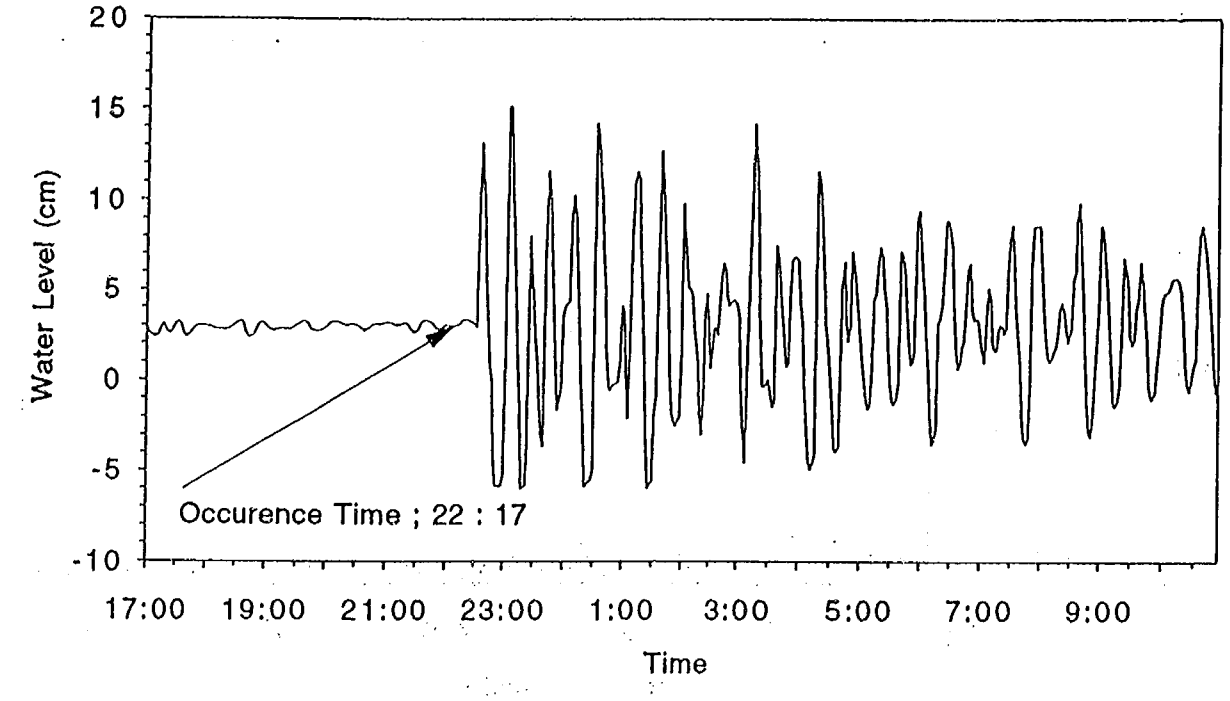


Kaiun bridge observation point

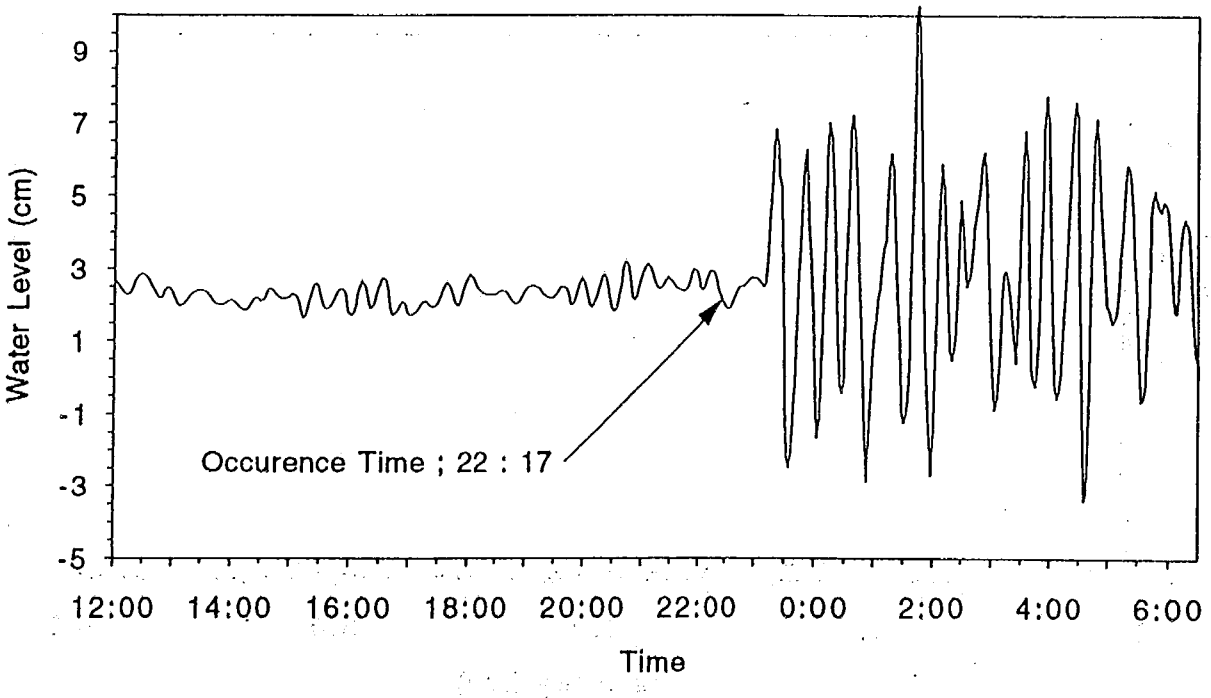
Koitoi bridge observation point

Haboro harbor

Figure 9 Running spectrum

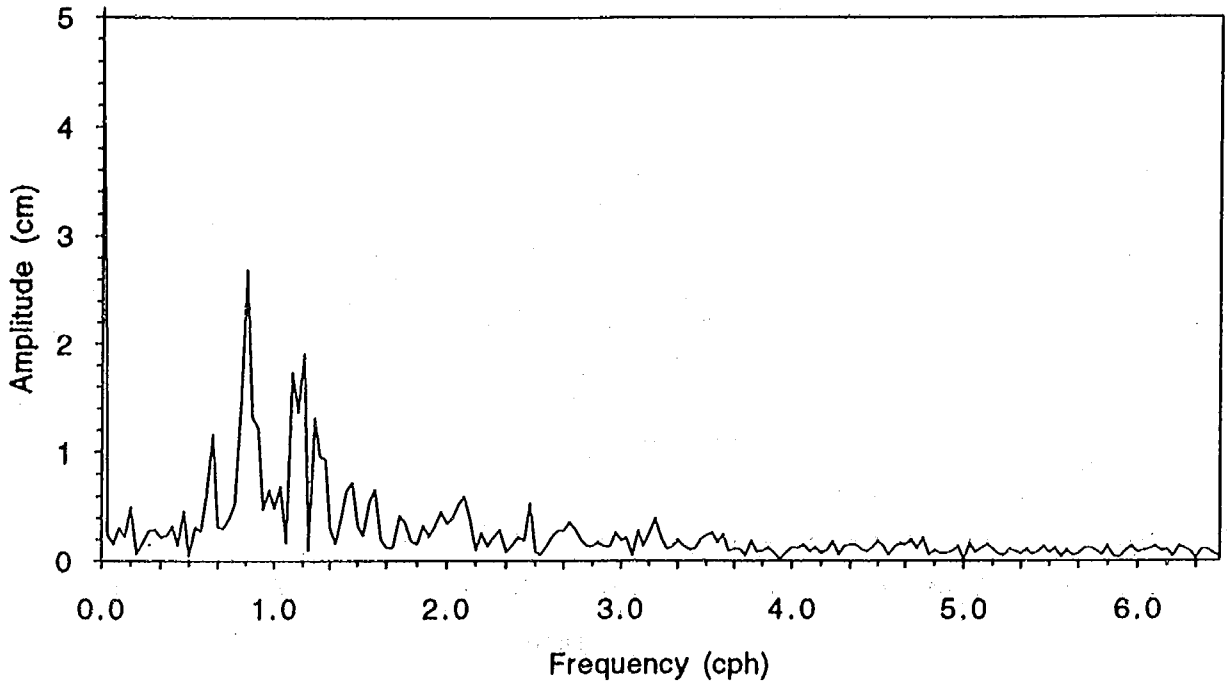


Iwanai harbor

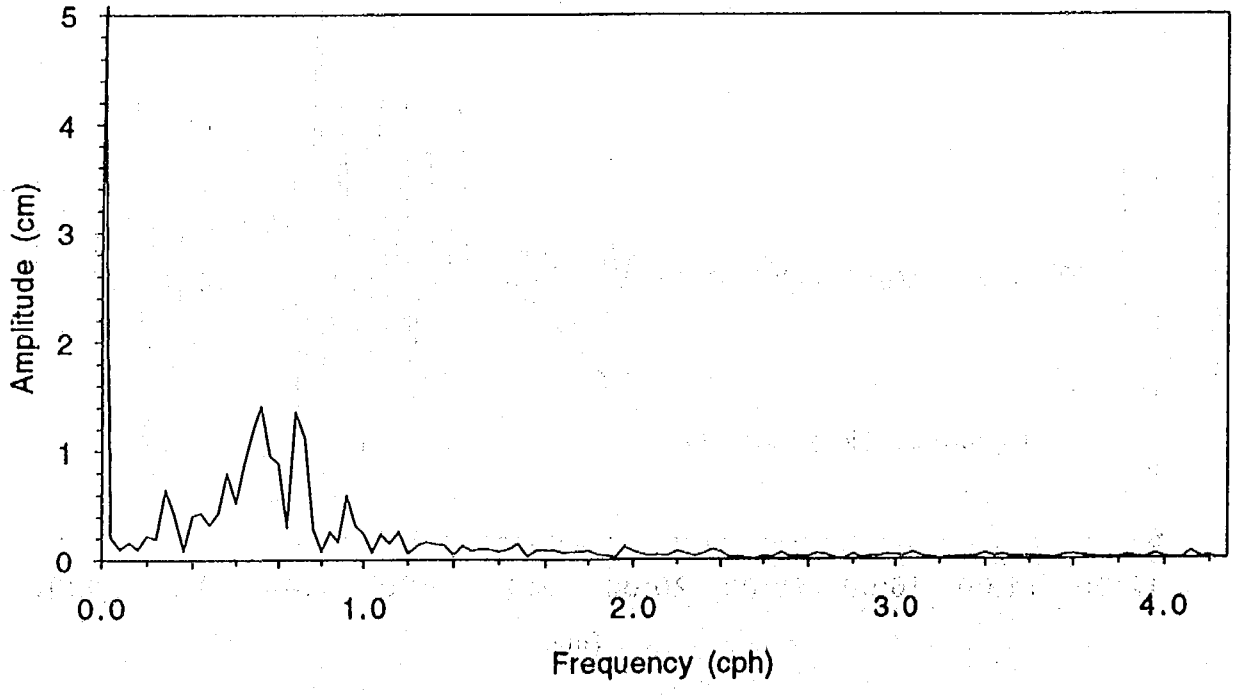


Rumoi harbor

Figure 10 Wave profiles of the tide level before and after the earthquake



Iwanai harbor



Rumoi harbor

Figure 11 Fourier amplitude on the day of the earthquake

Appendix

Abstract

Task Committees Reports

Report of Task Committee on
(A) STRONG-MOTION DATA AND APPLICATIONS

Date: May 16, 1995.
Place: Public Works Research Institute, Tsukuba, Japan

Attendees:	Japan side –	S. Iai (Chairman)	(PHRI)
		E. Mochizuki	(MRI)
		K. Ohtani	(NIED)
	U.S. side –	G. Brady (Chairman)	(USGS)
		R. McCarthy	(CA SSC)
		J. Ake	(BuRec)

1. Objective and Scope of Work

The objectives of the Task Committee are (1) to coordinate and promote sharing of strong motion earthquake data among researchers and practicing engineers, and (2) to develop techniques and exchange information for evaluating the destructive effects of earthquake motion.

The scope of work includes:

(1) instrumentation,
(2) recording, processing and analyzing strong-motion data,
(3) engineering characterization of ground motion,
(4) design applications, and
(5) seismic zonation.

The activities of the Task Committee include:

(1) regular exchange of data and publications,
(2) creating procedures for the dissemination of significant strong-motion digital data with regard for the rights and expectations of (a) owner, (b) the users of data and (c) the earthquake engineering community,
(3) planning and conducting T/C workshops and meetings, and
(4) coordinating relevant research activities.

2. Accomplishments

(1) Plans are well underway to conduct a Workshop on Strong-Motion Data/Local Site Effects in January, 1996, Yokosuka. Funding has been provided by the Japanese Government, including funding for 15 non-Japanese attendees.

(2) Northridge strong-motion data from USGS and CDMG programs are available on Internet . The address for USGS is : anonymous ftp@agram.wr.usgs.gov.

(3) NIED has received a large government grant funding the installation of 1000 instruments through out Japan, centralized data collection and Internet dissemination.

3. Future Plans

(1) Co-sponsors of the Workshop in Japan are sought in the US for individual attendees. Details of the type of preparatory work to be performed by all attendees for comparison purposes will be decided. This homework has been the driving element in previous successful workshops.

Report of Task Committee on
(B) TESTING AND EVALUATION PROCEDURES FOR BUILDING SYSTEMS

Date: May 16, 1995
Place: Public Works Research Institute, Tsukuba, Japan

Attendees:	Japan Side –	K. Ohtani (Chairman)	(NIED)
		I. Nishiyama	(BRI)
	U.S. Side –	H. Lew (Chairman)	(NIST)
		S. Sweeney	(CERL)

1. Objective and Scope of Work

The objective of the Task Committee is to develop rational test procedures and to collect performance data of dynamic response of structures through laboratory testing of prototype structures and field testing of structures in situ.

The scope of work includes:

(1) Plans and conducts workshops and joint meetings to identify research topics and develops joint research programs.
(2) Coordinates research projects carried out by various laboratories in the U.S. and Japan. Facilitates publication of research results and implementation of findings in codes and standards.
(3) Facilitates exchange of research personnel, technical information and available testing facilities.
(4) Develops uniform testing procedures including test loading history for case of comparison of results of tests carried out by various researchers, and for establishment of data base.
(5) Develops guidelines for interpretation of test results in consideration for design of structures.
(6) Develops methodology for evaluation and interpretation of physical test results.

2. Accomplishments

(1) The third phase of the U.S. Precast Seismic Structural Systems Program (PRESS) has been initiated in 1995 with several universities participating in the program,
(2) The fourth U.S. Technical Coordinating Committee (TCC) meeting on PRESS was held in May 1995 at San Diego, CA. Effective and timely transfer of PRESS research results into practice was discussed.

(3) The research program on Composite and Hybrid Structures (CHS) in Japan was initiated in 1993 Experimental and analytical work is being carried by the Building Research Institute and by several universities and construction companies. The Japan Structural Consultant Association is undertaking an applications study for implementing research results into practice.

3. Future Plans

(1) The second U.S.–Japan Joint Technical Coordinating Committee Meeting on Composite and Hybrid Structural Systems (CHS) will be held in June 1995 at Berkeley, CA.

(2) The Joint Research Program on CHS will be initiated in the U.S. in 1995. The National Science Foundation will select a principal investigator of the program in July 1995.

(3) In support of the International Decade for National Disaster Reducation (IDNDR) Program, techniques will be explored to disseminate findings of completed Joint Research Projects, such as masonry and precast concrete structures, which were carried out under the auspices of T/C "B" to countries of high sesmic risks.

(4) To maximize the usefulness of research date, it is desirable, to establish standards for test procedures, documentation and retrieval of test data. A joint workshop is proposed to be held before the 29th Joint Panel Meeting to discuss this topic.

Report of Task Committee on
(C) DESIGN, EVALUATION AND IMPROVEMENT OF STRUCTURES

Date: May 16, 1995
Place: Public Works Research Institute, Tsukuba, Japan

Attendees:	Japan Side –	H. Yamanouchi (Chairman)	(BRI)
		Y. Kitagawa	(BRI)
		K. Kawashima	(TIT)
		M. Suzuki	(PWRI)
		H. Otsuka	(PWRI)
		K. Yokoyama	(PWRI)
		H. Okada	(BRI)
		H. Sato	(PWRI)
		J. Rodrigues	(PWRI)
	U. S. Side –	K.P.Chong (Chairman)	(NSF)
		N.Raufaste	(NIST)
		B.Bienkiewicz	(CSU)
		H.S.Lew	(NIST)

1. Objective and Scope of Work

The objective of the Task Committee is to develop disaster mitigation policies and programs which will improve the performance of new structures and the capacity of existing structures in resisting wind and seismic forces. In order to establish adequate evaluation of performance, each country will coordinate development of condition assessment, screening, and structural analysis and design methodologies. Enhance performance can be obtained by the intelligent renewal, repair and retrofit of exiting buildings and other structures. Structures will be analyzed and instrumented, and then evaluated after disasters. Also, effective utilization of new advanced materials and structural systems, associated with appropriate design methods, will provide excellent structural performance in the life cycle.

The scope of work includes:

(1) Exchanging information, planning, and hosting workshops on new design technologies, evaluation technologies, and repair and retrofit techniques.
(2) Studying new materials and methods for repairing and retrofitting existing structures and for new construction.
(3) Developing a uniform system for screening and analyzing wind and seismic resistance capacity of structures in each country.
(4) Developing reliable condition assessment systems for new and existing structures.

(5) Evaluating masonry, precast concrete and composite/hybrid building structures: and providing documentation for post – disaster evaluation of performance.

(6) Coordinating research projects in the U. S. and Japan to minimize duplication and maximize benefits.

2. Accomplishments

(1) The UJNR Panel members on the U.S. and Japan sides jointly investigated the structural damage due to the 1995 Hyogo–Ken Nanbu Earthquake (Kobe).

(2) The BRI has initiated a three–year research and development program on Performance Based Structural Design System from the fiscal year of 1995.

(3) The NSF five–year initiative on Composite and Hybrid Structures – a U.S.–Japan Cooperative Earthquake Engineering Program was released and principal investigators will be chosen in July 1995 for the 1995 fiscal year. This Panel coordinates the bilateral research.

3. Future Plans

The following planning was performed on Design, Evaluation and Improvement of Structures.

(1) The second workshop on "Structural Control and Intelligent Material Systems" is being planned in the U. S. during 1996, in coordination with T/C "G".

(2) U. S. –Japan Workshop on smart materials and structures will be held at the University of Washington on December 4–5, 1995 funded by NSF.

(3) Develop a reliable system for screening and analyzing wind and seismic resistant capacity, and improve instrumentation and expert systems to provide condition assessment of existing structures.

(4) Compile a database of advanced materials/systems that have potential for improving structural performance of new construction, as well as for use in rehabilitating and strengthening existing buildings.

(5) Investigate new design methodologies based on required structural performance which also will address advanced materials and systems. In order to effectively take this new approach, BRI will propose to have an ad–hoc meeting to establish a U. S.–Japan joint study group of members from appropriate institutions in each country.

(6) Develop design guidelines for applying advanced structural and materials systems to be used for composite and hybrid structures under the joint U.S. /Japan Cooperative Research Program.

(7) Continue to encourage participation by private industry, consulting engineers, universities, national and local government agencies involved in instrumentation, evaluation, condition assessment, and retrofit and strengthening of existing buildings for seismic and wind resistance.

(8) In response to a growing recognition of high loses caused by extreme winds in the U.S. and Japan, it is proposed to initiate the feasibility study for establishing a new

4. Other Activities

(1) The BRI formed a feasibility study group involving eighteen construction companies for promoting research programs on "Building Safety and Related Infrastructure Improvements" under the framework of the "New Economic Partnership between the U. S. and Japan".

(2) Continued U.S. research sponsored by NSF developed reports on seismic rehabilitation and retrofit strategies, including innovative techniques for strengthening existing buildings and bridges.

(3) An updated report on Civil Infrastructure Systems – Strategic Issues has been published by NSF. Continue development of NSF's Civil Infrastructure Systems Research Program, including strong emphasis on evaluation and improvement of structures.

(4) NSF targeted $ 3M for a new initiative on Systematic Change in Urban Infrastructure including innovative design, evaluation, improvement and renewal of the urban civil infrastructure. The deadline is May 15, 1995 and awards are being made in the fiscal year of 1995.

(5) A NSF funded International Symposium on Civil Infrastructure Systems Research is scheduled for September 25–28, 1995 in Seoul, Korea. Researchers from U.S., Japan, Korea and other countries will be participating.

(6) NSF works with Japan Science and Technology Agency (STA/NISTP) on Smart Materials research planning by STA.

Report of Task Committee on
(D) EARTHQUAKE ENGINEERING FOR DAMS

Data: May 16, 1995.
Place: Public Works Research Institute, Tukuba, Japan

Attendees:	Japan Side –	A.Nakamura (Chairman)	(PWRI)
		T.Fujisawa	(PWRI)
		Y.Kato	(PWRI)
		I. Nagayama	(PWRI)
		J. Kashiwai	(PWRI)
		Y.Yamaguchi	(PWRI)
	U.S.Side –	W. E. Roper (Chairman)	(COE)
		A. G. Franklin	(WES, COE)

1. Objective and Scope of Work

The Objective of this Task Committee (T/C) is to develop technical insights into better understanding of the response of dams to seismic effects. The T/C will plan, promote, and develop research initiatives to assist in assuring seismic safety and economical protective countermeasure against earthquake loading for these structures. Its scope of work includes:

(1) Methods of analysis for seismic design of dams.
Comparison of design methods between U.S. and Japan.
Investigation and dynamic analysis methods as tools (modeling, calculation codes).
(2) Dynamic characteristics of dam construction materials.
Strength and deformation characteristics during earthquakes (concrete, soil and rock).
(3) Analysis of observed behavior of dams during earthquake.
Investigation of the mechanism of damages against earthquake loading.

Application of the analysis of the observed behavior during earthquake to the earthquake-resistant design.

2. Accomplishments

(1) Dr. Krinitzsky, Dr. Hall, Dr. Koester, Waterways Experiment Station (WES), U.S. Army Corps of Engineers, visited Hanshin Area to study the seismic effects of the 1995 Hyogoken – Nanbu Earthquake to dams and other hydraulic facilities from January 24th to 31st, 1995. They are exchanging further information with Japanese side.

(2) Dr. N.Matsumoto (PWRI) visited the US Bureau of Reclamation(USBR) and the Waterways Experiment Station(WES) on March 13 and 14, 1995, to discuss feasibility of cooperative research, to exchange technical information on geotechnical earthquake engineering and earthquake engineering for dams, and to present a report on the Hyogo-ken-nanbu Earthquake.

3. Future Plans

(1) Exchange of the results of research/investigation and technical information about dam earthquake engineering is encouraged, and feasibility of joint research and investigation is in continuous consideration.

(2) Exchange visits to the institutes concerned, of scientists and engineers between U.S. and Japan, is to be extended for the effective communications.

(3) In accordance with the progress of the activities (1) and (2), T/C(D) will hold a Workshop on State-of-the Art Review of US-Japan Research on Earthquake Engineering for Dams in the United States in 1996.

Report of Task Committee on
(F) DISASTER PREVENTION METHODS FOR LIFELINE SYSTEMS

Data: May 17, 1995.
Place: Public Works Research Institute, Tukuba, Japan

Attendees:	Japan Side –	Y. Koga (Chairman)	(PWRI)
		H. Otsuka	(PWRI)
		J. Hoshikuma	(PWRI)
	U.S. Side –	H. S. Lew (Acting Chairman)	(NIST)
		J. Malilay	(CDC)
		S. Sweeney	(CERL)

1. Objective and Scope of Work

The objectives of the Task Committee are to improve: 1) the performance of lifeline systems during earthquakes and 2) engineering and other seismic countermeasures including the capability in damage estimation techniques and inspection procedures.

The scope of work includes:

(1) Planning and conducting workshops on lifeline systems
(2) Facilitating exchange of technical information
(3) Promoting development of design guidelines and standards for lifeline systems

2. Accomplishments

(1) Organized a joint post–earthquake reconnaissance effort for the 1995 Hyogo–ken Nanbu earthquake (Kobe). Both the Japan and U.S. team members collaborated closely in field investigations which took place in mid–February 1995.

Results of joint investigations, including those related to the performance of lifeline systems, will be presented at meetings, workshops, and conferences.

3. Future Plans

(1) Hold the 6th Joint Workshop on Disaster Prevention for Lifeline Systems, 18–19 July 1995, Osaka, Japan. The workshop will focus on the R&D related to the topics given above, with special emphases on the lessons learned from the 1995 Hyogo–ken Nanbu (Kobe), and the 1994 Northridge earthquakes.

(2) Encourage collaborative research and development in the following areas:
   - Performance prediction and damage assessment of lifeline systems
   - systems approach to lifeline performance
   - soil–structure interaction
   - geographic information systems (GIS)
   - cost–effective ground improvement techniques for underground structures

(3) Encourage and strengthen current efforts in both countries to establish seismic design guidelines and standards for lifeline systems. Existing UJNR channels should be fully utilized to facilitate the exchange of relevant information concerning guidelines and standards development. Possible collaboration of joint development of guidelines and standards for lifeline systems should be pursued.

Report of Task Committee on
(G) Structural Control and Intelligent Material Systems

Date: May 16, 1995
Place: Public Works Research Institute
Tsukuba, Japan

Attendees:	Japan Side –	Y. Kitagawa (Chairman)	(BRI)
		K. Kawashima	(TIT)
		H. Okada	(BRI)
		H. Otsuka	(PWRI)
		J. Rodrigues	(PWRI)
		H. Sato	(PWRI)
		M. Suzuki	(PWRI)
		H. Yamanouchi	(BRI)
		K. Yokoyama	(BRI)
	U. S. Side –	K. Chong (Acting Chairman)	(NSSF)
		B. Bienkiewicz	(CSU)
		N. Raufaste	(NIST)
		H. S. Lew	(NIST)

1. Objective and Scope of Work

The objectives of the Task Committee are to: (1) develop research plans in control of equipment and structures and in high performance structural and material systems; (2) implement control techniques for motion reduction or modification; (3) implement use of advanced materials in actual design and construction of buildings and other infrastructure systems under seismic or wind environments; (4) promote U.S.–Japan cooperation in structural control and intelligent material systems research; (5) bring together govemmental, academic, and industrial participants in joint pursuit of these efforts; and (6) contribute to IDNDR by organizing joint research and other technical activities in structural control and intelligent material systems research on the basis of intemational cooperation.

The UJNR T/C "G" works closely with other organizations to provide the leadership in this emerging research by facilitating the exchange of technical data and information through UJNR mechanisms. The scope of work includes :

(1) Providing technical assistance, consultation and coordination of UJNR affiliated

research organizations in the initiation, development, and execution of their programs in research areas.

(2) Promoting Joint govemment–university–industry collaborative efforts to facilitate technology transfer and practical implementation.

(3) Sponsoring and conducting inter–disciplinary workshops and meetings to identify key areas of research and opportunities for cooperation, and to exchange new knowledge and experience in practice.

(4) Developing promotional and demonstrative activities to stimulate public awareness and interest in this field of research.

(5) Providing information useful for the establishment of performance standards, design specification, guidelines and code recommendations for application in new construction as well as retrofit/rehabilitation of existing structures.

(6) Promoting research in intelligent material systems, sensors, actuators, optimal control system design, and encourage laboratory and field experiments of prototype and full–scale structures.

2. Accomplishments

(1) The NSF Research on Structural Control, held a coordination meeting in conjunction with the First World Conference on Structural Control in Pasadena, Califomia on August 1994 with major participation by Japan and U.S. Panel Members. The proceedings was published by the University of Southern Califomia in 1994.

(2) "Second Intemational Conference on Intelligent Materials" co–funded by NSF and other U.S. agencies, was held in June 1994 in Williamsburg, VA.

(3) At BRI, research program on structural control and intelligent material systems using self–diagnosis and self–repairable materials has been initiated in April 1994.

(4) A research program on intelligent seismic structures has been initiated at PWRI from April 1995. This research is to develop new technology using self–diagnosis materials and self–repairable materials.

(5) A joint research program for active control of bridges is being carried out through T/C "G" and "J" by PWRI, NSF, FHWA, NIST, NCEER, and UC Irvine.

(6) A joint research program on active and hybrid control of building is being performed by BRI and NCEER.

(7) NSF works with STA (Japan Science & Technology Agency) on "Smart Materials" research planning by STA.

(8) A new NSF research initiative on sensor and sensors system for power systems and other civil infrastructure systems was issued for requesting final proposals by April 1995. EPRI and NSF and co–funding this initiative.

3. Future Plans

(1) Under NSF sponsorship, a U.S.–Japan workshop on smart materials and strucutres will be held at the University of Washington on December 4–5, 1995. Another workshop on "Structural Control and Intelligent Materials Systems" is planned to be conducted in late 1996 in cooperation with T/C "C".

(2) Efforts for U.S.–Japan cooperative research projects on seismic response control involving PWRI, BRI, NSF and industries from both sides are continuing. Research cooperation between the U.S. and Japan will be actively pursued using UJNR and other inter– governmental mechanisms.

(3) Joint research projects on active and hybrid control of structures, such as bridges and buildings, will be continued and developed by PWRI, BRI, NCEER, CUREE, and others.

(4) In cooperation with T/C "J", the 4th U.S.–Japan workshop on Earthquake Protective Systems for Bridges is being scheduled in 1996 in Japan. Proposed topics will be expected to include: (1) innovative protective systems: (2) design methods for seismic isolated/menshin bridges: (3) full–scale verification of performance: (4) comparative design examples, and (5) smart/high performance structural materials and system. T/C "G" will play a supportive role in the workshop.

(5) NIST will document a state–of–the–art review of active control systems and evaluate those available technology for use by designers.

4. Other Activities

(1) A joint ASME, JSME, and PVP conference on seismic base isolation will be held at Honolulu, Hawaii, on July, 1995.

Report of Task Committee on
(H) SOIL BEHAVIOR AND STABILITY DURING EARTHQUAKES

Date : May 17, 1995
Place : Public Works Research Institute,Tsukuba,Japan

Attendees :	Japan side –	R. Hagiwara (Chairman)	(PWRI)
		O. Matsuo	(PWRI)
		C. Minowa	(NIED)
		H. Mizuno	(BRI)
	U.S. side –	A.G. Franklin (Chairman)	(WES)

1. Objective and Scope of Work

Government agencies responsible for public works must assure seismic safety and provide economical protection against earthquake hazards.

The objective of the Task Committee is to assist in meeting these needs by enhancing the available technology for predicting the dynamic behavior of soils, analyzing dynamic soil–structure interaction, and modifying the earthquake behavior of foundations and earth structures to assure their safe performance during earthquakes.

In accordance with the objective, the scope of work includes :

(1) Present technical papers at annual joint panel meetings on technological developments and on state–of–the–art and practice related to soil behavior and stability during earthquakes.
(2) Exchange information and technical data relating to field performance, research, and methods of practice.
(3) Plan and conduct programs of cooperative research and/or workshops in coordination with the proposed or ongoing programs.
(4) Make other needed efforts including exchange of researchers between U.S. and Japanese research institutions, publication of research results and recommended practice.

2. Accomplishments

(1) T/C(H) held its 4th U.S.–Japan Workshop on Soil Liquefaction:Remedial Treatment of Potentially Liquefiable Soils at the Public Works Research Institute (PWRI) in Tsukuba,4–8 July 1994. PWRI published the Workshop Proceedings.

(2) The National Research Institute for Earth Science and Disaster Prevention (NIED), the Building Research Institute (BRI), and Wayne State University (WSU) have initiated a cooperative research program "Physical and Numerical Simulation of Structural Damages Due to Liquefaction and Development of Countermeasure Techniques" (1994–1998) under the auspices of UJNR Panel on Wind and Seismic Effects.

(3) Dr. N. Matsumoto of PWRI visited the US Bureau of Reclamation (USBR) and the Waterways Experiment Station (WES) on March 13 and 14, 1995, to discuss feasibility of cooperative research, to exchange technical information on geotechnical earthquake engineering and dam earthquake engineering, and to present a report on the Hyogo–ken–nanbu Earthquake.

3. Future Plans

(1) The Port and Harbour Research Institute (PHRI) and WES will publish the English version of the "Handbook on Remedial Measures for Reclaimed Land Soil Liquefaction" and deliver it to the Panel members and participating organizations in 1995.

(2) NIED, BRI and WSU will continue a cooperative research program "Physical and Numerical Simulation of Structural Damages Due to Liquefaction and Development of Countermeasure Techniques" (1994–1998). NIED will complete construction of a Large–scale Shear Box by the end of fiscal year 1995.

(3) WES will complete construction of a Large–scale Centrifuge within the next several months, and PWRI is planning to initiate construction of a Large–scale Centrifuge and Shaking Table in fiscal year 1995. T/C (H) will develop plans for information exchange and cooperation on Centrifuge Experimentation during the next year.

(4) T/C (H) tentatively plans to hold a workshop on the Use of Centrifuge Experiments for Research on Soil Behavior and Stability During Earthquakes in conjunction with the Joint Panel Meeting in the U.S. in 1998.

Report of Task Committee on
(I) STORM SURGES AND TSUNAMI

Data: May 17, 1995
Place: Public Works Research Institute, Tukuba, Japan

Attendees:	Japan Side –	S. Tanaka(Chairman)	(PWRI)
		S. Sato	(PWRI)
		E. Mochizuki	(JMA)
		T. Konishi	(JMA)
	U.S. Side –	W. E. Roper(Acting Chairman)	(COE)
		H.Yeh	(Univ.Wash.)
		C.Smith	(Mineral Management)

MISSION STATEMENT

1. Objective and Scope of Work

The objective of this T/C is to mitigate damages from storm surges and tsunamis through shared technologies, research, information sharing, and cooperative work. Storm surges are caused by hurricanes and typhoons. Tsunamis are caused by underwater earthquakes, volcanic activities and land slides. Both hazards may cause serious disasters along coastal region.

The scope of work of this T/C is as follows:

(1) Exchange results of research on storm surge and tsunami occurrence, generation, propagation, and coastal effects. This includes observations on historical, current, and theoretical tsunamis. Of particular interest is the effort by U.S. and JAPAN to acquire deep ocean tsunami measurements.

(2) Exchange results and status of countermeasure against storm surge and tsunami activities including analysis of the problem, planning, warning, and engineering approaches.

(3) Exchange information on development of technologies such as computer programs to predict travel times, land–fall locations, run–up heights, and wave characteristics, improved instrumentation, and use of satellite communications for detection and warning.

(4) Facilitate dissemination through exchanges of literature, technical reports at joint meetings, special workshops, joint projects, and direct interaction among participants.

2. Accomplishments

(1) The joint workshop with Task Committee (K) was held in Berkeley on January 17–19, 1995. The proceedings was printed by Japan side and are being distributed to all the participants and to the Secretaries–General of both sides.

3. Future Plans

(1) 1996 will be the centennial anniversary of the great Sanriku Earthquake and tsunami in Japan and the 50th anniversary of the April 1, 1946 Aleutian earthquake and tsunami. These events led to the establishment of warning system and much of current activity in this field. The Task Committee is planning for a Tsunami Symposium which will be held in Hawaii in April 1996.

4. Others

(1) The Storm surge research community is less well organized and lacking the specialty societies, journals, and international organizations to define and stimulate work in the field. The Task Committee (I) can help fill this gap.

(2) The tsunami problem is less severe in the U.S. than in JAPAN which leads to a smaller community of researchers. There are few U.S. researchers focusing on tsunamis at any specific location; thus highlighting the importance of T/C periodic meetings and workshop.

Report of Task Committee on

(J) WIND AND EARTHQUAKE ENGINEERING FOR TRANSPORTATION SYSTEMS

Data: May 17, 1995

Place: Public Works Research Institute, Tukuba, Japan

Attendees:	Japan side –	K. Yokoyama (Chairman)	(PWRI)
		M. Nakano	(PWRI)
		K. Nishikawa	(PWRI)
		S. Unjo	(PWRI)
		Y. Kimura	(PWRI)
		M. Ishida	(PWRI)
	U.S. Side –	J.D. Cooper (Chairman)	(FHWA)
		B. Bienkiewicz	(CSU)

1. Objectives and Scope of Work

The objectives of this Task Committee are to: (1) plan, promote, and foster research on the behavior of highway bridges when subjected to wind and seismic forces and (2) disseminate research results and provide specifications and guidelines based on the Task Committee's findings. Surface transportation systems play a vital role in the movement of goods and people. Highway bridges are especially influenced by the forces of wind and earthquakes because of their open exposure to those forces.

The scope of work includes:

(1) Focus research on highway bridges without limitation on their size and function.

(2) Investigate existing and new bridge designs and the behavior of whole bridge systems and/or single components of a bridge.

2. Accomplishments

(1) Mr. Mark Yashinsky, California Department of Transportation, was a guest researcher at the Earthquake Engineering Division, PWRI, from April 1, 1994 to August 29, 1994 working on the seismic design method of bridges.

(2) Dr. Philip Yen, FHWA, was a guest researcher at the Earthquake Engineering Division , PWRI, from March 12 to 31, 1995 to work on seismic design, and also participated in the International Workshop on Seismic Design of Bridges held at PWRI on March 13 & 14,1995. Mr. Michael Britt, FHWA, was a guest researcher at PWRI and the Honshu–Shikoku Bridge Authority from May 9, 1994 to April 25, 1995

working on the design method of bridges.

(3) Conducted joint field investigation of the January 17, 1995 Hyogo-ken Nanbu Earthquake. Engineers representing FHWA, CALTRANS, NSF, USGS, NIST, and Corps of Engineers joined engineers from PWRI, Hanshin Expressway Public Corporation, Japan Highway Public Corporation and the Ministry of Construction to study damages to transportation structures. The investigation, which was part of the larger UJNR joint investigation into earthquake damage, focused on highways and bridges, transit structures, airports, and ports and harbors. Reports are pending.

3. Future Plans

(1) Conduct the 11th U.S.-Japan Bridge Engineering Workshop in Tsukuba, Japan, May 30-31, 1995, after the 27th joint Panel meeting.

(2) Conduct the 12th U.S.-Japan Bridge Engineering Workshop in U.S., in 1996.

(3) Conduct the Third U.S.-Japan Workshop on Seismic Retrofit of Bridges within two years in Japan. The workshop will focus on practical repair methods of damaged bridges and seismic retrofit measures.

(4) In cooperation with Task Committee (G), the 4th U.S.-Japan workshop on Earthquake Protective Systems for Bridges is being scheduled within two years in Japan. Topics are expected to include: (1) innovative protective systems: (2) design methods for seismic isolated/menshin bridges: (3) full-scale verification of performance: (4) comparative design examples, and (5) smart/high performance structural materials and system.

(5) Continue to investigate and exchange technical information on improved seismic retrofit and strengthening procedures for highway bridges based on experimental, analytical, and field studies. This exchange should include information on maintenance of existing bridges.

(6) Continue experimental research on the seismic performance of bridge piers and columns, and encourage research on seismic isolation and hybrid control of bridges in cooperation with Task Committee (G).

(7) Encourage a research study on seismic, aeroelastic, and aerodynamic response of cable-supported bridges with emphasis on behavior of composite materials, cable inspection, vibration control, and corrosion protection.

(8) Continue the coordinated research study to compare the seismic design criteria for bridges in Japan and the U.S. and discuss the method and analysis procedures for bridge column design. Continue information exchange on the application of the limit state design method.

(9) Encourage a coordinated research study on seismic response and control, system identification techniques, nondestructive evaluation of bridge structures, use and performance of structural materials including new materials, and performance of

jointless bridges.

(10) Task Committee (J) recommends both sides perform a study on the feasibility of creating a new Task Committee on Design For Wind and Wind Hazard Mitigation.

Report of Task Committee on
(K) WIND AND EARTHQUAKE ENGINEERING FOR OFFSHORE AND COASTAL FACILITIES

Data: May 16, 1995
Place: Public Works Research Institute, Tukuba, Japan

Attendees:	Japan side –	T. Uwabe (Chairman)	(PHRI)
	U.S. Side –	C. Smith(Chairman)	(MMS)
		J.Malilay	(NCEH)
		H.Yeh	(Univer. of Washington)

1.Objective and Scope of Work

Criteria for the design of offshore and coastal facilities may differ greatly from their onshore counterparts. These differences can arise due to their unique design or mass distribution, to the fluid/structure or wind/structure interaction, to the placement of foundation elements in or on soft, fully saturated soils that can be subject to large hydrodynamicpressures, and to the lack of specific environmental data or the engineering experience that has been developed for most onshore sites.

The objective of this Task Committee is to develop technical insights necessary to mitigate damage to offshore and coastal facilities due to extreme wind and seismic effects. The Task Committee will plan, promote, and develop research initiatives to meet this objective, and will disseminate the results of their researc
h for incorporation into future specification or design guidelines.

The scope of work includes:

(1) Sponsoring and conducting workshops and meetings to identify key area of research, opportunities for cooperation, and the exchange of knowledge.
(2) Predicting strong ground motions for offshore and coastal sites including assessing the effects of basin geometry, linear, and nonlinear local geological effects using actual seafloor response measurements.
(3) Determining the dynamic response and the interaction of structure/foundation/soil systems to seabed motions and/or extreme wind forces.
(4) Assessing the dynamic response and behavior of various operational facilities mounted on offshore and coastal structures.
(5) Developing assessment methodologies for seismicity and other characteristics of potential seismic sources (e.g.faults) for offshore and coastal sites in regards to how

these conditions relate to structural design criteria.

(6) Promoting the implementation of new research results into current design and construction processes.

(7) Developing research efforts to include laboratory and field programs to obtain data on the response of offshore and coastal facilities to extreme wind and seismic forces.

(8) Creating performance standards, design specifications, guidelines, and code recommendations for application to new construction as well as remedial action for existing facilities.

2. Accomplishments

(1) Conducted 2nd U.S./Japan Workshop on Wind and Earthquake Engineering for Offshore and Coastal Facilities at the University of California,Berkeley,California on Janualy 17 – 19, 1995. This was a joint workshop with Task Committe(I) Storm Surge and Tsunami.

(2) The Japan side hosted Mr. Martin L. Eskijian of California State Land Commision to Kobe port to investigate the damage caused by the Hyogo-ken-nanbu Earthquake.

3. Future Plans

(1) The first and second Workshop Proceedings will be published and made available to the U.S. side and Japan side T/C members, and copies will be provided to both sides Secretaries-General.

(2) Develop workshop agenda of the third U.S./Japan Workshop on Wind and Earthquake Engineering for Offshore and Coastal Facilities in Japan in May 1997.

(3) Coordinate, where possible, on-going research on wind and earthquake engineering for offshore and coastal facilities of interest to the members of the Task Committee.

Technical Site Visits

PANEL ON WIND AND SEISMIC EFFECTS

Technical Site Visits 15 and 20–27 May 1995

by
Noel J. Raufaste
Secretary–General, U.S.–side Panel on Wind and Seismic Effects
Building and Fire Research Laboratory
National Institute of Standards and Technology

Introduction

Japan is composed of four main islands; Hokkaido, Honshu, Shikoku, and Kyushu and further south the small island of Okinawa. The islands are divided into10 Districts: Hokkaido; Tohoku, Kanto, Hokuriku, Chubu, Kinki, Chugoku, Shikoku, Kyushu, and Okinawa. Within these districts are 47 Prefectures. Districts are analogous to federal administrative regions (e.g. New England) and Prefectures to States. Except for Hokkaido and Okinawa Districts, the other eight districts have a Regional Construction Bureau which reports to the Ministry of Construction (MOC). These Bureaus construct and maintain highways, flood control works, dams, and bridges. Prefectures' design and construction work is funded by the National Government and by their own jurisdictions.

In addition, there are several public corporations responsible for specific construction projects. The corporations participating in the technical site visits include the Trans–Tokyo Bay Highway Corporation, the Japan Highway Public Corporation, the Honshu–Shikoku Bridge Authority, and the Hanshin Expressway Public Corporation. They report to the MOC. Each receive a small percent of funding required for their construction projects as direct funding from the National Government. Loans from the National and Prefecture Governments and from private sources make up the remaining 90 to 95 percent of construction monies needed for each project. These loans must be repaid with interest within 30 to 40 years depending on original negotiations. Revenues from toll roads, fees from parking areas, and rent from expressway associated facilities are used to pay off construction loans.

To gain a perspective of the MOC's public works construction funding; in 1991 its budget was 21 trillion yen ($247 billion). For the same year, Japan's National Budget represented 70.3 trillion yen ($827 billion). MOC receives about 30 percent of the National Budget for public works construction. Note: conversions from yen to dollars are based on the May 1995 rate of 85 yen equal $1.00.

During the 27th Joint Panel Meeting, 12 technical sites were visited in three Japanese Districts –– Kanto, Chuubu, and Kinki. Summaries of each are presented below.

Summary Technical Site Visits

1. **Trans–Tokyo Bay Highway.** The Trans–Tokyo Highway is a 15–km toll highway that runs across the central portion of Tokyo Bay connecting Kawasaki City located between Tokyo and Yokohama Cities with Kisarazu City, Chiba Prefecture on the east side of Tokyo Bay. The project consists of two 5–km long tunnels starting at the Tokyo side (City of Kawasaki) then rising through a man–made island serving as a transition to a 5–km long bridge to Kisarazu City. Presently, construction will accommodate two–2 lane highways with space for a future third pair of lanes. This work is under the

supervision of the Trans-Tokyo Bay Highway Corporation (TTBHC) and the Japan Highway Public Corporation (JPHC). The highway system is expected to be completed in 1996.

When the project is completed the driving distance between these two cities will be reduced from 110 km to 30 km and the travel time will be shortened by 75 percent. Similarly the distance between Tokyo and Kisarazu will be reduced by 45 km.

The delegation visited the two man-made islands and the bridge. The Kawasaki island, is located 4.6 km from the Tokyo-Yokohama shore line. It is in 28 m of water. Since the sea bed is extremely soft to a depth of 30 m, the soil had to be stabilized by sand compaction. The island consists of a 98 m diameter diaphragm wall extending 117 m from the water surface to the sea bottom. Its thickness is 2.8 m. This structure will ultimately serve as the ventilation tower. The ventilation tower's base dimensions are: wall thickness, 4 m; height, 75 m; and bottom slab thickness, 6 m. Two of the four locations where the tunnel excavation has been initiated are located at both sides of this tower base, one at the Tokyo-Yokohama shore line, and one at the second man-made island.

A 50 m steel trestle structure protects the main island's ventilation tower. It was towed to the site by a crane-barge as 14 sections, sunk, and secured to steel piles. After excavating the tunnels, the ventilation tower will be divided into seven floors on the inside to accommodate tunnel ventilation equipment, tunnel cross overs, and fire fighting equipment.

Tunnel construction is performed by eight pressurized slurry shield tunneling machines each weighing 3200 tons. The production goal for each machine of 150 m per month has generally been achieved. There has been some production problems initially which were corrected. The tunnel diameter is 14.1 m. The twin tunnels are 28 m apart and 60 m below the water surface. When completed this will be the longest vehicle traffic tunnel in the world. Over 500 workers are engaged at this site.

The Kisarazu Tunnel-bridge Interface Island, 650 m long and 100 m wide, was the second island visited. The soil at this site was replaced with sand and gravel and it includes a 750 m ramp from the sea floor connecting the tunnel sections to the bridge system. The island has a protective system of 48 circular steel pile structures that are 37 m high, filled with sand, and capped with concrete. Fill work is similar to that performed at the Kawasaki man-made island. Steel moles are constructed on either side of the descending ramps. Armored riprap, rubble stones, and wave dissipating concrete blocks protect the embankment.

Tunneling proceeds in 1.5 m increments where automated assembly systems install 11 precast wall lining segments for a 1.5 m ring. Each concrete segment measures 4 m by 1.5 m and is 0.65 m thick and weights 10 tons. Reinforcement bars are coated with vinyl. Furnace slag is mixed with the concrete to reduce corrosion of the reinforcement bars. Water tight membranes surround the tunnel walls. Both islands are designed for a 4.3 m high wave (after construction) and 3.8 m (during construction). TVs monitor for material defects and the structure's performance during earthquakes.

The bridge exiting the Kisarazu man-made island is 4.4 km in length. The bridge's superstructure sits on 42 Y-shaped piers of which 12 are in deep water. These piers were assembled at fabrication yards and transported to the work site where a floating crane set them into place. The footings were anchored to steel piles. Its base is

reinforced concrete set on steel pipe piles. The 12 deep water piers are steel and contain a special titanium cladding over a 5 m section in the splash zone to protect against corrosion. A thin layer of copper was placed between the 1 mm titanium sheet and the steel pier. The hot rolling process used squeezes out the molten titanium–copper inter–metallic compound which oxidizes with the residual air forming a bond of 180 MPa or higher. The Nippon Steel Research Laboratory played a key role in this innovative development. The cladding process was the first ever used in a construction application. The remaining 30 piers are reinforced concrete with steel sheet pile foundations. Cathodic protection is installed in the reinforced concrete to protect reinforcing steel from corrosion.

The bridge–girder is separated into sections spanning 10 piers with the longest span measuring 240 m. The girder is 22.9 m wide. High damping rubber bearings and other types of rubber bearings were used for the bridge piers. Variable concrete strengths were used throughout the project:

Tunnel segment	48 MPa
Road section	24 MPa
Ventilation Building	24 MPa

Much attention was given to designing the highway against earthquakes. The elbows at each of the horizontal ends of the tunnels are potential weak points. Elbows are flexible for about 10 cm at segment joints which change roadway slope.

Overall this is one of the largest public works projects that Japan has undertaken. The overall construction cost is projected to be 1.5 trillion yen ($18 billion). The cost is split 81% from TTBHC and 19% from JHPC. Of the 81% from TTBHC: 6.3% is from capital; 41.1% from government bonds; 25.6% from private loans and loans from the Japan Development Bank; and 26.6% from official loans. It is projected that the project will pay for itself over a thirty years. The expected first year traffic volume is 33,000 vehicles per day and it is expected to grow to 64,000 vehicles per day after 20 years. One way crossing toll will cost 5000 yen ($60.00).

One of the principal reasons for the more expensive long tunnel option over a longer bridge system was the vessel traffic. There are over 1,400 ships per day that move through this passage. Even though the cost of tunnel construction was 3 to 4 times more expensive than the bridge system, because of the potential impact on navigation and also to reduce environmental impact, the more expensive tunnel option was selected.

2. Kangawa Bridge. The Kangawa Bridge is located on the Joshin–etsu National Expressway, the North–South route across Nagano Prefecture, Chuku District, to link Tokyo with Nagano. The bridge is on a 47.5 km section of the expressway near Ueda City about 50 km south–east of the Nagano City, the site of the 1998 Winter Olympics. It is the longest Japanese arched bridge consisting of 20 arch spans totaling 714.5 meters in length. The arch type design was selected for this bridge to eliminate expansion joints and shoes which require high maintenance and to blend with the surrounding hilly landscape. The bridge was designed with two traffic lanes expanding to four lanes in the future. Bridge construction was initiated in October 1992;

completion is scheduled for November 1995.

Its 714.5–meter 20–arch span range from 26.5 m through to 37.7 m. Sixteen spans are reinforced concrete continuous solid web arches. Three spans are continuous framed rib arches and one span consists of a reinforced concrete solid web arch.

The bridge construction involves the erection of reusable steel arch centering to construct the curved arch ribs. The piers are built on top of the foundation; a crane lowers the centering and aligns it between the two piers. When the centering has been assembled, steel reinforcement for the arch is put in place and formwork assembled. Nine hundred tons of concrete are required to make a 36.5 m span. When the arch sections are completed, soil is packed in the space formed by the arches and the side walls. The solid web arches are filled with soil which helps reduce traffic–induced vibrations and noise.

The framed rib arches are the tallest and longest three spans of the bridge. They are located on the central part of the bridge with the total length of 162 m and the elevation reaching up to 52.5 m above the foundation level. The bridge's arch ribs and side walls are structurally separated. The arch ribs are inserted between the side walls on both sides and are linked to the side walls with concrete reinforced steel. The PC steel is fixed into the side of the side walls passing through polyvinyl chloride tubes embedded in the archrib. This technology permits movement in the arch ribs. The thermal expansion of the bridge spans is absorbed by vertical movement of the arches. As a result, there is no limitation on the number of the bridge arch–spans that can be linked together. This is the first Japanese bridge design to use this technology.

3. **Nagano Olympic Stadium.** Two constructed facilities were visited; the Main Figure Skating Auditorium Building (under construction) and the Ice Hockey Stadium "A" (one of two Olympic Ice Hockey Stadia that will be used in the 1998 Olympics). Its seating capacity is 8,000.

The Figure Skating Auditorium roof was constructed using the Lift–Up Method. This method permits construction of the steel roof at floor level. It is then lifted to the roof elevation by a jacking system and connected to the exterior wall tension rings forming the frame–work. A computer controlled hydraulic system maintains proper elevation of he roof structure during the lifting process. The jacking system consisted of 12 lifting devices positioned at the periphery of the roof structure. The roof is a hyperelliptical dome with a short axis of 92 m and a long axis of 104 m. All electrical and mechanical equipment was installed on the floor within the complete roof prior to jacking. The total jacking weight was 1,400 tons. This roof structure provided for a column free surface area of 16,000 m^2. The roofing material is stainless steel panels covered with fluorine paint to reduce oxidation. This unheated roof is designed for 80 cm snow load.

The total cost of the facility was 10 billion yen ($118 million). The costs were shared by the National Government 50%; 25% from the Prefecture, and 25% from the city of Nagano.

The second facility visited was the completed Ice Hockey Stadium "A". This attractively designed facility consists of four curved steel beams about 3 m by 9 m supporting a welded tubular steel truss roof system. The roof consists of dual tubular trusses that form a space frame with dimensions of 120 X 100 m (total floor area is 24,900 m^2). The height of the roof is 35 m. Lighting, air conditioning, ventilation ducts were installed within the beams. As in the ice skating auditorium, this roof was lifted

into place after its construction at the floor level. The stadium's seating capacity is 12,000.

The facility's cost was 14.1 billion yen ($169 million). It too was funded by the National Government at 50%; 25% from the Prefecture, and 25% from the city of Nagano.

4. **Abo Tunnel.** Construction of the Abo Tunnel follows years of surveys and planning dating back to 1964. There was need to permit smooth traffic flow over a snowy mountain year around (now road closed 1/2 of time due to snow and rock falls). The tunnel reduces driving distance from 15.6 km to 6.3 km along the route through Takayama to Matsumoto between Gifu and Nagano Prefectures of the Chubu District. The overall tunnel length is 4.3 km divided almost in half between the two prefectures.

Since there was much uncertainty about geology of the mountain (this site is an active volcanic region) an investigation tunnel was first drilled. This tunnel permitted a feasibility study of the geological conditions, ability to study methods to construct the main tunnel, and allowed transportation of material to eastern end (Nagano Prefecture) for use there. Based on this early information the main tunnel was raised by 50 m to avoid some of the hottest rock. The main tunnel was curved southward to avoid an ancient volcanic crater. The investigation tunnel indicated high water seepage. Later, during the drilling of the main tunnel, water infiltration collapsed 700 m of tunnel wall. Rockfalls caused further delays. Installing tunnel drainage lowered the ground water level to 30 m above the tunnel so work could proceed. Temperature at the tunnel face was kept reasonably low by spraying water and using air conditioning. The rock temperature reached 75° C; often temperatures were about 60° C. A low–velocity zone (P wave velocity 2.7 km/sec down to 1 km/sec) was treated by digging a small side tunnel first. Prevention of ceiling cracks was important. To prevent collapse of the tunnel, ceiling rock bolts, up to 6 m in length were used.

The main tunnel is constructed 90 m on center with the investigation tunnel. It was excavated by using the upper heading and short bench method. The face is drilled by two 3–boom hydraulic drills. The tunnel lining consists of shotcrete on the rockface, covered with waterproofing membrane, 5 cm rigid polyurethene foam insulation material applied over the waterproofing membrane followed by secondary concrete lining. Drilling of the main tunnel was recently completed.

A ventilation shaft, constructed by Mitsui Corporation, used down blasting and cutting method. Drilling is about 50% completed (drilled down about 450 m). The ventilation shaft measures 9.1 m in diameter. For each depth increment, a rapid–cure lining was first placed followed by a permanent lining. The finished shaft is 7.5 m in diameter.

In light of the danger from drilling in this hostile environment, a variety of safety methods were initiated. The tunnel is secured at all times during construction relying on past tunneling experiences and best practices. Construction required removing the threat of volcanic gases (hydrogen sulphide and methane) and the threat of any sudden inrush of hot water by using chemical grouting. To ensure the stability of the concrete lining, high durability concrete was used. Training was provided to ensure safe use of explosives.

Tunnel work is performed in three shifts and the vertical shaft in 2 shifts. The initial construction cost estimate in 1988 was 60 billion yen ($706 million); it has risen to 80 billion yen ($941 million). To date, expenditures total about 52 billion yen ($612

million). Work is expected to be completed in 1996. The automobile toll will cost 900 yen ($10.60).

5. **Historic Post Towns, Temples, and Pagodas.** Historic preservation and restoration of National Landmarks in Japan is taken seriously. An example is the Tsumago Post Town site visited by the delegation. Few historic properties remain in excellent condition due in part to humid conditions; most buildings are fire threats as they are constructed of wood. Several locations are designated as Protected Area for the Preservation of Traditional Buildings by the Japanese Government. Landscape is improved by removing electricity poles from the main road and television antennae from roofs of houses.

Principal pagodas and temples as Horyuji and Todaiji illustrate the measures needed to protect and preserve such national treasures. Horyuji was recently listed on the World Heritage by UNESCO. It is considered the oldest wooden temple in the world. A Nara Prefecture official hosting the delegation, pointed out an early technology used to reduce damages to pagodas from earthquakes. In construction, floors are suspended around a massive central timber post hanging from the roof (which also supports the spire), thus providing a measure of stability against earthquake shaking. The Ministry of Education is responsible for protecting traditional buildings listed on the National Register and for national landmarks. Funding from entrance fees and endowments are used for general maintenance of these buildings and their grounds.

6. **Awaji Island -- Epicenter of Hyogo-ken Nanbu Earthquake.** Several sites were visited on Awaji Island, Kinki District, to better understand the seismological, social/engineering aspects, and implications of this M7.2 Earthquake. On January 17,1995 at 0546 (JST) a magnitude 7.2 (Mw 6.9) earthquake occurred near Kobe, Japan. The epicenter of the Hyogo-ken-Nanbu Earthquake was located at 34.60 degrees North and 135.05 degrees East; its focal depth was 14 km. The focus of the event was near the north end of Awaji Island in the Akashi Strait on the Nojima Fault. Rupture proceeded in a bilateral fashion approximately 10 km to the southwest and 20 km to the northeast. Rupture duration was approximately ten seconds. The sense of motion on the fault plane (or planes) is generally right lateral strike-slip with some localized vertical offset. Surface rupture was observed for approximately 9 km on Awaji Island. Three sites were visited by the panel, > 1 m of lateral and about 1 m of vertical slip were observed at all three sites. More than 1800 aftershocks were recorded within the first two months following the main event, approximately 200 were large enough to be felt.

Trenching investigations on the Nojima fault as a result of this earthquake suggest the last event occurred about 1000 years ago and average surface slip per event is about 1 m. In terms of magnitude and source parameters, this event was very similar to the 1989 Loma Prieta, CA earthquake.

Devastating damage occurred in the greater Kobe area as a result of this earthquake. However, on Awaji Island surprisingly little damage was evident at sites within a few hundreds of meters of the fault trace. The northern end of Awaji Island is composed of granitic rocks, generally a very thin veneer of young, surfical materials is present. On the island 38 people died, 831 were injured, and about 1700 homes were destroyed as a result of the earthquake. The worst damage on the island appeared to be confined to areas near the coast where the thickest sequence of young alluvium was observed (Hokudan-town).

Within the greater Kobe area 5,497 people were killed and 36,820 injured during the earthquake (as of 31 March 1995). Approximately 180,000 homes were destroyed or severely damaged. Major damage to water and pipelines, port facilities (as a result of liquefaction), bridges and highways occurred. Current estimates of total damage is over $100 billion. The zone of most significant damage (JMA intensity VII) within the city proper was an elongate area lying between the granitic mountain front of the Rokko Mountains and Osaka Bay. This is the area where the thickness of young alluvial materials is 10–20 m. This zone lies to the southeast of the fault plane as inferred from aftershock data. Widespread liquefaction in both natural and man–made materials was widespread in the port area.

Many of the same types of structures that were destroyed in the Kobe area exist within a few ten's to hundreds of meters of the fault trace on Awaji Island. This puzzling observation has been reported previously. While some directivity or focusing of energy to the northeast may have occurred, most evidence currently available suggests differing site conditions and a large near–field velocity pulse as the causative mechanisms for the damage in Kobe. Japanese investigators are pursuing this line of research with some degree of success at the present time. Continued effort at understanding this phenomenon is vitally important to defining zones near active faults that could be susceptible to large ground motions with spectral content especially damaging to engineered structures. Continued interaction and collaboration between Japanese and U.S. researchers will hopefully provide additional insight into this important problem.

7. **Akashi–Kaikyo Bridge.** The Kobe–Naruto highway route which connects the main island of Honshu and the southern island of Shikoku is the eastern most route of three north–south traffic routes approved in the 1969 comprehensive Japan national development plan to stimulate local commerce and facilitate the industrial development of the region. A second central route, which connects Kurasiki on Honshu Island with Sakaide on Shikoku Island was completed in 1988. A third route further to the west, Onomichi–Imabari Route, will connect the Hiroshima greater metropolitan area with the Matsuyama area when completed in 1999.

The 81 km long Kobe–Naruto Route is marked by the construction of two major suspension bridges including the world's longest, the Akashi–Kaikyo bridge. This bridge, currently under construction, connects the Kobe area of Honshu with Awaji Island, the sixth largest island in Japan. A second major bridge on this route, the Ohnaruto Bridge, was completed in 1985 and connects Shikoku Island with the southern end of Awaji island. When the Kobe–Naruto Route is completed in 1998, this link of modern highways, interchanges, and bridges will provide access to greatly expand the economy of Awaiji and Shikoku islands. Construction of the Akashi–Kaikyo Bridge began in 1988 at an estimated cost of 400 billion yen ($4.7 billion). To date, the cost estimate has risen to 470 billion yen ($5.5 billion). More than 100 construction contractors are involved with the building of the bridge. This 4 km bridge crosses the Akashi Straits between Honshu and Awaji. A 1500 m wide main shipping lane into the inland sea is traversed by about 1,400 ships per day. This 3,910 m bridge was constructed in 110 m deep water with 4.5 m/sec tidal currents. Design for 80 m/sec wind speeds and a potential 8.5 Richter magnitude earthquake 150 km distant from the site had to be considered by the Honshu–Shikoku Bridge Authority (the bridge owner). Geology of the bridge site includes layered alluvium and diluvium deposits over hard "Akashi" or "Kobe" layer. Granite protrudes at the Awaiji anchorage.

Total length of the bridge will be 3,910 m from anchorage to anchorage. The main

span will be 1990 m with two side spans of 960 m each. The bridge roadway surface will be constructed on top of a 14 m deep by 35.5 m wide truss girder system suspended from main cables passing over two steel towers which rise 297 m above the mean sea level. A 65 m clearance will be maintained over the shipping lane. The 1.12 m diameter main cables were already erected by the prefabricated strand method. Approximately 200,000 tons of steel will be used in the superstructure and 1.42 million cubic meters of concrete for the substructure.

Anchorages measures 63 m by 84 m in plan, extend into the "Kobe" and granite layers at the site, which required special foundation construction technology. The Honshu anchorage had to be embedded 61 m below sea level and required the anchorage excavation to be performed in open air. Therefore, an 85 m diameter circular slurry wall, 2.2 m thick, was constructed and subsequently used as a retaining wall. Excavation within the slurry wall was followed by the placement of roller compacted concrete to complete anchorage foundation construction. The Awaji anchorage foundation was constructed using steel pipes and earth anchors to support the surrounding soil. The excavated foundation was filled with specially flowing mass concrete. Both anchorages were completed with the construction of a huge steel supporting frame used to anchor the main suspension cable strands.

Main tower piers were constructed in the Akashi Strait. The tower pier foundations were designed to transmit 120,000 tons of vertical force to bedrock, approximately 60 m below the water surface. The foundation was constructed using the newly developed "laying down caisson" method. Steel Caissons, 80 m in diameter and 70 m in height were towed to the tower sites, submerged, and set on the pre–excavated seabed. Pier foundation construction was completed with placement of concrete. Next, the main steel towers were erected on the concrete piers. Each main tower height is 282.8 m and was erected by stacking 30 approximately 10 m high prefabricated steel segments on top of each other. The segments are formed with three separate cells in plan view. Special procedures were used during fabrication of each segment to assure tight tolerances for proper tower alignment. The tolerances were maintained using laser measuring technologies for controlling all dimensions. The technology resulted in no major erection problems during field bolting and splicing the steel tower segmenting together. An independent, self supporting 160 ton tower crane was used during tower erection. Tuned mass dampers were attached to each tower at varying stages of completion to reduce wind driven tower motion and reduce tower vibration in the event of an earthquake.

Prior to stringing the cable, a pilot hauler rope was attached to each anchorage and placed over the tower tops by helicopter. The pilot rope was used to suspend the catwalk from which work on the main cable erection would proceed. The main cables which have a 1:10 sag ratio were erected using the "prefabricated strand method". Cable strands, comprised of 127–5.23 mm diameter galvanized wires were factory fabricated in 4,085 meter lengths. High strength wire with 180 kg/mm^2 tensile strength was used rather than the standard 160 kg/mm^2 wire. Each strand was transported to the construction site where it was pulled from one anchorage over the saddle of each tower and fastened to the opposite anchorage frame. This procedure was repeated 289 times to fabricate each main cable. Each main cable was separated at the anchorage by a splay saddle prior to attachment to the steel anchorage frame inside the anchorage to equally distribute cable tension in the foundation. A specially designed cable squeezing machine was used to compress the 290 parallel wire strands into the final 1.12 m diameter cable. Cable bands were placed to circumferentially compressed the cable and to maintain the circular shape. Finally, suspender cable hangers were

attached to the main cable for supporting the main stiffening truss.

Hangar cables or ropes have been factory fabricated from bundled 7 mm in diameter, 180 kg/mm^2 parallel wire strands. Because the higher strength wire was used, two rather than the usual four hanger ropes were required to support the panel points of the stiffening truss girders. As of 23 May 1995, the first two hanger ropes had been attached to the main cable.

Steel stiffening truss girder panels are being fabricated off site and will be transported by barge to the bridge tower piers, lifted to roadway elevation, and transported by traveler crane to the proper location for connection to the suspender ropes. This procedure will allow the uninterrupted use of the busy shipping lane of Akashi Straights. Stiffening truss erection is scheduled to begin in June 1995.

Several unique technologies were developed to support the design and construction of the Akashi–Kaikyo Bridge. The aerodynamic stability of long suspension bridges pose major challenges to designers. To verify the design of the world's longest suspension bridge, the Honshu–Shikoku Bridge Authority under an agreement with the Public Works Research Institute, designed and constructed the worlds' largest wind tunnel facility and tested full section models in laminar and turbulent wind flow. Other innovations resulting from wind tunnel testing include; installation of vertical plates at bottom center of the highway deck to increase flutter speed. Methods to improved prediction of flutter speed and gust response will be used in future bridge designs. Complete details on the wind tunnel facility and the design, fabrication, and testing of the full section bridge model are contained in past Proceedings of the UJNR Panel on Wind and Seismic Effects.

A second unique technology developed for use on the Akashi–Kaikyo Bridge was the use of parallel wire strand for cable fabrication and erection. Rather than using spinning methods for structure cable fabrication, individual parallel wire strands were fabricated off site, transported to the bridge site and strung parallel to each other to form the main cable. The advantage of using this method is the strands are continuous from anchorage to anchorage and eliminate the inplace spinning of cables, thus reducing the probability of accidents occurring. In order to use the parallel wire strand method, a unique cable squeezing machine was designed to form the parallel strands into the final circular shape.

The use of a higher strength wires, 180 kg/mm^2, reduced the number of strands required, thus saving erection time and cost. Use of the higher strength wire also reduced the number of suspender ropes from four to two needed to connect each stiffening truss panel point to each cable hanger attachment on the main cable. This accounts for reduced erection time and cost savings.

Of particular interest was the performance of the bridge in the 17 January 1995 Hyogo–ken Nanbu Earthquake which provided a full scale test of the tower response. The complete bridge structure is designed to resist a 150 km distant, 8.5 Richter magnitude earthquake. Fortunately, erection of the bridge stiffening truss had not begun. The Nojima fault zone passes between the towers of the bridge and caused a permanent lateral and vertical offset of the Awaji tower and anchorage. Ground fault rupture was visible on the northern tip of Awaji Island, approximately 2 km from the Awaji anchorage. The Awaji tower displaced 1.3 m to the west while the Awaji anchorage displaced 1.4 m to the west. The net result was 0.8 m increase in span length between the main towers and a 0.3 m increase in the southern side span length. The

Awaji tower pier displaced 0.2 m vertically downward while the Awaji anchorage rose by 0.2 m. The sag in the main cable was reduced by 1.3 m.

The earthquake caused a one–month delay in the construction schedule during which the bridge was carefully inspected for damage. This lost time is planned to be made up during the remaining three year construction period allowing the bridge to be opened to traffic on schedule. The increased distance between towers will be accommodated by the redesign of the two center stiffening panels each of which will be 0.4 m longer than originally designed. Other minor damage was inflicted to the cable squeezing machine which was quickly repaired. Anchorages, piers, and towers were otherwise undamaged.

The bridge has been under construction for seven years. In spite of the dangers associated with this type of construction project, elaborate safety procedures have paid off. To date, two accidents have occurred resulting in five injuries and no deaths, a world class safety record.

One–way tolls on the completed bridge will cost 5,000 yen ($60.00) a seemingly high cost to travel to work daily. Its companion bridge, the Seto Ohashi Bridge completed in 1988, has experienced about 1/2 of the number of expected drivers (will the Akashi–Kaikyo bridge experience the same fate?)

8. Matsumura–Gumi Corporation Technical Research Institute. The Matsumura–Gumi Laboratory features an instrumented, base–isolated building which was shaken by the 17 January 1995 Hyogo–ken Nanbu Earthquake. This facility will be one of the first entries in our to–be–developed database on seismic performance of base–isolated buildings.

This laboratory site is about 17 km north of central Kobe and about 35 km northeast of the earthquake epicenter. It is inland of the Rokko Mountains and away from the coastal plain of Kobe where the most serious damage occurred. The foundation is on Tertiary Era sandstone and mudstones of the Kobe Group. The region was considered before the January earthquake, to be of relatively low seismicity.

The building itself is a three–story reinforced concrete structure, 10 m by 16 m in plan and 12.5 m high. It is attached by expansion joints to an adjacent office building, which also is three–stories in height but of conventional steel frame construction and with conventional foundations. The base isolators are circular rubber laminated with steel plates. They are arrayed in two rows of 4–supports; the corner bearings are 700 mm diameter and the inner ones 600 mm. The bearings were placed after the building was constructed upon dummy steel bearings, by jacking up the building. Such construction will permit easy future replacement of the bearings, either as a maintenance measure or for trial of another type of bearing.

The structure is instrumented with strong–motion accelographs at foundation level, on the floor, and on the roof. Accelographs also are placed at the roof level of the adjoining steel–frame structure. Peak acceleration values were as follows:
Evidently, there was no great reduction of the peak acceleration of the first floor of the base–isolated building, but there was significant attenuation of frequencies above 1 Hz in the records on the first floor and roof as compared to the foundation record. There also was a much smaller response at the roof as compared to the adjacent buildings which was however of different construction. At the end of earthquake shaking, there

	N–S (gals)	E–W (gals)	U–D (gals)
Roof, adjacent building	965	677	368
Roof	198	273	334
1st Floor	148	253	266
Foundation	272	265	232

was a small but apparently unmeasured residual displacement of the structure, which was restored by horizontal jacking.

Matsumura–Gumi operates a structural research facility. One of its test facilities is a tri–directional test machine and a 2,000 ton/m reaction wall.

Most of Matsumura–Gumi Corporation's customers are hospital and condominium owners. Matsumura–Gumi estimate buildings design and construction will be 5 to 15 percent more costly (when using their base isolation system) than a conventional foundation (an approximate doubling of the structural related costs).

9. Port of Kobe. The Port of Kobe handles the largest volume of container cargo in Japan. With its extensive pier facilities and container berths on two man–made islands, Port and Rokko Islands, the Port of Kobe plays a vital role in the economic growth of Japan.
As a result of the earthquake, many pier structures and container berths sustained severe damage that essentially crippled the functioning of the port. Most gantry–cranes which handle container cargo suffered structural damage due to ground failure caused by liquefaction of soil. Three main bridges which connect the city of Kobe to Port and Rokko Islands sustained varying degrees of damage. It is estimated that the total cost of reconstruction could reach 500 billion yen ($ 6 billion) of which the Japanese government is providing 200 billion yen ($ 2.4 billion). The Ministry of Transport of Japan expects to complete the reconstruction of the port facilities within 2 years.

Ten specific damage sites were viewed by the U.S. delegation. The extent of damage was explained by engineers from the Port and Harbor Research Institute and the Third District Port Construction Bureau and site visits were made to Rokko Island and Naka Pier to inspect damages.

The general area of the Kobe port was shaken severely due to its close proximity (within 2–3 km) to the fault zone. A maximum recorded horizontal acceleration on small structures built on the top of Maya pier was about 700 gal (700 cm/sec sec). Overall failure of the port facilities can be categorized into three groups:

1. Most piers and container berth facilities sustained damage due either to ground settlement or lateral spread cause by severe liquefaction. Practically, all perimeter areas of two man–made islands were liquefied.
2. Reinforced concrete structures that are more than 20 years old and built on the piers had suffered major damage with many compression members failing in shear.
3. Gantry–cranes on Port and Rokko Islands which handle containers failed due to ground failures, either settlement, lateral spread or a combination of both. Typically, gantry–cranes either toppled or partially collapsed with their legs buckled.

Port and Rokko Islands were built using fill material excavated from nearby Rokko Mountain. The material consists mainly of decomposed granite. The extent of liquefaction on Rokko Island was greater than Port Island because the fill used for Rokko Island had more fine material than the fill used for Port Island. Sand compaction piles will be used to improve the liquefied areas before quay–walls are reconstructed.

10. Kobe City Damage. Most of the buildings severely damaged in the 17 January 1995 Hyogo–ken Nanbu Earthquake have been demolished and removed, leaving empty lots to mark their past existence. Still there is much evidence of damage waiting for repair or demolition. There are many graphic examples of shear failures in concrete frames. For example, Kobe's old City Hall (constructed in 1960) remains standing waiting for demolition since its sixth floor collapsed dropping the full structure above by one story. The plans for the entire water system were stored on the sixth floor of old city hall. Lack of duplicate plans significantly impaired the recovery efforts following the earthquake. Adjacent to it is the new City Hall, completed in 1989, which suffered little damage.

Although there are numerous empty lots and buildings abandoned or under repair, there are many more that survived the earthquake and the information that can be learned from them is equally significant.

The delegation inspected a damaged reinforced concrete building under construction on Matsuno Street, Nagata Ward of Kobe city. The earthquake occurred when the ninth floor of this nine–story RC shear–wall building was under construction. The structure has no basement and is supported on concrete piles. The damage survey showed that the building tilted to one direction about 15 cm at the ninth floor level which resulted in an uplift of 5 cm at the top of the pile cap located diagonally opposite corner.

The building was planned for 3 commercial stories below 6 stories of dwelling units. Concrete shear walls had door openings, which reduced the shear–resistance capacity, and shear walls did not continue through the commercial stories. All shear walls sustained severe damage; typically diagonal cracks were evident throughout the structure. Some beams also sustained shear failures near the beam–column joints particularly those supporting the discontinuous walls. The irregular framing system is considered disadvantageous for earthquake resistant, and the structure did suffer severe structural damage. However, collapse did not occur in a severe earthquake, so the intent of the code was met. Incidentally, the adjacent steel frame building of equal height was completed in January 1995 and showed no apparent damage.

The owner of the building opted for repair rather than replacing the building although the repair cost would be as much as 50 percent of the replacement cost. This decision was based on economic consideration ––repairing the building will reduce the time required to complete it for occupancy. Epoxy injection technique will be used to repair the cracks.

A large number of city blocks in Nagata Ward were damaged by fire during the earthquake. This area was cluttered with old two– to three–story buildings. Typically the first story is used for shoe manufacturing and the upper floors for dwelling. Fire leveled these buildings which had large quantities of highly flammable liquid and combustible materials. The delegation viewed a variety of buildings in the fire–damaged areas.

11. Hanshin Expressway Damages. Soon after the earthquake, officials from the

Hanshin Expressway Public Corporation (HEPC) began inspecting the Hanshin Expressway Route 3's concrete piers for damage. To investigate subsurface damage piers, 50 of the expressway's 700 piers were excavated to their foundations. Some cracking was observed around piles and footings but overall they were determined to be structurally acceptable. Emergency repairs were required immediately after the earthquake to prevent additional damage to the expressway and for safety during strong aftershocks. Temporary pier repairs consist of encasing the pier with a steel jacket and filling between the pier and steel with concrete. Where the superstructure remains, it will be supported by temporary bracing until the pier work is completed when base isolators will be installed. Concrete piers will be replaced by removing existing concrete, lap splicing new reinforcement to existing ones. New concrete piers will be redesigned and constructed in place. Steel piers are being repaired in place. Buckled sections are straightened and strengthened by adding welded stiffener plates over the buckled areas. Steel piers also are being evaluated to determine if filling with concrete will improve performance. HEPC does not expect to perform extensive repairs to the elevated superstructure. Steel sections are removed and sent to fabricators for straightening or reconstruction. Some of the collapsed sections will be completely replaced.

The most significant change in the overall repair work will be in the bearings. HEPC plans to use base isolator bearings in the repaired expressway whenever possible as determined by existing conditions (necessary clearance) and analysis. HEPC installed rubber and rubber/steel laminated isolator bearings in a section of Route 5, further to the east, five years ago. Although the data from instrumentation has not been analyzed, the section appears to have performed well, according the HEPC. A publication on the performance of the experimental section of Route 5, using rubber bearings and rubber/steel laminated bearings, is expected to be published in about 12 months.

The Hanshin Expressway repair work is being performed by 54 contractors; 27 working on the substructure (footings and piers) and 27 on the superstructure. Computerized databases are used for project management of design, scheduling, construction, and tracking work. HEPC does not offer incentives for contractors to develop and deploy new technologies for completing the job faster, or at less cost, or for improved quality. HEPC studies the problem, identifies in detail the work required to be done to solve the problem then hires constructors to perform the work. Too, there was no use of automated equipment handling methods beyond the conventional systems. Since space is limited and traffic severe, the mission is to complete the job as fast as possible without considering how to use new technologies.

A damaged bridge on Route 5 was visited. It suffered bearing failure but no other damage. The bearing was replaced in-situ. The Rokko Island Double-deck Bridge also suffered bearing failure, with 3 m lateral displacement. The bridge deck slid partially off its supporting pier. The approach span moved with the bridge deck and twisted. The approach span is being repaired at the fabricators. The bridge was lifted by barge cranes back into place. Bearings will be replaced temporally in-situ. Buckled steel members on the bridge superstructure are being repaired. The bridge is expected to open during the fall on 1995.

The loss of two major east-west routes between Kobe and Osaka has created serious transportation problems. Expediting the repairs on Route 5 by replacing bearings in-situ will alleviate some traffic congestion. Future analysis however is planned to determine if an improved bearing design is possible.

Repairs are projected to cost 230 billion yen ($2.7 billion) for this 27 km section of Route 3. Route 3 is expected to be completed by the end of 1996. Route 5 repair work is scheduled to be completed in the fall of 1995. These routes are badly needed by residents as they are coping with extensive traffic problems which require 3.5 to 4 hours to drive the 30 km route between Osaka and Kobe.

As a short note to get a flavor of the work performed by MOC Public Corporations, the Hanshin Expressway Public Corporation (HEPC) is reviewed. HEPC was created in 1962 using capital investment funds operating between Osaka–Kobe–Kyoto to construct and manage this urban tollroad network. HEPC will construct conventional roads when part of an urban planning project related to construction of the toll road. For sense of scale, 1993 tolls from the Hanshin Expressway was about 124 billion yen ($1.5 billion) received. This income covers payment of principal and interest on borrowed funds, road construction costs, and operating costs such as road maintenance, salaries, etc. About 90% of borrowed funds are raised by issuing bonds and 10% from loans (6% banks and 4% from National and local governments).

In 1985 MOC established provisions for carrying out environmental assessments of urban expressways. Final planning is not started until public opinion has been consulted. Attempts are made to achieve sustainable development such as: the expressway is designed to visually harmonize with its urban surroundings; sound barriers are used and highway joints improved to reduce amount of noise and vibration; land purchased extending 10–20 m from road edge used to plant trees and other greenery. In cases where homes still have excessive noise from highways, the National Government provides subsidies to home owner for sound insulation, special windows, and air conditioners. Residents too are compensated for loss of sunlight when an expressway obstructs sunlight. Also, when television reception is affected, residents are provided with antennas. HEPC introduced the "Miniway", a mobile temporary overpass (modular trailers) allowing traffic to pass above the area being repaired by driving on the roofs of the trailers.

12. Kansai Airport. The airport opened on 4 September 1994, after 71/2 years of construction. It is located in the southeast part of Osaka Bay about 4 km off the coast of Osaka. It is a 510 ha man made island measuring 4.4 km by 1.25 km. Its single air strip is 3.5 km by 60 m with a 4–story passenger terminal, a 90 m control tower, support buildings, a field maintenance hanger, and a 3.75 km double deck access bridge (6 automobile lane upper deck and two train track lower deck) connecting with Osaka. The bridge is the world's longest dual–function truss bridge. Its steel box girder has cathodic protection against corrosion.

The island fill material was transported by ship from mountains on the nearby mainland and from island sites, crushed near the source, delivered to barges on the sea coast by belt conveyors, and barged to the reclamation site. Poor strata under the island required designing for settlements of up to 11 m. The island, located in water varying from 16–19 m in depth, required over 180 million m^3 of fill material. To design against liquefaction from potential seismic events and to control future settlement, sand drain piles each 40 cm in diameter spaced 2.5 m apart are driven into the alluvial clay layer. Over 11 km of sea walls form the periphery of the island.

The cost for its design and construction total 1.5 trillion yen ($17.6 billion) paid by the National and Regional Governments and from private grants.

The passenger terminal building is designed of steel frame and partial–steel–frame

ferroconcrete construction. A floating foundation with 870 jacks is used to raise the building as needed to compensate for settlement differentials. This differential settlement system is an innovation that levels floors of all facilities to account for land settlement. The facilities are constructed on reclaimed soil, sandwiched between a 2.5 m thick iron ore layer, and a mat foundation. The settlement measuring system monitors settlement based on water level in an array of detectors. Hydraulic jacks with capacity of 300 kg/cm^2 each are used (4 for the terminal building and 2 for the airline operation buildings and other service buildings) to raise the structure. Leveling is manually performed by increasing the building height 1 cm at a time and installing steel shims until the floor is level. Since construction, the passenger terminal has been raised 10 cm.

During the 19 January 1995 earthquake the instrumentation installed in the passenger terminal recorded horizontal accelerations of 270 gals and 500 gals at its 1st floor and roof respectively. No noticeable damage occurred other than a segment on the ANA Hangar roof. The ANA hangar is a field maintenance facility; it does not have heavy load equipment such as overhead or gantry cranes. The building is a double bay frame with post tensioned trusses. The building measures 120 m by 100 m by 34 m high (effective dimensions are 114 m by 96 m by 26 m) and 27 m high interior clear space. The hangar doors consist of 28 sliding double leaf panels each weighing 15 tons. The doors are pinned at the top but only three base slots are installed to lock the doors in-place to help reduce damage during strong winds. The hangar roof is designed to support 30 cm snow load; its slope ratio is 1.6:60. The roof weighs 2,200 tons. Its settlement correction system follows the jack up method for pillars, floors, and the single slide rail following leveling practices used in the passenger terminal. Since the floor has no columns, screw jacks are built into the floor requiring a person to wind down on a 7.5 cm screw jack to create at least a 1.5 cm gap permitting space to inject grout. The screw grid is a 2 by 4 m pattern. The hangar cost of 4 billion yen ($47 million) is not counted in the overall airport expense.

Public Works Research Institute
Ministry of Construction
1, Asahi, Tsukuba-shi Ibaraki-ken, 305 JAPAN
TEL.0298-64-2211, Fax.0298-64-2148